Chapter 1

Electric Power Engineering, Systems, and Networks

Solution To Economic Load Dispatch Problem Using particle Swarm Optimization Method

Mr. S. Mohammad Rafee Dr. Shankarappa F Kodad

ABSTRACT

This paper presents the solution to Economic Load Dispatch problem using Particle Swarm Optimization Method. Economic Load Dispatch Problem is allocating loads to plants for minimum cost while meeting the constraints. It is formulated as an optimization problem of minimizing the total fuel cost of all committed plant while meeting the demand and losses. In this paper Economic Load Dispatch problem described mathematically as a minimization of problem of minimizing the total fuel cost of all committed plants subjected to the constraints. This paper presents minimizing the allocation of total fuel cost and transmission losses using the PSO. This is a new optimization method which optimizes the objective function by using less memory.

INTRODUCTION

Economic Load Dispatch problem is allocating loads to plants for minimum cost while meeting the constraints. Copious works had been done to solve this problem for plants having continuous fuel cost equations. But little work has been done so far if the plants have either piecewise quadratic fuel cost equations(multiple fuel cost equations) or piecewise linear fuel cost equations(combined cycle cogeneration plant), little work has been done so far. Since the fuel cost equations are discontinuous and different it is very difficult to find a global solution. Though some investigations were reported in the literature on the multiple fuel options, yet much remains to be done. Lin and Viviani[1] have attempted this problem with hierarchical approach of incremental cost for various combinations of fuel cost equations iteratively. Rajaram and Ramraj[2] approached this problem with some improvement. RB Kelkar and RC Desai[3] tackled the problem with dynamic programming . though the procedure of finding the global as well as all possible solution , it is suffering the curse of dimensionality when the number of plants is increased. In this paper a unique approach is presented to solve this problem.

The results obtained by the present method are given in tables 2 and 3. The results are compared in table 4 with the results

obtained by other methods. This algorithm uses PSO with quadratic programming. This paper is divided in to four parts. The first part explains the problem, the second part outlines the transformation of variables technique, third one deals with PSO and fourth part is concerned with numerical examples. This algorithm is finding the most economic allocation for any demand. The results are compared with other existing methods.

PROBLEM STATEMENT

Where Uij and Lij are the upper and lower limits for ijth plant and Dis the real power demand on the system.

To determine the transmission losses either load flow or Bmn cosfficients are considered. The problem can be formulated as minimizing the overall cost function.

$F_N(D) = \sum_{i=1}^{N} Fci$; Uij≤ Pij ≥Lij

$$\sum_{i=1}^{N} Pij = D + Pl$$

$$Pl = \sum_{i=1}^{N}\sum_{j=1}^{N} Pi\ Pj\ Bij \quad (2)$$

TRANSFORMATION VARIABLES TECHNIQUE

For economic load dispatch of plants having continuous fuel cost equations the equal incremental cost criteria is used to allocate the loads of them. The fixed cost does not play any role in that case. But in case of plants having discontinuous fuel

Consider a power plant with N units and m discontinuous quadratic or linear fuel cost pieces. For each unit the fuel cost equations for ith plant with jth piece is expressed in quadratic form as

$$Fci(Pij) = AiiPij^2 + Bij\ Pij + Cij$$

Uij < Pij <Lij (1a)

Aij=0, if it is alinear piece. (1b)

cost equations the fixed cost coefficients can play a role to commit a particular piece that plant. So some normalization to be implemented in such to assign priority between them. The following procedure is carried out for plants. For any plant piece having highest fixed cost (Cij) is chosen and fixed costs of other also normalized to that value by the following substitution. Let the maximum value of fixed cost be Ci_{max} for ith plant. Make a substitution Pij = Xij+ Kij for all other pieces of that plant such that the following relation is obtained.

$$AijKij^2 + BijKij + Cij = Cimax \quad (3a)$$

Suppose Kij is not a real number, and then ahoose some other value, which is greater or smaller than $Cimax$ which can give real value for Kij. Now the problem been transformed as below.

$$Fci(Xij) = aijXij^2 + bijXij + cij \text{ Rs/Mw/h} \quad (3b)$$

$$uij < Pij < lij$$

$$aij = Aij, bij = 2AijKij + Bij,$$

$$cij = AijKij^2 + BijKij + Cij = Cimax$$

$$uij = Uij - Kij, lij = Lij - Kij \quad (3c)$$

From the given data of the piecewise quadratic or linear cost functions are normalized by transformation of variable technique and the incremental cost lines are calculated.the incremental cost lines are different and continuous. If the Kth plant have m quadratic pieces, given as

$$2\,ak1\,Pk1 + bk1 = \lambda k1(lk1 < Pk1 < uk1)$$

Table 1 B_{mn} Coefficients for test system

0.0000750	0.000005	0.0000075
0.0000050	0.000015	0.0000100
0.0000075	0.000010	0.0000450

$$2\,ak2Pk2 + bk2 = \lambda k2(lk2 < Pk2 < uk2)$$
$$2\,akmPkm + bkm = \lambda km(lkm < Pkm < ukm)$$

Then the piece having lowest incremental cost limit is given a priority level of 1. In the same way the quadratic or linear pieces are arranged in ascending order based on incremental cost limit. Since the incremental cost lines are discontinuous and different, a Particle Swarm Optimization programming method along with transformation of variables technique is used to find the optimal solution.

PARTICLE SWARM OPTIMIZATION PROGRAMMING

The PSO is an effective optimization method to find the global minimum if the objective function is quadratic and the constraints are linear. Quadratic programming is used recursively from the lowest incremental cost region to highest incremental cost region to find the optimization allocation. Once the limits are found and the data is rearranged in such a way that the incremental cost limits of all the plants are ascending order.

For meeting any demand the algorithm is explained in the following steps

1. Assume all the plants are operating at lowest incremental cost limits that is with pieces with priority level of 1.
2. Substitute Pi = Li+(Ui- Li) Xi, where $0 \leq Xi \leq 1$ and make the constraints linear by omitting the higher order terms.
3. Solve the Economic Load Dispatch using PSO programming recursively to find the allocation and incremental cost for each plant within limits of that plant.
4. If there is no limit violation for plant for that particular piece, then it is a local solution.
5. If for any allocation for a plant , it is violating the piece limit, then replace that piece by the next piece for that particular plant.
6. Repeat steps 2,3,4 till a local solution is achieved.

7. Once a local solution is found check and compare that the incremental cost limit of any other piece of that plant can have the same incremental cost. If it is so, replace the piece with new one and find once again a local solution using steps 2,3,4,5.
8. Once all local solutions are found, the best allocation giving minimum cost is the global solution.

SIMULATION AND RESULTS

Example 1

A test system with three two thermal plants and one combined cycle cogeneration plant is considered[6]. The fuel cost equations of the system are given below.

$$F1 = 0.001562\,P1^2 + 7.92 + 561, \quad 100 \le P1 \le 600$$

$$F2 = 0.001942\,P2^2 + 7.92 + 310, \quad 100 \le P2 \le 400$$

$$F3 = 8.517P3 + 62.7, \quad 50 \le P1 \le 63.75$$

$$=605.67, \quad 63.75 \le P3 \le 82.75$$

$$= 9.18P3 + 6.289, \quad 82.875 \le P3 \le 93.75$$

$$= 1452.84, \quad 93.75 \le P3 \le 157.5$$

$$= 17.62\ P3 - 1660, \quad 157.5 \le P3 \le 200$$

Table 2 Comparison of results obtained by Micro Genetic Algorithm and Proposed method for two thermal plants and one CCCP

Micro genetic Algorithm						Proposed Method				
Demand	**Pg1**	**Pg2**	**Pg3**	**PI**	**Cost**	**Pg1**	**Pg2**	**Pg3**	**PI**	**Cost**
869	399.78	310.62	176.84	18.24	8368.47	374.577	353.764	157.5	16.84	8191.8
750	286.48	393.99	80.41	12.55	7267.82	308.100	296.53	157.5	12.13	7072.92

This algorithm is applied to this system. It is found that this algorithm not only

faster it is more efficient , accurate and reliable. The new algorithm is applied to the above problem. It is compared with Micro genetic algorithm[5] and the results in Table 2.

Table 2 Comparison of results obtained by Micro Genetic Algorithm and

Proposed method for two thermal plants and one CCCP.

A test system having ten plants each with three fuel options distributed in three areas is considered. The system is found to have minimum and maximum generation capacity of 1353MW and 3695MW, respectively. The load demand is assumed to vary between 2400MW and 2700MW in steps of 100MW. The results obtained by the present method are given in Table 3. The results are compared in Table 4 with the results obtained by other methods.

Example 2

Table 3 Optimum Allocation of proposed method for test system

plant	2400	2500	2600	2700
1	189.74000	206.51900	216.54400	218.24400
2	202.34300	206.45000	210.90500	211.66200
3	253.89500	265.73000	278.54400	280.72200
4	233.04500	235.95000	239.09600	239.63100
5	241.82900	258.01700	275.51900	278.49700
6	233.04500	235.95300	239.09600	239.63100
7	253.27400	268.86300	285.71700	288.58400
8	233.04500	235.95300	239.09600	239.63100
9	320.38300	331.48800	343.49300	428.52100
10	239.39600	255.05600	271.98600	274.86600
Incremental cost	0.42825	0.46276	0.50007	0.53739
Cost	481.72200	526.23800	574.38000	623.80900

Table 4 Comparison with other methods for test system 2

Demand	Results of Ref.9	Results of Ref.1	Results of Ref.3	Results of Proposed method
2400	488.46	487.91	481.73	481.720
2500	526.16	525.69	526.23	526.238
2600	573.52	574.28	574.39	574.380
2700	625.22	623.81	623.80	623.809

The advantage of the proposed method over GA

It takes comparatively less memory and time.

(1) It is certain to find the global minimum since the objective is quadratic ally convex function, but the GA is not certain to find global minimum all the time.
(2) This method meets all the constraints and does not require any penalty to be imposed for constraint violation, unlike GA.

CONCLUSION

The advantage of this method is that it is straight forward, faster and has the ability to find multiple solutions. Since it is robust and faster it can be considered for real time implementation.

REFERENCES

1. C E Lin and G L Vivianib. 'Hierarchical Economic Dispatch of Piecewise Quadratic Cost Functions.'' *IEEE Transactions on PAS*, vol PAS-103, no 6, June,1984.

2. N Ramaraj and R Rajaram. 'Analytical Approach to Optimize Generation Schedule of Plant with Multiple Fuel Options.'' *Journal of The Institution ofEngineers (India)*, vol 68, pt EL December 1987, p 106.

3. R B Kelkar and R C Desai. 'Easy Approach to Generation Scheduling with Multiple Fuel Options.''*Journal of The Institution of Engineers (India)*,

vol 80, pt EL December 1999, p 96.

4. S Baskar, P Subbaraj and M V C Rao. 'Hybrid Genetic Algorithm Solution to Economic Dispatch Problem with Multiple Fuel Options.' *Journal of The Institution of Engineers (India), vol, 82*, pt EL December 2001, p 177.

5. P Vengatesh, P S Kannan and Anu devi. 'Application of Micro Genetic Algorithm to Economic Load Dispatch.' *Journal of The Institution of Engineers (India), vol 82*, pt EL, September 2001, p 155.

6. S S Rao. 'System Optimization.'' *Wiley Eastern Publication*, New York, 2000.

7. L.K.Kirchmayer. 'Economic Operation of Power System.'*John Wiley and Sons, New York, 1984.*

8. Hadi Saadat. 'Power System Analysis.' *TATA McGRAW-Hill Publications*, New Delhi,2001.

9. N Ramaraj and K Nagappan. 'Analytical Method to Optimize Generation Schedule.'' *Journal of The Institution of Engineers (India), vol 66*, pt EL 6,1987, p 240.

Systems, Reactive Power Compensation.

Email: mdrafee1980@gmail.com

Dr. Shankarappa F. Kodad: He is from India. He has done his PhD in Energy Systems field. Now is working as a Professor in Aurora Engineering College, Hyderabad, India. He has published papers in various international journals and conferences.

Mr. S. Mohammad Rafee **M.Tech** **:** He is from India **.** Presently he is working as a Lecturer in Electrical Department in Al Jabal Al Gharbi University, Libya. He has published 7 papers in national and international conferences. His area of interest is Intelligent Protection, Harmonic Analysis in Power

Genetic Algorthims Optimization Approach for Three-Phase Passive Filter Design

Hazem Zubi
Electrical and Electronic Engineering Department
University of Bath
Bath, BA2 7AY, UK
hz224@bath.ac.uk

Rod Dunn
Electrical and Electronic Engineering Department
University of Bath
Bath, BA2 7AY, UK

Abstract

A new approach to designing improved broadband passive harmonic filters (IBFs) for such applications as direct on-line, adjustable-speed drives is
proposed, which employs genetic algorithms (GAs). The method is based on frequency domain modeling of the system. The success of the method requires accurate representation of the load harmonics. By using the proposed
GAs program, it becomes possible to quickly find the optimized power quality indices that will minimize filter size and harmonic resonance problems. The paper illustrates the potential performance of optimal IBFs using computer simulation to validate GA-assisted filter designs for 5.5 kW and 55 kW ASDs.

Index Terms-- ASD, broadband filter, design, Genetic algorthims (GAs), harmonic, power factor, rectifier, THD.

I. INTRODUCTION

djustable speed drives (ASDs) are widely used for driving AC motors in many industrial variable-speed applications [1], [2].Within these, the 6-pulse diode/thyristor rectifier, which is frequently connected direct-on-line to provide the input DC voltage-bus for the inverter, injects current harmonics into the AC power network. The harmonics excite resonances in power-system components, increase distribution transformer and line losses, produce voltage distortion at the point of common coupling (PCC) and cause a number of other detrimental effects within the power system and within other connected equipment. National standards authorities and electric power utilities have, therefore, introduced

mandatory standards in an attempt to limit the adverse effects of the increasing numbers and capacity of nonlinear, rectifier loads now being connected [3], [4]. The standards essentially place limits on the current-harmonic levels that may be injected into the AC network. For this reason, it is now more important than ever for equipment manufacturers and users to become adept at designing AC-side filter for use before the rectifier of ASDs.

Generally, for three-phase rectifier ASD systems harmonic mitigation techniques can be categorized as shown in Fig. 1. The purpose of these is to make the input current nearly a pure sinusoidal waveform,

so as to reduce the overall total harmonic distortion (THD). Passive filtering is the most widely employed method [5], [6].
Active filters are still avoided in most applications due to their high cost and complexity [7]. Phase multiplication (12 and 18 pulse) converters have low efficiency, large size, and high cost [8]. The three-phase boost type (AC-DC) PWM rectifier has superior performance compared to conventional diode or thyristor bridge rectifiers. However, designing a proper controller for it is generally a challenging task [9]. For PWM- Voltage Source Rectifiers (PWM-VSR), benefits like power regeneration, low harmonic distortion, unity power factor, and controlled DC link can be obtained. However, the topology complexity and high cost are the main drawbacks and make it impractical in many applications [10].

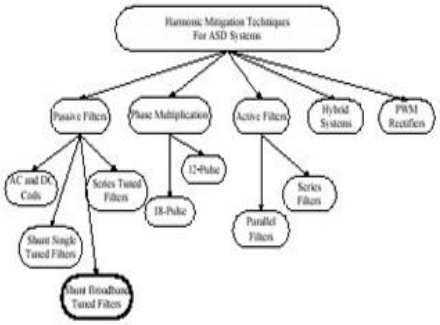

Fig.1. Classification of harmonic mitigation techniques for ASDs systems.

Among the various types of passive harmonic filters that exist, only the shunt tuned and broadband filter structures yield high power quality and allow systems to meet IEEE 519 and other recent standards. Since tuned filters carry the risk of forming a lightly damped resonant circuit, their application requires a relatively high degree of expertise.
Also the design rapidly increases in cost and complexity since multi-stage filters (one for each dominant harmonic frequency) are required. In contrast, the recently developed broadband harmonic filters are free of both the harmonic resonance problem, and structural complexity. Therefore, broadband filters appear to be a more practical approach to limiting harmonic-current injection. Input current Total Harmonic Distortion (THD) levels less than 10% and input power factor values near unity can be obtained with the broadband filter structures. In particular, the recently developed improved broadband filter (IBF) has superior overall performance and its applications have been increasing rapidly. However, the design process for determining the IBF parameters is complex. With input and output power quality requirements and filter efficiency, cost and size requirements, there are a large number of conflicting constraints to be optimized which complicate the design process and impede reaching the most effective design. At the present time, there are few publications on IBF design. Available material, largely filter manufacturer datasheets, does not give parameters and only provides performance data. One linear optimization searching method for the filter parameters was introduced in [11]. The linear nature of this searching method could be considered as the main drawback. This is due to the fact that linear method can be easily trapped in local optima.

Mathematical optimization methods have been used over the years in designing conventional shunt passive filters.
However, for IBF topology, the solution can not be easily obtained by these methods. This is due to multi-objective, discontinuous nature of the solution space.

Considering the fact that the optimal solution can not be simply achieved by mathematical optimization techniques, it has been essential to use an optimization technique with a robust searching capability. The genetic algorithm method is one of few that have the following features: the ability to store and use human knowledge to judge the solutions; the ability to learn and adapt from one solution point to another; a high likelihood of searching most of the solution space.

In this work, the IBF operating principle and its design principles are reviewed. A novel design algorithm using GAs is used to find the optimal power quality indices that can be obtained while keeping the filter size small and avoiding harmonic-excited resonance. The method is applied to ASDs of different power rating and based on frequency domain modeling the system. Finally, the performance of the IBF filtered ASD system is evaluated and its superior performance is proven analytically with the aid of detailed computer simulations. Overall, this paper proposes a new approach for the IBF design which reduces the filter size (cost) and demonstrates the IBF's superior performance. In order to validate the efficacy of the GA method, a comparison of the filter size given by a previous design method is presented.

II. IBF OPERATING AND DESIGN PRINCIPLES

The basic LC broadband filter, shown on Fig. 2(a), involves a simple structure with relatively large components [12]. The filter is free of the harmonic resonance problem. However, in particular at no-load the filter output voltage becomes excessive that may lead to rectifier or filter failure [13]. Also the power factor is largely leading at all load conditions. Trade-off relations between input current THD and power factor are strong. Thus, the filter does not yield overall a satisfactory performance. To overcome the deficiency of the LC broadband filter, the improved broadband LLCL filter (IBF), shown on Fig. 2(b), has been developed such that the basic LC filter problems are eliminated [14], [15]. As shown in Fig. 2(b), splitting the L filter of the simple LC broadband filter into two elements
(Li and Lf) the filter input-to-output behavior is altered.
Further, a 3-5% smoothing reactor (Lo) is inserted between the rectifier terminals and the filter output terminals. Filter capacitors Cf are usually delta connected and damping resistors Rd are connected to Cf (shown later in the system equivalent circuits) to damp the voltage/current peaks during line-side switching transients.

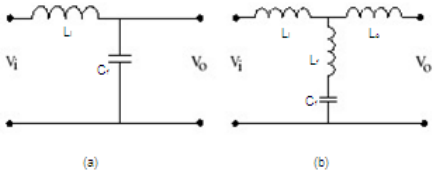

Fig.2. Broadband filter configurations (a): LC type, (b): LLCL type.

With an appropriate design, at the dominant rectifier current harmonic frequencies, the large input reactor (Li) provides high impedance, with respect to the shunt filter impedance, over a wide frequency range and gives a high impedance ratio as shown in Fig. 3... In consequence, all the rectifier current harmonics will be impeded by the line and diverted to pass through the shunt filter. Not only does Li block the current harmonic flow from the rectifier to the
AC line, but it also minimizes the effect of the line voltage harmonics on the rectifier (i.e. provides harmonic isolation between the source and the rectifier) and on the

shunt filter. Therefore, Li blocks the current harmonic flow either way.

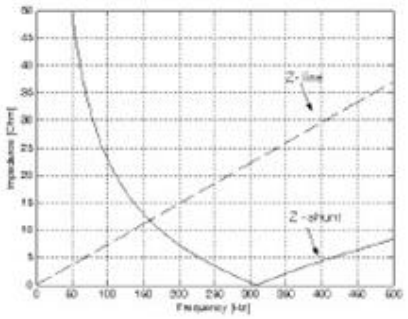

Fig.3 Line and shunt branch impedances of IBF (5.5 kW system).

The filter parallel-resonant frequency fp involving Li-Lf- Cf is defined in the following.

$$f_p = \frac{1}{2\pi\sqrt{(L_i + L_f)C_f}} \quad \dots\dots\dots (1)$$

The parallel-resonant frequency is selected between the fundamental frequency and the first dominant rectifier current harmonic which is the 5th harmonic such that harmonic resonance related overvoltage stresses are avoided. The filter capacitor Cf improves the input power factor while Lf is partitioned with Li such that there is no overvoltage at the rectifier terminals (unlike the LC filter) and no-load to full-load filter output voltage change is confined within a specified range.

Filter components Lf and Cf are connected in series to provide very low series impedance to the dominant rectifier current harmonics and short circuit them through its path.

The series resonant frequency fs is defined in the following.

$$f_s = \frac{1}{2\pi\sqrt{fC_f}} \quad \dots\dots\dots (2)$$

The output reactor (Lo) is a current smoothing reactor that makes the rectifier current waveform less discontinuous, resulting in lower current harmonics. It reduces the rectifier current THD significantly (4% Lo reduces the THD by 50%); and, hence, produces less harmonic current/voltage stress on the shunt branch components Lf and Cf, leading to smaller, lower cost and more efficient filter structure.

III. IBF DESIGN METHOD

In the IBF design procedure; there are five filter parameters (Li, Lf, Lo, Cf, and Rd) that must be determined.

With various power quality requirements along with filter efficiency, cost and size, the design is limited. Therefore, the design process is a complicated duty.

The power quality design constraints considered are the input current THD, input power factor, and filter output voltage regulation, which are all defined in the following.

$$THD = \frac{\sqrt{\sum_{h=2}^{N} I_h^2}}{I_1} \dots\dots\dots (3)$$

$$PF = \frac{I_1}{I} \times cos\varphi \dots\dots\dots (4)$$

$$\Delta V_o\% = \frac{V_{o-NL} - V_{o-FL}}{V_{o-NL}} \times 100 \dots (5)$$

In (3) and (4), I1 is the line-current fundamental component, Ih terms are the line-current harmonic components, and I is the line current, all rms values. In (4), ϕ is the displacement angle between the fundamental line- voltage and line-current components. In (5), VO-NL is the no-load filter output voltage and VO-FL is its full-load value, both fundamental frequency and rms values.

In the design, the first parameter Lo is

selected as 4% reactor.

$$L_o = 0.04 \times \frac{V_{LR}^2}{\omega_e \times P_R} \dots\dots\dots (6)$$

In the above equation, ωe is the line radial frequency. VLR and PR are the rated line-to-line voltage and power respectively. With this choice, the rectifier full-load current waveform becomes well defined (practically its shape is independent of power ratings). Therefore, the rectifier current fundamental component and the dominant harmonic current components can be approximated as shown in Table
I.

Closed form formula calculation of the remaining filter parameters (Li, Lf, Cf, and Rd) based on the performance indices (3), (4), and (5) involves extremely complex mathematics (if possible at all). However, if initial filter parameters are available, it is possible to calculate the filter performance indices via some mathematical models. Then filter parameters 3-D space can be scanned efficiently to find the optimized performance indices. Due to the nature of the design problem, previously explained, the GA optimizing searching method is utilized.

TABLE I
RECTIFIER CURRENT RATIOS

Current ratios (%)	I(%)
I1/I1	100
I5/I1	34
I7/I1	9.5
I11/I1	7
I13/I1	3.5
Higher order terms	neglected

IV. GENETIC ALGORITHM (GA)

The GA is a search mechanism based on the principle of natural selection and population genetics. An increasingly better approximation of the desired solution can be produced by applying the principal of survival of the fittest. In each generation, a new set of approximations of the solution are chosen according to fitness evaluation. The more 'fit' the approximation is, the higher likelihood it has to be selected to reproduce the next generation by using operators borrowed from natural genetics. Thus, the population of solutions is improved from one generation to the next with respect to their fitness evaluation. So, the least fit individuals are replaced with new offspring, which come from a previous generation, and which are better suited to the evolution of the environment.

Fig. 4 shows the Genetic Algorithm Flowchart used in this work. In the first step, a set of possible random solutions is created or initial solutions range can be specified. Every solution in the population (which can also be called an individual or a chromosome) is represented by a string of numbers that in turn represent the number of variables in the problem. Every variable is encoded in a suitable coding format (binary, integer, etc.).

In the second step, every chromosome is applied to the fitness function (also called the objective function) to produce an output of fitness values. In accordance with their fitness values a probabilistic technique, such as the
Roulette Wheel [16], is used to select the chromosomes that will contribute to the production of the next generation. The reason for this selection process is to keep the best and most fit chromosomes and

increase the number of their offspring in the next generation, eliminating the least fit chromosome. Having selected the parents, the crossover process then takes place by the exchange of genetic information between the selected chromosomes in order to form two new chromosomes (also referred to as children or offspring). This helps to avoid sticking in local optima. In order to ensure that GA will search different zones of the search space, a mutation is applied by randomly selecting and changing the structure of a limited number of chromosomes.

This process is repeated until all solutions converge into one optimum solution [17].

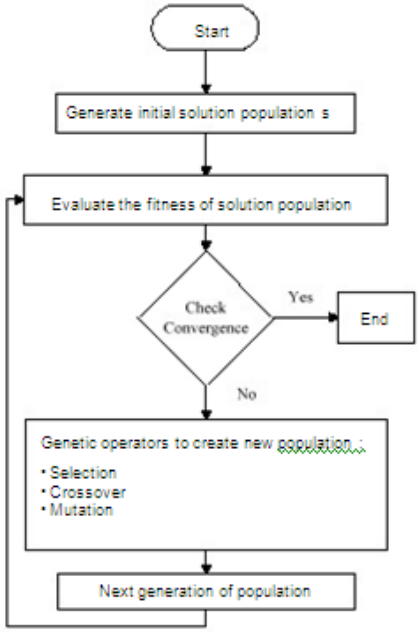

Fig. 4 Genetic Algorithm Flowchart

A. Problem Formulation

The main goal of this optimization problem is to design the improved broadband filter that yields optimal system power quality indices, small filter size and minimal harmonic resonance problems. The power quality indices considered in this optimization problem are THD, PF and ΔV%. The use of these factors facilitates obtaining a design with acceptable filter parameters.

The main filter elements which dominate the design size and performance of the IBF are the inductances Li, Lf, and the capacitance Cf.

B. Chromosome Encoding and Selection

As mentioned before, the values of the inductance Li, Lf, and the capacitance Cf play a very important role in the design of the improved broadband filter and ASD system performance. Therefore, they are considered in the structure of the chromosomes used in this optimization problem.

001	110	100
L_i	L_f	C_f

Fig.5 Chromosome structure utilized in GA.

As seen in Fig. 5, the number of variables in each chromosome represents the values of the line inductance Li, and filter inductance Lf, and the filter capacitance Cf, respectively.

C. Crossover and Mutation

The crossover method used in this study is a single point crossover. Different values of crossover fraction, varied from 10% to 100%, and mutation rates from 1% to 10% have been used in this research project to compare the performance of the proposed GA program. A range of population sizes from 50 to 200 and different numbers of generations varied from 100 to 700 were utilized.

A relatively wide range of GA operators was initially used until experience was gained observing their effects. It was found that an appropriate mutation rate will speed

up the evolution process and shorten the searching time of GAs. High crossover fractions (80%) and low mutation rates (2%) achieve the best convergence. These GA operators are applied to 200 generations with 100 populations for each generation. In modern computers, this computational requirement is completed in a few seconds.

D. Fitness F unction

The objective of the fitness function illustrated by (7) in the proposed GA program is to find out the minimum line current THD, minimum voltage regulation and the maximum line PF.

$$Fitness = THD + \Delta V_o + (1/PF) \dots (7)$$

Every chromosome in the current generation will be examined by the above fitness function. To calculate the filter performance indices (THD, ΔVo and PF) in the fitness function via some mathematical models, an accurate design method is required.

V.ACCURATE COMPUTATIONAL METHOD

The evaluation of the filter performance indices for a given set of parameters Li, Lf, Cf proposed by the GA solution will be through an accurate design method. The approach is based on utilizing highly accurate filter-ASD system equivalent circuits (in the frequency domain) and evaluating the filter performance for the given set of parameters. Therefore, the whole drive system must be modeled accurately. For steady-state performance investigation, the frequency domain model of the total system involving the AC line, the broadband filter, and the rectifier is established. At steady state the ASD is modeled with equivalent impedance or current source elements, depending on the frequency considered. Fig. 6 and Fig. 7 show the fundamental frequency model and the harmonic model of the system at full-load (rated power).

In the fundamental frequency equivalent circuit, the ASD
is reflected to the AC side of the rectifier as an R-L impedance circuit. Since the DC bus capacitor of an ASD is typically very large and decouples the inverter dynamics from the rectifier side, the drive (DC bus capacitor, inverter, motor load, etc.) is modeled with an equivalent DC resistor. This DC resistor, DC bus capacitor, and rectifier are all reflected to the filter side as the equivalent load resistor RL and inductor LL. The equivalent resistor value is found from the assumption that the filter is lossless and its terminal voltage is equal to the nominal voltage. The rectifier commutation effect and output voltage drop are represented with LL which has been found empirically [18].

These parameters are defined as follows:

$$R_L = \frac{V_{LR}^2}{P_R} \dots \dots \dots (8)$$

$$L_L \cong L_i + L_o \dots \dots \dots (9)$$

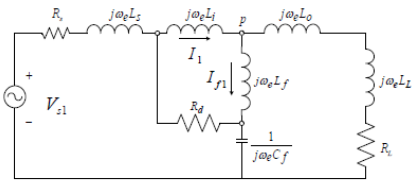

Fig. 6 Full-load fundamental frequency model of the ASD system.

The full-load equivalent circuit can also be utilized for no-load system modeling by setting RL larger than the shunt impedance by an order of magnitude. The full-load

fundamental-frequency current value is calculated as follows.

$$I_R = \frac{V_{LR}}{\sqrt{3}R_L} \dots\dots\dots (10)$$

In the harmonic equivalent circuit of Fig. 7, the rectifier side is modeled with a harmonic current source and the grid is represented with a harmonic voltage source. The grid voltage harmonics are selected depending on the utility grid properties. The rectifier current harmonic ratios are chosen from Table I, and the harmonic currents are found by multiplying the harmonic current ratio with the fundamental component current (I1=IR from (10)). For each harmonic frequency, the effect of the line-voltage harmonics and rectifier-current harmonics on the circuit is found by superposing the magnitude (pessimistic approach) of the resulting voltages (or currents). The simplified approach yields satisfactory results.

With the rectifier and its nonlinear behavior replaced by linear circuit elements and the sources, the steady-state equivalent circuit becomes a linear circuit where closed form calculations and analysis can be made. With all the parameters defined, the circuit can be completely analyzed and performance predicted.

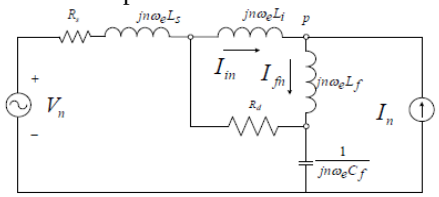

Fig.7 Full-load harmonic frequency model of the ASD system.

The damping resistor Rd is neglected in the steady-state conditions. Its selection criteria are related to transient conditions and are explained in [11].

VI. GENETIC ALGORITHM OUTPUT

For given ASD ratings and power system parameters, based on the system equivalent circuits, the filter- component values for Li, Lf, and Cf are initially proposed in a GA MATLAB M-file [19] based computer program. The initial range of values is estimated by the linear design method utilized in [11]. The program implements the derived formulas, calculates the impedances, then voltages, and currents followed by performance calculation (THD, PF, ΔVo). Based on the performance obtained, every set of solution (chromosome) in the current generation will be examined by the fitness function of (7). The filter parameters are varied until the objective of the fitness function is met with suitable convergence. Fig. 8 shows that the optimized solution is obtained in generation number 43 and the whole population ultimately converges toward the optimized solution. The corresponding 5.5kW ASD power rating filter parameters obtained are Li (10.1mH), Lf (8.1 mH) and Cf (16.6 F). The corresponding series resonance frequency fs and parallel resonance frequency fp values are 250Hz and 167Hz, respectively. The fp value shows that the harmonic resonance problem risk is negligible for the system. Other ASD power rating results will be presented and compared to the linear method results in the next section.

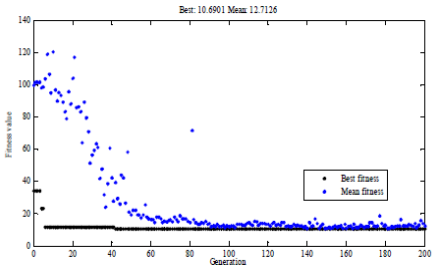

Fig.8 Best and mean fitness function values in GA for 5.5kW ASD system.

VII. SYSTEM PERFORMANCE EVALUATION

The proposed design method with the GAs searching technique was evaluated for ASDs of various power rating.

The utility line was considered to have 3% voltage THD.

The grid impedance was considered to be negligible compared to the input inductance Li. Best fitness value involves system power quality indices of line current THD < 6.5%, line PF > 0.98 and filter output voltage regulation

< 3.2%. For the same power quality indices criteria applied to the linear searching method, filter parameters obtained have higher values. The filter parameters obtained with

both methods for 5.5 and 55kW power rating ASDs are shown in Table II. Reductions of (5-15) % in the input inductance Li and (15-20) % in filter capacitance Cf have been achieved. Consequently, the filter inductance Lf will increase to keep the series resonance frequency (fs) within its desired and effective values. Nevertheless, the value of Lf is much smaller than Li for all power ratings. Since the input inductor is carrying the full line-current while the filter inductor is carrying only the harmonic-current components, a reduction in Li results in smaller filter size (cost). The filter capacitor reduction is also very effective in reducing the size (cost), improving the system power factor characteristics, and reducing output voltage regulation from no-load to full-load.

TABLE II.
IBF C OMPONENT VALUES.

PR (kW)	5.5		55	
Searching method	Linear	GA	Linear	GA
Li (mH)	10.6	10.1	1.138	0.99
Lf (mH)	6.0	8.1	0.598	0.75
Cf Δ (F)	21	16.6	208	180

Tables II and III allows a comparison between the performance of the two searching methods. As the tables indicates, the GA algorithm is capable of finding smaller values for the more bulky filter components that will achieve better power quality indices .

TABLE III.
PERFORMANCE COMPARISON

Searching method	THDI (%)	PF	Vo (%)
Linear	6.5– 6.75	0.95– 0.96	3.75-4.0
GA	6.0 - 6.5	0.98- 0.99	3.0- 3.2

With the filter parameters being determined, the IBF based system performance is evaluated. IBF performance characteristics are obtained based on detailed computer simulations utilizing Ansoft-Simplorer [20]. For the 5.5kW ASD system, the full-load line current and rectifier current simulation waveforms are shown in Fig. 9, while the full- load line-current and the supply phase-voltage

simulation waveforms are shown in Fig. 10. The line current has a
5.5% THDI value and the line power-factor is 0.987 leading at full-load conditions. These results are in close correlation with the equivalent circuit based estimation method results shown in Table III. They also verify the accuracy of the parameter determination method.

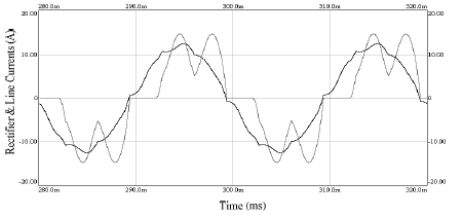

Fig.9 Full-load line (bold) and rectifier current simulation waveforms for 5.5kW ASD system.

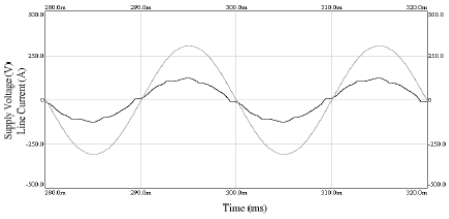

Fig. 10 Full-load line current (bold) and supply voltage simulation waveforms for 5.5kW ASD system (current scale: 10x).

The IBF line-current THD and line power-factor performance characteristics, from no-load to full-load, are shown in Fig. 11 and Fig. 12 for the power ratings considered. From nearly 50% load to full load, over a wide range the IBF based system provides high overall power quality performance. The input-current THD is at an acceptable level over the full operating range. The IBF based drive is substantially improved in terms of the harmonic injection to the connected AC network, making the drives impact on the connected power-system and other users in the vicinity of the PCC absolutely minimal. The power factor approaches unity at rated load and thus the IBF filter aids minimizing the reactive power requirement of the drive.

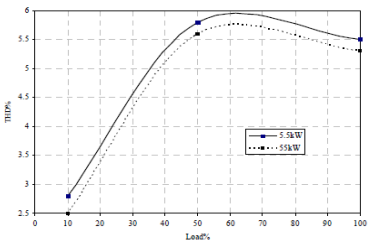

Fig.11 The load current dependency of the IBF line current THD.

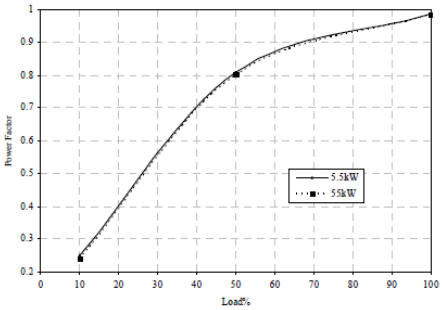

Fig.12 The load current dependency of the IBF line power factor.

VIII. CONCLUSIONS

The genetic algorithm design method, which has been described in this paper, can play an important role in the optimization of IBFs for industrial motor drives. The method allows a high standard of power-quality indices to be achieved with a set of filter components likely to have minimal bulk and cost overall. The design case-studies presented have shown that the

method is robust and has produced advanced designs, with lower filter size and cost, when compared to the results obtained by linear searching technique for the same power quality system requirements.

The new and simple frequency-domain equivalent- circuit-based analytical method for the improved broadband filter design is developed by using the GA. The method is efficient, accurate, and results in reduced filter size and cost along with less risk of harmonic-excited resonance problems.

The optimal filter parameters were validated in detailed computer simulations to obtain the IBF performance. The performance characteristics illustrate that the IBF had very low input current THD (<6%) and near unity power factor at full load.

The IBF system is a strong candidate for improving power quality demanding applications.

IX. REFERENCES

[1] B. K. Bose, "Energy, Environment, and Advances in Power Electronics," IEEE Trans. on Power Electronics, vol. 15, pp.688- 701, 2000.

[2] A. Savolainen, "Driving Towards a Better Future," ABB Review, Zurich, Tech. Rep. (34 – 38), 4, 2004.

[3] IEEE Recommended Practices and Requirements for Harmonic Control in Electric Power Systems, IEEE Std. 519-1992.

[4] R. C. Dugan, M. F. McGranaghan, Electrical Power Systems Quality, 2nd Edition, McGraw-Hill, 2002, p.282.

[5] S. Hansen, P. Nielsen, P. Thogersen, F. Blaabjerg "Line side harmonic reduction techniques of PWM adjustable speed drives-A cost-benefit analysis," in Proc. 2000 Nordic Workshop on Power and Industrial Electronics Conf., pp. 271-277.

[6] J. C. Das, "Passive filters –potentialities and limitations," IEEE
Trans. on Industry Applications, vol. 40, pp.232-241, Jan./Feb 2004,.

[7] B. Singh, K. Al-Haddad, A. Chandra, "A review of active filters for power quality improvement," IEEE Trans on Ind. Electronics, vol. 46, pp. 960-971, October, 1999.

[8] L. L. Grigsby, The Electrical Power Engineering Handbook, CRC Press, 2000, pp. 361-366.

[9] B. Yin, "Performance comparison of voltage mode control and current mode control of a three-phase PWM rectifier based on a dual SISO model," in Proc. 2006 IEEE Industrial Electronics Society
32nd Annual Conf., pp. 2220-2226.

[10] J. R. Rodriguez, J. W. Dixon, J. R. Espinoza, J. Pontt, P. Lezana, "PWM regenerative rectifiers: state of the art," IEEE Trans. On Industrial Electronics, pp. 5-22, Feb. 2005.

[11] A. M. Hava, H. Zubi, "Improved broadband harmonic filter design for adjustable speed drives," PEDS 2005, Malaysia, in press.

[12] M. M. Swamy, "Passive harmonic filter systems for variable frequency drives," U.S.Patent 5 444 609, Aug., 1995.

[13] M. M. Swamy, S. L. Rossiter, M.C. Spencer, M. Richardson, "Case studies on mitigating harmonics in ASD systems to meet IEEE519- 1992 standards," IEEE-IAS Conf. Rec., 1994, Vol.1, pp. 685 – 692.

,

[14]http://www.mtecorp.com/matrix. html

[15] A. M. Munoz, Power Quality, Mitigation Technologies in a Distributed Enviroment, Springer-Verlag London Limited, 2007,pp.152-153.

[16] D. E. Goldberg , Genetic Algorithm in Search, Optimization and Machine Learning ,Addison-Wesly, 1989.

[17] R. C. Bansal Dr. "Optimization Methods for Electric Power Systems: An Overview," International Journal of Emerging Electric Power Systems: Vol. 2 : Iss. 1, Article 1021 March 12, 2005.

[18] H. Zubi, "Design of Broadband Harmonic Filters for Power Rectifiers," M.Sc. dissertation, Dept. Elec. Eng, Univ. Middle East Technical, 2005.

[19] MATLAB 7.6, Mathworks Inc.," 2008.

[20] Ansoft-Simplorer, V7.0 (SV), 2004.

T he Libyan Arab International Conference on Electrical and Electronic Engineering LAICEEE 23-26/10/2010

Field Study of Protection against Direct Lightning Stroke

Dr. Fathi O. Hareb, Samah Abd asalam dweher
Academy of Graduate Studies Tripoli – Libya
School of Eng. Department of Electric and computer
(Code number of paper 102116**)**

Abstract

Lightning Phenomenon is a transient, high current discharge, due to the accumulation of charges in clouds.

This paper discusses the nature and causes of the phenomenon of lightning and Principle of lightning. Using Early Streamer Emission Method to design a lightning protection system. Then we start designing the protection system by using the early streamer Emission method. Once the level of the protection mainly depending, by the radius of the selected area which, measured according the Levels of the protection, and it found at Level one. The radius of the protected area can be covered at this level found equal to 78.58 m, of the electrical power systems against direct lightning strokes. The petroleum plants at Tripoli selected as a case study.

Applying two different techniques of lightning protection systems that can be used to protect the site. Then comparing between the two methods.

By using the protection level and the radius of the protected area of the study case, the numbers of protection units

required to cover the plant are four towers.

Key words: ESE - Early Streamer Emission Method, NC-Tolerable lightning frequency, RSM – Rolling Sphere Method, LAT- Lightning Air Terminal.

Introduction

Lightning, considered as a spectacular meteorological phenomenon, is one of the most fascinating events in the world.

Benjamin Franklin first constituted the preliminary scientific and systematic understanding of lightning phenomenon in 1752 that used a kite in order to verify that lightning is really a stream of electrified air. Interestingly when Benjamin Franklin experimented with the electric kite, there were no very tall structures and high-rise buildings like we observed today. However, until today over more than 200 years the Benjamin's lightning rod is still the most

internationally accepted Lightning Air Terminal (LAT). [1]

Aim of the paper:

1- To identify the suitable system event the direct lightning.

2- Applying two different techniques used for lightning protection.

Early Stream Emission and Rolling Sphere Methods for design lightning protection system for oil storage plant in Tripoli.

3- Comparing between the two methods of design and choosing the suitable system.

Literature review

Chew,T.P.1979**.** Discussed the lightning protection mechanism and concerned with the study of the mechanism of lightning protection. The main interest lies in the study of the performance of a radioactive lightning rod as compared with that of a conventional Franklin rod. Corvine, A. 1982 discussed the lightning protection for building structures. And reviews alternative arrangements of lightning arresters and concludes that the field performance of devices using radioactive isotopes. Bent, R. B 1986. Present the Lightning protection for building, towers, and Personnel. The purpose of a lightning rod and the basic requirements for lightning protection for building and towers are discussed. Other types of protection such as an overhead wires are discussed a long with radioactive systems. In addition to the elimination schemes. And the effects of lightning on persons and animals are also review.

Berger, G.2005**.** Present a comparison between Franklin rod and ESE. The conventional Franklin rod has been tested and then compared to an air terminal using an Early Streamer Emission (ESE) triggering device designed to enhance the Protection area of the Franklin rod. Extensive tested have shown that a high voltage pulse ESE air. Terminal is more effective then the conventional Franklin rod commonly used in the standards.

Methodology.

1- Study the concept of lightning.

2- Collecting available data from Lightning Meteorological. Authority concerning numbers of lightning monthly in Libyan.

3- Site measurement of the case study as, site area, oil tank diameters and height, and other factors needed for design.

4- Design a suitable of lightning protection system for Libyan oil site in Tripoli.

Design calculation.

- **Assumption:**

1- The site Located within a space containing structures or trees of the same height or taller C1 (Environmental coefficient) = 0.25

2- Structure coefficient C was taken C2 =0.5

3- High value or particularly flammable the site of the sited case C3 Structure contents coefficient = 3.0

4- Site occupation normally occupied C4 (Structure occupancy coefficient) = 1.0

5- Consequences on the environment **C5** (Lightning consequences coefficient) = 10.0

1-Using the Early Streamer Emission System.

When Applying ESE method some factors must be taken as mansion in the assumption such as C1, C2…andC5, to calculate the lightning tolerable lightning frequency (Nc), and the Expected lightning frequency (Nd) as followed

:

1- Determination of Tolerable Lightning frequency Nc:

- "Nc" = $5.5 * 10^{-3} / c$ (1)
- C2 = 0.5 (All structures are metal)
- C3 = 3.0 (Content of tanks is oil, which is explosive)
- C4 = 1.0 (Tanks are Normally occupied)
- C5=10.0 (There is consequences on the environment). Let

C=C2.C3.C4.C5=0.5*3.0*1.0*10.0
= 15.0

2- Tolerable lightning frequency:
"Nc" = $5.5 * 10^{-3} / C = 367 * 10^{-6}$

3-Determination of expected lightning frequency Nd:
The expected lightning frequency:

$Nd = Ng\ max. * Ae * C1 * 10^{-6}$ (2)

a- Ng_{max} (Lightning flash density (flashes/year/km^2) can be determined by :

$Ng_{max.} = 0.04\ (T)^{1.25}$ (3)

Where:
T is the number of thunderstorm days per year.
The site is located has, 9days thunderstorm per year
(T= 9) therefore, $Ng_{max} = 0.6235$
b- The equivalent collection area "A_e" is equal to the area of the site plus 25% for structures close to the site battery limits. The Equivalent collection area "A_e" can be determined by:

$\mathbf{A_e} = 400*100*1.25 = 50000\ m^2$

c- The site is located within a space containing structures of the same height or taller C1= 0.25
From the points a, b, and C, the expected lightning frequency Nd, as the following.
$Nd = 7.79375*10^{-3}$
According to value of (Nd & Nc) we found Nd > Nc; this means that the protection is required for the concerned site.
4-Determination of the effectiveness factor E by

$$E = 1 - \frac{N_C}{N_d}$$

(3)
E = 0.953 (i.e. the associated Protection level is at level one, the initiation distance D is, 20 meter.

5- Protection radius Determination Rp.
The protection radius of an E.S.E. Lightning conductor can be determined as following: [2]

$$R_P = \sqrt{h(2d-h) + \Delta l(2D + \Delta L}$$

(4)
Where: h = 5 m, D = 20 meters and
Δl = 60 (supplier's technical data for the E.S.E Lightning conductor) Therefore, Rp = 78.58 m, figure 1show the location of the ESE tower of the case study, and figure 2 present the tower installations.

2-Using Rolling Sphere method:

Striking distance (R) between the leader and the protection system depended on the current in the following lightning stroke. The striking distance increases with the lightning current according to the formula.[3]

$R = 10\ I^{0.65}$ (5)

Where; I in kA, and R in meters.

Table 1 Calculation results of Striking Distance

I_0 (KA)	$R=2*I_O +30\ (1-e^{-I_0/6.8})$	$R=9.4\ I_0^{2/3}$	$R=10\ I_0^{2/3}$
20	68.42	69.26	73.68
40	109.91	109.94	116.96
60	150.0	144.06	153.26
80	190.0	174.52	185.66
100	230.0	202.52	215.44
120	270.0	228.69	243.2
140	310.0	253.44	269.62

160	350.0	277.04	294.72
180	390.0	299.67	318.79
200	430.0	321.47	342.0

1-Calculations:
By using table 1.

1- In the first step we select current I= 10 KA

$R= 10(10)^{0.67}$

R= 64.41 (m)

2- In the second step we select current I= 20 KA

$R= 10(20)^{0.67}$

R= 73.68 (m)

3- In the third step we select current I= 40 KA

$R= 10(40)^{0.67}$

R= 118.4 (m)

Assume the minimum value of lightning current. I= (20KA) the system design (Rolling sphere method) is shown in Figure 3 The radius of imaginary sphere equal to **(**73.68m).

Comparison between two methods

After applying the two methods, ESE and RS on the site. The different between them as the following:

The rolling sphere method is difficult to apply and more complex

1- Structures and result in over design.

2- This method is very expensive compared to ESE.

3- It make partially protection site.

The advantage of ESE lightning conductor compared to Rolling Sphere method the protected area is bigger than area of (RS).

From this we found that ESE the best method as it covers a large

Protected area and cheaper than the Rolling sphere method.

Hence we have chosen the (ESE) method for applying in oil site.

Conclusions

Based on the average data of monthly and annual lightning in different areas over Libya obtained by the Libyan Meteorological Authority, it has been found that. Libya is considered as a low exposed area to the lightning strokes compared to other area over the world.

And by comparison the two methods of Lightning protection system found:

1- The estimated method RS results are very close to the calculation method ESE.

2- The two results fit the design consideration of protection towers.

3- This means that the design obtained for protecting the oil storage tanks site is approved by the methods.

4- This Study of lightning strokes protection the first done for Libyan oil sites.

References

[1] M. A. Uman and V. A. Rakov, A Critical Review of No conventional Approaches To Lightning Protection, American Meteorological Society, December 2002..

[2] Paul Hardarker "No more bolts from the blue,"IEE Review, September 1997.

[3] Donald G. Fink / H. Wayne Beaty "Standard Handbook for Electrical Engineers", Thirteenth Edition, McGRAW-HILL, INC., 1993.

[4] Lightning Eliminators & Consultants "Lightning Strike Protection, Criteria,

Concepts and Configuration "Report No. LEC-01-86, May 1995
[5] Walter J. Ros " Critical Issues in Distribution System Surge Protection" IEEE Transaction on Industry Applications, volume 24 , no. 2 March/April 1988.
[6] Dr. R. S. JHA "A Course in High Voltage Engineering ", DHANPATRAI & SONS, January 1981.

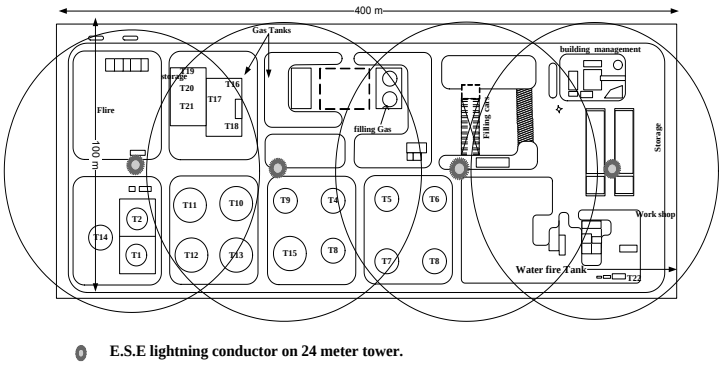

Fig.1- illustrate the distributions of 4 towers predicted by ESEM

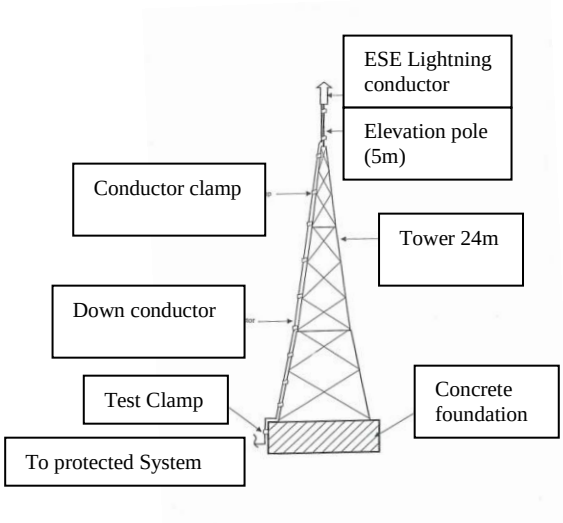

Fig.2, show the installations of the tower

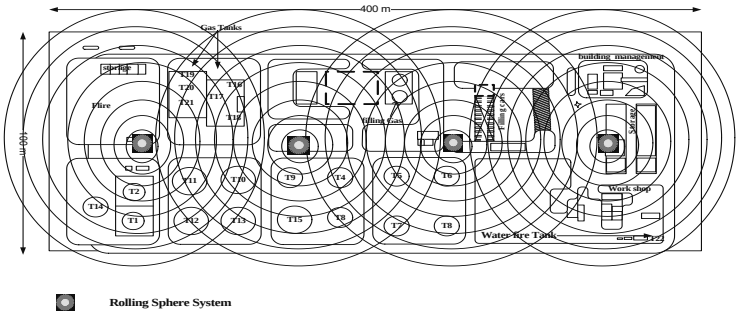

Fig. 4.6. distribution the Rolling Sphere method on the oil site

Fig.3, show the distributions of 4 towers predicted by RSM

Ability of FACTS Devices to Improve Transient Stability of Power Systems

Sattar Jaber Al-Isawi
Dept. of Electromechanical Eng.
High Institute for Industry
sattarjaber@yahoo.com

M. Abd-Elhameed
Dept. of Electrical Eng.
7-October University
m_a_elhameed@yahoo.com

Abstract

This paper proposes a new control strategy of flexible ac transmission system (FACTS) devices to improve the transient stability limit of power system. It is proposed to assess the ability of FACTS devices damping controllers in enhancing power system stability. The paper focuses in two different types of FACTS devices. First is a series device depends on thyristor controlled reactor, namely the thyristor controlled series capacitor (TCSC). The other one is the most recent developed FACTS devices that depend on voltage source converters, namely the unified power flow controller (UPFC). The contribution of these two devices, and their damping controllers, in system damping is analyzed from the point of view of damping and synchronizing torque coefficients.

This paper presents a simple method of evaluating the transient stability of a large power system in the presence of these two types of (FACTS) devices, which are represented by an equivalent circuit model. The model is then carefully interfaced to the power network to obtain the system reduced admittance matrix which is needed to generate the machine swing curves. The complex voltage at two end buses of the circuit model is also evaluated during simulation to implement various existing control strategies of FACTS devices and to update the reduced admittance matrix. The effectiveness of the proposed method of generating dynamic response and hence evaluating transient stability of a power system in the presence of various FACTS devices is tested on the M-IB system. The results obtained with various FACTS devices are also compared and discussed

Index Terms: Transient stability, flexible ac transmission system (FACTS), thyristor controlled series capacitor (TCSC), unified power flow controller (UPFC).

1. INTRODUCTION

Power flow through an AC line is a function of the phase angle, line end voltages and line impedance, and there is little or no control over any of these values. The consequences of this lack of fast and reliable control are stability problems, power flowing through other than the intended lines, the inability to fully utilize the transmission resources, undesirable Var flows, higher losses, high or low voltages, cascade tripping and long restoration times. With FACTS devices one can control the

phase angle, the voltage magnitude at chosen buses and/or line impedance. Power flow is electronically controlled and it flows as ordered by the control center using FACTS devices which include Static Var Compensators (SVC), Thyristor Controlled Series Capacitors (TCSC), Thyristor Controlled Phase Angle Regulators (TCPAR), Static Compensators (STATCOM), Static Series Synchronous Compensators (SSSC), Universal Power Flow Controllers (UPFC) [1]. There are a amount of work reported in the literature in the area of FACTS devices and power system operation [2,3,4,5, 6, 7,8].

2. MATHEMATICAL MODEL

This section describes the machine dynamic equations and a simple circuit model of FACTS devices.

In order to establish the relationship between the internal quantities of different machines in the power system, a common reference frame (D, Q) which rotates at synchronous frequency of the steady state network currents is considered. This selection is based on those derived in [9]. This selection has many advantages, the important one is that the angle δ between the d-q frame of each machine and the selected D-Q frame is itself the rotor angle that is between the system slack bus and the q-axis of the generators. Each individual machine can be referred to the general reference frame as:

$$\begin{bmatrix} v_{Di} \\ v_{Qi} \end{bmatrix} = \begin{bmatrix} \cos\delta_i & \sin\delta_i \\ -\sin\delta_i & \cos\delta_i \end{bmatrix} \begin{bmatrix} v_{di} \\ v_{qi} \end{bmatrix} \quad (1)$$

Or symbolically as

$$v_{Ni} = [T_{ii}]v_{mi} \quad (2)$$

Where

$$T_{ii} = \begin{bmatrix} \cos\delta_i & \sin\delta_i \\ -\sin\delta_i & \cos\delta_i \end{bmatrix} \quad (3)$$

The dynamics of rotor angle δ and velocity ω is described by the so called swing equations:

$$d\Delta\omega/dt = (1/2H)(T_m - T_e - D\Delta\omega) \quad (4)$$

$$d\,\delta/dt = \omega_o\Delta\omega$$

where $\Delta\omega = \omega-\omega_o$ is the deviation, in rad/s of rotor angular velocity from synchronous velocity $\omega_o = 2\pi f_0$, H is the p.u. inertia constant, D is the damping coefficient , T_m and T_e are the p.u. mechanical and electromagnetic torque, respectively.

The loads are converted to equivalent impedances or admittances. Thus if a certain load bus has a voltage V_L, power P_L, reactive power Q_L, and current I_L, flowing into a load admittance $Y_L = G_L + jB_L$, then:

$$P_L + j\,Q_L = V_L\,I_L^* \quad (5)$$

Substituting for I_L^*

$$P_L + j\,Q_L = V_L[\,V_L^*\,(G_L - jB_L\,)] \quad (6)$$

or

$$P_L + j\,Q_L = |\,V_L|^2\,(G_L - jB_L\,) \quad (7)$$

The equivalent load admittances are connected between the load buses and the references node. Thus the admittance bus matrix for each network condition may be constructed.

2.1 DYNAMIC MODEL OF M-IB SYSTEM EQUIPPED WITH TCSC

To study the effect of TCSC to damp the mechanical modes of a synchronous machine, machine connected to infinite bus through two parallel transmission lines with TCSC, shown in Figure 1, will be studied. V_1 is the machine terminal voltage and V_∞ is the infinite bus voltage. The machine is equipped with a static exciter, and the system data and equations are given in Appendix B. Dynamic model of the machine and the exciter is established in [10].

Third order model for the machine is used, assumptions of this model are found in [10]. In this model amortisseur effects are neglected, so that the damping controller will be designed at the worst case. Also, transformed induced voltages are neglected compared to the speed voltage terms in the stator and network voltage equations, and transmission lines transients are neglected.

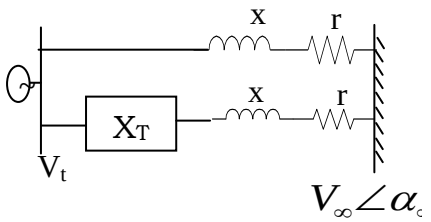

Fig.1: Machine-infinite bus system with TCSC

For the line with the TCSC, let $X_{ew} = X_e + X_{TCSC}$, the network equation can be written as

$$v_{abc} = v_{\infty abc} + r_e i_{abc} + L_{eq}\dot{i}_{abc} \qquad (8)$$

Using Park transformation and the assumptions of the third order model of the machine [11]

$$V_{0dq} = V_\infty \begin{bmatrix} 0 \\ -\sin(\delta - \alpha_\infty) \\ \cos(\delta - \alpha_\infty) \end{bmatrix} + r_e I_{0dq} - X_{eq} \begin{bmatrix} 0 \\ -I_q \\ I_d \end{bmatrix} \qquad (9)$$

Linearizing the above equation we get,

$$\Delta V_d = -V_\infty \cos(\delta_0 - \alpha_\infty)\Delta\delta + r_e \Delta I_d + X_{eq0}\Delta I_q + I_{q0}\Delta X_{TCSC} \qquad (10)$$

$$\Delta V_q = -V_\infty \sin(\delta_0 - \alpha_\infty)\Delta\delta + r_e \Delta I_q - X_{eq0}\Delta I_d - I_{d0}\Delta X_{TCSC} \qquad (11)$$

Equations 7 and 8 are the machine terminal voltage equations that include the effect of the TCSC dynamics on the system.

2.2 MODELING OF MACHINE-INFINITE BUS SYSTEM WITH UPFC

Consider the M-IB system shown in Figure 2.

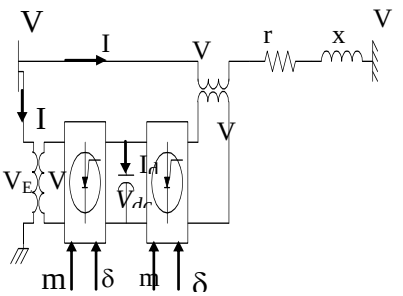

Fig.2: A UPFC installed in a single-machine infinite-bus power system

By applying Park's transformation [9] and ignoring the resistance and transients of the transformers of the UPFC, from the phasor diagram, the following d-q equations of the UPFC are obtained.

$$V_{Ed} = -\frac{1}{2} m_E V_{dc} \sin(\delta - \delta_E) \quad (12)$$

$$V_{Eq} = \frac{1}{2} m_E V_{dc} \cos(\delta - \delta_E) \quad (13)$$

$$V_{Bd} = -\frac{1}{2} m_B V_{dc} \sin(\delta - \delta_B) \quad (14)$$

$$V_{Bq} = \frac{1}{2} m_B V_{dc} \cos(\delta - \delta_B) \quad (15)$$

$$\Delta V_d = \Delta V_{Ed} + r_E \Delta I_{Ed} + x_E \Delta I_{Eq} \quad (16)$$

$$\Delta V_q = \Delta V_{Eq} + r_E \Delta I_{Eq} - x_E \Delta I_{Ed} \quad (17)$$

3.RESULTS

The machine-infinite bus system Shawn in Figs(1,2) studied with the TCSC and with the UPFC. Three phase fault is applied at the bus 2 for 80 msec and removed without any change in network configuration. Figs(3,4) show the generator rotor speed oscillations with and without FACTS device . The addition of FACTS have improved the damping of generator rotor speed oscillations.

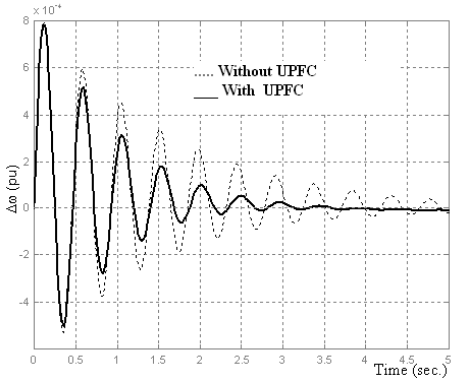

Fig. 3: Generator rotor speed oscillation damping with and without UPFC

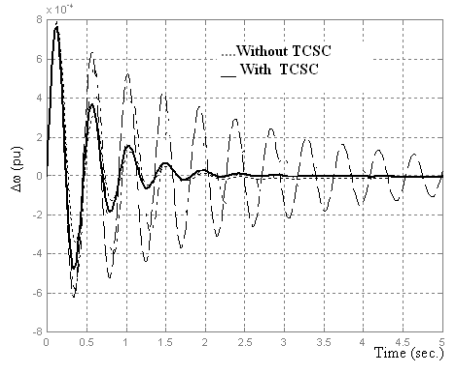

Fig. 4: Generator rotor speed oscillation damping with and without TCSC

The figures clearly indicates that the system is more stable with FACTS device also the effect of damping control UPFC best of TCSC .

4. CONCLUSIONS

A simple and general method of generating the dynamic response and hence determining the first swing stability of a power system in the presence of various FACTS devices is presented. First a

FACTS devices and their associated transmission line are considered and represented by an equivalent circuits model where the shunt admittances depend on control parameters of the UPFC. The parameters of the circuits model are then carefully evaluated (in each integration step) based on the control
strategy used and interfaced to the power network. The circuits model can also be used to represent a STATCOM or an SSSC by choosing proper values of control parameters of the UPFC and TCSC. The effectiveness of the proposed method is tested on the SMIB system using two different control strategies and consistent results are found. The proposed method of generating the system response is very general and can easily be applied to a large power system with various FACTS devices using different control strategies.

REFERENCES

[1] Nadaraja M. , Claudio A. C. , John R. , and Graham J. R. , “Coparison of PSS, SVC, and STATCOM Controllers for Damping Power System Oscillations”, IEEE Transaction on Power System, Vol. 18, No. 2, pp. 786-792, May 2003.

[2] Chuan-Te Chang, Yuan-Yih Hsu, “Design of an ANN Tuned Adaptive UPFC Supplementary Damping Controller for Power System Dynamic Performance Enhancement”, Journal of Electrical Power Systems Research (66), pp. 259-265, 2003.

[3] M.A. Abido, Y.L. Abdel-Magid, “Coordinated design of a PSS and an SVC-based controller to enhance power system stability”, Journal of Electrical Power and Energy Systems (25), pp. 695-704, 2003.

[4] Sidhartha Panda and Narayana Prasad Padhy," Power System with PSS and FACTS Controller: Modelling, Simulation and Simultaneous Tuning Employing Genetic Algorithm", International Journal of Electrical, Computer, and Systems Engineering 1;1 © www.waset.org Winter 2007.

[5] M. H. Haque, "Evaluation of First Swing Stability of a Large Power System With Various FACTS Devices", IEEE Transactions On Power Systems, Vol. 23, No. 3, pp. 1144-1151, August 2008.

[6] M. H. Haque, "Improvement of First Swing Stability Limit by Utilizing Full Benefit of Shunt FACTS Devices", IEEE Transactions On Power Systems, VOL. 19, NO. 4, pp. 1894- 1901, November 2004.

[7] P. Yan and A. Sekar, "Steady-state analysis of power system having multiple FACTS devices using line-flow-based equations", IEE Proc.-Gener. Transm. Distrib., Vol. 152, No. 1, pp. 31-39,January 2005.

[8] Seungwon An, John Condren, and Thomas W. Gedra, " An Ideal Transformer UPFC Model, OPF First-Order Sensitivities, and Application to Screening for Optimal UPFC Locations", IEEE Transactions On Power Systems, Vol. 22, No. 1, Pp.68-75, February 2007.

[9] S. Y. Ge and T S Chung, “Optimal power flow incorporating Power Flow Control Needs in Flexible AC Transmission Systems”, IEEE Transaction on Power System, Vol. 14, No. 2, pp. 738-744, May 1999.

[10] C.R. Fuerte-Esquivel, E. Acha and H. Amprez-Pêrez, “A Thyristor Controlled Series Compensation Model foe the Power Flow Solution of Practical Power Networks”, IEEE Transaction on Power System, Vol. 15, No. 1, pp. 58-64, Feb. 2000.

[11] C.R. Fuerte-Esquivel, E. Acha and H.

Amprez-Pêrez, “ A Comprehensive Newton-Raphson UPFC Model for the Quadratic Power Flow Solution of Practical Power Networks”, IEEE Transaction on Power System, Vol. 15, No. 1, pp. 102-109, Feb. 2000.

[12] S.O. Faried1 R. Billinton and S. Aboreshaid," Probabilistic technique for sizing FACTS devices for steady-state voltage profile enhancement", Published in IET Generation, Transmission & Distribution, ISSN 1751-8687, Received on 14th August 2008, Revised on 21st January 2009.

UPFC Steady State Performance to Improve Power System Operation

Mohamed Ali Shatwan
Deptm. of Electromechanical Eng.
The High Institute for Industry
Libya-Misrata
Shatwan57@yahoo.com

Sattar Jaber Al-Isawi
Deptm. of Electromechanical Eng.
The High Institute for Industry
Libya-Misrata
sattarjaber@yahoo.com

Abstract: In this paper, steady state models of the Universal Power Flow Controller (UPFC) is investigated. In steady state, model of the UPFC may consists of two equivalent voltage sources (with controlled magnitude and phase angle) in series with the transformers' impedance. These sources represent the shunt and the series branches of the UPFC. Incorporate of this model in the load flow of the power system will be discussed and applied to a sample system. power transfer capacity is investigated for systems with UPFC. The combined effects of equipment constraints, system topology and installation locations on the UPFC real power transfer is studied. The P-Q characteristics of UPFC operation under different sets of constraints are determined. The admissible operational ranges of UPFC control outputs are investigated, and the maximum power transfer and the maximum admissible range of power flow change are also found.

Key Words: FACTS, UPFC, Power Flow, Modeling, Controls.

1. INTRODUCTION

Power flow through an AC line is a function of the phase angle, line end voltages and line impedance, and there is little or no control over any of these values. The consequences of this lack of fast and reliable control are stability problems, power flowing through other than the intended lines, the inability to fully utilize the transmission resources, undesirable Var flows, higher losses, high or low voltages, cascade tripping and long restoration times. With FACTS devices one can control the phase angle, the voltage magnitude at chosen buses and/or line impedance. Power flow is electronically controlled and it flows as ordered by the control center using FACTS devices which include Static Var Compensators (SVC), Thyristor Controlled Series Capacitors (TCSC), Thyristor Controlled Phase Angle Regulators (TCPAR), Static Compensators (STATCOM), Static Series Synchronous Compensators (SSSC), Universal Power Flow Controllers (UPFC) [1]. There are a amount of work reported in the literature in the area of FACTS devices and power system operation [2,3,4,5, 6, 7,8].

2. UPFC MODEL FOR POWER FLOW SOLUTION

Several publications have appeared in the open literature, which describe the basic operating principles of the UPFC. In [9], A. Nabavi Niaki and M. R. Iravani decoupled the sending and receiving ends of the UPFC. The former is transformed into a PQ bus while the latter is transformed into a PV bus. The active and reactive power loads in the PQ bus and the voltage magnitude at the PV bus are set at the values to be controlled by the UPFC. The active power injected into the PV bus has the same value as the active power extracted in the PQ bus since the UPFC and the coupling transformers are assumed to be lossless. A standard load flow is carried out to determine the nodal, complex voltages at the UPFC terminals. After load flow convergence, an additional set of nonlinear equations, relating the various UPFC parameters, is solved by iteration. This sequential method is simple, however, since the UPFC parameters are computed after the load flow converged, there is no way of knowing during this iterative process whether or not the UPFC parameters are within limits.

C.R. Fuerte-Esquivel, E. Acha and H. Amprez-Pêrez introduced a comprehensive UPFC model [4]. The UPFC model is a straightforward extension of the power flow equations and, hence, it is suitable for incorporation into an existing Newton Raphson load flow algorithm. The UPFC equivalent circuit used to derive the steady state model is shown in Figure 1.

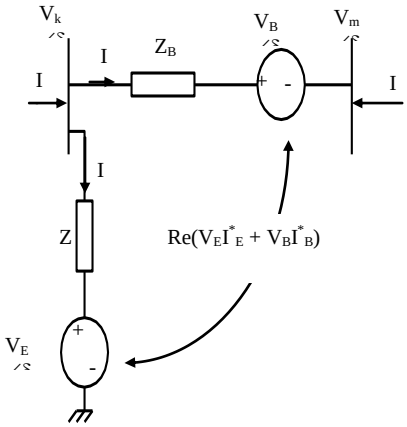

Fig.1: UPFC equivalent

The equivalent circuit consists of two ideal voltage sources representing the fundamental Fourier series component of the switched voltage waveform at the AC converter terminals. The source impedances included in the model represent the positive sequence leakage inductances and resistances of the coupling UPFC transformers.

The variable phase angle of the series injected voltage determines the mode of power flow control. If δ_B is in phase with the nodal voltage angle δ_k, it regulates the terminal voltage. If δ_B is in quadrature with respect to δ_k, it controls the power flow, acting as a phase shifter. If δ_B is in quadrature with the line current angle then it controls the power flow, acting as a variable series compensator. At any other value of δ_B, the UPFC operates as a combination of voltage regulator, variable series compensator and phase shifter.

2.1 MODIFICATION OF THE BUS ADMITTANCE MATRIX

The general transfer admittance matrix is obtained by applying Kirchhoff current and voltage lows to the electric circuit shown in Fig.1 and is given by

$$\begin{bmatrix} I_k \\ I_m \end{bmatrix} = \begin{bmatrix} y_B + y_E & -y_B & -y_B & -y_E \\ -y_B & y_B & y_B & 0 \end{bmatrix} \begin{bmatrix} V_k \\ V_m \\ V_B \\ V_E \end{bmatrix} \quad (1)$$

$$\Delta Y_{bus} = \begin{matrix} \\ k \\ m \end{matrix} \begin{matrix} \begin{matrix} k & m & B & E \end{matrix} \\ \begin{bmatrix} Y_{kk} & Y_{km} & Y_{kB} & Y_{kE} \\ Y_{mk} & Y_{mm} & Y_{mB} & 0 \end{bmatrix} \end{matrix} \quad (2)$$

The original Y_{bus} of the system before installing the UPFC is modified to include the UPFC model by adding ΔY_{bus} to it, and in this case the number of columns of the new Y_{bus} will increased by two corresponding to V_B and V_E.

Assuming a loss free converter operation, the UPFC neither absorbs nor injects active power with respect to the AC system. The active power demanded by the series converter is supplied from the AC power system by the shunt converter via the common DC link voltage. The DC link voltage, V_{dc}, must remains constant so that the stored energy in the capacitor would not changed. Hence, the active power supplied to the shunt converter, P_E, must satisfy the active power demanded by the series converter, P_B, i.e.

$P_E + P_B = 0.0$

Where

$$P_B = -real(V_B^* I_B) = -real(V_B^*(V_k - V_m - V_B)Y_{mB})$$
$$= V_B^2 G_{mB} - V_B Y_{mB} V_k \cos(\theta_{mB} + \delta_k - \delta_B) + V_B Y_{mB} V_m \cos(\theta_{mB} + \delta_m - \delta_B) \quad (4)$$

$$P_E = -real(V_E^* I_E) = -real(V_E^*(V_k - V_E)(-Y_{kE}))$$
$$= -V_E^2 G_{kE} + V_E Y_{kE} V_k \cos(\theta_{kE} + \delta_k - \delta_E) \quad (5)$$

$$P_B + P_E = V_B^2 G_{mB} - V_E^2 G_{kE} - V_B Y_{mB} V_k \cos(\theta_{mB} + \delta_k - \delta_B) + V_B Y_{mB} V_m \cos(\theta_{mB} + \delta_m - \delta_B) + V_E Y_{kE} V_k \cos(\theta_{kE} + \delta_k - \delta_E) \quad (6)$$

2.2 FORMATION OF THE JACOBIAN MATRIX

The UPFC linearized power equations are combined with the linearized system equations corresponding to the rest of the network,

$$[\Delta f(x)] = [J][\Delta x] \quad (7)$$

Where $[\Delta f(x)] = [\Delta P_k \ \Delta P_m \ \Delta Q_k \ \Delta Q_m \ \Delta P_{mk} \ \Delta Q_{mk} \ \Delta(P_B + P_E)]^T$, $[\Delta x]$ is the solution and [J] is the Jacobian matrix.

2.3 INITIAL LOAD FLOW SOLUTION OF THE UPFC VARIABLES

Engineering judgment indicates that for the simple case in which no controlled buses or branches are present, 1.0 pu voltage magnitude for all PQ buses and 0^0 voltage angle for all buses provide a suitable starting condition. However, if controllable devices are included in the analysis, the issue is not as a clear cut as the case above. For the UPFC, a set of equations which give initial estimates can be obtained from the nodal and constraint UPFC power flow

equations by assuming lossless converter valves and coupling transformers operation and null nodal voltage angles [4].

2.3.1 Series source initial conditions

For specified nodal powers at node m, P_{mref} and Q_{mref}, the solutions of the active and reactive power equations at this node give

$$\delta_{B0} = \arctan\left(\frac{P_{mref}}{Q_{mref} - \frac{V_{m0}}{X_B}(V_{m0} - V_{k0})}\right) \quad (9)$$

$$V_{Bo} = \left(\frac{X_B}{V_{m0}}\right)\sqrt{P_{mref}^2 + \left(Q_{mref} - \frac{V_{m0}}{X_B}(V_{m0} - V_{k0})\right)^2} \quad (10)$$

X_B is the inductive reactance of the series source.

2.3.2 Shunt branch initial conditions

An equation for initializing the shunt source angle can be obtained by solving equations (4, 5) and it is given by

$$\delta_{E0} = -\arcsin\left(\frac{(V_{k0} - V_{m0})V_{B0}X_E \sin(\delta_{B0})}{V_{E0}V_{ko}X_B}\right) \quad (8)$$

Where X_E is the inductive reactance of the shunt source. When the shunt converter is acting as a voltage regulator, the voltage magnitude of the shunt source is initialized at the target voltage value and then is updated at each iteration. Otherwise, if the shunt converter is not acting as a voltage regulator, the voltage magnitude of the shunt source is kept at a fixed value within its limits.

3. LOAD FLOW FOR A SIMPLE SYSTEM WITH UPFC

The machine-infinite bus system studied last chapter with the TCSC will be studied with the UPFC. The system is redrawn in Figure 2. UPFC has to control the voltage of bus 2 to be 1 pu, and the power flow through the line 3-2 to be P_{32} = -0.5 pu and Q_{32} = -0.1 pu, bus # 1 is the slack bus with $|V_1|$ = 1 pu. The value of the UPFC transformers impedance are $Z_E = Z_B$ = 0.01 + J0.025 pu. The solution is obtained after 5 iterations with a mismatch of $1.5224*10^{-6}$. Load flow results for the system are given in Table 1, it is worth noting that the series injected voltage value is small compared to shunt injected voltage.

To investigate the ability of the UPFC to control power flow, the scheduled power through line 2-3 is altered for the same loading on the system as given in the first column of Table 2. The series and shunt injected voltages by the UPFC to obtain the required level of load flow across the line is also shown in the Table 2.

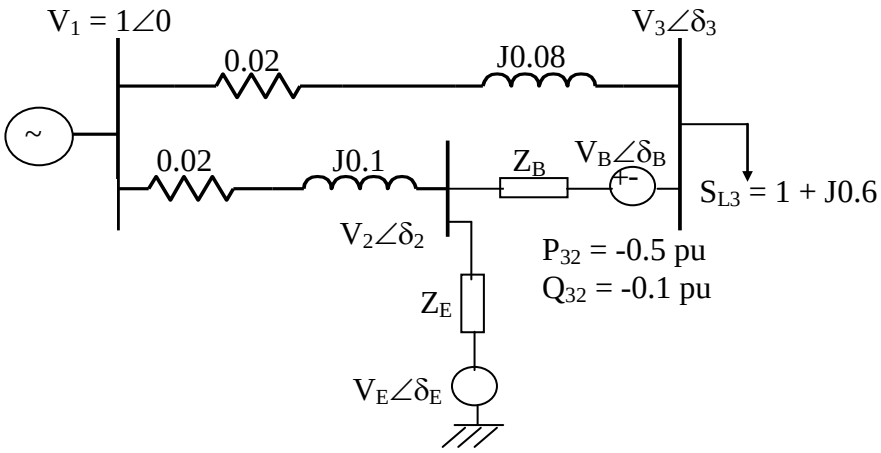

Fig. 2: Three bus system with UPFC (All values are in pu)

Table 1: Load flow output data for the system

Bus	|V|	δ	P	Q	UPFC Data
1	1	0	1.0198	0.4568	$V_B = 0.056\angle -38.046^o$
2	1	-3.0166^o	0	0	$V_E = 1.0055\angle -3.0974^o$
3	0.9467	-1.8160^o	-1	-0.6	

Table 2: Load flow output data for the system with different controlled power by the UPFC

Initial power	V_3	δ_2	δ_3	P_1	Q_1	UPFC Data
$S_{32} = -0.5 - j0.1$	0.946	-3.0^o	-1.8^o	1.019	0.456	$V_B = 0.0560\angle -38.046^o$ $V_E = 1.0055\angle -3.0974^o$
$S_{32} = -0.6 - j0.2$	0.958	-3.6^o	-1.4^o	1.020	0.325	$V_B = 0.0599\angle -61.535^o$ $V_E = 1.0084\angle -3.7777^o$
$S_{32} = -0.7 - j0.2$	0.96	-4.2^o	-0.9^o	1.023	0.305	$V_B = 0.0779\angle -71.796^o$ $V_E = 1.0087\angle -4.3911^o$
$S_{32} = -0.8 - j0.3$	0.971	-4.9^o	-0.6^o	1.026	0.182	$V_B = 0.0927\angle -84.316^o$ $V_E = 1.0115\angle -5.0748^o$
$S_{32} = -0.9 - j0.4$	0.982	-5.5^o	-0.2^o	1.032	0.064	$V_B = 0.1108\angle -92.942^o$ $V_E = 1.0141\angle -5.7605^o$

It is noticed that, although the magnitude of the series injected voltage is low, the required active power flow is achieved. This is because the flow of active power is most controlled by the series injected voltage angle. The value of the series injected voltage to transfer power of –0.9-j0.4 pu is $0.1108\angle -92.942^{o}$ pu. The limiting values of the magnitude of the injected voltages are self-explanatory, the series injected voltage limit is taken as 0.25 pu and that of the shunt branch lies between 0.9 and 1.1 pu in [7], while in [1] the series injected voltage limit is specified as 0.4 pu. Both series and shunt voltages' angles have no limitation i.e., $0 \le \delta_B \le 2\pi$ and $-\pi \le \delta_E \le \pi$. The ability of UPFC to control the line power can be investigated by examining Figure 3.

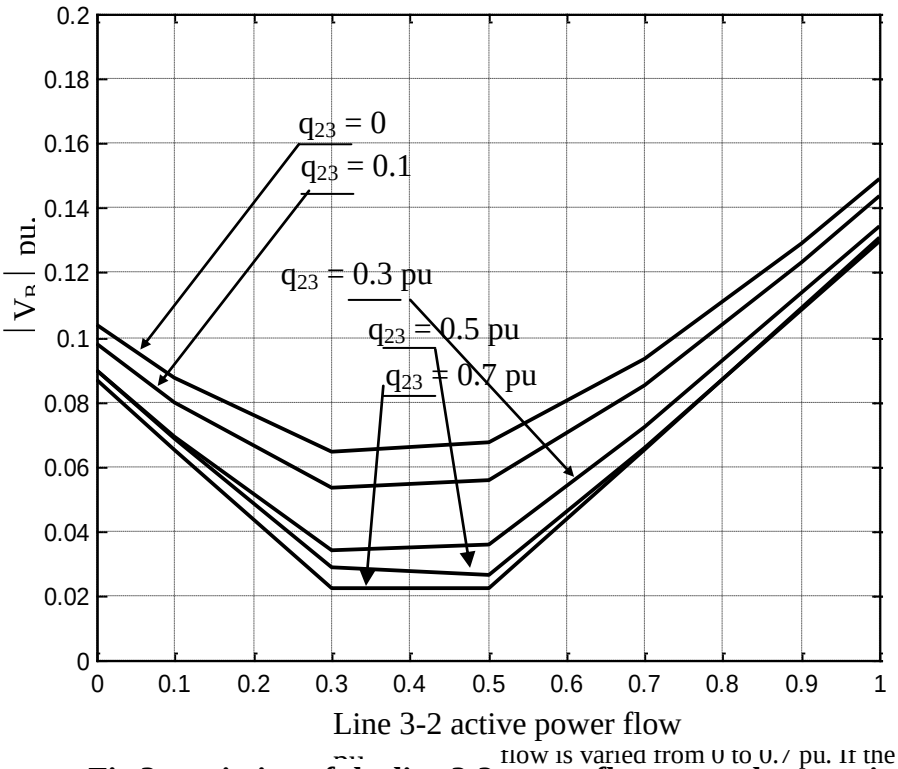

flow is varied from 0 to 0.7 pu. If the

Fig.3: variation of the line 3-2 power flow w.r.t. the magnitude of the series injected voltage from the UPFC

magnitude limit of the series injected voltage is taken as 0.25 pu, the line power flow can be increased to 1 pu when reactive power flow is 0.7 pu without violating that limit. This illustrates the role of the UPFC as a powerful device to control transmission line power flow.

4. UPFC FOR THE MULTI-MACHINE POWER SYSTEM

The UPFC for the system shown in Figure 4. The UPFC is installed to control the power through line 4-5 to be -1-0.3i pu, and to control the voltage of bus 4 to be 1 pu. Load flow with the UPFC is performed and solution is obtained after 7 iterations. The results are shown in Table 3. The UPFC calculated data are given in Table 4.

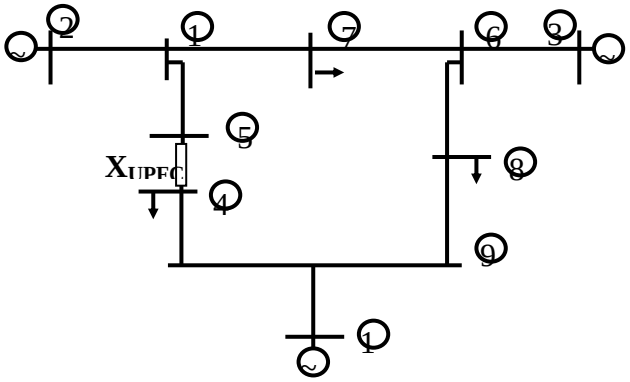

Fig 4: System under Study with the UPFC

Table 3: Base case load flow bus data with the UPFC

Bus	V_t (p.u.)	θ (degree)	P_g (p.u.)	Q_g (p.u.)	P_l (p.u.)	Q_l (p.u.)
1	1.0	0.0	0.7672	0.0118	0.0	0.0
2	1.025	23.7843	1.63	0.0874	0.0	0.0
3	1.025	13.3389	0.85	0.0263	0.0	0.0
4	1	-7.5515	0.0	0.0	0.0	0.0
5	1.0088	16.0638	0.0	0.0	0.0	0.0
6	1.0247	10.6205	0.0	0.0	0.0	0.0
7	1.0097	12.7669	0.0	0.0	1	0.35
8	0.9851	-0.9592	0.0	0.0	0.9	0.3
9	1.0003	-2.5321	0.0	0.0	0.0	0.0
10	1.0245	18.2172	0.0	0.0	1.25	0.5

Table 4: Base case UPFC data

V_B (p.u.)	θ_B (degree)	V_E (p.u.)	θ_E (degree)
0.4365	-88.5165	0.9989	-7.4977

4. CONCLUSIONS

The major contributions of paper are

1-FACTS devices do not provide new transmission capability but they certainly remove constraints and enable improved use of existing transmission network, and are capable of fast control.

2-This paper introduced a detailed analysis of UPFC model and how these model effect of load flow for both single machine infinite bus and multi-machine power systems.

3- UPFC is improved Power System Operation.

REFERENCES

[1]R. Mihalic, " Power Flow Control with Controllable reactive series elements", IEE Proc., Gener. Transm. Distrib., Vol. 145, No. 5, pp. 493-498, Sept. 1998.

[2]P. Yan and A. Sekar, "Steady-state analysis of power system having multiple FACTS devices using line-flow-based equations", IEE Proc.-Gener. Transm. Distrib., Vol. 152, No. 1, pp. 31-39,January 2005.

[3]Salim. Haddad, A. Haddouche, and H. Bouyeda,"The use of Facts devices in disturbed Power Systems Modeling, Interface, and Case Study", International Journal of Computer and Electrical Engineering, Vol. 1, No. 1, pp. 1793-8198, April 2009.

[4] C.R. Fuerte-Esquivel, E. Acha and H. Amprez-Pêrez, "A Thyristor Controlled Series Compensation Model foe the Power Flow Solution of Practical Power Networks", IEEE Transaction on Power System, Vol. 15, No. 1, pp. 58-64, Feb. 2000.

[5]Juan S. R., and Aurelio M. ," Periodic Steady State Solution of FACTS Devices Based on SPWM VSCs", IEEE International Symposium on Industrial Electronics (ISlE 2009),Seoul Olympic Parktel, Korea July 5-8, 2009.

[6]Juan Segundo-Ramírez and Aurelio Medina," Modeling of FACTS Devices Based on SPWM VSCs", IEEE Transactions On Power Delivery, Vol. 24, No. 4,pp.1815-1823, October 2009.

[7] H. Cai, Z. Qu, and D. Gan, "Determination of the Power Transfer Capacity of a UPFC with Consideration of the System and Equipment Constraints and of Installation Locations", IEE Proc., Gener. Transm. Distrib., Vol. 149, No. 1, pp. 114-120, Jan. 2002.

[8]Arefeh D. S. , Ervin S. , Gerd B. ," Optimal Location of Series FACTS Devices to Control Line Overloads in Power Systems with High Wind Feeding", Paper accepted for presentation at 2009 IEEE Bucharest Power Tech Conference, June 28th - July 2nd, Bucharest, Romania, 2009.

[9]A. Nabavi N. and M. R. Iravani, "Steady-State and Dynamic Models of Unified Power Flow Controller for Power System Studies", IEEE Transaction on Power Systems, Vol. 11, No. 4, Nov. , pp. 1937-1943, 1996.

Assessment of Electrical Power Network of Tajoura Research Center Using Power Quality Phenomena and indices.

Dr. Bashiri; Milad Ahmed
National Authority for Scientific Research
Libya

Eng. Segayer, Ali Mehemmed
Tajoura Research Center
Libya

Eng. Nuraddin M. Giali
Electrical Engineering Department
University of El-Fateh, LIBYA

Abstract

Electricity is very different from any other product it is generated far from the point of use, fed to the grid and arrives at the point of use . The quality of delivered power at the point of use is not an easy task and there is no way that sub -standard electricity can be withdrawn from the supply chain and rejected by the customer due to quality problems. The Quality of Power is therefore of concern to all and it must be monitored continuously and its quality established in “real Time".

Tajoura Research Center (*TRC*) is a very strategic research facility and contains many important industrial and electrical loads that must to be operated as a group to fulfill the requirements and the needs of the Center. Faults on the Electrical or the Industrial system can be a malfunction in the questioned system or may be a power quality related problem; and a failure of any load such as central ventilation or water circulation system or one of the substations have a great diverse effect.

In Fulfillment to the above and the recent established Power Quality Project at (*TRC*) ; this paper presents faults due to power quality phenomena and how they are assessed using Power Quality Indices (PQI) ; so that the operational condition of the REWDRC electrical and Industrial network will evaluated; and a recommendation of safe operation against power quality disturbances and faults will be pointed out through a continues monitoring of PQI as a result of this Project.

Introduction

Electrical power is the most essential raw material used by commerce and industry today. It is an unusual commodity because it is required as a continuous flow it cannot be conveniently stored in quantity and it cannot be subject to quality assurance checks before it is used. Electric power is not often thought of as raw materials, but it is vital to virtually all types of manufacturing. The Quality of Power is therefore of concern to all and it must be monitored continuously and its quality established in “real Time [1]. In reality, of course, electricity is very different from any other product it is generated far from the

point of use, fed to the grid together with the output of many other generators and arrives at the point of use via several transformers and many kilometers of overhead and possibly underground cabling. The quality of delivered power at the point of use is no easy task and there is no way that sub-standard electricity can be withdrawn from the supply chain and rejected by the customer due to quality problems.

Power Quality Indices (PQI)

Characterizing power quality levels on power systems has become extremely important with increased sensitivity of customer load equipment to momentary interruptions, voltage sags and transient voltages. Calculation of number and duration of oversteps of soft and hard limits and their consequences make the basis for evaluation of Indices of quality (IQ) set for a distribution network. By establishing a unique system of numerical indices of quality and the software tools for their evaluation, it is possible to evaluate both, operation quality and alternative projects quality in the course of network planning process [1].

For some industries and utility companies monitoring systems are often installed to determine the energy consumption, but for many of these the cost of power disruption can overweight the energy costs. Power quality indices should be monitored with energy consumption, and for these needs many new power quality-monitoring systems have the capabilities of monitoring all indices and all aspect of electrical network and plays an important role in total quality management system [1]. Using power quality indices a new technique converts accumulated power monitoring data into a single number called the power quality index, which you can track overtime. By trending this index, you get an advance warring of deteriorating situations that could lead to system failure.

TRC Power Quality Project:

Tajoura Research Center (TRC) is a very strategic research facility and contains many important and critical industrial and electrical loads that must to be operated as a group to fulfill the requirements and the needs of the Center in the operation of the main research facility of the center which

a 10 MW reactor. Faults on the Electrical or the Industrial system can be a malfunction in the questioned system or may be a power quality related problem; and a failure of any load such as central ventilation or water circulation system or one of the substations have a great diverse effect on the operation of the main research facility (reactor). In this Project faults due to power quality phenomena will be studied and assessed using PO phenomena and PQI so that the operational condition of the TRC electrical and Industrial network will evaluated; and a recommendation of safe operation against power quality disturbances and faults will be pointed out through a continues monitoring of PQI as a result of this project.

Measurement Procedure

In choosing a measuring and monitoring points; Legislative documents and standards prescribe that power quality parameters and indices should be monitored at the point of delivery to the customers [3] (i.e. point of common coupling PCC) so, for a large number of substation at the TRC (which are 7 substations) means the 10 kV side of the main substation and 30 kV side which is also a PCC with General

Electricity Company of Libya (GECOL). Considering the fact that in TRC there are 7 such substations, its noticeable such system would be a large and a lot of work must be done to monitor it at once. The best convenient location of measurement appears to be as said the 10 kV and 30 kV substation and in this way it is possible to cover all substations, as well as to collect all the information about state of power quality that flows into distribution network, It is also a point where commonly most customers can monitor quality of power delivered from transmission system[7].

At TRC network in each substation there are at the most two transformers, and each one can power its part or some selected loads, so it is logical to put monitoring instruments on secondary side of transformers 30/10 kV which is 10 kV busbars. A another suitable location for monitoring is also the overhead incoming lines leading to the 30 kV which is at the 30 kV busbars in the substation which is also a PCC between the National Grid and the center network. With what have been stated a measurement locations were selected as such (30 kV and 10 kV busbars) and the instruments were installed and powered on in accordance to their technical specifications and setup using the network technical diagrams and specifications.

Selection of instruments was based on the capability, type of measurement and the results of the initial survey of power quality .Two sets of VQREG-7 (12 channels in total) were installed at the 30 kV substation busbars and one TRANSNAL-16 (16 channels) plus one VQREG-7(6 channels) were installed at the 10 kV substation busbar.

Having arrived to the weekly indices for voltage variation, voltage imbalance, THD and power factor, it is then necessary to combine theses indices into a single number or index that could indicate the overall performance of each measured location for each week or they can be for each month getting the yearly index. To do this, a process is necessary to express each of the indices with the same unite. Two proposed possible methods of doing this are[7]:
Each index could be normalized with respect to the network average value for that index. Alternatively, each index could be normalized or compared with respect to

the specified tolerance limit value for that parameter[4]. Normalization with respect to a system average is appropriate if the aim is to rank sites across the network, where as normalization or comparison with respect to specified tolerance limit value is more appropriate if the objective is to establish conformance with a specified limit value.

Measurement analysis methods

Based in the above initial consideration and the selection of primary indices; it was decided to work in the following methods of analysis[6]:-

- Method 1:-From the measured data; indices were selected, normalized and trended in order to make a comparison between measurement locations.
- Method 2:-From the measured data; indices were compared to their limit value to check the operational condition of the network.
- Method 3:-Examining the time profile of some selected measurement channels at each location and diagnosis any problems that can be seen and may be recommended for mitigation.

A- Method of Normalization

Using the data results through the period of 12-22/05-2008 and using the selected indices to be trended, so each index can be normalized to substation or substation section average value for that index aiming to see the trend of each index in each measurement location. and also to compare these trends between locations. Table (1) shows the normalized indices for 30kV substation[7].

Table 1 Normalized Indices for 30 kV

	30 kV-1ST SECTION			30 kV-2ND SECTION		
	A	B	C	A	B	C
THD	0.8122	0.6706	0.7239	1.214	1.0658	0.9774
Vdev	1.124308	1.070085	1.135374	0.886389	0.886389	0.897455
P.F	1.089	1.078	1.079	1.11	1.076	1.10
Vunbal	0.544	0.544	0.544	0.4563	0.456	0.456
Pst	1.53	1.62	1.65	1.623	1.639	1.608

For the normalized indices values for the 10 kV substation and it's outgoing feeders at substation 10k-1st section as were also calculated and as shown in table (2) These calculated values for the two substations are plotted asshown in figure (1) and (2)

As can be seen from these graphs the amplitude of each index to each measurement location and the dominant index can be seen.

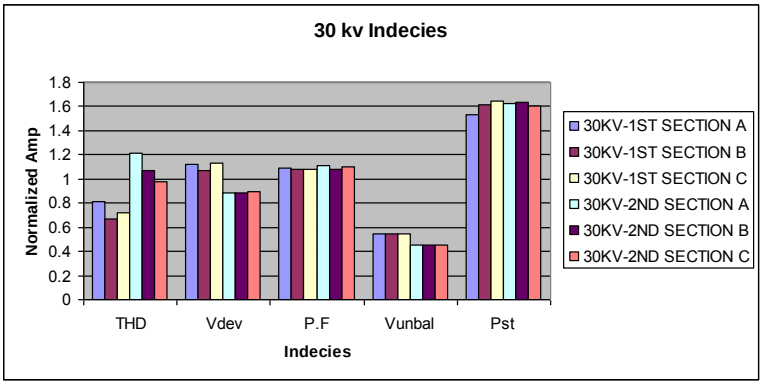

Figure 1 Normalized Indices for 30 kV

Table 2 Normalized Indices for 10kV-1st section substation Feeders

	A	B	C	Sub1	Sub2A	Sub3A	Sub5-1	Sub7
THD%	1.54	1.78	1.59	1.60	3.07	2.33	1.95	4.38
IA AVG	1.64	1.61	1.59	0.46	0.28	0.55	0.33	0.16
THD3%	1.51	5.26	5.26	2.03	6.96	1.17	5.19	3.56
THD5%	1.56	1.50	1.50	1.62	2.88	2.41	1.99	3.66
IR PST	1.01	1.00	1.00	0.99	0.99	0.99	0.99	0.99

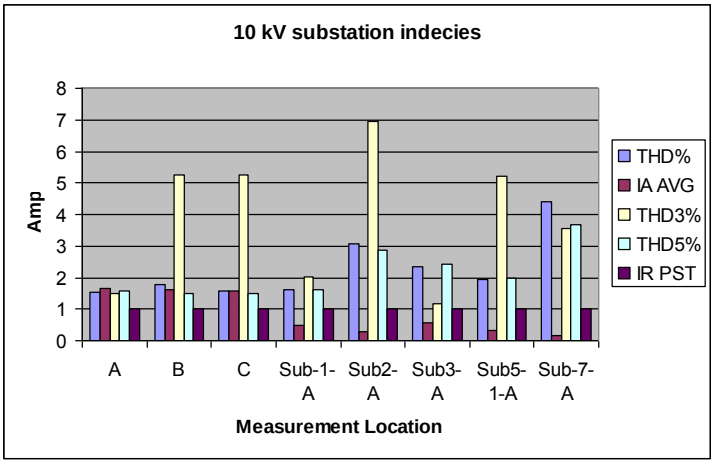

Figure 2 Normalized Indices for 10kV substation Feeders

For example in substation 30k we can see easily that harmonic index for section 2 is higher than section 1 and the voltage regulation of section 2 is much better than section 1. At 10 kV substation and it's outgoing feeders we see higher harmonic content at substation #7 and the higher THD3% at substation 2. These measurement locations they will be re-

measured again and a comparison of these indices with the new measurement will be done and the condition of each location will be assessed. As stated previously the aim of the normalization method is trending data over time and the benefits behind this method is to see what are the locations need concern or predicative maintenance action; i.e. power quality mitigation. Therefore; monitoring indices for the 30 kV substation , 10kV substation, and feeders of the distribution substations at 10kV substation were calculated for the first week and they will trended for the next measurement period, aiming for a monthly index and then a yearly index. In this way clearly the operating condition from the point view of power quality indices is achieved; however the more indices are assigned; the larger scale of monitoring the operating condition.

B- Method of Severity Limit

The method of severity limit is a comparison of 95% measured values of each index with the international standards. The aim of this method is to assess each index and to know the operation condition of the network in general. If the limit of an index exceeds the international standards then a process of mitigation and correction can be done after knowing the possible sources leading to higher value of this index. Table (3) below shows the indices for each measurement location at 30 kV and 10 kV substations along with the severity limits and it's clearly shown that all the indices are below the limit however the voltage deviation index exceed the planning limit. For the 10kV substation outgoing feeders indices of monitoring were selected and tabulated as shown in Table (4)

From the above measurement data and with the use of the international standards IEC 61000-X-X for each index one can draw the following statements:-

The voltage deviation indexes were below the severity limit but they exceed the planning limit. Harmonic index they still below the severity limit at 30 kV; however one should be cautious about this measured value without real measurement at lower voltage level.

Table: 3 REWDRC network Severity limit indices-10kV-1st section substation and outgoing feeders

Index	limit	A	B	C	Sub-1-1-A	Sub2-1A	Sub3-1-A	Sub5-1-A	Sub-7-A
THD%	8%	2.959	2.959	2.987	5.18	9.965	7.569	6.337	14.206
THD3%	5%	0.218	0.501	0.57	1.345	4.594	0.774	3.427	2.353
THD5%	5%	2.917	2.374	2.887	5.23	8.854	7.421	6.122	11.25
10 PST	1.0	0.479	0.408	0.617	0.236	0.236	0.236	0.238	0.236

Location	Voltage Deviation index			Harmonic % index			Vub	P.F
	A	B	C	A	B	C		
30 kV- 1st Section	.058	.055	.059	3.32	2.71	2.93	0.56	.811
30 kV- 2nd Section	.046	.046	.046	4.97	4.32	3.99	0.47	.794
10KV- 1st Section	.081	.081	.076	2.96	1.77	2.30	0.36	.826
Severity Limit	± 10%			8%			2%	-

Table: 5 REWDRC network Severity limit indices-30 &10 kV substation

This result is shown when this index is measured at the feeders of 10kV substation and it's clearly values exceed the limit. Voltage Imbalance measured values are well below the severity limit. 3% Harmonic index, values need special attention at substation#2, #5 since they are almost close to the alarming level. Pst 99% flicker index is higher at the 10kV substation and this is due to the switching of circuit breakers and transformers tap changer. As can be seen the objective of this method is to see where the sources are
of the problems. In analyzing the sources of these problem one need to study the load types at each substation and perform another measurement at each load to see which have the higher effect so that correction can be made. This will be studied briefly at the next analysis method.
studied briefly at the next analysis method.

were power quality related and the load

C-Method of verifying time profile of the measured channels

As stated previously analyzing further to the sources of these indices is beyond the scope of this paper; however the use of this method is to illustrate the severity of some power quality problems and to present other factors might be of use for mitigation such as the time factor. In order to have a grasp of what is going on from the time profile or from the statistical data one has to know what are the load types at each substation. Each load type has its own effect; for example switching would raise the flicker and voltage variation, where as nonlinear load would raise the harmonic contents and so on.

As stated previously through this research an initial survey was performed; this initial survey summarizes some problems which

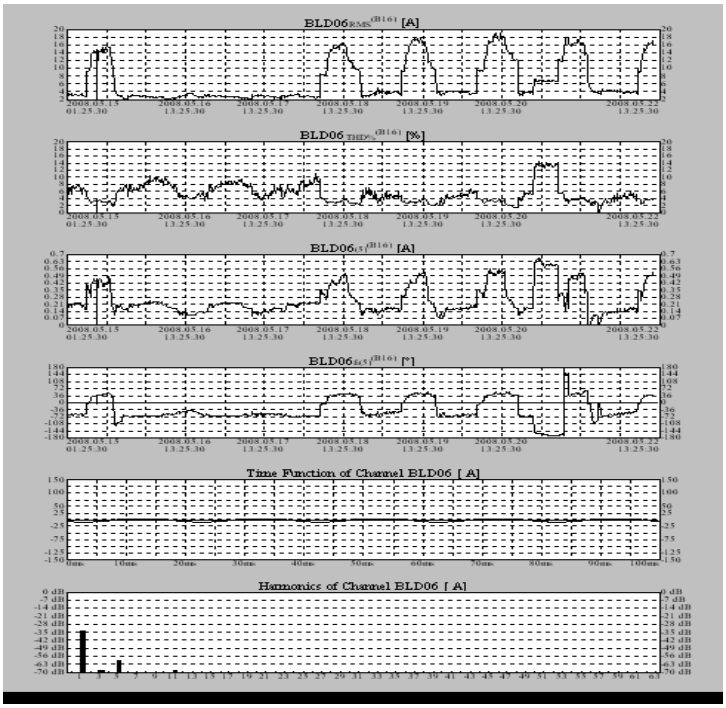

Fig(3) Measurement time profile of substation #2

types at each substation. Load types and identification is very important in order to analyze the spectral waveform of the measured data. With reference to method of severity limits and the origin of the problem one could illustrate some finding from the time profile of the measurement data. One can not illustrate all the events but for instance the harmonic content at substation #2 which supplies machine tools shop, CNC machine, exterior lighting, office building and

food service machines (grills, frying equipments….etc) clearly the harmonic content is justified since all these loads are source of harmonic . From the graph one can clearly see the content of the 5% and 3% harmonics and time of occurrence of theses contents.

Conclusions

In this paper a brief introduction to the power quality phenomena and indices was introduced along with the application of power quality phenomena and indices in assessing the power network at TRC. No doubt power quality phenomena and indices is a new trend in the industry to assess the electrical network using the operation parameters and avoiding any problems that leads to sudden shutdowns or failure. As it have been stated, the work in this research was to assign some indices to assess the network; however and as it have been

known; the most trouble part in any power quality project is the huge data collection and the way of presenting this data in order to give an inside view of the network so no matter how many indices you put in there is a lot that is left and the most important in any work such as this one, you must always know your enemy which is 90% is the load.

Some important indices were assigned to assess the network and the selection of these indices was based upon an initial survey report and from an immediate measurement results. This assessment was done through assigning indices at each measurement location and through the use of three methods of analysis aiming to trend data over time, checking the severity limits and identifying the sources. As it has been illustrated some indices were exceeding the severity limit where as some need to be compared with the next measured programme and notice their trending. In conclusion a lot of benefits were gained through this work experimentally, theoretically and this work is a true application of vertical transfer of technology hoping for the horizontal transfer.

References

[1]. Bishiri. M,Segayer.A, Fadel.A, Sherwali,A, Sori.A, Biao.A,Zobi.H, "Over view of Power Quality Phenomena" ,Fourth Libyan Arab International Conference on Electrical and Electronics Engineering, March20-23, 2006, Tripoli.

[2]. Bishiri. M, Segayer. Ali, Fadel A, Sherwali,A, Sori.A,Biao.A,Zobi.H "Predicative Maintenance Using Power Quality Indices", Fourth Libyan Arab International Conference on Electrical and Electronics Engineering , March20-23,2006,Tripoli.

[3]. D.Brooks,R.C Dugan, Marek Waclawiak, Ashock Sundaram "Indices foe Assessing Utility Distribution System RMS Varation Performance" .IEEE Transactions on Power Delivery, vol.13,np1, January 1998,pp.254-259.

[4]. Electrical Power Systems Quality, Roger C.Dugan, Mark F. McGranaghan ,H.Wayne Beaty, McGraw-Hill's,New York,1995-45698.

[5]. Application of Power Quality Indices, Summer Meeting, July 16,1998,San Diego.Bergeron,Roger "Canadian Electrical Association Approved Quality Indicies"IEEE

[6]. IEEE Std 1159-1995,Recmmended Practice on Monitoring Electric Power Quality, Working Group on Monitoring Electrical Power Quality of SCC22-Power Quality, Draft6, November 1994.

[7]. A study of Electrical Power Network of Renewable Energies and Water Desalination Research Center Using Power Quality Phenomena and indices. By: Ali Mohammed Segayer. A dissertation submitted to The Department of Electrical Engineering/power Systems In Conformity with the Department Requirements as partial Fulfillment for the Degree of Master of Engineering Science .Academy of Graduate Studies,2007.

[8]. R.S.Thallam, G.T.Heydt "Power Acceptability and Voltage Sag

Indices in the Three Phase Sense" IEEE PES Summer Meeting, July 2000, Seattle, WA

[9]. Understanding Power Quality Problems Voltage Saga and Interruptions, Math H.J.Bollen. McGraw-Hill's, New York,1996-45698

[10]. Power Quality Energy Efficiency Guide Technical Editing and Power Quality Subject Expert: Brad Gibson P.Eng., Cohos Evamy Partners, Calgary, AB Mr. Scott Rouse, P.Eng., MBA, CEM, Energy @ Work, Power Quality Fact sheet 3. E newsreo.co.uk

[11]. IEEE P1159: 1995. IEEE Recommended Practice for Monitoring Electric Power Quality. IEEE Stds. Coordinating Committee 22 on Power Quality. 1995. IEEE 1346:1998 Recommended practice for evaluating electric power system compatibility with electronics process equipment.

[12]. IEC 61000-4-30, 2003, Power quality measurement methods

[13]. IEC 61000-3-6:1996 – Assessment of Emission Limits for Distorting Loads in MV and HV Power Systems, technical report type 3.

[14]. IEC 61000-3-7:1996 – Assessment of Emission Limits for Fluctuating Loads in MV and HV Power Systems, technical report type 3.

[15]. IEC 61000-4-7, 2002, General guide on harmonics and interharmonics measurements and instrumentation for power supply systems and equipment connected thereto.

[16]. Cigre 1992 Paper 36-203. A. Robert, J. Marquet on behalf of WG36.05, 1992: Assessing voltage quality in relation to harmonics, flicker and imbalance

Field investigation to the integrated system of protection ,control and practical implementation

Eng. Mariem Elforjani
E-mail: mm_hf02@ yahoo.com
Eng. Abdullhamid Antar
hamid_antar@ yahoo.com
General Electrical Company
Dr. Hamid . H. Sherwali
Dr. Ali .H. Enfais
Electric & Electronic Engineering Dep.
ali_infis@yahoo.com

Abstract

In the last few years a variety of utility oriented software based digital devices with communication capabilities have emerged. Some utilities have been quick to recognize the advantages of these new products and an increasingly large number of these devices are being installed in substations toady. In order to make full use of this new technology, a means of collecting and organizing the data produced by these new products is needed locally in substations furthermore, access to this data must be provided to outside users.

The source data now available in modern substation consists of fault reports, fault locations, metered quantities, equipment status, station alarms and sequence of events (SOE) data. This data is required by different utility groups at multiple locations.

The paper presents and describes the integration of substation protection, control and data acquisition. It is a new concept for data integration where the substation field data recoded by monitoring and protection equipments. The paper will discuss detailed requirement for the integration process and how intelligent electronic devices (IED) is used to supplement remote terminal unit (RTU) and data for supervisory control and data acquisition system (SCADA). The paper will include the benefits gained and improvements on (SCADA) and other applications. The paper discussions will be based on field data as set and recorded from a one of the substations provided with the software based devices.

Introduction:

The centralization of network operation needs remote access to the electrical substations separated over the entire electrical grid as power plants or Transmission substations for monitoring and control via centralized system (SCADA).

SCADA stands for Supervisory Control and Data Acquisition system. That based originally on collecting data for each feeder in the substation consists of switchgear status, Alarms and measurements that are taken as an output of static relays, contactors and sensors (transducers) respectively. The data collected is then concentrated in a slave device called Remote Terminal Unit (RTU) containing a standard communication interfacing protocol allowing it to transmit all the Substation data through used communication media to the master centralized control Center usually called Regional Control Center (RCC) in which all substation data are displayed in a single line diagrams and recorded in lists in historical archive for the operator to monitor the substation in real time mode and responds to the events by sending back some control signals to adjust the substation to the operational situation planned and needed by the utility.

The substation static devices have been effectively influenced by the development of communication technology permitting using high speed automated devices called Intelligent electronic devices (IEDs) connected via reliable high speed communication protocols in peer-to-peer connection.

Electric utilities, especially in developed countries, as well as for LIBYA, continuously encounter the challenge of providing reliable power to the end-users at competitive prices. Due to several reasons such as equipment failures, accidents, power disturbances and outages in substations occur and often result in long service interruptions. Thus, the substations should be properly controlled and

monitored in order to take the necessary precautions accurately and in less time. In this respect, substation automation, which is the creation of a highly reliable, self healing power system that rapidly responds to real time events with appropriate actions, ensures to maintain uninterrupted power services to the end users. [1]

As the equipments and devices in the substation became more and more microprocessor based devices (protection relays, fault recorders …etc). The Intelligent Electronic Devices (IEDs) communicating over high-speed communication links have been introduced to the world of substation automation and the role of the substation System Integrator has changed dramatically. The principal cause of this change is the paradigm shift from a system with unilateral control of slave devices by a single master to one implemented by a fully distributed

architecture, which includes the capability for peer-to-peer communication between IEDs and SCADA server via local Area Network.

Centralized SCADA Systems

SCADA (supervisory control and data acquisition) refers to the combination of telemetry and data acquisition. SCADA encompasses the collecting of the information, transferring it back to the central site, carrying out any necessary analysis and control and then displaying that information on a number of operator screens or displays. The required control actions are then conveyed back to the process.

In modern manufacturing and industrial processes and off course power network utilities, telemetry is often needed to connect equipment (remote node) and systems (master station) separated by large distances, range from a few meters to thousands of kilometers. Telemetry is used to send commands and receives monitoring information from these remote locations.

SCADA systems have been introduced as there have been control systems. Firstly they utilized data acquisition by means of panels of meters, lights and strip chart recorders. The operator manually operating various control knobs exercised supervisory control. These devices were and still are used to do supervisory control and data acquisition on plants, factories and power facilities.

As the requirement for smaller and smarter systems grew, sensors were designed with the intelligence of PLCs and DCSs. These devices are known as IEDs (intelligent electronic devices). The IEDs are connected on a field bus, to the PC. They include enough intelligence to acquire data, communicate to other devices, and hold their part of the overall program. Each of these super smart sensors can have more than one sensor on-board. Typically, an IED could combine an analog input sensor, analog output, PID control, communication system and program memory in one device.[3]

Fundamental principles of modern SCADA systems

In the early days of data acquisition, as the electronic intelligent devices have been introduced and widely used to mange different substation equipments and bay protection for monitoring and operate distance, differential, bus bar protection … etc. and With the advent of the CPU and other electronic devices, manufacturers incorporated digital electronics into relay logic equipment. The PLC or programmable logic controller is still one of the most widely used control systems in industry and partially in power network, the PLCs were distributed and the systems became more intelligent and smaller in size.

As the need to monitor and control more devices in the power utilities grew, DCSs (distributed control systems) are used as local substation SCADA systems. [3]

RTU H/W configuration and functionality

An RTU can be thought as communication equipment that used basically as a data concentrator and equipped with a communication protocol programs to establish path connection with the master centralized station.

RTU configuration

From the operation point of view, the RTU is an electronic device resides in the substation (node), equipped with several input and output cards in which all telemetry Input/output data for that node are hardwired. Furthermore RTU is microprocessor based equipment containing some application programs for digital and analog data processing, addressing and allocation. It contains as well several protocol programs to permit it to communicate with the centralized SCADA system through a communication card using interfacing protocol. Briefly, its main task is data concentrator and telecommunication interface equipment.

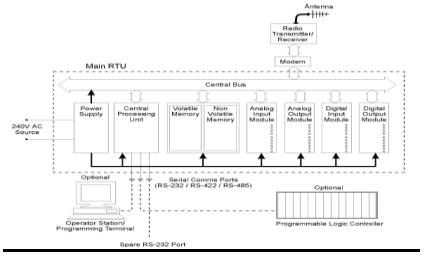

RTU Application programs

RTU S/W and applications, comprises firmware, system configuration and setup, Error management, communication and protocol interfaces as well as RTU database management and data allocations normally resides in a non volatile RAM.

Typical application programs that can run in the RTU are:

Small sized RTUs generally have less than 50 to 75 analog and digital signals, medium sized RTUs have less than 300 digital and analog inputs. RTUs, having a capacity greater than this can be classified as large.

A typical RTU configuration is shown below:

• Analog loop control (e.g. PID).

• Protocol interfaces applications

• Configuration and diagnostic tools for:

• System setup

• Hardware and software setup

•application code development/management/operation.

• Error logs.

• Remote and local operation.

Each module should have internal software continuously testing the systems I/O and hardware. Diagnostic LEDs should also be provided to identify any faults or to diagnose failure of components. It is important that all these conditions are

communicated back to the central station for indication to the operator.

Testing and maintenance

Many manufacturers provide a test box to test the communications between the RTU and master stations, and also to simulate a master station or RTU in the system.

The typical functions provided on a test box are:

• Message switches: Toggle switches simulating messages that the user wants to send to the RTU or master station.

• Message indicators: Display of transmitted data and received controls.

• Mode of operation: The user selects one of three modes of operation, test box in eavesdropping mode between RTU and master station, test box to RTU, test box to master station. An additional self-test mode is often provided.

There are other features provided such as continuous transmissions of preset messages. Often the test box is interfaced to a PC for easier display and control of actions. [3]

Typical requirements for an RTU system

In the writing of a specification, the following issues should be considered:

Hardware:

Individual RTU expandability (typically up to 200 analog and digital points)

• Off the shelf modules

• Maximum number of RTU sites in a system shall be expandable to 255

• Modular system – no particular order or position in installation (of modules in a rack)

• Robust operation – failure of one module will not affect the performance of other modules

• Visible status LEDs

• Local fault diagnosis possible. Remote fault diagnostics option

• Status of each I/O module and channel (program running/failed/ communications OK/failed)

• Modules all connected to one common bus

• Ease of installation of field wiring and Ease of module replacement

The RTU is normally installed in a remote location with fairly harsh environmental conditions considering dust, vibration, rain, salt and humidity.

Software (and firmware)

• Compatibility checks of software configuration of hardware against actual hardware available

• Log kept of all errors that occur in the system both from external events and internal faults

• Remote access of all error logs and status registers

• Software operates continuously despite powering down or up of the system due to loss of power supply or other faults

• Hardware filtering provided on all analog input channels

• Application program resides in non volatile RAM

From Remote Terminal Unit to Substation Automation

In case of conventional substation control system, this is implemented just by adding a remote terminal unit RTU in the substation, acting as a node which takes the needed data from some marshaling kiosk and transfer it to the network control center, respective connective commands from the network control center to some output contacts at the process. The RTU itself has, apart from pure communication handling, only the tasks to time stamp incoming data, and to assure the safety of outgoing commands by means of one out of N criteria supervision and the select before operate principle. So essentially it is just digital conversion and serialization device.

The advances in microprocessor technology lead also to more and more functionality of control devices, introducing the PLC (programmable logic control) that can be included within an RTU that became programmable using the function charts according to IEC 61131 standard languages, advances in communication technology lead to distributed RTUs. This typically consists of some core device containing the NCC protocol processing and the PLC functionality, and remote I/O cards for binary as well as analog data. Also a direct connection of CTs and VTs via analog inputs can be added to omit separation amplifiers and transducers. Thus, the RTU becomes a very basic SA system. Nevertheless its central or master slave related architecture causes some restriction to its functional capabilities, performance and availability.

In a complete SA system using DCS architecture, the RTU functionality is reduced to a station level gateway to the network control center (NCC), which could run even independent from the station level HMI, enhancing the overall system availability.

Digital Control Systems:

Substation automation (SA) is used for controlling, protecting and monitoring of the network[1]. Digital Control System (DCS) is a local SCADA system based on a main server and HMI Client connected to a bay manager in local Area Network via a HUB. The bay Computer (manager) communicates to the protection relays

(IEDs) through serial RS232 or fiber optic communication for substation protection and measurement data. Substation equipments status, controls alarms and CTs, VTs can be directly connected to the bay manager.

DCS system configuration

From a logical point of view, SA systems comprise three levels, the *station level* with the substation host, the substation HMI and the Gateway (GW) to the remote Network Control Center (NCC), the *bay level* with all the control and protection units and the *process level* with more or less intelligent process interfaces to the switchgear. [5]

All implemented levels are interconnected by serial communication links, whilst fiber optic communication link can be used. There is not only vertical communication between the levels (e.g. between bay and station level), but also horizontal communication within the level (e.g. in the bay level between bay units for functions like interlocking). Logical scheme of the three levels of a Substation Automation system shown in (Figure 4.1)

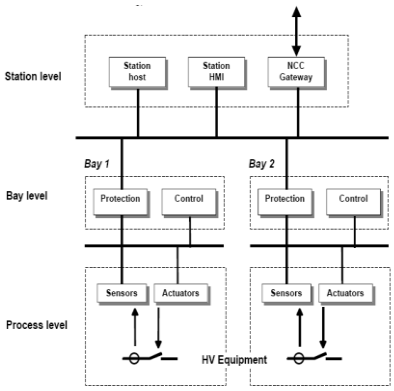

Figure 4.1 Logical DCS system structure

4.2 SA SCADA functionality

SA Operative functions are those typical SCADA functions that directly enable operator to control the substation.

4.2.1 Monitoring and Supervisory functions

The monitoring and supervisory functions enable operator to:

1.Show the status of the process (substation equipments status).
2.To alarm about errors and dangerous situations.
3.To archive data for later evaluation of process performance or failure analysis.
4.Reconstruct the system using Disturbance recording.
5.Get time stamp accuracy in ms. (field time).
The typical monitoring functions are:

- Event management.
- Alarm management.
- Data storage and archiving.
- Disturbance recorder and system reconstruction.
- Log management.

Control Functions

Enables the operator or automatic function (e.g. Automatic voltage Regulator) to control switchgear equipments to:

1. Open or close circuit breaker, disconnector, or earth switch (single and sequence switching).

The execute command here is subject to certain conditions that assure no damage accurse if the control action is conducted:

2. Device supervision will detect failures and block the

A .Hard wired interlocking in process level and software interlocking in HMI level using (PLC) language that generate a state to enable or disable control action.
A .When closing a breaker, synchrocheck function will verify both sides voltages synchronism before the breaker is closed.
b.A controlled object may be blocked if it is put into maintenance mode.
c.The privilege of an operator is checked if he wants to control an object.
d.The substation must be in remote mode to enable control from SCADA centralized system or in local mode to enable control from substation bay level.

3. Rise or lower transformer taps changer (manually or via AVR application).
4. Send a set point to adjust generating unit power capacity.
5. Set Tagging: open/close inhibition, work permission and sanction for test.
6. Update not renewed statue or missing measurement replacement when absence of telemetry data.
7. Parameterize Authentication and user operation area and access permissions.

Benefits of using DCS

Each utility, in their effort to automate existing substations, should focus on two considerations that influence the optimum control of its power system management business.

Technical point of view

Technical enhancements built into modern automation system IEDs provide timely data to support the utility's business functions, facilitate upgrading to add or modify IED functions, diagnose and remedy problems in a timely manner, and maintain accurate documentation of substation's functional configuration.

• From a business point-of-view, future substations must provide accurate, timely, and trusted information to the power control centers and the information technology centers.

• Unlike an existing conventional system that requires many labor-intensive changes in the secondary equipment to add additional functions, new multi-function IEDs provide the capability to add functions to the existing primary equipment without rewiring.

• The ability to diagnose in real time problems in modern systems, and provide accurate information

about the system, shortens the time required for diagnosis, results in a faster restoration time after a fault and increases the reliability of the substation.

• Today, utilities face difficulties in documenting all changes and upgrades to the network. In other words, "As Built" documents that reflect the actual site conditions of the secondary equipment might not be available. New numerical systems provide the capability to automatically document the system configuration during installation, and therefore an "As Built" electronic documentation is updated continuously.[7]

Financial point of view

From a business point of view, operation and maintenance costs should be significantly reduced to justify the cost of substation automation.

Savings in operational cost may be realized by

• Remote control of substation equipment, thereby eliminating the need to man the substation for local control.

• Faster fault location and clearance, resulting in shorter supply interruption time, which is directly related to cost.

• Rapid identification of control and protection equipment failure, allowed by timely remedial corrective action. This is enabled by sequential switching and expert systems that can perform sophisticated functions faster and more precisely than human operator.

• Better and more co-ordinated network control functions as voltage/VAR control, network reconfiguration, and supply reestablishment after faults.

Savings in maintenance cost may be realized by

• Elimination of periodic testing and inspection of electromechanical relays and meters.

• Reducing the time and effort to troubleshoot problems associated with less-complex wiring schemes.

• Software-based equipment testing, which if integrated into the substation automation system, requires less time and effort to isolate and fix equipment problems.

• Primary equipment condition monitoring to reduce regular maintenance schedules of primary equipment. For example, new IED's may have features that provide information about the number of times the feeder breaker operated on fault conditions and the total current that was switched. This information can be used to determine when to maintain the breaker.

• Continuously monitoring and diagnosing the entire substation installation, and then planning just-in-time maintenance rather than maintenance based on a predefined schedule.

Savings in retrofit installation cost (compared to conventional wiring) begins

with well-designed automation architecture. The use of a substation LAN is the major opportunity to reduce installation cost.

- Substation automation using digital signal processing does not require the extensive copper cabling that is required between bays in a substation and control room in existing conventional substations. Only fiber optic cabling is needed for communication between primary equipment and its local bay control cubical, either directly or through a process bus.

- With modern secondary equipment, a number of functions can be performed in one IED whereas in conventional equipment many different units are required. Using multi-function IEDs requires less space than using conventional single-function IEDs. [7]

Experience and possibilities for evolution

Installations

Table below shows total number of high voltage (400 KV, 220 KV) and plant substation (11 KV) Substation Automation operation per year in Libya.

Table 1.Total number of systems in operation

Scope in 2010	2009	2008	2007	2005	2004
219	60	59	55	26	19

Of the quantities shown, approximately 30% corresponds to new substations, and 70% to refurbishment of existing ones.

More, and another way of medium voltage substations (66/30/11 KV substations), GECOL started a new huge project for constructing a new 10 distributed Control Centers around the country to enhance the distributed power network performance, reduce the maintenance cost and respectively the network outages that influences on the network grid reliability availability.

In this project each control center will control substations relays on its responsibility, each substation is equipped with new full SA functional protection devices (IEDs) using new substation communication standards for substation equipments inter connections in both process and bay levels configuration, All telemetry data sent and received in the SA are connected to the master control center through a gateway as the substation level, comprising state of the art communication interfaces.

GECOL is looking forward to enhancing its power network grid and associated system by installing new and refurbishing existing substation with new SA recent technology. Using the IEC 60870-5-104 offer the opportunity to use the future up coming feature of using the WAN (wide Area Network) that permit accessing the SA through the internet web site for system enhancement with more third party application, substation browsing on the net reducing the maintenance cost and satisfying the customer with more efficient services.

Technical experiences

The main aspects that had to be solved at the early stages of the implementation of SA systems were:

a) Lack of knowledge and training of the personnel for commissioning, operation and maintenance.

b) Too long commissioning times due to the difficulties of coordinating the many different people involved in each project.

c) Lack of standardization of the new substation automation engineering.

d) Difficulties to perform complete system acceptance tests at the vendor's factory.

e) Considerable effort was dedicated to debug some minor interoperability / interchangeability problems in the used protocols due to the mixing equipment form different manufacturers in the same installation.

At the present, there still are some aspects that can be improved, such as:

a) Dependency on the manufacturers for reparations and small modifications.

b) Replacement parts availability: A 20 year guarantee is required from the manufacturers, but this may not be practical taking into account the fast evolution of the technology.

c) Need for improvement of the rudimentary level of tools and utilities for graphic design, logic debugging, system configuration maintenance, automatic back-ups, etc.

d) Excessive number of software version changes.

Economical aspects

A clear aspect is the reduction of the investment costs. The main reasons are the simplification of racks and panels, the reduction of the required space and the reduction of inter panel wiring.

A second real cost reduction aspect is the reduced maintenance of the secondary side devices, due to the self-monitoring capabilities of the systems.

Other generally supposed economic advantages are the opportunities for reduction of the maintenance of the primary side equipment and exploitation costs. In this respect, no evidence of such benefits has been experienced, mainly because no condition monitoring based maintenance applications are being used presently. [2]

Why do existing substations need to be automated?

1.This is best understood by identifying typical modern substation automation capabilities and architectures that have the potential to improve power delivery control, protection and supervision functions. Each utility, in their effort to automate existing substations, should focus on two considerations that influence the optimum control of its power system management business.

2.Savings in operational cost may be realized by

Remote control of substation equipment, thereby eliminating the need to man the substation for local control.

- Faster fault location and clearance ,resulting in shorter supply interruption time, which is directly related to cost.
- Rapid identification of control and protection equipment failure, followed by timely remedial corrective action. This is enabled by sequential switching and expert systems that can perform sophisticated functions faster and more precisely than human operator.
- It's more co- ordinate network control functions as voltage/VAR control, network reconfiguration, and supply reestablishment after faults.
- Savings in maintenance cost may be realized by
- • Elimination of periodic testing and inspection of electromechanical relays and meters.
- Reducing the time and effort to troubleshoot problems associated with less-complex wiring schemes.
- Software-based equipment testing, which if integrated into the substation automation system, requires less time and effort to isolate and fix equipment problems.
- Primary equipment condition monitoring to reduce regular maintenance schedules of primary equipment. For example, new IED's may have features that provide information about the number of times the feeder breaker operated on fault conditions and the total current that was switched. This information can be used to determine when to maintain the breaker.
- Continuously monitoring and diagnosing the entire substation installation, and then planning just-in-time maintenance rather than maintenance based on a predefined schedule.

Conclusion

The SA infrastructure comprising numerical protection and control devices allows a new maintenance approach for T&D equipment and provides cost effective solutions for

- On-line monitoring of primary and secondary substation equipment
- Diagnostics to determine the need for maintenance
- Reliability-centered maintenance and condition based asset management

The benefits are reduction of operation and maintenance costs as well as improved service quality and overall power system availability

The integration of protection and control is a way to minimize installation and maintenance complexity by reducing the number of IEDs in a substation. Thorough research studies have indicated that the

integration of protection and control functions will even increase the system reliability. The improvement arises largely from the reduced amount of hardware, wiring and interfaces between equipment that are enabled by integrated solutions.

References

[1] VOLKER Lohma,. "integrated substation automation enable new strategies for power t&d", ABB Power Automation Ltd, Baden/Switzerland

[2] AbdelHamid Mohammed ANTER, "Transferring From RTU to DCS

", comilack2009

[3] BAILEY David, WRIGHT Edwin, "Practical SCADA for Industry", , 2003

[4] K.P.Brand, V.Lohmann, W.Wimmer, "Substation Automation Handbook", UAC 2003, ISBN 3-85759-951-5, 2003 (www.uac.ch)

[5] KLAUS-Peter Brand, "the specification of iec 61850 based substation automation systems", ABB Switzerland Ltd, Baden, Switzerland, Marco Janssen, AMEC SPIE Special Services, Breda, The Netherlands

[6] Experiences and Plans, 58th Annual Conference for Protective Relay Engineers, "Automation of HV Substations in Iberdrola", Texas A&M University", April 7th, 2005.

Monitoring Power Quality Voltage Variations, Sag, Swell and Flickers Based on Wavelet Technique

Dr. Salah Kanoon
Computer Engineering Dep.
Faculty of Engineering, Al-Fatah University
E-mail: Kanoun_99 @Yahoo.com

Dr. Hamid . H. Sherwali
Electric & Electronic Engineering Dep.
Faculty of Engineering, Al- Fatah University
E-mail: Hsherwa@ EE.EDU.LY

Eng. AbdulBadee ali Awin
General Electrical Company
Of Libya
GECOL
E-mail:abdawin@ yahoo.com

Eng. Faroq ali awin
Electric & Electronic Engineering Dep.
Faculty of Engineering,
Al- Fatah University
E-mail:
faroqawin@yahoo.com

Abstract:

This paper presents an automatic system for the detection and classification of power quality disturbances, namely sag, swell and flicker. A detailed description of the multi-resolution wavelet transform technique is presented, and an elaboration on how it is used to detect and classify different disturbance instances is given. Matlab was used in this research to implement the different algorithms. The choice of Mtalab was based on the fact that it is one of the best tool for rapid prototyping that is available to researches in the academic environment.

Keywords: Power quality; wavelet transform; Multi-Resolution Analysis (MRA); neural network, Monitoring, Pattern recognitition.

1) Introduction

Recently, Power quality has become an important issue in power systems. Several years ago the demand for a good power quality has been increased and has become a requirement for some industries.. The reason is mainly due to the increased use of digital processors in Various types of equipment, such as computer terminals, Programmable logic controller, diagnostic systems, etc.

Most of these devices are quite susceptible to disturbances of the incoming alternating voltage waveform. Poor power Quality (PQ) may cause many problems for affected loads, Such as malfunction, failure, instabilities, short life time, etc.

Poor power quality is normally caused by power-lined disturbances, such as impulses, notches, momentary interruptions, wave shape faults, voltage swell/sag, harmonic distortion, and flicker, resulting in failure of end-use equipment. In order to improve power quality, the sources and causes of such disturbances must be known before appropriate mitigating actions can be taken.

A feasible approach to achieve this aim is to incorporate detection capabilities into monitoring equipment so that events of interest will be recognized, captured, and

classified automatically. Thus, good performance monitoring equipment must have functions which involve the detection, localization, and classification of transient events. To monitor electrical power quality disturbances, short timed is discrete Fourier transform (STFT) is most often used. But for non-stationary signals, the STFT does not track the signal dynamics properly due to the limitations of fixed window width chosen a priority thus, STFT cannot be used successfully to analyze transient signals comprising both high and low frequency components.

On the other hand, the discrete wavelet transform And multi-resolution analysis provides a short window for High frequencies components and long window for low frequency components, thus closely monitoring the characteristics of non-stationary signals.

In this paper, we used multi-resolution wavelet transform based neural classifier to automatically detect, and classify sag, swell and flicker disturbances. The structure of the system that was used is described below.

2) Systems components

The system's hardware consists of a voltage sensors, National Instruments data acquisition card (DAQ) model PCI 260+ and a personal computer (PC).

The systems software starts with acquiring the voltage samples of a specific window size from the power lines , then it extracts the features of the samples data from the 12-level resolution wavelet transform. , and finally classifies the feature vector of the sampled window as a sag, swell, flicker or pure.

Wavelet technique and program designing:

I. Wavelet Transformer (WT):

The wavelet technique is more suitable than the Fourier one, especially when signals are non-stationary. Wavelet algorithms process data on a different scale (level) or resolution. In wavelet analysis, the scale that we use to look at data plays a special role. A basis function varies in scale by chopping up the same function or data space using different scale sizes.

The continuous wavelet transform was developed as an alternative approach to the short-time Fourier transform to overcome the resolution problem. By using Mathematical Tools where a signal or function f(t) can be analyzed or processed as expression in a linear combination of a set of orthonormal functions $\Psi l\,(t)$

$$f(t) = \sum_{l \in Z} c_l \Psi_l(t) \qquad (1)$$

where t is time, l is an integer index, and c_l is the expansion coefficients that may be calculated, for continuous-time signals, by the inner product (or scalar product):

$$c_l = \langle f, \widetilde{\Psi}_l \rangle = \int_{-\infty}^{\infty} f(t) \widetilde{\Psi}_l^*(t)\, dt \qquad (2)$$

or for discrete-time signals,

$$c_l = \langle f, \tilde{\Psi}_l \rangle = \sum_{k=-\infty}^{\infty} f(k)\tilde{\Psi}_l^*(k) \qquad (3)$$

In wavelet, The continuous wavelet transform (CWT) is defined as follows:-

$$CWT_X^{\Psi}(\tau, s) = \Psi_X^{\Psi}(\tau, s) = \frac{1}{\sqrt{|s|}} \int X(t)\psi^* \left(\frac{t-\tau}{s}\right) dt \quad (4)$$

As seen in the above equation, the transformed signal is a function of two variables, τ and s, the translation and scale parameters, respectively, and the function Ψ(t) is called the mother wavelet.

In today's world, computers are used to do most computations. It is apparent that neither the FT, the STFT, nor the CWT can be practically computed by using analytical equations, integrals, etc. It is therefore necessary to discrete the transforms. As in the FT and STFT, the most intuitive way of doing this is simply sampling the time-frequency (scale) plane.

Sampling the plane with a uniform sampling rate sounds like the most natural choice. In the case of Wavelet Transformer, a fast algorithm is actually available to compute the wavelet transform of a signal, the discrete wavelet transform (DWT).

For the wavelet expansion

$$f(t) = \sum_j \sum_k c_{j,k}\Psi_{j,k}(t) \qquad (5)$$

where j and k are integer indices and $\Psi_{j,k}(t)$ are the wavelet functions that form an j,k orthogonal basis. The set of coefficients $c_{j,k}$ is called the discrete wavelet transform (DWT) of f(t) function, and can be calculated by

$$c_{j,k} = \int f(t)\Psi_{j,k}(t)dt = \langle f(t), \Psi_{j,k}(t) \rangle \qquad (6)$$

The DWT analysis the signal at different frequency bands with different resolutions by decomposing the signal into a coarse approximation and detailed information. DWT employs two sets of functions, called scaling functions and wavelet functions, which are associated with lowpass and highpass filters, respectively. The decomposition of the signal into different frequency bands is simply obtained by successive highpass and lowpass filtering of the time-domain signal.

The translation and dilation operations applied to the mother wavelet are performed to calculate the wavelet coefficients, which represent the correlation between the wavelet and a localized section of the signal. The wavelet coefficients are calculated for each wavelet segment, giving a time-scale function relating the wavelets correlation to the signal.

From Equation 5 the wavelet expansion has the form

$$f(t) = \sum_j \sum_k c_{j,k} \Psi_{j,k}(t) = \sum_k a_{J_0,k} \varphi_{J_0,k}(t) + \sum_{j=J_0}^{\infty} \sum_k d_{j,k} \Psi_{j,k}(t) \quad , \quad t \in \mathcal{R} \quad (7)$$

where J_0 is a non-negative integer. This expansion is similar to that by Fourier analysis showing a linear combination of wavelet coefficients, ($a_{J_0,k}$, $d_{j,k}$), a set of basis functions $\varphi_{J_0,k}(t)$, called scaling functions, and $\Psi_{j,k}(t)$. Sets $a_{J_0,k}$ and $d_{j,k}$ are the discrete wavelet transform (DWT) of f(t) and can be calculated by

$$a_{J_0,k} = \langle f(t), \varphi_{J_0,k}(t) \rangle \quad (8)$$

$$d_{j,k} = \langle f(t), \Psi_{j,k}(t) \rangle \quad (9)$$

In practice, the wavelet expansion must be truncated at $j= J–1$ such that

$$f(t) = \sum_{k=0}^{2^{J_0}-1} a_{J_0,k} \varphi_{J_0,k}(t) + \sum_{j=j_0}^{\infty} \sum_k d_{j,k} \Psi_{j,k}(t) \quad , \quad t \in \mathcal{R} \quad (10)$$

In this expression, the first sum is a coarse representation of f(t), where f(t) has been replaced by a linear combination of 2^{J_0} translations of the scaling function $\varphi_{J_o,0}$.

The remaining terms are the detailed representation. For each j level, 2^j translations of the wavelet $\Psi_{j,k}$ is added to obtain a more detailed approximation of f(t).

The DWT is implemented using multi-resolution analysis (MRA) to decompose a given signal into scales with different time and frequency resolution. MRA, as implied by its name, analyses the signal at different frequencies with different resolutions. Every spectral component is not resolved equally as was the case in the STFT.

Application Of Discrete Wavelet Transformer (DWT) to detect voltage variations:

Multi-wavelet transform is a new concept in the framework of wavelet transform but has some important differences. In particular, where as wavelet transformer has an associated one scaling (level) function and wavelet function, multi-wavelet has two or more scaling functions and wavelet functions.

A. Multi-Resolution Analysis technique (MRA) :

The first main characteristic in DWT is the Multi-Resolution Analysis (MRA) technique that can decompose the original signal into several other signals with different levels (scales) of resolution Figure(1). From these decomposed signals,

the original time-domain signal can be recovered without losing any information.

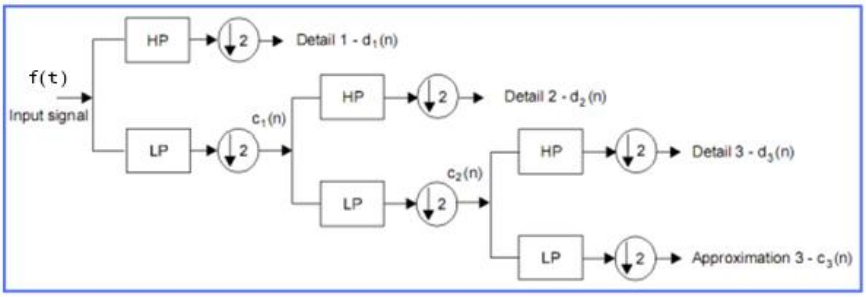

Figure (1) : three-level decomposition tree of MRA

The recursive mathematical representation of the MRA is as follows:

$$a_j = d_{j+1} \oplus a_{j+1} = d_{j+1} \oplus d_{j+2} \oplus d_{j+3} \oplus \ldots\ldots \oplus d_{j+n} \oplus a_{j+n}$$

Where:

$\mathbf{a_{j+1}}$: approximated version of the given signal at scale j+1

$\mathbf{d_{j+1}}$:detailed version that displays all transient j+1 phenomena of the given signal at scale j+1

$\oplus$:denotes a summation of two decomposed signals

n : is the decomposition level

hence, we observe MRA is designed to give good time resolution and poor frequency resolution at high frequencies and good frequency resolution and poor time resolution at low frequencies. This approach makes sense, especially when the signal at hand has high-frequency components for short durations and low-frequency components for long durations. Fortunately, the electrical signals that are encountered in practical applications are often of this type.

B. Wavelet based feature extraction model:

In this paper DWT and multi-resolution analysis have been used to build the model. By return to equations (5) and (10):

$$f(t) = \sum_{k=0}^{2^{J_0}-1} a_{J_0,k}\varphi_{J_0,k}(t) + \sum_{j=j_0}^{\infty}\sum_{k} d_{j,k}\Psi_{j,k}(t) \quad , \quad t \in \Re$$

where in MRA, any time series f(t) can be completely decomposed In terms of the approximations, provided by scaling functions $\boldsymbol{\varphi_m(t)}$ and the details, provided

by the wavelets $\psi_{m}(t)$, where $\varphi_{m,n}(t)$ and $\psi_{m,n}(t)$ are defined as the following:

$$\varphi_{m,n}(t) = 2^{\frac{-m}{2}}\varphi(2^{-m}t - n) \quad (11a)$$

$$\psi_{m,n}(t) = 2^{\frac{-m}{2}}\psi(2^{-m}t - n) \quad (11b)$$

The scaling function is associated with the low-pass filters with filter coefficients h(n), and the wavelet function is associated with the high-pass filters with filter coefficients g(n).

$$\varphi(t) = \sqrt{2}\sum_{n} h(n)\varphi(2t - n) \qquad n \in Z$$

$$\psi(t) = \sqrt{2}\sum_{n} g(n)\varphi(2t - n) \qquad n \in Z$$

Where h(n) and g(n), are sequences that represent discrete filters and Z is the set of all integers.

$$g(n) = (-1)^n h(1-n) \qquad (12)$$

The two Equations represent the DWT algorithm. Sequence f(n), the digitalized version of f(t), is decomposed by the MRA where we used MatLab tools box version 7.0.

The decomposition procedure starts with passing a signal through these filters. The approximations are the low-frequency components of the time series and the details are the high-frequency components.

Multi-resolution analysis leads to a hierarchical and fast scheme. This can be implemented by a set of successive filter banks as shown in Figure (2), where h(n) and g(n) are the low-pass and high-pass filters as defined in (11a-b) & (12).

The symbol **2** means the down sampling with a factor of 2, n is the coefficient index at each decomposition level. Considering the filter bank implementation in Figure (1), the relationship of the approximation coefficients and detail coefficients between two adjacent levels are given as

$$cA_j(k) = \sum_{n} h(2k - n)cA_{j-1}(n) \quad (13a)$$

$$cD_j(k) = \sum_{n} g(2k - n)cD_{j-1}(n) \quad (13b)$$

where $\boldsymbol{cA_j}$ and $\boldsymbol{cD_j}$ represent the approximation coefficients and detail coefficients of the signal at level j, respectively.

In this way, the decomposition coefficients of MRA analysis can be expressed as

$$[\boldsymbol{A_0}] \leftrightarrow [\boldsymbol{cA_1}, \boldsymbol{cD_1}]$$

$$\leftrightarrow [\boldsymbol{cA_2}, \boldsymbol{cD_2}, \boldsymbol{cD_1}]$$

$$\leftrightarrow [\boldsymbol{cA_3}, \boldsymbol{cD_3}, \boldsymbol{cD_2}, \boldsymbol{cD_1}]$$

$$\leftrightarrow \cdots \boldsymbol{and\ so\ on} \qquad (\boldsymbol{14a})$$

Which correspond to the decomposition of signal f(t) as $\mathbf{f(t) = A_1(t) + D_{1(t)}}$

$$\mathbf{= A_2(t) + D_{2(t)} + D_{1(t)}}$$

$$\mathbf{= A_3(t) + D_{3(t)} + D_{2(t)} + D_{1(t)}}$$

$$=$$

$$\cdots \textbf{ and so on} \qquad (\mathbf{14b})$$

Where $A_i(t)$ is called the approximation at level *i*, and $D_i(t)$ is called the details at level *i*, Since both the high-pass filter and the low-pass filter are half band, the MRA decomposition in frequency domain for a signal sampled with the sample frequency f_s can be demonstrated in Figure (2).

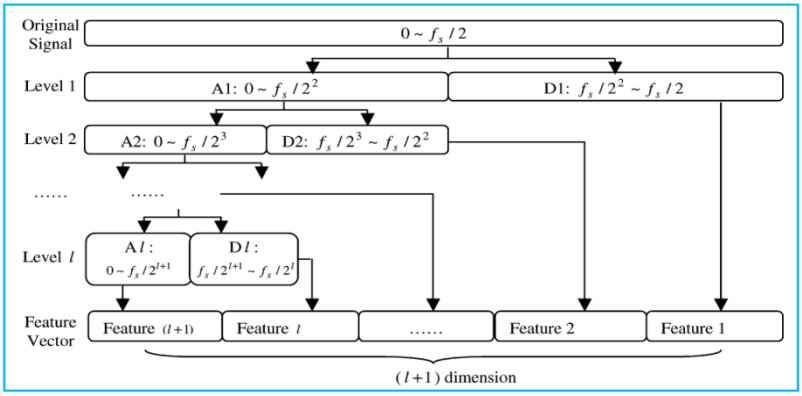

figure (2) MRA analysis and feature construction

- **Energy equation for details decomposition level:**

$$ED_i = \sqrt[2]{\frac{1}{N}\sum_{j=1}^{N}\left|D_{ij}\right|^2}$$

$$= \left(\frac{\left\|D_{ij}\right\|^2}{N}\right)^{\frac{1}{2}}, \qquad i = 1, \dots, l \quad (15a)$$

In order to reduce the feature dimension, we will not directly use the detail $D_i(t)$ and approximation $A_i(t)$ information for future training and testing. Instead, we propose to use ΔE_i as a new input variable for (NN) Neural Network classification.

Where E_i is the energy at each decomposition level, and ΔE_i is the difference in energy distribution between the distorted signal and the pure one see figure (7). The energy at each decomposition level is calculated using the following equations:

analysis. Figure (3) shows data flow in the proposed wavelet feature extraction.

Where the feature ΔE_i calculated by equation (16a-b):

$$\Delta E = E_{\text{distroted signal}} - E_{\text{pure signal}} \quad (16a)$$

Form 1 to **l** level :-

feature vector **distorted signal** **pure signal**

$$\begin{bmatrix} \Delta ED_1 \\ \Delta ED_2 \\ \vdots \\ \Delta ED_l \\ \Delta EA_{l+1} \end{bmatrix} = \begin{bmatrix} ED_1 \\ ED_2 \\ \vdots \\ ED_l \\ EA_{l+1} \end{bmatrix} - \begin{bmatrix} ED_1 \\ ED_2 \\ \vdots \\ ED_l \\ EA_{l+1} \end{bmatrix} \quad (16b)$$

- **And energy equation for approximations decomposition level:**

$$\mathbf{EA_j} = \sqrt[2]{\frac{1}{N}\sum_{j=1}^{N}|A_{lj}|^2} = \left(\frac{\|\mathbf{A_{lj}}\|^2}{\mathbf{N}}\right)^{\frac{1}{2}}, \quad (\mathbf{15b})$$

Where i=1, …, **l** is the wavelet decomposition level from level 1 to level **l**. N is the number of the coefficients of detail or approximate at each decomposition level.

In this way, for a **l** level wavelet decomposition, we construct a (**l** +1) dimensional feature vector for future

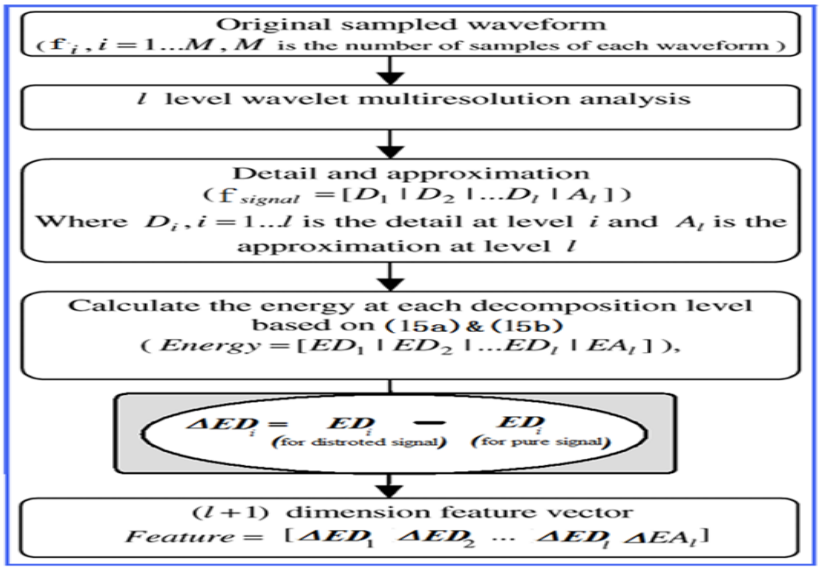

Figure (3) Wavelet based feature extraction.

C. The Selection Of Wavelet

One of the key factors in the application of DWT is the selection of the most appropriate wavelet function depending on the type of disturbance to be detected and analyzed. As a general rule shorter wavelets are best suited for detecting fast transients, while slow transients are better detected using longer wavelets.

Daubechies wavelet has been applied widely since it is sensitive for non-stationary signal. Because Daubechies wavelet has characteristics of orthogonality, compact support and fast arithmetic, so Daubechies wavelets is very suitable for detecting oddity of signal.[10]

D. Simulation and data generation:

The aim of the simulation is to produce typical power waveforms of different disturbances as well as pure AC. One advantage of simulation is the ability to produce as many as possible waveforms that represent different power quality disturbance with different level of noise. This will enable the classifier to be trained (Exposed) to almost every possible disturbance that could ever happen. Another clear advantage is the ability to test the recognition rate of the classifier with a huge data set. The different parameter that were used for the generation of simulated signals is shown in Tables 1&2: simulation of disturbed signals (pure sinusoid, sag, swell & flicker) can be generating by using a disturbed signal modeling (parametric equations) in tables (1&2):

Table (1):

Parametric equations for simulation of disturbed signals

Event	Equation
Pure sinusoid	$v(t) = \sin(\omega t)$
Sudden sag	$v(t) = (1 - \alpha_{ss}(1(t - t_b) - 1(t - t_e)))\sin(\omega t)$
Sudden swell	$v(t) = (1 + \alpha_{sw}(1(t - t_1) - 1(t - t_2)))\sin(\omega t)$
Harmonics	$v(t) = \begin{pmatrix} \alpha_{h1}\sin(\omega t) + \alpha_{h3}\sin(3\omega t)\ldots \\ +\alpha_{h5}\sin(5\omega t) + \alpha_{h7}\sin(7\omega t + \cdots) \end{pmatrix}$
Flicker	$v(t) = (1 + \alpha_f \sin(\beta_f \omega t))\sin(\omega t)$
Oscillatory transient	$v(t) = \begin{pmatrix} (\sin(\omega t) + \alpha_{osc}\exp(-(t - t_b)/\tau_{osc}))\cdot \\ \ldots \sin(\omega_{nosc}(t - t_b)) \end{pmatrix}$

Table (2):

Parameters variation in simulated signals

Event	Parameters variation
Pure sinusoid	Amplitude: 1 Frequency: 50 Hz
Sudden sag	Duration: $(t_2 - t_1) = (0–9)T$ Amplitude: $\alpha_{ss} = 0.3–0.8$
Sudden swell	Duration: $(t_2 - t_1) = (0–8)T$ Amplitude: $\alpha_{sw} = 0.3–0.7$
Harmonics	Order: 3, 5, 7 Amplitudes: 0–0.9
Flicker	Frequency: (5–10) Hz Amplitude: $\alpha_f = 0.1–0.2$
Oscillatory transient	Time const: 0.008–0.04 s Frequency: 100–400 Hz

Data generation by parametric equations is very advantageous to test the classifier ability to recognize different patterns. It is possible to change training and testing signal parameters in a wide range and in a controlled manner. The simulated signals are very close to the real situation. On the other hand, different signals belonging to the same class gave possibility to estimate generalization ability of classifiers based on neural networks.

MATLAB was used to generate 100 different test cases for each disturbance type **(i.e sag, swell & flicker).**

These data sets were used to train neural network and test its performance. Figure (4) shows the generated signals.

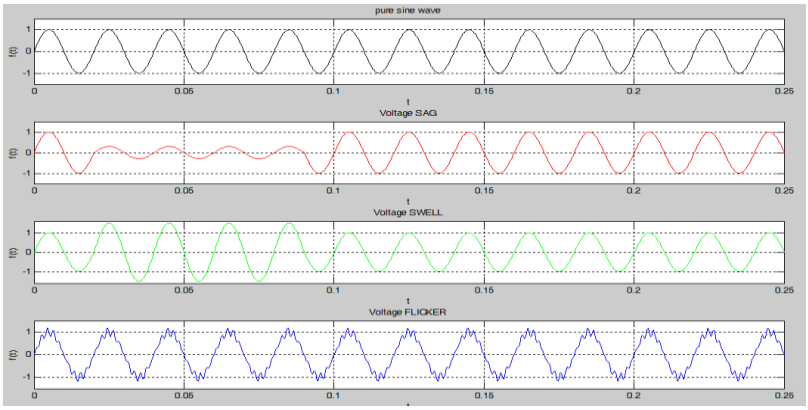

Figure (4) shows the signals generated by MATLAB

II. Detection Program

The monitoring voltage variations, sag, swell and flicker based on wavelet analysis can be realized by using MATLAB program version 7.0, its consists of two parts, part one is simulation part and part two to analyzing the data storage of real signal to detect and classify the voltage variation, sag, swell and flicker. This paper also discusses how to apply toolbox of MATLAB to made a monitoring program that has a detection and classification features.

i. Part one (simulation part)

The program steps of this part are:

- **Step1:** Generating signals close to the real situation of pure sinusoid, sag, swell and flicker by using the parametric equations in table (1), the sampling frequency used is 3.2 kHz and 100 different cases of disturbed signals for each type of sag, swell & flicker.

- **Step2:** Apply MRA on the simulated signals to detect the pure sinusoid, sag, swell and flicker features represented as details & approximation coefficients by using Daubechies wavelet (db5) Where we used **wavedec( )** as wavelet decomposition function and **wrcoef( )** as reconstruction function. Figure (6) shows the simulation results of extracting feature of flicker and swell as examples.
- **Step3:** Calculate energy at each decomposition level based on equations (15a-b).
- **Step4:** Calculate ΔE_i base on equation (16a-b) and save the results to be as inputs to Neural network.
- **Step5:** Train the neural network by feeding input the features generated from previous step to its input. Matlab provides a complete neural network toolbox. **MLP** type feed-Forward back-propagation was used in this paper. The Matalb code is as follows:

```
net = newff(  );

net.trainPara
 m.epochs = 4850


net = train( );
```

In this paper, NN is designed to recognize the following types of power quality disturbances: pure sinusoidal, voltage sag, voltage swell and flicker. The training parameters and structure of MLP are shown in Table (3). They were selected to obtain best performance, such as the number of hidden layers, the size of the hidden layers and type of the activation functions. Figure (5) shows the training performance.

- **Final step:** saving the training results to used it in part two where this part detect and classify the data storage of real signal.

Table (3) Training parameters and the structure of the MLP used in this paper:

ARCHITECTURE	
The number of layers	4
The number of neuron on the layers	Input:13, output:4, hidden layers:5
The initial weights and biases	Random
Activation functions	Sigmoid
TRAINING PARAMETERS	
Learning rule	Feed-Forward Back-Propagation
Train parameters epochs	4850
Mean-squared error	1E-13

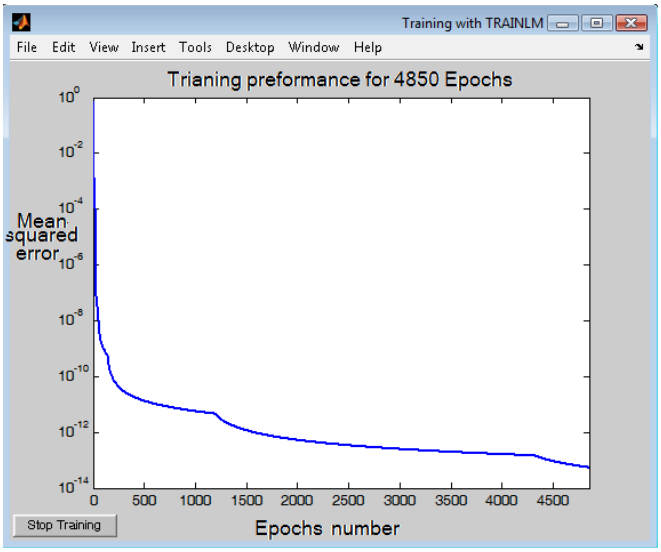

Figure (5) The training performance of neural network in this research.

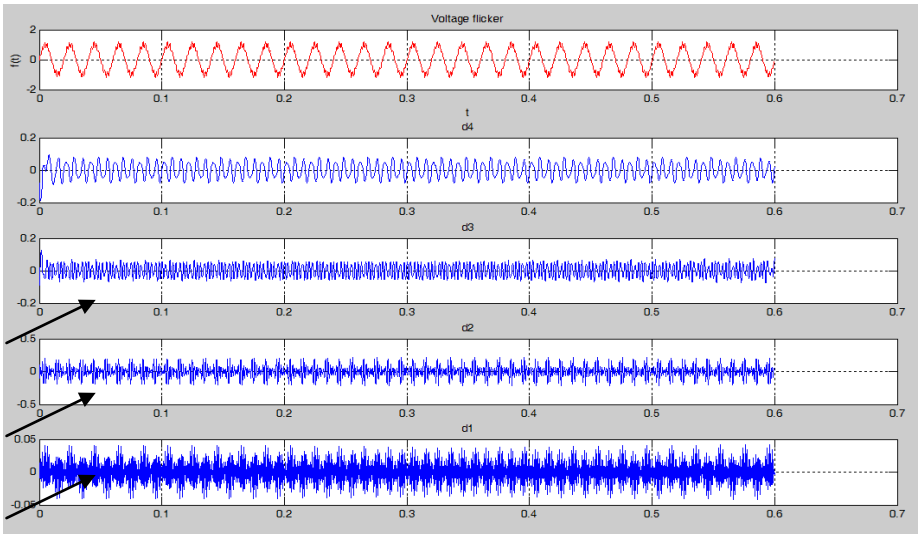

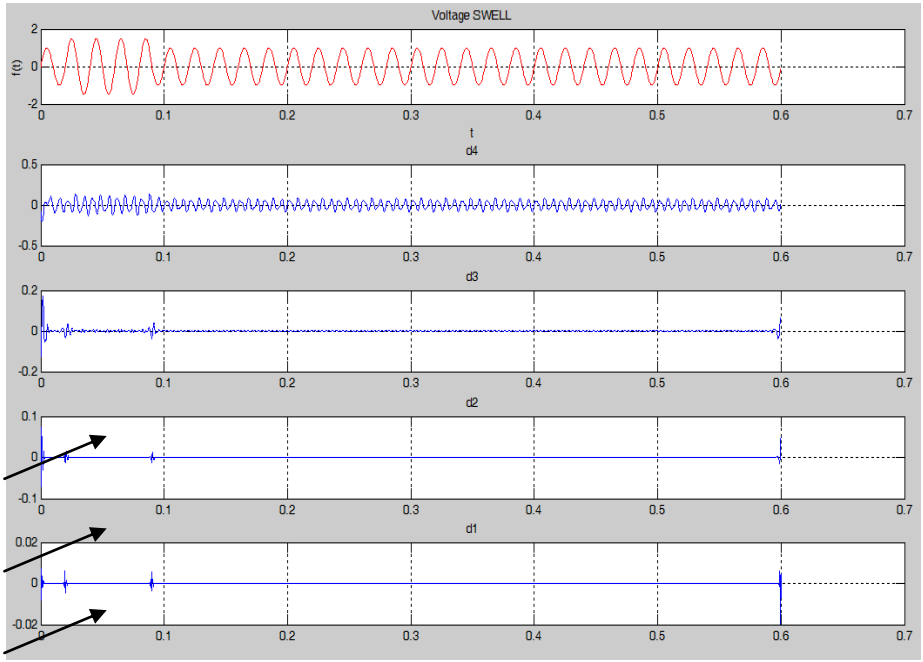

Figure (6) simulation results of extracting feature of flicker & swell

This part of program will be displayed time and location of voltage variation on the signal.

4. Testing Results of NN:

After training the computer we have to testing the results by generating new different signals looks like as we have done before, where randomly 100 signals of each disturbance type entered to testing neural networks. Table (4) shows the classification performance of NN.

ii. Part two (analyzing of data storage)

This part has not been completed yet and it is still being developed. is not finished yet and it's still under preparing, Its consists of three stages as follows:

- Stage one: Acquiring the real signal by DAC, processing and storing the data.
- Stage two: Detect the presence of any voltage variation and classify as either a sag, swell or flicker.
- Stage three: Store the detected event.

Table (4) Classification results for the wavelet-based neural network in this paper:

TYPE		TESTING				Overall Accuracy 98.75%
		pure sinus-oidal	Voltage Sag	Voltage Swell	Voltage Flicker	
SIMULATION RESULTS	pure sinusoidal	10	2	0	1	
	Voltage Sag	0	97	0	0	
	Voltage Swell	0	0	100	0	
	Voltage Flicker	0	0	0	98	
	Other	0	1	0	1	
accuracy		100%	97%	100%	98%	

5. Experimental results and conclusions

o Energy distribution

We can categorize two properties of energy distribution of the given distorted signals:

1) When Sag or Swell occurs, ΔE5, ΔE6 & ΔE7 will show obvious variations. The difference of them:
   - Voltage sag has amplitude between 0.1 p.u and 0.9 p.u.
   - Voltage swell has amplitude between 1.1 p.u and 1.8 p.u.

2) When the voltage suffers a transient disturbance of the low-frequency elements such as voltage flicker, ΔE1, ΔE2 & ΔE3 will show obvious variations.

o Parametric equations (Signals simulated):

1) Signal modeling by parametric equations for classifier test was advantageous in some aspects. It was possible to change testing and training signal parameters in a wide range and in a controlled manner.

2) Signals simulated in that way were very close to reality.

3) During the detecting and classifying PQ disturbances, 100 different cases for every type of PQ disturbance waveforms are generated by Matlab 7.0. The disturbances include voltage sudden sags, sudden swells and flickers, Before classifying the disturbances, we decompose the sample disturbance digital signals using Daubechies wavelet (Db5).

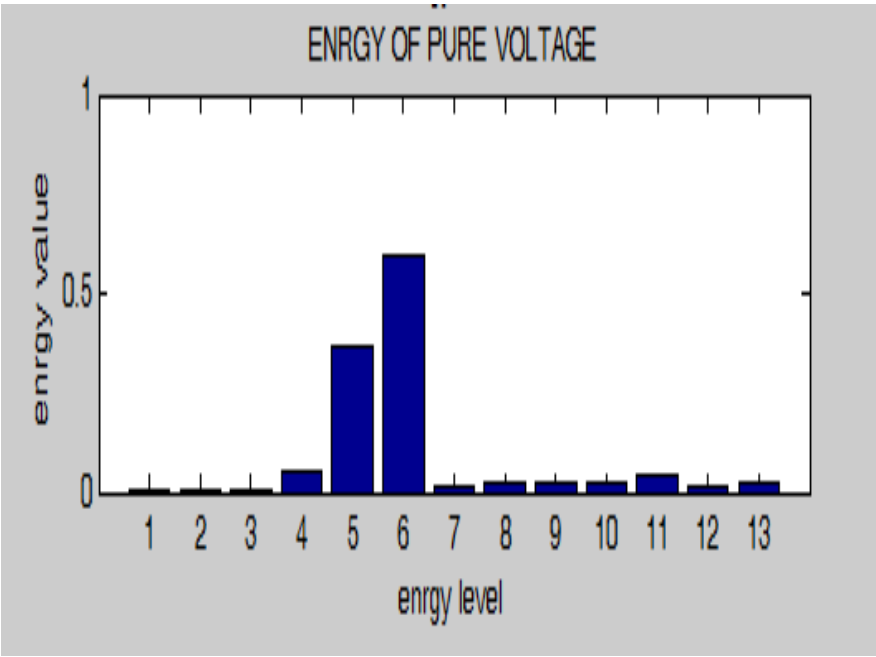

Figure (7a) Detailed Energy Distribution of pure signal

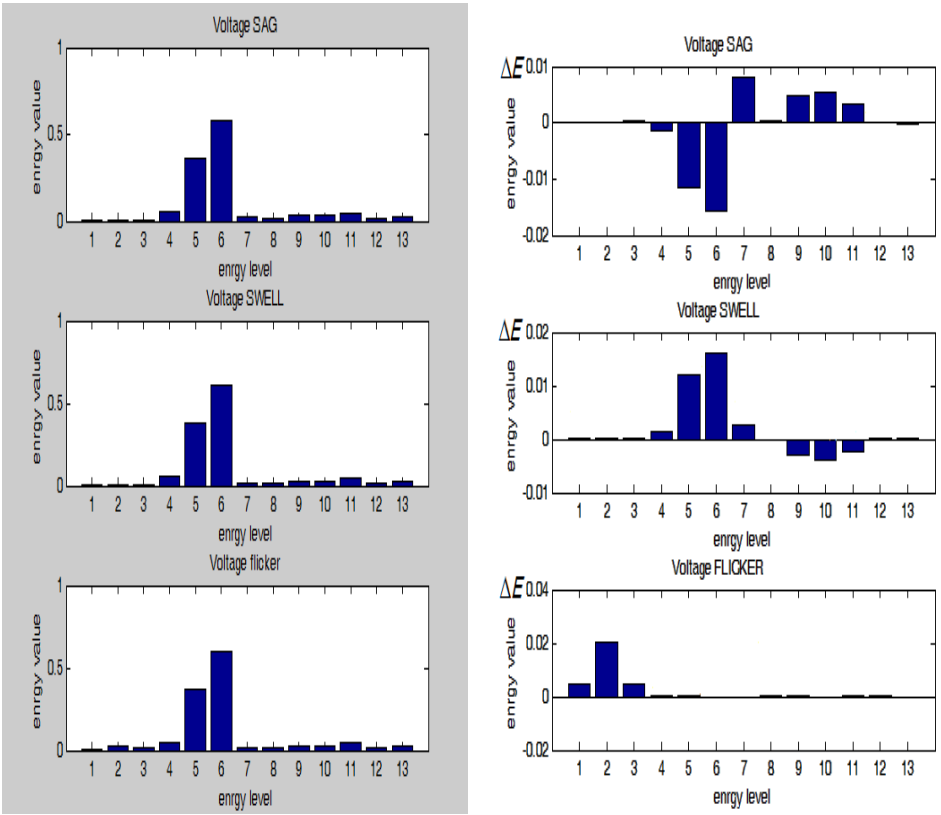

Figure (7b) Detailed Energy Distribution & ΔE of sag, swell and flicker

6) References

[1] S. Suja, Jovitha Jerome, **"Power Signal Disturbance Classification Using Wavelet Based Neural Network",** SERBIAN JOURNAL OF ELECTRICAL ENGINEERING Vol. 4, No. 1, June 2007, 71-83.

[2] M. Karimi, H. Mokthari, and M. R. Iravani, **"Wavelet based on line disturbance detection for power quality applications",** IEEE Transactions on Power Delivery, vol. 15, no. 4, pp. 12121220, October 2000.

[3] Murat Uyara, Selcuk Yildirima, Muhsin Tunay Gencoglub, **"An effective wavelet-based feature extraction method for classification of power quality disturbance signals",** www.ieeexplore.ieee.org, *2002*

[4] A.M. Gaouda, S.H. Kanoun, M.M.A. Salama, A.Y. Chikhani, **"Wavelet-Based Signal Processing Techniques For Disturbance Classification and Measurement",** www.*ieeexplore.ieee.org*

[5] A.M. Gaouda, S.H. Kanoun, M.M.A. Salama, A.Y. Chikhani, **"Pattern Recognition Applications For Power System Disturbance Classification",** *www.engg.uaeu.ac.ae, 2002*.

[6] Murat Uyara, Selcuk Yildirima, Muhsin Tunay Gencoglub, **"An effective wavelet-based feature extraction method for classification of power quality disturbance signals",** www.ieeexplore.ieee.org, *2002*

[7] Ricardo Lima, Damia´n Quiroga, Claudio Reineri, Fernando Magnago, **"Hardware and software architecture for power quality analysis",** 29 March 2006.

[8] Vaclav Matz, Tomas Radil, Pedro Ramos, A. Cruz Serra, **"Automated Power Quality Monitoring System for On-line Detection and Classification of Disturbances",** Instrumentation and Measurement Technology Conference – IMTC 2007, Warsaw, Poland, May 1-3, 2007.

[9] M. Karimi, H. Mokthari, and M. R. Iravani, **"Wavelet based on line disturbance detection for power quality applications",** IEEE Transactions on Power Delivery, vol. 15, no. 4, pp. 12121220, October 2000.

[10] Zhenmei Li, jin Shen, Peiyu Wei, Tianze Li, **"A voltage fluctuation and flicker monitoring system based on wavelet transform",** 2008 workshop on power electrics and intelligent transportation system.

Hybrid Particle Swarm Optimization Algorithm for Optimal Capacitor Placement and Sizing in Unbalanced Radial Distribution Systems

Abdelsalam A. Eajal
Electrical & Electronic Engineering Department
University of Sirte
P.O. Box 633 Sirte-Libya
Tel. +2185460157 / Fax. +2185465461
EAJAL2000@yahoo.com

Abstract-This paper employs a hybrid particle swarm optimization algorithm to locate shunt capacitors with optimal sizes in an unbalanced radial distribution system (unbalanced-RDS). A discrete version of particle swarm optimization (PSO) is combined with a three phase radial distribution power flow algorithm (RDPF). The former is employed as a global optimizer to find the best combination of locations and sizes of shunt capacitors, while the latter is utilized to satisfy the power flow equations. The problem is formulated as a constrained nonlinear integer programming problem with both the capacitor location and size being discrete values. The objective is to minimize the cost of the total real power loss and that of the installed capacitors while satisfying the operating constraints imposed on the system. A 13 bus-unbalanced radial distribution system (13bus-RDS) is tested to validate the proposed method. The test results show the effectiveness of the developed algorithm in solving the optimal capacitor placement and sizing problem.

Index Terms- shunt capacitors, distribution systems, particle swarm optimization.

I. INTRODUCTION

CAPACITORS are widely installed in distribution systems to reduce power losses, improve voltage profiles, and release the system capacity [1]. Achieving such benefits depends greatly on placing and sizing the capacitors properly. Studies have shown that about 13 % of generated power is consumed as losses [2]. Moreover, in distribution systems, the voltage tends to drop along long feeders causing more power losses. Including capacitors in the distribution system will boost voltage profiles back within allowable limits. Furthermore, proper installation of capacitors will release additional kVA capacity. Capacitor placement and sizing are well studied areas of research. The Capacitor Subcommittee of the IEEE Transmission and Distribution Systems Committee has issued 10 bibliographies on power capacitors dating back to 1950s [2]. In 1968, Duran employed a dynamic programming technique to solve the capacitor placement problem [3]. The goal was to maximize the savings due to the loss reduction through proper installation of shunt capacitors while minimizing shunt capacitors costs. The problem was formulated as one of

maximization with a return function of total real power loss savings minus the cost of the capacitors to be installed. The only constraint considered was the total reactive current injection of the node at which a shunt capacitor was to be installed. The optimal solution was obtained using a multistage optimization process. In [4] , Baran obtained the optimal location, type, and size of shunt capacitors in two separate steps. The problem was divided into a master problem, to optimize the capacitor location, and a slave problem, to optimize the capacitor size. The objective was to minimize energy loss and real power loss while taking the capacitor cost into account. The inclusion of energy loss into the objective function required accounting for load profile variations over a certain period of time. The load profile was assumed to change in discrete steps. Considering the changes in load profile allowed for accommodation of capacitors of switched type. Baran [1] formulated the optimal capacitor sizing problem as one of nonlinear programming. The outputs of shunt capacitors were optimized such that the cost of real power losses was reduced while keeping the cost of shunt capacitors methods, Chen solved the optimal capacitor placement and sizing problem by ignoring the discrete nature of capacitor banks and then the optimal solution was rounded up to the nearest integer value.

With the arrival of heuristic optimization methods, a new era of solution methods to the optimal capacitor placement and sizing problem had begun. Huang adopted an immune system algorithm to properly select the locations and ratings of capacitor banks [8]. The objective was to minimize the energy loss while keeping bus voltages within acceptable operating limits and the cost of capacitor banks at a minimum. Das applied genetic algorithms to find the at a minimum. A solution method based on I-phase-II-phase feasible directions was employed. Grainger et al optimized the locations and ratings of fixed shunt capacitors such that the maximum capacity was released [5]. The optimal solution was achieved using a new voltage-dependent method.

Chiang et al reformulated the conventional capacitor placement and sizing problem [6]. The objective function was classified as a non-differentiable function adding more challenges to the conventional optimization algorithms. A simulated annealing algorithm was applied to minimize the constrained non-differentiable objective function. Chen proposed a systematic approach to optimally locate and rate shunt capacitors while taking the mutual coupling effects into account [7]. The consideration of such effects was a step forward towards considering the unbalanced nature of distribution systems. The results showed that neglecting mutual coupling effects would result in oversizing of shunt capacitors and thus raising real power losses in the system. Like in many early

optimum locations and sizes of fixed and switched capacitors while varying the load level [9]. The problem was formulated as a minimization of the energy loss and the cost of shunt capacitors to be installed while maintaining voltage profiles within allowable limits. Another heuristic optimization technique used is the ant colony algorithm. Annaluru developed a multilevel ant colony algorithm to solve the capacitor placement and sizing problem [10]. A Newton-Raphson power flow method was employed to calculate the cost function. Newton-Raphson method is known for its time consumption (i.e. LU decomposition and forward-backward

substitution of the Jacobian matrix). Prakash and Sydulu combined loss sensitivity indices with the PSO algorithm to minimize real power losses and enhance voltage profiles [11]. Loss sensitivity factors were used to determine the sequence in which candidate buses were considered. Incorporating loss sensitivity reduced the computational time of the optimization process significantly. Once the potential locations of capacitor banks were determined, a PSO algorithm was employed to find the best locations and ratings of capacitor banks. AlHajri et al proposed a discrete PSO algorithm to optimally locate and rate a fixed single-phase capacitor in a balanced radial distribution system [12]. The problem was classified as a nonlinear integer optimization problem with both comprised the savings due to the released capacity, released power demand, reduction in the energy loss, and reduction in the installation cost of shunt capacitors.

II. PROBLEM STATEMENT AND FORMULATION

The optimal capacitor allocation and sizing problem is formulated as a constrained nonlinear optimization problem with both the capacitor location and the capacitor reactive power injection being discrete values. The objective function considered in this research is to minimize the cost of the total real power loss in unbalanced radial distribution systems (unbalanced-RDS) and that of the capacitors to be installed while satisfying the constraints imposed on the system. The objective function is described by the following equation:

$$\min F_T = F_P + F_C \qquad (1)$$

potential capacitor location and size being discrete. The PSO algorithm was able to find the best combination of the capacitor location and size simultaneously. The objective was to minimize real power losses while bus voltages were kept within permissible limits.

Heuristic optimization techniques provide an attractive feature and that is hybridization. For example, a hybrid fuzzy-genetic algorithm was developed to maximize the overall savings [13]. The fuzzy algorithm was used to select the best locations of shunt capacitors, while the genetic algorithm (GA) was utilized to find the best ratings of those capacitors. The problem was formulated as a maximization programming problem. The objective function

Where the first term of (1) stands for the cost of the total real power loss and given by:

$$F_P = K_P \sum_{i=1}^{Nb} Ploss_i \qquad (2)$$

Where

K_P : the cost of the total real power losses ($/kW/year).

Nb : the total number of branches in the system.

$Ploss_i$: the real power loss of the branch i.

The second term of (1) represents the total cost of the shunt capacitors to be installed and given by:

$$F_C = K_C \sum_{i=1}^{Nc} Q_i \qquad (3)$$

Where

K_C : the cost of the capacitor to be installed ($/kVAR/year).

Nc : the total number of the capacitors.

Q_i : the reactive power injection of the installed capacitor at node i.

The objective function mentioned in (1) is subject to equality and inequality constraints. The equality constraints are the nonlinear power flow equations of the RDS written in a vector form as:

$$H(x,u)=0 \qquad (4)$$

n : the total number of buses in the RDS.

The inequality constraints associated with the shunt capacitors are given by:

$$Q_i \le LQ_0 , \qquad L=1,2,...,Nc \qquad (6)$$

Where

Q_0 : the smallest capacitor size available.

III. THREE PHASE RADIAL DISTRIBUTION POWER FLOW

The radial distribution power flow algorithm (RDPF) for unbalanced-RDS adopted in this study is developed by Teng [14]. This algorithm is based on the backward-forward sweep technique. Moreover, it models the special features of RDS such as a radial network topology, large number of branches and nodes, and high R/X ratio. Two matrices are formed to obtain the power flow solution, namely $[BIBC]$ and $[BCBV]$. The $[BIBC]$ matrix represents the relationship between the bus current injections and branch currents, while the $[BCBV]$ matrix describes the relationship between branch currents and bus voltages. One unique feature of RDPF algorithm is that the power flow solution is obtained only by using matrix multiplication. In other words, the RDPF algorithm employs the Kirchoff's current and voltage laws KCL and KVL to form the two matrices $[BIBC]$ and $[BCBV]$ respectively. The multiplication of the two matrices results in matrix $[DLF]$ that is used to obtain the power flow solution. The flow chart of the RDPF algorithm is depicted in Fig. 1.

Where

x : the state variables vector.

u : the control variables vector.

The inequality constraints are the bus voltages to be maintained within permissible limits (i.e. $\pm 10\%$ of the swing bus voltage).

$$V_i^{\min} \le V_i \le V_i^{\max} \qquad (5)$$

Where

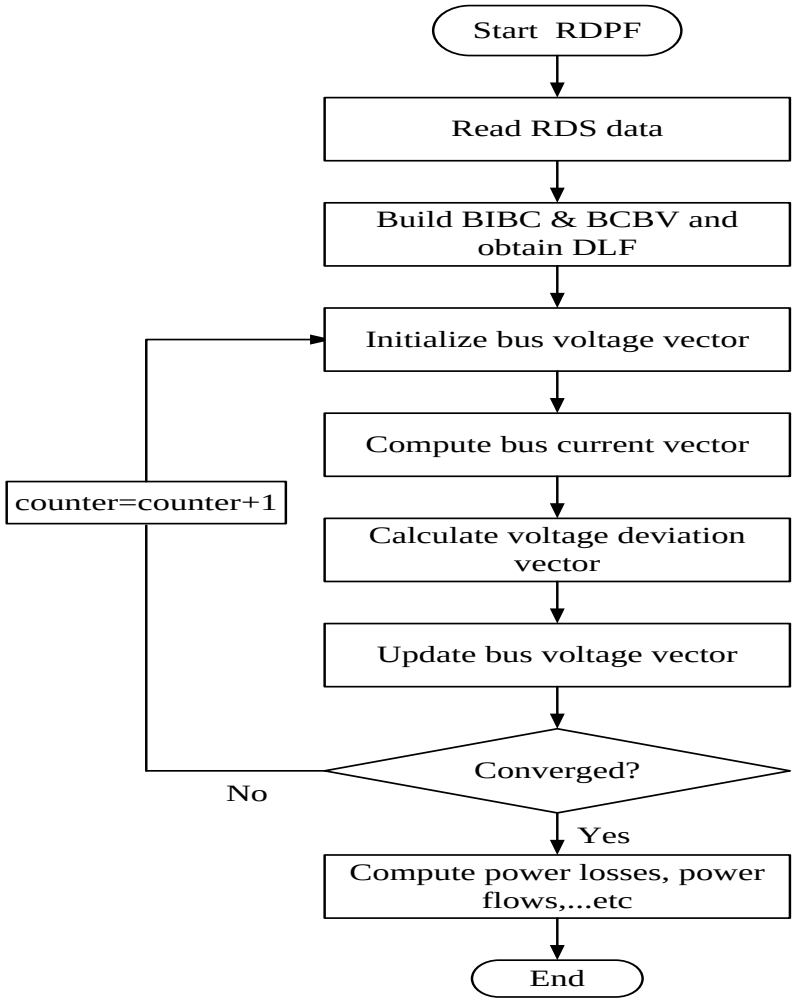

FiG
1 The flow chart of the radial distribution power flow

IV. PARTICLE SWARM OPTIMIZATION

Particle swarm optimization PSO is a meta heuristic optimization technique developed in 1995 by Kennedy and Eberhart [15]. Like other evolutionary technique, PSO is a population based algorithm inspired by bird flocking and fish schooling. In its infancy, PSO was used to solve unconstrained continuous optimization problems. A lot of research has been done since then to improve the first version of PSO to handle nonlinear constrained optimization problems with both discrete and continuous variables [16].

The fundamental idea behind PSO is that a randomly generated population called a swarm consists of individuals called particles, potential solutions. The particles fly through a D-dimensional search space with random velocities. Each particle updates its velocity and position according to the following equations:

$$v_{id}^{k+1} = w v_{id}^{k} + c_1 r_1 (pbest_i^k - x_{id}^k) - c_2 r_2 (gbest^k - x_{id}^k) \quad (7)$$

$$x_{id}^{k+1} = x_{id}^{k} + v_{id}^{k+1} \quad (8)$$

Where

w : the inertia weight.

c_1, c_2 : acceleration constants.

r_1, r_2 : two random numbers in the range of [0,1].

$pbest_i^k$: the best position ever visited by particle i at the kth iteration.

$pbest_i^k = (pbest_{i1}^k, pbest_{i2}^k, ..., pbest_{id}^k, ..., pbest_{iD}^k)$.

$gbest^k$: the global best position among all the particles.

$gbest^k = (gbest_1^k, gbest_2^k, ..., gbest_d^k, ..., gbest_D^k)$.

The basic concept of PSO is illustrated in Fig. 2. Each particle modifies its velocity and position according to its own flying experience and that of the rest of the swarm. If any particle, say particle i, is randomly placed in a two dimensional search space at the point x_i^k, it flies through the problem space with random velocity v_i^k. This particle remembers its best position achieved so far ($pbest_i^k$), shares the information with the other particles, compares its best position with those of other particles, and stores the best position achieved in the entire swarm as $gbest^k$.

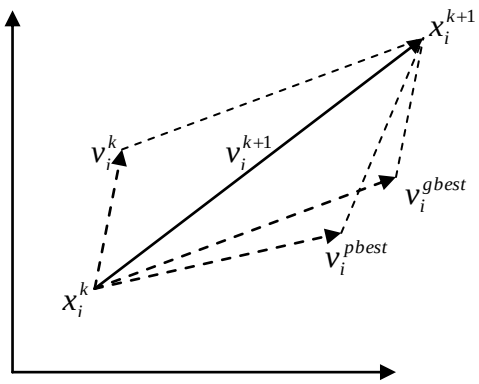

Fig. 2 The PSO concept

Table I lists the main elements of the PSO algorithm and their descriptions.

TABLE I
THE MAIN ELEMENTS OF THE PSO ALGORITHM WITH THEIR DESCRIPTIONS

Element	Description
Particle's position x_i	A possible solution represented by a D-dimensional vector. $x_i = (x_{i1}, x_{i2}, ..., x_{id}, ..., x_{iD})$.
Swarm	A group of particles initialized randomly that tends to cluster together as they move towards the global best position.
Particle's velocity v_i	The velocity at which the *i*th particle flies in a D-dimensional search space. $v_i = (v_{i1}, v_{i2}, ..., v_{id}, ..., v_{iD})$.
Inertia weight w	A control parameter that controls how much impact the previous velocity has on the current velocity of the *i*th particle.
Acceleration constants c_1 and c_2	Those parameters that pull the *i*th particle toward $pbest_i$ and $gbest$ positions.
Best particle's position $pbest_i$	The particle's best position associated with the best fitness value has ever visited.
Particle's fitness value $f(x_i)$	The fitness function that the *i*th particle compares with those of the other particles to enhance its flying experience.
Global best position $gbest$	The best position has ever encountered by all particles.
Stopping criteria	The conditions under which the search process for the optimal solution terminates.

algorithm [12] with a radial distribution power flow algorithm (RDPF) for unbalanced-RDS. The former is used as a global optimizer to determine the best

The pseudo code of the basic PSO algorithm is illustrated in Table II.

TABLE II
THE PSEUDO CODE OF THE BASIC PSO ALGORITHM

Set PSO parameters
Set iteration counter $k = 1$
For each particle {
Randomly generate a position vector and a velocity vector
Measure the fitness value of each particle $f(x_i^k)$
Store the best personal position as $pbest_i^k$
}
Record the particle with the best fitness value as $gbest^k$
Do {
For each particle {
Update the position vector and velocity vector
Evaluate the fitness value $f(x_i^{k+1})$ and compare it with the particle best position $pbest_i^k$
}
Record the particle with the best fitness value as $gbest^{k+1}$
Set $k = k + 1$
} While the maximum number of iterations is not reached

V. HYBRID PARTICLE SWARM OPTIMIZATION

The developed hybrid particle swarm optimization algorithm (HPSO) combines a discrete version of the PSO combination of the bus location on which a capacitor to be installed and the size of that capacitor. The latter is employed to minimize the load flow equations, the

equality constraints, (i.e. bus current mismatch equations). The inequality constraints are handled by preserving a feasible search space throughout the optimization process (i.e. forcing the entire swarm to fly through the feasible region only) [17].

The developed HPSO algorithm starts with generating a swarm of particles randomly in the feasible region of the search space. As previously stated in section IV, each particle is associated with two vectors, the position vector and the velocity vector. The position vector of each particle represents a potential solution to the problem at hand. The feasible swarm is passed to the RDPF subroutine as initial guess to minimize bus current injection mismatch equations. Each particle recalls its best position associated with the best fitness value (i.e. the total cost). Each particle records the best position achieved by the entire swarm. The update process of particles' positions results in continuous values of particles' positions. Thus, discretization of particles' position vectors is made. Once the updated particles' positions are discretized, the particles go through a feasibility check to ensure that no particle flies outside the feasible region [18] . The flow chart in Fig. 3 illustrates the HPSO algorithm that combines the PSO algorithm with the RDPF algorithm.

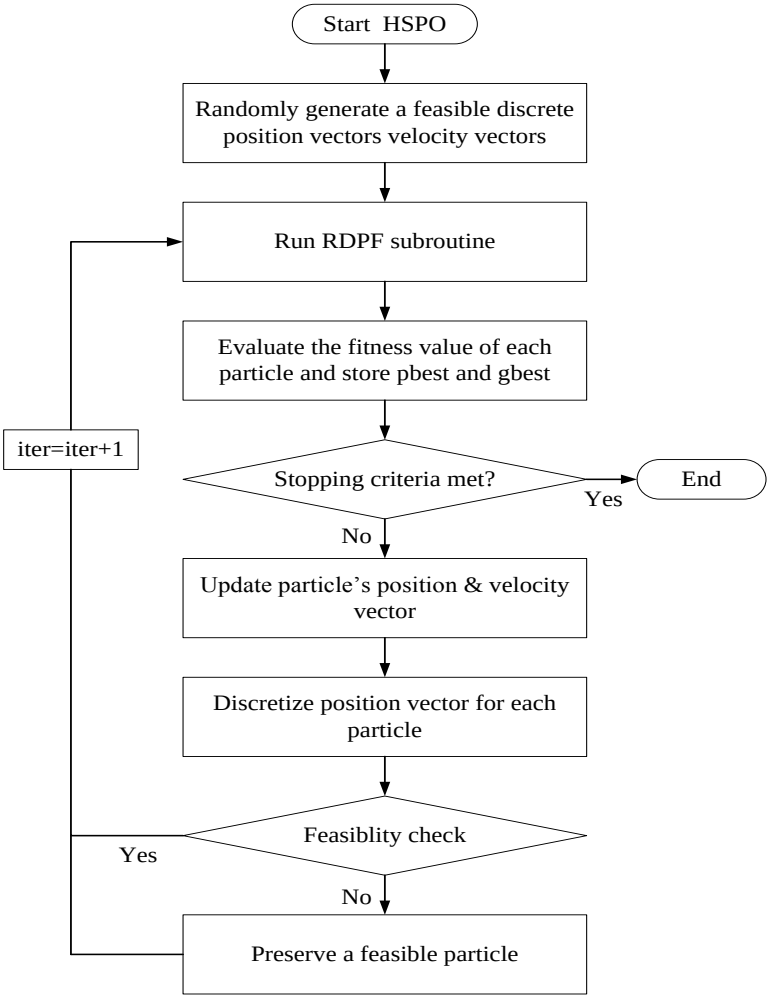

Fig. 3 The flow chart of the HPSO algorithm

VI. TEST RESULTS AND DISCUSSION

The proposed algorithm (HPSO) was implemented in MATLAB® computing environment on a Dell Laptop with Intel® Pentium® M processor of 1.86 GHz and RAM of 1 GB. The HPSO was tested on an unbalanced-13-bus radial distribution system (unbalanced-13-bus-RDS) whose single line diagram is shown in Fig. 4. The unbalanced-13-bus-RDS consists of single, double, and three phase lines and loads. The total real and reactive power demand are 3464.1 kW and 1568.9 kVAR respectively. The system loads are of two types, distributed loads and spot loads. A complete description of the system is found in [19]. The MVA base value is 10 and the line to line base voltage is the same as the feeder nominal voltage 4.16 kV.

The number of shunt single phase capacitors to be installed is not to exceed five banks of a discrete size of 150 kVAR each while maintaining the bus voltages within permissible limits (i.e. ± 10 % of the nominal bus voltage). The HPSO parameters were tuned to enhance the convergence characteristics for the given system. A swarm size of 20 particles and

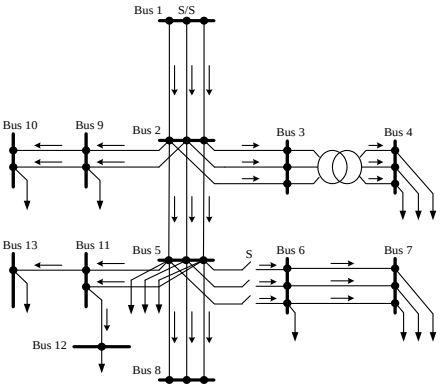

Fig. 4 An unbalanced-13-bus radial distribution system

system will bring the violated bus voltages back within the allowable limits. Voltage profiles before and after capacitor inclusion are reported in Table IV.

TABLE III
RESULTS FOR CASES 1&2

	Case 1	Case 2
Minimum Bus Voltage (p.u)	0.8944	0.9339
Maximum Bus Voltage (p.u)	0.9856	0.9993
Reactive Power Injection (kVAR)	—	$Q_{6c} = 600$
Real Power Losses (KW)	192.4208	179.1373
Total Cost ($/year)	32,327	30,227
Net Savings ($/year)	0	2100

acceleration constants of 2.0 were selected. The cost of real power losses is taken as 168 $/kW/year, while the cost of the installed capacitor is a function of the capacitor size [20]. The HPSO algorithm selected the phase c of bus 6 to be the optimal location for a single phase capacitor with an optimal size of 4×150 kVAR.

To investigate the impact of capacitor installation on voltage profiles, real power losses, and net savings, two cases are studied:

- **Case 1** represents the system before capacitor installation.
- **Case 2** represents the system after capacitor installation.

Results for cases 1and 2 are tabulated in Table III. From the results obtained, installing a shunt capacitor of 600 kVAR at phase c of bus 6 will reduce the total real power losses from 192.4208 kW to 179.1373 kW and profit the utility 2100 $/year. Also, including a capacitor in the TABLE IV

VOLTAGE PROFILES FOR CASE 1& CASE 2 ,OF THE OPTIMAL PLACEMENT AND SIZING OF ONE SHUNT CAPACITOR

Bus	ϕ	Case 1 $\lvert V \rvert$ (p.u)	Case 2 $\lvert V \rvert$ (p.u)
1	a	1.0	1.0
	b	1.0	1.0
	c	1.0	1.0
2	a	0.9674	0.9638
	b	0.9812	0.9688
	c	0.9505	0.9919
3	a	0.9644	0.9609
	b	0.9792	0.9668
	c	0.9477	0.9892
4	a	0.9411	0.9373
	b	0.9602	0.9479
	c	0.9288	0.9703
5	a	0.9499	0.9413

	b	0.9845	0.9598
	c	0.8999	0.9837
6	a	0.9499	0.9413
	b	0.9845	0.9598
	c	0.8999	0.9837
7	a	0.9426	0.9339
	b	0.9856	0.9610
	c	0.8964	0.9801
8	a	0.9499	0.9413
	b	0.9845	0.9598
	c	0.8999	0.9837
9	b	0.9699	0.9576
	c	0.9539	0.9953
10	b	0.9660	0.9537
	c	0.9578	0.9993
11	a	0.9485	0.9398
	c	0.8970	0.9808
12	a	0.9432	0.9345
13	c	0.8944	0.9782

The convergence characteristics of the proposed HPSO algorithm for case 2 in the optimal placement and sizing of one shunt capacitor problem is illustrated in Fig. 5. Figure 5 indicates the convergence speed of the developed solution methodology in finding the global optimal solution of the capacitor allocation and sizing problem.

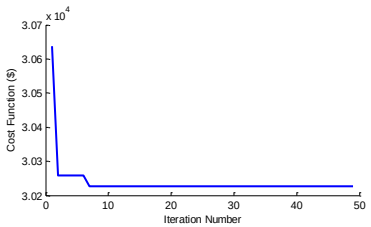

Fig. 5 Convergence characteristics of the HPSO algorithm for case 2

In order to do more testing on the developed HPSO algorithm, the capacitor placement and sizing problem is extended to multiple capacitors. Three single phase capacitors are considered instead of one capacitor. The maximum reactive power injection of these capacitors is not to exceed the total reactive demand of the system.

A swarm size of 25 particles and acceleration factors of 2 each were selected.

The developed HPSO algorithm was able to find the optimal locations and ratings of three shunt capacitors such that the overall cost was minimized. The simulation results are reported in Table V. As can be seen the optimal locations of the three shunt capacitors are phase b of bus 5, phase a of bus 6, and phase c of bus 6, while the optimal sizes of these capacitors are 300, 450, and 600 kVAR respectively. The proper installation of these capacitors results in 14.26 % reduction in the total real power loss and 6.831 % improvement in the voltage profile. In addition, inclusion of three shunt capacitor in the system would save the electric utility 4258 $/year.

TABLE V
RESULTS OF THE OPTIMAL PLACEMENT AND SIZING OF THREE SHUNT CAPACITORS IN A 13-BUS-RDS

	Case1	Case2
Minimum Bus Voltage (p.u)	0.8944	0.9555
Maximum Bus Voltage (p.u)	0.9856	0.9945
Reactive Power Injection (kVAR)	–	Q_{5b} =300 Q_{6a} =450 Q_{6c} =600
Real Power Losses (kW)	192.4208	164.9870
Cost Function ($/year)	32,327	28,069
Net Savings ($/year)	–	4258

Voltage profiles of the 13-bus-RDS before and after installation of three shunt capacitors are listed in Table VI.

The convergence characteristics of the developed HPSO algorithm for cases 2 in the optimal placement and sizing of three shunt capacitors problem is depicted in Fig.6.

TABLE VI
VOLTAGE PROFILES OF A 13-BUS-RDS FOR CASES 1 AND 2,OF THE OPTIMAL PLACEMENT AND SIZING OF THREE SHUNT CAPACITORS

Bus	ϕ	Case1	Case2
		$\|V\|$ (p.u)	$\|V\|$ (p.u)
1	a	1.0	1.0
	b	1.0	1.0
	c	1.0	1.0
2	a	0.9674	0.9869
	b	0.9812	0.9857
	c	0.9505	0.9804
3	a	0.9644	0.9839
	b	0.9792	0.9837
	c	0.9477	0.9777
4	a	0.9411	0.9606
	b	0.9602	0.9647
	c	0.9288	0.9589
5	a	0.9499	0.9887
	b	0.9845	0.9934
	c	0.8999	0.9610
6	a	0.9499	0.9887
	b	0.9845	0.9934
	c	0.8999	0.9610
7	a	0.9426	0.9814
	b	0.9856	0.9945
	c	0.8964	0.9574
8	a	0.9499	0.9887
	b	0.9845	0.9934
	c	0.8999	0.9610
9	b	0.9699	0.9744
	c	0.9539	0.9839
10	b	0.9660	0.9705
	c	0.9578	0.9878
11	a	0.9485	0.9873
	c	0.8970	0.9581
12	a	0.9432	0.9820
13	c	0.8944	0.9555

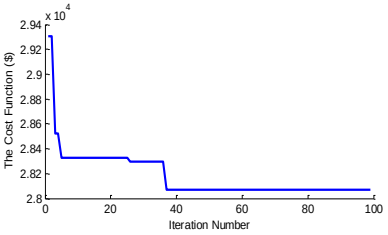

Fig. 6 Convergence characteristics of the HPSO algorithm for case 2 in the optimal placement and sizing of three shunt capacitors

VII. CONCLUSION

This paper proposed a hybrid PSO algorithm (HPSO) to solve the optimal capacitor placement and sizing problem for unbalanced radial distribution systems. The HPSO algorithm integrates a three phase radial distribution power flow (RDPF) with a discrete particle swarm optimization algorithm. The problem was formulated as a constrained nonlinear integer programming problem with both the capacitor location and the capacitor size being discrete values. The developed HPSO algorithm was tested on an unbalanced-13-bus-RDS. The research findings verify the effectiveness of the proposed approach in solving such an exhaustive nonlinear integer optimization problem.

VIII. REFERENCES

[1] Baran, M. and Wu, F., "Optimal sizing of capacitors placed on a radial distribution system," *IEEE Transactions on Power Delivery, vol.4, no.1,* pp. 735-743, 1989.

[2] Ng, H. N., Salama, M. M. A. and Chikhani, A. Y., "Classification of capacitor allocation techniques," *IEEE Transactions on Power Delivery, vol.15, no.1,* pp. 387-392, 2000.

[3] Duran, H., "Optimum number, location, and size of shunt capacitors in radial distribution feeders A dynamic programming approach," *IEEE Transactions on Power Apparatus and Systems, vol.PAS-87, no.9,* pp. 1769-1774, 1968.

[4] Baran, M. E. and Wu, F. F., "Optimal capacitor placement on radial distribution systems," *IEEE Transactions on Power Delivery, vol.4, no.1,* pp. 725-734, 1989.

[5] Grainger, J. J. and Lee, S. H., "Capacity release by shunt capacitor placement on distribution feeders: A new voltage-dependent model," *IEEE Transactions on Power Apparatus and Systems, vol.PAS-101, no.5,* pp. 1236-1244, 1982.

[6] Chiang, H. D., Wang, J. C., Cockings, O. and Shin, H. D., "Optimal capacitor placements in distribution systems: I. A new formulation of the overall problem," *IEEE Transactions on Power Delivery, vol.5, no.2,* pp. 634-642, 1990.

[7] Chen, C. S., Hsu, C. T. and Yan, Y. H., "Optimal distribution feeder capacitor placement considering mutual coupling effect of conductors," *IEEE Transactions on Power Delivery, vol.10, no.2,* pp. 987-994, 1995.

[8] Huang, S. J., "An immune-based optimization method to capacitor placement in a radial distribution system," *IEEE Transactions on Power Delivery, vol.15, no.2,* pp. 744-749, 2000.

[9] Das, D., "Reactive power compensation for radial distribution networks using genetic algorithm," *International Journal of Electrical Power and Energy Systems, vol.24, no.7,* pp. 573-581, 2002.

[10] Annaluru, R., Das, S. and Pahwa, A., "Multi-level ant colony algorithm for optimal placement of capacitors in distribution systems," *Congress on Evolutionary Computation,* pp. 1932-1937, 2004.

[11] Prakash, K. and Sydulu, M., "Particle swarm optimization based capacitor placement on radial distribution systems," *IEEE Power Engineering Society General Meeting,* pp. 1-5, 2007.

[12] AlHajri, M. F., AlRashidi, M. R. and El-Hawary, M. E., "A novel discrete particle swarm optimization algorithm for optimal capacitor placement and sizing," *Canadian Conference on Electrical and Computer Engineering,* pp. 1286-1289, 2007.

[13] Prasad, P. V., Sivanagaraju, S. and Sreenivasulu, N., "A fuzzy-genetic algorithm for optimal capacitor placement in radial distribution system," *ARPN Journal of Engineering and Applied Science, vol.2, no.3,* pp. 28-32, 2007.

[14] Teng, J. H., "Network-topology-based three-phase load flow for distribution systems," *Proc. Natl. Sci. Counc. ROC(A), vol.24, no.4,* pp. 259-264, 2000.

[15] Kennedy, J. and Eberhart, R., "Particle swarm optimization," *IEEE International Conference on Neural Networks,* 1995.

[16] Hu, X., Shi, Y. and Eberhart, R., "Recent advances in particle swarm," *Proceedings of 2004 Congress on Evolutionary Computation, vol.1,* pp. 90-97, 2004.

[17] Coath, G. and Halgamuge, S. K., "A comparison of constraint-handling methods for the application of particle swarm optimization to constrained nonlinear optimization problems," *The 2003 Congress on Evolutionary Computation,* 2003.

[18] AlRashidi, M. R. and El-Hawary, M. E., "Hybrid particle swarm optimization approach for solving the discrete OPF problem considering the valve loading effects," *IEEE Transactions on Power Systems, vol.22, no.4,* pp. 2030-2038, 2007.

[19] Task Force on Harmonics Modeling and Simulation, "Modeling and simulation of the propagation of harmonics in electric

power networks part II: Sample systems and examples," *IEEE Transactions on Power Delivery, vol.11, no.1,* pp. 466-474, 1996.
[20] Baghzouz, Y. and Ertem, S., "Shunt capacitor sizing for radial distribution feeders with distorted substation voltages," *IEEE Transactions on Power Delivery, vol.5, no.2,* pp. 650-657, 1990.

An Interactive Program for Overhead Transmission Line Design Using MATLAB

Salem Kurdi
kusalem@yahoo.com

Bashir M. Jomaa
bashir.jomaa@yahoo.com

Abstract

This paper presents an interactive computer program for three phase's overhead transmission line design using MATALB. This program can be used a self learning tool to understand the course material offered in class in order to enhance students understanding to the subject of the first introductory course in the field of electrical power engineering. This first course is normally given as a core course to all electrical engineering students. Most of the existing text books in power system analysis nowadays cover the Electrical line design only and describe the line performance very efficiently with very few power text books which treat the mechanical line design part. Therefore the electrical engineering students with power engineering major are often graduated from school without having sufficient background concerning the mechanical line design features such as; line sag, the mechanical tension at the tower and the conductor sag due to temperature variations or line loading, conductor thermal limit ….etc. This program is also equipped with an additional feature to compute the line sequence impedances and the line sequence capacitances. Using this program the students will then be able to compute the line sequence parameters for both the single circuit as well as the double circuit tower configuration, with and without ground wire. This program has been also provided with a built in data base library to most of the available power line conductors. Therefore the power engineering students will then be able to grasp the transmission line course contents in more depth and to use the program as a self learning tool for line design and line modeling performance.

Keywords : Line inductance, capacitance, sag , tension, transposition , sequence impedances and sequence capacitances, electric and magnetic field.

Introduction

Visualization of the solution of complex problems reinforces the basic principles learned via the traditional methods. The reinforcement is greater if the students from the beginning are exposed to such facilities. such as Graphical representation of solving equations that describe the physical system. This in turn will reinforce and accelerate the students learning and understanding to the field concept [1]. The effect of changing system parameters, topology, boundary and initial conditions provides a dramatic reinforcement to the mathematical description and to the

analytical system knowledge a power student acquires in the classroom.
This new developed program with the new added features using MATLAB with the graphical user interface facilities is a modification to the previous effort that was accomplished and published earlier by the author and his colleagues in 1989 [2]. The previous work was initiated by introducing four independent interactive programs for power engineering students covering mainly four different topics; load flow, short circuit , stability and line sequence impedances and sequence capacitances calculation. This paper will present a transmission line program which will help students to understand the material given in class for the core course taken during their undergraduate program.
The developed program is a user friendly, highly interactive during both the data entry phase and during the execution phase where the user can visualize the input data and see it on the screen. He or she can check, change, modify or completely erase the data so easily. The program solution can also be visualized.

A number of applications will be presented in a sequential order to present the usefulness of the program. Following this methodology the program can be very useful in class and as well as at home for better, faster and user friendly tool.

The subject of transmission line design is extensive as is the detailed modeling, since the overhead transmission line is a major component in power system. Therefore, the availability of a well developed and easy computer program for students, instructors and line designers is very essential.

Subject background and the need for Transmission line program

The new undergraduate students registering for the first time in the first electrical power engineering course is very much interested primarily to understand the transmission line principles such as; the line inductances per unit length , the line capacitance per unit length and the line resistance per unit length. Once all these line parameters are taken in class and understood then the line impedance, line admittance can be calculated based on a given and know system frequency. To model such a line in a particular study the line length must be also know. Since the line model varies with the line length. Different line models are available. Therefore students should be aware of such line models. The appropriate line model selection will depend on many factors such as; line length; steady state or transient condition, normal or faulted situation.
The three phase transmission line theory is given to undergraduate students as a core course. In this course the students will be exposed to the basic theoretical background with some line modeling details.
The line basic components such as; line inductance and line capacitance can be easily computed for a given line conductors and given tower configuration. Most of the time the homework assignments given to students during the course are devoted to a single circuit tower configuration without ground wire and assuming the line is completely transposed [3]
In some cases the undergraduate students will be given the appropriate techniques and the short cut approach without going in deep details in the analysis on how to deal with double circuit tower configuration and how to take into consideration the influence

of ground wire. During the course work the undergraduate students are given in class enough background to be used to compute the positive sequence inductance and positive sequence capacitance assuming the line is completely transposed. Under such condition the effect of ground wires are usually neglected [2,3,4] Very often during the lecture a brief discussion concerning the transposition concept is covered. The majority of students in class may or may not be familiar with the deep understanding of the need for line transposition and what are the real impacts on line performance in case the line is not transposed. What will be the effect on line impedance and line capacitance? When the line should be transposed? The students may raise many other questions such as what are the meanings of line sequence impedance, line sequence capacitances. Why do we need to get such sequence impedances? What do we mean by transmission line unbalance ……..etc?.

The answers to all these questions and others can be shown and explained with typical applications as will be described below.

Application#1

The first application will be devoted to develop user confidentiality session between the students and the program. The students will be asked to do the following assignments:

Turn the computer on and do call the transmission line program. The student is expecting to see a display on the screen with four options: these four options are:

- Electrical Design
- Mechanical design
- Thermal limit and line loading capability
- Environmental effects

A decision has to be made by the student to choose either a single circuit tower or double circuit tower

Let us now assume that the student selects the single circuit option; a new display will be shown on the screen as indicated in fig.1

This screen shows a large number of information that will guide the students step by step to insert the input data. The information required to be inserted on the screen are in itself very useful and are designed in a way to help the student to be well guided to accomplish his goal very successfully such as:

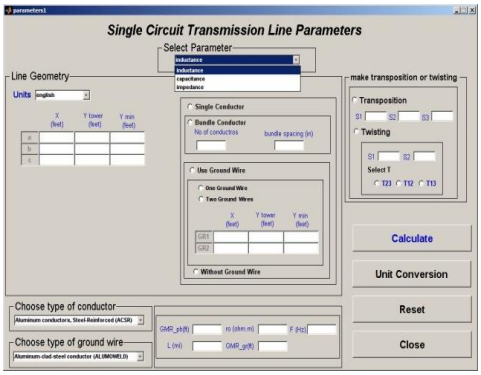

Fig.1 A single circuit tower line input data parameters.

- Choice of the type of the line parameters to be calculated first for example; line inductance, line capacitance or line impedance:
- Choice of the type of units to be used in the calculation ; metric or English
- For a single conductor, the student must click on single conductor option and for the bundle conductor the student must click on the bundle conductor and then he should insert the number of the bundle conductors;2,3,4.…etc . The spacing

between sub-conductors must be also specified.

- Tower configuration; the student should also insert the positions of the three phase conductor on tower. Therefore the three phase conductors should be inserted and specified as an (x,y) coordinates .

The student should also have been selected the conductor name from the beginning; and from the stored and the available data base library in the program an automatic display for all the data needed for the inductance, capacitance and impedance calculation will be shown on the screen such as: Conductor geometric mean radius, conductor radius, conductor resistance….etc

If the circuit has a ground wire, then the name of the ground wire should have been also selected with the same procedure similar to the phase conductor. The location of the ground conductor should have been decided and an automatic fill in information will be displayed at the appropriate space provided for the ground wire, such as; ground wire resistance, ground wire geometric mean radius and ground wire radius.

Let us now be very specific and let us assume that the following home work assignment is given to the student as:

Application# 2

A 400kv three phase single circuit completely transposed line , is composed of a single conductor per phase ACSR 1,272,000cmil, 45/7 Bittern conductor per phase with the tower configuration as shown in fig.6 Use the developed program and compute the following : The line inductance L , The line Capacitance C , The line Impedance Z

The required input data to the program are:

Conductor name: Bittern, CSA 1,272,000 ACSR

Single conductor /phase, line completely transposed

Let us go back to the screen display of fig.1 and select the conductor name as given above

Let us also insert the tower configuration shown in fig.2 and let us select also the completely transposed line option as normally mentioned in the course. No ground wire information is provided therefore; no ground wire exists. Let the English units; inches and feet are selected for this calculation

Let us calculate first the Line inductance by clicking on the inductance option

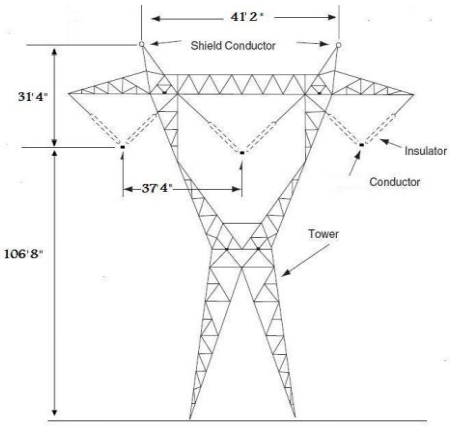

Fig.2 A 400 kv single circuit tower configuration.

The solution to this application will be shown on the screen as indicated in fig.4

The students can now compare the computed values with the value obtained using the formula that he took in class: where

L = 0.2 x ln (GMD/GMR) mH/km

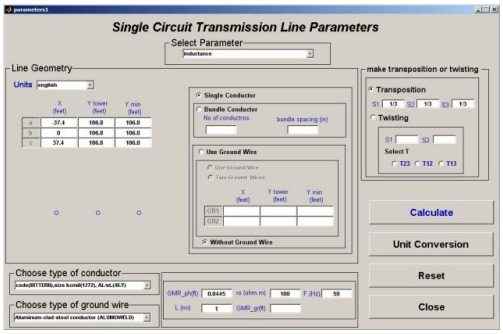

Fig.3 A single circuit inductance input data.

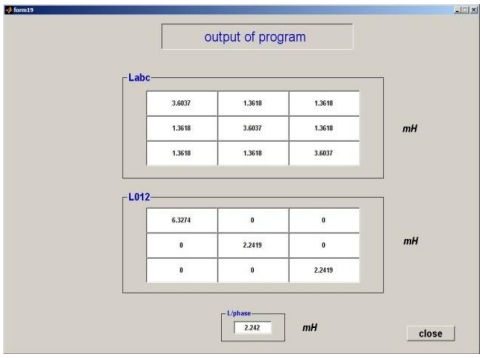

Fig.4 A single circuit inductance results.

GMD = (D_{ab} x D_{bc} x D_{ca})$^{(1/3)}$ where D_{ab} is the distance between phase a and phase b and D_{bc} is the distance between phase b and phase c and D_{ca} is the distance between phase c and phase a and the **GMR** can be taken from the input data display shown in fig.3. The student can now go back and run the program again by choosing the capacitance option calculation. The solution output is displayed on the screen as shown in fig.4

The student can now check and compare this computer solution output with what he learned in class where:
C= 0.0556 / ln (GMD/r) µ F/km

GMD is the same value used in the inductance calculation.
Let us continue with the same example and let us compute the line impedance Z
The student can now go back to the same input data screen and click the impedance option .using the mouse. The computer output results are displayed on the screen as shown in fig.5

The student can now check this value with what he also learned in class Z= R+j(ωL) where ω = 2Л f L

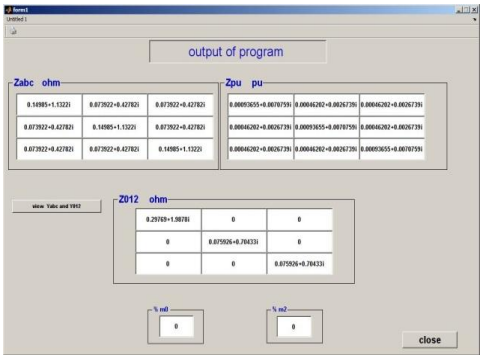

Fig.5 A single circuit impedance results.

Application#3

Let us replace the single conductor used in the previous application by 2 sub-conductors per phased (ACSR 636,000 CMIL ROOK) conductors which have the total cross sectional area of aluminum as one Bittern conductors. Assume the line spacing is the same as in the previous. Therefore the bundle conductor option will be activated.
These home work objectives are:

- To teach students the benefits of using bundle conductors in overhead transmission line. The program can be

used in this case to compute both line inductance as well as line capacitance.

- The second objective of the program is to check the influence of line length on the line equivalent circuit. We teach students in class that if the transmission line length is up to 50mi Then the effect of capacitance is neglected and only the series impedance will be considered [2,3]
- If the line length is greater than 50mi and up to 150mi then the medium model representation is used and in case of long line which is greater than 150mi then the long line representation is used.

This exercise will be used to accomplish the above objectives. The student should go to the same input data screen as described earlier and select from the conductor type the one with the conductor name ROCK. He should then click the mouse and insert 2 as the number of sub-conductors per phase and insert the space between the bundle conductors and repeat the same calculation for L, C and Z. The relevant circuit model will then be displayed on the screen

The student can now run the program by changing the line length to 80mi and 200mi respectively. Figures.13 and 14 show the impact of choosing the medium line length on the impedance calculation module where the medium line representation T and Π models will be displayed accordingly..

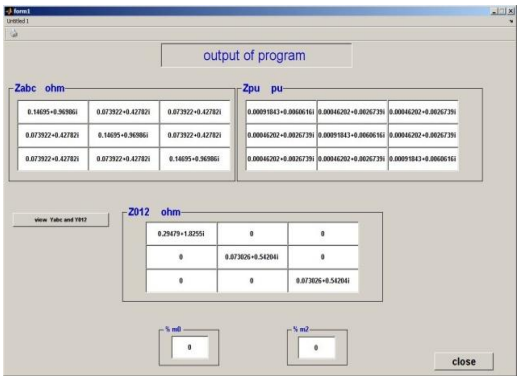

Fig.6 impedance results with bundle conductors.

Figures.7 show the effect of choosing long line length on impedance calculation module, and the long line representation Π model will be displayed.

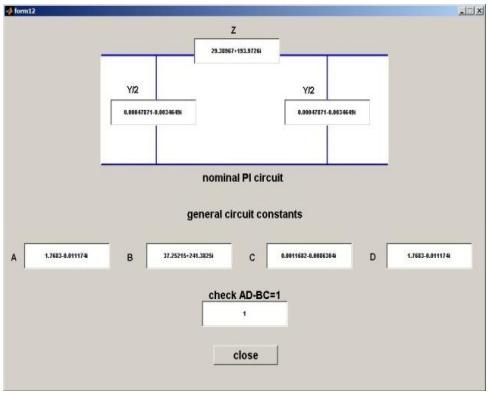

Fig.7 long line Π model.

Application#4

This program application will be devoted to the mechanical design Part of the transmission line where the theoretical part of this material is normally given in the second course for students specialized in electrical power engineering power .in the University. Part of the course material

deals with the analysis of sag and tension subject of the transmission line conductor This part is also very important in overhead transmission theory. The material of this subject is essential and is given only for power engineering students major in order to complete all the required information for transmission line theory.. The continuity and quality of electric service system depend largely on whether the three phase conductors have been properly installed. Thus, a design engineer must determine in advance the amount of sag and tension of the conductor at the support due to line load and at a given temperature, maximum wind, and possible ice loading. The student should be given in class all the mathematical background. The equation related to tension at the line support and its relation with temperature variation
Normally the students should be aware of the following two basic equations [4] :

Tension equation:

$$EA\alpha(t_2 - t_1) + \left\{W_1^2 L^2 \frac{EA}{24T_1^2}\right\} - T_1 = \left\{W_2^2 L^2 \frac{EA}{24T_2^2}\right\} - T_2 \quad (1)$$

Where:

E = modulus of elasticity
A=conductor cross-sectional area
α=coefficient of linear expansion
t_1= initial temperature
t_2=final temperature
W_1= initial conductor weight
W_2=final conductor weight
T_1=initial conductor tension
T_2=final conductor tension
L = Span length

Sag Equation:

$$d = \frac{W_1 L^2}{8T_2} \quad (2)$$

The above two equations were programmed using MATLAB. Fig.13 shows the basic mechanical design interface screen.

Application#5

This application is meant to enhance the course material relating to sag and tension calculation. If for example the student selects the ROOK conductor as presented in the previous example then the entire conductor's data needed for sag and tension calculation will be filled in its exact position from the conductor's data base library. Fig.14 shows both the required input data as well as the program output display where the relation between both sag and tension against temperature variation are displayed. A second option for the output results can be displayed in table form giving the values of tension and sag versus temperature upon the user request.

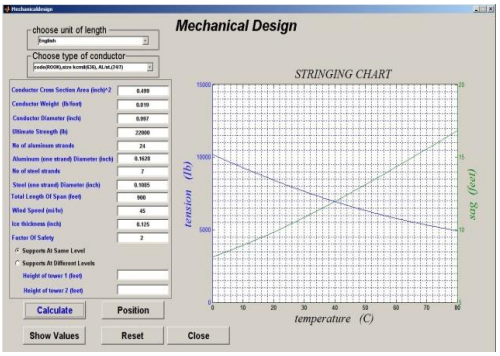

Fig.8 Mechanical design model.

Application#6

The thermal rating of an overhead transmission line is also another important term used in the power transmission and distribution field industry which indicates the maximum current that the line or cable can transfer without overheating. The thermal rating is a function of the weather conditions seen along the line, including wind speed, wind direction, air temperature, and sun radiation.

The undergraduate students are seldom exposed to such types of topic in class during their undergraduate studies except for a few students who had or will have a chance to do their BSC project in power system studies during the final semester. Therefore preparing the undergraduate students to such types of technical terms and real life practice will broaden and open their minds to further and more practical and technical terms in this field.

Heat balance equation

The conductor thermal current rating in wind, neglecting any voltage regulation consideration can be expressed by the following heat balance equation as given in [5]:

Heat generated [I^2R conductor power loss] =

Heat lost by convection (watts/km) + heat lost by radiation (Watts/km) – heat gained by solar radiation (Watts/km)

$$I^2R_{20}\{1+\alpha(t+\theta)\} = 387(V.d)^{0.448}.\theta + \pi.E_c.S.d.\{(t+\theta+273)^4-(t+273)^4\}-\alpha_s.S.d \text{ (Watts/km)} \quad (3)$$

Where I = conductor current rating in ampere

R_{20} = conductor resistance at 20°C

α = temperature coefficient of resistance per °C

t= ambient temperature °C

θ = temperature rise (t_1 initial temperature and t_2 final temperature

αs = solar absorption coefficient (vary from 0.6-0.9) an average value is 0.8

S= intensity of solar radiation watts/km

d= conductor diameter

V= wind velocity normal to conductor in m/s

E_c= emissivity of conductor , typical value = 0.3 for bright conductor and 0.9 for black aluminum ACSR

The average value is 0.6

S= Stefan Boltzmann's Constant = 5.7×10^{-8} watts/m^2

For preliminary design purpose 0.5-0.6 m/s wind speeds are used[ ] . Higher wind speeds would lead to higher rating

A practical example will be presented using the developed program for the above equation to show students the application and the results of such type of topic through application 7

Application#7

Compute the thermal current rating for the overhead line under the following operating conditions, the line voltage is 132kV and the line power is 40 MVA

Assume the following operating condition:

Maximum operating temperature =75°C

Maximum ambient air temperature = 40°C

Conductor maximum resistance= 0.1441 ohm/km

Conductor diameter =1.953cm

Emissivity = 0.6

Solar absorption coefficient = 0.8

Solar radiation intensity = 1000W/m2

Wind velocity = 0.418 m/s

Let us input the required data for the heat balance equation module and select the thermal limit module The program output results will be displayed as shown in fig.9

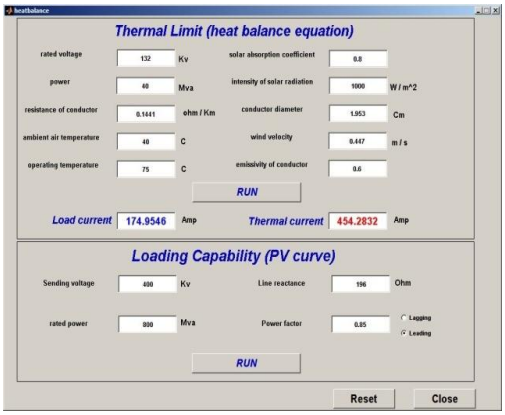

Fig.9 Solution of heat balance equation and PV curve.

Application#8

The power versus voltage curve or as is normally abbreviated as PV curve is the most widely used curve in voltage stability analysis today. The PV curve is formed by varying system load or power transfer and plotting it against voltage for a given power factor. The PV curve can provide real power and voltage margins using the knee of the curve as reference point. PV Curves at constant power factor are used to get maximum power transfer at critical voltage. The application of PV curve in voltage stability studies is enormous [6].

The objectives of this section to expose the both the undergraduate students as well as the graduate students to the importance of supplying reactive power at the consumer‘s location rather than attempting to supply reactive power from a great distance. Therefore a radial line where at the near end there is a voltage support but at the far end of the line there is a complex power load without a generator or capacitor bank to maintain the voltage at the far end. Thus the student will see how the voltage at the far end of the line varies with the load and with the power factor too.

The program can also be used to draw the PV curve for different power factors. In this display three power factors are shown (0.85 leading, 0.85 lagging, and unity power factor) and the results are shown in fig.10

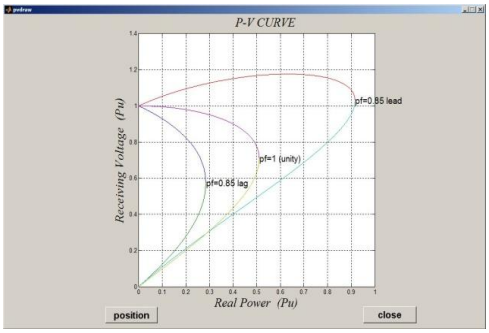

Fig.10 PV curve results.

Line Sequence Impedances and sequence capacitances calculation

This section will introduce the students to application of the developed program to the course material which is normally given to graduate students The background material of the course contents can be found in the text book ”Analysis of faulted power system” by Paul M. Anderson.[7] The developed program computes the transmission line impedance matrix and capacitance matrix for three phase transmission line single circuit and double circuit tower configuration with and without ground wire and taking into account the following option:

- Line not transposed
- Partially transposed line
- Completely transposed line
- Twisted line
- The sequence impedance and the sequence capacitances can be obtained for every option of the above mentioned cases.

- The electrostatic and the electromagnetic balance factors are also computed for each transposition cycle option

With this program the student will be able to understand the covered material given in class. At the same time the students will be able to understand and to practice different transposition cycles easily. They will understand and grasp the material given in class much faster. The impact of transposition on the impedance and capacitance matrix elements will be computed and assessed. The impact of transposition on the sequence matrix elements will be seen and evaluated. We do feel very strongly that explaining such transposition cycle options for the transmission line cannot be handled and understood easily by solving examples on the blackboard. Therefore having a computer program which has such features will help explaining this subject and reinforce the classroom lectures. The following applications will demonstrate this idea.

Application#9

In this assignment the students will be asked to compute the line impedance matrix and the line capacitance matrix for two types of tower configuration; a single circuit tower and double circuit tower configurations, with and without ground wires. The following cases have to be exercised:

1. A single tower configuration calculation
   - Computing the line impedance matrix without ground wire
   - The line impedance matrix With ground wire
   - Assuming the line partially transposed
   - The line completely transposed
   - The line sequence impedance with line not transposed
   - The line sequence impedance with the line partially transposed
   - The line sequence impedance with the line completely transposed
2. Repeating all of the above for double circuit tower configuration

Assignment 9.1

Compute the phase self and mutual impedances of the 69kv line shown in fig.11 Assume f=60c/s and the wires are 19 strands 4/O, hard drawn copper conductor. Ignore the ground wire assume the line length is 40 mile long.

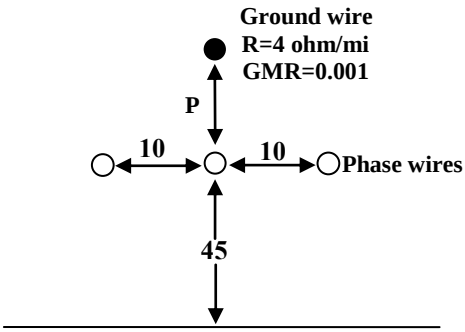

Fig.11 line configuration of a 69 Kv circuit.

Select the conductor name from the data base library and follow the previous procedure and insert the conductor coordinates as indicated in the appropriate locations. Run the program by selecting the single conductor option with no ground wire.

Fig.12 shows the Z_{abc} matrix with both actual values and with per unit. The line sequence impedance matrix is also displayed.

The impedance matrix elements for the single circuit three phase transmission line

without ground wire can be expressed as [1]

$$[Z_{abc}] = \begin{bmatrix} z_{aa} & z_{ab} & z_{ac} \\ z_{ba} & z_{bb} & z_{bc} \\ z_{ca} & z_{cb} & z_{cc} \end{bmatrix} \quad (4)$$

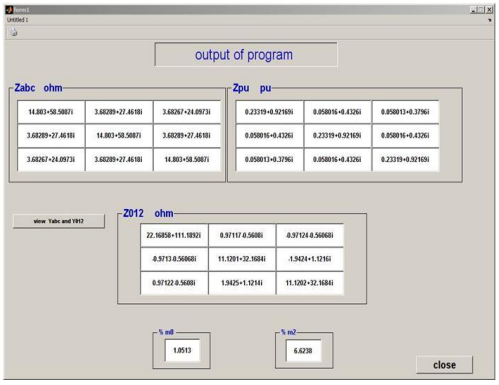

Fig.12 impedance results without transposition.

Where:

$Zii = (ri + rd) + j\omega ln\ De/Dsi$ Ω / unit length

$Zij = rd + j\omega ln\ De/Dij$ Ω / unit length

Where :

ri = the line resistance per phase Ω / unit length

rd (the earth resistivity) = $9.869 \times 10^{-4} f$ Ω/km

Dsi = Conductor self geometric mean radius GMR

De = 2160 √ ρ/f ft. Where ρ is the earth resistivity.

If no actual value exist for ρ it can be assumed 100

Dij = The distance between conductor i and j

For those who are interested in this subject and to get further details should consult reference [1].

The line sequence impedance matrix can be expressed as :

$$[Z_{012}] = [A]^{-1}[Z_{abc}][A] = \begin{bmatrix} z_{00} & z_{01} & z_{02} \\ z_{10} & z_{11} & z_{12} \\ z_{20} & z_{21} & z_{22} \end{bmatrix} \quad (5)$$

Where A is the symmetrical components matrix and can be expressed as :

$$[A] = \begin{bmatrix} 1 & 1 & 1 \\ 1 & a^2 & a \\ 1 & a & a^2 \end{bmatrix} \quad (6)$$

$$[A]^{-1} = \begin{bmatrix} 1 & 1 & 1 \\ 1 & a & a^2 \\ 1 & a^2 & a \end{bmatrix} \quad (7)$$

Assignment 9.2

Compute the Z_{abc} matrix with the line partially transposed where; S_1=8 miles, S_2=12 miles, S_3=20 miles. Fig.24 shows the output results for the full Z_{abc} matrix and the sequence impedance matrix Z_{012}

When the line is partially transposed the mutual elements of the Z_{abc} matrix get closer to each other and the difference between the mutual elements of the matrix get smaller. The same remarks are also valid for the sequence impedance matrix

Assignment 9.3

Compute the impedance Z_{abc} matrix and the sequence impedance matrix for the same

line assuming complete transposition cycle where S_1=13.333 mile , S_2 = 13.333 miles and S_3=13.333 mile

Fig.13 displays the full impedance Z_{abc} matrix and the full sequence impedance matrix Z_{012} for this case.

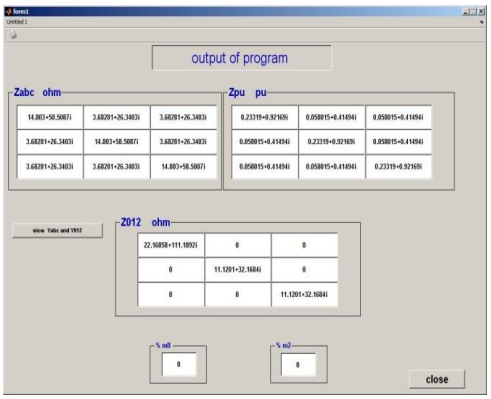

Fig.13 The sequence impedance results with completely transposed line

The student can now compare and see the differences between the impedance and the sequence impedance matrices elements. These differences can be explained as follows:

When the line is not transposed, there exists a coupling between the sequence impedances matrices elements. The coupling between the sequence impedances elements vanishes once the line is completely transposed. This phenomena is strongly needed for system studies.

Assignment 9.4

Repeat the previous application, taking into account the presence of the ground wire.

Fig.14 shows the output results for the Z_{abc} matrix and the sequence impedance matrix Z_{012}.With the presence of the ground wire.

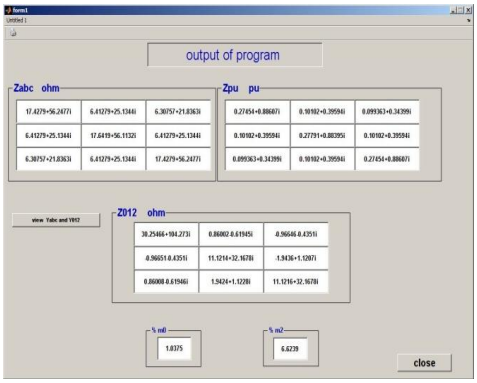

Fig.14 impedance results without transposition and with ground wire.

.

By comparing both applications we will observe the following

- The positive and negative impedances Z_{11} and Z_{22} are unchanged by the addition of the ground wire.
- The zero sequence impedance is changed. The real part R_{00} is increased by about 40% and the imaginary part X_{00} has decreased by about 7%.
- The off-diagonal terms are changed but not by a significant amount.

Similar applications can be also tried for double circuit tower configuration as shown below:

Application#10

Compute the impedance Z_{abc} matrix and the sequence impedance matrix for the double circuit 345Kv un-transposed line shown in figure 15 below

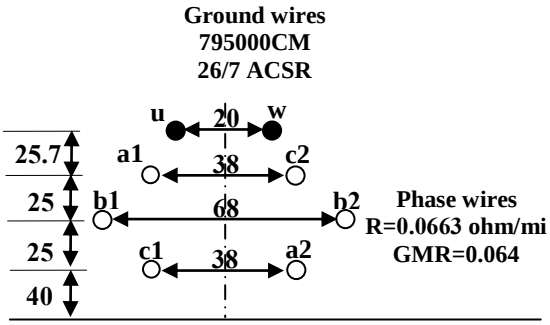

Fig.15 line configuration of a 345 Kv circuit.

Fig.16 shows the input data for the double circuit electrical design module and Fig.17 shows the output results for the Z_{abc} matrix and the sequence impedance matrix Z_{012}.

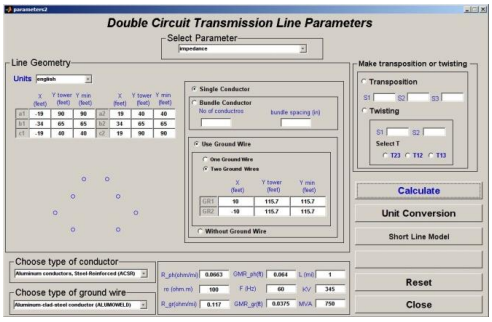

Fig.16 A double circuit impedance calculation.

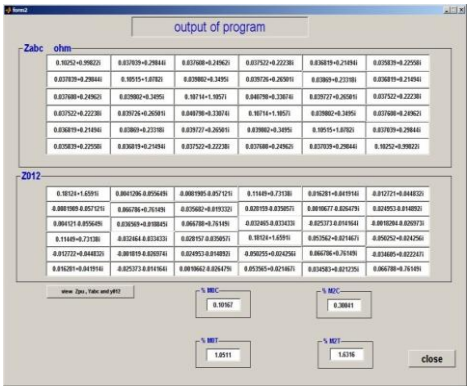

Fig.17 A double circuit impedance results.

Application#11

This example will present the program application to the computation of the self and mutual capacitance matrix for a double circuit tower configuration. For the case of a double circuit line with or without ground wires, the problems become complicated because of the presence of so many charges.

Using the method of charge images simulation
[1] we can write the voltage equation in terms of potential coefficients matrix as:

$$[V] = [P][q] \quad (8)$$

Where:

V = the voltage vector.

q = the charge vector.

P = the potential coefficient matrix.

The elements of the potential matrix are defined as follows:

$$P_{ii} = \frac{1}{2\pi\varepsilon} \ln\left(\frac{H_i}{r_i}\right) \quad (9)$$

$$P_{ij} = \frac{1}{2\pi\varepsilon} \ln\left(\frac{H_{ij}}{D_{ij}}\right) \quad (10)$$

Where:

P_{ii} and P_{ij} = the self and mutual potential coefficients

H_i= distance from Conductor i to its image i'

H_{ij}= distance from Conductor i to the image of Conductor j

D_{ij}= distance from Conductor i to Conductor j

r_i= radius of Conductor i.

ε = the permittivity of the medium.

Equation.8 can be written for double circuit transmission line as:

$$\begin{bmatrix} V_{a1} \\ V_{b1} \\ V_{c1} \\ V_{a2} \\ V_{b2} \\ V_{c2} \end{bmatrix} = \begin{bmatrix} P_{a1a1} & P_{a1b1} & P_{a1c1} & P_{a1a2} & P_{a1b2} & P_{a1c2} \\ P_{b1a1} & P_{b1b1} & P_{b1c1} & P_{b1a2} & P_{b1b2} & P_{b1c2} \\ P_{c1a1} & P_{c1b1} & P_{c1c1} & P_{c1a2} & P_{c1b2} & P_{c1c2} \\ P_{a2a1} & P_{a2b1} & P_{a2c1} & P_{a2a2} & P_{a2b2} & P_{a2c2} \\ P_{b2a1} & P_{b2b1} & P_{b2c1} & P_{b2a2} & P_{b2b2} & P_{b2c2} \\ P_{c2a1} & P_{c2b1} & P_{c2c1} & P_{c2a2} & P_{c2b2} & P_{c2c2} \end{bmatrix} \begin{bmatrix} q_{a1} \\ q_{b1} \\ q_{c1} \\ q_{a2} \\ q_{b2} \\ q_{c2} \end{bmatrix} \quad (11)$$

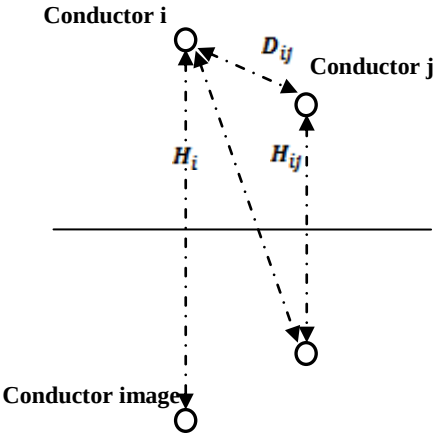

Fig.18 Transmission Line Geometry

The transmission line capacitance matrix C can then be determined by taking the matrix inversion of the P matrix as:

$$C = P^{-1} \quad (12)$$

$$[C] = \begin{bmatrix} C_{a1a1} & C_{a1b1} & C_{a1c1} & C_{a1a2} & C_{a1b2} & C_{a1c2} \\ C_{b1a1} & C_{b1b1} & C_{b1c1} & C_{b1a2} & C_{b1b2} & C_{b1c2} \\ C_{c1a1} & C_{c1b1} & C_{c1c1} & C_{c1a2} & C_{c1b2} & C_{c1c2} \\ C_{a2a1} & C_{a2b1} & C_{a2c1} & C_{a2a2} & C_{a2b2} & C_{a2c2} \\ C_{b2a1} & C_{b2b1} & C_{b2c1} & C_{b2a2} & C_{b2b2} & C_{b2c2} \\ C_{c2a1} & C_{c2b1} & C_{c2c1} & C_{c2a2} & C_{c2b_2} & C_{c2c2} \end{bmatrix}$$

The sequence capacitance matrix can be obtained with a similar approach to the sequence impedance approach discussed earlier as:

$C_{012} = A_2^{-1} C A_2$ (13)

Where:

A_2 =

A	0
0	A

(14)

The sub-matrix **A** is the 3 x 3 symmetrical components matrix and the sub-matrix **0** is a 3 x3 zero matrix.

A_2^{-1} =

A^{-1}	0
0	A^{-1}

(15)

The sub-matrix A^{-1} is the inverse of the A matrix

For those who are interested in more detailed analysis of this section should consult reference [1]

Environmental Effects

The importance of minimizing the environmental effects of overhead transmission lines has increased substantially due to increasing use of extra and ultra high voltage levels. The overhead transmission lines introduce electric and magnetic fields, which have to be taken into consideration during the line design stage. The study of the field effect (induced voltages and currents in the conducting bodies) is becoming crucial as the operating voltage level of transmission line have increasing due to the economic and operation benefits involved [8].

The environmental effects model allow the user to

compute the electric and magnetic field under the transmission line at ground surface or at any point in the space under the line, also the model allow the user to change many line parameters that effect the magnitude of the electric and magnetic field levels.

The electric fields related to the charges on the conductors and the magnetic fields related o the currents in the line. Both fields induce voltage in objects that are in the vicinity of the line corridors.

Electrostatic induction

The electric field produce by extra and high voltage lines induces currents in objects and nearby fences which are in the area of the transmission lines corridors. The effects of electric fields from transmission lines becomes of increasing issue as the line voltage gets higher. Electric field, related to the three phase transmission lines voltage are the primary cause of induction to vehicle, building, and other objects. Human being is also affected with exposure to electric discharges from charged objects in the field of lines. The resultant electric field in the nearby of a transmission line can be obtained using the module with this developed program. The students can use the program and compute and assess the magnitude of the electric field to different conductor arrangement, different voltage levels and also for different tower configuration. A demonstrated example will show such type of application as presented in homework assignment 9.

.

Application#12

Considers a three-phase, single-circuit transmission system with the following parameters:

- Operating voltage level is 525 kV line-to-line rms voltages.
- Each phase consists of three sub-conductors 3.3 cm diameter each and spaced by 45 cm.
- Nearest phase conductor to the ground is 10.6 m high from the ground level.
- Separation between each two adjacent phases is 10 m.

Three tower configurations will be studied; namely **Flat** (Horizontal), **Vertical**, and **Equilateral Delta** configurations as shown

in Figure19 below. Selecting the Environmental effect module from the program Menu and clicking on the appropriate tower configuration for the circuit under study. The relevant circuit and tower input data for this type of calculation should be inserted as indicated Figure 20 presents the final generated results for the electric field variations at ground level. The final results for the three selected tower configurations are found to be exactly similar to the results published in reference [8]. The maximum electric field strength does occur at a distance just outside the outer conductors of the three phase circuit. The strength of the electric field decreases as we move further from the tower center

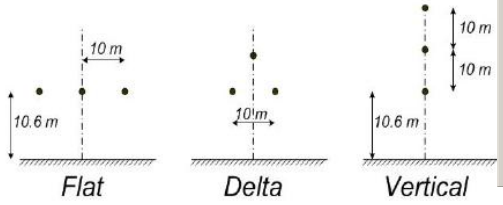

Fig.19 Single three-phase circuit configurations.

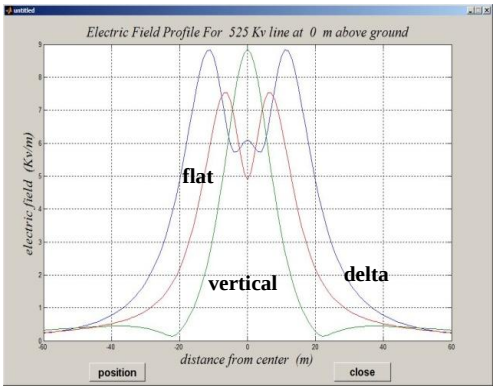

Fig 20 Electric field profile at the ground level for the three-phase single-circuit configurations.

Magnetic field induction

The magnetic field strengths are related to the three phase current passing through the conductors which induce voltage in objects that have a considerable length parallel to the line, such as fences, pipeline, and telephone lines. The students will now be able to use this program to compute and to check the magnetic field strength due to the three phase transmission lines as will be shown in the next application

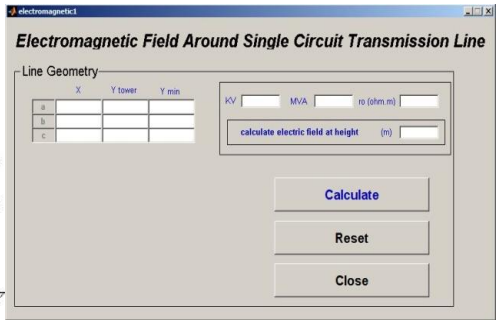

Fig.21 magnetic field around single circuit transmission line model.

Application#13

For the three circuit configuration given in the previous application, calculate the magnetic field at ground level. Assume the line is delivering 2400 MVA.

Fig.22 shows the program results for the magnetic field profile for the three selected circuit tower configuration. It is clear that the maximum magnetic field do occur at the center of tower and decay fast as we go outside the line corridor and further from tower center.

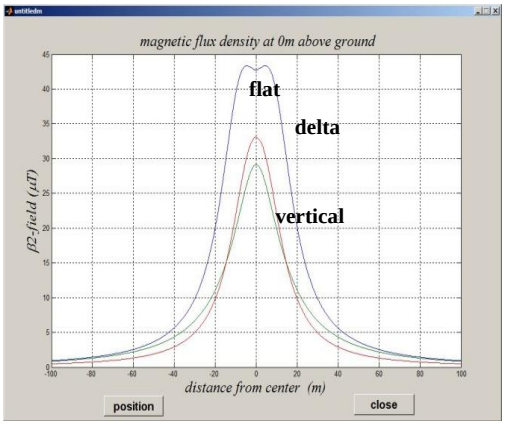

Fig.22 magnetic field density at ground level

Conclusion

The developed program in this paper presents many valuable features which can support the instructors in class in order to explain and teach the course material related to the three phase transmission line theory and design very effectively. A number of selected topics from the course material which are normally given in class are programmed and presented to enhance and modify the existing classical lecturing approach in class to more active one and using this program the classroom then becomes similar to a laboratory. This developed program will help the instructors to present the class material easily and it well help the students also to easily understand the class lectures effectively.

Both undergraduate students and graduate students will be able to learn and to compute the following: Transmission line parameters; line inductance and line capacitance, line impedance, the effect of line transposition, line twisting on the computed line parameters. Electrostatic and electromagnetic unbalance factors, PV curve, line thermal limit, electric field and magnetic field calculation and other line features can now be computed and assessed . The student's interaction with the instructors during the class lectures and simulation will make the classroom more live.

Using this program the instructor will be able to present many examples in class provided a computer is available which will be difficult or impossible to be presented in class without having such facilities due to lecture time constrain. The instructor will then be able to assign and defer the longer homework problems for students to be done at home or through mini projects during the course

References

1. Jomaa B. and others ;"Interactive Computer Programs For Electrical Power Engineering Students Part IV: Interactive Calculation of Transmission Line Seq. Impedance and Seq. Capacitance" Proceedings of the Second Libyan Arab International Conference on Electrical and Electronic Engineering March 1989
2. Glover and Sarma ; Power system analysis and design. Second Edition McGraw Hill
3. Grainger J , Stevenson W: Power System Analysis; McGraw Hill international 1994
4. Saadat Hadi, Power System Analysis.
   McGraw Hill international 1999
5. Bayless , Transmission and Distribution Electrical Engineering Reference book
6. Burgen Arthur, Power system Analysis,

Prentice Halt Series in Electrical and Computer Engineering
7. Anderson Paul , Analysis of Faulted Power System; , Iowa State University press , Ames Iowa 1970
8. Electric Power Research Institute; Transmission Line Reference book 345Kv and above / Second Edition

A Review of High Impedance Fault Detection on Power System Network

A. Abohagar M.W. Mustafa

Faculty of Electrical Engineering, Universiti Teknologi Malaysia, 81310 Skudai, Johor, Malaysia

Abohagar74@yahoo.com, wazir@fke.utm.my

Abstract:

High impedance faults (HIFs) are, in general, difficult to detect through conventional protection such as distance or overcurrent relays. This is principally due to relay insensitivity to the very low level fault currents and/or limitations on other relay settings imposed by HIFs. This type of fault usually occurs when a conductor touches the branches of a tree having high impedance or when a broken conductor touches the ground. In the case of an over current relay, the low levels of

current associated with HIF are below the sensitivity settings of the relay. Although HIFs, is uncommon, must nonetheless be accurately detected and removed. This is more so in view of the fact that apart from threatening the reliability of the electric power supply. Arcing is usually associated with these faults which poses a risk of fires and endanger life through the possibility of electric shock. This paper reviews some of the methods for detecting high impedance faults of various areas on power systems

1. INTRODUCTION

Rapid growth of electric power systems over the past few decades has resulted in a large increase of the number of lines in operation and their total length. These lines are exposed to faults as a result of lightning, short circuits, faulty equipments, mis-operation, human errors, overload, and aging. Many electrical faults manifest in mechanical damages, which must be repaired before returning the line to service. The restoration can be expedited if the fault location is either known or can be estimated with a reasonable accuracy. Faults cause short to long term power outages for customers and may lead to significant losses especially for the manufacturing industry. Fast detecting, isolating, locating and repairing of these faults are critical in maintaining a reliable power system operation.

High impedance fault detection is a long standing problem. The fault natures have been studied since the early 1970's [1] with

the hope of finding some characteristics in the waveforms for practical detections. The high impedance faults result when an unwanted electrical contact is made with a road surface, sidewalk, sod, tree limb, some other surface or object which restrict the flow of fault currents to a level below that reliably detectable by conventional protection devices. Such faults can be earthed or phase faults. HIFs on electrical transmission and distribution networks involve arcing and/or nonlinear characteristics of fault impedance, which cause cyclical pattern and distortion.

2. HIFs Characteristics and Detection Challenge

High impedance faults have two main characteristics [1]: the low fault currents and arcing. The first characteristic is happened because these faults produce little or no fault current. The second characteristic of high impedance faults is the presence of arcing phenomena as a result of air gaps due to the poor contact made with the earth or with an earthed object. These air gaps create a high potential over a short distance and arcing is produced when the air gap breaks down. However, the sustainable current level in the arc is not sufficient to be reliably detected. Part of this is due to the constantly changing conditions of the surface supporting the arc and maintaining high impedance. Therefore, a random electrical behavior is an associated feature with the high impedance faults. As the arcing often accompanies these faults, it further poses fire hazard and therefore the detection of such faults is critically important.

Detection of high impedance faults with high reliability is a great challenge for protection engineers. The protection reliability is measured by dependability and security. A high level of dependability occurs when the faults are correctly recognized. On the other hand, a high level of security occurs when the faults are not falsely indicated. A high dependability forces a lower security level and vice versa. The dilemma is to find a sensitive high impedance detector with conserving on the protection security.

High impedance faults produce current levels ranging from 0 to 50A. Typically, HIF exhibits arcing and flashing at the point of contact. When the fault current is less than 50 **A,** it is unlikely that conventional protection will operate. Table I provides typical fault currents for downed conductors on different types of surfaces [2] where the system voltage is 12.5kV.

Surface	Typical fault current (A)
Dry asphalt or sand	0
Wet sand	15
Dry sod	20
Dry grass	25
Wet sod	40
Wet grass	50
Reinforced concrete	75

Table I. Typical Fault Currents on Various Surfaces.

3. Detection Techniques

In a power system, most faults are detected by increasing the current flow

towards the fault point. This method has been successfully used to detect and protect against these low impedance faults. For HIF on transmission and distribution systems, the high impedance fault does not result in a substantial increase in current and hence they cannot always be detected [1].

Most of the work on high impedance faults has focused on the development of a sensitive detector to detect and clear such faults. Some of the techniques used standard relaying inputs and others required special equipment [2].

3.1 Signal processing Based Methods:

The availability of powerful microprocessors and signal processing algorithms has led to a wide range of new techniques to identify waveforms associated with high impedance faults. The fault feature extraction is carried out using different filters such as FFT, and Kalman Filter, [3, 4]. Although, the network waveforms are not stationary due to disturbances. Therefore, FFT is not suitable for well-timed tracking and it is important to use an appropriate signal processing technique such as wavelet transform. Recently, wavelet analysis has been [3] used in several applications in the power systems. For example fault detection and classification considering high impedance types have been enhanced when the wavelet analysis is considered. Marek Michalik et-al [5] introduced an effective algorithm of arcing fault detection in distribution networks with the application of a wavelet transform technique. The protection algorithm developed observes the phase displacement between wavelet coefficients calculated for zero sequence voltage and current signals at a chosen high-level frequency. The final decision in regards to feeder switching off (or alarm issuing) is met either with a deterministic logic scheme or with the use of a neural net trained especially for that purpose. T.M. Lai et-al [6] presented a practical pattern recognition based algorithm for electric distribution high impedance fault detection. The scheme recognizes the distortion of the voltage and current waveforms caused by the arcs usually associated with HIF. The analysis using discrete wavelet transform yields three phase voltage and current in the low frequency range which fed to a classifier for pattern recognition. The classifier is based on the algorithm using nearest neighbor rule approach. C.H. Kim et-al [7] described a novel fault-detection technique of high-impedance faults in high-voltage transmission lines using the wavelet transform, **t**he techniques is based on using the absolute sum value of coefficients in multi-resolution signal decomposition (MSD) based on the discrete wavelet transform (DWT). A fault indicator and fault criteria are then used to detect the HIF in the transmission line. In order to discriminate between HIF and no-fault transient phenomena, such as capacitor and line switching and arc furnace loads, the concept of duration time (i.e., the transient time period), is used. Finally, disadvantages of using conventional Fourier transform-based techniques (those which rely totally on spectrum analysis of Fourier transform) do not possess the inherent time information associated with fault initiation. Also disadvantages of using wavelet transform is more complex than other signal processing techniques, and the scale coefficients and wavelet coefficients that obtained from the wavelet transform have no readily discernable physical properties,

and this makes it difficult to interpret the result.

3.2 Artificial Intelligence and Statistical Analysis Based Methods:

There are several artificial intelligent (AI) methods such as Artificial Neural network (ANN), Fuzzy Logic (FL), Expert System (ES) and Genetic Algorithm (GA), etc. By using these methods, the time factor is substantially reduced and human mistakes are avoided. Therefore, many researchers used AI based methods in power systems fault detections. Ref [3,8,9] have applied neural network techniques as classifier with fast Fourier transform as feature extractor for the high impedance fault detection, Fourier analysis yields low order harmonic vectors of the three phase residual current, voltage admittance and power which are then fed to a neural network. However the classification rules of neural network are unreadable, so that the network cannot be adjusted using engineering experience. Ref [10 to 12] developed further a practical artificial neural network based relay algorithm for electrical distribution high impedance fault detection. S.M.A Salem et-al [13] presents the application of Fuzzy ARTMAP to investigate a long outstanding problem of arc type fault detection in electric systems. Here, a collection of dominant key harmonic signals forms the basis for a ‘feature’ or ‘diagnostic’ vector instead of a single dominant harmonic signal, but this method also requires a long measurement data for HIFs identification.

3.3 Hybrid based method

Almost all of the above methods detect faults based on one algorithm. Some have investigated the use of hybrid methods that locate faults based on more than one algorithm to achieve a more accurate estimation of the faulted section.

M.R. Haghifam et-al [14] a novel method for high-impedance fault (HIF) detection in distribution systems is presented, Wavelet transform and principal component analysis are used for feature extraction. A fuzzy inference system is implemented for fault classification and a genetic algorithm is applied for input membership functions adjustment.

M.T. Yang et-al [15] this work presents a novel protection scheme by combining wavelet transform with neural networks, for detecting and identifying normal switching operations and HIFs, Discrete wavelet transformations are initially applied to extract distinctive features of the voltage and current signals, and are transformed into a series of detail and approximation wavelet components. The coefficients of variation of the wavelet components are then calculated. This information is sent to the training neural networks to identify an HIF from the operations of the switches.

T.M. Lai et-al [16] this paper is used the Discrete Wavelet Transform as well as frequency range and RMS conversion to apply pattern recognition based detection algorithm for electric distribution high impedance fault detection. The aim is to recognize the converted RMS voltage and current values caused by arcs usually associated with HIF.

A.R. Sedighi et-al [17] a new HIF detection method that uses wavelet transform and statistical techniques is presented, Wavelet transform is used for the

decomposition of signals and feature extraction, feature selection is done by principal component analysis and the classifier is used for classification.

M. Sarlak et-al [18] a new pattern recognition based algorithm is presented to detect high impedance fault in distribution networks, To extract the best feature set of the generated time frequency features, two methods including Principle Component Analysis (PCA) and Linear Discriminate Analysis (LDA) are used and then Support Vector Machines (SVM) is used as a classifier to distinguish the HIFs considering with and without broken conductor from other similar phenomena such as capacitor banks switching.

H.M. Jabr et-al [19] a novel wavelet-FIRANN based technique is proposed for detecting High Impedance Faults in distribution systems, this technique uses the Discrete Wavelet Transform as a preprocessing stage for feature extraction which prepares the data for the artificial neural network stage. The ANN used in this work is of the Finite impulse response artificial neural network (FIRANN) type. The inputs to the FIRANN are selected to be the details' coefficients of the voltage waveform as measured at the relaying point.

Although the use of hybrid technique can enhance the detection of HIFs and overcome some limitations of other techniques, but it has some disadvantages such as system complexity and cost incensement.

Conclusion

This paper has presented an overview of HIFS detection on transmission and distribution power system and summarized various detection fault strategies.

High impedance faults occur on transmission and distribution power systems when low current faults are not detected by conventional overcurrcnt protection. Such faults may persist indefinitely causing a hazard to personnel and equipment. Extensive research on the nature of these faults and means to detect them has been conducted on utility systems. Many research has been conducted to reduce the chance of a- high impedance fault occurring and to improve the chance of detecting those faults which do occur. While some progress has been made, a complete solution has not been found. Regardless of whether it is technically possible and economically feasible to substantially improve high, impedance fault detection. The use of a high impedance fault detector could introduce operational problems including more frequent and longer service outages. These costs must be weighed against the benefits of improved fault detection.

REFERENCES

1. 1. Report of PSRC Working Group D15 “High Impedance Fault Detection Technology” March 1996.
2. 2. L. Li M.A. Redfem, **“**Review of Techniques to Detect Downed Conductors in Overhead Distribution Systems”. Developments in Power System Protection, Conference Publication No.479 *0* IEE 2001.
3. 3. K.Gayathri and N. Kumarappan, “Comparative Study of Fault Identification

and Classification on EHV Lines Using Discrete Wavelet Transform and Fourier Transform Based ANN" International Journal of Electrical, Computer, and Systems Engineering 2;2 © www.waset.org Spring 2008.

4. S.R. Samantaray, P.K. Dash,S.K. Upadhyay, "Adaptive Kalman filter and neural network based high impedance fault detection in power distribution networks" 0142-0615/$ - see front matter _ 2009 Elsevier Ltd. All rights reserved. doi:10.1016/j.ijepes.2009.01.001.
5. Marek Michalik, Waldemar Rebizant,, Miroslaw Lukowicz, Seung-Jae Lee,and Sang-Hee Kang "High-Impedance Fault Detection in Distribution Networks With Use of Wavelet-Based Algorithm" *IEEE Transaction on Power Delivery, Vol. 21, No. 4, OCTOBER 2006*.
6. 6. T.M. Lai, L.A. Snider, E. Lo "Wavelet transform based relay algorithm for the detection of stochastic high impedance faults" *0378-7796/$ – see front matter © 2006 Elsevier B.V. All rights reserved. doi:10.1016/j.epsr.2005.12.021.*
7. 7. Chul-Hwan Kim, Hyun Kim, Young-Hun Ko, Sung-Hyun Byun, Raj K. Aggarwal and Allan T. Johns "A Novel Fault-Detection Technique of High Impedance Arcing Faults in Transmission Lines Using the Wavelet Transform" *IEEE TRANSACTIONS ON POWER DELIVERY, VOL. 17, NO. 4, OCTOBER 2002*.
8. 8. M. M. Eissa, G.MA. Sowilam and A. M Sharaf, "A New Protection Detection Technique for High Impedance Fault Using Neural Network" *1-4244-0557-2/06/$20.00 ©2006 IEEE.*
9. 9. P.S Bhowmik, P. Purkait and K. Bhattacharya, "A Novel Wavelet Transform Aided Neural Network Based Transmission Line Fault Analysis Method", 014-0615/$-see front matter/2009 Elsevier Ltd.All rights reserved.
10. 10. L.A. Sinder, Y.S. Yuen, " The Artificial Neural Network Based Relay for the Detection of Stochastic High Impedance Faults", *Neurocomputing, Volume 23, 1998, PP243-254*
11. 11. Marek Michalik, Mirosław Łukowicz, Waldemar Rebizant, Seung-Jae Lee and Sang-Hee Kang, "New ANN-Based Algorithms for Detecting HIFs in Multigrounded MV Networks*", IEEE TRANSACTIONS ON POWER DELIVERY, VOL. 23, NO. 1, JANUARY 2008.*
12. Hassan Khorashadi Zadeh, "An ANN-Based High Impedance FaultDetection Scheme: Design and Implementation", *International Journal of Emerging Electric Power Systems* Vol. 4 [2005], No. 2, Article 1.
13. Syed Muhammad Atif Saleema, Adel M. Sharaf, "A FUZZY ARTMAP BASED HIGH IMPEDANCE ARC FAULT DETECTION SCHEME", *978-1-4244-1643-1/08/$25 © 2008 IEEE.*
14. 14. M.-R. Haghifam, A.-R. Sedighi and O.P. Malik, "Development of a fuzzy inference system based on genetic algorithm for high-impedance fault detection", *IEE Proceedings online no. 20045224 doi:10.1049/ip-gtd:20045224.*
15. 15. M.T. Yang∗ and J.C. Gu∗∗ "Using Wavelet Transform and Neural Network Detection High-Impedance Fault", *International Journal of Power and Energy Systems, Vol. 27, No. 3, 2007.*
16. 16. T. M. Lai, L. A. Snider, E. Lo and D. Sutanto, "High-Impedance Fault Detection Using Discrete Wavelet Transform and Frequency Range and RMS Conversion*", IEEE TRANSACTIONS ON POWER DELIVERY, VOL. 20, NO. 1, JANUARY 2005.*
17. 17. Ali-Reza Sedighi, Mahmood-Reza Haghifam, O. P. Malik and Mohammad-Hassan Ghassemian, "High Impedance Fault Detection Based on Wavelet

Transform and Statistical Pattern Recognition*", IEEE TRANSACTIONS ON POWER DELIVERY, VOL. 20, NO. 4, OCTOBER 2005.*

18. 18. M. Sarlak and S. M. Shahrtash, "High Impedance Fault Detection in Distribution Networks Using Support Vector Machines Based on Wavelet Transform", *2008 IEEE Electrical Power & Energy Conference.*
19. 19. H. M. Jabr, *Student member, IEEE*, A. I. Megahed, " A Wavelet-FIRANN Technique for High-Impedance Arcing Faults Detection in Distribution Systems", *Presented at the International Conference on Power Systems Transients (IPST'05) in Montreal, Canada on June 19-23, 2005 Paper No: IPST05 – 035.*

Static Synchronous Series Compensator to Improve Power Oscillation Damping

M. K. Jalboub, H. S. Rajamani, A. M. Ihbal, A. A. Ammar
School of Engineering, and Design and technology
Bradford University, Bradford, BD7 1DP, UK
M.K.JALBOUB@Bradford.ac.uk
H.S.RAJAMANI@Bradford.ac.uk
A.M.I.IHBAL@Bradford.ac.uk
Amer642002@yahoo.com

Abstract-The Static Synchronous Series Compensator (SSSC) is a series device of the Flexible AC Transmission System (FACTS) family using high power electronics to control power flow and improve Power Oscillation Damping (POD) on power grids. POD can influence the power system locally, partially, or thoroughly. This paper investigates the possibility of using SSSC on a power system in case of weakly coupled networks in order to improve POD. To evaluate effects of SSSC, a POD controller is proposed. Several scenarios are examined on this system and results are presented. The system is simulated in Matlab (Simulink). The results shows that by using SSSC devices, POD has considerably improved and power transfer capability has increased for both normal and contingency operations.

Keywords: FACTS, SSSC, POD Controller, Weak power system, Matlab (Simulink)

1-INTRODUCTION

A common dynamic phenomenon for any power system is the power oscillation which can influence the power system operation after a disturbance arises. This phenomenon increases the risk of instability and decreases the power transfer capability particularly in a weak transmission system. The concept of power oscillations damping improvement by means of dynamic series compensation was first introduced in [1]. After that smith [2, 3] proposed that the electromechanical power oscillation can be improved by switching a series capacitor in and out after fault occurrences mechanically. The combination of series and shunt compensation schemes can be used to improve both static and dynamic qualities of an EHV power transmission system as stated in [4]. New types of power transmission equipment have emerged due to advent of the high power semiconductor devices such as, the Static VAR Compensator (SVC) and the Controlled Series Capacitor (CSC) can be materialized to damp electromechenical power oscillation [6, 7]. Recently, the development of Flexible AC Transmission System (FACTS) devices increases power transfer capability as well as damping

performance of the power system [4-11]. STATic synchronous COMpensator (STATCOM) has the ability to improve the system damping as well as voltage profile of the power system [7-10]. Static Synchronous Series Compensator (SSSC) is more capable of handling power flow control, improvement of transient stability and damping of power oscillation [11, 12]. The Unified Power Flow Controller (UPFC) combines the features of both STATCOM and SSSC. Damping improvement is usually achieved by the use of a Power System Stabilizer (PSS) [13, 14]. A traditional PSS is a local power compensation device and cannot damp out all oscillation modes. The most effective alternatives are the FACTS devices. Among these devices is the advanced Static Synchronous Series Controller (SSSC) [11, 12]. The SSSC was first initiated by Gyugyi [15]. The application of SSSC for power oscillation damping, stability enhancement, and frequency stabilization can be found in [16-19]. In this paper the power oscillation damping (POD) controller based on the establishment of the liberalized Phillips–Heffron model [20, 21] of a power system installed with a SSSC controller is proposed in coordination with SSSC for power oscillation damping improvement.

2-The SSSC

The SSSC controller is a Voltage-Source Converter (VSC) based compensator that consists of a solid-state VSC with several Gate-Turn Off (GTO) thyristor switches, or any other semiconductor switches with turn-off capability valves, dc capacitor or storage device, a coupling transformer, and a controller. The SSSC is used to generate or absorb reactive power from the line, and hence can be regarded as a transmission line power flow controller. In reality, if the losses of the SSSC are neglected, it generates a quasi-sinusoidal voltage of variable magnitude in quadrature with transmission line current on its output terminal. Therefore, the injected voltage emulates a capacitive or inductive reactance in series with a transmission line, which increases or decreases the total effective reactance of the transmission line, resulting in a decrease or increase of the power flow in the transmission line. The SSSC can be viewed as analogous to an ideal synchronous voltage source as it produces a set of three-phase voltages at the desired fundamental frequency of variable and controllable amplitude and phase angle. However, the SSSC can be regarded as synchronous generator, because it can generate or absorb reactive power from the power system and can, independently from reactive power, generate or absorb real power if an energy storage device is connected instead of the dc capacitor used in the SSSC. The SSSC is typically used to provide only reactive power exchange with the AC system, neglecting the small amount of real power that is used to cover the circuit and switching losses. The SSSC can be used to exchange real power with the ac system if the dc capacitor is replaced with an energy storage system. Fig.1(a) shows a single line SSSC circuit where a VSC is connected to the utility power system through a series coupling transformer. Fig. 2(b) The SSSC is regarded as a controllable voltage source. Fig.1(c) shows the different operating modes for real and reactive power exchange of the SSSC with the power system.

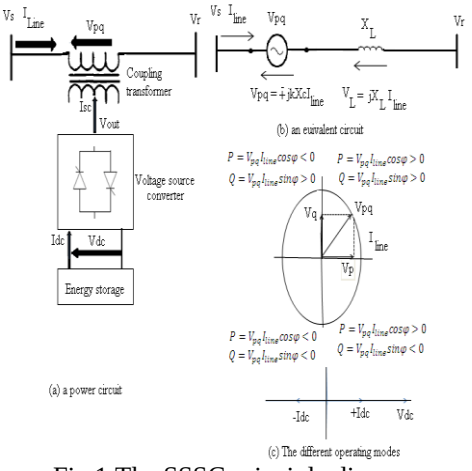

Fig.1 The SSSC principle diagram

3-The SSSC Control Strategy

The four different ways of SSSC operation are given [7]. In this paper, automatic, power flow mode is used for real power control. The injected voltage V_{pq} is perpendicular to the line current I_{line} and the phase angle of I_{line} is ahead of V_{pq}. A series injected voltage of the appropriate magnitude and angle are required to achieve real and reactive power flow control [20]. This injected voltage can be divided into components which are inphase and in-quadrature with the line current. The real power is controlled using the reactive voltage and the reactive power is controlled using the real voltage. By using Fig. 2 which show the simplified two machine power system, the mathematical relationships for of conventional PI controller for power flow control and voltage of bus C control are developed.

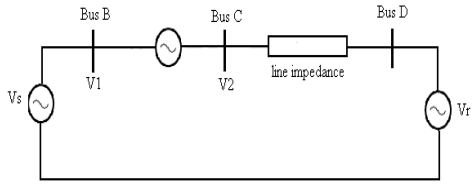

Fig.2 Simplified two machine power system

4-Power flow control algorithm

The real power control can be achieved by control of reactive voltage of series injected voltage V_{pq}. The differential equations for the current at bus C in the d-q frame are given in [20, 21]:

$$\frac{di_D}{dt} = (-R * wb / x)i_D - w_0 i_Q + w_0 / x(v_D^c - v_D^d) \quad (1)$$

$$\frac{di_Q}{dt} = (-R * wb / x)i_Q - w_0 i_D + w_0 / x(v_Q^c - v_Q^d) \quad (2)$$

Here: $v_D^c = v_D^b + e_D^{pq}$ (3)

$$v_Q^c = v_Q^b + e_Q^{pq} \quad (4)$$

Where *wb* is the base frequency and w_0 is system frequency. The subscripts '*D*' and '*Q*' represent the variables in d-q frame. $v_{pq}, [v_D^b, v_Q^b], [v_D^c, v_Q^b]$ and $[v_D^d, v_Q^d]$ are the components of voltage at buses *B*, *C* and *D* resp. For the simplification, it is assumed that the sending end voltage V_S is kept constant at the receiving end or at bus *D* and its approximately equal to that at bus *C* of the system with SSSC, therefore, control of power at bus *C* can be applied. The feedback signal is readily available.

The real power at bus *C* in d-q frame of reference is:

$$P^c = v_Q^c * i_D + v_Q^c * i_Q \qquad (5)$$

The injected real and reactive voltage in d-q frame can be written as:

$$e_R = e_D^{pq} * cos(\varphi^2) - e_Q^{pq} * sin(\varphi^2) \qquad (6)$$

$$e_P = e_D^{pq} * sin(\varphi^2) - e_Q^{pq} * cos(\varphi^2) \qquad (7)$$

Where: $\varphi^2 = tan^{-1}(i_D / i_Q)$ (8)

5-Bus Voltage control algorithm

The voltage at bus *C* of the simplified system shown in Fig. 2 is algebraically related to that voltage at bus *B* and the injected reactive power for power flow control by the following relationships:

$$v^c = \sqrt{\{(v_D^c)^2 + (v_Q^c)^2\}} \qquad (9)$$

$$v^c = \sqrt{\{(v_R^b + e_R^{pq})^2 + (v_P^b + e_P^{pq})^2\}} \qquad (10)$$

$$v_R^b = v_D^b * cos(\varphi^1) - v_Q^b * sin(\varphi^1) \qquad (11)$$

$$v_P^b = v_D^b * sin(\varphi^1) + v_Q^b * cos(\varphi^1) \qquad (12)$$

The real voltage e_P^{pq} to be injected to obtain the desired voltage at bus C can be easily calculated. The SSSC does not exchange any real power with the system. However, some real power is drawn to compensate the SSSC losses. The *DC* side capacitor voltage V_{dc} is described by the dynamic equation as:

$$\frac{dV_{dc}}{dt} = (-g_c * w_b / b_c) * V_{dc} - (w_b / b_c) * i_{dc} \qquad (13)$$

Where g_c and b_c are the conductance and susceptance of the *DC* capacitor resp. The conventional power flow controller block diagram can be developed by using the equations '(1)-(13)'. Fig. 3 Shows the injected series voltage controller.

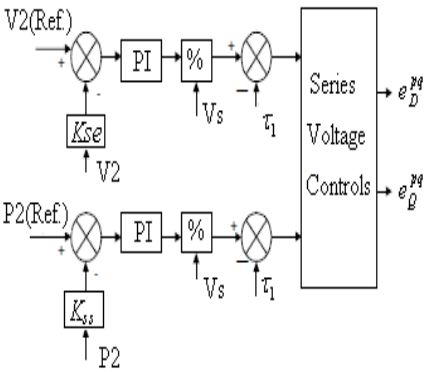

Fig. 3 Injected series voltage controller

The signals τ_1 and τ_2 are applied to transform receiving end bus reference to the bus B reference. The gain K_{se} and K_{ss} optimized by using Nonlinear Control Design (NCD) Matlab block set. By adjusting the gain of the feedback system damping ratio can be improved. The maximum and minimum voltage limits are chosen for the safe operation of the SSSC under the abnormal condition.

6-Power System oscillation (POD) Damping Controller

To improve the damping of power system oscillations, a damping controller is provided [22, 23]. The POD controller can be considered as comprising of two cascade connected blocks. The speed deviation signal is derived from the difference of measured power at FACTS device location and the set of mechanical input power and the error signal is integrated and multiplied by 1/M. The second block comprises a lead-lag compensator. The transfer function block diagram of POD controller is shown in Fig.4.

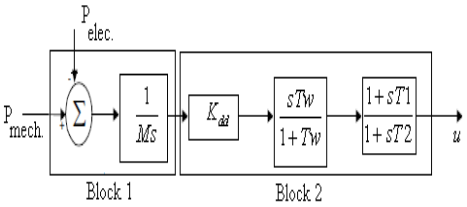

Fig.4 Transfer function block diagram of POD

The parameters of POD controller is optimized by NCD, so as to achieve the desired damping ratio of the electromechanical mode and compensate for the phase shift between the control signal and the resulting electric power deviation. The output of POD modulates the reference setting of power flow controller. In Fig.3, the deviation signal ΔP2 is replaced by ΔP2+u in order to include the POD for improvement of dynamic performance and in case of multi-machine system, the deviation signal ΔP2 is replaced by:

$\Delta P2+K_{POD}(\Delta w1-\Delta w2)$, where $(\Delta w1-\Delta w2)$ is the difference of speed deviations of generator 1 and generator 2.

7-Test System Description

Fig.5 shows a simple power system 500 KV network grid equipped with SSSC rated at 100 MVA connected in series with transmission line L1 designed and simulated in Matlab (Simulink). The power system grid consists of two power generation substation and one major load center at bus B3. The first power station M1 has a rating of 2550 MVA, the other power station M2 has a rating of 1400 MVA . The load centre is approximately 2200 MVA modeled using three-phase series load. M1 power station is connected to this load by two transmission lines L1 and L2. L1 is 300 km long and L2 is split into equal segment (L2-1 and L2-2) each of 160 km long. M2 is also to the load centre by 60 km transmission line L3. The SSSC is connected in series to L1 through B1 and is capable of injecting up to 10% of the nominal voltage. The SSSC injects a voltage V_{pq} in series with the transmission line where it is connected. As the SSSC does not use any active power source, the injected voltage must stay in quadrature with line current. Fig.6 shows the test system which is a Matlab-based model of a SSSC Connected in series with transmission line 1.

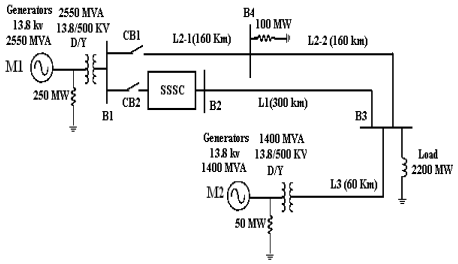

Fig.5 The single line diagram representing a 500 kv power system equipped with Series SSSC

8-Experements

- Test 1: SSSC is bypass (measure the active power P at bus 2).
- Test 2: SSSC is connected and the injected voltage V_{inj} is set 0.05 p.u.
- Test 3: Dynamic response of SSSC. The SSSC injected voltage reference is setby POD controller whose output is connected to the V_{qref} input of the SSSC. V_{qref} is set as follows: Initially V_{qref} is set 0 p.u, at t = 0.1 s.
- Test 4: Power oscillation damping of SSSC, to compare the test system with and without POD control.
- Test 5: SSSC is subjected to three phase faults at the middle of line 2.

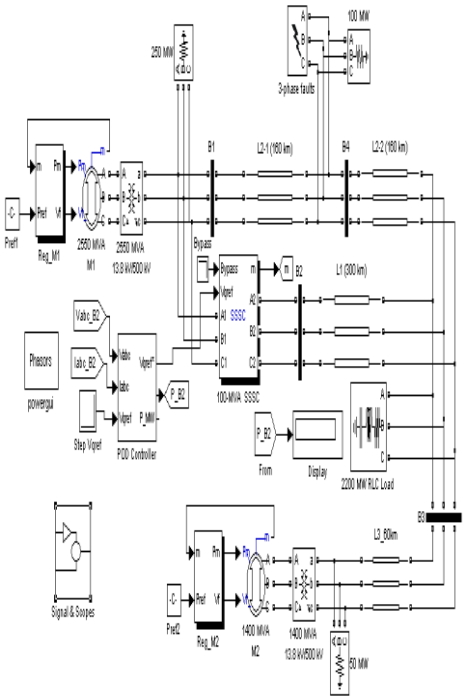

Fig.6 test system Matlab-based model

9-Simulation Results & Discussion

The following figures shows the operation of our test system when the SSSC is connected in series with line at bus B2, with and without the POD controller, and the effect of POD on the system subjected to three-phase faults at B4.

Fig.7 shows the test system operated without SSSC, the total active power flow towards the major load is measured at bus 2 (P_B2) flow on line 1 is 738 MW.

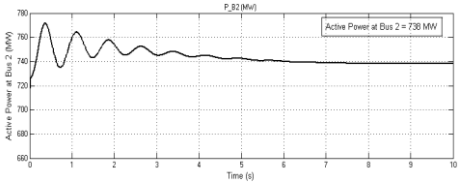

Fig.7 Normal operation of test system without SSSC

Fig.8, shows the operation of the test system when SSSC is connected in series with transmission line 1 and is capable of injecting up to 10 % of the normal voltage system, as we can see from the figures, the transmitted power at B2 is varying between 740 MW and 820 MW in accordance to the reference injected voltage of the SSSC. The active power is increased to 788MW.

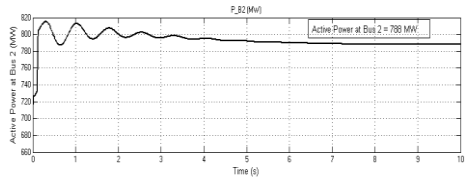

Fig. 8 SSSC is connected to the test system

Fig. 9, Shows the dynamic response of the test system. With POD is still disabled, The simulatrd result shows that the SSSC regulator follows very well the reference signal depending on the injected voltage.

The measured active power flow at B2 is incresed to 818 MW.

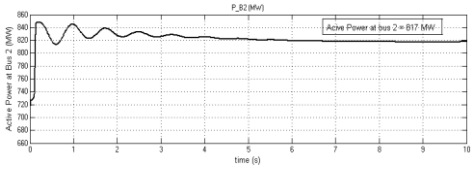

Fig.9 Test system operation with POD disabled

Fig.10 shows the effect of POD on the test system. As we can see from the figure, The SSSC with POD controller is a very effective tool to damp power oscillation.

Fig.11, Shows the effect of POD controller on test system operation when it subjected to three-phase faults at the middle of line 2. As we can see from the figure, The SSSC with POD controller is a very effective tool to damp power oscillation.

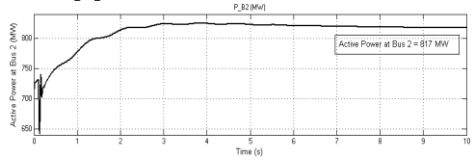

Fig.10 Test SystemWith SSSC and POD

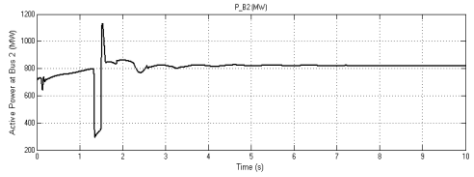

Fig.11 the Effect of POD controller on test system operation

10-Conclusion

This paper presents the transient stability improvement by a SSSC controller. The proposed controller is based on the establishment of the liberalized Phillips–Heffron model of a power system installed with a SSSC controller. The effectiveness of the proposed SSSC controller for improving transient stability performance and its design by the methods proposed in the paper are demonstrated by a weakly connected example power system subjected to three-phase fault. The result shows that the effectiveness of the proposed controller and their ability to provide good power oscillation damping. In addition, the effectiveness of the proposed SSSC controller to suppress power system oscillations and to improve the power transfer capability of the test system is also shown.

11- References

[1]E.W. Kimbark: "Improvement of system stability by switched series capacitors", IEEE PAS (1966), Vol. PAS-85, No.2, pp.180-188.

[2]O.J.M.Smith:"Power system transient control by capacitor switching", IEEE PAS (1969), Vol. PAS-88, No.1, pp.28-35.

[3]O.J.M. Smith, Webster, R.H.: "Series capacitor switching to quench electromechanical transients in power systems", IEEE PAS (1971).

[4]E. Iliceto, and Cinieri, E. "Comparative analysis of series and shunt Compensation schemes for AC transmission systems,:, IEEE PAS VOLPAS-90, No.2, pp-427-433 (1977), Vol. PAS-96, N0.6, pp. 1819-1830.

[5] A. Olveghd, Ahlgren, L., Frank, H., "Thyristor-controlled shunt copacitors for improving system stability", CIGRE SC 32-20, Paris 1976.

[6] Olweghd, A., Walve, K., WAglund, G., Frank, H., Torseng, S.: "Improvement of transmission capacity by thyristor controlled reactive power", IEEE PAS (1981). VoLPAS- 100, No.8, pp.3930-3939.

[7] L. Gyugyi, "Dynamic compensation of ac transmission lines by solid-state synchronous voltage sources", IEEE Trans. Power Delivery, 19(2), 1994.

[8]P.Rao , M.L. Crow ,Z.Young , " STATCOM control for power system voltage control application", IEEE Trans. Power Delivery ,15,2000, pp.1311-1317.

[9]H.Wang, F.Li, "Multivariable sampled regulators for the coordinated control of STATCOM ac and dc voltage" , IEE Proc. Gen. Tran. Dist.,147(2) ,2000,pp. 93-98.

[10]A.H.M.A Rahim , M.F.Kandlawala ," Robust STATCOM voltage controller design using loop shaping technique", Electric Power System Research, 68,2004,pp.61-74.

[11]K.Sen,"SSSC-Static synchronous series compensator : Theory modeling and pplication.", IEEE Trans. on Power Delivery, 13(1): 241-246, January 1998.

[12]L.Gyugyi, C. Schauder, and K.Sen , "Static Synchronous Series Compensator : A solid state approach to the series compensation of transmission lines.", IEEE Trans. on Power Delivery ,12(1):406-417, Jan. 1997.

[13] P. Kundur, *Power System Stability and Control*, New York, McGraw-Hill, 1994.

[14] M. J. Gibbard, "Robust design of fixed-parameter power system stabilizers over a wide range of operating conditions," *IEEE Trans. On Power Systems*, Vo1.6, No. 2, pp. 794-800, May 1991.

[15] L. Gyugyi, C.D. Schauder, and K.K. Sen, "Static synchronous series compensator: a solid-state approach to the series compensation of transmission lines," *IEEE Trans. on Power Delivery*, Vo1. 12, No. 1, pp.406-417, Jan. 1997.

[16] K R Padiyar and K Uma Rao, "Discrete control of series compensation for stability improvement in power systems," *Electrical Power & Energy Systems*, vol. 19, no. 5, pp. 311-319, 1997.

[17] R. Mihalic and I. Papic, "Static synchronous series compensator—a mean for dynamic power flow control in electric power systems,"*Electric Power Systems Research*, vol. 45, pp. 65–72, 1998.

[18] D. Menniti, A. Pinnarelli, N. Scordino and N. Sorrentino, "Using a FACTS device controlled by a decentralised control law to damp the transient frequency deviation in a deregulated electric power system,"*Electric Power Systems Research*, vol. 72 pp. 289–298, 2004.

[19] I. Ngamroo, J. Tippayachai and S. Dechanupaprittha, "Robust decentralised frequency stabilisers design of static synchronous series compensators by taking system uncertainties into consideration,"*Electrical Power and Energy Systems* vol. 28, pp. 513–524, 2006.

[20]K.R. Padiyar ,A. M. Kulkarni, "Development and Evaluation of controls for unified Power flow controller", IEEE Trans. on Power Delivery,13(4),Oct.1998,pp.1348- 1354 .

[21] N.G. Hingorani , L. Gyugyi " Understanding FACTS : Concepts and Technology of Flexible AC Transmission Systems", IEEE Power Engineering Society, IEEE press, Delhi 2001.

[22] Hai Feng wang, " A Unified model for the Analysis of FACTS devices in damping power system oscillation-part-III,UPFC ",IEEE Tran. on PD, 15(3),July 2000,pp.978-983.

[23]N.Tambey and M.L.Kothari, "Damping of power system oscillations with unified power flow controller(UPFC)" ,IEE Proc. Gen. Tran.& Distr. Vol.150,No.2, March 2003,pp 129-140.

Effective Use of Composite Insulators on WAHA OIL Company's Electrical Transmission and Distribution Systems

Dr. Abdulhamid T. El-Gammudi
Alfatah University

Eng. Salem Zwawi
Waha Oil Company

1. Abstracts

Waha Oil Company's (WOC) electrical distribution system consists of 138 KV transmission lines and 34.5 KV well distribution network, using suspension and tension towers. Ohio brass anti fog, open profile and composite insulators are used for insulation. Performance analysis of the three types of insulators were performed, where Ohio brass anti fog were used in the early 1960's with erection of first tower. Its performance was not satisfactory at all. The W.O.C electrical system was subjected to frequent failures primarily due to insulators failure attributed to pollution accumulation on its surfaces, resulting in oil production loss. Open profile type were introduced in the early 1990's, the failure rate was reduced but still is not up to the acceptable level. These two types of insulators required continuous costly cleaning and maintenance work in addition to the high cost of loss of production.

In 2003 silicon rubber insulators (SIR) were introduced to the high voltage transmission lines for testing period which lasted four years. The insulators proved its excellent performance in heavily polluted environment in terms of failures rate (0% without cleaning). Therefore, a full replacement program of the old two types of insulators with SIR insulators started from 2007 up to now. As of today 90% of 138 KV transmission lines insulators and 93% of 34.5 KV wells distribution network insulators have been replaced. So far no single failure has been reported due to composite insulators failure. Cost analysis no doughtily showed cost saving earned from using the composite type insulators, millions of dollars has been earned within one year span.

2. Introduction

WAHA Oil Company (W.O.C) operates an extensive system of oil and gas production which produces approximately thirty two different reservoirs into fourteen satellite processing facilities and eleven main processing complexes.

Once processed, oil production from the reservoirs is transported through transmission system involving five main line pumping stations to the Es-sider terminal facility for sale. Additionally WOC process associated gas and gas condensate, provides water and gas injection and oil necessary utilities and support services for its production operations. The prime motive power for all of these activities is electrical consequently WOC is entirely dependent on its ability to generate and maintain sufficient and reliable electrical power to produce, process and move its products to market. Without

adequate and reliable power, the many electrical powered devices from motors to heating elements used to produce and process its raw products will not operate.

3. Description of WOC electrical distribution system

WOC electrical network consist of 138KV transmission lines Used to interconnect the main generation stations and load stations, and 34.5KV well distribution network which provides electrical power to all electrified wells and other accessory equipments.

3.1 Types of overhead line towers used

Suspension towers (AR).
Tension towers (ER).
Dead end towers (well feeder tower).
Suspension towers with double circuit line (AAR).
Tension towers with double line (EER).

3.2 Types of insulators used

a- Anti fog (smoke 3) Specification:

Manufacturer	Ohio bras
Cat. No.	47316 (smoke 3)
fitting	bull & sockets
leakage distance	18 inch
M &E rating	20,000 pound
ANSI M&E category	15,000 pound

b- Aerodynamic (Open Profile) Specification:

Ball&socket class	ANSI Class 52.5
Test strength	80 KN
Leakage distance	330mm
Disk diameter	360 mm
Ball to socket	146 mm
Power frequency flashover (dry)	75KV
Power frequency flash over (wet)	55 KV
Corrosion protection	Zinc Sleeve
Compliance to standard	ANSI C29.2
Factory testing	ANSI C29.1

c- Silicon Rubber Insulators (SIR) Specification:

i. 34.5KV well distribution

type RODURFLEX, HTV Generation III blue house
Manufacturer Lab Insulators GMBH & Co KG Wunsiedel Germany
Minimum Creepage distance 1850 mm
arcing distance approx. 465 mm

Electrical data

50% lightning imp. flashover voltage positive 300 KV
50% lightning. imp. flashover voltage negative 310 KV
Power frequency flashover voltage wet 150 KV
Power frequency flashover voltage dry 170 KV

Mechanical data

Specified mechanical load tension 89.0 KN
Routine test load tension 45.0 KN
Weight approx. 3.2 KG
Test acc. To ANSI C29.11

ii. 138KV transmission lines

type RODURFLEX, HTV Generation III blue house
manufacturer Lab Insulators GMBH & Co KG, Wunsiedel, Germany
minimum Creepage distance 4495mm
arcing distance approx. 1330 mm

Electrical data

Power frequency flashover voltage wet 85 KV

Mechanical data

Specified mechanical load tension	120 KN
Routine test load tension	60 KN
Weight approx	6.7 KG
Test acc. to	IEC 61109

4. Nature of Electrical Failures in Waha Electrical System

The majority of power failure occurs in transmission and distribution systems are mainly due to flashover of insulators and bushings because of pollution contamination [1], climate conditions and other causes such as crow nesting on tower structure. Most of contanimination material is not good conductors in completely dry conditions, when pollutants become wet by fog, dew or mist, the resistivity drops, and the leakage currents increase significantly devolving high voltage across dry bands which eventually flashover increasing further, the leakage currents causing further partial flashover until a complete breakdown of the insulation occurs. These evidently leads to damage to the equipment (transformers, bushings, insulators……etc), loss of oil and gas production and Degrading the whole electrical system and becoming unreliable.

Anti fog type insulators were used in the early 1960's with the erection of the first tower, the performance was not satisfactory. WOC electrical system was subjected to frequent failure resulting in oil and gas production loss. This type of insulators requires frequent cleaning and maintenance.

Open profile type insulators were introduced to WOC in early 1990's. The Open profile is more suitable for desert environment than the anti fog type. The failure rate was reduced but not up to the acceptable level. These two types of insulators required continuous cleaning and expensive maintenance work.

5. Performance analysis of the composite insulators

Composite insulators have been accepted by many electric utilities around the world for use in overhead power transmission lines especially in heavily contaminated areas to reduce contamination flash over rate and maintenance cost in comparison with traditional ceramic counterparts [2]. Polymer materials such as silicone elastomers hydrocarbon elastomers and epoxy resins are being increasingly used instead of porcelain and glass for out door insulation applications, such as line insulators, bushings, hollowing core insulators, cable terminations, etc. mostly due to its advantages such as:

- Light weight = lower construction and transportation costs
- Vandalism resistance = less gunshot damage.
- High strength to weight ratio = longer span/ new tower design (compacted towers)
- Unexplosive housing = improved safety for staff in the station and for the installation equipment.
- hydrophobic surfaces = unlike porcelain and glass these polymers have low surface free energy which makes the surface of the polymers inherently hydrophobic (water repellent) surfaces present a higher resistance to leakage current flow than porcelain or glass surfaces (hydrophilic surfaces) [3]. They also require higher current and commensurate energy dissipation to initiate the well known phenomenon of dry band arcing which, ultimately, is responsible for material

degradation in form of tracking and erosion. The lower leakage current and consecutive lower probability of dry band formation requires a higher applied voltage to cause flash over. In one word, due to the hydrophobic surface, the polymer materials typically offer much better contamination performance than porcelain and glass.

6. WAHA Field Experience

In 2003, Waha decided to put these insulators on one of the most polluted lines which Zaggut- Samah line for actual environment conditions for a trial. 230 silicone rubber RODURFLEX insulators were installed on 138 KV Zagut –Samah Line, and 840 units were installed at different location on Waha 34.5 KV distribution system. The purpose of the trial was to find out the behavior of these insulators on real life operation and see if any flash over due to contamination occurs.

The insulators were checked by field operators regularly for any changes or damages, since the installation it was found no surface changes nor flash over reported.

In August 2008 a sample of 34.5 KV and 138 KV RODURFLEX insulators were sent to the manufacturer (Lapp Insulators GMBH Co. KG, Wunsiedel Germany) for tests and laboratory inspections in order to evaluate the performance of installed insulators. (The tests were witnessed by co-writer of this paper). The samples were inspected and tested to verify its field performance, the following features were inspected:

- analysis and identification of the pollution layer,
- visual inspections and evaluation of insulator status,
- electrical type tests according to IEC 61109,
- evaluation of the hydrophobic of the silicone housing,
- verification of SML according to IEC 61109.

7. Test and Inspection Results

High temperature vulcanizing (HTV) silicone rubber housing of both insulators appeared as light- medium polluted in general. The pollution layer is not even, some parts of the housing are heavily polluted. Hydrophobicity transfer mechanism is fully active.

ESDD/NSDD measurements of pollution taken from the heavily polluted sides showed NSDD = 3, 0 mg/cm^2 and ESSD = 0.01 mg/cm^2.

No damage, no punctures, no traces of tracking and erosion, no signs of aging was found. Chemical analysis of pollution layer revealed a light composition of Mgo, NaCl, K_2O and Fe_2O_3 (from natural pollution, sand, soil) an impact of industrial pollution is not yet significantly visible.

The results of the electrical type tests showed no significant degradation of the electrical insulation took place, the samples still performing electrically very well.

The results of the mechanical tests showed that ultimate tensile breaking loads (UTS) were 143 KN for the 138 KV unit where the SML = 120 KN, and 109 KN for the 34.5KV unit with SML = 89 KN, thus no mechanical degradation was found. Both RODURFLEX insulators performed very well in this environment that is characterized by heavy to very heavy pollution sites. It can be confirmed that after more than three years of service in these harsh environment, neither mechanical and electrical degradations nor any other ageing effects (e.g. UV ageing) were detected [4]. Accordingly starting

from 2008 upward WAHA have changed about 90% of 138 KV insulators and 93% of 34.5 KV insulators.

8. Effect of Introducing RODURFLEX to WAHA Electrical System

Tables (1-3) were prepared by WAHA showing the number of outages and the consequent oil production losses, and the cost of cleaning ceramic insulators. There is a considerable gain as a result of replacing the old ceramic insulators with silicon rubber insulators, the gain comes in two ways, the first is due to the huge reduction in electric failures which leads to increase in oil production, the second is the saving in insulators cleaning which increases as the rate of insulators replacement increase. Over the period Oct. 07 to Oct. 09, the total amount of saving equal to 27,053,407 LYD[5].

Table (1): number of failures and production losses per year for the period 07 to 09

Comparison of Electrical Failures

Area	System	Oct. 07- Oct. 08		Oct. 08- Oct. 09	
		Failures	Production Losses bbls.	Failures	Production Losses bbls
Waha	138 & 34.5 Kv	85	164,764	54	70,630
Gialo	138 & 34.5 Kv	31	192,331	13	21,522
Dahra	138 & 34.5 Kv	20	32,883	24	35,586
Samah	138 & 34.5 Kv	32	136,619	20	87,803
Total		168	526,597	111	215,541

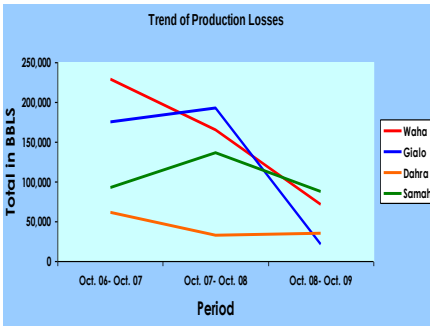

Fig (1): oil production losses due to electric outages for the period Oct. 06 to Oct. 09.

Table (2): production saving due to replacement of old insulators by SIR.

GAIN PRODUCTION SAVINGS

	LOSS PRODUCTION DUE TO ELECTRICAL FALUIRE bbls	PRODUCTION GAIN in BBLS	GIANED EARNINGS IN LYD IBBL=70 LYD
2008	526,597	311,056	21,773,920
2009	215,541		

Table (3): reduction in cleaning cost with the advance in SIR installation.

CLEANING COST SAVINGS

YEAR	2008	2009	savings
LYD	3,290,154	1,288,980	2,001,174
US$	3,861,683.400	1,512,888	2,348,795

9. Conclusions

1. RODURFLEX rubber insulators (138 KV, 34.5 KV) have been used in WAHA OIL COMPANY electrical system since 2004 without cleaning and with no flashover contributed to the operation of such insulators.
2. 27,000,000 LYD has been earned for only one year span.
3. RODURFLEX rubber insulators were tested at high voltage plant of the manufacturer after three years of operation, the test results revealed that the insulators performance was as new insulators.

10 Recommendations

1. It is highly recommended to use Silicon Rubber Insulators for all Libyan transmission and distribution networks that encounter similar environmental conditions as WAHA.
2. It is recommended that all old type insulators (Glass, Ceramic) are to be replaced with RODURFLEX Rubber insulators.

References

[1] A.T. El-Gammudi," The Degradation of Porcelain and Glass Insulators", The First Magarebi Symposium on Insulators Pollution, 10-12 Apr. 1995,Tripoli, Libya.

[2] A.T. El-Gammudi," Material Degradation and Ageing of Silicon Rubber Insulators", The Third Libyan Arab International Conference on Electrical and Electronic Engineering , 25-28 March 1996, Tripoli, Libya.

[3] J. M. Seifert, W. Hubl, " Hydrophobicity effect of silicon housed composite insulators and its transfer to pollution layers", Iraklion Symposium, Kreta, Greece, 26&27th April, 2001.

[4]Lapp Insulators Examination report 252/08

[5] Waha daily failure reports of the period from OCT.07 to OCT.09

A methodology for solving Var/voltage problems in the western Algerian transmission system

M. Khiat, A.Chaker, D.Rehiel, Z.Frioui
Laboratory SCAMRE, ENSET Oran, Algeria
Khiat2_2000@yahoo.fr

Abstract

This paper describes the methodology adopted to deal with the Var dispatch and voltage violation problems. This flexible methodology combining heuristic and numerical techniques has been successfully used to determine a suitable strategy for the operation of the western Algerian transmission / subtransmission system. The injection of shunt capacitors at target buses, optimization step and corrective actions at specific transformer taps and synchronous generators with considering heuristic rules allows to maintain the voltages in the whole network within the required limit and to reduce the active power losses. Finally, field results corresponding to the worst case reported up to date are analyzed to show the validity of the proposed procedure.

Keywords: Voltage problems, heuristic rules, optimization

1. Introduction

Quality and security of electric energy supply requires that proper attention be paid to Var dispatch and voltage control. Reactive power management can be defined as the control of the generator voltages, the variable transformer tap settings, the compensation and switchable shunt element, the Var injection in synchronous and static Var compensators (eg, Facts devices). Additionally when security is not concern there is still an economic incentive to reduce active power losses by rescheduling reactive power sources and shifting transformer taps.

In Algeria, the electric power supply is based in three regions: the western, the eastern and the central regions. Because of its large distance from the main poles, the southern region is not connected to the main network.

Presently, the control of the reactive power and voltage is one of the most important concerns of the Algerian electricity company (Sonelgaz). The Algerian system (220 and 60 kV system) possesses many buses radially connected to the main grid, certain consumption areas being remotely located from injection buses. It is also characterized by long transmission lines, an uneven distribution of reactive power reserves among available generators, and an insufficient number of shunt capacitors. As a consequence, operators are routinely facing severe voltage problem, and the Var dispatch has become one of the most relevant concerns in the control center for the western Algerian transmission system.

In this paper, we focus our interest on the western Algerian network (220 and 60 kV system) that is connected to Morocco by the Oujda station (bus n°12) at the west and by the Oued Sly station (bus n°13) at the center. In this network, severe voltage problems are traditionally encountered (*especially in the 60 kV electrical network for which operators are routinely facing low voltages*), as well as local reactive power shortages. In order to prevent these problems, very efficient optimization programs can be used [1], [2], [3]. Besides expert systems [4], [5], [6], heuristic (i.e. knowledge-based) methods [1], [5], Metaheuristic methods [10] and other branches of AI technology (e.g. fuzzy logic) have also been proposed regarding *var/voltage* control. Our methodology has consisted in the development of an optimization program that allows two-fold control of the system and the integration the heuristic rules. First, if one or several emergency voltage limits are violated, then identify the most effective shunt capacitors and compute the amount of reactive power that should be injected, in steps of 5 MVAR, with considering the heuristic rules. Second, reschedule generator reactive powers and transformer taps so to minimize active-power losses. If other violations occur, fine tuning is achieved through additional appropriate control steps. The advantage of our user-friendly methodology combining heuristic and numerical techniques is to establish a practical number of control variables, to solve efficiently the problem of voltage violations and to reduce loss powers.

In section 2, we present the methodology adopted. Section 3 and 4 describe in more detail how voltage problem are solved by heuristic method and active power losses are reduced respectively. Finally, implementation and some results obtained on the western Algerian network are presented and compared to those of a results Sonelgaz company in section 5.

2. Overview of the methodology adopted

Var/Voltage optimization and control is one the most important security and service quality indexes. The system behaves differently depending on which limit is exceeded. Several papers have presented methods for solving Var/voltage problems: knowledge-based, sensitivity-based and heuristic rule- based [1], [4], [5], [6], [10]. In the present work, the basic methodology for solving Var/ voltage problems is as follows:

1. Load flow by Newton Raphson in polar form.

2. Determine the buses that undergo the most severe voltage violations (target buses).

3. Identify the most effective shunt capacitor (s) and compute the amount of reactive power that should be suitably injected, in steeps of 5 MVAR, to solve those violations with considering heuristic rules.

4. Optimization process with fixed shunt capacitors.

5. If other less important voltage violations occur at buses, use appropriate control steps for the adjacent transformer tap and/or the nearest reactive power of generator, i.e with considering heuristic rules.

$$t_i^{new} = t_i^{optimal} \pm \Delta t_i \quad (1)$$

$$Q_i^{g,new} = Q_i^{g,optimal} \pm \Delta Q_i \quad (2)$$

Where Δt is the control step applied of transformer taps and ΔQ the control step applied for generator reactive powers. Typical and initial values of Δt and Δq are 0.01 p.u .

6. Actualize new voltages with a load flow.

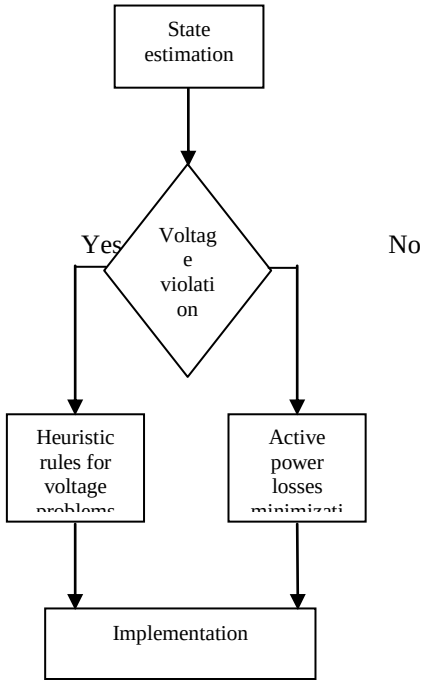

Figure1. Overview of the methodology adopted

3. Heuristic rules for voltage problems correction

To facilitate the resolution of voltage violations and to assist the operator, one can introduce rules that one call « heuristic rules ».These rules are established in a particular or general manner according to a particular experience. The correction process depends on the voltage violations in the upper or lower limit and network exploitation state (normal or contingency). According to the experience acquired, some rules of correction of the voltage violation have been determined.

3.1 Rules correction for voltage violation

IF there is no voltage violation
THEN the process ends.
IF there exists a voltage violation.

- to identify the largest voltage violation
- to select voltage according to their level of violation

THEN to correct voltage according to the upper or lower limit.

When the lower limit is exceeded, the correction for voltage violation in order of preference is as follows:

- to switch off lines that were formerly switched,
- to disconnect the reactances,
- to increase the voltage of production groups,
- to connect the condensers,
- to increase voltage on transformer taps.

If, the voltage violation persists, a diversion of load has been made.

When the upper limit is exceeded, the correction for voltage violation in order of preference is as follows:

- to decrease the voltage of production groups
- to connect the reactances .
- to open the lines whose disconnection is permissible
- to decrease voltage on transformer taps

Once the process of adjustment is selected, the new voltage has to be actualized.

IF it remains no voltage to correct
THEN the process ends.

Moreover, the treatment of the various controls offers an effective and quick solution to the following questions:

- What is the most adequate control to correct a given limit violation?
- What are the most effective control variables?
- What is the necessary variation of the control variable, in order to obtain the desired correction without inducing new violations?
- Should we use one control or various and simultaneous controls?
- What coordination between the controls is needed in order to correct the same violation?

An answer could be provided to these questions by using heuristic and/or numerical rules, thus:

- Always use the geographically nearest control, until the voltage is corrected. If this is sufficient, one can move to the next control.
- Always grant priority to the use of generators, to the transformers, and then to the batteries, in that order.
- Establish a criterion, which would allow us to classify and compare the effectiveness of the various controls.
- Establish an optimisation process under certain constraints.

3.2 Heuristic rules on the means of control

3.2.1 Production groups

Production groups are well situated to satisfy needs in reactive energy compensation. Furthermore, their dynamic performances allow them to face the abrupt demand fluctuations. However, they can only partially compensate the reactive loads by reason important voltage falls in order to create reactive energy transits. Their adjustment of the tension and management of the reactive power are insured by groups. Their action is coordinated in time (primary adjustment) and in the space (secondary adjustment)

3.2.2 Backup generators

The main objective of the backup generators is to provide energy during rush hour or in case of emergency. However, connecting the backup generators to the network must be undertaken in extreme situations in order to produce reactive power to increase voltage.
The general rules for connecting or disconnecting the backup generators are as follows:

Connection

IF $V_k << V_k^{min}$ (*emergency*)
AND load tendency is favourable,
AND generator is not in service,
AND generators, transformers, and condenser batteries cannot resolve the violation,
AND when it connected and does not consume reactive power,
THEN connect the backup generator.

If the backup generator is connected to the network, it functions in the same way as any other generator.

Disconnection

IF $V_k >> V_k^{max}$ (*emergency*)

AND minimum time has elapsed, during which the generator has been connected,
AND load tendency is favourable,
AND it has been started in order to increase the voltages,
THEN disconnection the backup generator.

3.2.3 Transformer taps

Network voltage variations are closely linked to the fluctuations of the reactive power in the system of production, transport and distribution.
These voltage variations are set out of sources of reactive power, and by the transformer taps.

A transformer taps is a connection point along a transformer winding that allows the number of turns to be selected. By this means, a transformer with a variable turn ratio is produced, enabling voltage regulation of the secondary side. Selection of the tap in use is made via a tap changer mechanism. A mechanical on-load tap changer (OLTC), also known as under-load tap changer (ULTC) design, changing back and forth between tap position 2 and 3. Because interrupting the supply is usually unacceptable for a power transformer, these are often fitted with a more expensive and complex on-load tap-changing mechanism. OLTC may be generally classified as mechanical, or as electronic, which in turn may be either assisted or solid state.
The proposed rule determines the tap position of the ULTC transformer to maintain the voltage within the permissible limits as much as possible.

IF $V_i < V_i^{min}$
AND generators is not capable to solve the violation,
AND load tendency is favourable,
AND tap position is not adequate,
THEN change the tap position of the ULTC transformer.

IF $V_i > V_i^{max}$
AND load tendency is favourable,
AND change the tap position does no provoke other voltage violation,
THEN change the tap position of the ULTC transformer.

3.2.4 Condensers

They allow to insure the maintenance of the tension and to limit active losses. General rules obeying the connection or the disconnection of these elements are as follows:

Connection

IF $V_i < V_i^{min}$
AND generators and transformers utilisation are not capable to solve the violation
AND load tendency is favourable,
AND connection does no provoke other voltage violations
THEN connect the condensers.

Disconnection

IF $V_i > V_i^{max}$
AND load tendency is favourable,
AND the disconnection does no provoke other voltage violation,
THEN disconnect the condensers.

3.2.5 Reactances

They are used to compensate reactive energy provided at slack hours by lines. The general rules that govern these devices are:
Connection:

IF $V_i > V_i^{max}$

AND generators and transformers use are not capable to solve the violation,
AND load tendency is favourable,
AND its connection does not give rise to a lower violation more severe than the upper violation being solved
THEN connect the reactance.

Disconnection

IF $V_i < V_i^{min}$
AND load tendency is favourable,
AND its disconnection does not lead to new violations,
THEN disconnect the reactance.

3.2.6 Lines

There exists a very strict condition for the opening of some lines. It is the last resort to use. During weak demands, the opening of the line is made only near the knot where the voltage is superior to its limit.

Disconnection

IF $V_i >> V_i^{max}$
AND load tendency is favourable,
AND other controllers cannot solve the violation,
AND the transit of a lower power than a percentage of its total capacity,
AND the time from the last switching exceeds a threshold,
THEN open the line.

Connection

IF the line was disconnected to correct voltage violation,
AND load tendency is favourable,
AND the placement in service does not provoke a great voltage to the upper limit tensions,
THEN connect the line.

3.2.7 FACTS devices

An attempt will be made to assess whether the use of this equipment is interesting and profitable in some cases as there are, in this domain, no standardised solutions, except the FACTS which are commonly used. The two principal reasons that justify the installation of FACTS devices in electric networks are:

- Increase of dynamic stability limits (*transitory stability*, *voltage stability*).
- Effective mastering of the low of energy and very Var/voltage problems.

4. Optimization: formulation and solution

4.1 Formulation of the problem

Assuming that the active power generation has been schedule according to the economic dispatch solution, it is possible to minimize active power losses by properly adjusting, within acceptable limits, generator voltage magnitudes, transformer taps and switchable Var sources. In this process, allowable bounds on certain dependent variables, like the load bus voltages and the generator reactive powers, should be enforced as well. Although it is customary in conventional load flow to consider generator voltage magnitudes as control variables and the respective reactive powers as dependent variables, the roles of these two variables can be interchanged in the optimization process, as long as the power flow equations are satisfied. The advantage of this procedure is twofold:

-All bus voltages magnitudes belong to the state vector. There are no present PV

buses and no need to distinguish between both types of buses.

- Reactive power limits are more easily modeled when the associated variables are explicitly handled. Otherwise, functional inequality constraint would appear. Mathematically, for a network with n buses, the active power loss minimization problem can be stated by resorting to the following set of vectors:

- Dependent or state vector: composed of the n bus voltage magnitudes v and of the $n-1$ bus phase angles δ relative to the slack bus:

$$x = [v, \theta] : (2n-1) \times 1 \qquad (3)$$

- Independent or control vector: composed of the n_g controllable reactive power injection and of the n_t transformer tap changer ratios:

$$u = [Q, t] : (n_g + n_t) \times 1 \qquad (4)$$

- Parameter vectors: comprise the $(n - n_g) \times 1$ load bus, the reactive power injection vector, Q_i and the $(n-1) \times 1$ active power injection, p_i:

5.2 Method of solution

The optimization process considered in this work, is the minimization of the total active power losses, with shunt capacitors fixed, $u = [Q_i^g, t_i]$ and $x = [V_i, \theta_i]$, which can be formulated as:

$$Min \ : \ P_L(V_i, \theta_i, t) \qquad (5)$$

Subject to:

(1) The net active and reactive power flow equations :

$$\Delta P_j = \sum_{j=2}^{n} V_i \cdot V_j \cdot (G_{ij} \cdot \cos\theta_{ij} + B_{ij} \cdot \sin\theta_{ij}) - P_i^g + P_i^c = 0 \qquad (6)$$

$$\Delta Q_j = \sum_{j=2}^{n} V_i \cdot V_j \cdot (G_{ij} \cdot \sin\theta_{ij} - B_{ij} \cdot \cos\theta_{ij}) - Q_i^g + Q_i^c = 0 \qquad (7)$$

(2) The physical limits on the reactive power of generators :

$$Q_{i,\min}^g \le Q_i^g \le Q_{i,\max}^g \qquad i = 1,....n_g \qquad (8)$$

(3) The physical limits on transformer taps:

$$t_{\min} \le t \le t_{\max} \qquad i = 1,....n_t \qquad (9)$$

(4) The voltage magnitude limits at all buses:

$$V_i^{\min} \le V_i \le V_i^{\max} \qquad i = 1,...n \qquad (10)$$

Where:

$$P_L = \sum_{i}^{n} \sum_{j}^{m} - G_{ij} . (V_i^2 + V_j^2 - 2 . V_i . V_j . \cos\theta_{ij}) \qquad (11)$$

We use the "Reduced Gradient" (*the constrained Gradient is obtained from the "augmented Lagrangian" function L and the Kun-Tuker conditions for the minimum*) together with an iterative method. The inverse transpose of the jacobian matrix can be calculated by using sparse vectors techniques. The active power productions are considered as fixed (except for the slack bus). From vector Gradient $\nabla_u L$ of Q and t we obtain the new different values of the reactive power generated and the

transformer tap. At each iteration, with the new values of reactive power and the transformer tap, we actualize the new voltages with the Newton Raphson power-flow solution.

This iterative procedure terminates as the the rate of decrease of the objective function, evaluated by the load flow, and is found to be less than a certain tolerance.

5. Implementation and results

The one-line diagram of the western Algerian 220/60kV transmission/subtransmission system is shown in Fig.2 (*appendix*). Its main data and operational limits are summarized in Table I and Table II. Among the several scenarios tested, the worst case has been, selected to better illustrate the capabilities of the methodology adopted. The weakness of the 60 kV portion, predominantly radial in the lower right-hand side area, leads to a voltage profile which, at peak loading, to close to voltage collapse for certain buses.

TABLE I: MAIN DATA OF THE WESTERN ALGERIAN SYSTEM

Parameter	Values
Load buses	64
Generator buses	4
Lines	78
Transformer taps	12
Shunt capacitors	8
Active load demand	MW
Reactive load demand	541.1MVAR
Total active losses	29.18 MW

TABLE II: LIMITS OF CONTROL V ARIABLES AND BUS VOLTAGES

Magnitude	**Lower**	**Upper**
Voltage/ 220I	0.99 p.u	1.11 p.u
Voltage /60kV	0.95 p.u	1.10 p.u
Taps (20 steps)	0.90 p.u	1.10 p.u
Q_{shunt} (10 steps)	0.00	10 MVAR
Q^g_1	-250 MVAR	500 MVAR
Q^g_9	-90 MVAR	180 MVAR
Q^g_{23}	-30 MVAR	70 MVAR
Q^g_{36}	-20 MVAR	36 MVAR

For the considered power system, two cases are provided. The first one corresponds to the actual data of the Sonelgaz Company (*case 1*), while the second one is related to our simulation results (*case 2*). For each case, we provide the variation of the voltage for the different buses (Fig.1.). The desired voltage for the 60 kV network has to be in the range of 0.95 to 1.1 p.u., while for the 220 kV network, this range is 0.99 to 1.11 p.u.. Figure.1 shows how the voltage magnitudes evolve through the different phases of the proposed methodology, for the 9 buses whose voltage is initially below the lower limit.

From Fig.1c, one can see that a severe violation voltage occurs at target buses 46, 67 and 68 (0.*759 p.u, 0.765 p.u, 0.697 p.u respectively*) for case 1. Raising the tree voltages whose magnitude is under 0.85p.u constitutes the most urgent task. The recommendation at this phase consist of connecting 10 Mvar, 5 Mvar and 10 Mvar at buses 46, 67 and 68, respectively (*as reported in Table 3*). In this case the application of the heuristic rules is necessary. Using these data (fixed capacitors), we obtained by optimization procedure described in section 4, reactive

power of the generators (*Table 4*) and transformers tap changes ratios.

However, we have found that other less important voltage violations are still observed at buses 17, 24, 60, 64 and 66 (1.115, 1.131, 0.911, 1.128 and 1,111, respectively). To avoid these violations, the final procedure of our simulation approach is used. In particular, appropriate control actions have been applied to 3-17, 9-23 and 10-24 transformer taps with considering heuristic rules.

TABLE III: SHUNT CAPACITORS IN [MVAR]

Bus	Case n°1(Mvar)	Case n°2(Mvar)
38	5	5
46	0	10
53	10	10
59	10	10
	10	10
60		
61	10	10
67	0	5
68	0	10

TABLE IV: REACTIVE POWER OF GENERATION[MVAR]

Bus	Case n°1(Mvar)	Case n°2(Mvar)
1	405.1	401.4
9	81.3	38.8
23	16.8	29.6
36	36.0	17.6

TABLE V: TRANSFORMER TAPS

Buses	Case n°1(p.u)	Case n°2(p.u)
1-14	0.98	0.93
2-15	1.00	0.95
3-16	0.97	0.97
3-17	0.97	0.92
4-18	0.97	0.95
5-19	0.97	0.97
7-20	0.98	0.94
8-21	0.98	0.95
8-22	**0.98**	**0.96**
9-23	1.00	0.99
10-24	0.98	0.90
11-25	0.96	0.90

The calculations show that all voltages are then in the desired limits (Fig. 1b, 1c, case 2) if these control actions are +0.02, -0.03 and +0.04 for 3-17, 9-23 and 10-24 transformer taps, as compared to the final values given in Table 5.

Finally, a comparison between case 1 and case 2 shows that this operation process also results in a decrease of the total active power losses from 29.18 to 23.18 MW (20%).

6. Conclusion

This paper is focused on the Var/voltage control problems of the western Algerian transmission/subtransmission system. In the last few years, the operators have frequently faced widespread voltage violations, especially at the subtransmission level, and a tool capable of helping them in systematically solving those problems is clearly needed. This tool combines heuristic rules procedures, mainly intended to handle special situations and discrete devices, with efficient numerical

techniques, in order to determine in which sequence, and to what extent , the available controllers should be rescheduled. In case there are no voltage problems, a list of feasible control action are recommended in an attempt to reduce active power losses. This procedure is based on methodology that mainly includes three main aspects:

(i) a suitable injection of shunt capacitors in target buses or critical buses with considering the heuristic rules;

(ii) an optimization process involving two control variables, namely the reactive power of the synchronous generators and the transformer taps change ratios.

(iii) a fine tuning process consisting in the application of appropriate control steps for the transformer taps and/ or the reactive power of the generators with considering the heuristic rules.

According to the obtained results, the proposed approach gives good results. The advantages of this method are: optimal solution, flexibility and customized solution.

This procedure allow us to determine a strategy that results in keeping the voltage within the required limits as well as in a significant reduction of the total active power losses.

References

[1] J.L. Martinez Ramos, A.Gomez Exposito, "A Hybrid Tool Assist the Operator in Reactive power /Voltage control and Optimization", *IEEE Trans, On Power System,vol10(2),1999, pp.760-768.*

[2] D.Thurakan., K. Parthasaraty. , D. L. Prior, Improved Algorithm for optimum reactive power allocation ", *Electric power and energy systems. Vol 6, 1984, pp. 72-74.*

[3] T. Tran-Quoc,J.C. Sabonnadiere, N. hadj-Said, R.Feuillet, "Voltage-Var control in the Vietnam power system",*3 th PSCC in Trodheim,1999, pp 1023- 1029* .

[4]Y. Tamura, H.Sasaki H, "Expert System Applied to Voltag-Var Control Final Report", *N°139,1991 , pp.109-131*

[5]SP.Sing, GS.Raju, AK.Gupta. " Sensibility based expert system for Voltage control in power system ", *Electrical power & Energy system, 1999.*

[6] A. Gomez Exposito, J.L. Martinez Ramos J.L, " Sensitivity-Based Reactive Power Control for Voltage " , *IEEE Trans, On Power System, vol8,n°3,1993,pp.937-945.*

[7] J.G Rolim., L.J.B Machado., M.R. Irving, "Switching to control Voltage problems: a hybrid approach" *Electric power and energy system, vol19,N°1,1997, pp69-74.*

[8] W.M. Lebow and al, " Optimization of reactive volt- Ampere (VAR) sources in system planning ", *Vol1, EL-3729 research project 2109-1, Final report, November 1984.*

[9]Y.Wallah , "Calculations and program for power system networks" *Prentice-Hall, Inc., Englewoo cliffs.*

[10]S.Chetih, M.Khiat, A. Chaker, "Means optimization of reactive Power compensation using the particle swarm optimization PSO Method: Aplication in the Western Algerian transmission system", *International Review of Electrical Engineering (IREE), vol. 4 n. 4,* July-August 2009, pp. 622 – 49.

Appendix

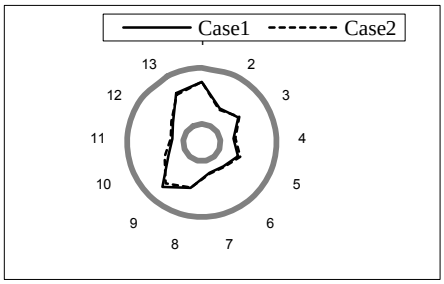

a)

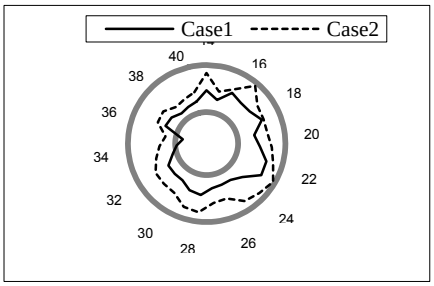

b)

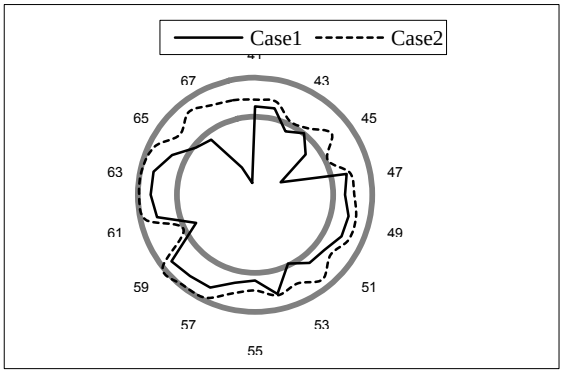

c)

Fig.1: (a) Voltages profile for buses 1-13, 220 kV.
(b) Voltages profile for buses 14-40, 60 kV.
(c) Voltages profile for buses 41-68, 60 kV.

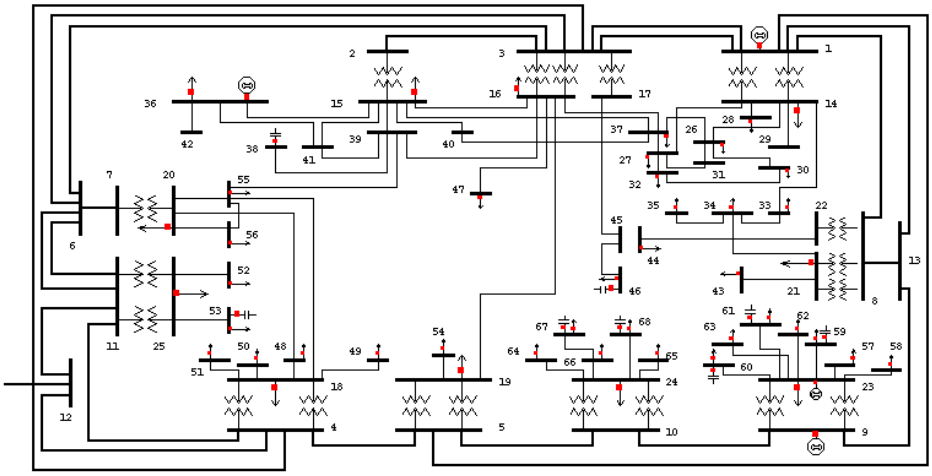

Fig.2: Western Algerian 220/60kV transmission/sub-transmission system.

Electricity load profiling for the UK Domestic Buildings

A. M. Ihbal[1], H. S. Rajamani[1], M. K. Jalboub[1], M. A. Elgadal[2], M. M. Hebal[3]

[1]School of engineering, Design and Technology University of Bradford, Bradford, BD7 1DP, UK
[2]The Higher Institute of Training for Trainers, Regdaleen, Libya
[3]The Higher Institute of Water Affairs, Alajelat, Libya
A.M.I.Ihbal@Bradford.ac.uk
H.S.Ramani@Bradford.ac.uk
M.K.Jalboub@Bradford.ac.uk
elgadal58@yahoo.com
mohammedihbal@yahoo.co.uk

Abstract

A better understanding of the behaviour of daily load profiles is desirable since the load shape, as well as the daily peak load is vital factors in planning the electricity distribution networks, optimal production capacity and pricing of electricity.
This paper presents a method of generating realistic electricity load profile data for the UK domestic buildings. The domestic space heating and domestic hot water are excluded in this study. The information and results of previous investigations and works that is available in public reports and statistics are used as input data when modeling of domestic energy. A questionnaire survey was conducted which included questions regarding the following aspects: the number of people living in the household, their age, employment and the general times of use of appliances and occupancy in the household.
The daily energy demand load profile of each appliance can be predicted using this method. A measured data set is also applied for comparison, and verification. Our analysis shows that the generated load profiles have a good agreement with real data.
The daily load profile from individual dwelling to community can be predicted using this method. The analysis shows the power requirements of each electrical appliance and helps to determine the suitability of applying renewable energy.

Keywords: electricity consumption; Load profiles; Domestic buildings; Appliances; microgeneration; demand response.

1. Introduction

The identification of the pattern of energy uses of a house and the prediction domestic load profile is essential in order to match load shape to power generated. In the UK, the domestic energy-consumption can be divided into three categories: space heating, domestic hot water, lighting and appliance. The use pattern varies depending on many determinants, such as weather,

household composition, income, behaviour patterns of occupants; etc. Occupants influence the use of electricity of dwellings by the number of electrical appliances they own and throughout their use of the appliances.

The demand per time interval is the sum of many consuming appliances. The demand of a typical appliance connected to the grid is not continuous over time. Generally, appliances will be switched on or switched off or will be operated on partial load depending on the time of the day, day of the week, seasonal influence and activity level etc. This results in a fluctuating electricity demand during a day and during a week. There are such many factors that influencing the occupancy pattern such as:

- The number of occupants.
- The getting up time in the morning and the sleeping time.
- The unoccupied period during the day.

There have been numerous investigations dealing with domestic electricity consumptions and load profiles in the UK [1-7]. A monitoring campaign was undertaken by Newborough [1] where the energy demand data of 30 homes have been obtained in order to modulate electricity demands emanating from individual dwellings to reduce the peak demand. A survey data among a sample of more than 1000 adults has been conducted and a questionnaire was designed in the south-east of England in order to collect information from consumers about environment, Ownership of appliances, Usage-patterns, and etc [2]. The result of this study, such as ownership level, and total energy consumption of certain appliances are generally used when modeling of domestic energy is carried out for the UK. A simple method of formulating load profile (SMLP) for UK domestic buildings was presented by R. Yao and K.A. Steemers [3]. The input data of the model was based mainly on public reports and statistics, such as the composition of households and average energy consumption of appliances per capita. The UK average size household (3 persons) was selected as an example of the implication of this method. A measurement of electrical energy consumption profiles for social sector in the UK, obtained over a period of 2 years was presented by Kreutzer [4]. The measurements were all obtained at 5 minute intervals. Annual energy consumptions, daily and overall profiles were derived for the dwellings from the data. An occupant survey was undertaken among the people living in the monitored dwellings in order to create a link between the energy consumption profiles and socio-economic factors. The monitored dwellings were categorised on the subject of floor area, number of occupants and ownership level of appliances.

Paatero and Lund [5] presented a method for creating domestic electricity load profiles at individual household level. It is based on a bottom-up model where the household load composes individual appliances/appliance groups. The input data of the model was based mainly on public reports and statistics. Yigzaw, et al [6] studied The patterns of electricity consumption and how occupancy and dwelling characteristics affect domestic electricity use for 27 homes in various locations throughout Northern Ireland (city, town and village). The results of this study showed that there is a strong correlation between average annual electricity consumption and floor area.

The Swedish Energy Agency recorded appliance consumption data of individual appliances for 400 households in order to

understand where and how measures should be taken to increase the number of energy efficient appliances in the homes. [7].
In this study, a method to generate load profiles for household electricity consumption is presented.

2. Methodology

The identification of the pattern of energy uses of a house and the prediction domestic load profile is essential in order to match load shape to the power generated, and also to predict the possible impact of any energy management action directly on the daily load profile. The generated Load profile is based on engineering assumptions as to the kind of appliances owned and lighting that are inside the house and when the occupants are expected to turn them on. The different households have different life styles, which mean the shape of total load profile will vary from house to house and day to day. The inputs of electricity demand profile generator are:

- The Census Demographic results, which care available from the UK Office for National Statistics (ONS) [8].
- The annual electricity consumption such as ownership level of appliances, and total energy consumption of certain appliances, which can be obtained from the results of survey among a sample of over 1000 adults which has been conducted mainly in the south-east of England regarding the socio-economic aspects of energy use [2].

Due to the lack of data about household occupancy pattern, it is necessary to make assumptions for the most common scenarios of household occupancy pattern in the UK. An Excel program is developed in order to generate domestic load profile for different consumption scenarios.

2.1 Household composition

The UK has a population of 61 million in 2008 and a total of 25 million households with an increase of almost 0.6 per cent on 2006. Since 1971 the population has increased by 5.0 million. The average household size is 2.4. Table1 and table 2 list the UK composition of households in 2008 and the type of households respectively [8].

Table 1 Percentage of UK household size [8]

No. of persons in the household	Percentage
1	29%
2	35%
3	16%
4	13%
5	2%
6 or more	2%
Total	100%

Table 2 Type of household

Type of household	Percentage share (%)
Single adult	15
Single retired adult	15
Two adults	29
Two adults with children	21
Two retired	6
Three adults or more	14
Total	100

2.2 Annual Electricity Consumption

The information of the average daily consumption for major appliances in the UK household carried out by Mansouri [2]. The information gives the type and the

average annual consumption per household per day, the average annual consumption per capita per day and the ownership level. Table 3 lists the average energy consumption of appliances in the UK.
The database gives the type and the average annual consumption per household per day, the average annual consumption per capita per day and the ownership level. The daily appliance energy consumption for different types of household can be calculated based on per capita daily energy-consumption data.

Table 3 average energy consumption of electrical appliances in the UK [2]

Appliance	Average annual consumption per household (kwh/day)	Average annual consumption per capita (kwh/day)	Ownership level (%)
Electric hob	1.33	0.39	37
Electric oven	0.74	0.22	56
Microwave Oven	0.23	0.07	74
Refrigerator	0.82	0.33	53
Freezer	1.9	0.55	55
Television	0.91	0.27	97
Video recorder	0.3	0.09	76
Dishwasher	1.72	0.48	16
Washing Machine	0.8	0.2	88
Tumble Driers	0.78	0.28	49
Electric Kettle	0.78	0.28	5
Iron	0.3	0.09	100
Vacuum Cleaner	0.15	0.04	100
Miscellaneous	1.1	0.33	100
Computers	0.5	0.3	75

2.3 Domestic appliance Category

Domestic appliances could be grouped as: brown goods, cold appliances, cooking appliances, wet appliances, and miscellaneous appliances. The domestic appliance categories in the UK are listed in table 4.

Table 4 Domestic appliances

Brown goods	Electric consumer goods : TVs, VCRs, etc.
Cold appliances	Refrigerators, freezers, and combined fridge-freezer.
Cooking appliances	electronic ovens, electric hobs, kettles, and microwaves, etc.
Wet appliances	Washing machines tumble dryers, and dishwashers.
Miscellaneous appliances	Vacuum cleaners, irons, electric showers, PCs, etc.
Lighting	Lights

The following assumptions have been made in order to generate appliances load profile:

1. All Cooking appliances are electric powered.
2. All households have an electric kettle, freezer and a refrigerator
3. No appliance is left on standby
4. Each household has only one of each appliances listed above.
5. The space heating and hot water systems are provided by means of natural gas. Although the boiler uses electric powered burner, the electric consumption of this burner is too small and has not been considered

2.4 Electric lighting patterns

The electric light depends on the occupancy pattern and is highly influenced by daylight condition (season) and the presence of active occupants. The electric lighting energy consumption can be calculated by using the following equation:

$$El = N_b \times E_{rb} \quad (1)$$

Where: N_b is the number of light bulbs per household distributed between bedrooms, kitchen, living room, bathrooms and others and E_{rb} is the energy rating per bulb per hour.

2.5 Occupancy Pattern of Household

The usage pattern is associated to the occupied period. For example, when there is nobody at home; most appliances will not be used. In daily appliance electricity profile, the occupants use practically low power (e.g. fridge-freezer) during the night, may wake up and have breakfast, leave the house during the morning and then may come again around mid-day for lunch, in the evening, the meal is cooked, television is switched on and showers are taken, etc. The total energy load profile can vary significantly from day to day and house to house depending on each household's life style. The occupancy pattern could be influenced by such many factors such as:

- The number of occupants.
- The getting up time in the morning and the time of going to bed.
- The unoccupied period during the day.

Due to the lack of data about household occupancy pattern, it is necessary to make assumptions for the most common scenarios of household occupancy pattern in the UK according to the household type. The six common scenarios are as follows:

Scenario 1: single adult household, the occupier is a full time working and the unoccupied period is from 09.00 to 18.00.
Scenario 2: Single retired Adult, the house is occupied all the time.
Scenario 3: Two retired, the house is occupied all the time.
Scenario 4: Two adults, the occupants in the house all have full-time job. The unoccupied period is from 09.00 to 18.00.
Scenario 5: Two adults with children, one occupant has a full time job and the other adult may have a part time job in the morning in order to take care of the children after school. The unoccupied period is from 09.00 to 13.00.
Scenario 6: Three adults or more, the unoccupied period is from 13:00 to 18:00. Two of the members have a full time job; the other one has a part time job in the afternoon session.

3. Generating a Typical Load Profile

A typical load profiles for UK average size households using different scenarios have been performed. The daily electricity consumption load profiles of electric appliances have been calculated for a winter and summer seasons

The calculation of daily energy-consumption of each appliance can use the following equation:

$$E_a = N \times \sum A \qquad (2)$$

Where $\boldsymbol{E_a}$ is the daily energy-consumption of household delivered by appliances; N is the number of occupants and A is the appliance energy consumption per capita.

3.1 Allocation of Households

In order to allocate a number of different household types which represent the community, the number of houses was assumed based on the national UK household percentage share, then the number of households for each household type was calculated.
The number of houses is allocated randomly and assumed to be equal 400. Table 5 lists the projected number of households of the assumed community.

Table 5 the projected number of households

Type of household	**Percentage Share**	**Projected No. of household**
Single adult	15%	60
Single retired Adult	15%	60
Two adult	29%	116
Two adult with children	21%	84
Two retired	6%	24
Three adult or more	14%	56
Total	100%	400

3.2 Time of Use Probability Profiles

In order to create sensible load profiles, knowledge of occupancy patterns is required. The occupancy information was limited, so simpler assumptions have been made for each scenario. Although the demand for appliances (refrigerators and freezers) normally varies during the duty cycle of the appliance, the assumption of constant load is assumed to be sufficiently accurate, the remaining appliances will have discrete events where the device is switched on and utilised. The usage Pattern and Probability of Occurrence of each appliance was distributed randomly based on the occupancy period. The lighting was dealt separately.

3.3 Electricity Demand Profile Generator

The random profile generator is an Excel program that aims to simulate the random action of the household at half hourly basis in order to generate electrical load profiles that match the consumption target. The electricity demand profile generator is based on probability that enable us to predict the possibility of each consumer to operate a number of appliances on a certain time of the day for different occupancy types by describing the behaviour of each appliance by a normal distribution probability between (0& 1).
Each appliance's random profile for each scenario will be generated using Random Number Generator technique (RNG). The aggregation of random profiles for all appliances will generate a daily electric appliances load profile for a known scenario. The daily appliance energy consumption for different occupancy scenarios can be calculated at half hourly basis based on the information of daily average end use electric appliance energy consumption for an average size household, per capita daily energy-consumption and the ownership

level. An Excel program is developed in order to generate the electricity demand profile for different household types. Fig 1 shows the framework of generating the community load profile. The inputs of generating the domestic load profile are:

- Daily energy-consumption for each appliance;
- Ownership of each appliance;
- Occupied period.

The load profile for the whole community was calculated using the equation:

$$Load_{community} = \sum_{j=1}^{6} E_{aj} \qquad (3)$$

Where; $Load_{community}$ the load profile for the whole community; $\boldsymbol{E_{aj}}$ is the half hourly load profile of household of type j. Fig 1 shows the framework of generating a typical community load profile.

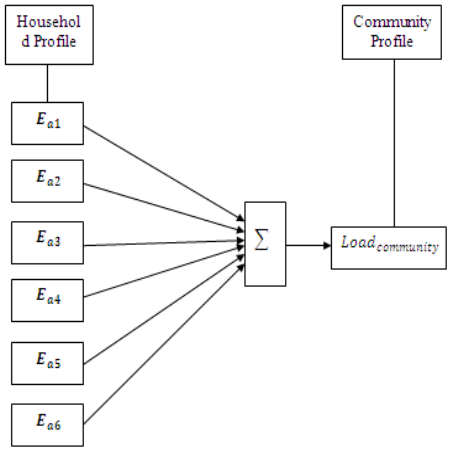

Fig 1. Framework of producing a typical community load profile

3.4 Results of Modelled Data

A typical load profile for UK households for different common scenarios has been performed using the mentioned method. The daily energy-consumption load profiles of electric appliance and lighting loads have been calculated individually for a winter and a summer weekday case. The total daily electricity demand profile for the community is generated by aggregating the load profiles of the common six scenarios.

The average half hourly daily consumption for a single household ore each household type(scenario) is calculated by dividing the total electricity consumed by the entire number of households for each scenario at a specific time by the total number of households for the same scenario at the same time.

The average load profile for a single household for the six scenarios is calculated by averaging the summation of the averages of all scenarios. The modeling results of the half hourly daily electricity consumption load profiles for a single adult household excluding and including lighting for winter season, The modeling results of the half hourly daily electricity consumption load profiles for each household type, the total half hourly daily electricity demand profile for the community and the average hourly daily consumption for a single household are shown in fig 2, fig 3, fig 4 and fig 5 respectively.

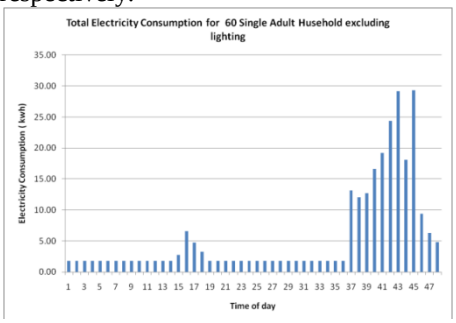

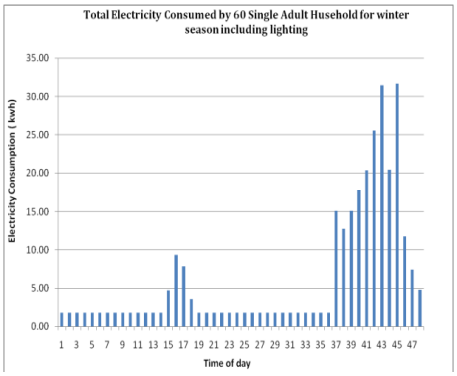

Fig 2. Daily electricity load profile for single adult households

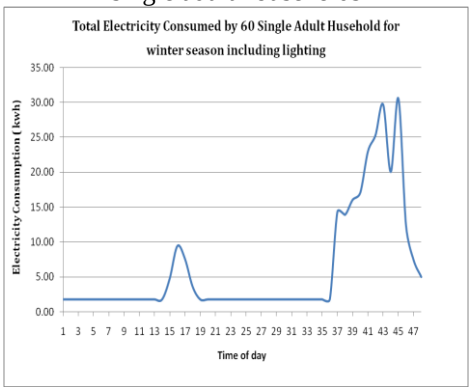

(Scenario 1)

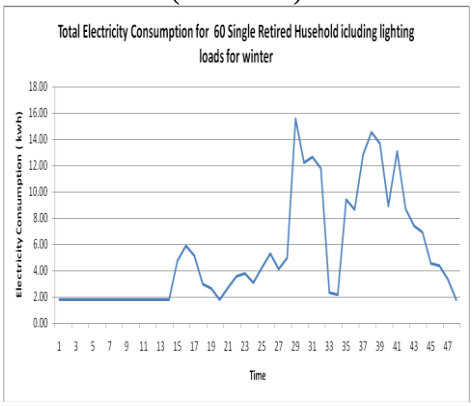

(Scenario 2)

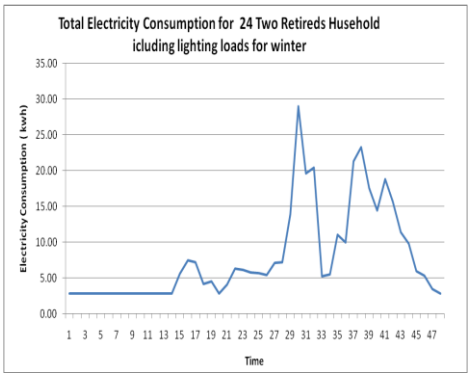

(Scenario 3)

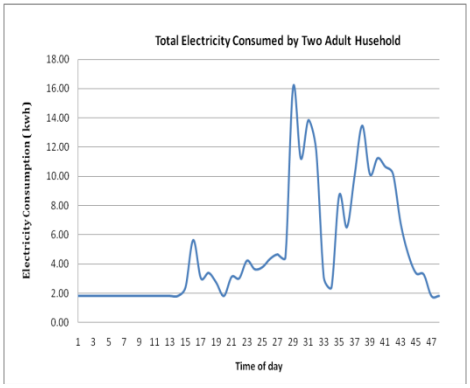

(Scenario 4)

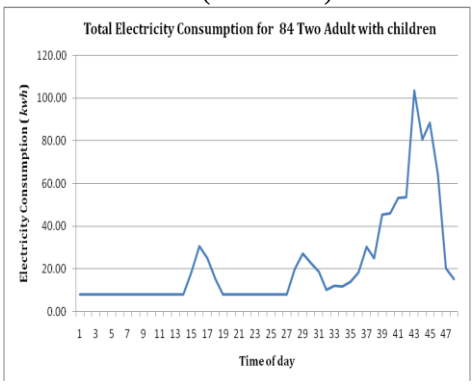

(Scenario 5)

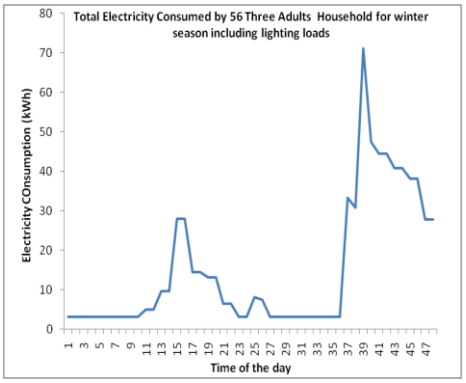

(Scenario 6)

Fig 3. Daily electricity consumption load profiles for each household type.

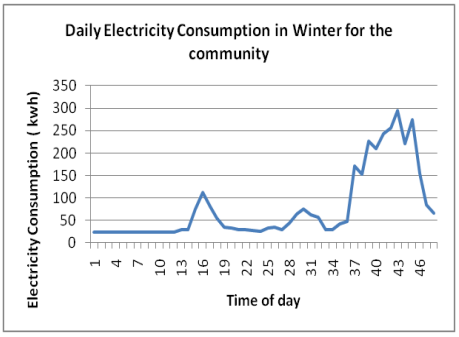

Fig 4. Daily Electricity Consumption in winter for the whole community

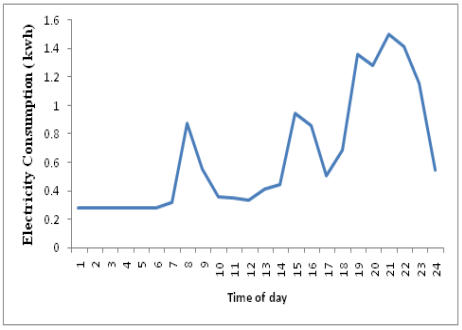

Fig 5. Average hourly daily consumption for a single household

4. Comparison of Generated Profiles with Measured Data

During the period between December 2003 and February 2004, Yigazw G. Yohanis and others performed electricity measurement using a half-hour load meter for 27 dwelling in Northern Ireland to obtain an understanding of how occupancy and dwelling characteristics affect domestic electricity use [6]. When compared the average daily consumption for one household for the six scenarios (fig.5) with the average daily annual electricity consumption measured by Yigazw [6], we can note that, there is a good agreement between the both curves and the general patterns are still clearly captured by the model, for example, the minimum consumption is occurring between 1.00 and 6.00 am (unoccupied periods), for the latter the consumption is almost the same from about 9.00 a.m. to mid-night. The maximum consumption is occurring between 18.00 and 22.00. The average daily electricity consumption from the generated model data is about 11 KWh in the winter season, and about 13 KWh from a national load profile [3]. The profile from modeled data is slightly lower than the national profile; because it is related only to the domestic appliance and does not include the space heating and hot water systems load (the assumption is that they are provided by means of natural gas).

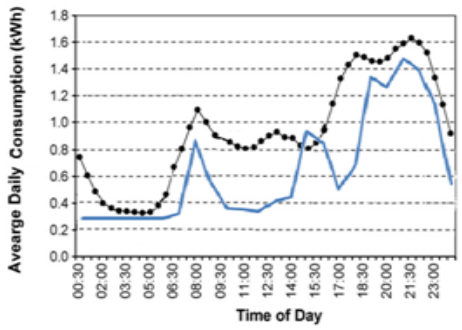

Fig 6. Comparison of the hourly load profile

5. Conclusion

This paper presents a method of generating realistic electricity load profile data for the UK domestic buildings. This method is based on the information and results of previous investigations and works that is available in public reports and statistics.

Six scenarios which present the behavioural characteristics and common occupancy pattern in the UK households have been proposed to regenerate the diversity in electricity consumption between households. The half hourly daily load profiles for assumed community of 400 households have been generated for the various scenarios and then the average electricity consumption for individual house has been calculated. The generated load profiles show a good agreement compared with the UK households load profiles.

This method has allowed the creation of typical seasonal and lifestyle activity profiles from statistical data. These profiles could be useful for predicting the future electricity demand. The daily load profile from individual dwelling to community can be predicted using this method. The analysis shows the power requirements of each electrical appliance and helps to determine the suitability of applying renewable energy.

References

[1] M. Newborough, P. Augood, Demand-side management opportunities for the UK domestic sector, IEE proceedings generation transmission distribution, 1999, 283-293

[2] I. Mansouri, M. Newborough, D. Probert, Energy Consumption in the UK Households: Impact of Domestic Electrical Appliances, Applied Energy 54 (3) (1996) 211-285

[3] R. Yao, K.A. Steemers, A method of formulating energy load profiles for domestic buildings in the UK, Energy and Buildings 37 (2005) 663-671

[4] N. Kreutzer ، I. Knight, Social housing electrical energy consumption profiles in the United Kingdom, submitted to Energy and Buildings (2007).

[5] J.V. Paatero, P.D. Lund, A model for generating household electricity load profiles, International Journal of Energy Research 30 (5) (2006) 273–290.

[6] Yigzaw G.Yohanis, Jayanta D. Mondol, Alan Wright, and Brian Norton, Real-life energy use in the UK: How occupancy and dwelling characteristics affect domestic electricity use, Energy and Buildings 40 (2008) 1053–1059.

[7] P. Bennich and A. Persson, proceedings of the Methodology and First Results from End-Use Metering in 400 Swedish Households Energy Efficiency in Domestic Appliances and Lighting (EEDAL) conference London (June 2006).

[8] Social trends, No. 39-2009 edition, Office of National Statistics, Available at:http://www.statistics.gov.uk/ theme_social/Social_Trends39/Social_Trends_39.pdf.

Functionality Evaluation of the SCADA/DMS for the Libyan

Distribution Electric Network

A.M. Gumaidh, A. Almndls, and H.Swayah

The General Electric Company of Libya (GECOL)

Gumaidh@Lycos.com

ABSTRACT:- *GECOL is a state owned company in charge of the generation, transmission and distribution of electrical power for the entire country of Libya. Today, GECOL: peak demand 5282MW (Sept. 2009). Following its strategy to invest and modernize its electric network, GECOL commissioned in 2010 its new Distribution Control System, delivered and installed by Siemens. This new control center system combines in the same SCADA/DMS (supervisory control and data acquisition/distribution management system), the monitoring and control facilities for the entire network, from medium voltage 30/66kV substations to distribution feeders. This is a real-time information system for all operation activities in a modern distribution control room. It improves the information made available to the operators, field crew personal, customer service representatives, and, ultimately, to the end customers. Nowadays, control and supervision is not anymore an isolated activity, but has to be performed aligned with corporate function of planning, assets inventory, maintenance, and customer management. It is within this context that GECOL is running new distribution control centers, located at different sites within the country and with a complete SCADA/DMS/NA functionality. The paper deals with the development of an interface between a SCADA/DMS system and electric network components. The capability and applications functions that are supported by the system are explained and broadly discussed. It also aimed to share the collaborative experience and present key features of this successful project implementation. Finally the paper discusses the benefits envisioned by GECOL when operating their network with this new system and the short-term network and system evolutions perspectives.*

Introduction

Distribution Automation and Management System provides modern tools for the distribution power network's security and economical operation. It guarantees power quality, perfecting facility management as well as increasing working efficiency and providing a series of solutions for the distribution automation system, [1]. SCADA systems are globally accepted as a means of real-time monitoring and control of electric power systems, particularly

generation and transmission systems. RTUs (Remote Terminal Units) are used to collect analog and status telemetry data from field devices. SCADA software and operator GUI (graphical user interface) are engineering applications that act on the data, historian software, and other components. DMS functionality is relatively new; DMS also extends to the efficient management of planned work and normal electrical operations. DMS is also typically associated with receiving real-time status and analog points from the distribution system, and the generation of supervisory control commands to distribution breakers, switches and recloses, switched capacitor banks, voltage regulators, and load tap changers (LTCs). The importance of DMS will increase as additional amounts of customer generation, energy storage, and demand response are placed on distribution systems. DMS is receiving a lot of attention because it can provide solutions to many challenges that distribution organizations face today. Table 1 below contains a listing of DMS applications, functionality and benefits.

Table.1 Indicates the Application, Functions and Benefits of DMS Systems

Applications	Functions	Benefits
Load Flow Analysis	Determination of Currents and Voltages per Phase for the entire N.W	Improve; awareness, asset utilization, contingency planning.
Load Allocation and State Estimation	Telemetered or Historical measurements and calculation of power flows	Improve load flow & State estimation calculations Notification of Voltage violation
Fault Location	Identifying of fault locations	.Improve Crew efficiencies
Switching Restoration	Establishing Isolation and Restoration Schemes	Increase Reliability and Operation Efficiency.
Control of Volt/VAR	Monitoring and Control of Capacitors bank, Regulators to reduce System Losses	Improve Voltage Profile and reduce Customer demand at Peaks.
Line Unloading	Calculation of load Transfer Options and Overload Reduction	Longer Equipments Lifetime and Higher assets Utilization.
Remote Switching	Feeder Reconfiguration	Reduce System Losses

In order to gain full benefits of the installed SCADA/DMS system, GECOL has digitally upgraded its protection and substation equipments for the entire distribution electric network, this is briefly described below.

1.0 Digital Adaptation of Substations

With the developments of computer technologies and electric technologies, the real-time and reliable network communication technologies satisfying the requirements of protective functions and the electronic technologies adapting to instrument transformers, switches and server environment has become mature. A digital substation means a substation whose information acquisition, transmission, processing and output process has been completely digitalized, [2]. Therefore the substation adaptation work needed is to introduce the concept of integrated protection and control for each bay where each bay will have feeder manager "FM" which will be responsible of all protection and data acquiring, also a distance digital protection relays were utilized for feeders and differential digital protection relay for transformers, those devices (FM and digital protection relays) were connected through standard IEC protocol to a RTU to gather all required data for the relative DCC data exchange.

1.1 Digital Protection Relays

Traditional distribution electric network (DEN) systems comprised of a huge number of distribution command panels with built-in switches, instruments, and buttons and light boards. Sum of interlocking and control functions were done with separate subsystems. An overall remark for those systems was that there were a lot of protection, control and monitoring subsystems running, a lot of wiring made introducing a demanding maintenance. So complex systems were requesting space what resulted in construction of large buildings. Any substation adaptation or reconstruction work to be done was a big problem due to the fact that works would effect a lot of subsystem, [3].

New types of protection relays (devices with a microprocessor) did solve a lot of practical problems from the past and introduced a lot of new features. With their open architecture they have enabled parallel operation with the relays of different manufacturer and operation with existing, classic protection devices. New types of protection relay are used for the protection, control, measuring and supervision of medium voltage networks. Having a CPU as the most important part, a lot of advanced functions are controlled and monitored by software modules supporting their open architecture. A block diagram of substation SCADA sub-system is shown in figure.1

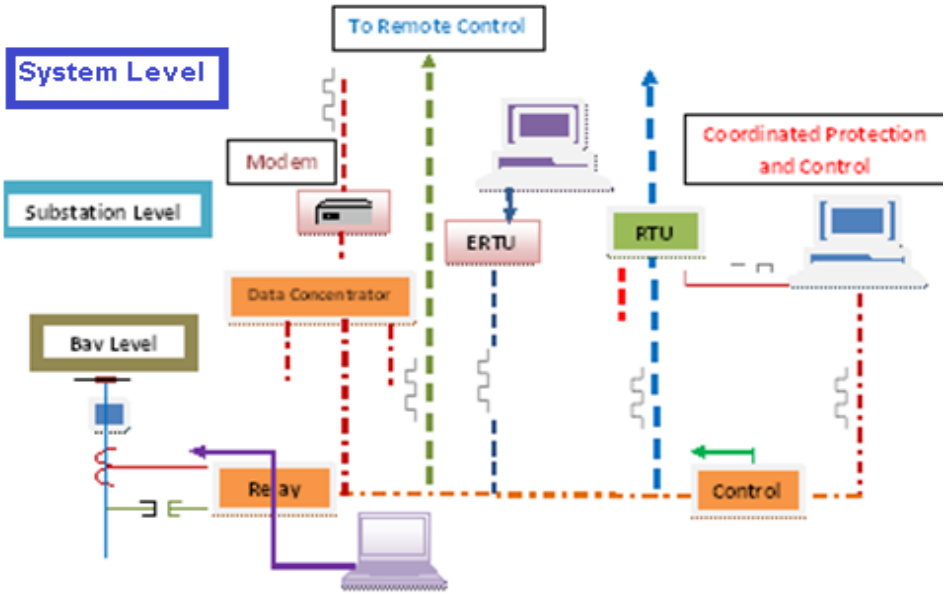

Fig.1 Block diagram of a SCADA system incorporating numeric relays

2.0 System Hardware Configuration.

The SCADA/DMS hardware configuration is based on a redundant high speed Ethernet LAN, where all servers, workstations and other peripheral equipment (printers, video-projector…) are connected, [4]. A full Windows configuration was chosen, using windows operating systems on all the servers and work stations. This hardware configuration includes the following building blocks:

- Two SCADA/DMS servers running in hot-standby mode, dedicated to the SCADA/DMS functions and to the server part of the User Interface Subsystem.
- One Historical server dedicated to the long term archiving. This includes a total capacity of around 300 GB.
- One Development server, being the repository for the whole system (Database, Displays, Source Code). From this server the system can be 100% re-built and delivered.
- Two Front-End computers, running in load-sharing mode, in charge of the management of the communication links with the RTUs.
- Workstations (Operator and Engineer Consoles).

In addition, the following LAN/WAN and peripheral equipment are used:

- Printing equipment (B&W and color laser printers).

- Two LAN switching equipment, allowing up to 24 Ethernet connections each.
- One Firewall Router allowing a secure connection with GECOL corporate LAN.
- One VPN router for remote maintenance purpose.
- One GPS clock distributing accurate time to all Servers & Workstations.
- A complete video-projection system allowing to call-up SCADA/DMS displays from any workstation on the wallboard.

The following diagram, figure.2 provides a graphical summary of this hardware configuration.

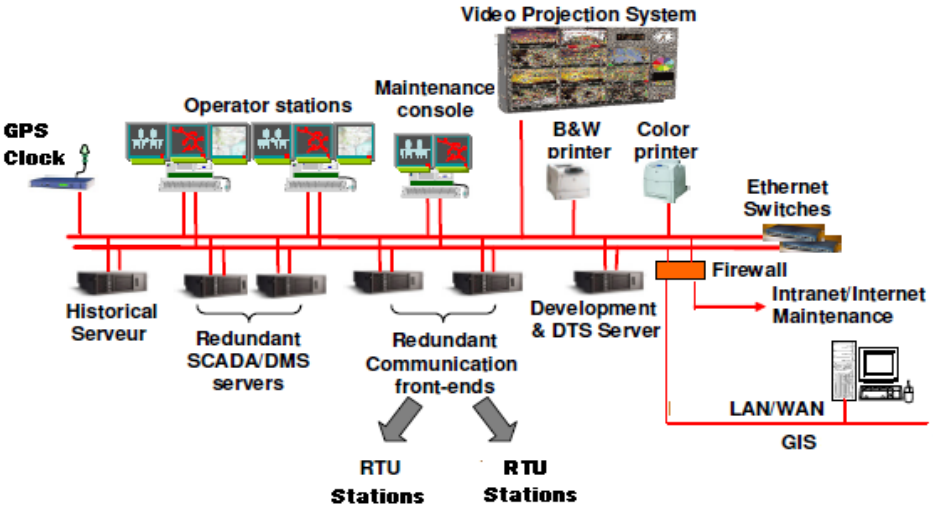

Fig.2. Represents the System Hardware Configuration

The SCADA/DMS system, provides in the same user interface the capabilities to annotate the network with tags, to follow up work which is done in the field, and to issue remote control operations.

3.0 Graphical Modeling Tool

After initial database conversion a Graphical Modeler was installed and used as central modeling tool for distribution network portions. This graphical tool allows editing and maintaining at the same time SCADA data, network data, and graphical diagrams representing the network, see figure.3. The network is divided into pieces called sub-networks. Each sub-network is covered by one graphical modeler source file. Each source file can be edited separately allowing multiple operators to work in parallel.

The graphical modeling environment uses a library of predefined symbols used by the operator to build the diagrams. Figure.4 represents an example of sub-network for

Tripoli's Distribution Control Center (DCC). Operators maintain database and displays by update drawings of the network, using drag/drop to create new components, and edit the connectivity graphically, thus avoiding errors. Connectivity is maintained while objects are moved around in the graphical environment. Automatic routing facilities with various options are available for these connectors. Once the model is complete, appropriate tools are available to populate the on-line environments with updated data and displays.

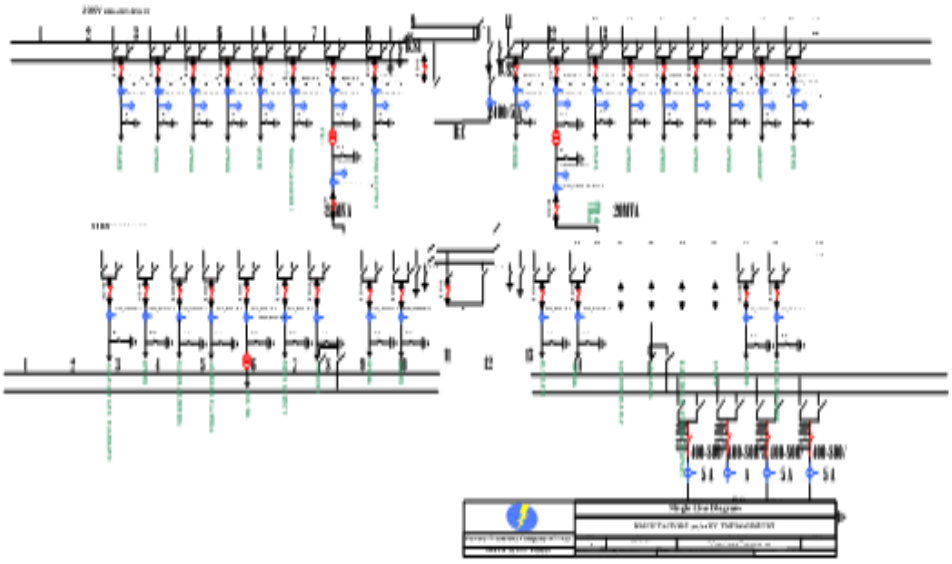

Fig.3. Representation of substation's single line diagram

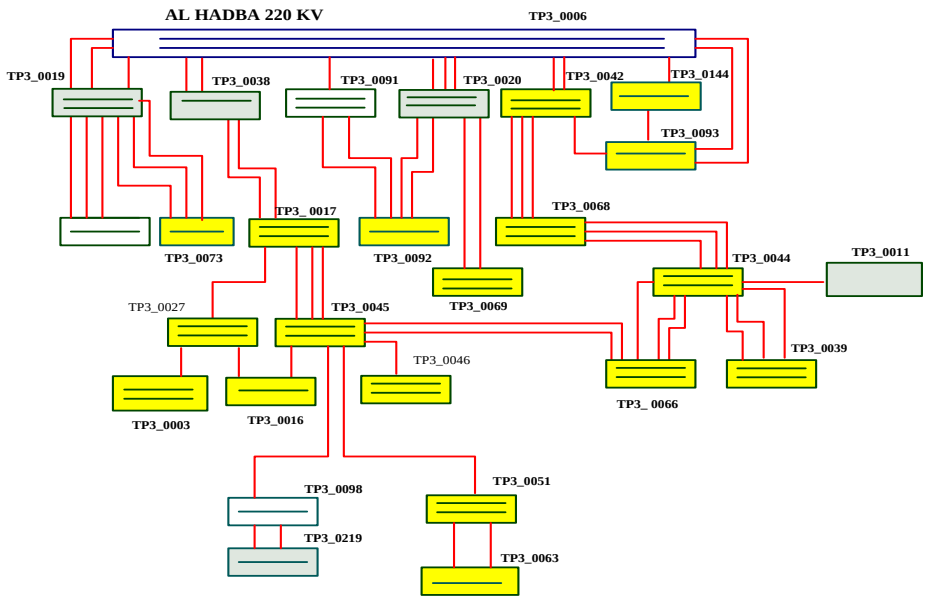

Fig.4 Shows an example of of sub-network for Tripoli DCC.

4.0 System Output and User Interface

Graphical User Interface (GUI) software running on the work station is designed to leverage the same user interface and is used for SCADA and DMS functions. The SCADA/DMS system provides the latest Web technologies and provides the best integration with the Windows environment. It provides all the features expected from a modern GUI software, like multiple viewports management, easy configuration and call-up of pre-defined display arrangements (rooms), pop-up pictures, pull-down menus, multiple fonts, efficient panning and zooming, support for scripting, etc…

In the same user interface the capabilities to annotate the network with tags, to follow up work which is done in the field, and to issue remote control operations, figure.5 show a snapshot of the system output.

5.0 Telecommunication Network and protocols

Data acquisition system is composed of a set of hardware and software connected together and supporting the transfer of information from the field equipment to the control centers:

- Two SCADA/DMS servers (master and standby), supporting the real-time database and data exchange with operators consoles.
- Two communication front end servers connected on the same LAN. These front-ends are responsible for the data polling of the various RTUs.
- Telecommunication lines :
  - Optical Ground Wire (OPGW)

- Under Ground Fiber Optic (UGFO)
- Power Line Carrier (PLC)
- Various types of Remote Terminal Units (RTUs) already installed in primary stations and small feeder RTUs in MV/LV kiosks.

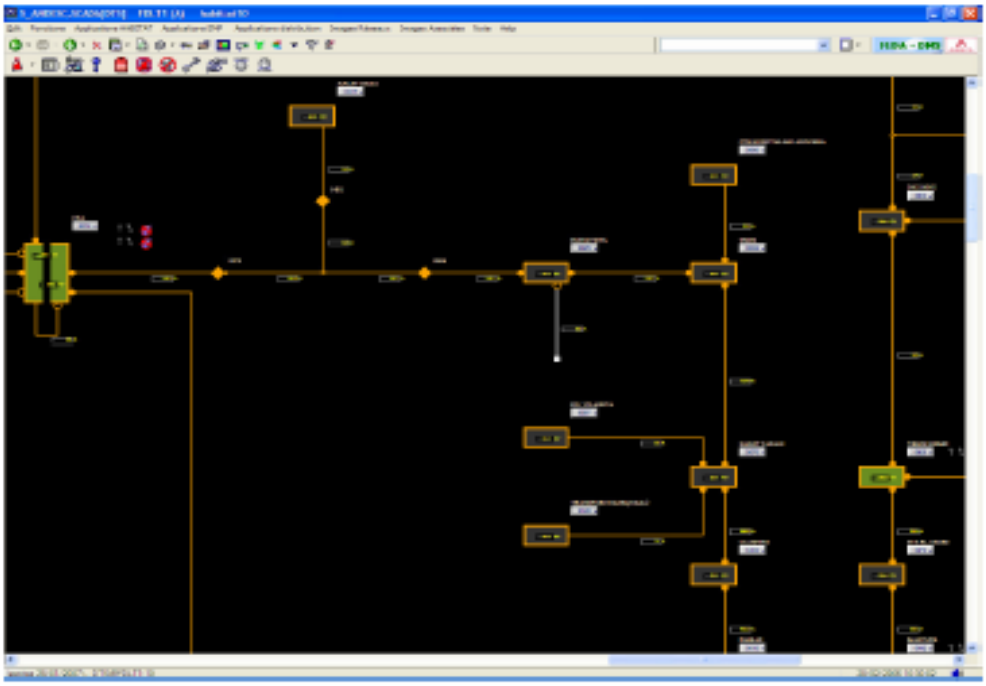

Fig.5 Shows a Snapshot of system output (User Interface).

In this system architecture, main SCADA/DMS servers are managed independently from the communication servers. RTU polling task is downloaded to the communication front-end equipments. The core application within front end processors is a powerful server whose main purpose is to distribute communication processing and to allow management of RTU. VoIP technology was considered when implementing the overall communication system, [5].

Conclusion and Remarks

GECOL derives several gains from this new unified system. Improved operation as it covers both transmission and distribution network and simplified configuration and extension. In addition, GECOL benefits from the load flow calculation which allow save operation and closer to the limits. This will help to solve a situation where network extensions of 11% to 13 % per year are scheduled. GECOL will also benefits from

the Dispatching Training Simulator (DTS), which is used to train operators and also for network model updates preparation and analysis. The system has now been used for several months to GECOL satisfaction, and a number of further evolutions are being discussed. Implementing state-of-the art solutions will enable the utility to meet all customer services challenges. Operators accepted well the new DCC system. An efficient and intuitive user interface helped them to quickly get familiar with the system's functionality. The use of dynamic network coloring functions of temporary modifications and tags has stimulated their interest in the system, bringing them a clear operation view of their network. To make full use of SCADA/DMS functions, the developed system should be interfaced to spatial data produced by GIS system.

References

[1] ***Mäkinen A., Järventausta P., Verho P, Rinta-Opas A.***, *Comprehensive Development of Power Quality Management and Evaluation Of Voltage dip problems. Proceedings of the 17th International Conference On Electricity Distribution (CIRED 2003), Barcelona, Spain.*

[2]. ***A. M. Gumaidh, J. M. fathalla and A.M. Yahya***, *Advanced Distribution Automation System for Electric Utility, ICEE'09 3rd International Conference on Electrical Engineering Algeria 19-21 May 2009* .

[3]. ***S. Micin*** , *Application Of Numerical Relay For Protection Elements Of Power System, University of Novi Sad, FTN, Novi Sad, Serbia, 2006;*

[4]. ***D. Popovic, R***. *Memarovic: Design Of Integrated Data Base For Distribution Management System, UPEC – Thessaloniki, Greece, 1 – 3 September, 2003;*

[5]. ***A .M. Gumaidh and etl***, *"Telecommunication Infrastructure for Power Control and IT Networks "The Arab Electricity Journal, No.13.May.2007 PP.63-70.*

Chapter II

Automatic Control Systems and Engineering

Identification and Control of Nonlinear Systems Using Artificial Neural Networks (Radial Basis Function Network)

Tripoli - Libya

Amer Elhadi Elshibani

The higher institute soqalkamis - Electrical department

Amrrshibanii@yahoo.com

Abstract. The aims of this paper are the identification and control of non-linear systems using artificial neural networks (RBFN), and comparison between the PID controller and RBFN controller. The direct adaptive control method is considered in this work for controlling the non-linear dynamic models. Examples of identification and control the non-linear system will simulate and the results will discussed revealed that the response of the desired signal was fully dependent on the learning factor's value. The RBF network consists of one input layer, one output layer and only one array of hidden nodes called centers. The RBF network is a simple architecture and moreover, the training of the network is faster than the MLP network. One reason the RBF is very fast, is that learning is divided into two stages. Learning in the hidden layer selecting centers and widths and the learning in output layer for selecting the weights.

Keywords: Identification, Control, Non-linear Systems, Radial Basis Function Network (RBFN), Hidden layer, Centers, Widths, Learning.

1 Introduction

The RBF network used for identification and controlling of non-linear dynamic systems. This type of network consists of fully interconnected layers: one input layer, at least one hidden layer which have an activation function and one output layer. Various non-linear plants were tested and very good results were obtained. Three different plants will used as examples to show the properties of the RBF network. These examples have been chosen in order to get the accuracy of the RBF network. Fig.1 is a block diagram of a series-parallel model. The output of the plant and the network are compared and the resulting error is used to update the network parameters (centers, width and weights).

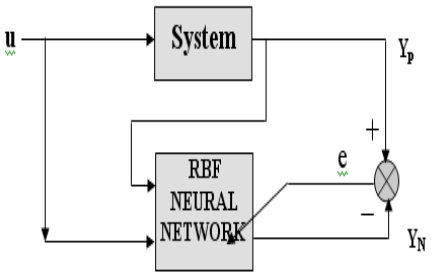

Fig.1 Series-Parallel identification schemes

The direct adaptive control method is considered in this paper for controlling the non-linear dynamic models due its simplicity and robustness, especially when the proper parameters are selected. One limitation which might affect the performance of the controller is the choice of the learning factor (η) which controls the convergence of the LMS algorithm.

2. Radial basis function network structure

The RBF neural network has a feed forward structure consisting of three layers as shown in Fig. 2.

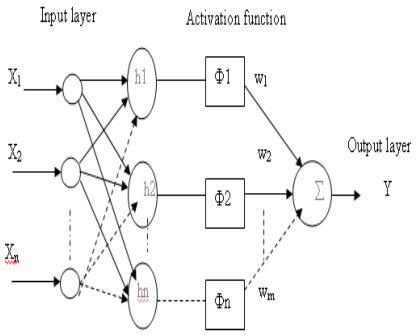

Fig.2 Radial Basis Function Structure

The input layer passes the input data to the hidden layer. The hidden layer consists of an array of nodes and each node contains a parameter vector called a center. The output layer is only a set of weighted linear combinations of the activation function. The only adjustable parameters• in the output layer are the weights. The output vector y is given by:

$$Y = \sum_{j=1}^{N} W_j \Phi_j \quad \text{-------- (1)}$$

Where (w_j) is the weight of the (j^{th}) node and (Φ_j) is the activation function. The hidden node calculates the distance between the center and the RBF network input vector, and then passes the result through the non-linear activation function (Φ) to the output layer.

The Gaussian activation function can be written as:

$$\Phi_{j(x)} = \exp\left(-\frac{\sum_{i=1}^{n} (xi - cj)^2}{\sigma j^2}\right) \quad \text{------ (2)}$$

$$i = 1,2,3,\ldots,n, \quad j = 1,2,3,\ldots,m$$

Where (Φ_j) is the output of the (j^{th}) unit in the hidden layer, (Xi) is the input data to the network, (c_j) is the center of the j^{th} unit in the input space, (σj) is the width of the Gaussian function, (m) is the number of centers and (n) the dimension of the input space.

3 Learning in the radial basis function network

The first learning stage involves selecting the centers and the widths in the hidden layer. The second stage is to adjusting the weights in the output layer.

3.1 Selection of the centers (c)

The clustering algorithm procedures are:

1. The objective of clustering algorithm is to categorize or cluster the data.

The classes must be found from the correlation of an input data set.

2. The clustering is a way of grouping similar patterns and separating dissimilar (different) ones.
3. Clustering in such a case involving identifying the number of classes and assigning individual datum membership of these classes.

4. The vectors in the same cluster are similar which means that they are close to each other in the input space.

The K-means clustering algorithm is used for selecting the number of the centers, this algorithm have been used in this work because of its simplicity and ability, to produce good results. To show the clustering results of this algorithm a hypothetical example is considered, with one input node, three centers and one output node. The input data shown in Fig.3 and the input data clustered as depicted in Fig.3.

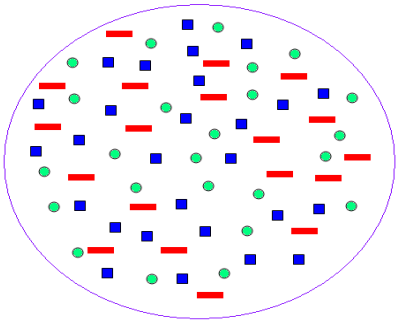

Fig.3 Input data

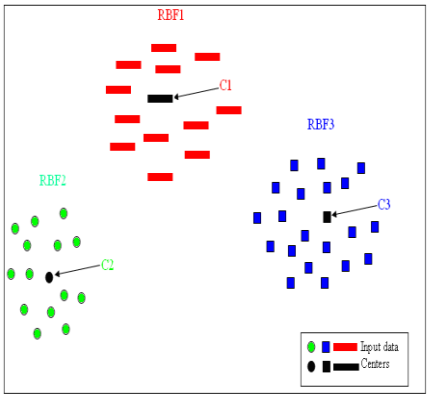

Fig. 4 Clusters data using K-means algorithm

3.2 Width selection (σ)

The most common method used is the Euclidean distance measure. This method is widely used because it is simple to calculate and more reliable. The shortest distance between vector X and vector C is the Euclidean distance which is defined as:
$E_{dist} = [\sum^{n} [xi - c_i]^2]^{0.5}$ …….(3) Where n is the vector dimension and E_{dist} is the Euclidean distance.

3.3 Output layer learning (Least Mean Squares method)

The LMS rule for adapting the weights:

1. Initialization of the weight vector.

$$\hat{W}_j(1) = 0$$

2. Calculate the network output.

$$\hat{W}_j(n+1) = \hat{W}_j(n) + \eta(y_d(t) - y(t))g_j(n)$$

Where *y(n)* is the output of the network, g_j are the Gaussian output, $\hat{W}_j(n)$ are the previous weights originally set to zero and $\hat{W}_j(n+1)$ are the updated weights

4 Identification of nonlinear systems

4.1 The plant considered for identification is a non-linear model (DC motor armature control) governed by the difference equation:

$$Y(k) = 1.885\, y(k-1) - 0.8868\, y(k-2) + 0.00009\, u(k-1) + 0.00000923\, u(k-2) \text{…….(4)}$$

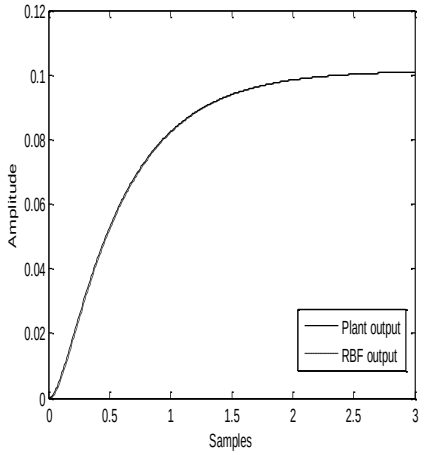

Fig. 5 Plant output, RBF output

4.2 The plant considered for identification is a non-linear model governed by the difference equation:

$$Y(k)=0.9847Y(k-1)+0.001527U(k-1) \ldots(5)$$

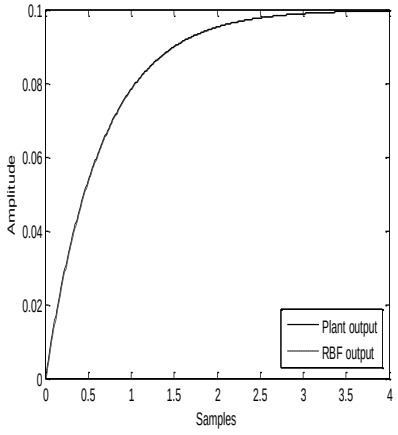

Fig. 6 Plant output, RBF output

4.3 The plant considered for identification is a non-linear model governed by the difference equation:

$$Y_p(t)=0.5y_p(t-1)+f[u(t-1)]\ldots.(6)$$

Where the unknown non-linear function has the form

$$f[u] = (u - 0.7)\, u(u + 0.3).$$

4.3.1 Testing the model using random centers

The centers of the radial basis function network have been set to a random and the width parameter (σ) has been set by a guess to a value of 1 and the weights were adjusted by least mean squares algorithm. The plant and the RBF output and the difference between them (i.e., the error term) are shown in Fig.7 and Fig.8, this error is very high and is due to inadequate selection of the RBF parameters. This procedure, therefore, is undesirable.

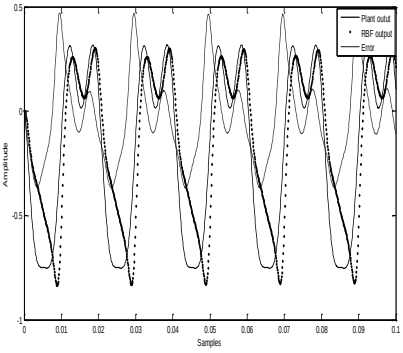

Fig. 7 plant output, RBF output and the error term

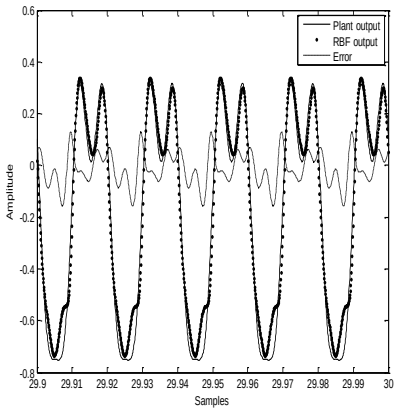

Fig. 8 plant output, RBF output and the error term after the weights were tuned

4.3.2 Testing the model using clustering centers

Here, the K-mean clustering algorithm was used to tune the centers, the $\sigma = \| C_i - C_j \|$ was used to compute the widths and the weights were adjusted by least mean squares algorithm. The plant and the RBF output and the difference between the net and the plant output signal (i.e., the error term) are shown in Fig.9.

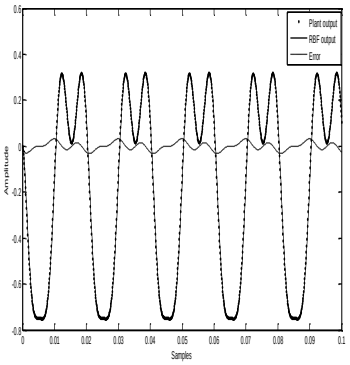

Fig.9 Plant output, RBF output and the error term

From the figure (9) we note that the error is very small due to adequate selection of the RBF parameters. This procedure, therefore, is desirable.

5 Nonlinear Systems Control using Radial Basis Function

The direct adaptive control (or the on-line) method is used to overcome the problems associated with the off-line approach. In this method, the neural network learns during the *on-line* feed forward control period. As shown in Fig.10, the controller network is placed in front of the plant, whereby the net output control signal $\hat{u}_c$ is an input to the plant.

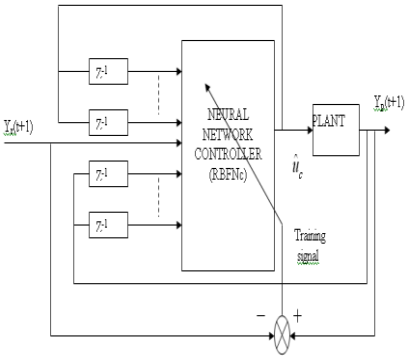

Fig. 10 Direct adaptive control configuration

The control signal can be realized as:

$$\hat{U}_c(t) = \mathrm{RBFN_c}[X^C(t)]$$

Where:

The desired reference signal $y_r(t+1)$ was used instead of the unknown $y(t+1)$, this can be rewritten as:

$$X^C(t)=[y_r(t+1), y(t), .., y(t-n+1), u(t-1), \ldots, u(t-m+1)]^T \quad \ldots..(7)$$

During the training of the network, the centers are assumed selected, presumed to have been prior to training and are given as

$Cji = [C_{11}\ C_{12}\ \ldots.\ C_{1n})]^T$ ….(8)

i = 1, 2… n & j = 1, 2… m

Where n is the network input space dimension and m is the number of centers (hidden units) with $m \leq n$. It is recommend that the width between the centers is also selected, remembering that the same number of centers and the width value obtained during the modeling are used for the purpose of controlling the system. Therefore, only the weights of the networks are adapted using the LMS algorithm to decreases the error between the reference signal $y_r(t+1)$ and the actual out put $y(t+1)$ in every iteration step.

After the learning process is finished, the connection weights between the output layer and the hidden units will have been adjusted so that $y_r(t+1) \cong y(t+1)$ The learnt inverse model may then be able to take a desired response and calculate an appropriate control signal $\hat{u}_c$,

$X^C(t)=[y_r(t+1),y_r(t),.,y_r(t-n+1),\ u(t-1),\ldots, u(t-m+1)]^T$…...(9)

The direct adaptive control method is considered in our work for controlling the non-linear dynamic models due its simplicity and robustness, especially when the proper parameters are selected. One limitation which might affect the performance of the controller is the choice of the learning factor (η) which controls the convergence of the LMS algorithm. Care must be taken by the user when selecting this value; the correct value can be selected according to the experience or by a trial and error procedure.

5.1 Simulation examples:

Here the centers and the width between the centers of the RBFNc are selected before training. By passing the training input signals through the selected 10 RBFNc nodes, the network controller is configured in the same way as shown in Fig. 11. Assuming the optimal width has been selected, and then the optimal output layer weights are found using the least mean square LMS algorithm. The weights vectors are initially set to zero and the learning factor is varied depending on the behavior of the desired input.

5.1.1 An electrical model (DC motor armature control)

The electric circuit of the armature and the free body diagram of the rotor are shown in figure (11).

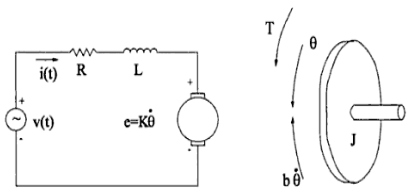

Fig. 11 The electric circuit of the Dc motor model

The system described by the following open loop transfer function:

$$\frac{\Omega}{V} = \frac{K}{(JS + b)(LS + R) + K^2}$$

We will assume the following values for the physical parameters:

The moment of inertia of the rotor (J) = $0.01\ kgm^2/s^2$

The damping ratio of the mechanical system (b) = 0.1 Nms.
The electromotive force constant K= 0.01 N m / Amp.
The resistance (R) = 1 ohm.
The inductance (L) = 0.5 H.
The input (V) is source voltage.
The output (Ω) is rotational speed (rad/sec).

5.1.1.1 Design requirements:
With an input voltage of 1 Volt, the steady-state error of the motor speed should be less than 1%, settling time less than 0.4 sec and no overshoot.

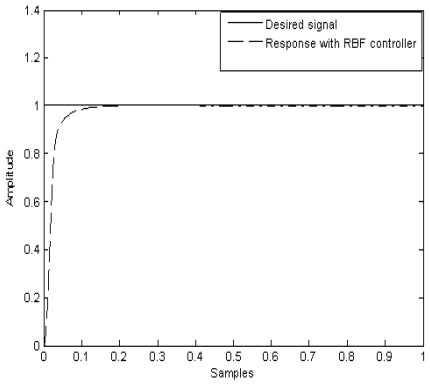

Fig. 12 Response of DC motor model (speed) with RBF and PID controller

As shown in figure (12), RBF controller satisfied the design requirements.

5.1.2 The system is subjected to some square wave set point.

The plant considered for controlling is a non-linear model governed by the equation:

$$(1 – 1.21 Z^{-1} + 0.374 Z^{-2}) Y(t) = Z^{-1}(-0.212 Z^{-1} + 0.269 Z^{-2}) g_u(t) \ldots\ldots\ldots\ldots\ldots\ldots\ldots\ldots (10)$$

Where $g_u(t)=3U(t)–0.315U^2(t)$.

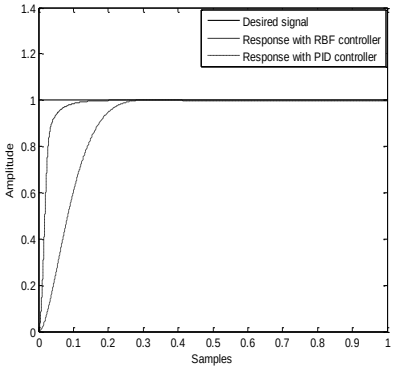

Fig. 13 Actual and desired signals

6 Comparison between the PID controller and RBFNc

The plant considered for controlling is a non-linear model (DC motor armature control) governed by the difference equation:

$$Y(k) = 1.885\, y(k–1) – 0.8868\, y(k–2) + 0.00009\, u(k–1) + 0.00000923\, u(k–2) \ldots\ldots..\ldots (11)$$

The design requirements for the DC motor model that has an overshoot less than 1%, the steady state error less than 1% and the settling time less than 0.3 seconds.

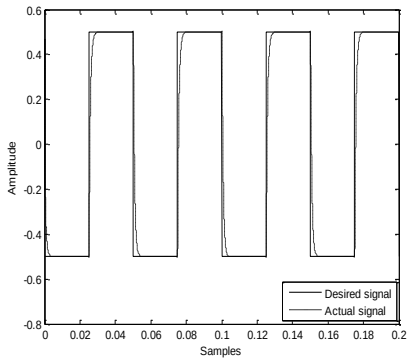

Fig. 14 Model response with PID controller and RBFNc

7 Conclusion

The Radial Basis Function Network (RBFN) is introduced on-line to identification and control of the non-linear dynamic systems, where the network weights were adapted using least mean squares method (LMS) and the network centers were selected using K-mean clustering algorithm. As a result, the on-line RBF algorithm is an effective algorithm for identification and control of nonlinear systems. Both controllers PID and RBF were satisfied the design requirements, but the RBF controller has fast response, good performance and ability in controlling of nonlinear system. The results have also shown that the on-line RBF neural network controller is an effective and robust algorithm.

8 References

[1] Haykin S., (1999), "Neural Networks, A Comprehensive Foundation", Prentice-Hall Inc, second edition.

[2]Sanchez J., (1996), "Adaptive Predictive Control", department of energy systems, Technical University of Madrid.

[3] Moody J. and C. Darken, (1989), "Fast learning in Networks of Locally-Tuned Processing Units", neural computation, Vol. 1.

[4] Fu L., (1994), "Neural Networks in Computer Intelligence", university of Florida.

[5] Bose K. N. and P. Liang, (1996), "Neural Network Fundamentals with Graphs,
Algorithms and Applications", McGraw-Hill series in Electrical and Computer Engineering.

[6] Hu H. Y. and J. Hwang, (2002), "Hand book of Neural Network Signal Processing", by CRC press LLC.

[7] Phillips L. C. and H. T. Nagle, (1995), "Digital Control System Analysis and Design", third edition.

[8] Jax I. and K. Jed, (1992), "Numerical Analysis", first edition.

[9] S◌oderstro◌m T. and P. Stoica, (1989), "System Identification", London.

[10] Mammone J. R., (1994), "Artificial Neural Networks for Speech and Vision", New Jersey, USA.

Identification of Nonlinear Systems using parametric and Non-Parametric Methods

Tripoli - Libya

Amer Elhadi Elshibani

The higher institute soqalkamis - Electrical department

Amrrshibanii@yahoo.com

Abstract. The aims of this paper are the identification of non-linear systems (a dual tank system) using parametric and non-parametric methods such as reaction curve method, over damped 2nd order system method, Auto-Regressive Exogenous (ARX) model, Auto-Regressive Moving Average Exogenous (ARMAX) model, Box-Jenkins (BJ) model, simple least squares (SLS) method and compare between them; and design a graphical user interface (GUI) to implement the results.

Keywords: System identification, Non-linear System, Parametric, Non-Parametric, Graphical User Interface.

1. Introduction

System identification is a problem that arises in many disciplines where a mathematical model is researched for a physical system; system identification is a basic problem in control theory, because in almost any application of control, the model is not completely specified. Since most processes in the real world are nonlinear to some extent, nonlinear models may be required to achieve acceptable prediction accuracy. From engineer's points of view, a good nonlinear modeling should have good model structure and good flexibility as well.

In recent years, there have been proposed many nonlinear modeling and identification methods. In this paper there is a good nonlinear modeling Box-Jenkins model. The goal of the identification is to search mathematical model of real plant, when we have a measured signal of the dual tank system, some parametric and non-parametric methods are applied on the filtered signal to obtain the mathematical model of the dual tank system.

2. Problem Formulation

The system in consideration consists of two interconnected water tanks linked together by an orifice. The water is fed into the system using an electrical water pump, the pump switched ON to move the water level in tank one to certain level. As a result, the water level in tank two will rise

with a certain rate until it reached a steady state level. The scheme of the system is given in Figure 1. The inlet water quantity is denoted by q_i, the outlet quantities are q_1 and q_2 respectively. The water levels are denoted by L_1 and L_2. The cross sections of a dual tank are A_1 and A_2. The cross sections of the tubes are denoted by R_1 and R_2.

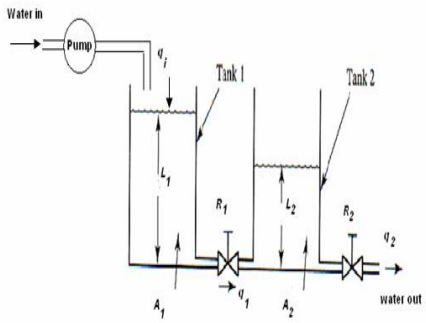

Fig. 1 Block diagram representing a dual tank system

The goal of the identification is to search mathematical model of a real plant. It is achieved by a step response. As input we have pump which works with the same efficiency during all the time. It simulates a step function. In output, we have level of liquid of tank two. As shown in Figure 2, two signals are obtained; the first one was the measured signal from the dual tank system. As we notice, the measured signal is noisy, in order to remove noise from the measured signal we have used polynomial curve fitting algorithm, In this case the seventh order polynomial is used which is quite good approximation as we can notice in second signal .

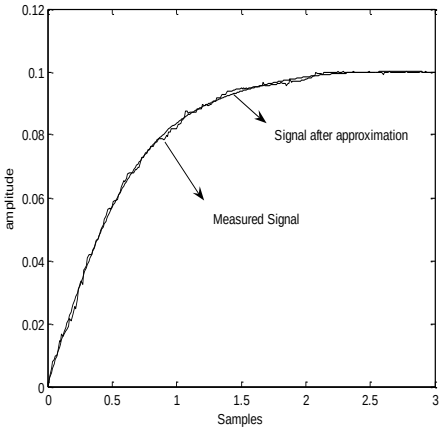

Fig. 2 measured signal from a dual tank system and signal after approximation

3. Identification of a dual tank system using Non parametric methods:

3.1 Identification using reaction curve method

Once the model structure is defined, the next step is to choose the correct value for the parameters using reaction curve method. Matlab program have been used to compute the reaction curve method, where step input is applied to the process and the output is recorded.

The step response of the process is shown in Figure 3.

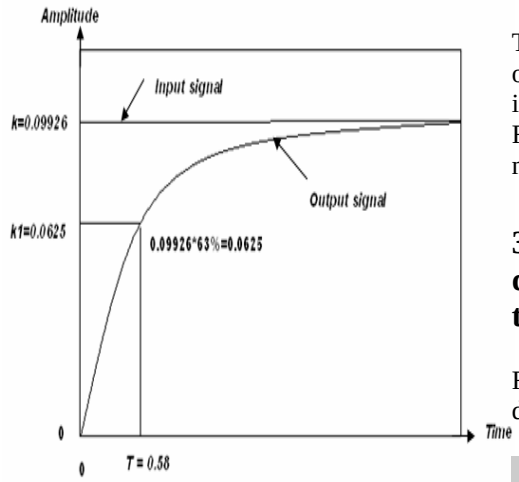

Fig. 3 Reaction curve method

The measured signal for a dual tank system and the model response which is identified by using reaction curve method are shown in Figure 4.

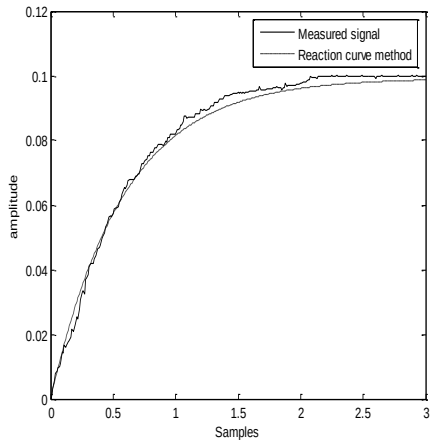

Fig. 4 meas. signal of a dual tank system and reaction curve method

Error is counted:

δ = measured signal – model response = 0.5722

The reaction curve method is probably one of the most popular methods used in industry for identifying objects. From the Figure above we see that the reaction curve method can describe the process dynamics.

3.2 Identification using over damped 2nd order system with no time delay

Figure 5 demonstrates a graphical method for determining the system parameters.

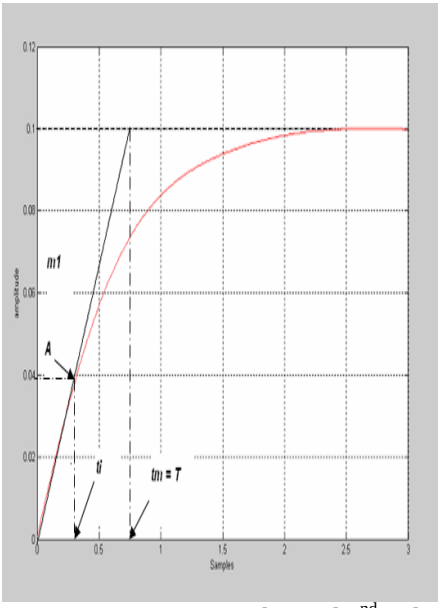

Fig. 5 over damped 2nd order system with no time delay

So, by using the Figure 5 and some procedures the model system parameters can be obtained and when the value of ζ near to zero and then reduce the system to first order system:

$$G(s) = \frac{K}{(1+TS)} = \frac{0.1}{(1+0.73S)}$$

The measured signal for a dual tank system and model response which is identified by using first order system is shown in Figure 6.

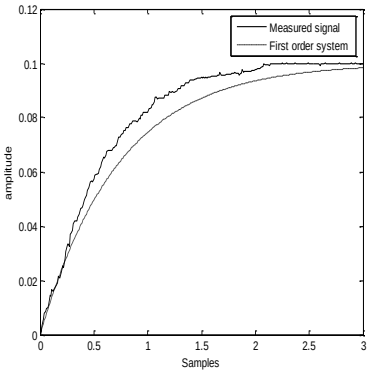

Fig. 6 meas. signal & 1st order model response

Error is counted:
δ = measured signal – model response = 1.6279

From the Figure above, this method can describe the process dynamics but it is worse than another identification methods.

4. Identification of a dual tank system using parametric methods:

4.1 Identification using autoregressive exogenous input model (ARX).

This section describes how identification of the dual tank system using ARX model, where the model is usually written as

$$A(z).(t)=B(z).U(t–nk)+d(t)….(1)$$

The measured signal for a dual tank system and the response of the model which is identified by using ARX model are shown in Figure 7.

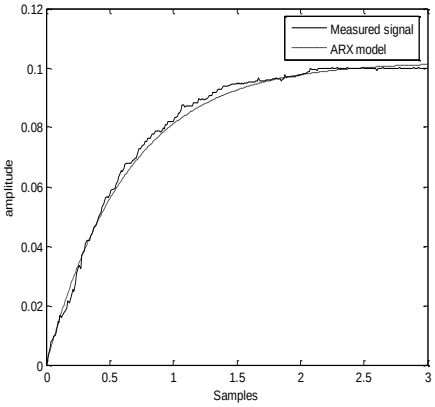

Fig. 7 meas. signal &ARX model response

Error is counted:
δ = measured signal – model response = 0.3974

From the Figure above we see that the ARX method worse the Box-Jenkins method (see figure 9), but it is better than another identification methods.

4.2 Identification using autoregressive moving average exogenous input model (ARMAX).

This section describes how identification of the dual tank system using ARMAX model, where the model is usually written as

$$A(z).Y(t) = B(z).U(t – nk) + C(z).d(t).....(2)$$

The measured signal for a dual tank system and the response of the model which is identified by using ARMAX model are shown in Figure 8.

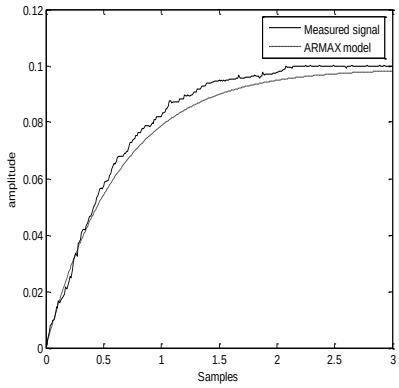

Fig. 8 meas. signal & ARMAX response

Error is counted:
δ = measured signal – model response = 0.9979

From the Figure above we see that the ARMAX method can describe the process dynamics but it is worse than ARX and Box-Jenkins methods.

4.3 Identification using Box-Jenkins model (BJ).

This section describes how identification of the dual tank system using Box-Jenkin model, where the model is usually written as:

$$Y(t)=B(z).U(t-nk)+\frac{C(z).d(t)D(z)}{F(z)} \quad \text{------ (3)}$$

The measured signal for a dual tank system and the response of the model which is identified by using Box-Jenkins model are shown in Figure 9.

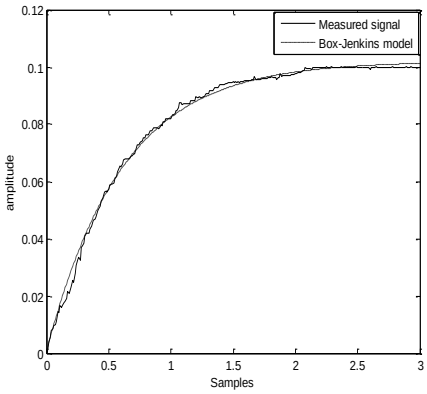

Fig. 9 meas. signal & B-J model response

Error is counted:
δ = measured signal – model response = 0.2973

From the Figure above, if we compare this method with others identification methods, it is better one.

4.4 Identification using simple least squares method (SLS).

Consider a real plant and it is mathematical model shown in Figure 10.

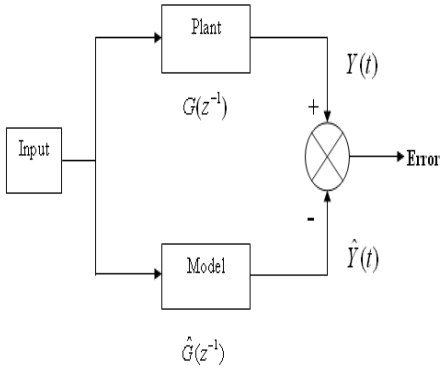

Fig. 10 Real plant and it is mathematical model

The real plant involves unknown aspects to the designer; it is a dynamics are expressed as G (Z^{-1}). Suppose that the plant dynamics can be approximated by the following transfer function:

$G(z^{-1})= \hat{Y}(z^{-1})/U(z^{-1})$ …….(4)

$Y(N) = \Phi(N)\,\theta + e(N)$ ……..(5)

Where:

- Y(N) is output vector
- Φ(N) is measurement matrix.
- θ is parameter vector to be estimated.
- e(N) is error vector.
- N is the number of data points.

The system considered is a dual tank system;
Let us assume second order model:

$$\hat{Y}_k = -a_1 y(k-1) - a_2 y(k-2) + b_1 u(k-1) + b_2 u(k-2) \quad (6)$$

Therefore a second order model can describe the process dynamics as shown in Figure 11, and the model that is used for controller design is

$$\hat{Y}_k = -a_1 Y(k-1) - a_2 Y(k-2) + b_1 U(k-1) + b_2 U(k-2) \ldots\ldots\ldots (7)$$

$$\hat{Y}_k = 0.74Y(k-1)+0.23Y(k-2)+ 0.2U(k-1)-0.18U(k-2) \ldots\ldots (8)$$

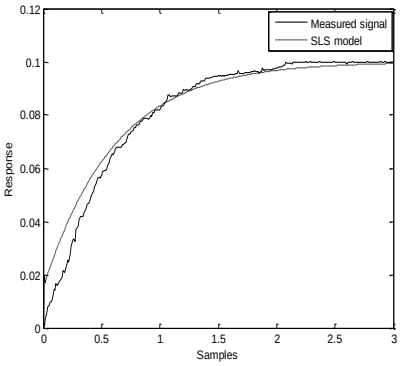

Fig. 11 meas. signal& SLS model response

Error is counted:
δ = measured signal – model response = 2.73

From the Figure above and error, if we compare this method with others identification methods, it is not good method for system identification.

5 Design a graphical user interface (GUI):

The components of the GUI such as buttons, text fields, sliders, and menus. When the GUI is designed, it should be intuitively obvious to the user how its components function; for example, when you change any value and click an OK button, your settings are applied and the dialog box is closed. Fortunately, most computer users are already familiar with GUIs and know how to use standard GUI components. When you run GUI and then click on the first part of GUI (Measured Signal & signal after approximation button) results as shown in Figure 12.

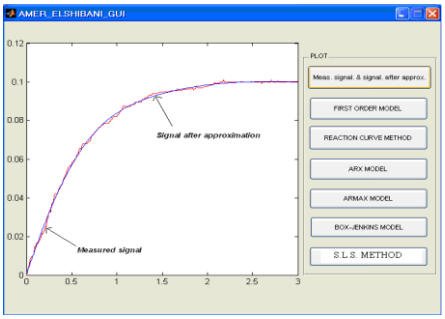

Fig. 12 GUI

6 Conclusion

In conclusion, the system in consideration was the dual tank system; the system exhibited the industrial processes. At the beginning of this paper, the data obtained from the dual tank system was filtered using polynomial curve fitting algorithm to remove the noise, and then two non-parametric methods and four parametric methods has been used in system identification, and then the response of Box-Jenkins (B.J) model shows the (B.J) model is an accurate method of modeling system behavior, that is mean when the results of these methods were compared; the winner was Box-Jenkins model.
The Graphical User Interface (GUI) has been used to implement and present the results of the identification methods, the GUI enable the user to operate the application without knowing the commands would be required by a command line interface.

7 Future Work

To get an in-depth view of system identification, more realistic view of the capabilities of system identification can be reached; in addition other models should also be explored, such as the Output Error (OE) and others.

8 References

[1] Sۏoderstroۏm T. and P. Stoica, (1989), "System Identification", Prentice Hall International, London.
[2] Pratap D., (1999), "A Quick Introduction for Scientists and Engineers", department of mechanical engineering Indian institute of science, Oxford University.
[3] Chi. T., (1992), "Analog and Digital Control System Design", State University of New York.
[4] Ogata K., (1997), "Modern Control Engineering", third edition Newcastle Upon Tyne, UK. Department of Electrical and Electronic Engineering.
[5] MATLAB 6.5.1 Release 13,(2000 – 2004), toolbox user's guide.
[6] Sanchez J., (1996), "Adaptive Predictive Control", department of energy systems, Technical University of Madrid.
[7] Jax I. and K. Jed, (1992), "Numerical Analysis", first edition.
[8] Leigh J., (1985), "Applied Digital Control Theory", design & implementation, second edition.
[9] Phillips L. C. and H. T. Nagle, (1995), "Digital Control System Analysis and Design", third edition.

Design and Simulation of an Adaptive Intelligent Control System for Direct Current Drive

Ali Madi*, Abduelbaset Goweder**, Abubaker Kashada** and Abdulmenim Guwaeder*

* Electrical Engineering Dept., Surman Institute for Comprehensive Professions Surman, Libya, Madi112003@yahoo.com. & N2730468@yahoo.co.uk

** Computer Engineering Dept., Surman Institute for Comprehensive Professions Surman, Libya, agoweder@yahoo.com & aokashada@yahoo.co.uk

Abstract: The paper presents an adaptive intelligent control method to overcome effects of some indeterminate and undealt factors that a DC .drive is suffered. In the speed loop, we use a three-layer neural networks through a backpropagation (BP) algorithm out of line learning to realize the fuzzy-control tactics. We use unit neuron through Hebb algorithm on-line dynamic learning to realize adaptive mechanism. The simulation is based on a MATLAB6.0 neural networks toolbox with simulink. The results of the simulation show that adaptive intelligent control method enables the system to have good dynamic and stability performance. The proposed method develops the use of simulink in the field of electrical drive of adaptive intelligent control.

Key words: DC motor, neural networks, and adaptive control.

1 Introduction

The performance of a DC drive system is effected by some indeterminate and undeal factors, for example, the changes of moment of inertia, the change of amplificative multiple for controlled object and driving device, etc. How does the Controller automatically change self-parameters to keep good performance of a system? One of many methods is to use adaptive intelligent control. In order to check correctness and effectiveness of the scheme, we use simulation experimentation. The senior

languages BC or VC can be used for our simulation. Also, we can use MATLAB directly for simulation. The paper uses MATLAB6.0 to realize Simulation.

2 Scheme Design of Adaptive Intelligent Control

2.1 Adaptive Intelligent Control System

The construction of adaptive intelligent control for a DC drive system is shown in Fig.1.

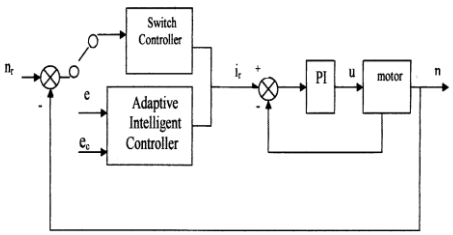

fig.1 DC drive System of adaptive intelligent control

controller with switch controller. When the motor is in starting stage, the switch controller acts on. After the speed reaches a given value, adaptive intelligent controller acts on.

2.2 The Construction of Adaptive Intelligent Controller

The construction of an adaptive intelligent controller is shown in Fig.2.

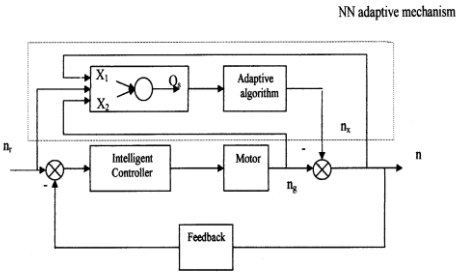

fig.2 Construction of adaptive intelligent controller

Where, intelligent controller is realized by fuzzy-neural networks controller (FNC),the adaptive mechanism consists of the neuron predictor, model-distinguish and adaptive algorithm.

3.2 Design of Adaptive Intelligent Controller

3.2.1 Intelligent controller

Intelligent controller uses a three-layer front neural network of 3-4-1 construction. Two inputs are the speed deviation (e) and the rate of the deviation (e_c). The output is current-giving value i_r. The neural networks determine their weight values through the BP algorithm out-line learning. The training data of neural networks are determinated by the system specifications following

performance and resist-disturbance performance through fuzzy control rules.

3.2.2 Adaptive Mechanism

Adaptive mechanism is the most characteristic part of all links for a DC drive system. Its main function is that the system can automatically change self-parameters and control rules to maintain high performance. For example, if moment of inertia is changed in a large scope, or mathematical models of controlled object is changed, output speed keeps unchanged. This function is not able to realize if only depends on the control of front-series controller (intelligent controller). Because the summarization and inference of mankind experience, dividing language variables into group, selecting membership function of language variables, learning of neural networks, etc. Can not avoid having large or small errors, during design and realization of intelligent ontroller. Therefore, control rules of intelligent controller can not suit controlled object. After introduced neuron adaptive mechanism, as the system operates, the models-distinguish is more and more approximative controlled object. Control rules are also modified more and more suitale to controlled object. So that, the system itself is able to regulate to satisfactory working condition.

Since adaptive mechanism uninterruptedly distinguishes controlled object on-line during system operation, selecting the construction of neural networks is required to suit working performance on line learning and to learn fast. Therefore, the system uses the neuron dynamic learning to realize distinguishing function on line. The construction of neuron predictor and model-distinguish is shown in Fig.3.

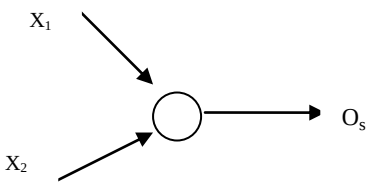

Fig.3. Neuron of adaptive mechanism

Where:

x_1, x_2: are the inputs of the neuron

O_s: is the output of the neuron.

We use linear simulative function. Its slope equals 0.1; its characteristic can be represented as:

$$\text{if} \quad \begin{cases} O_s=0.1(w_1x_1+w_2x_2) \\ O_s>1 \quad \text{then } O_s=1 \\ O_s<-1 \quad \text{then } O_s=-1 \end{cases} \quad (1)$$

Because the neuron of adaptive mechanism needs uninterruptedly learn on-line during system operation. The Hebb algorithm was selected as a learning supervisory algorithm.

$$\begin{cases} \Delta w_2 = \eta 2\,(d-O_s)\,x_2\,O_s \\ \Delta w_1 = \eta_1\,(d-O_s)\,x_1\,O_s \end{cases} \quad (2)$$

$$w_1 = w_1+\Delta w_1$$

$$w_2 = w_2+\Delta w_2$$

Where: d is ideal output of the neuron i.e. teaching signal; η_1, η_2 are learning factor.

The following equations describe the learning factors:

Working process is divided into distinguishing and modifying processes. For example, during the k order distinguishing process, input sample of the neuron is the speed $n_g(k-1)$ without adaptive control and the speed n(k-1), expectance output is the speed n(k). We use [n_g (k-1), n(k-1), n(k)] as training samples and use supervisory Hebb learning algorithm to realize dynamic study. In equations (1) and (2), we use $x_1=n_g(k-1)$, $x_2=n(k-1)$, d=n(k) instead. After dynamic learning, we can get modified weight values w_1 and w_2. Thus, the information of mathematic models about controlled object are kept in these weight values.

Modifying process is divided into two stages. Thus are predictive stages and error reverse-transfer stage, (or adaptive algorithm stage). For example, in predictive stage of the k order the neuron is in positive calculating condition

$$n(k+1)=0.1[w_1n_g(k)+w_2n(k)] \quad (3)$$

Where: n_g (k) is output of front intelligent controller; n (k) is the k-order speed output of the system.

In error-reverse transfer stage the output of adaptive mechanism is determinated according to predictive error between predictive speed n (k+1) and speed giving value n_r.

$$n_x=-0.1(O_s-d)\,w_1 \quad (4)$$

Where: O_s=n (k+1), it is predictive value,

$d=n_r$, it is speed giving value.

The final output of the K-order for adaptive intelligent controller is the sum of the k-order control value for front

intelligent controller and the k-order output of adaptive mechanism.

$$n(k) = n_g(k) + n_x \quad (5)$$

In summary, neural networks adaptive mechanism regulates control rules according to modifying the output of front intelligent controller. Thus, the design of adaptive intelligent controller is completed well.

3 Simulation for realizing control tactics

The requirement of dynamic performance for a DC drive system is to be as high as the development of science and technology. Thus, modern control technology is widely used in the field. Consequently, the paper uses adaptive intelligent control. The Simulink and neural networks toolbox based on MATLAB 6.0 plat form provide better environment for building models and simulation of complex and high-performance dynamic system.

3.1 Simulation Construction Drawing

A block diagram of the system simulation construction drawing of adaptive intelligent control in simulink is shown in Fig.4.

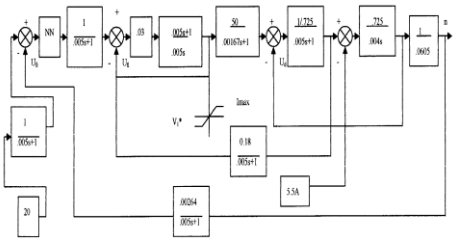

Fig.4 System simulation construction drawing

Building adaptive intelligent controller needs to design through neural networks toolbox and transfers into the model block in simulink environment. First, we use net= newff function to build three-layers front Bp networks of an intelligent controller, then we sequentially need to use net. train Parma. goal to establish training objective error, to use net=init (net), net=train (net, p, t) (where p,t is input and output sample vector data) to train neural networks. After finishing training, we use sim function and sample data to simulate trained neural networks. Finally, we use gensim function to transfer designed object of neural networks into simulink type.

In the same way, we can build the neuron of adaptive mechanism and transfer it into simulink type. Then, we

take simulink types of intelligent controller and adaptive mechanism to build subsystem in simulink, as neural networks model unit in Fig.4.

3.2 Simulation Results

We carried out the simulation corresponding to general PI control and adaptive intelligent control for speed controller under the following situations: Motor parameter

(as the resistance) changes from Ra to (1+10%)Ra, supply voltage changes from rated value U_N to 50% U_N, the load of the motor suddly changes from zero to rated value, speed giving value equals 3800rpm.

One Part of simulation curves are shown in Fig.5 and Fig.6

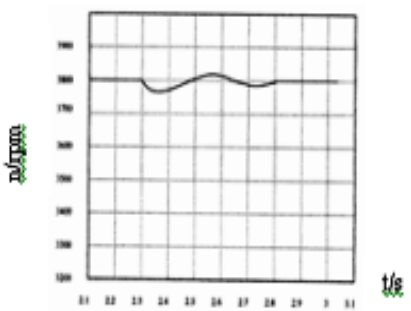

Fig.5. Speed simulation response in general PI control

t/s

(n_r = 3800 rpm, when t = 2.3 s , $\Delta T_L = T_{LN}$)

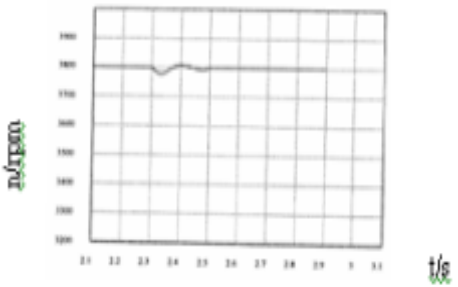

Fig.6. Speed simulation response in adaptive intelligent control

(n_r = 3800 rpm, when t = 2.3 s , $\Delta T_L = T_{LN}$)

Table 3.2 shows a comparison between PI control and adaptive intelligent control.

Table.3.2. Anti-interference Performance Comparison.

	PI control		Adaptive Intelligent control	
	ΔC_{max}(rpm)	t_f (s)	ΔC_{max}(rpm)	T s)
$\Delta T_L = T_{LN}$	28 rpm	0.49	9	0.19
ΔU_d=½U_N	10.36 rpm	0.21	4	0.1

Where: ΔC_{max} is maximum dynamic speed drop, t_f is recovery time.

The results of the simulation show that the speed of the motor can be kept in

stability level when operating conditions of the motor change. After we use adaptive intelligent control the system has better adaptive stability

The reason behind that is in PI control the parameters of speed regulator can not be changed with the changes of operating condition. While, in adaptive control they can automatically change. Because neural network has these functions which were trained before they are used as speed regulator. Except for this reason, attached component nx (refer to fig.2) can compensate the change of the speed deeply.

4 Conclusion

In this paper, neural networks toolbox and a simulink are combined to successfully carry out the simulation of an adaptive intelligent control method for a DC motor drive system.

The results of the experiments conducted in this research show that the adaptive intelligent control method used in a DC motor drive system has a high performance and the system keeps in a steady-state.

5 -Reference

[1] Fan Zheng-qiao Ma shutong. New control method of adaptive fuzzy-neural networks for Brush less D.C. Motor, Journal of Beijing University of Aeronautics and Astronautics Vo1.26 No.1, 2001,1: 34-37.

[2] C.B.Gray, Electrical machines and drive systems, John Wiley & son, jnc. New York, 1989.

[3] Sigeru Omatu, etc, Neuro-Control and its applications, Advances in industrial control, springer-Verlag London Limited 1996.

[4] Y.S. Dung, C.M. Liaw, and M . S. Ouyang, "Adaptive speed control for induction motor drives using neural networks", IEEE Trans. On Industrial Electronics, vol. 42, no.1, Feb. 1995.

Fuzzy PI- smith predictor process controller

A Tahir El Hashani , Shukri Doghman
High institute of industrial technology, Engila ,
thashani@yahoo.com sdoghman@hotmail.com

Abstract

Despite the PID controllers are the most popular controllers used in industrial control process. They don't perform well, or even failed to control the plant with significant time-delays. Consideration of this problem led to the development of predictive control strategies. Predictive control dose not mean a specific controller design, but it gives a set of ideas to develop control strategies. The predictive control technique that has the most attention in the control of long time delayed plants and used almost exclusively in the process industries is the Smith Predictor Controller.
The air-cooled heat exchanger system based on PI plus Smith Predictor Controller was implemented. Comparative evaluation with respect to classical PI and Fuzzy controls was presented to validate the controller design. The fuzzy controllers with seven membership function and forty nine rules were used as an attempt to observe the performance over the classical PI controller used. During design and evaluate the Fuzzy PI- Smith Predictor Process Controller with the effect process parameter uncertainties and/or disturbances, the fuzzy logic controller achieved much smoother response with higher accuracy. It proved better solutions and faster response over the conventional control design techniques. The simulation results are presented to test the robustness of each designed method used.

Keywords: *fuzzy control design, Smith Predictor Controller.*

1- Introduction

A fuzzy control system is a control system based on Fuzzy logic - a mathematical system that analyzes analog input values in terms of logical variables that take on Continuous values between 0 and 1, in contrast to classical or digital logic, which operates on discrete values of either 0 or 1 (true and false). Fuzzy logic is widely used in machine control. The term itself inspires certain skepticism, sounding equivalent to "bogus logic", but the "fuzzy" part does not refer to a lack of rigour in the method, rather to the fact that the logic involved can deal with fuzzy concepts - concepts that cannot be expressed as "true" or "false" but

rather as "partially true". Although genetic algorithms and neural networks can perform just as well as fuzzy logic in many cases (in fact, certain neural networks can be shown to be mathematically equivalent to certain fuzzy logic systems, fuzzy logic has the advantage that the solution to the problem can be cast in terms that human operators can understand, so that their experience can be used in the design of the controller. This makes it easier to mechanize tasks that are already successfully performed by humans. Fuzzy control is very simple conceptually. They consist of an input stage, a processing stage, and an output stage. The input stage maps sensors other inputs to appropriate at membership function, and truth values. The processing stage is based on a collection of logic rules in the form of IF-THEN statements, where the IF part is called the "antecedent" and the THEN part is called the "consequent". The output stage converts the combined result back into a specific control output value. Typical fuzzy control systems have dozens of rules.

The input variables in a fuzzy control system are in general mapped into by sets of membership functions similar to this, known as "fuzzy sets". The process of converting a crisp input value to a fuzzy value is called "fuzzification". A control system may also have various types of switch, or "ON-OFF", inputs along with its analog inputs, and such switch inputs of course will always have a truth value equal to either 1 or 0, but the scheme can deal with them as simplified fuzzy functions that are either one value or another.

Given "mappings" of input variables into membership functions and truth values, the microcontroller then makes decisions for what action to take based on a set of "rules", each of the form:

IF first input is large AND second input is not very fast THEN output is slightly decreased.

The two input variables that have values defined as fuzzy sets. The output variable is also defined by a fuzzy set that can have values like "static", "slightly increased", "slightly decreased", and so on. This rule by itself is very puzzling since it looks like it could be used without bothering with fuzzy logic, but remembers the decision is based on a set of rules:

All the rules that apply are invoked, using the membership functions and truth values obtained from the inputs, to determine the result of the rule. This result in turn will be mapped into a membership function and truth value controlling the output variable.These results are combined to give a specific ("crisp") answer, the actual output, a procedure known as "defuzzification".This combination of fuzzy operations and rule-based "inference" describes a "fuzzy expert system". Traditional control systems are based on mathematical models in which the control system is described using one or more differential equations that define the system response to its inputs. Such systems are often implemented as "PID controllers" (proportional-integral-derivativ controllers). They are the products of decades of development and theoretical analysis, and are highly effective. If PID and other traditional control systems are so well-developed, why bother with fuzzy control? It has some advantages. In many cases, the mathematical model of the control process may not exist, or may be too "expensive" in terms of computer processing power and memory, and a system based on empirical rules may be more effective.

Furthermore, fuzzy logic is well suited to low-cost implementations based on cheap sensors, low-resolution analog-to-digital converters, and 4-bit or 8-bit one-chip microcontroller chips. Such systems can be easily upgraded by adding new rules to improve performance or add new features. In many cases, fuzzy control can be used to improve existing traditional controller systems by adding an extra layer of intelligence to the current control method.

In this work the fuzzy PI controller will be considered instead of classic controller.
The PI smith predictor controller in comparison with fuzzy PI- smith predictor is also investigated.

2- Smith predictor Controller

The dynamic behaviour of many industrial processes contains inherent time-delay. Processes with time-delay are inherently difficult to control. i.e. It is difficult to achieve satisfactory performance. Much effort has been expended in to researching the design of effective control techniques for time-delay plants. As PID type controllers fails to control such plants. Perhaps the best known alternative technique in the control of long time delayed plants is the smith predictor controller. Smith (1959). proposed the PI plus smith predictor approach which represented an important breakthrough for controlling systems with time delays. Smith's approach enabled larger loop gains to be used and allows conventional PI controllers to be tuned to the levels which could have been attained when using a PI controller on the plant without time-delay. The attractive feature of this technique is that it eliminates the time delays from the characteristic equation of the closed-loop system and thus converts a time-delayed control problem into one without any time-delays. This is basically achieved by the inclusion of a mathematical model of plant in a minor feedback loop around the conventional controller to stabilize the system and to predict the effect of current control actions on the actual plant outputs.
However, when mismatches in the model occur, the smith predictor controller can exhibits very poor stability properties. This important problem motivated several researchers to develop techniques that quantify the Smith predictor controller robustness to modelling errors.
The robust stability and robust performance of the Smith predictor controller is investigated by. Designing Fuzzy PI - smith predictor controller for process plants uncertainties. This research considers the commonly used controller and plant model in process control. The PI controller and the stable first-order plus dead-time model because of their wide spread usage in industries.
Apredicative controller lies in the requirement of an assumed model of the process to be controlled.

3- Smith Predictor Controller Configuration and Analysis.

Since the great majority ofindustrial processes have an associated time-delay, due either to distance-velocity lags, that exist for instance in heating system, transportation equipment (conveyors. pipelines), or by the time required for chemical reactions to occur etc, these kind of processes are significantly more difficult to control.

Early researchers addressed the problem of controller design for process plants with time-delay by correlating PID controller setting with model gain, time- constant and time-delay. Low loop gains were required to avoid instability when time constant were small compared to time-delay, leading to poor system performance. The shortfalls of PID-type controller to control long time-delayed processes, argued the researchers to look for alternative control techniques. Perhaps the best-known alternative technique that has received the most attention in the control of long time-delayed plants is the Smith predictor. The common configuration of smith predictor control system is shown Fig. (1) where C(s) denotes the transfer function of the controller, P(s) is the actual time-delayed plant, M(s) is the model of the plant without time-delay and D(s) is the model time-delay. In order to construer the smith predictor controller shown in Fig. (1), it is necessary to select a process model and to design the controller C(s). The controller C(s) is usually taken to be a PI or PID controller or any lead-lag network and it must be designed so that the system is robust with respect to errors between the actual process and the model. The first order lag plus dead-time model has been used to represent the process.

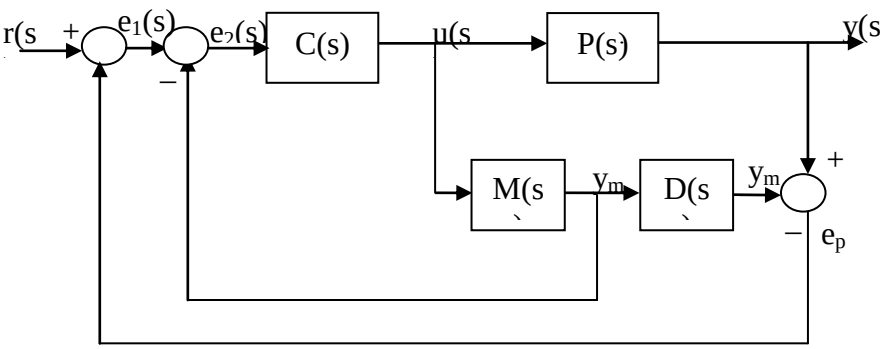

Fig. (1) Smith Predictor Control System

From Fig. (1) the closed loop transfer function is expressed by:

$$G_c = \frac{y}{r} = \frac{C\ P}{1+C[M+P-M.D]} \quad (1)$$

Where:

$$P(s) = \frac{K}{T_p\ S+1} e^{-s\,Td}$$

$$M(s) = \frac{K_m}{T_m S+1} \qquad D(s) = e^{-sTd_m}$$

Where
K and K_m denote gain; T_p and T_m denote time constant; Td and Td_m denote the pure time delay.
The primary controller adopted in this design is a conventional PI-controller of the form:

$$C(s) = k_p + \frac{k_i}{s} = k_p\,(1+\frac{1}{T_i s}) \quad (2)$$

When the model of the plant M(s) and the corresponding time-delay D(s) matches the actual time-delay plant P(s), then the over all transfer function of the closed loop from r(s) to y(s) is given by:

$$G_c(s) = \frac{y(s)}{r(s)} = \frac{C(s)P(s)}{1+C(s)M(s)} \quad (3)$$

From the above transfer function, it can be observed the characteristic equation does not contain the delay term and the controller can be designed as if the system was delay-free.
In order to discuss the relationship of the smith predictor controller with the classical feedback control, evident that
system as shown in Fig. (3), where the relationship between C(s) and the standard feedback controller k(s) is given by:

$$K(s) = \frac{C(s)}{1+C(s)M(s)[1-D(s)]} \quad (4)$$

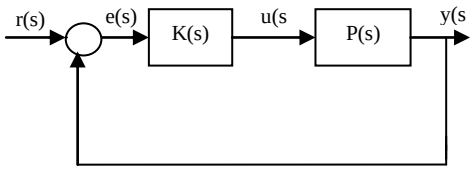

Fig. (3) Feedback Control Systems

4- System Modeling.

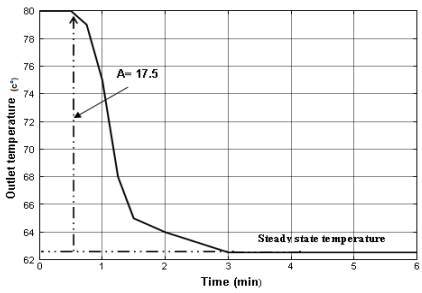

Fig. (4) Step response of the system model

Therefore, the estimated transfer function model is:

$$G(s) = \frac{-0.875e^{-0.75s}}{1+0.55S} \quad (5)$$

5- Fuzzy PI-Smith Predictor

The response as shown in Fig. (4) indicates some time delay and exponential response which could be first order model.

The outlet liquid temperature y (t) can be controlled by varying the speed of the cooling fan as shown in Fig. (4).

The system model represented by the air-cooled heat exchanger system.

The fuzzy logic control designed to control the air- cooled heat exchanger system, it utilizing seven membership functions, and forty nine rules as show in Fig. (5).

	Change rate of error (e_c)							
Error (e)		NB	NM	NS	ZO	PS	PM	PB
	NB	NM	NM	NM	NM	NM	NM	NM
	NM	PM	NS	NS	NS	NS	NS	PM
	NS	PS	NS	ZO	ZO	ZO	PS	PS
	ZO	NB	NS	ZO	ZO	ZO	PM	PB
	PS	NS	ZO	ZO	ZO	ZO	ZO	PB
	PM	NS	ZO	ZO	ZO	ZO	ZO	PS
	PB	PB	PB	PB	PB	PB	PB	PB

Fig. (5) Rule base table

Controller.

The inputs to the fuzzy system are error2 (e_2 (k)) and changes rate of error (e_{c2}).

Where

$(e_1(k)= r(k)-e_p(k))$, $(e_2(k) =e_1(k)-y_m)$,

$(e_{c2}(k)= e_2(k)- e_2(k-1)/Ts)$ (6)

Ts= sampling time and the output of fuzzy system is u (k).The fuzzy output is used for Smith Predictor as shown in Fig. (6). The error, change rate of error, and output membership function as shown in Fig. (7), Fig. (8) and Fig. (9) respectively.

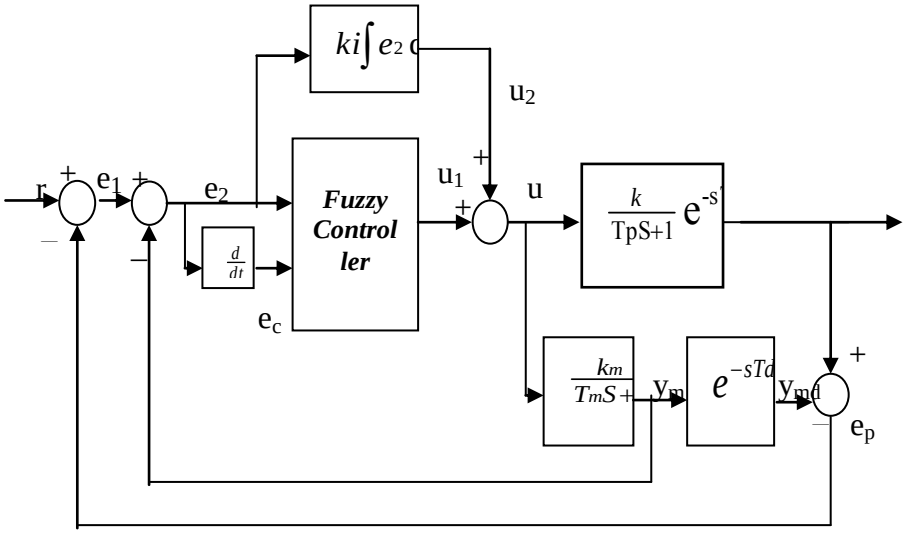

Fig. (6) Fuzzy-PI Smith Predictor Control System

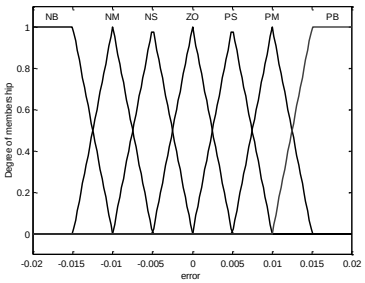

Fig. (7) Error membership function

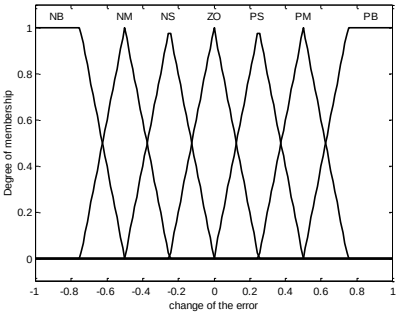

Fig. (8) Change rate of error membership function

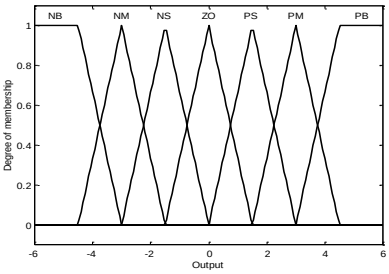

Fig. (9) Output membership function

Fig. (10), shows the simulation response for PI / Fuzzy PI-smith predictor controller.

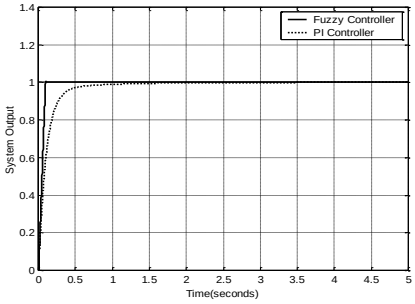

Fig. (10) PI / Fuzzy Controller response

6- Effect of Disturbances on Air-Cooled Heat Exchanger System

The air- cooled heat exchanger system designed is based on classical and fuzzy control to stabilize the system. To check the system performance and robustness of fuzzy logic control system, the comparison with classical control method is designed under the effect of disturbances.

The disturbances d(s) is added to the model as shown in Fig. (11).

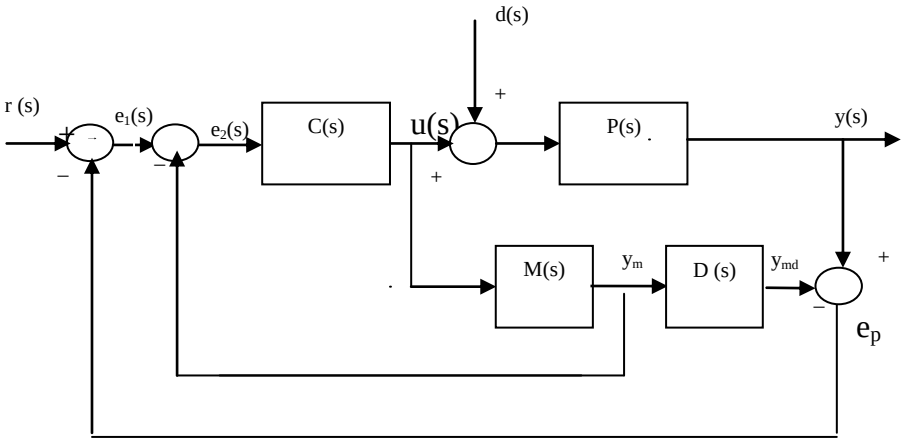

Fig. (11) Smith Predictor Control System

The disturbances model is defined by the equation (7) and as shown in Fig. (12)

$$d(s) = A\sin(\pi * Ts) \quad (7)$$

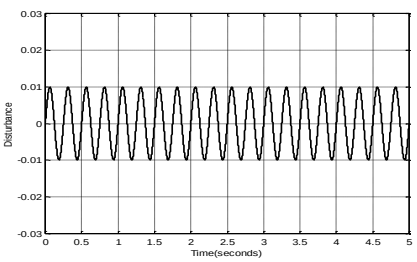

Fig. (12) Disturbances response

The system under the effect of disturbances as shown in Fig. (13) .

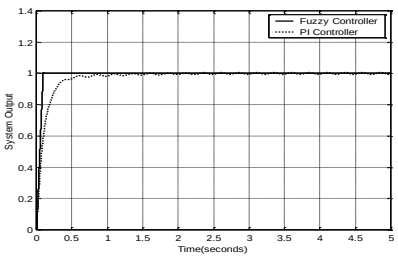

Fig. (13) System response by adding disturbances

7- Evaluation of Fuzzy PI- Smith Predictor Controller

An evaluation the performance of fuzzy PI desirable was carried to control simple air-cooled heat exchanger model. Here comparison of a fuzzy controller with that of classical controller is shown

To show the benefit of fuzzy PI controller several types of system parameter uncertainties were considered as shown in Table (1).

Table (1) several types of system parameter uncertainties

Case1	K and T_P Changed by 10%
Case2	K and T_P Changed by 50%
Case3	K and T_P Changed by 100%

The simulation results of PI / Fuzzy PI-smith predictor controller for the cases from1 to3 are shown in fig (14) to fig (16)

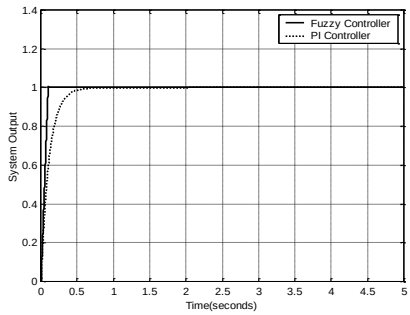

Fig. (14) Case 1

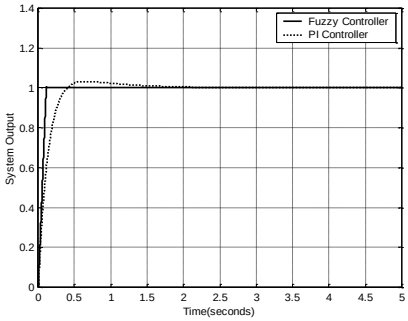

Fig. (15) Case 2

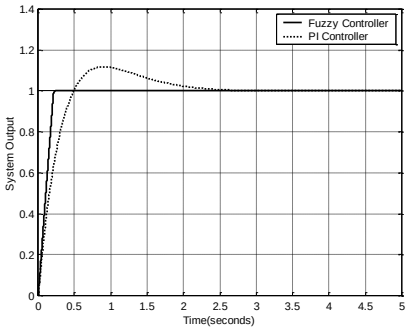

Fig. (16) Case 3

8- Conclusions

The classical and fuzzy logic controls design with smith predictor controller was used to investigate the performance and robustness of a model under the effect of uncertainties and disturbances.

Smith predictor controller as a form of model based predictive control has been carried out, SPC constitute an alternative approach for controlling long time delay plants.

The system has been designed using two approaches, first designed by a combining of classical PI control and smith predictor control for air-cooled heat exchanger system. Second was based on fuzzy

controller and smith predictor for the same system.

The robustness of fuzzy logic controller designed for air-cooled heat exchanger model, the comparison with classical PI controller has been carried out with the system uncertainties and under the effect of disturbances.

To test the benefit of fuzzy logic controller, several types of uncertainties has been considered.

From the simulation results, the proposed robust controller (Fuzzy logic Controller), has a better performance achieves a much smoother response, and provides a higher accuracy of process model compared to a classical PI controller.

References

[1] Anderson and Moore J.(1969) " linear Optimal Control " (Englewood Cliffs.NJ:prentice Hall).

[2] Astrom K.J. and Ho W.K. (1992), "Toward intelligent PID control" Automatica, vol.28, pp.1-9

[3] A Tahir EL Hashani jiang Yu Xian "Optimization of fuzzy heading hold autopilot using genetic algorithms". ICOM05.

[4] Brosilow. C. B. (1979), The structure and design of Smith Predictors from the viewpoint of inferential control. Joint American Control Conf. ,Denver

[5] Clark D.W. Mohtadi C. and Tuffs, (1987), "Generalized predictive control" Automatica. Vol.23, no.2, pp.137-160.

[6] Clark, (1988), "Application of generalized predictive control to industrial processes". IEEE Contr.Syst.Mag.vol.8,pp.49-55.

[7] Channon et l.(1996), Journal of Systems & Control Engineering, 210(1): 51-63.

[8] Cutler C. R. and B .L. Ramaker (1980), " Dynamic Matrix Control ", a Computer Control Algorithm, Proceedings of the Joint Automatic Control Conference.

[9] Homaifar, A. and McCormick, E. (1995). "Simultaneous Design of membership functions and rule sets for fuzzy controllers using genetic algorithms". IEEE Transactions on fuzzy systems, pp 129-139.

[10] k.M. Passino and S. Yurkovich , (1998). " Fuzzy Control " , Addison Wesley Longman;

[11] Langton C G. (1996), " Artificial life " . The philosophy of artificial life". Boden M A editor. Chapter 1. Pp.34-94. pp. ISBN: 0-19875154-0.

[12] landau. ID, (1995). "Roust digital control of system with time delay". Int. J control, vol. 62,325-347.

[13] laughin, D. L. Rivera, D. E. and Morari, M. (1987), " Smith predictor design for robust performance " . International Journal of Control.

[14] Richalet, (1993), " Industrial application of model based predictive control" Automatica, Vol. 29, pp 1251-1274.

[15] Smith. O J. M. (1959), "Feedback Control System". McGraw Hill. New York.

[16] Takagi and M. Sugeno, (1985). "Fuzzy identification of systems and its application to modelling and control", IEEE transactions on systems, Maan, and Cybernetics vol 15. pp. 116-132.

.

Appliances Control Using Mobile Phone

Manhal J. Alhelaly, Ayad A. Mousa, Abdelhamid M. Raheel.
Faculty of Engineering
Omer Al-Muktar University
Al-Beida, Libya
manhalmail@yahoo.com

Abstract - In many cases it is desirable to turn on or off some appliances, such as air conditioning and heating units before arriving home, this is known as home automation systems. This project uses the Dual-Tone Multi Frequency (DTMF) technique used in touch tone telephones, to control multi- electronic devices from long distances using the mobile phone. A practical application case for this system was implemented to control four electronic devices. A test to detect the DTMF signal received from different mobile phones was also carried out. The DTMF decoder was tested for accurate detection of the presence of these tones under various conditions. The automation features of this work makes it possible for homeowners to remotely control a large number of appliances, indoor and outdoor lamps and lights, landscape sprinkler timers and more using their mobile phones.

1.Introduction

The remote control used in home automation systems, is a wonderful feature that everyone would like to enjoy, if they were not expensive to install, maintain, and able to be used from long distance. The mobile phones and Touch-Tone telephones use the DTMF. That was developed initially for telephony signaling. Each key-press on the phone keypad generates DTMF signal consists of two tones that must be generated simultaneously. Using the DTMF technology, the system in this project will control multi electronic devices from long distance using the mobile phone. This system allows the user to control and known the present state of home appliances by cell phone, it can be done by send signal over the cell phone (Control Phone) to other cell phone in the home (Home-Based Phone), this cell phone is connected to an interface circuit detects the DTMF signals and give it the access to a control unit which controls the home devices and turn the power of these devices On or Off. A design of a home applia-nces control system using cell phone presented in this project is shown in Figure 1.

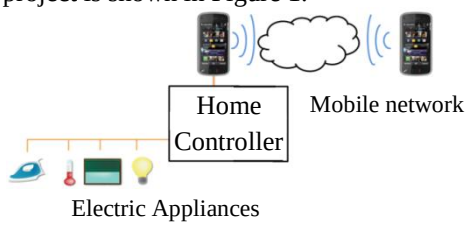

Figure 1 Appliances Control Using Mobile Phone

The Home Controller divided into two units which is, the DTMF detection unit, and the device control unit, these units consists of many sub-circuit blocks, beginning with the DTMF decoder, 4-16 line decoder/de-multiplexer, some D-flip-flops, relay driver circuits, feedback circuitry, etc.

2. DTMF Detection Unit

DTMF detection is the main object before starting to control the appliances. We discuss below the DTMF signaling and detection, and later we will show the integrated circuit we use in this project, and how to get its output on 16 different output line.

DTMF generation is based on a 4×4 grid matrix shown in Figure 2. This matrix represents 16 DTMF signals including numbers 0–9, special keys * and #, and four letters A–D. The letters A–D are assigned to unique functions for special communication systems.

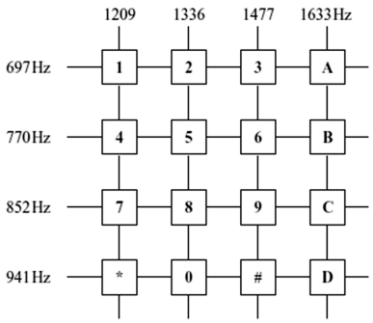

Figure 2 Telephone keypad matrix

The DTMF signals are based on eight specific frequencies defined by two mutually exclusive groups. Each DTMF signal consists of two tones that must be generated simultane-ously. One is chosen from the low-frequency group to represent the row index, and the other is chosen from the high-frequency group for the column index [2].

The implementation of a DTMF signal involves adding two finite-length digital sinus-oidal sequences with the later simply generated by using look-up tables or by computing a polynomial expansion [1]. By pressing a key, for example number 3, it will generate a dual-tone consist of 697 Hz for the low group, and 1477 Hz for the high group, as shown in Figure 3.

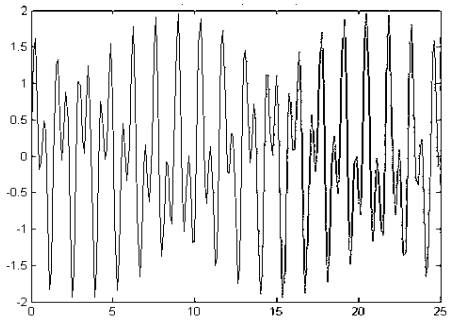

Figure 3 Symbol “3” [697,1477]Hz

The decoder must detect the DTMF signals under various conditions such as frequency offsets, power level variations, DTMF reception timing incons-istencies, etc. DTMF decoder implementation requirements are detailed in ITU-T Q.24 recomm-endation.

The implementation of DTMF decoder involves the detection of the DTMF tones, and determ-ination of the correct silence

between the tones. In addition, it is necessary to perform additional assessments to ensure that the decoder can accurately disting-uish DTMF signals in the prese-nce of speech. For North America, DTMF decoders are required to detect frequencies with a tolerance of ±1.5%. The frequencies that are offset by ±3.5% or greater must not be recognized as DTMF signals. For Japan, the detection of frequencies has a tolerance of ±1.8 %, and the tone offset is limited to ±3.0 %. Another requirement is the ability to detect DTMF signals when two tones are received at different levels. This level difference is called twist. The high-frequency tone may be received at a lower level than the low-frequency tone due to the magnitude response of the communication channel, and this situation is described as a forward (or standard) twist. Reverse twist occurs when the received low-frequency tone has lower level than the high-frequency tone. The final requirement is that the receiver must avoid incorr-ectly identifying the speech signal as valid DTMF tones. This is referred as talk-off perform-ance [2].

The integrated DTMF decoder is the device that receives the incoming DTMF data and converts it into a respective 4-bit binary coded decimal (BCD) numbers as shown in the Table 1.

Table 1 The respective DTMF data into BCD digits

F_{low}	F_{high}	Key	Q_4	Q_3	Q_2	Q_1
697	1209	1	0	0	0	1
697	1336	2	0	0	1	0
697	1477	3	0	0	1	1
770	1209	4	0	1	0	0
F_{low}	F_{high}	Key	Q_4	Q_3	Q_2	Q_1
770	1336	5	0	1	0	1
770	1477	6	0	1	1	0
852	1209	7	0	1	1	1
852	1336	8	1	0	0	0
852	1477	9	1	0	0	1
941	1209	0	1	0	1	0
941	1336	*	1	0	1	1
941	1477	#	1	1	0	0
697	1633	A	1	1	0	1
770	1633	B	1	1	1	0
852	1633	C	1	1	1	1
941	1633	D	0	0	0	0

The CM8870 is a full DTMF receiver that integrates both band split filter and decoder functions into a single 18-pin DIP. Its filter section uses switched capacitor technology for both the high and low group filters and for dial tone rejection. Its decoder uses digital counting techniques to detect and decode all 16 DTMF tone pairs into a 4-bit BCD code. External component count is minimized by provision of an on-chip differe-ntial input amplifier, clock generator, and latched tri-state interface bus. Minimal external components required

include a low-cost 3.579545 MHz crystal, a timing resistor, and a timing capacitor. It can also inhibit the decoding of fourth column digits.

To have the BCD output on 16 different lines, we feed the DTMF decoder output to a 4-16 line decoder like IC74154. This IC takes the BCD number and decodes. According to that BCD number it selects the active low output line from 1 to 16 which is decimal equivalent of the BCD number present at its input pins. To get a logical high output, the output of the IC74154 needs to get inverted. This inversion is carried out by an inverter, like the hex inverter IC 7404. This IC inverts the data on its input terminal and gives inverted out-put.

3.Control Unit

The Device Control unit designed for this project consists of device switching section, device status feedback section, and relay driver circuit.

The Device Switching section consists of a tri-state buffer and flip-flops. The tri-state buffer contains independent gates each of which performs a buffer function. The outputs have the 3-STATE feature. When control signal is at high state, the outputs are nothing but the data present at its input terminals. When control signal is at low state, the outputs are held at high impedance state, so no output will be available at the output terminal.

The main object of the device switching section, is giving access to the relay drive circuit when needed to turn On/Off the controlled devices.

Before and after changing the present status of the device On/Off, it's important to check the status of the device. The control unit will give a feedback tone after switching On any device, this help us to check the device status.

This status feedback circuitry, utilizes a dual input AND gate, When the both inputs are high that indicates that the device is switched ON, then the output of the AND gate goes logic high state. This output is fed to the beep generator. When we press the key the feedback tone is heard. This feedback tone is heard only when the device is switched ON. After switching OFF the device, this tone is not heard.

The beep tone generator produces a beep tone of audible frequency. This unit is constru-cted using a 555 timer chip. Here it is wired as an astable multi-vibrator with a few external com-ponents like resister and capacity-or, required along with the timer 555 chip set. This frequency comes in the audible range betw-een 40 to 650 Hz. It should be less than 650 Hz otherwise it will mix up with the DTMF tone.

In order to switch the appliances On or Off, small board type relays were used. Since the output of the D flip flop is normally +5 V or it is the voltage of logic high state, we cannot use this output to run the device or appliances. Therefore here we use relays which can handle a high voltage of 230 V or more, and a high current in the rate of 10 A to energize the electromagnetic coil of the relays +5 V is sufficient. We use four SRD-05VDC- SL-C relays to switch On/Off four different devices.

4.Overall System Design

A Design of a home appliances control system using cell phone presented in our project is referring to Figure 1 as a block diagram, let's begging with the two cell phones one remote cell phone which called Control phone, this phone control the system after a call is made by only press the buttons that generate the DTMF signal; and the other home cell phone which called home-based phone because it's based in the home with the home controller board; the home controller is divided into two parts, DTMF detection unit, and the control unit.

Once the user call to the home-based phone, in order to control the home appliances, the home-based phone answer the call automatically, if the user is the one who is recorded in the white list program, that we use for the system security.

After that the user can accesses to the system, check the current status of the devices, and change the state of any device (On/Off).

The overall system design is shown in figure 4.

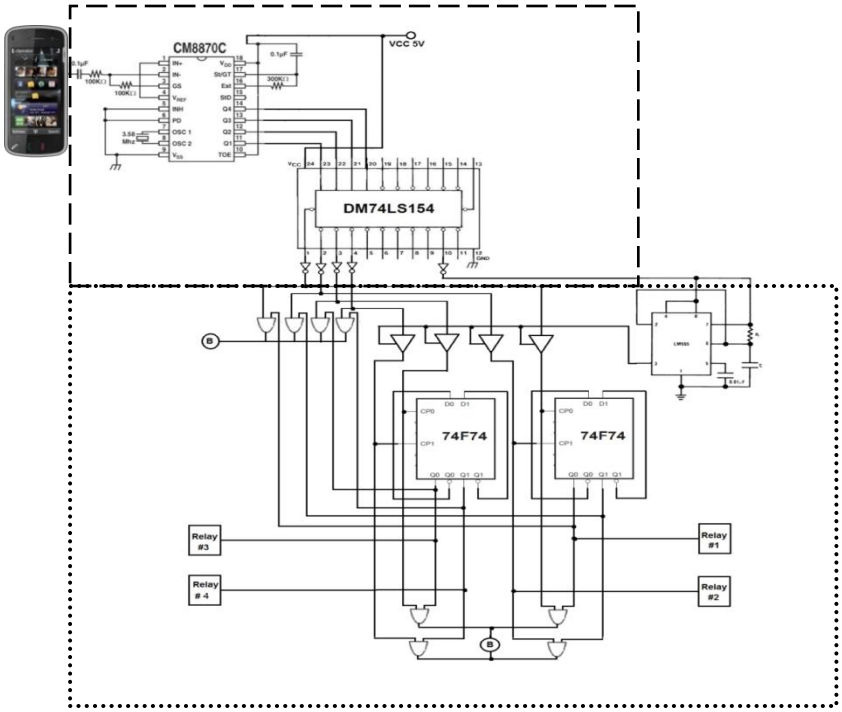

Figure 4 Home Controller Block Diagram

DTMF Detection Unit

Control Unit

1st and 2nd Status Feedback

As discussed before, the DTMF detection unit constructs of DTMF decoder, 4-16 line Decoder/de-multiplexer, and inverter to invert the output of the 4-16 line Decoder/de-multiplexer.

The control unit consists of device status check section, device switching section, device status feedback section, and relay driver circuit.

Before switching On/Off any device, to avoid any confusion about the device present status of the output, we can check the status of any device by fed the BCD decoder inverted output (the button that the user pressed) and the output line of the respective device (from the relay circuit) to independent block of And gates, where the output of the And gates is connected to the beep tone generator (B), that generates a beep if the respective device in the ON state.

After checking the device status, the tri-state buffer mode can be changed by making the control input high. This is done by pressing the "0" key. When this key is pressed the output of the 4-16 line decoder goes low. This gives a triggering pulse to the monostable multi-vibrator which is built around the LM555. This will keep the output high for about 5 seconds. In this time interval the output of the tri state buffer will be the signal at its input terminal. Now the device code of the chosen relay (1, 2, 3 or 4) whose status is to be altered is again pressed. The output of the tri-state buffer is latched by using a D flip-flop. After a period of 5 s the output of the LM555 monostable multi-vibrator goes low and puts the tri state buffer in the high impedance state. Therefore to change the status of any other device to be done we must press again "0" key to make the tri-state buffer act as input‑output state and the respective code of the device is pressed.

The output of the tri-state buffer is latched by using a D flip-flop. This D flip-flop is used in the toggle mode. For each positive going edge of the clock a pulse will trigger the flip flop. The output of the tri-state buffer is connected to the clock input, and the inverted output connected to the D input, this will make the D flip-flop invert its output each time a trigger pulse applied from the tri-state buffer. The main reason to use the D flip-flop is to keep the status of the tri-state buffer output after it disabled. The beep tone generator constr-ucted using a 555 timer chip wired as an astable multi-vibrator with a few external components, required along with the timer 555 chip set.

5. The System Features

This system can control up to 10 devices, it may be any electric or electronic appliances, and each device is given a unique code. There is no risk for false switching, it makes accurate switching any false switching the device are not done. This system doesn't cost a lot of money, and it's easy to implement. Before changing the state of the device we can confirm the present status of the device. The system gives an acknowledgement tone after switching on the devices to confirm the status of the devices. Its highly secured system using the white list programs on the home-based phone to block any other call from controlling the home appliances. This system can be controlled by multi users, this feature refer to user choice.

6. Future Work

For a future work it will be useful to develop programs for the mobile devices to give more control options and security control. And we suggest devel-oping the system using PLCs or Microcontrollers instead of the control unit, to give more reliab-ility and control options, as temp-erature control, security and more computational work so the sys-tem can do more than just turn On/Off the devices.

References

[1] Sanjit K. Mitra, *Digital Signal Processing*, Second Edition, McGraw-Hill, University of California, International Edition, 2002.

[2] Sen M Kuo, Bob H Lee, Wenshun Tian, *Real-Time Digital Signal Processing Implementations and Applications*, Second Edition, John Wiley & Sons, Ltd, 2006.

[3] www.datasheetcatalog.com

[4] Gunter Schmer, *DTMF Tone Generation and Detection: An Implementation Using the TMS320C54x*, Application Report, Texas Instrument, May 2000

Simulation Of The Different Position On The E-Type Round Diaphragm And The Length Of The Beam

Dr. M. M. Bakush [*] **Abdalla I. Fadel**[*] **Ahmed J. Abogarir**[*]
Adel A. Abosdial [**]

[*] **Dept. of Electrical and Electronic Engineering, Al-Fateh University-Libya.**
Phone: +21825385942, Email: abougarir@yahoo.com

Dept. of Electrical and Computer Engineering, Naser NationUniversity-Libya. Phone: +218925238263, Email: **adel1880@yahoo.com**

Abstract

This paper studies a resonant silicon sensor whose elementary sensing component is the E-type round diaphragm, and the final sensing component is the silicon beam resonator is attached to the E-type round diaphragm. The relationship between the basic natural frequency of the beam resonator and the measured acceleration are calculated and simulated by using the above finite element modeling and Matlab. Because of the fact that beam is located on the different position on the E-type round diaphragm and the length of the beam, the outer radius of the E-type round diaphragm are varied respectively. The related analyses and investigations are carried out. Some important results on the relationship between the basic natural frequency of the beam resonator and the measured acceleration are obtained. Finally, based on the differential output scheme of the resonant sensor and some related criteria, a set of appropriate parameters for the above sensing structure of the sensor is determined for measuring the acceleration.

1. Introduction

Silicone resonant sensors have developed rapidly in past decade. Many experts in sensor paid special attention to this technology.

The main advantage of the silicon microstructure resonant sensors is the advantage of generalized resonant sensors, such as direct digital output (without A/D converters), because the sensors whose output is in the form of variable frequency are called quasi-digital because it is very easy to obtain a digital output from them. The output of digital sensors is in the form of discrete steps or states. The output of digital sensors does not require an Analogue to Digital convector and their output is easier to transmit than analog sensors. The output of digital sensors is also more repeatable, reliable, and has long-term stability. They have low hysterics and high repeatability which is often more accurate and precise .The advantages of silicon

material is that they have excellent mechanical properties, posses high strength, no mechanical hysterics. Moreover they have ability to batch process at low cost and the compatibility of mechanical and electrical properties. Meanwhile, due to their high working frequency, the dynamic characteristics of silicon resonant sensors are much better than those of conventional resonant sensors[1].

2. Structural Sketch and Sensing Mechanism of Microstructure Silicon Accelerometer

Fig.1 shows the structural sketch of a microstructure silicon resonant sensor for measuring acceleration. Fig 2 shows the mathematical model of the sensing structure. The preliminary sensing unit of the microstructure silicon accelerometer micro-sensor for measuring the acceleration is an E-type round diaphragm, where **A** is the outer radius, **B** is the inner radius, and **H** is the thickness of the diaphragm, respectively.

The measured acceleration within $(-100,+100)\,m/s^2$, (a<0 F>0 ,a>0 F<0) acts perpendicularly to the lower plane of the E-type round diaphragm and yields the radial and circular stresses of the diaphragm. The final sensing unit is one pair of beams (resonator beam1 and beam2: ***L*** is the length of the beam, **b** is the width of the beam, and **h** is the thickness of the beam, see Fig.2) which are attached to the upper plane of the E-type round diaphragm. The location of the beam1 and beam2 are along the radial direction of the E-type round diaphragm. Beam1 is located at the outer edge and beam 2 at the inner edge.

As compared with the round or square diaphragm, the E-type round diaphragm is one of the advanced elementary sensing units in silicon microstructure resonant sensors. Its major advantages are such that the stress concentrations on the effective annular sensing area, flexible stress distribution designing, easier to achieve the differential measuring scheme in order to increase the sensitivity and reduce some disturbances such as temperature, random vibration, etc. In addition, the advantage of the above sensing structure is that the beam resonator of very high Q factor because they can be packaged within a vacuum housing.

The location of beam 1 and beam2 are along the radial direction of the E-type round diaphragm (see Fig.1). beam l is located at the outer edge $r \in (A\text{-}L \sim A)$, and beam 2 at the inner edge $r \in (B \sim B+L)$. However, it is very important for the silicon resonant sensor to design and select the optimal parameters of the sensing structure to measure the different acceleration ranges. Based on the sensing mechanism of the sensor, the FEM model of the sensing structure is established in details in [2].

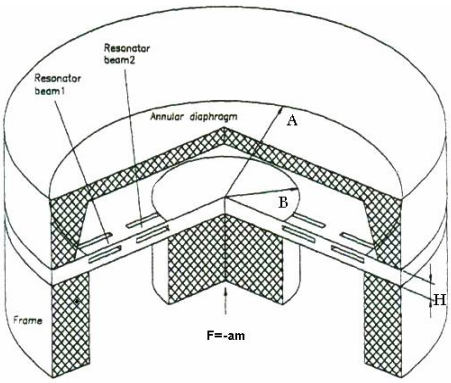

Fig.1 : The structural sketch of a silicon resonant sensor for measuring acceleration

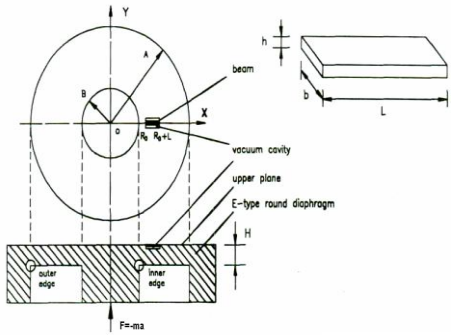

Fig. 2: The mathematical model of sensing structure

3. Stresses On The Upper Plane of The E-Type Round Diaphragm

The differential equation of the round diaphragm which is measuring by a acceleration can be written as following[2]:

$$\frac{d}{dr}\left[\frac{1}{r}\frac{d}{dr}\left(r\frac{dw}{dr}\right)\right]=\frac{Q}{D} \qquad (1)$$

Where $D=\dfrac{EH}{12(1-\mu^2)}$

$$Q=\frac{F}{2\pi r},$$

$$F=-ma,$$

$$m\approx\rho\pi(H_s B^2+HA^2)$$

Where w is the normal displacement of the E-type round diaphragm, D is the flexural rigidity of the diaphragm, Q is the shearing force of the circle of radius r of the diaphragm, r is radial coordinate of the diaphragm in polar coordinate, F is the inertial force caused by the measured acceleration a, m is the effective sensing mass, H_S is the height of the sensing cylinder and E ,ρ, μ are Young's modulus, density and Poisson ratio of the sensing structure respectively. It should be pointed out that the positive direction of the measured acceleration a and the corresponding inertial forces are shown in Fig 2. If the amount of the above both variables is a positive, the actual direction of the above variable is the same with that in Fig 2. And if the amount of the above both variables is a negative, the actual direction of the above variable is opposite from that in Fig.2. The boundary conditions at the inner and outer edges of the E-type diaphragm are as follows[3,4]:

$$r=B \qquad \frac{dw}{dr}=0 \qquad (2\text{-a})$$

$$r=A \qquad w=\frac{dw}{dr}=0 \qquad (2\text{-b})$$

From equ9ations (1) and (2,a,b), the normal displacement of the E-type round diaphragm w can be obtained. Then the radial stress $\sigma_r(r)$ and circular stress $\sigma_\theta(r)$ of the E-type round[5].

$$\sigma_r(r)=-\frac{3F}{4\pi H^2}\left[(1+\mu)S\right] \qquad (3\text{-a})$$

$$\sigma_\theta(r)=-\frac{3F}{4\pi H^2}\left[(1-\mu)S\right] \qquad (3\text{-b})$$

Where

$$S = 2\ln R + 2 + C - \frac{C}{R^2}$$

$$K = \frac{B}{A}$$

$$C = \frac{-2K^2 \ln K}{1-K}$$

$$R = \frac{r}{A}$$

4. Reckoning Model of The Beam

Fig. 3 shows the mathematical model of the beam. The axial and normal vibrating displacements u(s,z,t) and w(s,t) of beam at an arbitrary point in Cartesian coordinate can be written as[4]:

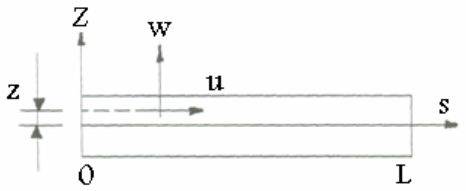

Fig. 3: The mathematical model of the beam

$$u(s,z,t) = -z\frac{dw(s)}{ds}\,Cos\,\omega t \qquad (4\text{-a})$$

$$w(s,t) = w(s)\,Cos\,\omega t \qquad (4\text{-b})$$

Where s , z are axial and normal coordinates of the beam in Cartesian coordinate, **ω** [rad/s], **w(s)** are natural frequency and its corresponding vibrating shape along the axial direction of the beam. Energy expressions of the beam resonator are as follows[5] :

The potential energy:

$$U = M\int_s \left[\frac{d^2 w(s)}{ds^2}\right]^2 ds \qquad (5)$$

Where $M = \dfrac{Ebh^2 Cos^2\,\omega t}{24}$

and S is the integrated length of the beam.

The kinetic energy

$$T = X\int_s [w(s)]^2\, ds \qquad (6)$$

Where $X = \dfrac{\rho bh\omega^2\, Sin^2\omega t}{2}$

and **ρ** is density of the sensing structure In addition, the initial potential energy of the beam, which is caused by $\sigma_s^0(s)$, is

$$U_o = N\int_s \sigma_s^o \left[\frac{dw(s)}{ds}\right]^2 ds \qquad (7)$$

Where $N = -\dfrac{bh\,Cos^2\,\omega t}{2}$

From Fig.2and equations(3,a,b), according to the above analyses

$$\sigma_s^o(s) = \sigma_s(R_o + S) \qquad (8)$$

Then the total potential energy of the beam is

$$U_T = U - U_o \qquad (9)$$

In equation (7) if $\sigma_s^0(s)$ is a constant, we can directly obtain the analytic relationship

between the frequency and the initial axial stress can be directly obtained from equation (10). In this thesis, we present the FEM equation to solve the relationship between the natural frequency of the beam resonator and the measured acceleration.

$$\omega = V1 \times V2 \qquad (10)$$

Where

$$V1 = \frac{22.4h}{L^2}\left(\frac{E}{12\rho}\right)^{0.5}$$

$$V2 = \left(1 + 0.295\frac{\sigma_s^o L^2}{E h^2}\right)^{0.5}$$

Beside on the above related equation we can divide the element along the axial direction of the beam (Fig.4, N is the total number of the beam element.) Introducing the dimensionless length:

$$\chi = (s - S_j)/\boldsymbol{l}, \text{ and } \boldsymbol{l} = 0.5(S_{j+1} - S_j).$$

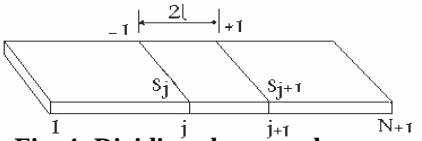

Fig. 4: Dividing element along the beams axial direction

Then map of domain $s \in [S_j, S_{j+1}]$ is $\chi \in [-1, +1]$. For the displacement of the jth element, introducing the second order Hermite interpolation.

$$w_j(s) = w_j(x) = X_2^O G_2 \mathsf{a}_j \qquad (11)$$

where

$$X_2^O = [1 \quad \chi \quad \chi^2 \quad \chi^3 \quad \chi^4 \quad \chi^5]$$

$$\mathsf{a}_j = [\mathrm{w}(-1) \quad w'(-1) \quad w''(-1) \quad w(+1) \quad w'(+1) \quad w''(+1)]^T$$

$$G_2 = \frac{1}{16}\begin{bmatrix} 8 & 5\iota & \iota^2 & 8 & -5\iota & \iota^2 \\ -15 & -7\iota & -\iota^2 & 15 & -7\iota & \iota^2 \\ 0 & -6\iota & -2\iota^2 & 0 & 6\iota & -2\iota^2 \\ 10 & 10\iota & 2\iota^2 & -10 & 10\iota & -2\iota^2 \\ 0 & \iota & \iota^2 & 0 & -\iota & \iota^2 \\ -3 & -3\iota & -\iota^2 & 3 & -3\iota & \iota^2 \end{bmatrix}$$

From equation (5) ~ (9),(11) we can obtain the element potential energy, kinetic energy and initial potential energy caused by the initial stress, in the domain $s \in [S_j, S_{j+1}]$:

$$U^j = A_1 \int_{-1}^{1} a_j^T G_2^T X_2^{2T} X_2^2 G_2 a_j dx \qquad (12)$$

Where

$$A_1 = \frac{Ebh^3 \cos^2 \omega t}{24t^3}$$

$$X_2^2 = \frac{d^2}{dx^2} X_2^o$$

$$T^j = A_2 \int_{-1}^{1} a_j^T G_2^T X_2^{oT} X_2^o G_2 a_j dx \qquad (13)$$

Where

$$A_2 = \frac{\rho bh\omega^2 \sin^2 \omega t}{2}$$

$$U_o^j = A_3 \int_{-1}^{1} A_4 \, a_j^T G_2^T X_2^{1T} X_2^1 G_2 a_j \, dx \quad (14)$$

Where

$$A_3 = \frac{bh \cos^2 \omega t}{2t}$$

$$A_4 = \sigma_s^o \left[S_j + (\chi + 1)t \right]$$

$$X_2^1 = \frac{d}{dx} X_2^o$$

Then we obtain the element stiffness matrix:

$$K^j = A_5 \int_{-1}^{1} G_2^T \, X_2^{2T} X_2^2 \, G_2 \, dx \quad (15)$$

Where

$$A_5 = \frac{Ebh^3}{12t^3}$$

The element mass matrix:

$$M^j = \rho bht \int_{-1}^{1} G_2^T \, X_2^{oT} \, X_2^o \, G_2 \, dx \quad (16)$$

The element initial stiffness matrix:

$$K_o^j = \frac{bh}{t} \int_{-1}^{1} A_4 \, G_2^T X_2^{1T} X_2^1 G_2 dx \quad (17)$$

The element total stiffness matrix:

$$K_T^j = K^j + K_o^j \quad (18)$$

From equation (18) and (16), we can obtain the assembly stiffness matrix K and assembly mass matrix M in the local domain $s \in [0, L]$. Then the finite element equation is the follow:

$$\left(K - \omega^2 M \right) a = 0 \quad (19)$$

Where the assembly nodal vector a consists of all a_j.

For actual structural feature of Fig 2, the boundary conditions of beam are as follows:

$$\begin{aligned} s = 0, \;\; & w(s) = w(s)' = 0 \\ s = L, \;\; & w(s) = w(s)' = 0 \end{aligned} \quad (20)$$

From equation (19) and (20), we can obtain the natural frequency and the corresponding vibrating shapes[6,7].

5. Calculations The Location of The Beam

The main investigations are the varying laws of the measured acceleration - frequency relationship for the beam resonator as the thickness *H*, outer radius *A* for the E-type round diaphragm and the corresponding length of the beam *L* are varied accordingly. In order to get some generalized results of the measured acceleration frequency relationship for the beam resonator, some related parameters are selected follows:

Referenced value for the inner radius of the E-type round diaphragm is as $B = 1.4 \times 10^{-3} m$. Referenced values for the width and the thickness of the beam are as $b = 50 \times 10^{-6} m$ and $h = 5 \times 10^{-6} m$. And the thickness of the E-type round diaphragm is as H= 30×10^{-6} m .The sensor is made of silicon, *E*= 1.3 x10^{11} pa, ρ = 2.33xl0^3 kg/m^3, μ =0.17.

Basic Natural Frequency for zero acceleration a = 0

Table1 and Fig.5 shows the basic natural frequency *f*(0)of beam with the measured zero acceleration a = 0. From this Table and fig, we can get results: the basic natural frequency of the beam, for the zero acceleration a = 0, decreases with increasing the length of the beam L as the inner radius of the E-type round diaphragm B is a constant.

Table 1 :The basic natural frequency of the beam with a=0 for the different L

$L\times10^{-3}$ m	0.40	0.45	0.50	0.55	0.60
f(0) (Hz)	244745	189134	153561	126914	106648

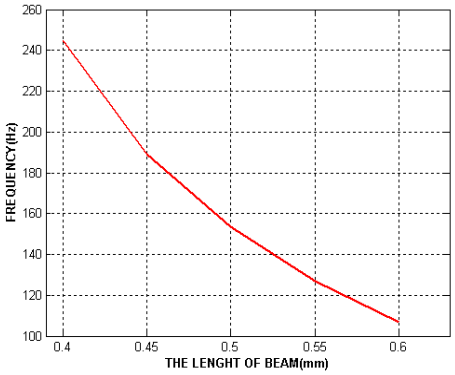

Fig. 5: basic natural frequency of beam with a=o for different L

Then, the length of the beam L should be increased if it is required to decrease the basic natural frequency for the zero acceleration a = 0. From the below Tables and the below Figures, we can get the following results:

The variation of the basic natural frequency of the beam decreased with increasing the length of the beam, while the relative variation (sensitivity) of the basic natural frequency increases with increasing the length of the beam for the given parameters of the E-type round diaphragm.

The variation of the basic natural frequency of the beam and the relative variation (sensitivity) of the basic natural frequency of the beam is increased with increasing the outer radius of the E-type round diaphragm as the inner radius of the E-type round diaphragm is constant.

The variation of the basic natural frequency of beam2 is more than that of beam1 And the above tendency decreases with increasing the ratio B/A and decreases with increasing the length of the beam [8,9].

Table 2 :The variation frequency (Hz) of Beam1 for the different A,L

$A*10^{-3}m$	THE LENGTH OF THE BEAM ($L\times10^{-3}$ m)				
	0.4	0.45	0.50	0.55	0.60
3.5	4354	4123	3790	3654	3498
3.6	4489	4240	3878	3719	3567
3.7	4521	4387	4115	3968	3811
3.8	4611	4456	4343	4190	4047

Table 3: The variation frequency (Hz) of Beam2 for the different A,L

$A*10^{-3}m$	THE LENGTH OF THE BEAM ($L\times10^{-3}$ m)				
	0.4	0.45	0.50	0.55	0.60
3.5	-4867	-4732	-4587	-4310	-4165
3.6	-5032	-4898	-4778	-4521	-4282
3.7	-5499	-5389	-5181	-4942	-4679
3.8	-5921	-5765	-5594	-5352	-5083

Table 4: The relative frequency variation (sensitivity) of Beam1 for the different A,L

$A*10^{-3}m$	THE LENGTH OF THE BEAM ($L\times10^{-3}$ m)				
	0.4	0.45	0.50	0.55	0.60
3.5	1.778%	2.150%	2.487%	2.879%	3.279 %
3.6	1.834%	2.240%	2.525%	2.930%	3.345 %
3.7	1.847%	2.319%	2.680%	3.127%	3.573 %
3.8	1.884%	2.356%	2.828%	3.301%	3.795 %

Table 5: The relative frequency variation (sensitivity) of Beam2 for the different A,L

$A*10^{-3}m$	THE LENGTH OF THE BEAM ($L\times10^{-3}$ m)				
	0.4	0.45	0.50	0.55	0.60
3.5	-1.988%	-2.501%	-2.987%	-3.396%	- 3.905 %

3.6	-2.056%	-2.601%	-3.112%	-3.562%	-4.01%
3.7	-2.246%	-2.849%	-3.374%	-3.894%	-4.387%
3.8	-2.634%	-3.048%	-3.643%	-4.217%	-4.766%

Table 6: The variation frequency (Hz) of Beam1 for the different A,L

$A*10^{-3}m$	THE LENGTH OF THE BEAM ($L\times10^{-3}$ m)				
	0.4	0.45	0.50	0.55	0.60
3.5	-4277	-4167	-3822	-3755	-3532
3.6	-4310	-4245	-3987	-3858	-3716
3.7	-4576	-4378	-4234	-4114	-3980
3.8	-4789	-4567	-4489	-4364	-4236

Table 7: The variation frequency (Hz) of Beam2 for the different A,L

$A*10^{-3}m$	THE LENGTH OF THE BEAM ($L\times10^{-3}$ m)				
	0.4	0.45	0.50	0.55	0.60
3.5	5076	4954	4312	4211	4034
3.6	5134	5099	4620	4342	4270
3.7	5376	5177	4994	4719	4452
3.8	5743	5470	5378	5085	4814

Table 8: The relative frequency variation (sensitivity) of Beam1 for the different A,L

$A*10^{-3}m$	THE LENGTH OF THE BEAM ($L\times10^{-3}$ m)				
	0.4	0.45	0.50	0.55	0.60
3.5	-1.747%	-2.203%	-2.487%	-2.964%	-3.311%
3.6	-1.761%	-2.244%	-2.596%	-3.040%	-3.484%
3.7	-1.869%	-2.314%	-2.757%	-3.242%	-3732%
3.8	-1.956%	-2.414%	-2.923%	-3.439%	-

					3.972 %

Table 9: The relative frequency variation (sensitivity) of Beam2 for the different A,L

$A*10^{-3}m$	THE LENGTH OF THE BEAM ($L\times10^{-3}$ m)				
	0.4	0.45	0.50	0.55	0.60
3.5	2.073%	2.619%	2.808%	3.317%	3.782 %
3.6	2.097%	2.695%	3.009%	3.421%	3.826 %
3.7	2.196%	2.737%	3.252%	3.718%	4.175 %
3.8	2.346%	2.892%	3.502%	4.007%	4.514 %

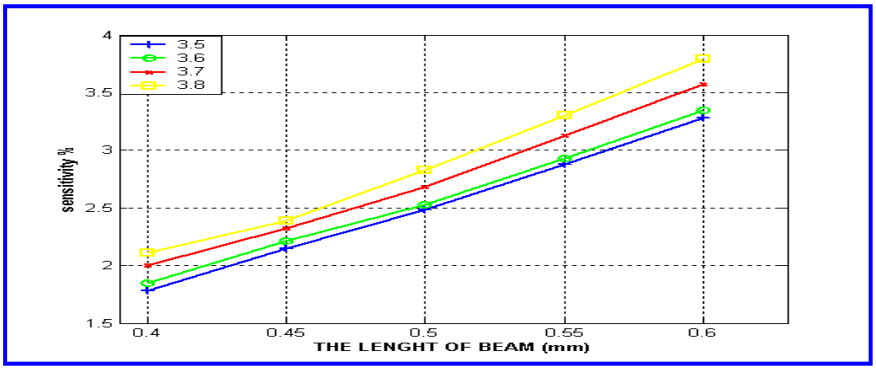

Fig. 6 : The relationship between the relative frequency variation (sensitivity) of beam1 and the length of beam

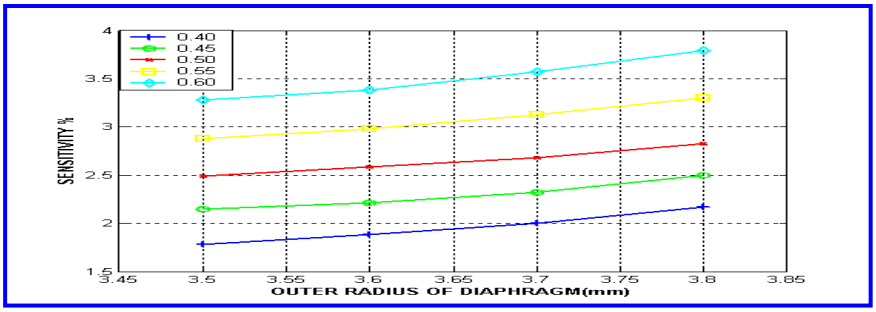

Fig 7: The relationship between the relative frequency variation (sensitivity) of beam1 and the outer radius of diaphragm A

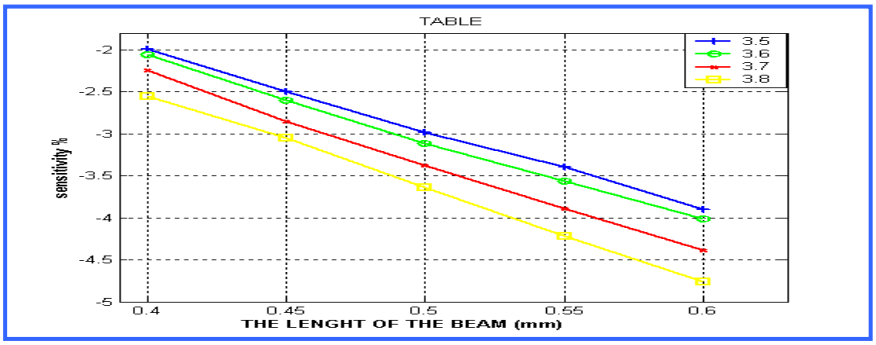

Fig. 8:The relationship between the relative frequency variation (sensitivity) of beam2 and the length of beam

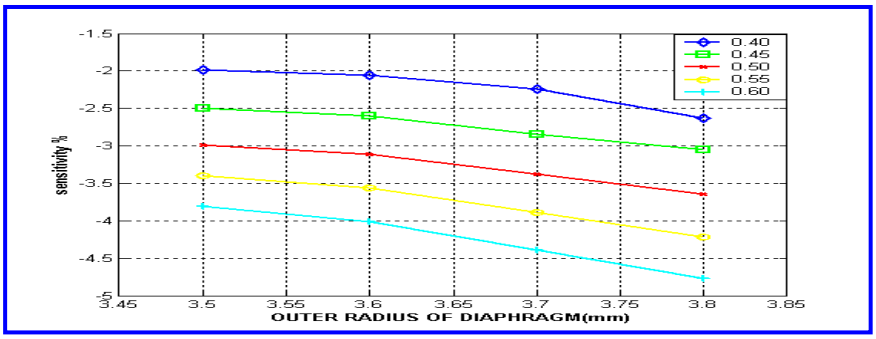

Fig. 9: The relationship between the relative frequency variation (sensitivity) of beam2 and the outer radius of diaphragm

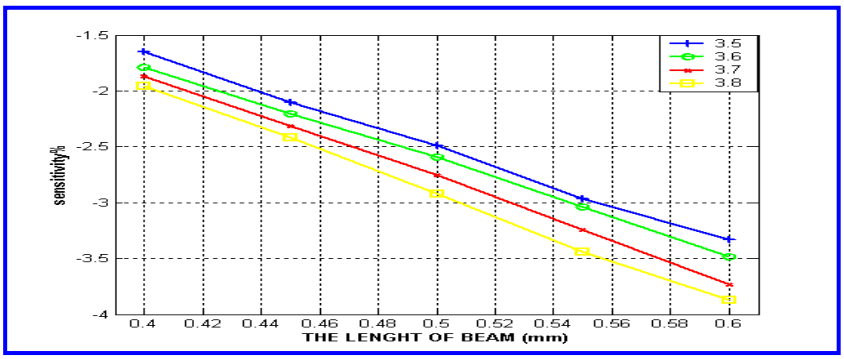

Fig. 10 :The relationship between the relative frequency variation (sensitivity) of beam1 and the length of beam

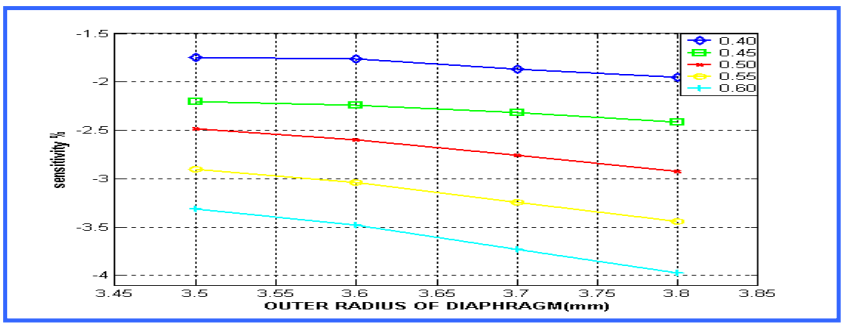

Fig. 11: The relationship between the relative frequency variation (sensitivity) of beam1 and the outer radius of diaphragm A

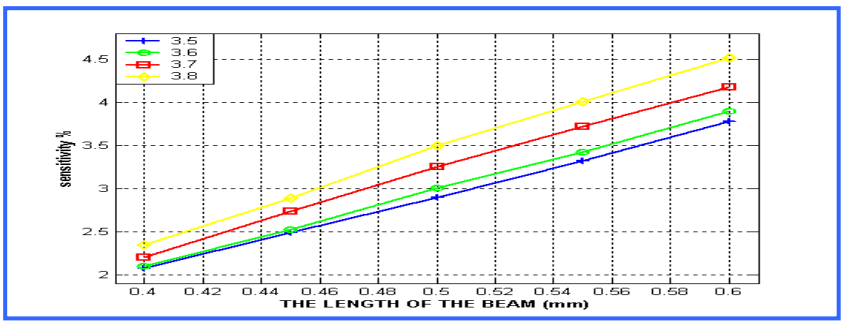

Fig. 12: the relationship between the relative frequency variation (sensitivity) of beam2 and the length of beam

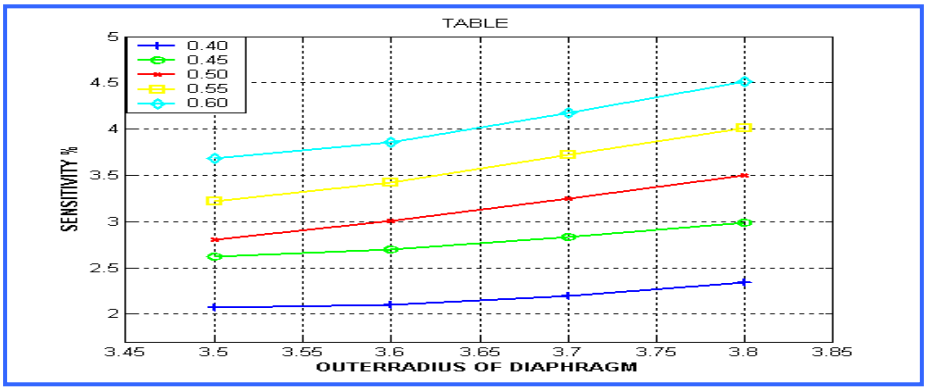

Fig 13 the relationship between the relative frequency variation (sensitivity) of beam2 and the outer radius of diaphragm A

6. Conclusion

The modeling and simulation for a novel resonant silicon micro-sensor are carried out in this paper. The elementary sensing component of the micro-sensor is the E-type round diaphragm and its final sensing component is the beam resonator which is attached to the E-type round diaphragm.

The sensor is made of silicon, E = 1.3×10^{11}pa, $\rho=2.3\times10^{3}\ kg/m^{3}$, $\mu=0.17$. The inner radius is as B = $1.4\times10^{-3}\ m$ and the thickness of the E-type round diaphragm is as $H=30\times10^{-6}\ m$. The width and thickness of the beam are $b=50\times10^{-6}\ m$ and $h=5\times10^{-6}$. Assuming the measured acceleration $a\in(-100,+100)\,m/s^{2}$, corresponding inertial force are $F\in(+1.3,-1.3)\times10^{-2}\ N$ to $F\in(+1.304,-1.304)\times10^{-2}\ N$ as the outer radius of the E-type round diaphragm are $A=(3.5,3.6,3.7,3.8)\times10^{-3}\ m$ and the frequencies of the beam are $f(0)$= (244745,189134,153561,126914, 106648) Hz for measured acceleration a=0 as the length of the beam L = (400, 450, 500, 550, 600) $\times10^{-6}$ m respectively.

Then the simulation results are as follows:

The frequency range for Beam1 is (149327~ 157675)Hz which located at the outer edge the measured acceleration as within (-100,+100) m/s^{2} ,the frequency range for Beam2 is (158555~ 148380)Hz which located at the inner edge the measured acceleration as within (-100,+100) m/s^{2}. In addition to the variation and relative variation or the sensitivity of the basic natural frequency of the beam1 $\Delta f(-100\,m/s^{2})$ = -4234 Hz, $\Delta f(+100\,m/s^{2})$ = 4115 Hz,

$\beta(-100\,m/s^2)$=-2.757%,
$\beta(+100\,m/s^2)$ = 2.680%,
$f(0)$=153561Hz. And the variation and relative variation or the sensitivity of the basic natural frequency of the beam2
Δf $(-100\,m/s^2)$ = 4994Hz,
$\Delta f(+100\,m/s^2)$ = -5181 Hz,
$\beta(-100\,m/s^2)$=3.252%
$\beta(+100\,m/s^2)$=-3.374%
$f(0)$=153561Hz. Moreover, as the differential frequency output of the above accelerometer between Beam1 and Beam2 is
(-9228, 9295)Hz

References

[1] P. Parsons, A. Glendinning and D. Angelidis, "Resonator Sensor for High AccuracyPressure Measurement Using Silicon Technology," Schlumberger Industries Aerospace.Transducer Division, IEEE AES Magazine, pp. 45-48, July 1992.

[2] G.Gautschi chapter 9, piezoelectric Sensor (2001) 731-8621-g27z .

[3] Shangchun Fan, Guangyu Liu, Man Hyuna Lee, Finite-element modeling and simulation on a novel microstructure silicon accelerometer with direct frequency output, SPIE Volume 3087, 1997.

[4].Baltes,W.Gopel,J.Hesse,“SensorsUpdate”,Volume7,Sensortechnology;Applications; Markets(1998).

[5] Ljubisa Ristic, "Sensor Technology and Devices", Artech House Boston, London (1994).

[6] S. Middelhock, Quo vadis silicon sensor, report, 1996.

[7] S. Middelehoek, Quo vadis silicon sensors & Actuators, A 41-42 (1994) 1-8.

[8] H.Baltes,W.Gopel, J.Hesse"Sensors Update",Volume 4 Sensor technology; Applications; Markets (1998).

[9] Shangchun Fan, Guangyu Liu, Man Hyuna Lee, Finite-element modeling and simulation
on frequency characteristics of the silicon beam resonator attached to an E-type round diaphragm for measuring the concentrated force, Sensors and Actuators, A63 (1997), 169-176.

Study The Effects of Noise on The Identification of MIMO Systems

Dr. M. M. Bakush* Eng. Abdunaser M. Abdusamad**
Electrical & Electronic Engineering Department
Alfateh University
**Tel*: +218912200263, E-mail: mbakush @yahoo. co. uk
***Tel*: +218913671071 E-mail: nsssser1970 @yahoo.com

Abstract

To study the effects of noise for any MIMO systems, it's necessary to have a model for it, that will describe the system behavior, this could be done by a system identification process, which is used for a construction of a different models structure for a certain system, and then compared with each other to choose the best model of them.
In this paper the principle of the SI techniques is used for a nonlinear MIMO system (5-inputs, 3-outputs) which is a(Process of Ethane-Ethylene Destillation) and also to see the effects of noise for the models produced.

I. Introduction

The requirement of SI from operating input-output data, is basically for estimating the system, or the parameters of the system, or to build a model that will adequately describe the system behavior.
To construct a model for any system from it's input/output data by a SI techniques, it's involves 4-basic steps:

1.The data:
The input-output data are sometimes recorded during a specifically designed identification experiment.
In other cases the user may not have the possibility to affect the experiment, but must use Data from Normal operation of the system.
2. A set of models:
a set of candidate models is obtained by specifying within which collection of models that are going to look for a suitable one. This is the most important, and at the same time, the most difficult choice of the system identification procedure . In most cases linear models are used, without reference to the physical background of the system. Such a model set, is called a black box model.
3. Model validation process:
In this process the data is divided in two parts, one for estimation and the other for validation, and from the compression between the models which use the estimation data by a validation data set, it could be decided that the model is accepted or not.
4. Determining the "best" model:
From a set of models which can reproduce the measured data with an acceptable level.

II. MIMO Systems

The systems with the input signal has m-components, and output signal has p-

components are called multivariable systems.

If the p-components of the output signal is collected with a p-dimensional column vector $y(t)$ and similarly construct an m-dimensional input vector $u(t)$, also let the disturbance $e(t)$ be a p- dimensional column vector.

Then the basic system description becomes as in the following equation:

$$y(t)=G(q)u(t)+H(q)e(t) \qquad (1)$$

where, the $G(q)$ is the transfer function matrix of dimension $p\times m$ and $H(q)$ has dimension $p\times p$, this means that the i, j entry of $G(q)$ which denoted by $G_{ij}(q)$ is the scalar transfer function from the input number j to the output number i.

III. MIMO System Identification

The following system is a chemical system with five inputs and three outputs, the system is a process to distillate the ethane-ethylene component from each other, by using a SI technique wants to construct a model for this system, which will describe the system behavior, and during this operation the effect of noise will be discussed.

- **Process of Ethane-Ethylene Distillation (destill. system)**

***System Description*:**

The number of data samples is (90-sample), 5-inputs, 3-outputs system as shown in fig(1), the system consists of 4 series, the 1st series is free of noise, the 2nd series is with 10% additive white noise, the 3rd series is with 20% additive white noise, and the 4th series is with 30% additive white noise and want to construct a model for each series, then discus the results obtained.

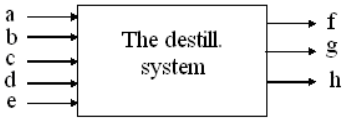

fig(1) Ethane-Ethylene Destillation System

Where:

Number of data Samples: 90

Sampling Time: 15 S.

Inputs:

a: ratio between the reboiler duty and the feed flow.

b: ratio between the reflux rate and the feed flow.

c: ratio between the distillate and the feed flow.

d: input ethane composition.

e: top pressure.

Outputs:

f: top ethane composition.

g: bottom ethylene composition.

h: top-bottom differential pressure.

The system equation is:

$$\begin{bmatrix} Y_1(s) \\ Y_2(s) \\ Y_3(s) \end{bmatrix} = \begin{bmatrix} H_{11}(s) & H_{12}(s) & H_{13}(s) & H_{14}(s) & H_{15}(s) \\ H_{21}(s) & H_{22}(s) & H_{23}(s) & H_{24}(s) & H_{25}(s) \\ H_{31}(s) & H_{32}(s) & H_{33}(s) & H_{34}(s) & H_{35}(s) \end{bmatrix} \begin{bmatrix} U_1(s) \\ U_2(s) \\ U_3(s) \\ U_4(s) \\ U_5(s) \end{bmatrix} \qquad (2)$$

and the transfer of the system matrix is:

$$H(s)=\begin{bmatrix} H_{11}(s) & H_{12}(s) & H_{13}(s) & H_{14}(s) & H_{15}(s) \\ H_{21}(s) & H_{22}(s) & H_{23}(s) & H_{24}(s) & H_{25}(s) \\ H_{31}(s) & H_{32}(s) & H_{33}(s) & H_{34}(s) & H_{35}(s) \end{bmatrix} \qquad (3)$$

the block diagram of the system is shown in fig(2).

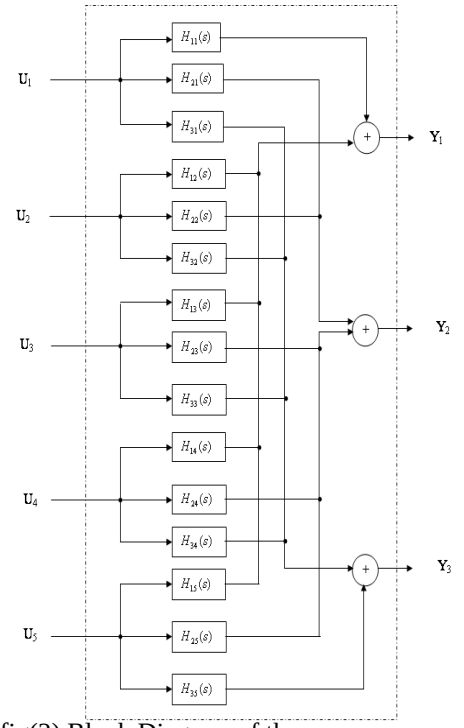

fig(2) Block Diagram of the Ethane-Ethylene System

A. *System Without Noise: (Original System)*

The original data for the destill. System is a data taken as a free of noise and want to construct a model for it.

the data is divided into a matrix of 90 rows × 9 column as follows:

Column 1: time-steps.
Column 2: Input A.
Column 3: Input B.
Column 4: Input C.
Column 5: Input D.
Column 6: Input E.
Column 7: Output F.
Column 8: Output G.
Column 9: Output H.

- ***System Analysis:***

1st by examining the data to remove any trends and outliers, and select useful portions of the used data.

1.**Examining the data**:

To check the data by plotting the outputs with the inputs, as shown in fig(3), and fig(4). Plot(zaa(:,1,1)) plot the input U_1 vs. 1st output Y_1.

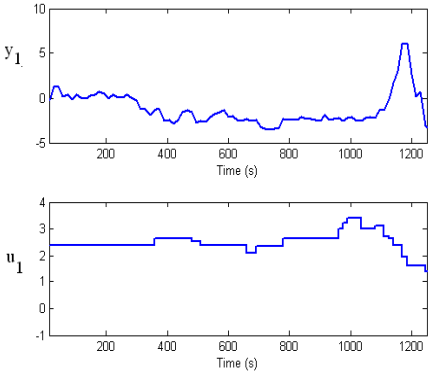

fig(3) The input U_1 vs. output Y_1

Plot(zaa(:,1,3)) plot the input U_3 vs. the 1st output Y_1

Plot(zaa(:,2,4)) plot the input U_4 vs. the 2nd output Y_2

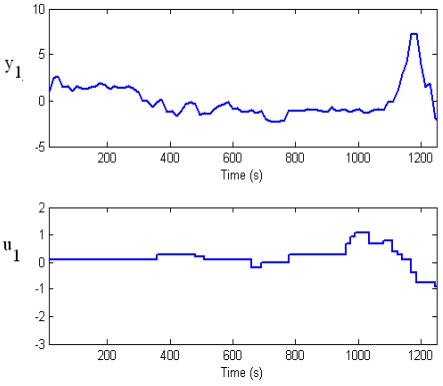

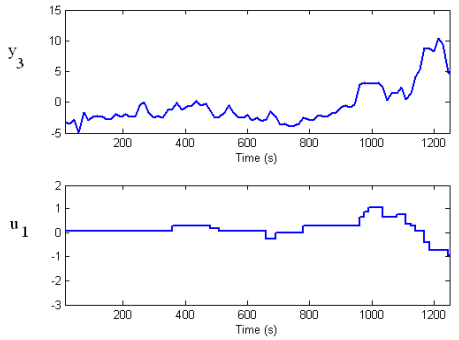

fig(4) The input U_1 vs. output Y_1 &U_1 vs. Y_3

As seen from the figures above, there is no trends or any outliers in data may effect on constructing the system model.

- ***Preliminary Analysis of Data:***

The Preliminary Analysis of Data, is used by estimating the Non-Parametric Models, for the system to try to know any information may help the user, to choose the suitable parametric model, and during the work for the black-box models, so the Preliminary Analysis of Data will not give any information about the system.

- ***Parametric Analysis of Data***:

The simplest way to get started on a parametric estimation routine is to build a state-space model where the model-order is automatically determined, using a prediction error method. To estimate a model using the **pem** technique, yields:

mp = pem(zaa(1:60)); where mp is the state-space model.

State-Space model: X(t+Ts) = A x(t) + B u(t) + k e(t)

Y(t) = C x(t) + D u(t) + e(t)

A =

	$x1$	$x2$	$x3$	$x4$
$x1$	−0.0974	−1.985	−0.810	−0.185
$x2$	−0.186	−0.785	−0.123	0.0234
$x3$	0.577	1.936	0.971	−0.228
$x4$	−0.630	−0.053	−0.502	0.3954

B =

	$u1$	$u2$	$u3$	$u4$	$u5$
$x1$	2.470	−2.906	−782.4	921.5	−157.3
$x2$	1.355	−1.038	485.6	496.1	−640.6
$x3$	−2.935	3.312	−923.7	−462.7	194.7
$x4$	−0.976	−0.826	−1720	1341.3	555.9

C =

	$x1$	$x2$	$x3$	$x4$
$y1$	−0.0003	−0.0001	−0.0005	−0.0001
$y2$	−0.0001	0.0004	−0.0001	0.0002
$y3$	−5.779	−0.0017	−0.0003	4.0991

D =

	$u1$	$u2$	$u3$	$u4$	$u5$
$y1$	0	0	0	0	0
$y2$	0	0	0	0	0
$y3$	0	0	0	0	0

K =

	$y1$	$y2$	$y3$
$x1$	691.4	394.2	401.8
$x2$	−280.6	−513.04	408.2
$x3$	−349.2	−869.5	−624.3
$x4$	−336.2	549.5	456.3

x(0) =

$x1$	0.751
$x2$	2.167
$x3$	−2.106
$x4$	−2.376

Estimated using PEM from data set z

Loss function 4.07423e-021 and FPE 3.6668e-020

Sampling interval: 15 s.

The following figure(5) shows the comparison between the state-space model mp, and the validation data set.

- ❖ Compare (zv,mp) the validation data with the state-space model mp.

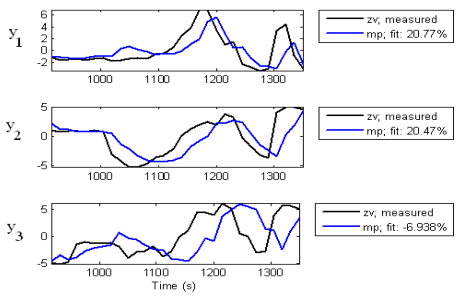

fig(5) Simulation of model output compared vs. validation data set

As seen from the fig(5),the model is acceptable at the output y_1 for the validation data, and does a reasonable job also for y_2 but it's far from y_3. And this, is due to the number of data samples very low 90 samples.

- ***Single-Input-Single-Output (SISO) Models:***

  Due to the number of data samples is very low (90), and also the state-space model obtained dose not give a good results , this will cause, the user must try to found an acceptable models better than state-space model. The ARX models is obtained as follows:

- Estimating using ARX models:

  Knowing the delays for each input/output and by selecting the best orders, the suitable arx model with 3-poles, 2-zeros, and zero delay will be constructed.

  As seen from the following figure, mm1, mm2, and mm3 gives the best arx models for the system.

  mm1 = arx(ze(:,1,3),nn); %ARX models

  mm2 = arx(ze(:,2,4),nn);

  mm3 = arx(ze(:,3,5),nn);

  where nn = [3 2 0]

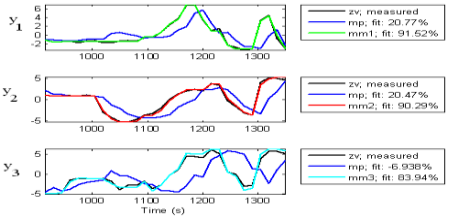

fig(6)Comparing the arx models with the validation data set

Also the same work is done for the other models structure (ARMAX; OE; BJ):

Finely, compare these models with the MIMO model mp and with the measured data (validation data set) as it clear in a following figure.

compare(zv,mp,mm1,mm2,mm3,mb1,mb2, mb3,md1,md2,md3,mo1,mo2 ,mo3)

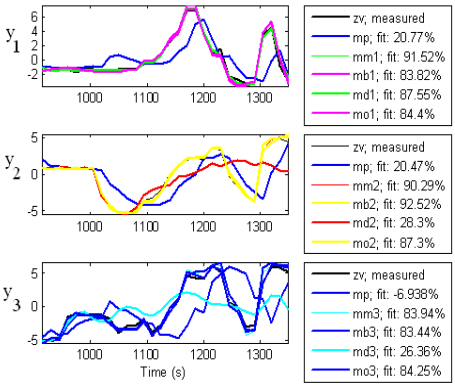

fig (7) Comparing the predictions of models (arx,armax,oe,bj,mp) on validation data set

Conclueding Remarks:

In this case for a dealing with the 5-input, 3-output system, It's clear that the prediction error method gives an acceptable state-space model structure, this due to the number of data samples is low, only 90 samples. But a SISO models structure give a better conclusion for all the outputs.

From the comparison between the models used it could be seen that mm1 (ARX) and md1(ARMAX) models gives the best fit of the first output (top ethane composition), while mb2 (BJ) and mm2 (ARX) models gives the best fit of the second output (bottom ethylene composition) and mo3 (OE) and mm3 (ARX) models gives the best fit of the third output (diff. pressure between top and bottom).

B. System With 10% Noise:

A 10% additive white noise is added to the system, then by the same work which is done in part A, the models is constructed as it seen in fig(8).

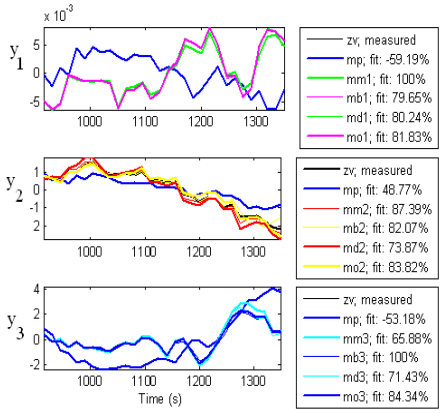

fig (8) Comparing the predictions of models (arx,armax,oe,bj,mp) on validation data set

From fig(8), It's clear that the prediction error method gives a good state-space model only on the output Y2 but it's not acceptable for both Y1&Y3, this is due to the effect of 10% added white noise, but still dealing with 60 samples for estimation, and we expect that this model will improve, if the no. of estimation data is increased up to 62 samples instead of 60, on the other hand by a looking for the other models, found that mm1 (ARX) model gives the best fit of the first output (top ethane composition), while mm2 (ARX) and mo2 (OE) models gives the best fit of the second output (bottom ethylene composition) and mb3 (BJ) and mo3 (OE) models gives the best fit of the third output (diff. pressure between top and bottom.

C. System With 20% Noise:

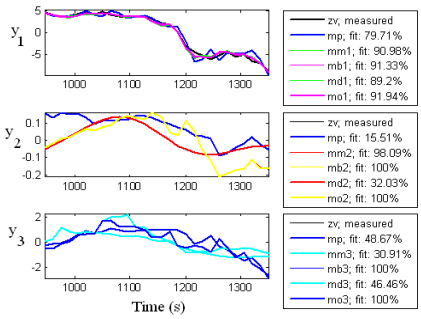

fig(9)Comparing the predictions of models (arx,armax,oe,bj,mp) on the validation data set

It's clear that the prediction error method (mp)gives a good state-space model for all the outputs, this is due to increasing the no. of data samples at estimation, and the effect of the added 20% noise cause that the 60 samples are not suitable for the estimation, and the number of the estimation data must increase by 2 data samples to get an acceptable results, on the other hand by a looking for the other models, it could be found that mo1 (OE) and mb1 (BJ) models gives the best fit of the first output (top ethane composition), while m02 (OE) and mb2 (BJ) models gives the best fit of the second output (bottom ethylene composition) and mb3 (BJ) and mo3 (OE) models gives the best fit of the third output

D. *System With 30% Noise:*

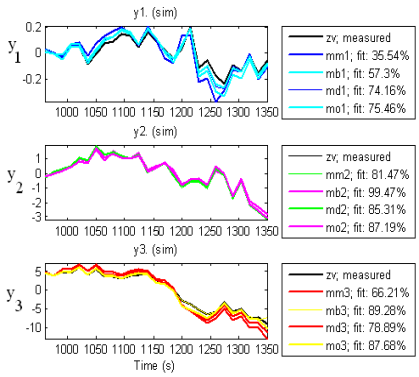

fig(10) comparing the predictions of models (arx,armax,oe,bj) with the validation data set.

when the percent of noise reach 30% the prediction error model(mp) cannot follow the system by any change of the no. of estimation data samples, and this due to the effect of noise which causes to increase the range of error between ze & zv . on the other hand, the SISO models gives a good fit for the system, and the effect of added noise is still small. By looking to fig(10) it found that mo1 (OE) model gives the best fit of the first output (top ethane composition), while mb2 (BJ) model gives the best fit of the second output (bottom ethylene composition) and mb3 (BJ) and mo3 (OE) models gives the best fit of the third output (diff. pressure between top and bottom).

IV. Conclusion

This paper interested to study the principles of system identification for MIMO systems, the deferent methods used, how to choose the best model from a set of candidate models, and the effect of noise for a construction of model structure.

- The key conclusion in multi-variable system identification is the kind of data used, which it depends on, (the number of data samples, the effect of noise), and the number of inputs and outputs for the system.
- The nonparametric methods is seen as preliminary experiments, to know the time-domain performance like delay time, settling time, …. etc, and what the model order to be selected, this will help the user for what the suitable parametric method should be used.
- In the parametric model estimation, there is no a closed form used to calculate the model parameters, but the work is done from an algorithms.
- In constructing parameter estimates for a dynamic models that include noise, the least squares method is not good scheme, in this case Maximum-likelihood is the suitable method used.
- The State-space model is the best model used to represent MIMO system identification, due to, it is not give information about the system parameters only, but also gives a good information about the state and will give a good results when the number of data samples are high, and the percent of noise is low.
- The results obtained from the OE & BJ models are approximately the same, this is due to the kind of noise used (white), while BJ will give a more accurate models when a hard noise is used.

VI. References

1) Torsten Soderstrom & Petre Stoica **"System Identification"** 1989
2) Lennart Ljung University of Linkoping sweeden **"System Identification"** Theory for the User.1987

3) Tohru Katayama **"Subspace Methods for System Identification"**.2005
4) System Identification Using Black-Box Modeling Technique.2008
5) Lennart Ljung **''From Data to Model A Guided Tour of System Identification''** Department of Electrical Engineering Linkoping University S-581 Linkoping, Report Lith-ISY-R-1652.2005
6) Y.Zhu(Editor) **''Multivariable System Identification for Process Control''** October 2001.
7) Lennart Ljung **''System Identification Toolbox for Use with Matlab''**, Versions 2005, 7.4 (R2007a).

LOAD AND LINE DISTURBANCE'S EFFECT ON BUCK DC-DC CONVERTER'S PERFORMANCE UNDER SLIDING MODE CONTROL TECHNIQUE

Mohsen M. Elhimdi
Tajoura Research Center,
Tajoura Libya
elhimdim@yahoo.com

Dr. M.M. Bakush
EE Department Al_Fateh University, Tripoli
Libya
m.bakush@.ee.edu.ly

Abstract

This paper examines disturbance effect on both load and input voltage on the behavior of buck DC-DC converter. The converter utilizes sliding mode control technique to achieve stability and operating in continues conduction mode (CCM). Sliding mode controller design procedure for the converter haven outlined. System simulation model was built and tested; results based on these simulation shows excellent performance and good robustness against load variation as well as input voltage variation.

Key words Sliding Mode Controller; Disturbance; Converter

1 Introduction

Sliding Mode Control (SMC) methodology which is a particular type of Variable Structure Control System (VSCS) that was initiated in former Soviet Union in the late 1950's and is considered as one of the most popular approaches to control variable structure systems (VSS). Sliding mode controller application to power converter goes

back to 1983, where Bilalovic *et al*. applied SMC to DC/DC converters and in 1985 Venkataramanan *et al*. presented a comprehensive study on the application of SMC to the three basic topologies (Buck, boost and buck boost). Detailed SMC literature review is presented in [1].

2 Sliding Mode Controllers

The general system with scalar control can be represented in the following form [2]:

$$\dot{X} = f(x,t,u) \qquad (1)$$

Where x is a column vector and f is a function vector both of these vectors are of dimension n , u is the control input that can influence the system motion. If f is discontinuous on the manifold given by $S(X,t)=0$, thus f can be rewritten as:

$$f(X,t,u) = \begin{matrix} f^+(x,t,u^+) & for \quad S(x) \to 0^+ \\ f^-(x,t,u^-) & for \quad S(x) \to 0^- \end{matrix} \qquad (2)$$

while the scalar discontinuous control input is given by:

$$u = \begin{matrix} u^+ \, for & s(x) > 0 \\ u^- \, for & s(x) < 0 \end{matrix} \qquad (3)$$

Then the system is in sliding mode if its representative point RP moves on sliding surface given by: $S(x,t) = 0$.

In second-order system case such as buck converter, the sliding manifold can be chosen as a linear combination of state variables, which will results in a simple controller for practical implementation [2].

$$S(X) = C_1 X_1 + X_2 = 0 \qquad (4)$$

Where C_1 is a positive parameter known as the sliding coefficient. Three conditions must be obeyed in order for sliding mode can be achieved, namely, existence condition, reaching condition, and stability condition [1].

2.1 Existence condition

Sliding-mode existence condition requires phase trajectories of the two substructures corresponding to the two states of the control input u ={0, 1} to be directed toward the sliding manifold [2]; in other words the distance from the RP to the sliding line must be decreasing with time in both sides of the sliding manifold (*S>0* and *S<0*) . In mathematical terms this condition is expressed by:

$$S.\dot{S} < 0 \qquad (5)$$

2.2 Reaching condition

Reaching condition (reachability) is guaranteed if the representative point, RP located in the phase plane region that is reserved of one substructure has its steady state placed on the region reserved for the other substructure and vice versa [2]. Therefore, RP will eventually hit the sliding manifold

2.3 Stability condition

Since system dynamic in sliding regime is confined to the sliding manifold Eq. (4); system stability is granted by choosing a positive sliding coefficient C_1. This can be proved by realizing the fact that at the sliding manifold $S(x,t) = 0$, hence;

$$\begin{aligned} C_1 X_1 + X_2 &= 0 \\ C_1 X_1 + \dot{X}_1 &= 0 \end{aligned} \qquad (6)$$

The solution for this first order deferential equation is given by:

$$X_1(t) = X_1(t_0) e^{-C_1(t-t_0)} \qquad (7)$$

Therefore, for $X_1(t)$ to decay to zero (equilibriums point); the sliding coefficient C_1 must be positive. Furthermore, in the SMC operation, sliding coefficient is very crucial since it sets the dynamic response of the system with a first order time constant system equal $\tau = \frac{1}{C_1}$.

3 Equivalent Control

Performance of variable structure system VSS operating in sliding mode control; can be significantly simplified through equivalent control method [3], [4]. This method is based on replacing the discontinuous control signal u with an equivalent continuous low-frequency control signal u_{eq}, which will maintains system progress on the sliding surface. The method of obtaining equivalent control is as follows [1].

When the system $\dot{X} = f(x,t,u)$ is in ideal SM operation, the representative point RP will always be moving along the sliding manifold;

$$S(x,t) = 0 \quad \Rightarrow \dot{S}(x,t) = 0 .$$

Therefore, if the equivalent control produces a trajectory which is exactly equivalent to the trajectory's motion of an ideal SM operation; then the state trajectory equation can be expressed as:

$$\dot{S}(x,t) = G.f(x,t,u_{eq}) = 0 \qquad (8)$$

Where $G = \dfrac{\partial S}{\partial x}$ is a gradient vector.

System motion equation can be obtained by solving (8) for u_{eq} and substituting in system equation.

$$\dot{X} = f(x,t,u_{eq}) \qquad (9)$$

4 Mathematical model of buck converter

Buck DC/DC converter shown in Fig. (1) is non-linear time varying system; it is the simplest among DC/DC converters topologies (Buck, Buck boost and buck boost). Designing a SMC for such converter requires state-space model description of the converter in terms of suitable control variable (state variable). For simple practical implementation; controllable states are chosen as output voltage error and its derivative which is the voltage error dynamics [5]. These states are continuous and accessible for measurement; therefore they are quite suitable for SMC application.

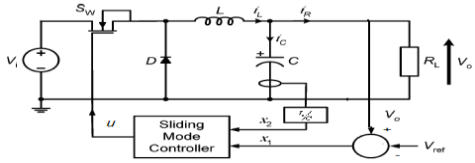

Fig. 1 Basic buck converter under Sliding mode controller

The mathematical model of buck converter in terms of the following state variable:

$$X_1 = V_o - V_{ref} \qquad (10)$$

$$X_2 = \frac{dX_1}{dt} = \frac{d(V_o - V_{ref})}{dt} = \frac{I_c}{C} \qquad (11)$$

Is expressed as:

$$\dot{X}_1 = X_2$$

$$\dot{X}_2 = -\frac{X_1}{LC} - \frac{X_2}{RC} - \frac{V_{ref}}{LC} + \frac{V_{in}.u}{LC} \qquad (12)$$

4.1 SMC for buck DC-DC converter

SMC methodology for buck converter is based on cascade control structure; where two control loops are used [4]; one for output voltage (outer loop), and the second for inductor current (inner loop); combination of these two loops represent the Sliding Mode Controller; design procedure can be summarized in the following steps:

Step one Select suitable system's state variable and derive the mathematical model.

Step two choose a logic control signal u which will enforce representative point RP toward the sliding manifold $S(x,t)=0$, and consequently enforce inductor current to track reference current.

$$u=\begin{cases}1 & for\ S(x)<0\\ 0 & for\ S(x)>0\end{cases} \qquad (13)$$

Step three: Based on the selected state variable chosen in step one; the control criterion, which is the desired steady state output of the converter should be set. Obviously the control criterion is to achieve zero output error; therefore at steady state, state variable will be:

$$X_1=0 \quad \Rightarrow \dot{X}_1=\frac{I_c}{C}=0 \qquad (14)$$
$$X_2=\dot{X}_2=0$$

Step four: Constructing the sliding function, since control criterion require zero current through the capacitor, thus, at steady state inductor current must equals to load current; therefore the sliding function can be expressed as the difference between inductor current I_l in the dynamic region (nonlinear control part) and desired (reference) steady state inductor current I_l^* (linear control part).

$$\begin{aligned}S(x)&=I_l-I_l^*\\&=I_c+I_R-I_l^*\\&=CX_2+\frac{V_o}{R}-\int\frac{V_l}{L}dt\\&=CX_2+\frac{(X_1+V_{ref})}{R}+\int\frac{((X_1+V_{ref})-V_{in}u)}{L}dt\end{aligned} \qquad (15)$$

Where $V_l=(V_{in}u-V_o)$ is the voltage across the inductor.

Step five: Derive the expression for equivalent control u_{eq} by solving $\dot{S}(x,t)=0$ and using control criterion equation (14).

$$\dot{S}(x,t)=C\dot{X}_2+\dot{X}_1-\frac{(V_{in}u_{eq}-X_1-V_{ref})}{L}=0$$

$$u_{eq}=\frac{V_{ref}}{V_{in}} \qquad (16)$$

Step six: by substituting Eq. (16) into Eq. (15) sliding function in terms of state variables is obtained.

$$S(x,t)=CX_2+\frac{(X_1+V_{ref})}{R}+K\int X_1dt \qquad (17)$$

Where $K=a/L$ is the linear sliding coefficient (proportional gain), L is the inductor value in Henries and (a) is a constant. Choosing low value for (a) will reduce the overshoot but will increase steady state error; therefore this value must be set by the designer depending on the application and beast performance.

Step seven: Eq. (17) is used to construct the SMC shown in Fig. (2).

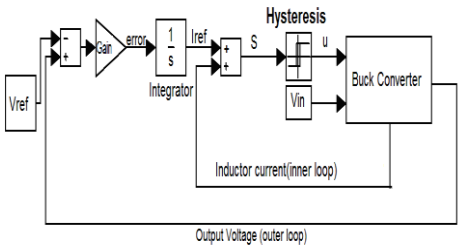

Fig. 2 SMC structure for buck DC-DC converter

5 Simulation results and discussions

Simulation model for buck DC-DC converter is designed according to Eq. (25).

Selected converter parameters [4] are given in table 1

Table 1 Buck Converter parameters

Parameter	Symbol	Value
Input voltage	V_{in}	20 volts
Output voltage	V_o	12 Volts
Capacitor	C	10 μF
Inductor	L	1 mH
Load resistance	R	2.4 Ω
Switching frequency	F_s	100 kHz

Before any disturbance can be applied to the system, a number of simulation tests were done under different linear sliding coefficients K till finest performance (shortest transient time and minimum state error) is achieved as shown in Fig. (3).

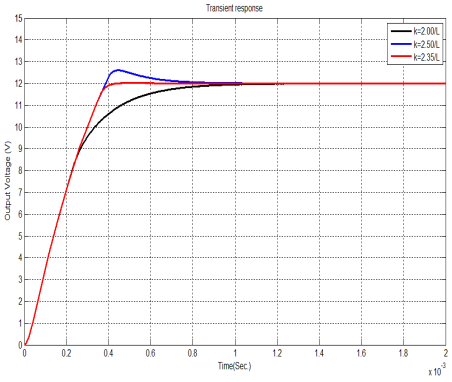

Fig. 3 Linear sliding coefficient (K) effect on system transient response.

5.1 Load disturbance

Simulation model was tested under load variation, where the load resistance is altered from 2.4 Ω to 8.4 Ω for 10 ms. starting at *t=0.01sec.* , Fig. (4) Shows output voltage, inductor current and load wave forms. It can be observed that system exhibit overshoot of about 8V and settling time of about 0.001sec before reestablish stability at 12Vand 1.43A as expected. However, when load is back to nominal value at time *t=0.02*sec, inductor current and output voltage experience smaller disturbance before stabilizing at 5A and 12V respectively.

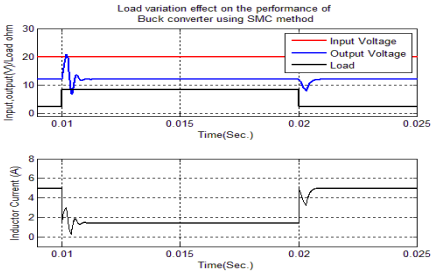

Fig. 4 Load disturbance's effect on buck converter's performance under SMC method.

5.2 Input disturbance

Input disturbance's effect on buck converter dynamic behaviour, under sliding mode control is simulated. A step-up input from nominal value 20V to 25V at time *t=0.050sec*. Also step-down input from nominal value 20V to 15V at time *t=0.054sec*. Simulation result is shown in Fig. (5a) and Fig. (5b) respectively; from these two figures, it's clear that the control signal's instant switching frequency changed to accommodate for input disturbance before its effect reaches the output. Therefore, neither the output voltage nor inductor current was affected by input variation.

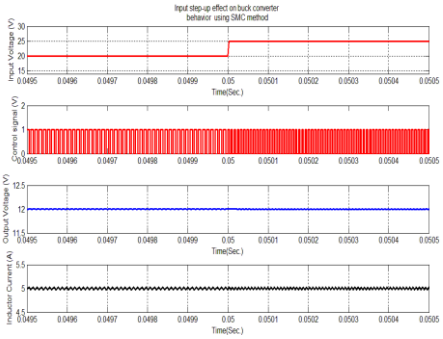

Fig. 5a Step-up input effect on buck converter output behavior using SMC

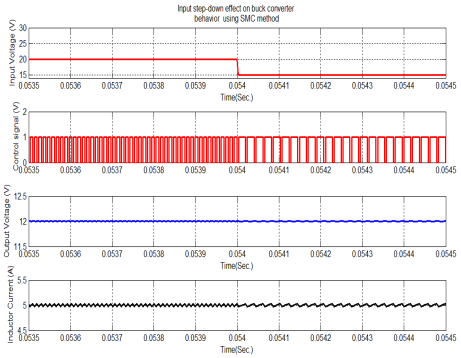

Fig. 5b Step-down input effect on buck converter output behavior using SMC

6 Conclusions

Sliding mode control represents a powerful tool to enhance performances of power converters, such as buck DC-DC converter. In this paper a buck converter simulation model is designed based on a sliding mode controller. The model was tested under load as well as input disturbance. Simulation results showed that Load disturbance has high effect on buck output voltage behavior before stabilizes to desire level where as input disturbance has negligible effect on output voltage as well as load current.

References

[1] Siew-Chong Tan, Y. M. Lai, Chi K. Tse "*General Design Issues of Sliding-Mode Controllers in DC–DC Converters*"; IEEE Transaction on Industrial Electronics, Vol. 55, No.3, March 2008

[2] G. Spiazzi, P. Mattavelli, L. Rossetto "*Sliding mode control of DC-DC Converters"*

[3] R. Venkataramanan,: "Sliding-mode control of Power converters," PhD thesis California Institute of Technology Pasadena, California, 1986

[4] E.h.E. Bayoumi, A Simplified Method for Controlling Dc-Dc Converters Using Sliding Mode Control**,** Proceedings of the 22nd lasted international conference modeling, identification, and control, February 10-13,2003, Innsbruck, Austria

[5] Siew-Chong Tan, Y. M. Lai, Martin K. H. Cheung, Chi K. Tse*; "On the Practical Design of a Sliding Mode Voltage Controlled Buck Converter";* IEEE transactions on power electronics, vol. 20, no. 2, march 2005

LOAD AND LINE PERTURBATION EFFECT ON BUCK DC-DC CONVERTER'S PERFORMANCE UNDER PID CONTROLLER

Mohsen M. Elhimdi
Tajoura Research Center,
Tajoura Libya
elhimdim@yahoo.com

Dr. M.M. Bakush
EE Department Al_Fateh University, Tripoli
Libya
m.bakush@.ee.edu.ly

Abstract load and line Perturbation's effect on buck Dc-Dc converter's performance under PID controller is presented in this paper. The procedure to stabilize the converter; by selecting and designing a suitable compensator type based on open loop frequency response is introduced in details. The K-factor approach to place Compensator's poles and zeros is explained. Finally, a simulation model is designed using the presented approach, simulation showed a high performance system with sufficient stability margin and good disturbance rejection.

Key words Buck converter; PID compensator.

1. Introduction

The buck converter circuit is shown in fig.1 [1] is a class of switching converters, which are widely used to supply well regulated power in electrical power systems. This type of converters offers high efficiency as compare to linear regulators.

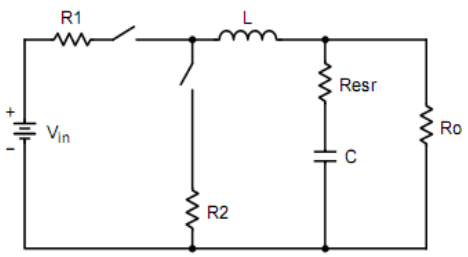

Fig.1 Buck DC-DC converter.

Feedback control loop of buck converter shown in fig. 2 [1] consists of three stages; power stage $G_p(s)$, Pulse Width Modulation stage (PWM) stage (these two stages are commonly grouped as the modulator) and the compensator stage $G_c(s)$. Many papers were published on buck stability and optimization [1], [2], [3]. This paper investigate load and line perturbation effect on buck performance through computer simulations model.

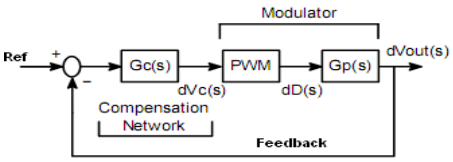

Fig.2 Buck converter feedback loop.

2. Modulator transfer function

Modulator transfer function $A_{\mathrm{mod}}(s)$ can be expressed as [1].

$$\frac{dV_{out(s)}}{dV_c(s)} = \frac{V_{in}}{V_{st}} \frac{R_{esr}CS+1}{LC[S^2+(\frac{1}{R_oC}+(\frac{R+R_{esr}}{L}))S+\frac{1}{LC}]} \quad (1)$$

Assuming $R_o >> R_{esr}$ and $R_o >> R$ where $R = DR1+(1-D)R2)$ and D is the duty cycle. The term in the brackets in the denominator is in the form of second order characteristic equation ($S^2 + 2\xi\omega_0 S + \omega_0^2 = 0$) from which two poles can be defined located at

$$\omega_0 = \frac{1}{\sqrt{LC}} \qquad \Rightarrow f_p = \frac{1}{2\pi\sqrt{LC}} \quad (2)$$

Plus a zero which introduced by ESR located at

$$\omega_z = \frac{1}{R_{esr}C} \Rightarrow f_z = \frac{1}{2\pi R_{esr}C} \quad (3)$$

Typical buck modulator open loop frequency response is shown in Fig. 3. [1]. The figure shows that bellow f_p gain is constant and minimum phase shift. From f_p to f_z, gain falls at -40 dB/decade due to the effect of complex conjugate poles introduced by LC filter, meanwhile phase tends toward -180 degrees. Beyond f_z the zero introduced by R_{esr} will cancel the effect of one pole, therefore gain curve will fall at -20 dB/decade only while phase curve toward -90 degrees.

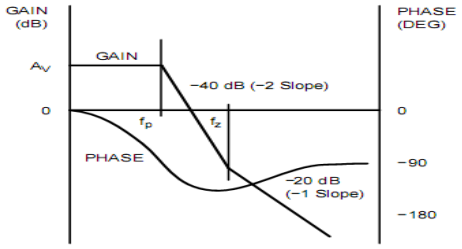

Fig. 3 Typical Gain/Phase buck modulator open loop response.

Buck converter specifications are given in table 1

Table 1 Buck parameters

Description	Parameter	Value
Input voltage	V_{in}	20 V
Output voltage	V_o	12 V
PWM saw tooth	V_{st}	2.0V
Capacitor	C	10 μF
Inductor	L	1 mH
Load resistance	R_o	2.4 Ω
Equivalent series resistance	R_{esr}	0.07 Ω
Switching Freq.	F_s	100 kHz

3. Stability criterion

In order to accomplish precise and tight output voltage regulation; feedback loop with suitable compensator network $G_c(s)$ must be incorporated. The compensator should accomplish the following stability criterion [4]:

A) High gain at low frequency region to guarantee accurate output voltage regulation and to minimize the steady state error.

B) Crossover frequency f_c should be in the range $0.1f_s < f_c < 0.2f_s$; where f_s is converter switching frequency to insure fast response to transients, such as sudden load change

C) Typical phase margin range from 45^O to 60^O for fast stable system.

4. Compensator design using K factor approach.

Compensator's objective is to stabilize the feedback system (converter) in addition to quickly response to regulate the output voltage against input or load variation. Therefore, compensator Gain/Phase ought to be shaped such that when integrated with open-loop gain/phase will satisfy stability requirements. Type III (PID) compensator is the most suitable for stabilizing buck converter; its implementation will result in superior transient response. The compensator transfer function includes one pole at the origin and two zero-pole pairs; however, for optimum performance consideration, coincident zero-pole placement form will be implemented. This form enhances the phase boost curve by making it narrower and the amount of phase boost is increased. Fig. 4 [1] shows compensator network and its frequency response (un-coincident form) Fig. 5 shows frequency response in coincident zero-pole placement form.

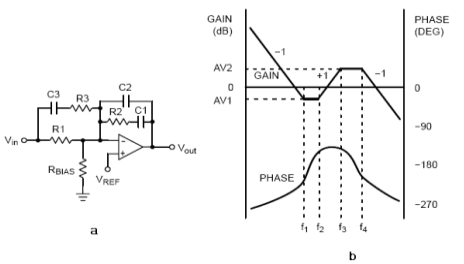

Fig.4 Type-III (PID) compensator network and its frequency response

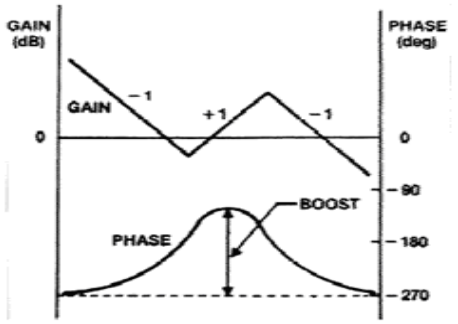

Fig. 5 Type III (PID), frequency response of coincident zero-pole placement form.

Compensator transfer function in coincident zeros poles form is given by:

$$\frac{V_{out}}{V_{in}} = Comp\_G\,\frac{(S+\omega_z)^2}{S.(S+\omega_p)^2} \qquad (4)$$

where;

$$Comp\_G = \frac{R_1 + R_2}{R_1 R_2 C_2} \qquad (5)$$

The K factor method [3],[4],[5] is a powerful mathematical stabilization tool which places pole(s) and zero(s) to crossover at a particular frequency with a precise phase margin, the concept was introduced in 1980s by D. Venable. It is a measure of gain reduction at low frequencies and increase of gain at high frequencies by controlling the position of pole(s) and zero(s) of the compensator networks, the procedure requires choosing

the desired crossover frequency f_c and the amount of phase margin needed at f_c then by applying the K factor concept, locations of poles and zeros can calculated such that f_c is the geometric mean between their respective locations where phase boost is maximum. For type III compensator the two zeroes are placed below crossover by a factor of $\sqrt{K}$, and the two poles above crossover by the same amount as illustrated in Fig. 6 [5].

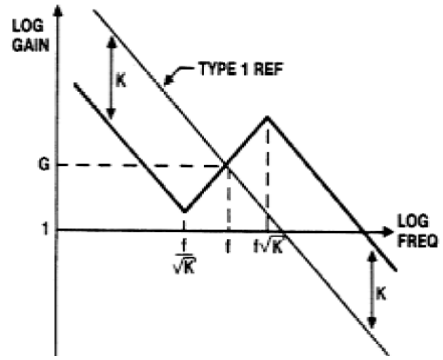

Fig. 6 Zeros and poles placement in Type III compensator using K factor approach.

Total Phase boost from coincide zeros at $f_z = f\sqrt{K}$ and coincide poles at $f_p = f_c/\sqrt{K}$ is given by [5]:

$$\phi_{boost} = 2[\tan^{-1}(\sqrt{K}) - \tan^{-1}(\frac{1}{\sqrt{K}})] \quad (6)$$

Using the trigonometric identity:

$$\tan^{-1}(X) + \tan^{-1}(\frac{1}{X}) = 90^0 \quad (7)$$

Equation (6) can be expressed as:

$$\phi_{boost} = 4\tan^{-1}(\sqrt{K}) - 180^0 \quad (8)$$

By solving for K yields:

$$K = [\tan(\frac{\phi_{boost}}{4} + 45^0)]^2 \quad (9)$$

Compensator design procedure can be summarized as follows:

Step 1: From open-loop bode plot; determine the phase shift PS and modulator gain margin G_m at the selected crossover frequency f_c.

Step 2: Determine required Compensation G at the chosen crossover frequency which is given by:

$$G = 10^{(-G_m/20)} \quad (10)$$

Step 3: Calculate the total Phase boost (ϕ_{boost}) required by the compensator which is equal to:

$$\phi_{boost} = \text{PM-PS-90} \quad (11)$$

Step 4: Determine K factor from equation (9) and calculate compensator network components using table 2 [2]:

Table 2: Compensator's components value

	Type–I	Type–II	Type–III
R_1	User–Selected		
R_2	Not Used	$\frac{K^2}{K^2-1}GR_1$	$\frac{\sqrt{K}}{K-1}GR_1$
R_3		Not Used	$\frac{R_1}{K-1}$
C_1	$\frac{1}{2\pi f_c GR_1}$	$\frac{K^2-1}{K}\frac{1}{2\pi f_c GR_1}$	$\frac{K-1}{2\pi f_c GR_1}$
C_2	Not Used	$\frac{1}{K}\frac{1}{2\pi f_c GR_1}$	$\frac{1}{2\pi f_c GR_1}$
C_3		Not Used	$\frac{K-1}{\sqrt{K}}\frac{1}{2\pi f_c R_1}$

5. Buck simulation model using type III (PID) compensator

Switching frequency is set at 100 kHz; crossover frequency15 kHz, and phase margin PM 60 degrees. From modulator open loop bode plot shown in Fig. 7; at crossover frequency the phase shift is PS= -152 degrees and the gain margin $G_m = -19.6$, using equation (10) and (11), G=9.5499, ϕ_{boost}=122 degrees. Therefore, Appling equation (9) K=14.95., R_1 was set to 5k, R_2 and C_2 were calculated using table 2; compensator gain is calculated from equation (5). Compensator transfer function is given:

$$\frac{V_{out}}{V_{in}} = 1.3457e7 \frac{(S+2.3474e4)^2}{S.(S+3.6443e5)^2} \quad (12)$$

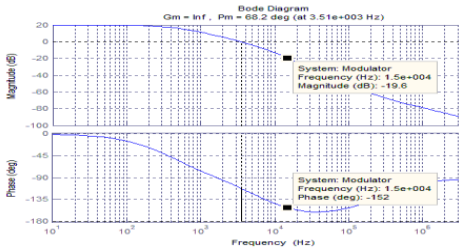

Fig. 7 Converter uncompensated Open loop bode plot

Fig. 8 shows compensated open loop frequency response where phase margin is 60 degrees at crossover frequency response as expected.

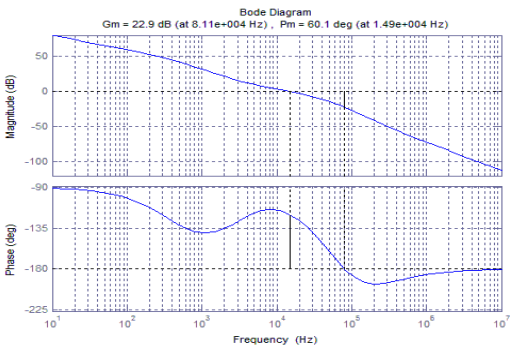

Fig. 8 Converter compensated Open-loop bode plot.

6. Simulation results and discussion

Simulation model is designed to simulate load and line perturbation effect on buck converter performance. The model is shown in Fig. 9.

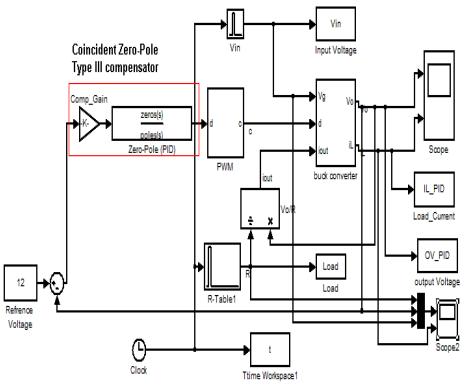

Fig. 9 Simulation model for buck converter using PID controller.

The Simulation model for buck converter using PID controller is tested under load and line perturbation as follow:

Case 1: Load variation

Simulation started with nominal load resistance of 2.0 Ω, then after system reached stability a step load change to 8.4 Ω at time=0.01 sec. Simulation waveforms for; input voltage, output voltage, load resistance and inductor current are shown in Fig. 10. From this figure, its is clear that output voltage experience high overshoot when step load is applied, however system was able to recover rapidly to steady state (12 volts) in about 0.0025 sec. due to fast dynamic response. Inductor current waveform also shows undershoot but recover to new steady state value of about 1.43A as expected.

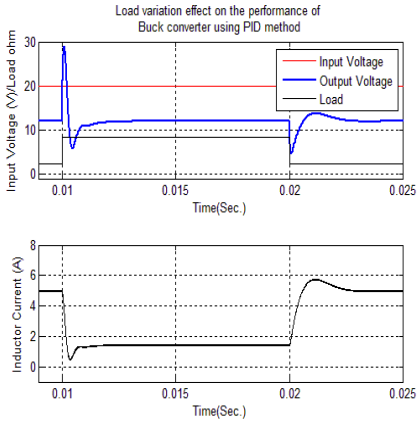

Fig.10 Load variation's effect on buck converter behavior.

Case 2: Line variation

In this case simulation started with nominal input voltage of 20 volts, then at time=0.04 sec. a step change is introduced into the input voltage; where the input was step-up to 25 volts. Simulation result is shown in fig. 11. As it can be seen from this figure that both; the output voltage and inductor current exhibit an overshoot when the input is up, then stabilized to the expected values 12 volts and 5 A respectively in less 0.005 sec. Also from the same figure one can observe that, when the input is back to nominal value at time=0.06 sec, both output voltage and inductor current waveforms experience undershoot before stabilizing back to steady state values.

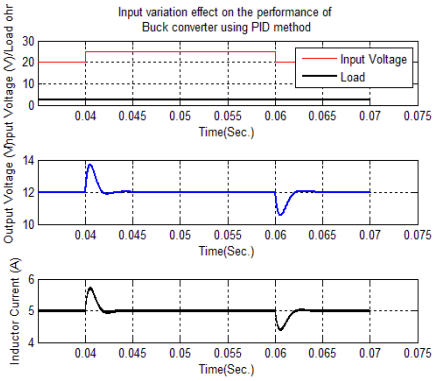

Fig. 11 Input voltage variation's effect on buck converter behavior.

7. Conclusion

This paper focused on type III (PID) compensator design for buck DC-DC converter in order to minimize load and line perturbation effect on converter performance. The chosen Compensator type has two zero-pole pair in addition to a pole at the origin, and for optimum performance; it is designed such that there are two coincident zeroes and two coincident poles symmetrically placed around crossover frequency. The K factor approach is used to place compensator's poles and zeros. Results from simulation module showed good dynamic response and system was able to promptly reestablish steady state performance following

disturbance that is caused by either input or load variation.

References

[1] W.H. Lei, T.K. Man, *"A General approach for optimizing dynamic response for bock converter "*

[2] Doug Mattingly "*Designing Stable Compensation Networks for Single Phase Voltage Mode Buck Regulators*", Intersil, Technical Brief December 2003

[3] Venable Technical Paper #3 "*Optimum Feedback Amplifier Design for Control Systems"*

[4] Ned Mohan, Tore M. Undeland, William P. Robbins, "*Power Electronics: Converters, Applications, and Desig*n", 3rd Edition, Wiley

[5] H. Dean Venable *"The K Factor: A new mathematical tool for stability analysis and synthesis"*

APPROXIMATION OF STANFORD ROBOT PARAMETERS USING NEURAL NETWORK

Paper code number 102518

Ali Lesewed
The higher institute of electronics,
Beni Walid -Libya
ali_lesewed@yahoo.com

Mostafa Alfillani
The higher institute of electronics,
Beni Walid-Libya

Abstract

The paper describes applications of feedforward neural network and back propagation learning method for calculation of mathematical model for Stanford robot. The model is based on the Lagrange-Euler formulation and described by a set of nonlinear differential and algebraic equations. A numerical example has shown the comparison of neural model and robot manipulator.

Keywords: Stanford robot, dynamic model, neural nets.

1 Introduction

The model of Stanford manipulator is nonlinear, and subject to structured and unstructured uncertainties. Structured uncertainties are caused by imprecision in the manipulator link properties like length and unknown loads, whereas unstructured uncertainties are caused by friction and disturbances [10]. Due to such problems mentioned previously, it is very hard to approximate the parameters of the real robot precisely.

The capability of the neural network (NN) to approximate arbitrary nonlinear functions and to learn through examples makes it the main tool of many useful applications in robotics and control engineering [6,8]. For this reason, employing neural net is a proper tool for the calculation of robot models. This approach has great advantage of easy and quick modeling of nonlinear functions that are inherent in the robot manipulator.

In this article, the model of Stanford type robot has been approximated using neural net technology. In section 2, Lagrange-Euler equation is presented for model of robot dynamics. In section 3, the feedforward neural net proposed for model approximation is structured and explained. In section 4, the numerical results are presented for evaluation. The last section is devoted to remarks and conclusions.

2 Model of robot manipulators

The dynamic equation of a robotic manipulator with n-degree of freedom can be described by a differential nonlinear matrix Lagrange-Euler or Newton-Euler equation [1,2,3].

$$M(y)\ddot{y} + D(y,\dot{y}) + G(y) = \tau \qquad (1)$$

where $y \in R^n$ is the vector of joint position, $\tau \in R^n$ is the vector of generalized torque inputs, $M(y) \in R^{n\times n}$ is the symmetric positive definite inertia matrix, $D(y,\dot{y}) \in R^n$ is the vector characterizing Coriolis and centrifugal forces, $G(y) \in R^n$ is the gravitational force vector, $\dot{y}$ and $\ddot{y}$ are vectors of joint velocity and joint acceleration respectively. In reality, a robotic manipulator is always affected by unknown factors such as frictions and disturbances but in our equation these factors have been ignored.

The following equation is a discrete time model of robot derived from the above Lagrange-Euler equation:

$$y(k+1) = 2y(k) - y(k-1) + A[y(k), y(k-1)] + B[y(k)] + C[y(k)]\tau(k) \qquad (2)$$

Where

$$A[y(k), y(k-1)] = -T_p^{\,2} M^{-1}[y(k)] D[y(k), y(k-1)]$$
$$B[y(k)] = -T_p^{\,2} M^{-1}[y(k)] G[y(k)]$$
$$C[y(k)] = T_p^{\,2} M^{-1}[y(k)]$$

and $A \in R^n$, $B \in R^n$, $C \in R^{n\times n}$ are matrices whose entries are nonlinear functions with unknown parameters. The derivatives were approximated using the following rectangular forward/backward approximation:

$$\dot{y}(t) \cong \frac{y(t) - y(t - T_p)}{T_p},$$

$$\ddot{y}(t) \cong \frac{\dot{y}(t + T_p) - \dot{y}(t)}{T_p} \qquad (3)$$

where T_p is sampling time, $t=kT_p$, and k is discrete time.

In order to obtain the output position of robot model (2), the unknown model parameters A, B and C should be approximated by using the neural network.

3 Feedforward neural network

The feedforward [5] type neural network has been constructed with nonlinear and linear neurons in the first and second layer, respectively as shown in Fig. 1. We have used one of the most typical activation functions (sigmoidal tangent function) for nonlinear neurons [6,9].

$$y = f(v) = \frac{2}{1 + e^{-2v}} - 1 \qquad (4)$$

where

$$v = \sum_{k=1}^{n} w_k x_k + b_k \qquad (5)$$

and x_k, w_k, b_k are input signals to the network, weights and biases of the neuron respectively.

We have used the back propagation method [10] for the calculation of the model parameters of Stanford robot with six degree of freedom. The mathematical basis for the back propagation algorithm is

the optimization technique known as gradient descent [4]. The Standard of the robot parameters are given in [1]. During the learning stage of the network, the reference positions and the torque of the robot were applied as input signal to the network whereas the predicted model output y_n was obtained from NN as shown in the Fig 1. The back propagation rule was applied for network learning according to algorithm 1.

Algorithm 1.

Step 1. Initialize weights (w_k) and biases (b_k) for the neural network (set to small random values).

Step 2. Apply the sequence of reference positions and torque $\{y(1),\tau(1),\ldots\ldots,y(N),\tau(N)\}$ as the input signal to the neural net, where N is the length of the input signal.

Step 3. Calculate network output $y_n(k)$, $(k=1,2,\ldots\ldots,n)$, where y_n denotes the approximated model output.

Step 4. Using back propagation learning rule for calculation of network parameters minimizes the performance index.

$$J = \frac{1}{2}\sum_{k=1}^{N}\left[y(k) - y_n(k)\right]^2 \qquad (6)$$

After learning, we have tested the obtained neural net. During the testing, the reference position $y(k)$ and torque $\tau(k)$ was applied as input and based on the calculated parameters $A_N(k)$, $B_N(k)$, and $C_N(k)$ the predicted positions of the robot $y_n(k+1)$ was obtained as the output from the network according to NN structure presented in Fig. 1.

4 Numerical results

The robot Stanford with six degree of freedom was approximated by using neural network with one hidden layer nonlinear and output layer linear neurons. The number of neurons in the input layer was 8 neurons and the number of neurons in output layer depends on the number of elements in matrices *C, A* and *B* which are 36, 6, 6 neurons respectively as shown in Fig. 1. In order to show the generalization capability of neural network, the input data for the neural network has been grouped into two data sets for (i) learning and (ii) testing of the neural net respectively. The learning stage lasted for 500 learning iterations and the network had to simulate the output of robot neural model time $t=5$ [sec] with sampling time T_p=0.01 [sec], then the length of input data is 500. The input trajectory for learning and testing was described as the follows:

Learning data:

$$y_i(t) = A(1-\cos(\omega t)) \qquad (7)$$

Where ω=1/3, A=114.6 and i=1,2,.....6

Testing data:

$$y_i = A\cos(\omega t) \qquad (8)$$

Where $\omega=\pi$, A=114.6 and i=1,2,.....6

The input (ref. signal) and output (torque) from the robot, obtained according to scheme of robot control system and then could be used to learn the NN as shown in Fig.2. and 3. The approximated positions of the robot can be obtained from the network and compared with the reference positions of the robot manipulator movement as depicted on Fig. 3.and Table 1. When the network had been learned, one can observe that the output of the NN tracks the reference signal (7) as shown on

Fig. 3. From Table 1, you can notice that the maximum error between the reference position of joint number 2 (e.g) and the approximated position for the same joint not exceed $0.0.866^{o}$ which is acceptable error. The other group of data set (8) was used for neural net testing as mentioned previously. In this case the trajectory position of robot has been applied to the network and the output from the network can be recorded and compared with the position of robot model (2). One can notice from Fig. 4 that the approximated output of the NN model can follow the reference positions of the robot precisely. Table 2 shows that the maximum error for joint number 2 and the approximated position for the same joint after testing the network not exceed 3.61^{o} which is satisfactory error for NN under the testing stage.

5 Concluding remarks

One can see that employing the neural network it is quite possible to obtain robot neural model which output is very close to the real robot, in spite of nonlinearity phenomena of the robot manipulator. It seems that in order to use the presented algorithm effectively, the neural network should be learned with rich data and more learning iteration should be done. We would like also to mention that an increasing number of neurons should give smaller errors and lead to improvement the results of robot neural model. It was easy to train the neural net to model the parameters of the real robot because we need only the information about the position of the robot manipulator which can be measured by position sensors and the control signal (torque) from the regulator. We plan further research to synthesize the control system based on the approximation robot parameters obtained from NN.

References

[1] R. P. Paul, *Robot Manipulators: Mathematics, Programming and Control.* Cambridge, Massachusetts: MIT Press, 19981.

[2] K. S. Fu, R. C. Gonzalez, C. S. Lee, *Robotics: Control, Sensing, Vision and Intelligence.* McGraw-Hill, 1987.

[3] J. J. Craig, *Introduction to Robotics.* Addison

Wesley, second ed., 1989.

[4] L. Fausett, *Fundamentals of Neural Networks: Archi*tectures, *Algorithms and Applications.* New Jersey: Prentice Hall International, 1994.

[5] Demuth H., Beale M., *Neural network toolbox user's guide.* The MathWorks, Inc., Natick, Massachusetts, USA, 1994.

[5] F. L. Lewis, S. Jagannathan, A. Yesildirek. *Neural Network Control Robots Manipulators and Nonlinear Systems.* Taylor and Francis Press, 1999.

[6] Kurek J. E., *Calculation of robot manipulator model using neural net.* European Control Conference ECC '99, Karlsruhe Germany, 1999.

[7] Kurek J. E., *Neural net model of robot manipulator.* Neural Computation NC '99, Vienna, Austria, 1998.

[8] Wildner C., Kurek J. E., *Calculation of robot model using neural nets and evolutionary algorithm.* Mechatronics, Robotics and Biomechanics, Hrotovice, Czech Republic, 2003.

[9] Shenghai H., Marcelo H., *Neural network controller for constrained robot manipulators.* Proceeding of the

IEEE International Conference on Robotics and Automation, San Francisco, CA, USA, pp. 1906-1911, May 2000.

[10] Limin P., Peng-Yung W., *Neural Fuzzy Control System for Robotic Manipulators.* the IEEE Control Systems Magazine, pp. 53-63, February 2002.

Table 1. Maximum error between (y) and (y_n) after 500 learning iterations (Learning stage)

Joint number	1	2	3	4	5	6
Error [^{o}]	0.0785	0.0866	0.0610	0.0731	0.0923	0.0785

Table 2. Maximum error between (y) and (y_n) after (Testing stage)

Joint number	1	2	3	4	5	6
Error [^{o}]	3.4120	3.6100	3.360	3.412	3.563	3.4122

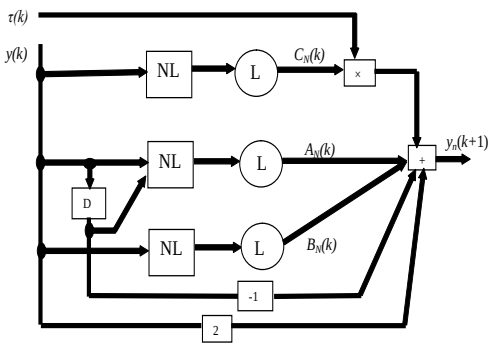

Fig. 1. The structure of feedforward neural network (D is a delay)

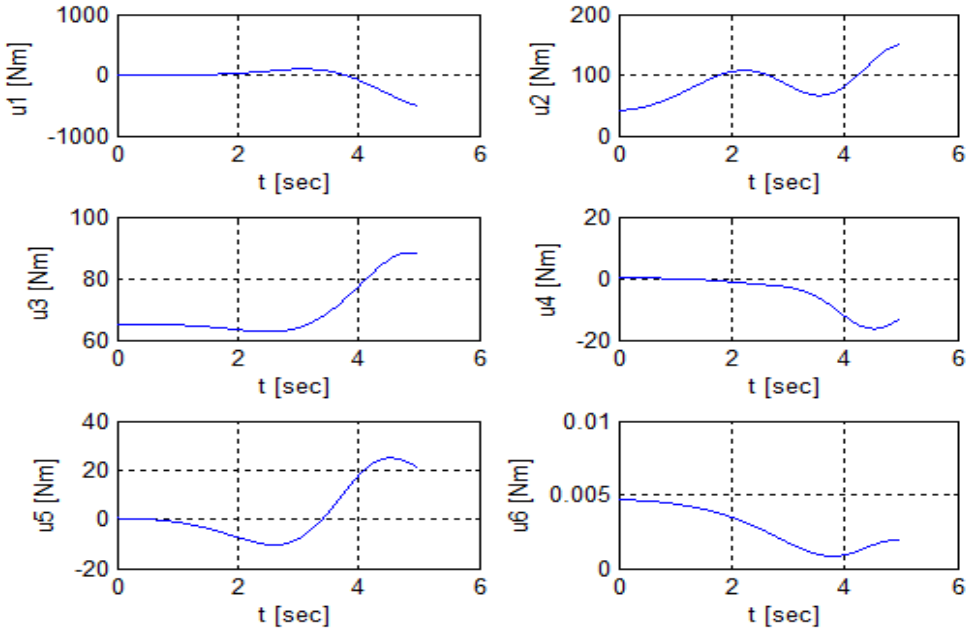

Fig. 2. Input torque=τ to Stanford robot, set of learning data.

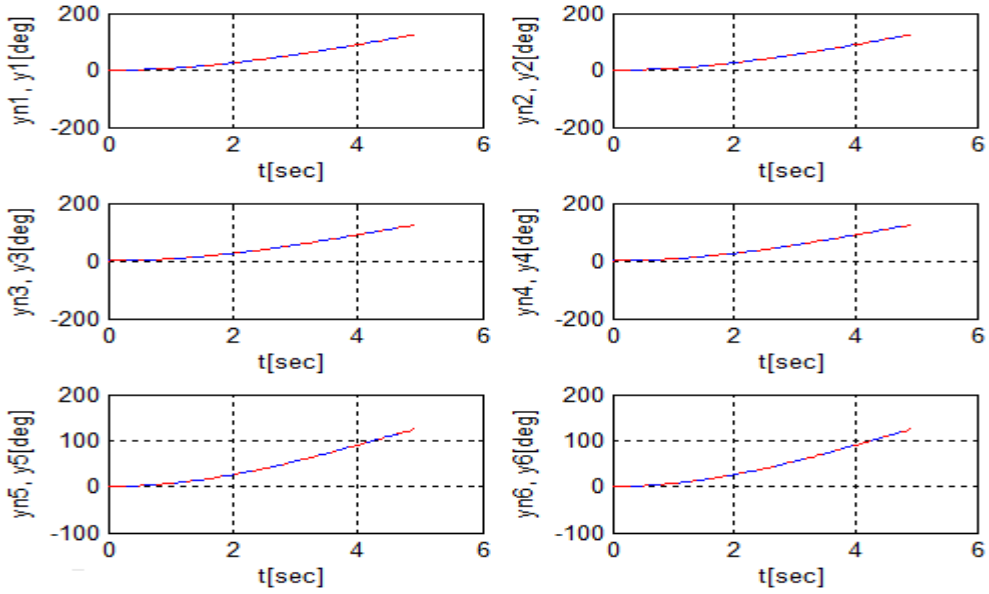

Fig. 3. The reference position (y) and (y_n) output of NN (learning stage).

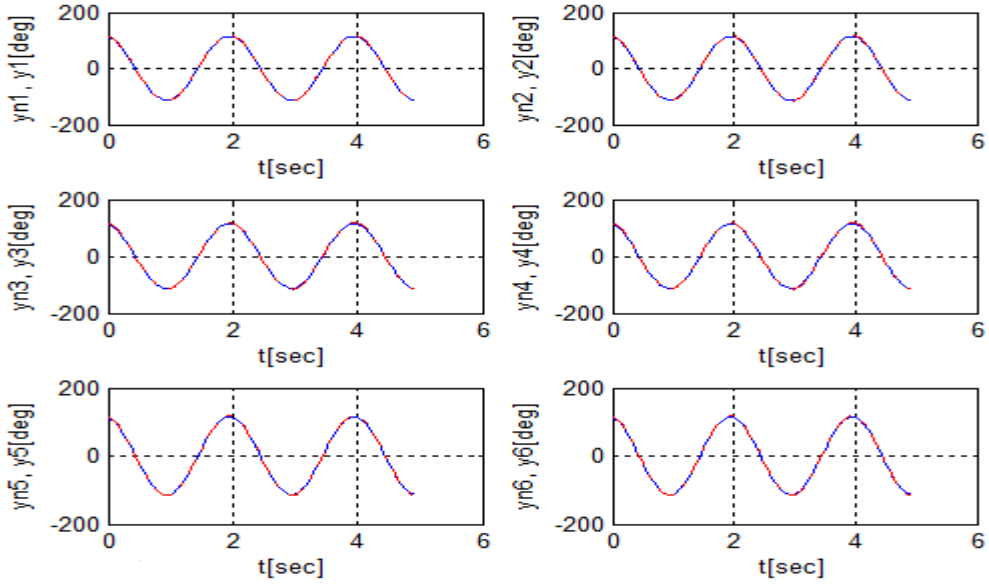

Fig. 4. The reference position (y) and (y_n) output of NN (Testing stage).

Advanced Fuzzy Logic controller based Mirror-Image-Character-Recognition OCR

Santosh Kumar Henge, Niranjan Shrivastava, Laxmikant Ramakrishna
Department of Electrical & Electronic, Faculty of Engineering, Al-Tahadi University, Sirte, Libya
Email: hingesanthosh@gmail.com, nirshree@gmail.com, lux_rcr1@rediffmail.com

Abstract

While digitalizing the document, Most of the individuals are using the OCRs (OCR: Optical Character Recognition) technique and researchers proposed techniques for OCRs, they are trying to reduce inconvenience while digitalizing the data. They use OCRs which is saving relevant documents to Data Base DB. However, there are inconveniences in general OCR. That is, text should be entered to Data Base and processed after classifying text segments, text sentences, one by one is realized, and whole document is recognized through OCR. While performing so, the noise/ reverse Image of the text/ content in background of the front text, which is acting as an obstacle for OCR engine, resulting in time consuming performance, if background noise / reverse images are improperly filtered. In other way it is advantageous when the front text is completely bypassed after its content is recognized and concentrated only on the back ground text/ Reverse Image text. In order to overcome this obstacle, we made an effort to recognize the Reverse-Printed characters, using Advanced Fuzzy Logic Control algorithm and discussed i.e. on, Reverse-Printed-Characters-Recognization (RPCR) / Mirror-Image-Character-Recognition (MICR) OCR technique. This OCR system saves abstracted characters to DB after extracting only equivalent and necessary characters from a large amount of documents by using Gaussian membership based Fuzzy Logic Control algorithm, that is one of Artificial intelligent network. This recognization produces the same output pattern regardless of the orientation, position, and size of the input pattern on both the sides of the document. The recognization has the advantage of being simple. This makes it computationally efficient and fast, which in turn makes it appropriate for on-line and offline implementations. In the process of development of the algorithm the preprocessing, segmentation, character recognition and post-processing modules were discussed.

Key words:
OCR, Fuzzy based ORC, RPCR, MICR Document, DBs

Background; The motivation

Imaging if someone wants to know or read or listen to the stuff in set of papers enclosed in the cover or in a book without turning the pages around, by just keeping the papers set or the book closed beneath

the set of sensors. It may be possible to listen to the content of the stuff which is enclosed in the cover or in the book. How? if we keep the set of papers beneath the array of the sensors or the Imaging camera/ photogrammetry camera, we can obtain the skeleton image of the text, on the top page, when this image is processed by the OCR engine the text is recognized and displayed on the monitor which can be read aloud by the text to speech converter in the system also. The skeleton of the text image is obtained for bottom layer page too, the top page text would be easily recognized by the OCR-engine, but the difficulty arises when the image in reverse direction or the text appears as it is appearing in the mirror and the texture stuff may be in different direction and orientation (in different quadrants). As shown in the figure 1.

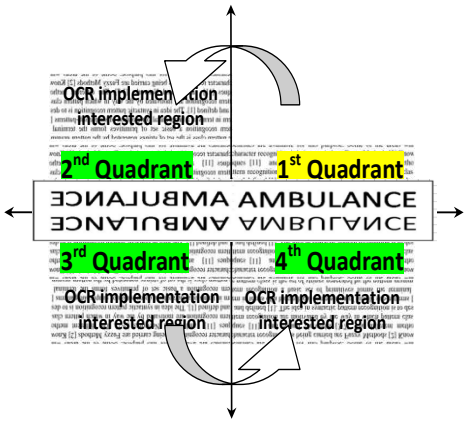

Figure 1; OCR Implementation areas, Quadrant 2,3and 4 where the text is in reverse and appearing as in mirror image

1. Introduction

In this paper we have concentrated on processing of the reverse characters Mirror Image Text which is appearing as printed on both sides of transparent or semi-transparent sheet. We are interested in discussing character recognization engine in four different quadrants i.e. quadrant 1-4, where the processing of the text is required depending upon orientation, direction of the text etc.

. This paper describes the suppression of front layer 1st quadrant components or the top layer characters first quadrant text, and enhancement of the bottom layer 2nd quadrant components or back layer or second quadrant text, in which the reverse image of the text or the character is seen. This technique is based on independent component analysis (ICA). Similarly the 3rd and 4th quadrant components also. The concept of Mirror Image Text (MIT) detection or Reverse Text (RT) layer detection is introduced to detect and identify the text character appears as in the mirror image or back layer of the paper, when seen from the front side or the front layer is completely bypassed like having the printouts on both sides of transparent sheet

2. Earlier Work

Many researchers done considerable amount of work behind processing of camera-held images [1] online, offline character recognization OCRs. Many

researchers have proposed their own methods for character, text detection, and methods for character, text location, and extraction of the text from images [2]. Experience in optical character recognition (OCR) of the text in images suggests that one doesn't get good recognition accuracy without proper enhancement of the imaged text. Several image enhancement techniques [2, 3] have therefore been developed. Many of these techniques have been modeled as the binarization problem that classifies image pixels as either background or foreground pixel [4]. Some other techniques considered through and other effects to model the enhancement problem as multi-class one.

.Execution of ICA gives foreground, middle layer and background as independent components. Foreground (more specifically character parts) information contained in each component is then identified and integrated Though use of ICA in digital signal processing is widespread, its use in image processing, in general, and document image analysis, in particular is also most common. ICA-based approaches have already been implemented to give encouraging results in different DIA tasks [5 - 7]. This paper presents an advancement of ICA research where an ICA-based approach models the image enhancement as a 1-class problem. Pixels are assumed to belong to one of two sources namely, foreground layer, and background layer. Since the mixing patterns for these pixels are not known, their separation into different classes is viewed as a blind source separation problem.

3. Working Methodology:

The image containing text has been processed under the three main following processes, i.e. pre processing, processing and execution of the selected text image as shown in the figure 2.

1. Text in image detection/ identification,
2. Text layout or orientation identification,
3. Quadrant classification of the text based on the orientation of the text
4. Segmentation
5. Character processing applying the Gaussian Fuzzy process
6. Post Processing/ Analysis

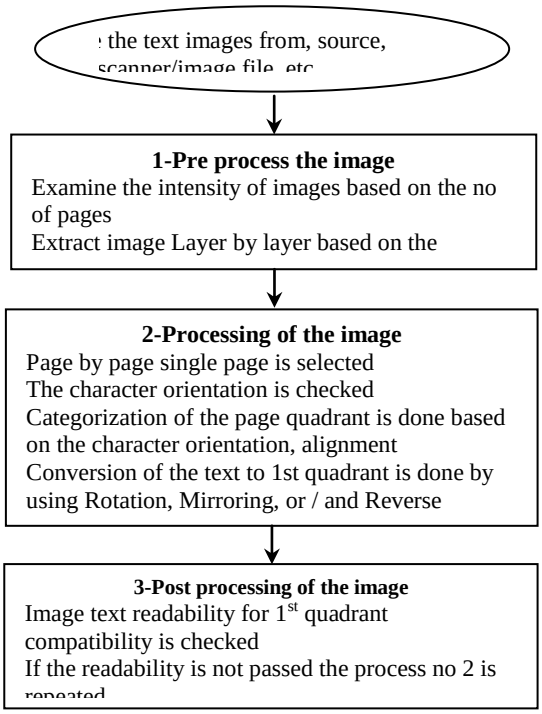

Figure 2 process flow diagram

The whole word has been divided in the small characters by over segmenting it. These characters can be as small as possible. As per the analysis, the probability of error-some recognition is more if the character segment size is more and will continue to be less, as the character size is lesser But the processing time is inversely proportional to the character size. Figure 3.1 to 3.3 shows the examples where various Characters with different sizes have been shown.

Figure 3.1 Single layer Telugu texts in all four quadrants which is not in data base of the OCR

Figure 3.2 Single layer alphanumeric texts in all four quadrants

In figure 3.1 a text of south Indian Telugu language is shown which would be rejected by the OCR, because it is not in the OCR engine database. The system fails in early stage. In figure 3.2 alpha numeral is shown which would detected by the OCR engine because the English is in the OCR engine database. In figure 3.3 text in English alphabets is shown which is in four different quadrants.

The figure contains 3 different processed images.

The first/ top one is processed and tried to show only top layer of the text in 4 quadrants. Here OCR is needed to process directly in first Quadrant and make orientation and layer adjustments in 2nd 3rd and 4th quadrant.

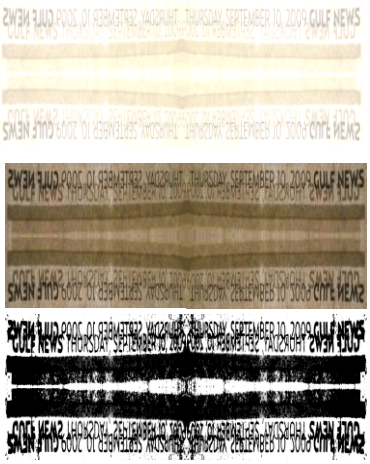

Figure 3.3 Dual layer texts in four quadrants front layer of text highlighted in top figure, two layers 4 quadrants shown in middle figure , back layer 4 quadrants shown in bottom

The second image is processed and tried to show both the front layer and back layer of the paper in 4 quadrants totally the OCR is needed to process 2 + 6 = 8 quadrants, two direct implementation and six times OCR need to process the Image orientation and other things

3.1 The text in front layer First Quadrant here text is in normal position no OCR image adjustments are needed, text in top position present in top (TOP-TOP) position and bottom of the text is in bottom (BOTTOM-BOTTOM) position. Here OCR image text adjustments are not needed.

3.2 The text in front layer Second Quadrant is Mirror image of First Quadrant text which is not in direct readable form, which is appearing as if it is seen in the mirror with text in top position present in top (TOP-TOP) position and bottom of the text in bottom (BOTTOM-BOTTOM).position Here OCR image adjustments are needed.

3.3 The text in the front layer third Quadrant is Mirror image of second Quadrant text which is not in direct readable form, which is appearing as if it is seen in the mirror with text in top position present in bottom (TOP-BOTTOM) position and bottom of the text in top (BOTTOM-TOP).position Here OCR image adjustments are needed

3.4 The text in the front layer fourth Quadrant is Mirror image of third Quadrant text which is not in direct readable form, which is appearing as if it is seen in the mirror with text in top position present in top (TOP-TOP) position and bottom of the text in top (BOTTOM-

BOTTOM).position Here OCR image adjustments are needed

This is all text direction adjustments in front layer of the text of four quadrants similarly the OCR is needed to process the text image depending upon the orientation of the direction and rotation of the text

3.5 The text in back layer First Quadrant is Mirror image of second Quadrant text of back layer which is not in direct readable form, which is appearing as if it is seen in the mirror with text in top position present in top (TOP-TOP) position and bottom of the text in bottom (BOTTOM-BOTTOM).position Here OCR image adjustments are needed. Text is in reverse direction left to right o OCR image adjustments are needed

3.6 The text in back layer Second Quadrant here text is in normal readable position no OCR image adjustments are needed here text in top position present in top (TOP-TOP) position and bottom of the text in bottom (BOTTOM-BOTTOM) position. Here OCR image text adjustments are not needed.

3.7 The text in the back layer third Quadrant is Mirror image of back layer second Quadrant text which is not in direct readable form, which is appearing as if it is seen in the mirror with text in top position present in bottom (TOP-BOTTOM) position and bottom of the text in top (BOTTOM-TOP).position Here OCR image adjustments are needed

3.8 The text in the back layer fourth Quadrant here text is Mirror image of back layer third Quadrant text which is not in direct readable form, which is appearing as if it is seen in the mirror with text in top position present in top (TOP-TOP) position and bottom of the text in top (BOTTOM-BOTTOM).position Here OCR image adjustments are needed

4. Implementation

One may ask where and how fuzzy logic is implemented. here with the quadrants location and quadrants differentiation method the set of rules are known and which are the feeds for fuzzy logic controller [8 - 9] fuzzification rules, these cases and conditions would be implemented as the if cases and for each individual quadrant the processing action is to be done is written as the then-corresponding action Fuzzy-neural network having the four layers (input, fuzzification, inference and defuzzification) have been used.

4.1 Fuzzy sets

Can be effectively used to represent linguistic values such as low, young, and complex. A fuzzy set can be defined mathematically by assigning to each possible individual in the universe of discourse a value representing its grade of membership in the fuzzy set to a greater or lesser degree as indicated by a larger or smaller membership grade. The fuzzy set is represented as where x is an element in X and $\mu A(x)$ is a membership function of set A which defines the membership of fuzzy set A in the universe of discourse, X

4.2 Fuzzy Membership Functions

A fuzzy set is characterized by a membership function which associates with

each point in the fuzzy set a real number in the interval [0, 1], called degree or grade of membership. The membership function may be triangular, trapezoidal, Gaussian etc. A triangular membership is described by a triplet (a, m, b), where 'm' is the modal value, 'a' and 'b' are the right and left boundary respectively. The trapezoidal membership function (shown in Figure. 4) is defined as follows.

$$\mu_Z(x_k, \gamma_k) = \begin{cases} 1 & x_k \in [u_k, U_k] \\ 1 - \max(0, \min(1, \gamma_k(u_k - x_k))) & x_k \prec u_k \\ 1 - \max(0, \min(1, \gamma_k(x_k - U_k))) & x_k \succ U_k \end{cases}$$

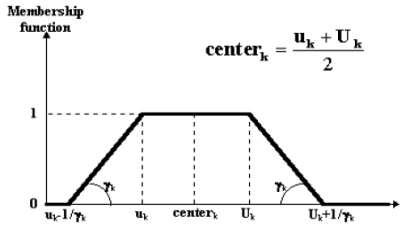

Figure 4. Trapezoidal Membership Function for μ Z (xk, γ k)

Another fuzzy membership function that is often used to represent vague, linguistic terms is the Gaussian which is called Gaussian membership function (shown in figure 5) is defined as follows.

$$\mu_Z(x_k, \gamma_k) = \exp\left(-\frac{1}{2} \cdot \frac{(x_k - \text{center}_k)^2}{\gamma_k^2}\right)$$

$$\text{center}_k = \frac{u_k + U_k}{2}$$

with $\gamma_k > 0$ for any $k \in \{1, 2, ..., n\}$

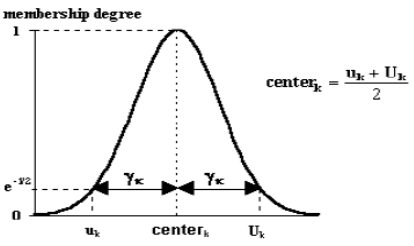

Figure 5. Gaussian Membership Function for μ Z(xk, γ k)

4.3 Gaussian Bell curve sets

Give richer fuzzy system with simple learning laws that tune the bell curve variance. The Gaussian Function is represented by "(equation 1),"

$$\mu_{A_i}\langle x \rangle = Gaussian\langle x, c_i, \sigma_i \rangle = e^{-(x-c_i)^2/2\sigma_i^2}$$

Where c_i is the center of the i^{th} fuzzy set and σ_i is the width of the i^{th} fuzzy set.

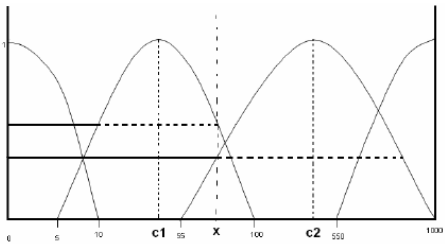

Figure 6. Representation of DATA Cost driver using Gaussian Membership Function

We define a fuzzy set for each linguistic value with a Gaussian shaped membership function μ is shown in Figure 5. We have defined the fuzzy sets corresponding to the various associated linguistic values for each variable / parameter of interest it may be character intensity, orientation, layout or anything.

In this research, a new fuzzy effort estimation model is proposed by using Gaussian function to deal with linguistic data or text image quadrant position analysis, and to generate fuzzy membership functions and rules for further processing the membership functions Primitives have been added to find form a character, which

is part of the lexicon. The word is not said to be recognized till it is tested with lexicon containing root words with an efficient algorithm [7]. The system working model is designed as shown in the flowchart Figure no 2, the process no 2 is repeated till the whole text is reached to quadrant no1, i.e. till the text is arranged page by page in readable mode.

5. Discussion

The proposed algorithm presented, got the versatility in implementation while constructing an OCR system, our system can scan the text in different directions and orientation, there is no need to change the layout of the scanning textured image every time. The scanning of multiple papers at a time is permitted.

The proposed method is an effective method and outperforms the other methods in the complex textured background situation. Disturbances due to the textured background are well avoided or considered as an advantage, in our method than the other ones. So that binarised image can be better recognized by OCR.

6 Future scope

The 4 quadrant reverse text image recognization/ reverse character image recognization can implemented in any scanner/ virtual instrument if the text image is readily available, it can be implemented either using the math tool or the LabVIEW VI GUI

7. References

[1] D. Doermann, J. Liang, and H. Li, “Progress in Camera-Based Document Image Analysis”, Proc. ICDAR'03, 606-616, 2003.

[2] C. Wolf, J.-M. Jolion, F. Chassaing, “Text Localization, Enhancement and Binarization in Multimedia Documents”, Proc. ICPR'02, vol. 4, 1037-1040, 2002.

[3] S.-S, Kuo, M.V. Ranganath, “Real Time Image Enhancement for Both Text and Color Photo Images”, Proc. of ICIP, vol. 1, 159-162, 1995.

[4] G. Leedham, C. Yan, K. Takru, J.H.N. Tan, and L. Mian, “Comparison of some thresholding algorithms for text/background segmentation in difficult document images,” Proc. ICDAR’03, 859-863, 2003.

[5] A. Hyvarinen, J. Karhunen, and E. Oja, “Independent Component Analysis”, Wiley, New York, 2001.

[6] A. Tonazzini, L. Bedini, and E. Salerno, “Independent component analysis for document restoration”, IJDAR, 7(1), 17–27, 2004.

[7] Leonard J. Jowers A, James J. Buckley B, Kevin D. Reilly A, “Estimation of f-COCOMO model parameters using optimization techniques,”

[8] Zadeh. L. A., Fuzzy Sets, Information and Control, Volume 8, 1965, pp. 338-353.

[9] Ch. Satyananda Reddy, KVSVN Raju, An Improved Fuzzy Approach for COCOMO’s Effort Estimation using Gaussian Membership Function JOURNAL OF SOFTWARE, VOL. 4, NO. 5, JULY 2009, pp452-459.

FUZZY LOGIC CONTROL OF DC MOTOR DRIVE SYSTEM

Abdalla Idres Fadel* **Ahmed Jaber Abogarir***
Hamza Ramadan Elkony* **Hatem Abdalla Fadel ***

*** Dept. of Electrical and Electronic Engineering, Al-Fateh University-Libya.**
Phone: +21825385942, Email: abougarir@yahoo.com

Abstract

The DC motor drives still in competition in industrial application, because of it's high performance, robustness, and its lower cost compared with AC drives. Ponteryagin Minimum principle is applied in this paper to study the optimal parameters of the separately excited DC motor at steady state mode of operation, where the minimum losses are accomplished. The dynamic behavior of the separately excited DC motor also studied applying Fuzzy Logic Control (FLC) taking the optimal steady state results as a boundary condition for starting and final operation points. Also the fuzzy logic dynamic results will be compared to proportional integral differential (PID) controller. Also the sensitivity analysis are performed to assure the system stability. The expected results will be of value to many industrial applications for reducing energy consumption and enhancing the DC drive performance.

1. Introduction

In recent years, fuzzy logic controllers which are based on fuzzy set theory have been used in growing numbers of application in artificial intelligence computer science, control engineering, decision theory, pattern recognition, robotics and aircraft control. A fuzzy control system is implementing a part of a human operator's expertise which does not lend itself to being easily expressed in PID-parameters or differential equations but rather in situation or action rules. FLC dose not require parameter estimation [1,2]. In this paper, a fuzzy logic controller is designed to control the speed of a separately-excited DC motor. In some applications, DC machines are much more adaptable to adjustable speed service than AC machines. Indeed, the ready susceptibility of DC motors to adjustment of their operating speed over wide ranges and by variety of methods is one of the important reasons for the strong competitive position of DC machinery is modern industrial applications[3,4].

2. Formulation of Optimal Control Problem

A steady state optimal control for the separately excited DC motor applied voltage to minimize the energy losses it found for any desired state operating conditions, which is defined by a given motor speed and load torque demand. The pontryagin state function from optimal control theory is used in this analysis. The steady state optimal control problem can be formulated as follows: To find the optimal applied voltages to DC motor, which

produce minimum motor losses, at a given motor shift speed and load torque. Following the optimal control procedure a performance index or a quadratic function representing the motor power losses in terms of the applied voltages. The various losses for DC motor, and the direction of energy flow, are shown in figure 1 [5].

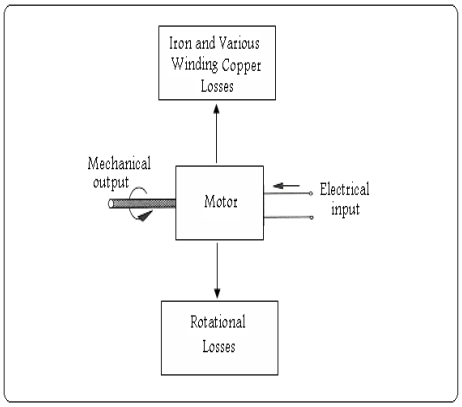

Fig 1: Direction of power flow in DC motor

The major losses consist of copper losses P_{cu} , brush losses P_e and iron losses P_{fu}. Since the iron and brush contact losses are more less than copper losses then will negligible. Consider the function L for the total losses is defined as

$$L = P_s = R_a I_a^2 + R_f I_f^2 \qquad (1)$$

where I_c , I_f , R_a and R_f are the armature and field current and resistance. In steady state the electromagnetic torque can be considered equal to the load torque

$$T_e = T_L = K_t I_a I_f \qquad (2)$$

Where K_t is torque constant . This equation is used as constraint that must be satisfied for all time during steady state. Also at steady state all terms containing the time derivative operator vanish. Thus the motor currents are expressed in terms of the applied voltage [6].

$$I_a = \frac{V_a - e_g}{R_a}, I_f = \frac{V_f}{R_f},$$
$$e_g = K_V \omega I_f \qquad (3)$$

Using last equations the loss function and the torque can be expressed in terms of the motor applied voltage as following

$$L = \frac{1}{R_a R_f^2}(R_f^2 V_a^2 - 2R_f K_V \omega V_f V_a + K_V^2 \omega^2 V_f^2) + \frac{V_f^2}{R_f} \qquad (4)$$

$$T_e = T_L = \frac{K_t V_f}{R_a R_f^2}(R_f V_a - K_V \omega V_f) \qquad (5)$$

Equation (5) is used as a constraint for the optimization problem , which can written as

$$g = 0 = \frac{K_t V_f}{R_a R_f^2}(R_f V_a - K_V \omega V_f) - T_L \qquad (6)$$

The pontryagin H-function is formed as

$$H = L + \lambda\, g \qquad (7)$$

Where λ is a Lagrange multiplier. Substituting (4) and (6) for L and g in (7) yields

$$H = \frac{1}{R_a R_f^2}(R_f^2 V_a^2 - 2R_f K_V \omega V_f V_a + K_V^2 \omega^2 V_f^2) + \frac{V_f^2}{R_f} + \lambda\left(\frac{K_t V_f}{R_a R_f^2}(R_f V_a - K_V \omega V_f) - T_L\right) \qquad (8)$$

The state function H is a function of the speed ω , the Lagrange multiplier λ and the applied voltage Va. The Lagrange multiplier λ is a real number chosen in such a way that the optimality conditions are satisfied.

3. Necessary and Sufficient Conditions For Optimality

The optimum values of the voltage are obtained by minimizing the value of the H-function. from equation (7) if the constraint is satisfied, then $H = L$, and the minimum of L is then found when the minimum of H is obtained [7].

To determine the minimum of H , the extremals for H are found and these are checked to see if they minimize H the necessary conditions for minimum H are:

$$\frac{\partial H}{\partial V_a} = 0,\ \frac{\partial H}{\partial \omega} = 0\ ,\ \frac{\partial H}{\partial \lambda} = 0 \qquad (9)$$

From equation (8) the necessary conditions can writes as :

$$\frac{\partial H}{\partial V_a} = \frac{2}{R_a} V_a - \frac{2K_V V_f}{R_a R_f}\omega + \lambda \frac{K_t V_f}{R_a R_f} = 0 \qquad (10)$$

$$\frac{\partial H}{\partial \omega} = \frac{-2K_V V_f}{R_a R_f} V_a + \frac{2K_V^2 V_f^2}{R_a R_f^2}\omega + \lambda \frac{K_t K_v V_f^2}{R_a R_f^2} = 0 \qquad (11)$$

$$\frac{\partial H}{\partial \lambda} = \frac{K_V V_f}{R_a R_f} V_a - \frac{K_t K_V V_f^2}{R_a R_f^2}\omega - T_L = 0 \qquad (12)$$

After the above equations are solved for extremals of H , then these are checked to see if they satisfy sufficient conditions for minimum H . From equations (11) and (12)

$$\lambda = \frac{-2R_a R_f^2}{K_V K_t} \qquad (13)$$

Substituting (13) in (10) we get

$$V_a = \frac{K_V V_f}{R_f}\omega + \frac{R_a R_f}{K_t V_f} T_L \qquad (14)$$

4. The System (Model) and Results

A $15-hp$ $2000-rpm$ separately excited DC motor, the field circuit resistance is $R_f = 147\,\Omega$, the armature circuit resistance is $R_a = 0.25\,\Omega$, and the voltage constant of the motor is $K_V = K_t = 0.7032\,V/A-rad/s$. The viscous friction is negligible and the armature current may be assumed continuous and ripple free. Find the optimal values of the voltage that giving the required speed at this bounders ($100\ rad/s$ - $200\ rad/s$). The next figures shows the analysis was done over a speed range from $100\ rad/s$ to $200\ rad/s$. The figures 2 and figure 3 shows the relation between optimal armature voltage and speed at different values for the field voltage and the torque respectively.

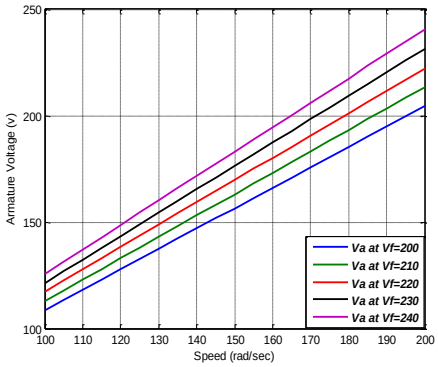

Fig. 2 : Optimal armature voltage at different field voltage

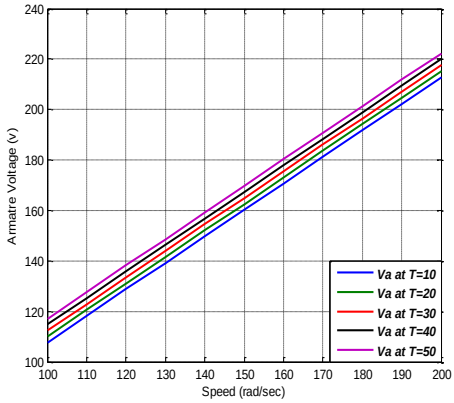

Fig. 3 : Optimal armature voltage at different load torque

5- DC Motor Model

The DC motor is supplied from DC chopper. The motor parameters used in simulation program are given in table 1 [8].

Table 1 : DC Motor parameters used in simulation

Rated armature voltage	$205\ V$		
Rated armature current	$57\ A$		
DC-chopper voltage	$220\ V$		
Rated roter speed	$200\ rad/s$		
Rated torque	$50\ N.m$		
R_a	$0.25\,\Omega$	L_a	$0.02\ H$
J	$0.28\ Kg.m^2/s^2$	β	$0.02\ N.m.s$
$K_t = K_v$	$0.732\ V/A-rad/s$	$K\phi$	$0.95\ N.m/rad$

The simulation time is taken $4.0\,s$. The motor started at full-load without control. The motor speed and the motor current are shown in figure 4 and 5 respectively. From the speed figure 4 we note that, there is overshot , and there is disturbance in the speed and the current figures. The function of the FLC is to minimize the speed

overshoot and maintain the speed nearly constant specially during the disturbance period.

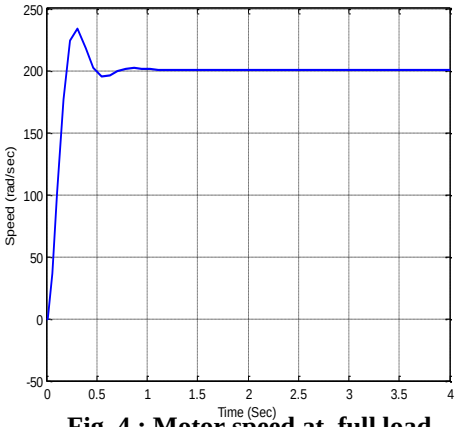

Fig. 4 : Motor speed at full load without control

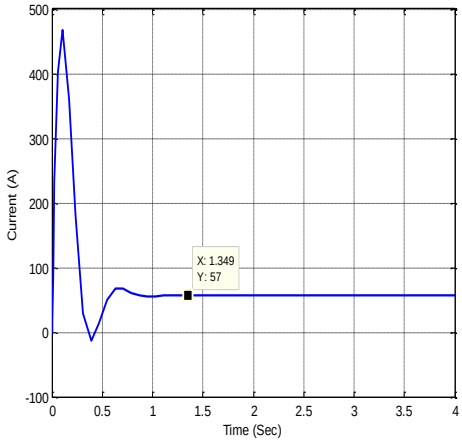

Fig. 5 : Motor current without control

6. Speed Control Using FLC

To improve the motor speed response, FLC is used to control the duty cycle by α ,where α is the angular value that determining the duty cycle of DC-DC converter as shown in figure 6. From this figure, the power circuit consist of DC chopper that drives a separately-excited DC motor. The speed loop has a voltage limiter to limit the armature voltage around $205\,V$.

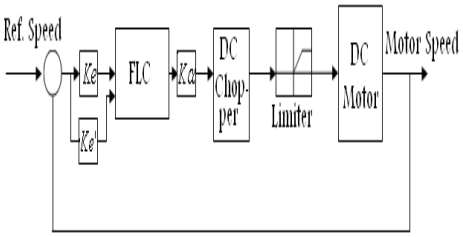

Fig. 6 : Block diagram of speed control system

The FLC scaling factors Ke , Ke' and $K\alpha$ are tuned several times using the knowledge about the nature of e & e' and also by using trial and error until the best or optimal performance is achieved. The scaling factors are set at: $Ke = 1/150$ $Ke' = 1$ $K\alpha = 15000$. Each fuzzy variable e , e' and α is quantized to seven triangular membership functions $\left\{ \begin{matrix} N_B, & N_M, & N_S, & Z, \\ P_S, & P_M \text{ and } P_B \end{matrix} \right\}$ with over lapping as shown in figure 7 and the table 2 shows the controller rules:

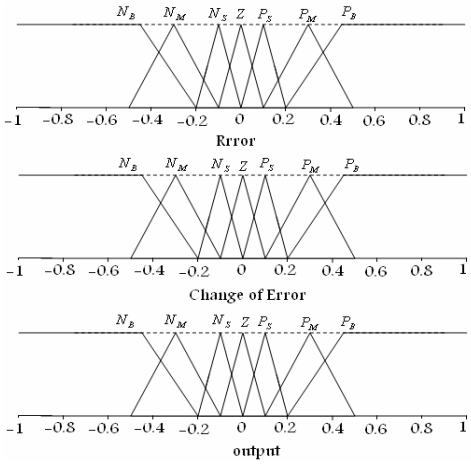

Fig. 7 : Membership functions for the fuzzy variable

Table 2 : Rule table for the speed control system

e \ e'	N_B	N_M	N_S	Z	P_S	P_M	P_B
N_B	P_B	P_B	P_B	P_B	N_M	Z	Z
N_M	P_B	P_B	P_B	P_M	P_S	Z	Z
N_S	P_B	P_M	P_S	P_S	P_S	Z	Z
Z	P_B	P_M	P_S	Z	N_S	N_M	N_B
P_S	Z	Z	N_M	N_S	N_S	N_M	N_B
P_M	Z	Z	N_S	N_M	N_B	N_B	N_B
P_B	Z	Z	N_M	N_B	N_B	N_B	N_B

7. Design Fuzzy Logic Controller With Matlab

The matlab and simulink are one of the most popular and worldwide used simulation software packages. Since matlab contains the fuzzy logic toolbox (FLT) that allows the designer to create and test new fuzzy control designs. Matlab FLT is a program tool for working with fuzzy logic systems. FLT contains fife main tools: FLS editor, membership functions editor, rule editor, rule viewer, and surface viewer.

7.1 FIS Editor

The FIS editor is a tool in FLT, where the number of inputs, names of input, and output variables, as well as the type of fuzzy controller (Mamdani or Sugeno) is determined as shown in figure 8. Selection of a Mamdani-type fuzzy controller assumes that linguistic values of the output variable are regular fuzzy sets. Selection of a Sugeno-type fuzzy controller assumes that linguistic values of the output variable are singletons. In this work Mamdani-type was used.

The FIS editor also serves for selection of a fuzzy inference method and it enables the choice of aggregation operator that gives a different type of a compositional output fuzzy set [9]

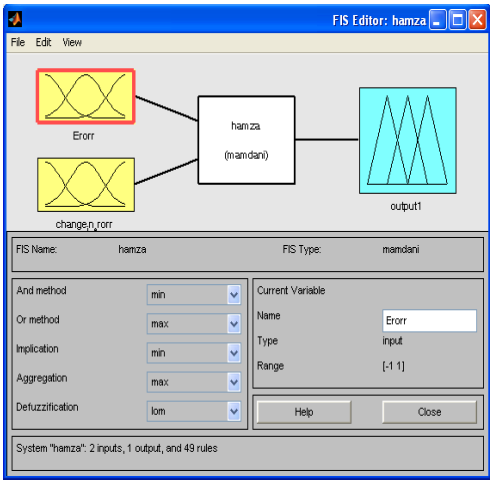

Fig. 8: FIS Editor

7.2 Membership Function Editor

Membership function editor shown in figure 9 of DC motor drive system controller enables definition of membership function forms for the inputs and the output, and allows setting of boundary parameters for each membership function. The designer can choose from eleven standard

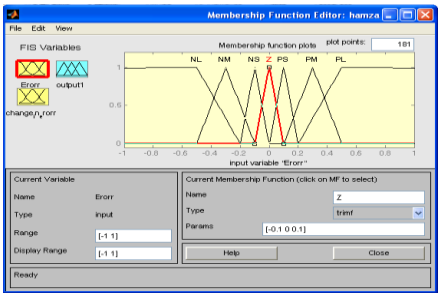

Fig. (9-a) : Error Input

Functions (triangle, trapeze, bell, Z-shape, S-shape, Gauss,etc..).The tool allows definition of the functions range, name of functions, and the range of display. Also, new membership functions can be added [9].

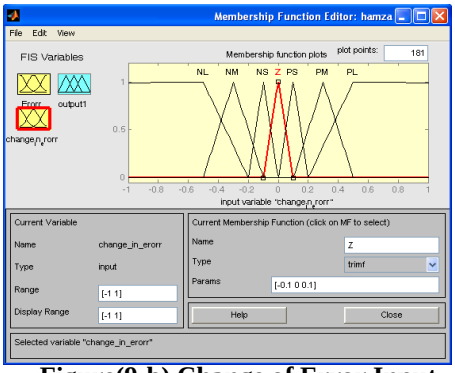

Figure(9-b) Change of Error Input

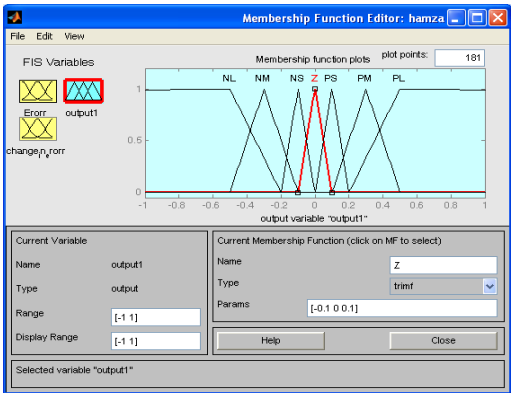

Figure (9-c) Output

7.3 Rule Editor

The rule editor for editing the list of rules that defines the behavior of the system. Rule editor shown in figure 10 serves for insertion of new fuzzy rules. Rules can be inserted in forms of text, symbols. Before insertion of rules, fuzzy membership functions must be defined [9].

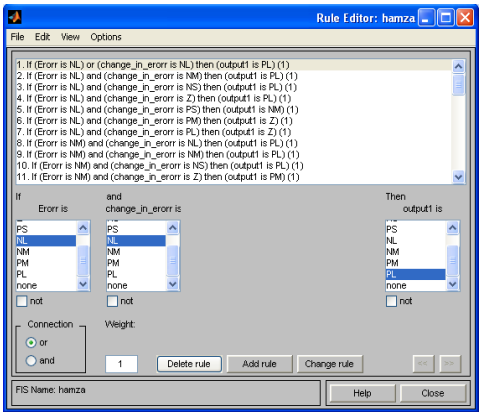

Fig. 10: Rule Editor

7.4 Rule Viewer

Rule viewer shown in figure 11 is a tool that provides a more detailed insight into the fuzzy inference process of a system controller. Row represents one fuzzy rule containing tow input membership functions and one output membership function. In this way all fuzzy rules create a table with tow corresponding columns. Actual values of fuzzy controller inputs, depending on selected features of fuzzy inference, yield different contributions to the crisp fuzzy controller output, which can be simultaneously registered in the rule viewer window. This tool allows the designer to make analysis of the inference system and decide about the controller parameter setting [9].

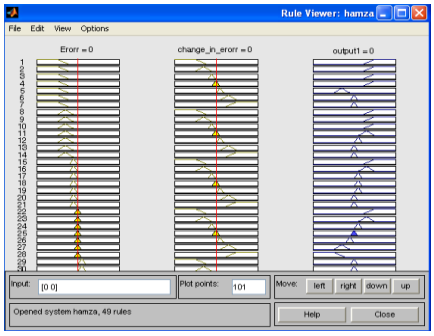

Fig. 11: Rule Viewer

7.5 Surface Viewer

The surface viewer is used to display the dependency of the output on the input that is, it generates and poles an output surface map for the system. Figure 12 shows the surface viewer.

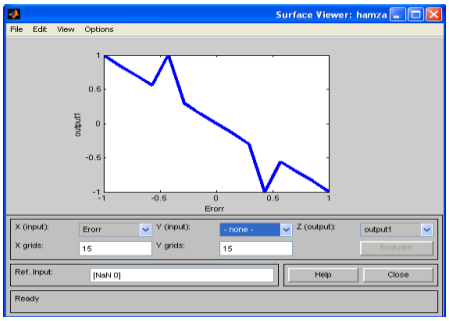

Fig. 12: The Surface Viewer

The figure 12 shows the operation map of the FLC according to the results that defined for a certain system operation. If any rules are changed according to any operating condition, then this map is changed as well [9].

8. Simulation Model and Results

The simulation model of the DC motor drive system control using FLC and PID controllers are shown in the next figures 13 and 14 respectively also this figures shows nonlinear signals as saturation , backlash and random signal to assure the system stability. The motor speed using FLC and PID during simulation time is shown in figure 15 and 16 respectively. Compared with the motor speed without control shown in figure 4, FLC controls the speed at a required constant value with more less than overshoot and rise time. Also the comparison between FLC and PID is shown in the next table 3, where note that the rise time, setting time and speed overshoot at using FLC are best.

Table 3: Performance comparison of FLC and PID controlled drive system

	FLC	PID
Rise Time (s)	0.1975	0.3
Setting Time (s)	0.45	0.6
Speed Overshot (rad/s)	5.2	5.6

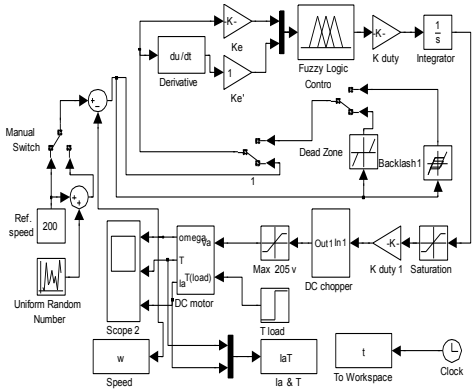

Fig. 13:Simulation model of DC motor control system using FLC

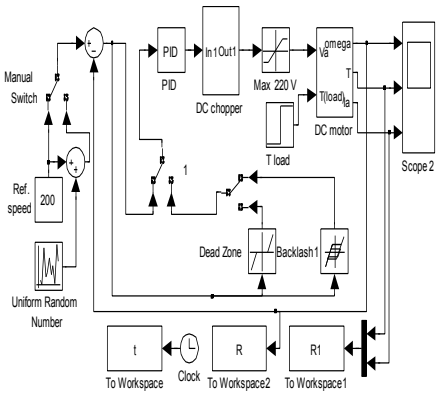

Fig. 14 : Simulation Model of DC Motor Control System Using PID.

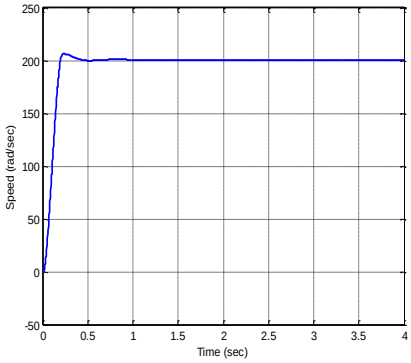

Fig. 15: Motor speed with FLC

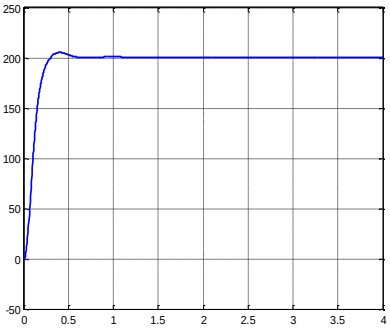

Fig. 16 : Motor speed with PID controller

9. FLC Sensitivity

Study was conducted to demonstrate the effect of non-linearity signals on the performance of FLC, using the same DC motor drive and FLC & PID parameters. And then compared FLC with PID by effecting this signals. The comparison results are shown in the next figures. From this figures note that the DC motor performance with FLC was not effected by the nonlinear signals.

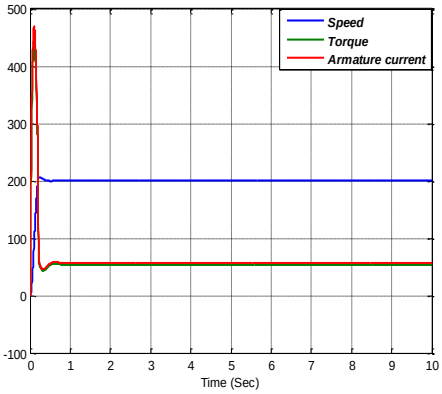

Fig. 17 : FLC with random signal

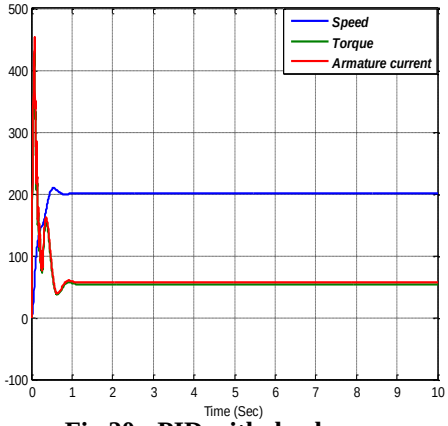

Fig.20 : PID with dead zone

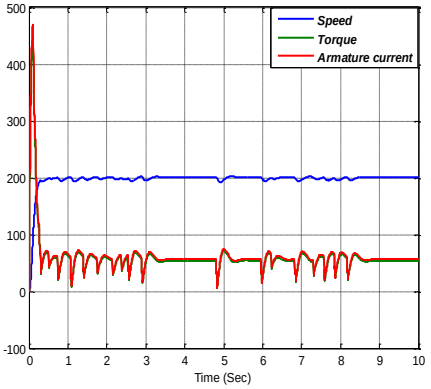

Fig. 18 : PID with random signal

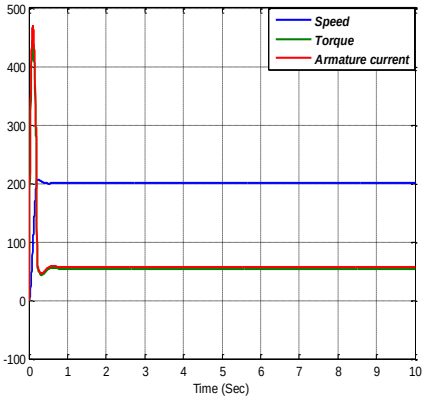

Fig. 21 : FLC with backlash

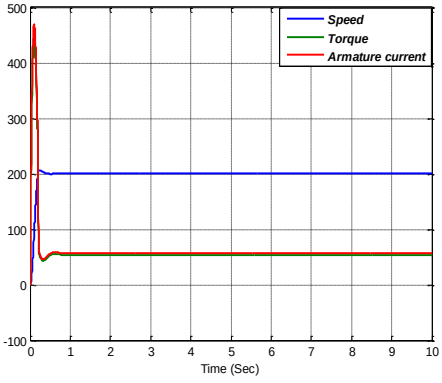

Figure 19 : FLC with dead zone

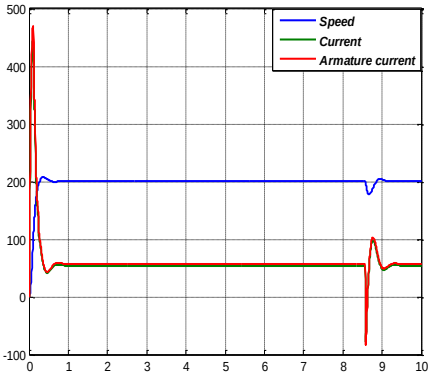

Figure 22 : PID with backlash

10. Conclusion

Speed control of motor drives is an important concern in many industrial applications and research in this aspect focuses on application of different speed methods that can results in a higher motor drive performance during steady state and dynamic modes. This paper concentrates on application of fuzzy logic controller to DC motor drives based on optimum boundary conditions at steady state operating mode. The steady state optimal voltages and speeds of separately-excited DC motor are derived using open-loop control and Lagrangian function method for optimization. The results are used as a boundary condition in motor dynamic simulation applying fuzzy logic control. A DC-DC converter (chopper) is also used in the system model as controlled power supply. The simulation is based on Matlab AND simulink that simulates the motor drive system with fuzzy logic controller. The simulation results of the motor drive system shows a higher motor performance that compared with the conventional PID controller when FLC is applied. The motor performance shows better stability and robustness.

References

[1] Dimiter Driankov, Hans Hellendoorn, and Michael Reinfrank, "An Introduction to fuzzy control," ISBN 0-387-56362-8 Springer- Verlag Berlin Heidelberg, 1993.

[2] Gilberto C.D. Sousa, and Bimal K. Bose, " A Fuzzy Set Theory Based Control of A Phase-Controlled Converter DC Machine Drive," IEE Trans. Ind. Appl., Vol. 30,No. 1, PP. 34-44, Jan/Feb.,1994.

[3] A.E. Fitzgerald, Charles Kingsley, and Stephen D. Umans, "Electric Machinery," ISBN 0-07-707708-3, McGraw-Hill, Fifth edition, 1992.

[4] S.K. Sen, " Electric Machinery," First edition, pp. 461-467, 1989.

[5] J.D. Edwards, "Electrical Machines And Drives," ISBN 0-333-53650-9, first edition, 1985.

[6] Muhammad H. Rashid, "Power Electronics",Prentice-Hall International, Inc., ISBN 0-12-581650-2., Academic press all rights reserved 2001

[7] Donald E. Kirl, " Optimal Control Theory" Prentice-Hall, INC. Englewood cliffs, New Jersey, 13-638098-0, 1970. PP 163-177

[8] K. P. Gokhale, and G. N. Revankar, "Microprocessor-Controlled Separately Excited DC motor Drive System," IEE proc., Vol. 129, Pt.B, No. 6, November 1982.

[9] The Works Inc. Matlab General Help, Fuzzy Logic Toolbox.

Modeling and Control of A Half Car Active Suspension system

Y.M. Sam and Abdulhamid Abohagar
Faculty of Electrical Engineering,
Universiti Teknologi Malaysia,
81310 Skudai, Johor, Malaysia
Abohagar74@yahoo.com, yahaya@fke.utm.my

Abstract:

The purpose of this paper is to present a modeling and control of the active suspension system using Proportional Integral Sliding Mode Control (PISMC) techniques. The objective of designing the controller for the car suspension system is to reduce the traditional design as a compromise between ride and handling by directly controlling the suspension forces to suit the road and driving conditions. In this paper a new mathematical model is presented which will give a much more complete mathematical representation of active suspension system for the half car model. In order to achieve the desired ride comfort and road handling and to solve the mismatched condition, a proportional integral sliding mode control will be utilized to deal with the system uncertainties. Mathematical analysis for reach ability and stability of the controller will be derived. Finally, a simulation of a half-car active suspension system will be carried out using a MATLAB/SIMULINK software.

Keywords: Half car suspension system, proportional-integral sliding mode control, mismatched condition

1. INTRODUCTION

A vehicle suspension system is a mechanism that separates the vehicle body from the wheels of the vehicle so that the handling and the comfort of the driver can be improved and the road noise, bumps, vibrations can be isolated reasonably well. The objective of a suspension system is to maximize the passenger ride comfort and vehicle road quality. The performance of the suspension system can be evaluated the characteristics above. These characteristics deal with regulation of the body movement, the regulation of suspension movement and the force distribution. Ideally the suspension should isolate the body from road disturbances and inertial disturbances associated with cornering and braking or acceleration. Furthermore, the suspension must be able to minimize the vertical force transmitted to the passengers comfort. These are the major challenges currently faced by the automotive industry. To overcome the above problem active suspension system has been proposed by

various researchers [1-3]. Active suspension system is more effective to ride comfort of passengers. This type of suspension systems has the capability to adjust itself continuously to changing road conditions. It "artificially" extends the design parameters of the system by constantly monitoring and adjusting itself, thereby changing its character on an ongoing basis. The main difference between the active suspension system and the conventional suspension system is that it is able to inject energy into the system, as well as store and dissipate it. In the past years various control strategies such as backsteeping method [2], sliding mode control [4], LQR [5], H∞ control [6] and fuzzy control [7] have been proposed to meet such needs as the balance between ride comfort and road handling robustness against model uncertainty. In this paper we will consider a model of half car active suspension system and discuss the performance of the PISMC technique in terms of body acceleration and wheel deflection. To demonstrate the effectiveness and robustness of the proposed control scheme, computer simulation was performed and presented in this paper.

2. DYNAMIC MODEL OF THE ACTIVE SUSPENSION SYSTEM

The model of the half-car active suspension system that shown in figure 1 has been used by [7], in the design of active suspension system. From figure 1 it can be observed that the active suspension system for half car model is consists of the front and rear wheels and the axles that are connected to the half portion of the car body, while the tyers are modeled as simple spring without damper and two actuators connected to each front and rear suspensions.

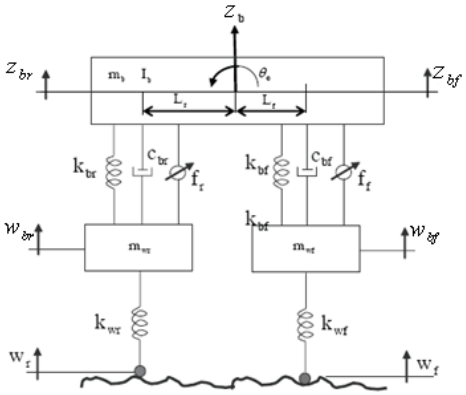

Figure 1 A half car active suspension model

where I_b is the mass moment of inertia for the vehicle body, m_b is the mass for the vehicle body, m_{wf} and m_{wr} are the mass of the front and rear wheels, respectively, Z_{bf} and Z_{br} are the vertical displacements of the vehicle body at the front and rear suspension locations, respectively. Z_{wf} and Z_{wr} are the vertical displacements of the vehicle body at the front and rear wheels, respectively, θ_0 is the rotary angle of the vehicle body at the center of gravity, f_f and f_r are the active controls at the front and rear suspensions, respectively, w_f and w_r are the irregular excitations from the road surface, L_f and L_r are the distances of the front and rear suspension locations, respectively, with reference to the center of gravity of the vehicle body, and $L_f + L_r = L$.

By applying Newton's second law and using the static equilibrium position as the origin for both the displacement of the center of the gravity and angular displacement of the vehicle body, the motion equations for the active suspension system of the half car model can be derived as follows,

$$\frac{m_b}{L}(L_f\ddot{z}_{bf}+L_r\ddot{z}_{br})+c_{bf}(\dot{z}_{bf}-\dot{z}_{wf})+k_{bf}(z_{bf}-z_{wf})+c_{br}(\dot{z}_{br}-\dot{z}_{wr})+k_{br}(z_{br}-z_{wr})-f_f-f_r=0 \quad (1)$$

$$\frac{I_b}{L}(\ddot{z}_{bf}-\ddot{z}_{br})+L_f\left[c_{bf}(\dot{z}_{bf}-\dot{z}_{wf})+k_{bf}(z_{bf}-z_{wf})-f_f\right]-L_r\left[c_{br}(\dot{z}_{br}-\dot{z}_{wr})+k_{br}(z_{br}-z_{wr})-f_r\right]=0 \quad (2)$$

$$m_{wf}\ddot{z}_{wf}-c_{bf}(\dot{z}_{bf}-\dot{z}_{wf})-k_{bf}(z_{bf}-z_{wf})+k_{wf}(z_{wf}-w_f)+f_f=0 \quad (3)$$

$$m_{wr}\ddot{z}_{wr}-c_{br}(\dot{z}_{br}-\dot{z}_{wr})-k_{br}(z_{br}-z_{wr})+k_{wr}(z_{wr}-w_r)+f_r=0 \quad (4)$$

The state space representation of active suspension system of the half car model may be written as:

$$\dot{z}_{hm}(t)=A_{hm}z_{hm}(t)+B_{hm}u_{hm}(t)+G_{hm}w_{hm}(t) \quad (5)$$

where, $A_{hm}(t)$, $B_{hm}(t)$,$u_{hm}(t)$,$G_{hm}(t)$ and $w_{hm}(t)$ are:

$$A_{hm}=\begin{bmatrix} a_{h11} & a_{h12} & a_{h13} & a_{h14} & a_{h15} & a_{h16} & a_{h17} & a_{h18} \\ a_{h21} & a_{h22} & 0 & 0 & a_{h25} & a_{h26} & 0 & 0 \\ a_{h31} & a_{h32} & a_{h33} & a_{h34} & a_{h35} & a_{h36} & a_{h37} & a_{h38} \\ 0 & 0 & a_{h43} & a_{h44} & 0 & 0 & a_{h47} & a_{h48} \\ 1 & 0 & 0 & 0 & 0 & 0 & 0 & 0 \\ 0 & 1 & 0 & 0 & 0 & 0 & 0 & 0 \\ 0 & 0 & 1 & 0 & 0 & 0 & 0 & 0 \\ 0 & 0 & 0 & 1 & 0 & 0 & 0 & 0 \end{bmatrix} \quad (6)$$

$$B_{hm}=\begin{bmatrix} b_{h11} & b_{h12} \\ b_{h21} & 0 \\ b_{h31} & b_{h32} \\ 0 & b_{h42} \\ 0 & 0 \\ 0 & 0 \\ 0 & 0 \\ 0 & 0 \end{bmatrix} \quad (7)$$

$$u_{hm}(t)=[f_f \quad f_r]^T \quad (8)$$

$$G_{hm}=\begin{bmatrix} 0 & 0 \\ g_{h21} & 0 \\ 0 & 0 \\ 0 & g_{h42} \\ 0 & 0 \\ 0 & 0 \\ 0 & 0 \\ 0 & 0 \end{bmatrix}$$

$$w_{hm}(t)=\begin{bmatrix} w_f \\ w_r \end{bmatrix} \quad (9)$$

From the equations (7-9) the elements of the disturbance input matrix G_{hm} is not in phase with the actuator input matrix B_{hm}, i.e. Rank $[B_{hm}] \neq$ rank $[B_{hm} , G_{hm}]$, therefore the

system does not satisfy the matching condition.

The system state variables are assigned in the following: $z_1 = z_{bf}$ is the front body displacement, $z_2 = z_{wf}$ is the front body velocity, is the front wheel displacement, is the $z_3 = z_{br}$ front wheel displacement, $z_4 = z_{wr}$ is the front wheel velocity, $z_{51} = z_{bf}$ is the rear body displacement, $z_6 = z_{wf}$ is the rear body velocity, $z_7 = z_{br}$ is the rear wheel displacement, $z_8 = z_{wr}$ is the rear wheel velocity, $z_9 = f_f$ is the front actuator force, and $z_{10} = f_r$ is the rear actuator force. For more details for the state equations of the half car model and non-zero elements for A_{hm} ,B_{hm} and G_{hm} as shown in Appendix A.

3. CONTROLLER DESIGN

Linear Quadratic Regulator (LQR) and a proportional integral sliding mode control (PISMC) schemes are employed to compare the performance between the two controllers for the active suspension systems.

3.1 LQR CONTROLLER DESIGN

Linear Quadratic Regulator (LQR) is a powerful concept of optimally controlling linear system commonly used for vehicle system control. This technique results in a simple control structure with an optimal state-feedback controller which can easily be obtained from the solution of the algebraic Riccati equation.

First of all let us consider a state variable feedback regulator:

$$u = -Kx \quad (10)$$

Where K is the state feedback gain matrix, the optimization procedure consists of determining the control input u, which minimizes the performance index J. The performance index J, represents the performance characteristic requirement as well as the controller input limitations.

The performance index J penalizes the state variables and the inputs; thus, it has the standard form:

$$J = \int_0^\infty x(t)^T Qx(t) + u(t)^T Ru(t)dt$$

Where Q and R are positive definite, being called weighting matrices.
The gain matrix K is computed form:

$$K = R^T B^T P \quad (12)$$

Where the matrix P is evaluated being the solution of the Algebraic Riccati Equation (ARE):

$$AP + A^T P - PBR^{-1} B^T P + Q = 0 \quad (13)$$

Then the feedback regulator is:

$$u = -(R^{-1} B^T P)x \quad (14)$$

Equation (5) for the optimal closed-loop system, being used for computer simulation, can be written in the form of:

$$\dot{x} = (A - BK)x + Gw \quad (14)$$

3.2 PISMC CONTROLLER DESIGN

The Proportional Integral Sliding Mode Control (PISMC) method which is consists of combination of the proportional integral sliding surface and the controller design which is designed to control MIMO system, the MIMO system is represented by the active suspension system for half car model.

The design procedure of the Sliding Mode Control can be broken into two parts.

3.2.1 Sliding Surface Design

The proportional integral Sliding surface for a half car model is defined as:

$$\sigma(t) = C_h x_h(t) - \int_0^t [C_h A_h + C_h B_h K_h] x_h(\tau) d\tau \quad (16)$$

Where B_h is the input matrix, C_h and K_h are constant matrices, C_h is nonsingular, while K_h is chosen such that: (A+BK) less than zero. For half car model the active suspension system has two sliding surfaces. Let the sliding surface for front and rear suspensions be defined as; $\sigma_{hf}(t)$ and $\sigma_{hr}(t)$, respectively.

3.2.2 Controller Design

The control law is broken into the linear part and the nonlinear part. The linear part is equal to the equivalent control u_{heq} and the nonlinear part is equal to the switching input control u_{hs}. For the half car active suspension model, the control input of the sliding mode control can be written as:

$$u_h(t) = u_{heq}(t) + u_{hs}(t) \quad (17)$$

$$u_h^{eq} = K_h x_h(t) - [C_h B_h]^{-1} C_h f_h(x,t)$$

Where the equivalent control $u_{heq}(t)$ is,

$$u_h^{eq} = K_h x_h(t) - [C_h B_h]^{-1} C_h f_h(x,t) \quad (18)$$

Then the switching control $u_{hs}(t)$ is selected as follows:

$$u_{hs}(t) = (C_h B_h)^{-1} \rho_h \operatorname{sgn}(\sigma_h(t)) \quad (19)$$

Obviously form equation (19), the switching control is nonlinear and discontinuous. So, the chattering effect caused by the $\operatorname{sgn}(\rho_h(t))$ function may be replaced by the continuous function. Hence the switching control becomes:

$$u_{hs}(t) = -(C_h B_h)^{-1} \rho_h \frac{\sigma_h(t)}{\| \sigma_h(t) \| + \delta_h} \quad (20)$$

Where δ is the boundary layer thickness which is selected to reduce the chattering problem and ρ_h is the design parameter which is specified by the designer. Therefore, the proposed conventional sliding mode controller for the half car active suspension model is given as follows:

$$u(t) = Kx(t) - [CB]^{-1} Cf(m_b, t) - (CB)^{-1} \rho \frac{\sigma(t)}{\| \sigma(t) \| + \delta} \quad (21)$$

Where ρ > 0, and the appropriate value for the matrix C in equations (20) and (21) are chosen by trial and error approach.

4. SIMULATION RESULTS AND DISCUSSION

The mathematical model of the system as defined in Eq. (5) and the proposed proportional integral sliding mode controller (PISMC) in Eq. (21) were simulated on computer. For comparison purposes, the performance of the active suspension system using PISMC controller is compared to the linear quadratic regulator (LQR) control approach and also with the passive suspension system.

The numerical values for the model parameters are taken from [6] and are as follows:

m_b = Mass of the car body = 1794.4 kg

I_b = Moment of inertia for the car body = 3443.05 kgm^2

m_{wf} is Mass of the front wheel = 87.15 kg

m_{wr} is Mass of the rear wheel = 140.04 kg

k_{bf} is Stiffness of the front car body spring = 66824.2 N/m

k_{br} is Stiffness of the rear car body spring = 18615 N/m

k_{wf} is Stiffness of the front car tyre = 101115 N/m

k_{wr} is Stiffness of the rear car tyre = 101115 N/m

C_{bf} is Damping of the front car damper 1190 N$_s$/m

C_{br} is Damping of the rear car damper 1000 N$_s$/m

L_f *is* Distance of the front suspension referenced to the center of gravity of the gravity of the car body (m) = 1.271

L_r is Distance of the rear suspension referenced to the center of gravity of the car body (m) = 1.713

In the study, the following typical road disturbance is used: where (*a = .055m)* denotes the bump amplitude (see Fig. 2).

$$w_f(t) = \alpha\ (1-\cos 8\pi t) \text{ if } 0.5 \le t \le 0.75 \quad (22)$$

$$w_r(t) = \alpha\ (1-\cos 8\pi t) \text{ if } 3 \le t \le 3.25 \quad (23)$$

This type of road disturbance has been used by [2,8] in their studies. Furthermore, the maximum travel distance of the suspension travel used is ±11cm as suggested by [2].

The value of the matrix gain K for LQR and PISMC controllers are chosen as [see Appendix A].

And matrix C for PISMC is, C=

$$\begin{bmatrix} 11.0532 & 0.1941 & 1.0842 & -1.2047 & 1 & 1 & 1 & 5 \\ 1 & 2 & 20 & 2 & 1 & 5 & 4 & 1 \end{bmatrix}$$

$$\rho_{hf} = 1000 \quad , \quad \sigma_{hf} = 10 \quad , \quad \rho_{hr} = 10 \ , \ \sigma_{hr} = 1$$

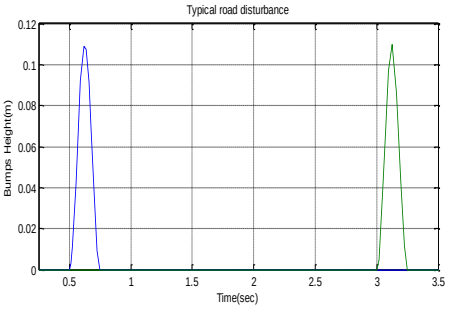

Figure 2 Typical Road Disturbances

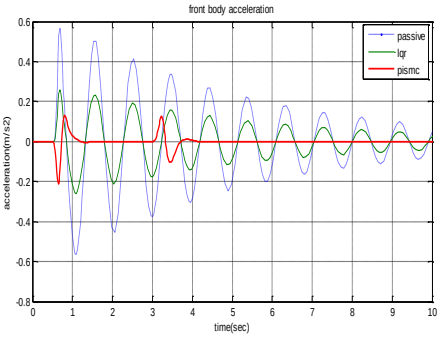

Figure 3 Front Body Accelerations

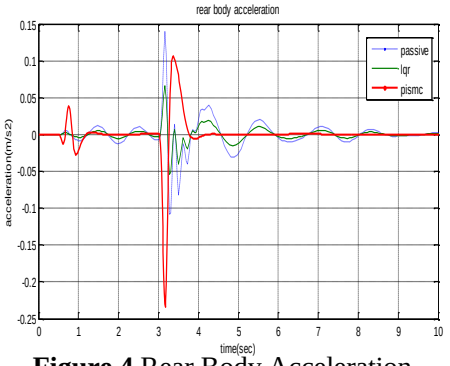

Figure 4 Rear Body Acceleration

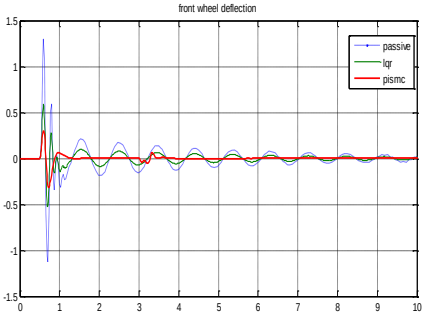

Figure 5 Front Wheel Deflection

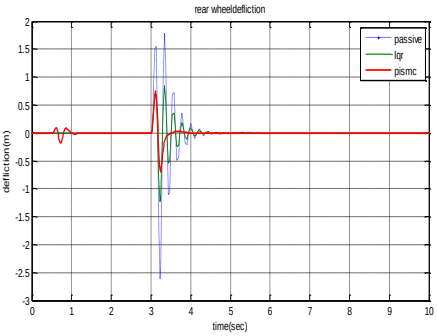

Figure 6 Rear Wheel Deflections

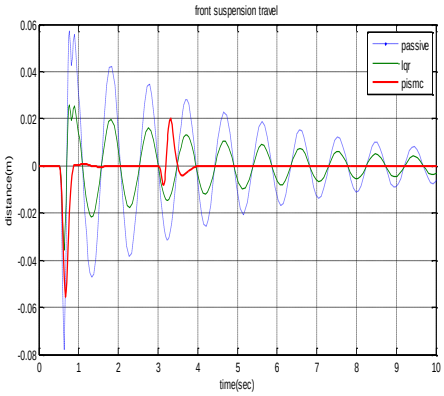

Figure 7 Front Suspension Travel

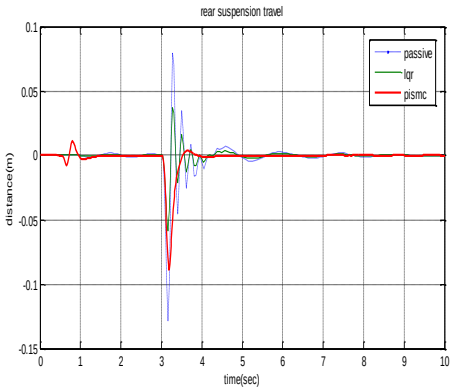

Figure 8 Rear Suspension Travel

In order to fulfill the objective of designing an active suspension system, to increase the ride comfort and road handling, there are two parameters to be observed in the simulation. The two parameters are the body acceleration and wheel deflection. The body acceleration for the front and rear suspensions for the active suspension system using LQR and PISMC controllers and also the passive suspension system are shown in Figures 3 and 4.The results show that the PISMC technique perform much better as compared to the LQR and the passive suspension, we can see that from the peak limitation of the acceleration in the sliding mode case is less than 0.2 (m/s^2). That's insure the force driven to the passenger is very small. Thus, the passenger comfort performance is much better. Figures 5 and 6, show that the PISMC approach has a better tyre deflections to road surface contact, hence directly improved the car handling as compared to the LQR method and the passive suspension system. Since the ride comfort is trade-off with the tyre deflection so the car handling is slightly improved an accepted.

Figures 7 and 8 show the front and rear suspension travel of the active suspension system using LQR and PISMC and the passive suspension system. The results show that the PISMC technique performed better as compared to the LQR and the passive suspension. Furthermore, the suspension travel of both controllers is within the distance of ± *8 cm*.

5. CONCLUSION

This paper is presented new methods which are LQR and PISMC that has been designed for the half car active suspension system. The proposed PISMC approach is capable in improving the ride comfort and road handling of the active suspension for the half car model as compared to the LQR approach and the passive suspension system. Increasing the ride comfort will make the driver and passengers of that particular car more comfortable and relax through a journey. Whereas, increasing the road handling will make the car more stable and can avoid skidding especially when the car is cornering and breaking. Furthermore, the proposed proportional integral sliding mode controller showed great achievement in enhancing the ride comfort and road handling of the active suspension system for the half car model.

REFERENCES

1.Alleyne, A. and J.K. Hedrick, "Nonlinear Adaptive Control of Active Suspensions," *IEEE Trans. Control .System. Technology*, Vol. 3, pp. 94-101 (1997).

2. D'Amato, F.J., and D.E. Viasallo, "Fuzzy Control for Active Suspensions,"

Mechatronics, Vol. 10, pp. 897- 920 (2000).

3. Esmailzadeh, E. and H.D. Taghirad, "Active Vehicle Suspensions with Optimal State-Feedback Control," *J. Mech. Sci.*, pp. 1-18 (1996).

4. Lin, J.S. and I. Kanellakopoulos, "Nonlinear Design of Active Suspension," *IEEE Contr. Syst. Mag.*, Vol. 17, pp. 45-59 (1997).

5. Tseng, T. and Hrovat, D., 1990. Some Characteristics of Optimal Vehicle Suspensions Based on Quarter-Car Model, *Proceedings of the 29th IEEE Conference on Decision and Control*, Honolulu, Hawaii: IEEE, 2232-2237.

6. Yahaya Bin Md. Sam. *Modeling and Control of Active Suspension System Using PI Sliding Mode control*. PhD thesis , Universiti Teknologi Malaysia. 2004.

7. Yamashita, M., Fujimori, K., Hayakawa, K. and Kimura, H., 1994. Application of H-infinity Control to Active Suspension Systems, *Automatica*, 30(11): 1717-179

8. Yoshimura, T., A. Kume, M. Kurimoto, and J. Hino, "Construction of an Active Suspension System of a Quarter Car Model using the Concept of Sliding Mode Control," *J. Sound Vib.*, Vol. 239, pp. 187-199 (2001).

9. Yoshimura, T., K. Nakaminami, M. Kurimoto, and J. Hino, "Active Suspension of Passengers Cars using Linear and Fuzzy-Logic Controls," *Contr. Eng. Prac.*, Vol. 7, pp. 41-47 (1991).

APPENDIX A

$$a_{h11} = \frac{-Lc_{bf}}{m_b(L_f + L_r)} - \frac{L^2{}_f Lc_{bf}}{I_b(L_f + L_r)}$$

,

$$a_{h12} = \frac{Lc_{bf}}{m_b(L_f + L_r)} + \frac{L^2{}_f Lc_{bf}}{I_b(L_f + L_r)}$$

$$a_{h13} = \frac{-Lc_{br}}{m_b(L_f + L_r)} + \frac{LL_f L_r c_{br}}{I_b(L_f + L_r)}$$

,

$$a_{h14} = \frac{Lc_{br}}{m_{bf}(L_f + L_r)} - \frac{LL_f L_r c_{br}}{I_b(L_f + L_r)}$$

$$a_{h15} = \frac{-Lk_{bf}}{m_b(L_f + L_r)} - \frac{L^2{}_f Lk_{bf}}{I_b + (L_f + L_r)}$$

$$a_{h16} = \frac{Lk_{bf}}{m_b(L_f + L_r)} + \frac{L^2{}_f Lk_{bf}}{I_b(L_f + L_r)}$$

$$a_{h17} = \frac{-Lk_{br}}{m_b(L_f + L_r)} + \frac{LL_f L_r k_{br}}{I_b(L_f + L_r)}$$

$$a_{h18} = \frac{Lk_{br}}{m_b(L_f + L_r)} - \frac{LL_f L_r k_{br}}{I_b(L_f + L_r)} \qquad a_{h25} = \frac{k_{bf}}{m_{wf}} \ ,$$

$$a_{h26} = \frac{-(k_{bf} + k_{wf})}{m_{wf}}$$

$$a_{h21} = \frac{c_{bf}}{m_{wf}} \ ,$$

$$a_{h22} = \frac{-c_{bf}}{m_{wf}} \ ,$$

$$a_{h31} = \frac{-Lc_{bf}}{m_b(L_f + L_r)} + \frac{LL_f L_r c_{br}}{I_b(L_f + L_r)} \qquad a_{h35} = \frac{-Lk_{bf}}{m_b(L_f + L_r)} + \frac{LL_f L_r k_{br}}{I_b(L_f + L_r)}$$

$$a_{h32} = \frac{Lc_{bf}}{m_b(L_f + L_r)} - \frac{LL_f L_r c_{bf}}{I_b(L_f + L_r)}$$

$$a_{h33} = \frac{-Lc_{br}}{m_b(L_f + L_r)} - \frac{L^2{}_r Lc_{br}}{I_b(L_f + L_r)} \qquad a_{h37} = \frac{-Lk_{br}}{m_b(L_f + L_r)} - \frac{L^2{}_r Lk_{br}}{I_b(L_f + L_r)}$$

$$a_{h34} = \frac{Lc_{br}}{m_b(L_f + L_r)} + \frac{L^2{}_r Lc_{br}}{I_b(L_f + L_r)} \qquad b_{h11} = \frac{L}{m_b(L_f + L_r)} + \frac{L^2{}_f L}{I_b(L_f + L_r)}$$

$$a_{h43} = \frac{c_{br}}{m_{wr}} \qquad a_{h44} = \frac{-c_{br}}{m_{wr}} \ , \qquad a_{h47} = \frac{k_{br}}{m_{wr}}$$

$$a_{h48} = \frac{-(k_{br} + k_{wr})}{m_{wr}} \ , \qquad g_{h21} = \frac{k_{wr}}{m_{wf}} \ , \qquad g_{h42} = \frac{k_{wr}}{m_{wr}}$$

$$b_{h12} = \frac{L}{m_b(L_f + L_r)} - \frac{LL_fL_r}{I_b(L_f + L_r)} \qquad b_{h21} = -\frac{1}{m_{wf}}$$

$$b_{h31} = \frac{L}{m_b(L_f + L_r)} - \frac{LL_fL_r}{I_b(L_f + L_r)} \qquad b_{h42} = -\frac{1}{m_{wr}}$$

,

$$b_{h32} = \frac{L}{m_b(L_f + L_r)} + \frac{L^2{}_fL}{I_b(L_f + L_r)}$$

LQR,

K =

$$\begin{bmatrix} 20.4527 & 37.9965 & 2.9295 & 0.0674 & 71.3249 & -121.2562 & -16.7904 & 5.9735 \\ 3.1670 & 0.1521 & 40.5343 & 46.8391 & 15.1987 & 3.6052 & 47.7956 & -123.5472 \end{bmatrix}$$

PISMC,

K =

$$\begin{bmatrix} 21320 & 7020 & -5140 & 340 & 39270 & 164210 & -40980 & -24260 \\ -6610 & -680 & 57600 & 61900 & -2279 & -95990 & 240370 & 275650 \end{bmatrix}$$

A Robust H_∞ Controller for Power System Stabilization

* Nasr Emhemmed Shtawa

*nasrshtawa@yahoo.com

* Department of Electrical and electronic Engineering, Faculty of Engineering, Afateh University, Tripoli - Libya

ABSTRACT

In this paper a new approach to the design of power system stabilizer (PSS) for a synchronous generator is presented. The approach is based on a robust H_∞ control for power system stabilization. The uncertainties in power system modeling and operations are considered at designing of PSS. The bounds of power system parameter are determined over a wide range of operating conditions. These bounds are used to design a robust H_∞ power system stabilizer. A sample power system, composed of a synchronous generator connected to infinite bus-bar through transmission line is simulated. The digital simulation results show that the proposed robust H_∞ PSS can achieve good performance over a wide range of operating conditions. Moreover, a comparison between power system responses at a variety of operating conditions using the PSS based on linear quadratic regulator (LQR) approach and the proposed robust H_∞ is presented.

1. INTRODCTION

Power system stabilizers (PSSs) have been widely used as supplementary controllers to provide extra damping for synchronous generators in electrical power system. Conventional power system stabilizer (CPSSs) are used to damp out small signal oscillations and they are designed based on a model which is linearized around a particular operating point. Conventional design tunes the gain and time constants of the PSS, which are mostly lead-lag compensator, using modal frequency techniques [1]. Such designs are specific for a given operating point; they do not guarantee robustness for a wide range of operating condition [2].

Modern control methods were extremely successful because they could be efficiently implemented on computers, they could handle multi-input-multi-output system, and they could be optimized[3]. This paper proposes a robust output feedback controller design for damping power system oscillations.

The robustness can be defined as the ability of the controller to maintain the stability of the system over a wide range of operating condition. One way of ensuring system robustness is to take into consideration at the design stage, the various uncertainties that arise in the system due to inaccuracy of the mathematical model, the system parameter variations, neglected dynamics etc. Modern robust controls theory such as and theory can be used to damp power system oscillations with system uncertainty. One of the important in optimal control design is the choice of the weighting functions. Weighting function are necessary to achieve a trade-off between the conflicting design requirements such as small sensitivity and complementary sensitivity. However, there is no systematic procedure yet available for selecting these weighs [1].

The formulation and solution procedures are explained on how to choose proper weighting functions that reflect the robustness and performance goals. Also, synthesis is carried out in two stages. First, in what is called the formulation procedure to robust for modeling errors and weighting. Second, in what is called the solution procedure, and the weights are iteratively modified until an optimal controller. Time response simulations are used to validate the results obtained. The effectiveness of such controllers is examined at different extreme operating conditions. The present paper uses robust approach to design a robust power system stabilizer applied on synchronous machine connected to an infinite bus through a transmission line. The essential feature of the proposed power system stabilizer PSS is that it is simple, easy to implement, and it is not sensitive to the external disturbances and power system parameter variations[3-7].

2. POWER SYSTEM MODEL

The linearized model of the studied power system consisted of synchronous machine connected to an infinite bus through a transmission line is obtained in a an interconnected power system between automatic voltage regulation and load frequency control. The state space formulation can be obtained as follows :

$$\dot{\Delta\delta} = \Delta\omega \tag{1}$$

$$\dot{\Delta\omega} = -\left(\frac{K_1}{M}\right)\Delta\delta - \left(\frac{D}{M}\right)\Delta\omega - \left(\frac{K_2}{M}\right)\Delta E'_q + \left(\frac{1}{M}\right)\Delta T_m - \left(\frac{1}{M}\right)\Delta P_d \tag{2}$$

$$\dot{\Delta E}_q = -\left(\frac{K_4}{T'_{d0}}\right)\Delta\delta - \left(\frac{1}{K_3 T'_{d0}}\right)\Delta E'_q + \left(\frac{1}{T'_{d0}}\right)\Delta E_{fd} \tag{3}$$

$$\dot{\Delta T}_m = -\left(\frac{1}{T_t}\right)\Delta T_m + \left(\frac{1}{T_t}\right)\Delta P_g \tag{4}$$

$$\dot{\Delta P}_g = -\left(\frac{1}{RT_g}\right)\Delta\omega - \left(\frac{1}{T_g}\right)\Delta P_g + \left(\frac{1}{T_g}\right)U_2 \tag{5}$$

$$\dot{\Delta E}_{fd} = -\left(\frac{1}{T_A}\right)\Delta E_{fd} - \left(\frac{K_A K_5}{T_A}\right)\Delta\delta - \left(\frac{K_A K_6}{T_A}\right)\Delta E_q' + \left(\frac{K_A}{T_A}\right)\Delta U_1 \tag{6}$$

where;

$$A=\begin{bmatrix} 0 & \omega_0 & 0 & 0 & 0 & 0 \\ -\frac{K_1}{M} & -\frac{D}{M} & -\frac{K_2}{M} & \frac{1}{M} & 0 & 0 \\ -\frac{K_4}{T'_{d0}} & 0 & \frac{-1}{(K_3 T'_{d0})} & 0 & 0 & \frac{1}{T'_{d0}} \\ 0 & 0 & 0 & \frac{-1}{Tt} & \frac{1}{Tt} & 0 \\ 0 & -\frac{1}{(RT_g)} & 0 & 0 & \frac{-1}{T_g} & 0 \\ -\left(\frac{K_4K_5}{T_A}\right) & 0 & -\left(\frac{K_AK_6}{T_A}\right) & 0 & 0 & \frac{-1}{T_A} \end{bmatrix}$$

$$X=\begin{bmatrix} \dot{\Delta\delta} \\ \dot{\Delta\omega} \\ \dot{\Delta E'_q} \\ \dot{\Delta T_m} \\ \dot{\Delta P_g} \\ \dot{\Delta E_{fd}} \end{bmatrix} \qquad B=\begin{bmatrix} 0 & 0 \\ 0 & 0 \\ 0 & 0 \\ 0 & 0 \\ 0 & 1/Tg \\ \frac{K_A}{T_A} & 0 \end{bmatrix} \quad (7),$$

The parameters and coefficients of A matrix and B vector are defined in ref. [2].

3. H_∞ Power System Stabilizer Design

The H_∞ solve the small-gain infinity-norm robust control problem; i.e., find a stabilizing control K(S) for a system plant P(s) as shown in Fig.2. The compensation configuration depicted in Fig.1 will be referred to as the standard compensator. The objective is to design a controller K(s), for the plant P(S) such that the input/output transfer characteristics from the external input vector w to the external output z is desirable, according to some engineering specification. Then, the following fundamental relations:

$$y(s)=\frac{G(s)K(s)}{1+G(s)K(s)}\ r(s)+\frac{1}{1+G(s)K(S)}\ d(s)-\frac{G(s)K(s)}{1+G(s)K(s)}\ n(s) \quad (8)$$

The complementary transfer function

$$T(s)=\frac{G(s)K(s)}{1+G(s)K(s)}$$

Also, the sensitivity transfer function

$$S(s)=\frac{1}{1+G(s)K(s)}$$

The following set of weighting function is chosen to define the desired robustness and performance goals. Augmentation of the weightings system $W1, W2, W3$ (state-space form) into two-port plant can be calculated by calling MATLAB function “augment” as follows:

[A,B1,B2,C1,C2,D11,D12,D21,D22]=augment(sys_g,sys_W1,sys_W2, sys_W3,DIM) (9)

Where:

Sys_W1:=[aw1 bw1;cw1 dw1]

Sys_W2:=[aw2 bw2;cw2 dw2]

Sys_W3:=[aw3 bw3;cw3 dw3]

Sys_g : power system parameters.

Any of the above weightings can be removed by setting sys_W1 or sys_W2 or

sys_W3 equals to zero, a non dimensional state space. Also, the DIM is a dimension of the system under study and weightings W1, W2, W3 as :

$$DIM = [xg \quad xw1 \quad xw2 \quad xw3]$$

Where xg : no. of states of the system $G(s)$,

xw1 : no. of states of (W1(s)=0, if sys_w1=[zero])

xw2 : no. of states of W2(s)….etc…,. after computing of the system TSS_P and SS_U by using the MATLAB function $mksys$ as follows :

$$TSS_p = mksys(A, B1, B2, C1, C2, D11, D12, D21, D22)$$

Computes the H_∞ controller $F(s)$ and the controller parameterization $K(s)$using the loop shifting formulas formed by wrapping feedback $U(s)$

Around $K(s)$ as :

[SS_CP,SS_CL,HINFO,TSS_K]=Hinf(TSS_P) (10)

the output data :

Controller $F(s) = SS\_CP$,

Closed loop = SS_CL and feedback TSS_K

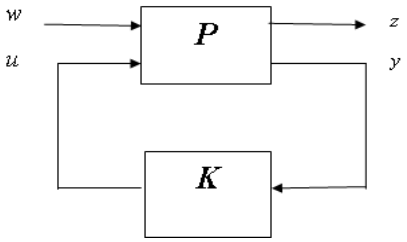

Fig. 2: Standard compensation configuration

5. LQR Control Feedback

The design of the power system stabilizer based on linear-quadratic regulator LQR control for continuous-time systems as follows:

[K, S, E] = LQR (A, B, Q, R, N)

(11)

The optimal gain matrix K is calculate such that the state-feedback law u= -Kx minimizes the cost function

$$J = Integral \quad (X'QX + u'Ru + 2*X'Nu)dt$$

Subject to the state dynamics

$$\dot{X} = AX + Bu.$$

The matrix N is set to zero when omitted. Also returned are the Riccati equation

solution S and the closed-loop eigenvalues E:

$$SA + A'S - (SB + N) R^{-1} (B'S + N') + Q = 0, \quad (12)$$

$$E = EIG\ (A - B * K) \quad (13)$$

7. DIGITAL SIMULATION RESULTS

Choosing the machine parameters at nominal operating conditions as ref. [2] ;

The A matrix at nominal load (P=1.0, Q=0.25 pu.) is evaluated and calculated sa Eqn.(7). By selecting the weights W_1, W_2 and W_3 to give best performance after the iteration of MATLAB program.

The weights W_1, W_2, and W_3 to give best performance as following :

$$W_1(s) = \begin{bmatrix} \frac{100S+0.63}{0.1S+30} & 0 \\ 0 & \frac{100S+0.63}{S+300} \end{bmatrix}$$

,

$$W_2(s) = \begin{bmatrix} \frac{50S^2+0.3S+6}{1106S^2+166S+1106} & 0 \\ 0 & \frac{1.5S^2+2S+7}{5S^2+S+4} \end{bmatrix}$$

$$W_3(s) = \begin{bmatrix} \frac{0.1S^2+0.107S+4}{100S^2+5000S+4500} & 0 \\ 0 & \frac{0.01S^2+0.072S+3}{0.1S^2+40S+60} \end{bmatrix}$$

Solving Eqn.(11), for the H_∞controller feedback K(S) using U(S)=0 (default) and by using Riccati equations the performing H_∞ existence tests:

1. D_{11} is small enough
2. State-feedback (P) Riccati A-B2*F is stable (P >= 0)
3. Output- injection (S) Riccati A-G*C2 is stable (S >= 0)

After applying the robust H_∞controller to the interconnected power system represents in Eqn.(8), the feedback controller matrix Tss_K can be calculated from Eqn.(11). Fig.2 depicts the power system model in a block diagram after adding the proposed controller. Using the value of feedback matrices obtained in Eqn.(11), the dynamic stability of linearized studied power system subjected to load disturbances is simulated on the computer using the program in Matlab Package. Moreover, the feedback LQR controller using for comparison is calculated from Eqn. (12) . Figs 2,3 show the rotor speed deviation response and rotor angle deviation response due to 0.01pu. load disturbances with both LQR and robust H_∞controller at lead power factor load(1,-0.25). The eigenvalues of the studied power system at variety of operating conditions with and without controllers is shown in table [1].

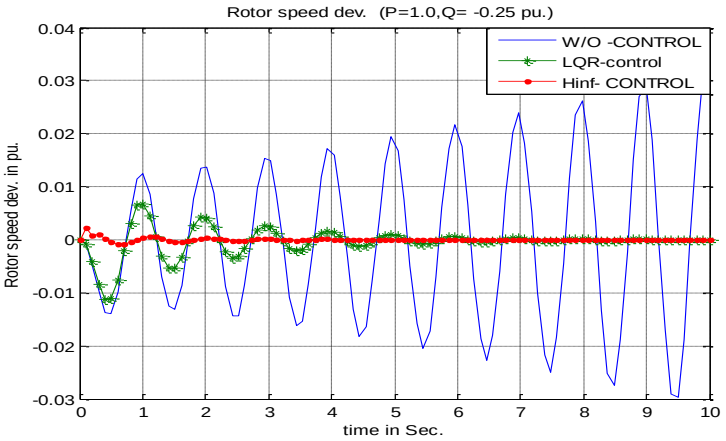

Fig.(2): Rotor speed dev. Response due to 0.05 pu load disturbance with and without (LQR & H_INFINITY) controller at (P=1, Q=-0.25pu)

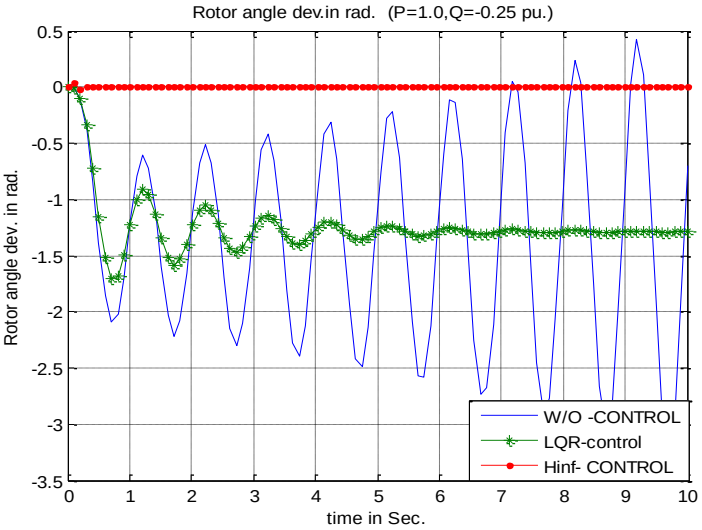

Fig. (3): Rotor angle dev. Response due to 0.05 pu load disturbance with and without (LQR & H_INFINITY) controller at (P=1, Q=-0.25pu)

X_d =1.6; X_q=1.55 ; $X_{d'}$=0.32 ; X_e= 0.4p.u , M=10; T_{do}= 6; D=0; T_A=0.06 ; K_A=25;

Tt=0.27 ; Tg= 0.08 ; R=1/(Tg*6.86) ;. $\omega_o = 377$

Table 1: Eigen values calculation with and without (LQR & H_∞) controllers.

Operating point	Without controller	With LQR controller	With H infinity controller
P=1, Q=-0.25 pu. Lead power factor	+0.1033 + 6.3047i + 0.1033 - 6.3047i -14.9008 -12.4804 -2.4303 -3.7285 unstable	-14.9060 -13.1803 -0.4950 + 6.3372i -0.4950 - 6.3372i -2.2020 -4.1167	-398.49 -300.00 -300.00 -13.03 + 30.84i -13.03 -.3.084i -49.08 -31.41 +12.67i -31.41 – 12.67i -15.01 -0.67 + 6.80i -0.67 – 6.80i -0.08 + 1.00i -0.08 – 1.00i -2.12 -0.92 -1.51

8. CONCLUSION

The present paper introduces a new application for design of a robust PSS Based on H_∞. The proposed PSS needs only bounds of system parameters. The sample single machine –infinite bus connected to load frequency control power system is simulated to the study of the effectiveness of proposed robust H_∞-PSS for subjected to variety of load and system parameters variations. A comparison between the control action of PSSs designed using robust H_∞ and LQR controller are studied and obtained. The digital results show the powerful of the proposed robust H_∞-PSS in sense of fast damping electromechanical oscillations and small settling time with change of system operating conditions and parameters.

9. REFERENCES

[1] M. K. El-Sherbiny and D. Mehta " Dynamic stability, part I, investigation of the effect of different loading and excitation system" IEEE Trans. Power Appar. Syst., PAS-92(1973), PP 1538-1546.

[2] *Ali M. Yousef* " Efficient methods for enhancing power system operations" Ph.D thesis, Faculty of engineering, Assiut university, Assiut, Egypt 2003.

[3] M. K. El-Sherbiny, A.I.Saleh and A.A.M.El-Gaafary " Optimal Design of An Overall Controller of Saturated Synchronous Machine Under Different Loading", IEEE Transaction of power Apparatus and System, Vol.PAS-102,No.6,June 1983

[4] M.K. El-Sherbiny , G. El-Saady and Ali M. Yousef "Robust controller for power system stabilization" IEEE MEPCON'2001, Helwan University, Cairo, Egypt, December 29-31,2001, PP. 287-291.

[5] M.K. El-Sherbiny , M. M. Hassan, G.El-Saady and Ali M. Yousef " Optimal pole shifting for power system stabilization", Electric Power Systems Research Journal, No.66 PP. 253-258. 2003

[6] S. C. Tripathy, R. Balasubramanian and Zahid Jamil " Interaction of Voltage and Frequency Control Loops and Optimization of Parameters", IE(I) Journal-EL, Vol. 62, paper No. UDC 621-316-2, October 1981.

[7] A. Abdel- Fatah “ Analysis and design of magnetic levitation control systems” M. Sc. Thesis, Assiut university, 1994.

LQR Based a UAV Pitch Controller System Design

Mustafa R. Abozaid

Abstract

In this paper, an automatic control system design based on Linear Quadratic Regulator has been implemented on longitudinal flight dynamics of an UAV. It has been aimed to suppress the sustained oscillations resulted from the very close complex conjugate poles pair to the imaginary axis. In the following parts, the open loop response of the full mode longitudinal flight dynamics of the desired UAV is studied and then LQR controller has been designed.

Keywords—LQR, UAV, Longitudinal Flight Dynamics,, Short period mode

Introduction

In recent years, the desire of obtaining information about unreachable, distant places has increased. This desire sometimes has risen as a need of observation of damage caused by natural phenomenons (such as storms, earthquakes, floods …), sometimes as a need of commercial issues, sometimes as a need of strategic location and border security of countries. As a result of these necessities, solutions have also occurred in scientific environment immediately and perhaps one of the most important results of this need is the design, modeling and automatic control system design of Unmanned Aerial Vehicles (UAVs) [1].

In daily life, starting from agriculture up to defense related issues; UAVs have a wide range of application areas. Even if, in the recent years they have been used in defense technologies or combat missions, they have also been widely used in observatory purposes such as determining the damage caused by natural phenomenon's or exploration of arctic places where human-being cannot reach. Moreover, they have also been extensively used in reconnaissance and intelligence gathering issues as well. In this kind of events precision, functionality and stability of the vehicle is playing a vital role in accomplishment of the mission.

Longitudinal Model of UAV— The first step in designing a controller for any physical system is to characterize the dynamics of that system. The dynamics of any aircraft can be decoupled into lateral dynamics and longitudinal dynamics [2,6]. The lateral dynamics are the aircraft's response along the roll and yaw axes. The lateral modes are generally excited with aileron and rudder inputs. The longitudinal dynamics are the response of the aircraft along the pitch axis. The aircraft's response in velocity to thrust is also included in the longitudinal dynamics.

Since pitch control is a longitudinal problem so, only the longitudinal dynamics will be considered in this paper.

The longitudinal dynamics mode of interest here is the short period mode. Nearly all of the aircrafts are experiencing different kind of forces and moments as a result of external disturbances during the flight. Some of these disturbances are happening in a very short period of time and could have a great effect on the system itself. Considering that this kind of short period oscillations occurs in such a short period of time, the forward velocity of the aircraft could be assumed constant. The equations of motion for short period approximation in longitudinal taken from [3]

Z :

$$\left(\frac{mu}{Sq}s - C_{z\alpha}\right)\alpha'(s) - \frac{mu}{Sq}s\,\theta(s) = Cz_{\delta e} \quad (1)$$

M :

$$-\left(\frac{\bar{c}}{2u}C_{m\dot{\alpha}}s + C_{m\alpha}\right)\alpha'(s) + \left(\frac{I_{yy}}{Sq\bar{c}}s^2 - \frac{\bar{c}}{2u}C_{mq}s\right)\theta(s) = Cm_{\delta e}$$

In compact form

$$\begin{bmatrix} (\frac{mu}{Sq}s - C_{z\alpha}) & -\frac{mu}{Sq}s \\ -(\frac{\bar{c}}{2u}C_{m\dot{\alpha}}s + C_{m\alpha}) & (\frac{I_{yy}}{Sq\bar{c}}s^2 - \frac{\bar{c}}{2u}C_{mq}s) \end{bmatrix} \begin{bmatrix} \alpha'(s) \\ \theta(s) \end{bmatrix} = \begin{bmatrix} Cz_{\delta e} \\ Cm_{\delta e} \end{bmatrix} \quad (2)$$

Where,

u = perturbation velocities in X axis,

u' = u/u_0 = Change of velocity in longitudinal flight,

α'= w/u_0= Change of angle of attack in longitudinal flight,

θ = Change of pitch angle from equilibrium condition.

C_{xu} = Change in F_x due to change in forward velocity.

C_{xa} = Change in F_x due to change in angle of attack.

$C_{z\alpha}$ = Change in F_z due to change in angle of attack.

$Cz_{\delta e}$ = Elevator displacement with respect to **y**

C_{zq} = Change in F_z due to change in pitching velocity.

C_{zu} = Change in F_z due to change in forward velocity

$C_{m\alpha}$ = Change in pitching moment due to change in angle of attack

C_{mq} = Change in pitching moment due to pitching rate.

The characteristics properties of Hezarfen UAV and stability derivatives are presented in the tables below [1].

Table 1: Characteristic Properties of Hezarfen UAV.

Symbol	Description	Value	Unit
m	Mass	5	kg
U_0	Velocity	20	m / sec
g	Gravity	9.807	m /sec^2
S	Wing Area	0.4205	m^2
b	Wing Span	1.7	m
$\bar{C}$	Chord length	0.235	m
ρ	Air Density	1.226	Kg / m^3
Iyy	Moment of inertia	0.1204	Kg. m^2
q	Dynamic pressure	245.2	Kg / m. sec^2
AR	Aspect Ratio	6.8728	

Table 2 Stability Derivatives and inputs Hezarfen UAV

Symbol	Value	Symbol	Value
C_{xu}	- 0.0264	Cm_{ad}	- 0.0348
Cx_a	0.4367	C_D	0.0132
Cz_u	- 0.9512	C_L	0.4756
Cz_a	- 0.1381	C_W	- 0.4756
Cz_{ad}	- 0.0348	$C_{x\delta e}$	0
Cz_q	- 3.3	$C_{z\delta e}$	-0'71
Cm_a	- 0.0312	$C_{m\delta e}$	-0.71
Cm_q	- 3.3		

For homogeneous solution and by inserting numeric values Eq.(2) becomes

$$\begin{bmatrix} (0.9701\ s+0.1381) & -0.9505\ s \\ (0.0002\ s+0.0312) & (0.00497\ s^2+0.0194\ s) \end{bmatrix} \begin{bmatrix} \alpha'(s) \\ \theta(s) \end{bmatrix} = 0 \quad (3)$$

Where the determinant of Eq.(3), which yields to the characteristic equation of short period approximation, is as

$$0.0048\,s^3+0.019\,s^2+0.0323\,s=0 \quad (4)$$

$$s(s^2+3.9583s+6.7292)=0$$

A closer look at Eq.(4), shows a presence of a pole at the origin, which is leading the system to be a marginally stable one. The natural frequency and damping values of short period approximation were obtained as in Eq.(5).

$$\left.\begin{aligned} \xi_{spa} &= 0.763 \\ \omega_{n\,spa} &= 2.59 \quad rad/s \end{aligned}\right\} \quad (5)$$

From Eq.(5), it can be said that the short period approximation behavior of the UAV is satisfactorily damped and the natural frequency is noticeably good.

From Eq.(3), and by using the Cramer's Rule, the following $\frac{\theta(s)}{\delta_e(s)}$, is obtained

$$\left(\frac{\theta(s)}{\delta_e(s)}\right)_{spa} = \frac{(-0.6887\,s-0.0758)}{0.0048\,s^3+0.019\,s^2+0.0323\,s}$$

$$\left(\frac{\theta'(s)}{\delta_e(s)}\right)_{spa} = \frac{-143.48(s+0.11)}{s(s^2+3.9583s+6.7292)} \quad (6)$$

The open loop transfer function consists of aircraft transfer function in series with the servo actuator transfer function $(\frac{10}{s+10})$ for the approximated short period mode is found to be as follows:

$$\left(\frac{\theta(s)}{\delta_e(s)}\right)_{spa} = \frac{6.887\,s+0.758}{0.0048\,s^4+0.067\,s^3+0.2223\,s^2+0.323\,s} \quad (7)$$

$$\left(\frac{\theta(s)}{\delta_e(s)}\right)_{spa} = \frac{1435\,s+157.9}{s(s^3+13.96\,s^2+46.31\,s+67.29)}$$

The corresponding bode plot is shown in Fig.(1). The presence of the pole at $S=0$ in Eq.(7) mathematically represents a pure integration. As a result, if δ_e is a step then, the output θ will be the integral of this

constant and will approach infinity as time approaches infinity.

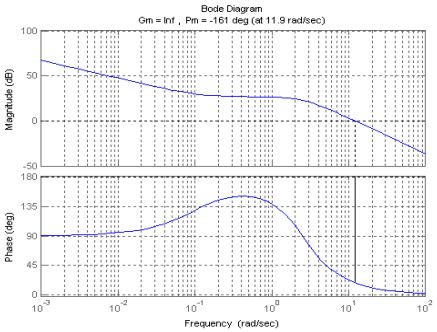

Figure 1: Bode Plot of $\left(\frac{\theta(s)}{\delta_e(s)}\right)_{spa}$

From the plot of the step response of $\left(\frac{\theta(s)}{\delta_e(s)}\right)_{spa}$ shown in Fig.(2), the effect of pole at the origin can be clearly seen which caused the system to be easily unstable. So, some kind of control is needed to move the pole away from the origin and hence maintain the system stability,

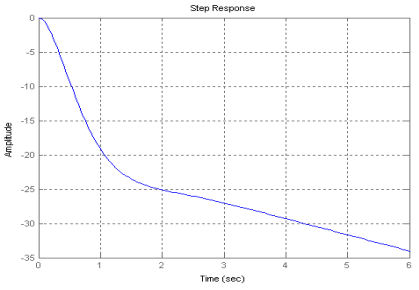

Figure 2: Step response of $\left(\frac{\theta(s)}{\delta_e(s)}\right)_{spa}$

Linear Quadratic Regulator (LQR)

This section of the paper depicts the application of linear quadratic regulator to the longitudinal flight motion of an unmanned aerial vehicle (UAV) for the pitch control. The principle objective for LQR control is to minimize certain cost function which is called performance index[4]. The design of quadratic optimal controller based on such quadratic performance index requires the determination of the elements of the matrix feedback gain matrix "K" by using the following Matlab command:

$$[K, S, E] = lqr(A, B, Q, R) \qquad (8)$$

Where

Q is the state cost matrix

R is the performance index matrix

A, B are the state space representations of the system.

Eq.(8) calculates the optimal gain matrix K such that the state-feedback law **u =-k x** minimizes the quadratic cost function **J(u),** which is described by[4]:

$$J(u) = \int_0^\infty \left(x^T Q x + u^T R u\right) dt \qquad (9)$$

In addition to the state-feedback gain K, lqr returns the solution S of the associated Riccati equation[5].

$$\mathbf{P}A + A^T\mathbf{P} + Q - \mathbf{P}BR^{-1}B^T\mathbf{P} = 0 \qquad (10)$$

and then solving for the controller gain K

$$K = -R^{-1}B^T\mathbf{P} \qquad (11)$$

Where **P** is a positive definite matrix.

The state space representation of the pitch to elevator deflection is obtained by converting the transfer function, relating the pitch angle to the elevator deflection its state space form.

LQR Controller Design

The first step in designing LQR controllers is to put the desired plant into its state space form. The open loop transfer function was transformed to state space form using an associated Matlab command and the state space form of the

approximated short period mode is found to be as follows:

$$A = \begin{bmatrix} -13.9583 & -46.3125 & -67.291 & 0 \\ 1.0000 & 0 & 0 & 0 \\ 0 & 1.0000 & 0 & 0 \\ 0 & 0 & 1.0000 & 0 \end{bmatrix}$$

$$B = \begin{bmatrix} 1 & 0 & 0 & 0 \end{bmatrix}^T \quad (12)$$

$$C = \begin{bmatrix} 0 & 0 & 1435 & 157.9 \end{bmatrix}$$

$$D = [0]$$

$$\text{Controlability} = 10^3 * \begin{bmatrix} 0.0010 & -0.0140 & 0.1485 & -1.4940 \\ 0 & 0.0010 & -0.0140 & 0.1485 \\ 0 & 0 & 0.0010 & -0.0140 \\ 0 & 0 & 0 & 0.0010 \end{bmatrix} \quad (13)$$

(13)

Rank (Controllability) = 4

$$\text{Observolability} = 10^4 * \begin{bmatrix} 0 & 0 & 0.1435 & 0.0158 \\ 0 & 0.1435 & 0.0158 & 0 \\ 0.1435 & 0.0158 & 0 & 0 \\ -1.9869 & -6.6449 & -9.6550 & 0 \end{bmatrix} \quad (14)$$

(14)

Rank (O_t) = 4

With such observability and controllability analyses, it has been proved that the short period mode of the longitudinal UAV system is both controllable and observable, which grants the opportunity to use an observer in the control system design process.

$$K = \begin{bmatrix} 11.5 & 226.9 & 1398.8 & 157.9 \end{bmatrix} \quad (15)$$

Fig.(3) shows the response of the LQR controller, from which it is clearly noticeable that the LQR controller meets the desired requirements with a maximum percentage overshoot of about 6, settling time of about 0.7sec and almost zero steady state error.

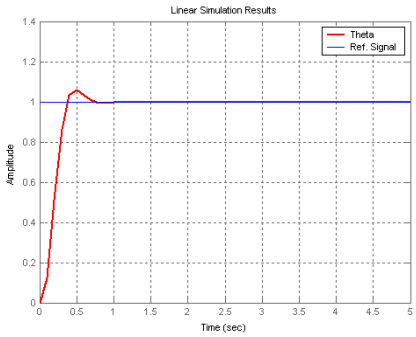

Figure 3 : LQR Controller for Short Period Mode

To test the system reliability, a step input signal with varying amplitude was applied to the system input and the system behavior was observed. From Fig.(4), it is clear that the tracking of the LQR controller acceptable and that the LQR controller responses very well

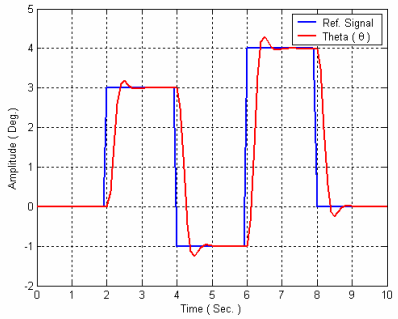

Figure 4: Tracking Signal of LQR Controller

A way to investigate the performance of the system is to disturb the system and observing the system behavior. The disturbance and the system response are shown in Fig.(5), from which it is clear that the disturbance affects the system instantly, but the LQR controller responses very well and returns the system to the desired situation

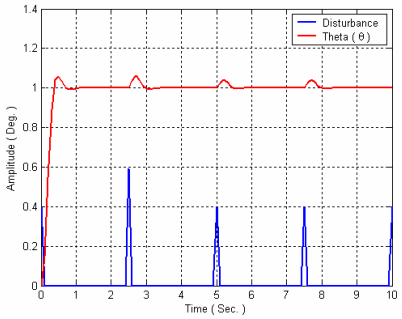

Figure 5: Disturbance Rejection Of LQR Controller

Table (3) lists the calculated eigenvalues with and without the LQR controller. From the table, it is clear that the presence of the LQR controller moves the poles of the system to the left away from the imaginary axis and hence improves the damping as shown in Table (3), and hence a good robustness of the LQR controller was achieved.

Table 3 Calculated Eigenvalues of the Short Period Mode

Without Control	With LQR Control
0	-0.1099
-10.0000	-13.0810
-1.9792 + 1.6769i	-6.1379 + 8.4930i
-1.9792 - 1.6769i	-6.1379 - 8.4930i

Conclusion

The Linear quadratic Regulator (LQR) controller was designed for the UAV based on the mathematical model. Open and closed loop computer simulations were conducted to analyze the response of the mathematical model and to aid the controller design.

From the closed loop time domain results, it is clear to note that the optimal LQR control system design is able to shape the open loop dynamics so that the settling time and the percentage overshoot lie within the desired limits with almost zero state error.

Due to its well response in getting optimum response in tracking sudden changes in the system ant due to its robustness in improving the system stability. LQR controller may be used instead of the old control techniques used in designing UAV autopilots,

References

[1] K. Turkoglu, E. M. Jafrov, Application of H_∞, Loop Shaping Robust Control design on Longitudinal Dynamics of Hezarfen UAV with classical PI and Pole placement Methods: A Comparison Analysis, WSEAS Transactions on Systems, Issue . Vol.6, January 2007

[2] J.Roskam, Airplane Flight Dynamics and Automatic Flight Control, Part I, 2nd ed., Darcorporation, Newyork,1998

[3] John H. Blakelock., Automatic Control of Aircraft and Missiles, 2nd ed.,Wiley Interscience, 1991.

[4] Ogatta, Modern Control Engineering, 3rd ed Prentice-Hall, 1997

[5] Graham C. G , et el, Modern Control System, University of New Castle,1st ed., 2000

[6] B. Etkin, L. D. Reid, Dynamics of Flight: Stability and Control,3rd ed., Wiley & Sons, Inc, USA,1996

A new s Adaptive PID Controller Incorporating A Radial Basis Function Neural Network for Non-linear Systems

Ali S Elfllah*, Ali S. Zayed* and Mahmoud Elfandi*

*Department of Electrical & Electronic Engineering, 7Th of April University, Sabrata, Libya.

**Department of Electrical & Electronic Engineering, Alfateh University, Sabrata, Libya.

Corresponding author's E-mail: : m_elfandi@hotmail.com

Abstract

This article presents a new non-linear PID adaptive controller algorithm incorporating a radial bases function (RBF) neural network based generalised learning model (GLM) . The GLM assumes that the unknown non-linear plant is represented by an equivalent model consisting of a linear time-varying sub-model plus a non-linear RBF neural networks sub-model. The parameters of the linear sub-model are identified by a recursive least squares algorithm with a directional forgetting factor, whereas the unknown non-linear sub-model is modelled using the RBF neural network resulting a new non-linear controller with a generalised minimum variance performance index. In addition, the proposed controller has a PID structure and overcomes the shortcomings of other linear designs and provides an adaptive mechanism which ensures that both the closed-loop poles and zeros are positioned at their pre-specified places. It can track set-point changes with the desired speed of response, penalises excessive control action, and can be applied to non-minimum phase systems and unstable systems. Example simulation results using a non-linear plant model demonstrate the effectiveness of the proposed controller.

Keywords: *PID control, zero pole-placement control, self-tuning control, Nonlinear control, Neural networks.*

1. Introduction

Since the inception of self-tuning control (STC) by Astrom and Wittenmark [1] and Clarke and Gawthrop [2], much attention has been devoted to control system based on linear models. These linear self-tuning controllers have been remarkably successful in controlling many non-linear processes by treating them as time-varying linear processes. Despite these successes, linear self-tuning controllers may not perform well for rapid, large changes in the operating point of the plant.

Over the last two decades or so, there has been much progress in modelling and controlling nonlinear systems with neural networks [3,4]. This is due to their proven ability to learn arbitrary non-linear mappings [5] which has been effectively

utilized to represent the controller non-linearity. Other advantages inherent in neural networks such as their robustness, parallel architecture and fault tolerant capability act as further incentives.

In particular, the neural network technique is highly effective for controlling complex non-linear systems when we have no complete model information, or even when considering a controlled plant as a black box [6].

On the other hand, significant work to-date has also been done on the conventional linear, generalised minimum variance controller (GMVC), which was originally developed by Clarke and Gawthrop [2]. It was extended to achieve pole-placement by Allidina and Hughes [7] and modified to have a PID structure by Cameron and Seborg [8] and Yusof *et al.* [9]. More recently, in work by Zayed [3-5], the GMVC has been modified to a robust controller which can be used either as a PID controller or as an adaptive pole-placement controller through the use of a switch.

In industrial sectors, many machines and processes need optimal control (e.g., the steel industry, food industry, chemical industry, textile industry). The difficult problem in the control of these industrial processes is the non-linearity of their models and it cannot be solved by traditional generalised minimum variance control techniques. The application of linear control theory to these plants relies on the key assumption of the small range of operation in order for the linear model to be valid. When the required operation range is large, a linear controller is likely to perform unsatisfactorily. For this reason, it seems appropriate to extend generalised minimum variance control to plants with non-linear models and with plant/model mismatch. This can be done by incorporating the inherent non-linearity of the process into the control design.

However, in spite of developed modern control techniques like fuzzy logic controllers or neural networks controllers, the so called three-term proportional-integral-derivative (PID) controllers are still considered as the dominant controllers in the process control industries. The domination of PID controllers is owing to the simplicity of their structure, robustness and the ease of implementation.[3,4,5, 9,10,11].

For this reason, current trends in the area adaptive control are towards incorporating the flexibility of nonlinear minimum variance control and the simplicity of PID control structures.

In this paper a new nonlinear PID control algorithm is proposed which builds on the works of Zayed *et al*. [3, 10] and Zhu *et. al*. [11, 12]. In the proposed controller an unknown non-linear plant is represented by an equivalent generalised learning model (GLM), consisting of a linear time-varying sub-model plus a non-linear sub-model. Models of this type (GLM) have previously been shown to be particularly useful in an adaptive pole-placement based control framework by Zhu *et al*.[11]. In this work, the non-linear controller is designed to incorporate a new PID zero-pole placement structure, in which the parameters of the linear sub-model are identified by a standard recursive algorithm, whereas the non-linear sub-model is estimated using the Radial Basis Function (RBF) neural network.

The paper is organised as follows: the derivation of the control law is discussed in section 2. In section 3, a simulation case study is carried out in order to demonstrate

the effectiveness of the proposed controller. Finally, some concluding remarks are presented in section 4.

2. Derivation of the new control law

In deriving the control law it is considered that the plant being investigated can be described by:

$$A(z^{-1})y(t) = z^{-k}B(z^{-1})u(t) + f_0(Y,U) \quad (1)$$

Where $y(t)$ and $u(t)$ are respectively the measured output and the control input at the sampling instant t, k is the integer-sample dead time of the process, and $f_0(Y,U)$ is potentially a nonlinear function. Therefore the equivalent model is a combination of a linear time varying submodel plus a non-linear submodel as shown in figure(1). The polynomials $A(z^{-1})$ and $B(z^{-1})$ are respectively of orders n_a and n_b. The polynomial $A(z^{-1})$ is assumed to be monic. In what follows, the z^{-1} notation will be omitted from the various polynomials to simplify the presentation.

The generalised minimum variance controller minimises the following cost function:

$$J = E\{(Py(t+k) + Qu(t) - Rw(t) - Hf_0(.,.))^2\} \quad (2)$$

Where $w(t)$ is the set point and $P(z^{-1})$, $Q(z^{-1})$, $R(z^{-1})$ and $H(z^{-1})$ are user-defined transfer functions in the backward shift operator z^{-1}. $E\{.\}$ is the expectation operator.

The control law which minimises J is:

$$u(t) = \frac{[Rw(t) - (\frac{F'}{P_d})y(t) + (H - E')f_0(.,.)]}{(EB + Q)} \quad (3)$$

where E' is of order $(k-1)$, and the order of F' is $(n_a + n_{p_d} - 1)$ where $(P = \frac{P_n}{P_d})$ and n_{p_d} is the order of P_d.

The polynomials E' and F' are obtained by solving the least square identity

$$CP_n = AP_dE' + z^{-k}F' \quad (4)$$

equation (3) can also be expressed as:

$$u(t) = \frac{[R'w(t) - F'y(t) + H'f_0(.,.)]}{q} \quad (5)$$

$$\left.\begin{array}{l} R' = P_dR \\ \text{where } q = P_dE'B + QP_d \\ H' = P_d(H - E') \end{array}\right\} \quad (6)$$

R', q and H' are still user defined transfer functions since they depend on the transfer functions R, Q and H, respectively.

We further assume that q can also be expressed as [4,5]: $q = \Delta[\frac{q_n}{q_d}]$ (7)

(2)

We can see clearly from equations (4) and (7) that the controller denominator has now conveniently been split into two parts:

1) An integrator action part (Δ) required for PID design.

2) An arbitrary compensator ($\frac{q_n}{q_d}$) that may be used for pole-placement and pole-zero zero placement design.

2.1 Pole zero-placement design

If we substitute for $u(t)$ given by equation (5) into the process model given by equation (1) and make use of equations (6) and (7), we obtain

$$(q_n \Delta A + z^{-k} q_d B F^{'}) y(t) = z^{-k} q_d B R^{'} w(t) + (z^{-k} H^{'} B q_d + \Delta q_n) f_0(.,.) \quad (8)$$

It is obvious from equation (8) that at steady state the output $y(t)$ equals the constant reference command $w(t)$ when:

$$R^{'} = F^{'}\Big|_{z=1} \quad \text{and} \quad H^{'} = \Delta = (1 - z^{-1}) \quad (9)$$

If we assume $\overline{B} = q_d B$ and $\overline{A} = \Delta A$, then equation (8) becomes:

$$(q_n \overline{A} + z^{-k} F^{'} \overline{B}) y(t) = z^{-k} q_d B R^{'} w(t) + \Delta(z^{-k} B q_d + q_n) f_0(.,.) \quad (10)$$

We can now introduce the identity:

$$(q_n \overline{A} + z^{-k} F^{'} \overline{B}) = T \quad (11)$$

where T and q_d are respectively the desired closed loop poles and zeros, and q_n is the controller polynomial. For equation (11) to have a unique solution, the order of the regulator polynomials and the number of the desired closed loop poles have to be [3, 4, 5]:

$$\left.\begin{aligned} n_f &= n_{\bar{a}} - 1 \\ n_{q_n} &= n_{\bar{b}} + k - 1 \\ n_T &\le n_{\bar{a}} + n_{\bar{b}} + k - 1 \end{aligned}\right\} \quad (12)$$

Where $n_{\bar{a}}$, $n_{\bar{b}}$, n_{q_d} and n_{q_n} are the orders of the polynomials $\overline{A}$, $\overline{B}$, q_d and q_n, respectively, n_T and k denote the number of desired closed loop poles and the time delay. Also, $n_{\bar{b}} = n_{q_d} + n_b$ and $n_{\bar{a}} = n_a + 1$. By using equation (10) and (11) we obtain:

$$y(t) = \frac{z^{-k} q_d B R^{'}}{T} w(t) + \frac{\Delta(q_n + z^{-k} B q_d)}{T} f_0(.,.) \quad (13)$$

As can be seen from equation (13) above, clearly, the closed loop poles and zeros are in their desired locations. We can also see clearly from equations (3), (10) and (6) that the transfer functions P_n, P_d, Q, R and H change at every sampling instant in order to satisfy the condition in equation (11). However, it is not necessary to explicitly calculate these user-defined polynomials [3,4,5].

The pole-zero placement can also be achieved by assuming that:

$$q = \Delta q_n \quad \text{and} \quad R^{'} = q_d R_0^{'} = q_d F^{'}(1)[q_d(1)]^{-1} \quad (14)$$

where q_d is the desired closed loop zeros.

By using (5), (6) and (14) the closed loop system becomes:

$$(q_n \overline{A} + z^{-k} F^{'} B) y(t) = z^{-k} B q_d R_0^{'} w(t) + \Delta(z^{-k} B + q_n) f_0(.,.) \quad (15)$$

Now we can introduce the identity:

$$(q_n \overline{A} + z^{-k} F^{'} B) = T \quad (16)$$

It is obvious that the order of the polynomial q_n becomes:

$$n_{q_n} = n_b + k - 1 \quad (17)$$

It is clear from equation (15) and (16) that both closed loop poles and zeros are now at their desired positions.

As can be seen in figure (1), a recursive least squares algorithm is initially used to estimate the parameters *A* and *B* (equation (1)) of the linear sub-model. Then a Radial Basis Function (RBF) neural network is used to approximate the non-linear part $\hat{f}_0$. The actual non-linear function is detected as follows:

$$\hat{f}_0(.,.) = y(t) - \hat{y}(t) = y(t) - \varphi^T(t)\hat{\theta}(t) \quad (18)$$

where θ is the parameter vector, $\varphi \in \Re^m$ is the data factor and $\hat{y}(t)$ is the output of the RLS estimator.

$$\hat{f}_0 = \sum_{j=1}^{n} w_j g_j + b \quad (19)$$

$$\delta_w = \eta g_j \hat{f}_0[1 - \hat{f}_0]\varepsilon[\tilde{x} - \hat{f}_0] \quad (20)$$

$$\varepsilon[= \tilde{x} - \hat{f}_0] \quad (21)$$

$$w_j(t) = w_j(t-1) + \delta_w \quad (22)$$

$$g_j = \exp(-\sum_{i=1}^{l} \frac{\|x_i\|}{(2\sigma_j)^2}) \quad (23)$$

$$\tilde{x} = y - \hat{y} \quad (24)$$

where w_j is the hidden, δ_w is the change in weights, η is the learning rate, x_i is the inputs, c_j is the mean, $l = n_a + n_b$, g_j is the input of hidden layer and $\hat{f}_0$ is the output of RBF neural networks.

2.2 Nonlinear PID control Design

As a result of the robustness, simplicity of their structures, ease of implementation and remarkable effectiveness in regulating a wide range of processes, it is highly desirable to use PID control as a means of introducing the procedures employed in pole-zero placement derived above.

The most commonly used PID controller is the velocity form [4,5,8,9,10] which can be expressed as:

$$\Delta u(t) = K_I w(t) - [K_P + K_I + K_D]y(t) - 2) - [-K_P - 2K_D]y(t-1) - K_D y(t-2) \quad (25)$$

For more details about the derivation of the above equation (25), see [5].

If we assume that the degree of $F(z^{-1})$ is equal to 2

$$F'(z^{-1}) = f_0' + f_1' z^{-1} + f_2' z^{-2} \quad (26)$$

and switch off the pole-placement and zero placement polynomials q_n and q_d respectively, we then can easily show that [9, 12]:

$$K_P = -(f_1' + 2f_2') \quad (27a)$$

$$K_I = f_0' + f_1' + f_2' \quad (27b)$$

$$K_D = f_2' \quad (27c)$$

It can be seen from (24) that if the order of $F(z^{-1})$ is one then a PI controller is achieved. In the situation where $F(z^{-1})$ is of order two then a PID controller is obtained. A PID controller plus additional control action is then achieved if its order is more than two [5].

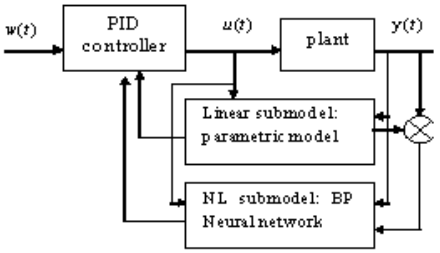

Figure (1): control system structure

2.3 Non-linear Controller Algorithm summary:

The proposed non-linear pole-zero placement based control algorithm can be summarised as:

step 1. Select the desired closed-loop system poles and zeros polynomials T and q_d .

step 2. Read the new values of $y(t)$ and $w(t)$.

step 3. Estimate the process parameters $\hat{A}$ and $\hat{B}$ using least squares algorithm.

Step 4. Compute $\hat{F}'$ and $\hat{q}_n$ using (11) or (16).

Step 5. compute the PID parameters using (27a), (27b) and (27c).

Step 5. Compute R' using (9) or (14).

Step 6. Compute $f_0(.,.) = y(t) - \hat{y}(t)$, where $\hat{y}(t)$ is the output of the linear sub-model.

Step7. Apply the RBF network to obtain $\hat{f}_0(.,.)$ by using equations (18-24).

Step 8. Compute the control input using (5).

Steps 1 to 7 are to be repeated for every sampling instant.

3. Simulation Results

The objective of this section is to study the performance and the robustness of the closed loop system using the technique proposed in section 2.1. A simulation case study is carried out in order to demonstrate the ability of the proposed algorithm to locate the closed-loop poles and zeros at their desired locations under set point changes. The simulation example was performed over 600 samples with the set point changing every 100 sampling instants. Consider the following non-minimum phase and unstable process treated previously by Zhu *et al.*[11,12]:

$$y(t) = \frac{1.5\sin[y(t-1)]y(t-1)}{1+y(t-1)^2+y(t-2)^2} + 1.1y(t-1) - 1.2u(t-1) + 2u(t-2) \quad (28)$$

The set point changes from 5 to 10. The desired closed loop poles polynomial and zeros were selected as follows: $T = 1 - 0.65z^{-1}$ and $q_d = 1 + 0.7z^{-1}$.

A RBF neural network is used to approximate the model error $f_0(.,.)$, which has three layers, the hidden layer with 6 neurons and the output layer with one neuron. The forgetting factor was selected as: $\lambda = 0.98$. All the initial condition weights are selected to be small. Comparative evaluation with well-established nonlinear PID pole placement controller proposed by Zhu and Warwick [11].

In order to see clearly the effect of the zeros in the performance of the closed loop system, the controller is arranged to work as either a PID pole-placement (PIDPP) proposed in [11] or as PID zero pole placement (PIDZPP) proposed in this paper , as follows:

a) From (0^{th} up to 250^{th} sampling time) only the pole placement controller is on-line.

b) The pole-zero placement controller is switched on from (251^{th} to 600^{th} sampling time).

The output and the control input are shown in the figures (2a) and (2b).

It is clear from the figures (2a) and (2b) that, the transient response is shaped by the choice of the polynomial T and ensures steady state error to zero. It is also obvious that excessive control action which resulted from set-point changes, is tuned after using zero-pole placement from the sampling interval 251, onwards.

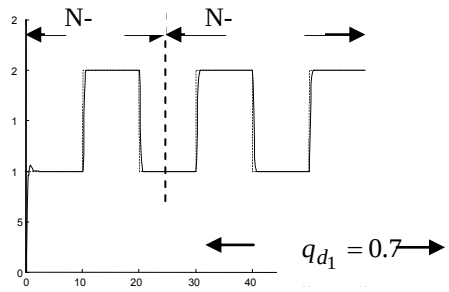

Figure (2a): the output using suitable

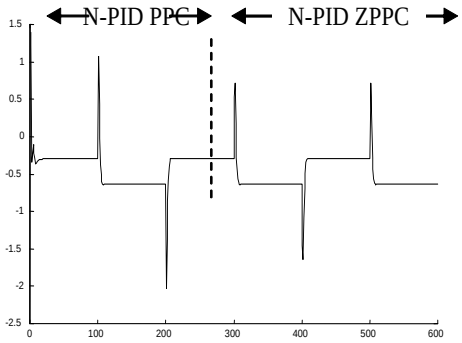

Figure (2b): the control input using suitable q_d

In order to see the effect of the zeros on the closed loop performance, the desired closed-loop poles polynomial is fixed as before and only the closed loop zeros is changed as follows: $q_d = 1 - 0.68z^{-1}$. The output and control input are shown in figures (3a) and (3b). Figure (4) shows the estimates of the non-linearity $f_0(.,.)$.

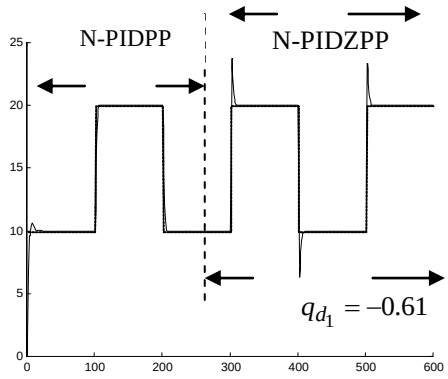

Figure(3a): the output using unsuitable q_d

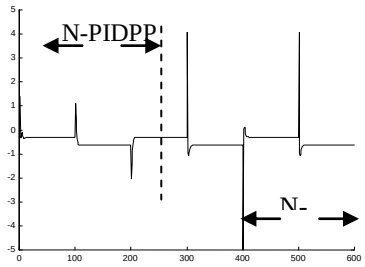

Figure(3b): the control input using unsuitable q_d

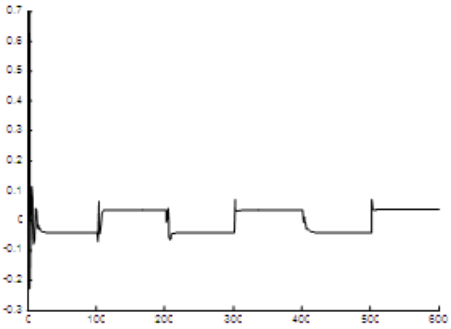

Figure(4): the estimates of the nonlinearity $f_0(.,.)$

It is clear from figures (3a) and (3b) that changing the polynomial q_d significantly affects the closed loop performance.
Excessive control input results if an unsuitable q_d is selected.

Therefore, the closed loop performance is determined by selecting the user-defined polynomials $T(z^{-1})$ and $q_d(z^{-1})$. The transient response is shaped by the choice of the desired closed loop poles polynomial T, while the desired closed zeros polynomial q_d can be used to reduce the magnitude of control action or to achieve better set point tracking [15,16,17].

4. Conclusions

In this article, a new non-linear algorithm is developed which combines the benefits of both the PID and pole-zero placement along with GLM framework. In the GLM the unknown non-linear plant is assumed to represented by an equivalent model composed of a simple linear sub-model plus a non-linear sub-model. The parameters of the linear sub-model are identified by a standard recursive least squares with a directional forgetting factor algorithm, whereas the non-linear sub-model is approximated using radial bases function RBF neural network. The resulting adaptive controller provides an adaptive mechanism, which ensures that *both* the closed loop poles and zeros are placed at their pre-specified positions. The non-linear PID control design was successfully tested on simulated non-linear model. The results presented here indicate that the controller tracks set point changes with the desired speed of response, penalises the excessive control action, and can deal with non-minimum phase systems. The transient response is shaped by the choice of the pole polynomial $T(z^{-1})$, while the zero polynomial $q_d(z^{-1})$ can be used to reduce the magnitude of control action or to achieve better set point tracking [9,13,14,15].
In addition, the controller has the ability to ensure zero steady state error.

Acknowledgment

The authors are indebted to Dr Amir Hussain, University of stirling, Scotland, (Uk) and Professor Mike Grimble of the

Industrial Control Centre, University of Strathclyde, Glasgow, UK for highly stimulating discussions and their insightful comments and suggestion.

References

[1] K. J. Astrom and B. Wittenmark. "On self-tuning regulators," *Automatica* , 9**,** pp. 185-199,1973.

[2] D. W. Clarke and P. J. Gawthrop. "Self-tuning control," *Proc. Inst. Electr. Engineering,* Part D, vol. 126, pp. 633-640, 1979

[3] A. Hussain, A. S. Zayed and L. S. Smith, "A New Neural Network and pole placement Based Adaptive composite selftuning controller modified minimum-variance stochastic self-tuning controller with pole-zero placement," Proceeding 5th IEEE International Multi-topic Conference (INMIC,2001), Lahore, 28-30 December, 2001,267-271.

[4] A. S. Zayed, A. Hussain and R. Abdullah, "A novel multiple-controller incorporating a radial basis function neural based generalized learning model," *Nerocomputing*, vol. 69, pp. 2006.

[5] A. S. Zayed, "Novel linear and non-linear minimum variance techniques for adaptive control engineering," *PhD Thesis*, Stirling University, Stirling, U.K., 2005.

[6] W. Yu and A. Poznyak, "Indirect adaptive control via parallel dynamic neural networks" *IEE Proc. Contol theory Appl.*, vol. 146, pp.25-30, 1999.

[7] A. Y. Allidina and F. M. Hughes, "Generalised self-tuning controller with pole assignment," *Proc. Inst. Electr. Engineering, Part D*, vol. 127, pp. 13-18, 1980.

[8] F. Cameron and D. E. Seborg, "A self-tuning controller with a PID structure" *Int. J. Control*, vol. 38, pp. 401-417, 1983.

[9] R. Yusof, S. Omatu, "A multivariable self-tuning PID controller," *Int. J. Control.* 57, pp. 1387-1403, 1993.

[10] A. S. Zayed "MinimumVariance Based Adaptive PID Control Design," *M.Phil Thesis*, Industrial Control Centre, University of Strathclyde, Glasgow, U.K., 1997.

[11] Q. Zhu, Z. Ma and K. Warwick, "A Neural network enhanced generalised minimum variance self-tuning proportional, integral and derivative control algorithm for complex dynamic systems," *Proc instn Mech Engs*, vol. 216, pp. 265-273, 2002.

[12] Q. Zhu, Z. Ma and K. Warwick, "Neural network enhanced generalised minimum variance self-tuning controller for nonlinear discrete-time systems," *IEE Proc. Contol theory Appl.*, vol. 146, pp. 319-326, 1999.

[13] P. E. Wellstead, J. M. Edmunds, D. Prager and P. Zanker, Self-tuning pole/zero assignment regulators," *Int. J. Control*, vol. 30, pp. 1-26, 1979.

[14] A. S. Zayed, A. Hussain and L. S. Smith, "A modified minimum-variance stochastic self-tuning controller with pole-zero placement,"Proceeding 5th IEEE International Multi-topic Conference (INMIC,2001), Lahore, 28-30 December, 2001, 252-256.

[15]A. Zayed, A. Hussain and L. Smith, "A New Multivariable Generalised Minimum-variance Stochastic Self-tuning with Pole-zero Placement," International Journal of Control and Intelligent Systems, 32 (1), 35-44, 2004.

[16] H. R. Sirisena and F. C. Teng, "Multivariable pole-zero placement self-tuning controller," *Int. J. Systems Sci*., vol. 17, No.2 pp. 345-352, 1986.

[17] S. Puthenpura and J. MacGregor, "Pole-zero placement controllers and self-tuning regulator with better set-point

tracking," *Proc. Inst. Electr. Engineering*, Part D, vol. 134, pp. 26-30, 1987.

Neural Structure and Fuzzy Thinks for Non-linear Systems Control

Ali A. Abdulaziz, Assoc. Prof., EEE, Sirte University
P.O.Box 609 Sirte, Email: aliazizbakkar1957@yahoo.com

Key Words:- ANNIMC (Artificial Neural Network Internal Model Control), IMC (Internal Model Control), GPC (Generalized Predictive Control), ARMAX(Autoregressive Moving Average with eXogenous), ANNARMAX (Artificial Neural Network Autoregressive Moving Average with eXogenous), NRNGPC (Newton Raphson Nonlinear Generalized Predictive Control)

Abstract:-

The limitations or eventually the impossible use of conventional control techniques over modern life needs increase, gives a continuous, and speedup encourages for research centers to look for a reliable non-conventional control system design that can cope with most of limitations of available conventional control techniques. In the last few years, the idea of using model-based self-tuning predictive control, neural-based control, and fuzzy-based control, which are all a non-conventional techniques, becomes a promise and give encourages for research centers to give more effort and importance to such research studies.

The work in this approach has been presentenced in my Thesis work which has been done at the Newcastle Open Tyne University [1]. The Thesis presents an approach to the development of neural-based control which is suitable for solving non-linear control problems. In this sense, the inefficiencies of using fixed learning parameters search techniques within back-propagation learning algorithm are analyzed and it demonstrated with the aid of a number of test problems to justify the investigation of more robust and powerful new recursive self-tuning back-propagation algorithm using on-line tuning strategies.

The paper elaborate the idea of using neural-based fuzzy control strategies and aims to obtain a frame of work by which the conventional model-based predictive control technique which is directly incorporates plant models (i.e. forward and inverse) in a conventional internal model control structure IMC [8] to provide a non-conventional non-linear IMC structure. The procedure involves training a back propagation feed-forward neural network to represent a plant inverse, then the learnt plant inverse net is used with its inverse model as a direct inverse controller in a model-based predictive control strategy to form a neural-based IMC (ANNIMC) control system. Because, the closed loop performance characteristic of any conventional IMC structure (such as settling time) is related directly to controller parameters; this gives the possibility for on-line tuning using fuzzy logic strategy for both plant model and inverse. Finally, the proposed control structure is compared in simulation level with a conventional non-linear GPC [11] to confirm robustness. The obtained results were very attractive.

1.0: Introduction

IMC technique [8] has been developed to provide an alternative to the classical feedback control structure with an advantage that the closed loop stability of a control system is assumed simply by choosing a stable IMC controller. Also, the closed loop performance characteristics (such as settling time) is related directly to the controller parameters which makes on-line tuning of the IMC controller very convenient, [2, 3]. Consider the familiar feedback control arrangement shown in figure-1. The P(z) and C(z) blocks represents the discrete form for the plant and controller transfer functions, respectively, where, w(z) and ζ(z) are the set-point and disturbance added to the closed loop system, respectively.

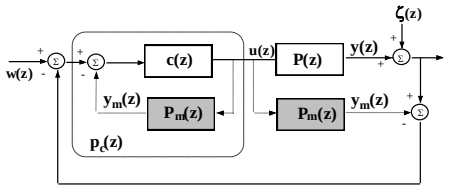

Figure-1:- Discrete-time feedback control structure.

For an entirely equivalent step, if we modify the feedback control structure given in Figure-1 by a one given in Figure-2, the obtained control structure is a conventional internal model control (IMC) structure. The shaded area represents the IMC control algorithm loop to be designed by software or hardware.

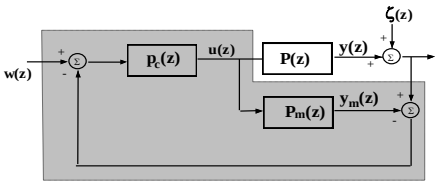

Figure -2:- Conventional IMC structure.

Therefore, any conventional feedback control system can be restructured to the IMC control structure. Furthermore, any IMC can be put back into a conventional feedback control format by defining:

$$c(z) = \frac{P_c(z)}{1 - P_c(z)\,P_m(z)} \qquad (1)$$

The advantage over conventional structure is that the IMC controller $P_C(z)$, is much easier to design than the classical feedback c(z) [8]. Also, in the IMC structure, the robustness can be design in a very explicit manner this is partly due to the feedback signal e(z) which is:

$$e(z) = (1 + (P(z) - P_m(z))\,P_c(z))^{-1}\,\varsigma(z) \quad (2)$$

Therefore, when a perfect model exists the feedback signal e(z) is equal to just the disturbance ζ. This demonstrates that the IMC system is an open loop control strategy in a deterministic environment (i.e., no model uncertainty and/or unknown input noise), and the feedback signal is only needed because of the uncertainty problem [3]. Also, the closed loop performance characteristics (such as settling time) is related directly to the controller parameters which makes on-line tuning of the IMC structure is very convenient.

In this paper, we consider that: The control signal u(z), and the corresponding plant output y(z), may be represented respectively as:

(3)

$$u(z) = \frac{P_c(z)}{1 + P_c(z)(P(z) - P_m(z))}(w(z) - e(z))$$

$$y(z) = \varsigma(z) + \frac{P(z)\,p_c(z)}{1 + P_c(z)(P(z) - P_m(z))}(w(z) - e(z)) \qquad (4)$$

Now, if we assume; $P(z) \cong P_m(z)$, then, P(z) will give a perfect control action if

$$P_c(z) = \frac{1}{P_m(z)} \qquad (5)$$

According to the above properties, if a good plant model is available, the closed loop system will achieve exact set-point tracking despite unmeasured disturbances acting on the plant. In practice, however, a perfect model can never be obtained, also under model uncertainty the infinite gain which may be required for perfect control would lead to sensitivity problems. However, to cope with such problems, a linear filter is usually added to conventional IMC structure to keep the control system robust [4], but it will move away from perfect control action. All such design problem can be eliminated by using non-conventional techniques like neural and fuzzy control structures.

The idea of using neural networks as a non-linear IMC control system was proposed by many authors, like [5]. However, none of them appears to have fulfilled the basis of the conventional IMC design steps given by [8] which based on that, the real plant output must be use to obtain the true inverse representation rather than that of using the plant model output, and that, the plant model be the inversion of the plant inverse.

In this study, we relate our design steps to those given by [8]. The obtained control system is a non-linear form of an IMC structure.

Although, for non-linear systems, general guidelines are not available on how to design a feedback control system with a stable closed loop performance, the IMC is significant because the stability and robustness properties of the structure can be analyzed and manipulated in a transparent manner, even for non-linear systems. Thus the IMC structure provides a general framework for linear and non-linear system control. The ability of using conventional IMC structure for non-linear systems control has been demonstrated by [7], see the non-linear IMC structure given in figure -3.

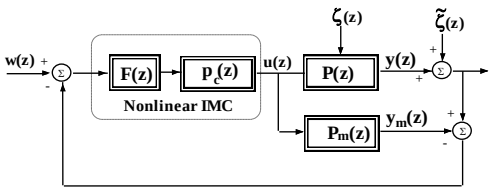

Figure-3:- Non-linear conventional IMC control structure.

A very important difference between linear and non-linear systems may be emphasized in that:- For linear systems, disturbances are usually added at the output, and it can be (ζ =0, $\neq$0) because of the Superposition Principle which states that:- $P(u+\tilde{\zeta}) = Pu + P\tilde{\zeta} = Pu + \bar{\zeta}$, with

$$\bar{\zeta} = P\zeta \qquad (6)$$

Therefore, in the non-linear IMC case, when discussing robustness, not only modeling errors but also the expected disturbances have to be considered.

It is intuitively obvious that a feedback controller with infinite gain is necessary to achieve the performance stipulated by the property of perfect control in the IMC structure. Hence, the control system suggested by (5) will suffer from stability problems. That is, in the non-linear IMC design procedure the control gain should be reduced by employing an IMC filter F(z), in series with the non-linear IMC controller figure-3 [7]. The primary reason for adding a non-linear filter element is to introduce robustness in the overall IMC structure by

appropriately reducing the loop gain. Moreover, when the plant is non-linear, by definition the inverse operator is defined in the range of the operator space; consequently the inverse operator is not defined for inputs outside the range of the operator space. Hence, there is no assertion that the error signal will belong to the operator space. The non-linear filter element has been introduced to filter the external noise and to perform some type of on-line tuning by rapidly changing signals in order to reduce the transient response.

2.0: Neural-based IMC Control (ANNIMC) Design

The characteristics of back propagation feed-forward neural networks (FFNN) are relevant to provide a general framework for non-linear IMC control structure because of the following features [1]:

(i)- It is able to represent arbitrary non-linear relations.

(ii)- It can adapt and learn in both off-line and on-line stages.

(iii)- It can transform information internally by allowing data fusion with both quantitative and qualitative signals.

(iv)- It allows fast processing for large scale dynamic systems because of their parallel distributed processing architecture.

(v)- The internal architecture provides a degree of robustness through fault tolerance and noise filtration.

Such above features are a motivations for using FFNN for learning both the input and output relationship of any non-linear plants governed by the NARMAX model. The direct extension of a classical IMC structure to an artificial neural network IMC (ANNIMC) is addressed in this paper, the obtained structure is as in figure-4. The non-linear operators P, NN_m, and NN_C represent the real plant, plant model, and controller, respectively.

Based on the possibility of using real plant output to obtain the true inverse representation rather than that of using the plant model output as outlined in [1] is governed in this paper work. Moreover, it is imperative that the plant model be the inversion of the plant inverse.

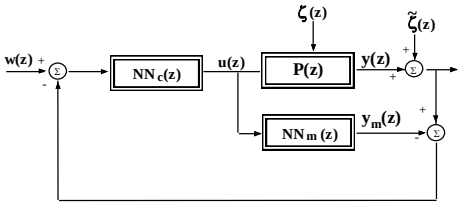

Figure-4:- Simplified structure of an ANNIMC control structure.

However, according to conventional IMC properties, if a good plant model is available, the closed loop system will achieve exact set-point tracking despite unmeasured disturbances acting on the plant. Therefore, the ANNIMC structure provides a direct method for designing a non-linear feedback control system if a neural-based plant model is exist. Note that the non-linear filter block F(z) in figure-3 is considered to be a trivial element, that is because the neural-based controller NN_C is inherently acting as a non-linear filter, [1].

2.1: ANNIMC Design Steps

To achieve a robust ANNIMC control system, the real plant output signal must be used for learning the plant inverse. Then the perfect control signal may be obtained if the controller is a true inverse representation of the plant model. Hence, it is imperative that the plant inverse be learnt from the plant itself. Now, if we denote, P as a plant, M as a plant model, and C as a

controller, then, the following relationship must exist:

$$C = \frac{1}{M} \qquad (7)$$

Corollary: *Using the feed-forward identification approach, the condition in (7) cannot be met because the plant model cannot give the exact output value for implementing the system inverse* [1]. *Hence, in ANNIMC, the Plant model is chosen as the inverse of the controller.*

Equation-11 can be rewritten as:

$$M = \frac{1}{C} \qquad (8)$$

and

$$C = \frac{1}{P} \qquad (9)$$

In other words, it is proposed that the plant inverse in the ANNIMC design structure must be determined directly from the real plant. Hence, using (7) the controller must be known in advance to get the plant model However, in this work, the two design steps that have been described previously in the conventional IMC design [8] are followed for the ANNIMC implementation. The first step involves designing a direct inverse controller for optimal set-point tracking (inverse modeling). Then the second step is to use the direct inverse control structure to train the plant operator model (forward modeling). Finally, the learnt plant models (plant model and its corresponding plant inverse) are incorporated to form the ANNIMC control system

2.2: Plant Inverse Identification

Using (7), if the plant is invertible then the inverse model (controller) of the plant can be obtained to some desired approximation by a neural model, NN_C , network structure. The procedure for system inverse identification is very important step, and is the basic step for control design strategy. The learnt inverse model NN_C is then can be used as a direct inverse controller, figure -5.

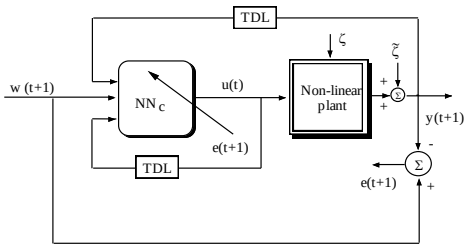

Figure-5:- On-line inverse model identification.

Here, the TDL represents a tapped delay line. It corresponds to all input-output data lags of the non-linear plant. This gives:

$$V_{on}^{c}(t) = [w(t+1), y(t), ..., y(t-n+1), u(t-1), .. \cdots, u(t-m+1)]^{T} \qquad (10)$$

Where-n represents plant order, and m≤n. The controller output therefore may be represented as:

$$u(t) = NN_c[w(t+1), y(t), . ., y(t-n+1), u(t-1), ..., u(t-m+1)] \qquad (11)$$

Conceptually, the direct inverse controller monitors the difference between desired and actual output data of the plant as a cost function to manipulate the control signal by adjusting connection weights of the neural controller structure in order to minimize the error difference that may make the plant output converge towards the desired output. Here, the topology of the neural-based controller structure is of one hidden layer feed-forward net. Number of input, hidden, and output nodes is function of the input data vector given in (10), [9]. Thus, if the number of hidden nodes is denoted by N,

then the controller network output u(t), (11) may be rewritten as:

$$u(t) = \sum_{i=1}^{N_c} x_i \Theta_i \qquad (12)$$

Here, the subscript c indicates those parameters are related to the controller. N is the total number of hidden nodes, and θ_i represent the connection weights between a hidden unit-i and the output. The variable x_i represents the activated output of the hidden nodes. For example for hidden node-i, the activated output may be represented as:

$$x_i = \sum_{j=1}^{n+m} \tanh(x_j^c \theta_j + \beta_j) \qquad (13)$$

Where xj represents the jth input from the input data vector (10). β_j represents the node threshold for the hidden node-j.

However, using (11), the inversion problem can be formulated as a problem of solving an operator equation in which the given operator represented by an inverse model NN_C maps the input data vector

$$[w(t+1), y(t), ...,y(t-n+1), u(t-1),...,u(t-m+1)]^T$$

to u^*. Therefore, the problem is to solve the equation which is represented by:

$$NN_c . u^* = w^* \qquad (14)$$

An iterative method was used to solve (14). In this method, at each time instance t, the objective of the controller is to find an input u^* which will produce plant output y(t+1) equal to the desired output w^*=w(t+1). The recursive form of the control signal therefore, may be represented as:

$$u(t) = u(t-1) + \psi(w(t+1) - y(t+1)) \qquad (15)$$

Where, Ψ is the learnt weight gain to be selected by the updating algorithm using fuzzy strategy on-line. Fuzzy strategy has been based on the internal relation between learning parameters which has been mentioned in my Thesis work [1].

2.3: Plant Model Identification

Previously, we chose to use the plant inverse rather than the plant model inverse as a controller for the reasons described before. The learnt inverse is then used for training the plant model figure -6. Recall that, the TDL represents the tapped delay line for the input and output data lags. It corresponds to all input and output data lags for the non-linear plant [1]. The NN_C and NN_m represent the neural network controller (plant inverse) and the plant model, respectively.

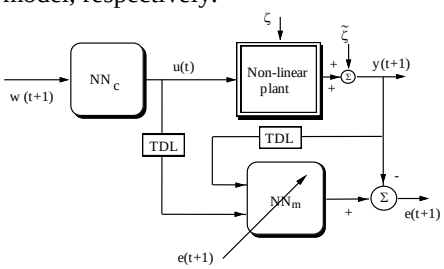

Figure-6:- On-line Plant model identification.

The general form of the input data vector is:-

$$V_m(t) = [y(t), y(t-1), ... , y(t-n+1), u(t), ..., u(t-m+1)]^T \qquad (15)$$

The output of the neural-based model $\hat{y}$ (t+1) may then be represented as:

$$\hat{y}_m(t+1) = NN_m[y(t), ... , y(t-n+1), u(t), ..., u(t-m+1)] \qquad (16)$$

The topology of the neural-based plant model NN_m is of one hidden layer feed-forward net. The number of hidden nodes is denoted by N, and the plant model output

by y_m (t+1), equation -16 may be rewritten as:

$$y_m(t+1) = \sum_{i=1}^{N_m} x_i^m \theta_i^m \qquad (17)$$

Here, m subscript indicates a parameter related to the plant model, and θ_i represent the connection weight between hidden unit-i and the network output. The variable x_i represents the activated output of the hidden nodes. For example for hidden node-i, the activated output may be represented as:

$$x_i = \sum_{j=1}^{n+m} \tanh(x_j^m \theta_j + \beta_j)$$

(18)

The error difference between the actual system output y(t+1) and the model output y_m(t+1) is thus:-

$$\begin{aligned} e_m(t+1) = f[&y(t), y(t-1),... \\ &, y(t-n+1), u(t),... \\ &, u(t-m+1)] - \\ &NN_m[y(t), y(t-1),... \\ &, y(t-n+1), u(t),... \\ &, u(t-m+1)] \end{aligned}$$

(19)

The output of (19) is to be used for optimizing the connection weights of the identification model, NN_m to minimize the specified cost function governed by:

$$\phi_i^m(t+1) = \theta_i^m(t) - \varepsilon\left(\frac{\partial J(\Theta)}{\partial \theta_i}\right)$$

(20)

Where ε represents the learning rate parameter, and $\Theta = [\theta_1, \theta_2, ..., \theta_n]$ is the connection weigh matrix.

2.4: ANNIMC Control Mechanism

The plant inverse network NN_C and the plant model network NN_m are incorporated in the given IMC frame to form the ANNIMC control system structure as it is illustrated in figure -7. The control objective is then to find a control signal (u) which will produce a model output y_m(t+1) equal to the desired output w(t+1) by minimizing the prediction error (e) which is the error difference between plant output and model outputs. That is

$$e(t+1) \triangleq y(t+1) - y_m(t+1)$$

(21)

From the representation given in figure-7, if the exact plants model, NN_m, and the inverse, NN_C, exist, the recursive control signal which may keep the prediction error at each time instance asymptotically minimum is:

$$u(t) = u(t-1) + \Psi(e(t+1))$$

(22)

Therefore, the control signal is automatically evaluated by selecting the optimum control gain, Ψ, of the control performance surface which is represented by the weight matrix of the inverse model.

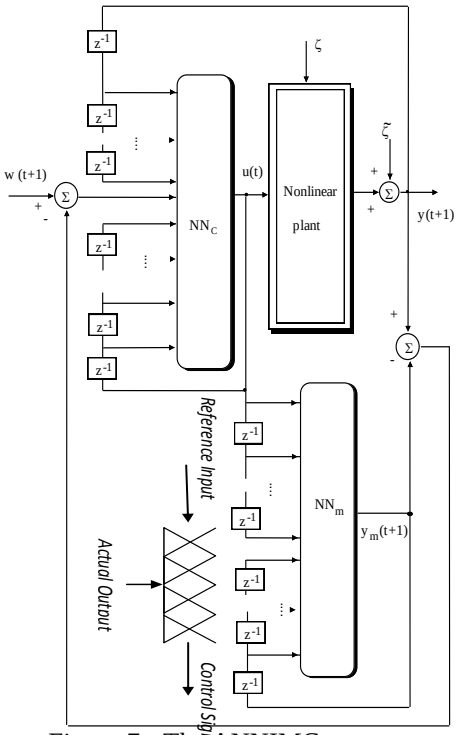

Figure-7:- The ANNIMC structure.

3.0: Simulation Study Results

Two different non-linear plants were used as examples to show the performance of the ANNIMC compared to conventional non-linear control techniques.

Example-1:- A first order non-linear plant governed by the difference equation:

$$y_p(t) = 0.8y_p(t-1) + f[u(t-1)] \qquad (23)$$

Where the unknown non-linear function in the plant is assumed to be:

$$f[u] = (u - 0.8)u(u + 0.5) \qquad (24)$$

The control objective is to control the relationship between the controlled input and the controlled output of the non-linear system so that the controlled output tracks the desired output (set-point changes). The desired output was selected to be a square wave function with a frequency of 50 Hz.

To compare the ANNIMC behavior with other non-linear control strategies, the non-linear generalized predictive controller (NLGPC) algorithm [11] was selected in this case. In NLGPC, the approach taken was to employ a one-step Newton-Raphson method to calculate iteratively the non-linear roots and then to apply the linear GPC [6] for the rest of the control problem. The overall cost function was governed by:

$$J(N_1, N_2) = \sum_{j=N_1}^{N_2}[y(t+j) - w(t+j)]^2 + \sum_{j=1}^{N_u}\lambda(j)[\Delta x(t+j-1]^2 \qquad (25)$$

Here, N_1 and N_2 represent the minimum and the maximum prediction horizons. λ, is a cost applied to the control input, and w the desired output. The signal x(t) is obtained by minimizing (25). The linear control signal is considered to be governed by [12]:

$$x(t) = x(t-1) + g^T(w - h) \qquad (26)$$

Where g is the first row of $(G^TG + \lambda I)^{-1}G^T$. For more details see [14] . Although, the control signal x(t) acts as a solution to the linear predictive control problem, it is an output of a non-linear polynomial operator f(.) where

$$x(t) = f\{u(t)\} \qquad (27)$$

Where, u(t) is the required control signal for the linear part of the system. Hence, the problem is to solve equation -27. The solution was obtained by using the Newton-Raphson recursive method so that :

$$u_{n+1}(t) = u_n(t) - \frac{f\{u_n(t) - x(t)\}}{f'\{u_n(t)\}} \qquad (28)$$

The subscript-n denotes the order of iteration. The first 800 samples of the set-point, system output, and the controlled input signal of the NLGPC simulation for example-1 are shown in figure -8.

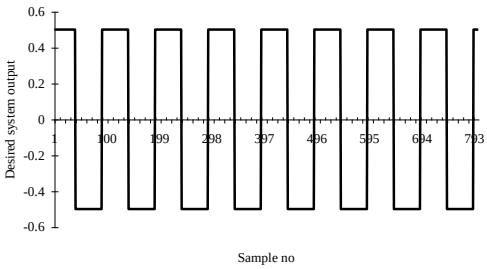

(a): The desired output.

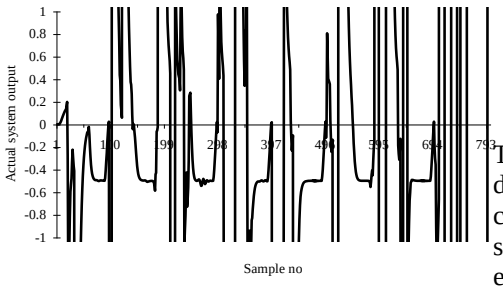

(b): The actual system output.

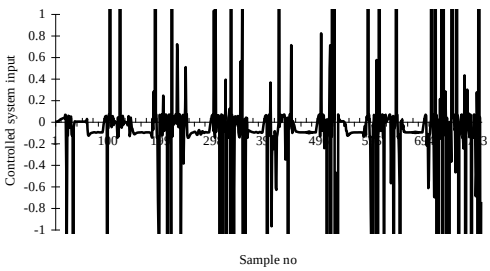

(c): The controlled input signal.

Figure-8: Example-1: The non-linear GPC responses.

It can be reported that the control strategy using the Newton-Raphson method [11] was not successful in such class of non-linear systems.

The ANNIMC was then implemented after the plant model NN_m(4-12-1) and the plant inverse NN_c(4-12-1) nets were learned. The number of hidden nodes was calculated according to the topology discussed [9]. In this case, the hidden nodes required were 12 for each of the plant model and its inverse. The following are the ANNIMC settings used:-

1- The learning rate parameter, ε, was set initially to 0.009.
2- The initial weights were set initially to 0.3.
3- The momentum learning factor was set to 0.5.
4- The maximum jump factor for the steepest descent was set to 1.5.
5- The learning rate jump factor was set to 0.03.

The first 500 samples of simulations for the desired output, actual output, and the controlled input signal of the ANNIMC are shown respectively in figure-9. It can easily be seen that the ANNIMC strategy has effectively tackled the problem of non-linearity for such non-linear systems.

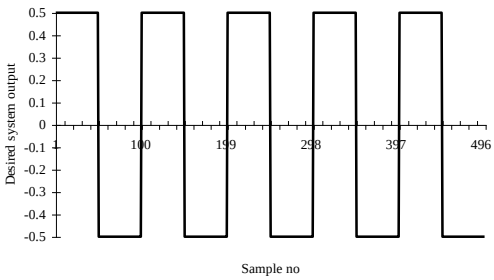

(a): The desired output.

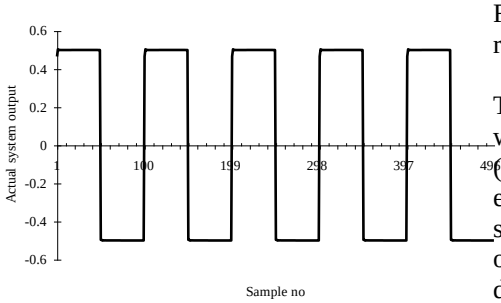

(b): The actual output.

Figure-9: Example-1: The ANNIMC responses.

The robustness of the ANNIMC structure was observed by adding a sinusoidal signal (0.05 sin (20t)) to the plant output of example-1. Figure -10 shows the first 500 samples of the desired output, the actual output, and the control signal when a disturbance is added between 100-300 samples. It can be clearly seen that the ANNIMC performed well.

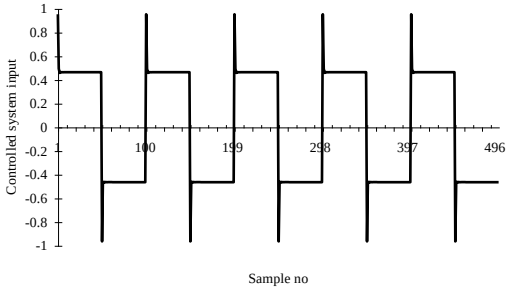

(c): The controlled input signal.

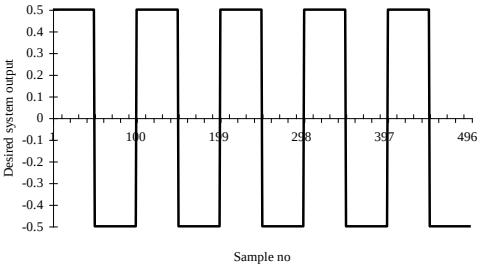

(a): The desired output.

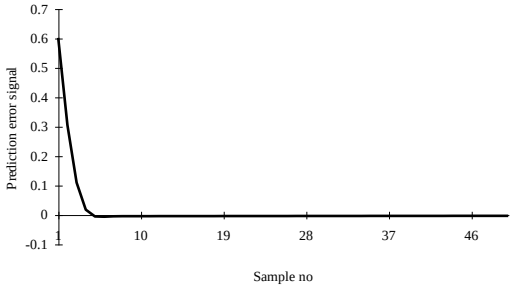

(d): The prediction error.

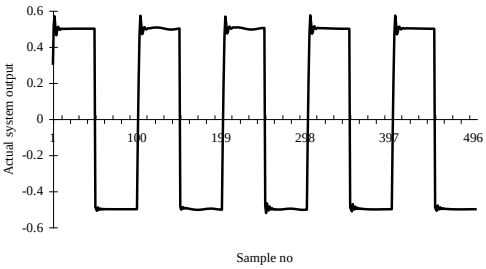

(b): The actual system output.

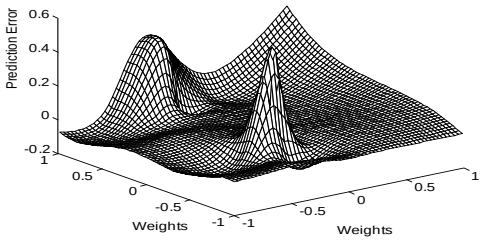

(e): The control performing surface.

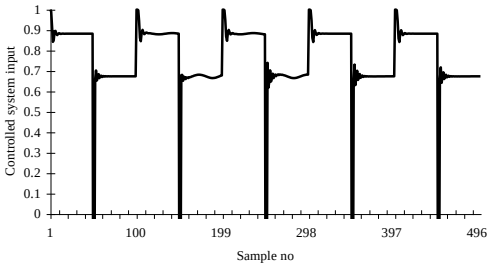

(c): The controlled input signal.

Figure-10: Example-1, The ANNIMC, with external noise (0.05 sin (20t)).

Example-2: A second order non-linear system governed by the following difference equation:

$$y_p(t) = \frac{y_p(t)}{1 + y_p(t)^2} + f[u(t)] \qquad (29)$$

Here, the unknown non-linear function in the plant is assumed to be

$$f[u(t)] = u^3 \qquad (30)$$

The same control objective given in example-1 was also considered for this example. The desired output was selected to be a square wave function with a frequency of 50 Hz. The results using NLGPC for the first 800 samples of iteration are shown in figure -11.

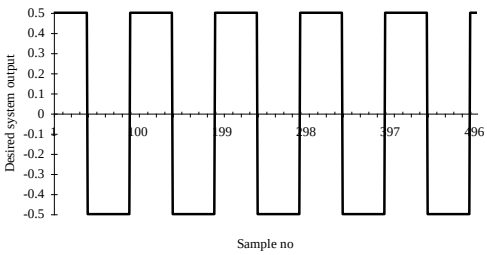

(a):The desired output.

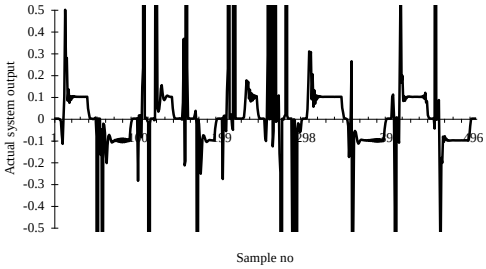

(b): The actual system output.

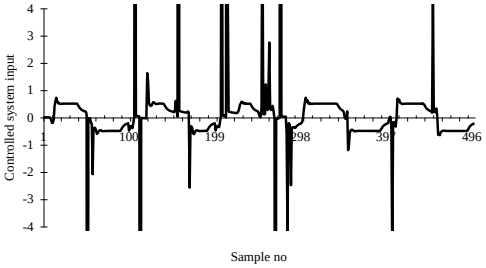

(c): The controlled input signal.

Figure-11: Example-2: The NLGPC responses.

In this non-linear system, example-2, the behavior of the NLGPC was also not satisfactory; this is due to the system non-linearity. The results obtained with the ANNIMC with the same system are shown in figure-12.

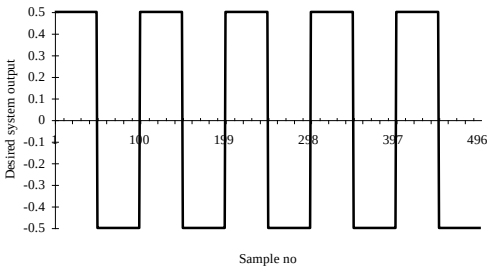

(a): The desired output.

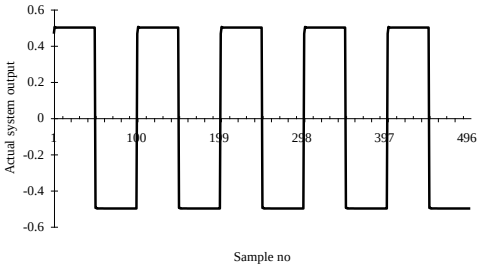

(b): The actual system output.

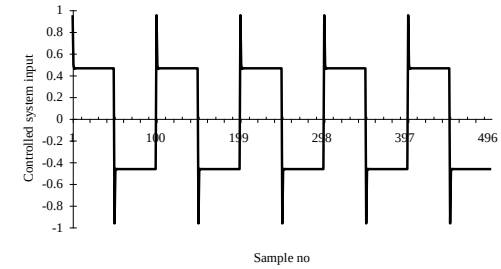

(c): The controlled input signal.

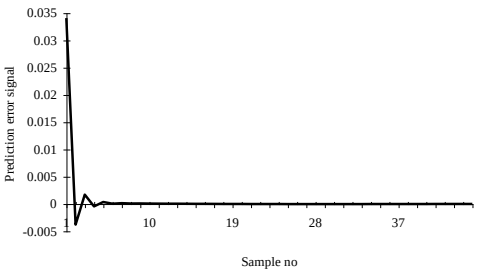

(d): The prediction error.

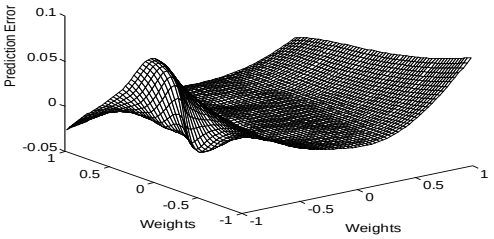

(e)

Figure -12: Example-2: The ANNIMC responses.

Now, in order to show how can fuzzy control helps for on-line tuning of system models it is important to control the effect of parameterization (parameters tuning). Here, two parameters are very important for tuning; the learning rate-ε, and the excessive use of neurons in hidden layers. The simulation results of the effects of the two above mentioned parameters for both system examples are shown (example-1) in figures 13, 14.

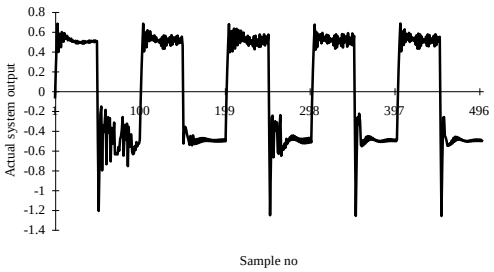

(a): The actual system output.

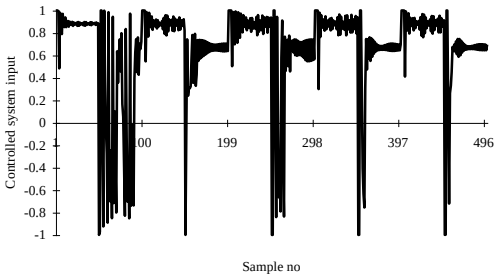

(b): The controlled input signal.

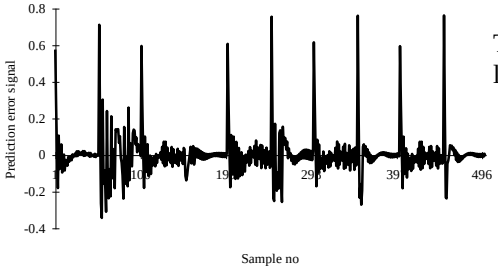

(c): The prediction error.

Figure-13: Example-1: With ε=0.052.

.

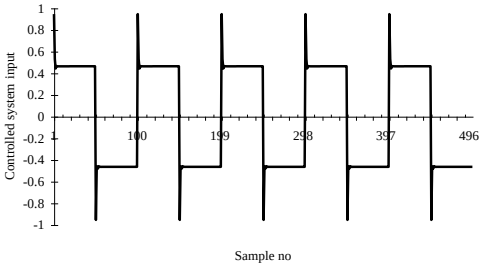

(a): The controlled input signal.

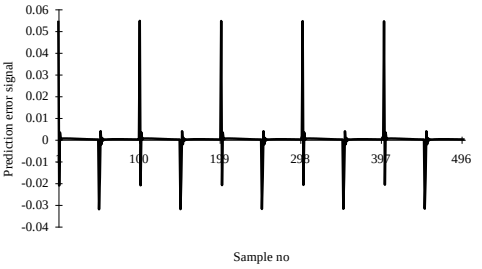

(b): The prediction error.

Figure -14: Example-2: With e=0.002.

The excessive use of neurons in hidden layers is shown in figure-15.

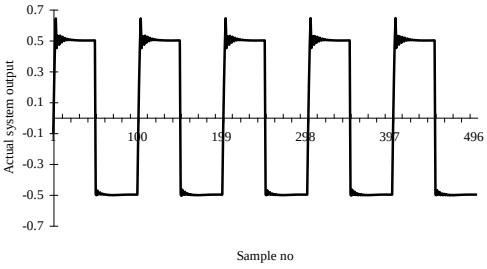

(c): The actual system output.

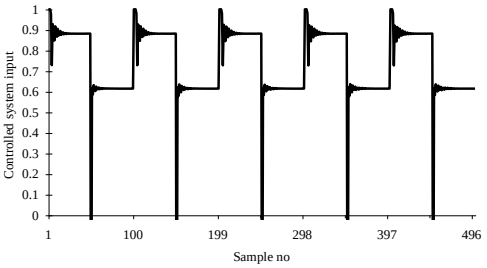

(d): The controlled input signal.

Figure-15: The effects of over-parameterization with example-1.

4.0: Conclusion

The idea of using artificial neural networks with fuzzy thinks is presented in this paper [10]. The idea is mainly based on how model-based predictive control strategy which directly incorporates plant models (i.e. forward and inverse) in a control structure can be provided by conventional IMC. The technique has been developed to provide an alternative to the classical feedback control structure with an advantage that the closed loop stability of the control is assumed simply by choosing a stable IMC controller. The design steps were based on the possibility of using real plant output to obtain the true inverse representation rather than that of using the plant model output. Finally, the two obtained nets (plant and inverse models) are incorporated in linear IMC structure to form a non-linear IMC (ANNIMC). The performance of the proposed non-linear control system has been compared with other well known non-linear controllers; Newton-Raphson non-linear GPC [11].
Finally, the on-line tuning using fuzzy techniques has been liked to assess the merits of the ANNIMC strategy, additional analysis was made to the overall performance and robustness of the control system. In this analysis, the effects of external noises and the effects of the excessive use of hidden nodes, and learning rate were discussed.

5.0: References

[1]:-Abdulaziz. A. A, "Neural-based controller development for solving nonlinear control problems", PhD thesis, Newcastle Upon Tyne University, U.K, 1994.

[2]:-Boquette. B. W. "Non-linear Control of Chemical Processes: A Review", Ind. Eng. Chem. Res. Vol. 30, No. 7, pp. 1391-1413.

[3]:-Morari, M. and Zafiiou, E., "Robust Process Control", Prentice-Hall, Inc., 1994.

[4]:-Brosilow, C. B. "The Structure and Design of Smith Predictors from the Viewpoint of Inferential Control", Joint Auto. Control Conference Proceedings, Denver, Colorado, USA.

[5]:-Bahat, N. and T. J. McAvoy, "Use of Neural Networks for Dynamic modeling and Control of Chemical Process Systems", Compt. Chem. Eng. Vol. 14, pp.573-583, 1990.

[6]:-Clarke, D. W. and P. J. Gathrop, . "Selft-uning Controller",Proc. IEE, Vol.122, No. 9, pp, 929-934, 1975.

[7]:-Economou, and M. Morari, . "Internal Model Control: Extention to non-linear systems", Ind. Eng. Chem. Process Des. 25, pp, 403-411, 1986.

[8]:-Garcia C. E., and M. Morari, . "Internal Model Control: A Unifying Review and Some New Results", Ind. Eng. Chem. Process Des. 25, Vol. 21, pp, 308-323, 1982.

[9]:-Abdulaziz. A, "New Approach to selftuning Back Propagation algorith", المجلة العلمية جامعة التحدي، سرت, 2003.

[10]:-Abdulaziz. A, " التحكم بالنظم اللاخطية باستعمال المنطق غير المحدود و الشبكات الذهنية", المجلة العلمية جامعة التحدي، سرت, 2007.

[11]:-Zhu, Q., K. Warick, and Douce J "Adaptive Generalized Predective Controller for Non-linear Systems", IEE, Proc. D. Vol. 138, No. pp, 33-4-, 191.

[12]:-Ästrom, K.J., (1970), "Introduction to Stochastic Control Theory", Academic Press, London..

Paper NO. 102551

Self-Correct Intelligent Control Based On Fuzzy-Neural Networks

Abduelbaset Goweder
Computer Engineering Dept.
Surman Institute for Comprehensive Professions Surman, Libya
agoweder@yahoo.com

Ali Mustafa Ali Madi
Electrical Engineering Dept.
Surman Institute for Comprehensive Professions Surman, Libya
madi112003@yahoo.com

Jamal . A. Almashal
Electrical Engineering Dept.
Surman Institute for Comprehensive Professions Surman, Libya
jamal_Almashal@yahoo.co.uk

Abstract:

Abstract: In order to achieve high performance for a DC drive system, this paper presents a self-correct intelligent method. A three-layer neural network is used to achieve fuzzy control tactics through a back propagation algorithm out-line learning. An on-line method is used to regulate the parameters of measured and proportional factors of the proposed system. The performance of the proposed system is measured using different operating stages. The simulation is carried out using Semolina Dlatform based on Matlab6.0 and combined with neural network toolbox. The simulation results have shown that the self-correct intelligent control method can increase dynamic and static performance of the system. It also motivates the use of Semolina in the area of self-correct intelligent control drives.

Keywords *self-correct, neural networks and DC drive*

Note:

This paper is included in the conference program but not published because the revised copy after introducing the reviewed comments did not arrive in the specified Time

FUZZY BASED GENETIC ALGORITHM FOR FLIGHT LINEAR AND NONLINEAR STABILIZATION

ALI MOHAMED s.ELMELHI
(Electrical Department. Alfateh University
Tripoli Libya
e-mail ali_elmulhi@yahoo.com

Abstract

The fuzzy logic strategy is a part of intelligent control theory and is applied to many industrial systems. Recently, this design methodology has been applied successfully to synthesize robust controllers for various aerospace applications. In this paper, we want to prove that the fuzzy pd controller can deal with the perturbations caused due to the effect of structured and un-structured uncertainties. In addition, this design method can also deal with the kinematics coupling and keep the nominal performance without significant degradation. Genetic algorithm is presented here in order to improve the system nominal performance where the settling time and steady state error are reduced. The linear and nonlinear simulation results for the launch vehicle's attitude control motion showed the effectiveness of this design method in comparison with classical pd design.

Keywords: *fuzzy control design, genetic algorithm, flight dynamics, linear control design.*

Nomenclatures

m: mass
μ_p: mass propellant
G: gravitation force
d, S: diameter and surface area

g: acceleration due to gravity
T, v propellant force and launch vehicle speed.
α , β : angle of attack and sideslip
ρ air density.
Q *dynamic pressure;* $Q = 0.5\rho v^2$

C_y^{α} *aerodynamic lift force coefficient due to* α

C_z^{β} *aerodynamic side force coefficient due to* β

C_x *aerodynamic drag coefficient.*

L *aerodynamic lift force,* $L = 0.5\rho v^2 S C_y^{\alpha} \alpha$.

D *aerodynamic drag force,* $D = 0.5\rho v^2 S C_x$

Y *aerodynamic side force,* $Y = 0.5\rho v^2 S C_y^{\beta} \beta$

ϑ, ψ, ϕ *pitch, yaw, and roll angles*

θ, σ *path and heading angle.*

q, r, p *body axis pitch, yaw, and roll rates.*

$\delta_q, \delta_r, \delta_p$ *elevator, rudder, and aileron deflection angles*

$m_z^{\alpha}, m_y^{\beta}$ *damping moment coefficient due to angle of attack and sideslip angle respectively*

m_z^q, m_y^r, m_x^p *damping moment coefficient due to pitch, yaw and roll rates* J_x, J_y, J_z moment of inertia about body axis x, y and z

A_i, B_i the inputs fuzzy sets

k_{α} control moment coefficient

p_q, p_{α} damping moment coefficients due to pitch rate and angle of attack respectively

I Introduction

A fuzzy logic controller proposed by Zadeh [1] incorporates uncertainty and abstract nature of human decision-making into an action mechanism. Reasoning by fuzzy logic, such system flexibility implements functions in near human terms, i.e. IF-THEN linguistic rules, it also provides a good reliability and capability in dealing with nonlinear systems that are ill-defined or time varying [2]. Several studies had been proved that, the fuzzy logic controller is an appropriate method for controlling complex systems [3], [4], [5]. Fuzzy logic control for missile autopilot design has also been studied and it was applied to improve the system robustness when the effect of the parameter variations is considered [6]. Recently, the fuzzy control scheme is proposed to design a high-angle-of-attack flight system for a super-maneuverable version of an F-18 aircraft, where its hybrid structured can meet both given robustness and performance requirements [7].Genetic algorithm is used to automate and introduce objective criteria in defining fuzzy controller parameters [8], [9], [10]. This approach is more powerful and high-dimensional searching spaces in comparison with other techniques such as neural networks [11].

Based on the previous work as mentioned above, we focused to emphasize that under the nominal case where there were no perturbations, the fuzzy pd control design method can achieve a high nominal performance. In addition, the degradation on the performance due to the effect of structured, un-structured uncertainties and kinematics coupling can also be reduced. However, the genetic algorithm for fuzzy parameters optimization is presented in order to improve the system nominal and robust performance. To test the effectiveness of fuzzy pd controller, the linear and nonlinear simulation results for attitude control motion of the launch vehicle are presented at the end of this paper.

II Plant Model

The equations of motion used in this paper to carryout the linear and nonlinear simulation are written below. These are derived according to the assumption that the earth is flat, non-rotating, no

disturbances included, and the launch vehicle motion is symmetrical.

Fig.1 shows the body frame $[x_p, y_p, z_p]$ and the wind frame $[\ x_a, y_a, z_a\ ]$ geometric diagram for the considered launch vehicle, and according to the Newton's law of translation and rotation motions, the following nonlinear equations of motions are summarized: [12]

$$\frac{dm}{dt} = -\mu_p \qquad (1)$$

$$m\dot{v} = T\cos\alpha - D - mg\sin\theta \qquad (2)$$

$$mv\dot{\sigma} = T\cos\vartheta\sin\beta - Y \qquad (3)$$

$$mv\dot{\theta} = T\sin\alpha + L - mg\cos\theta \qquad (4)$$

$$\frac{d\vartheta}{dt} = q \qquad (5)$$

$$\alpha = \vartheta - \theta \qquad (6)$$

$$\frac{d\psi}{dt} = r \qquad (7)$$

$$\beta = \psi - \sigma \qquad (8)$$

$$\frac{d\phi}{dt} = p \qquad (9)$$

The rotation equation of motion can be written as a combination of linear and nonlinear contributions:

$$\dot{q} = \left(\frac{m_z^{\alpha} QSd}{J_z}\right)\alpha + \left(\frac{m_z^{q} QSd^2}{J_z v}\right)q + M_z^{\delta_q}\delta_q + \frac{(J_x - J_y)}{J_z}pr \qquad (10)$$

$$\dot{r} = \left(\frac{m_y^{\beta} QSd}{J_y}\right)\beta + \left(\frac{m_y^{r} QSd^2}{J_y v}\right)r + M_y^{\delta_r}\delta_r + \frac{(J_z - J_x)}{J_y}pq \qquad (11)$$

$$\dot{p} = \left(\frac{m_x^{p} QSd^2}{J_x}\right)p + M_x^{\delta_p}\delta_p \qquad (12)$$

With;

$$M_z^{\delta_q} = \max\left(\frac{m_z^{\alpha} QSd}{J_z}\right)$$

$$M_y^{\delta_r} = \max\left(\frac{m_y^{\beta} QSd}{J_y}\right) \qquad M_x^{\delta_p} = 0.8dT$$

And the kinematics' coupling considered in this paper can be expressed by the following simple three equations.

$$\dot{\vartheta} = q + \phi\, r$$
$$\dot{\psi} = r - \phi\, q \qquad (13)$$
$$\dot{\phi} = p + \psi\, q$$

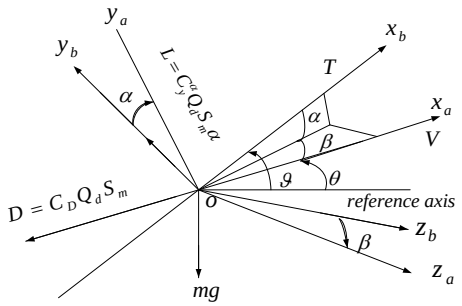

Fig.1 Vehicle coordinates system

III Fuzzy Control Logic

The schematic diagram of the fuzzy pd controller for pitch, yaw and roll autopilots is shown in Fig.2 below. These three autopilots are considered in order to stabilize the launch vehicle in three planes and to carryout the effect of kinematics coupling on the nominal system performance as well. The all crisp variables of errors $[e_\alpha, e_\beta, e_\phi]$, and change of errors

$[\dot{e}_\alpha, \dot{e}_\beta, \dot{e}_\phi]$ are first converted into the fuzzy variables to serve as conditions for a rule-base or an inference engine. In three fuzzy pd controllers, the control actions $[u_\alpha, u_\beta, u_\phi]$ are inferred from the interpretation of the membership functions of errors AND/OR those of change of errors. So as illustrated in the block diagram shown below, the inputs to fuzzy controllers are errors, change of errors, and the outputs are control actions to the three actuator models. According to the symmetrical assumption and due to the existence of roll autopilot which keep the roll angle and roll rate to be nearly zeros, therefore, the pitch and yaw autopilots are approximately identical.

For the purpose of simplicity, and due to the concentration on the attitude stabilization problem, the rest of this study will continue with the assumption that only the results and design procedures that related to the pitch fuzzy autopilot of the launch vehicle are presented.

To design fuzzy pd controller, the following three stages are required.

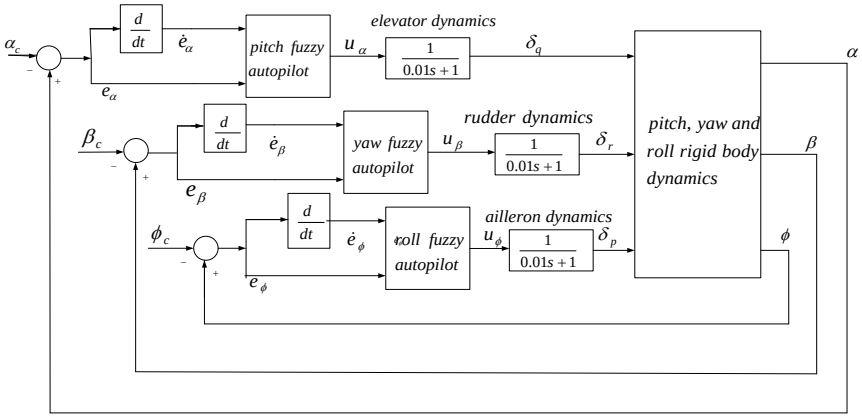

Fig.2 General block diagram of fuzzy pd controller for three channels.

1-Fuzzification interface

In this level, main idea is to design membership functions of inputs e_α , and $\dot{e}_\alpha$. The membership functions of these two inputs are selected here as a triangular type with maximum value is equal to one. Seven fuzzy subsets are used to accomplish this design, which can be expressed by the following seven linguistic variables.

NB: Negative Big
NM: Negative Medium
NS: Negative Small
ZE: Zero
PS: Positive Small

PM: Positive Medium
PB: Positive Big

2- Decision making logic

The decision making logic is the kernel of the proposed controller. And according to the designed membership functions, 49 fuzzy rules R_{49} must be decided. These rules can be represented by the following general statement:

R_i : *if* e_α *is* A_i *and* $\dot{e}_\alpha$ *is* B_i, *then* u_α *is* C_i

Where, the "*and*" logic can be realized by the following minimum operation, i.e. $\mu_i = \min(A_i, B_i)$

3-Defuzzification interface

The next and last step is the defuzzification process which computes the output value by the center of area method written in (14). [13]

$$u_\alpha = \frac{\sum_{i=1}^{n} \mu_i C_i}{\mu_i} \qquad (14)$$

Where, C_i denotes the center of the membership function of the consequent rule i, and n is total number of rules. In case of conventional pd controller, the control action can be represented mathematically as

$$u_{pd} = k_p\, e_\alpha + k_d\, \dot{e}_\alpha \qquad (15)$$

Where k_p and k_d are the proportional and derivative gains to be adjusted until the desired values of gain and phase margins are satisfied. And in order to carryout the nonlinear simulation presented at end of this paper, these gains are designed at different linearized operating points along the trajectory envelope.

Genetic Algorithm

A simple genetic algorithm has four steps, population size, Reproduction, Crossover, and Mutation. Reproduction is a process in which a new generation of population is formed by random selection from the existing population. Crossover is responsible for producing new trial solutions. Under this operation, two strings are selected to produce new off-spring by exchanging portions of their structures. These new off-springs may then replace weaker individuals in the next generation. Mutation is applied with a low probability ranging from 0.001 to 0.05, and the main function of the mutation is to add perturbation to find a new solution in the searching space.

The index called integral of absolute control signal and error is considered here where its minimum value at one given generation number reflects the optimal values of the parameters that need to be obtained. The general mathematical model for such an evaluation cost function is given as

$$J = \sum_{k=1}^{n} \left[w_1 e_\alpha + w_2 \left(u_\alpha(k) - u_\alpha(k-1) \right) \right] \qquad (16)$$

With w_1 , w_2 are the scaling weighting functions and k denotes the iteration parameter. Then the fitness function can be defined as

$$F = \frac{1}{\left(J + \varepsilon_o \right)} \qquad (17)$$

Where; ε_o represents the small positive constant used to avoid the numerical error of dividing by zero.

The genetic algorithm operators that are selected to achieve our design requirements can be explained briefly as follows.

1- Generation gap selection method

In this method of selection, a proportion of the existing population is replaced by newly created offspring. For example a generation of 0.5 means that, 50% of the present generation is replaced by other new formed offspring, where the individuals to be replaced may be chosen randomly or based on their evaluations, so that the worse members of the population are being replaced by good ones.

2- Uniform crossover

In this type of operator, there is a probability p_c that the offspring will take a real value from the corresponding positions of either parent. For example, when $p_c = 0.5$ the offspring take on values from parents with equal likelihood, while $p_c = 0 \; or \; p_c = 1$ creates offspring that are closes to the parents.

3- Gaussian mutation

In this type of mutation, if the value x'_k is selected for mutation from the following chromosome

$$X = x_1, x_2, ..., x_k, ...x_l$$

Where x_k have values in the constraint $\left\{U^k_{\min}, U^k_{\max}\right\}$, so the mutated value x'_k can be calculated as follows

$$x'_k = \frac{U^k_{\min} + U^k_{\max}}{2} + \frac{U^k_{\max} - U^k_{\min}}{6} \times \left(\sum_{i=1}^{12} r_i - 6\right) \qquad r \in [0,1]$$

And the new chromosome after mutation will be

$$X' = x_1, x_2, ..., x'_k, ...x_l$$

IV Simulation Results

In this study, the tasks for both the classical and fuzzy pd controllers were to track the step command in linear simulation and desired angle of attack trajectory in the case of nonlinear simulation. The comparison between them is accomplished based on the following linear and nonlinear analysis.

1- Linear Analysis

Under the case, when the short period motion is considered, the relation between angle of attack α and input elevator deflection δ_q at one selected operating point $(t = 5\,\text{sec})$ can be expressed by following transfer function

$$\frac{\alpha}{\delta_q} = \frac{k_\alpha}{s^2 + p_q s + p_\alpha}$$

With;

$k_\alpha = 48.3588$, $p_q = 0.2066$, and $p_\alpha = 1.1196$

In fuzzy pd control design, the parameters including the widths and centers of the membership functions for the error e_α and change of error $\dot{e}_\alpha$ with the fuzzy rule centers are adjusted until the step response of the angle of attack with high performance is achieved. For the case when the classical pd controller is used, the

parameters k_p and k_d are tuned in order to obtain the desired phase margin, $PM = 40^o$, and gain margin, $GM = 26db$. The values of pd gains which can satisfy these required margins are, $k_p = 1.49, k_d = 0.149$. The step response of the angle of attack using both design methods is shown in Fig.3, where it is observed that the fuzzy pd controller can provide a high performance level in comparison with the classical pd design. This is due to the lower settling time, minimum steady state error and zero overshoot that can be obtained using fuzzy pd control design method.

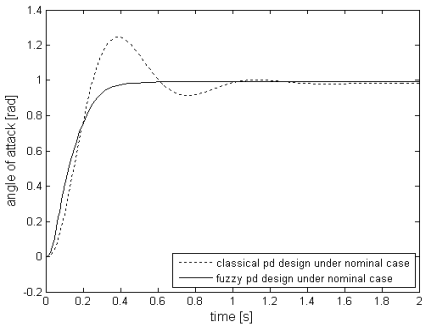

Fig.3 step response under the nominal case

The genetic algorithm is considered to optimize the fuzzy pd parameters in order to obtain a better level of performance. Where after 200 numbers of generations as shown in Fig.4, the optimized membership functions for the error e_α and change of error $\dot{e}_\alpha$ are obtained as shown in Fig.5 and Fig.6 respectively. In addition, the rule centers are also optimized and they are tabulated in two dimensional fuzzy relation matrix as shown in Table (1). Consquently, the step response of the angle of attack under the nominal case before and after optimization is shown in Fig.7 where it is seen that, using genetic algorithm this response is optimized in which minimum settling time and lower steady state error are obtained.

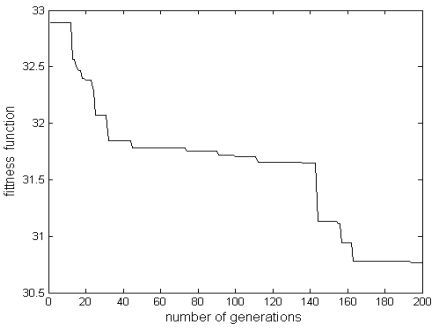

Fig.4 fitness function versus number of generations

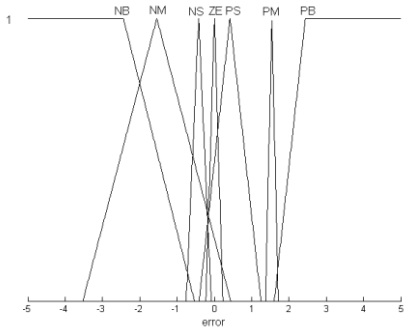

Fig.5 membership functions for error e_α

Based on these design parameters for classical and fuzzy pd controllers the effects of the following three perturbations on the nominal system performance are considered.

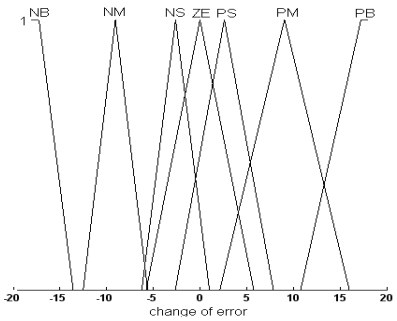

Fig.6 membership functions for change of error $\dot{e}_\alpha$

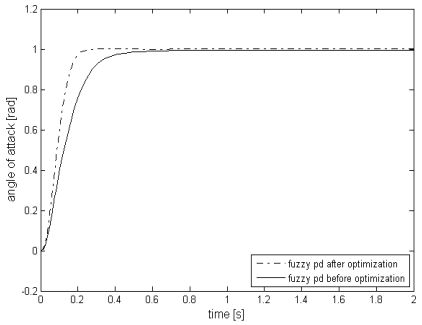

Fig.7 step response before and after optimization

Table (1) optimized fuzzy relation matrix

e_α \ $\dot{e}_\alpha$	*NB*	*NM*	*NS*	0	*PS*	*PM*	*PB*
NB	8.951	9.414	7.029	8.489	4.170	3.826	0
NM	9.406	7.771	9.143	5.696	2.842	0	- 3.827
NS	9.500	9.799	4.959	2.017	0	- 2.842	- 4.170
0	7.444	6.773	1.766	0	- 2.017	- 5.696	- 8.489
PS	5.406	1.032	0	- 1.766	- 4.959	- 9.143	- 7.029
PM	3.638	0	- 1.032	- 6.773	- 9.799	- 7.771	- 9.414
PB	0	- 3.638	- 5.406	- 7.444	- 9.500	- 9.406	- 8.951

- **Structured Uncertainty**

One parameter variation is considered here in order to carryout this type of uncertainty, that is due to the damping moment coefficient p_q. The effect of this parameter on the system nominal performance when it is fluctuated from its nominal value can be illustrated from the angle of attack trajectories shown in Fig.8. It is concluded that, the fuzzy pd controller keeps high performance, where a significant degradation in the performance due to large overshoot is observed in case of classical pd design.

- **Unstructured Uncertainty**

This type of uncertainty includes the input actuator model error dynamics, which can be represented by the two multiplicative transfer functions with time constants $0.05\,s$ and $0.1\,s$ respectively. The primary effects of these uncertain dynamics are an additional phase lag and high frequency gain attenuations, which cause the degradation in the nominal performance and may cause instability. The effect of the first multiplicative transfer function for both design methods is shown in Fig.9 where the fuzzy pd controller can achieve better performance than classical pd one. The second multiplicative transfer function destabilizes the system in case of classical pd design where as in the same time fuzzy pd controller is found to be more robustly stable and it can keeps the system stability as shown in Fig. 10.

- **Kinematics Coupling**

The kinematics coupling based on the model written in (13) is another serious perturbation effect on the system performance. And its effect on both design methods can be seen in Fig.11 where it is

observed that fuzzy pd controller can keep the system performance in the acceptable level while a large degradation in the nominal performance occur in case of other design method.

2- Nonlinear Analysis

In order to carryout nonlinear simulation, the equations of motion written in section II are simulated according to the data given for the considered launch vehicle. And to carryout this type of analysis, a typical angle of attack trajectory between -4^o to $+2^o$ is presented here. In this simulation only the nominal case and effect of worst un-model dynamics due to the multiplicative transfer function with time constant $0.1\,s$ is considered. From Fig.12 it is seen that, both design methods can achieve a command tracking, where fuzzy pd can satisfy a high tracking accuracy especially when there is a peak variation of the desired angle of attack trajectory. The effect of the multiplicative transfer function with time constant $0.1\,s$ is illustrated in Fig.13. It is observed that the fuzzy pd can keep tracking without degradation while instability occurs in case of classical pd design method.

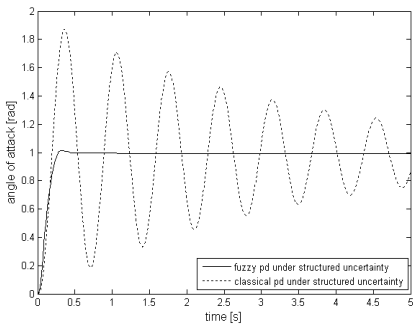

Fig.8 step response due to structured uncertainty

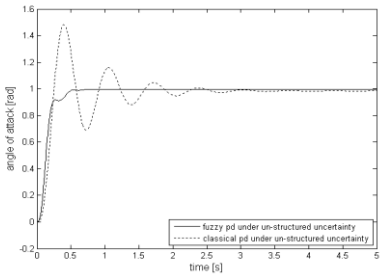

Fig.9 effect of the un-structured uncertainty with time constant $0.05\,s$

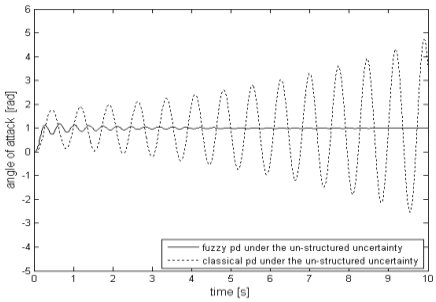

Fig.10 effect of the un-structured uncertainty with time constant $0.1\,s$

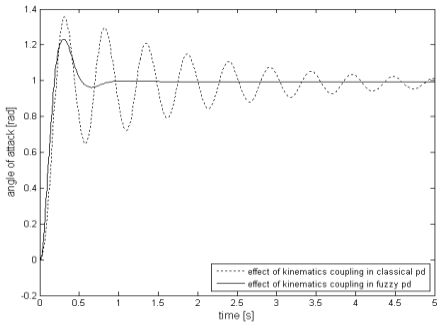

Fig.11 step response under the effect of the kinematics coupling

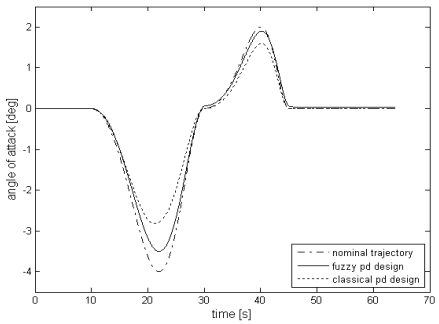

Fig.12 non-linear simulation in nominal case

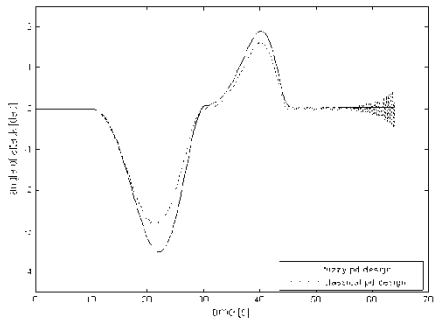

Fig.13 non-linear simulation under the effect of un- structured uncertainty with time constant $0.1\,s$

VI Conclusion

A fuzzy pd control design method is presented in this paper. From the linear and nonlinear simulation results, it was concluded that this design method can achieve a higher robust performance under the effect of the structured, un-structured uncertainties and kinematics coupling in comparison with the classical pd design. Furthermore, the nominal performance has been improved by optimizing the fuzzy pd parameters by using genetic algorithm optimization method. This study encourages to apply fuzzy control logic in flight control design where the high performance and robustness are the main requirements under the nominal and perturbed conditions.

References

[1] Zadeh. L. A, Fuzzy Sets[J]. *Information and control*, 1965, 8: 338-353.

[2] R.M. Tong, A control engineer reviews of fuzzy control[J]. *Automatica*, 1977, 13: 559-569.

[3] ASSILIAN.S, MAMDANI. E.H, An experiment in linguistic synthesis with a fuzzy logic controller[J]. *International.Journal.Man Machine Studies*, 1977, 7: 1-13.

[4] KING. P.J, MAMDANI. E.H, The application of fuzzy control systems to industrial processes[J]. Automatica, 1977, 13: 355-242.

[5] MAMDANI. E.H, Application of fuzzy algorithms for control of a simple dynamic process[C], Proceeding .IEE, 1974, 121: 1585-1588.

[6] Schumacher. W. K, K. Liu, An Appropriate Application of Fuzzy Logic: A Missile autopilot for dual control implementation[C] // Proceedings of the IEEE International Symposium Intelligent Control, Columbus, OH, U.S.A, 1994, :93-98.

[7] Tae. Hyun. Won, Dall. Seop. Song, Sae. Kyu. Nam, Man. Hyung. Lee, A design for fuzzy control for high performance aircraft[C] // Proceedings of the IEEE International Symposium on Industrial Electronics, 1999, 3: 1141 – 1146.

[8] GOLDBER. D.E, Genetic algorithms in search, optimization and machine learning. Addison-Wesley, 1989.

[9] K.F. Man, K.S.Tang,S, K wong, W. A. Halang, Genetic Algorithms for Control and Signal Processing. Springer Verlag London, 1997.

[10] C.L. Karr, Genetic Algorithms for Fuzzy Controllers[J]. *AI Expert*, 1999, 6:26 – 33.

[11] J. S. Jang, Self – Learning Fuzzy Controllers Based on Temporal Back Propagation[J]. IEEE Transactions on Neural Networks, 1992, 3(5): 1992.

[12] Ali Mohamed Elmelhi, Flight Vehicle's Stabilization Based Fuzzy Logic Control Design and Optimization, ph. d thesis, Beihang university, Biejing, china, Nov.2005.

[13] Kevin. M. Passino, Stephen. Yurkovich, Fuzzy Control. U.S.A, Copyright, Addison Wesley, California, 1998.

Robust Dynamic Inversion Design for Flight Control System

ALI MOHAMED.S.ELMELHI

Alfateh University

ali_elmulhi@yahoo.com

Abstract. Dynamic inversion is a feedback linearization control law design in which feedback is used to simultaneously cancel the system dynamics and achieve a desired dynamics response characteristic. Robust dynamic inversion obtained by coupling μ - synthesis with dynamic inversion through the inner/outer loop is presented here in order to achieve a large robustness to the uncertainties. In this paper, this design methodology is used to tolerate the uncertainty due to effect of the kinematics coupling, and remove the requirements of gain scheduling during all flight envelope. To demonstrate the effectiveness of this design method, the comparison with gain scheduling design is carried out from the robust point of view. This can be achieved by testing the effect of the kinematics coupling on the system nominal performance when the linear and non linear simulations are carried out.

1- Introduction

Robust dynamic inversion has been widely studied in flight control designs. It has been used as a design method for controlling super-maneuvering control law for the F18 high angle of the attack research vehicle [1]. Many of the other researchers are focusing their attention on applying this technique for different flight control problems such as in [2], where control of the aircraft using feedback linearization and μ - synthesis techniques to achieve a high performance and robust to parameter variation has been studied. In [3], the dynamic inversion yields a better performance with minimum control deflections comparing to the gain scheduling "GS".

Robust dynamic inversion obtained by coupling μ -synthesis with dynamic inversion can improve the robustness and reduce the complexity that results due to the requirement of robust controller scheduling. The basic philosophy of this paper is to carry out the comparison between GS and robust dynamic inversion based on the effect of the kinematics coupling on the system nominal performance. In addition, it has been proved that, by using a nonlinear simulation, one controller is sufficient to achieve the nominal and robust performance requirements in complete trajectory envelope.

2 Plant Model

The simplified equations of motions due to the assumption that, the earth is flat, no disturbances included, and the flight vehicle is symmetrical can be written as

$$m\dot{v} = T\cos\alpha - D - mg\sin\theta \quad (1)$$

$$mv\dot{\theta} = T\sin\alpha + L - mg\cos\theta \quad (2)$$

$$\dot{\alpha} = q - \frac{1}{mv}\left[T\sin\alpha + L - mg\cos(\vartheta - \alpha)\right] \quad (3)$$

And

$$\frac{dm}{dt} = -\mu_p \qquad \frac{d\vartheta}{dt} = q \qquad \frac{d\phi}{dt} = p$$

where m represent the mass, μ_p the propellant flow rate, v the launch vehicle speed, T the propellant force, α the angle of attack, D the aerodynamic drag force, g the acceleration due to gravity, θ the flight path angle, ϑ the pitch angle, L the lift force, q the pitch rate, p the roll rate and ϕ the roll angle.

Due to a symmetrical assumption, and existing of the roll autopilot which stabilizes a roll motion to make the roll rate $p \approx 0$ and roll angle $(\phi \approx 0)$, the equation of motions for the yaw dynamics and moments are neglected and we assume that both the pitch and yaw autopilots are approximately identical.
The pitch and roll moment equations can be written as in the following form:

$$\dot{q} = \frac{\left(M_z^{\alpha}\alpha + M_z^{q}q + M_z^{\delta_q}\delta_q\right)}{J_z}$$

$$\dot{p} = \frac{\left(M_x^{p}p + M_x^{\delta_p}\delta_p\right)}{J_x}$$

Where δ_q, δ_p represent the elevator, and aileron deflections. $M_z^{\delta_q}, M_x^{\delta_p}$ the aerodynamic pitch and roll moments due to δ_q and δ_p deflections, M_z^{q}, M_x^{p} the aerodynamic moments due to pitch and roll rates respectively and J_x, J_z are the moment of inertia about body axis x and z.

3 Robust Dynamic Inversion Control Law Structure

Due to a limited space, the design procedure using μ-synthesis and GS are omitted and the reader should refers to [2], [4], and [5] for more details. And due to the same reason, the simulation results related to the roll autopilot are not included as well. The robust dynamic inversion control law is derived here to obtain a closed loop system which can satisfy the robust performance and stability requirements. The structure of the robust dynamic inversion for pitch autopilot can be illustrated by the block diagram shown in Fig.1, where the roll autopilot has the same configuration with different weighting functions that needed to design the robust controllers K_{ϕ} and K_p in order to achieve the stability and performance requirements for

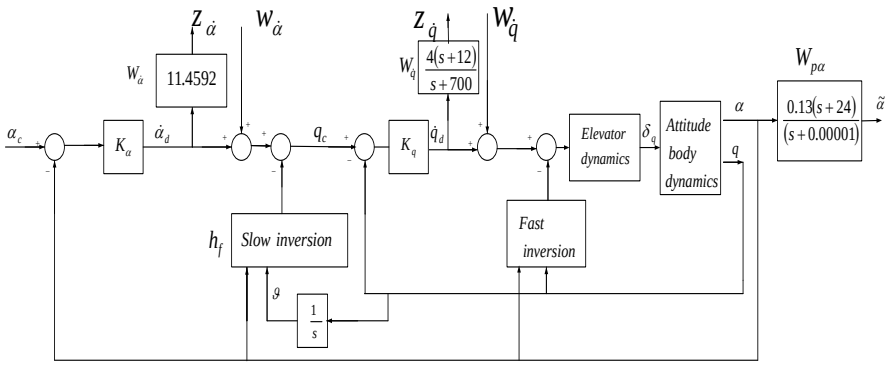

Fig.1.Structure for pitch autopilot using robust dynamic inversion

the roll motion. The weighting function $W_{\dot q}$ is designed to reflect the effects of uncertainties, the weighting function $W_{p\alpha}$ is considered to reflect the relative importance of the various frequency ranges for which the performance of angle of attack is desired, and the weighting function $W_{\dot\alpha}$ is design to achieve the frequency domain of $\dot\alpha$ in order to limit the pitch rate amplitude. $\dot\alpha_d$, and $\dot q_d$ represent the desired angle of attack and pitch rate obtained from the outer and inner loop respectively. All the weighting functions and the input/output variables $[z_{\dot\alpha}, w_{\dot\alpha}, z_{\dot q}, w_{\dot q}, \tilde\alpha]$ are shown here in order to design the robust controllers K_α, K_q and they are not considered during the design procedures for the inner and outer loop dynamic inversion as we will see in the next two subsections. For more details about how to design K_α, K_q and K_p, the reader again refer to [2], and [4] as mentioned before.

3.1 Outer Loop Dynamic Inversion

This represents the first stage of dynamic inversion, where the angle of attack α, and roll angle ϕ can be written in the following general state form:

$$\dot x = R + h_f \qquad (4)$$

With $x = [\alpha \quad \phi]^T$, $R = [q \quad p]^T$,

$$h_f = -\frac{1}{mv}\begin{bmatrix} T\sin\alpha + L - mg\cos(\vartheta - \alpha) \\ 0 \end{bmatrix}$$

So the outer loop pseudo-control input can be defined as

$$\dot x = u_x \quad \text{And} \quad u_x = R + h_f \qquad (5)$$

Now the body rate inner loop command R_c can be computed by an outer loop as

$$R_c = \begin{bmatrix} \dot{\alpha}_d & \dot{\phi}_d \end{bmatrix}^T = u_x - h_f \quad (6)$$

With $u_x = K_x(x_c - x)$

$$x_c = \begin{bmatrix} \alpha_c & \phi_c \end{bmatrix}^T$$

$$K_x = \begin{bmatrix} K_\alpha & K_\phi \end{bmatrix}^T$$

Where, K_α and K_ϕ are the outer loop robust controllers for pitch and roll autopilots respectively which are designed by using $\mu-$synthesis, and $\dot{\phi}_d$ represents the desired roll angle.

3.2 Inner Loop Dynamic Inversion

In this case a dynamic inversion involves the body angular rates q and p . An inner loop pseudo control input is defined by

$$\dot{R} = u_R \quad , \quad u_R = f(x, R, \hat{\delta})$$

So the body angular rate dynamics can be approximated as

$$\dot{R} = f(x, R, \hat{\delta}) \approx \hat{F}(x, R) + \hat{B}\begin{bmatrix} \hat{\delta}_q \\ \hat{\delta}_p \end{bmatrix} \quad (7)$$

With

$$\hat{F}(x, R) = \begin{bmatrix} \hat{F}_q \\ \hat{F}_p \end{bmatrix}, \hat{B} = \begin{bmatrix} \frac{M_z^{\delta_q}}{J_z} & 0 \\ 0 & \frac{M_x^{\delta_p}}{J_x} \end{bmatrix},$$

$$\hat{F}_q = \frac{\left(M_z^{\alpha}\alpha + M_z^{q}q\right)}{J_z}, \hat{F}_p = \frac{\left(M_x^{p}p\right)}{J_x}$$

Performing an approximate dynamic inversion, the control input $\hat{\delta}$ is

$$\hat{\delta} = \begin{bmatrix} \hat{\delta}_q \\ \hat{\delta}_p \end{bmatrix} = \hat{B}^{-1}\left(u_R - \hat{F}(x, R)\right) \quad (8)$$

$$u_R = \begin{bmatrix} \dot{q}_d & \dot{p}_d \end{bmatrix}^T = K_R(R_c - R) \quad (9)$$

With $R_c = \begin{bmatrix} q_c & p_c \end{bmatrix}^T$

and $K_R = \begin{bmatrix} K_q & K_p \end{bmatrix}$

Where K_q and K_p are the inner robust controllers for pitch and roll autopilots obtained by using μ -synthesis, and $\dot{p}_d$ represents the desired roll rate.

4 Simulation Results

4.1 Linear Analysis

In order to carryout a linear analysis, the nonlinear model given in section 2 is linear zed at different operating points on the trajectory envelope [6]. And consequently, both the angle of attack and roll angle transfer functions are obtained. And their

dynamics at some instant operating point are given by

$$\frac{\alpha}{\delta_q} = \frac{48.35}{s^2 + 0.125s + 39.607}$$

$$\frac{\phi}{\delta_p} = \frac{19.93}{s(s + 0.8570)}$$

The actuator model for the elevators is considered as the first order transfer function with time constant 0.01 sec. The simplified model dynamics of the kinematics coupling used here can be expresses as

$$\dot{\vartheta} = q + \phi r \quad \dot{\psi} = r - \phi q$$

$$\dot{\phi} = p + \psi q$$

With r , ψ represent the yaw rate, and yaw angle respectively. And due to the symmetry assumption, so we assume that $(\psi \approx \vartheta, r \approx q)$.

Under the nominal case, the robust dynamic inversion can achieve a high performance where the response with zero overshoot and very small steady state error in comparing to GS design can be obtained as shown in Fig.2 and Fig.3 respectively. In addition, the effect of the kinematics coupling on the system performance in both design methods is considered. In case of robust dynamic inversion, this effect can be tolerated and good tracking performance can be achieved as shown in Fig.2. Where, under the same amount of coupling, a large degradation in performance due to overshoot and large settling time is observed in GS design as illustrated in Fig.3.

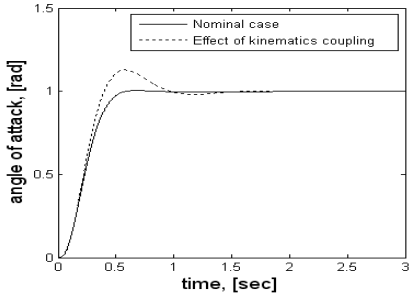

Fig.2 Linear simulation in robust dynamic

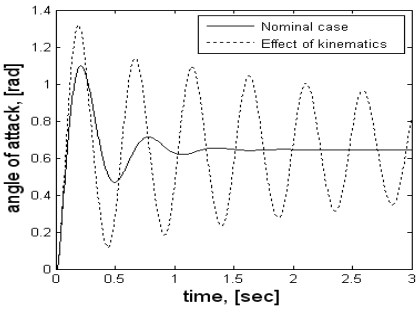

Fig.3. Linear simulation in GS

4.2 Nonlinear Analysis

The nonlinear model in section 2 is simulated based on some available typical data [6]. The main objective here is to prove that, one controller is sufficient to achieve a required performance during complete flight trajectory in case of robust dynamic inversion, a typical trajectory of angle of attack is considered in order to carryout the nonlinear simulation. Where, only one robust controller is considered during all trajectory envelope and can achieve a high robust performance under the effect of the kinematics coupling.

Fig.4 shows that, the robust dynamic inversion can deal with the effect of coupling and keep an accurate tracking in

comparing to the design using GS in which a large degradation in the tracking accuracy is observed as shown in Fig.5.

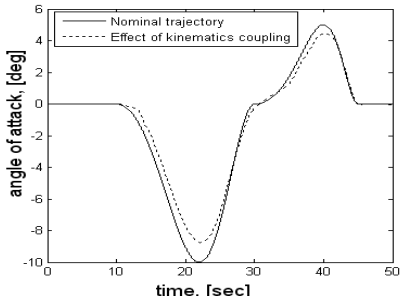

Fig. 4 Nonlinear simulation in robust dynamic inversion

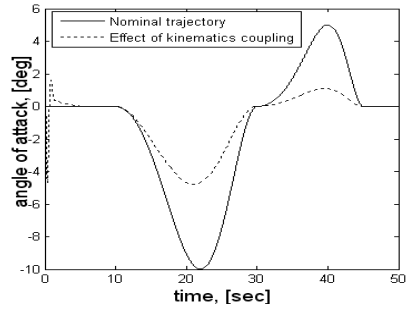

Fig.5 Nonlinear simulation in GS Design

5 Conclusion

Robust dynamic inversion methodology has been presented in this paper. Where, a higher robust performance and stability can be achieved in comparison to GS design method. This design procedure has been carried out by incorporating μ - synthesis through the inner/outer loop structure of dynamic inversion in order to enhance the performance and robustness goals of the closed loop system. The main advantage of this design approach that, it can minimize the degradations on the system nominal performance obtained due to effect of the kinematics coupling. In addition, the design complexity of the high order robust controllers can be reduced by removing the requirements of gain scheduling where one controller is sufficient during all flight trajectory.

References

[1] DALE, ENNS., DAN, BUGAJSKI., RUSS, HENDRICK., GUNTER, STEIN.: Dynamic Inversion: an evolving methodogy for flight control design. Int.J.control. 59 (1994) 71-91.

[2] JACOB, REINER., GARY, J,BALAS., WILLIAM, L, GARRARD.: Flight Control Design Using Robust Dynamic Inversion and Time-scale Seperation. Auomatica. 32 (1996) 1493-1504.

[3] S, Antony, snell., Dale, F, Enns., William, L., Garrard, Jr.: Nonlinear Inversion Flight Control for a Super-maneuverable Aircraft. Journal of Guidance, Control And Dynamics. 15 July-August (1992) 976-984.

[4] Doyle.: structured uncertainty in control system design. Proceeding. of 24th conference. on Decision. Control (1985) 260-265.

[5] JOHN, H,BLAKELOCK.: Automatic Control of Aircraft and Missiles, Copyright by John Wiley and Sons, Inc (1991).

[6] Ali Mohamed Elmelhi, Flight Vehicle's Stabilization Based Fuzzy Logic Control Design and Optimization, ph. d thesis, Beihang university, Biejing, china, Nov.2005.

Digital and Analogue PID Controller for Heat Process System Based on a Microcontroller

Mahmoud Ali Osman [1] Mahmoud Mansour Al-Fandi [2]

1-Department of computer engineering, 2-Department of Electrical & Electronic Engineering,

Faculty of Engineering, Al-Fateh University , Tripoli, Libya

Abstract:-This paper presents an application of real time control for controlling a PT326 Process Trainer laboratory equipment. Firstly, an interfacing data acquisition card is developed based on microcontroller. Secondly, a conventional three term controller PID is implemented based on Zeigler-Nichols tuning method. Control of the process has been implemented in real time using the Matlab environment. Experimental results regarding the performance of the real time control are included in a comparative study.

Keywords**: -** Real Time Control Systems, Data acquisition, Microcontrollers

I – Introduction

The PIC is a good choice for producing interesting, but achievable, projects which incorporate a good balance between hardware and software design. Microcontrollers are important because they make electronic circuits cheaper and easier to build. Hardware circuits can be replaced with a microcontroller and its software, reducing the number of components required. The software element (control program) can be reproduced at minimum cost, once it has been created. So the development costs may be higher, but the production cost will be lower in the long run. Serial communication is the most common low-level protocol for communicating between two or more devices. Normally, one device is a computer, while the other device can be a modem, a printer, another computer, or a scientific instrument such as an oscilloscope. As the name suggests, the serial port sends and receives bytes of information in a serial fashion - one bit at a time. These bytes are transmitted using either a binary (numerical) format or a text format. The data acquisition hardware is connected to the computer using a serial port, this device is composed of a PIC micro controller 16F876A, and MAX232 which is used to make compatible the signals transmitted by the PIC to the computer, in others words it translates the binary signal sent by the PIC into RS232 protocol[11]. The serial port is harder to interface than the parallel port. In most cases, any device is connected to the serial port will need the serial transmission converted back to parallel and this can be done by using UART(univeral asynchronous reciver transmitter). On the software side, there are many more registes to attend to than on a standard parallel port [1].

Microcontrollers have in built SCI (serial communication interfaces) which can be used to talk to the outside world. Serial communication reduces the pin count of these PIC's. Only two pins are commonly used, transmit data (TXD) and receive data (RXD) compared with at least 8 pins for an 8 bit parallel method [1],[11]. Many PIC chips incorporate analogue inputs so that they can be used in control systems with input sensors which produce a voltage, current or resistance change in response to an environmental variation[10].

II- Process Trainer PT326 (Feedback's Process Trainer PT326)

The **PT 326** is a self-contained process control trainer. The PT 326 which is built by Feedback Instruments Ltd. (UK). Process Trainer PT326 which available at the department of computer Engineering as shown in Figure (1), it incorporates a plant and control equipment in a single unit. In this equipment, a blower draws air from the atmosphere and forces it through a heater grid. The air temperature is detected downstream of the grid by a bead thermistor before being returned to the atmosphere. The detecting (bead thermistor) and correcting (heater) elements have been placed sufficiently far apart to facilitate the investigation of "lag" time. A bead thermistor fitted to the end of a probe can be inserted into the air stream any of three points along the tube, spaced by 28mm, 140mm, and 279 mm from the heater. The control action corresponds to a signal from o to + 10 volts which is converted in a variable power supply to the grid. The desired temperature may be set in a range from 0C to 80C. A toggle switch provides an internal step increase to the desired temperature signal. The PT 326 may be configured to run with either open-or closed-loop control. The process trainer also allows the connection of an external controller[3]. Process control simulator PCS327 (Feedback UK) as shown in Figure (2) provides multi – propose controller with full package it perform the three main kinds of controller(P,PI,PID) and give real simulate to what actual can be happen, its useful in this work in the comparison between the real time control system of the heat process trainer PC326 and PCS 327.The interfacing between the heat process PT326 and the computer was handled by data acquisition card developed by the authors, this card is based on PIC16F876A microcontroller which is programmed to convert from analog to digital and the opposite.

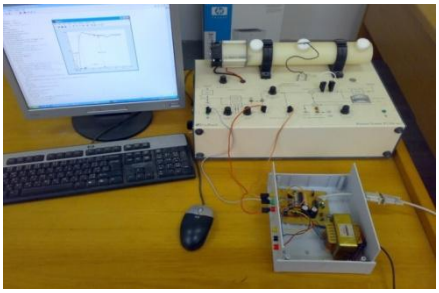

Figure (1) Data Acquisition Card Connected by Serial Port of the PC and PT326

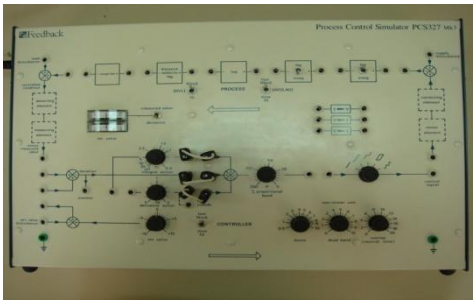

Figure (2) PID Analogue Controller PCS 327

III- Serial Port Interface

The original serial port interface standard was given by RS-232, which stands for Recommended Standard number 232. The term "RS-232" is still in popular use, and is used when referring to a serial communication port that follows the TIA/EIA-232 standard. RS-232 defines these serial port characteristics:

- The maximum bit transfer rate and cable length.
- The names, electrical characteristics, and functions of signals.
- The mechanical connections and pin assignments.

Primary communication is accomplished using three pins: the Transmit Data pin, the Receive Data pin, and the Ground pin. Other pins are available for data flow control, but are not required. Other standards such as RS-485 define additional functionality such as higher bit transfer rates, longer cable lengths, and connections to as many as 256 devices. Serial ports consist of two signal types: data signals and control signals. To support these signal types, as well as the signal ground, the RS-232 standard defines a 25-pin connection. However, most PC's and UNIX platforms use a 9-pin connection. In fact, only three pins are required for serial port communications: one for receiving data, one for transmitting data, and one for the signal ground [10],[11].

The device MAX-232 includes a charge pump, which generates + 10 V and – 10 V from a single 5 V supply. This I.C. also includes two receivers and two transmitters in the same package which is handy in many cases for someone only wants to use the Transmit and Receive data Lines.

IV Hardware development based on microcontroller.

Data acquisition channel is divided into two parts one is an input data acquisition channel and the other is an output data acquisition channel, the data acquisition channel hardware has digital inputs, analog inputs, digital outputs and analog outputs. The full circuit as shown in Figure (4) containing input and output circuit which consists of a microcontroller PIC16F876A and Max232. Max232 is important to connect between the microcontroller and the serial port, because process trainer PT326 voltage range between 0-10Volt and the microcontroller does not take more than 5Volt, there are two circuits using operational amplifiers to decrease the voltage to the half before it get into the microcontroller and increase the voltage to double after get out the microcontroller Figure (3) shows these circuits. The amount of the resisters depend on the required rate for example $R_f = 1k\Omega$ and $R_{in} = 2k\Omega$ to decease the voltage to the half and $R_f = R_{in}$ to give double the voltage $\mathbf{V_{in}}$ [2] .

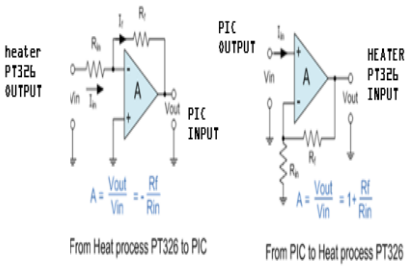

Figure (3) Multiplier and Divider Circuits Using Operational Amplifier

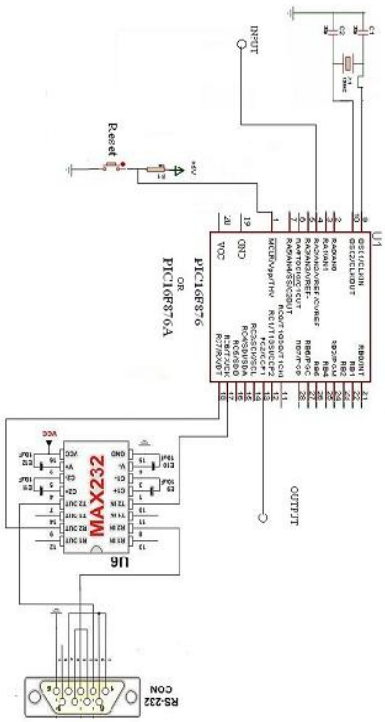

Figure (4) Hardware Interfacing Using Microcontroller PIC 16F876A

V The MATLAB commands for writing and reading data from serial port:

The main commands used in this work are summarized as follows [9]:

- Create a serial port object — create the serial port object **s** associated with serial port COM1. **s = serial ('COM1');**
- Configure property values — configure the input buffer to accept a reasonably large number of bytes, and configure the baud rate to the highest value supported by the scope. **s.InputBuffer s.BaudRate = 4800**
- Connect to the device — Connect **s** to the Heat process PT326. Because the default value for the ReadAsyncMode property is continuous ,data is asynchronously returned to the input buffer as soon as it is available from the instrument. ,**fopen(s)**
- It can be verified the number of values read with the **BytesAvailable**.,**s.BytesAvailable property**

Reading Binary Data

The using of the fread function is to read binary data from the device. Reading binary data means that it will return numerical values to MATLAB. The use of fgetl, fgets, and fscanf functions to read data from the device, and format the data as text. ,**out = fread(s,69);**

Writing Binary Data

The use of the fwrite function is to write binary data to the device. The fwrite

function is used to write text data to the device as follows .,**fwrite(s,out);**

Disconnect and clean up

When there is no need to **s**, it has to be disconnected from an instrument and it has to be removed from memory and from the MATLAB workspace and this is done as follows . ,**fclose(s)**,**delete(s)**, **clear s**

VI Digital PID Controller

In order to form a basis of comparison the process was first controlled using an analogue three term controller. This was achieved by connecting the heater process and the analogue controller, since they were specifically designed for use with each other. The analogue controller could then be replaced by a digital controller, and the response to a step input compared with the response of the analogue controller. The three terms controller are set in accordance with Zeigler-Nichols tuning rules. Most process loops where the plant transfer function has not been completely defined are controlled by the PID algorithm or one of its variations. There were a number of possibilities all of which derived from the basic continuous algorithm [4],[7],[8].

$$U(t) = K_P\,[e(t) + \frac{1}{T_I}\int e(t)dt + T_D\,\frac{de}{dt} + UO \quad \ldots\ldots \quad (1)$$

Where, K_P = Proportional gain, T_I = Integral time constant, T_D = Derivative time constant ,e(t) = Error signal,

U(t) = Controlled output signal, U_O = U(0) is the controlled output at t = 0.

The terms T_D is related to K_D and T_I is related to K_I as follows: $K_D = K_P\,T_D$, $K_I = \frac{K_P}{T_I}$

Hence equation (1) reduces to equation (2)

$$U(t) = K_P\,e(t) + K_I\int e(t)dt + K_D\,\frac{de}{dt} + UO \ldots \quad (2)$$

Some algebraic manipulation was required to obtain a convenient solution, hence the continuous algorithm shown in equation (2) can be written as :

$$U(n) = K_P\,e(n) + K_I\sum_{n=1}^{k}\frac{T_S}{2}(e_n + en-1 + KDTSen - en-1 \ldots \quad (3)$$

Where T_S = sampling period , K_I = Integral gain, K_D = Derivative gain, n = 1,2,3,…, k

This form of algorithm most convenient one for microprocessors and microcontrollers use[5]. The variable e_{n-1} is the value of the previous sample of the error. The new value e_n then replaces the old e_{n-1} at the next sampling interval. The counter timer circuit interrupt time of the microcontroller as a real time clock was used to provide a variable sampling rate T_S.

The minimum permissible sampling rate was found to be 40 m.sec and from equation (3) if we define the term by

$$K_F = K_I * T_S \quad \ldots\ldots\ldots \quad (4)$$

However, in order to make K_F as small as possible, and consequently the smaller the sampling period is, the only chance

available to us is to vary K_I while T_S is kept as a constant,

Where, $T_S = 40$ m.sec. ,Hence

K_F reduces to $K_F = 40 \times 10^{-3} * K_I$ ….. (5)

Where K_I has to be smaller by a factor than the Ziegler- Nichols recommended settings thereby enabling us to obtain an equivalent system response to both digital controller and the equivalent continuous

(analogue) controller under the same process conditions.

VII Real Time Results

In order to test the data acquisition card developed by the authors a comparison between continuous (analogue) and digital control was made based on the continuous (analogue) simulator PCS327 . The experimental results were taken when the temperature input was 40^0 which is equal to 5V, and detector probe is inserted in the third position (279mm) and sampling rate .

of the digital controller was 60 m.sec. and the initial value of the error was zero, the fan velocity and the ambient temperature were assumed constant. Figures (5), (6), and (7) show comparison between PCS327 PID continuous or analogue controller and digital controller of the real time control system that was performed in this work based on the Ziegler-Nichols tuning, as a reference PCS327 was a little bit better than the real time

From these results comparison can be made between the digital controller and the continuous controller and it concludes that the integral gain K_I (T_I) of the digital controller has to be smaller than the Ziegler-Nichols recommended settings, therefore the smaller the sampling period is, and the closer the system response to the continuous one, But generally speaking, the difference is small and the real time control system has proven that it's capability of performing high level PI(PID) controller in relative to analogue controller PCS327

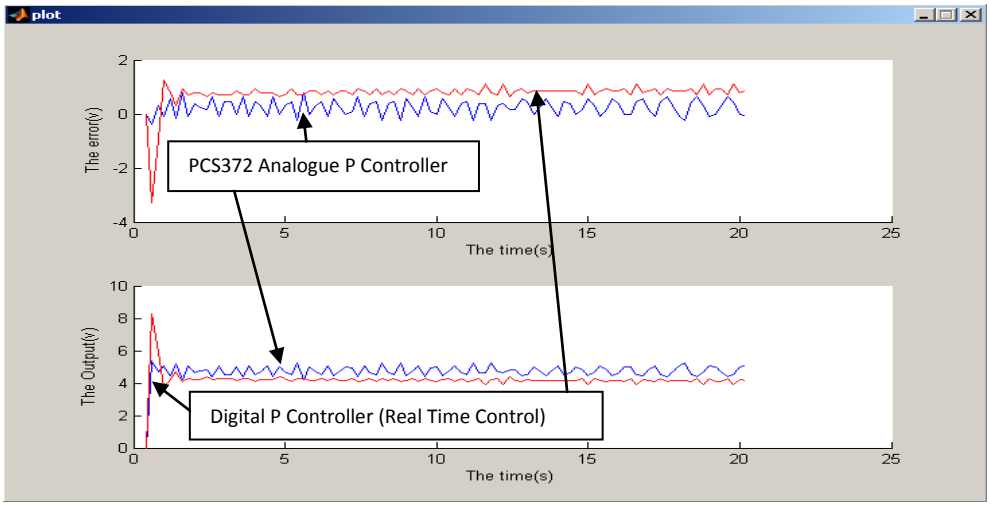

Figure(5) Digital P Controller versus Analogue P controller, K_P=1

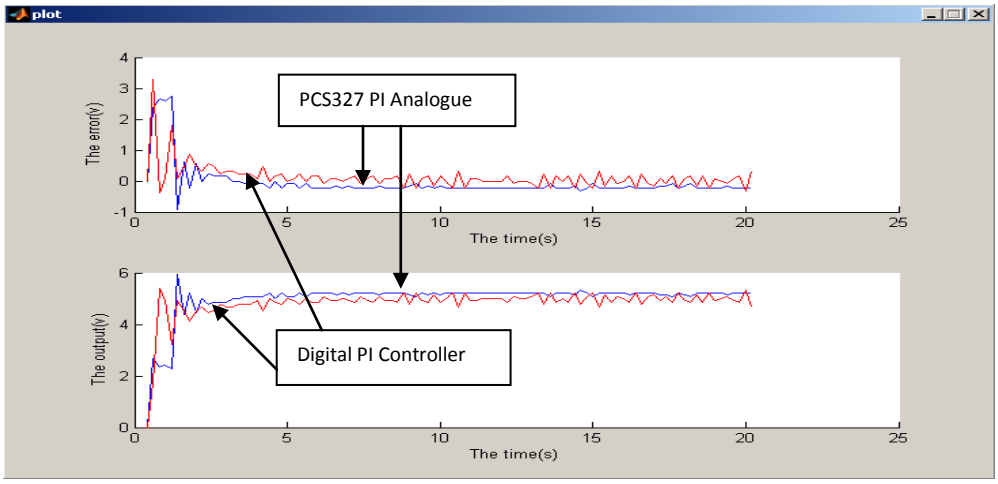

Fig (6) Output time response of Digital

PI Controller versus Analogue PI controller

PI Continuous controller(K_p = 1.3 , T_I=0.8), PI Digital controller (K_P=1 , K_I = 0.5)

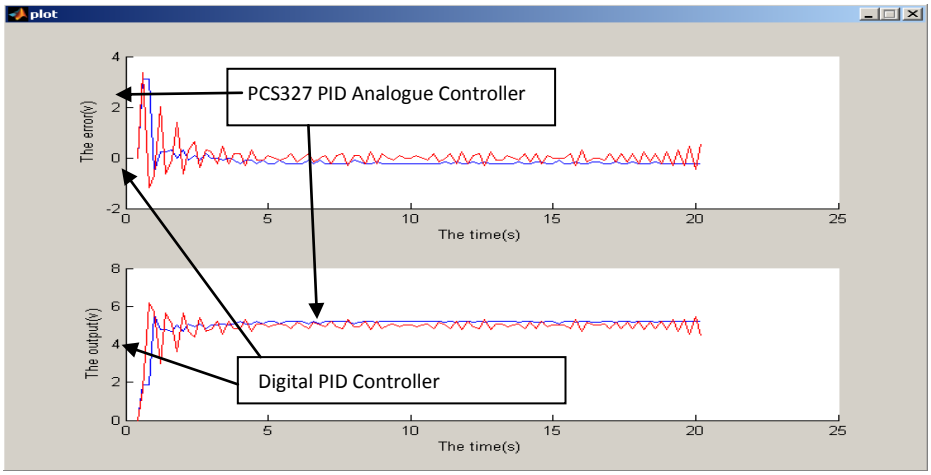

Fig (7) Digital PID Controller versus Analogue PID controller

Analogue PID controller (K_P =1.5, T_I =0.7 , T_D =0.2) , PID Digital Controller (k_p =1.5, k_I=0.3 , K_D =0.15)

V III Conclusions

A very flexible basic controller has been developed using microcontroller 16F867 system which could be implemented with very little effort on any suitable process to provide single loop direct digital control. Minor modifications would be required to the software to convert this generally applicable unit into one for specific use, such as standby or multi-process control. A comparison between continuous and digital control was made. It is therefore the digital controller developed which provides very effective control.

It is possible to use microcontroller 16FXXX chips system facilities for real time operation by using an interrupt signals provided by the counter timer circuit (CTC). It is possible by using a PID controller and by selecting the adequate values for their respective gains through the PC keyboard to have a zero steady state error and very fast response for the stated sampler interval.

References

[1]. Jan Axelson, "Parallel Port Complete", 1st edition, john Wiley & Sons Inc, 1999.

[2]. Nuri Agab " Applications of Adaptive Control Using Neural Networks In On Line of Real Time Control Systems" MSc Dissertation, Department of Computer Engineering, Faculty of Engineering, Al-Fateh University, Tripoli, Libya, Spring 2010

[3]. Feedback instrument limited, "PT326 data sheet" , 1974.

[4]. Benjamin C. Kuo, "Automatic Control systems", 7th edition, John Wiley Inc., 2001.

[5]. A. O'Dwyer, "PI and PID controller tuning rules for time delay process", 2nd edition, An Imprint of Addison Wesley Longman Inc, 2002.

[6]. R. Hedjar, "Online adaptive control of non-linear plants using neural networks with application to temperature control system" , J. King Saud Univ. Vol. 19, Comp.& Info. Sci., pp. 75-94, Riyadh (1427H./2007).

[7]. Roland S. Burns, "Advanced control engineering", 1st edition, Planta Tree, 2001.

[8]. M.Sam Fadali, "Digital control engineering analysis and design", 1st edition, Elsevier Inc, 2009.

[9]. MATLAB, "Help of the language of technical computing", The MathWorks, Inc, 2006.

[10]. Martin Bates," PIC Microcontrollers An Introduction to Microelectronics",2nd edition, Elsevier, 2004.

[11]. Interfacing the Serial / Rs232 port V5.0, http://www.senet.com.au/~cpeacock.

Chapter III

Electrical Machines, Generation of Electric Energy, and High Voltage Engineering

Intelligent Techniques for Three-Phase Induction Motor Inter-Turn Short Circuit Faults Diagnosis Based on Voltage and Current Unbalance Percentage

Prof. B. M. saied
Dr Y. M. Y. Ameen
Electrical Dept., Engineering college, Mosul University

Abstract:

Stator faults count a high percentage of three-phase induction motor problems. In fact, the detection of this type of faults in its early stages is not easy, and many of detection tools may be considered inefficient tools. Identification of fault needs human expert and continuous interpretation of extracted fault feature. In order to automate the on-line diagnosis process and to avoid the requirement of the expert human, intelligent techniques can be used and developed. In this paper, an intelligent fuzzy inference system (FIS) based on both the magnitude of the voltage unbalance percentage, UV%, and current unbalance percentage, UI%, is proposed and implemented. The proposed FIS is used to diagnose the inter-turn short circuit faults of three-phase induction motor. The system takes into account the current unbalance due to unbalance problem in the supply voltage, and the current unbalance due to deterioration in the stator windings. The proposed system is implemented and verified by developing an automatic computerized on-line diagnostic system which is acquiring motor line voltages and currents. A three-phase 1.1 Kw, 380 V, 50 Hz squirrel cage type induction motor is re-wounded such that many taps are obtained, in order to perform many deliberately different fault conditions. The proposed FIS is effectively detected the low-level deterioration (approximately 0.5% and upwards) of stator winding turns under normal and abnormal supply voltage condition. The proposed method can be used, with other techniques, to increase the reliability of the diagnosis system.

Keywords: (Fuzzy Inference system, Fault diagnosis, Induction motor faults, inter-turn short circuit, symmetrical components)

1. Introduction.

Induction motors are the most popularly and most widely used electrical machines, because of their relatively low manufacturing cost, robust construction and ease of control. It have dominated the field of electromechanical energy conversion by having 80% of the motors in use [Wan, 2001]. In fact, induction motors are the critical component of many industrial processes. They are often used in hostile environments and sensitive applications such as nuclear plants, aerospace and military applications, where the reliability must be at high standard. Although induction motors are reliable, they may encounter several failures due to

operating conditions. These failures of the induction motors may lead to harmful consequences such as: additional maintenance costs and unscheduled downtimes that result in lost production and financial income. In order to reduce these consequences and preventing occurrence of the catastrophic fault, on-line condition monitoring and fault diagnosis techniques are used. In recent years, the condition monitoring and fault diagnosis of the induction motors have moved from conventional techniques toward artificia intelligent (AI) techniques, which have many advantages. When AI techniques are used, fault diagnosis can be achieved without an expert human. In addition, on-line diagnosis processes can be fully automated [Saied, 2006].

In general, induction machine failure surveys have found the most common failure mechanisms in three-phase induction machines as shown in Figure 1. It can be categorized according to the main components of machine, stator related faults, rotor related faults, bearing related faults and other faults [Thomson, 2001]. In fact, about 38% of all reported induction machine failures fall in to stator faults category. The incipient of stator winding faults, in its early stage, is often due to insulation breakdown between two adjacent turns in a coil for the same phase; this is called a turn-to-turn or inter–turn short circuit fault. Therefore, this type of fault will produce an extra heat, and imbalance in magnetic filed of the machine. The local extra heat between two shorted turns or more will cause further damage to the neighbor turns insulation until occurrence a catastrophic failure, such as phase failures, phase to phase failures, phase to ground failures , or phase to phase to ground failures.

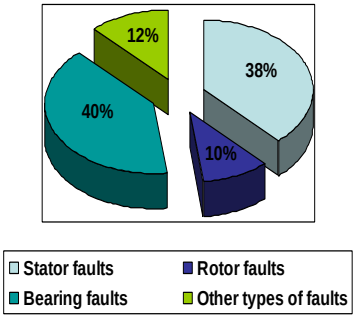

Figure 1: General classification of three phase induction motor faults

2. Condition monitoring based on symmetrical components techniques.

For a three-phase induction motor the symmetrical component technique is used to analyze the unbalance in machine circuit, supply voltages or/and currents by converting the unbalance system to three balance system called positive sequence, negative sequence and zero sequence. The positive sequence components (V_{A1},V_{B1},V_{C1}) have equal magnitudes and are displaced by 120^o with vector relation A-B-C. The negative sequence components (V_{A2},V_{B2},V_{C2}) also have equal magnitudes and phase displacement by 120^o, but out of phase rotation is C-B-A. Zero sequence components (V_{A0},V_{B0},V_{C0}) have equal magnitudes with no phases displacement. The phase value is the vector of its positive, negative, and zero sequence components as expressed in the following equations.

$$\left.\begin{aligned}\vec{V}_A &= \vec{V}_{Ao}+\vec{V}_{A1}+\vec{V}_{A2}\\ \vec{V}_B &= \vec{V}_{Bo}+\vec{V}_{B1}+\vec{V}_{B2}\\ \vec{V}_C &= \vec{V}_{Co}+\vec{V}_{C1}+\vec{V}_{C2}\end{aligned}\right\} \quad \ldots\ldots (1)$$

Where the magnitudes of the symmetrical components are equal and therefore they are as follows*:*

$$\left|\vec{V}_{A1}\right| = \left|\vec{V}_{B1}\right| = \left|\vec{V}_{C1}\right| = V_1$$

$$\left|\vec{V}_{A2}\right| = \left|\vec{V}_{B2}\right| = \left|\vec{V}_{C2}\right| = V_2 \qquad \ldots.(2)$$

$$\left|\vec{V}_{A0}\right| = \left|\vec{V}_{B0}\right| = \left|\vec{V}_{C0}\right| = V_0$$

The above equations are also true for current by replacing I instead of V. Also these equations can be simplified by making proper substitutions, as follows:-

$$\begin{vmatrix}\vec{V}_A\\ \vec{V}_B\\ \vec{V}_C\end{vmatrix} = \begin{vmatrix}1 & 1 & 1\\ 1 & a^2 & a\\ 1 & a & a^2\end{vmatrix} \begin{vmatrix}\vec{V}_{Ao}\\ \vec{V}_{A1}\\ \vec{V}_{A2}\end{vmatrix} \quad \ldots(3)$$

Where :

$$a = e^{j120} = -0.5 + j0.866$$

$$a^2 = e^{j240} = -0.5 - j0.866$$

The sequence components can be obtained by solving the last matrix and become as:

$$\begin{vmatrix}\vec{V}_{Ao}\\ \vec{V}_{A1}\\ \vec{V}_{A2}\end{vmatrix} = \frac{1}{3}\begin{vmatrix}1 & 1 & 1\\ 1 & a & a^2\\ 1 & a^2 & a\end{vmatrix} \begin{vmatrix}\vec{V}_A\\ \vec{V}_B\\ \vec{V}_C\end{vmatrix} \qquad \ldots.(4)$$

Thus, if the three-phase voltages and currents are known, then the symmetrical components can be calculated. Generally, the presence of a negative sequence component indicates some level of unbalance. The magnitude of this unbalance is usually represented as a percent of unbalance based on the positive sequence value. Therefore, the voltages unbalance factor (*UV*) and current unbalance factor (*UI*) given as shown below [Kohler, 2002]:

$$UV = \frac{V_2}{V_1} * 100\% \quad \ldots (5)$$

$$UI = \frac{I_2}{I_1} * 100\% \ \ldots (6)$$

While the existence of a zero-sequence component indicates some level of neutral

current flowing during line-to-ground fault.

On the other hand, if the stator circuits are not symmetrical, and are connected to a symmetrical voltage supply, the stator currents will be unbalanced. In this case each phase can exhibit a different impedance to each current sequence. Because of the neutral point of a wye-connected induction motor is normally not grounded, or the motor is delta connected, therefore only positive and negative sequence impedances are existed, while the zero sequence impedance is not presented.

Since induction motor normally operates at slip less than 5 percent, therefore the negative sequence impedance of the induction motor is much less than the positive sequence impedance. Consequently, a low level of negative sequence voltage will produce a high level of negative sequence current relatively. For induction motor fault detection based on negative sequence current monitoring, the last point is considered a significant problem. The negative sequence current will change with changing of the supply unbalance percentage due to switching of single-phase loads or for other reasons unrelated to incipient failure in the motor. However, it is well known that the machine deterioration in its early stages produces small levels of negative sequence current. Therefore, more than one source changes the negative sequence current level. The last reason makes using of this technique alone an unreliable tool [Sottile, 2002].

3. Inter-turn short circuit Diagnosis Based On Fuzzy Inference System.

In order to overcome the weak point of using negative sequence current monitoring alone and to automate the diagnosis processes , a diagnosis system of inter-turn short circuit fault of the induction motor stator circuit is proposed and implemented in this study by utilizing Mamadani-type fuzzy inference system. The magnitude of the voltage unbalance percentage, UV% and current unbalance percentage, UI%, are defined as input variables for the Fuzzy based diagnosis system. They are first of all "fuzzified" and translated in the interval [0,2.5]for the first input, UV%, and [0,10] for the second input, UI% . The input variables are assigned the names UV and UI. Trapezoidal Fuzzy membership functions are defined to handle the input variables as illustrated in the Figures 2a and 2b. The limits of each function are adjusted based on the behavior of the input variables UV and UI determined experimentally by symmetrical components analysis for both machine voltages and currents as illustrated in the next section.

The linguistic values for the first input set, UV, are defined as being: zero(ZE), very low (VL), low (LO), medium (ME), high (HI), and very high (VH). While the linguistic values for the second input set, UI, are defined as : zero(ZE), very low (VL), low (LO), high low (HL), medium (ME), high (HI), high high (HH), very high (VH), and X high (XH), XXhigh (XXH).

In terms of Fuzzy terminology, the variables UV and UI are the antecedent (input variables) and the number of stator shorted turn is the consequent (output variable). The latter is associated to nine membership functions which map the output of the following Fuzzy set (linguistic values): healthy or zero turn defected (ZE), three turns defected (3TURN), five turns

defected (5TURN), nine turns defected(9TURN),thirteen turns defected (13TURN), seventeen turns defected (17TURN), twenty two turns defected (22TURN), twenty seven turns defected (27TURN), thirty or more turns defected (30TURN). The linguistic fuzzy relation rules between the input and the output fuzzy sets are described in Table 1. Sixty rules are deduced for this application according to our knowledge base and experience from the practical simulation of the inter-turn short circuit faults as described lately in the previous section.

Trapezoidal membership functions are also defined for the output variable (Short_Turn) as can be seen in Figure 2c. The output range for this variable is defined between the ranges [0-30]. A three-dimension plot for output variable (Short_Turn) at different input fuzzy sets is shown in Figure 3. For the defuzzification process of this system, the Centroid method is used.

4. Experimental Verification.

An automatic computerized on-line monitoring system is developed to acquire motor line voltages and currents. Firstly, a three-phase 1.1 Kw, 380 V, 50 Hz squirrel cage type induction motor is re-wounded such that many taps are obtained, in order to perform many deliberately different fault conditions. The rewinding motor specifications are listed in Appendix A. However, the motor is considered as a model to study and analyze the motor performance under stator inter-turn short circuit faults. After that, the motor is connected to three-phase variable voltage supply, then the three-phase voltages and currents are sampled, acquired, and recorded by using data acquisition card type Advantech PCI-1710 . A computer function is written in MATLAB programming language and used to compute the RMS magnitude and phase angle for each phase voltage and current signal. Another computer function is written to receive the calculated values from the first function in order to deduce the symmetrical components for both voltages and currents.

However, several tests are performed on the model by shorting different number of turns. Table 2 shows sample of these tests and their corresponding voltage unbalance percentages, UV%, and current unbalance percentage, UI%. The calculated values of UV% and UI%, are fed as input variables for the proposed fuzzy system. The output results of this system are compared with the corresponding database, which obtained experimentally. Figure 4 shows an example sample of, sixty rules with their membership functions at values of the input variables, (UV%=0.19 and UI%=1.56). The output defuzzified value is the number of defected inter-turn (Short_Turn≈3).

The input values of the Fuzzy systems can be seen in the second and third column of Table 2 and corresponding values for the output variable Short_Turn are shown in the fourth column. The associated linguistic values are in the fifth column of this Table. In this connection, it is clear that the value of (UI) for the normal case is relatively somewhat high (UI=1.1) although the value of the UV is low, i.e. the supply voltage is balanced; this is due to some asymmetry in the stator winding as a result of the manual re-winding of the machine. From the results shown in table 2, it is clear that the proposed FIS is effectively detected the low-level deterioration (approximately of 0.5% and upwards) of stator winding turns per phase under normal and abnormal supply voltage condition. The proposed method can be

used, with other techniques, to increase the reliability of the diagnosis system.

4. Conclusion.

From these results, it can be concluded that the proposed Fuzzy system based on the voltage unbalanced percentage and current unbalanced percentage can be considered an acceptable reliable diagnosis tool for the inter-turn fault detection and its severity evaluation. The proposed FIS is effectively detected the low-level deterioration (approximately 0.5% and upwards) of total stator winding turns per phase. The system take into account the current unbalance due to supply voltage unbalance problem, and the current unbalance due to deterioration in the stator windings. The presented method can be used, with other techniques such as park vector approach, effective negative impedance and motor current signature analysis (MCSA), to increase the reliability of the diagnosis system. Diagnosis based on FIS is automated and on-line decision compared with conventional approaches, which need to a person operates the diagnosis and detection processes and who is very well aware of different kinds of faults occurring in the machine. The practical results show using FIS technique, accurate decision for evaluating number of inter-turn short circuit, which is difficult to be perform with other techniques. It is clear that the error in evaluation of the number of defective turns is less than (0.5 turn) for the worst case, which is considered a reasonable error.

5. References

J.Kohler, J. Sottile, and F. Trutt, 2002 "Condition monitoring of stator windings in induction motors: part I-Experimental investigation of the effective negative-sequence impedance detector" IEEE Transactions on Industry Applications, VOL. 38, NO. 5, pp.1447-1453.

B. M. Saied , and Y. M. Y. Ameen, 2006 " Artificial Neural Networks for Three-Phase Induction Motor Fault Detection and Diagnosis Using Stator Current Concordia Pattern" Sixth International Philadelphia Engineering Conference (IPEC) on Computational Aspects and Their Applications in Electrical Engineering, September 19-21,2006,Amman, Jordan.

J. Sottile, F. Trutt, and J. Kohler, 2002. "Condition monitoring of stator windings in induction motors: part II-Experimental investigation of voltage mismatch detectors", IEEE Transactions on Industry Applications, VOL. 38, NO. 5, pp. 1454-1459.

W. T. Thomson, and M. Fenger, 2001 "Current signature analysis to detectinduction motor faults", IEEE Industry Applications magazine, pp.26-34.

T. W. Wan, and H. Hong, 2001 "An on-line neuro-fuzzy approach for detecting faults in induction motors", Electrical Machine Drives Conference, IEMDC 2001, Cambridge, MA, pp.878-883.

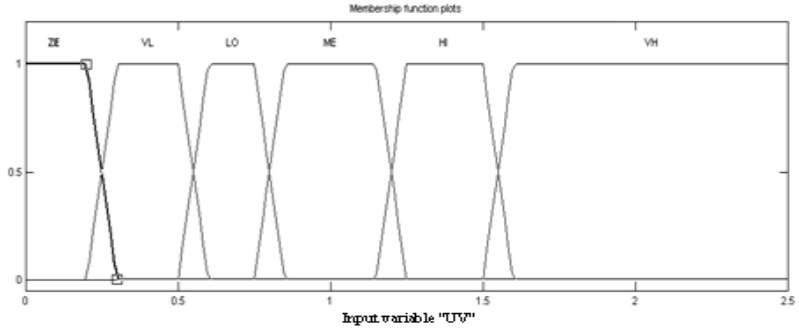

(a)

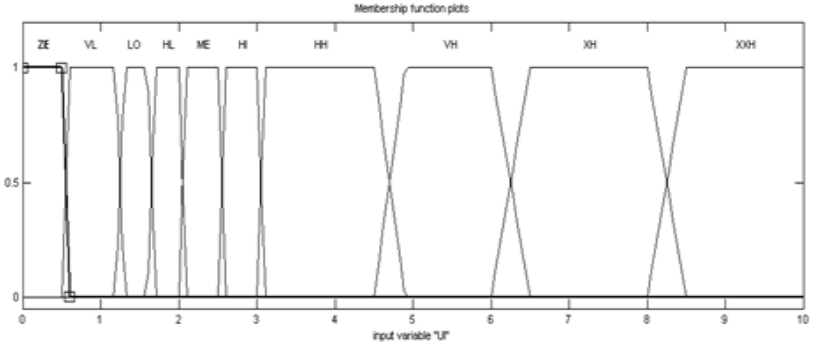

(b)

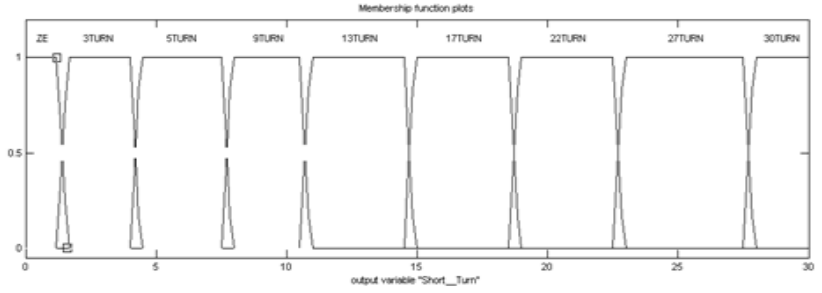

(c)

Figure 2: Membership functions. (a): for the first input (UV) .
(b) for the second input (UI) .
(c) for the output variable (Short_Turn).

Table 1: The linguistic fuzzy relation rules between the input and the output fuzzy sets

No.	Inputs		Output
	Voltage unbalance percentage(UV %)	Current unbalance percentage (UI%)	No. Of deffected turns(Short_Turn)
1,2	ZE	ZE,VL	ZE
3	ZE	LO	3 Turn
4	ZE	HL	5 Turn
5	ZE	ME	9 Turn
6	ZE	HI	13 Turn
7	ZE	HH	17 Turn
8	ZE	VH	22 Turn
9	ZE	XH	27 Turn
10	ZE	XXH	30 Turn
11-13	VL	ZE,VL,Lo	ZE
14	VL	HL	3 Turn
15	VL	ME	5 Turn
16	VL	HI	9 Turn
17	VL	HH	13 Turn
18	VL	VH	17 Turn
19	VL	XH	22 Turn
20	VL	XXH	27 Turn
21-25	LO	ZE,VL,LO,HL,ME	ZE
26	LO	HI	3 Turn
27	LO	HH	5 Turn
28	LO	VH	9 Turn
29	LO	XH	13 Turn
30	LO	XXH	17 Turn
31-36	ME	ZE,VL,LO,HL,ME,HI	ZE
37	ME	HH	3 Turn
38	ME	VH	5 Turn
39	ME	XH	9 Turn
40	ME	XXH	13 Turn
41-47	HI	ZE,VL,LO,HL,ME,HI, HH	ZE
48	HI	VH	3 Turn
49	HI	XH	5 Turn
50	HI	XXH	9 Turn
51-58	VH	ZE,VL,LO,HL,ME,HI, HH,VH	ZE
59	VH	XH	3 Turn
60	VH	XXH	5 Turn

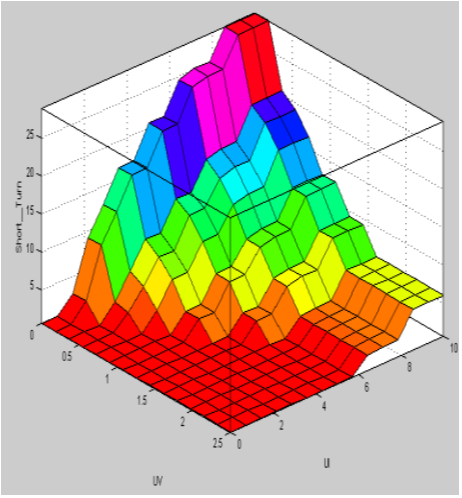

Figure 3: Three dimension plot for Short_Turn output with

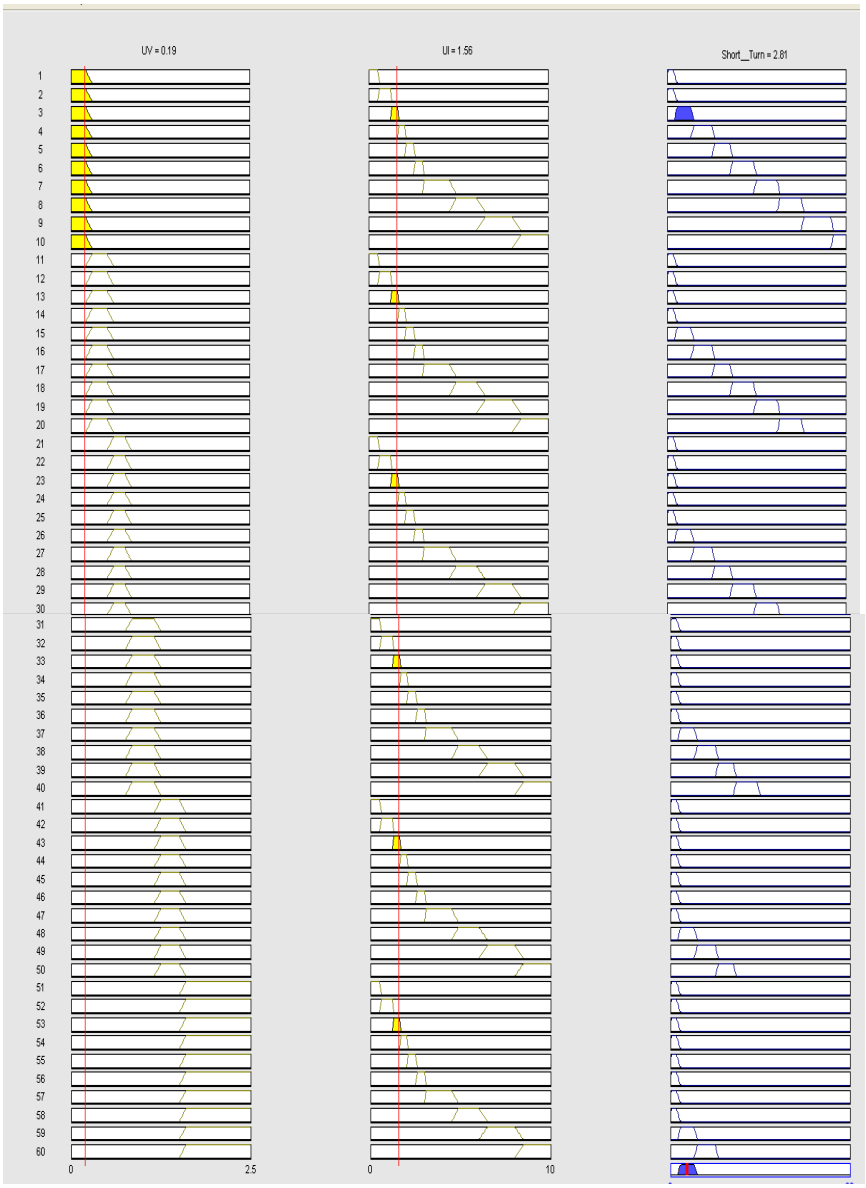

Figure 4: Rules and memberships distribution for certain inputs.

Table 2: Input and out put values for the proposed fuzzy based diagnosis system for inter turn short circuit

Actual condition	**Input**		**Output**	
	UV	UI	Short_Turn	Diagnosis condition
Health (No defected turn)	0.18	1.10	0.48	No defected Turn
3 Turn defected	0.19	1.56	2.81	3 Turn defected
5 Turn defected	0.22	1.7	5.44	5 Turn defected
9 Turn defected	0.15	2.25	9.22	9 Turn defected
13 Turn defected	0.18	2.95	12.70	13 Turn defected
17 Turn defected	0.21	3.66	16.52	17 Turn defected
22 Turn defected	0.21	5.84	21.3	21 Turn defected
27 Turn defected	0.16	7.29	26.2	26 Turn defected
30 Turn defected	0.23	9.10	29.3	29 Turn defected

Appendix A
Specification of the Inter-Turn Short Circuit Induction Motor Model

Manufacture: Siemens.

Input Voltage 3-phase 380V.

Delta Connected Connection.

Full load Current =2.8A.

Supply Frequency= 50Hz.

No. of Poles = 4 pole.

Rated speed = 1410RPM.

Rated Motor Power =1.1Kw.

No. of Stator Slots =36 slot.

No. Rotor Slots= 28 bars.

Back Motor Bearing: A6004.

No. of Turns per Slot=100 turn.

Turns per phase=600 turn

Figure A.1: Top and Front view of the inter-turn short circuit induction motor model (different taps)

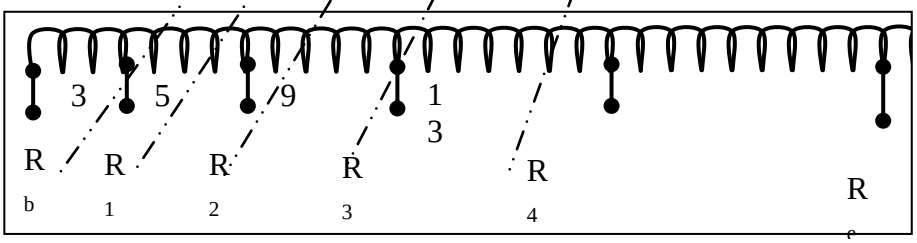

Figure A.2: The taps terminals of the phase R turns

Flux–Weakening Operation for Electric and Hybrid-Electric Vehicle Propulsion System

[*]Aiman Nouh
aimannouh@hotmail.com

[*]Faisal A. Mohamed
elabdli@hotmail.com

[*] Omar Al-Mukhtar University , Faculty of Engineering – El-Baida – Libya

Abstract—The electric propulsion is considered as a promising technology because it allows proposing a solution technically feasible and economically viable. This technology appears in three main groups of Electric Vehicles (EV): Battery Electric Vehicles (BEV), Fuel Cell Electric Vehicles (FCEV) and Hybrid Electric Vehicles (HEV). These types of vehicles require extended-speed, constant-power operation from the propulsion system (Flux-weakening operation). This paper investigates, in first time, the analysis of this phenomenon for the permanent magnet motor. And in the second time, it proposes a structure of rotor, adapted to this type of operation, using Flux2D software.

Keywords—electric vehicle, hybrid electric vehicle, motor drives, permanent magnet motors, flux weakening, extended speed, constant- power, Flux2D software.

I. INTRODUCTION

Environmental and economical issues are the major driving force in developing electric vehicles for urban transportation [1][2]. The exhaust emissions of the conventional internal combustion engine (ICE) vehicles are the major source of urban pollution that causes the greenhouse effect leading to global warming [1].

In this paper, firstly, we analyze the phenomenon of flux weakening by presenting a theoretical study which will enable us to know the various parameters, the various limits of operation. Then, by using the Flux2D software, two structures of motor have been done. The first describes a structure of bicycle motor which we know its parameters. The second comprises modifications with an aim of having a correct operation in mode of demagnetization.

Finally, we give the results obtained by comparing the two studied motors and by showing the influence of the parameters on the flux density and torque.

II. MOTOR RATING AND DESIGN

The tractive force (F_T) in an electric vehicle is supplied by the electric motor in overcoming the road load (F_R) [1][8]. The equation of motion is given by

$$k_m m \frac{dv_x}{dt} = F_T - F_R \qquad (1)$$

Where k_m is the rotational inertia coefficient and it has typical value between 1.08 and 1.1 dimensionless. $\frac{dv_x}{dt}$ is the acceleration of vehicle.

The desired power rating of the electric motor can be calculated from the above equations based on the system constraints of initial acceleration, vehicle rated velocity and vehicle maximum velocity. The desired torque at the wheels of the vehicle can be obtained from the power relation:

$$Power = T_T \omega_{wh} = F_T v_x \qquad (2)$$

Where T_T is the tractive torque in (N.m) and ω_{wh} is the angular velocity of the wheel in (m/sec). The angular velocity and the vehicle speed related by

$$v_x = \omega_{wh} r_{wh} \qquad (3)$$

Where r_{wh} is the radius of the wheel in meters.

The torque-speed profile of an electric motor has three regions; constant torque, constant power and natural characteristics regions as shown in figure 1. The constant torque region extends up to the rated or base speed of the motor when the rated power condition of the motor is reached. The constant power region is the field weakening region that helps extend the operating speed of the motor beyond its rated speed. The motor fails to maintain the rated power beyond this region and the speed drops according to the natural characteristics of the motor [3][6][7]. A good efficiency in the field weakening region is of extreme importance in electric vehicles.

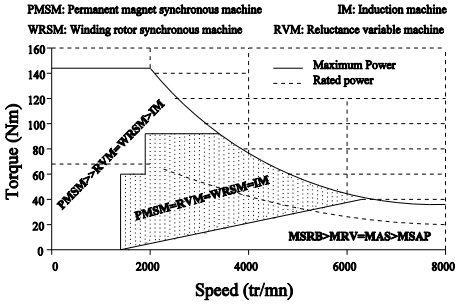

FIG. 1: Torque-Speed curve

The advantages of permanent magnet synchronous motor (PMSM) compare to other types of motor are high and constant torque even at stillstand, higher efficiency and better cooling conditions resulted from very low rotor losses; the main drawback is the relatively high cost [5]. Nowadays, due to the continuously reduction of the prices of PMSM's and theirs easier control algorithms especially in low speed range, this type of the motor is more and more popular in several vehicle applications of very wide power range [9][10].

III. FLUX-WEAKENING

In order to modeling the PMSM, the machine equations in the rotor reference frame are used. The flux, current and voltage equations of the PMSM model may be written shortly in space vector notation as [4][8]:

$$\lambda_d = L_d i_d + \lambda_m \qquad (4)$$

$$\lambda_q = L_q i_q \qquad (5)$$

$$i_{dq} = i_d + j i_q = i_{dq} \exp(j\Theta_e) \qquad (6)$$

$$v_{dq} = v_d + j v_q = v_{dq} \exp(j\Theta_e) \qquad (7)$$

$$v_d = R_s i_d + \frac{d\lambda_d}{dt} - \omega_s \lambda_q \qquad (8)$$

$$v_q = R_s i_q + \frac{d\lambda_q}{dt} + \omega_s \lambda_d \quad (9)$$

Where i_d, i_q, v_d, v_q, L_d, L_q, λ_d and λ_q are the d-, q-axis components of the stator current, voltage, inductance and flux linkages, respectively, λ_m is the flux linkage due to the rotor magnets linking the stator, R is the stator resistance, ω_s and Θ_e are the electrical angular velocity and the electrical angle of rotor position.

The electric torque equation of the PMSM, neglecting the damping effect, is:

$$T_e = \frac{3p}{2}[\lambda_m i_q - (L_q - L_d) i_d i_q] \quad (10)$$

Where p is the number of pole pairs.

For operation above the base speed, the air-gap flux is weakened by the demagnetizing effect due to the d-axis armature reaction [1][9].

There are constraints when a PMSM is fed through an inverter. These constraints can be expressed as [8]:

$$i_s = \sqrt{i_d^2 + i_q^2} \le I_{\max} \quad (11)$$

$$v_s = \sqrt{v_d^2 + v_q^2} \le V_{\max} \quad (12)$$

Where $I_{\max}$ and $V_{\max}$ are the available current and voltage of the inverter and motor.

IV. DESIGN WITH FLUX2D

Flux2D is a computer program to analyze and design of devices, based on the finite elements method. It treats the magnetic, electric or thermal states. These states give access to many global or local variables as like field, flux, potential, energy, force, etc.

In this section, two PMSMs have been integrated in the Flux2D software. The first is a reversed structure bicycle motor (the rotor is external). Its rotor magnets are surface mounted and radial flux as shown in figure 2.

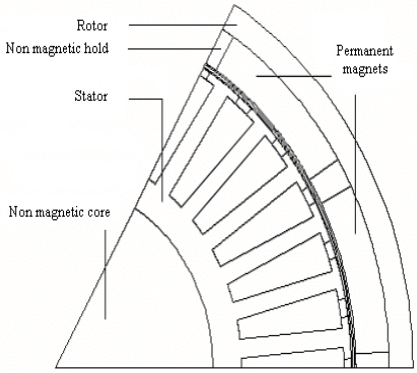

FIG. 2: The bicycle motor

This contribution proposes some modifications on the bicycle motor to obtain a second motor. The modified motor has a structure very close to that of the bicycle motor. Figure 3 shows this new structure.

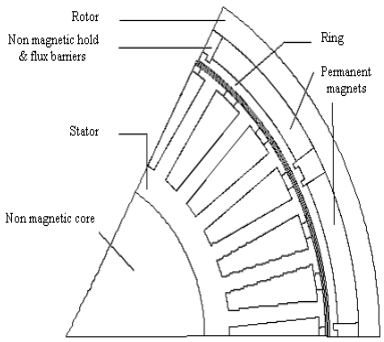

FIG.3: The modified PMSM

We preserved the diameters of the rotor and stator cylinder. The thickness of magnet was decreased. We added barriers of flux between the magnets and a magnetic ring following the same principle adopted by [8]. The thickness of the air-gap did not change and the material used for the ring is identical to that of the rotor cylinder.

These modifications make it possible to reduce the resulting flux by applying a current i_d, to increase the value of reactance X_d, and to have a ratio of (L_q/L_d) lower than one, therefore a good power-factor, a relative sufficient armature reaction and finally to protect the magnets against demagnetization.

V. RESULTS AND DISCUSSION

In order to execute the simulation under Flux2D, some steps should be done before. These steps are geometry description, circuit description, mesh realization, physical properties, and parameters definition [11].

Figures 4 and 5 show a comparison of flux lines between the bicycle motor and the modified motor. The new structure has flux lines less than the bicycle motor at the teeth level.

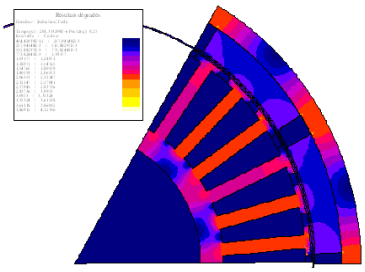

FIG. 6: Flux density bicycle motor

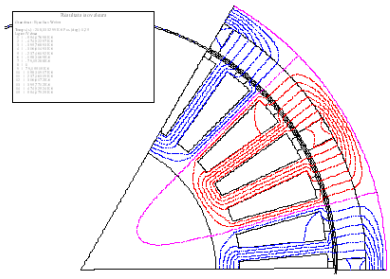

FIG. 4: Flux lines – bicycle motor

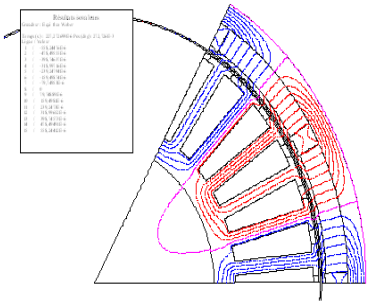

FIG. 5: Flux lines – modified motor

Figures 6 and 7 illustrate a comparison of flux density between the two motors. The modified motor is less saturated but the thickness of magnet is lower a millimetre (thickness of magnetic ring).

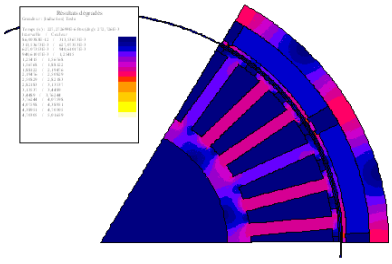

FIG. 7: Flux density - modified motor

We can observe the influence of stator teeth on the values of flux density in the air-gap as shown in figures 7 and 8. Where (h_a) is

the thickness of magnet and (ent.) is the air gap length. The shape of flux density curve depends on the relative position of the rotor compared to the stator.

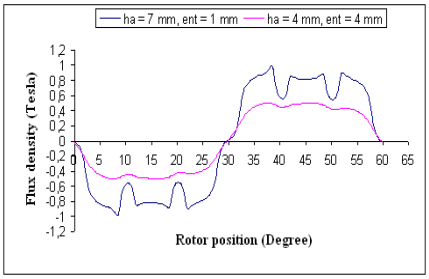

FIG. 8: Flux density - bicycle motor

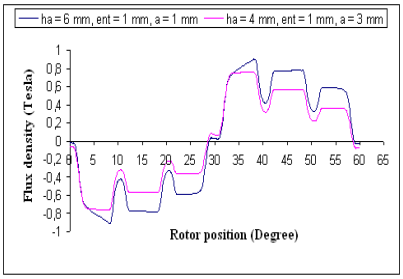

FIG. 9: Flux density - modified motor

The static torque depends directly on the structure of the motor but also on the dimensioning and the energy supply [12]. Figures 9 and 10 present a comparison of the variation of the static torque according to the rotor position at rated current and with various values of magnet thickness.

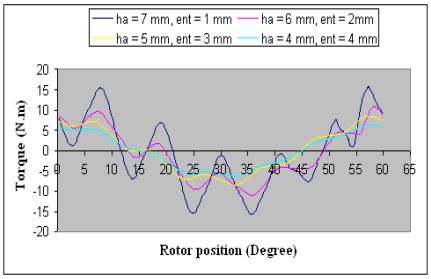

FIG. 10: Torque - bicycle motor

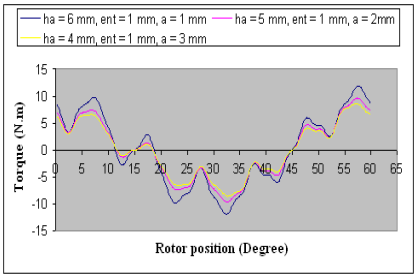

FIG. 11: Torque - modified motor

Figure 11 shows the variation of inductance according to the position of the rotor for the bicycle motor. We can see that this structure has an inductance not depending on the position of the rotor (the inductance of the d-axis is equal to the inductance of q-axis).

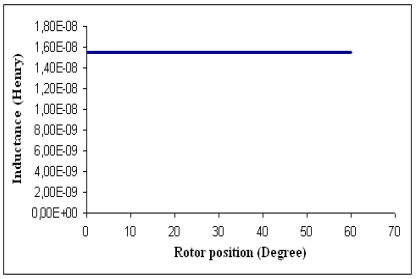

FIG. 12: Inductance - bicycle motor

The inductance of the modified motor depends on the rotor position as shown in figure 12. This enables us to make the flux weakening operation. It was not the case with the first motor.

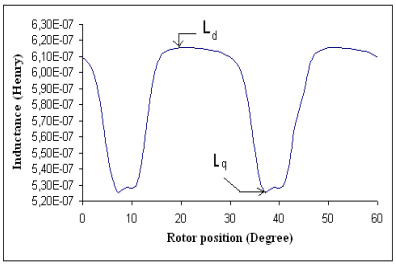

FIG. 13: Inductance - modified motor

VI. CONCLUSION

The flux weakening operation of the permanent magnet synchronous motor was very interesting because it touches all the fields of electrical engineering as well the study of the machines as the study of the speed variation using power electronics.
In this paper, we have limited our study to simulation by using Flux2D only. Cost involved in design, development and control of motors with extended speed operation was not considered in this paper.

VII. REFERENCES

[1] I. Husain, Electric and Hybrid Vehicles: Design Fundamentals, CRC Press, 2003.

[2] C. C. Chan, K. T. Chau, Modern Electric Vehicle Technology, Oxford University Press, 2001.

[3] T.M.Jahns, Flux-Weakening Regime Operation of an Interior Permanent Magnet Synchronous Motor Drive. IEEE Trans. on I.A., Vol.IA-23.N°4, pp.681-689 July / Aug. 1987.

[4] S. Morimoto, Y. Takeda, T. Hirasa, K. Taniguchi, Expansion of Operating Limits for Permanent Magnet Motor by Current Vector Control Considering Inverter Capacity. IEEE Trans on I.A., Vol.26, N°5, pp. 866-871 Sept. / Oct. 1990.

[5] Z. Q. Zhu, D.Howe, Instantaneous magnetic field distribution in permanent magnet brushless dc motors, part III: effect of stator slotting. IEEE Transactions on magnetics, Vol. 29, no. 1, January 1993.

[6] W. L. Soong, T. J. E. Miller, Practical Field-Weakening performance of the Five Classes of Brushless Synchronous AC Motor Drive. EPE Brighton, Vol. 5, pp.303-310. 13-16 September 1993.

[7] H. Yin, J. M. Lin, Z. JIN, Comparison on Characteristics of PMSMs with Different Parameters. For Flux – Weakening Operation. Conf. ICEM, Vol 2, pp.1-5. Paris, Sept. 1994.

[8] L.Xu, L.Ye, L.Zhen, A.EL-Antably, A New Design Concept of Permanent Magnet Machine for Flux Weakening Operation. IEEE. Transaction on Industry Applications Vol. 31, Issue 2, pp. 373-378. March/April 1995.

[9] A. Ackva, A. Binder, K. Greubel, B. Piepenbreier. Electric Vehicle Drive with Surface-Mounted Magnets for Wide Field-Weakening Range. Proceedings of 7th European Conference on Power Electronics and Applications EPE'97, Trondheim 1997.

[10] N. Bianchi, S. Bolognani, M. Zigliotto. High Performance PM Synchronous Motor Drive for an Electerical Scooter. IEEE Trans. On Industry Applications, Vol. 37, No. 5, 2001.

[11] Flux2D, Version 7.50, Notice d'utilisation générale. CEDRAT, 10 Chemin de Pré Carré – Zirst, 38246 MEYLAN Cedex France. Septembre 2000.

[12] A. N'DIAYE, C. ESPANET, A. MIRAOUI, J.M. KAUFFMANN. "Torque ripple reduction of PM motors through an optimal feeding". Modeling Identification and Control, Proceedings, Vol.1, pp. 113 – 118. February 2001.

Harmonic distortion phenomena related to power electronic Loads in Distribution System

Abdul wahab Ibrahim Naser
7th April University- Faculty of Engineering- Electronic & Electrical Engineering Department

Abstract

All business types, commercial, industrial, goverment and energy / utility have a concern with power quality. The reliable and continuos delivery of " expected quality" electricity is critical for proper daily operations.from a manufacturing facility to a brokerage frim, the need for utility grade or better power exisits.Further , with more digital technologies instaled on the load,"highnine" type power requirerments keep increasing . Environments in harmonic content can place serious burdens on power distribution systemes and the equipments to which it is connected. The problem of harmonics penetration in Libyan local distribution systems has been significantly growing during the last few years due to increased of nonlinear loads, such as arc furnaces, static power convertors, electronic rectifiers and inverters, (include computers, adjustable speed drives, and UPS systemes, TV's ,Video recorders, Printers, Micro wave ovens, etc.) which generate harmonic currents that may produce excessive harmonic distortion on the supply system.

An assessment of the harmonic found in office distribution systems such Dat Elemad complex(in Tripoli capital) as a case study yielded sevreal conclusions useful in power quality and in the design of electrical distribution systems Spcially power factor. This paper describes the status of new source casuing harmonic distortion through the uitilites distribution system and consumers. Measurements on several of power common coupling (PCC) at several substations of GECOL (General Electrical Company Of Libya) supplying the complex has been caried out to determine significant amounts of harmonic currents or voltages existed in the distribution system. Subsequent calculations and load profile analysis for the case study appeared sigificant levels of harmonics, power analyser used to record waveforms and give the magnitude of harmonics compeared with (IEC) standrads, harmonic mitigation has been pointed out thertically to decrease the impacts.

Key words – harmonic sources, standrads, limits, harmonic analysis, harmonic mitigation.

1. Introduction

The Important items of Harmonic distortion phenomena.

- ***Harmonic*** : *Is a sinusoidal component* of periodic wave which has a frequency that is an integral multiple of the fundamental frequency " Figure (1.1) .To the electrical engineer, harmonics are voltages and currents, which appear on the electrical system at frequencies that are integral multiples of the generated frequency

$$h = n\,p \pm 1 \quad ,,, \quad I_h = \frac{I_l}{h}$$

Where :

h : Harmonic order **,** I_h : Harmonic current . ***P*** : Number of pulses or rectifires **„**

I_l: Load current

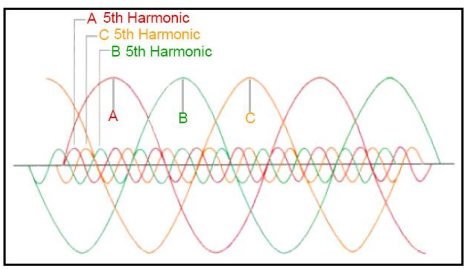

Fig(1.1) shape of a distorted wave

- **Inter-Harmonic:** " Between the harmonics of the power frequency voltage and current, further frequencies can be observed which are not an integer of the fundamental **".**
- **-Total Harmonic Distortion (THD),** " Is the RMS values of individual harmonic currents, voltages expressed as a percentage of the fundamental RMS current , voltage **".**

$$THD\ \% = \frac{\sqrt{\sum_{h=2}^{h=\infty} (M_h)^2}}{M_{fundamental}} \times 100\ \%$$

2.Impactes of harmonic distortion

Harmonics can lead to power system inefficiency. Some of the negative ways that harmonics may affect plant equipment are listed as:

1-Conductor Overheating: a function of the square rms current per unit volume of the conductor. Harmonic currents on undersized conductors or cables can cause a "skin effect", which increases with frequency and is similar to a centrifugal force. **2.Capacitors:** can be affected by heat rise increases due to power loss and reduced

b- Power system harmonic model

life on the capacitors. If a capacitor is tuned to one of the characteristic harmonics such as the 5th or 7th, overvoltage and resonance can cause dielectric failure or rupture the capacitor.

3.Fuses and Circuit Breakers: harmonics can cause false or spurious operations and trips, damaging or blowing components for no apparent reason.

4.Transformers: have increased iron and copper losses or eddy currents due to stray flux losses. This causes excessive overheating in the transformer windings. Typically, the use of appropriate "K factor" rated units are recommended for non-linear loads.

5.Generators: have similar problems to transformers. Sizing and coordination is critical to the operation of the voltage regulator and controls. Excessive harmonic voltage distortion will cause multiple zero crossings of the current waveform.
Multiple zero crossings affect the timing of the voltage regulator, causing interference and operation instability.
6.Utility Meters: may record measurements incorrectly, resulting in higher billings to consumers.
7.Drives/Power Supplies: can be affected by misoperation due to multiple zero crossings. Harmonics can cause failure of the commutation circuits, found in DC drives and AC drives with silicon controlled rectifiers (SCRs).
8.Computers/Telephones: may experience interference or failures.**[** Bulletin No. 8803PD9402, August, 1994]

3- Power factor implementation.

Voltage and current harmonics produced by nonlinear loads increase power losses, and therefore have a negative impact on electric utility distribution systems and the exact components.

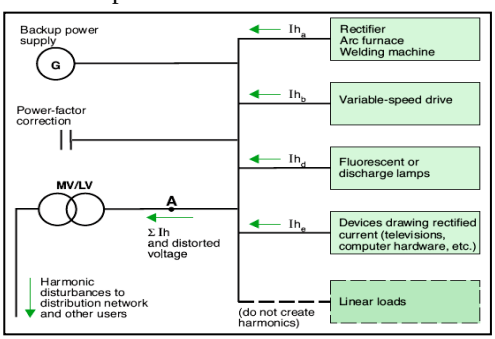

a-Flow of harmonic currents in a distribution network

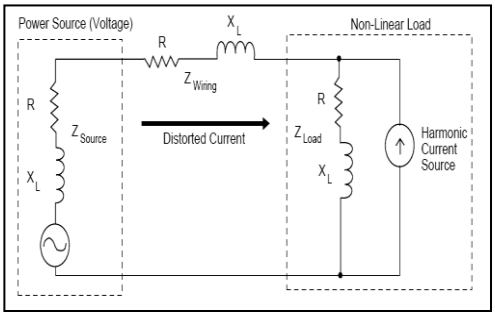

b - non-linear load and power supply modeling

While relationship between harmonics and losses is very complex and difficult to generalize, the well established concept of power factor does provide some measure of the relationship, and it is useful when comparing the relative impacts of nonlinear loads–providing that harmonics are incorporated into the power factor definition. The power factor in sinusoidal situations could be explained as the concept of power factor originated from the need to quantify how efficiently a load utilizes the current that it draws from an AC power system. Consider, for example, the ideal sinusoidal situation shown in Figure (3-1)[4].

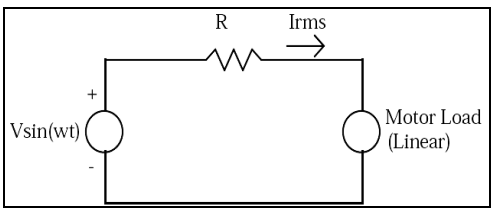

Fig.(3-1) *Power System with Linear Load*

The voltage and current at the l

$v(t) = V_1 \sin(\omega_o t + \partial_1$ …… (3-1)

$i(t) = I_1 \sin(\omega_o t + \theta_1)$ ……...(3-2)

Where:

V_1: peak values of the 50/60 Hz voltage.

I_1: peak values of the 50/60 Hz current.

∂_1 : relative phase angle.

θ_1 :relative phase angle.

The true power factor at the load is defined as the ratio of average power to apparent power, or:

$$PF_{true} = \frac{P_{avg}}{S} = \frac{P_{avg}}{V_{rms} I_{rms}} \quad \text{..... (3-3)}$$

For the purely sinusoidal case, (3-3) becomes:

$$PF_{true} = PF_{disp} = \frac{P_{avg}}{\sqrt{P^2 + Q^2}} = \frac{\frac{V_1}{\sqrt{2}} \frac{I}{\sqrt{2}}}{\frac{V_1}{\sqrt{2}} \frac{I}{\sqrt{2}_1}} \cos(\delta_1 - \theta_1) = \cos(\partial_1 - \theta_1) \quad (3\text{-}4)$$

Where:

PF_{disp} **:** displacement power factor.

$(\partial_1 - \theta_1)$**:** power factor angle**.**

Therefore, in sinusoidal situations, there is only one power factor because true power factor and displacement power factor are equal[4]. For sinusoidal situations, unity power factor corresponds to zero reactive power Q, and low power factors correspond to high Q. Since most loads consume reactive power, low power factors in sinusoidal systems can be corrected by simply adding shunt capacitors.

Now, consider nonsinusoidal situations as shown in figure (3-2), where network voltages and currents contain harmonics[4].

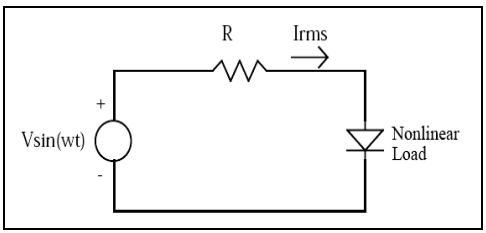

Fig. (3-2) Power System with Nonlinear Load

While some harmonics are caused by system nonlinearities such as saturation, most transformer harmonics are produced by power electronic loads such as adjustable-speed drives and diode bridge rectifiers. The significant harmonics (above the fundamental, i.e., the first harmonic) are usually the 3rd, 5th, and 7th multiples of 50/60 Hz, so that the frequencies of interest in harmonics studies are in the low-audible range. When steady-state harmonics are present, voltages and currents may be represented by Fourier series of the form:

$$v(t) = \sum_{k-1}^{\infty} V_k \sin(k\omega_o t + \theta_k) \text{ …….(3-5)}$$

whose *rms* (root mean square) value of voltage can be shown to be:

$$V_{rms} = \sqrt{\sum_{k=1}^{\infty} \frac{V_k^2}{2}} = \sqrt{\sum_{k=1}^{\infty} V^2{}_{krms}} \text{ ….(3-6)}$$

The average power is given by:

$$Pavg = \sum_{k=1}^{\infty} V_{krms} I_{krms} \cos(\partial_k - \theta_k) = P_{1avg} + P_{2avg} + P_{3avg} + ..., \quad (3\text{-}7)$$

where we see that each harmonic makes a contribution, plus or minus, to the average power. Frequently-used measure of harmonic levels is total harmonic distortion (or distortion factor), which is the ratio of the rms value of the harmonics (above fundamental) to the rms value of the fundamental, times 100%, or:

$$THD_v = \frac{\sqrt{\sum_{k=2}^{\infty} V^2_{krms}}}{V_{1rms}} \times 100\% \text{ [4]} \quad (3\text{-}8)$$

Power factor (P.F) is comprised of two components. The first is the phase shift induced between the sinusoidal input voltage and current due to either the inductive or capacitive nature of the load and is referred to as the displacement power factor (DPF). DPF is defined as the cosine of the phase shift angle phi (φ). The second component is due to non-linear characteristics of the load and is referred to as the distortion factor. It is expressed as a function of the load's total harmonic distortion (THD). The load's power factor is the product of its distortion factor and its displacement power factor.

$$P.F = \frac{1}{\sqrt{1+THD^2}} \cos(\phi) \quad \text{…….(3-9)}$$

Where:

P.F : Power factor.

THD : Total harmonic distortion .

cos Ø : Displacement power factor (DPF).

Basic electronic ballasts are non-linear loads with high levels of THD and a low power factor. This can be corrected with additional electronic circuitry added to the ballast, but with a number of trade-offs. Historically, most hard wired lighting ballasts have been power factor corrected to 0.9 P.F. since it was considered likely that large commercial buildings will result in a dense aggregation of ballasts.

Typically these densely ballast populated commercial buildings were illuminated with fluorescent lamp ballast systems with a high input Watt rating per fixture and potentially a high input VA rating [19].

4.Implementation of standards and application criteria:

In the area of power quality has become very evident on GECOL networks, harmonic distortion is one of the key issues in the design of many types of circuits . There are two distinct thought processes that can be applied to limit the amount of harmonics that are presented in power systems, favored by: 1- ***International ElectroTechnical Commission*** **(IEC)** is a series of limits that is appropriate for application at the terminals of any particular nonlinear load labeled under **IEC 1000-3-6**, **EN61000-3-2**, Harmonic Current. 2- ***Institute of Electrical and Electronics Engineers*** **(IEEE**) and the basis for **IEEE 519-1992** [2]. These new techniques consist of non-linear components that are used to control the load current. The current became distorted, i.e. deviates from the ideal sinusoidal waveform, and can be described by harmonic and interharmonic currents[2]. Mostly new electronic devices are more sensitive to voltage variation than linear loads[2].

Maximum Harmonic Current Distortion in % of I_L Individual Harmonic Order (Odd Harmonics)[1,2]						
I_{SC}/I_L	<11	11≤h≤17	17≤h≤23	23≤h≤35	35≤h	TDD
<20[3]	4.0	2.0	1.5	.6	.3	5.0
20 < 50	7.0	3.5	2.5	1.0	.5	8.0
50 < 100	10.0	4.5	4.0	1.5	.7	12.0
100 < 1000	12.0	5.5	5.0	2.0	1.0	15.0
>1000	15.0	7.0	6.0	2.5	1.4	20.0

5. Arc Furnace standards and application criteria

Under unbalanced condtions of electrode arcing , there could be significant occur under balanced conditions could be incrased under unbalanced arcing, amounts of third harmonic and their multiples. Also, fifth ,seventh harmonics

6. Transformers and derating standards and application criteria

Saturation of iron magnetic circuit of transformer is its only inherent characteristic that tends to distort the wave shape of power system . If saturation exisits, the application of sinusoidal voltage to a transformer will produce nonsinusoidal exciting current. linear capability , depending on harmonic in transformer load current .

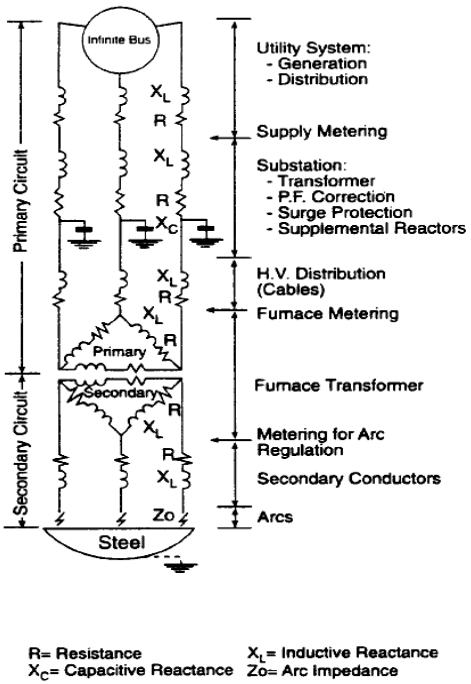

Simplified Schematic of the ac EAF Arc Circuit [8]

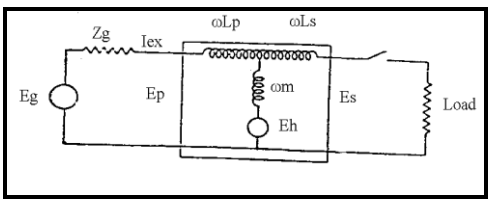

Equivelent circuit for analysis harmonic voltages and currents due to satusration in a transformer.

The increased use of nonliner loads on electric power systems has caused concern for possible reduces transformer life . By using transformer derating factor, the

transformer will have capability to supply nonliner load current with out lossing normal life expectancy . That is the capability of transformer with a given nonlinear load which causes heating in the

Measurments and monitoring of harmonics in transformers load currents in local distribution system must be caried out frequently for calculations and statistical analysis of the K factor variation for various transformers .More detailed calculation of K factor rating transformer and more detailes are explained in chapter three.

The ANSI/IEEE C57.110-1986 (IEEE Recommended Practice for Establishing Transformer Capacity Where Supplying Nonsinusoidal Load Currents) states that a transformer subject to nonsinusoidal load current having more than 5% total harmonics distortion needs to be derated. Also uniform methods for determine the capacity of transformers to supply nonsinusoidal load currents of known characteristics without loss, normal life expectancy was established [11].

The effect of harmonic current on transformer is namely derating factor (K), expressed mathematically as **:**

$$k = \frac{\sum_{h=1}^{N} I_h{}^2 h^2}{\sum_{h=1}^{N} I_h{}^2}$$

h : Harmonic order.
N : Maximum hrmonic order.
$\boldsymbol{I_h}$: Harmonic current .
K: Derating factor.

hottest spots equal to the value at rated linear load . In another way , the transformer operates at a certain percentage of its

And the maximum permissible rms nonsinusiodal load current per unit of rated rms load current .

$$I_{\max}(P.U) = \frac{\sqrt{1 + MaxP_{ec-r}}}{1 + K \times MaxP_{ec-r}} \quad \ldots(6\text{-}2)$$

Where:
K : Derating factor
$\boldsymbol{Max\ P_{ec\text{-}r}}$: The eddy current loss in the area of maximum loss density in per unit of rated secondary winding I^2.R loss .
$\boldsymbol{I_{max}\ (P.U)}$: Maximum permissible rms nonsinusiodal load current per unit of rated rms load current . And the winding eddy current losses for exisiting transformer.

7- Offices Load Results

Dat Elemad -Offices Complex, Libyan central bank are chosen as good examples to illustrate the total harmonic distortion limits belongs such load type of non linear load.

7-1 Dat Elemad -Offices Complex

The results has been obtained regarding to common coupling points chosen according to voltage levels 11KV,0.4KV.

7-1-1 High Voltage Side : Three sites of high voltage 11KV has been chosen:

1. **PCC_1** (***Main input feeder from Elwatania 30KV substation)***

The current drawn at delta side approximately balanced, steady state voltage received, Maximum Total harmonic distortions equal (3.6%) recorded at 3:36 AM, it is within the limit

which is equal (5%) figure (4-3), optimum Power factor, the total harmonic distortion on phases L_1, L_2 extremely high about (5.54%) recorded at 6:21 AM on 19th/o5/2005 that is because of disconnected high inductive and capacitive load type , as the resistive load type increases the value of total harmonic distortion decreases .

VTHD	IEEE
19.8	5

Spectrum of voltage harmonic

Harmonic order	% of fund .	IEEE
5	12	3%
7	6	3%
17	16	3%
19	4	3%

(VTHD%)distortion percentage of voltage Field measurments of total harmoni

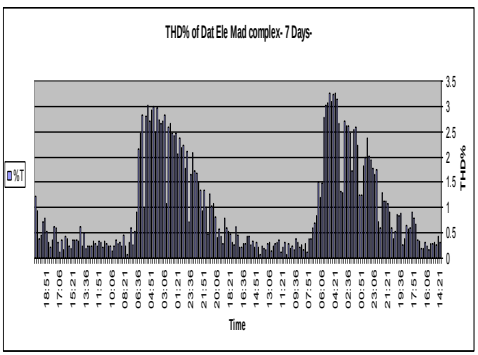

Max THD% : (3.6%), - IEEE limit = 5 % THD% of PCC_1 (Main input feeder from Elwatania 30KV substation) Dat Elmaed Complex-7day

2. **PCC_2 (Main input feeder from Elfanadek 30KV substation)**

Maximum Total harmonic distortion shown at early mooring about (4.51%)

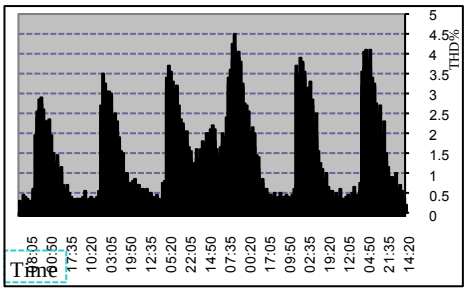

Max THD% : (4.51%), - IEEE limit = 5 % THD% of PCC_2 (Main input feeder from Elfanadek 30KV substation) Dat Elmaed Complex-7day

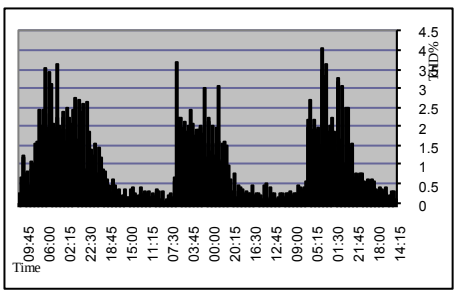

Max THD% : (4.07%), - IEEE limit = 5 % THD% of PCC_3 (Main out Feeder 11kv from complex substation to towers 4,5)-7days

7-1-2 Low Voltage Side: Tow sites of low voltage 0.4KV has been chosen.

1. PCC_4 (Main out put feeder low voltage side of tower number 1 transformer)

Maximum total harmonic distortion percentage above limits it's about (7.03%) recorded at 5:15AM on 24th/05/2007 figure

(4-6), all phases inducing harmonic distortion approximately equal increased at night period specially when the resistive load switched off where multi of electronic devices still connected even at night, the current drawn seems to be unbalancing that is because some of new load modification has been installed with unbalanced distributed , at the weekend the drawn of current reaches to minimum values certainly at night this one of the factors contributing the transformer of high capacity (1000)KVA emission percentage of harmonic distortion ,also with unbalanced phases the ability of flowing neutral current to high values about (220 amps) causing undesirable harmonic orders induced, good power factor, most of unwanted orders induced (3^{rd},5^{th},7^{th}) that is because hundreds of single and three phase electronic devices with different pulses.

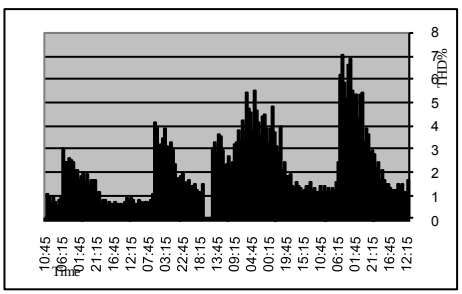

Max THD% : (7.03%), - IEEE limit = 5 %
THD% of PCC4 (Main out put feeder low voltage side of tower number 1 transformer)-4days

2 . PCC $_5$ (Main out put feeder low voltage side of tower number 3 transformer)

Maximum total harmonic distortion percentage above limits it's about (7.42%) recorded at 5:34AM on 25^{th}/05/2007 figure (4-7), other observations seems to previous tower because they are same design and extremely same load.

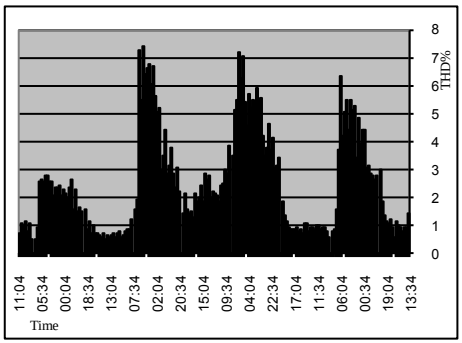

Max THD% : (7.42%), - IEEE limit = 5 %
THD% of PCC4 (Main out put low voltage feeder side of tower 3 transformer)-4 days

7-2 Libyan Central Bank

This case study has been chosen to show perfectly how much the values of total harmonic distortion increases effected by the type of electronic offices loads, the maximum total harmonic distortion THD% reaches (93.03%) figure (4-8), this results were taken along one week period and no filters were connected, from observations and investigations related the reason behind hugh new electronic devices under installation as central control of all Libyan banks was the reason behind , anther reason makes THD% increases types of special electronic printing and photocopy machines used.

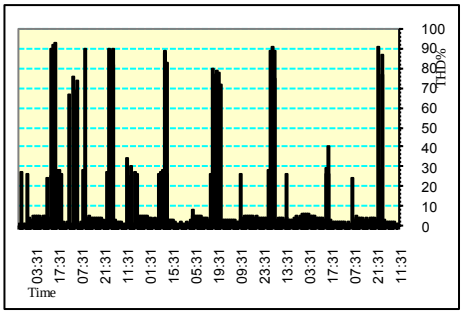

Max THD% : (93.03%), - IEEE limit = 5 %
THD% of Libyan Central Bank -7 days

8- Harmonic Mitigation

There are many ways to reduce harmonics, ranging from variable frequency drive designs to the addition of auxiliary equipment, two main points discussed first the types of mitigation could be used for minimizing the influence of affected harmonic distortion in the networks, second solutions and mitigation methods used to over come the THD% found through measurements[29].

8-1 Power System Design [30]

Harmonics can be reduced by limiting the non-linear load to 30% of the maximum transformer's capacity. However, with power factor correction capacitors installed, resonating conditions can occur that could potentially limit the percentage of non-linear loads to 15% of the transformer's capacity. By using the following equation to determine if a resonant condition on the distribution could occur by :

$$h_r = \sqrt{\frac{KVA_{SC}}{KVAR_C}} \quad \text{.....(5-1)}$$

$\boldsymbol{h_r}$: Resonant frequency as a multiple of the fundamental frequency.

$\boldsymbol{kVA_{SC}}$: Short circuit current at the point of study.

$\boldsymbol{kVAR_C}$: Capacitor rating at the system voltage.

If h_r equals or is closed to a characteristic harmonic, such as the 5^{th} or 7^{th}, there is a possibility that a resonant condition could occur.

8-2 Pulse Converter Front End [30]

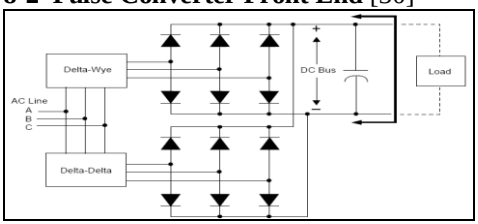

Typical Twelve-Pulse Front End Converter for AC Drive

5-1-3 Pulse Converter Front End

In this configuration, the front end of the bridge rectifier circuit uses twelve diodes instead of six. The advantages are the elimination of the 5th and 7th harmonics to a higher order where the 11th and 13th become the predominate harmonics. This will minimize the magnitude of harmonics, but will not eliminate them. The disadvantages are cost and construction, which also requires either a Delta-Delta and Delta-Wye transformer, "Zig-Zag" transformer or an autotransformer to accomplish the 30° phase shifting necessary for overall drive system efficiency rating because of the voltage drop operation. This configuration also affects associated with the transformer configuration requirement. Figure (5-1)

illustrates the typical elementary diagram for a 12-pulse converter front end.

8-3 Delta-DeltaandDelta-Wye Transformers [30]

This configuration uses to separate utility feed transformers with equal non-linear loads. This shifts the phase relationship to various six-pulse converters through cancellation techniques, similar to the twelve-pulse configuration.

8-4 Isolation Transformers [30]

An isolation transformer provides a good solution in many cases. The advantage is the potential to "voltage match" by stepping up or stepping down the system voltage, and by providing a neutral ground reference for nuisance ground faults. This is the best solution when utilizing AC or DC drives that use SCRs as bridge rectifiers.

8-5 Line Reactors [30]

More commonly used for size and cost, the line reactor is the best solution for harmonic reduction when compared to an isolation transformer. AC drives that use diode bridge rectifier front ends are best suited for line reactors. Line reactors (commonly referred to as inductors) are available in standard impedance ranges from 1.5%, 3%, 5% and 7.5%.

8-6 Harmonic Trap Filters [30]

It´s used in applications with a high non-linear ratio to system to eliminate harmonic currents. Filters are tuned to a specific harmonic such as the 5th, 7th, 11th, etc. In addition, harmonic trap filters provide true distortion power factor correction. Filters can be designed for several non-linear loads or for an individual load, as shown in Figure (5-2)[29].

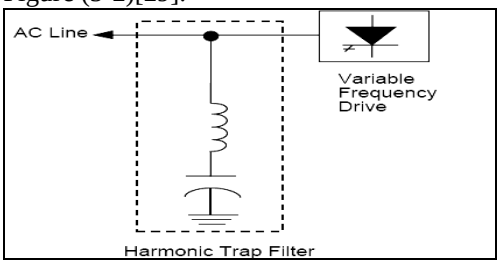

Typical Harmonic Trap Filter Configuration

8-7 New Technique of The Passive Filter Design

The main objective of a filter, in general, is that the value of the quality factor of the filter must be optimum at lowest costs and lowest losses. These factors are usually contradicting. The objective of our study is to put a technique to optimize the design criteria of the filter, hybrid active power filter configuration shown in figure (5-3). The mathematical analysis aiming at derivation of equations to obtain the cost and the losses of the filter as a function of quality factor.

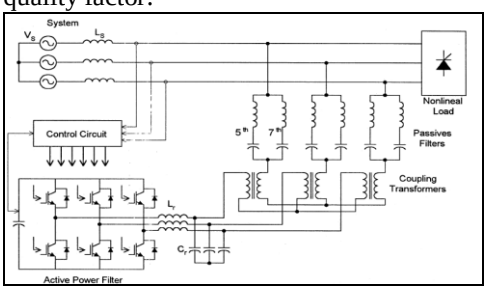

Hybrid active power filter configuration.

8-7-1 Types of Filters

Harmonic filters are the most common

solution to prevent the unwanted harmonic currents from flowing back through the power system by diverting them through a low impedance shunt path with a very little flowing back into the rest of the system. Thus minimizing the voltage distortion caused by any nonlinear loads. It is probable to use more than one filter to keep the harmonic distortion under its allowable limit [10]. Shunt filters are shown in figure (5-4-a,b,c) such as:

- **Single tuned filter**.
- **High-pass filter**.

Single tuned filter absorbs nearly all the harmonic currents of tuning frequency with low harmonic distortion. In principle, a single tuned filter is installed for each harmonic to be limited. They are connected to the bus bars for which harmonic voltage reduction is specified. Together they form a filter bank.

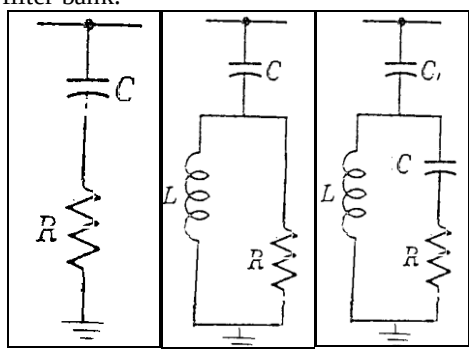

(*a*) **(*b*)** **(*c*)**

High-Pass-Filters (a) For 1st- order (b) For 2nd- order (c) For 3rd- order

Conclusion

Traditional power electronic system are the main reason for harmonic pollution. Most variable speed drive applications get its power via AC to DC convertor. Normally phase controlled thyristor convertors have been extensively used because of their control simplicity. However, the line currents drown by such convertors have distorted waves those posses harmonics. On the other hand the harmonic contents vary randomly because they are load dependent. Clearly there is need to reduce eliminate these harmonics associated with the existing traditional power electronics schemes. Harmonic current components increase power system losses, cause an excessive heating in rotating machinery, can create significant interference with communication circuits, and cause an excessive heating in power systems components such as cables, capacitors and transformers. Harmonic measurements for different load types and different bus voltages are studied. Proliferation of non-linear loads the makes power harmonics are more apparent and ascendant . Controlling and monitoring industrial system designs and their effects on utility distribution systems are a potential problem for the industrial consumer, who is responsible for complying with the IEEE 519-1992 recommended practices and procedures. Industrial facilities should include a system evaluation, including a harmonic distortion analysis, while planning facility construction or expansion. Vendors of non-linear loads such as variable frequency drives can provide services and recommend equipment that will reduce harmonics in order to comply with the revised IEEE 519-1992 guidelines.

Recommendations

1. It is advised for the General Electric Company (GECOL) to do a harmonic study for customers with nonlinear loads which produce harmonics then recommend and encourage customers to install a harmonic filters if the harmonic results exceed the standard-limits.

It is advised also, that if the customer does not install a harmonic filter, GECOL must enforce the customer to pay a penalty.

2. Customer with nonlinear loads that produce harmonics should perform harmonics study to find out if their systems exceeding the limit of the harmonic standards or not .

References

[1] J. Arrillaga, D.A. Bradley, P.S. Bodger, *Power System Harmonics*, John Wiley & Sons Ltd., 1985.

[2] IEEE Standard 519-1992, *Recommended Practices and Requirements for Harmonic Control in Electrical Power Systems*, The Institute of Electrical and Electronics Engineers, 1993.

[3] "Limits for Harmonics in the Electricity Supply System" Prepared by: Abu Dhabi Distribution Company, Al Ain Distribution Company, Abu Dhabi Supply Company for Remote Areas (RASCO), Version 1.0,30th November 2005.

[4] Proc. of the EPRI Power Quality Issues & Opportunities Conference (PQA'93), San Diego, CA, November 1993.

[5] Nokian capacitors Ltd,(*Harmonic filtering makes electrical power work more efficiently*) www. Nokiancapacitors .com

[6] IEEE Working Group on power systems Harmonics, "power system harmonics: An overview," IEEE Transactions on power Apparatus and systems, V 01. PAS.

[7] CEI/IEC 1000-2-1:1990, "Electromagnetic Compatibility", Part 2: Environment, Sect. 1: Description of the environment – Electromagnetic environment for low-frequency conducted disturbances and signalling in public power supply systems. First Edition, 1990-05

[8] Connecting Non-linear Loads to Public Electricity Systems- a Guide to G5/4. By Geoffrey Hensman, Power Engineering Journal, April 2002

[9] J. Arrillaga, B. C. Smith, N. R. Watson, A. R. Wood, *Power System Harmonics*, John Wiley & Sons Ltd., 1997.

[10] Siemens, Electrical Engineering Handbook Transmission And Distribution .

[11] G.Goldberg "Behavior of Apparatus Under the influence of voltage and current Harmonics" Bull Soc R BeIge Electr (Belgium), Vol. 91, No. 4, pp 225-235.

[12] J . ARRILLAGA, D.A BRADIET AND P.S BODGER " POWER SYSTEM HARMONICS ". 1985.

[13] R.C. Dugan, D.T. Rizy, "Harmonic Considerations for Electrical Distribution Feeders", National Technical Information Service, Report No ORNL/Sub/81-95011/4 (Cooper

Power Systems as Bulletin 87011, “Electrical Power System Harmonics, Design Guide.

[14] AN SI/IEEE C- 57. 11 0 - 1986 (reaffirmed December 1992) "Recommended practice For Establishing Transformer capability when supplying Non-Sinusoidal line current.

[15] Dr. M. SHAKER, SHAKER Consultancy Group "Effects of Harmonics on The Power Systems" 1995.

[16] Arab union of producers, Transporters And Distributors of Electricity. The international Conference on Electricity - Distribution [CIRED] 1996.

[17] G.T. Heydt, "The impact of Energy saving Technologies on Electric Distribution system power quality ", in proceedings of IEEE international Symposium on Industrial electrics , pp 176-181,25-27 May 1994, Santiage,chile.

[18] F.V.Topalis,"Efficiency of Energy Saving Lamps and Harmonic Distortion in Distribution Systems "IEEE Transaction on Power Delivery , vol. 8, no. 4, October 1993,pp2038-2042 .

[19] R. Areseeau , M.oullette, "The effects of supply Harmonics on the performance of compact Fluorescent lamps "IEEE on power delivery , VO. 8 , No. 2, April 1993,pp473- 479.

[20] D.J. Pileggi, E.M. Gulachenski, C.E. Root, T.J. gentile, A.E Emanual, "The Effect of Modern compact fluorescent lights on voltage distribution ", in IEEE- PES summer meeting Seattle, July1992, page92 .

[21] "Harmonic distortion And power Factory assessment In City Street Gas discharge lamps "IEEE Transaction on power delivery vol. 11, No. 2 , April 1996.

The Impact of Static Eccentricity on the Induction Machine Stator Currents

Dr. Saleh S. Hamad Elawgali
Sirte University, Faculty of Engineering
Department of Electrical and Electronics Engineering
P.O. Box 633 Sirte-Libya
Tel. +218-5460157 / Fax. +218-5465461
E-mail: elawgali2002@yahoo.com

Abstract:

Current spectrums of a four pole-pair, 550 kW induction machine were calculated for the cases of full symmetry and static eccentricity. The calculations involve integration of 93 electrical plus four mechanical ordinary differential equations. Electrical equations account for variable inductances affected by slotting and eccentricities. The calculations were followed by Fourier analysis of the stator currents in steady state operation. Zooms of the current spectrums, around the 50 Hz fundamental harmonic as well as of the main slot harmonic zone, were included. The spectrums included in the full contribution will refer to both calculated and measured currents.

Key words:

Induction machine, diagnostics, current spectrum, harmonics.

1. Introduction

Induction machines are responsible for conversion of about 65% of electrical energy produced all over the world into mechanical energy. Hence, diagnosing such machines is a very important issue.
Mature procedures have been elaborated by many researchers [1], [2], [3] dealing with diagnosing cage asymmetries. Development of these procedures can be supported by induction machine models recognizing only the fundamental harmonic. In contrast to This paper, will present the effect of the static eccentricity on the spectrum of the induction machine stator currents. The this, the models admitting static or/and dynamic
eccentricities have to be based on poly-harmonic models.

The calculations presented in this paper as well as in [4], [5] are based on the poly-harmonic model accounting for static and dynamic eccentricity, stator and rotor slotting, parallel branches as well as cage asymmetry. In addition, in [6] the effect of the polluted supply voltage on the current spectrum was accounted for as well.

paper will also present the spectrum in case of healthy machine and demonstrate the difference between the two cases via

comparing the harmonics contained in stator current spectrums in each case. The spectrums presented in this paper rely on calculations performed with special software (AS2).

The program for dynamic simulation consists of four base classes [7]:

- Class Pa1 calculates mainly leakage inductances.
- Class In16 calculates self and mutual main inductances accounting for true stator winding configuration as well as for slotting and eccentricity.
- Class De18 calculates derivatives of the inductances, with respect to rotor angle.

2. Full Symmetry

In order to provide reference basis the calculations have been performed for the case of fully symmetrical machine (no eccentricity). The full spectrum of the stator line current is shown in figure 1. It contains the 50 Hz fundamental harmonic as well as the main slot harmonic Slh, of the frequency of about 1140 Hz, and amplitude of about -33dB. The frequency of the main slot harmonic can be predicted by the following formula [8]:

$$\left| f_1 + h \cdot NR(1-s)n_s \right| \qquad (1)$$

Where: the supply frequency f_1 =50 Hz, the parameter h =1 [9], N_R = 88, the slip s = 0.00846, and the synchronous speed n_s = f_1/p = 12.5 revolutions per second. In addition, the spectrum contains the second slot harmonic, of the frequency of about 2130 Hz, which is out of our interest.

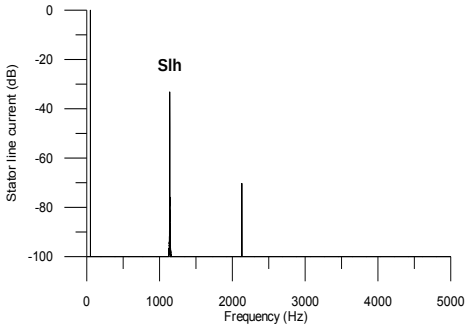

Figure1. Spectrum of the stator current (full symmetry)

3. Static Eccentricity

In this case the spectrum of the stator line current i_A will be demonstrated, considering that the rotor axis is shifted by a certain value of the geometrical air gap thickness toward the first coil group of the stator phase A [10], [11].

Fig. 2.a refers to the case of 50% static eccentricity. The spectrum of the stator line current contains a pair of harmonics in the main slot zone, as compared to just the main slot harmonic Slh in the case of full symmetry (fig.1). This new twin harmonic (tw) is spaced by about 100 Hz to the left of the main slot harmonic Slh, as shown in fig. 2.b. Its frequency is about 1040.7 Hz and its amplitude about -75 dB that gives clear evidence for the static eccentricity. The frequency of the twin harmonic, tw, can be predicted by the following formula [8]:

$$\left| f_1 - h \cdot NR(1-s)n_s \right| \qquad (2)$$

Where: the supply frequency f_1 = 50 Hz, the parameter h = 1 [9], the no. of rotor slots NR = 88, the slip s = 0.0084558, and the synchronous speed $n_s = f_1/p$ = 12.5 revolutions per second.

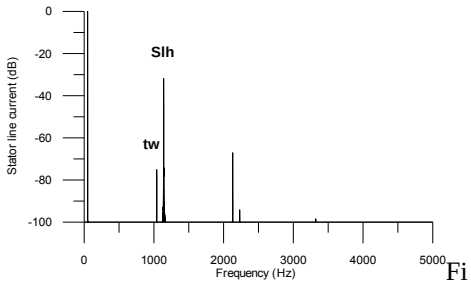

Fig.2.a Spectrum of the calculated stator current
(50% static eccentricity)

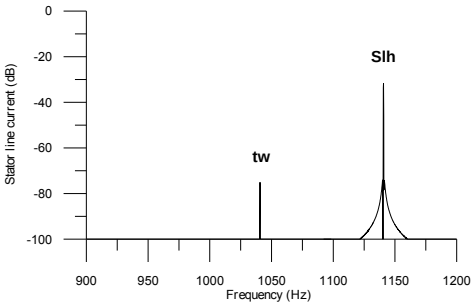

Fig.2.b Zoom of the main slot harmonic zone
(50% static eccentricity)

Further calculations were performed for the cases of 60% and 70% static eccentricity. The spectrum of fig.3 refers to the case of 60% static eccentricity. In this spectrum the twin harmonic tw is clearly visible, to the left of the main slot harmonic Slh, having now higher amplitude (-70 dB) as compared to (-75 dB) in the previous case of 50% static eccentricity. In practically the same manner, the twin harmonic tw is present; to the left of the main slot harmonic Slh, in the spectrum of fig.4, which refers to the case of 70% static eccentricity. The amplitude of the twin harmonic again increased, reaching now the level of about -65 dB, as a result of increment of the static eccentricity degree. That proves the possibility of relying on the twin harmonic as a clear sign for existence of the static eccentricity.

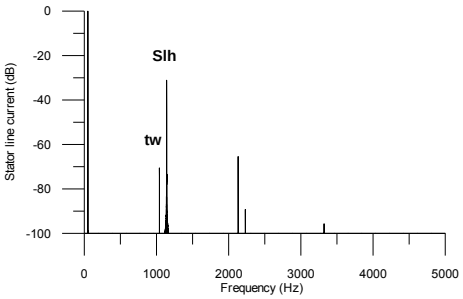

Fig.3 Spectrum of the calculated stator current
(60% static eccentricity)

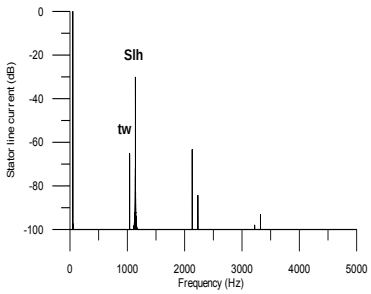

Fig.4 Spectrum of the calculated stator current(70% static eccentricity)

4. Case Studies

Spectral analyses have been performed for a number of currents really registered in the industry. The currents analyzed refer to a number of four pole pairs, 550kW induction machines, labeled in the industry as WS. The registered currents have been taken from the data base owned by the

Chair of Electrical Machines, AGH University of Science and Technology.

Among all the cases analyzed, there were some cases found to show up some static eccentricity. In the following there are two examples of the really measured currents, referring to the WS, 550 kW, machines, (files names 1WS2U2 of 22.09.2005 and 3WS2U2 of 19.10.2005).

These two cases were classified as static eccentricity ones, due to the presence of the twin harmonic tw, to the left of the main slot harmonic Slh, as shown in figs. 5c and 6.c. It delivers clear evidence for the static eccentricity in these cases. Hence, these two cases were classified as showing up pure static eccentricity.

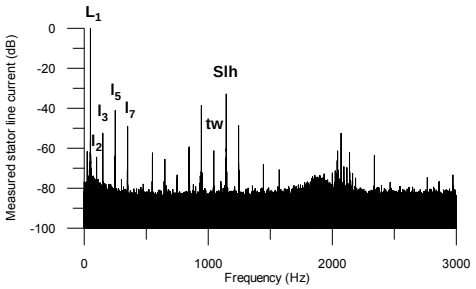

Fig. 5.a Spectrum of the measured stator current (1WS2U2 of 22.9.2005)

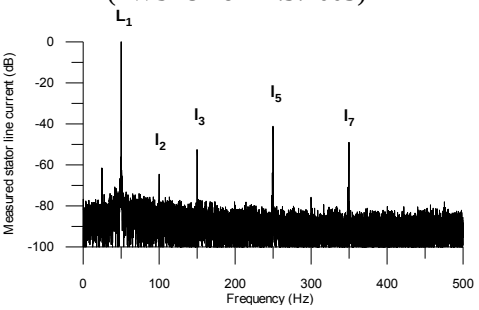

Fig. 5.b Zoom around 50 Hz of the measured stator current (1WS2U2 of 22.9.2005)

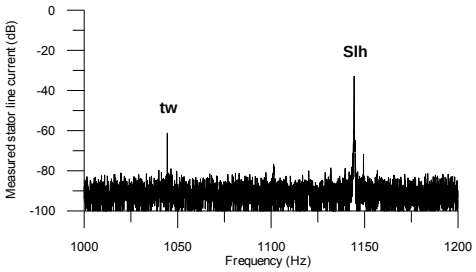

Fig. 5.c Zoom of the main slot harmonic zone of the measured stator current (1WS2U2 of 22.9.2005)

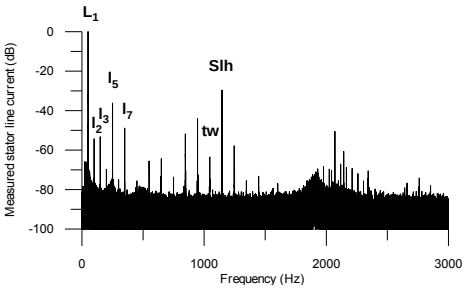

Fig. 6.a Spectrum of the measured stator current (3WS2U2 of 19.10.2005)

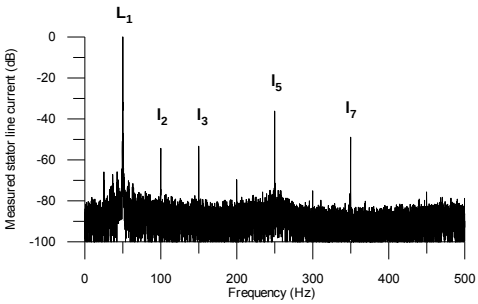

Fig. 6.b Zoom around 50 Hz of the measured stator current (3WS2U2 of 19.10.2005)

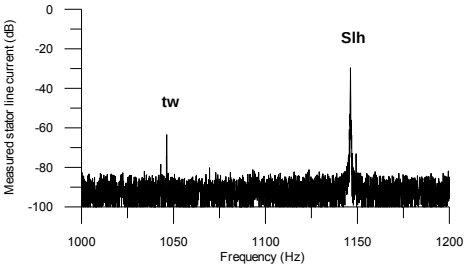

Fig. 6.c Zoom of the main slot harmonic zone of the measured stator current (3WS2U2 of 19.10.2005)

5. Conclusions

1. The main slot harmonic is present in all calculated current spectrums, referring either to the symmetrical or asymmetrical machines, practically independent on whether the machine is affected by static eccentricity.

2. The experience gathered from performing a lot of calculations allowed to conclude that to secure visibility of the harmonics bearing information about static eccentricity, it is recommended to calculate the current spectrums down to -100 dB with respect to the 50 Hz fundamental harmonic.

3. The calculations proved that the main slot harmonic zone is, from diagnostic point of view, the most important zone, as it contains diagnostic information, in form of the most important diagnostic harmonic. In addition, the main slot harmonic zone is cleaner as compared to the fundamental harmonic zone, normally polluted by many other harmonics like higher harmonics of the supply system.

4. Pure static eccentricity is characterized by a pair of 100 Hz spaced harmonics in the main slot harmonic zone. This pair of harmonics consists of the main slot harmonic which is always present, independently of the static eccentricity, and the twin harmonic which gives evidence for the static eccentricity.

5. The amplitude of the twin harmonic is affected by the degree of the static eccentricity, and generally, it is quite conspicuous whenever the degree of the static eccentricity trespasses 50% of the air gap length.

REFERENCES

[1] Bellini, A., Filippetti, F., Franceschini, G. and Tassoni, C. “Towards Correct Quantification of Induction Machines Broken Bars Through Input Electrical Signals”, International Conference on Electrical Machines (ICEM’2000), pp. 781-785, 28-30 August 2000, Espoo, Finland.

[2] Bellini, A., Filippetti, F., Franceschini, G. and Tassoni, C. (2001), “Quantitative Evaluation of Induction Motor Broken Bars by Means of Electrical Signature Analysis”, IEEE, Transactions on Industry Applications, Vol. 37 No. 5, pp. 1248-55.

[3] A. Lebaroud, A. Bentousi, A. Kkhezzar, M. Boucherma. “Effects of Broken Bar of InductionMotor

with Stator Asymmetry and DistortedSupply ", International Conference on Electrical Machines (ICEM'2004), pp. 795-796, 5-8 September 2004, Cracow, Poland.

[4] Saleh Elawgali. "Effect of Combined Eccentricities on the Spectrum of Induction Machine Currents", XL International Symposium on Electrical Machines (SME'2004), pp. 457-462, 15-18 June 2004, Hajnowka, Poland.

[5] Saleh Elawgali. "Current Spectrums of a 3.15 MWInduction Machine Based on Diagnostic Oriented Calculations ", Elektrotechnika i Elektronika, AGH Uczelniane Wydawnictwa Naukowo-Dydaktyczne, pp. 14-26, Krakow 2004, tom 23. zeszyt 1.

[6] Saleh Elawgali. "Effect of Eccentricities and Cage Asymmetry on the Induction Machine Currents, Considering Deformation of Supply Voltages", International Conference on Electrical Machines (ICEM'2004), pp.443-444, 5-8 September 2004, Cracow, Poland.

[7] J. Rusek, "Computer Implementation of Induction Machine Dynamical Model Accounting for Broken Bars, Eccentricities, Slotting and Parallel Branches", International Conference on Electrical Machines (ICEM'2000), pp. 868-872, 28-30 August 2000, Espoo, Finland.

[8] Rusek, J. "Category, Slot harmonics and the Torque of Induction Machines", The International Journal for Computation and Mathematics in Electrical and Electronic Engineering, COMPEL, Vol. 22 no. 2, 2003, pp. 388-409.

[9] J. Rusek, "Categorization of Induction Machines Resulting from Their Harmonic-Balance Model", Electromagnetics, 23, pp. 277-292, 2003, Taylor & Francis.

[10] Devanneaux, V., Kabbaj, H., Dagues, B., and Faucher, J., "An Accurate Model of Squirrel Cage Induction Machines Under Static, Dynamic or Mixed Eccentricity", IEEE International Symposium on Diagnostics for Electric Machines, Power Electronics and Drives, SDEMPED, 1-3 September 2001, Grado-Italy, pp. 121-126.

[11] Thomson, W. T. and Barbour, A. "On-Line Current Monitoring and Application of A Finite Element Method to Predict the Level of Static Air-Gap Eccentricity in Three-Phase Induction Motors", IEEE Transaction on Energy Conversion, Vol. 13, No. 4, December 1998, pp. 347-354.

Three Phase Induction Motors: Phase Imbalance Severity Evaluation Based on Acoustics Measurements and Energy Calculations

R. Shnibha, A. Albarbar, G. Ibrahim, A. Badri

Department of Engineering& Technology,

Manchester Metropolitan University,

Manchester, M1 1GD UK

Abstract:

Three phase induction motors are at the core of most engineering processes. In general, they are inherently reliable because of their mechanical simplicity and require very little attention, except at infrequent intervals when the plant is shutdown for inspection. Nevertheless, like any electromechanical system, electric motors do fail. Unanticipated failure can lead to consequential damage and very costly downtime. Hence, early and accurate fault detection and diagnosis through a reliable condition monitoring system are key.

Supply voltage fluctuations or imbalance between the phases can cause operational problems such as overheating which leads to winding insulation over-stress. There are a number of common methods based on vibration and power parameters which provide an indication of such incipient faults.

In the research work presented here an air-borne acoustic based monitoring technique is investigated and used to detect three phase induction motor phase imbalance and evaluate its severity. A novel method based on the short-time Fourier transform (STFT) and energy contained in selected frequency bands is proposed. The reliability and repeatability of the proposed method is examined and compared with the vibration and power parameter based methods. The experimental work was carried out using a 1.1kW variable speed three phase induction motor with varying output load (No load, 25%, 50%, 75% and 100% load) at varying phase imbalance (5, 10, 15, 20 and 25 V drops).

It was concluded the proposed method offers a reliable and inexpensive condition monitoring tool which can be implemented with real-time monitoring systems.

1. Introduction

Condition monitoring and condition based maintenance aim at increasing machine availability, performance, reducing consequential damage, increasing machine life, reducing spare parts inventories and reducing break-down maintenance. Induction motor faults such as winding faults, unbalanced stator and rotor, broken rotor bars, eccentricity and bearing faults have been studied. Several studies have shown that 30%-40% of induction motor failures are due to stator winding breakdown. Slow fluctuations in the supply voltage or even imbalance between the phases can cause operational problems such as overheating which leads to winding

insulation over-stress. As a thumb rule, for every 3.5% voltage unbalance per phase, the winding temperature increases by 25% in the phase with the highest current. Transient voltage conditions result in reduced winding life [1]. There are a number of common vibration and power parameter based methods for detecting such faults and to provide an indication of incipient faults. The concept of using the motor as a transducer and measuring the current consumed from each phase has been used in condition monitoring. It has the major advantage that it does not required direct access to the motor being monitored. The line current can be easily monitored with either a current (clamp-on) transformer or a Hall-effect transducer. This method is commonly called motor current signature analysis (MCSA) [2]. Several researchers have used per-phase current to detect and diagnose eccentricity [3], broken rotor bar [4-6] and bearing problems [7, 8]. Park's vector approach and finite element method techniques were used by Benbouzid to investigate MCSA [9]. In ref. [10] Acosta et al., combined MCSA and extended Park's vector approach (EPVA) for fault detection and diagnosing induction motor stator and rotor related faults.

The measurement of machine vibration has long been one of the most popular techniques for machine condition monitoring. Structural vibration has a long-established theoretical background through traditional dynamics and control theory. The vibration of either the motor stator core or end-caps can be easily monitored by an accelerometer which is usually mounted on the motor. There have been many practical demonstrations of the capability of vibration monitoring to detect a wide range of motor faults; these include shaft eccentricity/ misalignment [11,12], bearing faults [12], looseness [13], rotor imbalance [6], and broken rotor bar [6,12,13]. In ref. [14] Liang et al showed that both current spectra and vibration spectra are able to reveal broken rotor bars faults.

Conventional techniques involving vibration may not be able to detect a growing fault due to the low impact energy generated by the small relative movement of components. As an alternative to accelerometers, the acoustic emission (AE) technique has been widely used in the fault diagnosis. AE is a high frequency analysis technique which was initially developed as a non-destructive testing (NDT) tool to detect crack growth in materials and structures. Today AE is increasingly being used as a means of monitoring the health of industrial machines. Rao [15] has provided a review on the state-of-the-art of AE technology in machine condition monitoring. Yoshioka [16] has shown that AE techniques can detect defects before they appear in the vibration acceleration range and can also identify possible sources of AE generation during a fatigue life test of thrust ball bearing.

Microphones are commonly used as transducers in acoustic monitoring to acquire data on acoustic signals and/or noise waveforms in many condition applications, including induction motors. Microphones are sensitive devices with the advantages of wide frequency response range and easy installation.

Analysing the measured signal using conventional signal processing techniques such as fast Fourier transforms (FFT) does not always achieve adequate results. E.g. time information is lost when transforming to the frequency domain. When looking at a Fourier transform of a signal, it is impossible to tell when a particular event took place. In an effort to determine when

and at what frequencies a signal event occurs, Gabor [17] derived the short-time Fourier transform (STFT).

The STFT represents a sort of compromise between the time and frequency based views of a signal. It provides some information about both when and at what frequencies a signal event occurs. STFT is based on application of a time window in determining the localisation of the spectrum in the time domain [17]. In ref. [18] Jorado et al., concluded that the discrete STFT is more suitable for harmonic analysis and by selecting a small window length, the STFT is able to detect transients within noisy data. Wang et al., presented a comparative study of two types of time-frequency domain analysis methods to the ultrasound pulse-echo signals of steel pipe defects [19]. In ref. [20] an experimental study showed that using the STFT for fault diagnosis and classification in induction motors, where the faults were broken rotor bars and broken end rings, increased accuracy rates.

It was noted that much of the work carried out has dealt with detecting phase imbalance faults at higher degrees of severity, e.g. voltage drops of 10% and over. The novelty of this work lies on detecting very low phase imbalance related faults.

This paper is organized as follows. In the second section the proposed signal processing technique is introduced. Numerical simulation and method validations are presented in Section 3. Section 4 describes the test rig, the instrumentations and data collection. Results discussions and conclusions are presented in Sections 5 and 6 respectively.

2. Conventional and the proposed signal processing technique

Measurements taken by sensors are usually raw data; therefore to extract some machinery condition information one has to use signal processing techniques. In general, there are three main signal processing techniques: time domain, frequency domain and time-frequency domain.

2.1 Time domain

One of the simplest detection and diagnostic approaches is to analyse the measured signal in the time domain. A number of statistical parameters can be extracted such as root mean square (RMS), peak, crest factor, kurtosis, skewness, etc. The choice of such approaches depends on the nature of the signal and the required information.

2.1.1 Root mean square (RMS)

The RMS value of the signals is expressed in Equation 1.

$$RMS = \sqrt{\frac{1}{N}\sum_{i=1}^{N}(x_i^2)} \qquad (1)$$

Where x_i is the i-th member of signal x and N is the number of points for signal x

2.1.2 Crest factor (CF)

It is defined as the peak value of the signal divided by the RMS value of the signal. The CF measures the spikiness of a signal and is used to characterise signals containing repetitive impulses in addition to a lower level continuous signal.

2.1.3 *Kurtosis*

It looks at the fourth moment of the spectral amplitude difference from the mean level. A mathematical definition of kurtosis is given by [21].

$$K = \frac{N*\sum_{i=1}^{N}(x_i-\bar{x})^4}{\left[\sum_{i=1}^{N}(x_i-\bar{x})^2\right]^2} \quad (2)$$

where $\bar{x}$ is the mean value of the samples.

2.2 *Frequency domain*

The signal could be transformed into frequency domain using Fourier analysis. Analysing data in the frequency domain is especially valuable as signal frequency features are directly interpretable in terms of machine components.

Spectrum analysis is the usual method in transforming raw data into frequency domain. Its mathematical formula is:

$$X(f) = \int_{-\infty}^{\infty} x(t)e^{-2\pi ift}\,dt \quad (3)$$

Where *x(t)* is the signal in the time domain, *X(f)* is its Fourier transform and *f* the frequency.

Therefore, the FT determines the strength/energy of a particular frequency component. In practical applications, the measured signal is not continuous, but sampled at time intervals (sampling frequency). Therefore discrete Fourier transforms (DFT) are required.

For real-time measurements, Fourier transforms have three main hardware limitations. First, the captured sensor signals are not free of noise. Second, the data only has a finite number of samples. Third, a digital computer can only evaluate the Fourier transform at a finite size of frequency interval. All of these hardware limitations reduce the accuracy in analysing the various frequency components of a signal.

2.3. Time-Frequency domain

Clearly, true signal representation in joint time and frequency domains is desirable and will maximise condition feature extraction capabilities. It is possible to view both time and frequency information simultaneously in the time-frequency plot. Hence the change in particular frequency components may be related to particular instances in time, allowing the possibility of improved fault location. There are many algorithms for achieving a time-frequency plot such as the STFT, Wigner-Ville distribution and wavelet transform.

2.3.1 Short-time Fourier transform (STFT):

As described in the previous section, the FFT provides the frequency information of a signal, however without time information. One way of getting a time-frequency representation is to apply the short-time Fourier transform STFT. The principle of the STFT is to divide a time signal into equal length sub-blocks by using a sliding window function and perform the Fourier transform on each of the sub-blocks separately (Eq. 4)

$$STFT = \int_{-\infty}^{\infty} x(t)w(t-\tau)e^{-jwt}\,dt \quad (4)$$

where ω(t) is the window function.

As a result the STFT can extract the frequency information of a signal while maintaining time information. However, the STFT reduces the frequency resolution of the signal because the STFT divides the signal into smaller sub-blocks with less observation time. Hence the frequency and time resolution of the STFT technique depend on the length of the window. A longer window means higher frequency resolution but lower time resolution, while

a short window means lower frequency resolution but higher time resolution.

2.4. The proposed method

Most studies for condition monitoring are focusing on conventional techniques which are based on statistical analysis of the signal in the time domain to detect any damage in the induction motor. RMS, crest factor, kurtosis and figures of merit parameters have been considered for this technique. Each parameter has been defined in detail in the references [21, 22].

The proposed method is based on using STFT and subsequently calculating the energy levels of certain frequency bands; rotor frequency, power supply frequency and their sideband zones. Equation 5 mathematically expresses this novel method:

$$TE = \int_{f_1}^{f_2} STFT(t,f)\,df\,dt \quad (5)$$

where TE is the frequency band total energy level, f_1 and f_2 are the lower and upper frequency boundaries, respectively

3 Numerical simulation

Conventional analysis using statistical parameters and the Fourier transform of a periodic, stationary and deterministic signal, cannot take into account the temporal variation of the spectral characteristics of a non-stationary signal. Consider the two signals shown in Figure 1. The first signal is represented in Equation (6):

$$f_1(t) = \sin(2\pi 25t) + \sin(2\pi 90t) + \sin(2\pi 150t) \quad (6)$$

This signal has frequencies of 25, 90 and 150 Hz at any instant in time; therefore it could be described as a stationary signal. Figure 1(a) represents a 1000*ms* period of this signal and its frequency spectrum is shown in Figure 1(b).

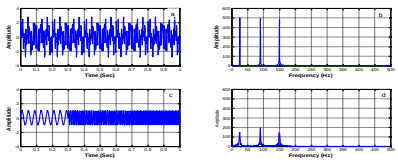

Figure 1 Time and frequency domain representation of the two signals f_1 and f_2. (a) f_1 in time domain, (b) f_1 in frequency domain, (c) f_2 in time domain and (d) f_2 in frequency domain

A non-stationary signal f_2 contains the same frequency components as f_1 but in three discrete and different time intervals.

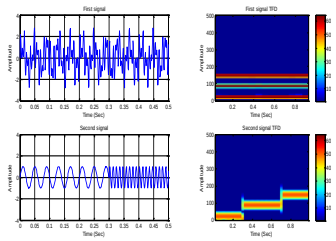

A 1000*ms* length of this signal is plotted in Figure 1 (c) and its spectrum is plotted in Figure 1 (d). The time interval 0 to 350 ms contains a 25 Hz sinusoid, the interval 350 to 700 ms contains a 90 Hz sinusoid, and the interval 700 to 1000 ms contains a 150 Hz sinusoid as described in Equation (7).

$$f_2(t) = \begin{cases} \sin(2*pi*25*t) \ldots\ldots 0 \le t \le 350 \\ \sin(2*pi*90*t) \ldots\ldots 350 \le t \le 700 \\ \sin(2*pi*150*t) \ldots 700 \le t \le 1000 \end{cases} \quad (7)$$

Comparing the signals represented in Figure 1, both of the signals include the same frequency components, but while Figure 1 contains all three signals at all

times, the second contains the signals over different time intervals, the time domain representations are completely different. In the frequency domain, apart from the jagged noise along the bottom of the scale (introduced due to the sharp transition from one frequency to the next), f_2 is almost identical to f_1. This is because the Fourier transform does not take time information into account. The Fourier transform simply identifies all frequencies contained in the signal, but it does not provide the information regarding the time when those spectral components appear. Therefore, the Fourier transform is not a suitable technique for non-stationary signals.

Figure 2 Time and frequency domain representation of the two signals f_1 and f_2 (a) f_1 time domain, (b) f_1 time- frequency domain, (c) f_2 time domain and (d) f_2 time-frequency domain

In order to accurately represent the frequency information contained in a nonstationary signal, a technique that presents time information and frequency information needs to be used, producing a signal spectrum in the time-frequency domain.

Time-frequency analysis is a novel signal processing method making it possible to see both the time and frequency information at the same time. It displays the combined results from the time and frequency analysis in a two or three-dimensional way which plots the amplitudes against time and frequency axes as shown in Figure 2. Comparison of Figure 2(b) and Figure 2(d) reveals that signals f_1 and f_2 can easily be distinguished.

Comparing the signals represented in Figure 3, both signals include the same frequency components and both have an amplitude "spike" inserted at the same instant. Figure 3(a) contains all three signals at all times, while Figure 3(b) contains the three signals in sequence. I.e., the time domain representations are completely different. In the frequency domain f_2 is very similar to f_1 because the Fourier transform does not take time information into account. When time-frequency analysis used, see Figures 4(b) and 4(d), that signals f_1 and f_2 can easily be distinguished and the time information on the presence of the spikes is presented.

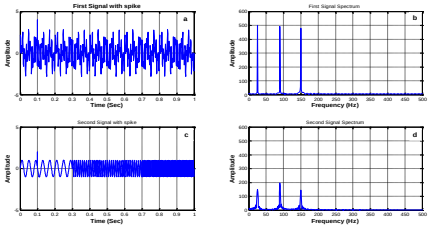

Figure 3 Time and frequency domain representation of the two signals f_1 and f_2 with spike. (a) f_1 in time domain, (b) f_1 in frequency domain, (c) f_2 in time domain and (d) f_2 in frequency domain

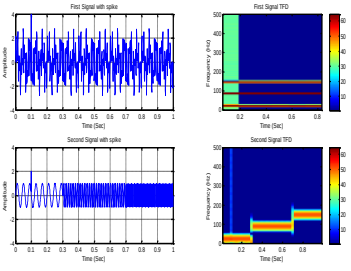

Figure 4 Time and frequency domain representation of the two signals f_1 and f_2 with spikes. (a) f_1 time domain, (b) f_1 time-

frequency domain, (c) f_2 time domain and (d) f_2 time- frequency domain.

Using this technique to analyse vibration and airborne acoustic signals emitted by electromechanical machinery enables us to link every event observed in the time-frequency plane to one excitation source. It is then possible to measure the energy of each event and to quantify the part of each excitation mechanism in the emitted signals to those sources on the outer surfaces of the machinery.

To describe this temporal variation of induction motor airborne acoustic signals, an evaluative spectral analysis must be performed using time-frequency methods. Such methods are a good tool for describing the spectral contents of a transient signal, by their nature normally highly nonstationary, as a function of time. They enable several patterns superimposed in time and/or in frequency, within the same transient signal, to be located and separated in the time – frequency plane.

An efficient time-frequency method should allow us to:

1- Locate at each point of the structure the responses inherent to each source of excitation,

2- Analyse the frequencies associated with each source of excitation, and

3- Measure the contribution of each source of excitation in terms of energy.

4 Instrumentation and data collection

The schematic diagram for the test rig and instrumentations is shown in Figure 5. It comprises a 1.1kW variable speed induction motor, a DC Generator and a resistor bank to act as a load and to dissipate the electrical energy. The instrumentation consisted of an accelerometer, current transducer and a condenser microphone. The current sensor module of (PR 30) measuring range was from 0 to 30A, output sensitivity is 100mV/A, resolution ±1mA. Accelerometer sensitivity is 100mV/g. The output of the accelerometer is filtered and amplified via a charge amplifier. The measured data is then transferred to the computer using 24-bit resolution data acquisition. The sampling frequency was set to 50k Hz.

The developed Labview based system allows the user to monitor and store machine variables, and subsequently a Matlab code was used for further signal processing.

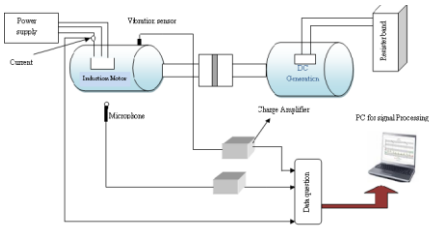

Figure 5 Schematic diagram of induction motor test rig

5 Experimental Result

The motor was tested at 1500 rpm and 100% load in a healthy condition and then under four different phase imbalance voltage of 5, 10, 15, 20 and 25 V; these represented 2%, 4%, 6%, 8% and 10% respectively, of the main nominal voltage level. A number of statistical methods were applied to the measured current, vibration and acoustic signals; see Figure 6. The applied statistical signal processing includes RMS, CF and Kurtosis. No sufficient and reliable condition related

information can be observed even in the case of 10% voltage imbalance.

The measured signals were transformed into the frequency domain, where the frequencies of their main components were indentified; see Figures 7 to 9. Three frequency components could be determined within the vibration signal. The current spectrum, Figure 7, doesn't show condition related information in all cases and the spectrum was mainly dominated by the 50Hz mains frequency and its harmonics. In Figure 8 (vibration) the first frequency component is at 25 Hz, rotor rotation speed. The second is at 50 Hz, due to the power supply or the second harmonic of rotor running speed. The third was at 100Hz, which could be the second harmonic of power supply frequency or fourth harmonic of the rotor frequency. There was a slight increase in the amplitudes of these components.

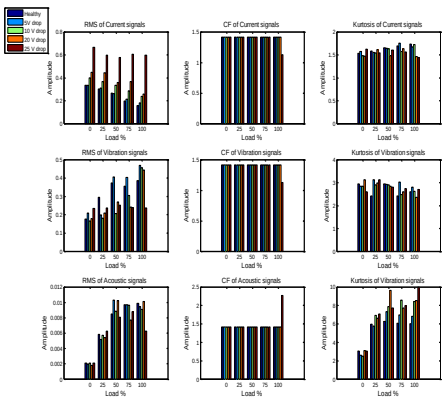

Figure 6 Time domain parameters

Figure 9, represents the spectral domain analysis of the measured acoustic signals, frequency components similar to those in the vibration signals are seen. These amplitudes are not significantly different from those of the normal motor harmonics. Clearly, spectral analysis of the measured current, vibration and acoustic signals has failed to provide sufficient information about the motor condition and the severity of the phase imbalance.

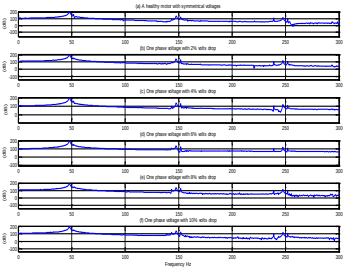

Figure 7 Measured current signal in frequency domain, at 100 % load

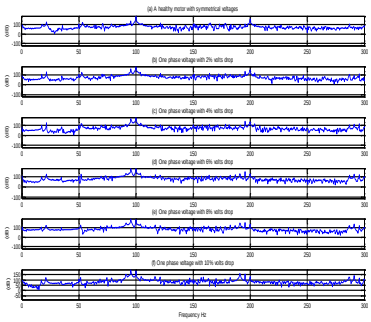

Figure 8 Measured vibration signal in frequency domain, at 100 % load

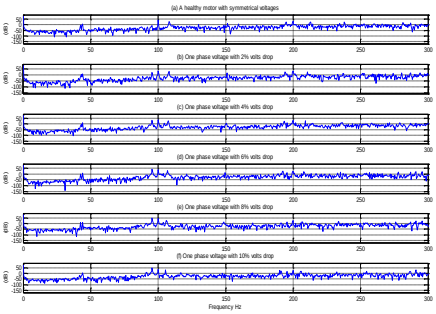

Figure 9Measured acoustic signal in frequency domain, at 100 % load

In an effort to extract phase imbalance severity information the method described above was applied to the measured acoustic signals. Figures 10 and 11 present the STFT analysis of the acoustic signals when running at 1300 rpm and 1500 rpm respectively. The frequency components identified are the same as those identified in the acoustic and vibration spectral domain; however STFT is more sensitive and has better localisation capabilities than conventional Fourier analysis.

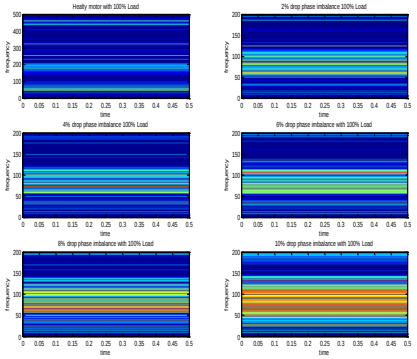

Figure 10 STFT acoustic signals at 100% load, various imbalance phase faults at 1300rpm

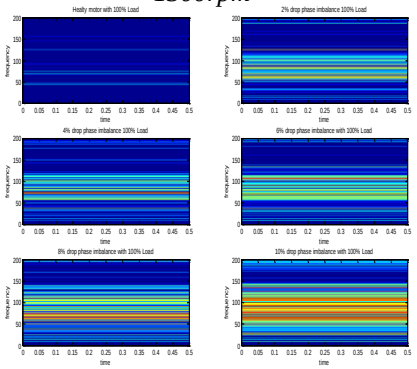

Figure 11 STFT acoustic signals at 100% load, various imbalance phase faults at 1500rpm

The energy levels were calculated for the motor running frequency (20 to 40 Hz), supply frequency (45 to 60 Hz) and the frequency band from 80 to 100 Hz. Figures 12, 13 and 14 show the energy for all cases. It can be seen that there is a direct relationship between the fault severity and the energy levels for both speeds. The curve gradually rises as imbalance phase increased; it is a linear increase between 2% to about 7% fault severity especially for the speed of 1300rpm.

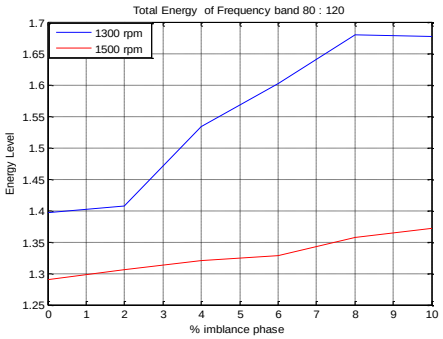

Figure 12 Energy levels of twice power

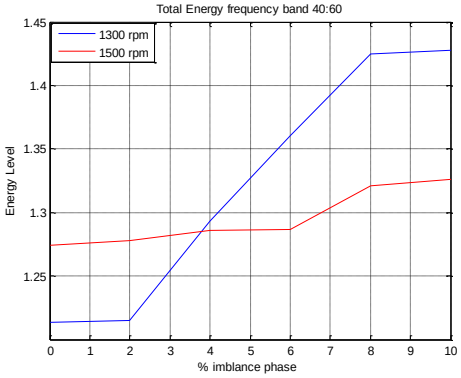

Figure 13 Energy levels of rotor rotation speed frequency band

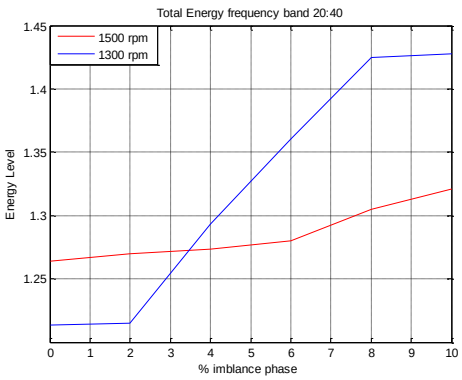

Figure 14 Energy levels of power supply frequency band

Conclusion

In this work the results of raw data obtained from physical machine parameters are presented. FT and STFT are used to present the results in the frequency domain and joint time-frequency domain. Time domain analysis could be used to obtain the motor condition qualitatively using RMS value, crest factor and Kurtosis. For primary investigation, time domain analysis provides a rough assessment and is not appropriate for fault classification and ranking. Frequency domain analysis of the acoustic signals provides detailed information of the spectrum and may reveal some hidden features of short duration. The alternative approach to such non-stationary signals is the STFT that provides useful information about any signal in the time domain for different bands of frequencies. It is concluded there is a big advantage in using STFT and the energy levels calculations as a voltage imbalance severity evaluator.

References

1- Siddique. A., Yadavan, G.S., B. Singh, 2005, "A review of stator fault monitoring techniques of induction motors." *IEEE Transactions on Energy Conversion*, Vol. 20, No. 4, pp. 106-113.

2- Kilman, G.B. and Stein, J. 1992. "Methods of motor current signature analysis". Proc. Int. *Conf. on Electrical Machines and Power Systems*, pp 463-474.

3- Thomson, W.T, Rankin, D. and Dorrell, D.G. 1999. "On-line current monitoring to diagnosis air gap eccentricity in large three phase induction motor". *IEEE Trans. on Energy Conversion*, Vol. 14, No. 4, pp. 1372-1378.

4- Walliser, R.F. and Landy, C.F. 1994. "Determination of interbar current effects in the detection of broken rotor bars in squirrel cage induction motor". *IEEE Trans. on Energy Conversion*, Vol. 9, No. 1, Dec., pp. 152-158.

5- Rankin, D.R. 1995. "The industrial application of phase current analysis to detection rotor winding faults in squirrel cage induction motors". *Power Engineering Journal*, Vol 9, pp 77-84.

6- Arthur, N. and Penman, J. 2000. "Induction machine condition monitoring with higher order spectra". *IEEE Trans. on Industrial Electronics*, Vol. 47, No. 5, pp. 1031-1041.

7- Schoen, R.R., Habetler, T.G., Kamran, F. and Barthheld, R.G. 1995. "Motor bearing damage detection using stator current monitoring". *IEEE Trans. on Industrial Application*, Vol. 31, No. 6, pp. 1274-1279.

8- Eren, L. and Devaney, M.J. 2001. "Motor bearing damage detection via wavelet analysis of starting current transient". *IEEE Instrument Measurement Magazine*, Vol. 3, pp. 1797-1800.

9- Nandi, S., Toliyat, H.A., Xiadong, L. 2005. "Condition monitoring and fault diagnosis of electrical machines - A review." *IEEE Trans. on Energy*

Conversion, Vol. 20, No. 4, Dec., pp. 719-729.

10- Acosta, G., Verucchi, C. and Gelso, E. 2004. "A current monitoring system for diagnosing electrical failures in induction motor". *Mechanical Systems and signal Processing*. Vol. 20, Issue 4, May 2006 pp. 953-965.

11-Dorrell, D.G., Thomson, W.T. and Roach, S. 1997. "Analysis of air gap flux, current and vibration signals as a function of the combination of static and dynamic air gap eccentricity in 3 phase induction motors". *IEEE Trans. on Industry Applications* , Vol. 33, No. 1, pp. 24-34.

12-Seker, S. 2000. "Determination of air gap eccentricity in electric motors using coherence analysis". *IEEE Power Engineering Review*, Vol. 20, No. 7, pp. 58-50.

13- Finley, W R, Hodowanec, M M and Holter, W G, 2000. "An analytical approach to solving motor vibration problems". *IEEE Transactions on Industrial Application*, Vol. 36, No. 5, pp. 1467-1480.

14-B. Liang, A.D. Ball, S.D. Iwnicki, 2001 "Asymmetrical stator and rotor fault detection using vibration, per-phase current and transient speed analysis". *Condition Monitoring and Diagnostic Management*, Elsevier Science Ltd.

15- R. Rao. 2003. "Advances in acoustic emission technology (AET): A state-of-the-art review". *COMADEM 2003*, pp. 1-18.

16- T. Yoshioka, A. Korenaga, H. Mano and T. Yamamoto. 1999. "Diagnosis of rolling bearing by measuring time interval of AE generation". *Journal of Tribology*, Trans. ASME, 121, 468-472.

17-K. Darowicki, A. Zielinki. 2001. "Joint time-frequency analysis of electrochemical noise". *Journal of Electroanalysis Chemistry*, 504, 201-207.

18-F. Jurado, J. Seanz. 2002. "Comparison between discrete STFT and Wavelets for the analysis of power quality events". *Electric Power Systems Research*, 62, pp. 183-190.

19- Y.M Wang, Y.H. Kang, X.J. Wu. 2006. "Application of STFT and HOS to analysis magnetostrictively generated pulse-echo signals of a steel pipe defect". *NDT&E International*, 39, pp. 289-292.

20- H. Arabaci, O. Bilgin. 2009. "Neural network classification and diagnosis of broken rotor bar faults by means of short time Fourier transform". Proc. Int. *Multi-Conference of Engineering and Computer Scientists*, Vol 1

21- A. Pareya, M. El Badaouib, F. Guilletb, N. Tandon. 2006. "Dynamic modelling of spur gear pair and application of empirical mode decomposition-based statistical analysis for early detection of localized tooth defect". *Journal of Sound and Vibration* 294 pp. 547–561.

22. P. Vecer, M. Kreidl and R. Smid. 2005. "Condition indicators for gearbox condition monitoring systems". *Acta Polytechnica*. Vol. 45, No.6, pp. 35-43.23.

Performance analysis of internally reformed solid oxide fuel cell-gas turbine hybrid systems

Abdullatif Musa*, Mosbah Talbi
Marine Engineering Department, Faculty of Engineering,
Al-fateh University, Tripoli, Libya
E-mail:Musa.Abdullatif@yahoo.com

Abstract

Solid oxide fuel cell (SOFC) is considered extremely suitable for electrical power plant applications. The high temperature (HT) and intermediate temperature (IT) SOFC performances are calculated using numerical models that are built in Aspen customer modeller and integrated in Aspen Plus™ for the internally reformed (IR) fuel cells. In this study, two types of combined cycles are proposed and investigated: a combined cycle consisting of a two-staged combination of IT-SOFC and HT-SOFC, and another consisting of two stages of IT-SOFC. Moreover, the effects of various parameters such as operating temperature, current density, fuel recirculation rate, and cell pressure on the system performance are evaluated. The simulation results show that the cycle efficiency increased when cell pressure, fuel utilization rate and fuel recirculation rate increase. Furthermore, two stages IT-SOFC system together with gas turbine can lead to highly efficient power cycle.

Keywords: SOFC; Combined cycle; Performance; Cycle analysis

1. Introduction

Fuel cells convert chemical energy into electrical energy and have the advantage of a continuous supply of reactant gases. Fuel cells used for stationary energy production are typically high temperature cells. A combined cycle consisting of two or several stages of SOFC is recently being investigated as a means to increase the SOFC share of power production and thus increase the efficiency of the cycle. The United States Department of Energy (DOE) has investigated ways to achieve a power generation efficiency of 80% and has proposed a multi-staged fuel cell system with five serial stages of fuel cells in order to reduce the regenerative heat for fuel and air, and to extend the operating temperature range of fuel cells. Power generation system consisting of two-staged externally reformed SOFCs with serial connection of low and high temperature SOFCs is investigated. The results show that the power generation efficiency of the two-staged SOFCs is 50.3% and the total efficiency of power generation with gas turbine is 56.1% under standard operating conditions [1]. This demonstrates the advantages of the proposed two-staged SOFC cycle.

The operating temperature of HT-SOFC is between 950 and 1000°C because the YSZ solid electrolyte has low ionic conductivity at lower operating temperatures. The high operating temperature causes many serious problems, such as physical and chemical degradation of the electrode materials, and so it is

desirable to develop SOFCs operating at or below 800°C. Such operating temperatures can be achieved by using an extremely thin but dense YSZ electrolyte or a more conductive electrolyte [2]. Several recent works focused on intermediate temperature SOFC.

Hydrogen is not freely available in nature. As a result hydrogen is most of the time produced from fossil fuels. Due to the high temperature in the high temperature fuel cells (SOFC or MCFC) and the water production during the electrochemical reaction, SOFCs can allow for internal reforming. This means that natural gas is directly fed into the fuel cell, where it will convert to hydrogen. The heat necessary for this reforming reaction is delivered by the electrochemical reaction in the cell. In previously paper [3], the performance of internal and external reforming molten carbonate fuel cell (MCFC) systems was investigated. The simulations show that the internal reforming MCFC system is more efficient than the external reforming MCFC system.

In this paper, thermodynamic models for internally reformed intermediate and high temperature SOFCs are developed. These fuel cells are combined in different ways in order construct single-staged and two-staged fuel cell systems combining different cell types. The aim of the paper is to find the best configuration for a single-staged or a two-staged combined internally reformed system.

2. Cycles description

The SOFC cells currently in operation are fuelled with natural gas. The high temperature inside the cell stacks allows for reforming the methane directly inside the cell if steam is provided at the inlet. The heat necessary for this reforming reaction is delivered by the electrochemical reaction in the cell. The pure methane (CH_4) fuel is provided at atmospheric conditions. Part of the anode gases is recycled in the cycles because the anode gases contain the steam needed for the reforming reaction. This is a way of avoiding a steam generator in the cycles as it was adopted by [1]. The characteristics of the systems are given in Table 1.

2.1 IT-SOFC/HT-SOFC combined cycle

Figure 1 is a diagram of the combined cycle consisting of IT-SOFC and HT-SOFC. In this cycle the anode flows of the IT-SOFC and HT-SOFC are connected in parallel while the cathode flows are connected serially. Methane is admitted into the heat exchanger H/E2 to preheat the methane. The preheated methane is split into two equal parts, one of which is mixed with the recycling anode gases of the IT-SOFC stack; the mixture is supplied to the anode side of IT-SOFC stack. The other part of the preheated methane is mixed with part of the recycling anode gases of the HT-SOFC stack and then delivered into the anode side in the HT-SOFC stack. The compressors (C1 and C2) are used to compensate the pressure drop through the SOFC stacks. In both SOFC stacks the remaining part of anode gases is recycled to the combustor. The heat released in the combustor is used to heat the burned gas, which then passes to heat exchangers H/E3 and H/E1, the gas turbine, and heat exchanger H/E2, respectively. The compressed air from the compressor (AC) is supplied to the heat exchanger (H/E1). The hot burned gas in the heat exchanger H/E1 provides the heat necessary to preheat the cathode inlet gases of the IT-SOFC stack. The composition of the cathode gases at the IT-SOFC outlet was taken as the HT-SOFC inlet condition. In the heat exchanger H/E3, the cathode outlet gases of the IT-

SOFC stack are heated further before flowing into the cathode side of the HT-SOFC stack. The cathode gases of the HT-SOFC stack are recycled to the combustor.

2.2 Two-stage IT-SOFC combined cycle

The two-staged IT-SOFC combined system is similar to the IT-SOFC/HT-SOFC combined cycle (Fig. 1) but does not include heat exchanger H/E3. Instead of the HT-SOFC stack, there is another IT-SOFC stack.

Table 1: Input parameters and the assumptions made for the SOFC systems

Setting parameter	Value
Current density	0.250 Acm^{-2}
Active cell area	250 m^2
Total fuel utilisation rate	85 %
Steam-to-carbon ratio	2
Fuel recirculation rate	55 %
Gas turbine and pump isentropic efficiencies	85 %
Compressors isentropic efficiency	80 %
Pressure drop in combustor	0.2 bar
Pressure drop in SOFC	0.01 bar
Pressure drop in heat exchangers	0.02 bar
Gas turbine and compressors mechanical efficiencies	98 %

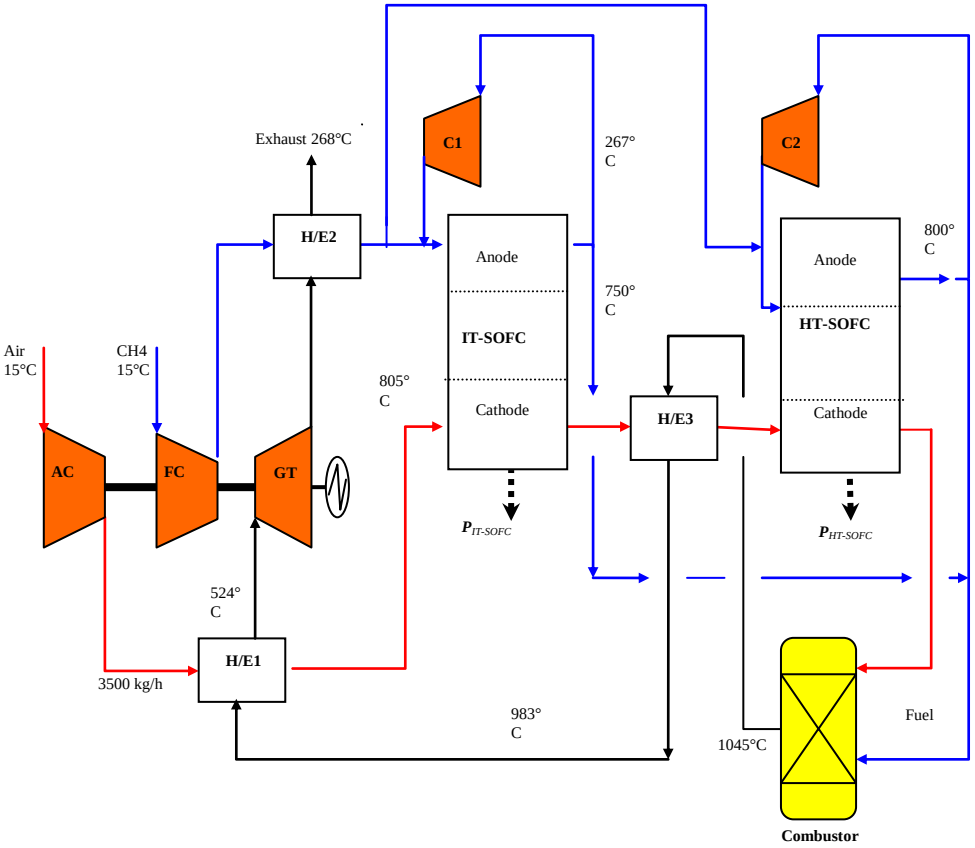

Fig. 1- Configuration of the IT-SOFC/HT-SOFC combined cycle (AC: air compressor; FC: fuel compressor; GT: gas turbine; H/E: heat exchanger).

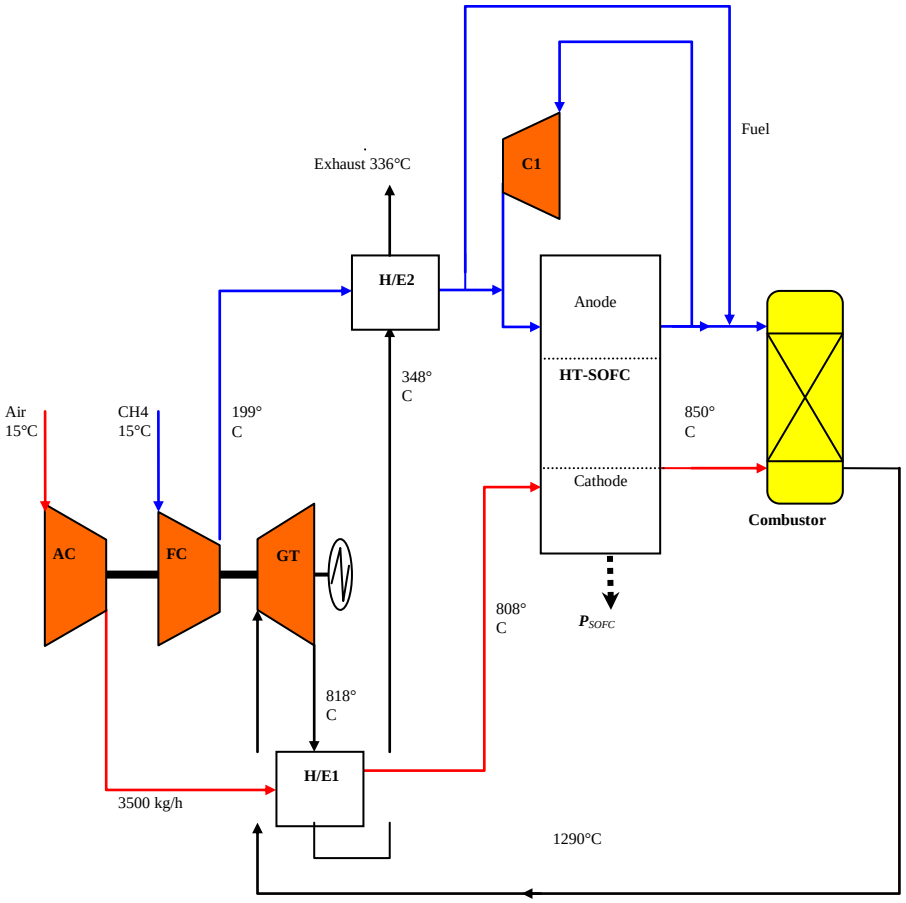

Fig. 2- Configuration of the single-staged HT-SOFC/GT system

2.3 Single-staged HT-SOFC cycle

The single-staged HT-SOFC system (Fig. 2) is similar to the IT-SOFC/HT-SOFC combined cycle (Fig. 1) but there is no IT-SOFC stack. The combustor exit gas is sent to a gas turbine, heat exchanger H/E1, and heat exchanger H/E2, respectively. In heat exchanger H/E2, the hot effluent of burned gas provides the heat necessary to preheat methane, which is split into two parts. The first part is mixed with the recycling anode gases and supplied to the anode side of the stack. The remaining part of the preheated methane is introduced into the combustor. The compressor (C1) is used to compensate the pressure drop through the SOFC stack.

3 Thermochemical aspects: water gas shift reaction and methane reforming

In the models, the chemical reactions are assumed to be in equilibrium, *i.e.* that they occur instantaneously and reach the equilibrium condition spontaneously at each position.

For SOFC models the electrochemical reactions are as follows:

$$\tfrac{1}{2}O_2 + 2e^- \rightarrow O^{2-} \text{ cathode} \qquad (1)$$

$$H_2 + O^{2-} \rightarrow H_2O + 2e^- \text{ anode} \qquad (2)$$

$$H_2 + \tfrac{1}{2}O_2 \rightarrow H_2O \text{ overall reaction} \qquad (3)$$

The high temperatures inside the HT-SOFC and the IT-SOFC stack can make it possible to reform the methane directly inside the cell if steam is provided at the inlet. The chemical reactions of fuel reforming and water-gas shift are as follows:

$$CH_4 + H_2O \Leftrightarrow CO + 3H_2 \qquad (4)$$

$$CO + H_2O \Leftrightarrow CO_2 + H_2 \qquad (5)$$

The electrochemical and water-gas shift reactions are exothermic, whereas fuel reforming is a strongly endothermic reaction.

4. Description of the HT-SOFC and IT-SOFC models

The fuel cell is treated as a single control volume to which the steady state flow energy equation is applied with the assumption of negligible change of kinetic and potential energy. In order to determine cell performance, the overpotential must be deducted from the Nernst potential (E), which represents the ideal performance.

$$V_{cell} = E - V_{loss} \qquad (6)$$

where

$$E = \frac{RT}{2F}\ln K + \frac{RT}{2F}\ln\left(\frac{p_{H_2}\, p_{O_2}^{1/2}}{p_{H_2O}}\right)$$

4.1 Evaluation of the overpotential HT-SOFC

The overpotential, which is a very important parameter in the analysis of fuel cell performance, is expressed by activation (V_{act}), ohmic (V_{ohm}) and concentration (V_{conc}) overpotentials. Activation overpotential, which estimates losses due to slow electrochemical kinetics, is calculated as follows:

$$V_{act} = ai\exp\left(\frac{b}{T}\right) \qquad (7)$$

In this equation, $a = 2.83\times10^{-4}\ \Omega\text{cm}^2$ and $b = 8360$ K are the coefficients obtained by Solheim from experimental data from Umimura [4].

Ohmic overpotential, which estimates losses associated with ionic and electronic resistance throughout the fuel cell, can be calculated according to [5].

$$V_{ohm} = iR_t \qquad (8)$$

The resistance of all materials used in the SOFC components can be calculated as follows:

$$R_t = \frac{a\delta \exp\left(\frac{b}{T}\right)}{A} \qquad (9)$$

Where a and b are constants that are specific to the materials. δ is the equivalent thickness of the diffusion layer, and A is the active area.

Concentration overpotential, which estimates losses due to mass transport limitations, becomes significant when amounts of current are drown from the cell, it can be calculated according to [5].

$$V_{conc} = -\frac{\bar{R}T}{n_e F}\ln\left(1-\frac{i}{i_L}\right) \qquad (10)$$

4.2 Evaluation of the overpotential in IT-SOFC

The model of the IT-SOFC stack used in this paper is based on an existing IT-SOFC model [2]. In this model the cell utilises an electrolyte with a thickness of 25 µm, a 50-µm thick cathode, and a 250-µm thick anode. The cells are assumed to be stacked between bipolar interconnect plates. In contrast to HT-SOFC, which uses a ceramic interconnect, the IT-SOFC uses a lower operating temperature that allows the use of metal alloys.

It is difficult to break down reported cell characteristics in these individual contributions, and in the present context where the aim is stack and system modelling, all cell losses are lumped together in one equivalent resistance. The cell resistance is assumed to have the following temperature dependence [2]:

$$R_{tot} = \mathrm{A}\exp\left(\frac{\Delta\mathrm{E}}{\mathrm{K}\times T}\right) \qquad (11)$$

Where T represents the cell operating temperature and K is the Boltzmann constant. The activation energy ($\Delta\mathrm{E} = 1.01\times10^{-19}$ J) and the pre-exponential factor ($\mathrm{A} = 2.98\times10^{-4}$) were chosen to fit the experimental data reported by [2].

4.3 Electrical power of the fuel cells

The electrical power produced by the fuel cell is calculated by:

$$\dot{W} = V_{cell} I \qquad (12)$$

The heat lost to the environment at equilibrium can be determined by evaluating the entropy rate balance for a control volume.

$$\dot{Q}_{cv} = T\left(\Delta S - \sigma_{cv}\right) \qquad (13)$$

Where:

$$\Delta S = \left(S^{\circ}_{H_2O} - S^{\circ}_{H_2} - \tfrac{1}{2}S^{\circ}_{O_2}\right) + \frac{R}{2}\ln\left(\frac{(p_{H_2})^2\, p_{O_2}}{(p_{H_2O})^2}\right)$$

The 'thermodynamic' entropy production, which is actually the irreversibility, is related to the electrochemical overpotential as [5]:

$$\sigma_{cv} = \frac{2F}{T}V_{loss} \qquad (14)$$

5. Cycle performance variables

The steam to carbon ratio is defined as the ratio between the mole flow rate of steam and the CH_4 mole flow rate to the anode.

$$S/C = \frac{\dot{n}_{H_2O}}{\dot{n}_{CH_4}} \qquad (15)$$

The fuel utilisation factor is defined by:

$$u_f = \frac{\dot{n}_{H_2 consumed}}{\dot{n}_{H_2 in} + \dot{n}_{COin} + 4\dot{n}_{CH_4 in}} \qquad (16)$$

The fuel cell efficiency (η_{FC}) is defined as the ratio of power produced by the fuel cell (IT-SOFC or HT-SOFC) to the lower heating value (LHV) of the total amount of fuel ($Q_{tot} = m_{tot} \times LHV$) supplied to the system.

$$\eta_{FC} = \frac{P_{FC}}{Q_{tot}} \qquad (17)$$

The net cycle efficiency (η_{net}) is defined as the ratio of the power produced by the fuel cells (P_{FCs}) and the turbine, minus the total compressor power, to the (LHV) of the total amount of fuel (Q_{tot})

$$\eta_{net} = \frac{P_{FCs} + P_{turb} - P_{comp}}{Q_{tot}} \qquad (18)$$

6. Results and discussions

6.1 Performance of the IT-SOFC/HT-SOFC combined cycle

In these simulations the effects of changing several operating parameters (such as operating temperature of IT-SOFC, current density, cell pressure, total fuel utilisation rate and fuel recirculation rate) on the efficiencies of IT-SOFC stack, HT-SOFC stack, and IT-SOFC/HT-SOFC combined cycle are investigated. In the analyses, the low line (-) indicates the efficiency of the HT-SOFC stack , the multiplication sign (×) indicate the efficiency of the IT-SOFC stack, the solid squares (■)indicate the efficiency added by both IT-SOFC and HT-SOFC, and the triangles (▲) indicate the net efficiency of the IT-SOFC/HT-SOFC combined cycle.

6.1.1. Operating temperature of the IT-SOFC

In the IT-SOFC/HT-SOFC combined cycle, increasing the operating temperature of the IT-SOFC decreased the electrolyte resistance in both SOFC stacks and increased the efficiencies of both IT-SOFC and HT-SOFC (Fig. 3).

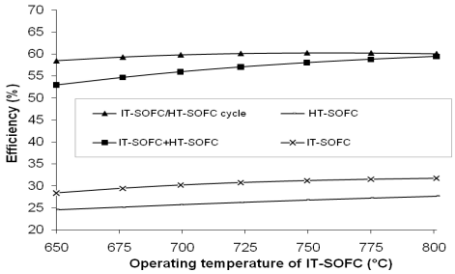

Fig. 3- Effect of operating temperature on net efficiency of IT-SOFC/HT-SOFC combined cycle.

The overpotential is lower in the IT-SOFC than in the HT-SOFC, and so the efficiency of IT-SOFC is higher than that of the HT-SOFC. In the gas turbine cycle, an increase in the operating temperature of the IT-SOFC led to a decrease in the turbine inlet temperature. Thus, turbine inlet temperature decreased with decreasing

turbine output. Since the increase in the efficiency of both SOFCs is larger than the decrease in the efficiency of the gas turbine, there is a net increase in the efficiency of the IT-SOFC/ HT-SOFC combined cycle.

6.1.2. Current density

Fig. 4 shows the changes in the net efficiency of the cycle with mean current density and gives an idea about the contribution of each cell and the gas turbine to the net efficiency in the IT-SOFC/HT-SOFC combined cycle. In the IT-SOFC/HT-SOFC combined cycle, increasing the current density increased the overpotential of SOFC, resulting in decreased efficiencies of IT-SOFC and HT-SOFC. In the gas turbine cycle, as the outlet temperature of the SOFC stacks increased with the increase of current density, the gas turbine inlet temperature increased together with the increasing turbine output. Because the decrease in the efficiency of both SOFCs is larger than the increase in the efficiency of the gas turbine, the net efficiency of the IT-SOFC/HT-SOFC combined cycle goes down.

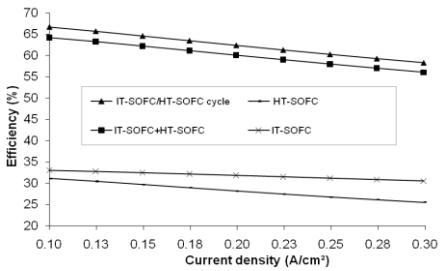

Fig. 4- Effect of current density on net efficiency of IT-SOFC/HT-SOFC combined cycle.

6.1.3. Cell pressure

Fig. 5 shows the changes in the net efficiency of the cycle with cell pressure. Raising the cell pressure caused an increase in the Nernst potential. Also increasing the operating pressure led to some decrease in the overpotential, resulting in an increase in the net efficiency in the IT-SOFC/HT-SOFC combined cycle. An increase in the compressors' outlet temperature due to the increase of the operating pressure caused an increase in the turbine inlet temperature, and consequently raised gas turbine output.

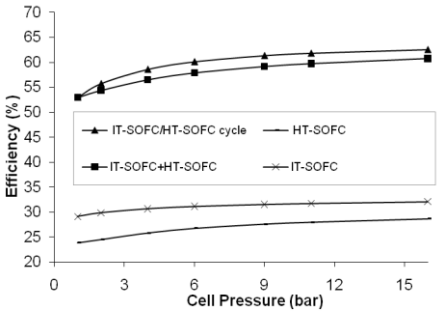

Fig. 5- Effect of cell pressure on net efficiency of IT-SOFC/HT-SOFC combined cycle.

6.1.4. Total fuel utilisation rate

Fig. 6 shows the changes in the net efficiency of the cycle with total fuel utilisation rate. The energy converted at the SOFC stacks increased with rises in the fuel utilisation rate. Due to the rise in the fuel utilisation rate, the electrical output of the SOFC stacks goes up. Therefore, the net efficiency of the cycle increased with increasing fuel utilisation rate.

6.1.5. Fuel recirculation rate

Fig. 7 shows the changes in the net efficiency of the cycle with fuel recirculation rate. Increasing the fuel recirculation rate lowered concentration in the outlet of the SOFC anode.

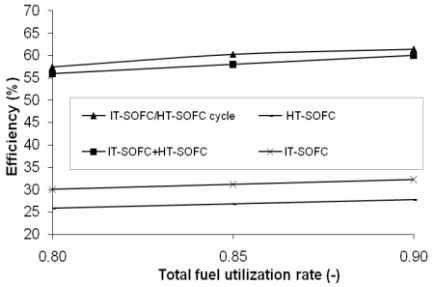

Fig. 6- Effect of total fuel utilization on net efficiency of IT-SOFC/HT-SOFC combined cycle.

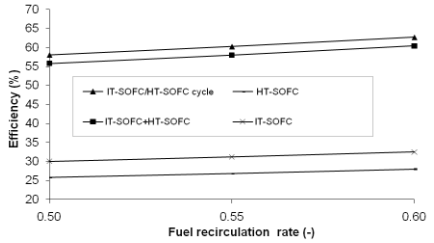

Fig. 7- Effect of fuel recirculation rate on net efficiency of IT-SOFC/HT-SOFC combined cycle.

This means that an increase in the mass flow rate of steam resulted in moving the reforming and gas shift reaction equilibrium to the H_2 side. Increases in the fuel recirculation rate led to increased electrical output of the SOFC stacks, and a slight increase in net efficiency of the cycle.

6.2 Comparison of performances between the combined cycles and the single-staged HT-SOFC cycle

The simulation of the single-staged SOFC cycle is done at 875°C and under the same standard operating conditions (Table. 1) used with the combined cycles.

Fig. 8 shows the changes in the total power of the cycles. The total power of the cycle is the power produced by the fuel cells and turbine, minus the compressors' power. Increasing the current density increased the fuel cell stacks overpotential, resulting in a decrease of the cell voltage. Since the increase in the current density is larger than the decrease in the cell voltage, the electrical outputs of the fuel cell stacks go up (Fig. 9). The two-staged IT-SOFC combined cycle has a higher total power than the IT-SOFC/HT-SOFC combined cycle. This is because the electrical output of the second stage IT-SOFC in the two-staged IT-SOFC cycle is higher than that of HT-SOFC in the IT-SOFC/HT-SOFC cycle.

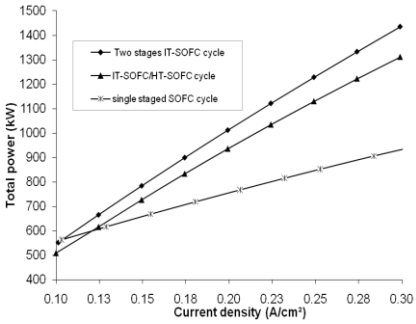

Fig. 8- Total power of the cycles as a function of current density.

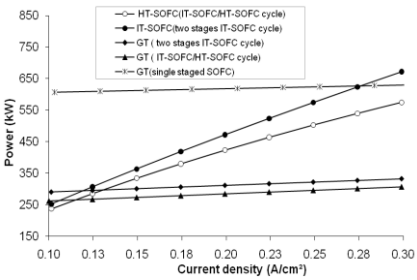

Fig. 9- Fuel cell stacks and gas turbine (GT) powers as a function of current density.

Also, the electrical output of gas turbine in the two-staged IT-SOFC system

is higher due to the increased turbine inlet temperature. The reason that the turbine inlet temperature of the IT-SOFC/HT-SOFC system is lower than the two-staged IT-SOFC system is that much heat is required to further increase the inlet cathode gas temperature in the IT-SOFC/HT-SOFC system.

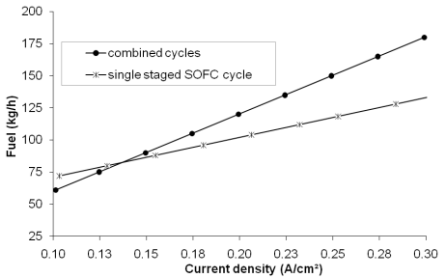

Fig. 10- Total fuel consumption in the cycles as a function of current density.

The total fuel consumption in both combined cycles is similar (Fig. 10). As efficiency is the ratio of total power to total fuel consumption, the efficiency is higher in the two-staged IT-SOFC combined cycle (Fig.11). Though the fuel consumption is lower in the single-staged SOFC cycle (Fig. 10), the total power is also lower, causing the reduction in efficiency.

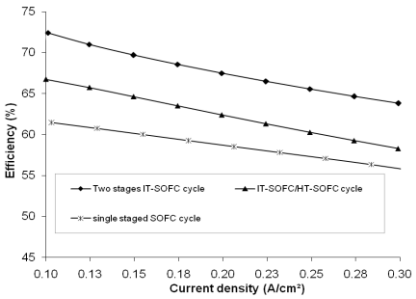

Fig. 11- Change of the net efficiency of the cycles with mean current density.

7. Conclusion

Two types of combined cycles are proposed and investigated: a combined cycle consisting of two staged combination of IT-SOFC and HT-SOFC, and another consisting of two stages of IT-SOFC. Moreover, the effects of changing several operating parameters such as operating temperature of IT-SOFC and current density on the efficiency of IT-SOFC/HT-SOFC combined cycle are evaluated.

The simulation results show that the cycle efficiency increased when cell pressure, fuel utilisation rate and fuel recirculation rate increase. Moreover, the two-staged SOFC system gave much higher net efficiency than the system with the single-staged SOFC. Two stages IT-SOFC system together with gas turbine can lead to highly efficient power cycle.

Nomenclature

F	faraday's constant (96487 kC kmol^{-1})
i	current density (A cm^{-2})
$\dot{Q}$	heat (kW)
p	partial pressure (Pa)
h	specific enthalpy (kJ kmol^{-1})
n	molar flow (mol s^{-1})
s	specific entropy (kJ kmol^{-1}K^{-1})
P_{FCs}	fuel cell stacks electrical power (kW)
R_t	ohmic resistance of HT-SOFC material (Ω m²)
i_L	limiting current density (A cm^{-2})
R_{tot}	cell resistance of IT-SOFC satck (Ω cm^{-2})
A_{cell}	active cell area (m²)
u_f	total fuel utilization
V_{cell}	cell voltage (V)
V_{act}	activation overpotential (V)
V_{ohm}	ohmic overpotential (V)
V_{conc}	concentration overpotential (V)

$\overline{R}$ universal gas constant (8.314 kJ $kmol^{-1}K^{-1}$)
S/C steam-carbon ratio

Greek letters

η efficiency (%)
$\dot{\sigma}_{cv}$ entropy production in a control volume (kW K^{-1})

Subscripts and Superscripts

0 at standard temperature and pressure
i initial
p product
R reaction or reactants

References

[1] Araki T, Ohba T, Takezawa S, Onda K, Sakaki Y. Cycle analysis of planar SOFC power generation with serial connection of low and high temperature SOFCs. J. Power Sources 2006; 158: 52-59.

[2] Plasson J, Selimovic A, Hendriksen P. Intermediate temperature SOFC in gas turbine cycles. J. ASME 2001; GT: 0091.

[3] Musa A, Steeman H, De Paepe M. Performance of internal and external reforming molten carbonate fuel cell systems. J. ASME 2007; 4: 65-71.

[4] Stiller C. Design, Operation and Control Modelling of SOFC/GT Hybrid Systems. Doctoral Thesis, Norwegian University of Science and Technology, Norway, 2006; pp. 41-42.

[5] Chan SH, Ho HK, Tian Y. Modelling of simple hybrid SOFC and Gas Turbine Power Plant. J. Power Sources 2002; 109: 111-120.

[6] Zhang, X., Chan, S.H., Li, G; Ho, H.K; Li, J; Feng, Z; "A review of integration strategies for solid oxide fuel cells", Journal of Power Sources 2010; 195:685-702.

[7] Chan SH, Low CF, Ding OL. Energy and exergy analysis of simple solid-oxide fuel cell power systems J. Power Sources 2002; 103: 188-200.

[8] Calise F, Dentice d'Accadia M, Palombo A, Vanoli L. Simulation and exergy analysis of a hybrid Solid oxide fuel cell (SOFC)-Gas Turbine system J. Energy 2006; 31: 3278-3299.

MATLAB /SIMULINK MODDLING OF STAND-ALONE SELF-EXCITED INDUCTION GENERATOR DRIVEN BY VARIABLE SPEED PRIME MOVER

Dr. Mustafa .A. AL-REFAI
Dept of Electrical and Electronic Engineering
Faculty of Engineering, Alfatah University
alrefai@ee.edu.ly

***Abstract*—** this paper presents simulation of stand-alone of self-excited induction generator driven by variable speed prime mover. The proposed dynamic model consists of induction machine, excitation capacitor and inductive load expressed in stationary reference frame with the actual magnetizing saturation curve of the induction machine. The aim of this paper is to develop and design stand-alone self-excited induction generator and to describe its loading analysis using Mallab/Simulink. Using the Matlab/Simulink environment in model development features high flexibility and makes it possible to adapt the model whatever is needed. The system has been simulated to verify its capability such as build-up voltage and stator flux-linkage response, stator phase current, electromagnetic torque and variation of magnetizing inductance both during dynamic and steady state with variable speed prime mover.

I. INTRODUCTION

HE Self Excited Induction Generator Tshown in Fig. 1 has gained considerable attention due to its application as a stand-alone generator using conventional and non conventional energy sources.

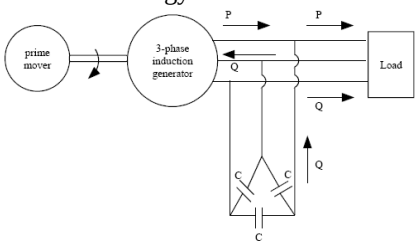

Fig .1 Self-excited induction generator.

Induction machine modeling has continuously attracted the attention of researchers not only because such machines are made and used in largest numbers but also due to their varied modes of operation both under steady and dynamic states. Induction machines operate both in motoring and generation modes. Recent exploitation of renewable energy systems such as wind and small hydro has led to use of grid connected and self excited induction generators. The essence of simulation of such complex machines such as Self Excited

Induction generator involves solving of complex equations of high order.

The induction generator self-excitation phenomenon has been well known since the beginning of the last century [1-2]. In recent years, self-excited induction generator has been widely used as suitable

power source, particularly in renewable power generating systems, such as in hydroelectric and wind energy applications, [3-6]. Self-excited induction generator offers certain advantages over a conventional synchronous generator as a source of isolated power supply. Reduced unit cost, brushless rotor (squirrel cage rotor), absence of DC power supply for field excitation, small seize, source, and ease of maintenance are among the advantages. Due to change emphasis on energy problems, development of suitable isolated power generators driven by unconventional energy sources such as wind, biogas etc., has recently assumed greater importance. The disadvantages of this type of generator are its relatively poor voltage and frequency regulation, and low power factor [7].

A three-phase induction machine can be operated as a SEIG if its rotor is externally driven by a suitable speed and a three capacitor bank of a sufficient value is connected across its stator terminals. When the induction machine is driven at the required speed, the residual magnetic flux in the rotor will induce a small e.m.f. in the stator winding. If the induced emf is sufficient, leading currents through the capacitors will circulate. The magnetic flux produced due to these currents would assist the residual magnetism in magnetizing the iron core of the induction generator. This would increase the machine main magnetic flux and larger emf will be induced. This in turn will increase both the currents and the flux. The induced voltage and the current will continue to rise until the reactive power supplied by the capacitors is balanced by the reactive power required by the induction machine, a condition which is essentially decided by the saturation of the magnetic cores. This process is thus cumulative and the induced voltage keeps on rising until saturation is reached [7-10].

The frequency and magnitude of voltage generated by the SEIG is highly influenced by the rotor speed, the excitation and the load [11-12]. The steady state analysis of the isolated SEIG has been extensively dealt with over the last decades. However, the literature on the analysis of the dynamic performance of the isolated self-excited induction generator, particularly under different loading conditions, appears to be somewhat sparse. This paper presents the design, simulation and analysis of the dynamic performance of stand-alone three-phase SEIG feeding general inductive load connected to its terminal using Mallab/Simulink. This method is applicable during both dynamic and steady-state of SEIG driven with variable speed prime mover. This method is based on the analysis of the dynamic α-β reference frame model of the SEIG with a general inductive load connected to its terminal. The mathematical modeling of SEIG, presented in section II, is based on stationary reference frame. A simulation Simulink Model consisting of the induction generator, the excitation capacitor, and inductive load is presented in section III. To validate the proposed model, simulation results is presented in section IV. Finally conclusions of the work are given.

II. MATHEMATICAL MODELLING OF THREE-PHASE SELF-EXCITED INDUCTION GENERATOR

Although the behavior of the induction machine may be described in any of the commonly used reference frames. [13] The voltage equations for each of them can be obtained from the voltage equations in arbitrary reference frame by assigning the appropriate speed to ω. For the stationary reference frame, ω=0, for the synchronous

reference frame, $\omega=\omega_e$, and for the rotor reference frame, $\omega=\omega_r$. Generally, the conditions of operation will determine the most convenient reference frame or analysis and/or simulation purposes. The stator reference frame is used when the stator voltages are unbalanced or discontinuous and the rotor applied voltages are balanced or zero. The rotor reference frame is used when the rotor voltages are unbalanced or discontinuous and the stator applied voltages are balanced. The stationary frame is used when all (stator and rotor) voltages are balanced and continuous. In this paper, the stationary reference frame $\omega= 0$ is used for simulating the self-excited induction generator (SEIG). With all rotor parameters quantities are referred to the stator. Fig. 2 shows the α-β equivalent circuit of the SEIG in stationary frame.

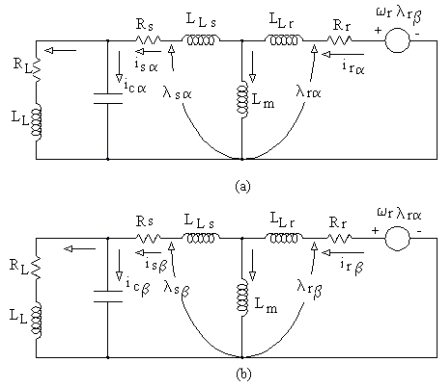

Figure.2 SEIG equivalent circuit (a) α-axis (b) β-axis.

The dynamic model of SEIG in the stationary α-β coordinate system attached to the stator is expressed by the following equations.

The stator voltage differential equatons:

$$v_{s\alpha} = R_s i_{s\alpha} + \frac{d}{dt}\lambda_{s\alpha} \quad \text{.....(1)}$$

$$v_{s\beta} = R_s i_{s\beta} + \frac{d}{dt}\lambda_{s\beta} \quad \text{.....(2)}$$

The rotor voltage differential equations:

$$v_{r\alpha} = R_r i_{r\alpha} + \frac{d}{dt}\lambda_{r\alpha} - \omega_r \lambda_{r\beta} \quad \text{....(3)}$$

$$v_{r\beta} = R_r i_{r\chi} + \frac{d}{dt}\lambda_{r\beta} + \omega_r \lambda_{r\alpha} \text{.....(4)}$$

Where:

R_s *and* R_r denote stator and rotor resistances referred to the stator, $v_{s\alpha}, v_{s\beta}, v_{r\alpha}, v_{r\beta}$ denote the $\alpha-\beta$ axis components of the stator, and rotor voltages referred to the stator respectively, $i_{s\alpha}, i_{s\beta}, i_{r\alpha}, i_{r\beta}$ represent the $\alpha-\beta$ axis component of the stator, and rotor currents referred to the stator respectively; $\lambda_{s\alpha}, \lambda_{s\beta}, \lambda_{r\alpha}, \lambda_{r\beta}$ represent the $\alpha-\beta$ axis components of the stator, and rotor fluxes referred to the stator respectively; and ω_r is the angular speed of the rotor.

The stator and rotor flux linkages expressed in terms of the stator and rotor current space vectors:

$$\lambda_{s\alpha} = L_s i_{s\alpha} + L_m i_{r\alpha} \quad \text{.....(5)}$$

$$\lambda_{s\beta} = L_s i_{s\beta} + L_m i_{r\beta} \quad \text{.....(6)}$$

$$\lambda_{r\alpha} = L_r i_{r\alpha} + L_m i_{s\alpha} \quad \text{.....(7)}$$

$$\lambda_{r\phi} = L_r i_{r\beta} + L_m i_{s\beta} \quad \text{.....(8)}$$

Substituting equations (5-6) into equations (1-4) then

$$v_{s\alpha} = R_s i_{s\alpha} + L_s \frac{d}{dt} i_{s\alpha} + L_m \frac{d}{dt} i_{r\alpha} \quad ..(9)$$

$$v_{s\beta} = R_s i_{s\beta} + L_s \frac{d}{dt} i_{s\beta} + L_m \frac{d}{dt} i_{r\beta} \quad ..(10)$$

$$v_{r\alpha} = R_r i_{r\alpha} + L_r \frac{d}{dt} i_{r\alpha} + L_m \frac{d}{dt} i_{s\alpha} + \omega_r \lambda_{r\beta} \quad .....(11)$$

$$v_{r\beta} = R_r i_{r\beta} + L_r \frac{d}{dt} i_{r\beta} + L_m \frac{d}{dt} i_{s\beta} - \omega_r \lambda_{r\alpha} \quad ...(12)$$

For a self excited induction generator, the voltage-current equations of the excitation capacitor are expressed in the stationary reference frame as:

$$V_{c\alpha} = \frac{1}{c}\int i_{c\alpha} dt + V_{c\alpha o} \quad .....(13)$$

$$V_{c\beta} = \frac{1}{c}\int i_{c\beta} dt + V_{c\beta o} \quad .....(14)$$

Where C denotes excitation capacitor.

The components of rotor flux linkage in the stationary reference frame can be written as follows:

$$\lambda_{r\alpha} = L_r i_{r\alpha} + L_m i_{s\alpha} + \lambda_{r\alpha o} \quad .....(15)$$

$$\lambda_{r\beta} = L_r i_{r\beta} + L_m i_{s\beta} + \lambda_{r\beta o} \quad .....(16)$$

Where:

$\lambda_{r\alpha o}$ *and* $\lambda_{r\beta o}$ are the remnant or residual rotor flux linkage along $\alpha - \beta$ axis

respectively.

Then with an electrical rotor speed of ω_r, the rotational voltage in the stationary reference frame can be described as follows:

$$\omega_r \lambda_{r\alpha} = \omega_r L_r i_{r\alpha} + \omega_r L_m i_{s\alpha} + \omega_r \lambda_{r\alpha o} \quad ...(17)$$

$$\omega_r \lambda_{r\beta} = \omega_r L_r i_{r\beta} + \omega_r L_m i_{s\beta} + \omega_r \lambda_{r\beta o} \quad ....(18)$$

Using the equivalent circuit of SEIG given in figure.1 and from last equations the following matrix model for SEIG could be formulated as follows:

$$\begin{bmatrix} 0 \\ 0 \\ 0 \\ 0 \end{bmatrix} = \begin{bmatrix} R_s + pL_s & 0 & pL_m & 0 \\ 0 & R_s + pL_s & 0 & pL_m \\ pL_m & \omega_r L_m & R_r + pL_r & \omega_r L_r \\ -\omega_r L_m & pL_m & -\omega_r L_r & R_r + pL_r \end{bmatrix} \begin{bmatrix} i_{s\alpha} \\ i_{s\beta} \\ i_{r\alpha} \\ i_{r\beta} \end{bmatrix} + \begin{bmatrix} v_{c\alpha} \\ v_{c\beta} \\ \omega_r \lambda_{r\beta 0} \\ -\omega_r \lambda_{r\alpha 0} \end{bmatrix} \quad ..(19)$$

The above equation can be written in the state space equations as follows:

$$ApI + BI + V = 0 \quad .....(20)$$

Where

$$A = \begin{bmatrix} L_s & 0 & L_m & 0 \\ 0 & L_s & 0 & L_m \\ L_m & 0 & L_r & 0 \\ 0 & L_m & 0 & L_r \end{bmatrix}, \quad B = \begin{bmatrix} R_s & 0 & 0 & 0 \\ 0 & R_s & 0 & 0 \\ 0 & -\omega_r L_m & R_r & \omega_r L_m \\ \omega_r L_m & 0 & \omega_r L_r & R_r \end{bmatrix}$$

$$I = \begin{bmatrix} i_{s\alpha} \\ i_{s\beta} \\ i_{r\alpha} \\ i_{r\beta} \end{bmatrix}, \quad V = \begin{bmatrix} v_{c\alpha} \\ v_{\beta} \\ \omega_r \lambda_{r\beta 0} \\ -\omega_r \lambda_{r\alpha 0} \end{bmatrix}$$

Using matrix inversion, equation (20) can be written as follows:

$$pI = -A^{-1}BI - A^{-1}V \quad (21)$$

From last equation, a set of first order differential equations in term of the stator and rotor currents can be obtained as follows:

$$pi_{s\alpha} = \frac{-L_r}{L}(_r R_s i_{s\alpha} + v_{c\alpha}) + \frac{L_m}{L}[\omega_r (L_m i_{s\beta} + L_r i_{r\beta} + \lambda_{r\beta 0}) + R_r i_{r\alpha}]$$

..(22)

$$pi_{s\beta} = \frac{-L_r}{L}(_r R_s i_{s\beta} + v_{c\beta}) - \frac{L_m}{L}[\omega_r (L_m i_{s\alpha} + L_r i_{r\alpha} + \lambda_{r\alpha 0}) - R_r i_{r\beta}]$$

…(23)

$$pi_{r\alpha} = \frac{L_m}{L}(_r R_s i_{s\alpha} + v_{c\alpha}) - \frac{L_s}{L}[\omega_r (L_m i_{s\beta} + L_r i_{r\beta} + \lambda_{r\beta 0}) + R_r i_{r\alpha}]$$

……,,,,,,……(24)

$$pi_{r\beta} = \frac{L_m}{L}(_r R_s i_{s\beta} + v_{c\beta}) + \frac{L_s}{L}[\omega_r(L_m i_{s\alpha} + L_r i_{r\alpha} + \lambda_{r\alpha 0}) - R_r i_{r\beta}] \quad ..(25)$$

Where:

$$p = \frac{d}{dt} \quad \text{and} \quad L = L_s L_r - L_m^2$$

$$L_s = L_{ls} + L_m \quad and \quad L_r = L_{lr} + L_m$$

Where:

L_{ls} and L_{lr} = stator and rotor leakage inductance respectively.

L_m = magnetization inductance.

The above differential equations given in equations (22) to (25) are also used when the generator is loaded. And for RL load the differential load voltage equation can be written as follows:

$$pv_{l\alpha} = \frac{1}{C} i_{c\alpha} = \frac{1}{C}(i_{s\alpha} - i_{l\alpha}) \quad .....(26)$$

$$pv_{l\beta} = \frac{1}{C} i_{c\beta} = \frac{1}{C}(i_{s\beta} - i_{l\beta}) \quad ....(27)$$

Where $i_{c\alpha} = i_{s\alpha} - i_{l\alpha}$ and

$i_{c\beta} = i_{s\beta} - i_{l\beta}$

Also the differential load load current can be written as follows:

$$pi_{l\alpha} = \frac{1}{L_L}(v_{L\alpha} - R_{L\alpha}) \quad .... (28)$$

$$pi_{l\beta} = \frac{1}{L_L}(v_{L\beta} - R_{L\beta}) \quad ....(29)$$

III. CHARACTERISTICS OF MAGNETISING INDUCTANCE

In the SEIG the variation of magnetizing inductance, L_m is the main factor in the dynamics of voltage build-up and stabilization of generated voltage for unloaded and loaded conditions. For the machine under investigation the magnetizing inductance characteristic as a function of magnetizing current is shown in fig 3. and it is a nonlinear function of magnetizing current, which can be represented by fifth order polynomial curve fit as in [14].

$$L_m = \frac{1}{120\pi}[-0.1175 I_m^5 + 1.918 I_m^4 - 11.074 I_m^3 + 25.387 I_m^2 - 19.662 I_m + 53.365] \, (H) \quad .....(30)$$

Where the magnetizing current is given by:

$$I_m = \sqrt{(i_{s\alpha} + i_{r\alpha})^2 + (i_{s\beta} + i_{r\beta})^2} \quad ...(31)$$

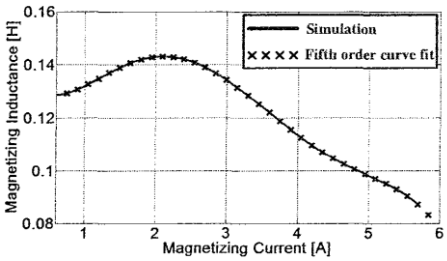

Fig .3 Variation of magnetizing inductance with magnetizing current.

Using equations (22) to (25) and (30) the electromagnetic torque developed by the SEIG can be computed using magnetizing inductance equation (30) and current components in equation (31) and can be expressed by:.

$$T_e = (\frac{3}{2}) \times \frac{P}{2} \times L_m \times (i_{s\beta} i_{r\alpha} - i_{s\alpha} i_{r\beta}) \quad ..(32)$$

Where P is the number of poles

IV. DESIGN OF CAPACITOR BANK OF SEIG

The value of the excitation capacitance must be greater than a minimum limit so that the magnetization current is sufficient for the operation in the nonlinear portion of the magnetization curve. For sustained self-excitation the value of L_m must be less than its unsaturated value and therefore the unsaturated value of L_m gives the minimum value of excitation capacitance below which the excitation takes place.

The capacitance of the capacitor bank is defined as follows:

$$C_{\min} = \frac{1}{\omega_r^2 L_m} \quad \text{.....(33)}$$

Therefore by substituting equation (30) into equation (33), the minimum capacitance required for build-up voltage at the rated speed and under no-load can be calculated and found to be 65 μF.

V. SIMULINK MODELING OF THREE-PHASE SELF EXCITED INDUCTION GENERATOR

SIMULINK has a wide selection of dynamic systems for modeling, analyzing and simulating. It also offers a graphical user interface for creating block diagram models. A system is configured in terms of block diagram representation from a library of standard components. In the middle of a simulation, algorithms and parameters can still be changed to get intuitive results, thus providing the user with a ready access learning tool for simulating many of the operational problems found in the real world. It also provides immediate access to the mathematical, graphical, and programming capabilities of MATLAB [15]. Here, the simulation of the three-phase induction generator has been done by considering the mathematical model of the generator given in Section II. The equations from (22) to (32) have been implemented in MATLAB/SIMULINK using different blocks. In order to have the induction generator self-excited, there must be a remnant magnetization in the machine. This is represented in the model by adding a constant magnetization value corresponding to the remnant value. In this paper the step by step modeling of SEIG using SIMULINK has been described. For simplicity reason the simulation program was built up modularly, using several sub-systems. In the framework of the simulation program there are several switches back and forth between simulation in SIMULINK, respectively computation and visualization taking the full advantages of the program. The main window of the simulation program is given in Fig. 4. Due to the lack of space here not all subsystems of the model can be presented in details.

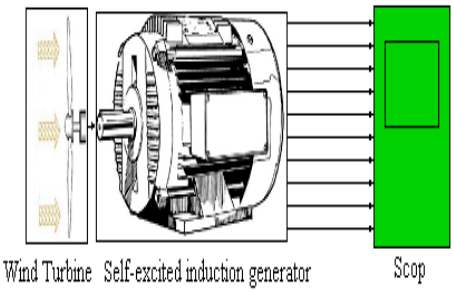

Fig. 4 Simulink Model of SEIG.

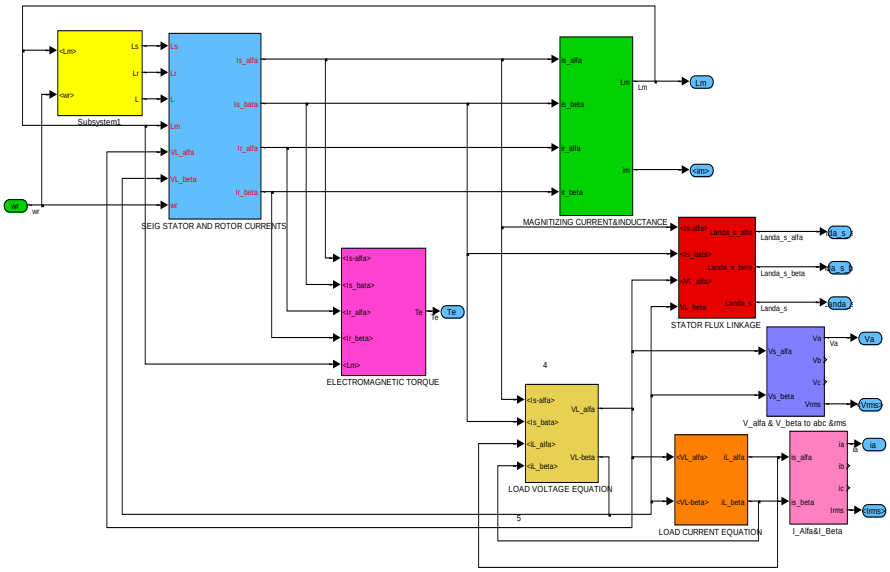

Fig. 5 Su-bsystem blocks of the SEIG model

.

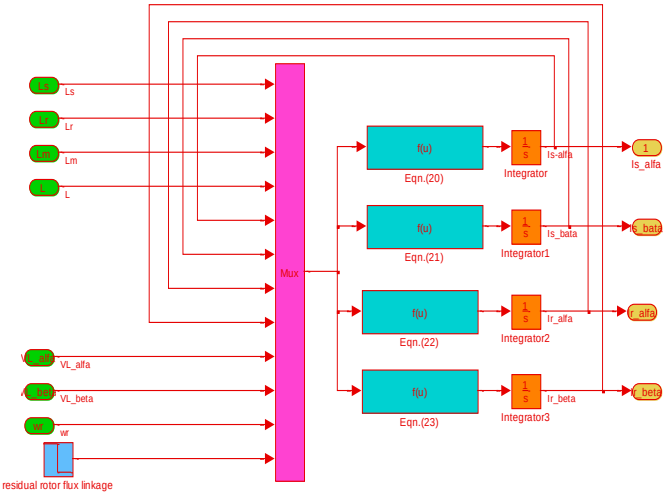

Fig . 6 Sub-system blocks of the stator and rotor currents.

I. SIMULATION RESULTS

Matlab/Simulink simulation software is used to predict the generated voltage from a given three phase self-excited induction machine rotating at a given speed with appropriate capacitors connected at the stator terminals. In this simulation prime mover speed is variable from 1000 rpm to 1500 and the capacitance is fixed. The SEING used for this purpose is a 1.5kW, 220/380V, 3-phase, 4-pole, start connected, 50 Hz, R_s =1.66Ω, R_r = 2.74Ω, L_{ls} =L_{lr}=11.4 mH, L_m=180mH. The simulation result shows that self-excitation can be identified and the effects of different values of initial conditions on self-excitation investigated.

It can be seen that the magnetizing current increases until its peak value, then start to decrease until reaches its saturated value as shown in figures 7. and 8. Figure 9. shows that the electromagnetic torque increases from 0 to -5 Nm during start-up processes. Figure 10. shows build up of stator generated voltage at the terminals of the SEIG during the start of self excitation. The start-up time is about 0.8. Figure 11. shows the effect of varying the drive speed of the stator terminal which seen it decreases by about 20% when the speed of the prime mover decreased by 10%. Fig 12. shows the phase current during start-up processing and at full-load.

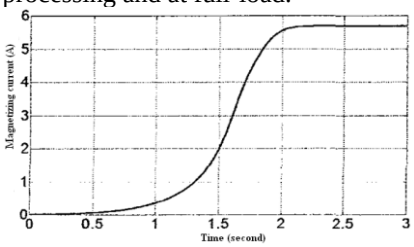

Fig. 7 Magnetizing current I_m (A).

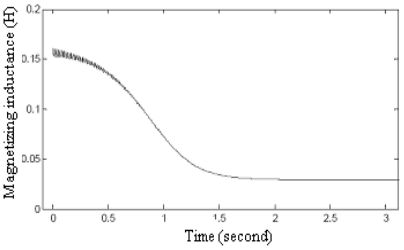

Figure. 8 Variation of magnetizing inductance with voltage buildup.

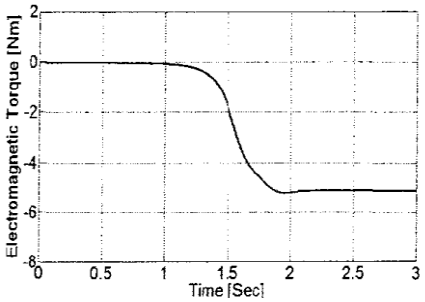

Fig. 9 Electromagnetic torque.

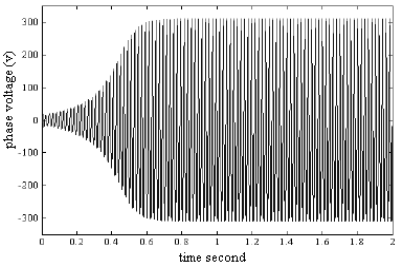

Figure .10 stator phase voltage build-up at speed 1500 rpm and no load.

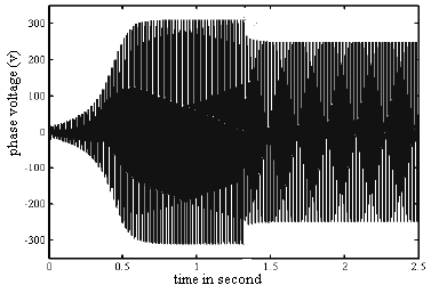

Figure .11 stator phase voltage build-up at speed 1350 rpm and no load.

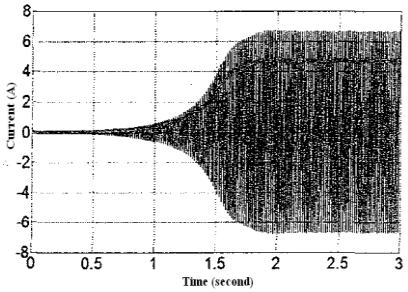

Figure .12 stator phase current with Resistive inductive load (RL) and at 1500 rpm.

II. CONCLUSION

An analysis on the dynamic performance of stand-alone self-excited induction generator driven by variable speed prime mover and feeding three-phase RL static loads is presented. The dynamic models of the SEIG as well as the models of RL load in the $\alpha-\beta$ axis stationary reference frame are given. The proposed dynamic model consists of induction machine, excitation capacitor and inductive load expressed in stationary reference frame with the actual magnetizing saturation curve of the induction machine. The connection of a load onto the SEIG terminals causes its excitation to decrease and thus, the SEIG to operate at lower magnetizing flux. The SEIG output voltage is highly influenced by the impedance and the power factor of the load. The simulation results have shown that, variation of magnetizing inductance and magnetizing current, electromagnetic torque, build-up voltage and current under speed variation. The model gives good dynamic and steady-state performance of SEIG. It is expected that the model presented in this paper would be widely applicable in any system where the induction machine is used as a generator.

REFERENCES

[1] BASSETT E. D., POTTER E. M., "Capacitive Excitation for Induction Generators" Elect. Eng., vol. 54, pp. 540-545, May 1935.

[2] WAGNER C. E., "Self Excitation of Induction Motors" Trans. AIEE, vol. 58, pp. 47-51, Feb. 1939."Analysis of self-excited induction generator", IEE Proc.C., 129(5)(1982),260-265.

[3] T. Ahmed, O. Noro, E. Hiraki, M. Nakaoka: Terminal Voltage Regulation Characteristics by Static Var Compensator for a Three-Phase Self-Excited Induction Generator: IEEE Trans. On Industry Applications, Vol. 40, No. 4, 2004, pp. 978–988.

[4] N. Ammasaigounden, M. Subbiah and M. R. Krishnamurthy, "Wind-drive self-excited pole-changing induction generator, IEEE Proc, B, 133 (5)(1986), 315-312.

[5]G. Grantham, D. Sutanto and B. Mismail, "Steady-state and transient analysis of self-excited induction generator", IEE Proc. B., 136(2)(1989), 61-68.

[6] T .F. Chan, "Self-excited induction generator driven by regulated and

unregulated turbines", IEEE Trans. , EC-11 (2) (1996), 338-343.

[7] Grantham, C., Sutanto, D. and Mismail, B., "Steady-State and Transient Analysis of Self- Excited Induction Generators", Proc. IEE, Vol. 136, Pt.B, No. 2, 1989, pp. 61-68.

[8] Elder, J.M., Boys, J.T. and Woodward, J.L., "Self- Excited Induction Machine as a Low-Cost Generator", IEE Proc. C, 131, (2), 1984, pp.33-41.

[9] Salama, M. H., and Holmes, P.G., "Transient and Steady-State Load Performance of Stand-alone Self-Excited Induction Generator", IEE Proc. - Electr. Power Appl., Vol. 143, No. 1, January 1996, pp. 50-58.

[10] Shridhar, L., Singh B., Jha, C. S., Singh, B. P., and Murthy, SM., "Selection of Capacitance for the Self Regulated Short Shunt Self Excited Induction Generator", IEEE Trans. on EC, Vol.10, No.1, March 1995, pp. 10-17.

[11] G.K. Singh: Self-excited induction generator research-a survey, Electric Power Systems Research, 69, 2004, pp. 107–114.

[12] A. Nesba, R. Ibtiouen, S. Mekhtoub, O. Touhami, N. Takorabet: Rectified Self-Excited *Induction* Generator as Regulated DC Power Supply for Hybrid Renewable Energy Systems, WSEAS Trans. on Circuits and Systems, Issue 11, Vol. 4, November 2005, pp. 1457–1463.

[13] Paul.C.Krause, Oleg Wasynczuk and Scott D. Sudhoff, Analysis of Electric Machinery, IEEE Press, 1994, ch. 3-4.

[14] T.Ahmed, K.Nishida and M. Nakaoka, Advance control for PWM converter and Variable-speed Induction Generator", IET Electric Power Applications, vol. 1 , pp239-347, March 2007.

[15]. Saadat, H., .MATLAB., [Online] 2001, Available: http://www.msoe.edu/~saadat/Matlab.

Performance of silicone rubber insulators in Libyan high voltage network

Dr. Abdulhameed Algammudy
Alfateh University
elgammudi@lttnet.net

Engr. Abdulmowla B. Ohaida
General Electricity Company of Libya
abdulmowla_ohaida@yahoo.com

1. Abstract

This paper deals with two samples of silicone rubber insulators have been exposed to the natural pollution for 6 years in continuously energized line working in Libyan transmission network. The test line is connecting between Khomes power station to Khomes switching substation, the site is considered to be the most polluted site in Libya .Several tests have been done on this type of insulators to the effect of Libyan environment on these insulators to decide if this insulator is suitable for working in the Libyan electrical grid.

2. Introduction

The first composite insulators, for which extensive use was made of polymeric materials appeared in the late 1960's. They are of the long rod design, have a better strength-to-weight ratio, and can be manufactured in longer length than their porcelain counterparts.

Although the cost of the insulators is a relatively small percentage of the cost of building a new transmission line, failure of this small component can result in serious economical consequences. A consequence resulting from the selection of an insulator of inferior quality or an insulator with characteristics not matching the service requirements can be far more than the cost of its premature enhancing coatings or frequent washing all have a significant economic impact. The repair and the daily cost of the unavailability of an important power line can reach hundreds of thousands of dinars.

The growth in the population density and the corresponding higher industrial and agriculture production increased the amount of pollution imposed on insulators. This made environmental stress one of the most critical factors to be considered in the selection of insulators. Moreover, modern electronic equipment and apparatus need a quality and continuity of supply not required previously, it is imperative that modern insulators have the highest achievable level of performance.

Libya is a wide geographical area and demographic distribution. It is divided to desert, mountain, and coastal regions. Therefore supplying the electric energy

to these regions requires long transmission lines at different voltage levels, with different weather condition and types of pollutions are encountered. These factors have to be taken in consideration when choosing the electric insulators. It is well known that the performance of an electric system are strongly affected by the accumulation of pollution on the insulator surface, moreover humid weather condition sometimes cause the insulators to flash over which leads to interruption of electric power or at least fluctuation in electric voltage. As a result decrease of the reliability of electric grid and in general a reduction in the electric power quality. The goal of this paper is to contribute in solving this problem.

3. Insulator materials

Consideration of the properties of the insulating materials to be used is important in the insulator design process. Not only dose the material have to be capable of accommodating high electric stresses over a long term, but it must also withstand often severe environmental effects imposed, such as ultraviolet radiation, contamination and lightning over-voltages. Further, it must possess sufficient tensile, compressive and cantilever strength to support the loads applied and maintain its mechanical integrity over the life of the installation in question. The common materials used in suspension insulators are porcelain, toughened glass and composite insulators.

3.1 Polymer Composites

The term 'composite' refer to insulators with a fiberglass core, which provides the mechanical strength, covered by a housing to protect the core from the environment and to yield the required electric characteristics. A wide variety of constructions and materials are used in the production of composites and thus generalizations of their characteristics can be misleading.

The two main families of housing materials used today are those which are ethylene propylene diene monomer (EPDM) based and those which are silicones (SIR), however, have a higher resistance to ultraviolet degradation and have the unique property of maintaining a hydrophobic (water repellent) surface even when severely contaminated. They are thus more popular for use in areas of significant marine and industrial pollution [1].

The positive features of composite insulators are:

- High tensile strength-to-weight ratio.
- Improved performance in highly polluted areas (silicone rubber type).
- An unattractive target for vandals and very resistant to projectile damage.
- Flexibility, providing better seismic capabilities and preventing cascade failure of post units.
- For apparatus bushing, avoidance of damage to surrounding equipment in the event of explosive of equipment.

The limitations of composite insulators are:

- Subject to leakage current erosion if incorrect material and/or dimensioning used.
- Possible electrical weakness (in some technologies) at the mould line (moulded construction only).

- Special care needed in design and manufacture to ensure the elimination of moisture ingress at interfaces.
- Deflection under load in certain applications[4].

4. Insulators Used in GECOL'S Network

In Libyan transmission line electric network there are two levels of voltages first is 220 kV which about 13000 km long and the second is 400 kV which is new network, it is about 400 km, figures (1 - 2) shows the geographical maps of the above levels of voltages.

Figure (1): geographical map of the Libyan 220 kV network

Figure (2): geographical map of the Libyan 400 kV network

As it illustrates in the geographical maps transmission line net work covers a long distance with different environments so it should perform will in all environmental conditions.

Both glass and porcelain are commonly used materials for insulators and have given good service history backed by years of manufacturing experience. There is little difference in the cost or performance between glass and porcelain. Toughened glass has the advantages for overhead lines that broken insulators tend to shatter completely upon impact and are therefore more easily spotted during maintenance inspections. In practice, the type to be used on overhead lines will depend partly upon the existing spares holdings and spares rationalization practices employed by the particular electricity company.

On the other hand, glass insulators are rarely used in substation practice since on shattering they leave only some 15 mm between the top metal cap and the pin. Porcelain insulators, which may be chipped or cracked but not shattered, are therefore preferred for substation use since access for replacement may require a busbar outage.

5. Flash-Over Statistics on a Western Libyan 220 kV Network for the years 2008 and 2009

Flash over on electric transmission lines can occur by many reasons, some of them related to insulators contaminations and many of another problems [2]. The data of lines outage for the western, southern and medial of 220 kV Libyan network for 2008 and 2009 has been taken from western control center. Also determined the time of the year and hours of the day where the insulators causes more problems. Figures (3 - 4) illustrate the number of monthly outages for the years 2008 and 2009. While

figures (5 - 6) shows the relation between the number of outages and the time of the day of its relation occurrence[6].

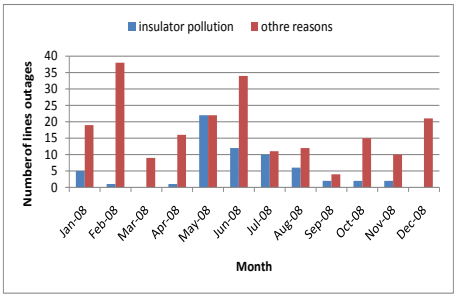

Figure (3): Number of lines outage due to insulators and other reasons in the year of 2008.

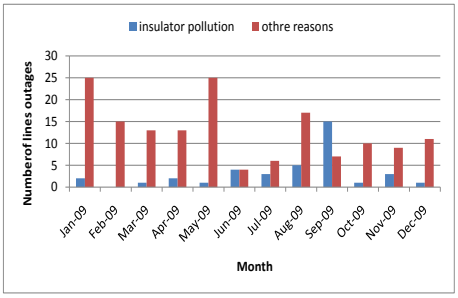

Figure (4): Number of lines outage due to insulators and other reasons in the year of 2009

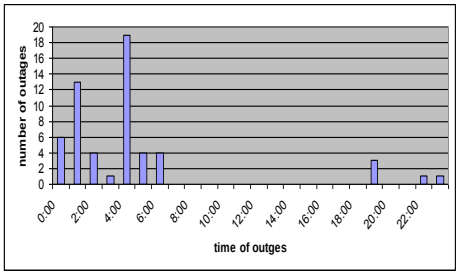

Figure (5): relations between the number of outages and the time of the day of outage in 2008.

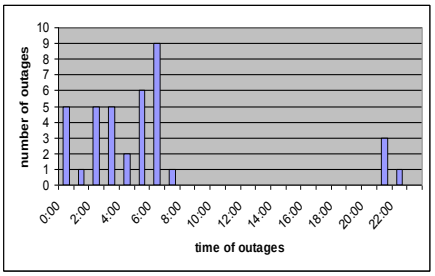

Figure (6): relations between the number of outages and the time of the day of outage in 2009.

From the figures (3 - 4) it's clear that the most of flash over in the transmission lines occurs between May and September, because the relative humidity is very high. Also from the western control center data figures (5 - 6) it's noted that most of outage due to insulator pollution occurs mainly on the coastal lines, and between med night and 6:00 A.m. Most of the outages occur between 5:00 – 6:00 Am. Where it is the highest during September due to the high relative humidity during this period of the year.

6. GECOL'S Remedy for Pollution Problems on T.L

(GECOL) adapted hand cleaning technique on high voltage transmission line insulators on disconnected line as shown in figure (7) , and by using fixed spry washing systems for insulators used in electric substations as shown in figure (8).

Figure (7): hand washing of 220 kV line insulators

Figure (8) fixed spry washing system in Tripoli east 220 kV S/S

To avoid the pollution problems GECOL created 12 departments for transmission line operation and maintenance allover the country, the main job of these departments is to maintain the electric transmission line.

7. Cost of Electric Transmission Line Network's Dry Hand Cleaning.

Regarding to the information from main department of transmission line operation and maintenance, there are 12 department in GECOL for operating and maintenance the Libyan high voltage T/L network, each of department has 30 people, to evaluate the cost the following hypotheses are used[7]:-

- There are 12 department each has 30 technician, the salary of each employee is approximately 400 LD per month.
- Each department have approximately five vehicles each one costs 50,000 LD.
- Each employee needs special clothes, safety belt, clamping stack, safety tools, they cost approximately 500 LD.

- All cleaning works done energized line, the average of 220 kV line capacity is approximately 80 MW. The line under cleaning is stay disconnected from 7 to 10 hours per day for 10 days, this is for 100 km lines.

From the previous data, the approximate cost of insulator cleaning in Libyan 220 kV network can be calculated as follows.

The salary of 30 employees per month is

$$30 * 400 = 12000 \text{ LD} \quad \ldots 1$$

The salary of 12 department employees per month is

$$12 * 12000 = 144{,}000 \text{ LD} \quad \ldots 2$$

The price of employee's equipments

$$30 * 12 * 500 = 180000 \text{ LD} \quad \ldots 3$$

The cost of vehicles for 12 departments is

$$5 * 12 * 50000 = 3000000 \text{ LD} \quad \ldots 4$$

The cost of line disconnection during insulator cleaning if the average price of kWh is 0.03 LD

$$80000(\text{kW}) * 0.03(\text{LD/kWh}) * 8(\text{h/day}) * 10(\text{days}) = 192{,}000 \text{ LD} \quad \ldots 5$$

The insulator cleaning consumes about 50 % of department of transmission line operation and maintenance effort, so the salaries per year are

$$144000/2 * 12 = 864000 \text{ LD} \quad \ldots 6$$

The employees' equipments are replaced every five years so its cost per year is

180000/5 = 36000 LD …7

The validity of vehicles are five years so it's cost per year become

3000000 /5 /2 = 300000 LD …8

There is no reliable data for calculation of energy loss during insulators cleaning of all Libyan 220 kV network but the calculation is made only for one line about 100 km long. The cost of energy loss is as for eq. (5) multiplied by the number of cleaning times per year which is from 2 to 3 times, therefore the cost per year is.

192,000 * 3 =576000 LD

This cost can be reduced or omitted if the disconnected line exists in ring network, so this calculation is true only when the network configuration is radial.
From eq. (6 – 8) we can calculate the cost of cleaning per year.

864000 + 36000 + 300000 = 1,200,000 LD … 9

The previous calculation shows that the insulators' cleaning costs GECOL about 1,200,000 LD per year, this is just the cost of cleaning services, excluding the cost of energy loss and the power quality problems, due to the forced outage. Accordingly, GECOL has to look for a solution for this problem, in year 2002 erected test line equipped with silicone rubber insulators. After 6 years of operation without any cleaning no flashover reported what so were.

8. Results of Insulator Testing

The General Electricity Company of Libya (GECOL) used silicone rubber insulators in a 220 kV test line. This line connects El-khoms power station with switching station it is 8.5 km long. The plan is test two samples of these insulators after five years in operation to understand the aging process. The insulators were inspected and tested at the laboratories and test facilities in the manufacturing company in Germany. Visual inspections, electrical type tests, pollution measurements and material tests were performed.

8.1 Material Investigations

The following points are checked

1- Fiber Reinforced Polymer (FRP): Glass Transition point Tg: is 108.3^{o}C, it's o.k. [spec. 100…115^{o}C].

2- FRP: Interlaminar Shear Strength (ILS): is 70.8 MPa it's o.k. [spec.>65MPa].

3- FRP: High Voltage Water Diffusion Strength (HD): class 2 (leakage current 98 μA) identical to IEC 61109, o.k. [Spec. HD2].

4- FRP: Dye Penetration Test: Passed acc. to IEC 61109, o.k. [Spec. IEC61109].

5- High Temperature Vulcanized silicone rubber (HTV): Hydrophobicty Test: Wettability Class (WC) =1-2.

The Wettability is the ability of a surface to be wetted by a liquid (e.g. water). The appearance on the insulator surface after mist exposure has to be identified with one of the seven wettability (hydrophobicity) classes (WC), which is a value between 1 and 7.
A surface with the WC value 1 is the most hydrophobic surface and a surface

with the WC value 7 is the most hydrophilic surface.
Two visual criteria are used to judge the WC value:
a) The shape of droplets;
b) The percentage part of the surface which is wetted.

8.2 Pollution Measurements

ESDD and NSDD were measured from pollution taken from failed insulator (lab. No. 3356/1-2). The determination was performed by means of the procedures described in IEC 60815-1 (2008).the results are visualized in figure 9.

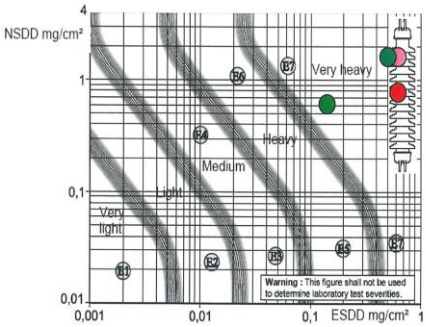

Figure (9): Results of ESDD/NSDD measurements Lab. No. 3356/1 and Lab. No. 3356/2

8.3 Specified Mechanical Load (SML) Verification Test

The SML verification test is in accordance with IEC 61109 (sample test) have been performed on both units together with the test for tightness of sealing and interfaces. Both tests were passed successfully for the SML=160kN. Test results[8]:

- UTS = 181 and 181kN.
- All four (4) sealing are sound and tight in acc. with IEC 61109.

Figure 10 shows the mechanical failure modes after SML verification test.

Figure (10): Lab. No. 3356/1-2: Mechanical failure modes after SML verification Test, UTS =181, 181kN, ball breakage, low scatter.

8.4 Visual Examination

The results of the visual inspection are recoded in the following pictures. No traces of ageing were found. No signs of electrical activity, corona or other surface discharges have been observed. No signs of tracking and erosion were found. The markings are still legible and not degraded. No ultra violet (UV) aging took place at the housing. The hosing of both insulators is fully sound, the end fitting zinc galvanization is still exceeding 85µm (IEC 61109). All four sealings were proven to be fully intact by means of IEC 61109 tightness test. the insulators could have remained in service for at least another 25 years. Life expectancy is > 30 years.

Figure (11): Appearance of insulator shank end fittings, both components are covered with fine dust and sand (Lab No. 3356/1).

Figure (12): Appearance of insulator housing, both covered with fine dust and sand. The pollution has a very strong adhesion to the blue silicone rubber (Lab No. 3356/1).

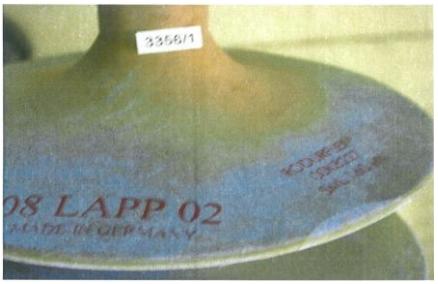

Figure (13): Lab.No. 3356/1 marking is still well legible. No UV degradation, no cracking or other traces of ageing.

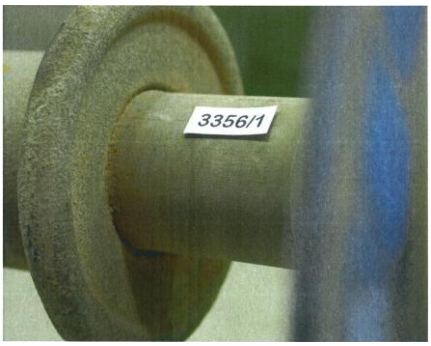

Figure (14): Lab.No. 3356/1 sealing area, sealing is full sound and intact.

Figure (15): Lab.No. 3356/1 Hydrophobicity EC=1-2 in acc. with IEC 62073.

8.5 Electrical Type Tests

Electrical type tests in accordance with IEC 61109 / IEC 60383 were repeated in order to evaluate the residual electrical insulation performance.

These tests are:

1- **Lightning impulse test.**

- Dry lightning impulse withstand voltage, positive.
- Dry lightning impulse withstand voltage, negative.
- 50 % Dry lightning impulse withstand voltage, positive.
- 50 % Dry lightning impulse withstand voltage, negative.

2- Wet switching impulse test.

- Wet switching impulse withstand voltage, positive.
- Wet switching impulse withstand voltage, negative.
- Wet switching impulse flashover voltage, positive.
- Wet switching impulse flashover voltage, negative.

3- Power frequency test.

- Wet power frequency withstand voltage.
- Wet power frequency flashover voltage.
- dry power frequency withstand voltage.
- Dry power frequency flashover voltage.

All the above tests are implemented on the two insulator test samples Lab N^{O}. (3356/1-2). The results are recorded in the Tables (1 - 3). Only a slight /minor decrease in wet switching impulse withstand voltage by -4.4%/-5% and in wet power frequency withstand voltage by 22.5%/25% have been found. The reductions which are caused by the VERY HIGH / EXTREME surface pollutions are not critical for long-term insulation performance of the 245kV OHTL.

Table (1) lightning impulse test

Test type	**Nominal values, or values acc. to specification**	**Test result Lab. No. 3356/1**	**Test result Lab. No. 3356/2**
Dry lightning impulse withstand voltage, positive	**1800 kV**	**1938 kV**	**1953 kV**
Dry lightning impulse withstand voltage,negative	**1800 kV**	**1960 kV**	**1985 kV**
50 % dry lightning impulse withstand voltage, positive	---------	**2016 kV**	**2031 kV**
50 % dry lightning impulse withstand voltage, negative	--------	**2038 kV**	**2064 kV**

Table (2) wet switching impulse test

Test type	**Nominal values, or values acc. to specification**	**Test result Lab. No. 3356/1**	**Test result Lab. No. 3356/2**
Wet switchig impulse withstad voltage, positive	**1050 kV***	**1006 kV**	**990 kV**
Wet switchig impulse withstad voltage, negative	**1050 kV***	**1004 kV**	**1005 kV**
Wet switchig impulse flashover voltage, positive	---------	**1092 kV**	**1074 kV**
Wet switchig impulse flashover voltage, negative	--------	**1089 kV**	**1090 kV**

*) Values acc. to IEC 60071 -1, table 3

Table (3) power frequency test

Test type	**Nominal values, or values acc. to specification**	**Test result Lab. No. 3356/1**	**Test result Lab. No. 3356/2**
Wet power frequency withstand voltage	**800 kV**	**620 kV**	**602 kV**
Wet power frequency flashover voltage	--------	**715 kV**	**708 kV**
Dry power frequency withstand voltage	--------	**1026 kV**	**1012 kV**
Dry power frequency flashover voltage	--------	**>1026 kV**	**>1012 kV**

It is clear from Tables (1 - 3) that the silicone rubber insulators showed no decrease or degradation in their performance after five years of operation in very hostile environment.

9 conclusions

The conclusions of this study are summarized in the following points:

1- Electric insulators are one of the main parts of over head transmission lines, they must meet two requirements, first is the electric insulation for the conductors, and the second is to provide mechanical support for the over head lines.

2- Insulators are subjected to various electric stresses of different origin such as operating voltages and an electric stroke waves due to lightning storms.

3- Most insulator types used in Libyan transmission network are porcelain and glass. These conventional insulators have encountered some problems when it operates in highly polluted areas.

4- The line outage statistics date of 2008 &2009 of western area show that there are many reasons of lines outage such as insulator pollutions, electric faults, over voltages, over currents ...etc.

5- Line outage due to insulators pollution problems mainly occurs between May and September, because in this period there are many sand storms blows (Gibly) and less rain falls and relative humidity is very high especially in the coastal area.

6- The time of the day of line outage due to pollution problems is between 12:00 at med night and 6:00 PM.

7- GECOL uses the hand washing techniques for transmission line insulators cleaning and fixed spry washing techniques for substation insulators.

8- Insulators cleaning costs GECOL approximately 1,200,000 LD per year.

9- The General Electricity Company of Libya (GECOL) used silicone rubber insulators in a 220 kV test line. This line connects El-khoms power station with switching station it is 8.5 km long. Two samples of these insulators tested after

five years in operation. Lab. No. 3356/1-2 were allocated to the sample

10- The silicone rubber insulators performed very well in OHTL. No failure (flash over or ageing damages) were observed or reported. The insulators show excellent service performance under extreme service pollution condition encountered in Khomes area. A minimum life-time of 30 years is expected. Mechanical and electrical performance was verified by the relevant type and sample tests.

11- These tests showed that silicone rubber insulator performs well in Libyan environment.

12- Adding to resistance to contamination there are many another feature of silicone rubber insulators when compared with conventional insulators (porcelain and glass), such as cost, lightweight, less maintenance, gun shooting (vandalism).

10 Recommendations

After 5 years of operation of silicone rubber insulators in Libyan electric grid in Khomes area the test results proved the superiority of this type of insulators above the regular insulators without the need of cleaning, which mean a valuable reduction in outages and maintenance cost. Therefore it's strongly recommended use of this type of insulators in Libyan high and medium voltage networks.

References

1- A. T. El-Gammudi, 'Material Degradation and Ageing of Silicone Rubber Insulators', Third Libyan Arab International Conference on Electrical and Electronic Engineering, 25-28 March 1996.

2- A. T. El-Gammudi, 'performance of 220 kV, Transmission Line Insulators in Tripoli Region', The Third Arabic National CIGRE Committee in Arab Countries Conference, 25-27 May 1999 Doha, Qater.

3- Colin Bayliss, “Transmission and Distribution Electrical Engineering”, Newnes, second edition 1999.

4- W.L. Vosloo, R.E. Macay, C. de Tourreil, The Practical Guide to Outdoor High Voltage Insulators, Crown Publications cc. Johannesburg, July 2004.

5- Polymer insulator training book, Pyungil Co. , Ltd.

6- The GECOL annual reports for 220 kV transmission line outages during 2008 & 2009, National control center and Western control center.

7- The GECOL reports for insulators cleaning, Transmission lines department, Dec. 2009 .

8- The insulators examination report 266/08, Dr. Jans Martin Seifert, 30/10/2008.

Chapter IV

Renewable Energy

Design Of New Street Lighting Lamp

Dr. Bilal Abdullah Nasir Assist Prof Hawijah Technical. Institute
Dr. Zaki Majeed Abdullah Lecturer Hawijah Technical Institute Foundation of Technical Education
Ministry of Higher Education
IRAQ, Mohammed H. Yasen, Engineer
Ministry of Electricity
Management of North Control Center
, Member, IEEE

Abstract

The developments in the technology of high power Light Emitting Diodes (LEDs) offer alternative replacement of the conventional street lighting lamps such as mercury vapour high pressure sodium types, with energy saving up to 90 % and a considerable reduction in carbon emissions.

LEDs offer a number of advantages when compared with the conventional street lighting lamps such as high energy saving, long life, high color index, no dust absorption and instant starting.

In this work a new street lighting lamp using a LED type is designed with its control circuit and implemented at the same street lighting pole and fixture. The model is tested to show its efficiency and power saving when compared with the high pressure mercury vapour street lighting lamp.

Can be supply this type from Solar Cells this type suppose renewable energy .

1-Introduction

During the last hundred years, electrical lighting sources have gone through a series of technology transitions. From early carbon filament lamps to the ever present tungsten filament incandescent lamps to the use of plasma discharge sources, such as fluorescent lamps, high pressure mercury vapor lamps(HPMVL), and metal halide lamps. A solid-state light emitting diode (LED) is bringing a new light source with different operating characteristics.

Recently, this type of lightsource has been commercially available for street lights as replacement for (125) watts high pressure mercury lamps at the same fixtures and poles [1].

LEDs were first introduced in the early 1960s as indicator lights and had efficiency of only (0.01) lumens per watt. By the 1980s, red LED performance had increased to more than (20) lumens per watt, and today produces more than (30) lumen per watt. LEDs are now used in many of applications and are available in several

colors and packages [2].

LEDs for street lighting applications packages a number of LED chips onto a coated printed circuit board and enclosed them in housing suitable for the environment. The LED fixture requires no ballast or capacitors like conventional street lights, rather it converts the line voltage to low voltage direct current with a small electronic power supply, either in the enclosure or mounted on the printed circuit board. LEDs have many advantages over conventional electric light sources, including low power requirements, long life time, small size, optical control and operating characteristics [3]. In many applications where LEDs are used today, the energy saving are at least 50% and up to 90% for applications where they replace in candescent or HPMV lights. The life time of the LED is up to 60000 hours. This is several times greater than the operating life time of conventional lights [3].

Internationally cities through out USA, Europe, China and South Africa now beginning to investigate and implement programs to try and make public street lighting more efficient by replacing traditional high intensity discharge lights with more energy efficient and longer life time white LED lights. White LEDs are very small, extremely efficient and robust as they do not

produce much heat and do not a fragile filament when compared with conventional high intensity discharge lights. Each LED area is usually smaller than one cm^2, so hundreds of them are used in an array to produce enough light for large applications [3].

Due to the above reasons, this paper deals with replacing the conventional high power street lamps, such as (125) w HPMV lamp, with a very low power white LED lamp. The LED lamp can be classified as low power LED (3 volts and up to 50 mA D.C. power) and high power LED (3 volts and up to 350 mA D.C. power). The selection of LED over head lamp units are designed to replace existing Mercury and Sodium street lamps using the same fixtures, poles and extended arms to hold the luminiares.

The developments in high power LED lighting technology offer a viable alternative to conventional street lighting with energy saving up to 90% and a considerable reduction in carbon emissions. High power LED offers a number of significant benefits [4]:

1. High lumen output: High power LED offers up to eight times more brightness than incandescent lamps.
2. Tremendous energy saving: High power LED light sources are extremely efficient returning at least 80% saving over conventional Sodium or Mercury lamps.
3. Long life: Operating for an average of 10 hours per day, LED has a life period of up to 13 years, or 50000 hours.
4. High color index: White LED has a unique color index providing brightness, true colors during the night time hours, and reducing glare or strobe effects common in conventional street lighting.
5. No dust absorption or yellowing: Because LED operates at low voltage and temperature; there is no reduction in brightness or yellowing over the life period of the LED.
6. Instant starting: Unlike Sodium lights, LED lights do not require a time delay to reach optimum brightness levels.

In this paper a new street lighting lamp using a LED type is designed with its

control circuit. This lamp is implemented and tested, to show the validity of the new model and the amount of power saving when compared with the conventional HPMV street lighting lamps.

The following sections deal with white LED lamp back-ground, types, characteristics, connections, colors, control circuit design, practical measurements and conclusions.

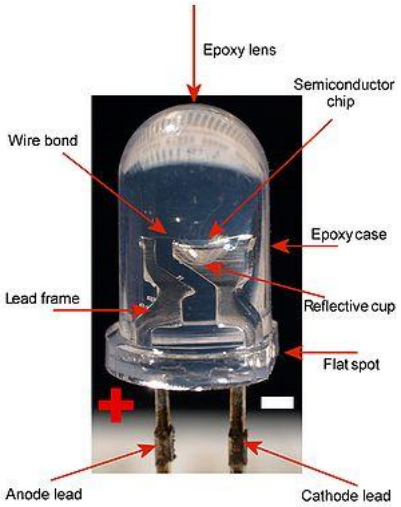

(a) Part of an LED

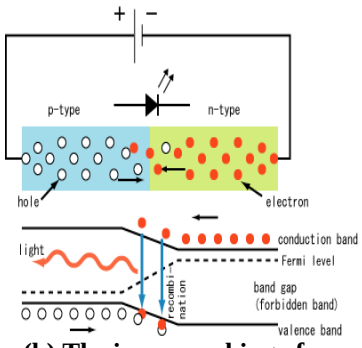

(b) The inner working of an LED

Figure (1) The LED construction and inner operation

2-LED lighting back-ground

The LED is discovered in the early 20th century, and introduced as a practical electronic component in 1962. All early devices emitted low-intensity red light, but modern LEDs are available across the visible, ultraviolet and infra red wavelengths, with very high brightness [5].

LEDs are based on the semiconductor diode, which consist of two semiconductor materials layered on a substrate. Powered by a low D.C. voltage (2-4 V), electrons released from the negative N-type layer combine with holes from the positive P-type layer. When electron-hole pairs combine, a photon of light is emitted from the active layer. The semiconductor is often called a chip. The chips can be packaged in variety of optical refracting forms to enhance the light output. The most common type has been the bullet-shape that incase the chip in area less than 1 cm^2 epoxy package [6].

The first practical visible-spectrum red LED is developed in 1962 by N. Holonyak, while working at General Electric Company [7]. M. George Craford, a former graduate student of Holonyak, invented the first yellow LED and improved the brightness of red and red-orange LED by a factor of ten in 1972 [8]. In 1976, T.P. Pearsall created the first high-brightness; high efficiency LED for optical fiber by inventing new semiconductor materials specifically adapted to optical fiber transmission wavelengths [9]. As the LED materials technology became more advances, the light output is increased. The invention and development of the high power white LED led to use for illumination [10]. In 1995, Alberto Barbieri at the Cardiff University investigated the efficiency and reliability of high-brightness LED demonstrated a very

impressive result by using a transparent contact made of Indium Tin Oxid (ITO) on Aluminium-Gallum-Indium Phosphide/Gallium Arsenide (Al Ga In P/ Ga As) LED. The existence of blue LEDs and high efficiency LEDs quickly led to the development of the first white LED, which employs a phosphor coating to mix yellow light with blue to produce light that appears white [11]. With the development of white lighting, high efficiency and high power LEDs, it has become possible to incorporated LEDs in illumination and street lighting, to replace the conventional light bulbs.

3-LED LIGHTING CONSTRUCTION AND TYPES

1) LIKE A NORMAL DIODE, THE LED CONSISTS OF A CHIP OF SEMICONDUCTING MATERIAL DOPED WITH IMPURITIES TO CREATE A P-N JUNCTION AS SHOWN IN FIGURE (1-A). THE CURRENT FLOWS EASILY FROM THE ANODE TO THE CATHODE. THE CHARGE CARRIERS (ELECTRONS AND HOLES) FLOW INTO THE JUNCTION FROM THE ELECTRODES WITH DIFFERENT VOLTAGES. WHEN AN ELECTRON MEETS A HOLE, IT FALLS INTO A LOWER ENERGY LEVEL, AND RELEASES ENERGY IN THE FORM OF PHOTON AS SHOWN IN FIGURE (1-B). THE WAVELENGTH OF THE LIGHT EMITTED AND ITS COLOR DEPENDS ON THE BAND GAP ENERGY OF THE MATERIALS FORMING THE P-N JUNCTION [12]. IN SILICON OR GERMANIUM DIODES, THERE IS NO OPTICAL EMISSION BECAUSE THESE MATERIALS ARE INDIRECT BAND GAP. THE MATERIALS USED FOR THE LED HAVE A DIRECT BAND GAP WITH ENERGIES CORRESPONDING TO NEAR-INFRARED, VISIBLE OR NEAR-ULTRAVIOLET LIGHT [13]. ADVANCES IN MATERIALS SCIENCE HAVE MADE POSSIBLE THE PRODUCTION OF DEVICES WITH SHORTER WAVELENGTHS, PRODUCING LIGHT IN A VARIETY OF COLORS.

THE MAIN TYPES OF LED ARE SHOWN IN FIGURE (2) AND CAN BE CLASSIFIED AS [14]:

1) MINIATURE (LOW POWER) LED WITHOUT LENS.

2) MINIATURE (LOW POWER) LED WITH LENS.

3) HIGH POWER LED WITHOUT LENS.

4) HIGH POWER LED WITH LENS.

5) IN ALL THESE TYPES, THE OPERATING D .C. VOLTAGE APPROXIMATELY 3 VOLTS, BUT THE RATED CURRENT IS (50 MA) IN THE LOW POWER LEDS AND (350 MA) IN THE HIGH POWER LEDS. THE PERFORMANCE CHARACTERISTICS FOR EACH TYPE ARE TESTED AND STUDIED IN THE FOLLOWING SECTION.

4-LED LIGHTING CHARACTERISTICS

THE 4-TYPES OF LED LIGHTING CLASSIFIED IN THE PREVIOUS SECTION ARE USED IN THIS PROJECT FOR STREET LIGHTING LAMP DESIGN. THESE 4-TYPES ARE TESTED TO PREDICT THEIR PERFORMANCE

CHARACTERISTICS. FIGURE (3) SHOWS THE PHOTOGRAPH OF THE EXPERIMENTAL TEST. THIS PHOTOGRAPH CONSIST OF VARIABLE D.C. POWER SUPPLY (1→12 V, 0→1A), DIGITAL AMMETER, DIGITAL VOLTMETER, FLUX METER, LED MODEL INSIDE A 2-INCHES DIAMETER OF PLASTIC TUBE AND WIRING CONNECTIONS. THE LED IS INTRODUCED INSIDE A WHITE PLASTIC TUBE FROM A CLOSED SIDE AND THE FLUX METER IS SUPPORTED AT THE OTHER END OF THE TUBE TO MEASURE THE LED OUTPUT LUMENOUS FLUX IN A LUX. THE TUBE HAS ONE FOOT LENGTH. A SUITABLE SERIES RESISTANCE (400→600Ω) IS CONNECTED IN SERIES WITH EACH TYPE OF TESTED LED, TO PROTECT THE WHITE LED FROM THE CURRENT FLOWS THROUGH IT DURING THE OPERATION.

FIGURES (4-7) SHOW THE PERFORMANCE CHARACTERISTICS OF THESE 4-TYPES OF WHITE LEDS. FROM THESE FIGURES, THE FOLLOWING POINTS CAN BE CONCLUDED:

1. HIGH POWER WHITE LED WITH A LENS (FIGURE.4) HAS A HIGH LUMINOUS FLUX AND HIGH POWER THAN THAT OF HIGH POWER LED WITHOUT A LENS (FIGURE.5), DUE TO IT HAS A LOWER DIODE RESISTANCE (APPROXIMATELY 45 Ω AT 3 V), HIGH DIODE CURRENT AT THE SAME DIODE VOLTAGE. THE LUMINOUS FLUX DEPENDS ON THE DIODE CURRENT BEFORE THE SATURATION.

2. LOW POWER WHITE LED WITHOUT A LENS (FIGURE.6) HAS A HIGH LUMINOUS FLUX AND HIGH POWER THAN THAT OF LOW POWER WHITE LED WITH A LENS (FIGURE.7), DUE TO THE LOW POWER LED WITHOUT A LENS HAS A LOWER DIODE RESISTANCE THAN THAT OF LOW POWER LED WITH A LENS AT THE SAME DIODE VOLTAGE.

3. THE LUMINOUS EFFICIENCY OF HIGH POWER WHITE LED WITHOUT A LENS IS HIGHER THAN THAT OF HIGH POWER LED WITH A LENS. ALSO THE LUMINOUS EFFICIENCY OF LOW POWER LED WITH A LENS IS HIGHER THAN THAT OF LOW POWER LED WITHOUT LENS.

DUE TO THE LUMENOUS FLUX OF THE LED IS THE IMPORTANT FACTOR IN THE DESIGN OF LED STREET LIGHTING LAMPS, IN THIS PROJECT, THE HIGH POWER WHITE LED WITHOUT LENS IS USED AS THE PREFERRABLE CHOICE.

5-LED LIGHTING COLORS AND MATERIALS [5]

THE CONVENTIONAL LEDS ARE MADE FROM A VARIETY OF INORGANIC SEMICONDUCTING MATERIALS. TABLE (1) SHOWS THE AVAILABLE COLORS WITH THE CORRESPONDING WAVELENGTH RANGE, VOLTAGE DROP ACROSS THE DIODE AND THE MATERIAL TYPE.

IN THE STREET LIGHTING A WHITE LIGHT IS USED TO OBTAIN A HIGH RENDERING INDEX [1, 2, 3, AND 4]. THERE ARE TWO WAYS OF PRODUCING HIGH INTENSITY WHITE LIGHT USING LEDS. ONE IS TO USE INDIVIDUAL LEDS THAT EMIT THREE PRIMARY COLORS-RED, GREEN AND BLUE, AND THEN MIX ALL THESE COLORS TO PRODUCE WHITE LIGHT. THE SECOND METHOD IS TO USE A PHOSPHOR MATERIAL TO CONVERT THE BLUE OR ULTRAVIOLET LIGHT OF LED TO A WHITE LIGHT LED IN THE SAME WAY OF A FLUORESCENT LIGHT BULB WORKS. THE PHOSPHOR METHOD OF

PRODUCING WHITE LIGHT IS STILL THE MOST POPULAR TECHNIQUE FOR MANUFACTURING HIGH INTENSITY WHITE LEDS.

TABLE (1) THE LED COLORS, WAVELENGTH, VOLTAGE DROP AND MATERIAL.

A. COLOR	B. WAVELENGTH [NM]	C. VOLTAGE [V]	D. SEMICONDUCTOR MATERIAL
E. INFRARED	F. $\lambda >$ 760	G. $\Delta V <$ 1.9	H. GALLIUM ARSENIDE (GAAS) ALUMINIUM GALLIUM ARSENIDE (ALGAAS)
I. RED	J. 610 $< \lambda <$ 760	K. 1.63 $< \Delta V <$ 2.03	L. ALUMINIUM GALLIUM ARSENIDE (ALGAAS) GALLIUM ARSENIDE PHOSPHIDE (GAASP) ALUMINIUM GALLIUM INDIUM PHOSPHIDE (ALGAINP) GALLIUM (III) PHOSPHIDE (GAP)
M. ORANGE	N. 590 $< \lambda <$	O. 2.03 <	P. GALLIUM ARSENIDE PHOSPHIDE (GAASP) ALUMINIUM GALLIUM INDIUM PHOSPHIDE (ALGAINP) GALLIUM (III) PHOSPHIDE (GAP)
	610	$\Delta V <$ 2.10	
Q. YELLOW	R. 570 $< \lambda <$ 590	S. 2.10 $< \Delta V <$ 2.18	T. GALLIUM ARSENIDE PHOSPHIDE (GAASP) ALUMINIUM GALLIUM INDIUM PHOSPHIDE (ALGAINP) GALLIUM (III) PHOSPHIDE (GAP)
U. GREEN	V. 500 $< \lambda <$ 570	W. 2.18 $< \Delta V <$ 4.0	X. INDIUM GALLIUM NITRIDE (INGAN) / GALLIUM (III) NITRIDE (GAN) GALLIUM (III) PHOSPHIDE (GAP) ALUMINIUM GALLIUM INDIUM PHOSPHIDE

			(ALGAIN P) ALUMINIUM GALLIUM PHOSPHIDE (ALGAP)
Y. BLUE	Z. 450 < Λ < 500	AA. 2.48 < ΔV < 3.7	BB. ZINC SELENIDE (ZNSE) INDIUM GALLIUM NITRIDE (INGAN) SILICON CARBIDE (SIC) AS SUBSTRATE SILICON (SI) AS SUBSTRATE — (UNDER DEVELOPMENT)
CC. VIOLET	DD. 400 < Λ < 450	EE. 2.76 < ΔV < 4.0	FF. INDIUM GALLIUM NITRIDE (INGAN)
GG. PURPLE	HH. MULTIPLE TYPES	II. 2.48 < ΔV < 3.7	JJ. DUAL BLUE/RED LEDS, BLUE WITH RED PHOSPHOR, OR WHITE WITH PURPLE PLASTIC
KK. ULTRAVIOLET	LL. Λ < 400	MM. 3.1 < ΔV < 4.4	NN. DIAMOND (C) ALUMINIUM NITRIDE (ALN) ALUMINIUM GALLIUM NITRIDE (ALGAN) ALUMINIUM GALLIUM INDIUM NITRIDE (ALGAIN) — (DOWN TO 210 NM)
OO. WHITE	PP. BROAD SPECTRUM	QQ. ΔV = 3.5	RR. BLUE/UV DIODE WITH YELLOW PHOSPHOR

6-LED CONNECTION [15]

A-CALCULATING THE LED SERIES RESISTOR VALUE:

LEDS MUST HAVE A RESISTOR IN SERIES TO LIMIT THE CURRENT FLOWS THROUGH THE LED TO A SAFE VALUE; OTHERWISE IT WILL BURN OUT ALMOST INSTANTLY. FROM FIGURE (8) AND BY USING THE OHM'S LAW, THE SERIES CURRENT LIMITING RESISTANCE CAN BE CALCULATED AS:

$$R = \frac{(V_s - V_D)}{I} \quad (\Omega) \qquad \ldots\ldots (1)$$

WHERE:

V_S=SUPPLY VOLTAGE (V)

V_D=LED VOLTAGE (V)

I= LED CURRENT (A)

R= CURRENT LIMITING RESISTANCE (Ω)

IF THE CALCULATED VALUE IS NOT AVAILABLE, CHOOSE THE NEAREST STANDARD RESISTOR VALUE WHICH IS GREATER, SO THAT THE CURRENT WILL BE A LITTLE LESS THAN THE RATED VALUE BUT THIS MAKE THE LED LESS BRIGHT.

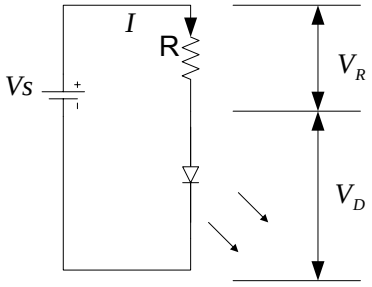

FIGURE (8) LED CONNECTION

B-CONNECTING LEDS IN SERIES AND PARALLEL:

IF SEVERAL LEDS ARE REQUIRED TO BE ON AT THE SAME TIME, IT MAY BE POSSIBLE TO CONNECT THEM IN SERIES. THIS PROLONGS THE BATTERY LIFE BY LIGHTING SEVERAL LEDS WITH THE SAME CURRENT AS JUST ONE LED. AS SHOWN IN FIGURE (9), ALL THE LEDS CONNECTED IN SERIES PASS THE SAME CURRENT, SO IT IS BEST IF THEY ARE ALL THE SAME TYPE. THE POWER SUPPLY MUST HAVE SUFFICIENT VOLTAGE TO PROVIDE THE NECESSARY VOLTAGE ACROSS EACH LED (ABOUT 3 VOLT) PLUS THE VOLTAGE DROP ACROSS THE CURRENT LIMITING RESISTOR. TO WORK OUT A VALUE OF CURRENT LIMITING RESISTOR (R), IT MUST ADD UP ALL THE LED VOLTAGES AND THIS IS USED AS V_D IN EQUATION (1).

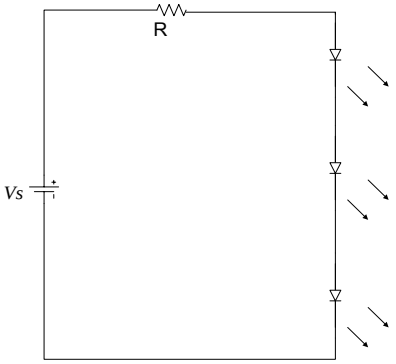

FIGURE (9) LEDS SERIES CONNECTION

CONNECTING SEVERAL LEDS IN PARALLEL WITH JUST ONE RESISTOR SHARED BETWEEN THEM IS GENERALLY NOT GOOD IDEA. IF THE LEDS REQUIRE SLIGHTLY DIFFERENT VOLTAGES ONLY THE LOWEST VOLTAGE LED WILL LIGHT AND IT MAY BE DESTROYED BY THE LARGER CURRENT FLOWING THROUGH IT. ALTHOUGH IDENTICAL LEDS CAN BE SUCCESSFULLY CONNECTED IN PARALLEL WITH ONE RESISTOR, THIS RARELY OFFERS ANY USEFUL BENEFIT, BECAUSE RESISTORS ARE VERY CHEAP AND THE CURRENT USED IS THE SAME AS CONNECTING THE LEDS INDIVIDUALLY. IF LEDS ARE IN PARALLEL CONNECTION, EACH ONE SHOULD HAVE ITS OWN RESISTOR, AS SHOWN IN FIGURE (10).

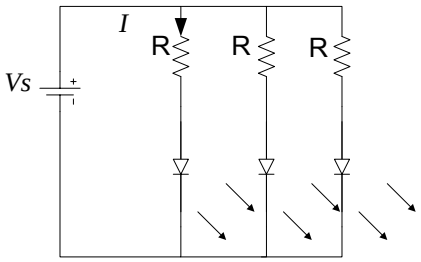

FIGURE (10) LEDS PARALLEL CONNECTION

IN THIS PROJECT, THREE SCHEMATIC DIAGRAMS ARE DESIGNED, IMPLEMENTED AND TESTED TO OBTAIN THE SUITABLE STREET LIGHTING LAMP. THE FIRST DIAGRAM IS SHOWN IN FIGURE (11), WHICH CONSIST OF (84) LOW POWER LEDS WITHOUT LENSES IMMERSED IN SERIES AND PARALLEL GROUPS INSIDE THE STREET LAMP FIXTURE. THE SECOND DIAGRAM CONSISTS OF (84) LOW POWER LEDS WITH LENSES IMMERSED INSIDE THE LAMP FIXTURE IN SERIES AND PARALLEL GROUPS, AS SHOWN IN FIGURE (12). THE THIRD DIAGRAM OF STREET LIGHT LED LAMP CONSISTS OF (84) LEDS OF HIGH POWER WITHOUT LENSES AS SHOWN IN FIGURE (13).

7-Designn and Implementation Of The Control Circuit For Street Lighting LED Lamp

The schematic diagram of control circuit is shown in figure (14). The circuit consists of the following parts:

1. A step-down transformer 220/18 V, 1 A is connected to 220 V, 50 Hz, single-phase A.C. power supply.
2. A bridge rectifier type LTKBJ408G to convert the transformer output into a D.C. voltage.
3. Smoothing capacitor of 25 V, 100 μF to smooth the converted output voltage of the bridge rectifier.
4. Stabilizer type 7812 with adjustable output voltage to feed the LED lamp from the A.C. supply during the night, through points 2 and 3 of the D.C., 12 V relay. The relay operation is indicated by a red LED lamp.
5. Stabilizer type 7812 with a constant output voltage to charge the D.C. supply battery. The capacity of the battery is 12 V, 12 AH, which is enough to feed street lighting LED lamp in case of emergency, when the A.C. supply voltage is disconnected. Also, the battery is used to feed the control circuit (comparators, transistor and relay) by a D.C. signal.
6. Two operational amplifiers type LM358 are used as comparators. The first comparator is used to compare the output voltage of the third stabilizer type 7812 (as reference signal) with that obtained from the light dependent resistance (L.D.R.) during the night. The output of the first comparator will be delayed about 1 minute before reaching the second comparator as an input signal. The delay circuit consists of resistance (1MΩ) and capacitor of 47 μF, and the time delay can be calculated as:

$$\tau = R * C \quad \ldots\ldots (2)$$

The output signal from the delay circuit will compared with the reference

signal of the second comparator.

7. A transistor of NPN type BD137 is used as a switch to control the operation of the second relay. The output signal from the second comparator will feed to the transistor to make it ON, and this will operate the LED lamp (from the A.C. supply or the D.C. battery) through the contacts of the second relay.
8. The operation of the first comparator is indicated by a red LED connected between the comparator and delay circuit.
9. The benefit of the delay circuit is to prevent the street lighting LED lamp from the disconnection during the night, when an abnormal light comes from a car or any source of light, which leads to a L.D.R. operation.

8- PRACTICAL MEASUREMENTS

IN THIS PROJECT FOUR SAMPLES OF LAMPS HAVE BEEN MADE FOR STREET ILLUMINATION, AND A COMPARISON HAS BEEN MADE TO PROVE THE EFFICIENCY OF EACH SAMPLE IN ORDER TO SELECT THE BEST ONE. THE COMPARISON HAS BEEN MADE BY MEASURING THE LIGHT AND THE POWER CONSUMED OF EACH LAMP. THE FOLLOWING FOUR SAMPLES ARE:

1. THE FIRST SAMPLE: A STREET LED LAMP WITH (84) LEDS WITHOUT LENS, WHITE COLOR, AND THE LEDS ARE CONNECTED AS SHOWN IN FIGURE (11) FASTENED ON THE FIXTURE, THE FIXTURE IS MOUNTED ON THE ARM OF THE POLE, SIX METERS ABOVE THE GROUND. THE LAMP POWER IS (4) WATT, 12 V DC, SUPPLIED FROM A CONTROL CIRCUIT AS IN FIGURE (14). THE LIGHT INTENSITY THAT REACHES THE STREET WAS MEASURED USING THE LUX-METER, THE LIGHTING WAS (40) LUX UNDER THE LAMP FIXTURE. FIGURE (15) SHOWS A PHOTO OF THE LIGHT WHEN THE LAMP OPERATED DURING NIGHT.

2. THE SECOND SAMPLE: A STREET ILLUMINATION LAMP HAS (84) LOW POWER LEDS WITH LENS AND A WHITE COLOR. THE LEDS CONNECTED AS IN FIGURE (12) AND FASTENED INSIDE THE FIXTURE. THE FIXTURE IS MOUNTED ON THE ARM OF THE LIGHTING POLE. THE POLE IS SIX METERS IN HEIGHT. THE LED LAMP POWER IS (5.25) WATTS, 12 V DC, A CONTROL CIRCUIT SUPPLY IT AS IN FIGURE (14). THE LIGHTING REACHES THE STREET WAS MEASURED BY THE LUX-METER, IT WAS (38) LUX UNDER THE LAMP FIXTURE. FIGURE (16) SHOWS A PHOTO OF THE LIGHT DURING THE LAMP OPERATION IN THE NIGHT.

3. THE THIRD SAMPLE: A STREET LIGHTING LAMP WITH (84) LEDS WITH HIGH POWER WITHOUT LENS, WHITE COLOR, THE LEDS CONNECTED AS IN FIGURE (13), FASTENED IN THE FIXTURE AND MOUNTED ON THE LIGHTING POLE. THE POWER OF THE LED LAMP IS (5.5) WATT, 12 V DC SUPPLIED FROM THE CONTROL CIRCUIT. THE LIGHT INTENSITY REACHES THE STREET UNDER THE LAMP IS (50)

LUX. FIGURE (17) SHOWS THAT IN A PHOTO DURING THE LAMP OPERATION IN THE NIGHT.

4. THE FOURTH SAMPLE: A CONVENTIONAL STREET LIGHTING LAMP, MERCURY VAPOUR, HAS A POWER OF (125) WATT, 220 V, FASTENED TO THE FIXTURE, AND MOUNTED ON THE LIGHTING POLE SIX METERS IN HEIGHT. THE LIGHT REACHES THE STREET UNDER THE LAMP IS (45) LUX. FIGURE (18) SHOWS THE LIGHT IN A PHOTO DURING THE LAMP OPERATION IN THE NIGHT. THE FOLLOWING TABLE SHOWS A SUMMARY FOR THE READINGS TAKEN FROM THE FOUR SAMPLES MENTIONED BEFORE.

TABLE (2) SUMMARY OF THE PRACTICAL READINGS

	MODEL TYPE	LAMP POWER (WATT)	LIGHT INTENSITY (LUX)
1	LOW POWER LED LAMP WITHOUT LENS	4.4	46
2	LOW POWER LED LAMP WITH LENS	5.25	38
3	HIGH POWER LED LAMP WITHOUT LENS	5.5	50
4	CONVENTIONAL MERCURY VAPOUR LAMP	125	45

THROUGH COMPARISON OF THE RESULTS IN THE TABLE, WE FIND THAT THE THIRD SAMPLE IS THE BEST AMONG THE OTHER SAMPLES IN CONSUMING POWER AND LIGHTING EFFICIENCY REACHES THE STREET.

9- CONCLUSIONS:

IN THIS RESEARCH THREE SAMPLES HAVE BEEN MADE OF WHITE LEDS LAMP, EACH SAMPLE HAS (84) LEDS DISTRIBUTED ON THE SURFACE AREA OF THE CONVENTIONAL STREET LIGHTING FIXTURE, BUT WITH DIFFERENT REFLECTORS. THE POWER CONSUMED HAS BEEN MEASURED FOR EACH LAMP AND THE INTENSITY OF LIGHT REACHES THE STREET.

A COMPARISON HAS BEEN MADE FOR THE THREE SAMPLES TO MEASURE THE POWER, EFFICIENCY AND THE LIGHT INTENSITY BY USING THE PERFORMANCE CHARACTERISTICS FOR EACH ONE. A COMPARISON HAS BEEN MADE AMONG THE THREE SAMPLES TYPE LED LAMP WITH CONVENTIONAL STREET LIGHTING LAMP TYPE MERCURY VAPOUR WITH (125) WATT, 220 V, USING THE SAME FIXTURES, POLES AND STREET.

THE COMPARISON SHOWED THAT LED TYPE LAMPS ARE BETTER THAN THE CONVENTIONAL LAMPS, WHICH HAVE HIGH POWER CONSUMED. THE LED LAMPS POWER IS BETWEEN (4-5.5) WATTS IN COMPARISON WITH (125) WATT FOR THE MERCURY VAPOUR LAMP. THIS SAVES POWER OF 95%, AND IN THE OTHER HAND THE LIGHT INTENSITY AND COLOR RENDERING OF LIGHT, SHOWED THAT LED LAMPS ARE BETTER THAN CONVENTIONAL LAMPS, ESPECIALLY HIGH POWER LED LAMP WITHOUT LENS, THE LIGHTING REACHES THE STREET IS (50) LUX WHILE MERCURY VAPOUR LAMP IS (45) LUX, AND THE LIGHT WAS WHITE FOR LED LAMPS, YELLOW FOR THE CONVENTIONAL MERCURY VAPOUR

LAMP LIGHT.

THE OUTCOME INTENSITY OF LIGHTING FOR LED LAMPS CAN BE IMPROVED BY IMPROVING REFLECTORS USED IN MANUFACTURING THE LAMP. WE NOTICED THAT THE REFLECTORS OF MERCURY VAPOUR LAMPS WERE BETTER THAN THE REFLECTORS MANUFACTURED FOR SPECIAL SAMPLES FOR LED LAMP, WHICH CAN SPREAD THE LIGHT OVER THE STREET AREA IN A BETTER WAY.

ACKNOWLEDGEMENT

THE AUTHORS WISH TO PLACE ON RECORD THEIR DEEP SENSE OF GRATITUDE AND THANKS TO RESEARCH AND DEVELOPMENT OFFICE/MINISTRY OF HIGHER EDUCATION//REPUBLIC OF IRAQ, FOR INITIATING, FINANCIAL HELPFUL, INVALUABLE ASSISTANCE, OFFERING THE CHANCE TO FINISH THIS WORK AND SUPPORT OF THE PROJECT THAT HELPED IN THE PROMPT COMPLETION OF THE RESEARCH.

REFERENCE

[1] PACIFIC GAS AND ELECTRIC COMPANY:" DEMONSTRATION ASSESSMENT OF LED STREET LIGHTING", FINAL REPORT PREPARED IN SUPPORT OF THE U.S. DOE SOLID-STATE LIGHTING, PP1-6, JANUARY, 2008.

[2] SAN DIEGO REGIONAL ENERGY OFFICE:" TECHNOLOGY ASSESSMENT OF LED FOR STREET AND PARKING LOT LIGHTING APPLICATIONS", PREPARED BY TETRA TECH EM INC., PP1-22, AUGUST, 2003.

[3] SUSTAINABLE ENERGY FOR ENVIRONMENT AND DEVELOPMENT PROGRAM:" EXPLORING LED STREET LIGHTING" VOL. 2, NO 3, PP1-2, SEPTEMBER 2008.

[4] ^CREE (NOVEMBER 19, 2008). ACHIEVES 161 LUMENS PER WATT FROM A HIGH-POWER LED. PRESS RELEASE. HTTP://WWW.CREE.COM/PRESS-DETAIL.ASP?I=1227101620851.

[5] ^[AB] E.FRED SCHUBERT, LIGHT-EMITTING DIODES, CAMBRIDGE UNIVERSITY PRESS, CHAPTER 1, 2003.

[6] ^…(2008) "MODELING THE RADIATION PATTERN OF LEDS"…(OPTICS EXPRESS). HTTP://WWW.OPTICS EXPRESS.ORG/VIEWMEDIA.CFM? ID=149957 OF SEQ=0.

[7] ^" NICK HOLONYAK, JR. 2004 LEMELSON-MIT PRIZE WINNER". LEMENSON-MIT PROGRAM. "

HTTP:// WEB.MIT.EDU/INVENT/A-WINNERS/A-HOLONYAK.HTML.

[8] ^"BRRIEF BIOGRAPHY-HOLONYAK, CRAFORD, DUPUIS" (PDF). TECHNOLOGY ADMINISTRATION .HTTP://WWW.TECHNOLOGY.GOV/MEDAL/ 2002/BIOS/HOLONYAK-CRAFORD-DUPUIS.PDF.

[9] ^T.P. PEARSALL, B.I. MILLER, R. J. CAPIK, AND K.J. BACHMANN:" EFFICIENT, LATTICE-MATCHED, DOUBLE-HETEROSTRUCTURE LEDS AT 1.1 MM FROM GAXIN1-X ASYP1-Y BY LIQUID-PHASE EPITAXY", APPLIED PHYS.LETT., VOL.28, PP499-501, 1979.

[10] ^"LED THERE BE LIGHT".

HTTP://WWW.ELECTROOPTICS.COM/FEATURES/JUNJU106/JUNJU106LEDS.HTML/.

[11] ^2006 MILLENNIUM TECHNOLOGY PRIZE AWARDED TO UCSB'S SHJI NAKAMURA".

HTTP://WWW.IA.UCSB.EDU/PA/DISPLAY.ASPX? PKEY=1475.

[12] ^ZHELUDEV, N. (2007). "THE LIFE AND TIMES OF THE LED-A 100-YEAR HISTORY"(PDF). NATURE PHOTONICS, VOL. 1, NO. 4, PP 189-192. DOI: 10.1038/NPHOTON. 2007.34.

HTTP://WWW.NANOPHOTONICS.ORG.UK/NIZ/PUBLICATIONS/ZHELUDEV- 2007.

[13] ^" THE FIRST LEDS WERE INFRARED "THE QUARTZ WATCH. THE LEMELSON CENTER.

HTTP://WWW.INVENTION.SMITHSONIAN.ORG/CENTERPIECESE/QUARTZ/INVENTORS/BIARD.HTML/, 2008.

[14] ^LED DESIGN

HTTP://WWW.ELEKTOR.COM/MAGAZINES/2008/FEBRUARY/POWER-TO-THE-LEDS.350167.LYNKX.

[15] JOHN HEWES 2009, THE ELECTRONICS CLUB, HTTP://WWW.KPSEC.FREEUK.COM/, LIGHT EMITTING DIODES/ LED.HTML/.

[16] AOUSS GABASH:" ELECTRICAL ILLUMINATION ENGINEERING", BOOK IN ARABIC, ALRADWAN PUBLISHING HOUSE, CHAPTER-13, 2006.

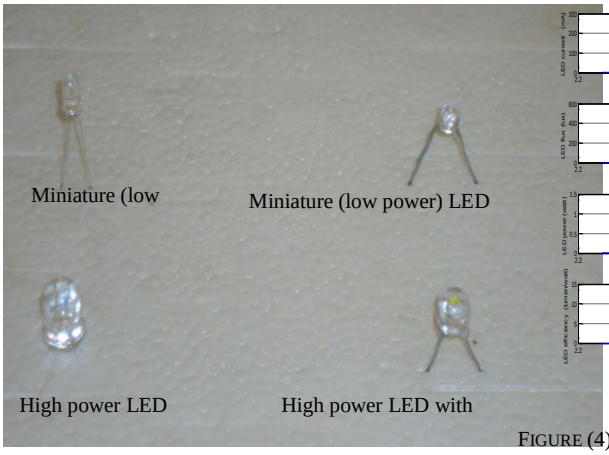

FIGURE (2) THE MAIN TYPES OF LED

FIGURE (3) THE EXPERIMENTAL TEST

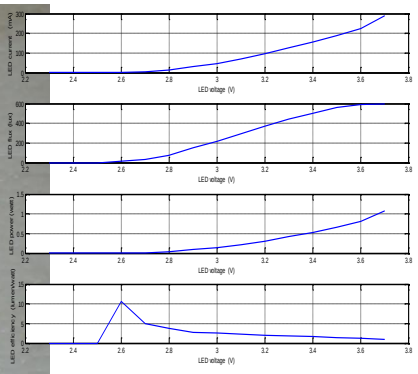

FIGURE (4) PERFORMANCE CHARACTERISTICS OF HIGH POWER LED WITH LENS

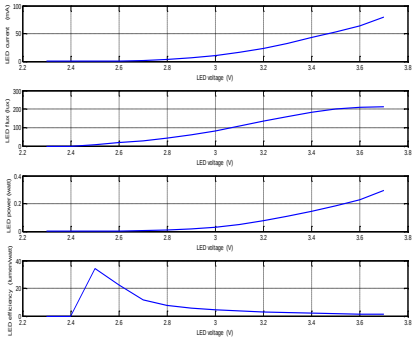

FIGURE (5) PERFORMANCE CHARACTERISTICS OF HIGH POWER LED WITHOUT LENS

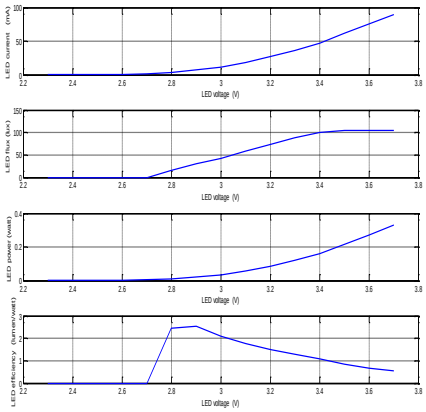

FIGURE (6) PERFORMANCE CHARACTERISTICS OF LOW POWER LED WITHOUT LENS

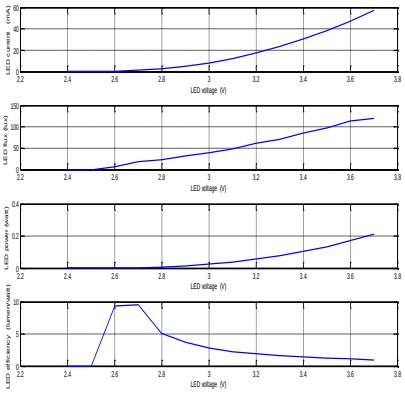

FIGURE (7) PERFORMANCE CHARACTERISTICS OF LOW POWER LED WITH LENS

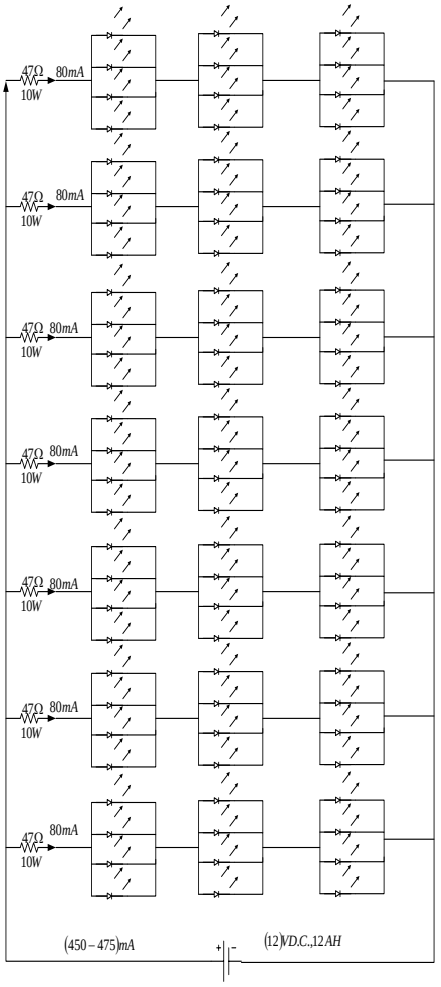

FIGURE (11) LED LAMP DIAGRAM OF (84) LEDS OF LOW POWER WITHOUT LENS

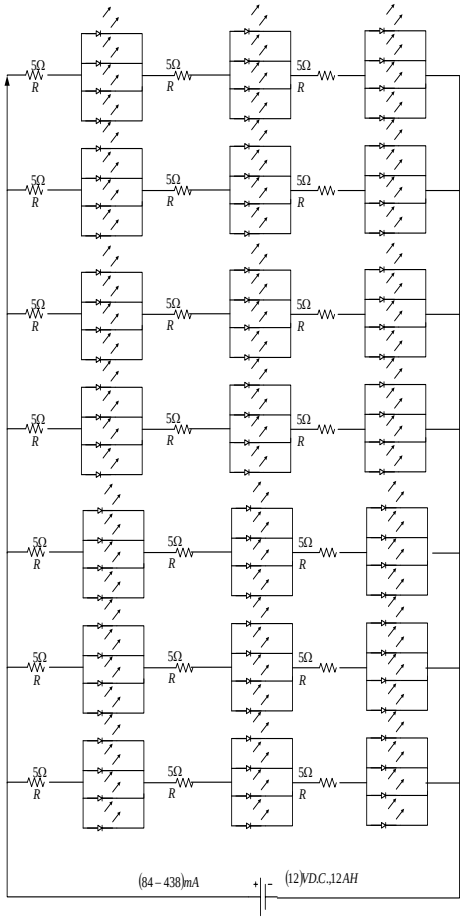

FIGURE (12) LED LAMP DIAGRAM OF (84) LEDS OF LOW POWER WITH LENS

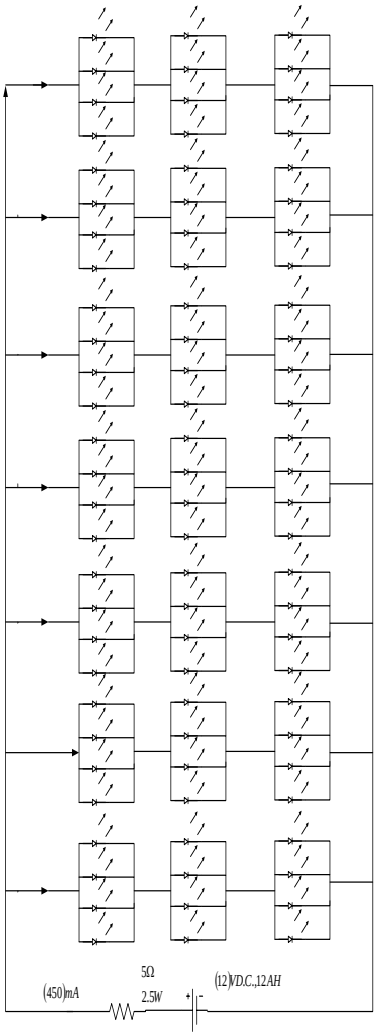

FIGURE (13) LED LAMP DIAGRAM OF (84) LEDS OF HIGH POWER WITHOUT LENS

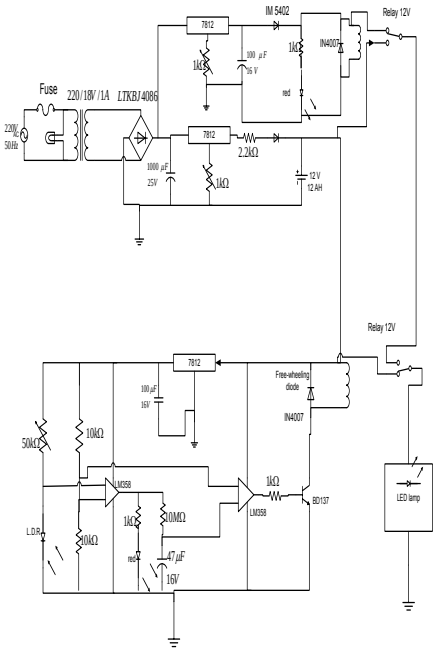

FIGURE (14) SCHEMATIC DIAGRAM OF THE CONTROL CIRCUIT

FIGURE (15) PHOTOGRAPH OF THE LOW POWER LED LAMP WITHOUT LENS MOUNTED IN THE FIXTURE ON THE POLE DURING THE NIGHT

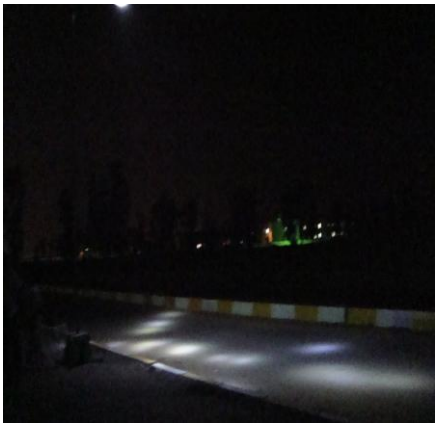

FIGURE (16) PHOTOGRAPH OF THE LOW POWER LED LAMP WITH LENS MOUNTED IN THE FIXTURE ON THE POLE DURING THE NIGHT

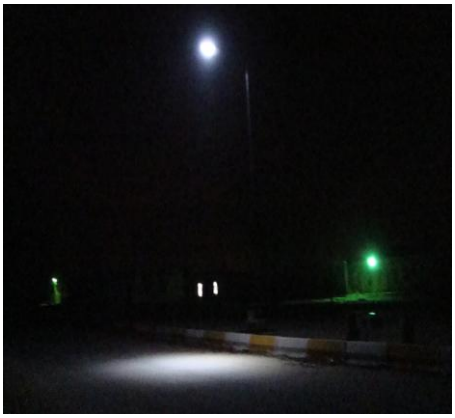

FIGURE (17) PHOTOGRAPH OF THE HIGH POWER LED LAMP WITHOUT LENS MOUNTED IN THE FIXTURE ON THE POLE DURING THE NIGHT

FIGURE (18) PHOTOGRAPH OF THE HIGH POWER LED LAMP WITH LENS MOUNTED IN THE FIXTURE ON THE POLE DURING THE NIGHT

How energy requirements of remote locations are met using renewable energy sources?

Professor Salman K Salman
Independent Consultant
sk.salman@btinternet.com

Abstract- This paper presents an investigation related to exploitation of renewable energy sources for meeting energy requirements of remote locations. This investigation is based on a practical project which was executed in collaboration between academia and industry. It is funded by the U.K. government, industry and local community. It involves design and installation of a prototype integrated renewable energy system which includes two 15 kW wind turbines, electrolyser and fuel cells together with the associated control equipment. It was installed at the furthest island of Shetland located at the north of Scotland, U.K. The philosophy upon which the design of this system based is summarised as follows: During times of high wind, the electricity generated by wind turbines is normally greater than that required by site electrical load. The excessive amount of generated electricity is stored into Hydrogen by utilising an electrolyser. On the other hand at times when wind is low which results in either no electric power or only a fraction of load demand, the remaining electric power required by load is obtained from the electricity generated by fuel cells using the stored Hydrogen as their input.

I. Introduction

The oil crisis of 1973 due to Arab-Israeli conflict has led to sharp increase in oil prices. This in turn has led industrial countries, for the first time, to seriously consider exploitation of renewable energy sources such as wind, solar, marine etc. In order to make this happening appropriate legislations have been put in place. For example in 1978 Public utility Regulatory Policies Act (PURPA) has been published in the USA. *This act has established the right for power producers (whether individuals or group of people) to use utilities' transmission and distribution networks to transmit electrical energy to another location*. The UK Energy Act which is similar to PURPA was published in 1983. Such legislations and other encouragement for competition have resulted in rapid increase of using renewable energy sources to drive small and medium electrical generators which are largely connected to utilities' distribution networks. However under certain circumstances such generators are also utilised to supply isolated networks. The latter is particularly common in remote locations which are far away form the Grid

and consequently its connection to the grid is expensive.

Exploitation of renewable energy sources (RES) has attracted and still continues to attract the attention of many countries world-wide. This is also helped by environmental pressures aiming at reducing CO_2 emission, which has recently become an important incentive for developing renewable energy sources globally. Recently it has been reported by the International Energy Agency that 46% global electricity would be from RES by 2050 [1], while Greenpeace International and European Renewable Energy Council forecasted the share of global electricity from RES would reach 77% by 2050 [2]. The share of global electricity from wind, according to Global Wind Energy Council would be 21-30% [3]. As with regard to solar, it was projected by Greenpeace International that electricity from solar would increase from 16 GW in 2008 to 180 GW of solar PV worldwide by 2030 [4]. Large percentage of electricity generated from RES would be non grid-connected. For example according to Greenpeace International about 40% of the 180 GW forecasted power systems solar electricity by 2030 would be non grid-connected.

In recent years several renewable energy systems have been developed to electrify remote locations in different parts of the world [5-6]. This paper presents an investigation related to exploitation of renewable energy sources to meet energy requirements of remote locations. This investigation is based on a practical project which was executed in collaboration between academia and industry. It was funded by the U.K. government, industry and local community. It involves designing and installation of a prototype integrated renewable energy system which includes two 15kW wind turbines, electrolyser and fuel cells together with the associated control equipment. It was installed at the furthest island of Shetland located at the north of Scotland, U.K.

The philosophy used in designing this system can be summarised as follows: During times of high wind, the electricity generated by wind turbines is normally greater than that required by site electrical load. Consequently the excessive amount of generated electricity is stored into Hydrogen by utilising an electrolyser. On the other hand at times when wind is quite/low which results in either no electric power or generation of only a fraction of load demand, the remaining electric power required by the load is obtained from the electricity generated by fuel cells using the stored Hydrogen as their input.

II. Site of the project

The system was developed and installed in Unst; the most northern island in Shetland located 200 miles from Scotland mainland. This makes it a truly remote area which is characterised by (i) having high wind energy resource. Fig. 1 shows a comparison between wind energy resource in Shetland and other locations in the UK and Denmark. It demonstrate that wind energy resource in Shetland is as twice as high the UK and Denmark locations [7] (ii) far from the grid and (iii) the cost of oil related products such as petrol and diesel could be as high as 20% more the UK

mainland. This has led to opting wind turbine as power source for the considered system.

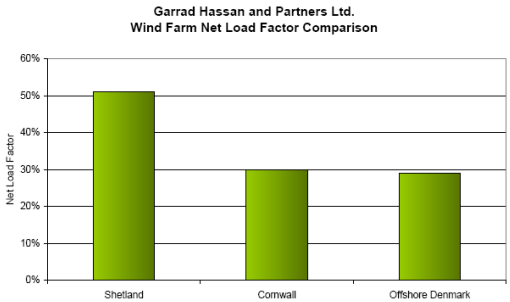

Fig. 1 Comparison between wind energy resource in Shetland, Cornwall (UK) and Denmark.

III. The design philosophy

The philosophy upon which the design of the system is based is summarised as follows: During times at which wind is high the electricity generated by system wind turbines is normally more than needed by electrical loads. The excessive amount of generated electricity is stored into Hydrogen by utilising an electrolyser. At times when wind is low and consequently the resultant generated electricity constitutes only a fraction of load demand. The remaining electric power required by the load is obtained from the electricity generated by fuel cells which uses the stored Hydrogen as their input. The Hydrogen generated by the system can also be used for other applications such as powering the project site small electric car.

IV. System Components

Fig. 2 shows the details of the system. It basically consists of (i) a renewable energy system which comprises from two wind turbines, 15kW each, (ii) back-up energy system based, on fuel cell technology where the adopted fuel cell is rated at 5kW, (iii) electrolyser for hydrogen production, (iv) hydrogen storage system and hydrogen dispenser, (v) two electrical load; the first in a form of electrical heating system which can be directly supplied from unregulated DC supply and the second is an AC load and (vi) energy management control system.

The unregulated AC power generated by the two wind turbines is rectified and smoothed to provide a DC supply of up to 30kW on a common DC bus. The unregulated DC bus power is then used to either supply the 9KW inverter, the storage heating system, or the electrolyser depending on weather and load requirements.

The management control system is specifically developed to prioritise the flow of power generated by the turbines. During periods of low electrical demand and high electrical energy, generated by the turbines during high wind, surplus energy is directed to the electrolyser for generating hydrogen which is stored in the pressurised storage

system. When the energy balance is reversed, the consumption of the load exceeds the electrical energy generated by the wind turbines. In this case, the fuel cell is operated. The fuel cell maintains the power supply to the AC circuit consumer unit through a 5kW inverter. During the time when the fuel cell is in operation, the electrolyser is switched off to minimise the parasitic loss in the system during light periods. However the wind turbine even in the event of low renewable power generation continue to system during light wind periods. However, the wind turbines even in the event of low renewable power generation continue to maintain the supply to the heating system. The latter is switched off only when there is no wind.

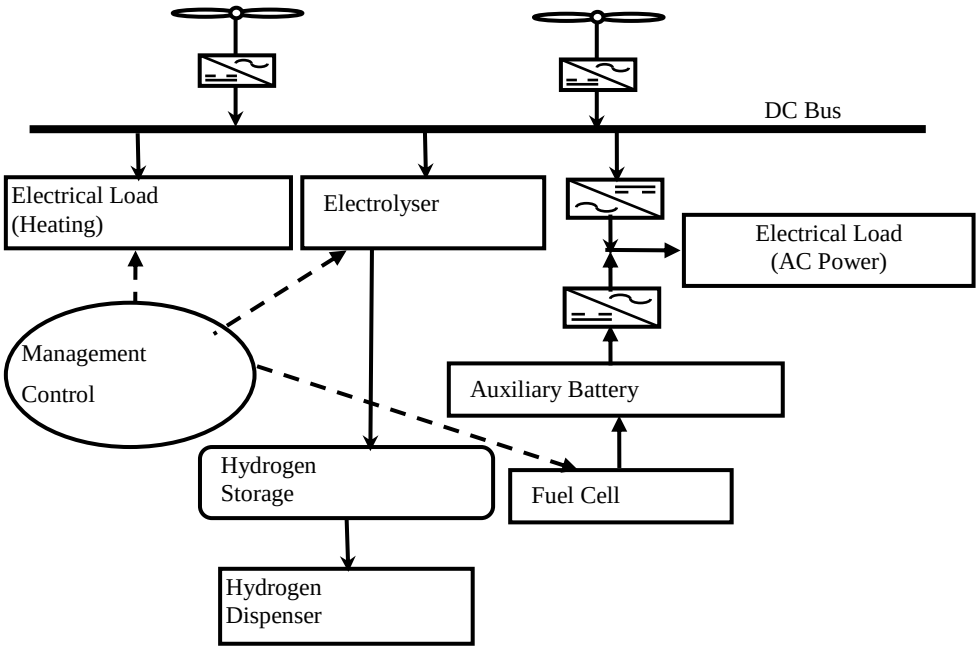

Fig. 2 Basic components of Unst integrated renewable energy system

V. Extracted mechanical power from wind

Theoretically the wind power available to be harvest by wind turbine is given by equation (1):

$$P_{th} = \frac{1}{2}\rho A v_w^3 \qquad (1)$$

Where, P_{th} is the theoretical wind power that can be converted to mechanical power by wind turbine, ρ is the air density [kg/m3], A is the area swept by wind turbine blade and v_w is the wind speed [m/s].

The rotor diameter of wind turbines used in this project is equal to 9.4m resulting in a swept blade area of 69.4 m^2.

The actual mechanical power that can be extracted from wind is equal to theoretical wind power multiplied by the power coefficient of wind turbine such that [8]:

$$P_w = \frac{1}{2}\rho \pi R^2 v_w^3 C_p(\lambda, \theta_{pitch}) \qquad (2)$$

Where, P_w is the actual extracted power from wind, R is the radius of wind turbine blade [m], and Cp is the power coefficient which is a function of tip speed ratio, λ, and blade pitch angle, θ_{pitch} [deg], where λ is given by:

$$\lambda = \frac{\omega R}{v_w} \qquad (3)$$

Where, ω is the angular speed of wind turbine blade.

Figs. 3 and 4 show the power curve and the power coefficient curve specific to the adopted wind turbines [9]. It can be seen from Fig. 4 that the optimum designed power efficiency for the selected wind turbine occurs at wind speed of 8 m/s. The efficiency of wind turbine below this optimum speed is not of great importance as there is not much energy available to be extracted from airflow. On contrary at high wind speeds wind energy in excess of the design limits of electrical generator must be shed by the turbine. The process of power shedding can be understood by examining Figs. 3 and 4 related to the turbine power curve and the efficiency respectively. It is evident from these two curves that by the time the turbine reaches its rated power of 15kW at approximately 10 m/s, its efficiency has dropped considerably which ensures regulating the turbine output. Having low turbine efficiency is particularly important at high wind speed region where wind energy is high and the extracted amount of energy must be limited to the rated power of generator otherwise it would be damaged.

The best way to demonstrate how the two curves work together is by reference to Fig. 5 which shows a sample of a record of wind speed versus time at the project site and the corresponding wind turbine output [10]. It can be seen that although wind speed between hours 25 and 30 continues to increase the turbine output remains almost constant at 14 to 15kW. During the same period wind speed varies between 17 m/s to 26 m/s. Referring to the efficiency curve of Fig. 4 it can be seen that the corresponding turbine efficiency is 7.5% to 2%. This means huge amount of wind energy is shed for the sake of protecting the generator from damage.

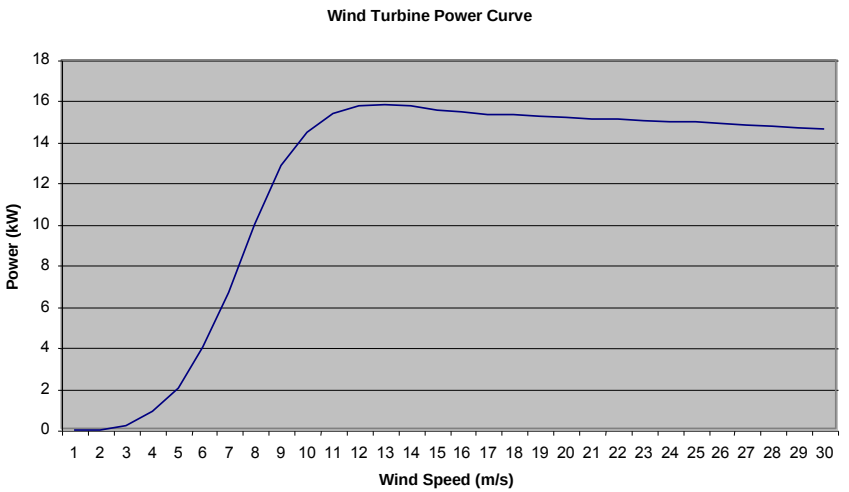

Fig. 3 Power curve for 15kW Proven wind turbine

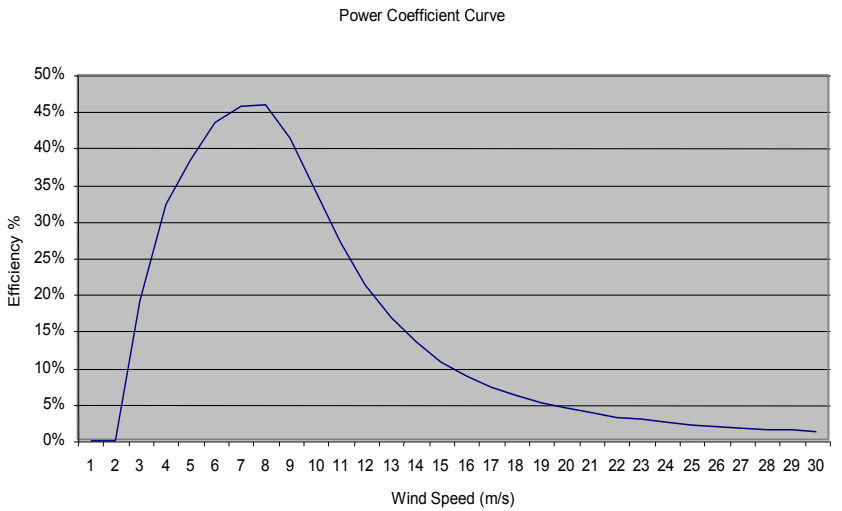

Fig. 4 Power Coefficient, Cp for 15kW Proven wind turbine

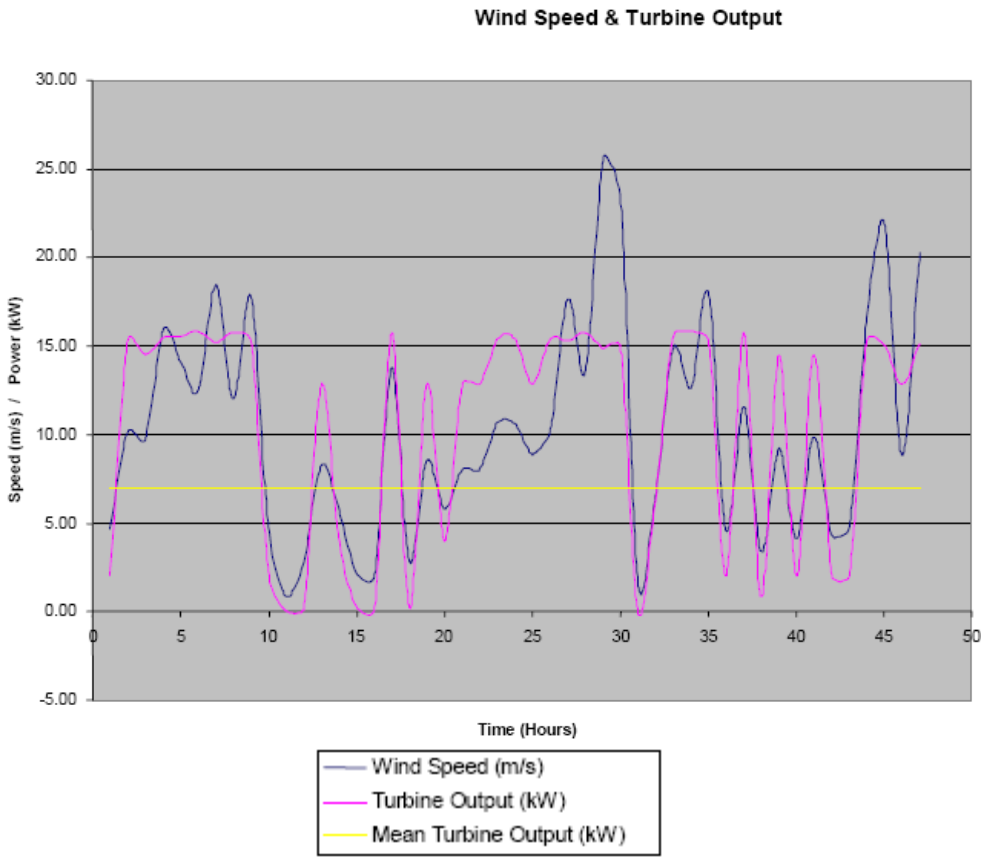

Fig. 5 Time-series wind speed and the corresponding simulated wind turbine power output.

VI. Renewable energy system for Middle East applications

The lessons and experience learned from Unst prototype renewable energy system [7] can be used for the development and installation of similar systems anywhere in the word including Middle East after taking into account local dominant renewable energy resource. It is obvious that the dominant renewable energy resource in Middle East is solar radiation which is available in huge quantity almost everywhere. Similar to Unst island coloration between the energy demand and energy resource also exists in Middle East. However the energy demand in case of Middle East is in a form of cooling during summer time as opposed to heating during winter in case of Unst. Therefore a renewable energy system that suits Middle

East environment would be similar to that shown in Fig. 4 but with replacing the wind turbines and its interfacing AC/DC rectifiers by Photovoltaic arrays, which normally generate DC voltage, and DC/AC inverters respectively. Further modification may be introduced depending whether there is a need for hydrogen applications. If this is not the case the back-up system based on generation of hydrogen and fuel cell technology may be replaced a back-up system based on batteries. Final decision regarding which of the two options is to be adopted should consider factors such a safety issues, economical considerations and staff training.

VII. CONCLUSION

Development of a prototype clean renewable energy system for electrical generation suitable for remote areas has been presented. The system was installed in Unst island which is located 200 miles from UK mainland which is characterised by having high wind energy resource compared to other locations in UK mainland and Europe. The system basically consists of a primary electrical generation source comprising of two 15kW wind turbine and a back-up electrical power source based on fuel cell technology. The latter is essential to meet the deficiency in the primary electrical power generation normally experienced at times when wind speed is low.

Modification of Unst renewable energy system to suit the clean energy resource available in Middle East which is solar radiation has also been discussed. This means the primary electrical generation source needs to be replaced by one which is based on photovoltaic solar panels. The back-up power source may be also by another one based on batteries depending on factors including whether the hydrogen is needed, safety issues and economical consideration.

VIII. References

[1] International Energy Agency “Energy technology prospective”, Paris, 2008

[2] Greenpeace International and European Renewable Energy Council “Energy [R]evolution: A sustainable global energy outlook”, Amsterdam and Brussels, 2008

[3] Global Wind Energy Council “Global wind energy outlook” 2008, Brussels.

[4] Crispin Aubrey, ed. (Greenpeace & EPIA) “Solar generation IV: Solar electricity for over one billion people and two million jobs by 2002”, 2007

[5] Arnaud Rte and Oystein Ulleberg, “The Utsira wind-hydrogen demonstration system in Norway: Analysis and optimisation using modelling tools”, EWEC 2009, Marseille.

[6] Tapan K et al “Stand-alone renewable energy system-based on hydrogen production”, Canada, http://www.ieahia.org/pdfs/res_uquebec.pdf (accessed on 29 January 2010)

[7] R.Gazey, S.K.Salman, D.D.Aklil-D’Halluin, “A field application experience of integrating hydrogen technology with wind power in a remote island location”, Elsevier Power Sources Journal, POWER-D-05-01096, February 2006.

[8] S. Heier, Grid Integration of Wind Energy Conversion System, Chichester, UK, John Wiley & Sons Ltd., 1998.

[9] Proven Energy Ltd, Proven WT15000 Wind Turbine, Advance Technical Specifications, http://www.provenenergy.com/index.php?option=com_content&task=view&id=21&Itemid=37

[10] Ross Gazy, "Design and development of an integrated prototype renewable hydrogen energy system", MPhil Thesis, Robert Gordon University, Aberdeen, U.K. 2006

SUSTAINABLE ENERGY SUPPLY USING CONCENTRATED SOLAR POWER AND WIND ENERGY.

Prashant Kumar Yelagi, Lecturer, Department of Civil, Faculty of Engineering, Sitre University, Sirte.
prashant.yelagi@gmail.com

Abstract:

Although Libya has a vast amount of Oil and natural Gas reserves for the energy need of the country and also for the export purposes, they will be over sooner or later; hence there is a need for an alternative sustainable energy source which is clean, efficient and cost effective. Lot of renewable energy sources like Biomass, solar PV cells, Hydro electric etc, are there but most of them are either not suitable for Libya or are not cost effective hence the third generation technologies like Concentrated Solar Power and Wind energy are the natural choices as they are clean, cost effective and are well suited for the Libyan conditions. Furthermore the countries geographical conditions are best suited for these technologies as Libya has plenty of sunshine hours thought the year and also the wind speed especially along the coast is sufficient for the wind energy to be developed.

1. Introduction

Libya is located on the northern edge of Africa(Approximately from 19^0 north to @33^0 N) with about 88% of its area considered to be desert. As an oil exporting nation Libya does not have any energy crisis immediately but the location and the availability of Solar insolation and wind speed makes Libya the natural choice for the renewable energy production, which can for the domestic consumption as well as for export purpose, and there is a huge demand from the European countries for the power which can be supplied from Libya.

The most ideal place for generation of solar energy is places where you get minimum of 2000kWh of sun light radiation /m2 annually which are usually near the equator up to 30^0 north and south and which has free land for the unit.

Renewable energy technologies like Hydro Power and Bio-Mass combustion is not viable for Libya as it lacks the resources , continuous flow of water and bio-mass supply. Photovoltaic's is not cost effective when the energy production on large scale is considered . That leaves us with two options i.e. Concentrated Solar Power and Wind Power which are ideal for Libya as it is located near the equator and lies below 30^0 N along with having a large part as Sahara desert .

2. Technology Assessment

There are four types of Concentrated Solar power technology namely
1.Parabolic trough
2.Central receiver (Power Tower)

3.Parabolic Dish
4.Fresnel Linear Reflector.

Concentrating Solar Power Plants produce energy / Electric power by converting the Sun's energy into high temperature heat using various mirrors or Len's configuration to concentrate Sun's rays to a Temperature of about 400^0 to 1000^0 C. For Solar Thermal Systems the heat is transmitted to a turbine or engine for power generation. Thermal plants consists of two major subsystems: one that collects solar energy and converts it into heat, and another that converts heat energy to electricity.

2.1 PARABOLIC TROUGH SYSTEM:

Parabolic trough systems comprise rows of trough shaped mirrors which direct solar insolation to a receiver tube along the focal axis of each trough. the focused radiation raises the temperature of the heat transfer fluid usually molten salt , which is used to generate steam. the steam is then used to power a turbine generator to produce electricity.

Fig. 1 Parabolic trough System.

2.2 CENTRAL RECEIVER (POWER TOWER):

Power tower systems consists of a field of thousands of sun tracking mirrors which direct insolation to a receiver atop a tall tower. A heat transfer fluid usually molten salt is heated in the receiver and is piped to a ground based steam generator. The steam drives a steam turbine-generator to produce electricity.

Fig. 2 Central receiver (Power Tower)

All CSP systems make use of direct normal component of solar radiation, that is, the radiation that comes directly from the sun and not the diffused sun light. Direct normal insolation (DNI) is available only on sunny days. Concentration of DNI allows a solar system to achieve a high working fluid temperature. The need to focus DNI requires that collector systems track the sun. Parabolic trough systems use single axis trackers to focus radiation onto a linear receiver whereas power towers systems use two axis trackers to track the sun . These trough and tower plant systems are best suited for relatively large plants 50 MW or larger.

2.3 PARABOLIC DISH:

Parabolic dish systems use a dish shaped arrangement of mirror facets to focus energy onto a receiver at the focal point of collector. A working fluid such as hydrogen is heated in the receiver, and drives a turbine or sterling engine. These are modular in nature, with single units producing power in the range of 10 kW to 35kW.These could be used in remote areas or may be used in a group for larger requirements.

Fig. 03 Parabolic dish.

Fresnel linear Reflectors are similar to parabolic trough systems as they also radiate the solar insolation to a receiver tube along the focal axis but in this case they use flat mirrors arranged in parabolic curve instead of trough shaped mirrors. This system are economical compared to trough systems as the installation cost is very low.

The solar flux concentration ratio typically obtained at the focal plane varies between 30-100 suns for the trough systems, 500-5000 suns for tower systems, and 1000-10,000 for dish systems. Higher concentration ratio's imply lower heat losses from smaller receivers and, higher attainable temperatures at the receiver.

3. Renewable energy Scenario

For the adoption of appropriate Sustainable Renewable energy production system it has to satisfy the following few things

3.1. Technology
3.2. Resources.
3.3 Cost effectiveness.
3.4 low Maintenance.
3.5 Environmental impact.

3.1 Technology:

The third generation technologies like CSP and wind turbine are still under development but are also adopted by a lot of countries, at the end of 2008 CSP provided only 436MW but by 2011 it may go up to 1000MW and by 2017 it is expected to increase by 17,000MW as Spain and USA are adding 10,000MW & 7,000MW. The current Electricity production using CSP is 560 MW and another 984MW plants are under construction and @7463MW of plants already been announced to be complete by 2014. Hence the Technology is available for the Production of Electricity using CSP.

3.2 Resources

Libya is located on the northern tip of Africa and lies between 19^0 N and 32^0 N latitudes, and @88% of land is considered to be desert with an daily average solar radiation on a horizontal plane of 7.1kWh/m2/day in the coastal region and 8.1 kWh/m2/day in the southern region with an average sun duration of more than 3500hours /year and the average wind speed at 40 meter height is between 6.75m/s to 7.5m/s. So the required resources and open land are available for Libya.

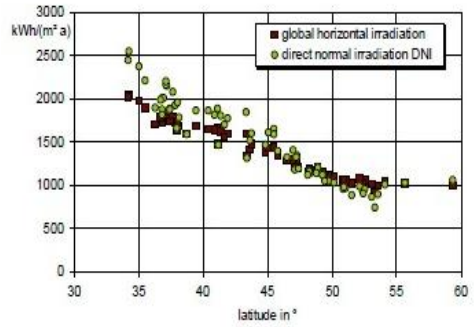

Fig. 4 Global Irradiation levels

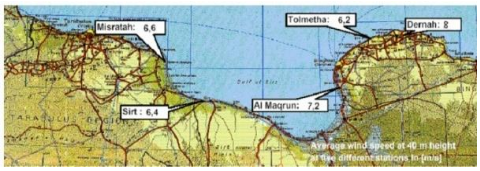

Fig. 5. Wind map of Coastal Libya

Using the 300kW reference turbine the measured data from Sirte gives 100% production of 613MWh/a and a capacity factor of 20%. which is similar to an average German site. Hence Libya has the Much needed Solar irradiation for the CSP and the wind speed along the coast for the wind Mill, hence it can plan Hybrid systems along the coast for better efficiency and pure CSP (Central Tower and Trough systems) along the southern border.

3.3 Cost Effectiveness

The production costs for CSP today is about 15cents/kWh in USA and may come down to 7cents/kWh in the coming years. The IEA (international Energy Agency) and for wind energy it is from 7cents/kWh to 15 cents/kWh study on cost competitiveness of selected renewable power technologies suggest that after small Hydro and Biomass the CSP ,Geo thermal and wind energy are the technologies that produce electricity within the retail consumer price range the figure below gives an idea of cost competitiveness which was conducted in 2006 but now the production cost for CSP has come down to about 15cents/kWh and is expected to reduce further to 7cents/kWh.

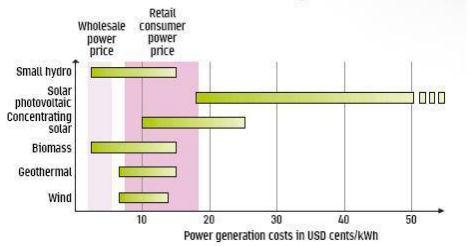

Fig. 6 Cost competitiveness of Renewable technologies

The levelized electricity costs for CSP and Photovoltaic's are indicating that the CSP is more cost effective that the photovoltaic in North Africa even with a 50% cost reduction in photovoltaic's and no cost reduction in CSP. For Libya the levelized electricity cost for CSP is around 0.12Euros/kWh where as the for photovoltaic's it's around 0.35euros/kWh and even with a 50% cost reduction it may come down to 0.18euro's/kWh which is higher than the present day cost of CSP. With more and more plants being under construction the levelized cost is expected to come down.

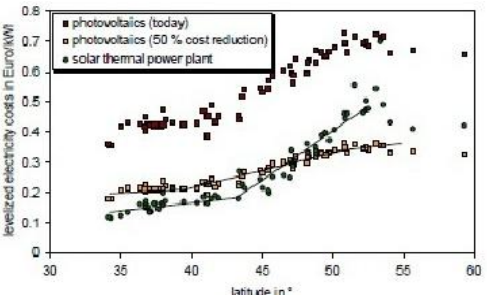

Fig. 07 Levelized Electricity costs

As the USA experience shows that the levelized cost of production will come down with increase in the production. the SEGS Plant LEC Experience curve shows a reduction in the production cost with increased cumulative megawatts installed. Hence as more plants are added in future and the cumulative capacity increases the cost will come down.

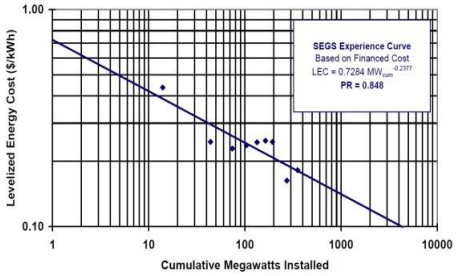

Fig. 08 Levelized cost of CSP in USA

3.4 Low maintenance

The CSP trough system plants need very less maintenance and the environmental impact is almost nil in comparison with the fossil fuel based production these units will not pollute the environment and are clean technologies.

4. Conclusion

After a detailed study of the technology available and the suitability for the country one can come to a conclusion that the possible options of sustainable renewable energy for Libya are CSP (Concentrated Solar Power) as Parabolic trough and Power tower and then Wind energy . The Southern part of the country has a large potential for CSP and along the coast hybrid systems can be proposed. CSP and wind energy along the coast of Libya can provide a sustainable continuous power supply for the domestic and export purposes.

Fig. 09 Proposed HVDC grid for Europe.

The picture shows the possibility of a combination of Conventional AC grid with High voltage DC grid (HVDC) which can be used in the transmission of electricity to trans-European Electricity scheme. As Europe needs electricity and Libya has a huge potential for the production from renewable energy sources like CSP and wind energy, it can be a potential energy exporter to the European market.

5-References.

[1] Ibrahim M Saleh: 2006, "prospects of renewable energy in Libya",
[2] Volker Quaschining, Manuel blanco Muriel : 2001, Solar Power-Photovoltaic's or Solar Thermal Power plants.
[3] L.Stioddard, J.Abecunas, and R. O'Connel : 2006, Economic,Energy, and Environmental benefits of Concentrating Solar Power in California.
[4] 2004: Wind Regimes of Africa.
[5] 2007: Renewables in Global Energy Supply. An IEA Fact sheet
[6] Henry W Price, Stephen Carpenter 1999: The Potential for Low Cost Concentrating Solar Power Systems. NREL.
[7] 2009: Concentrating Solar power, Greenpeace International, Solar PACES and ESTELA

An evaluation of the prospects for electricity production in Libya using Parabolic Trough Solar Thermal Generation

Abdussamad Emhemed
Petroleum Training & Qualifying Institute (PTQI)
Tripoli, Libya
E-mail: abdu_emhemed@yahoo.com

Abstract

The national plan in Libya adopted 10% target of renew-able energy to be brought into electricity production stream by 2020. Libya can tap the huge received solar energy resources by using Parabolic Trough technology which is the only mature and commercial CSP technology. In order to estimate reliably the required capacity to meet this target, forecasting scenarios for the electricity production have been built, based on historical data of electricity production for the last seven years. The required amount of electricity production to meet 10% target by 2020 is 5442GWh according to the first forecasted scenario with 6% annual growth rate, and 6939GWh according to the second one with 8% annual growth rate. SAM software provided by (NREL) is used to simulate the proposed 100MW Parabolic Trough unit with either water or dry cooling systems at Tripoli and other comparator locations in North Africa and Southern Europe. The annual electricity output for each proposed unit in Tripoli is about 224GWh and at the Southern part (Al Kufra) the net electricity output, taking in account the 3% transmission losses through HVDC lines, is more than 50% higher than for a unit in Tripoli. The total required capital cost for the proposed number of installed units in Tripoli is (8.65 – 11.8) billions US$ for both forecasted scenarios, whereas in Al Kufra the required capital cost is more than 50% lower than Tripoli. The levelized cost of energy is about 4¢/kWh lower in Tripoli than Palermo and Athens, whereas in Al Kufra this cost, in addition to HVDC transmission cost (about 1.5 ¢/kWh), is less than half of the cost in Palermo and Athens in the Southern Europe.

1) INTRODUCTION

1.1. Study Background

The existing electricity gene-ration technologies are mainly dependent on burning fossil fuel which is probably considered the main contributor to GHG emissions. Currently, a big movement towards renew-able energy resources has been recorded since Kyoto Protocol establishment in (11 December 1997) and targets has been set to achieve GHG emissions re-duction by tapping the available renewable resources.

The huge amount of energy received due to solar irradiation on the earth is the largest renewable energy resource, which can supply many times the present demand for the whole globe if it is utilized and tapped sensibly. Currently, two methods of solar

energy utilization are available in the energy market. The first method is using photovoltaic solar systems which convert the scattered and diffuse sunlight to electricity directly. The second method is using Solar Thermal Systems which convert the direct sunlight into heat to produce steam for driving the turbine to generate electricity. The Sunbelt regions which mainly have the desert-like climatic conditions are the most suitable places to install these technologies. Figure 1.1 shows the world's best locations for concentrating solar power such as inland of Australia, the Middle East, the Sahara desert of North Africa, the South-western United States and the Atacama Desert of Chile (SCHTOTT, 2008).

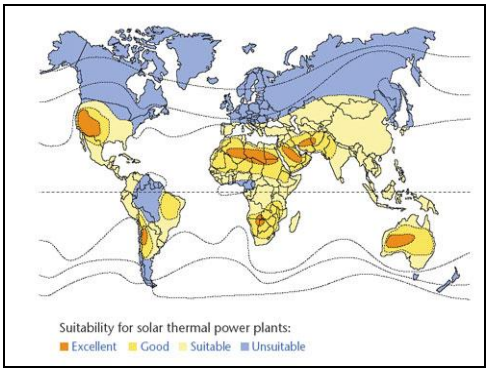

Fig (1.1): The availability of implementing CSP over the world (Source: Schott Solar)

A study carried out by German Aerospace Centre (**DLR**) suggests a promising scenario for the future of solar thermal technology, if utilized in the Sunbelt area. Figure 1.2 introduces this scenario; the biggest red square on the left (300 km × 300 km) shows an area of desert that, if covered with concentrating solar power plants, would provide electricity that would be equivalent to the entire current world energy consumption. The middle-sized square (126 km × 126km) shows a corresponding area for the European Union (as it was with 25 countries in 2004). The smallest square is the corresponding area for the Middle East and North Africa (55 km x 55 km) (TREC, 2008).

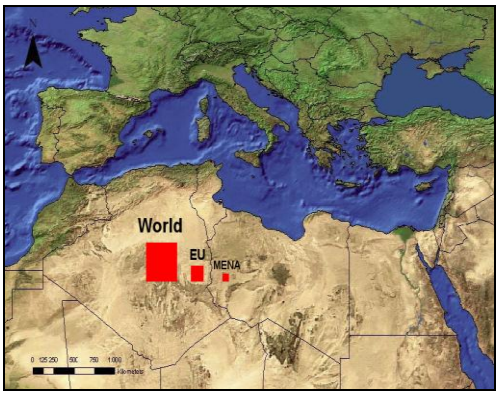

Fig (1.2): **DLR** future scenario of CSP in North Africa
(Source: German Aerospace Centre (**DLR**), 2005)

1.2. Potential of Solar Energy in Libya

There is a huge potential of renewable energy sources in Libya due to its geographical and climatic conditions. The most important renewable energy source is solar energy, since Libya enjoys as shown in figure (1.3) the daily average solar radiation on a horizontal plane about (7.1kWh/m^2/day) on the coast and (8.1kWh/m^2/day) in the South, and the average annual sun duration is more than 3500 hours per year (MEDELEC, 2008).

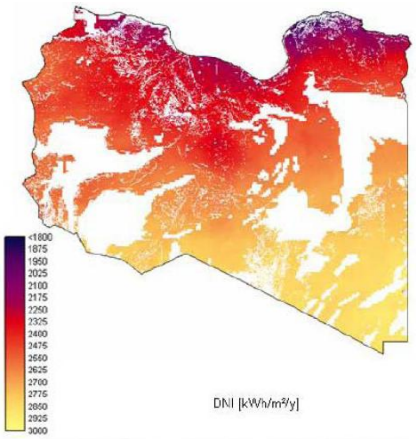

Fig (1.3): Solar Radiation Availability (Source: Renewable Energy in Libya, 2008)

1.3. Electricity Production in Libya

The existing 10 electricity generation plants provide 6612 MW total installed generation capacity in 2007, and most of these are installed on the coast which is considered the most inhabited area in Libya. The electricity production reached 25,514 GWh in 2007 with 6.34% growth rate in com-parison with 2006, and is set to increase in the coming years. Table (1.1)

shows the growth of electricity production from 1998 to 2007 (GECOL annual report, 2007).

Table (1.1):- The generated electricity over the last ten years

Year	Electricity Production (GWh)	Growth Rate (%)
1998	13,528	-
1999	14,407	6.50
2000	15,496	7.56
2001	16,111	3.97
2002	17,531	8.81
2003	18,942	8.05
2004	20,202	6.65
2005	22,450	11.38
2006	23,992	6.87
2007	25,514	6.34

(Source: GECOL annual report, 2007)

1.4. Schematic & Components of Parabolic Trough Systems

Parabolic trough system as shown in figure (1.4) consists of long parallel rows of reflectors (typically, glass mirrors) that are curved to form a trough which are used to concentrate sunlight on the receiver (EUROPEAN COMMISSION, 2007).

Fig (1.4): The main components of Parabolic Trough system
(Source: H. Price, 2006)

The receiver tube fixed at the focal line of the reflector to absorb the reflected sunlight, and this receiver takes the form of a pipe treated with a low-e coating encased in a glass cylinder, the space between the pipe and glass cover is evacuated. Trough technologies are based on the principle of single-axis sun tracking, and in the typical design of this system the receiver is fixed to the Trough. These rows are arranged along a north-south axis and they rotate from east to west over each day. Parabolic troughs can achieve concen-tration ratios (ratio of solar flux on the receiver to that on the mirrors) of between 10 and 100. A heat transfer fluid or HTF (typically, an oil), which also called Heat Collection Element (HCE), is circulated through the receiver to absorb the solar heat. The HTF can be heated to temperatures of up to 400-500 $^{\circ}$C (GREENPEACE, 2005). Then this fluid is pumped to a heat exchanger where its heat is transferred to water or steam. The parabolic trough can collect up to 60% of the incident solar radiation and has

achieved a peak electrical conversion efficiency of 21% (net electricity generation to incident solar radiation) (F.M.Tellez, 2006).

Parabolic Trough Plants has different configuration structure such as solar only, solar with thermal storage system or solar hybrid with fossil fuel. Hybrid solar thermal power plants can use fuel in addition to solar energy to generate heat; in this system solar fields feed their heat energy into a conventional generation unit with a steam turbine, so they can be com-bined without any problem with fossil fuel (hybrid power plants). However, the possibility of including thermal energy storage system (TES) to the Parabolic Trough Plants indicates this Schematic structure as the most attractive configuration, since it is a 100% renewable system and can generate electricity during periods of no or low solar radiation. Figure 1.5 shows the structure of Parabolic Trough Plant with Thermal Storage. Also, there are two kinds of cooling systems that can be attached to Parabolic Trough Plants; the first kind is water cooling system which is suitable for locations near the sea or water sources. The second kind is called (Dry Cooling) without using water for cooling which is considered the most suitable type, since the most promising locations for implementing CSP technology are arid areas where water is scarce.

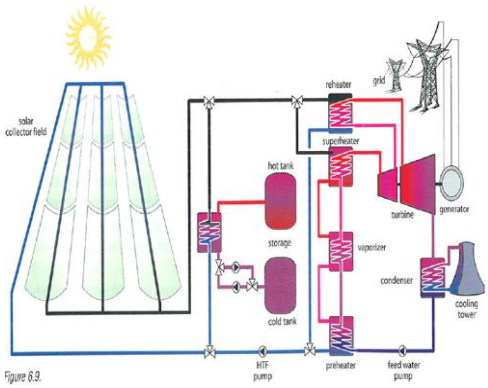

Fig (1.5): Schematic of a parabolic trough power plant with thermal storage
(Source: A guide for installers, architects and engineers, 2005)

Currently most of the existing, under construction or planned CSP plants are adapting Parabolic Trough technology due to the well-proven experience from SEGS plants in California. In Spain and the US at present a large number of plants, many at 50 MW or bigger are being constructed or planned. Also CSP projects are underway in Italy (Archimedes project) and several states in Northern Africa and the Middle East, including Egypt, Algeria, Morocco and Abu Dhabi (A. Maccari, 2006).

1.5. The objective of the study

An evaluation of the 10% planned target of renewable energy share in the electricity generation sector in Libya, and to what extent can Parabolic Trough technology with thermal storage system (the only

comm.-ercial solar thermal technology) contribute in this scenario by 2020, based on the current electricity generation capacity and anticipated demand.

2) - SCOPE OF WORK

2.1. Introduction

The process of this study is divided into two parts which are combined at the end to gain the final results. In the first part historical data of the Libyan electricity production are used to forecast the required electricity quantities in Libya by 2020. In the second part a computer simulation tool (SAM software Version 2.5) will be used as the main method to analyse the use of solar thermal technology in the study area and determine the amount and cost of the energy output.

2.2. Data Collection

The required data for this study are divided into two kinds of secondary data obtained from different sources. The first type of data is historical data of the electricity demand and production of Libya. The second is meteorological data in computer format for some locations in Libya or com-parative locations.

2.2.1. Historical Data of Electricity production

All the available data about the generated electricity in Libya throughout the period (2002 to 2007) are collected from the published annual reports by GECOL. These reports provide us with adequate information about the generated electricity and the recent increase rate, since the electricity market in Libya is dominated by GECOL (monopoly). A calculation based on these historical data and adoption of a flat increase rate which has been recorded in this period can help us to anticipate the future electrical production for 2020. Also, we gather all the available studies of the fore-casting scenarios about the future electricity generation of Libya. A comparison of all these scenarios is useful for choosing a suitable increase rate to calculate the total electricity production in 2020 and con-sequently the 10% share of renewable energy.

2.2.2. Meteorological Data

The meteorology data is an essential element in the evaluation of any renewable energy resource or project. The meteorology data base gives a variety of climate parameters such as the wind speed, direct normal irradiation and the number of sunny hours per day which can affect the energy output. In this research weather data in EnergyPlus weather format are used with Solar Advisor Model software to carry out the simulation for the suggested locations. This weather data are available for 1042 locations in the USA, 71 locations in Canada, and more than 1000 locations in 100 other countries throughout the world. The weather data are classified by World Meteorological Organization (WMO) for many regions and countries as following:

- Africa (WMO Region 1)
- Asia (WMO Region 2)
- South America (WMO Region 3)
- North and Central America (WMO Region 4)
- Southwest Pacific (WMO Region 5)
- Europe (WMO Region 6)

This weather data for these regions and countries are available and can be down-loaded from U.S Department of Energy, Energy Efficiency and Renewable Energy, EnergyPlus Energy Simulation Software. Figure 2.1 shows the Energy-Plus data from weather station in the study area Tripoli/Libya (U.S Department of Energy, 2009).

Fig (2.1): the Energy Plus data from weather station in the study area Tripoli/Libya (Source: GoogleEarth, 2009)

2.3. Comparison between Libyan & Egyptian Locations

The available EnergyPlus meteorological data in a computer format for Libya is limited just to the capital city of Tripoli. The problem of the scarcity of meteorological data for different locations in Libya can be overcome by considering comparative locations which have the same climate and weather conditions in the same region. As an example, a comparison between Al Kufra in the South of Libya and Aswan in the South of Egypt is shown in Figure (2.2). The Monthly Averaged Direct Normal Radiation (kWh/m2/day) are seen to be quite similar at both locations.

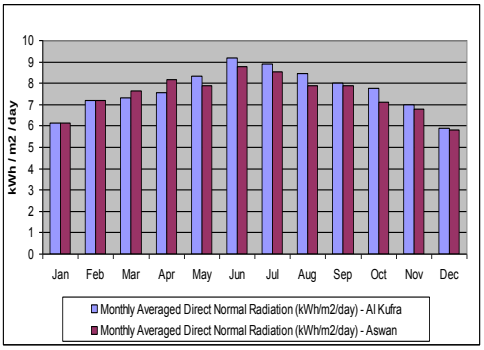

Fig (2.2): The Monthly Averaged Direct Normal Radiation for Al Kufra and Aswan (Source: ATMOSPHERIC SCIENCE DATA CENTER, 2009)

2.4. Methods and techniques

The methodology process of this research is divided into two parts which are combined at the end to gain the final results. In the first part a historical data of the Libyan electricity demand and production will be used to forecast the required electrical demand and production of Libya by 2020. In the second part a computer simulation tool (SAM software Version 2.5) will be used as the main method to analyse the use of solar thermal technology in the study area and determine the amount and cost of the energy output.

2.4.1. Anticipating Scenarios of the Electricity production by 2020

A simple calculation is carried out to anticipate the electrical demand for Libya by the year 2020 based on the historical data for the growth of the electricity demand during the last seven years. According to this data an average growth rate 7.5% has been recorded during this period. Adopting 8% growth rate of the electrical demand can give more realistic scenario for forecasting the electrical

demand by 2020. The results of this scenario can be compared with other ready scenarios to conclude the suitable scenario which will be used to calculate the 10% share that comes from renewable energy by 2020.

2.4.2. Solar Advisor Model simulation tool (Version 2.5)

Solar Advisor Model (SAM) is simulation software for solar energy technologies which has been developed in 2006 by National Renewable Energy Laboratory (NREL), in con-junction with Sandia National Laboratory and in partnership with the U.S. Department of Energy (DOE) Solar Energy Technologies Program (SETP). Figure 2.3 shows the main interface of SAM software.

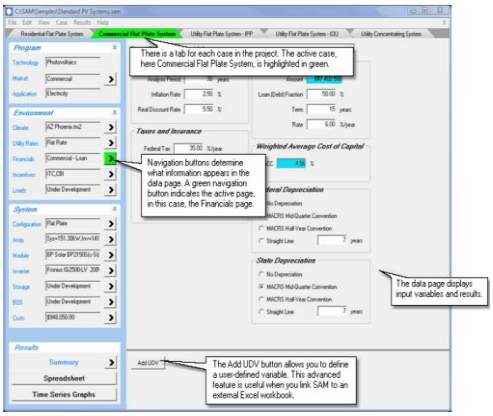

Fig (2.3): The main interface of Solar Advisor Model (SAM) software (Version 2.5)
(Source: Solar Advisor Model user guide, Version 2.5, 2008)

Several types of solar power technologies can be simulated by Solar Advisor Model in different financing types from residential to utility-scale. The current available technologies represented by SAM are concentrating solar power (CSP) as parabolic trough and dish-Stirling systems, in addition to Photovoltaic (PV) flat plate and concentrating systems. More technologies to be added in future versions such as residential solar water heating and CSP solar tower systems. (NREL, 2009).SAM software is considered as one of the most important elements with some market factors in supporting the program's Solar America Initiative (SAI) and planning for the Solar Energy Technologies Program (SETP). The use of SAM as a simulation tool does not required a complete knowledge of all the program components, since the designer of this software had set technical and cost default values which represent baseline values of these components. These default cost values for Parabolic Trough systems is likely to be realistic because of the limited number of installed plants which means limited cost data as well. The analysis of all solar technologies by SAM is carried out using a consistent methodology with financing and cost assumptions. SAM offers several performance and financial output parameters that help the solar developers and decision makers to evaluate any solar project. The most important parameters are Levelized Cost of Electricity (LCOE), system annual and monthly output, System capital and operating and maintenance (O&M) costs, Peak and annual system efficiency and Hourly system production (NREL, 2009).

2.5. Configuration of the proposed CSP plant with SAM

The structure of SAM simulation tool is divided into three parts (program, Environment and System) which are illustrated in the following tables and graphs. Table 4.1 shows the economic and

financing parameters for the proposed 100 MW Parabolic Trough Plant in our research. The third part of the proposed configuration with SAM simulation tool is related to the technical side of the proposed Parabolic Trough Plant in this study.

3) - RESULTS

3.1. Results of Forecasting scenario for the Libyan future electricity production

The results of the first part is represented the electrical production of the study area (Libya) in two scenarios with different growth rate. A summary of the final results of these two scenarios for the forecasted electrical production are included in table (3.1).

Table (3.1): The Three Forecast Scenarios of Electrical Production at 2020

Scenario	1	2
Annual Growth Rate	6%	8%
Forecasted Electricity Production by 2020 (GWh)	54419.53	69389
10% RE Share of 2020 Electricity Production (GWh)	5442	6938.9

3.2. Results of SAM simulation for Tripoli

This section illustrates the results of the simulation of the proposed 100MW Parabolic Trough Plant in the study area (Tripoli) with two configuration cases the first one with water cooling system and the second one with dry cooling system**.**

3.2.1. Levelized Cost of Energy (LCOE)

The simulation case of Tripoli by SAM comes up with LCOE results which are illustrated in figure (3.1). For the water cooling configuration case the difference of LCOE between the real and nominal is 4.68 ¢/kWh, and for the Dry cooling configuration this LCOE difference is higher 5.01 ¢/kWh. Also, the real LCOE is higher with the dry cooling configuration with 1.21 ¢/kWh, and it is the same for the nominal LCOE is higher as well with 1.54 ¢/kWh.

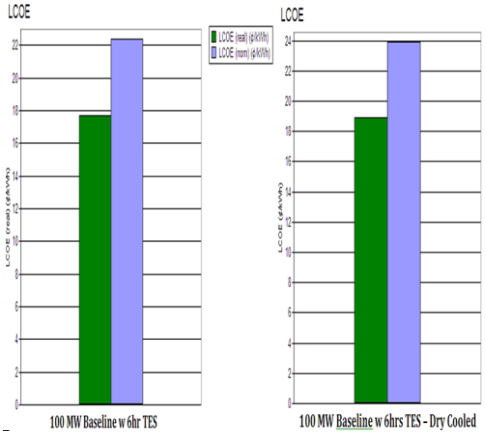

Fig (3.1): A comparison of the LCOE for the two configurations

3.2.2. Annual Energy Flow

The annual energy flow results are illustrated in figure (3.2) in MWh starting from the received solar radiation incident on the collector (Qdni) and ending with the Net Electricity Generated Availability which is one of the most important key results. There is a huge difference between received solar energy and the net utilized

energy due to the heat losses through conversion cycle. Also, this difference is higher in the dry cooling configuration which means that the amount of the net electricity generated is lower than the water cooling configuration.

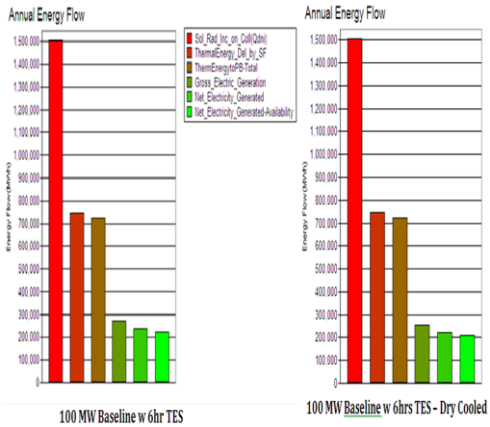

Fig (3.2): Distribution of the annual energy flow for both configurations

3.5. Comparison of SAM simulation results for different locations in Southern Europe and North Africa

The same proposed con-figuration of Parabolic Trough Plant with SAM software has been applied on different locations in Southern Europe region (Palermo & Athens) and in North Africa (Cairo & Aswan), in addition to Tripoli the main location of our study. The comparison of the results output of the electricity amount and cost at these locations, which is shown in figure (3.3), gives an idea about the difference of electricity generation by CSP technology between Europe and North Africa. The big difference of the output and cost will encourage the European countries to co-operate with their neighbours and open a new era for these countries of clean electricity export instead of oil and gas.

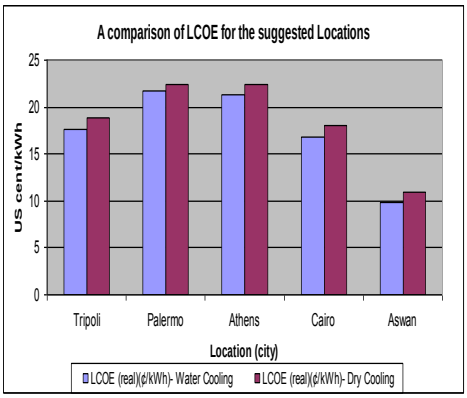

Fig (3.3): LCOE cost for different locations in Southern Europe & North Africa

4) – CONCLUSIONS

Based on the historical data of electricity production and some other published scenarios, a forecasted scenario for the required electricity production in 2020 has been built with two different annual growth rates (6% and 8%). The required amount of electricity production to meet the 10% target by 2020 is 5442GWh according to the lower forecasted scenario with 6% and 6939GWh according to the higher forecasted scenario with 8% annual growth rate.

SAM software is used to simulate our proposed 100MW Parabolic Trough unit with water and dry cooling systems at Tripoli and other comparator locations in the Southern part of Libya such as Al Kufra. As data for this part of Libya is sparse, this was simulated using an available data set for Aswan in Egypt, which was demonstrated to have similar climatic con-ditions and almost identical latitude. Also the same simulation case is applied for two locations in Southern Europe (Palermo & Athens) in order to compare the cost of the generated electricity per KWh on both sides of the

Mediterranean Sea by the proposed technology.

The key conclusions of this study, which were obtained as a result of building the forecast scenarios and applying the simulations, are:

- The annual electricity output for each proposed unit (which has 470.30 m^2 of Solar Collector Assembly (SCA) area and the total solar field area is 871,936 m^2) in Tripoli is 223.7GWh with water cooling system, and the required number of units to produce the required electricity for the 10% target is 24.33 units for first forecasted scenario or 31 units for the second scenario. With dry cooling system the electricity output is slightly lower with 209.2GWh per unit annually and 26 units for first scenario or 33.2 units for the second scenario are required. At the Southern part (Al Kufra) the net electricity output, taking in account the 3% transmission losses through HVDC lines, is more than 50% higher than Tripoli (353 GWh) although the used configuration is limited to dry cooling because of water scarcity there. The required number of installed units is less than Tripoli and it is 15 units for the first forecasted scenario and 19 units for the second scenario.

- The capital cost for one proposed unit is about 355 million US$ and, therefore, the total required capital cost for the proposed number of installed units in Tripoli is (8.65 – 9.25) billions US$ for the first forecasted scenario and (11 – 11.8) billions US$ for the second scenario. This required capital cost is approximately equal to the Libyan oil export revenue for (9.2 – 12.6) days/year for the proposed ten years period. For a site in the Southern part of Libya the required capital cost is more than 50% lower than Tripoli with (5.33 – 6.75) billions US$ which is equal to the Libyan oil exports revenues for (5.7 – 7.2) days/year for the same period.
- The levelized cost of energy is about 4¢/KWh lower in Tripoli than Palermo and Athens, whereas in Al Kufra this cost in addition to HVDC transmission cost (about 1.5 ¢/KWh) is less than half of the LCOE in Palermo and Athens in the Southern Europe. This cost difference can be increased significantly if this electricity could be exported to central Europe which will increase interest in exporting clean electricity generated in North Africa desert to Europe.

References:

[1]. A. Maccari, 2006, "The Thermo-dynamic Solar Project," ENEA

[2]. ATMOSPHERIC SCIENCE DATA CENTER, Surface meteor-ology and Solar Energy, A renewable energy resource web site, NASA's Earth Science Enterprise Program, http://eosweb.larc.nasa.gov/cgi-bin/sse/sse.cgi

[3]. EU Commission, 2007, Concentrating Solar Power FROM RESEARCH TO IMPLEMENT-ATION,

[4]. F.M.Tellez, 2006, " High Concentrating Solar Power Technologies," in AECI

[5]. GECOL, 2007, General Electricity Company of Libya Annual Report, GECOL

[6]. Google Earth, 2009, [accessed in 18-07-2009],

http://www.energyplus.gov/weatherdata/1_africa_wmo_region_1/zip/LBY_Tripoli_IWEC.zip

[7]. GREENPEACE, ESTIA, September 2005, Solar PACES, EXPLOITING THE HEAT FROM THE SUN TO COMBAT CLIMATE CHANGE, Concentrated Solar Thermal Power – Now!

[8]. H. Price, 2006, Parabolic Trough Technology Overview, (NREL) National Renewable Energy Laboratory, USA

[9]. MEDELEC, 2008, General Electricity Company of Libya (GECOL), THE 16th ANNUAL MEETING Casablanca 20-21 March, www.auptde.org/NewSite/UploadFiles/Activityfile/158.ppt

[10]. National Renewable Energy Laboratory (NREL), Science & Technology, Solar Advisor Model (SAM), [accessed in 12-06-2009], https://www.nrel.gov/analysis/sam/

[11]. Planning and Installing Solar Thermal Systems, A guide for installers, architects and engineers, 2005

[12]. Renewable Energy in Libya: Present Situation & Future Initiatives, www.auptde.org/NewSite/UploadFiles/Activitypaperfile/369.pdf

[13]. SCHOTT, 2008, SCHOTT memorandum on solar thermal power plant technology, SCHOTT AG, Mainz

[14]. Solar Advisor Model user guide, Version 2.5, 11/12/2008

[15]. TREC, 2008, CLEAN POWER FROM DESERTS**,** the 'DESERTEC' scenario for Europe, the Middle East and North Africa—EUMENA, Developed by the 'TREC' inter-national network of scientists and engineers

[16]. U.S Department of Energy, Energy Efficiency and Renewable Energy, EnergyPlus Energy Simulation Software, [accessed in 15-06-2009], http://apps1.eere.energy.gov/buildings/energyplus/cfm/weather_data.cfm

CO2 Emission Factor for the electricity generation systems in Libya

Prepared by: Eng. Mohammed R.Zaroug
Planning & studies department in Renewable Energy Authority of Libya (REAOL)
Tel: +218 926456185 Fax: +218 213408602
E-mail: Mohmnl1037480@yahoo.com

Abstract
The generation of electricity in Libya relies on the burning of fossil fuels (oil & natural gas). National statistics indicate that the electricity sector is one of the main emitters of carbon dioxide (CO2). Up to date, the CO2 emissions from electricity system are only estimated and a few of power plants have continuous emissions measuring capability, this shows the need to calculate the CO2 emission factor for Libyan power system to know the real amount of CO2 emitted by power plants. In this study the calculation based on one of international methodologies which approved by The Clean Development Mechanism Executive Board, and using most recently available information which have been collected and reviewed by General Electricity Company of Libya (GECOL). The results of this study can be used to calculate the exact amount of CO2 emitted by power plants in Libya, and also to estimate the amount of emission reductions that will be realized by Clean Development Mechanism (CDM) projects in power sector.

1. Introduction

Electricity can be generated from a different primary energy sources, two-thirds of the world's electricity comes from burning of fossil fuels. The combustion of fossil fuels release CO2 and other greenhouse gases (GHG) to the atmosphere, the amount of emissions varies from one fuel type to another (coal, oil or natural gas) and they are calculated using the emission factors which expressed in kg of CO2 per KWh or tons per MWh of electricity produced.

In general, there are several options to limit the CO2 emissions from electricity generation include:

- Increasing the use of renewable energy,
- Use fuels with lower CO2 emission per KWh produced,
- Increase the efficiency of both electricity production and end-use.

In Libya, the electricity is generated by thermal power plants using oil and natural gas, national statistics indicate that the power sector is responsible for more than (38%) of total emissions in the country. In this study, the CO2 emission factor for Libyan power system is made in accordance with "Consolidated baseline

methodology for grid-connected electricity generation from renewable sources" and " Tool to calculate the emission factor for an electricity system". In this methodology the CO2 emission factor is determined by calculating the combined margin emission factor (CM) of the electricity system.

2. Electricity Sector Overview

The electricity system in Libya is run by the state-owned General Electricity Company of Libya (GECOL). GECOL is responsible for generation, transmission and distribution of electricity in Libya. In 2009, the total electricity produced is around 30 TWh comes from 14 main power plants with overall installed capacity of 6.2 GW. Fig (1) shows the growth of electricity generation in Libya during last decade

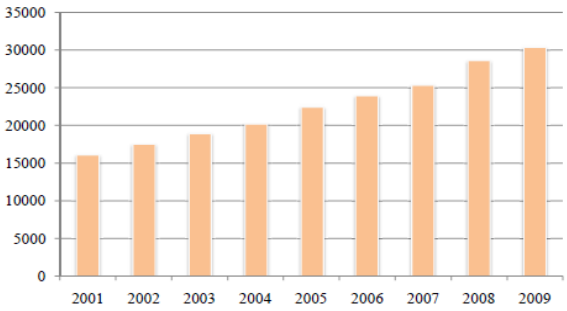

Fig (1) Electricity generation in Libya (2001-2009)

The electricity is generated by thermal power plants using natural gas (NG), light fuel oil (LFO) and heavy fuel oil (HFO) as shown in Fig (2). The last annual report of GECOL indicates that, the residential sector is the main consumer of electricity in the country followed by the industrial , commercial and agriculture sectors as shown in Fig (3)[1].

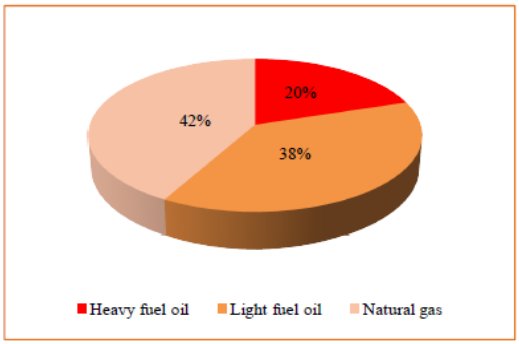

Fig (2) Electricity generation by fuel type

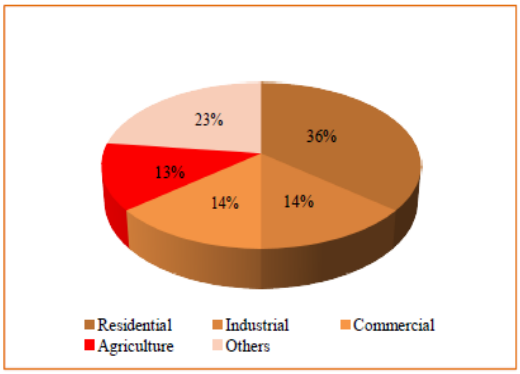

Fig (3) Electricity consumption per sector

Although Libya is a large country with a relatively small population, access to electricity in Libya is almost 100%. In recent years, the growth rate of Libya's electricity demand is increased rapidly; the peak demand reached 5.28 GW in 2009 [1], and is expected to reach 6 GW in 2010 and 18 GW in 2020. The growth of electricity demand is driven mainly by increase in residential consumption, economic growth and the large projects announced by the government. With regarding to the environmental issues, the power sector is one of the main emitters of CO2 in Libya and responsible for more than (38%) of total emissions [2].

3. Methodology used

In this study the CO2 emission factor for the electricity system in Libya was calculated using "Consolidated baseline methodology for grid connected electricity generation from renewable sources (ACM0002)" [3] and "Tool to calculate the emission factor

for an electricity system, version 02" [4] which approved by The Clean Development Mechanism Executive Board of United Nations Framework Convention on Climate Change (UNFCCC). In this methodology the CO2 emission factor is determined by calculating the combined margin emission factor (CM) of the electricity system. The CM is the result of a weighted average of two emission factors; the operating margin (OM) and the build margin (BM) of the electricity system. This methodology provided four options to calculate the operating margin emission factor, the choice depending on availability of data. However, in this study the simple operating margin method is used and the main data needed include:

- Type and amount of fuel consumed by power plants;
- CO2 emission coefficient of fuel and
- Net electricity delivered to the grid.

For build margin additional informations are required so as to identify power plants capacity additions in the electricity system that comprise 20% of the system generation and that have been built most recently.

3.1. The Simple Operating Margin (OM) Method

The simple operating margin (OM) Method can only be used if low-cost/must-run resources (hydro, wind, solar and nuclear) constitute less than 50% of total grid generation, The simple OM emission factor is calculated as the generation-weighted average CO2 emissions (kg of CO2 per KWh or tons per MWh) of all generating power plants serving the system not including low-cost/must-run power plants [5].

The calculation based on fuel type, total fuel consumption and the net electricity supplied to the grid as explained in equations (1), (2).

$$\text{CO}_2\text{ emission (Natural gas)} = \text{Fuel consumption over } (10^3\text{ toe}) \times \text{Net calorific value } (\text{TJ}/10^3\text{ toe}) \times \text{C emission factor } (\text{tC/TJ}) \times \text{Fraction of C oxidized} \times \text{Mass conversion factor } (\text{tCO}_2/\text{tC}) \quad (1)$$

Using the data of Libyan power system which given in Annex (1) for natural gas in year 2007 and specifications of natural gas which given in Annex (4).

CO2 emission (natural gas) = 3,539.26 X 42 X 15.3 X 0.995 X 3.66 = 8,298,262 tCO2

Repeating for fuel oil, the CO2 emission is 12,734,888 tCO2, taking the total for year 2007 to 21,033,150 tCO2. Then,

$$\text{CO}_2\text{ emission factor for operating margin} = \text{Sum of CO}_2\text{ emission for operating margin } (\text{tCO}_2) \div \text{Total grid electricity generated for operating margin (MWh)} \quad (2)$$

CO2 emission for operating margin = 21,033,150 ÷ 23,266,536

=0.904 tCO2/MWh

This is repeated for years 2008 and 2009 using the data which given in Annexes (2),(3) and the results are summarized in table (1).

Table (1) The average OM emission factor
For Libyan power system

Year	2007		2008		2009	
Fuel type	Nat.gas	Fuel oil	Nat.gas	Fuel oil	Nat.gas	Fuel oil
Fuel consumption (10^3 toe)	3539.26	4015.47	3387.66	4561.54	3127.98	5115.68
NCV (TJ/10^3 toe)	42	42	42	42	42	42
C emission factor (tC/TJ)	15.3	20.8	15.3	20.8	15.3	20.8
Fraction of C oxidized	0.995	0.990	0.995	0.990	0.995	0.990
Mass conversion factor (tCO2/tC)	44/12	44/12	44/12	44/12	44/12	44/12
CO2 emissions per fuel type (tCO2/yr)	$8.30*10^6$	$12.73*10^6$	$7.94*10^6$	$14.47*10^6$	$7.33*10^6$	$16.22*10^6$
Total CO2 emissions (tCO2/yr)	$21.03*10^6$		$22.41*10^6$		$23.56*10^6$	
Total electricity generated (MWh/yr)	23,266,536		27,248,375		28,606,802	
Annual grid OM	0.904		0.822		0.823	
Average grid OM	**0.849**					

3.2. The Build Margin (BM) Emission Factor

The build margin emission factor is calculated as the generation-weighted average emission factor (tCO2/MWh) of the sample of build margin power plants, where the sample group consists of either:

- The five power plants that have been built most recently, or
- The power plants capacity additions in the electricity system that comprise 20% of the system generation (in MWh) and that have been built most recently [5].

In this study, the first option was chosen .Therefore, the chosen build margin sample group is; Khoms Gas Turbine, Tripoli South, West Mountain, Zawia and Benghazi North power plants. And the CO2 emission for the build margin is obtained using total fuel consumption and the net electricity supplied to the grid for build margin sample group in year 2009 as explained in equations (3),(4).

Table (2) Build margin power plants

Power plant	Type of generation	Commission date	Capacity (MW)	Net electricity Produced (GWh)	Fuel consumption (10^3 toe)	
Khoms	Gas turbine	1995	600	2,595.98	Light fuel oil	248.92
					Natural gas	595.20
Tripoli South	Gas turbine	1994	500	2,007.55	Light fuel oil	714.76
West Mountain	Gas turbine	2005-2006	624	3,341.34	Light fuel oil	72.51
					Natural gas	1,042.11
Zawia	Combined cycle	2000-2007	1440	6,941.23	Light fuel oil	1,449.70
Benghazi North	Combined cycle	1995-2007	915	5,062.12	Light fuel oil	385.01
					Natural gas	705.80
Total				**19,948.21**		**5,214.01**

The build margin emission factor for Libyan power system is calculated for five power plants that have been built most recently which indicated in table (2). Using equations (3) , (4) and the data of Libyan power system which given in Annex (3) for natural gas in year 2009 and specifications of natural gas which given in Annex (4).

$$\text{CO}_2 \text{ emission (Natural gas)} = \text{Fuel consumption over } (10^3 \text{ toe}) \times \text{Net calorific value } (\text{TJ}/10^3 \text{ toe}) \times \text{C emission factor } (\text{tC/TJ}) \times \text{Fraction of C oxidized} \times \text{Mass conversion factor } (\text{tCO}_2/\text{tC})$$

CO2 emission (natural gas) = 2,343.11 X 42 X 15.3 X 0.995 X 3.667

= 5,493,731 tCO2

Repeating for fuel oil, the CO2 emission is 9,104,966 tCO2, taking the total for year 2009 to 14,598,697 tCO2. Then,

$$\text{CO}_2 \text{ emission factor for Build margin} = \frac{\text{Sum of CO}_2 \text{ emission for Build margin (tCO2)}}{\text{Total grid electricity generated for Build margin (MWh)}} \quad (4)$$

CO2 emission for build margin = 14,598,697 ÷ 19,948,205

= 0.732 tCO2/MWh

Therefore, the build margin (BM) emission factor for Libyan power system equals to (0.732 tCO2/MWh). and the results are summarized in table (3).

Table (3) The BM emission factor For Libyan power system

Year	2009	
Fuel type	Natural gas	Fuel oil
Fuel consumption (10^3 toe)	2,343.12	2,870.91
NCV ($TJ/10^3$ toe)	42	42
C emission factor (tC/TJ)	15.3	20.8
Fraction of C oxidized	0.995	0.990
Mass conversion factor (tCO2/tC)	44/12	44/12
CO2 emissions per fuel type (tCO2/yr)	$5.49*10^6$	$9.10*10^6$
Total CO2 emissions (tCO2/yr)	$14.60*10^6$	
Total electricity generated (MWh/yr)	19,948,205	
Grid BM	0.732	

3.3. The Combined margin CO2 emission factor

Using emission factors which calculated above for the operating margin(OM) and build margin(BM), the combined margin emission factor(CM) is calculated using the default OM: BM weighting of 75% : 25% as:

$$\begin{matrix}\text{CO}_2\text{ emission factor for combined margin} \\ (tCO_2/MWh)\end{matrix} = \begin{matrix}\text{CO}_2\text{ emission factor for the operating margin} \\ (tCO_2/MWh)\end{matrix} \times 75\% + \begin{matrix}\text{CO}_2\text{ emission factor for the build margin} \\ (tCO_2/MWh)\end{matrix} \times 25\% \quad (5)$$

Using the equation (5) and the results of operating margin and build margin which indicated in tables (1), (3).

CO2 emission factor for combined margin = 0.849 X 0.75 + 0.732 X 0.25

= 0.82 tCO2/MWh

Therefore, the CO2 emission factor for electricity system in Libya is (0.82 tCO2/MWh)

4. Conclusion and recommendations

- The emission of CO2 per kWh electricity produced varies among countries and depends on the mix of energy sources used to produce electricity.
- The statistics of International Energy Agency (IEA) for year 2007 show that, the average of CO2 emission factor for electricity systems in the world is (0.507tCO2/MWh), Africa (0.627tCO2/MWh) and Middle East (0.678tCO2/MWh), and Annex (5) gives the emission factor for electricity system in other countries.
- The CO2 emission factor for electricity generation system in Libya is (0.82 tCO2/MWh). (3)
- Based on the CO2 emission factor for electricity system which calculated in this study, The CO2 emitted by electricity system in Libya in 2009 is around (24,000,000 tCO2).
- The results of this study can be used to calculate the CO2 emission reductions of Clean Development Mechanism (CDM) projects in power sector. (3)
- It is necessary to establish a database for all units of power plants in Libya in order to facilitate the access to required data.
- Since the data of electricity generation is changing yearly, that is why it is recommended to update this study every year.

5. Acknowledgment

The author thanks Eng. Fathi M.Abugrad and Dr. Mohamed A.Ekhlat from Renewable Energy Authority of Libya (REAOL) for their comments and suggestions. And thanks Eng. Hasan

Kmeshi and Eng.Randa Turki from Production Management of General Electricity Company of Libya (GECOL) for their efforts in obtaining and verification of data.

References

[1] General Electricity Company of Libya, Annual Report 2009.

[2] National Oil Company (NOC) information, version 7, September 2007.

[3] Consolidated baseline methodology for grid connected electricity generation from renewable sources, ACM0002 Version11, CDM-Executive Board, UNFCCC.

[4] Tool to calculate the emission factor for an electricity system, version02, CDM-Executive Board, UNFCCC.

[5] Project Design Document for Zafarana Wind Power Plant Project, Mitsubishi UFJ Securities Clean Energy Finance Committee, May 2007.

Annexes

Annex (1) Data of Libyan power system (2007)
Source - GECOL

Electricity generated in Libya (2007)				
Power plant	**Type of generation**	**Type of fuel**	**Capacity (MW)**	**Power generation (MWh)**
Khoms (ST)	ST	HFO,NG	480	2,762,144
Khoms (GT)	GT	LFO,NG	600	2,590,686
Tripoli West	ST	HFO	500	1,011,669
Dernah	ST	HFO	130	279,123
Tobruk	ST	HFO	130	822,201
Abu kammash	GT	LFO	45	171,189
Tripoli south	GT	LFO	500	2,023,856
Zwitina	GT	LFO,NG	200	934,889
Kufra	GT	LFO	50	167,827
West Mountain	GT	LFO,NG	624	2,862,271
Zawia	CC	LFO	1440	3,938,435
Benghazi North	CC	LFO,NG	915	3,380,187
Musrata Steel	ST	HFO,NG	510	2,834,224
Sreer	GT	NG	75	118,799
Total			**6,199**	**23,897,500**

Annex (2) Data of Libyan power system (2008)
Source - GECOL

Electricity generated in Libya (2008)				
Power plant	**Type of generation**	**Type of fuel**	**Capacity (MW)**	**Power generation (MWh)**
Khoms (ST)	ST	HFO,NG	480	2,396,609
Khoms (GT)	GT	LFO,NG	600	2,886,090
Tripoli West	ST	HFO	500	1,106,085
Dernah	ST	HFO	130	691,366
Tobruk	ST	HFO	130	623,231
Abu kammash	GT	LFO	45	170,165
Tripoli south	GT	LFO	500	1,819,700
Zwitina	GT	LFO,NG	200	858,034
Kufra	GT	LFO	50	142,912
West Mountain	GT	LFO,NG	624	3,229,840
Zawia	CC	LFO	1440	6,733,261
Benghazi North	CC	LFO,NG	915	4,785,427
Musrata Steel	ST	HFO,NG	510	2,438,769
Sreer	GT	NG	75	282,798
Total			**6,199**	**28,164,287**

Year 2007			
Power plant	**Fuel consumption**		
	HFO (m^3)	**LFO (m^3)**	**NG (m^3)**
Khoms (ST)	491,176	3,480	258,047,200
Khoms (GT)	-	90,664	719,732,000
Tripoli West	348,547	16,843	-
Dernah	105,569	-	-
Tobruk	253,567	-	-
Abu kammash	-	116,746	-
Tripoli south	-	772,877	-
Zwitina	-	34	318,696,000
Kufra	-	103,478	-
West Mountain	-	103,960	843,676,078
Zawia	-	1,367,674	-
Benghazi North	-	187,069	825,367,707
Musrata Steel	360,062	-	424,552,400
Sreer	-	4,319	81,837,624
Total	**1,558,921**	**2,767,144**	**3,471,909,009**

Year 2008			
Power plant	Fuel consumption		
	HFO (m^3)	LFO (m^3)	NG (m^3)
Khoms (ST)	517,852	6,448	132,125,300
Khoms (GT)	-	305,385	666,962,000
Tripoli West	408,467	14,974	-
Dernah	244,103	-	-
Tobruk	197,504	-	-
Abu kammash	-	120,284	-
Tripoli south	-	723,870	-
Zwitina	-	14,181	300,285,000
Kufra	-	95,528	-
West Mountain	-	12,977	1,025,491,632
Zawia	-	1,534,438	-
Benghazi North	-	270,757	797,515,746
Musrata Steel	442,919	-	293,622,312
Sreer	-	2,006	107,186,696
Total	**1,810,845**	**3,100,848**	**3,323,188,686**

Annex (3) Data of Libyan power system (2009)
Source - GECOL

Electricity generated in Libya (2009)				
Power plant	Type of generation	Type of fuel	Capacity (MW)	Power generation (MWh)
Khoms (ST)	ST	HFO,NG	480	3,236,717
Khoms (GT)	GT	LFO,NG	600	2,603,953
Tripoli West	ST	HFO	500	1,206,401
Dernah	ST	HFO	130	625,888
Tobruk	ST	HFO	130	532,903
Abu kammash	GT	LFO	45	192,289
Tripoli south	GT	LFO	500	2,022,008
Zwitina	GT	LFO,NG	200	768,872
Kufra	GT	LFO	50	203,337
West Mountain	GT	LFO,NG	624	3,362,381
Zawia	CC	LFO	1440	7,143,020
Benghazi North	CC	LFO,NG	915	5,192,772
Musrata Steel	ST	HFO,NG	510	2,268,861
Sreer	GT	NG	75	334,425
Total			**6,199**	**29,693,827**

Annex (4) Specifications of natural gas and fuel oil
Source - GECOL & Intergovernmental Panel on
Climate Change (IPCC) Reference Manual

Variable	Fuel type	value
Density	Natural gas	0.793 Kg/m^3
	Heavy fuel oil	940 Kg/m^3
	Light fuel oil	841 Kg/m^3
Net calorific value (NCV)	Natural gas	10194 Kcal/m3
	Heavy fuel oil	10400 Kcal/kg
	Light fuel oil	10712 Kcal/kg
C emission factor	Natural gas	15.3 tC/TJ
	Heavy fuel oil	20.8 tC/TJ
	Light fuel oil	20.8 tC/TJ
Fraction of C oxidized	Natural gas	0.995
	Heavy fuel oil	0.990
	Light fuel oil	0.990
(1 toe= 41.868GJ)		

Power plant	Year 2009		
	Fuel consumption		
	HFO (m^3)	LFO (m^3)	NG (m^3)
Khoms (ST)	714,024	5,238	145,482,100
Khoms (GT)	-	274,676	583,872,000
Tripoli West	421,816	14,800	-
Dernah	227,293	-	-
Tobruk	209,172	-	-
Abu kammash	-	145,245	-
Tripoli south	-	788,719	-
Zwitina	-	1,980	275,357,001
Kufra	-	122,820	-
West Mountain	-	80,015	1,022,273,182
Zawia	-	1,599,693	-
Benghazi North	-	424,851	692,370,610
Musrata Steel	462,580	-	227,476,300
Sreer	-	15,167	121,622,303
Total	**2,034,885**	**3,473,204**	**3,068,453,496**

Annex (5) CO_2 emissions per MWh from electricity
Source - International Energy Agency (IEA)

	Country (2007)	t CO_2 / MWh			Country (2007)	t CO_2 / MWh
1	Canada	0.205		22	Egypt	0.450
2	USA	0.549		23	Algeria	0.597
3	Finland	0.230		24	Morocco	0.712
4	France	0.090		25	Tunisia	0.557
5	Germany	0.427		26	Bahrain	0.847
6	Greece	0.749		27	Iraq	0.811
7	Italy	0.388		28	Jordan	0.588
8	Norway	0.007		29	Kuwait	0.645
9	Austria	0.202		30	Lebanon	0.638
10	Spain	0.390		31	Oman	0.861
11	Sweden	0.040		32	Qatar	0.623
12	Switzerland	0.023		33	Saudi Arabia	0.736
13	Malta	0.923		34	Syria	0.606
14	Argentina	0.352		35	UAE	0.831
15	Brazil	0.073		36	Yemen	0.679
16	Cuba	0.849		37	Iran	0.536
17	India	0.928		38	Botswana	1.852
18	Pakistan	0.432		39	South Africa	0.845
19	China	0.758		40	Middle East	0.678
20	Japan	0.450		41	Africa	0.627
21	Korea	0.455		42	World	0.507

Chapter V

Biomedical Engineering

Monte Carlo simulation of electron and photon transport in the Elekta SL-25 linear accelerator head at the Tripoli Medical Center

رمضان مفتاح كريدان و خديجة عمر بن إبراهيم

قسم الهندسة النووية – جامعة الفاتح

kuridarm@yahoo.com

Abstract

Monte Carlo (MC) modeling of a linear accelerator is a prerequisite for Monte Carlo dose calculations in external beam radiotherapy. In this study, a simple and efficient model is developed for the Elekta SL-25 linear accelerator head using MCNP4C Monte Carlo code. A photon source model is developed in order to reduce the run time taken by the simulation of the electron beam source. Energy spectra and angular distributions of photons produced by electron interactions in the target are used for the new photon source description to the code. Using this model, percent depth doses (PDDs), and beam profiles are calculated for different field sizes. The results of MC calculations are compared with measurements. There is a good agreement between MC calculations and measurement for PDD curves. However, for beam profiles, differences range from 1to 2% in the flat region and up to 20% difference is seen for the out of field region. These results were acceptable according to the recommended criteria. Using the photon source model, the run time on a two GHz computer is decreased from days to hours in comparison to the

electron source model. Our study showed the presented model to be accurate and effective for MC calculations in radiotherapy treatment planning.

Introduction

The Monte Carlo (MC) method is widely accepted as the most accurate technique for calculating dose distributions in radiation therapy (the treatment of cancer tumors with ionizing radiation). In the MC method particles (neutrons, photons, electrons, etc) full description in terms of position, energy, direction, and tracks are randomly selected. Particle collision physics is relied upon in the process of determining the probability density function required for random sampling. The particle faith is decided accordingly. A large number of particle histories are run in order to obtain reliable statistics determined by the variance. The primary goal of radiation therapy is to maximize the dose to the tumor cells and to minimize the exposure of

the healthy tissue surrounding the tumor to radiation. The MC method is a statistical simulation technique for particle transport whose capabilities have progressed into many different areas of application since its introduction in the 1940s. Simulating the particle transport through the treatment head of a linear accelerator (linac) utilizing a MC based code is both a widespread and practical approach to determining detailed clinical beam characteristics such as the energy, angular and spatial distribution of particles which are needed to properly quantify dose. One particular and versatile MC code, the Monte Carlo N-Particle (MCNP) radiation transport code, developed by Los Alamos National Laboratory has been extensively used to model ionizing radiations for medical physics applications [1].

There are many papers about the Monte Carlo simulation of medical linacs (Verhaegen and Seuntjens, 2003) [2]. However, such linacs differ a great deal depending on the model and manufacturer and end user facility (Sheikh-Bagheri, D., Rogers, D.W.O., 2002 [3]; Fix et al (2001); [4]; Solberg TD et al., 2000, [5]). There is only one unpublished study in which the SL 25 linac at the TMC is simulated using the EGS code (Karima and tawfiq [6]). However, this code has its shortcomings and is incomparable to the capabilities of MCNP. Using the electron beam as a source is a time consuming task. Mesbahi (2006) used a simple point photon source model to replace the electron beam model for a similar linac [7]. This is far from real since photons are produced in at least four components of the linac and can not easily be approximated by a point source. Such volumetric sources are the subject of our model.

Modeling and simulation:

In this paper, a more realistic model is developed using the MCNP4C code for the Elekta SL-25 linear accelerator used by the radiotherapy department at the Tripoli Medical Center (TMC). The material composition of the linac head components is as follows: (a) Target (90% Tungsten and 10% Rhenium). (b) Base is a 100% Copper. (c) Collimators consist of 90% tungsten, 5% iron, and 5% nickel. (d) Flattening filters are made of highly pure stainless steel. (e) Two types of jaws: the top one has the same composition as the collimator and the lower one consists of an equal mixture of lead and antimony. A 6 MeV electron beam is produced, and bended orthogonal to at the linac head where photons (p) and electrons (e) are produced by different types of interactions. The resulting photons are mostly emitted downward through the head components until they finally reach their intended destination (the tumor). The photon spectra are characterized in a standard 10 x 10 cm2 field and subsequent dose calculations are made in a virtual water phantom. It is normally used in radiotherapy because it resembles the human tissue in terms of composition and radiation interaction characteristics. Energy fluence, percent depth dose (PDD) and beam profiles are calculated in the water phantom and are compared to measurements performed at the TMC linac. Collimators are made of shielding materials characterized by a strong absorption of gamma ray photons and their shape allows for the collimation of the emerging photons leaking from the target in a cone around the z-axis.. The conic shape of the flattening filter reduces the pencil like beam to a flat shape producing a uniform dose distribution at the tumor volume. The jaws are also supposed to absorb the unwanted side photons in order to protect the healthy

tissue. Figure 1 is a schematic representation of the SL 25 head and phantom.

Electrons interact with matter via elastic and inelastic scattering, Bremsstrahlung, and annihilation radiation. The first two types are predominant at low and intermediate energies and are associated with small energy losses and electron deflections. Bremsstrahlung photons emerge when high energy electrons are accelerated or decelerated in the atomic electric field of a high Z (atomic number) material e.g. tungsten. Two annihilation photons are emitted in two opposite directions upon the interaction of electrons and positrons with minimum energy of 0.511 MeV each. Photons on the other hand interact via mainly three mechanisms. First, photo electric absorption: the photon disappears completely and an orbital electron is emitted. Second, Compton scattering: the photon is scattered by a free electron resulting in loss of energy and direction. Third, pair production: the incident photon with minimum energy of 1.022 MeV interacts with the electric field of the atomic electrons leading to the annihilation of the photon and the creation of an electron and positron pair emitted in opposite directions. Therefore, electrons produce photons and photons produce electrons and hence the mode of interaction is a photon-electron (p-e) throughout the particle transport.

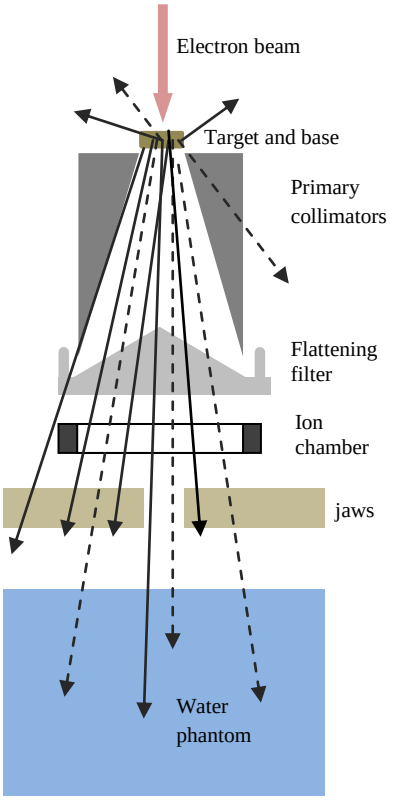

Figure 1- Schematic diagram for the axial view of the SL 25 head and water phantom for M C simulation

p → e - - →

The field area represents the tumor position. According to the size of the tumor the field size can be varied by altering the window size drawn by the motion of the jaws in the x and y directions. Therefore, different field sizes can be produced. In fact, complicated curved contours can be made to surround the area of the tumor in order to prevent healthy tissue from radiation damage. In this study a simplified variable size square fields are used. Figure 2 shows a field drawn by controlled opening of the jaws.

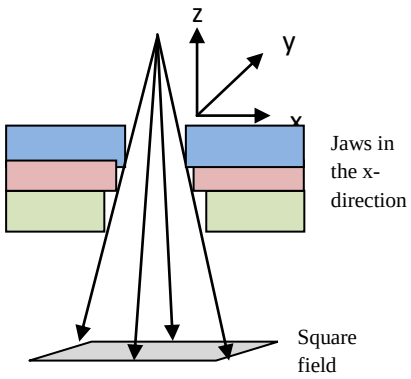

Figure 2- A square field size drawn by jaws motion

Measurements and calculations are performed in a water phantom. The 2mm radius 6 MV electron beam incident on the head of the Elekta SL-25 linac is simulated using MCNP4C MC code. Beam radius used in this study is recommended by many authors in previous studies [8]. Figure 3 and 4 are produced by the MC code and they clearly show the target (starting from top of figure 3), collimators, filter, ion chamber, and mirror in addition to jaws and phantom in figure 4.

Photon source model:

Two approaches are adopted for the source definition to MCNP: electron beam source and anisotropic photon source. The first one is of course more realistic. However, its prohibitive length of simulation time makes it unattractive. The run may take many days because of electron energy losses are so small during a collision. In the second one, the energy and angular dependence of photons and electrons

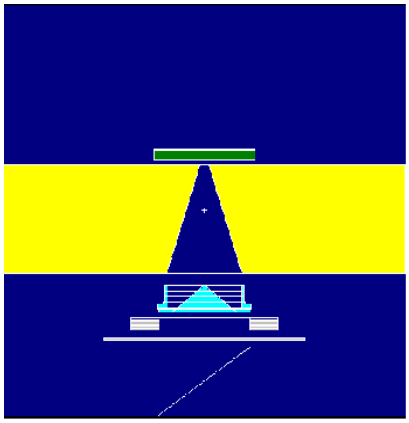

Figure 3- MC simulation plot of the Elekta SL25 head

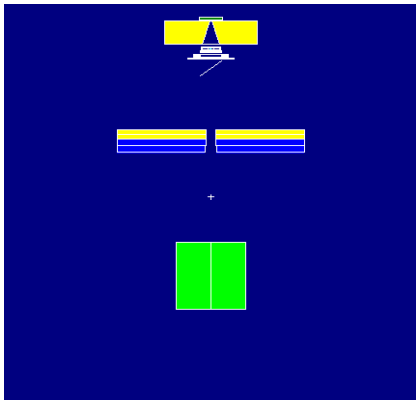

Figure 4- MC simulation plot of the Elekta SL25 head and virtual water phantom (bottom)

energy and angular distributions of scattered and un-scattered electrons emerging from target and base (figures 5 and 6) are used as a new source in order to produce the photon energy and angular distributions in the collimator and flattening filter. It was found that the amount of photon production in the collimator, and filter are of negligible importance as compared to that produced in the target.

Therefore, only the target and base are considered as a volume sources for photons replacing the electron beam in the particle transport. The target collisions flatten the spectrum and further base collisions brings it to the lower end as shown in figure 5. Figure 6 shows that most of the electrons are scattered in the forward direction.

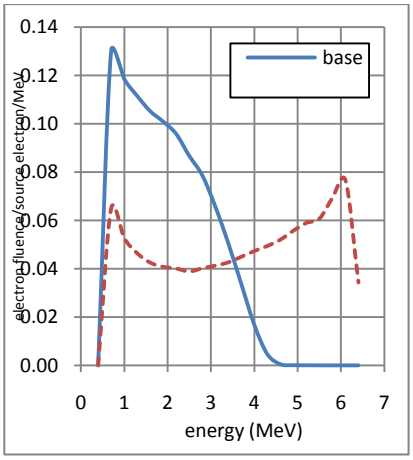

Figure 5- Energy distribution of electrons in the target and base

Direction is mainly determined by the polar angle (θ) and the azimuthal angle (φ). The azimuthal angle is sampled uniformly between 0 and 2π since photon emission is almost independent of this angle. Conversely, it is highly dependent on the polar angle in mainly the forward direction; therefore, the probability distributions in the cosine cones (μ=cosθ) are calculated. Ten angular bins of one degree each are taken in the forward direction and larger bins in the rest of the 4π space. Figure 7 simplifies this argument.

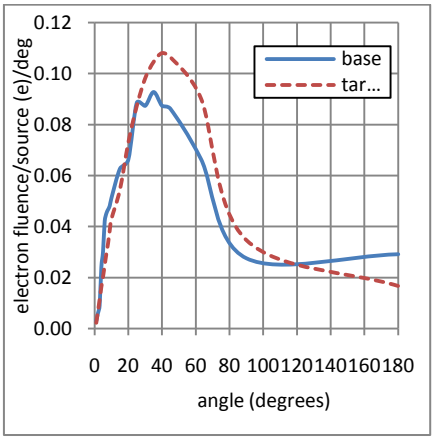

Figure 6- angular distribution of electrons in the target and base

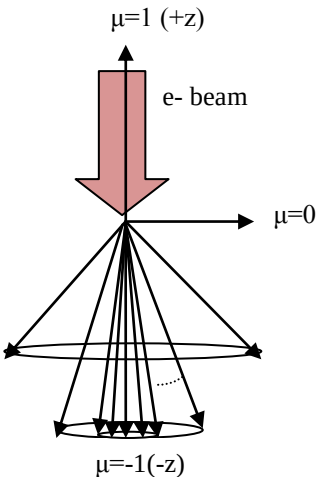

Figure 7- Polar cosine bins for photon source simulation

Figure 8 and 9 show the energy and angular distributions of such photons in the base and filter. Photons have a bottom peaked energy distribution and are forwardly directed. These distributions are used in the description of the photon source in the MCNP input file. Test runs are performed for the photon sources with and without energy cut off. Photon and electron energy cut-offs of 10 and 500 keV respectively are used in order to reduce drastically the simulation time. Early

optimization studies led to the conclusions that the particle energy contributions to the overall dose become insignificant below such values. Otherwise, the particles will be tracked indefinitely as long as they are not absorbed leading to such long simulation times.

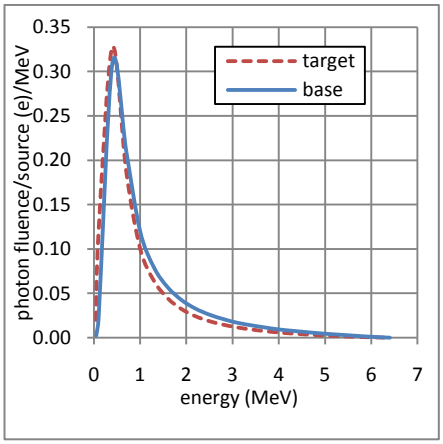

Figure 8- Energy distribution of photons in the target and base

By introducing energy cut offs a particle is killed by Russian roulette (randomly) and its weight is distributed between living particles (conservation of weight). Run time is reduced from hours to minutes.

short range. The location of the peak is dependent on the electron energy. In this case, it is around 1.6 cm below the surface. The PDD curve is obtained by normalizing all values to the maximum value at the peak.

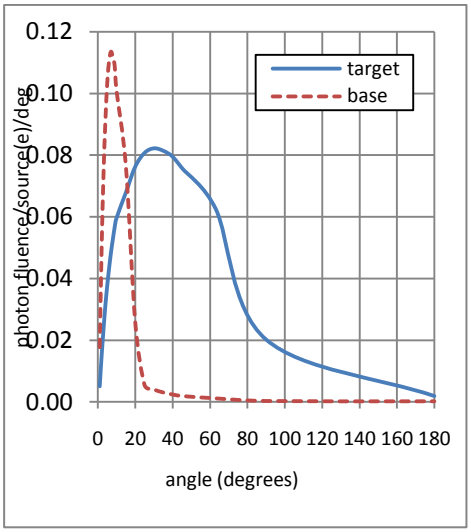

Figure 9- angular distribution of photons in the target and base

Percent depth dose and beam profile curves:

The percent depth dose (PDD) curve is obtained by recording the radiation dose for the field size of interest in the water phantom axially around the beam centerline. The appropriate voxel size should be determined by calculating doses in voxels of variable size. The effect of the size of the voxel on the value of the recorded dose is shown in figure 10. It can be concluded that a cylindrical voxel radius equal to the one tenth of the beam profile width is reasonable. That is a width of 2cm by 2cm in the x-y dimensions and a height of 2 mm in the z dimension is used for a 10 cm by 10 cm field. A peak appears just below the phantom surface in the PDD curves. It is caused by the build

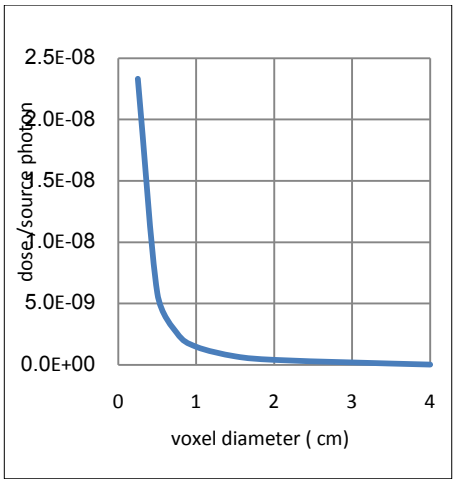

Figure 10- variation of dose with voxel size

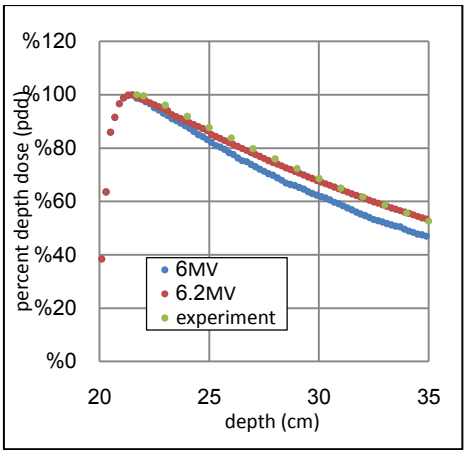

Figure 11- The percent depth dose for 6 and 6.2 MV electron beams and experiment in a 10×10 field size.

The exact mean energy of the electron beam incident on target is usually unknown and must be determined by calibrating the calculated PDD curve against the one obtained by experimental work. The primary electron beam energy exiting the flight tube is varied until the PDD curve for the standard 10×10 cm2 field size becomes within 1% from the experimental one. A final value for the primary beam energy of 6.2 MV satisfies this condition. The PDD curves are shown in figure 11. These results are obtained by the source models discussed above. The run times for achieving accuracy of less than 1% relative error are incomparable. The time required to complete a run using the electron of in a source model exceeds few days with a two GHz computer, while the photon model takes less than an hour.

and 25×25 cm2 field sizes are calculated and compared with measured data (figure 12 and 13). Notice that at smaller field size calculated and measured data depart from each other at lower depths. This is due to the diverging nature of the photon beam given a small voxel size of the 4 by 4 field. Beam profiles are calculated at a depth corresponding to the position of the peak in horizontal voxels perpendicular to the beam axis. The voxel size is 4×4×2 mm. Dose profiles are obtained by normalizing all values to the maximum value at the peak in a similar fashion to the PDD curve. A uniform distribution of dose in the specified field implies that a uniform dose is imparted to the tumor.

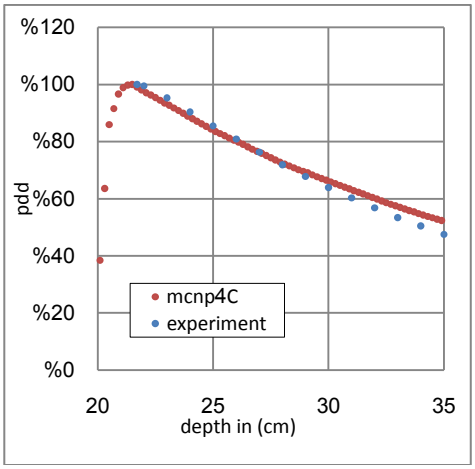

Figure 12- The calculated and measured PDD curves for 4×4 field size at 6.2 MV

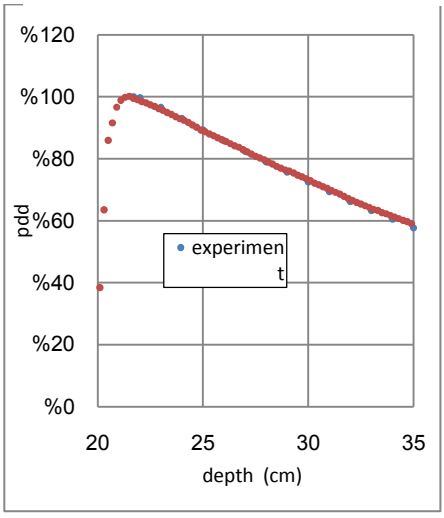

Figure 13- The calculated and measured PDD curves for 25×25 field size at 6.2 MV

The calculated and measured beam profile for a 10×10 field is presented in figure 14. Differences between calculation and experiment in the off-axis region range from 1% to 2% for both the electron source and photon source models. On the other hand, differences are quite high in the penumbra tail region (boundary between tumor and healthy tissue). However, calculation points fall quite sharp as compared to experimental ones, a more preferred behavior. Other profiles and PDD curves are also produced and there is no need to present them all here.

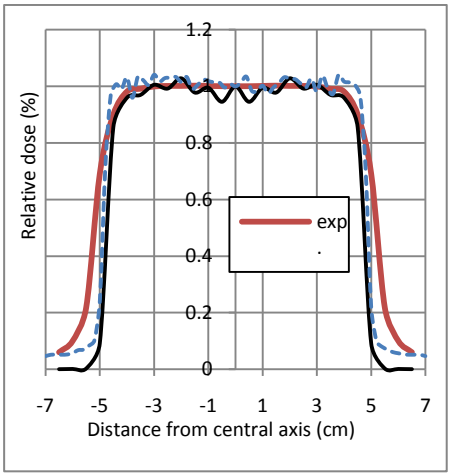

Figure 14- The calculated and measured beam profile curves for 10×10 field size at 6.2 MV

CONCLUSION

Precise modeling of the Linac head and a sufficiently large number of particle histories are required in order to reduce the statistical uncertainty and obtain accurate results in Monte Carlo dose calculations in radiotherapy. In this study, the Elekta SL-25 Linac head is simulated using published data. A volumetric photon source model as an alternative to the electron beam source model is proposed. It is found that MC calculations are in reasonably good

agreement with experimental results for the PDD curves and dose profiles. Our results are also in good agreement with the recommended criteria for photon beam models for dose calculation in radiotherapy [8]. In comparison to the electron beam model, the photon source model reduced the MC simulation runtime drastically from days to hours.

References

1. Briesmeister, J.F., 2000. MCNP—A general Monte Carlo N-particle transport code, Version 4C. Report LA-13709-M. Los Alamos National Laboratory, NM.
2. Verhaegen, F., Seuntjens, J., 2003. Monte Carlo modeling of external radiotherapy photon beams. Phys. Med. Biol. 48, R107–R164.
3. Sheikh-Bagheri, D., Rogers, D.W.O., 2002. Sensitivity of megavoltage photon beam Monte Carlo simulations to electron beam and other parameters. Med. Phys. 29, 379–390.
4. Fix MK, Stampanoni M, Keller H, Born EJ, Mini R, Ruegsegger P (2001) A multiple Source Model for 6 MV photon beam dose calculations using Monte Carlo. *Phys Med Biol, 1407-1427.*
5. Solberg TD, DeMarco JJ, Chetty IJ, Mesa AV, Cagnon CH, Li AN, Mather KK, Medin PM, Arellano AR, Smathers JB (2001) A review of radiation dosimetry application using the MCNP Monte Carlo code. *Radiochim Acta, 337-355.1-11.*
6. Elmasri, K. and Giadui, T. (2008) Modeling the Elekta SL-25 linear accelerator head using EGS code, MSc thesis, Nuclear engineering department, Alfateh University, Tripoli, Libya.
7. Mesbahi, A (2006), Development a simple point source model for Elekta SL-25 linear accelerator using MCNP4C Monte Carlo code, *Iran. J. Radiat. Res.; Vol. 4, No. 1, Summer 2006*
8. Venselaar J, Welleweerd H, Mijnheer B (2001) Tolerances for the accuracy of photon beam dose calculations of treatment planning systems. *Radiother Oncol, 191-201.*
9. Vassiliev, O.N., Titt, U., Kry, S.F., Po¨ nisch, F., Gillin, M., Mohan, R.,2006a. Monte Carlo study of photon fields from a flattening filter-free clinical accelerator. Med. Phys. 33, 820–827.

Integrated Electrochemical Microsensors for Biomedical Applications

Eithne Dempsey*[1], Ahmad Benkhial[1], Anna Tsigara[1], Ronan O'Reilly[1,] Rodica Doaga[1], Baljit Singh[1], Dhanraj Rathod[1] and Fathi Akkari[2] .

[1]*Centre for Research in Electroanalytical Technologies, Institute of Technology Tallaght, Tallaght Dublin 24,* [2]*Dept. Electronic Engineering, Institute of Technology Tallaght, Tallaght Dublin 24.*
*Corresponding author
00 353 1 4042862 (tel)
01 353 1 4042404 (fax)
Eithne.dempsey@ittdublin.ie

Abstract

Electrochemistry is a compatible mode of detection for chip based microscale analytical systems. Features such as sensitivity, inherent miniaturisation and compatibility with advanced microfabrication technologies enable portable applications at the point of care (bedside diagnostics, near patient monitoring). We have adopted a multi-disciplinary approach to the establishment of core platform technologies, bringing together physical chemistry, biochemistry, surface science and microfabrication/semiconductor technology, leading to production of innovative nano/microsensors for *in vitro* blood/urine diagnostic testing. Nano/microscale devices offer advantages of small sample volume, rapid response together with bio-functional adaptation leading to multianalyte determination for a range of disease states. This review will outline the approach taken with respect to the fabrication of thin film electrochemical cells with subsequent surface modification for analyte capture and signal transduction. Essential elements include the use of nano-materials as stable immobilisation matrices for chemical and bio-reagent entrapment (nanoassembly, nanosphere lithography), synthesis and functionalisation of nanostructured materials which act as catalytic surfaces within the sensing element, and finally microfluidic channel integration for sample handling. The determination of relevant parameters is achieved using a combination of experimental approaches such as cyclic and rotating disk voltammetry, surface characterisation (scanning electron microscopy, transmission electron microscopy), thus ensuring optimisation of the charge transport/kinetic properties of the films and overall analytical performance of the devices.

Introduction

Electrochemical sensors can be employed to detect a wide range of molecules, with applications in areas such as environmental/biomedical analysis and industrial process control. An electrochemical reaction is one involving the transfer of charge as part of a chemical reaction. Typical electrochemical reactions such as corrosion involve metal dissolution (oxidation) and oxygen reduction. Cyclic voltammetry [1] is the most widely used technique for acquiring qualitative electrochemical information. The power of cyclic voltammetry results from its ability to rapidly provide considerable information on the thermodynamics of the redox process and the kinetics of heterogeneous

electron transfer, coupled chemical reactions or adsorption processes [2]. It is often the first experiment performed in an electrochemical study. In particular, it offers rapid location of the redox potential of an electroactive species and convenient evaluation of the effect of media on the redox process.

In a typical experiment three electrodes are normally immersed within a cell containing an electrolyte. The working electrode (WE) acts as a transducer converting the transfer of electrons to/from the species in solution, into a detectable signal. The reference electrode (RE) provides a constant potential against which the potential of the WE is varied and the counter electrode (CE) provides an alternative route for the current to pass through the circuit (Figure 1).

Cyclic voltammetry involves applying a triangular wave form (Figure 2) to the electrode and recording the corresponding current.

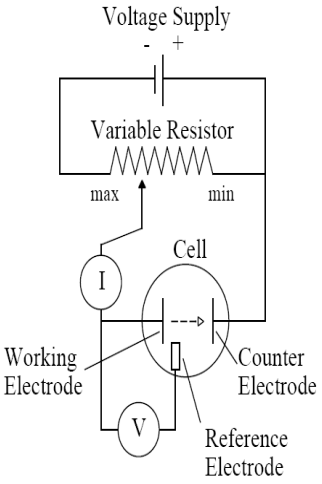

Figure 1: Potentiostat control unit.

This consists of sweeping the potential, at a constant rate in an unstirred solution, from an initial to a final potential, chosen to enable measurement of the formal potential E^o, of the analyte of interest. The current is then recorded as a function of potential.

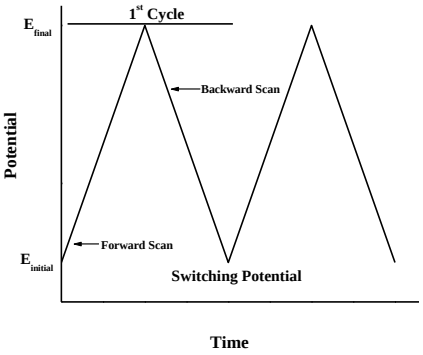

Figure 2: Potential-time excitation signals in a cyclic voltammetry experiment.

Amperometric electrochemical cells are based upon the detection of current produced by an electroactive compound during a non-spontaneous redox reaction. The application of an external potential (via a potentiostat control unit), causes oxidation/reduction of the analyte and the transfer of electrons, which are recorded as current, the magnitude of which is directly proportional to the concentration of the electroactive species.

Microsensors

A miniaturised electrochemical cell is referred to as a microsensor when the dimensions are reduced from mm to μm scale (microelectrode dimensions typically < 100 μm). During a redox reaction, the analyte is consumed in the area directly adjacent to the surface of the working electrode. To retrieve analytical data, the reaction must be sustained for a pre-

determined period of time and the consumed analyte replenished. Diffusion is the spontaneous movement of a species down a concentration gradient established within a defined region (diffusion layer) and the interface of the electrode and the electrolyte (Figure 3 (a)). As the diffusion layer increases and its dimensions exceed those of the working electrode, spherical diffusion dominates (Figure 3 (b)). Due to the increased quantity of species diffusing across the layer, a steady state is established where the rate of consumption can equal the rate of replenishment resulting in a sigmoidal voltammogram typical of a microelectrode response (Figure 3).

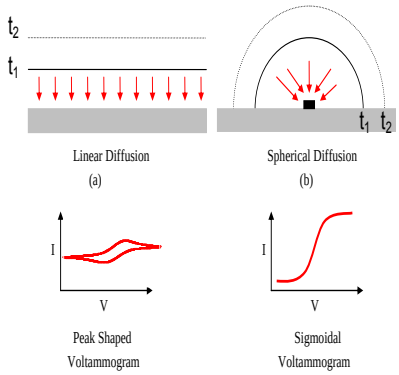

Figure 3: Comparison of diffusion profiles and corresponding cyclic voltammetric shapes for (a) macroelectrode and (b) microelectrodes.

Microelectrodes have several advantages over larger macroelectrodes e.g. rapid establishment of a steady state current, enhanced mass transport, improved S/N ratio and low ohmic drop.

Microfabrication

Fabrication of thin film microsensors involves the formation of permanent structures (25-250 nm thick) on a prepared substrate. Metallic thin films may be deposited over a template using sputtering, evaporation or electro deposition with the aid of standard photolithographic techniques [3,4]. Sensor configurations vary and some typical designs are shown in Figure 4. In particular, disk shaped microelectrodes display a spherical diffusion pattern while being compatible with standard microfabrication techniques.

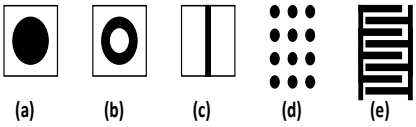

Figure 4: Commonly employed microelectrode (a) Disk (b) Ring (c) Band (d) Disk array (e) Interdigitated array

A working electrode array 64 individually addressable Pt microelectrodes (custom designed on a silicon substrate) has been developed in our laboratory using physical vapor deposition (scanning electron microscope image Figure 5). Electrochemical testing resulted in typical sigmoidal cyclic voltammograms with an increased current density due to the 8x8 25 μm Pt working electrode disk array (Figure 6). As confirmed experimentally, the current density achieved for such electrode arrays increases by a factor of N, where N is the number of electrodes within the array.

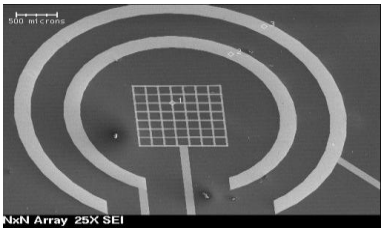

Figure 5: Scanning electron microscope image of an 8x8 microelectrode array (Pt

working electrode in centre surrounded by Ag/AgCl reference and Pt counter electrode**).**

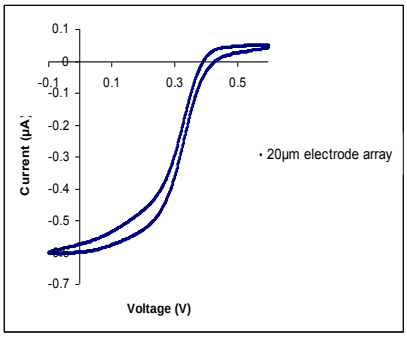

Figure 6: Corresponding cyclic voltammogram for thin film electrochemical device shown in Figure 5. Testing was carried out in 5 mM potassium ferricyanide as redox probe in 0.1 M KCl/ phosphate buffer at 100 mV/sec scan rate vs. Ag/AgCl.

Further recent work in our laboratory involved fabrication of an alternative linear design with disk shaped working, reference and counter electrodes via deposition of Cr (20 nm) and Pt (150 nm) metallic thin films, deposited on silicon by RF sputtering and resistant heated thermal evaporation respectively. This was followed by deposition of Ag on the reference electrode (250 nm) using chamber resistant heated thermal evaporation. Once the fabrication of counter, reference and working electrodes, contact pads and interconnections was completed, passivation was required to prevent galvanic corrosion of the metal multilayers and in order to delineate the active area of the device. The Ag thin film reference electrode was transformed to a Ag/AgCl layer using ferric chloride to oxidise the silver and form an insoluble layer of AgCl. This was required for a functioning reference system (maintenance of a stable potential was dependent on a constant chloride ion concentration in solution). Figure 7 shows the three electrode silicon microchip prior to microfluidic channel integration. The surface of the device can be modified with chemical/biological catalysts enabling a range of sensing applications (see below) while integrated sample delivery can be achieved via microchannels which enable mixing/filtration as required prior to analysis.

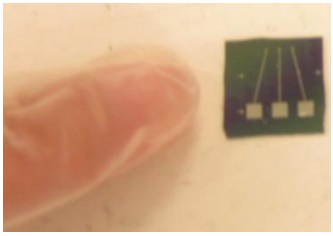

Figure 7: Microchip electrochemical cell in linear arrangement (0.0314µm^2 working electrode) scaled against an index finger**.**

Microfluidics

Microfluidics can be defined as the management, manipulation and analysis of fluids in structures on a micrometer (and lower) scale. The introduction of microfluidics offers several advantages including reduction in the reagents consumed, waste produced, cost per analysis, energy consumption and faster analysis time. The flow of fluid through a microfluidic channel is laminar, resulting in predictable fluid transport with no convective mixing (mass transfer is via diffusion only). The term “Lab-on-a-chip” was coined to describe an integrated microfluidic and electrochemical microsensor device which can execute multiple laboratory type functions on a

single planar platform. Advantages include the fact that tiny volumes of analytes/reagents are required, rapid analysis can be achieved with high reproducibility possible due to automation and mass production.

Lab-on-a-chip configurations include single or multiple channels/sensors [5,6]. Other components such as valves, pumps, switches may also be integrated and a recent review [7] charts the recent developments in micro total analysis systems.

Hydrodynamic flow is the primary method used to deliver a fluid sample in a microfluidic channel, where a pressure drop is created across the inlet and outlet of a channel via syringe pumps [8-13]. A recent review of micropumps outlines future prospects [14] in this area. Other delivery methods based on electroosmotic [15,16] and thermal-pneumatic flow [17], require additional components to be added to the microchannel device such as heat sensors/transducers, thus adding complications to the final device.

Microfluidic Channel Fabrication

For the implementation of the microfluidic system a reliable bonding process which does not affect the performance and properties of the components is required. Polydimethylsiloxane (PDMS) is an elastomeric material widely used in microfluidic devices [18,19] and the suitability of PDMS for the facile fabrication of a microfluidic enzyme modified electrochemical sensor has been demonstrated [20]. The advantage of electrochemistry for chip based analysis is that alignment of the electrodes with microfluidic elements is simplified and often directly microfabricated into channels using the same technology as the channels themselves. In addition, electrochemical detection does not require much off the chip instrumentation. Recent work within our group has involved the development of PDMS single channels (Figure 8) integrated with electrochemical cells for glucose detection – see further information below.

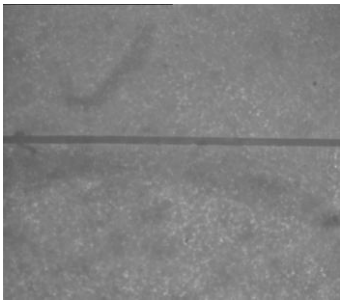

Figure 8: Filled PDMS microchannel 20 μm wide, 115 μm high. Total volume is 35 pm^3 for a 1.5 mm length channel.

Figure 9 shows the linear three electrode thin film microsensor (Pt disc 200 μm), as shown in Figure 7), formed within a channel patterned on the chip using photoresist (SU-8-50) with subsequent PDMS sealing. Alternatively, microchannels may be formed within an overlaid PDMS layer with inlet and outlet forming the required fluidic connections. To form a defined microchannel within the PDMS layer positioned onto the planar microchip device, a silicon wafer with patterned SU-8 photoresist was used as a mould on which a prepolymer of PDMS was poured. Following curing, the PDMS layer was peeled-off from the master to be placed onto the electrode chip and sealed (see Figure 10).

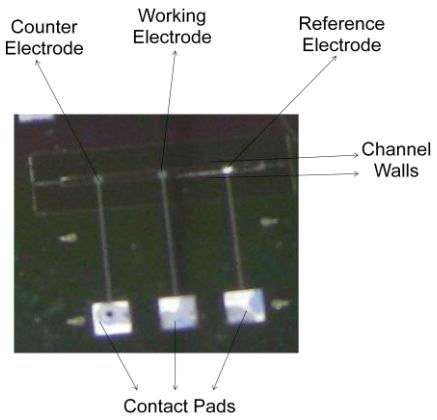

Figure 9: Components of the µ-fluidic chip prior to electrochemical testing.

The volume of the flow channel depended on the mould employed which ranged from 500-1000µm for a 14mm microchip. Once the PDMS layers are completed, two holes were drilled for insertion of needles allowing fluid delivery from a peristaltic pump (as employed during continuous monitoring glucose application – see further details below). A schematic of the total device is shown in Figure 11.

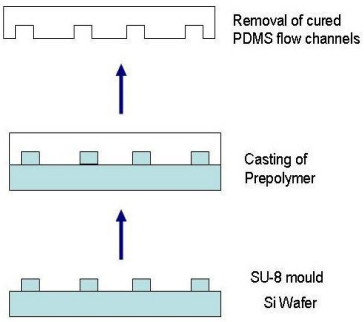

Figure 10: Preparation procedure for the PDMS microfluidic channel.

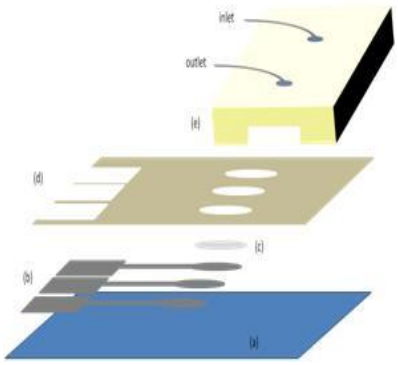

Figure 11: Exploded view of the three electrode system, (a) SiO_2 substrate, (b) Cr/Pt layer, (c) Ag Layer (d) SU8-5 passivation layer and (e) PDMS seal.

Microsystems and Miniaturisation

In analytical separation methods such as capillary electrophoresis (CE) or liquid chromatography physico-chemical characteristics that differ from one compound to another are exploited to effect separation of sample components into discrete zones before reaching the detector. CE separation is based on the differential electrophoretic mobilities of compounds in an electric field, determined by charge-to mass ratios of the compounds being analysed. This technique has been the primary method investigated for microchip separation platforms [21,22]. Electrochemical detection features sensitivity together with inherent miniaturisation of the detector and control instrumentation [23,24]. PDMS channels sealed onto planar glass slides with integrated on-chip electrochemical detection (see Figure 12) have been employed by our group for the separation of biologically and environmentally relevant species (endocrine disrupting compounds) [25,26].

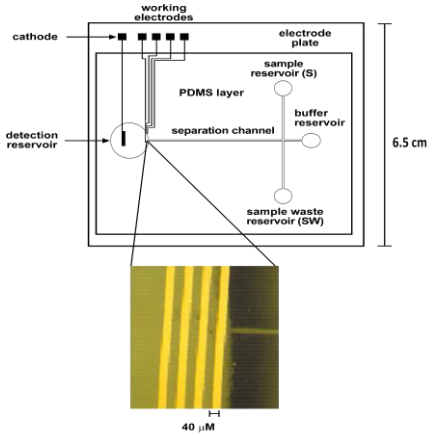

Figure 12: Microchip capillary electrophoresis device showing separation and injection microchannels together with 4x40 μm Au band electrochemical detection system.

Nanomaterials and Nanosensors

Nanotechnology can be defined as 'engineering at a very small scale' and this rapidly growing area may be applied to many areas of research and innovation. As biotechnology is also experiencing rapid growth, this creates exciting opportunities for new and highly applicable sensing strategies. Nanotechnologies involve the design, characterisation, production, and application of structures, devices, and systems by controlling their shape and size. Application areas include drug screening technologies, biocompatible materials, degenerative disease studies, self-assembled bio-structures, advanced medical imaging and bio-nano-sensors. Micro/nanosensors can be fabricated using "top-down" e.g. nanolithography, energy beams or "bottom up" approaches e.g. molecular assembly, layer by layer chemistry. Key drivers in nano(bio)sensors is in increased sensitivity, accuracy and precision.

This area takes advantage of advanced semiconductor technology which encompasses moving components as well as electrodes and electronics on a single chip. This also results in higher component density and chip functionality enabling multianalyte capability with lower power and high speed. At the nanoscale, surface to volume ratio increases and the more surface exposed, the more active the material becomes. If these properties are harnessed or new features imparted to them by chemically modifying their surfaces with specific molecules, these materials can be incorporated into larger devices e.g. sensors which can detect and measure e.g. pollution or key messengers within blood or urine.

Nanomaterials cross the boundary between nanoscience and nanotechnology and it is recognized that the size range that provides the greatest interest is <100 nm. For example, 2 g of 100 nm diameter spherical Al nanoparticles contains sufficient particles to give every human on the planet 300000 particles each [27]. Nanoparticles are known to exist in diverse shapes (spherical, star shaped, triangular, cubical, pentagonal, hexagonal, rod-shaped, shells, ellipsoidal) and cover a wide range of materials, polymers, metals, and ceramics.

Organic based particles include fullvarenes, carbon nanotubes, nanoshells and rods, dendrimers and liposomes, while inorganic include quantum dots, metal nanorods and nanoparticles. By optimising conditions during formation/synthesis, scientists and engineers can tune the resulting properties and, ultimately, design new and exciting materials.

Biosensors are analytical devices which incorporate a biological material such as an enzyme or antibody, integrated within a

physicochemical transducer which can be electrochemical. They yield a digital electronic signal which is proportional to the concentration of a specific target compound. The devices can be configured to enable continuous measurement (applications in diabetic control) or single use low cost strips for "one-shot" biosensors. The integration of recognition, signal transduction and processing on the nanoscale will enable increased sensitivity, selectivity, speed of analysis and miniaturisation with associated power saving. Design considerations for nanosensors are similar to those for traditional devices with respect to interface requirements, interferences and noise.

Nanomaterials offer excellent prospects for achieving bioanalysis with high sensitivity multiplexing capability. The formation of nanoparticle – biomolecule assemblies provide the basis for ultrasensitive detection while bioaffinity (e.g. immunoassays) or nanoprobes offer great potential for simplified detection of biomolecular interactions. Nanoprobes and nanobiosensor technology can enable detection within single cells allowing the study of cellular systems at the molecular level. Silicon based nanowires [28] could test nl volumes of blood for key biomarkers, or be employed as a basis for electrical communication with enzyme molecules [29]. Recent work in our group has involved an electrocatalytic approach to biomolecule detection with pM detection limits within a millisecond time domain [30, 31].

Nanosized magnetic materials have gained increasing interest for their properties, which have promising applications in various technologies such as information storage [32] medical diagnosis [33], and cell separation [34] Among these materials, magnetite (Fe_3O_4), an Fe^{2+} and Fe^{3+} complex oxide, is one of the most commonly studied super-paramagnetic nanoparticles, with unique mesoscopic physical and mechanical properties. Magnetite particles may be easily separable in solution and substances to which they have been attached can be readily separated from a reaction medium, or directed by an external magnetic field to site-specific drug delivery targets. They have been widely used for *in vivo* examination including magnetic resonance imaging, contrast enhancement, tissue specific release of therapeutic agents, hyperthermia, magnetic field assisted radionuclide therapy, as well as *in vitro* binding of proteins and enzymes [35-37]. Fe_3O_4 has recently been employed in biosensors for glucose, ethanol, and acetaminophen [38-40]. Magnetic nanoparticles have been functionalised with both amino-silanes and polyamidoamine (PAMAM), the latter type of binding introducing a dense outer amine shell through a cascade-type generation, enabling the coupling of biomolecular entities with enhanced stability [41,42].

Recent work in our group has involved the synthesis and functionalisation of magnetite nanoparticles (Figure 13 and 14), which enabled subsequent covalent attachment of cholesterol oxidase and cholesterol esterase for novel sensing of both cholesterol and its esters. The clinical analysis of cholesterol in serum samples plays a key role in the diagnosis and prevention of a large number of clinical disorders such as hypothyroidism, nephrosis, diabetes mellitus, myxedema, and obstructive jaundice. The desired total plasma cholesterol for an individual is less than 5.2 mM with elevated levels > 6.2 mM. Plasma cholesterol levels increase with age, and are

generally less in females relative to males [43].

Magnetic nanoparticles were synthesised by the thermal co-precipitation method using ferric and ferrous chlorides, and functionalised using 3-aminopropyltriethoxysilane (APES) and PAMAM with subsequent covalent attachment of cholesterol esterase and cholesterol oxidase. The enzyme attachment was analysed by FT-IR and UV spectroscopy, and confirmed by SEM surface analysis and by electrochemical investigations.

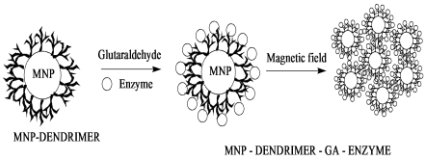

Figure 13: Attachment of enzymes to dendrimer modified magnetite nanoparticles.

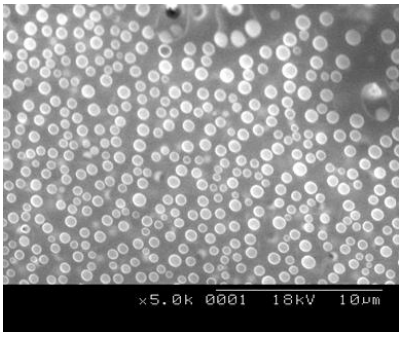

Figure 14: SEM image of PAMAM-magnetic nanoparticles bound to cholesterol oxidase, magnification X5.0 K, accelerating voltage of 18 kV, resolution 10 µm

Detection of free cholesterol and total cholesterol using the magnetite-modified biosensors offers the possibility of an alternative approach to cholesterol measurement. The best analytical performance for the free cholesterol biosensor was obtained using APES-functionalized magnetite with a sensitivity of 3.2 µA/mM when operated at 37 ^{0}C. In the case of the total cholesterol biosensor, the best analytical performance was obtained using PAMAM dendrimer-modified magnetite with a sensitivity of 2.32 µA/mM (see Figure 15 for typical CV response) The 3-aminopropyltriethoxysilane and especially the polyamidoamine dendrimer's ability to form a dense outer amine shell resulted in an efficient enzyme binding. The incorporation of mediators within the functionalised material is the focus of further related work in our group.

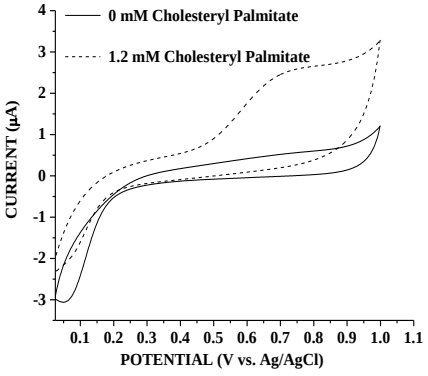

Figure 15: Cyclic voltammograms obtained for total cholesterol biosensor using the PAMAM-functionalized nanoparticles in a solution of 0.1 M KCl/PBS vs. Ag/AgCl at scan rate 5 mV/s, in the absence (solid line) and presence of 1.2 mM Cholesteryl palmitate (dotted line)

Another area of current interest within our team is NanoSphere Lithography (NSL) [44], a patterning tool for nanofabricated electrochemical surfaces, based on the self-assembly of polymeric (i.e. polystyrene) micro/nanobeads followed by e.g. evaporation of a metal layer and subsequent removal of the beads to reveal the patterned surface. The size and distance between the metal nanodots so formed may be manipulated by changing the diameter of the beads and the evaporation conditions. Recent work by researchers at ITT-Dublin has demonstrated this technology to deposit multi-element nanodots and nanomeshes (see Figure 16) using aluminum based on initial monolayer bead formation as confirmed using SEM (Figure 17).

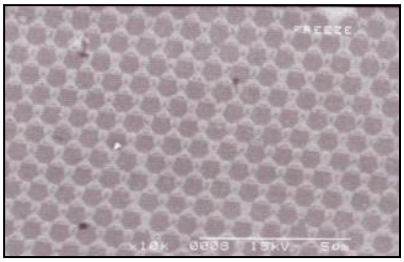

Figure 16: SEM image of Al patterned silicon via nanosphere lithography

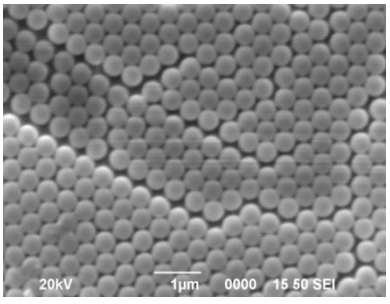

Figure 17: Monolayer of 500 nm polystyrene beads (0.4%w/v)) on a Ag sputtered layer on silicon wafers.

These surfaces are currently being evaluated as high surface area microelectrode arrays for biomedical applications such as glucose determination.

Glucose Sensors

The fabrication of a glucose sensor is an important area of research due to the fact that determination of blood and urine glucose levels in a rapid, convenient and precise manner is necessary for the diagnosis and management of diabetes mellitus [45, 46] Diabetes is a growing public health issue with no known cure. It is the fastest growing disease in the world and is expected to double in prevalence by 2050 (8% of all US citizens and 18% of all senior citizens are affected).

The most widely studied group of enzymes for electrochemical sensors are the oxidases, which under aerobic conditions, allow hydrogen peroxide from the reduction of dioxygen to be monitored amperometrically during the enzymatic reaction sequence. As the responses of oxygen/hydrogen peroxide based sensors are affected by fluctuations in the concentration of dissolved oxygen, electron mediators [47] e.g. quinones [48,49] ferrocenes [50] viologens [51] and Ru [52,53], have been employed to facilitate the electron transfer between the enzyme and electrode and to decrease the applied potential used to follow the enzyme catalysed reaction. Recently, we have synthesised and electrochemically evaluated the potential of a number of new osmium based complexes to act as mediators for glucose oxidase [54-56].

The application of enzymatic biosensors has been hindered by the inherent fragility of enzymes in addition to complex immobilization procedures which may

further decrease the stability of the biocomponent. Glucose oxidase (GOx) is widely used in the fabrication of glucose biosensors and though quite stable compared with other enzymes, is subject to thermal and chemical deformation during fabrication, storage or use.

A number of studies have been conducted to alleviate the drawbacks of enzymatic glucose sensors. Some research has focused on retaining and increasing the activity of the enzyme, whereas others have focused on the development of nonenzymatic catalysts [57-60]. Park et al [61] have reviewed this area recently and many non-enzymatic glucose sensors have been explored, but the selectivity and sensitivity of e.g. Pt-based sensors [62] are still a critical issue for practical applications. Many pure metals (including platinum) exhibit unsatisfactory sensitivity, selectivity and are affected by poisoning by adsorbed intermediates. It has been reported that that platinum surfaces modified by some heavy metals such as Ir/IrO_2, Pd, Pb, and Bi [63-67] showed good stability, increased sensitivity and catalytic activity for glucose oxidation. However, the dissolution and toxicity of the heavy metal elements prevent this method from being put to practical use.

Recent work in our laboratory [68] has involved synthesis of nanocomposites of ethylene glycol protected platinum nanoparticles prepared in the presence of activated carbon (AC), multi-walled carbon nanotubes (MWNTs) and carbon nanofibres (CNFs) at 20 % (w/w) Pt loading and their potential in non-enzymatic glucose sensing evaluated. Physical and electrochemical characterisation of these hybrid materials was enabled using transmission electron microscopy (TEM), X-Ray diffraction (XRD), thermogravimetric analysis (TGA) and cyclic voltammetry. The average platinum nanoparticle diameters, as determined from TEM & XRD measurements, were 2±1 to 3±1 nm. Figure 18 (a) and (b) shows transmission electron microscope (TEM) images of Pt decorated carbon nanofibres and multiwalled carbon nanotubes respectively, showing uniform distribution of nanoparticles and consistency of size achieved.

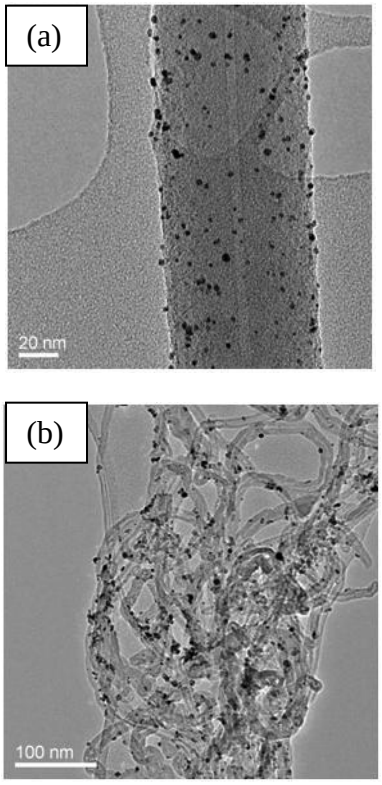

Figure 18: TEM images of (a) Pt nanoparticle decorated carbon nanofibres and (b) multiwalled carbon nanotubes.

Figure 19 shows the electrochemical characterisation of the typical Pt features confirming the presence of stable

nanoparticles on the surface of the support material. The electrochemically active surface area of the platinum nanoparticles were found to be 91, 78 and 128 m^2 g^{-1} for Pt-C, Pt-MWCNT and Pt-CNF respectively, as determined by the hydrogen adsorption/desorption phenomenon, using cyclic voltammetry in H_2SO_4. The nanomaterials were applied to the direct non-enzymatic quantization of glucose over its physiological range in the absence of enzyme glucose oxidase.

Hydrodynamic amperometry at E_{app} = 0.55 V vs. Ag/AgCl in phosphate buffer (pH 7.4) was employed and the materials responded linearly to glucose (at pH 7.4 298 K) over the range 0-20 mM (R^2=0.99) with sensitivity 1.07, 1.10 and 0.52 µA mM^{-1} cm^{-2} for Pt-C, Pt-MWCNT and Pt-CNF respectively.

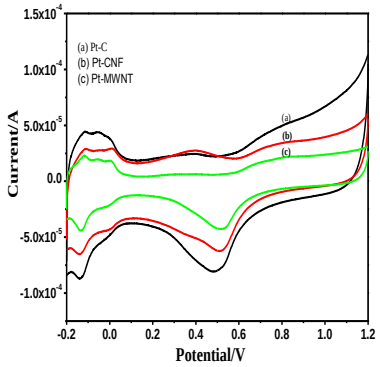

Figure 19: Cyclic voltammetry for (a) Pt-C, (b) Pt-CNF and (c) Pt MWNT in 0.1 M H_2SO_4 with hydrogen adsorption/desorption evident -0.2-+0.1 V vs. Ag/AgCl.

Applications of integrated electrochemical microchip for continuous glucose monitoring.

The linear arrangement thin film microsensor designed in our laboratory (Figure 11) was fabricated as described, and tested for continuous monitoring of glucose levels over physiologically relevant ranges. The completed microfluidic device, following curing of the outer PDMS layer, was connected to a peristaltic pump (Ismatec model PCI) via metallic needles. The flow rate was initially adjusted to 49.9µL/min and a phosphate buffer solution flow through the microchips was monitored for approximately an hour to ensure the systems sealing properties (see image Figure 20). Tests were also performed using variable flow rates between 43µL/min – 250µL/min. Prior to integration, the Pt disk working electrode was modified with crosslinked glucose oxidase together with a deposit Pt nanoparticles, enabling a unique combination of enzymatic and non-enzymatic glucose detection.

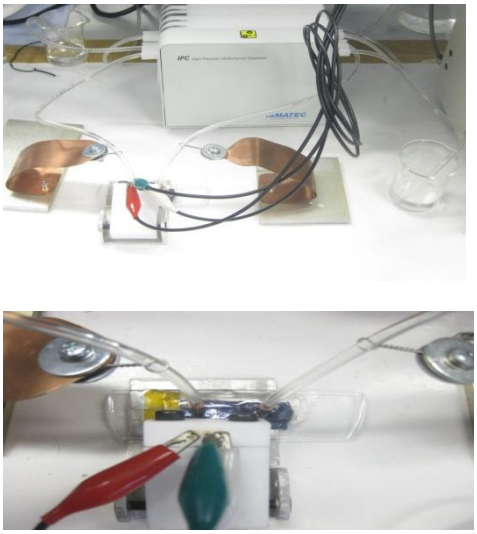

Figure 20: Electrochemical testing setup showing peristaltic pump, tubing, tubing holder, chip holder and connections to potentiostat.

The microfluidic microchips were tested using chronoamperometry for their response to glucose over the range 2mM to 20mM. Figure 21 shows the amperometry current response acquired for an ascending and descending cycle of 2mM additions of glucose in the flow system. The time interval between all increments in concentration was approx. 9mins. The flow rate was kept constant at 46.4µL/min throughout the recording and the applied potential was 0.7V vs. Ag/AgCl. Typical volumes within the channel is 50-80 µl. Heller and Feldman have recently given an account of electrochemistry in diabetes management [69] with emphasis on current state of the art Freestyle Navigator commercial continuous glucose monitoring system which employs glucose oxidase wired to a redox hydrogel of Os $^{2+/3+}$ (electron mediator). The sensor is replaced after 5 days continuous usage. Our three electrode microdevice operated reliably for 6 days with *in vitro* testing and >20 days using a single microelectrode device (data not shown), demonstrating the potential of this technology for selective and sensitive glucose detection over both the required time period and relevant physiological range.

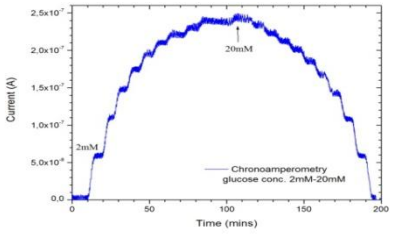

Figure 21: Hydrodynamic amperometric response for a integrated three electrode microchip – microfluidic system with additions of 2mM Glucose every 500secs.

Conclusions

Driven by the need for earlier, accurate diagnostic information to guide critical clinical decisions, technology advances including miniaturisation are enhancing the role of diagnostics in health care systems. Rapid blood tests performed at the point-of-care, together with wearable monitors for continuous monitoring are revolutionising the healthcare sector, providing immediate information which can influence the clinical decision process. Combining the unique specificity of bio-molecules with the sensitivity of electrochemical detection enables identification and accurate quantification of substances at ultra-trace levels in biological systems. The strategy of miniaturisation and integration of functional elements in analytical systems will continue to dominate progress in this field, with electrochemistry playing an important role due to its compatibility with standard micro-fabrication approaches. Nanobiosensors offer promise for multiple elusive goals in medical diagnostics. An immediate impact will be in companion diagnostics and theranostics where *in vivo* applications with therapeutic principles will employ multi-functional nanobiosensors. Other exciting developments in nanorobots/nanomedicine ensure that there will be a continuous drive for success within this multidisciplinary area, uniquely positioned at the interface of science and engineering.

References

[1] A.J. Bard, L.R. Faulkner, Electrochemical Methods, 2nd Edition, 2002.

[2] P.T. Kissinger, W.R. Heineman, Laboratory Techniques in Electroanalytical Chemistry, 2nd Edition, Marcel Dekker, Inc. 1996, 51-110

[3] J. C. McDonald, G.M. Whitesides, Accounts of Chemical Research 2002, 35(7) 491-499.

[4] C-H. Lin, G-B. Lee, B-W Chang, and G-L Chang, J. J. Micromech. Microeng. 2002, 12, 590-597.
[5] Y. Yoonhee, S. Y. Oh and J. K. Park, Enzyme and Microbial Technology 39 (2006) 1112-1127.
[6] H. Suzuki and R.Yoneyama, Sensors and Actuators B: Chemical 96 (2003) 38-45.
[7] A. Arora, G. Simone, G.B. Salieb-Beugelaar, J. Tae Kim and A. Manz Anal. Chem. 2010 ASAP
[8] Z. R. Xu, and Z. L. Fang, Analytical Chimica Acta 507 (2004) 129-135.
[9] S. Upadhyay, N. Ohgami, H. Kusakabe and H. Suzuki, Biosensors and Bioelectronics 21 (2006) 1230-1236.
[10] A.Yamaguchi, P. Jin, H. Tsuchiyama, T. Masuda, K. Sun, S. Matsuo and H. Misawa, Analytical Chimica Acta 468 (2002) 143-152.
[11] D. M. Spence, N. J. Torrence, M. L. Kovarik and R. S. Martin, The Analyst 129 (2004) 995-100.
[12] A. M Christensen, D. A. Chang-Yen and B. K. Gale, Journal of Micromechanics and Microengineering 15 (2005) 928-934.
[13] C. Amatore, M. Belotti, Y. Chen, E. Roy, C. Sella and L. Thouin, Journal of Electrochemical Chemistry 573 (2004) 333-343.
[14] MP. Woais, Sensors and actuators B 105 (2005) 28-38
[15] D. C. Duffy and G. M. Whitesides, Analytical Chemistry 70 (1998) 4974-4984.
[16] George M. Whitesides, Nature 442 (2006) 368-373.
[17] W. H. Song and J. Lichtenberg, Journal of Micromechanic and Microengineering 15 (2005) 1425-1432.
[18] Teruo Fujii, Microelectronic Engineering 61-62 (2002) 907-914,
[19] Adrian Plecis, Yong Chen, Microel. Engineering 85 (2008) 1334-1336.
[20] A. Yamaguchi, P. Jin, H. Tsuchiyama, T. Masuda, K. Sun, S. Matsuo and H. Misawa, Analytical Chimica Acta 468 (2002) 143-152.
[21] R. S. Martin, A.J. Gawron and S. M. Lunte, Anal. Chem. 72 (2000), 3196-3202,
[22] R. Kihura-Hanajiri, R.S. Martin, S.M. Lunte, Anal. Chem. 74 (2002) 6370-6377.
[23] L.A. Holland, N. Murray Harmony and S. M. Lunte, Electroanalysis 11, 5 (1999) 327-329.
[24] R.S. Pai, K.M. Walsh, M.M. Crain, T.J. Roussel, D.J. Jackson, R.P. Baldwin, R.S. Keynton and J.F. Naber, Anal. Chem. 8 (2009) 4762-4769.
[25] R. S. Martin, A. J. Gawron, B. A. Fogarty, F.B. Regan, E. Dempsey and S. M. Lunte, Analyst 126 (2001), 277-280. 14.
[26] A. Collier, E. Dempsey, D. Diamond, Joseph Wang, Anal. Chim Acta (2005) 550: 107-115.
[27] M. J. Pitkethly, Nanotoday, 7, (2004), 20-29.
[28] Beckman et al J. Applied Phys 96 (2004) 5921-5923.
[29] M.G. Georgeanopoulou Proc. Nat. Acad. Science 102 (2005) 2273-2275
[30] G. Munteanu, E. Dempsey, T. McCormac J. Electroanalytical Chemistry 638 (2010) 109-118. 4.
[31] G. Munteanu, E. Dempsey, T. McCormac, Journal of Electroanalytical Chemistry Volume 632, Issues 1-2, 1 July 2009, Pages 80-87 2009.
[32] A.J. Chakraborty, J. Magn. Mater., 204 (1999) 57.
[33] L. Josephson, C.H. Tung, A. Moore, R. Weissleder, Bioconj. Chem., 10 (1999), 186.
[34] S. Sieben, C. Bergemann, A. Lubbe, B. Brockmann, D. Rescheleit, J. Magn. Mater., 225 (2001), 175.
[35] G.K. Kouassi, J. Irudayaraj, G. McCarthy, Biomagnetic Research and Technology, 3:1 (2005) 1-10.
[36] A. Dong, N. Ren, Y. Tang, Y. Wang, Y. Zhang, W. Hua, Z. Gao, J. Am. Chem. Soc., 125 (2003), 4976.
[37] G.K. Kouassi, J. Irudayaraj, Anal. Chem. 78 (2006), 3234-3241.
[38] B-W. Lu, W.C. Chen, J. of Magn. and Magn. Mat., 304, (2006), 400-402.
[39] M.H. Liao, J.C. Guo, W.C. Chen, J. of Magn. and Magn. Mat., 304, (2006), p421-423.

[40] S.F. Wang, F. Xie, R.F. Hu, Sensors and Actuators B, 123, (2007), 495-500.
[41] S.Y. Shaw, Y.J. Chen, J.J. Ou, L.Ho, Enzyme and Microbial Technology, 39, (2006), 1089-1095. [42] B.F. Pan, G. Gao, H.C. Gu, J. of Colloid and Interface Science, 284, (2005), 1-6.
[43] S.P. Martin, D.J. Lamb, J.M. Lynch, S.M. Reddy, Anal. Chim. Acta 487, (2003), 91-100.
[44] D. Ingert, The Open Physical Chemistry Journal, 1, (2007) 10-17.
[45] S. Sotiropoulou, N.A. Chaniotakis, Anal. Bioanal. Chem. 375(1) (2003) 103-105.
[46] Y. Nakabayashi, M. Wakuda, H. Imal, Anal. Science 14 (1998) 1069-1076.
[47] A. Chaubey, B.D. Malhotra, Biosensors and Bioelectronics, 17 (2002) 441-456.
[48] T. Katu, H.I. Karan, Y. Okamoto, Anal. Chem. 66(8) (1994) 1231-1235.
[49] T. Ikeda, T. Shibatta, M. Senda, J. Electroanal. Chem. 261 (1989) 351-362.
[50] S.P. Hendry, M.F. Cardosi, A.P.F. Turner, Anal. Chim. Acta 281 (1993) 453-459.
[51] E. Katz, N. Itzhak, I. Wilner, J. Electroanal. Chem. 332 (1992) 357-363.
[52] H.O. Finklea, D.D. Hanshew, J. Am. Chem. Soc. 114 (1992) 3173-3181.
[53] E.V. Ivanova, V. S. Sergeeva, J. Oni, C. Kurzawa, A.D. Ryabov and W. Schuhmann, Bioelectrochemistry 60 (2003) 65-71.
[54] S. Warren, R. Doaga, T. McCormac, E.Dempsey, Electrochimica Acta, Volume 53, Issue 13, 20 May 2008, Pages 4550-4556. 12.

[55] S. Warren, T. McCormac, E. M. Mihaylova, E. Dempsey, Electroanalysis 18, 2006, 1778-1785. 16.
[56] S. Warren, T. McCormac and E. Dempsey, Bioelectrochemistry Volume 67, Issue 1, September 2005, Pages 23-35.
[57] E. Scavetta, S. Stipa, D. Tonelli, Electrochem. Commun. 9, (2007), 2838-2842.
[58] D. Foxx, E.E. Kalu, Electrochem. Commun. 9, (2007), 584-590.
[59] S.J Park, T.D. Chung, H.C.Kim, Anal. Chem. 75, (2003), 3046–3049.
[60] L. Meng, J. Jin, G. Yang, T. Lu, H. Zhang, C. Cai, Anal. Chem. 81,(2009) 7271–7280.
[61] S. Park, H. Boo, T.D. Chung, Anal. Chim. Acta 556, (2006), 46–57.
[62] Y.Y. Song, D. Zhang, W. Gao, X.H. Xia, Chem.- A Eur. J. 11 (2005), 2177–2182.
[63] L. Meng, J. Jin, G. Yang, T. Lu, H. Zhang, C. Cai, Anal. Chem. 81 (2009), 7271–7280
[64] P.H. Hindle, S. Nigro, M. Asmussen, A. Chen, Electrochem. Commun. 10, (2008), 1438–1441.
[65] J. Wang, D.F. Thomas, A. Chen, Anal. Chem. 80, (2008), 997–1004.
[66] J. Wang, G. Rivas, M. Chicharro, J. Electroanal. Chem. 439, (1997), 55-61
[67] G. Wittstock, A. Strubing, R. Szargan, G. Werner, J. Electroanal.Chem. 444, 1998, 61-73.
[68] D. Rathod, C. Dickinson, D. Egan and E. Dempsey, Sensors and Actuators B Chemical 143, Issue 2, 2010. 547-554
[69] A. Heller and B. Feldman, Accounts of Chemical Research 2010 43 (5), 631–641.

Multi-frequency Electrical Impedance Tomography: Image Reconstruction Using Bivariate Laguerre Functions

J. M. Mehalhal, A. M. Shallof and M. F. Bara

ABSTRACT

Electrical Impedance Tomography (EIT) is a technique which allows cross- sectional image related to the electrical impedance within an object to be reconstructed from a set of measurements made on the object surface in EIT.

EIT aims to image the conductivity distribution within a test object by making electrical measurements on the surface of the object. Some of the potential advantages of this technique are that:

a) It offers the possibility of an inexpensive, non-harmful imaging technique capable of being used in the intensive care environment for a range of physiological measurements.
b) It will be capable of characterizing tissues in a novel physiological way which should enable diseased tissues or abnormal function to be identified, and
c) It should be capable of imaging fast dynamic activity within the human body because data can be acquired rapidly.

In single frequency Electrical Impedance Tomography only the change in the real part of the conductivity can be imaged and not those of the imaginary part of the conductivity or of the absolute values. Multi-frequency Electrical Impedance Tomography has been proposed to solve this problem. In this paper, there is a new method using Laguerre function in multi-frequency electrical impedance tomography which has been developed, and full information contained in the complex tissue conductivity can be obtained.

1 .Introduction:

Electrical Impedance Tomography (EIT) is an ima-ging modality that estimates the electrical properties inside a volume from electrical measu-rements on its surface. By elec-trical properties, we mean spec-ifically the electric conductivity and permittivity.

The electric conductivity is a measure of the ease with which a material conducts electricity; the electric perm-ittivity is a measure of how readily the charges within a material separate under an imposed electric field. Both of these properties have seen much interest in medical applications for many years, because different tissues, or even the same tissue in different physiological states, have different conductivities and permittivities.

Possible biomedical appli-cations of EIT include monit-oring cardiac and pulmonary function, detection and quantification of intraperitoneal fluid ,

detection and charact-erization of tumors, monitoring cancer ablation procedures, stu-dying emptying of the stomach, studying pelvic fluid accu-mulation as a possible cause of pelvic pain, quantifying seve-rity of premenstrual syndrome by determining the amount of intracellular versus extracellular fluid, determining the boundary between dead and living tissue , and building forward models for bioelectric field inverse problems such as Electro/Magneto Encephalography (E/MEG) and Electr-o/Magneto Cardiography (E/MCG).

A variety of non-clinical applications of EIT are also possible. These include imaging multi-phase fluid flow, dete-rmining the location of mineral deposits in the earth, tracing the spread of contaminants in the earth , non-destructive evalu-ation of machine parts , and control of industrial processes such as curing and cooking .

EIT has many advantages over other medical imaging techniques. It is noninvasive, and it does not expose the patient to harmful X-rays or any other radioactive materials. It is safe for long term monitoring, cost-effective, and portable. In addition, EIT combined with other medical imaging techniques can provide increased diagnostic accuracy. For example, X-rays can only detect breast tumors that have an X-ray absorption density that differs significantly from that of the normal breast tissue. EIT is based on the contrast in elec-trical properties of the tissue and can thus be used to find or distinguish tumors that are undetectable or indisting-uishable by mammography .

In EIT the fundamental problem in the image reco-nstruction is that, in a general case, the electric current cannot be forced to flow linearly (or even along a known path) in an inhomogeneous volume condu-ctor; the current flow is dete-rmined by the impedance distribution within the object. Therefore, the inverse problem, computing the electrical conductivity and permittivity distribution in the object, is significantly more difficult than for a modality such as X-ray computed tomography where the photon paths are essentially straight lines. Additionally, the problem is ill-posed, meaning that large changes in impedance at the interior of the object may result in only small voltage or current changes at the surface [1] .

2. EIT Theory

The theory behind elec-trical impedance tomography is that by applying a constant current across a material the voltage distribution resulting on the surface will reflect the internal resistivity distribution. However, intuitively one will understand that multiple resistivity distributions can produce the same voltage distribution at the surface. Therefore the system is stimulated in multiple manners to constrain the possible resistivity distributions.

3. Data Collection Strategies

There are a number of variations of EIT that depend on whether one injects current (and measures voltage) or applies voltage (and measures current), and whether one uses the same or different electrodes for these two purposes. Many common acquisition systems stimulate the object under measurement by applying current and measuring resulting voltages, as this arrangement is less sensitive to the degrading effect of contact impedances . In the following, we describe some of the measurement methods that are used [16].

4. Forward Model for EIT

Electromagnetic phenome-na are governed by Maxwell's equation for the electric field E and the magnetic field H. These equations are:

$$\nabla \times E = \frac{\partial B}{\partial t} \qquad (1)$$

$$\nabla \times H = J + \frac{\partial D}{\partial t} \qquad (2)$$

where J denotes the current density, B the magnetic flux density (also called the magnetic induction), D the electric displacement, and the partial derivative is with
respect to time t.

The frequencies used in EIT systems are low enough so that the quasi-static Approximation holds, and thus we can ignore capacitive, propagation, and inductive effects [9]. The ACT3 system, for example, operates at 28.8 kHz, and is applied to bodies smaller than one meter in which the conductivity is generally less than one (Ohm-meter)−1 [10]. Under such quasi-static conditions, since the displacement current (∂D/∂t) is approximately zero we get

$$\nabla . J = 0 \qquad (3)$$

For current density J we have

$$J = \sigma E + J_s \qquad (4)$$

where σ is the conductivity of the medium. This equation states that the total current density J is the sum of the conduction current density σE and the "impressed current" density Js due to the internal sources [9]. In regular EIT systems all the sources are on the outer boundary of the object, so can be modeled as the boundary condition; therefore, Js = 0.

5. Conduction in Human Tissues

Tissue consists of cells with conducting contents surrounded by insulating membranes embedded in a conducting medium. Inside and outside the cell wall is conducting fluid. At low frequencies of applied current, the current cannot pass through the membranes, and conduction is through the extracellular space. At high frequencies, current can flow through the membranes, which act as capacitors. A simple model of bulk tissue impedance based on this structure, which was proposed by Cole and Cole [1941], is shown by (Fig. 1).

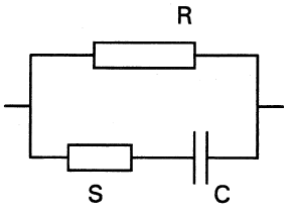

FIG. 1 The Cole-Cole model of tissue impedance.

Clearly, this model as it stands is too simple, since an actual tissue sample would be better represented as a large network of interconnected modules of this form. However, it has been shown that this model fits experimental data if the values of the components, especially the capacitance, are made a power function of the applied frequency ω . An equation which describes the behavior of tissue impedance as a function of frequency reasonably well is

$$Z = Z_\infty + \frac{Z_0 - Z_\infty}{1 + (j\frac{f}{fc})^\alpha} \qquad (5)$$

Where Z_0 *and* Z_∞ are the (complex) limiting values of tissue impedance low and high frequency and fc is a characteristic frequency. The value of α allows for the frequency dependency of the components

of the model and is tissue dependent. Numerical values for invivo human tissues are not well established.

Making measurements of the real and imaginary components of tissue impedivity over a range of frequencies will allow the components in this model to be extracted. Since it is known that tissue structure alters in disease and that

R, S, C are dependent on structure, it should be possible to use such measurements to distinguish different types of tissue and different disease conditions. It is worth noting that although maximum accuracy in the determination of the model components can be obtained if both real and imaginary components are available, in principle, knowledge of the resistive component alone should enable the values to be determined, provided an adequate range of frequencies is used. This can have practical consequences for data collection, since accurate measurement of the capacitive component can prove difficult.

Although on a microscopic scale tissue is almost certainly electrically isotropic, on a macroscopic scale this is not so for some tissues because of their anisotropic physical structure.

Muscle tissue is a prime example, where the bulk conductivity along the direction of the fibers is significantly higher than across the fibers. Although unique solutions for conductivity are possible for isotropic conductors, it can be shown that for anisotropic conductors unique solutions for conductivity do not exist. There are sets of different anisotropic conductivity distributions that give the same surface voltage distributions and which therefore cannot be distin-guished by these measurements. It is not yet clear how limiting anisotropy is to electrical impe-dance tomography.

Clearly, if sufficient data could be obtained to resolve down to the microscopic level (this is not possible practically), then tissue becomes isotropic. Moreover, the tissue distri-bution of conductivity, inclu-ding anisotropy, often can be modeled as a network of conductors, and it is known that a unique solution will always exist for such a network. In practice, use of some prior knowledge about the anisotropy of tissue may remove the ambiguities of conductivity distribution associated with anisotropy.

The degree to which anisotropy might inhibit useful image reconstruction is still an open question.

6. Image reconstruction using bivariate Laguerre function

In this section we use bivariate Laguerre function to find the sensitivity matrix of multi-frequency Electrical Imp-edance Tomography.

The successful imaging depends on the amount of information we acquire from the sensitivity matrix the vol-tage gradient of the sensitivity matrix based on the finite element. The voltage gradient is calculated in each element when current is passed in turn through each of individual drive-receive pair using Lagu-erre function and finite element method.

The finite element method is a numerical analysis techn-ique for obtaining approximate solution to a wide variety of engineering problems.

Due to its ability to model arbitrary geometries and vari-ous boundary conditions the finite element method is the

most common method currently used for the numerical solution of EIT problems.

In a continuum problem of any dimension, the field variable such as the electric potential in EIT, is define over an infinite number of values because it is a function of the infinite number of points in the body.

The finite element method first discretizes the medium under analysis into a finite number of elements collectively called a finite element mesh. Using finite element mesh and the following performability equation's to get complex sensitivity matrix [2].

$$P(x,t) = 1 - (e^{bt} \sum_{\substack{0 \le i \le \infty \\ 0<j<\infty}} p_{ij} l_{ij}(x,t)) \quad (6)$$

Where p_{ij} and $l_{ij}(x,t)$ are given by:

- Create the Markove generator matrix Q and reward matrix F :

$$Q = \begin{bmatrix} \nu & 0 \\ 0 & \nu \end{bmatrix} F = \begin{bmatrix} \psi & 0 \\ 0 & \psi \end{bmatrix} \quad (7)$$

Compute the Laguerre coefficient vector p_{ij} :

$p_{ij}=R_{ij}D$ (8)

$R_{ij}=[R_{i-1j} A+R_{ij-1} B+R_{i-1j-1}C]$ (9)

Where : $R_{00}=I$, $R_{01}=B$, $R_{10}=A$ (10)

$S=[KI+KF-2Q+2bI]^{-1}$ (11)

$A=S[K(I-F)-2(Q-bI)]$ (12)

$B=S[K(-I+F)-2(Q-bI)]$ (13)

$C=S[K(I+F)+2(Q-bI)]$ (14)

$D=2K^2Se^{\wedge}$ (15)

- Compute the Laguerre difference coefficient P_{ij} using eq.

$$p_{ij} = 2K \sum_{\substack{i+1 \le m \le \infty \\ 0 \le n < j}} (-1)^{i+m} \tilde{p}_{mn} \quad (16)$$

Where

$$\tilde{p}_{mn} = \begin{cases} \frac{1}{k^2}(p_{ij} - p_{i-1j}) & , i > 0 , j = 0 \\ \frac{1}{k^2}(p_{ij} - p_{i-1j}) & , i = 0 , j > 0 \\ \frac{1}{k^2}(p_{ij} - p_{i-1j} - p_{i-1j} + p_{i-1j-1}) & , i > 0 , j > 0 \end{cases} \quad (17)$$

-Find $l_{ij}(x,t)$ using eq. :

$$l_{ij}(x,t) = l_i(x) l_j(t) \quad (18)$$

$$i l_i(x) = (2i - 1 - kx) l_{i-1}(x) - (i-1) l_{i-2}(x) \quad (19)$$

- compute the performability using eq. :

$$P(x,t) = 1 - (e^{bt} \sum_{\substack{0 \le i \le \infty \\ 0<j<\infty}} p_{ij} l_{ij}(x,t)) \quad (20)$$

- Compute the adittmances matrix as:

$$\begin{bmatrix} Y_{11} & Y_{12} & Y_{13} \\ Y_{21} & Y_{22} & Y_{23} \\ Y_{31} & Y_{32} & Y_{33} \end{bmatrix} \begin{bmatrix} V_1 \\ V_2 \\ V_3 \end{bmatrix} = \begin{bmatrix} i_1 \\ i_2 \\ i_3 \end{bmatrix} \quad (21)$$

Successful imaging depends on the amount of information we acquire from the boundary measurements and the extracting information.

From equation (5.1) we assume the boundary condition as following:

$$\sigma \frac{\partial v}{\partial n} = \begin{cases} J & \text{on the electrodes} \\ 0 & \text{on the body air interface} \end{cases} \quad (22)$$

Where J is the current density , $\frac{\partial v}{\partial n}$ is the potential derivative normal to the surface and (□) is the conductivity using finite element method.

For triangle element we can express the current density as:

$$\begin{bmatrix} J_1 \\ J_2 \\ J_3 \end{bmatrix} = \begin{bmatrix} Y_{11} & Y_{12} & Y_{13} \\ Y_{21} & Y_{22} & Y_{23} \\ Y_{31} & Y_{32} & Y_{33} \end{bmatrix} \begin{bmatrix} V_1 \\ V_2 \\ V_3 \end{bmatrix} \quad (23)$$

But in 1996 Shallof and Barber show that:

$$V^* \, \sigma^* = J \quad (24)$$

$$V^* = \frac{J(\sigma_R - j\sigma_I)}{\sigma_R - \sigma_I} \quad (25)$$

Where (σ_R) and (σ_I) are the real and imaginary parts of the complex conductivity.

We assume that the value of the complex sensitivity matrix at the point is given by:

$$S^* = V_d^* . V_r^* \quad (26)$$

Where d and r are drive and receive electrodes.

From equation (24) to equation (26) we get the real sensitivity matrix is:

$$S = J_d \, J_r \quad (27)$$

And we get the complex sensitivity matrix is:

$$S^* = J_d \, J_r \left(\frac{(\sigma_R - j\sigma_I)^2}{(\sigma_R{}^2 - \sigma_I{}^2)^2}\right) \quad (28)$$

So from equation (27) and (28) we get:

$$^* = \alpha S + j\beta S \quad (29)$$

Where

$$= \frac{(\sigma_{ref})^4}{\left(\sigma_{ref}{}^2 + \grave{\sigma}_{ref}{}^2\right)^2} \left(1 - \frac{\grave{\sigma}_{ref}{}^2}{\sigma_{ref}{}^2}\right) \quad (30)$$

$$= -\frac{(\sigma_{ref})^4}{\left(\sigma_{ref}{}^2 + \grave{\sigma}_{ref}{}^2\right)^2} \left(\frac{2\grave{\sigma}_{ref}{}^2}{\sigma_{ref}{}^2}\right) \quad (31)$$

From equation (29) and the boundary voltage measurement, we get:

$$^* = (S^*)^{-1} . g^* \quad (32)$$

The sensitivity relationship between the changes in complex conductivity (*) and the changes in boundary measurements (g^*) is given by

$$_{}^* = (S^*)^{-1} \, g_p{}^* \quad (33)$$

To normalize change in conductivity to normalized change in boundary from we use the following:

$$g_n{}^* = \frac{g_p{}^*}{g_u} \quad (34)$$

$$\sigma_n{}^* = \frac{\sigma_p{}^*}{\sigma_u} \quad (35)$$

Thus from equation (33),(34) and (35) we get

$$_{}^* = (F^*)^{-1} . g_n{}^* \quad (36)$$

Where (F^*) is normalizes complex sensitivity matrix and ($. g_n{}^*$) is the normalized voltage measurements.

6. RESULT

The results are obtained from new method for multi-frequency electrical impedance

tomography image reconstruction using Laguerre functions. We use a finite element model consisting of 192 elements. Equation (29) are used to compute a complex sensitivity matrix. The sensitivity matrix value were computed using 16 interleave drive and receive electrodes. The dimension of the sensitivity matrix is 64 x 192 it has chosen the size of the object 0.1.

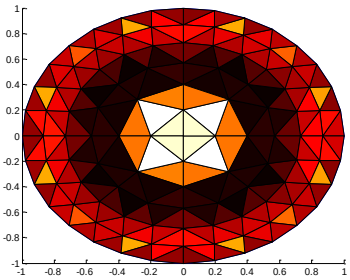

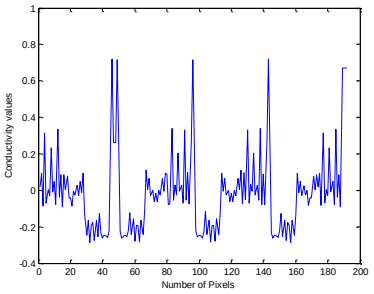

(New developed method image)

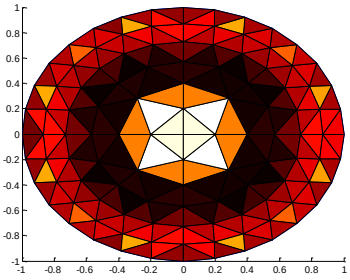

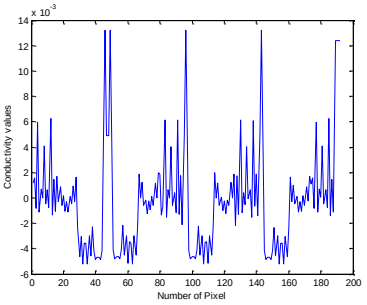

(Previous method image)

(a)

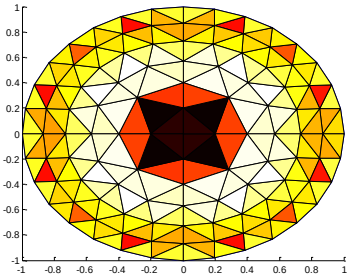

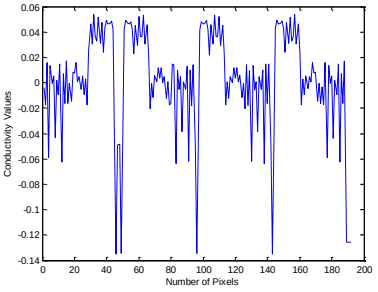

(New developed method image)

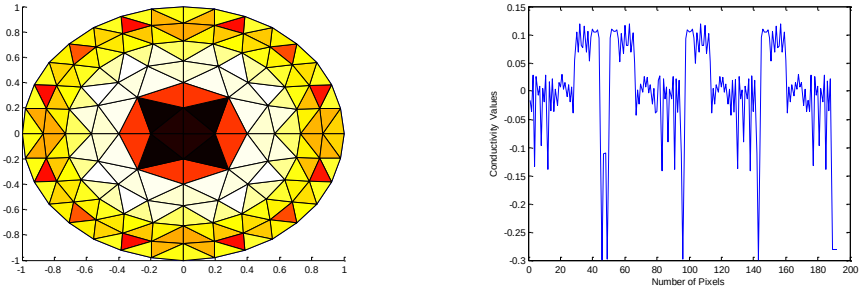

(Previous method image)

(b)

Fig. 6.2. Image reconstruction of the object at the center using frequency 9.6 KHz:

(a) Real part of conductivity, (b) Imaginary part of the conductivity.

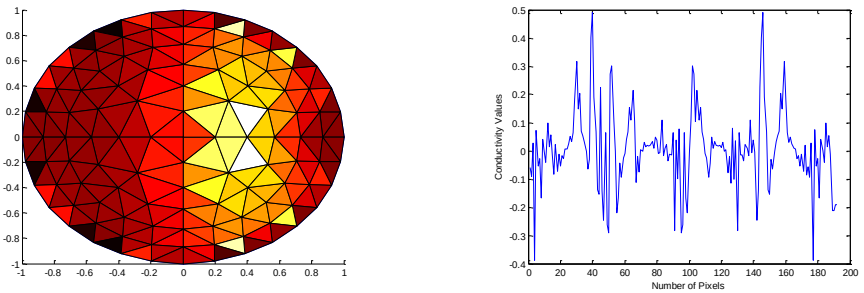

(New developed method image)

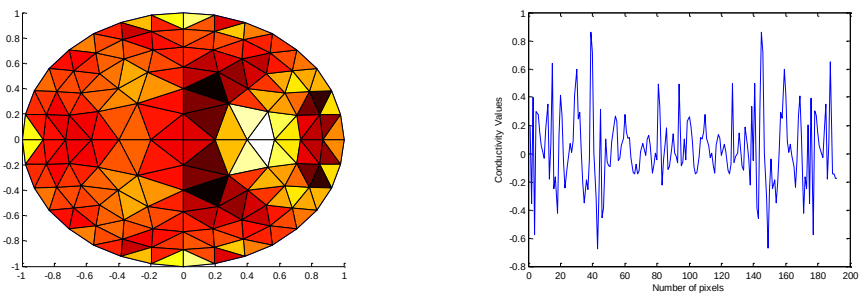

(Previous method image)

(a)

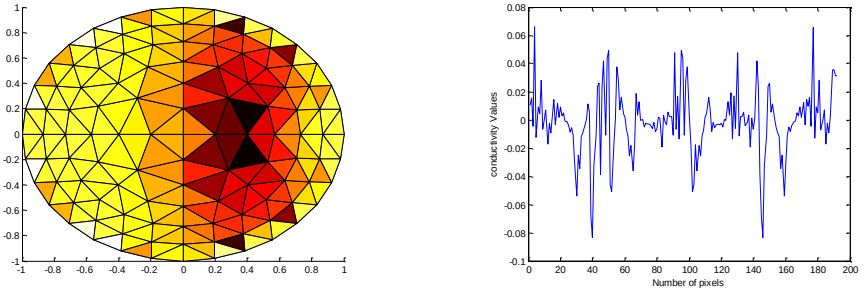

(New developed method image)

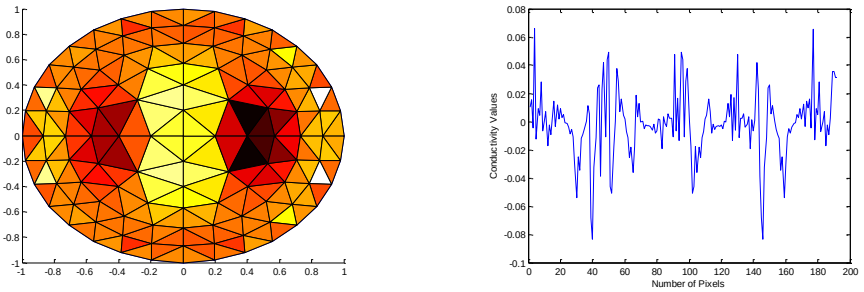

(Previous method image)

(b)

Fig. 6.3. Image reconstruction of the object at the center using frequency 9.6 KHz:

(a) Real part of conductivity, (b) Imaginary part of the conductivity,

7. CONCLUSION

7.1 Multi-frequency EIT advantage

Electrical Impedance Tomography (EIT) is a non invasive imaging technique with widespread applications in medicine and industry. It aims to image the conductivity distribution within an object by making electrical measurements on the surface of the volume. Some of the potential advantages of this technique are that:

I. It offers the possibility of an inexpensive non-harmful imaging technique capable of being used in the intensive care environment for a range of physiological measurements.

II. It will be capable of characterizing tissues in a novel physiological

way which should enable diseased tissues or abnormal function to be identified, and

III. It should be capable of imaging fast dynamic activity within the human body because data can be acquired rapidly.

Electrical impedance tomography at single frequency allows images of temporal changes in tissue impedance to be produced. Production of static images using data from human subjects is difficult. The main reason for this is that body shape and electrode position are more important determinates of transfer impedance measurements than is the distribution of tissue impedance.

Multi-frequency EIT offers the potential for making static images by producing images of changes in tissue impedance with frequency. Furthermore, by considering both real and imaginary parts of the conductivity, all information contained in the tissue is obtained.

In this thesis new method concerning multi-frequency electrical impedance tomography using Laguerre function has been developed.

The new developed method was applied in some models and compared with previous method it has been noted the following:

I. Acceptable results.

II. The image reconstruction which obtained from the new developed method is clearer and higher value of complex conductivity in the center and in the boundary for the different frequencies than the previous methods.

7.2 Future work

The future study will use regulation method to improve the image reconstruction and involves 3D multi-frequency EIT using Laguerre function.

REFERNCES

1. Shallof A. 1997, “Multi-frequency electrical impedance tomography for medical diagnostic image “ PhD thesis, University of Sheffield.
2. Shallof A. 1994, “Performability of real-time control system” PhD thesis, University of Sheffield.
3. Shallof A. and Barber D.,1996(a), “*Imaging the complex conductivity in electrical impedance tomography*,” IEEE international Conf. on Image Processing, PP 543-546.
4. Shallof A. and Barber D.,1996(b), “*Analytical soluation of complex conductivity in electrical impedance tomography*,” Advances in Electrical Impedance Tomography (Colloquium organized by IEE, Manchester, poster presentstion.).

5. J. Malmivuo and R. Plonsey, " Bioelectromagnetism, Principles and Applications of Bioelectric and Biomagnetic Fields ". Oxford University Press, 1995.
6. D.C. Barber. "Electrical Impedance Tomography." The Biomedical Engineering Handbook: Second Edition. Ed. Joseph D. Bronzino Boca Raton: CRC Press LLC, 2000.
7. Saeed Babaeizadeh 2006, "3-D Electrical Impedance Tomography for Domains with Piecewise Constant Conductivity " PhD thesis, Northeastern University Boston, Massachusetts.
8. Amani Mohammed Soliman 2007, "Multi-frequency Electrical Impedance Tomography: Image Improvement" M.Sc Thesis, Al-Fateh University.
9. R.M Gulrajani, "Bioelectricity and Biomagnetism". John Wiley & Sons, Inc.,1998.
10. M. Cheney, D. lsaacson, and J. C. newell, "Electrical Impedance Tomography" SIAM Review, Vol. 41, no. 1, pp. 85-101, 1999.
11. Kandel ER, Schwartz JH (1985): *Principles of Neural Science*, Elsevier Publishing, New York.
12. Nunez PL (1981): *Electric Fields of the Brain: The Neurophysics of EEG*, 484 pp. Oxford University Press, New York.
13. Thompson CF (1985): *The Brain - An Introduction to Neuroscience*, 363 pp. W. H. Freeman, New York.
14. Ganong WF (1991): *Review of Medical Physiology*, 15th ed., Appleton & Lange, Norwalk, Conn.
15. Barber DC, Brown BH (1984): "Applied potential tomography". *J. Phys. E.: Sci. Instrum.* 17: 723-33.
16. Cheng KS, Simske SJ, Isaacson D, Newell JC, Gisser DG (1990): "*Errors due to measuring voltage on current-carrying electrodes in electric current computed tomography*". *IEEE Trans. Biomed. Eng.* 37:(60) 60-5.
17. Molinari, M., 2003, "High Fidelity Imaging in Electrical Impedance Tomography", Ph.D. dissertation, University of Southampton, Southampton, United Kingdom.
18. Islam S. and Hany H. Ammar,(1991)*,"Performability Analysis of Distribution Real-Time Systems ",*IEEE Trans. Vol. 40,1239-1251.
19. G. J. Saulnier, R. S. Blue, J. C. Newell, D. Isaacson, and P. M. Edic, "*Electrical impedance tomography*", IEEE Signal Processing Magazine, vol. 18, no. 6, pp.31-43.2001.
20. K.-S. Cheng, D. Isaacson, J. C. Newell, and D. G. Gisser, "*Electrode models for electric current computed tomography*," IEEE Transactions on Biomedical Engineering, vol. 36, no. 9, September 1989.

21. H. Jain, D. Isaacson, P. M. Edic, and J. C. Newell 1997, " *Electrical impedance tomography of complex conductivity distributions with noncircular boundary*," IEEE Transactions on Biomedical Engineering, vol. 44, no. 11, pp. 1051–1060.

Design and Development of a portable Pulse Oximetry system with Data Logging Function

Mohamed A. Zaltum*, M. Shukri Ahmad, Ariffuddin Joret and M. Mahadi Abdul Jamil

Faculty of Electrical & Electronic Engineering, University Tun Hussein Onn Malaysia, Batu Pahat 86400, Johor, Malaysia

*Corresponding email: mzaltum@yahoo.com

Abstract

Heart is the most important part in human body. Hence, we always need to follow-up and diagnose its health condition. Heart rate (HR) and blood oxygen saturation (SpO_2) are important indicators directly related to heart-pulmonary system. Monitoring of HR and SpO_2 offers us a good indication of heart functionality. Therefore, developing homemade inexpensive devices for measuring HR and SpO_2 is very essential. Pulse Oximeter (PO) is an opto-electronic non-invasive medical instrument capable of measuring and recording the changes of HR and SpO_2 at the finger tip.

Keywords: Pulse Oximetry, Optical Sensor, Heart Rate level.

1. INTRODUCTION

Pulse oximetry is based on two principles; that the oxy-hemoglobin and deoxy-hemoglobin are different in their absorption of red and infrared light, and that the volume of the arterial blood in tissue changes as the pulse changes. With each heartbeat, the volume of the arteries becomes bigger before the blood goes in to capillaries. This change makes possible for oximetry to differentiate the arterial blood from all other absorbing substances [1]. Usually, in a pulse oximeter, two lights with different wavelengths are transmitted through the tissue [1]. Since both oxygenated and deoxygenated hemoglobin have different absorbance and reflectance properties, two different light sources are used. Oxygenated hemoglobin (HbO2) has the highest absorbance in the infrared region (850nm-1000nm), while deoxygenated hemoglobin (Hb) has a high absorbance in the red band (600 nm to 750 nm).This is why most present pulse oximeters use 940 nm infrared and 660 nm red light emitting diodes [1]. Figure 1 shows the absorption levels of oxygenated and deoxygenated blood at different wavelengths.

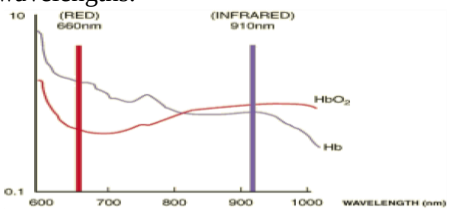

Fig 1: Absorption levels of oxygenated and deoxygenated blood at different wavelengths [2]

When light is emitted into the body tissue, some light will be absorbed by the skin, bones, and muscle tissue. This represents the static direct current (DC) component of the signal received at the photo detector receiver. The pulsatile flow in arteries and arterioles during diastole and systole will usually create some variation in light intensity. This will produce the AC part of the signal [3]. Both AC and DC components are shown in Figure 2.

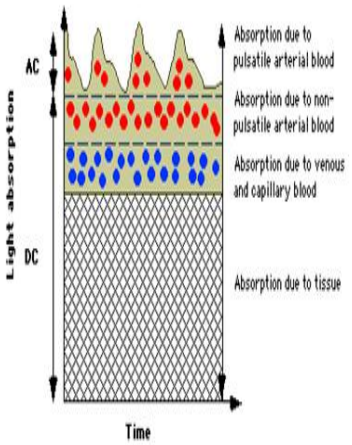

Fig 2: Diagram showing light absorption through living tissue [3]

2. MATERIALS & METHODS

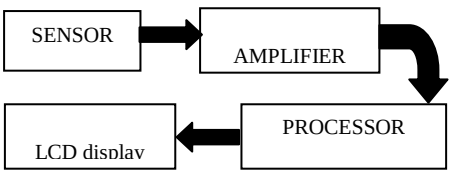

Fig3: Block diagram for Pulse Oximetry operation

Pulse Oximeter system consists of a probe (sensor), signal-processing unit (main device) and also a results displaying unit.

2.1 Sensor of Pulse Oximetry

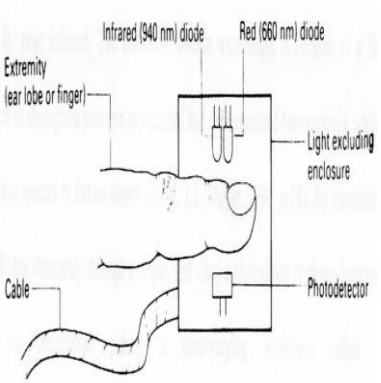

Fig 4: Diagram showing sensor orientation for light transmittance in the designed pulse oximeter [4]

Designed a low-cost Pulse Oximetry system consists of a probe (sensor); the sensing probe consists of two LEDs, and a photo-detector. The two LEDs used in the sensor part are the red (660nm) and infrared (940nm). The signal collected from the photo-detector (LDR&IR RECEIVER) will be supplied to a dual operational amplifier (LM358) the first output will be go to PIC16F877A to process the signal easy and get result, for the second output just for manually tests as show in figure 4.

2.2 Computing of Pulse Oximetry

The output signal from the dual amplifier will be further supplied to a Programmable Interface Controller (PIC16F877A) which will convert the current analogue signal into digital signal through the built-in Analogue to Digital Converter (ADC). However, this

converting process will require MICRO C programming software to generate the Hexadecimal file of the PIC before one can display the value of detected pulse rate and oxygen saturation in the blood. PIC 16F877A as show in figure 5.

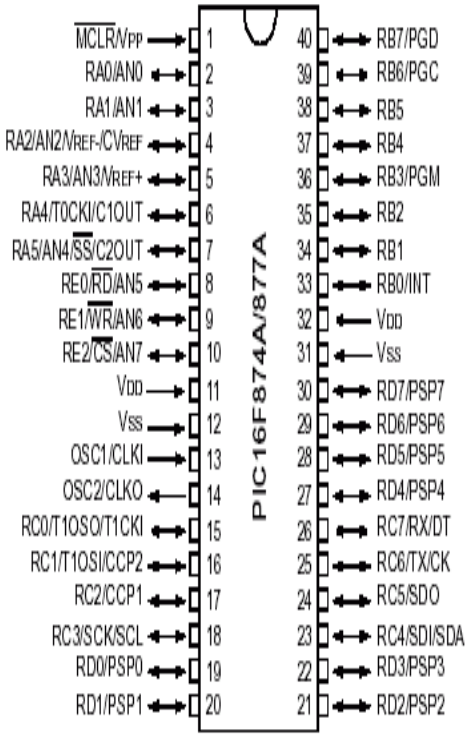

Fig 5: Details of PIC16F877A connections

[5]

2.3 Display of Pulse Oximetry

The PO will be displayed via a Liquid Crystal Display (LCD) screen. This shows that the newly developed PO system has extra capabilities in collecting the measured data such as the HR and SpO_2 which could be further analyzed and stored through the computer as show in figure 6.

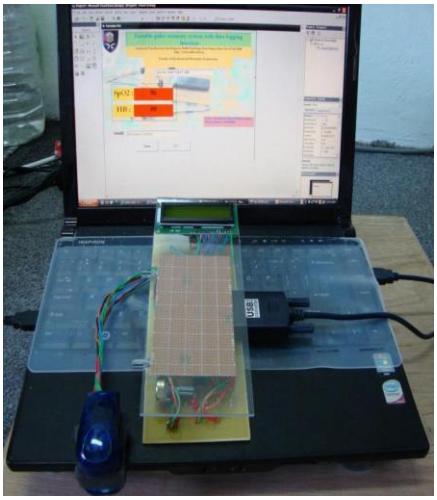

Fig 6: Diagram showing the designed Pulse Oximetry device connected to a computer

3. RESULTS AND DISCUSSIONS

From this study a portable PO system has been designed and developed. The system able to produce highly reliable results for both HR and also SpO_2. In developing the sensor part the use of super bright LED was useful since its capability to penetrate the skin layer with different color. Next, the LDR positioned near the LED were able to detect the light reflected at the fingertip during blood circulation and from this detection the output signal from LDR were in resistance and very small in value. Thus, there is a need for the signal to be amplified. The signal were then fed into the amplifier and further processed by the PIC. The next stage was to program the selected PIC. This required more efforts than the previous stage as the PIC needed boot loading then the micro C code was loaded into it. The PIC were programmed in order to functionalize the ADC converter

thus, converted the analogue signal into digital. Finally, the device was completed by the attachment of an LCD plus demonstrating the output reading from the device through the computer. From this, the user of this PO device could read their test results via an LCD as shown in figure 7. In addition, the test results were also recorder and displayed on a computer by Visual Basic as show in figure 8.

Fig 7: Display via a Liquid Crystal Display (LCD) screen

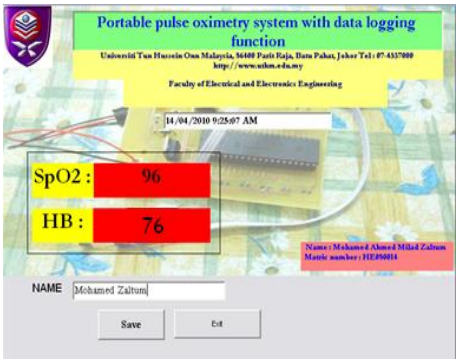

Fig 8: Display via Visual Basic on computer

3.1 Comparison between Standard System (DOLPHIN MEDICAL 2100 PULSE OXIMETER) & Proposed System

Once the PO device have been designed and developed, it is crucial to conduct a comparative analysis between the designed and the standard PO device.

Thus, the analysis will prove the reliability of the test results produced by the designed PO device. For this purpose three people with different skin color were selected such as (bright skin, fair skin and also dark skin).

The test results obtained for Mr. Mohamed Ramadan by Standard System and Proposed System at the same time under five different conditions which are (arriving at the lab, after rest, after exercise, after rest and then before leaving the lab). The conditions were the same for the entire people whom participated in this PO device testing. The results were then plotted in the following figure 9.

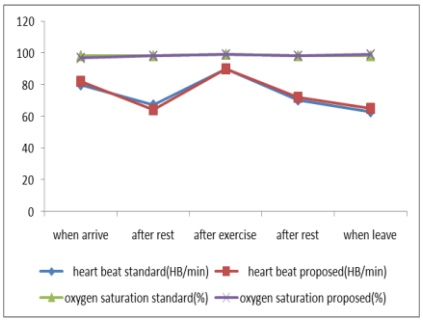

Fig 9: Results showing the output reading for pulse/oxygen level of Mr. Mohamed Alarqaa

The test results obtained for Mr. Wan Suhaimizan. The results were then plotted in the following figure 10.

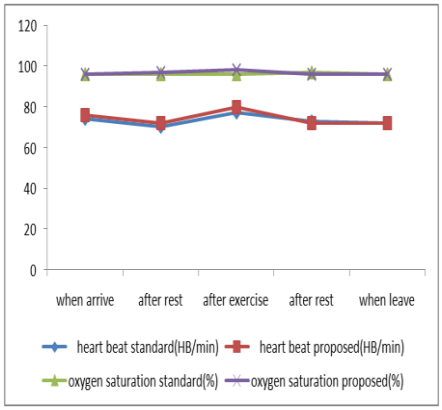

Fig 10: Results showing the output reading for pulse/oxygen level of Mr. Wan Suhaimizan

The test results obtained for Mr. Mohamed Zaltum. The results were then plotted in the following figure 11.

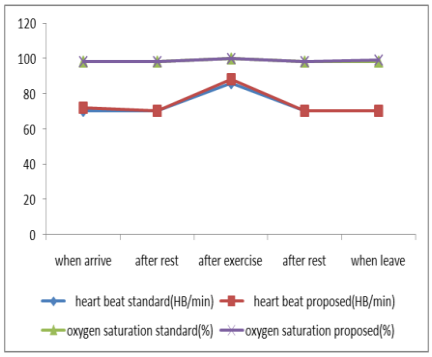

Fig 11: Results showing the output reading for pulse/oxygen level of Mr. Mohamed Zaltum

From the results obtained for the three people as shown in the graphs (Figure 9, 10 and 11) the developed PO device were capable of producing test result with very close to the standard device. In another words, it could be summarized that the developed PO device were able to produce the test results with a difference of 5% error state, which demonstrated that the device has a high level of accuracy when compared to the standard device. Next, the designed PO device was further tested for the reliability via a standard SpO_2 simulator. The tests were conducted for both HR and SpO_2 readings. The outcome of this test will be discussed in the next section.

3.2 Test Proposed System by SpO_2 Simulator (Index 2)

The results obtained from the standard system were compared with the SpO_2 simulator under two setting which are (70 heart beat per minute (HB/min) and 75 HB/min). These standard values were set with the SpO_2
device and compared with the standard system. It was discovered that the result from the standard system and also having less than 5% errors, as shown in figure 12. This again demonstrated the accuracy and reliability of the results as in the readings for the HB and SpO_2 that being produced by the PO device designed in this study.

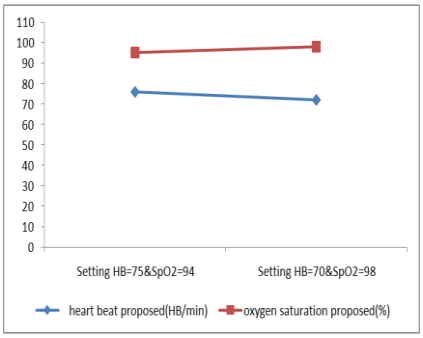

ig 12: Results produced by the SpO_2 Simulator (Index 2) and the Proposed System

4. CONCLUSIONS

Overall, the objective of this research has been achieved, since the result obtained from the developed PO device has less than 5% errors in comparison to the standard device. Therefore it is assured that the device were able to produce highly reliable test results for both the HR and SpO_2. Considering the high cost of the standard equipment, local ones as in this study the home-bulit PO device demonstrated the proof of concept where a much cheaper in cost can be produced. In addition, this PO device has the extra function of recording the test result for the user to come back at any time to analysis and

observe their test result again. Finally, these PO devices are suitable for personal in-home
usage, technical school and universities levels for educational and research purposes.

5. ACKNOWLEDGEMENT

The author would like to take his opportunity to express his heartfelt appreciation and thanks to his respectful supervisor, Dr. Muhamad Mahadi bin Abdul Jamil and co supervisor Mr. Muhammad Shukri bin Ahmad for their supervisions,encouragement, contradictive ideas, patience, guidance and invaluable advice, enabling the author to produce this paper.

6. REFERENCES

[1]. Ferrera, F. (2006). Design of low-cost instrument for pulse oximetry.

[2]. Hoff, D. Zhang, R. Stalter, T. & Carlson, M. (2003). Pulse Oximetry.

[3]. Deni, H. Muratore, D. M. Malkin, R A. (2005). Development of a Pulse Oximeter Analyzer for the Developing World. Proceedings of the IEEE 31st Annual Northeast Bio-engineering Conference. Pp. 227-228.

[4]. Moyle, J. (2002). Pulse oximetry. Second edition, BMJ Publishing Group. London, United Kingdom.

[5]. Microcontrollershop.com:product_ info, Retrieved on 20th of March, 2009. URL :(http://microcontrollershop.com).

[6]. Gupta, R.C. Ahluwalia, S.S. & Randhawa, S.S. (1995). Design and Development of Pulse Oximeter Proceedings RC IEEE-EMBS & 14th BMESI. Central Scientific Instruments Organisation, INDIA.

[7]. Oximeter: pulseox/applications, Retrieved on 10th of August 2008, URL: (http://www.oximeter.org).

[8]. Jovanov, A. Milenkovic, A. Basham, S. Clark, D. Kelley, D. (2004). Reconfigurable Intelligent Sensors for Health Monitoring: A Case Study of Pulse Oximeter Sensor. Proceedings of the 26th Annual International Conference of the IEEE EMBS, San Francisco, CA, USA. September 1-5, 2004.

[9]. Severinghaus, J. Honda, Y. (1987). History of blood gas analysis VII. Pulse Oximetry. J Clin Monit 1987 Apr 3 (2): pp.135-138.

[10]. Wieringa, F. Mastik, F. Boks, R. Visscher, A. Bogers, A. & Steen, A. (2007). In Vitro Demonstration of a SpO2-Camera. Computers in Cardiology. Vol. 34. Pp. 749-751.

The Study of Implantable Medical Device Based Wireless Biomedical Telemetry

Chandrasekhar Kandagatla
Faculty of EE Engineering
AP, INDIAkcs1011@gmail.com

Prabhu. G. benakop
Aurora Technological and Research Institute,
Sirte University, Sirte, LIBYA
pgbenakop@rediffmail.com

Abstract

Implantable medical devices (IMDs) have a history of outstanding success in the treatment of many diseases, including heart diseases, neurological disorders, and deafness. Today's aging population is driving wide-scale demand for more-advanced healthcare treatments, including wireless implant devices that can deliver ongoing and cost-effective monitoring of a patient's condition. New ultra-low-power radio-frequency (RF) technologies are spurring the development of innovative medical tools, from endoscopic camera capsules that are swallowed, to implanted devices that wirelessly transmit patient health data. Communication links between external programming devices (or base stations) and medical implants are critical to the success of IMDs.Historically, low-frequency inductive links (introduced in the early 1970s) have been the most prevalent method of communication. They typically operate in the tens to hundreds of kilohertz range, with data rates of 1–30 Kb/sec. These low-power systems, which can accommodate a small coiled antenna in the IMD, have proven to be robust and suitably reliable. However, antenna size and power limitations in implants result in a very low magnetic field strength for an IMD that is communicating with an external programmer. Therefore, inductive links are short range and often require the external programmer to have contact with the skin of the patient directly over the implant. To overcome these operating-range and low-data-rate limitations, new ultra-low-power RF technologies are being developed that operate at much higher frequencies, such as in the 433 and 915 MHz industrial, scientific, and medical (ISM) bands and the more recently allocated 402–405 MHz medical implant communication service (MICS) band. RF integrated circuit (RFIC) technology can now offer low power, reduced external component count, and higher levels of integration, which will open new markets for medical device manufacturers.

This article discusses the issues related to remote management of IMDs via the MICS band and presents guidelines for addressing these issues. A brief history of the MICS standard is presented, followed by an outline of the requirements driving RF medical technology. To enable use of the MICS band, medical devices require an ultra-low-power, high-performance transceiver. This article examines a transceiver IC designed specifically

for this purpose. The design considerations of implantable transceivers are presented, followed by a brief discussion of the architecture and important design features.

Keywords: IMD, ISM, Implantable, RF Transceiver

I. Introduction

Traditionally, communication systems in medical devices have used very short-range magnetic coupling. These systems require close coupling between the programmer and medical device and often have limited available data rate.

The 402-405 MHz Medical Implant Communication Service (MICS) band was recommended for allocation by ITU-R Recommendation SA1346 in 1998. The FCC established the band in 1999 with similar standards following in Europe [1,2]. The allocation of this band supports the use of larger range (typically 2 meters), high-speed wireless links. The MICS band overcomes the limitations of dated inductive systems and facilitates the development of next generation medical devices with improved patient health care. This is especially important given escalating health costs driving the usage of home monitoring.

The 402-405 MHz band was considered well suited for this service, due to the signal propagation characteristics in the human body, the compatibility with the incumbent users of the band (Meteorological aids such as weather balloons), and its international availability for this purpose.

To enable the use of the MICS band, medical devices require an ultra low power, high performance transceiver. This paper presents a transceiver integrated circuit (IC) specifically designed for this purpose. The design considerations of implantable transceivers are presented, followed by a brief discussion of the architecture and important design features.

I. Transceiver Design Considerations

The design of transceivers for medical devices is challenged by the following basic requirements:

- Low power consumption during 400 MHz communication is required. Implant battery power is limited, and the impedance of implant batteries is relatively high. This combination limits peak currents that may be drained from the supply. During communication sessions, current should be limited to <6 mA for most implantable devices.
- The transceiver must operate in a low-power sleep mode, with the capability to look periodically for a wake-up signal.
- Minimum external component count and small physical size are important factors. An RF module for a pacemaker must be no larger than ~5 x 5 x 10 mm. Furthermore, implant-grade components

are expensive, and using high levels of integration may significantly reduce costs. Integration has the additional benefit of increasing overall system reliability.

- Reasonable data rates are demanded; pacemaker applications are currently demanding >20 Kilobits/sec(kb/sec), with higher data rates projected for the future.
- High reliability in both data transmission and system operation.
- An operating range is typically >2 m because the MICS band is designed to improve upon the very-short-range inductive link. Longer operating ranges imply that good sensitivity is needed, because small antennas and body loss affect link budget and allowable range. Antenna matching and body loss can typically be more than 40 dB.
- Selectivity is required and interference must be rejected.

The MICS regulations provide additional requirements. This section discusses some of the key requirements.

The MICS regulations require a system to perform a clear-channel assessment (CCA) in which the user scans all 10 of the 300-kHz channels and is allowed to transmit on the channel with the lowest ambient signal level (the least-noisy channel). The user can also choose to transmit on the first available channel with an ambient power below a certain threshold (as defined in the standard). The MICS standard requires that the external programmer carry out the scanning process. For this reason, the IMD transceiver should support a low-power method of sniffing for the presence of an external programmer signal.

MICS regulations provide an exception to the CCA procedure in the event of an emergency medical event. For clinically significant medical emergencies, the IMD may transmit immediately on any channel. For example, if an implanted ECG monitor or pacemaker detects a cardiac arrest, the device could transmit immediately to a monitoring base station that, in turn, calls an emergency response service.

Given the important requirements defined above, it is essential that medical device designers and system architects meet the demands of RF medical implant communication.

An example of a transceiver IC specifically designed for implanted medical devices operating in the 402–405 MHz MICS band is shown in Figure 1. The concepts of duty cycling, ultra-low-power circuit design, and high integration levels are incorporated, with specific attention paid to the special needs of IMD systems. This example will be used to highlight the concepts introduced in the following sections.

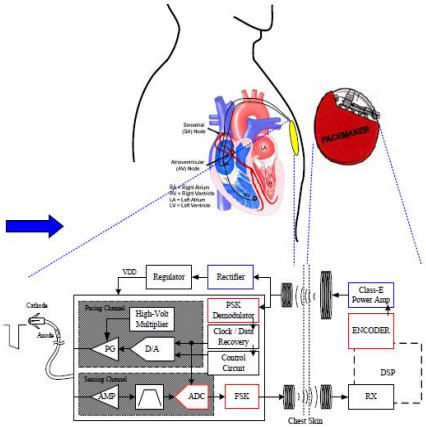

Figure 1. An implanted pacemaker uses the MICS band to communicate patient health and operating data to a base station, which transmits information to a physician's remote office(Ref.5)

A. Achieving Low Power Consumption

Medical devices can be divided into two categories: those that use an internal nonrechargeable battery (e.g., pacemakers) and those that couple power inductively (e.g., cochlear implants). The former heavily duty-cycle the operation of systems to conserve power. The transceiver is off most of the time. Therefore, the off-state current and the current required to periodically look for a communicating device must be extremely low (<1 µA). In both cases, low power (<6 mA) is also required for both transmit and receive.

The primary philosophy for saving power in IMD electronics (RF or otherwise) is the simple concept of duty-cycling: operate systems for a short time period and with minimum current. Furthermore, low leakage currents must be ensured when systems are disabled.

By operating systems quickly, fixed power-consuming overheads (such as support circuitry, synthesizers, clocks, biasing, and regulators) have less time to drain the battery. There is always a limit to applying this principle, because circuit complexity will rise, and total energy requirements will increase if the operating time is too short. Therefore, an optimal time period usually exists where the total energy consumed is minimized.

For RF communication systems in medical implants, duty-cycling may be applied to all phases of operation. The IMD transceiver sniffing and start-up should be duty-cycled. In addition, duty-cycling and short on-times may be exploited during the actual 400 MHz communication sessions.

B. Duty-Cycling Normal Transmission.

For minimum overall power consumption, defined in terms of joules per bit, it is recommended that implantable transceivers use the highest possible data rate that satisfies the application receiver-sensitivity requirements. Systems that require low data rates (even in the low kilohertz range) should buffer data, operate at the highest data rate possible, and exploit duty-cycling of the power states to reduce the average current consumption. Sending data in short bursts conserves power and reduces the potential time window for interference. In addition, the power supply decoupling

requirements are more forgiving in systems with high battery impedance.

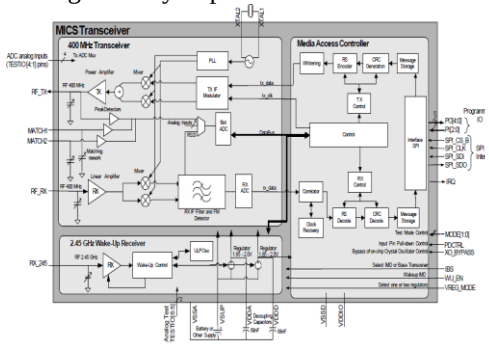

Figure 2. Highly integrated ultra-low-power MICS transceiver.(Ref.5)

The transceiver architecture presented in Figure 2 allows a user to select from a wide range of relatively high data rates (up to 800 Kb/sec) with varying receiver sensitivity. To facilitate this flexibility, the system uses frequency-shift-keyed (FSK) modulation with varying frequency deviations.

In low-power architectures, the modulation scheme should provide high data rates while supporting a simple radio architecture that meets the current consumption requirements. Quadrature amplitude modulation and Nyquist-filtered M-ary (or multiple) phase modulation both offer good bandwidth efficiencies. However, constant-envelope signals (i.e., FSK) are advantageous because they result in relaxed requirements on the linearity of the system. Of the available modulation schemes, FSK modulation has been found to provide a good compromise between data rate, complexity, and requirements on linearity.

FSK allows for a high-data-rate, low-power receiver. Note that more-complex modulation schemes are often seen in short-range RF communication standards, such as Bluetooth. These modulation schemes are not easily amenable to the truly ultra-low-power communication demanded by medical implants.

The design of the communication control should facilitate duty-cycling of the RF blocks when data are not ready to be transmitted. The transceiver in Figure 2 includes an integrated media access controller (MAC) that may be used to control the power state of analog circuitry when data communication is not immediately required or is being buffered. The MAC relieves the user of communication link control activities to the extent that the RF link is simply a memory-mapped peripheral.

C. Duty-Cycling Transceiver Wake-Up.

Most implant applications use the MICS RF link infrequently because of their overriding need to conserve battery power. In very-low-power applications, the transceiver spends most of the time asleep in a very-low-current state and periodically sniffs for a wake-up signal.

This sniffing operation should be frequent enough to provide reasonable start-up latency and, because it will occur regularly, it should consume a very low current. It should also be immune to noise sources that invoke an erroneous start-up. In this situation, an on-off keyed (OOK)

modulation scheme is recommended because the OOK scheme removes the need for a local oscillator and synthesizer in the receiver, both of which require time and power to start up.

The wake-up system shown in Figure 2 uses an ultra-low-power RF receiver to read OOK transmitted data. The receiver's main function is to detect the incoming signal from the programmer and then to activate the rest of the chip. The example shown may also be started directly by pin control, which allows either an external programmer to initiate communication or the implant itself to send an emergency communication.

D. Achieving High Data Integrity

For typical RF communications, given the plethora of noise and interference sources that exist, a reasonable design guideline is to assume a minimum raw radio bit-error rate of about 1 x 10^{-3}errors/bit. The MAC shown in Figure 2 includes forward error correction (FEC) using a Reed-Solomon block code and CRC error detection. The design of appropriate FEC codes is interesting, with trade-offs existing between power consumed by retransmission of packets and power consumed by additional coding capability. FEC codes also provide an overall trade-off between final bit-error rate and system power consumption.

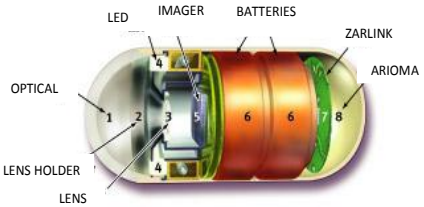

An ultra-low-power RF transmitter is a key component of the swallowable camera

For a 30% overhead in bits used for error correction and detection, for example, an improvement can be obtained in bit-error rate of many orders of magnitude from 1 x 10^{-3} to at least 1 x 10^{-4}errors/bit. This improvement equates to an average time between errors, given a data rate of 200 Kb/sec, of four years under the impractical scenario of continuous operation. As noted earlier, in order to save battery power, the RF link in most applications will be used rarely.

Reed-Solomon codes are especially good at correcting burst errors. In addition, high data rates offer the opportunity to minimize the probability of interference in burst-noise cases frequently observed in an RF environment.

From an analog RF standpoint, immunity from interference places constraints on channel and band filtering and on low-noise amplifier (LNA) linearity because of intermodulation. Immunity also limits synthesizer phase noise caused by reciprocal mixing. Such constraints are often in direct conflict with low-power design and require skilled RF analog IC design expertise.

In some systems, an external standing-acoustic-wave (SAW) filter may be appropriate. This is more easily accommodated in the external programmer, because it is usually subject to worse interference scenarios than the IMD. A SAW filter also does not suffer as severely from space constraints. The external programmer is more susceptible to interference due to two factors: the attenuation of an interferer through the body before reaching the implant, and the normally smaller available power received by the external programmer from the implant.

The MICS standard allows for a maximum transmitted power (in air) of 25 mW. The external programmer may easily radiate at this power level; however, this will not be the case for an implant due to large antenna losses, body losses, and limitations in available implant transmit power. Good power amplifier design is important for maximizing the available implant transmit power. Nevertheless, battery performance and current limitations in the implant are the ultimate limiting factors.

II. Conclusion

The design considerations for implantable RF communication systems require careful consideration of transceiver design, power consumption, and data integrity. Moreover, when designing an implantable RF communication system, it is essential to consider the issues related to remote management of these devices via the MICS band. The transceiver IC discussed in this article uses an architecture that provides the basic concepts of achieving low power and high data integrity.

These concepts will lead the way to high-performance, low-power RF communication. Such transceiver technology will facilitate clinically significant improvements in healthcare for the development of next generation of medical implants.

III. References

[1] FCC Rules and Regulations 47 CFR Part 95, Subparts E (95.601-95.673) and I (95.1201-95.1219) Personal Radio Services, November 2002.

[2] ETSI EN 301-839, Parts 1 and 2 and ETSI EN 301-489 Part 27.

[3] A. Rofougaran et al., “A single-chip 900-MHz spread-spectrum wireless transceiver in 1-_m CMOS—Part I: Architecture and transmitter design,” IEEE J. Solid-State Circuits, vol. 333, pp. 515–534, Apr. 1998.

[4] I. Vassiliou, “A single-chip digitally calibrated 5.15-5.825-GHz 0.18-µm CMOS transceiver for 802.11a wireless LAN,” IEEE J. Solid-State Circuits, vol. 38, no. 12, pp. 2221–2231, Dec. 2003.

[5] B. Razavi, “Architectures and circuits for RF CMOS receivers,” in Proc. IEEE Custom Integrated Circuits Conf., Santa Clara, CA, May 1998, pp. 393–400.

Random segmentation blocks algorithm for Gout Skin Detection and recognition

Hind Rostom Mohammed

Computer Department /Assistant Professor
College of mathematical and computer sciences / Kufa University/Iraq
hind_restem@yahoo.com

ABSTRACT

Gout is a disease of antiquity but is increasing once again in prevalence despite availability of reasonably effective treatments. This may be related to a combination of factors, including diet, obesity, and diuretic use. Allergic reactions, noncompliance, drug interactions, and sometimes inefficacy all limit the effective use of current hypouricemic agents. The objective of this paper is to show that for every color space there exists an optimum Gout skin detector scheme such that the performance of all these skin detectors schemes is the same and then process the Random segmentation blocks algorithm in order to recognition Gout skin A theoretical proof is provided and experiments are presented which show that the separability of the skin and no skin classes is independent of the color space and some parameters chosen (experimentation for 80 gout image for different types and 80 other Dermatological disorders images) for testing are Energy , Entropy , Average and Variance. 160 patient were randomly placed in three groups and treated topicaly along 7-weeks with either gout in foot or hand or other parts bodyThe recognition results for testing program by Random segmentation blocks algorithm shows superior efficacy for gout skin detection(the testing stage contain all 160 images to recognized only gouts images) .

key words: Gout ,gout stages, segmentation blocks, image processing , color space, energy.

1. Introduction

Gout is a metabolic disease that can manifest as acute or chronic arthritis, and deposition of urate crystals in connective tissue and kidneys. It can either manifest as acute arthritis or chronic tophaceous gout. Skin detection can be defined as the process of selecting which pixels of a given image correspond to human skin.

Skin detection is useful in, for example, face detection and face tracking for security and video indexing applications, model-based video coding. There are some difficulties when detecting skin pixels. Skin color is affected by ambient light which is unknown in many situations; different cameras produce different colors,

even from the same person, under the same illumination conditions; and finally, skin colors change from person to person.

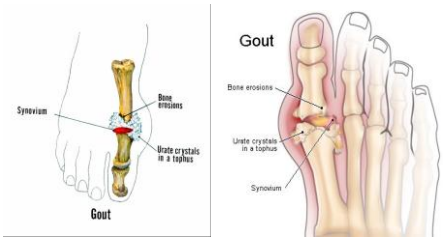

Figure(1):gout

There are new treatments for gout on the horizon, including febuxostat, a nonprime inhibitor of xanthine oxidase with a potentially better combination of efficacy and side effects than allopurinol. Diagnostic progress is being made in that ultrasound may offer a noninvasive means of diagnosing tophaceous deposits in and around joints[2]. The increasing prevalence of gout means that dermatologists will see more cutaneous manifestations of gout, including tophi, draining sinus tracts, panniculitis, and dystrophic calcifications.

The modifications needed to analyze the picture will be applied through the use of Oracle Intermedia and the images will be stored in an Oracle database. The same features will be used to apply modifications to the picture which are needed for skin detection and body measuring[1].

Gout occurs more frequently in men than women, at older age, with higher levels of uric acid, and in association with hypertension.

2. Acute Attack of Gout

When gout occurs, the joint tends to be extremely painful and is warm, red and swollen . The inflammation that is part of a gout attack is systemic, so that fever and chills, fatigue and malaise are not uncommonly part of the picture of a gout attack[4,5]. As with all other known types of arthritis, gout has particular joints it tends to attack. Gout especially favors the bunion joint, known as the 1st metatarso-phalangeal joint, which is the first joint involved in 75% of patients and is ultimately involved in over 90% of those with this condition.. The ankle, mid-foot and knee are also common locations for gout, as well as the bursa that overlies the elbow. Late in gout, if untreated, multiple joints can be involved, including the fingers and wrists[3,6]. The shoulder joint is very rarely involved by gout, and the hip essentially never. Several color spaces have been proposed in the literature for skin detection applications. Skin segmentation has many important applications related to finding and analyzing people behavior on images or video sequences. Some of these applications are visual tracking for surveillance, face detection, hand gesture recognition, searching and filtering image contents on the web and many others. In the case of Intelligent Human-Computer Interaction (IHCI), the capture and interpretation of the users motions and emotions is an important element to understand of his/her current cognitive state [7,8].

Skin Color Features Modeling skin color requires the selection of an appropriate color space and identifying the cluster associated with skin color in this space. HSI

space (Hue, Saturation and Intensity) was chosen since the hue and saturation pair of skin-tone colors are independent of the intensity component Thus, colors can be specified using just two parameters instead of the three specified by RGB space color (Red, Green, Blue). In order to find common skin tone features, several images involving people with different backgrounds and light conditions where processed by hand to separate skin areas[9].

Many texture classification schemes have been used for grey level images. Texture image segmentation is common in analysis of medical images, remote sensing scene interpretation, industrial quality control inspection, document segmentation, image recovery in databases, visual recognition systems, etc.

3. Random segmentation blocks algorithm

This segmentation problem is stated classifying the pixels of an input image in two groups: skin and non-skin pixels. An important requirement for automatic (or semiautomatic) skin detection systems is a trade off between correct classification rate and response time. The common approach to skin detection is using the skin colour as feature. we use a segmentation method that considers all RGB bands or other color spaces combinations. It also permits to difference among different color and texture combinations in the same image. The algorithm allows distinguishing among different textures with few changes on the same type.

Probability(p)=n(g)/m

g: color ; n: number of pixel with color (g);m: total number of pixel in image

Average ($\overline{g}$)=∑r ∑c I(r,c) / M……..(1)

I(r,c): color at coordinate (r,c)

Variance(v)
$= \sqrt{\sum_{g=0}^{l-1}(g-\overline{g})^2 + p(g)}$ ……..(2)

$\overline{g}$:average ;
l: number of colors in image

Entropy(E)
$= -\sum_{g=0}^{l-1} p(g) \times \log_2[p(g)]$ ……..(3)

Energy(En)
$= \sum_{g=0}^{l-1}[p(g)]^2$ ……..……(4)

color space [Y Cr Cb]

Y: is the luminous component; while Cb and Cr provide the color information

$$\begin{bmatrix} Y \\ Cr \\ Cb \end{bmatrix} = \begin{bmatrix} 16 \\ 128 \\ 128 \end{bmatrix} + \begin{bmatrix} 65.481 & 128.553 & 24.966 \\ -37.797 & -74.203 & 112.00 \\ 112.00 & -93.786 & -18.214 \end{bmatrix} \times \begin{bmatrix} R \\ G \\ B \end{bmatrix} \quad (5)$$

$$Y = 0.299R + 0.587G + 0.114B$$
$$C_r = R - Y$$
$$C_b = B - Y \quad (6)$$

YCrCb is an encoded nonlinear RGB signal, commonly used by European television studios and for image compression work.

Y – Luminance component, C – Chrominance

The user has the opportunity both to supply a variance image of the input and to receive a variance image of the smoothed output. (A variance image is an image of the variances,
that is the squares of the standard deviations, in the values of the input or output images.)

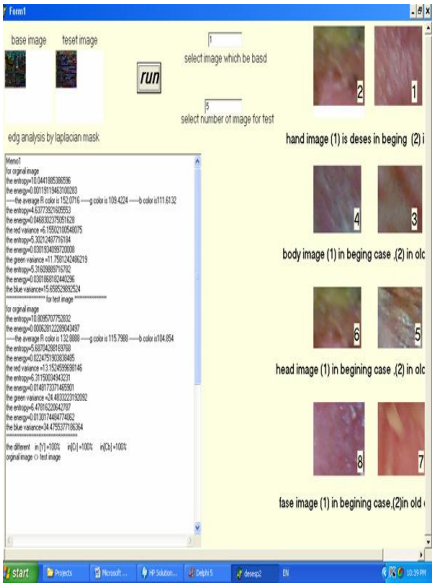

Figure(2):interface program

Table(1):image parameters which used in Random segmentation blocks algorithm with color space.

Parameter name	Parameter note
1-Average	Provide information about the contrast of the image high variance find high contrast
2-Variance	Provide information about the contrast of the image high variance find high contrast
3- Entropy	Measure of image information content, Provide information about the number of bit required to code the image
4- Energy	Provide Information about the data spread

For the case of basic RGB space, we applied the following simple explicit skin detection algorithm and works on all the image pixels for uniform daylight illumination: Normalized RGB – rg space

2D color space as 'b' component is redundant

b = 1 – g – r

Invariant to changes of surface orientation relatively to the light source

r =R/(R+G+B) ; g=G/(R+G+B) ; b=B/(R+G+B)…(7)

HSV, HSI, HSL (hue, saturation, value/intensity/luminance)

$$H = \arccos \frac{\frac{1}{2}((R-G)+(R-B))}{\sqrt{((R-G)^2+(R-B)(G-B))}} \quad ..(8)$$

S=1-3(min(R,G,B))/(R+G+B)…….(9)

V=1/3(R+G+B)……(10)

where R, G and B represent the value of pixel in the respective RGB color channel with values ranging from 0 to 255. For HSV and YCbCr spaces, a similar approach is followed. We retain luminance information by converting the image to gray levels. Next, we produce an initial over segmented image of regions by applying a morphological watershed method. If these histograms are similar, the region is considered as "skin region" and used as seed for a region growing algorithm applied on neighbor non-skin regions. Finally, the explicit skin detection algorithm is applied to each pixel of detected skin regions to discard False Positive (FP) skin regions when the percentage of skin pixels in a region is above an experimental threshold. The global proposed color based skin detection method is outlined by the algorithm pseudo code.

This paper explores the use of texture as a descriptor for the extraction of skin pixels in images. For this aim, we analyzed and compared a proposed color-based skin detection algorithm (using RGB, HSV and YCbCr representation spaces) with a texture-based skin location algorithm which used a measures with color spase are Energy , Entropy , Average , Variance to evaluate region features. We showed the usefulness of each skin segmentation feature (color versus texture) under different experiments that compared the accuracy of algorithms under the same set of hand segmented images.

4- Hybrid Systems

The original system contain two stages

1-random segmentation blocks

2- recognition the gout images

The segmentation blocks algorithm

1-input (original image)(F) .

- Get the red component (Fr) from F.
- Get the green component (Fg) from F.
- Get the blue component (Fb) from F.

2-input blocks size(N*N). ex:10*10

3-No. of blocks in each raw in Fr (X) =image width / N.

4-No. of blocks in each column in Fr(Y)=image height /

5-No. of blocks in image in Fr (Z) =X * Y.

6- for i = 1 to z

7-each block represent at

For j =1 to N

For k =1 to N

Bi(j, k) = Fr(m, m1)

M= 1 to image width

M1= 1 to image height

8- save in the table the number of block (Bi) and its block.

9- save the red blocks in image file (Fr).

10- repeat from step 1 to step to 8 on green component (Fg).

11- repeat from step 1 to step to 8 on blue component (Fb).

12- gathering the three components to represent the output image blocks

FF =Fr+Fg+Fr

Output :

1- image which contains the blocks.

2- table contains the blocks numbers and its blocks

The steps that moves the segmentation blocks as random for multi spatial image are:

1- input :1- image which contains the blocks.

2- table contains the blocks numbers and its blocks.

2- random (table).

3- for i= 1 to Z

4- get the new location of block (i) from the

random table.

5- put the block (i) in new location.

6- display the output image.

The number of blocks is =11*11=121 and

Size block=10*10

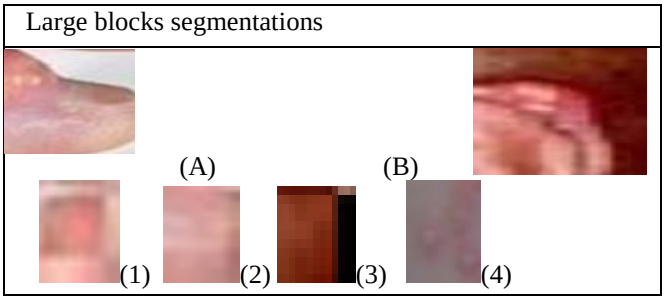

Figure(3): (A) ,(B) gout skin blocks images size 50*50 (2),(3), (4) gout skin blocks images size 10*10,(1) psoriasis skin block

Table(2):blocks segmentation after the random move number blocks

19	82	5	33	75	92	20	71	34	16	91
80	27	63	26	31	46	83	93	81	32	47
112	44	78	72	104	11	56	28	43	2	98
48	68	8	90	50	91	70	113	67	102	17
100	37	89	111	73	30	103	15	101	38	18
6	110	42	25	55	109	49	88	24	79	74
114	120	117	62	84	1	95	61	119	97	7
13	69	36	115	108	65	116	66	51	118	57
105	121	99	12	54	106	23	107	41	77	40
76	4	87	14	59	85	96	60	94	3	58
21	53	64	35	10	45	29	52	22	39	86

The formulation of the rules for classification based on segmentation is carried out by the context information and the classes relationships. Generally in higher hierarchy spectral information could yield good results, such as Energy, Entropy and Variance. To distinguish different objects which are very close spectrally form parameters .

Region for segmentation blocks and recognition

The method based to take the spatial arrangement of skin pixels into account during the detection stage to enhance the methods performance. Additional knowledge in terms of texture etc are required.

Many methods combines skin color detection with background subtraction to reduce falsely detected skin pixels. In this paper, we implemented three skin color detection methods and one background subtraction method [10].

(b)

Figure(4): (a) Original gout images (b) segmentation images Where the array contain =11*11=121 blocks and size block=10*10

Conclusion

Gout is a common disease and appears to be becoming more common over time. We are fortunate to have a strong armamentarium against this condition, with newer agents in development. In view of the effectiveness of our treatments, it is

important for a correct diagnosis to be made as early as possible, and therapy begun quickly when appropriate. Other conditions which can mimic gout, should be definitively ruled out through crystal identification in joint fluid whenever possible. For acute attacks of gout, a key is treating as quickly as possible and choosing a medication least likely to cause side-effects, with special attention to individual co-morbidities. For chronic prevention of gout, the essential message is that present treatments work in a huge majority of patients, and are generally well-tolerated. It is important for patients to understand the four stages of gout since the treatment of each is different. It is important for patients with gout to be carefully counseled to communicate any changes in the frequency of gout attacks to their practitioner. A primary care practitioner can often manage gout without a consultation with a rheumatologist, but consultation should be considered if the diagnosis is unclear, there is uncertainty as to whether or not to start uric acid-lowering medication, attacks continue to occur despite treatment, or possible medication side-effects are making treatment difficult.

The most important conclusions we draw are listed below:

1- Parametric skin modelling methods are better suited for constructing classifiers in case of limited training and expected target data set. The generalization and interpolation ability of these methods makes it possible to construct a classifier with acceptable performance from incomplete training data.
2- The methods that are less dependent on the skin cluster shape and take into account skin and non-skin colors overlap automatically constructed colors pace and classification rules skin classifier for large target datasets.
3- Evaluation of color space goodness 'in general' by assessing skin/non-skin overlap, skin cluster shape, etc. regardless to any specific skin modeling method cannot give the impression of how good is the color space suited for skin modeling, because different modeling methods react very differently on the color space change.

Used 80 images to build a general color model.

●Density is concentrated around the color line and is more sharply peaked at red than blue.

●Most colors fall on or near the space color line.

●There is a marked skew in the distribution toward the red corner of the color image .

It is possible that color spaces other than RGB could result in improved detection performance. The skin colors form a separate cluster in the RGB color space. Hence skin color can be used as a cue for skin detection in images and videos. The performance of different color space may be dependent on the method used to model the color for skin pixel. The recognition results by Random segmentation blocks algorithm shows superior efficacy for gout skin detection.

Table(3): Recognition the gout skin images results (testing stage same image or sub image)			
index	Parameter name	Image(1)parameters Image(5)parameters	Image(2)parameters Image(6)parameters
1	entropy	10.8095707752832	10.8095707752832
2	energy	0.0006281222890434 97	0.00628122289043497
3	average R color	132.8888	132.8888
4	average G color	115.7988	115.7988
5	Average B color	is104.854	is104.854
6	entropy	5.68704288169768	5.68704288169768
7	energy	0.0224751903838485	0.0224751903838485
8	red variance	13.1524599698146	13.1524599698146
9	entropy	6.31150034943231	6.31150034943231
10	energy	0.0148173371465901	0.0148173371465901
11	green variance	24.4833223192092	24.4833223192092
12	entropy	6.47816220642787	6.47816220642787
13	energy	0.0130174484774062	0.0130174484774062
14	blue variance	34.4755377186364	34.4755377186364

Table(4):Recognition the gout skin images results (testing stage)

index	Parameter name	Image(4)parameters	Image(7)parameters
1	entropy	9.88502155472831	10.0441885386596
2	energy	0.00147810826427482	0.0011911946310028
3	average R color	117.9236	152.0716
4	average G color	92.8496	109.4224
5	Average B color	81.946	111.6132
6	entropy	4.64209097460996	4.63773921605553
7	energy	0.0498367593261242	0.0468302375051628
8	red variance	6.27447267152303	6.15502100548075
9	entropy	5.43099133051117	5.30212487716184
10	energy	0.0293607706493251	0.0301934099720008
11	green variance	13.1198144806039	11.7581242486219
12	entropy	5.84579061572267	5.31609889716782
13	energy	0.0235562337711224	0.0301868182440296
14	blue variance	20.9089776801885	15.658529892524
15	the different in [Y] , in[Cr] and in[Cb]		the different in [Y] =100% [Cr] =99.9583506872137% [Cb] =99.9583506872137%

References

[1] Emanuil Rednic &Andrei Toma,Simple Skin Recognition with Oracle Intermedia", Body Building Science Journal, Vol. 2, No. 2, (2010).

[2] Fleck, M.M., Forsyth, D.A., Bregler, C.: Finding naked people. In: Proceedings of the European Conference on Computer Vision (ECCV). (1996)

[3] Abdel-Mottaleb, M., Elgammal, A Face detection in complex environments from color lmages. In: Proceedings of the International Conference on Image Processing (ICIP). (1999)

[4] Jones, M.J., Rehg, J.M., Statistical color models with application to skin detection. International Journal of Computer Vision (IJCV) 46(1) (2002)

[5] Burger, W., Burge, M.: Digital Image Processing, an Algorithmic Introduction Using Java. Springer (2008)

[6] Brand, J., & Mason, J., A comparative assessment of three approaches to pixellevel human skin-detection. In Proc. of the International Conference on Pattern Recognition, vol. 1,(2000).

[7] Brown, D., Craw, I., & Lewthwaite, J. 2001. A som based approach to skin detection with application in real time systems. In Proc. of the British Machine Vision Conference,(2001).

[8] Chai, D., & Bouzerdoum, A. A bayesian approach to skin color classification in ycbcr color space. In Proceedings IEEE Region Ten Conference (TENCON'2000), vol. 2,(2000).

[9] Raju M. Tugnayat, Nitin K. Choudhary & M.V.Sarode, Improvement in Recognition Techniques for Human Computer Interaction, 2010 International Journal of Computer Applications (0975 – 8887) Vol 1 , No. 6,(2010).

[10] A. Cheddad, J. Condell, K. Curran, P. M. Kevitt, "A skintone detection algorithm for an adaptive approach to steganography," Signal Processing, Vol. 89, No. 12,(2009).

A.Prof. Hind Rostom Mohammed is a A.Professor in Iraq/ Kufa University/ College of mathematical and computer sciences/ Sciences Computer Department . She received her B.Sc from Basra University/ sciences College /Computer science, 1990. Degree Obtained M.Sc.computer Seience from Babylon university,1999 , She was Director of Computer Department in Sciences Computer Department/ College of mathematical and computer sciences 2009-2010. She research focuses in computer architecture and organization, Neural network , Image processing, and speaker recognition . She has published many papers at international journals and conferences. Her research areas are Neural network ,Image compression, image recognitions.

Multi-frequency Electrical Impedance Tomography : Inequality constrains for image reconstruction

A. Shallof*, M. F. Bara* and D.C. Barber**, A.K.EL-Harbi***, A. Adwaib*

* Al-Fateh University, ** Sheffield University U. K. ,***7th April University

Email: a_shallof@yahoo.com

ABSTRACT

In order to take advantages of all information contained in tissue impedance it is necessary to consider not only the real part of conductivity but also the imaginary part. The real part of the complex conductivity always has positive values where as the imaginary part is always negative. The ability to consider least squares problems with linear inequality constraints allows us, in particular to have such constraints on the solution as non-negativity. The problem of determining whether or not a set of linear inequalities is consistent and if consistent finding some feasible vector arises in various contexts. In this paper least squares solution with

linear inequality constrains for multi-frequency image reconstruction are used and the solution obtained was tested with real data taken from the phantom with different object positions and acceptable results were found.

1. Introduction

Electrical Impedance Tomography (EIT) is a non invasive imaging technique with widespread applications in medicine and industry. It aims to image the conductivity distribution within an object by making electrical measurements on the surface of the volume. Some of the potential advantages of this technique are that[1][2]:

(a) It offers the possibility of an inexpensive non-harmful imaging technique capable of being used in the intensive care environment for a range of physiological measurements.

(b) It will be capable of characterizing tissues in a novel physiological way which should enable diseased tissues or abnormal function to be identified, and

(c) It should be capable of imaging fast dynamic activity within the human body because data can be acquired rapidly.

Electrical impedance tomography at single frequency allows images of temporal changes in tissue impedance to be produced. Production of static images using

data from human subjects is difficult. The main reason for this is that body shape and electrode position are more important determinants of transfer impedance measurements than is the distribution of tissue impedance.

Multi-frequency EIT offers the potential for making static images by producing images of changes in tissue impedance with frequency. Furthermore, by considering both real and imaginary parts of the conductivity, all information contained in the tissue is obtained.

The ability to consider linear least squares solution with linear inequality constraints allows us particular to have such constraints solution as non-negative conductivity values. In the literature there is no work addressed to the use of least squares with linear inequality constraints solution for EIT imaging. In this we use non-negative least squares MATLABE routines reconstruction problem. By this method the image quality is improved. The possibility of improving the reconstruction is based on the fact that the real part of conductivity is always positive and the imaginary part of the conductivity is always negative. In this paper we use real data from phantom studies to test linear least squares solutions with linear inequality constraints to improve image quality.

2.Non-negative least squares

The problem non-negative linear least squares is defined as the following:

Minimize $\|F\sigma - g\|$ subject to $\sigma \geq 0$

Here F is a given MXN sensitivity matrix and is a given data vector.

This problem always has a solution but it is non unique if the rank of is less than N .

The problem non-negative least squares is solved using the following Algorithm: [3-11]

On termination the solution vector satisfies

$$\sigma_j > 0 \qquad j \in p$$

$$\sigma j = 0 \qquad j \in z$$

And is a solution vector for the least squares problem

$$F_p \sigma \cong g$$

The dual vector satisfies

$$w_j = 0 \qquad j \in p$$

$$w_j = 0 \qquad j \in z$$

And

$$w = F^T (g - F\sigma)$$

Results

Based on the fact that real part of conductivity always has positive values we have applied non-negative least squares

MATLAB routines for different finite element meshes with different object positions. The algorithm of NNLS starts with a sets the possible basis vectors and computes the associated dual vector. It then selects the basis vector corresponding to maximum value in dual vector in order to

swap out of the basis an exchange for another possible candidate. This continues until the dual vector less than zero shown in figure 1 and 2. Used the negative sensitivity matrix so that a decrease in conductivity is shown as a positive change in the image.

Figure 3 shows the mesh consisting of 192 elements and the position of the object at the center and at the boundary. We modified this mesh into another mesh with the same elements of a different shape as shown in figure 4, to investigate how the shape affects the image but we obtained the same results.

Also we have used different meshes with different numbers centre of divisions to investigate how the center division number affects on the image reconstruction. The first mesh consist of 208 elements and more than four element divisions at the center as show in figure5 and the second one consists of 56 elements and more than four elements in the center as shown in figure 6 from these results we observe that the mesh with more than four central elements gives a better image than when a mesh with four central elements is used.

So it is clear that non-negative least squares using non-rotated data gives a solution but it is only applicable to certain meshes.

Such a solution is not a general one. Including rotated data provides a non-negative least squares solution for all types of meshes and a general results are obtained.

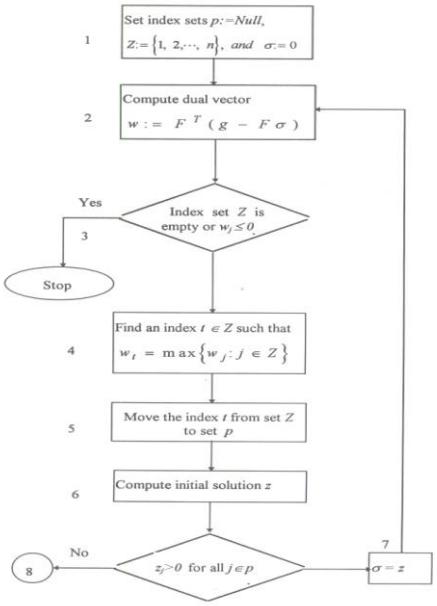

Fig 1 *Algorithm of NNLS*

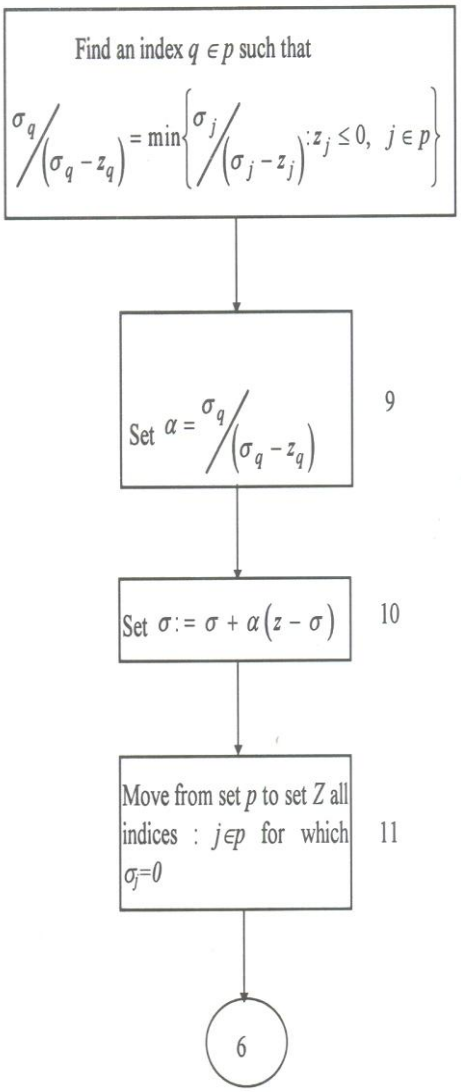

Fig 2 *Algorithm of NNLS* (last part)

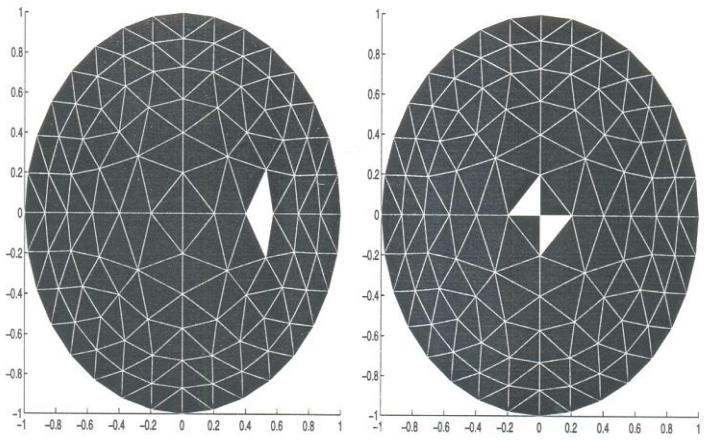

(a)

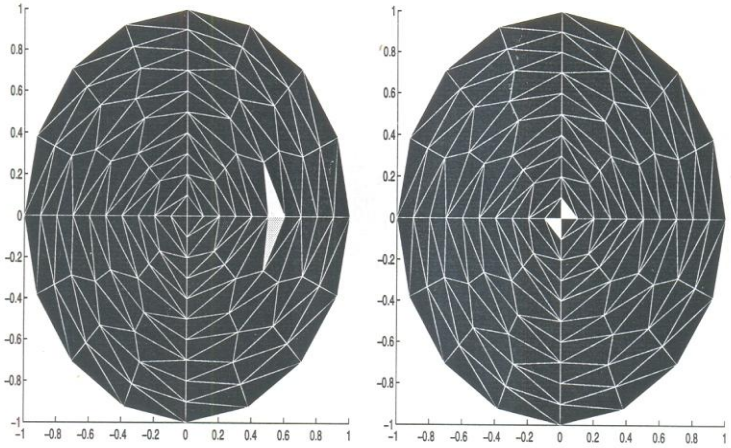

(b)

Fig 3 the object at the boundary and at the centre for different meshes: (a) 192 element (original shape) (b) 192 element modified shape

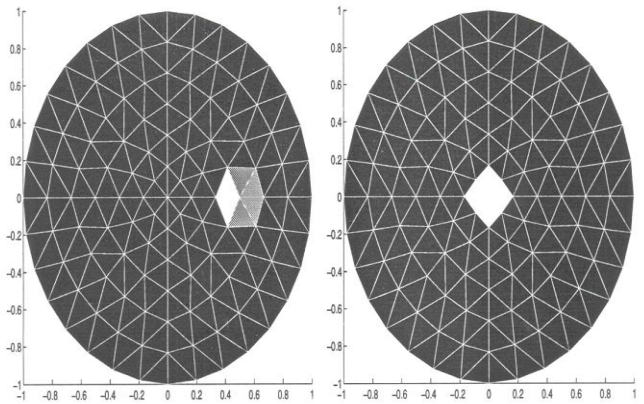

(a)

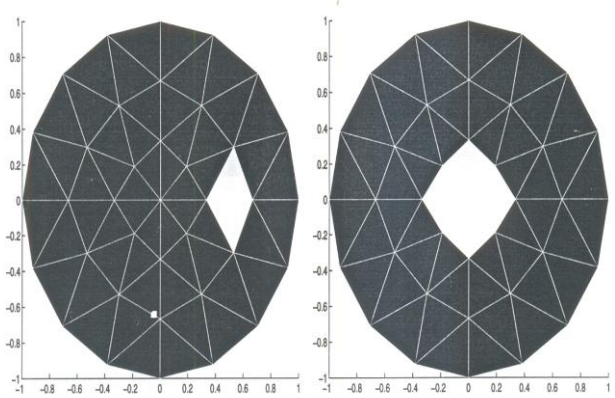

(b)

Fig 4 the object at the boundary and at the centre for different finite element meshes: (a) 208 element (b) 56 element

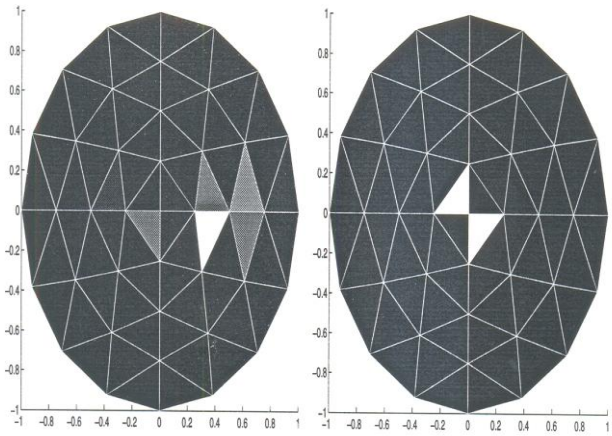

(a)

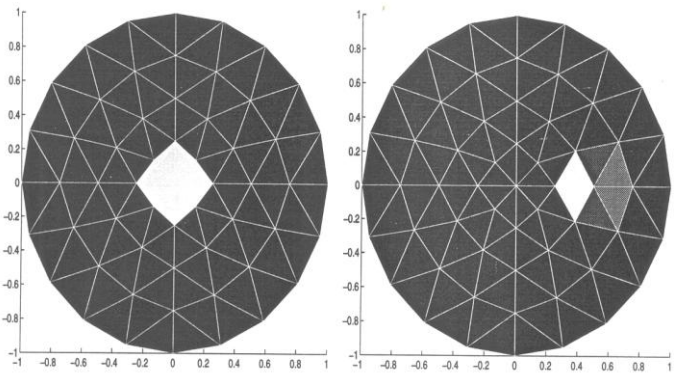

(b)

Fig 5 the object at the boundary and at the centre for different finite element meshes: (a) 64 element (b) 92 element

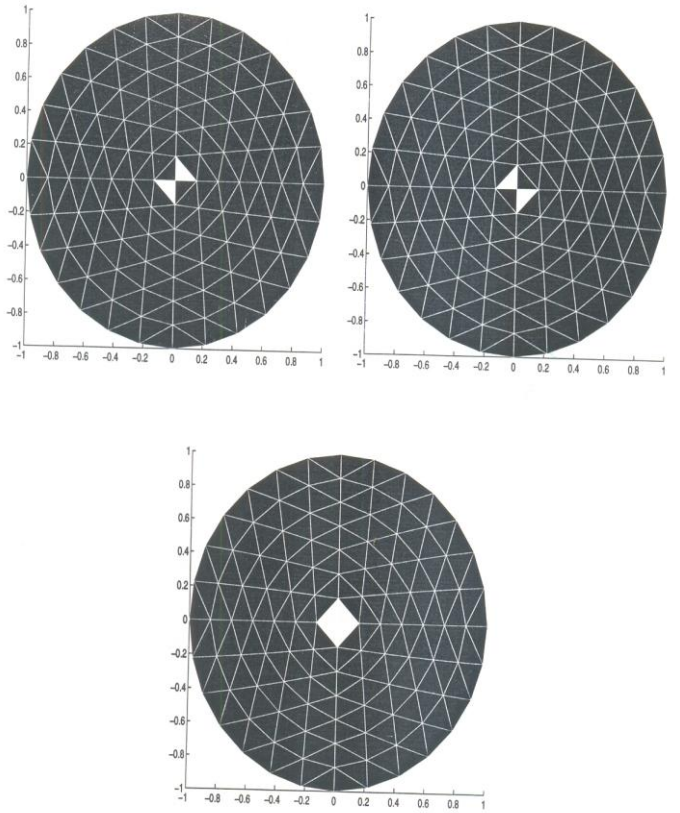

Fig 6 Final image obtained from rotated and non- data when the object at the centre

References

1. Barher D.C. and brown B.H. " *Electrical Impebancs Tomography*" special issue of clinical Physics . Meas.(preface), 1992
2. D.C. Barber and B.H Brown and I.L Freeston . "*Imaging spatial Distribution of Resistivity using Applied Potential Tomograph*". Electronics letters . vol . 19. pp.933-935, 1983.
3. Gill P.. Murrary w.. and Wright m, Practical Optimization .Academic press .London.UK. 1981.
4. James M..Smith G..Wlford J..1977. Appled Numerical methods for digtal Computation

with fortran and CSMP. Harper & Row . publishers . Inc.

5. John A. 1966, Numerical Analysis for computer, Reinhold . Publishing Corporation.
6. Lawson C. and Hason R, Solving least squares problems, prentice-Hall .Englewood Cliffs.1974.
7. Osborne E.. 1961. "*On least squares solution of Linear Equation*" J..ACM . vol .8. pp 628-636.
8. Peters G. and Wilkinson J.. 1970. "*The least squares problem and pseudoinverses* ." Comput . J..vol .13. pp 309-316.
9. Powell M, "*A survey of numerical methods of unconstrained optimization* ."SIAM Rev . vol 12. pp 79-97, 1970
10. Store J. "*On the numerical solution of constrained least squares problem* . "SIAM .J Numer .Ana.Vol.8. pp 382-411, 1971
11. William H..Brian P..sual A..and William T. Numerical Recipes (Fortran version). Cambridge University press, 1989.

Converting Binary Data To NRZ signal for RFID and Biomedical Applications

Gihad. A. Elamary, Member, IET, E.G. Chester

Abstract

In this work, we proposed a simple new circuit design to convert the binary data in to non return to zero (NRZ) signal. These techniques were applied in analogue modulation schemes for radio frequency identification (RFID) applications, and it may suitable for biomedical purposes. The proposed circuit steps down the input signal below a zero level by the value of $-V_{EE}$). The negative signal drives the transistor switch. The output of the switch provides a NRZ signal. The circuit has been designed for low power consumption and hand-held applications for biomedical purposes or RFID. Our proposed circuit has been simulated and evaluated by measurements of performance.

Keywords: NRZ, signal, RFID, security system, BPSK Modulator, Biomedical, Medical Health Care.

I. INTRODUCTION

RFID and Biomedical systems are wide by applied in wireless technology for communication between tags and reader. Modulated with analogue or digital schemes in near field, these technologies are rapidly applied today, for many applications such as wireless security systems, medical health care and implant sensors [1] [2] [3] [4]. Required for handle devices and low cost readers with high data rate, on the other hand the functionality is growing-up. The information data are transmitted and modulated with digital schemes such as BPSK, which has advantages over other schemes such as ASK or FSK [5]. The BPSK modulation has advantages which having a fixed carrier signal amplitude that provides a stable Wireless transfer power and independent data modulation [6]. However, this type of modulation needs a NRZ form signal, this technique is essential to convert the binary data into NRZ signal. To achieve a transition of the carrier (0, π), which is controlled by the input data, the BPSK signal can be represented mathematically in an analogue way as expressed in the equation (1). In addition, the data signal 'Data-input' m (t) has been generated by a PN sequence can be represented by Fourier series analysis as in equation (2) [7].

$$S_{BPSK}(t) = m(t)\sqrt{\frac{2E_b}{T_b}}\cos(w_{rf}t + \theta_{rf}) \quad (1)$$

$$PN(t) = \sum_{-\infty}^{\infty} c_n p(t - nT_c) \quad (2)$$

Where $m(t) = PN(t)$

Our purposed circuit has been interfaced to the modulator to provide a BPSK signal as demonstrated in Fig. 1.

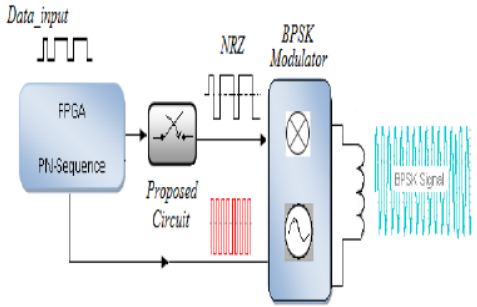

Figure 1: the proposed circuit with BPSK Modulator.

In practice the binary data m (t) is converted to a NRZ signal that maps the logic‘0’ to -1V (nominal) and the logic ‘1’ to +1V. This data signal has controlled the transition shift (0, π) for the carrier frequency signal, as shown in Figure 2.

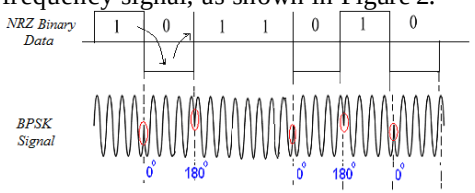

Figure .2 illustrates the BPSK waveform with respect to (NRZ) data state.

II. Theory Method Of The Circuit

The theory of the proposed circuit has been analysed and the principle of the pulse signal has been demonstrated in the block diagram has shown in Fig. 3. The mathematical analysis can be expressed in the equations that for the input and output data signals [8], [9]. The input pulse signal can be expressed in equation (3) with Fourier series analysis, and in the equation (4) is presented the processing of the inverter circuit of the square signal output.

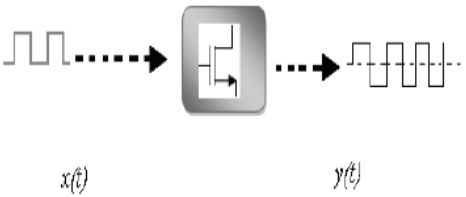

Figure 3: the block diagram of the NRZ convertor signals.

$$z(t) = \frac{2V}{\pi} \sum_{n-1}^{\infty} \sin(2\pi ft) \quad (3)$$

$$y(t) = \frac{4V}{n\pi} \sum_{n=odd}^{\infty} \frac{1}{n} \sin(2\pi ft) \quad (4)$$

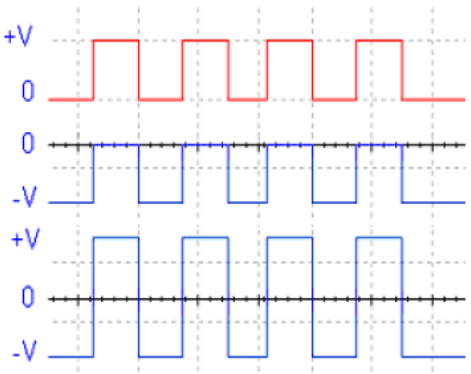

Figure 4: the waveforms of the pulse processing signals.

The external circuit been used as the input data source which generates a PN sequence, feed to clock driver circuit as booster for the output pulse signal, then inverted by the Inverter. After that it is stepped down to the negative level by Switched Capacitor Voltage Converter. The signal controlled the

gate of MOSFET-Transistor. The transistor is working as switch element in the circuit which combines the positive and negative pulse signals for performing the squared output signal. This output is applied in to the BPSK modulator, the output is filtered for transmission.

III. PROPOSED CIRCUIT DESCRIPTION

The proposed circuit has been demonstrated in Fig. 5. Generally it divided in to two parts. The first part is the external data source and clock driver, the second part is the inverter and the switch circuits. The control switch circuit consists of the integrator that is controlled by the negative voltage for step down the level of data signal as illustrated in Fig. 6. The negative pulse has driven the transistor switch for select the positive and negative pulses. In addition, the capacitor is used to blocking DC bias voltages.

However, the switch capacitor DC-DC voltage converter is capable for converting the positive DC voltage input (+V) to corresponding negative DC voltage (-V). The suitable package C7660 is used to work with the range (-1.5V) to (-10V) with low power consumption (200µA) from National semiconductor [10]. In practice, additional circuit has been modified to adjust the DC bias from (-0.5 V to -5V) to drive the integrator RC circuit (C, R3) to the right level.

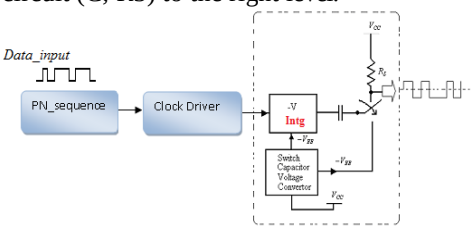

Figure 5: the proposed diagram for the converter binary data in to NRZ signal.

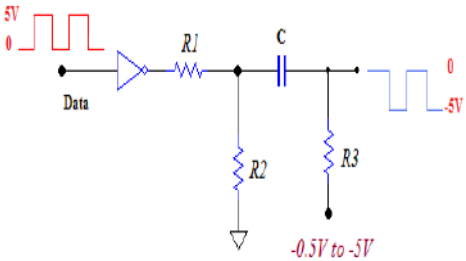

Figure 6: the level shifter circuit for driven the DC bias up to -5V

IV. SIMULATION CIRCUIT FOR NRZ

The proposed system design shown in Fig.5 has been simulated and evaluated to perform the NRZ signal; which is generating a bipolar signal as data source. The simulation results for the circuit have provided a square signal from the pulse signal as shown in Fig. 7. This is illustrated as the CH1 is presented the input data signal at 125Kbps, and the CH2 is presented the negative pulse signal. Finally the CH3 illustrates the square output signal. The circuit has been simulated with different frequencies to evaluate the performance of the circuit when tested up to 3Mbps over carrier frequency 13.56 MHz. The algorithm of the PN-sequence has been synthesized in VHDL code, there are many techniques can be implemented for generate the code sequence [11], which is used as data source either in reader part or tag and implant device, that simulates the command information. However, the PN sequence has been synthesised by VHDL code using Altera development kit [12].

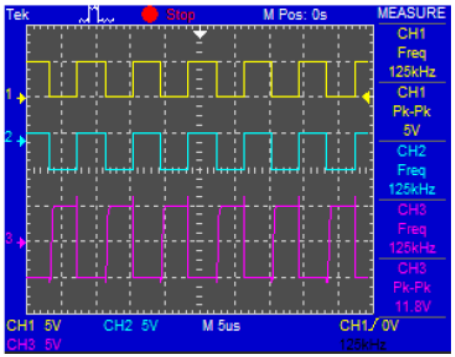

Figure 7: The simulation result of proposed circuit.

The waveform result has been demonstrated in Fig. 8. Where the block diagram of this code has been illustrated in Fig.9.

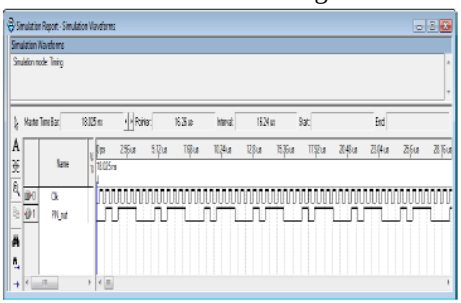

Figure 8: The simulated PN sequence by VHDL code.

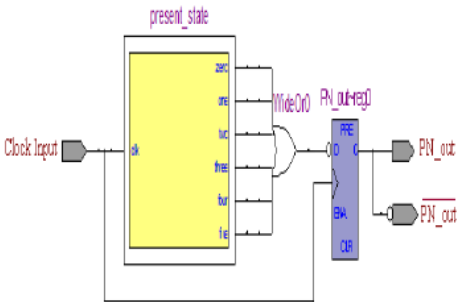

Figure 9: The block diagram of PN sequence generated By VHDL code.

V. EXPERIMENTAL RESULTS

The prototype circuit in Fig. 9 has been implemented and evaluated experimentally to generate a square bipolar signal. The data source has been synthesized with different clock frequencies using PN sequence signal. In our work we generated the PN signal by VHDL code. In addition, the desired carrier 13.56 MHz has been programmed by VHDL code. The lab setup measurements for our proposed circuit have been illustrated in Fig. 10. The first measurement result for the circuit has been performed for stepped down integrator RC as shown in Fig. 11, obviously the top CH1 is presented the input pulse signal; where the CH2 is presented the step down output signal.

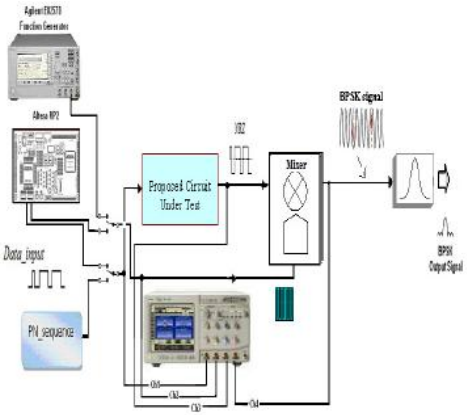

Figure 10: Lab setup test measurements for the proposed circuit Figure 11: The input pulse signal and step down pulse signal.

The second measurements have performed for the proposed circuit, which illustrated in Fig. 12, at data rate 256Kbps. However, the circuit has been tested up to 2.5Mbps.

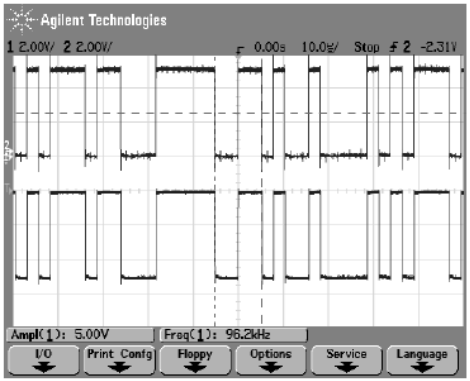

Figure 11: The input pulse signal and step down pulse signal.

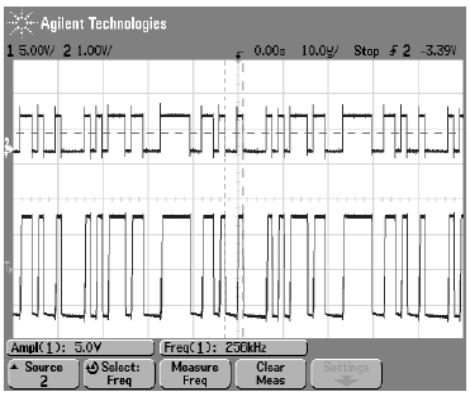

Figure 12: the output measurement results for NRZ signal.

VI. CONCLUSION

In this paper, we have demonstrated a new simple circuit design for generates the NRZ signal from binary data. It used control of the switch transistor (ST) to produce a square signal. The data are inverted and followed by negative circuit which consists of a passive integrator feed with negating voltage.

The switch transistor is clocked by negative pulse for selecting between positive and negative voltages. The output of the ST is a squared signal 'Bipolar base band digital signal'. Generally, we focus in this work to design a simple circuit for hardware implementation and low consumed power, which is able to work with battery. Conversely, the PN sequence has been carried out with VHDL using CPLED (EPM3064) as a part of the reader unit, to reduce the hardware. Finally the circuit can be working with higher frequency in microwave, when design in CMOS technology.

REFERENCES

[1] Klaus. Finkenzeller. 1999 "Fundamentals and application In contact less smart cards" Identification 2nd Edition ,2004,PP.61-159

[2] Cangialosi. A., Monaly. J. E,Yang. S. C. "Leveraging RFID in Hospitals: Patient life cycle and mobility perspectives" Communication Magazine, IEEE,Volume:45,Issue:9.2007,PP. 18-23

[3] Lahtela. A., Hassinen. M, Jylha.V "RFID and NEC in Healthcare: safety of hospitals medication care"PervasivelHealth.2008 IEEE.PP:241-244

[4] S. Huang, G. Horng, G. Jong "Intelligent Hospital Space Platform Combined with TFID and Wireless Sensor Network" IIH-MSP-2008.IEEE

[5] S. Sonkusale, Z. Luo "A complete Data and Power Telemetry System Utilizing BPSK and LSK signaling for Biomedical Implant "IEEE, 30th EMBS,2008

[6] Gihad. Elamary, Graeme. Chester, Jeff. Neasham "Experimental Digital BPSK Modulator Design with VHDL Code for Biodevices Applications" (251-255) BIOSTEC. Porto-Portugal, 14/17.01.2009 -IEEE.

[7] R. N. Mutagi "Pseudo noise sequences for engineering ".electronics & communication engineering journal. April 1996

[8] TAUB SCHILLING "Principle of Communication System". Pp 249~298

[9] SYED A. NASAR, HYGH.C.MADDOCKS "3000 solved problems in Electronic Circuit" Ed. New York: McGraw-Hill 1988, PP. 231-303

[10] Data sheet for the DC-DC convertor Available: http://www.national.com/mpf/LM/LMC7660.ht ml

[11] http://ieeexplore.ieee.org/iel5/7180/19335/00893288.pdf("IEEE standard VHDL Language Reference Manual").

[12] www.altera.com/literature/univ/upds.pdf (UP2-educationa board datasheet).

Modelling and Control Immune System against Simple Viruses

Fatma A. Alazabi [1] *Prof. Mohamed Zohdy* [1] *Zineb A. Alazabi* [2]
1. School of Electrical and Computer Engineering, Oakland University , Michigan, U.S.A

2. School of Electrical and Electronic Engineering, Alfateh University , Tripoli, Libya
.
e-mails:
faalazab@oakland.edu zohdyma@oakland.edu Zineb_alazzabi@yahoo.com

Abstract:
A new simple immune system model is proposed. The model presents the population of simple viruses, uninfected cells and infected cells with immune system effect (T cells & B cells). The comparison between this new model and other models is demonstrated. It's shown that it provides a proper model. Also, it gives good results in comparison.

Key words: Immune system, B cells & T cells, Biological modeling.

Introduction:
The human immune system has to cope with a lot of challenges both externally and internally. The major role is to defend the host against infections, a task that is clearly essential to any organism. At the same time, the immune system must create a tolerance to the recognition of "self " , recognize and fight any foreign invader, but it should not overreact, since inadequate responses may lead to adversity [1 2].
Part of the immune system, known as the adaptive immune system, has the ability to adapt to specific microbes and remember them so that it can react more efficiently if it encounters the same threat again. The adaptive immune system is mainly composed of T and B lymphocytes. In the humoral immune response, the B lymphocytes are activated to produce a soluble form of their antigen receptors called antibodies. Antibodies neutralize their target (the antigen) by binding to it. The cellular immune response is generated by T lymphocytes, which recognize fragments of proteins (peptides) expressed on the surface of the host cells. The peptides are bound to the Major Histocompatibility Class I (MHC I) and Class II (MHC II) molecules. The cytotoxic T lymphocytes (CTL) will kill infected cells that present non-self peptides bound to MHC I. The helper T lymphocytes recognize non-self peptides presented on MHC II, become activated, and generate cytokines that will skew the immune system towards more humoral or cellular responses. Both CTLs and B cells need this helper component to become fully activated [3].

Modelling the immune system:

1) Modelling population of the Virus, uninfected & infected cell without immune system effect:

- To model this we will use three equations where ***V*** is the number of virus particles, ***X*** is the number of uninfected cells, and ***Y*** is the number of infected cells [4]:

$$\frac{dV}{dt^*} = aY - bV$$

$$\frac{dX}{dt^*} = c - dX - \beta XV$$

$$\frac{dY}{dt^*} = \beta XV - fY$$

- In this system, ***b, d, and f*** are the death rates of viruses, uninfected cells and infected cells respectively .
- The terms ***a and c*** are the production rates of viruses and uninfected cells.
- The term ***βXV*** is the rate of infection.

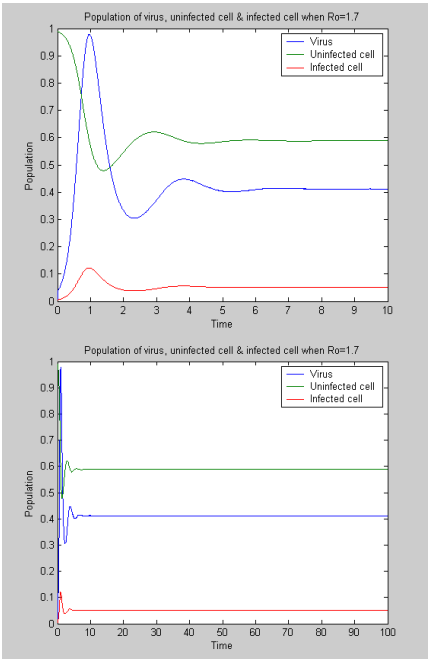

After substitution:

$$v = \frac{bf}{ac}V, x = \frac{d}{c}X, y = \frac{d}{c}Y, t = dt^*$$

We finally get:

$$\frac{dv}{dt} = \frac{\alpha}{\varepsilon}y - \frac{1}{\varepsilon}v$$

$$\frac{dx}{dt} = 1 - x - R_0 xv$$

$$\frac{dy}{dt} = R_0 xv - \alpha y$$

Where:

$$\alpha = \frac{f}{d}, \varepsilon = \frac{d}{b}, R_0 = \frac{\beta ca}{dbf}$$

R_0 *is called reproduction ratio of virus.*

- In the first case, we use the initial condition v(0)=0.005, x(0)=0.99, y(0)=0.005, and the parameters α=8, ε =0.00556, and R_0=1.7.
- In the second case, we use the initial condition v(0)=0.005, x(0)=0.99, y(0)=0.005, and the parameters α=8, ε =0.00556, and R_0=0.8.

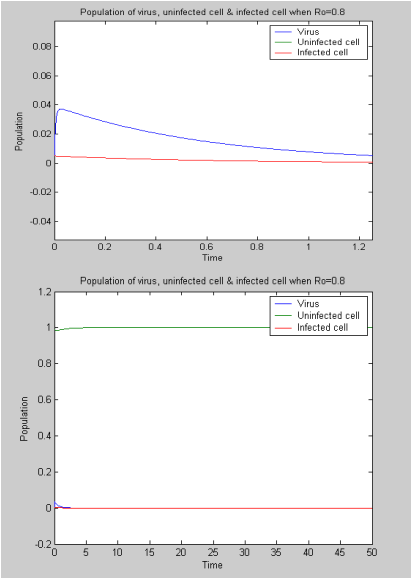

2) Modelling population of the virus, uninfected & infected cell with immune system effect (T cell effect:)

- To model this we will use four equations where V is the number of virus particles, X is the number of uninfected cells, and Y is the number of infected cells, T the number of T cells [4]:

$$\frac{dV}{dt^*} = aY - bV$$

$$\frac{dX}{dt^*} = c - dX - \beta XV$$

$$\frac{dY}{dt^*} = \beta XV - fY - \gamma YT$$

$$\frac{dT}{dt^*} = g - hT$$

- In this system, b, d, f, and h are the death rates of viruses, uninfected cells , infected cells and T cells respectively.
- The terms a , c and g are the production rates of viruses , uninfected cells and T cells.

- γYT is the rate at which the immune system (T cells) kills the infected cells.
- The term βXV remains the rate of infection.

After substitution:

$$v = \frac{bf}{ac}V, x = \frac{d}{c}X, y = \frac{d}{c}Y, t = dt^*, T_c = \frac{h}{g}T$$

$$\frac{dv}{dt} = \frac{\alpha}{\varepsilon}y - \frac{1}{\varepsilon}v$$

$$\frac{dx}{dt} = 1 - x - R_0 xv$$

$$\frac{dy}{dt} = R_0 xv - \alpha y - kyT_c$$

$$\frac{dT_c}{dt} = \lambda(1 - T_c)$$

Where:

$$\alpha = \frac{f}{d}, \varepsilon = \frac{d}{b}, k = \frac{\gamma g}{dh}, \lambda = \frac{h}{d}, R_0 = \frac{\beta ca}{dbf}, R_0^* = \frac{R_0\alpha}{(\alpha + k)}$$

R_0^* is called new reproduction ratio of virus.

- In the third case, we use the initial condition v(0)=0.005, x(0)=0.99, y(0)=0.005, Tc(0)= 0.3 and the parameters α=8, ε =0.00556, R_0=1.5, , k=0.1, and R_0^*=1.48.

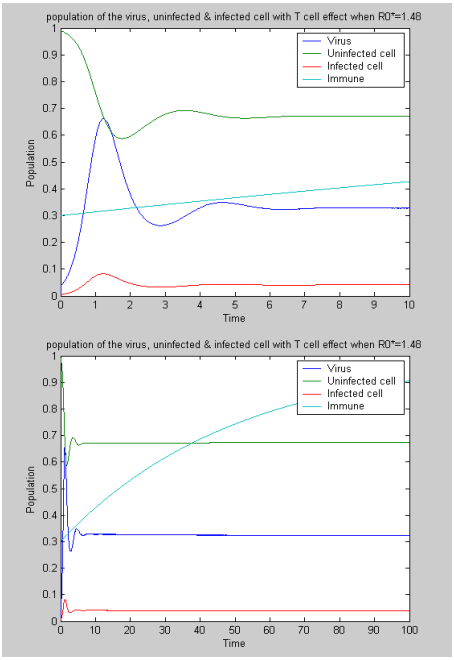

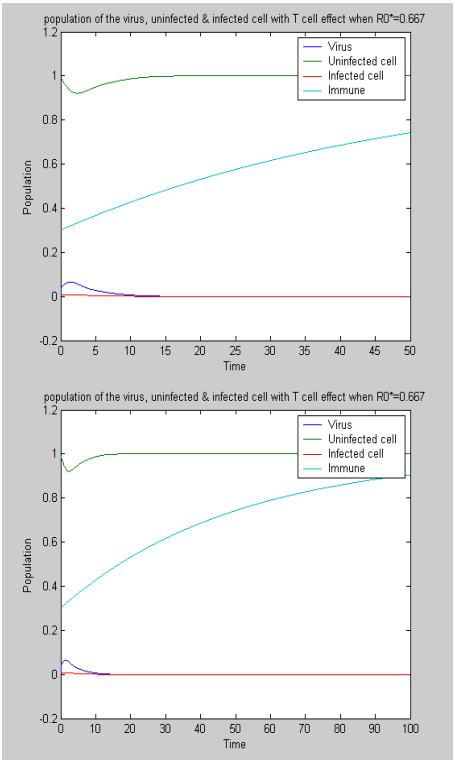

- *In the fourth case, we use the initial condition v(0)=0.005, x(0)=0.99, y(0)=0.005, Tc(0)= 0.3 and the parameters α=8, ε =0.00556, R_0=1.5, , k=10, and R_0*=0.667.*

$$\frac{dV}{dt^*} = aY - bV$$

$$\frac{dX}{dt^*} = c - dX - \beta XV$$

$$\frac{dY}{dt^*} = \beta XV - fY - \gamma YT - \mu YB$$

$$\frac{dT}{dt^*} = g - hT$$

$$\frac{dB}{dt^*} = e - LB$$

3) Modelling population of the Virus, uninfected & infected cell with immune system effect (T cell effect & B cell effect) ' New model'

- To model this we will use five equations where *V* is the number of virus particles, *X* is the number of uninfected cells, and *Y* is the number of infected cells, *T* the number of T cells, *B* the number of B cells :

- In this system, ***b, d, f, h and L*** are the death rates of viruses, uninfected cells , infected cells , T cells and B cells respectively.
- The terms ***a*** , ***c*** , ***g and e*** are the production rates of viruses, uninfected cells , T cells and B cells respectively.

- γYT is the rate at which the immune system (T cells) kills the infected cells.
- μYB is the rate at which the immune system (B cells) attacks the infected cells.

After substitution:

$$v=\frac{bf}{ac}V, x=\frac{d}{c}X, y=\frac{d}{c}Y, t=dt^*, T_c=\frac{h}{g}T$$

$$B_p=\frac{L}{e}B$$

$$\frac{dv}{dt}=\frac{\alpha}{\varepsilon}y-\frac{1}{\varepsilon}v$$

$$\frac{dx}{dt}=1-x-R_0xv$$

$$\frac{dy}{dt}=R_0xv-\alpha y-kyT_c-myB_p$$

$$\frac{dT_c}{dt}=\lambda(1-T_c)$$

$$\frac{dB_p}{dt}=\delta(1-B_p)$$

Where: $\alpha=\frac{f}{d}, \varepsilon=\frac{d}{b}, k=\frac{\gamma g}{dh}, \lambda=\frac{h}{d}, \delta=\frac{L}{d}, m=\frac{\mu e}{dL}, R_0=\frac{\beta ca}{dbf}, R_0^*=\frac{R_0\alpha}{(\alpha+k+m)}$,

R_0*is called newer reproduction ratio of virus.

- In the fifth case, we use the initial condition v(0)=0.005, x(0)=0.99, y(0)=0.005, Tc(0)= 0.3, Bp(0)=0.2 and the parameters α=8, ε =0.00556, m=1.5, R_0=1.5 ,k=0.1and R_0*=1.25.

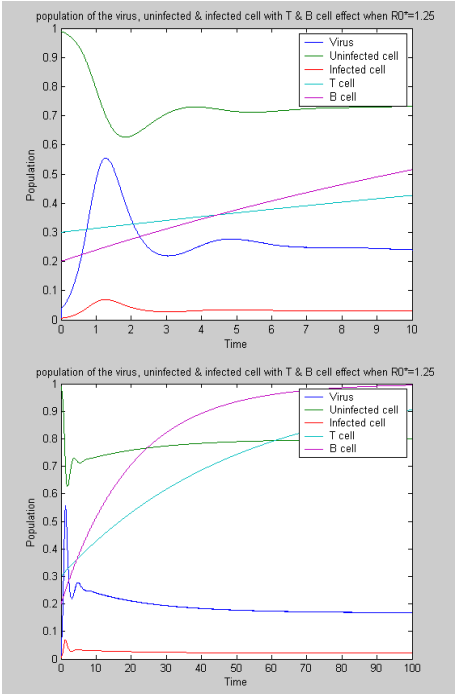

- In the sixth case, we use the initial condition v(0)=0.005, x(0)=0.99, y(0)=0.005, Tc(0)= 0.3, Bp(0)=0.2 and the parameters α=8, ε =0.00556, m=1.5, R_0=1.5, , ,k=10 and R_0*=0.615.

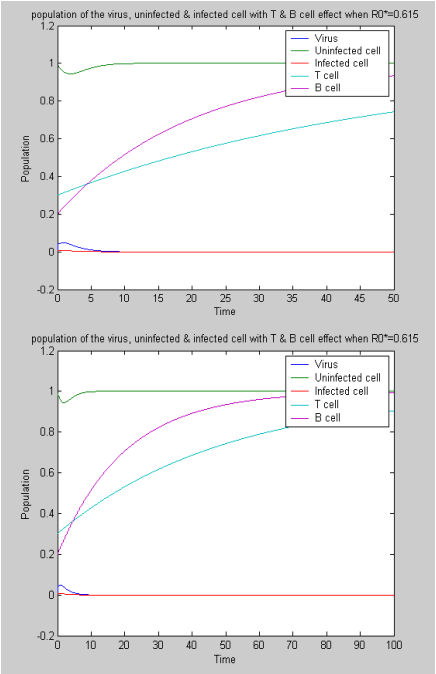

Conclusion:

In this paper, a new yet simple immune system model is proposed.. It's response is compared by Matlab simulation to illustrate the control effect of B & T cells submodels. The population of the virus is further decreased and population of the uninfected cell is increased by using these control effects.

In future, we will examine interacting B & T cells, application of nonlinear theory to make our model more realistic and use experiment data to refine model structure and parameters.

References:

1. Holmdahl, R., Bockermann, R., Backlund, J., Yamada, H.: The molecular pathogenesis of collagen-induced arthritis in mice - a model for rheumatoid arthritis. Ageing Res. Rev. , 135–147 (2002).

2. Burroughs, N.J., de Boer, R.J., Kesmir, C.: Discriminating self from nonself with short peptides from large proteomes. Immunogenetics 56, 311–320 (2004).

3. Nicolas R. , Can K., Sune F., Morten N., Claus L., Søren B., Ole L.: Modelling the human immune system by combining bioinformatics and systems biology approaches. J Biol Phys (2006) 32: 335–353.

4. Nicholas E.Britton: Essential Mathematical Biology, 2003.

Paper NO. 103325
Optical Density Measurements On The Examination of Colon Cancer Tissues

Rebah Emhmed Touati[1], Khaled A Sayeh Marghani[2], Tawfik Taher Ajaal[1]

[1] Department of Physics , The Academic for Higher Studies, and

Physics, Faculty of Science, University of Al-Fateh, Tripoli-Libya. [2]Department of

corresponding author: rbh_twaty@yahoo.co

Abstract:

Automated quantitative image analysis can help in cancer diagnosis and prognosis and, in general, optimize medical treatments managements and improve routine medical diagnosis. Early diagnosis can make big difference between life and death. Microscopic images from two tissue types, forty- four normal and fifty-eight cancers, was evaluated based on their ability to identify abnormalities in colon images. Optical density approach was applied to extract parameters that show cancer behavior on colon tissues images. Using statistical toolbox, a significant result of ($p<0.0001$) for the mean and the variance of the optical density parameter were detected, and only ($p<0.001$) for skewness optical density. Based on linear discrimination method, the obtained result shows 90 % accuracy for both sensitivity and specificity, and with an overall accuracy of 90 %.

Note:
This paper is included in the conference program but not published because the revised copy after introducing the reviewed comments did not arrive in the specified Time

Chapter VI

Education and Training in EE

Knowledge Management Model for Future Engineering Education

Niranjan Shrivastava, Santosh Kumar Henge, Laxmikant Ramakrishna
Department of Electrical & Electronic, Faculty of Engineering, Al-Tahadi University, Sirte, Libya

Email: nirshri@gmail.com, hingesanthosh@gmail.com, lux_rcr1@rediffmail.com

Abstract

In this research paper the author focuses on modeling of an interactive online educational infrastructure by introducing four major modules forming the Knowledge-Management (KM) module, Client/ Server applications (CS) module, Group Information Sharing (GIS) module, and an Interactive Workflow (IW) module. New technology tools like Internet/ Web/ Multimedia-based technology breakthroughs and accelerated availability of wide-bandwidth resource tools, for preparing Modern, Scientific, and Knowledge-based educational materials, present a unique opportunity to boost up the academic rigor and quality of modern education. Thus resulting in, increased participation, keeping in view of learner interest, it is exploring avenues for optimizing distance and time independent learning Delivery and Adaptive models. The present paper discusses the different types of block processes and procedures in support of each of these modules reflect different features of the online interactive enterprise. Proposed KM module is comprised of different types of knowledge associated with online educational infrastructure and different KM lifecycle components.

Key words: *Knowledge Management, Client/ Server, Group Information Sharing, Interactive and Adaptive Workflow.*

Introduction

New web-based technology breakthroughs and accelerated availability of wide-bandwidth tools and resources for preparing multimedia educational materials present a unique opportunity to boost academic rigor and quality of modern education, increase student interest and participation, and explore avenues for optimizing distant-learning delivery models.

This research focuses on modeling of an interactive online educational infrastructure (OEI) by introducing four major modules forming this OEI:

a) Knowledge Management (KM) module,
b) Client/Server Applications (CSA) module,

c) Group Information Sharing and Collaboration (GISC) module, and
d) An Interactive Workflow (IW) module.

The architectures, processes and procedures in support of each of these modules reflect different features of the online interactive enterprise and are used for assessment of the OEI outcomes.

Proposed KM module is comprised of eight types of knowledge associated with OEI, such as tacit, explicit, descriptive, procedural, reasoning, linguistic, presentation, and assimilative types, and of six KM lifecycle components, such as relevant knowledge reaction, capturing, refining, storing, managing, and disseminating.

Interactive Online Educational Infrastructure

- KM Module
- CSA Module
- GISC Module
- IW Module

The CSA module is mapped into the three major blocks:

- Inquiry applications (via the data/information repositories),
- Transaction-oriented services and applications (via access gateways and other web-based processors), and
- Consultative sessions (available through Internet, pagers, wireless phones, and web-enabled call centers).

These applications merely focus on supporting and automating different OEI processes and would provide limited contributions to the KM enterprises. The GISC module formalizes an Internet enabled support for all types of interactions between an online instructor and each student as well as between students themselves through utilization of readily available on the market GSS (Group Support Systems) software, such as information sharing, discussion groups, web collaboration, application sharing, and electronic brainstorming.

Knowledge Management Module of an Interactive Online Educational Infrastructure

Evolution of any profession has always been affected by the progress in science, applicable tools, standards, methodologies, and new discoveries. At the same time, technology and engineering fundamentals have been, are and always will be essential in supporting any progress in those and closely related fields.

Thus, it seems reasonable to suggest that a mission of a novel online model for modern education should focus on optimized knowledge management to maintain and balance two major types of technology and engineering knowledge:

o **Tacit knowledge** (technology and engineering expertise; design; know-how; engineering ethics, engineering values, and cultural aspects of technology and engineering profession; skills and collaborative teaming) and

o **Explicit knowledge** (technology and engineering fundamentals, major contributions to the particular field of engineering profession, technology and engineering standards, patents, established practices and successful engineering developments).

Optimized knowledge management structure includes two major blocks:

Technology and Engineering Knowledge Types block and Knowledge Lifecycle block.

Knowledge Management for Technology and Engineering Profession

- Explicit Technology and Engineering Knowledge

- Tacit Technology and Engineering Knowledge

In turn, **Technology and Engineering Knowledge** Types block might include:

- **Factual knowledge** (concerned with an accumulated wealth of past, present, future, orexpected topics associated with *what* in engineering),
- **Actionable knowledge** (concerned with processes and procedures essential in each engineering field for knowing *how*),
- **Judgmental knowledge** (concerned with knowing *why* in assessing complex engineering developments),
- **Communication knowledge** (concerned with means of communication with project teams, administration, standard-developing organizations, competition, government agencies, vendors, suppliers, research entities, manufacturing departments, and non-engineering supporting services),
- **Semantics knowledge** (concerned with interpreting contextual meaning of communication related to a new knowledge), and
- **Incorporative knowledge** (concerned with maintaining the engineering knowledge base current by improving on existing knowledge and thus optimally maintaining balance between the legacy and newly developed elements on knowledge in each particular engineering field).

Knowledge Lifecycle

- Technology and Engineering Knowledge Types
- Factual Knowledge
- Actionable Knowledge
- Judgmental Knowledge
- Communication Knowledge
- Incorporative Knowledge
- Semantics Knowledge

Examples for the particular field of Electrical and Electronic Engineering would include such Interactive Tutorials as "Advanced Instrument Control with LabVIEW", "Fast Fourier Transform", "Simulation Interface Toolkit", "Machine Vision and Scientific Image Processing", "Eliminating Accuracy Errors with Self-Calibration", etc. These particular interactive tutorials (offered by National Instruments1 and other providers) would be linked (through the required licensing agreements) with the database of the proposed interactive online model.

For the proposed Factual Knowledge subset, linkage to the well established web repositories might substantially increase effectiveness of the proposed model. One of the options might be the GlobalSpec2 web site with such categories as "Sensors, Transducers and Detectors", "Laboratory Equipment and Scientific Instruments", "Networking and Communication Equipment", "Industrial Maintenance", etc.

In the wide variety of technology, communications, information systems, and engineering professions, keeping students and professionals current in their field(s) of expertise becomes an issue of competitiveness and employability. That is why a cycling approach in maintaining a good knowledge management system is so

important: knowledge must be periodically updated to reflect changes in the relevant engineering and technology fields.

To this extent, a technology and engineering knowledge management lifecycle is suggested to include the following phases:

o **Relevant Knowledge generation** (new developments, new designs, new conceptual, logical, hardware and software introductions and implementations),

o **Knowledge assessment** (new and generated knowledge should be properly assessed and identified as valuable, relevant and be expressed in a reasonable format),

o **Knowledge stratification** (new knowledge must be analyzed to distribute it between the tacit and explicit domains),

o **Knowledge accommodation** (concerned with logistics of storing new knowledge in formats, locations and groupings for convenient access), and

o knowledge **currency update** (continued evaluation and verification of accuracy and relevancy of engineering knowledge).

Client/Server Applications Module

The Client/Server Applications module can be broken into the three major blocks:

- **query applications** (via data/information repositories),
- **online analytical processing** and transaction-oriented applications (via access gateways and other Web-based processors), and
- **collaborative** applications (available through Internet, pagers, wireless broadband services,and Web-enabled call centers).

It should be noted that inclusion of the collaborative applications block stems from the necessity toprovide enough support for meaningful and expedient exchange of information and ideas globally,
effectively and efficiently.

Group Information Sharing Module

The GIS module's objectives include utilization of readily available on the market Group Support
Systems groupware, such as information sharing, Web collaboration, application sharing, and electronic brain storming. With a background of currently available wireless technologies, special emphasis could be made on utilization of wireless Internet-based broadband access opportunities offered by different telecommunication carriers. For example, in USA the telecom companies such as Verizon, Sprint, T-Mobile, Singular, and AT&T start offering the broadband Internet access services that are reasonably priced, seamless, available anytime, anywhere (within continental USA), with high speeds of 300-500 Kbps (thousands of bits of information per second), reliable and appropriately
secured with an authentication and data protection support.

Interactive Workflow Module

Since the proposed online interactive infrastructure represents yet another example of a system model, then a concept of *modeling* should be inherent throughout its design and development stages. Thus, modeling might represent several conceptual perspectives; in case of the proposed online educational infrastructure, those perspectives might include three online educational engines:data oriented, process oriented, and time-dependent (emphasizing the dynamic nature of the data and information flow).

For example, for an online delivery of a course in Information Systems Methodologies, the Data Oriented perspective might concentrate on the following aspects:

- business data,

- logical database design,
- data taking into account construction tools to be used, and
- data taking into account construction design.

On the other hand, a Process Oriented perspective could be broken down conveniently into three distinct aspects:

- Activity performed in business area,
- User perceivable task, and
- Client/Server Applications Module
  - Query Applications
  - Online Analytical Applications
  - Collaborative Applications
- Construction design stage.

Finally, the time-dependent perspective (sometime called as behavioral oriented perspective) could be broken into four aspects, such as:

- event occurring in a business area,
- information system event,
- triggering condition, and
- initiation of transaction.

The first of these would address the MIS business analysis stage, the second and third would be related to the MIS system design stage, and the last would be associated with the construction design stage.

Conclusion :

Knowledge Management dealing with both business and engineering/technology issues. The latter ones included the topics in web development and design, database conceptual and logical design, engineering, and information technology competencies. Relevance of this experience to the proposed Online Interactive Model stems from the fact that in both instances – online transactional processes defining Electronic Business and Online Educational Infrastructure – dynamics, global nature of collaboration and competitiveness dominate and define the measure of success or even survival.

Bibliography

1. http://www.ni.com/events/tutorials/campus.htm
2. http://www.globalspec.com
3. www.worldwidelearn.com/continuing-education/engineering-cpe.htm

References

1. Alavi M., and Leidner D.E., (2001). “Review: Knowledge Management and Knowledge Management Systems: Conceptual Foundations and Research Issues”, MIS Quarterly, 25(1),Pp. 107-136.
2. Chantarasombat C., and Srisa-ard B., (2007). “Developing a Knowledge Management Modelfor Community Self-reliance”, Mahasarakham, Mahasarakham University, Education Journalof Thailand, 1(1), Pp. 83-94.
3. Churchman C., W., (1979). “The Systems Approach (revised and updated)”, New York: DellPublishing.
4. Davenport T.H., and Prusak L., (1998). “Working Knowledge”, Harvard Business SchoolPress,
5. Faculty of Education, (2006). “Faculty of Education Strategic Plans, 2006-2009”, Faculty ofEducation, Mahasarakham University.
6. Holsapple C.W., and Joshi K.D., (2004). “A Formal Knowledge Management Ontology:Conduct,

Activities, Resources, and Influences", Journal of the American Society forInformation Science and Technology, 55 (7), Pp. 593-612.
7. Nonaka I., and Takeuchi H., (1995). "The Knowledge-creating Company: How JapaneseCompanies Create the Dynamics of Innovation", New York: Oxford University Press, Pp. 20-25, 71-72.
8. Jennex M. E., (2005). "What is Knowledge Management?", The International Journal of Knowledge Management, 1(4), Pp. i-iv,
9. Kuofie M.H.S., (2005). "E-Management: E-Knowledge Management for Optimizing RuralMedical Services", The International Journal of Management and Technologies, 1(1), Pp. 37-50.
10. Office of Educational Standards Certification and Quality Assessment, (2007). "A Draft of a report on Results of External Quality Assessment in Round 2, Mahasarakham University",Office of Educational Standards Certification and Quality Assessment, Pp. 5,32-33.
11. Phanich Vicharn, (2005). "Know Management, a Practitioner Version", Bangkok Institute ofKnowledge Management for the Society (IKMPS), Pp. 1-4, 23-48.
12. Sinlarat P., (1998). "Principle and General Higher Education", Bangkok: ChulalongkornUniversity, Pp. 24-24.
13. Thinnalak Y., (2006). "Riddles of Local Wisdom", Bangkok: Withithat Institute, Pp. 1-17.
14. Yeamsang T., and Srisar-ard, B., (2007). "Developing a Knowledge Management Model of the Office of Mahasarakham Educational Service Area Zone 1", Proceeding The 1st InternationalConference on Education Reform 2007, Mahasarakham, Mahasarakham University, Pp. 225-234.
15. Wasi Prawet, (2002). "The Intelligence Network", Bangkok: Design, Pp. 21,
16. Wiig K., (1993). "Knowledge Management Foundations", Arlington, Texas: Schema Press, Pp.39-51.

An Assessment Study and the Design of E-learning System Strategy in Computer Science Department of Sirte University

Melvin Ballera
Sirt University
maballera@yahoo.com.ph

Ziyad Hazim Abid Jabbar
Sirt University
ziyadha68@hotmail.com

Abstract: In light of the great flood of information, change, and tremendous growth of development of knowledge, it has become necessary to think and adapt new technique in educating and training people through the use of global information network; the e-learning. E-learning is commonly referred to the intentional use of networked information and communications technology in teaching and learning. It is a procedural in character that aims to effect the construction of knowledge with reference to individual experience, practice and knowledge of the learner and pedagogical strategy. Today, Libyan educators have not fully implemented or not progressively implementing e-learning systems in the university curriculum.

This research aims to assess and evaluate the readiness and preparedness of e-learning implementation at Sirte University using several factors such as its technological infrastructure and communication backbone, student's readiness and needs, and technical know-how of its staff and the design of an e-learning architecture and strategy for the development and implementation of e-learning system. This research also the start of a series of papers related to e-learning as we progressively develop research on this field.

Keywords: *e-learning, curriculum, ICT, pedagogy*

Introduction

Change appears to be the only constant in the field of information and communication technologies and what was avant-garde two years ago is today passé (Naidu, 2006). The e-learning presentation of Brandon Hall in 1995 exponentially increased to its current 109 million related sites and becoming inevitably considered the fastest digital business and perfect area for educating people. If coping with such rapid change in the field is getting increasingly difficult and complex, it is even more difficult when one tries to simplify the concepts and processes and help academics and educators who have to grapple with effective educational delivery.

E-learning is commonly referred to the intentional use of networked information and communications technology in teaching and learning. For more in-depth definition, it is a procedural in character that aims to effect the construction of knowledge with reference to individual experience, practice and knowledge of the learner and pedagogical strategy. Normally, e-learning

is an educational training delivered in digital form to help learn the content, and improve organizational performance by training, educating and enhancing knowledge of group of learners. This educational technology provides a blended learning among the students and educators in university while trying to improve learning outcome. E-learning is rich in content, interactive and uses different media and delivered via the Internet, intranet/extranet, audio or video tape, satellite TV, and CD-ROM. It can be self face paced or instructor led and includes media in the form of text, image, animation, streaming video and audio.

As an evident of the success of e-learning, company profits increased steadily as predicted by Chambers in 2000 and more and more company adopted to e-learning environment (Barbara, 2002; van Dam, 2002; and eLearning Guild, 2006;Quin, 2009) for training their workforce in a different and diversified location. In education, several higher institutions migrated to e-learning, taking up the pedagogical strategy of McDonalds (2007), Mayes (2005) for its conceptualization cycle, Laurillard (2007) for its conversational model and Salmon (2004) for its moderation and instructional delivery while adapting the strategy of Carter and Lange (2005), Kent (2007) and Karrer (2009) implementation. Today, more and more university established their e-learning systems to support their learners at all levels. Thus adopting and adapting to "e-learning" is unavoidable for everyone in society and in particular in education setting (Collis & Moonen, 2005).

Like in most developing countries, the use of ICTs and implementation of e-learning in Libya are still in early stage. While some Libyan universities, such as Alfateh University, Garyounis University, and Sirt University have the basic ICT infrastructure (such as computers, Internet access, and a local area network), they still use the "traditional" model of education; this model is based on face-to-face interactions in and outside of, classroom between students and teachers, and learning activities that are only available on campus. Libyan Open Universities (LOPs) offer students the opportunity to study at home; however, the learning experiences are traditional too, as the universities rely largely on printed learning materials (Rhema & Miliszewska, 2010).

This research aims to assess and evaluate the readiness and preparedness of e-learning implementation at Sirte University using several factors such as its technological infrastructure and communication backbone, student's readiness and needs, and technical know-how of its staff and the design of a standard e-learning architecture and strategy for the development and implementation e-learning system.

ICT Infrastructure and Readiness of the University

Integrating ICT can help teachers and leaders expand learning possibilities to create effective contemporary learning environments where students and teachers use technology purposefully and flexibly to improve student learning outcomes. Widespread demand for this technology and increasing student numbers may, however, consume any future increase in capacity. Access to this infrastructure is therefore a

key determinant of a college's ability to deliver teaching and learning effectively.

At the university, there are 5 Computer Laboratory with 30 computers each; enough to cater the 250 students enrolled in Computer Science Department. Internet connection is limited only in 2 laboratories. Currently the total bandwidth is 10Mbps and expecting change in the near future. According to the survey, 90% of the students have internet connection in their house; enough to support the Internet based delivery of the e-learning system. Students are 100% digitally connected using mobile.

Local area networks (LAN specification improved steadily between and 2005 up to date and still upgrading. The college upgrades their LANs to make best use of the bandwidth with 100Mbs Ethernet and Wireless network. The computer per student ratio is 1:1 however it is not being maximized. Improvements in access to the Internet decline in the last few months of this year due to cable disruptions during building constructions. The target of one internet-connected for every permanent member of the teaching staff is not yet achieved, however all staff can access Internet using their respective account.

College intranets and networks continued to be extensively used for learning specifically for computer subjects married with applications in the laboratory. Almost 100% of the learning material used is at the discretion of individual teacher. According to the survey, the Internet is the most frequently used source of learning materials with 95% while the remaining 5% preferred books and stock knowledge. The reuse of e-learning materials is also taking place in the department. Interestingly, materials were likely updated before reuse. Given the extent of updating and repurposing identified, ease of modification is clearly a key element for materials reuse.

Students' access to a reasonably robust infrastructure gives access to electronic resources. Limited resources, taken up by individual enthusiasts, can begin to produce e-learning. However, management time has to be committed to facilitate access and to plan and set targets, and information has to flow from the teaching and learning process to the management process. Teaching staff also need access to ICT, and their competence and confidence with ICT need to be improved. They could then engage with e-learning and develop their own resources. All these developments need to be in place so that e-learning can be widely implemented and begin to transform teaching and learning.

Challenges for the Design of E-learning

Although admittedly young, Libyan is striving to fasten the development of e-learning with the help of UNESCO and various projects of the government. Libyan ICT is exponentially growing as shown in world ranking in networked readiness index and web assessment index (Ballera & Ziyad, 2010). Thus, Sirt University will take advantageously with these developments and plan to introduce an e-learning design and strategy. However, the university faces many challenges in terms of the implementation of ICT and e-learning in teaching and learning. These challenges are associated with: culture and language, technology, attitudes towards e-learning, curriculum design and development, and management support for e-learning initiatives.

Different people have different perceptions of ICT and e-learning based on their backgrounds. Notably, the design of e-learning must consider cultural differences and context sensitivity issues especially in its learning environment. For instance, in Libya, the design should consider appropriate reading directions, right-to-left to suit the Arabic language; likewise, text justification and navigation systems should be fixed on the left hand side. In addition, the choice of icons, symbols, objects, and colors needs to be carefully considered; for example, to many users in the Western countries will find an image of a dog on a Web page harmless, or indeed friendly, whereas users in Libya would find a similar Web page quite offensive (Rhema & Miliszewska, 2010).

The technology infrastructure as mention in the previous chapters is significantly considered, however in e-learning development, constant Internet connection needs to be uninterruptable. Moreover, networks design, hardware specifications, softwares, videos, audios and supporting data for the learners must be available. While computer laboratories are available in the university, the lack of adequate network facilities places serious restrictions on Internet access. The use of educational software within institutions is limited too due to unavailability of Arabic products in the market. Further, the technical support is almost unavailable, which leads to delays in installation, operation and maintenance of equipment and software and further discontinuance of users.

Student attitudes and motivation is a factor that affects students' satisfaction and capacity: "Highly motivated students perform well in most cases whereas non-motivated students tend to drop out" (Andersson & Gronlund, 2009). Personal motivation is one of the main reasons for success or failure in the integration of ICTs and adopting e- learning in the classroom setting. ICT increases student engagement because it provides opportunities to shift from teacher-centered to student-centered learning which attracts students and leads them to enjoying learning. However, many students, particularly those who struggle with computers, lack motivation for e-learning, because the lack of exposure makes it difficult for them to appreciate its potential benefits.

Curriculum is becoming more dynamic and interactive as a result of the many kinds of ICT based learning activities, projects and software applications (UNESCO, 2005). Hu and Webb (2009) stated that "regardless of the amount of technology and its sophistication, technology will not be used unless faculty members have the skills, knowledge and attitudes necessary to infuse it into the curriculum." The curriculum and pedagogical methods need to be modified and developed to employ ICT application effectively, and fit to e-learning setting (Andersson & Gronlund, 2009; Rhema & Miliszewska, 2010). At Sirte, the curriculum dated 2006 is obsolete and need to be reviewed and modified accordingly. The pedagogical scenarios for e-learning settings require assistance from educational developers with experience in e-learning; such expertise is not fully available at the university.

Without support from top management, an e-learning program will probably not survive. Teachers and Trainors generally are more motivated and committed when they feel supported and encouraged by the administrators. According to Mapuva

(2009), "Institutional leaders are a determinant factor, given their decision-making roles which could either make-or-break the e-earning projects by either facilitating or impeding its implementation within their institutions." So, administrative support can be regarded as essential to the successful adoption of ICTs into the educational processes. At Sirte University, the lack of ability to deal with educational problems will take some time due to understanding of the technical, financial, pedagogical, and administrative dimensions of ICTs in education.

E-Learning Strategy

An e-learning strategy is needed to help focus resources including infrastructure, staff development and support. There are many instances of good practice around the University, but there is insufficient support available. The University needs to build capacity and skills to be ready and able to respond quickly to, and benefit from, the fast moving changes of an increasingly networked world.

Sirt University needs to position itself well in Libyan academic level. There are many different visions and models for e-learning and its implementation, but a unique strategy is needed to suit its own mission and circumstances. The features and best practice and information from benchmarking exercises is considerably taken which served as guiding principles in creating e-learning strategy such as the work of Salmon (2005) and Norfolk (2009) in e-learning and pedagogical framework, Kent (2007) for its implementation, JISC (2007) for effective feedback and assessment and others. E-learning has the potential to transform teaching and learning at the university.

The following are specific aspects of ICT to be developed in Sirt are outlined as part of the strategic priorities.

Priority 1. Engaging and involving staff and learners – Information drive:
Computer Science Department will work with all stakeholders, partners and learners to continue to develop a common vision and understanding about the use of ICT in learning. Several classes will undergo with the beta version program to measure students performance. Student will have a technological innovation at the same time cultural immersion and eliminating language barrier. Staff members will continue to promote and support the leading edge developments by actively participating and involving with the whole process. Developers will work with partners through the university to facilitate and support the utilization of funding and infrastructure initiatives. A one year plan is needed for students to appreciate the new technology, as students' increases awareness, so is the management.

Priority 2. Building a common ICT infrastructure to support transformation and reform – the university current ICT infrastructure needed major revamp, so requesting for an immediate improvement to management is a surely thumbs down; management is hesitant in changing the current set-up especially when it involves cost and return of investment takes time. By gradually improving, management will be able to ready themselves and have ample time to think. For the ICT infrastructure specifically for e-learning implementation the BECTA (2007) standards will be used in a 5 year plan installment system modification. The BECTA developed by UK is a standardized system for technical

specification and institutional infrastructure for e-learning system. The university will develop a simple technical framework based on Becta to provide clear steps in managing learning environment.

Priority 3. Improved CS Curriculum and Course Content Management – the university needs to modify and change the curriculum to infuse the technological innovation in delivering education. Currently, several courses have been collided with other courses. The IT education is considered young since it started in the early year of 2000, pre-requisite and co-requisite must follow international standard to provide incremental learning. Teaching staff developed their own teaching materials without checking and monitoring content of other courses, a need for making standards. In developing the e-learning content, the university will coordinate with academic press and suppliers to make high quality digital content and learning resources available to schools and learners and consultation among peers

Today, most e-learning incorporate a learning content management system (LCMS), which is a set of software tools that enables the, storage, use and reuse of the subject matter content. Contemporary organizations recognize that the use of online learning management systems have the potential to significantly improve their image and value, as well as access to their services.

An LCMS might consist of a whole range of different software and systems that interrelate, share data and contribute to learning management. A VLE refers to a specific piece of software that enables learners and staff to interact, and includes content delivery and tracking. This is illustrated by Figure 1.

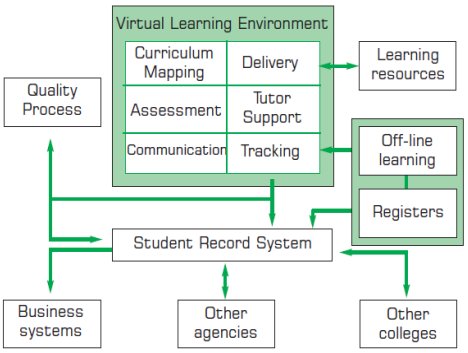

Figure 1. Learning Content Management System

Most LCMSs will have the following features: course content delivery capabilities; management of online class transactions; tracking and reporting of learner progress; assessment of learning outcomes; reporting of achievement and completion of learning tasks; and student records management. It is likely that the next generation of LMSs will have additional features such as better collaborative learning tools and better integration with other complementary systems, and with portable and wireless (mobile learning) devices. It is also suggested that the next generation of LMSs is going to be increasingly browser-based and less reliant on umpteen downloads or plug-ins on the user's desktop. They will have to be easier-to-use, more robust, scalable and more easily customizable. With the growing interest in the sharing of study materials, they are also likely to comply more with industry standards and with complementary systems.

Priority 4. Provide a Pedagogical Design for E-learning - it is widely acknowledged that the role and influence of information and communications technology on learning and teaching is optimized especially when it is skillfully integrated into the educational environment. For this to happen, we need to focus our attention foremost, on the careful design of the learning experience rather than the presentation of the subject matter content or the technology. This means careful orchestration of what the learners are going to do in the learning environment.

The university crafted its own e-learning environment design using four components and shown in Figure 2. The four components are pedagogical design, the graphical user interface and multimedia, the content management and feedback and assessment. The pedagogical design will be discussed in detailed and GUI while LCMs discussed in Priority No. 3 and feedback and assessment will be discussed in priority no. 5.

This concept of "learning by doing" has been popularized, among others, by Roger Schank and his collaborators and it is at the heart of pedagogical designs that stand to optimize e-learning (Schank, 1997). These pedagogical designs include "scenario based learning", "goal-based learning", "problem based learning", "case-based learning" (Carrol & Rosson, 2005), "learning by designing" (Newstetter, 2000), and "role-play-based learning". These pedagogical designs are grounded in the principles of constructivism and situated cognition, and in the belief that learning is most efficient and effective when it is contextualized and when it is based on real world or similarly authentic settings.

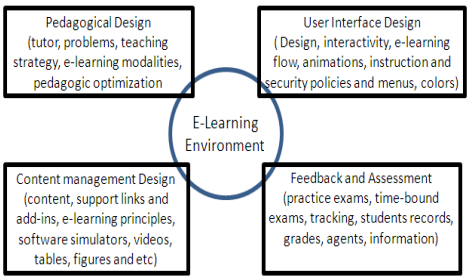

Figure 2. Core Components of E-Learning Environment – Pedagogic, GUI, CMD and Feedback and Assessment

E-learning with multimedia and graphical user interface is fashionable in virtual learning environment (Malayeri & Rezaei, 2004). These interfaces can improve quality of education by increasing attention of educational subjects and providing instructions when a learner is lost or provide help during problem solving. Adding some plug-ins in e-learning environment like relative sound, electronic noting, chat, colors combination, videos increases the curiosity and motivate the learners to continue navigating the environment. The university observed that students tend to become more interested in the learning process if they see computer applications and allowing them to interact with the environment.

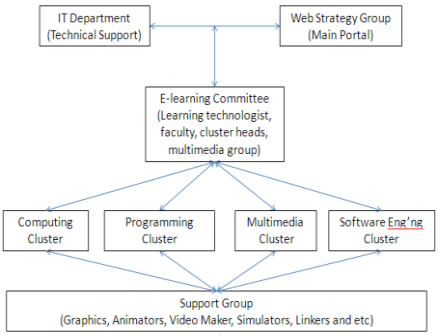

Figure 3. Operational Model of the E-Learning at Sirte University

The operation model in Figure 3 is used by the university as guiding principles, and responding to previous consultations involving e-learning strategies, we have developed an enabling organizational structure to support the development of e-learning to enhance the range of pedagogic uses of e-learning by staff and students. This structure consists of an e-learning committee, Learning Technologist, Faculty Learning Technologists, and departmental cluster heads. The University will also: provide and fully support a range of core technologies, and assist with evaluating peripheral technologies provide information and support to academic departments to help them decide on, implement and evaluate their e-learning developments, including the appropriate use of educational technologies, instructional/learning design, quality considerations and staff development needs and to provide appropriate staff development.

Priority 5. Provide an Assessment, Feedback and e-Moderation for Learners - Assessing learning outcomes is concerned with determining whether or not learners have acquired the desired type or level of capability, and whether they have benefited from the educational experience (i.e., have they learned, and how their performance has changed). A measure of learning outcomes requires learners to complete tasks, which demonstrate that they have achieved the standards specified in the learning outcomes. In order to ascertain the most realistic and valid assessment of performance, these task(s) have to be as similar to on-the-job conditions, that is, as authentic as possible (Naidu, 2006).

A major purpose of assessment in education is the improvement of learning. At the university, only quiz is used to measure the performance of the students. In the case of e-learning online assessment is necessary to be included in the design. A range of measures of achievement is necessary to assess the wide variety of skills and competencies that need to be acquired. It is important to clearly specify and communicate the basis for all assessment measures. When this is the case, assessment can serve as a powerful teaching tool.

Assessment activities are most effective when they are accompanied with feedback. At the simplest level, feedback is aimed at correcting errors in understanding and performance. However, like the assessment of learning outcomes, the provision of feedback is a lot more complex process. Feedback is usually designed to inform learners about the quality and/or the accuracy of their responses. This kind of feedback is specific and directly related to the performance of the prescribed task. It may be delivered directly to the learners, or mediated by information and communications technology. Feedback can be directed at different aspects of learning. Some feedback is primarily designed to influence affective learning outcomes such as motivation. Others might be directed at understanding of subject matter content.

Moderation of the learning process comprises supporting learning with the help of a variety of instructional interventions. It is an integral part of any educational context and is often carried out by teachers and tutors as well as students themselves. For e-learning, e-moderation refers to the acts of managing, facilitating and

engendering group based computer-mediated communication. Example, using the synchronous mode, even though the participants may be physically separated from one another, the communication takes place in real time (i.e., they are logged on at the same time and reacting to each other's comments as soon as these are received). At the university, they are studying the possibility of engaging such scenario while some disagree for the moment and wait till e-learning implementations is mature.

Priority 6. Provide ICT Training and Support for Practitioners and Developers – Using blended approaches, this will enable school staff to engage in more personalized training with increased choice of where and when they engage in learning. The university will facilitate networks for practitioners, making use of electronic communication and video conferencing to develop communities of professional learners. Thus, they will **d**evelop a flexible continued professional development program for all school staff.

In order to achieve the priorities above and to provide a coherent set of support structures and arrangements, the university will seek and create a dedicated team. This will be supported by funding mechanisms from the university. The team will oversee the development of all work related to the strategic priorities through project based implementation.

Conclusion

In this paper, we studied the current ICT infrastructure of Sirte university and students and technical capability of the staff members and found out that there are still a lot to be done in upgrading the information and communication technology of the university. Applying the Becta architecture for ICT, the university could afford to implement e-learning if given the chance to upgrade and update the current ICT setting. The five challenges has been addressed in e-learning development such as culture and language, infrastructure, motivation and student awareness, curriculum design and management supports. These challenges also incorporated in the 6-Plan priority for e-learning strategy of Sirte University.

References

Rhema, A & Miliszewska, Iwoma (2010). Towards E-Learning in Higher Education in Libya. Issues in Informing Science and Information Technology.

Ballera & Ziyad. (2010). E-Government in Libya: Benchmarking Against Best Practices. Appeared in the proceedings of First International Conference in Electronic Management. June 1-4, 2010, Tripoli Libya.

Quinn, C. (2009). Populating the LearnScape: e-Learning as Strategy. In M. Allen, Ed. Michael Allen's eLearning Annual 2009. Pfeiffer: San Francisco.

Andersson, A., & Grönlund, A. (2009). A conceptual framework for E-learning in developing countries: A critical review of research challenges. The Electronic Journal on Information Systems in Developing Countries, 38(2), 1-16.

Hu, L., & Webb, M. (2009). Integrating ICT to higher education in China: From the perspective of activity
theory. Education and Information Technologies, 14(2), 143-161.

Mapuva, J. (2009). Confronting challenges to e-learning in higher education institutions. International
Journal of Education and Development Using ICT, 5(3).

Brandon Hall (2007). www.brandon-hall.com
Laurillard, Diana (2007): The Conversational Framework - an approach to Evaluating e-Assessment Patterns in Terms of Learning Theory.
McDonalds (2007). Communication Report of McDonalds. www.mcdonalds.co.uk.
JISC (2007) 'Effective Practice with e-Assessment' www.jisc.ac.uk/.html
University of Kent (2007). E-learning Strategy.

Becta (2006) 'Emerging Technologies for Learning' www.becta.org.uk

Naidu, Sam (2006). E-Learning: A Guidebook of Principles, Procedures and Practices. Commonwealth of Learning. Educational Media Center for Asia

Mayes, T. (2006). Theoretical perspectives on interactivity in e-learning. In C. Juwah (Ed.),
Interaction in Online Education: Implications for Theory & Practice (pp. 9-26). New York:
Routledge.
Salmon, Gilly. (2005) 'Flying not flapping: a strategic framework for e-learning and pedagogical innovation in higher education institutions.' ALT-J, Research in Learning Technology Vol. 13, No. 3, September 2005, pp. 201-218.

Carter & Lange (2005). Successful e-learning Strategies: Interactive e-Learning for an Interactive Age.

Collis, B. A., & Moonen, J. (2005). An on-going journey: Technology as a learning workbench. Public address, University of Twente, Enschede, The Netherlands. Retrieved October 30, 2009 from http://www.BettyCollisJefMoonen.nl/rb.htm
Carrol & Rossan (2005). Toward even more aunthentic case-based learning. Educational Technology, November/December 45(6), 6-11.
Malayeri & Rezaei. (2004). Graphically E-learning and Its Benefits in Virtual Learning.
Van Dam, Nick. (2004). The E-Learning Fieldbook: Implementation Lessons and Case Studies from Companies that are Making E-Learning Work. McGraw Hill.
University of Iowa (2004). E-Learning Usage Pattern. How Faculty and Students Perceive E-Learning at the University of Iowa.
SALMON, G. (2004). E-moderating: The Key to Teaching and Learning Online (2nd ed.) London: Taylor & Francis.

Salmon, G.(2003). Etivities: The key to active online learning. London: RoutledgeFalmer.
Barbara M.O., 2002. Effective strategies to Assess the Impact of e-Learning. Proceeding of the e-Technologies in Engineering Education (eTEE'02), Aug. 2002, Davos, Switzerland, pp: 158-163
Clark, Ruth (2002). Six Principles of Effective e-Learning: What works and why. E-Learning Guild.
Newstetter, W.C. (2000). Guest Editor's Introduction. The Journal of the Learning Sciences, 9(3), 279-298.

Schank (1997). Virtual Learning: A Revolutionary Approach to Building a Hihgly Skilled Workforce. New York. McGraw Hill.

Reliability Analysis of Multi-Stage Flash Distillation Processes Based on Industrial and Operation History

Abdallah.A.Ezzedin
Department of Nuclear Engineering, Faculty of Engineering
Al-fateh University, Tripoli-Libya
Nora.R.Abozid
General Electrisity Company Of Libya
Generation department

Abstract

Reliability of Multi-stage flash distillation (MSF) processes are estimated using time – dependent fault tree analysis (FTA) of major critical systems. MSF is a water desalination processes that distills sea water by flashing a portion of the water into steam in multiple stages of what are essentially regenerative heat exchangers. MSF has been preferred over other processes for sea water desalination because of the relatively long experience gained in the operation of MSF plants. FTA is a formalized deductive analysis technique that provides a systematic approach to investigate the possible modes of occurrences of a defined system state or undesired event. Failure data of one the critical system of the desalting plant, the brine recirculation system are obtained from the operation records of an old plant which is still in operation in a relatively harsh environment. Industrial failure data are also used to complement historic data. The analysis shows areas where design improvements can be made to enhance MSF processes availability.

1. Introduction

Large quantities of water are required in many parts of the world for agricultural, industrial and residential uses. The world is becoming more and more aware of its shortage of fresh water. Availability of water supply systems which in incorporate desalination processes is greatly influenced by the reliability of the desalting plant and desalination equipments [(1)]. In many countries, MSF has been preferred over other processes for seawater desalination because of the relatively long experience gained in the operation of the plant. However, no large effort is taken to evaluate the reliability of a typical MSF plant. Such effort is required for improvement in future designs and for assessment of possible fixes to enhance the reliability of present designs. The approach employed here is to review design details of MSF processes in order to construct and evaluate fault trees for the critical systems in the plant such as the brine recirculation system (BRS). Fault tree is a logic diagram that simulates plant design and

performance. In other words, Fault tree analysis (FTA) has become indispensable tool for the reliability and safety analysis of a complex system such as the MSF plant [2]. Failure data obtained or extracted from actual operation and maintenance records of the plant are required for the analysis, since the plant operation and maintenance records are invaluable in assessment of failure rates and human factors [3]. The description of the general application of fault tree analysis is given in section two. Section three describes the analysis of the MSF plant system. The reliability analysis of the BRS is given in section four.

2. Fault tree analysis and its applications

2.1. Fault tree Analysis (FTA)

Fault Tree Analysis is a formalized deductive analysis technique that provides a systematic approach to investigate the possible modes of occurrences of a defined system state or undesired event. In other words, a fault tree is a logical diagram of the sequences of events, which lead from one or more causal events upward to one consequence or resultant single failure. This failure is called " Top Failure ", " Final Failure " or " system Failure ". Fault tree may be alternatively defined as a logical diagram, which traces top failure to basic failure causes. FTA consists of two major steps: (1) the construction of the fault tree and (2) its evaluation. The evaluation of the fault tree can be qualitative, quantitative, or both depending upon the scope and extensiveness of the analysis.

The objectives of fault tree analysis are: (1) to define critical paths in the accident analysis, (2) to calculate probabilities of failures leading to given consequences occurring in the system from one or a number of different initiating faults, and (3) to specify safeguard systems against damaging consequences for each branch of the tree [5].

2.2. Application of Fault Trees

After constructing the fault tree an evaluation of the critical path is carried out. A critical path (mode failure) is a smallest set of primary failures such that if all of these primary failures simultaneously exist, then the top failure exists. The mode failures of a fault tree can be obtained by number of methods. A detail description of the methods is given in references [3,5] . With knowledge of the mode failures of the fault tree, the evaluation can then proceed to obtain the probabilistic characteristics of the primary faituras, mode failures, and the top faiture.

In order to obtain this probability, the component behavior data in the form of failure rates $\lambda(t)$ and the repair times $\mu(t)$ are required as inputs to the system models. On the other hand, for any reliability analysis using fault tree study, the quantities $\lambda(t)$ and $\mu(t)$, or their equivalant, must be known for every primary failure of the fault tree . If the primary failure is the failure of a component, then $\lambda(t)$ and $\mu(t)$ are termed the component failure rate and component repair rate , respectively. From $\lambda(t)$ and $\mu(t)$, some probabilistic quantities may be obtained which quantify, or characterize, the particular primary failure. The probability $A(t_1,t)$ of the primary failure

first occurring in time t to t+dt, given it is not existing at time t_1 is given by

$$A(t_1,t)\ dt = \exp\left[-\int_{t_1}^{t}\lambda(t_2)dt_2\right]\lambda(t)dt; t_1 \le t \quad (1)$$

Where

$\lambda(t)\ dt$ = the probability of the failure occurring in time t to t+dt given the failure is not existing at time t.

It is clear from Equation (1) that the probability of the primary failure $F(t_1,t)$ occur from time t_1 to t is simply

$$F(t_1,t) = \exp\left[\int_{t_1}^{t}\lambda(t_2)dt_2\right]; t_1 \le t \quad (2)$$

In context of the defined failure, the failure probability is equivalent to unreliability.

With regard to repair, the probability that the primary failure is repaired at time t to t+dt, given it is existing at time t_1, $B(t_1, t)$ dt , is given by

$$B\ (t_1,t) = \exp\left[-\int_{t_1}^{t}\mu(t_2)dt_2\right]\mu(t)dt; t_1 \le t \quad (3)$$

Where

$\mu(t)\ dt$ = the probability of the failure being repaired in time t to t+dt given the failure is existing at time t .

The quantity A (t_1,t) and B (t_1, t) are termed the first failure distribution and the repair distribution, respectively. The term $F(t_1,t)$ is called the nonfailure probability .

There are two other primary failure characteristics, besides the above, which are essential for any reliability study or fault tree evaluation. The first characteristic is the primary failure intensity w(t), which is defined as

W(t) = the expected number of times the primery failure occurs at time t per unit time.

By using the definition, it is clear that the expected number of times the primary failure occures in any interval from t_1 to t , $w(t_1 ,t)$ is

$$w(t_1 ,t) = \int_{t_1}^{t} w(t_2)dt_2 \quad (4)$$

By assuming as initial condition that at t= 0 , the primary failure does not exist, an equation for w(t) in termes of the data for the primary failure can be obtained,

$$w(t) = A(0,t) + \int_0^t w(t_2)dt_2 \int_{t_2}^{t} dt_1 B(t_{2,}, t)A(t_1, t) \quad (5)$$

where A(0,t) is the contribution to w(t) from the first occurrence of the primary failure.

The second primary failure characteristic of interest is the primary failure existence probability q(t). The probability of the primary failure not existing at time t is merely 1- q(t). By using the definition of $\lambda(t)$ and w(t), it is clear that

$$W(t)= [1-q(t)]\ \lambda(t) \quad (6)$$

Or

$$q(t)= 1- \frac{w(t)}{\lambda(t)} \qquad (7)$$

It was stated previously that, a mode failure, or critical path, is the smallest set of primary failures such that if all these primary failures exist at time t the mode failure (and top failure) exists at time t .

Consider a particular mode failure that consists of n primary failures and let these constituent primary failures be designated with indices from 1 to n.

The first characteristic obtained for the mode failure will be the mode failure existence probability, Q(t), which is defined as:

Q(t) = the probability that the mode failure exists at time t.

Since the mode failure exists at time t if and only all its primary failure exists at time t, then

$$Q(t) = \prod_{j=1}^{n} q_j(t) \qquad (8)$$

More detail explanation for other mode failure characteristics is given in references[4,5].

2.3. PREP and KITT codes description

The PREP code is designed to accept an input description of the system's fault trees , generate the appropriate logical equivalent, and obtain the system's minimal cut or path sets. A minimal cut set is a smallest set of system components which when failed will cause the system to fail. A minimal cut set is defined to be in the failed or nonfunctioning state if and only if all of its components are in the failed state, and is defined to be in the nonfailed or functioning state if and only if at least one of its components is in the functioning state.

These minimal cut sets (failure mode) or the minimal path sets (success modes) can then be used by the KITT codes to obtain reliability information about the system. The PREP code is composed of two sections: TREBIL reads the input and generate the logical equivalent of the fault tree and MINSET obtains the minimal cut or path sets of the tree. Detailed description of the PREP code and its input data is given in Appendix(4).

After having obtained either the minimal cut sets or the minimal path sets, the fault tree is then evaluated by running the KITT code to obtain the probability characteristics of the components. These probability characteristics include:

1- the probability of the failure existing at time t (the " unavailability ")
2- the probability of the failure not occurring to the time t (the " reliability ")
3- the expected number of failures occurring to time t .
4- the failure rate at time t, and the failure intensity at time t (λ). Detailed description of the KITT code and its input data are given also in Appendix (4).

3. Analysis of the MSF plant system

3.1. General description of the plant

The MSF plant selected as a case study is a dual purpose type which produces 50 Mwe and 5 MGD of distilled water. The

general arrangement of the plant consists of six horizontal evaporator modules on asingle tier arrangement. There is a total of 42 stages which are divided into a heat rejection sectionand a heat recovery section. Detailed description of the selected plant is given in references [7,8].

3.2. Fualt tree analysis of the MSF plant

using detailed plant design, fault tree is synthesized to determine how the system could fail in terms of faults of basic consitituents of the system. Faults examined including failure modes of pipes, valves, pumps and electric power. In addition, human errors which could result in faulted components are also considered. The developed fault tree is based on the following assumptions [6]:

1. Loss of power affects both units.
2. Any failure identified on the fault tree was assumed to be of sufficient mangitude to constitute component failure. For example, pump failure, as it applies on the tree, results in sufficiently reduced flow to make the pump essentially unavailable.
3. All small pipes (1" diameter or less) are considered to be small enough that their rupture would not result in sufficient fluid loss to cause system failure.
4. Any monitors associated with valve position, pump flow, etc., are operable and provide adequate information for an operator to respond.
5. Piping failures resulting in a total catastrophic break are rare occurrences. However, significant leaks requiring repair or leaks in sensitive locations are more likely.
6. Human failurs include miscalibration and failure to remove the system from isolation after maintenance.
7. Loss of power and external causes are included but there is no development of these events in the fault trees.
8. Steam is provided by heat recovery from the power generation unit or from the boiler directly.

FTA starts with the event " desalination plant unavailable to produce sufficient distillate", since many types of failure modes contribute to this event which leads to unreliable plant operation through loss of water production. Also the analysis of the fault tree illustrates potential failure problems and shows the critical components, which would impact plant availability.

Failure of the MSF plant to produce sufficient distillate is assessed using the fault tree logic diagrams. Loss of steam and power are the common contribuators of the plant failur and the most important systems which represent the major problem areas in the plant are the following:

1- The seawater intake system (SIS).
2- Make-up WATER system (MWs)
3- The brine recirculation system (BRS).

In this study, the reliability analysis of the BRS using FTA is selected and presented in details in the next section.

4. Reliability analysis of the brine recirculation system (BRS)

4.1. Brine Recirculation Fault Tree

The flow diagram of the BRS is shown in figure (1) and the corresponding fault

tree is illustrated in figure (2) which is constructed by tracing through system operation and identifying possible single and multiple modes of equipment failures. By taking a good look to the system flow diagram, the following failures are identified:

1- Brine heater tubes damage or leaks
2- Brine recirculation pump fail
3- Flow control valve (FCV) prevent flow
4- Temperature control valve fail (TVC-1)

Also, the fault event code for the BRS is the letter C. Other fault event codes for the component which includes the component type and the identifier of the component and the type of failure are given in table (1)

To illustrate as an example, the primay event CMV007 X presented in the fault tree, C for the BRS, MV for the motor operated valve and 007 for the number of the valve and X for the fault type which in this case maintenance.

The fault tree shown in figure (2) represents the input to the PREP code. Eash uniqe primary event on the fault tree is assigned an arbitrary unique name. Eash gate is then coded on an input card. This card gives the name of the gates and/or primary event attached to the gate. Besides the fault tree, the input data necessary to use the PREP code are the component failure rate and repair time. These values are listed in table (2).

4.2. Results and discussion

Having obtained the minimal cut sets from the PREP code, KITT-1 code is then run to obtain the probability characterstics associated with the BRS fault tree.

The system differential characterstics resulted from KITT-1 code run are given below and plotted in figures (3)and (4) where the program output symbols are defined as follows :

T (hours) = t, time (in hours)

Q = the upper bound of the probability of system failure at time t.

FSUM = the upper bound of the probability of failure of one or more failures to time t.

Table (1) Fault Event Codes

code	Component	code	Failure type
PP	Pipe	A	Short circuit
TK	Tank	B	Poor vacuum
PM	Pump	D	Loss of steam
TG	Tube	E	Plugged
CV	Check valve	F	Leakage/ rupture
XV	Control valve	G	Test & maintenance outage
MV	Motor operated valve	I	Incorrect dosing
PV	Manual valve	K	Contamination of seawater
NZ	Nozzle		
MO	Motor	L	Loss of power

SC	Screen	N	Environmental cause
BH	Brine heater		
DS	Desuperheater	P	Does not open
LI	Level indicator	Q	Dose not remain open
BK	Circuit breaker		
MD	Module	U	Unavailable
PS	Pressure sensor	W	Loss of function
DE	Dearator	X	Maintenance fault
BL	Blower		
TV	Temperature control valve	y	Operator error
TI	Temperature indicator		

Table (2) Brine Recirculation System Failure Rates [3,9]

Event	Failure rate $*10^{-6}$(per hr) I	Repair time (hour)
Mechanical failure of BR pump	222	20
MOV fails to function	78	18
BH tube leakage	479	16
Mechanical failure of condensate pump	135	20
Motor fails to function	78	10
Poor control of desuperheater	17	15
Pipe leakage / rupture	52	16
Circuit breaker short	17	5
Pump valve fails to remain open	9	18
Test and maintenance errors on pump	52	5
Test and maintenance errors on valve	17	5
BH hot well leakage / rupture	17	16
Operator errors on pump	6500	5
Operator errors on MOV	6500	5
Pump line down for test and maintenance	3333	48
Conductivity indicator failure	6	5
Temperature indicator failure	6	5

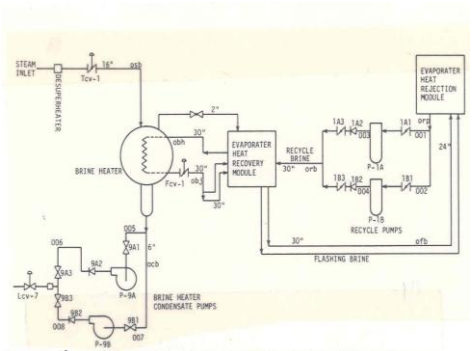

Figure (1). MSF, recirculation brine system flow diagram

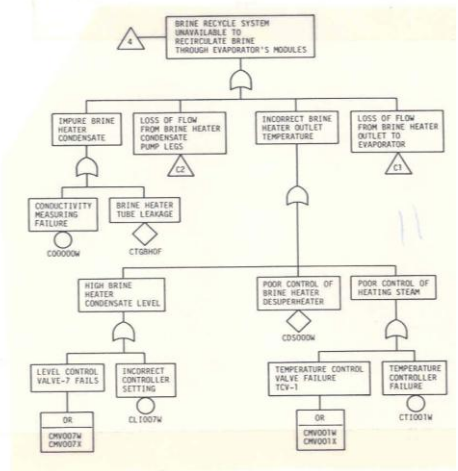

Figure (2) Brine recycle system fault tree diagram

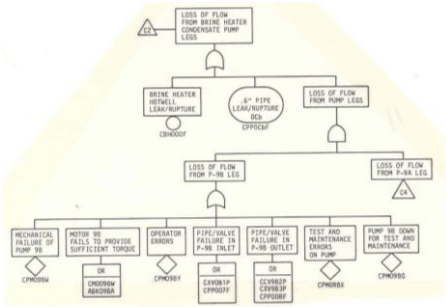

Figure (2) Brine recycle system fault tree diagram (continued)

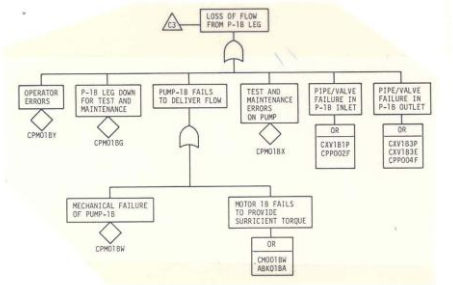

Figure (2) Brine recycle system fault tree diagram (continued)

The unavailability and the unreliability of the BRS of the MSF process is estimated from actual operating data using fault tree analysis. Table (2) presents the failure data for each component of the BRS. Both pumps; the recirculation pump and the condensate pump have the highest failure rates. Also, tubes in the brine heater have high failure rates. The characteristics of this system unavailability versus operation time is shown in Figure (3). A rapid rise in the unavailability which occurs at the early history of the system is followed by a constant high value after 50 hours. Tracing the BRS to the component level shows that recycle pumps and tube leakage are the

major contributors to the unavailability of the system. To a lesser extent, valves do effect the system unavailability. Pumps are the main source of system problems due to several causes such as inadequate design, maintenance and operation. Table (2) lists all contributors of failure to the system and the failure rates and repair times to each contributor. Pumps and tubes represent the most frequent cause of system unavailability.

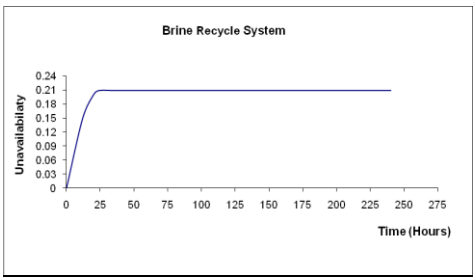

Figure (3) Unavailability characteristics for brine recycle system

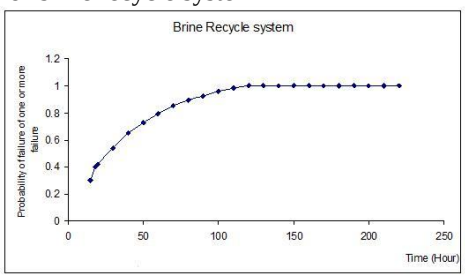

Figure (4) Probability of failure to time t.

Conclusion

The objective of this research is to present some safety features of MSF desalting plant. Availability of water supply systems is greatly influenced by the reliability of the desalting plant and desalination equipments. The unavailability of one of the important system considered, the BRS, is calculated to be 0.22 at the 50 hours mission period. The basic events and components which significantly affect the system reliability are pumps, human errors and motor operated valves. In order to improve system reliability, it is required to have a higher quality of these pumps. The other improvement should be the reduction of the human causing unavailability by using the certified form of procedures. In future, the study will be extended to the other critical systems of the plant for the purpose of calculation of the unavailability of the overall MSF plant. This value of the unavailability gives answers to the question capability of the plant to be able to produce either the amount of pure water at their expected cost, or operate satisfactory over all full expected life of the system.

References

[1] A. Unione , E. Burns and A.A.Husseiny , " reliability Analysis of desalination equipment, " Desalination, 32,225 (1980).

[2] A.Unione, E.Burns, and A.A.Husseiny , " MSF Desalination Plants Availability , Reliability and safety Analysis," desalination ,33 , 49 (1980).

[3] Reactor Safety Study, An Assessment of Accident Risks in U.S. commercial Nuclear Power Plants , U.S. Nuclear Regulatory Commission, Report Number Wash- 1400, 1975.

[4] W.E. Vesely and R.E.narum. PREPand KITT, Computer codes for the Automatic Evaluation of a

Fault Tree (IN-1349), Argonne code- center, Argonne, Illinois, 1975

[5] H.E. Lambert, " Fault Tree for Decision Making System Analysis ," University of clifornia, Lawrence Live more.

[6] El- Dessouky, H. Alatiqi, I. and Ettouney , H. , (1998) Process Synthesis, The Multistage Flash desalination system, Desalination , 115, 155-179.

[7] El-Saie , M.H.A., (1992), Technical developments of the MSF desalination process and its prospects for the future, pegional water desalination symposium, Al-Ain, united Arab Emirates, 15-17, Nov., vol.2,579-595.

[8] A. A. Husseiny , and I.I. Kutubi, " Performance Evaluation of MSF Plant , Proc.loth IDEA International congress on desalination and water reuse, Bahrin, Dec. 1981.

[9] Evaluation of the Reliability and Maintainability of desaling plants. Coulract no. 14-30-2848. department of Interior , Officie of saline water, Washington D.C., 1992.

Chapter VII

ورقات بحثية باللغة العربية
Arabic Papers

استخدام التقنية الحديثة في متابعة تنفيذ برامج شراكة التعليم التقني وسوق العمل

أ.د موسي محمد موسي
MMousa@LTTNET.Net
قسم الهندسة الكهربائية- كلية الهندسة
جامعة الفاتـــــــــــح
طرابلس – ليبيا

أ.جمعة علي الزوالي
Giumazwali@Gmail.com
إدارة شبكة المعلومات
كلية تقنيات الحاسوب

ملخص:

تقوم مؤسسات التعليم التقني، ، مثل بعض المعاهد العليا والمتوسطة التقنية، والمعاهد المهنية الأخرى بجهد كبير في بناء وتأهيل العديد من الكوادر المتخصصة، غير أن المفارقة أن هذه الجهود غالبا لا تؤتي ثمارها على الوجه المطلوب، خاصة عند الحديث عن تلبية حاجات سوق العمل من المتخصصين والعمالة الماهرة،ولعل من مؤشرات ذلك الاستمرار في الاعتماد على العمالة الوافدة من جانب ، ومن جانب آخر وجود بطالة بين الخريجين، بالإضافة إلى عزوف العديد من الشركات الأجنبية عن توظيف العمالة الوطنية بحجج متنوعة؛ منها ندرة التخصصات المطلوبة، وعدم الكفاءة وغيرها من الأمور الأخرى. إن هذه المعضلة تتطلب دراسة جادة من قبل المتخصصين، خاصة فيما يتعلق بتوفيرها واستخدام التقنيات الحديثة في متابعة تنفيذها بغية خلق تواصل فعال بين مؤسسات التعليم وسوق العمل.

تقدم هذه الورقة مناقشة عامة عن الإشكاليات القائمة بين مؤسسات التعليم وسوق العمل، ومقترح ببعض الحلول العملية لمعالجة هذه الإشكاليات المتمثلة في آلية تنفيذ البرامج المشتركة، و تقترح خوارزمية بآلية نمط التعاون في التنفيذ والذي ينبغي أن يكون بين عملية التعليم في المؤسسة والتدريب في سوق العمل بهدف تلبية حاجات سوق العمل، وتخلص الورقة إلى مجموعة من النتائج والتوصيات.

مقدمة:

على الرغم من الجهد الكبير الذي يبذل من قبل مختلف المؤسسات التعليمية، بغية تخريج دفعات من الشباب والفتيات وفي مختلف التخصصات التقنية، وعلى الرغم مما يصرف من أموال ضخمة على العملية التعليمية، إلا أنها في معظمها لا تزل لدى كثير من خبراء التعليم دون المستوى، فهي تقليدية في آلياتها، وروتينية في أدائها، وضعيفة في مخرجاتها ودون المستوى المطلوب [1]، إذ يلاحظ وجود ارتباك كبير وعلى عدة مستويات، منها على سبيل المثال لا الحصر: مستوى أداء المؤسسة التعليمية وضعف جودة مخرجاتها، وعدم وضوح الرؤية لدى الطلبة في تحديد ما يحتاجونه بالفعل أو وقوعهم تحت التأثير السلبي للأسرة أو المجتمع ككل، وسوق العمل الذي لا

يعرف بالضبط حاجته الفعلية من التخصصات والأعداد المطلوبة. السبب والتفسير المعقول والمقبول لذلك هو وجود نظام أو آلية عمل مفتوحة ربما تعرف مدخلاتها [2]، ولكن لا تعرف مخرجاتها بالضبط، ويفسر هذه الربكة وجود أعداد كبيرة من الطلبة تدرس تخصص محدد والذي أصلا قد يكون غير مطلوب في سوق العمل، أو قصور المؤسسة التعليمية في تعليم وتدريب طلابها على المعارف والمهارات التي يحتاجونها بالفعل، وغياب الشراكة الحقيقية بين سوق العمل ومؤسسات التعليم التقني.

إن هذه المعضلة تتطلب وضع حلول جذرية لها، إذ من غير المعقول أن تستمر الأمور هكذا، بدون آلية تنسيقية واضحة تنظمها وتحدد معاييرها، وشروط تنفيذها، فمن الضروري أن يكون هناك انسجاما بين كل مكونات العملية التعليمية التي تعد وتنتج الكوادر المتخصصة المختلفة، وبين مؤسسات سوق العمل التي تشكل بوتقة ومستوعبا هاما للخريجين الجدد.

برامج التعليم التقني المرتبطة بسوق العمل ومستوياتها:

المؤسسات التعليمية تعد العديد من الأطر الفنية، وفي مختلف التخصصات التقنية، وبرامج التعليم تتشعب من حيث نوعية التخصص، وتعدد وكمية المعارف، ونوعية المهارات العقلية والسلوكية والحركية، التي تعطى للطالب، والتركيز دائما على نوعية المنتج الذي يرغب في الحصول عليه، من هنا؛ كانت برامج التعليم تتفاوت في أسمائها، وتخصصاتها [3]، وحتى المدة الزمنية التي يحتاجها المتعلم للإلمام بالخبرة والمهارات المطلوبة، وعليه ينبغي إعادة النظر في برامج التعليم التقني بحيث تستجيب للمعايير التالية:-

الجوانب العملية في متطلبات الدراسة والممكنة بسوق العمل:

التعليم والتدريب بغرض الاستجابة لحاجيات سوق العمل يتميز عن غيره من أنواع التعليم والتدريب التقليدية المعروفة، منها أن تكون البرامج قصيرة، ومركزة، وعملية، أي أنها برامج تعليمية تقود المتعلم والمتدرب إلى اكتساب خبرة محددة وفي زمن قصير نسبيا، ويبين الجدول رقم(1) تفصيل بأنواع التخصصات العلمية والفنية ومتطلبات برامج التعليم والتدريب العملية لكل منها.

ينبغي لمن يرشح لهذا النوع من التعليم أو التدريب أن يتمتع بالخصائص التالية:

- اجتياز اختبار القدرات والمقابلة الشخصية.
- أن تكون لديه المعلومات والمهارات الأساسية للتخصص.
- أن يجيد اللغة الإنجليزية.
- أن يتمتع باللياقة الصحية المطلوبة لنوع التخصص التعليمي أو التدريبي.
- أن يكون مقيم بالقرب من موقع التعليم.
- أن يقبل العمل في أي مكان يكلف به.
- أن يلتزم بشروط العمل التي تحددها جهة العمل وبما لا يتعارض والقوانين واللوائح المعمول بها بالبلد.

آليات التنفيذ لبرامج التأهيل:

لتنفيذ هذا النوع من البرامج التعليمية أو التدريبية السريعة ينبغي إتباع سلسلة الإجراءات التالية:-

أولا- جهة سوق العمل:

1. تحديد التخصصات والأعداد المطلوبة.

2. تحديد مكان وشروط العمل (ساعات الدوام الرسمي).
3. تحديد طبيعة العمل.
4. تحديد المرتبات والمنح والعلاوات المرتبطة بتنفيذ العمل.
5. تحديد المزايا الإضافية.
6. تحديد نوعية التجهيزات والتي سيعمل عليها أثناء ممارسة العمل بصورة فعلية.
7. نوعية المهارات الحسية والسلوكية والذهنية المطلوبة.
8. تحديد مدة العمل ونوعية التعاقد (تعاقد-دائم، تعاقد-موسمي، تعاقد- خاص).
9. تحديد تاريخ مباشرة العمل.

جدول رقم 1، تفصيل بأنواع التخصصات العلمية والفنية ومتطلبات الجوانب العملية

نوع التخصص	تفصيل	نوع المهارات العملية المطلوبة	المدة الزمنية		المدة الكلية
			ساعة/يوم	أسبوع	ساعة
الحاسوب	- توظيف حاسوب، إدارة الحواسيب، شبكات معلومات، رسم هندسي.	- طباعة. - جداول الكترونية. - عرض الكتروني. - تركيب وتشغيل شبكات.	8	5	200 لكل تخصص
الاتصالات	- تشغيل محطات الأقمار الصناعية، الإذاعتين، إدارة منظومات المؤتمرات الالكترونية عن بعد،	تشغيل وصيانة	10	5	250 لكل تخصص
الميكانيكا العامة	- الخراطة، المقاشط، الفريز، التجليخ، NCM.	تشغيل وصيانة	8	7	280 لكل تخصص
الكهرباء العامة	- تركيب شبكات كهرباء منازل ومصانع، تركيب وصيانة خطوط الضغط العالي، المحولات والأبراج،	تشغيل وصيانة	7	7	245
مهن البناء	- تسليح وخشب، بناء، لياسة، تزليز ومايوركا، صب خراسانات، طلاء، روافع الخ..	تنفيذ عملي، إشراف ومراقبة	8	6	240

ثانيا- الجهة المكلفة بإعداد وتنفيذ البرنامج التعليمي أو التدريبي:

عند الاطلاع على الشروط التي حددها صاحب العمل في أولا، يتم المباشرة في التالي:

1. نشر إعلان للراغبين في الالتحاق بالبرنامج التعليمي أو التدريبي وعلى أن يتضمن التالي:
   أ. اسم البرنامج.
   ب. المدة الزمنية المقررة للتعليم أو التدريب.
   ج. مكان التدريب.
   د. الشروط التي يجب توفرها في المرشح.
   هـ. جهة العمل التي سيعمل بها الخريج.
   و. المهايا والميزات التي يوفرها برنامج التدريب.
   ز. المهايا والميزات التي توفرها جهة العمل عند اجتياز الاختبارات المقررة.
2. توزيع نماذج الترشح -على الراغبين، وأن يتضمن البيانات التالية:
   أ. اسم المرشح، وتاريخ ميلاده، وعنوانه السكني، والبريدي، وأرقام هواتفه.
   ب. خبراته السابقة، والأعمال التي يجيدها.
   ت. التخصص الذي يرغب العمل به.
3. فرز النماذج واختيار العناصر الجيدة (الاختيار الأول).
4. إجراء مقابلات شخصية وإجراء اختبارات المقدرة (الاختيار الثاني).
5. طلب شهادة صحية للمرشحين.
6. تحديد الأعداد المرشحة بدقة.
7. إعداد الحقائب التعليمية للمرشحين.
8. اختيار وتحديد المحاضرين والمدربين.
9. تحديد واختيار تجهيزات ومكان التدريب.
10. إبلاغ الجهة المستفيدة بالقيمة المالية للدورة بغية السداد.
11. المباشرة في التعليم والتدريب.
12. تحويل نتائج التقييم الأولي عن مستوى تقدم المتدربين إلى الجهة (الجهات) المستفيدة، أي جهات العمل.
13. إجراء اختبارات تقييم المهارات السلوكية والذهنية المرتبطة بنوع التخصص.
14. استلام رد جهة العمل عن النتائج الأولية.
15. تحويل المجموعة الممكن لها المباشرة في سوق العمل كجزء من البرنامج ألتأهيلي.
16. استلام تقييم جهة العمل عن الأداء.
17. استكمال البرنامج التدريبي بالمؤسسة.

18. إرسال النتائج النهائية إلى جهة العمل.

19. تعبئة نموذج تقييم الدورة ككل وتشمل:

أ. تقييم المتدربين.

ب. تقييم أعضاء هيئة التدريس والتدريب.

ت. تقييم الجهوزية ومدى تلبية التجهيزات لحاجة التدريب.

ث. تقييم النواحي الإدارية والإجرائية وأهم الايجابيات والسلبيات.

مقترح التنفيذ في حالة الشراكة مع سوق العمل:

كي يعمل هذا الأسلوب بنجاح، أي الشراكة, فإنه ينبغي أن تكون هناك علاقة وثيقة بين جهة العمل (سوق العمل) وجهة التدريب، ويكون ذلك من خلال الارتباط الوثيق بين الجهتين، وتواصل مستمر. كما ينبغي أن يكون هناك تعاقد يبين حقوق وواجبات كل طرف تجاه الأخر، ويحدد في التعاقد ما ينبغي فعله عمليا ومسؤولية كل جانب، ويجب أن يكون لدى جهة التدريب وبالتنسيق مع سوق العمل مكتب بحوث يحدد بالضبط طبيعة الاحتياجات الفعلية من الكوادر الممكن ترشحها وتنطبق عليها متطلبات سوق العمل ولفترة زمنية لا تقل عن 3 سنوات، وتكون آلية التنفيذ أو الشراكة بين سوق العمل والمؤسسات التدريبية على النحو التالي:-

- ينشىء بين الطرفين قناة اتصال فعالة، وتكون من مهام هذه القناة تحديد أولويات التخصصات المطلوبة لسوق العمل والأعداد وطبيعة المهارات الذهنية والسلوكية المطلوبة.
- تتفق الجهتان على معايير الجودة المقبولة للتعليم والتدريب، ويشمل ذلك كل ما يتعلق بالعملية التعليمية والتدريبية.
- بناء على المعلومات يتم إعداد الخطط اللازمة لتنفيذ المطلوب.
- تباشر المؤسسة التدريبية في عملية إعداد الكوادر المطلوبة (أنظر آليات التنفيذ المبينة أعلاه)، وعند انتهاء أي عملية التدريب تبلغ الجهة المعنية (سوق العمل) بجهوزية القوة المنتجة لمباشرة العمل، وكجزء من متطلبات التأهيل بالبرنامج التدريبي.
- تقوم الجهة المستفيدة بالتواصل مع المؤسسة التدريبية وذلك من خلال تزويدها بالبيانات الهامة عن مدى استفادة الجهة من القوة المنتجة، وما هي النقاط الإيجابية والسلبية المسجلة عن القوى المنتجة.
- يجتمع فريق من الجهتين لدراسة البيانات الخاصة بحالة المنتجين، وتحديد النقاط الإيجابية لتقويتها وتضمينها في البرامج اللاحقة لإكمال البرنامج، والنقاط السلبية لتجنبها.

تتكرر هذه الدورة عند نهاية كل برنامج تعليمي أو تدريبي وتخزن النتائج في قواعد بيانات يتم الاستدلال بها مستقبلا.

منهجية التطبيق باستخدام التقنيات الحديثة المتاحة.

تستخدم التقنيات المتاحة لتنفيذ الآليات المقترحة، وتشمل التالي:

تستخدم التقنيات المتاحة لتنفيذ الآليات المقترحة، وتشمل التالي:

1 - إدخال كافة البيانات المتعلقة باحتياجات سوق العمل ضمن قاعدة بيانات تكون مفتوحة (قراءة فقط) للمؤسسات التعليمية والتدريبية المختلفة التي تدخل في الاتفاق مع سوق العمل.

2 - إدخال كافة البيانات عن كل مؤسسات التعليم والتدريبي المختلفة، وبحيث يتم تحديد قدرات المؤسسات في تنفيذ البرامج التدريبية المختلفة، ونوعية التجهيزات المتوفرة الخ.. وتكون قاعدة البيانات مفتوحة من حيث الاطلاع لكافة الأطراف في سوق العمل.

3 - يتم التواصل بين الطرفين من خلال وسائل الاتصالات المتاحة ومنها:

- شبكة المعلومات الوطنية المؤمنة من كافة الأخطار[5] وتكوين شبكة افتراضية.
- شبكة المعلومات الدولية "الانترنيت" وتكوين موقع خاص بالبرنامج مع ضمان الحماية الضرورية تجنبا للاختراقات.
- التواصل عبر الرسائل القصيرة باستخدام الهاتف النقال وعقد مؤتمرات عن بعد.
- التواصل عبر جهاز الناسوخ.

4 - تختار جهة سوق العمل المؤسسة التعليمية والتدريبية التي ترغب في التعامل معها وإبرام عقد ويتم الاتصال بينهما بالخصوص.

5 - يتم التنفيذ وفق الآلية المقترحة كما جاء في آليات التنفيذ ومسؤوليات كل طرف أي أن تكون المعلومات والبيانات عن المتدربين وعن أماكن العمل بسوق العمل ضمن المعلومات المتبادلة بين الطرفين ويتم تحويل النتائج وكذلك ملاحظات العمل الكترونيا وتكون وصلات الربط فاعلة بينهما.

مقترح بخوارزمية تحدد آلية التعاون بين مؤسسات التعليم التقني وسوق العمل:

الخوارزمية المبينة في الشكل رقم(1) تبين آلية التعاون بين سوق العمل ومؤسسات التعليم التقني، والهدف دائما ضمان العلاقة الوثيقة بين الطرفين وبما يحقق المصلحة العليا للبلد.

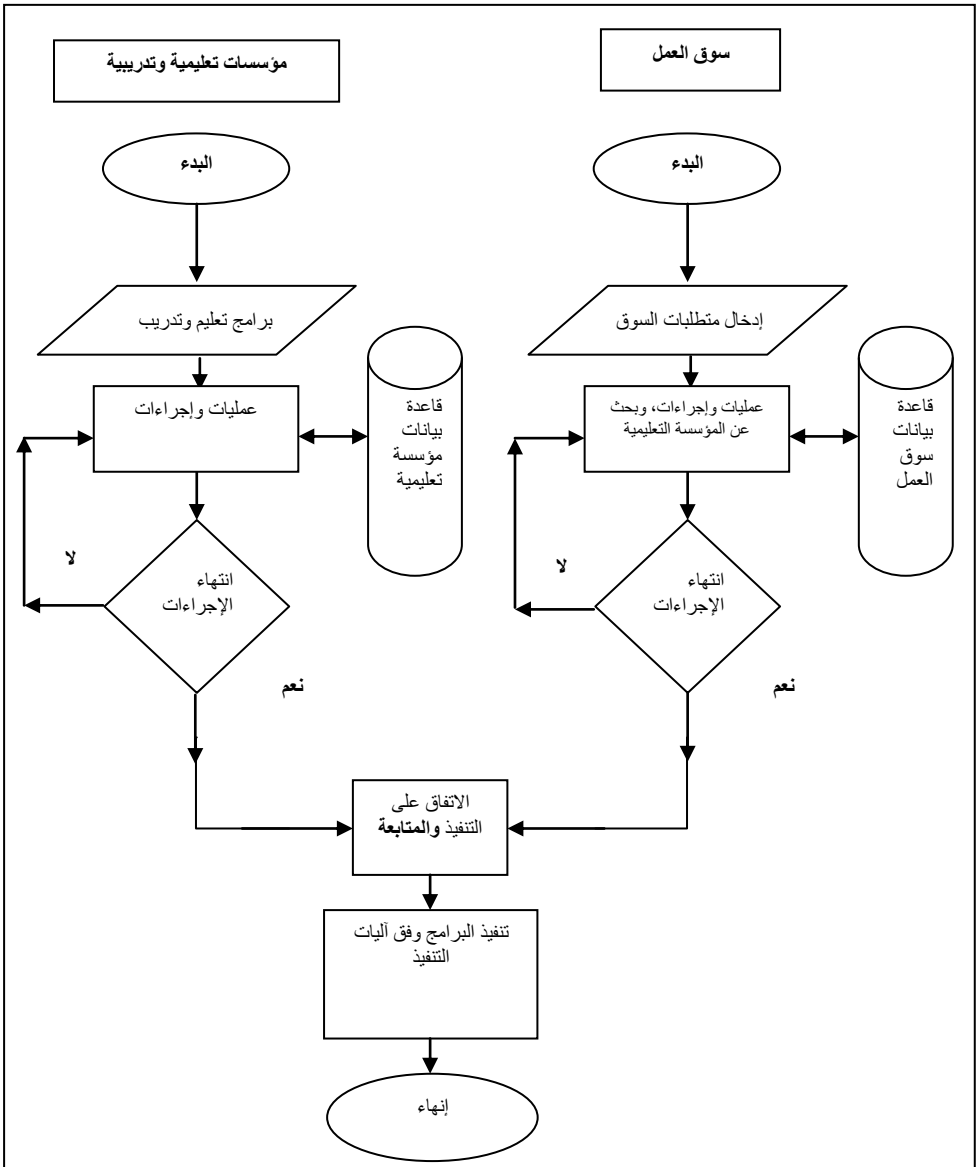
مؤسسات تعليمية وتدريبية
سوق العمل
البدء
البدء
برامج تعليم وتدريب
إدخال متطلبات السوق
عمليات وإجراءات
عمليات وإجراءات، وبحث عن المؤسسة التعليمية
قاعدة بيانات مؤسسة تعليمية
قاعدة بيانات سوق العمل
لا
لا
انتهاء الإجراءات
انتهاء الإجراءات
نعم
نعم
الاتفاق على التنفيذ والمتابعة
تنفيذ البرامج وفق آليات التنفيذ
إنهاء

شكل رقم(1)، خوارزمية تواصل بين سوق العمل والمؤسسات التعليمية والتدريبية

لاشك، فإن تطبيق هذه التجربة سينجم عنها العديد من الفوائد، ويوضح الجدول رقم(2) مقارنة لمؤشرات النجاح.

جدول رقم(2)، مقارنة لمؤشرات النجاح في التطبيق

المؤشر	الطريقة القديمة	الطريقة الجديدة (الشراكة)	ملاحظات
وجود العلاقة المباشرة	لا	نعم	العلاقة بين سوق العمل ومؤسسات التعليم التقني من خلال قواعد البيانات والتواصل
تقليل الهدر	لا	نعم	هنا الهدر في الوقت، الجهد، والمال أثناء العملية التعليمية والتدريبية
معرفة جودة برامج التعليم أو التدريب آنيا	لا	نعم	يمكن قياس جودة العملية التعليمية مباشرة من خلال تقييم مستوى الأداء للخريجين
إنجاز العملية التدريبية	إنجاز حسب الجدول	الأسرع في الانجاز	السرعة بسبب توفر الرد من جهة العمل الكترونيا
ضمان الحصول على وظيفة	لا	نعم	المئات من الخريجين يبقون بدون فرص عمل في النظام القديم
تطابق البرامج التعليمية والتدريبية مع حاجة السوق الفعلية	لا	نعم	بسبب ووجود المعلومات والبيانات المتبادلة بين الطرفين بصفة مستمرة
التواصل مع الخريجين	لا	نعم	الموقع الالكتروني وفرصة استخدامه من الخريجين

النتائج والتوصيات:

بسبب مد جسور التواصل بين سوق العمل ومؤسسات التعليم التقني، فإن الاستخدام الممنهج للتقنيات الحديثة سيترتب عنه نقلة موضوعية ستبعد كلا الجهتين عن الفوضى في حالة غيابه، ولعل أهم النتائج المتوخاة التالي:

1 - زيادة وتوسيع وتعميق دائرة ارتباط مؤسسات التعليم والتدريب التقني بصورة فعالة مع سوق العمل.

2 - التحقيق الفعلي لمبدأ الشراكة بين الجهتين (سوق العمل ومؤسسات التعليم والتدريب التقني) وبما يحقق المصلحة العليا للبلد.

3 - تقليل الهدر في المال والجهد والوقت والذي يمكن استثماره في التمكن من تعليم أعداد كبيرة لا يمكنها أن تنال تعليم أو تدريب عالي التخصصية وفق الأساليب القديمة.

4 - تفعيل استخدام التقنيات الحديثة بشكل إيجابي وتسخيرها لتحقيق مردود مادي ومعنوي مهم.

5 - إمكانية تطوير العملية التعليمية متاحة وذلك لوجود التواصل بين سوق العمل والمؤسسات التعليمية والتدريبية والخريجين وفرصتهم لتقديم ملاحظاتهم بالخصوص.

6 - يمكن تحقيق معايير الجودة في الأسلوب الجديد من خلال المعاينة المستمرة وتصحيح المسار حسب الاعتماد على التقنيات الحديثة.

7 - معايير التنافس ميسرة بين كافة الفرقاء لسهولة النفاد للمواقع الالكترونية المتاحة وهذا سيعمل على تحسين الجودة.

8 - لن يكون هناك بطالة للخريجين؛ بل ستزداد فرص حصولهم على مزايا وظيفية أفضل.

الخلاصة:

مما ورد بهذه الورقة نرى أن فرص نجاح الشراكة بالاعتماد على استخدام التقنية الحديثة المتاحة سوف يحقق ويعمل على إيجاد الشراكة الحقيقية وهذه لن ترضي سوق العمل فحسب بل تفتح آفاق وفرص جديدة أمام خريجي المؤسسات التقنية والتدريبية.

المراجع:

[1] أ.جمعة علي عبد الله الزوالي، "تنمية التعليم التقني في العالم العربي"، المجلة العربية للتعليم التقني، المجلد 21، العدد 1، ص 103-118، طرابلس- ليبيا، الطير (أبريل)، 2009م.

[2] أ.جمعة علي عبد الله الزوالي، هل هناك حاجة لتطوير آليات ومناهج التعليم التقني في البلاد العربية؟، المجلة العربية للتعليم التقني، المجلد20 ، العدد 1، ص 73-83 ، طرابلس – ليبيا، 2008م.

[3] أ.د عبد القادر الصادق عكي و أ.د موسي محمد موسي، منهجية حول إعداد وتصميم برنامج تدريبي لتدرج الخبرة للمهندسين بالقطاعات الخدمية والإنتاجية، المجلة العربية للتعليم التقني، المجلد 20، العدد3، ص 30-57، طرابلس – ليبيا، 2008م.

[4] أ.جمعة علي عبد الله الزوالي، أهمية استخدام المعلوماتية في التعليم التقني، المجلة العربية للتعليم التقني، المجلد20، العدد2، ص 92-112، طرابلس – ليبيا، 2008م.

[5] Dr. Mousa M. Mousa & Giuma A. Zwali, Security Aspects of Information Networks, The National Concern, The Proceeding of the Scientific Society of Libyan Engineers, PP119-136, Tripoli – Libya, 16-17.5.1998.

تعرض الإنسان للمجالات الكهرومغناطيسية المنبعثة من خطوط النقل ذات الجهد العالي

HUMAN EXPOSURE TO ELECTROMAGNETIC FIELDS RADIATED FROM HIGH VOLTAGE TRANSMISSION LINES

الأستاذ الدكتور / صلاح الدين عبد الستار محمد

قسم الهندسة الكهربائية . كلية الهندسة . جامعة الطائف . المملكة العربية السعودية

sabdelsattar@yahoo.com

ملخـص :

إن استخدام المعدات والأجهزة الكهربائية بالمنازل والمعامل والمختبرات والمكاتب وكافة أماكن العمل . التى تشع مجالات كهرومغناطيسية . يؤدي الي ارتفاع درجة التلوث الكهرومغناطيسي بتلك الأماكن مما يجعل مستخدميها أكثر تعرضا لتلك المجالات وبقيم عالية ولفترات ليست بالقصيرة مما يؤثر سلبا علي صحتهم. كما أن التوصيلات الكهربائية المنفذة بطريقة غير سليمة بالمنشآت المختلفة يصاحبها أيضا زيادة في قيمة المجالات الكهرومغناطيسية المنبعثة مما يؤدي الي ارتفاع درجة التلوث الكهرومغناطيسي واتساع مناطق التلوث. ومن ناحية أخري فإن النمو المتزايد للمدن والمجتمعات أدى إلى ظهور مجتمعات جديدة والزحف تجاه خطوط نقل وتوزيع الطاقة الكهربائية فأصبحت أماكن الإعاشة قريبة جدا من تلك الخطوط الكهربائية التى تشع مجالات كهرومغناطيسية التي قد تترك أثرا صحيا سيئا لمتعرضيها.

فى هذه الورقة يتم إلقاء الضؤ علي مشكلة التعرض للمجالات الكهرومغناطيسية بالوسط المحيط متضمنا عرض تأثير التعرض لتلك المجالات بالمناطق الملوثة كهرومغناطيسيا علي صحة الإنسان وكذلك أهم مصادر . بالوسط المحيط بنا . ملوثات البيئة كهرومغناطيسيا. كما يتم دراسة ومناقشة النتائج التي تم الحصول عليها بإجراء بعض القياسات لقيم المجالات المغناطيسية المنبعثة من مصادر التلوث الكهرومغناطيسي بالوسط المحيط بنا لتقنين وتحديد درجة التلوث. كما يتم

مقارنة النتائج بالمناطق الملوثة كهرومغناطيسيا بالقيم المرجعية للمجال المغناطيسى المسموح بها حتى يمكن تقييمها ومعرفة ما إذا كانت قيما آمنة للإقامة والعمل الدائمين أم غير آمنة.

كما يتم وضع بعض الاقتراحات والتوصيات التى تتعلق بالتصدى لهذه الظاهرة والتى تخص التلوث الكهرومغناطيسي الناتج من استخدامنا للكهرباء.

مقدمة :

إن للطاقة الكهربائية دورا كبيرا وفعالا في التنمية وذلك لاستخدامها على نطاق واسع في الحياة اليومية ويستعان بنظم التوليد والنقل والتوزيع لوصول الطاقة الكهربائية للمستهلك ، وعادة تكون محطات التوليد بعيدة عن مكان الاستهلاك فيتم نقل الطاقة الكهربائية بخطوط نقل هوائية ذات جهد عال. يكون مسار خطوط نقل الطاقة الكهربائية المعلقة عادة خارج المدن السكنية فنجد أنه يمر خارج المدن خطوط نقل الطاقة الكهربائية المعلقة ذات جهود مختلفة القيم. ونتيجة للزيادة المستمرة في عدد السكان ببعض المدن والتوسع العمراني المطلوب زادت المناطق السكنية وبدأ الزحف العمراني نحو حرم تلك الخطوط حتى أصبحت خطوط نقل الطاقة الكهربائية بالفعل داخل التجمعات السكنية. كما أن التقدم التكنولوجي الذي نعاصره حاليا أدي إلي زيادة الاعتماد علي الأجهزة الكهربائية مما أدي إلي زيادة تعرض السكان للمجالات الكهرومغناطيسية المنبعثة من هذه الأجهزة.

إن الأجهزة الكهربائية وخطوط نقل وتوزيع الطاقة الكهربائية تضخ مجالات كهربائية ومغناطيسية في الوسط المحيط لهذه المصادر وبالتالي فإن المستخدمين للأجهزة الكهربائية والأطفال بالحدائق والناس بالمباني والفلاحين بالحقول القريبة من هذه الخطوط يتعرضون للمجالين الكهربائي والمغناطيسي الناتجين من هذه المصادر[11-17] . وإنه لمن المعلوم لا يمكن استخدام جهاز كهربائي أو توليد ونقل وتوزيع الطاقة الكهربائية بدون توليد هذه المجالات ذات تردد 60/50 هرتز والذي يصنف تبعا للمجالات الكهرومغناطيسية منخفضة التردد (Extremely Low Frequency (ELF التي ثبت أن لها تأثيرا ضارا بصحة الإنسان[12,18,20-24] الذي يتعرض لها.

ومن حسن الحظ أن الأشجار والأجسام المؤرضة والمباني تعمل على حجب المجالات الكهربائية الناجمة من مصادر الانبعاث الكهرومغناطيسي بينما لا تحجب المجالات المغناطيسية. إن حجب المجالات المغناطيسية

ليس أمراً سهلاً ولكنه يحتاج لبعض المتطلبات الخاصة. ومما يزيد من خطورة التعرض للمجالات المغناطيسية أن الناس لا يشعرون بوجود المجال المغناطيسي ما عدا العالي نسبيا منه. ومن المعروف أن تعرض جسم الإنسان لمجال مغناطيسي ينتج عنه تيارات دوامية بالجسم تمر في حلقات أو دوائر عمودية على المجال المغناطيسي الناتج عن خطوط القوى الكهربائية ويكون لهذه التيارات الأثر الصحي السيئ على الجسم إذا تعرض لها[20,24] .

بإيجاز هناك تأثيرات سلبية ومخاطر ناتجة عن التعرض للمجالات الكهرومغناطيسية المنبعثة من مصادر الانبعاث الكهرومغناطيسي خاصة ذات الجهد العالي القريبة من المباني والساحات الشعبية والحدائق والمنتزهات والحقول وقرب تلك المصادر من التجمعات العمرانية الجديدة جعل قيم المجال الكهربائي والمغناطيسي ترتفع وقد تتعدى القيم المسموح بها مما يكون لها الأثر الضار بصحة الإنسان والحيوان والنباتات[11,20-24] خاصة عند زيادة الأحمال.

في هذا البحث يتم إلقاء الضوء علي مشكلة التعرض للمجالات الكهرومغناطيسي بالوسط المحيط بنا متضمنا تأثير التعرض للمجالات الكهرومغناطيسية بالبقاء بالقرب من مصادر ملوثات البيئة كهرومغناطيسيا. كما يتم دراسة ومناقشة النتائج التي تم الحصول عليها بإجراء بعض القياسات لقيم المجالات المغناطيسية المنبعثة من بعض مصادر التلوث الكهرومغناطيسية بالوسط المحيط بنا خاصة الأماكن القريبة من خطوط نقل وتوزيع الطاقة الكهربائية. كما يتم مقارنة النتائج التي تم التوصل إليها بالمناطق الملوثة كهرومغناطيسيا بالقيم المرجعية للمجال المغناطيسي المسموح بها حتى يمكن تقييمها ومعرفة ما إذا كانت قيما آمنة للإقامة والعمل الدائمين أم غير آمنة.

كما يتم وضع بعض الاقتراحات والتوصيات التي تتعلق بالتصدي لهذه الظاهرة والتي تخص التعرض للمجال المغناطيسي المنبعث من مصادر ملوثات البيئة كهرومغناطيسيا متمثلا في استخدام الكهرباء بجميع جوانبه.

خلفية الدراسة :

إن مصادر ملوثات البيئة كهرومغناطيسيا تشع مجالات كهرومغناطيسية (كهربائية ومغناطيسية) وقد وجد أن المجال الكهربائى يحجب بالمباني والأشجارعكس المجال

المغناطيسى والذي يعتمد أساسا على تيار تحميل الخط ومن المعروف أن هذه المصادر ذات تيارات كبيرة وعليه فإنها تشع مجالات كهرومغناطيسية وتكون قيم هذه المجالات مرتفعة بالقرب من المصدر وتتناقص مع زيادة البعد عن هذه المصادر. كما أن الزيادة في كمية الطاقة الكهربائية والتوصيل العشوائي للتوصيلات الكهربائية بالمنشآت السكنية والتجارية والتعليمية واستخدام الأجهزة والمعدات الكهربائية بصورة مفرطة كل ذلك يؤدي الي ارتفاع درجة خطورة التعرض للمجالات المغناطيسية واتساع رقعته مما يجعلنا نحذو حذو الكثير من الباحثين ونلقي الضؤ علي هذا الموضوع بالوسط المحيط بنا.

يحس الناس عادة بالمجالات الكهربائية العالية بينما معظم الناس لا يشعرون بوجود المجال المغناطيسي ما عدا العالي نسبيا منه. ومن حسن الحظ . كما ذكر سابقا . أن الأجسام تعمل على حجب المجالات الكهربائية بينما لا تحجب المجالات المغناطيسية وبالتالي لا تتأثر قراءات الأجهزة المستخدمة بجسم القارئ. ونظرا لصعوبة حجب المجالات المغناطيسية تم التركيز في هذا البحث علي المجالات المغناطيسية. إن التعرض للمجالات الكهربائية تسبب حثا كهروستاتيكيا في الأجسام التي تتعرض لها وينتج من هذا الحث تياراً[3، 4، 18، 24، 31] أما التعرض للمجال مغناطيسي فيكون في صورة تيارات دوامية بالجسم تمر في حلقات أو دوائر عمودية على المجال المغناطيسي الناتج عن المصادر. كما يكون لهذه التيارات الأثر الفسيولوجي على جسم الإنسان أيضا إذا تعرض لها[12, 18] .

ومن ناحية أخري لابد من التأكد من قيم المجالات المغناطيسية داخل تلك المبانى. وذلك تفاديا لما توصلت اليه بعض الدراسات بأن هناك تأثيرا على الإنسان عند تعرضه للمجالات الكهرومغناطيسية قد تصل إلى إصابته بالأمراض السرطانية. فقد لاحظ بعضهم[27] أن بعض الأطفال توفوا متأثرين بالأمراض السرطانية عند تعرضهم للمجالات الكهرومغناطيسية وقد وصلت نسبتهم إلى إصابة طفلين من كل ثلاثة أطفال وذلك بالمناطق القريبة من خطوط القوى الكهربائية والتى تبعد عنها حوالى 40 متر.

مما سبق يتضح أنه لابد من قياس المجالات المغناطيسية بالوسط المحيط بنا خاصة داخل المباني ومقارنتها بالقيم المسموح بها[32-35] .

القيم المرجعية للمجالات الكهرومغناطيسية:

يقاس المجال المغناطيسي بالجاوس وهو يساوى 10^{-4} تسلا وأيضا يساوى 0.0125 أمبير/ متر . وقد لوحظ أن جاوس واحد قد يسبب تياراً كثافته حوالي 100 نانو أمبير/سم^2 في الجسم المعرض له . كما لوحظ أن مجالا كهربائيا كثافته 1 كيلو فولت/متر يسبب تياراً كثافته حوالي 30 نانو أمبير/ سم^2 [9، 31] .

لقد أشار كثير من المهتمين بهذا الموضوع إلي أنه من الصعب أن يقال أن هناك قيمة معينة للمجال المغناطيسي تؤخذ كقيمة آمنة لتعرض الإنسان لقيم أقل منها وذلك لاختلاف القيم المرجعية من بلد لبلد آخر بل من مدينة لأخرى. لقد لوحظ أنه لا يوجد بالولايات المتحدة الأمريكية قيماً مرجعية موحدة لمستوى المجالات المغناطيسية[9, 18, 26, 32-35] فمعظم الولايات لم تضع قيماً محددة مسموح بها للمجالات المغناطيسية وقد حدد المؤتمر الأمريكي للصناعات الحكومية 10 جاوس كقيمة للمجال المغناطيسي المسموح تعرض العمالة له. وفى ولاية نيويورك الأمريكية وضعت القيمة 200 جاوس للمجال المغناطيسي عند حافة حق مسار خطوط الطاقة الكهربائية بينما ولايات أخرى مثل كاليفورنيا اعتبرت أن حد الأمان بالمدارس هو 1.2 ملي جاوس وفي مدينتي بريتوود تتسي وارفين كاليفورنيا حددت 4 ملى جاوس كأقصى قيمة آمان مسموح بها للمجال المغناطيسي. بعض تنظيمات المدن حددت قيمة المجال المغناطيسي المسموح بالتعرض له هو 2 ملى جاوس والبعض الآخر نزل إلي 1 ملي جاوس[10, 18, 32-35]. أما في سويسرا فأقرت القيمة 2.5 ملي جاوس هي القيمة المرجعية للتعرض للمجالات الكهرومغناطيسية[33] EMF/ELF.

كما هو واضح من الدراسات السابقة نلاحظ أن هناك تفاوت كبير من مكان لآخر بالنسبة لتحديد القيم المسموح بها للمجالات المغناطيسية[11, 18, 32-35] مما زاد من أهمية الموضوع خاصة وأنه يمس صحة الإنسان مباشرة. الأمر الذي يدعم اعتماد أقل هذه القيم المرجعية ولتكن 2 ملي جاوس كحد للإقامة والعمل الدائمين.

إجراءات القياس:

- لاختبار درجة التلوث الكهرومغناطيسي بأي مكان مثل المنازل وأماكن التعليم ، والشوارع والأماكن العامة ، والأماكن القريبة من مصادر التلوث الكهرومغناطيسي... الخ يجب قياس قيم المجال المغناطيسي بتلك الأماكن لمقارنتها بالقيم المرجعية الآمنة.
- أستخدم في قياس المجالات المغناطيسية جهاز القياس[35] المعروف باسم Magnetic Field Meter EMF/ELF

Meter, TM-191 ومدي القياس له هو 0.1 mG إلي 2000 mG. كما استخدم أيضا جهاز SPECTRAN NF 5010 spectrum analyzers لنفس الغرض والذي يقوم بتسجيل النتائج.

- تم إجراء القياسات للمجال المغناطيسي بأجهزة القياس علي ارتفاع 60 سم من سطح الأرضية بالمكان المعني.
- جسم الشخص القائم بإجراءات القياس لا يؤثر علي القيم المقاسة وذلك نظرا لضعف مقدرته علي حجب المجالات المغناطيسية.
- تم إجراء القياسات للمجال المغناطيسي بالمساحة الواقعة خارج المبني والواقعة بين الخط والمبني.
- تم إجراء القياسات للمجال المغناطيسي بالقرب من مصادر انبعاث المجالات المغناطيسية وبداخل المبني وخلال الجزء المواجه للخط وخلال طوابق المبني المختلفة.
- تمت القياسات عند تيار حمل معين.
- قيمة المجال المغناطيسي بالملي جاوس.
- قيمة المجال المغناطيسي . علي سبيل المثال ـ سوف تزيد بمقدار حوالي 65 % (أي تصبح قيمة المجال 1.65 من القيم التي تم قياسها عند حمل 130 أمبير) عندما يصبح تيار الحمل 215 أمبير وقت الذروة.

النتائج والمناقشات :

المجال المغناطيسي داخل شقة سكنية:

لتقييم قيمة المجال المغناطيسي الناتج من مصادر التلوث المغناطيسي الخارجي ولمعرفة قيم المجال المغناطيسي العادية والمحيطة بنا يتوجب علينا أولا قياس المجالات المغناطيسية داخل شقة سكنية بعيدة عن مصادر التلوث الخارجية. والشقة محل القياس تتكون من غرفتين للنوم وغرفة معيشة وغرفة مطبخ وحمامين بالإضافة إلي مدخل الشقة وطرقة مؤدية إلي الغرف ومضاءة بلمبات الفلوريسنت. والجدول رقم 1 يبين القيم المقاسة للمجال المغناطيسي داخل تلك الشقة السكنية بواسطة جهاز القياس الذي يوضع مباشرة بمكان القياس المعني.

جدول (1): قيم المجال المغناطيسي المعتادة داخل شقة سكنية بعيدة عن مصادر التلوث الخارجية.

المكان	المجال المغناطيسي (ملي جاوس)
مدخل الشقة	0.2 . 0.3
الطرقة المؤدية للغرف	0.3
المطبخ	0.2 . 5.1
الطرقة المؤدية للمطبخ والحمام الصغير	0.3
الحمام الصغير	0.3 . 3.3
الحمام الكبير	0.3
حجرة النوم 1	0.3
حجرة النوم 2	0.3

حجرة المعيشة	0.2 . 29.0

يتضح من هذا الجدول أن قيمة المجال المغناطيسي المعتادة داخل الشقة السكنية بدون تأثير مصادر التلوث الخارجية هي 0.2 ملي جاوس ما عدا الأماكن القريبة من مصادر التلوث الداخلية مثل الثلاجة والتلفزيون فقد تصل إلي 29 ملي جاوس.

ومن ناحية أخري فقد لوحظ أن قيمة المجال المغناطيسي بالأماكن المحتوية علي مصادر التلوث الخارجي تعتمد علي البعد عن تلك المصادر. فقيمة المجال المغناطيسي تزيد كلما قلت المسافة بين التلفزيون ومكان القياس من جميع جوانبه كما هو موضح بالجدول رقم 2. كما أن قيم المجال المغناطيسي تختلف من جانب إلي آخر حول التلفزيون وذلك بسبب مكونات التلفزيون الداخلية.

جدول (2): توزيع المجال المغناطيسي بالمنطقة المحيطة بالتلفزيون.

المسافة (سم)	أمام التلفاز	علي جانب التلفاز الأيسر (يمين المشاهد)	علي جانب التلفاز الأيمن (يسار المشاهد)
0	27	206	249
10	14	83	69
20	9	55	29
30	6	28	14
40	3.2	14	9
50	1.9	9	5
50	1.2	5	3
70	0.9	4	2
80	0.7	2	1.5

المجال المغناطيسي من حولنا:

الجدول رقم 3 يبين توزيع المجال المغناطيسي أمام مصدر آخر من مصادر التلوث بالمنطقة المحيطة بنا وهي لوحة توزيع كهرباء المنزل وهي لوحة توزيع ذات عرض 200 سم لتغذية عدد 16 شقة وتحتوي علي عدادات القياس ومدخل الكهرباء العام وأجهزة الحماية للشقق. ويتضح من هذا الجدول أن قيمة المجال المغناطيسي تبلغ أقصي قيمة لها عند موضع المغذي الرئيسي لهذه اللوحة (0 سم) وتقل كلما زادت المسافة عن هذا الوضع.

هذا وقد اتضح من القياسات ببعض الأماكن العامة أن قيمة المجال المغناطيسي العادية تتراوح بين 0.2 ، 0.5 ملي جاوس عدا الأماكن التي تحتوي علي مصادر تلوث كهرومغناطيسي فقد ترتفع القيمة إلي 22 ملي جاوس أو أكثر كما هو موضح بالجدول رقم 4.

جدول (3): توزيع المجال المغناطيسي أمام لوحة توزيع كهرباء منزل.

المسافة بعدا عن المدخل الرئيسي (سم)	قيمة المجال المغناطيسي (ملي جاوس)
- 50 (يمين)	5
0 (المغذي الرئيسي)	30
+ 50 (يسار)	18

100 +	15
150 +	10
200 +	7

المجال المغناطيسي أسفل بعض خطوط الجهد العالي:

الجدول رقم 5 يعرض القيم القصوى للمجال المغناطيسي أسفل بعض خطوط نقل وتوزيع الطاقة الكهربائية ذات الجهد العالي. وقد لوحظ أن قيمة المجال المغناطيسي المنبعث من تلك الخطوط تتناسب مع تيار الحمل وليس الجهد. كما أن قيمة تلك المجال تكون أكبر ما يمكن أسفل الخط وتقل كلما بعدنا عن محوره.

المجال المغناطيسي ببعض الأماكن القريبة من بعض خطوط الجهد العالي:

لقد لوحظ أن قيم المجال المغناطيسي بالمناطق القريبة من خطوط نقل وتوزيع الطاقة الكهربائية ليست بالقيم المعتادة طبقا لبعدنا عن تلك الخطوط. ولتقييم ذلك تم اختيار مبني قريب من أحد هذه الخطوط وتم إجراء القياسات خارجه وداخله كما هو موضح بالجداول 6 . 14.

جدول (4): قيم المجال المغناطيسي ببعض الأماكن العامة.

المكان	المجال المغناطيسي (ملي جاوس)
بعض المدارس	0,2 . 3,1
بعض المتاجر	0,3 . 9,2
بعض الشوارع	0,47 . 6,4
بعض أماكن الجامعة	0,2 . 22,4
بعض السيارات	0,2 . 18,2

جدول (5): أقصي قيمة للمجال المغناطيسي أسفل بعض خطوط الجهد العالي.

الخط	المجال المغناطيسي (ملي جاوس)
خط 500 كيلو فولت	106
خط 220 كيلو فولت	6,3
خط 132 كيلو فولت	6,3
خط 33 كيلو فولت	14
خط 11 كيلو فولت	3,6

ويتكون المبني محل القياسات من تسع طوابق (أرضي + ثمانية طوابق علوية) وهو قريب من خط جهد عالي ثلاثي الطور 132 كيلو فولت ذو حمل متغير من 60 إلي 215 أمبير (عند الذروة). ويقع هذا المبني شمال الخط وتبعد واجهته القريبة من الخط عن محور الخط (وسط الأوجه) مسافة متغيرة تتراوح بين 12 . 20 متر.

وقد تم إجراء القياسات للمجالات المغناطيسية داخل جدار المبني المواجه للخط مباشرة وعندما كان تيار الحمل 130 أمبير كما هو موضح بالجدول 6. ويتضح من هذه النتائج أن أقل وأقصى قيمة لشدة المجال المغناطيسي هي

2.5 ملي جاوس (بالدور الأرضي) و 6.5 ملى جاوس (بالطابق السابع العلوي) وهى قيمة غير آمنة نسبيا للإقامة الدائمة. ونظرا لأن المسافة بين موصلات الخط ونقطة القياس بالطوابق تقل مع زيادة ارتفاع الطابق عن سطح الأرض حتى الطابق السابع ثم تبدأ في الزيادة بعد ذلك فإن قيمة المجال تزيد مع ارتفاع الطابق حتى الطابق السابع ثم تبدأ في التناقص كما هو موضح بالجدول 6. والجدير بالذكر أن هذه القيم قابلة للزيادة مع زيادة تيار حمل الخط خاصة وقت الذروة.

الجدول 7 يعرض نتائج القياسات ولكن عند محور آخر داخل المبني وبالأدوار المختلفة والذي يبعد 5 م عن الجدار المواجه للخط مباشرة وعندما كان تيار الحمل 130 أمبير. وقيم المجال المغناطيسي عند هذا المحور أقل من نظيرتها المعروضة بالجدول 6 عند نفس الحمل.

ولتقييم حد أمان الإقامة بشقق هذا المبني والمواجهة للخط تم تقدير القيم المتوسطة لهذا المجال وذلك بإجراء القياسات بأحدي هذه الشقق بالمبني والمواجهة للخط وبالأدوار المختلفة عندما كان تيار الحمل 130 أمبير كما هو موضح بالجدول 8.

وبمقارنة تلك القيم بالقيم المسموح بها للإقامة الدائمة يتضح أنها قيما غير أمنة للإقامة الدائمة خاصة بحجرة النوم وبالبلكونة بتلك الشقق كما هو موضح بالجدولين 9 ، 10 علي التوالي. والجدير بالذكر أن درجة الأمان تقل مع زيادة تيار حمل الخط خاصة وقت الذروة.

جدول (6): أقصي قيمة متوسطة للمجال المغناطيسي داخل المبني وبالأدوار المختلفة داخل الجدار المواجه للخط مباشرة وعندما كان تيار الحمل 130 أمبير.

الطابق	المجال المغناطيسي (ملي جاوس)
الثامن	6.5
السابع	6.8
السادس	6.7
الخامس	6.6
الرابع	5.5
الثالث	4.8
الثاني	4.1
الأول	3.6
الأرضي	2.5

جـدول (7): أقصـي قيمـة متوسـطة للمجـال المغناطيســـي داخـــل المبنـــي وبالطوابق المختلفة عند محور يبعد 5 م مـن الجـدار المواجـه للخـط مباشـرة وعنـدما كـان تيـار الحمـل 130 أمبير

الطابق	المجال المغناطيسي (ملي جاوس)
الثامن	3.6
السابع	4.03
السادس	3.9
الخامس	3.7
الرابع	3.6
الثالث	3.4
الثاني	3.1
الأول	2.5
الأرضي	.

الجـدولان 11 ،12 يعرضـان توزيـع المجـال المغناطيسـي داخل أحد هذه الشقق والتي تقع بالطـابق الرابـع العلوي والمواجهـة للخـط وخـلال محورين أحدهما بجانب الجدار المواجه للخط مباشـرة (جـدول 11) والآخـر يبعـد مسـافة 5 م شمال المحور الأول ومتجهان من الشرق إلـي الغرب وعند تيار حمل 130 أمبير. ويتضح من هذه القيم أنها غير آمنة للإقامة الدائمة.

جدول (8): القيم المتوسطة للمجال المغناطيسي داخـل الشـقة بـالمبني والمواجهـة للخـط وبـالطوابق المختلفـة وعنـدما كان تيار الحمل 130 أمبير.

الطابق	المجال المغناطيسي (ملي جاوس)
الثامن	3.83
السابع	4.7
السادس	4.7
الخامس	4.5
الرابع	3.2
الثالث	3.1
الثاني	2.8
الأول	2.5
الأرضي	.

ولتقييم قيم المجال المغناطيسي خارج المبني تم إجراء القياسات خارج المبني خلال محورين يقعان بالمساحة بين المبني وبين الخط أحدهما من الجهة الغربية للمبني (جدول 13) والمحور الآخر بالجهة الشرقية للمبني (جدول 14) بداية

من أسفل الخط (0 م) متجها إلي المبني وعند تيار حمل 130 أمبير.

ويتضح من النتائج المعروضة بالجدولين 13، 14 أن قيم المجال المغناطيسي أسفل خط نقل الطاقة الكهربائية يزيد مع زيادة البعد عن محور الخط إلي أن يصل إلي أقصي قيمة له ثم يبدأ في النقصان متجها إلي المبني. هذا ويتضح أيضا أن قيم المجال المغناطيسي خارج المبني وخلال المساحة بين الخط والمبني هي قيما غير آمنة للمكث بها فترة طويلة.

جدول (9): المجال المغناطيسي وسط حجرة النوم القريبة من الخط وبالطوابق المختلفة وعندما كان تيار الحمل 130 أمبير.

الطابق	المجال المغناطيسي (ملي جاوس)
الثامن	4.2
السابع	4.3
السادس	4.35
الخامس	4.4
الرابع	3.3
الثالث	3.5
الثاني	3.2
الأول	2.6
الأرضي	.

مما سبق يتضح أن التنمية والتطور العمراني أدى إلى الزحف تجاه خطوط نقل وتوزيع الطاقة الكهربائية التي كانت خارج نطاق الكردون فأصبحت قريبة من أو تخترق التجمعات العمرانية بما فيها من مباني للعمل والسكن وكذلك الحدائق والمنتزهات. الأمر الذي أدى إلى التعرض للمجالات المغناطيسية الناجمة عن تلك الخطوط والتي قد يصل تأثيرها علي صحة الإنسان إلى درجة خطيرة.

جدول (10): المجال المغناطيسي بالبلكونة المواجهة للخط وبالأدوار المختلفة وعندما كان تيار الحمل 130 أمبير.

الطابق	المجال المغناطيسي (ملي جاوس)
الثامن	5.1
السابع	5.5
السادس	5.3
الخامس	5.2
الرابع	5.0
الثالث	4.5
الثاني	.
الأول	.
الأرضي	.

الخلاصة:

جدول (11): توزيع المجال المغناطيسي داخل شقة بالطابق الرابع العلوي بالمبني والمواجهة للخط وخلال محور داخل الجدار المواجه للخط مباشرة متجها من الشرق إلي الغرب وعندما كان تيار الحمل 130 أمبير.

الموضع من الشرق إلي الغرب	المجال المغناطيسي (ملي جاوس)
1	5.25
2	5.06
3	5.38
4	5.75
5	5.56
6	5.8

وطبقا لقياسات المجالات المغناطيسية بالوسط المحيط بنا خاصة أسفل وبالقرب من بعض خطوط نقل وتوزيع الطاقة الكهربائية مختلفة الجهد الكهربائي وكذلك داخل المباني القريبة من تلك الخطوط يمكن أن نخلص لما يلي:

1 –توجد مناطق كثيرة من حولنا خاصة حول الأجهزة والمعدات الكهربائية ذات درجة عالية من التلوث الكهرومغناطيسي.

2 –قيم شدة المجال المغناطيسي أسفل خطوط نقل وتوزيع الطاقة الكهربائية تعتبر قيما آمنة في حالة التعرض لها لجزء من الوقت وليس كل الوقت ولا تعتبر قيما آمنة للإقامة الدائمة بها.

جدول (12): توزيع المجال المغناطيسي داخل شقة بالدور الرابع العلوي بالمبني والمواجهة للخط وخلال محور يبعد مسافة 5 م عن الجدار المواجه للخط مباشرة ومن الشرق إلي الغرب وعندما كان تيار الحمل 130 أمبير.

الموضع من الشرق إلي الغرب	المجال المغناطيسي (ملي جاوس)
1	2.85
2	3.075
3	2.98
4	3.25

3 –قيم شدة المجال المغناطيسي داخل المباني القريبة من خط قوى 132 كيلو فولت لا تعتبر قيما آمنة للإقامة الدائمة والمستمرة بهذه المباني .

4 – تعتمد قيم شدة المجال المغناطيسي على قيمة تيار الحمل لهذا الخط.

التوصيات:

مما سبق يمكن اقتراح التوصيات التالية:

1 –عند التخطيط لتجمعات عمرانية جديدة يجب دراسة المنطقة المحيطة بها والقريبة منها بما فى ذلك خطوط نقل الطاقة الكهربائية ومعداتها وذلك قبل البدء فى التنفيذ .

2 –دراسة المدن الجديدة والمجتمعات العمرانية الجديدة التي أنشأت أخيرا والقريبة من خطوط ومعدات القوى الكهربائية وتقييمها ومعرفة ما إذا كانت آمنة للإقامة الدائمة بها أم لا.

3 – تنفيذ المسح الصحي والدراسات الصحية والفحوصات الدورية على قاطني هذه المجتمعات العمرانية الجديدة والقريبة من خطوط نقل الطاقة الكهربائية ومعداتها.

4 –عدم إقامة أية منشآت خاصة بالأطفال مثل الحدائق والمتنزهات والمستشفيات والمدارس بالقرب من خطوط ومعدات الطاقة الكهربائية .

5 – البدء في نقل خطوط القوى الكهربائية بعيدا عن وخارج نطاق المجتمعات العمرانية المقامة فعلا .

6 – تحديد حرم خطوط الطاقة الكهربائية الموجودة فعلا أو الخطوط التي سوف تنشا في المستقبل .

7 – التنسيق بين الجهات المختلفة المخول لها بالترخيص للبناء بحيث لا يصرح لمبنى وبعد الانتهاء من تشييده يكتشف أنه غير آمن لقربه من خطوط الطاقة الكهربائية .

8 – إضافة التلوث الكهرومغناطيسي إلى قائمة ملوثات الجو الخطرة .

9 –التأكيد على تخصيص جزء من إيرادات القطاع الخاص لمعالجة التلوث الكهرومغناطيسي.

10 – وضع قواعد تنظيمية موحدة لعملية تنظيم البناء بالقرب من خطوط القوى الكهربائية ومعداتها.

جدول (13): توزيع المجال المغناطيسي خارج المبني خلال محور يقع بالمساحة بين المبني وبين الخط من الجهة الغربية للمبني بداية من أسفل الخط متجها إلي المبني وعند تيار حمل 130 أمبير.

المسافة (م)	قيمة المجال المغناطيسي بالملي جاوس
0	0
2	0.6

1.2	4
10	6
13.4	8
26.4	10
2.8	12
2.6	14
2.6	16
2.8	18
2.8	20
2.6	22

2.2	4
2.4	6
3.0	8
3.3	10
3.0	12
2.7	14
2.6	16
2.3	18

شكر وتقدير:

يود الباحث يود يشكر جامعة الطائف بالمملكة العربية السعودية لدعمها المالي للمشروع البحثي رقم 43 . 428 . 1 موضوع هذه الورقة..

جدول (14): توزيع المجال المغناطيسي خارج المبنـــي خـــلال محـــور يقـــع بالمساحة بين المبني والخط من الجهـة الشرقية للمبنـي بدايـة من أسـفل الخـط متجهـا إلـي المبنـي وعند تيار حمل 130 أمبير.

المسافة (م)	قيمة المجال المغناطيسي بالملي جاوس
0	0.5
2	1.6

المراجع :

1. Adair. R., "Constraints on Biological Effects of Week ELF/EMF", Phys. Rev. A 43, pp. 1039-1049, 1991.
2. Adair. R., "Biological Response to Week 60 Hz Electric and Magnetic Fields Must Vary as the Square of the Fields Strength", Proc. Nat. Acad. Sci. 91, pp. 9422-9425, 1995.
3. Abdel-Salam M. and Abd-Allah H., "Transmission Line Electric Field Induction in Humans Using Charge Simulation Method," IEEE Trans. on Biomedical Engineering, Vol. 42, No. I 1, 1995.
4. Abdel-Sattar S., "Environmental Impact of HDVC Transmission Lines," Ph.D. Thesis, Assiut University, Egypt, 1982.

Background Paper, Amer. J. of Physics 64,pp. 974-981, 1996.
11. Laforest J., “Transmission Line Reference Book 345kV and above” EPRI, PloAlto, California, 1987, 2nd edition revised.
12. NIEHS Report, “Health Effects from Exposure to Power-Line Frequency Electric and Magnetic Fields”, NIH publication No. 994493, May 1999.
13. Final Report of Eskom Holdings LTD, "Electric and Magnetic Fields from Overhead Power Lines", 2006.
14. N. Abdul Rahman and W. N. Binti Mahadi, "Measurements and Simulations on ELF-EMF Magnetic Field Exposures from Multiple Electric Transmission Lines", International Journal of Emerging Electric Power Systems, Vol. 10, Issue 4, Article 7, 2009.
15. R. G. Olsen and P. S. Wong, "Characteristics of Low Frequency Electric and Magnetic Fields in the Vicinity of Electric Power Lines", IEEE Trans. On Power Delivery, Vol. 7, No. 4, 1992.
16. A. H. Hamza et. Al., "Environmental Pollution by Magnetic Field Associated with Power Transmission Lines", Energy Conversion and

5. Abdallah A. S., “Electric Fields from Transmission lines nearby populated areas in Egypt-Theory versus experiment” Proceeding ISH 99 Conference, London, UK, Vol. 2, August 23-27, 1999, PP. 11 9-122.
6. Bames F., “Some Engineering Models For Interactions of Electric and Magnetic Fields with Biological Systems”, Bioelectromagnetics Supplement 1, pp. 67-85, 1992.
7. Bracken T. and Patterson R., “Variability and Consistency of Electric and Magnetic Fields Occupational Exposure Measurements,” Journal of Exposure Analysis and Environmental Epidemiology, Vol. 6, pp. 355-374, 1996.
8. Bracken T. et al., “Recommendation for Guidelines for Personal Exposure Field Measurements,” U.S. Department of Energy, 1997.
9. William L. Cotton, Kai Ramsing and Charles Cai, “Design Guidelines for Reducing Electromagnetic Field Effects from 60 Hz Electrical Power Systems,” IEEE Trans. on IA Application, vol. 30, No. 6, 1994.
10. Hafemeister D., 'Tower Lines Fields and Public Health,”

Brain Cancer in the Offspring", Cancer Causes Control, 2o, PP. 945-955, 2009.
24. Stuchly M. and Zhao S., "Magnetic Field induced Currents in the Human Body in Proximity of Power Lines," IEEE Trans. on PRD, Vol. I 1, No. 1, 1996.
25. L. Vitale, "Guide to Solving AC Power EMF Problems in Commercial Buildings," Presented at the New York Interagency Engineering Council, May 1995, revised Dec. 1998.
26. Wertheimer N. and Leeper E., "Electrical Wiring Configurations and Childhood Cancer", American Journal of Epidemiology, 109, 273-284, 1979.
27. Zaffanella L., "Environmental Field Surveys," Enertech Consultants, Lee, Mass, USA, 1996.
28. Zaffanella L. and Kalton G., "Survey of Personal Magnetic Field Exposure, Phase 1: Pilot Study and Design," Enertech Consultants, Lee, Mass, USA, 1998.
29. Zaffanella L. and Kalton G., "Survey of Personal Magnetic Field Exposure, Phase II: 1000-Person Survey," Enertech Management, 34, PP. 2443 – 2452, 2002.
17. J. M. Bakhashwain et. Al., "Magnetic Field Measurement and Evaluation of EHV Transmission Lines in Saudi Arabia", proceedings of the International Conference on Non-Ionizing Radiation at UNITEN (ICNIR 2003)", 20-22 October 2003.
18. Nair I. et al., "Biological Effects of Power Frequency Electrical and Magnetic Fields," U.S. Congress, 1989.
19. Randa J. et al., "Catalogue of Electromagnetic Environment Measurements, 30-300 Hz", IEEE Trans. on Electromagnetic Compatibility, vol. 37, No. 1, pp. 26-33, 1995.
20. Sheppard A. and Eisenbud M., "Biological Effects of Electric and Magnetic Fields of Extremely Low Frequency", book, New York, 1977.
21. Sienkiewciz Z., "Biological Effects of Electromagnetic Fields", IEE Power Engineering Journal, pp. 131-139, June 1998.
22. "Electric Fields (EMF/ELF) can Kill", http://emfjournal.com, 16/3/2009.
23. P. Li et. Al., "Maternal Occupational Exposure to Extremely Low Frequency Magnetic Fields and the Risk of

to Taif University, Project No. 1-428-43, 200

Consultants, Lee, Mass, USA, 1998.

30. “Electrostatic and Electromagnetic Effects of UHV Transmission Lines,” ERRI, June 1978.
31. “The Electrostatic and Electromagnetic Effects of AC Transmission Lines,” IEE Tutorial Course, 1979.
32. "Electro Magnetic Field (EMF) – Hazardous to Our Health", http://www.mercola.com.
33. "EMF and RF Safely Levels – a Comparative Guide", www.scantech7.com.
34. NRPB Consultation Document, "Proposals for Limiting Exposure to Electromagnetic Fields (0 – 300 GHz", Comments from Professor Denis L. Henshaw, http://www.electric-fields.bris.ac.uk/dlhcomments.pdf, May 2003.
35. M. Bedja et. Al., "French Population Exposure to 50 HZ Magnetic Fields: Intermediate results",
36. International Colloquium on Power Frequency EM Fields – ELF/EMF", Sarajevo, Bosnia and Herzegowina, 2009.
37. S. Abdel-Sattar, "Power Line – Frequency Electromagnetic Fields Around us", Final Report

تقدير الإنتروبيا للغة العربية المكتوبة باستعمال نص القرآن الكريم

عبدالله أعبودة، خديجة أمبيص، الحسين سعد
abdulla.abouda@gmail.com
قسم الهندسة الكهربائية والإلكترونية– جامعة مصراتة
صندوق بريد 2478– مصراتة– ليبيا

الملخص

تحتوي مصادر البيانات المتقطعة على كميات معينة من المعلومات وتقدير هذه الكميات مهم جداً لعمليات إرسال البيانات وضغطها و حمايتها من التطفل عند الإرسال، النص المكتوب بأي لغة بشرية مفهومة يمكن اعتباره مصدر بيانات متقطعة، نصوص اللغة العربية المكتوبة تمثل مصدر بيانات متقطعة يمكن تقدير كمية المعلومات التي تحتويها. في هذا العمل نقوم بتقدير الإنتروبيا للغة العربية المكتوبة باستعمال إحصائيات من نص القرآن الكريم برواية حفص عن عاصم وبالرسم الإملائي، أولاً نستخرج البيانات الإحصائية من نص القرآن الكريم باستخدام برنامج حاسوب قمنا بإعداده ثم نستخدم هذه الإحصائيات لتقدير الإنتروبيا من الرتبة الصفرية إلى الرتبة الرابعة، النتائج المتحصل عليها تشير إلى الآتي، باعتبار أن الرموز الأساسية للغة العربية 45 رمز (الحروف بأشكالها وحركات التشكيل والفراغ) كانت الرتبة الصفرية 5.4919 بت لكل حرف، والرتبة الأولى 4.4273 بت لكل حرف، والرتبة الثانية 3.1516 بت لكل حرف، والرتبة الثالثة 2.4497 بت لكل حرف، والرتبة الرابعة 1.9426 بت لكل حرف، القيم المقدرة تشير إلى أن النص العربي يحتوي على فائض يصل إلى حوالي 50% عند مقارنة الإنتروبيا للرتبة الثالثة مع الأولى.

الكلمات الدليلية: الإنتروبيا، اللغة العربية، تشفير المصدر.

1 المقدمة

يُعتبر فرع نظرية المعلومات من أهم فروع علم الاتصالات والذي يهتم بطُرق قياس كمية المعلومات في المصادر المختلفة وطرق تشفير هذه المصادر سواءً لزيادة كفاءة ضغطها أو

تحسين طُرق إرسالها واستقبالها أو لحمايتها من محاولات التجسس. أول من تكلم عن نظرية المعلومات هو شانون عام 1948 في ورقته البحثية المشهورة "النظرية الرياضية للاتصالات" [1]. في هذه الورقة وضع شانون أساسات نظرية المعلومات بوضع مقياس دقيق لكمية المعلومات التي يحتويها أي مصدر وعُرفت هذه الكمية بالإنتروبيا (Entropy). باستعمال تعريفه لكمية المعلومات قام شانون بتقدير كمية المعلومات الموجودة في اللغة الانجليزية المكتوبة وقدرها بحوالي 1 بت لكل حرف، أي أنه لتمثيل نص باللغة الانجليزية نحتاج بت واحد لكل حرف [2]. نتيجة مقاربة باستعمال نفس العينة التي استعملها شانون قدمها كلاً من كوفر وكينج حيث وجدا أن الإنتروبيا للغة الانجليزية المكتوبة حوالي 1.25 بت لكل حرف [3]. لغات أخرى تم تقدير الإنتروبيا لها مثل اللغة البرتغالية والتي وجدت بأنها حوالي 4 بتات لكل حرف [4]. اللغة العربية المكتوبة أيضاً تم تقدير كمية المعلومات التي تحتويها ووجدت بأنها حوالي 4.21 بت لكل حرف [5]، هذا التقدير تم باستعمال نصوص من جرائد عربية وكان حجم العينة المدروسة حوالي 64000 حرف وتم اعتبار حروف اللغة العربية الأساسية 32 حرف بما فيها الفراغ.

في هذا العمل نعرض نتائج لتقدير الإنتروبيا للغة العربية المكتوبة باستعمال إحصائيات من عينة خاصة وهي نص القرآن الكريم وكذلك نأخذ في الاعتبار عدد أكبر من أشكال حروف اللغة العربية المكتوبة بالإضافة إلى حركات التشكيل التي تلعب دوراً مهماً في حالة نص القرآن الكريم. المتبقي من هذه الورقة مقسم كالآتي، المقطع 2 من الورقة العيار المتبع في اختيار الرموز المعتمدة في الدراسة وعلاقتها بالرسم القرآني، النتائج الإحصائية المتحصل عليها بالإضافة معروضة في المقطع 3، النتائج المتحصل عليها لتقدير الإنتروبيا للغة العربية معروضة ومناقشة في المقطع 4، خلاصة هذا العمل يعرضها المقطع 5.

2 الرموز المعتمدة والرسم القرآني

تُعامل أجهزة الاتصال أو التخزين الرقمية البيانات المدخلة إليها من أحرف وأرقام وأشكال مختلفة على أساس أنها رموز تم تمثيلها باستخدام أحد أنظمة التشفير المتعارف عليها عالمياً مثل شفرة الأسكي (American Standard Code for Information Interchange ASCII). في هذه الدراسة تم اعتماد كل الرموز التي يمكن تمثيلها باستخدام شفرة الأسكي، حيث وجد أن كل الحروف العربية من الألف إلى الياء بالإضافة إلى

الطرق المختلفة لرسم الهمزة وحركات التشكيل من الفتحة والكسرة والضمة والسكون والتنوين بأنواعه لها شفرات أسكي خاصة بها. الجدول 1 يبين قائمة بالرموز المعتمدة في الدراسة بالإضافة إلى شفرة الأسكي لكل رمز من هذه الرموز مُعبر عنه بالنظام العشري، بهذا الاختيار تصبح الرموز الأساسية للغة العربية 45 رمز مقسمة إلى 36 حرف هجاء و 8 حركات تشكيل والفراغ. تجدر الإشارة هنا إلى أن هناك عدد من الرموز التي تُستعمل في رسم القرآن الكريم ولكن ليس لها شفرات أسكي خاصة بها مثل الألف المحذوف وعليه فقد اعتمدت هذه الدراسة على تحليل نتائج الرسم الإملائي للقرآن الكريم بدلاً من طرق الرسم المتعارف عليها في علوم القرآن الكريم.

3 الإحصائيات المتحصل عليها

للحصول على الإحصائيات المطلوبة لحساب الإنتروبيا لدرجات مختلفة تم كتابة برنامج حاسوب يقوم بقراءة نص القرآن الكريم من ملف ويقوم باستخلاص عدد من الإحصائيات، الإحصائيات المستخرجة تمثل عدد تكرار ورود التركيبات المختلفة لرموز، مثلاً عدد مرات تكرار كل رمز معتمد في الدراسة في العينة المدروسة والذي يشار إليه في هذه الدراسة بإحصائيات الرتبة الأولى، عدد مرات تكرار التركيبات المخلفة لرموز مثل عدد مرات تكرار رمزين معتمدين في الدراسة والتي يشار إليها بإحصائيات الرتبة الثانية، وعدد مرات تكرار ثلاثة رموز معتمدة في الدراسة ويشار إليها بإحصائيات الرتبة الثالثة، وعدد مرات تكرار أربعة رموز معتمدة في الدراسة ويشار إليها بإحصائيات الدرجة الرابعة. عدد الإحصائيات المستخرجة وصعوبة الحصول عليها يزداد بشكل أُسي مع زيادة الرتبة، فمثلاً عدد الإحصائيات لرتبة الأولى 45 بينما عدد الإحصائيات لرتبة الثانية $45^2 = 2025$ ولرتبة الرابعة $45^4 = 4100625$.

الجدول رقم 1 يعرض نتائج إحصائيات الرتبة الأولى المتحصل عليها من نص القرآن الكريم، العدد الكلي لرموز في نص القرآن الكريم برواية حفص عن عاصم وبالرسم الإملائي كانت 680408 رمز وحجم هذه العينة معقول جداً مقارنة مع حجم العينة في المرجع [5] والتي كانت 64000 حرف بما فيها الفراغ، الـ 680408 رمز شكلت 77684 كلمة بمتوسط طول كلمة 7.7587 رمز، قد يلاحظ هنا أن متوسط طول الكلمة كبير نسبياً وهذا يرجع إلى أخذ حركات التشكيل في الاعتبار حيث أن كل الكلمات في نص القرآن الكريم لا تخلو من حركات التشكيل، من الجدول رقم 1 يمكن

ملاحظة أن احتمالية ورود الحرف (ؤ) هي 0.0011 وهي أقل احتمالية في الجدول، بينما أخذت الفتحة أكبر احتمالية ورود حيث كانت الاحتمالية 0.1750، أما بقية الرموز فتراوحت احتمالية ورودها ما بين 0.0011 و 0.1750.

إحصائيات الدرجة الثانية تمثل عدد مرات تكرار رمزين متتاليين في نص القرآن الكريم، على سبيل المثال عدد مرات تكرار الحرف (ا) وبعده الحرف (س) بشكل متتالي كانت 665 مرة، أما الحرف (ي) وبعده الحرف (ر) فتكرر 527 مرة، كذلك تكرر الحرف (ئ) وبعده حركة التشكيل الكسرة 787 مرة.

إحصائيات الرتبة الثالثة تتمثل في عدد مرات تكرار ظهور ثلاثة رموز وراء بعضها، مثل عدد مرات تكرار ظهور الحرف (ا) وبعده الحرف (ل) وبعده الحرف (س) والتي كانت 576 مرة، بينما تكرر ظهور الحرف (ن) وبعده (الضمة) وبعدها الحرف (س) 18 مرة، هناك بعض التركيبات التي كان عدد مرات ظهورها صفر مثل ظهور الحرف (خ) وبعده الحرف (ش) وبعده الحرف (ث).

إحصائيات الرتبة الرابعة تمثل عدد مرات تكرار ظهور أربعة رموز متتالية مثل ظهور الحرف (هـ) وبعده (الضمة) و بعدها الحرف (م) وبعده (الضمة) فتكرر 325 مرة. باستخدام برنامج الحاسوب تم استخراج إحصائيات كل التركيبات الممكنة لكن يصعب عرض كل النتائج خصوصاً الرتب الثانية والثالثة والرابعة وذلك لعدم توفر مساحة كافية في هذه الورقة.

4 نتائج الإنتروبيا

من الإحصائيات التي تم الحصول عليها في المقطع السابق تم تقدير الإنتروبيا للغة العربية للرتبة الصفرية والرتب الأولى والثانية والثالثة والرابعة. باعتماد 45 رمز أساسي للغة العربية يمكن تقدير الإنتروبيا لرتبة الصفرية للغة العربية من خلال التعويض في المعادلة (1) (في الصفحة الثاني عشر من هذه الورقة) حيث N تمثل عدد الرموز المعتمدة للغة العربية والتي تم اعتبارها في هذه الورقة 45 رمز، بالتعويض في المعادلة (1) كانت الإنتروبيا للرتبة الصفرية 5.4919 بت لكل رمز، هذه القيمة تمثل الحد الأدنى لمتوسط طول كلمات التشفير التي يمكن استعمالها للتعبير عن مخرجات هذا المصدر بأقل فائض على فرض أن خوارزمية الضغط المستخدمة تعتبر أن احتمالية ورود كل رمز من رموز المصدر متساوية.

لحساب الإنتروبيا لدرجة الأولى للغة العربية باستخدام الإحصائيات المتحصل عليها تم استعمال المعادلة (2) حيث $P(x_i)$ تمثل احتمالية ظهور الرمز x_i، بالتعويض بالقيم المستخرجة في المعادلة (2) وجد أن الإنتروبيا للرتبة الأولى تساوي 4.4273 بت لكل حرف، الإنتروبيا للرتبة الأولى تمثل الحد الأدنى لمتوسط طول كلمات التشفير الذي يمكن استعماله لتعبير عن مخرجات هذا المصدر إذا كانت خوارزمية ضغط هذه البيانات تفترض أن رموز المصدر مستقلة عن بعضها وذات احتمالات وقوع مختلفة، تشفير المصدر سوف يعمل على تخصيص أقصر شفرة لتعبير عن حركة الفتحة لأنها أكثر احتمالية ورود من غيرها من الرموز وسوف يعمل على تخصيص أطول كلمة تشفير لرمز (ؤ) لأن له أقل احتمالية حدوث.

الإنتروبيا للرتبة الثانية وجد أنها تساوي 3.1516 بت لكل حرف وتم حسابها بالتعويض بالإحصائيات المتحصل عليها في المعادلة (3) حيث $P(x_i, x_j)$ تمثل احتمالية ورود الحرف x_i متبوعاً بالحرف x_j. إذا كانت خوارزمية تشفير المصدر تفترض ترابط كل حرفين متتاليين فإن أقل متوسط طول كلمات تشفير يمكن استعماله لتعبير عن مخرجات هذا المصدر هو قيمة الإنتروبيا للرتبة الثانية، أما إذا كانت خوارزمية تشفير المصدر تفترض ترابط كل ثلاثة رموز متتالية فإن أدنى متوسط طول كلمات التشفير المستخدمة لضغط نص القرآن الكريم سيكون هو الإنتروبيا للرتبة الثالثة والتي وجدت أنها تساوي 2.4497 بت لكل حرف والتي تم الحصول عليها بالتعويض في المعادلة (4).

الإنتروبيا للرتبة الرابعة وجد أنها تساوي 1.9426 بت لكل حرف وهي تمثل أقل مستوى ضغط بيانات يمكن الوصول إليه إذا تم افتراض ترابط كل أربعة رموز متتالية.

بمقارنة نتيجة الإنتروبيا للرتبة الصفرية مع الإنتروبيا للرتبة الأولى يتضح أن هناك فائض يصل إلى حوالي 24%، أما بمقارنة الإنتروبيا للرتبة الثالثة مع الإنتروبيا للرتبة الأولى فإن نسبة الفائض تصل إلى حوالي 50%.

5 الاستنتاجات

نصوص اللغة العربية المكتوبة تمثل مصدر بيانات متقطع يمكن تقدير كمية المعلومات التي يحتويها، في هذه الورقة تم استخدام نص القرآن

الكريم برواية حفص عن عاصم وبالرسم الإملائي كعينة لتقدير الإنتروبيا للغة العربية ووجد أن نصوص اللغة العربية المكتوبة تحتوي على فائض كبير. تقدير الإنتروبيا لدرجات مختلفة لنصوص اللغة العربية المكتوبة مهم جداً لفهم طبيعة اللغة العربية وكذلك لعمليات ضغط وتشفير وإرسال النصوص العربية.

المراجع

[1] C.E. Shannon "A Mathematical Theory of Communication", *Bell System Technical Journal*, vol.27,pp.379-423, July 1948.

[2] C.E. Shannon "Prediction and Entropy of Printed English", *Bell System Technical Journal*, pp. 50-64, 1951.

[3] T.M. Cover and R.C. King. "A Convergent Gambling Estimate of the Entropies of English", *IEEE Transaction on Information theory*, vol. 24(4), pp.413-421, 1950.

[4] R.L. Manfrino, "Printed Portuguese (Brazilian) Entropy Statistical Calculation," *IEEE Trans. Inform. Theory (Abstract).* vol. it-16. pp. 122, January 1970.

[5] Wanas, M.A , Zayed, Al. Shaker, M.M., and Taha, E.H. "First-Second and Third Order Entropies of Arabic Text" *IEEE Trans. Information theory*, It-22(1),pp.123 ,January 1976.

جدول 1: إحصائيات الرتبة الأول لنص القران الكريم

الرمز	الرمز بالنظام العشري	عدد مرات التكرار	احتمالية الرمز	الإنتروبيا لكل رمز
الفراغ	32	77683	0.1142	0.3574
ء	193	1515	0.0022	0.0196
آ	194	1686	0.0025	0.0215
أ	195	9121	0.0134	0.0834
ؤ	196	769	0.0011	0.0111
إ	197	5086	0.0075	0.0528
ئ	198	1175	0.0017	0.0158
ا	199	43385	0.0638	0.2532
ب	200	11491	0.0169	0.0994
ة	201	2362	0.0035	0.0284
ت	202	10502	0.0154	0.0929
ث	203	1414	0.0021	0.0185
ج	204	3317	0.0049	0.0374
ح	205	4140	0.0061	0.0448
خ	206	2497	0.0037	0.0297
د	207	5991	0.0088	0.0601
ذ	208	4932	0.0072	0.0515
ر	209	12403	0.0182	0.1053
ز	210	1599	0.0024	0.0205
س	211	6012	0.0088	0.0603
ش	212	2124	0.0031	0.0260
ص	213	2072	0.0030	0.0255
ض	214	1686	0.0025	0.0215
ط	216	1273	0.0019	0.0170
ظ	217	853	0.0013	0.0121
ع	218	9405	0.0138	0.0854

غ	219	1221	0.0018	0.0164
ف	221	8747	0.0129	0.0808
ق	222	7034	0.0103	0.0682
ك	223	10497	0.0154	0.0928
ل	225	38190	0.0561	0.2332
م	227	26735	0.0393	0.1835
ن	228	27270	0.0401	0.1860
ه	229	14850	0.0218	0.1204
و	230	24813	0.0365	0.1742
ى	236	2593	0.0038	0.0306
ي	237	21975	0.0323	0.1599
ً	240	3683	0.0054	0.0408
ٌ	241	2491	0.0037	0.0296
ٍ	242	2604	0.0038	0.0307
َ	243	119054	0.1750	0.4400
ُ	245	37155	0.0546	0.2291
ِ	246	45657	0.0671	0.2615
ّ	248	22495	0.0331	0.1626
ْ	250	38851	0.0571	0.2358
المجموع	–––	680408	1.00	4.4273

(1)

$$H_0 = \log_2 N$$

$$H_1 = -\sum_{i=1}^{45} P(x_i) \log_2 P(x_i) \quad (2)$$

$$H_2 = -\sum_{i=1}^{45}\sum_{j=1}^{45} P(x_i, x_j) \log_2 P\left(x_i, x_j\right) - H_1 \quad (3)$$

$$H_3 = -\sum_{i=1}^{45}\sum_{j=1}^{45}\sum_{k=1}^{45} P(x_i, x_j, x_k) \log_2 P\left(x_i, x_j, x_k\right) - H_2 - H_1 \quad (4)$$

تقنيات التعدد لتحسين نظم الاتصالات اللاسلكية المستقبلية

بشير محمد بن رابحة **عبد الله اعبودة** **سعيد الختالي**

basher1963@hotmail.com abdulla.abouda@gmail.com elkhetali @ yahoo.com

الملخص

تقدم هذه الورقة توضيح لمفهوم وفكرة تقنية **التعدد** أو استخدام عدة مرسلات ومستقبلات (باستخدام عدة هوائيات في كل من المُرسِل والمُستقبِل Multiple-Input Multiple-Output **MIMO**) أو بشكل مختصر (تقنية **التعدد**) واعتبارها تقنية المستقبَل في مجال الاتصالات اللاسلكية , كما أنها توضح فائدة وأهمية هذه التقنية وكفأتها الكبيرة في تحسين الأداء والتغلب على التحديات المعروفة في مجال الاتصالات اللاسلكية مثل الخبو وتضاءل الإشارات الناتج عن مرور تلك الإشارات خلال عدة مسارات (multipath fading) ومحدودية نطاق الترددات (Bandwidth) وتزايد الاحتياج لرفع معدلات الإرسال للبيانات (demand for higher data rates) وغيرها . حيث سيتبين من خلال هذه الورقة أن أنظمة **التعدد MIMO** تستثمر وتستفيد من طبيعة أوساط النقل اللاسلكية بوجود العديد من المسارات للإشارة اللاسلكية بسبب الانعكاسات والانكسارات وغيرها بين المرسل والمستقبل وذلك لزيادة تعزيز دقة ووثوقية نقل المعلومات خلال القنوات اللاسلكية (Reliability) وزيادة معدلات تدفق البيانات أو السعة (capacity) وبالتالي رفع كفاءة استعمال حيز الترددات المتاح . أي أن تقنية التعدد تحول التأثير السلبي لتعدد المسارات المُميِز للقناة اللاسلكية والمسبب للخبو وتقلبه إلى نتائج ايجابية كبرى.

المقدمة

إن معدل إرسال البيانات للشبكات اللاسلكية في حدود 50 ميجا بت / ثانية , بينما للشبكات السلكية يزيد عن 1 جيجا بت / ثانية [1]. ومع أن التقنيات المستخدمة في مجال الاتصالات اللاسلكية تطورت بشكل كبير وتمت العديد من الأبحاث للرفع من أداء الاتصالات اللاسلكية والوصول بها إلى مستوى الاتصالات السلكية ولكن يظل الفارق بينهما كبير بل يزداد بشكل مستمر, وذلك لان الاتصالات اللاسلكية تتم عبر الفراغ وهو وسط نقل مشترك لعدد كبير جداً من التطبيقات والذي يؤدي إلى خبو وتضاءل الإشارات حسب طبيعة وسط النقل المكون من العديد من المسارات (multipaths) .

الجدير بالذكر أن الخواص المميزة للاتصالات اللاسلكية والمتمثلة في إمكانية الاتصال بين المستخدمين وهم في حالة حركة وتنقل تجعل منها الميزة الجذابة والمطلوبة لجميع المستخدمين.

وكنتيجة طبيعية لذلك حدث نمو هائل وتطور ملحوظ وسريع جدًا للتقنيات والخدمات والتطبيقات اللاسلكية المتنقلة والثابتة.

ولكن من جانب أخر فان الخواص المميزة أيضًا للاتصالات اللاسلكية تمثل التحدي الكبير الذي يواجه المختصين في هذا المجال من باحثين ومهندسين ومصممين والمتمثل في محدودية حيز الترددات المتاح والتغير المستمر لمواصفات القناة مع الزمن وأيضا الحاجة الملحة لزيادة معدل إرسال البيانات وتحسين الأداء وجودة الاتصال والمحافظة على القدرة وصغر حجم أجهزة الاتصال المحمولة وغيرها.

لذا فان تقنية **التعدد** MIMO والتي تشمل التنوع الفراغي (spatial diversity) وتشكيل الشعاع (beam forming) وكذلك الإرسال الفراغي المضاعف (spatial multiplexing SM) تعتبر الحل الأمثل لتحسين أداء الاتصالات اللاسلكية المستقبلية وزيادة سعاتها.

فباستخدام SM وهو استخدام عدة هوائيات في كل من المرسل والمستقبل وإرسال بيانات مختلفة على هوائيات الإرسال في نفس الوقت وعلى نفس التردد أي إضافة بعد أخر وهو **الفراغ** بالإضافة للأبعاد السابقة **التردد والزمن** وبالتالي يمكن مضاعفة وزيادة سرعة نقل البيانات حسب عدد حزم البيانات المُرسلة أو هوائيات الإرسال المُستخدمة [4,3,2]. فمثلاً إذا تم استخدام عدد 4 هوائيات إرسال (N_t) وعدد 4 هوائيات استقبال (N_r) فإنه يمكن نقل 4 حزم

من البيانات المختلفة على التوازي في نفس الوقت وعلى نفس التردد , أي زيادة سرعة النقل بمعدل 4 مرات أكثر من الحالة التقليدية وهي استخدام هوائي واحد للمرسل والمستقبل (نظام أحادي **SISO** Single-Input Single-Output) , حيث أن عدد مرات الزيادة ومضاعفة السعة (أو بمعنى أخر عدد الطبقات) يكون مساوياً لعدد هوائيات المُرسل المستخدمة (N_t) تقريبا [6,5].

2. نمذجة الإشارة وقناة التعدد

لنفرض أن لدينا نظام تعدد مكون من (N_t) هوائي إرسال و (N_r) هوائي استقبال كما في الشكل (1) , حيث يمكننا التعبير عن هذا النظام بمعادلة المصفوفات التالية:

$$\mathbf{y} = \mathbf{H}\,\mathbf{S} + \mathbf{z} \qquad (1)$$

حيث: $\mathbf{y}^{1\times Nr}$ هو متجه معبر عن الإشارات المستقبلة,

و $\mathbf{S}^{1\times Nt}$ هو المتجه المعبر عن الإشارات المرسلة بمتوسط صفر(μ_s=0) وتباين σ_s^2 ,

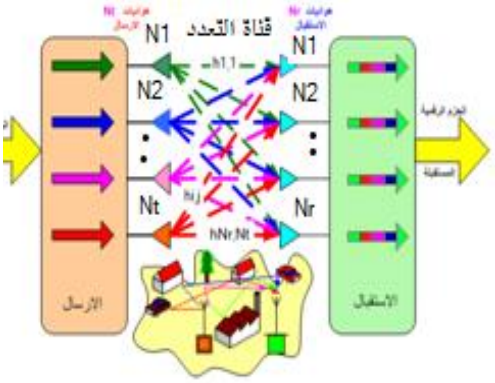

الشكل (1) يوضح تقنية التعدد باستخدام طريقة الإرسال الفراغي المضاعف SM .

و $\mathbf{z}^{1\times Nr}$ هو المتجه المعبر عن ضوضاء القناة بمتوسط صفر (μ_z=0) وتباين σ_z^2

و $\mathbf{H}^{Nt\times N\,r}$ هي المصفوفة المعبرة عن قناة التعدد وهي كالتالي :

$$\mathbf{H} = \begin{bmatrix} h_{1,1} & \cdots & h_{1,N_t} \\ \vdots & \ddots & \vdots \\ h_{N_r,1} & \cdots & h_{N_r,N_t} \end{bmatrix}$$

وكل عنصر مركب $h_{i,j}$ من عناصر مصفوفة القناة $\mathbf{H}$ يعبر عن قناة فرعية للإشارة المرسلة من هوائي المرسل j إلى هوائي الاستقبال i بحيث يكون $h_{i,j}$ كالتالي:

$$h_{i,j} = \alpha_{ij}\, e^{j\Phi ij} \qquad (2)$$

حيث α_{ij} يعبر عن توهين مسار الإشارة المرسلة و Φ_{ij} يعبر عن التأخير الزمني للإشارة المرسلة من هوائي المرسل j إلى هوائي المستقبل i .

ويعبر المتجه: $[h_{1,j} \quad h_{2,j} \quad \ldots \quad h_{Nr,j}]^T$ وهو عمود من أعمدة المصفوفة **H** عن البصمة الفراغية بين هوائي المرسل j وهوائيات المستقبل.

3. نظام التعدد لزيادة الوثوقية وتحسين أداء المنظومات اللاسلكية

لنظام التعدد امتياز مهم جدا لتحسين أداء الأنظمة اللاسلكية . فباستخدام عدة هوائيات في كل من المرسل والمستقبل (تكوين قناة تعدد) فان كفاءة استعمال الحيز الترددي ستكون أفضل بكثير من النظام الأحادي التقليدي . كما أن فكرة استخدام عدة هوائيات ستزيد من فرصة و إمكانية التنوع الفراغي (spatial diversity) لتقليل تأثير خبو القناة .

فكل زوج مؤلف من هوائي إرسال واستقبال سيعبر عن قناة فرعية لإشارة من المرسل إلى المستقبل. وإذا تم إرسال إشارات (حزم بيانات) تحمل نفس البيانات على هوائيات المرسل , ستمر هذه الإشارات خلال مسارات مختلفة إلى المستقبل , فسيكون لدينا عدة نسخ عند المستقبل مطابقة للإشارة المرسلة , وبالتالي سنحصل على استقبال أكثر دقة ووثوقية .

لتوضيح ذلك , ليكن وسط النقل اللاسلكي عديد الانتشارات أو المسارات (rich scatter) , وبفرض استخدام هوائي واحد للمرسل وعدد (N_r) من الهوائيات للمستقبل . في هذه الحالة ستمر الإشارة المرسلة من هوائي المرسل عبر N_r من القنوات الفرعية إلى هوائيات المستقبل. وبناءا على الافتراض بأن وسط النقل اللاسلكي بطبيعته عديد المسارات , فان حدوث الخبو (fading) سيكون مستقل (independent) للقنوات الفرعية المختلفة التي تسلكها الإشارة من هوائي المرسل إلى أي من هوائيات المستقبل. وسنحصل على أكبر كسب تنوع في هذه الحالة مقداره N_r. فعند قيمة SNR عالية نسبياً سينتج نقص كبير في متوسط احتمالية حدوث الأخطاء p للبيانات المستقبلة. أي ستكون النتائج التقريبية لاحتمالية حدوث الأخطاء في هذه الحالة مساوية للمقدار ($p = \frac{1}{(SNR)^{Nr}}$) بالمقارنة بالقيمة ($p = \frac{1}{SNR}$) للنظام الأحادي [7].

من خلال هذه القيم التقريبيـــة يتضـــح فائـــدة استخدام نظام التعدد في تقليل معدل حدوث الأخطاء وزيادة وثوقية النظام اللاسلكي.

وإذا تم استخدام عدد (N_t) من الهوائيات في المرسل وعدد (N_r) من الهوائيات في المستقبل وبفرض أن الوسط اللاسلكي متعدد المسارات , فإنه يمكننا الحصول على أقصى كسب تنوع (diversity gain) مقداره ($N_r N_t$) وهو العدد الكلي للقنوات الفرعية الممكنة بين المرسل والمستقبل , وسيكون متوسط احتمال حدوث الأخطاء p للبيانات المستقبلة في هذه الحالة تقريبا مساويا للمقدار ($p = \frac{1}{(SNR)^{NtNr}}$) [7].

إن استخدام تقنية التعدد ستعطي كسب تنوع فراغي يؤدي إلى تحسين وزيادة قيمة SNR وذلك بتطبيق واستخدام تقنيات الدمج للإشارات المستقبلة (combining techniques).

4. زيادة السعة أو معدل إرسال البيانات في نظام التعدد

نظرا لتحسين وزيادة قيمة SNR باستخدام تقنية التعدد , ومن خلال معادلة السعة لشانون وهي:

$$C = \log_2 (1+ SNR) \text{ bits/s/Hz} \quad (3)$$

فان سعة القناة تزداد باستخدام تقنية التعدد (أو كسب التنوع الفراغي) ولكنها زيادة لوغاريثمية

$$C \approx \log_2 (SNR) \text{ bits/s/Hz} \quad (4)$$

إن فوائد استخدام نظام التعدد ليست زيادة التنوع وتقليل حدوث الخبو للإشارة و معدل حدوث الأخطاء للبيانات المستقبلة وزيادة الدقة والوثوقية فقط بل له فوائد وميزات كبرى في زيادة درجات الحرية (أي زيادة السعة أو معدل إرسال البيانات) لمنظومات الاتصالات اللاسلكية وهو بالطبع من أهم الأهداف المطلوبة لتحسين أداء هذه المنظومات.

و بتحليل مصفوفة قناة التعدد **H** رياضيا لإيجاد القيم الذاتية (λ_i eigenvalues) أو القيم الأحادية (σ_i singular values) باستخدام طريقة Singular Value Decomposition) SVD) مثلاً , حيث ($\sigma_i=\sqrt{\lambda i}$) وأن عدد القيم الذاتية (أو الأحادية) هو الرتبة r (rank) لمصفوفة القناة **H**. وتكون رتبة المصفوفة **H** أكبر ما يمكن في حالة التساوي للمعادلة ($r \le \min (N_r , N_t)$) إذا كانت القنوات الفرعية مستقلة, أي أن جميع الصفوف والأعمدة لمصفوفة قناة التعدد **H** تكون مستقلة. وكلما قل تشتت القيم الأحادية

(σ_i) كانت مصفوفة القناة في وضع أفضل (well-conditioned) [8]. ويتم تحديد حالة قناة التعدد بإيجاد رقم حالة المصفوفة **H** (condition number) وهو يُعرّف بأنه النسبة بين أعلى قيمة أُحادية إلى أقل قيمة أحادية ($\frac{\max \sigma i}{\min \sigma i}$) , فكلما كانت هذه القيمة قريبة من الواحد (1) كانت حالة مصفوفة قناة التعدد أفضل. حيث تعبر قناة التعدد في هذه الحالة عن وجود عدة قنوات فرعية افتراضية حسب عدد القيم الأحادية وقيمها.

والفكرة هنا هي أمكانية استغلال هذه الظروف المتاحة في قناة التعدد بوجود مسارات متعددة , والاستغلال الأمثل لهذه الظروف يمكن بتطبيق تقنية SM باستخدام عدة هوائيات تكون المسافة بينها كافية (*على الأقل نصف الطول الموجي (λ/2) للموجة الحاملة حتى نحصل على مسارات مستقلة*) بكل من المرسل والمستقبل وإرسال حزم لبيانات مختلفة على هوائيات المرسل في نفس الوقت وعلى نفس التردد , فيبدو النظام في هذه الحالة وكأن البيانات المختلفة يتم إرسالها ونقلها على مسارات افتراضية متوازية من المرسل إلى المستقبل (أي يمكن تخيل افتراضياً أن وسط النقل اللاسلكي عبارة عن مجموعة خطوط نقل متوازية ويمكن إرسال بيانات مختلفة على هذه الخطوط) وينتج عن ذلك زيادة كبيرة في معدل إرسال البيانات حسب عدد هوائيات المرسل والمستقبل المستخدمة. وتكون حزم البيانات التي يمكن نقلها في نفس الوقت وعلى نفس التردد خلال قناة التعدد مساوية تقريبا لأقل عدد مستخدم من هوائيات الإرسال (N_t) والاستقبال (N_r), أي ($\min(N_t, N_r)$) وذلك حسب حالة القناة.

ومن هنا يتضح أن تطبيق الإرسال الفراغي المضاعف (SM) يكون مناسباً في حالة ظروف القناة اللاسلكية جيدة وتحتوي على العديد من المسارات بسبب الانعكاسات والتشتت الناتج عن الحواجز الطبيعية كالجبال والمباني والأشجار وغيرها , أي قناة عديدة المسارات , فيمكن توظيف هذه الظروف المتاحة واستغلالها (بدلا من اعتبارها مشكلة) وتطبيق عملية الإرسال المتزامن لحزم بيانات مستقلة ومختلفة في نفس الوقت وعلى نفس الحيز الترددي , وبالتالي نحصل على زيادة كبيرة في سعة النظام أو معدلات الإرسال للمنظومة اللاسلكية .

سعة القناة حسب صيغة شانون والتي تعرف بأنها أقصى معدل لإرسال البيانات عبر القناة بدون (أو بأقل) احتمالية للأخطاء , وبفرض أن

قناة التعدد معروفة جيدا للمستقبل , فإن سعة قناة التعدد المكونة من عدد N_t من هوائيات المرسل و N_r من هوائيات المستقبل تعطى بالمعادلة :[12,11,10,9]

$$C=\log_2 \det (I_{Nr}+ \frac{\rho}{Nt} \mathbf{H}\,\mathbf{H}^H) \qquad (5)$$

حيث : $\boldsymbol{\rho}$ هي SNR لكل قناة فرعية ,

و $^{Nr\times Nr}\mathbf{I}_{Nr}$ هي مصفوفة الوحدة ,

و **H** هي مصفوفة قناة التعدد,

و det هي محدد المصفوفة.

وبتحليل المصفوفة H رياضيا باستخدام طريقة تحليل المصفوفات SVD فانه يمكن إعادة كتابة المعادلة السابقة كالتالي :

$$C = \sum_{i=1}^{r} \log_2 (1+ \frac{\rho}{Nt} \lambda i) \qquad (6)$$

حيث r هي رتبة مصفوفة قناة التعدد,

و λi , $(i=1,2,\ldots,r)$ هي القيم الذاتية الموجبة للمصفوفة HH^H.

ومن هذه المعادلات يتضح أن استخدام طريقة الإرسال الفراغي المضاعف (SM) تمكننا من الحصول على زيادة بشكل خطي $\min(N_t ,N_r)$ لمعدل إرسال البيانات أو سعة القناة كما أنها تحتوي ضمنا على وجود كسب التنوع الفراغي بسبب تقنية التعدد والتي تعطينا زيادة في قيمة SNR وتقليل الأخطاء في البيانات المستقبلة.

5. النتائج

يوضح الشكل (2) منحنيات المقارنة بين سعة نظام التعدد والنظام الأحادي باستخدام برنامج المحاكاة بواسطة MATLAB باستخدام هوائي واحد لكل من المرسل والمستقبل لتمثيل النظام الأحادي واختيار عدد 2 و2 , 4 و4 , 8 و 8 هوائيات لكل من المرسل والمستقبل على الترتيب لتمثيل نظام التعدد بعدد هوائيات صغير ومتوسط وكبير حيث يوضح هذا الشكل فائدة استخدام نظام التعدد من خلال منحنيات السعة فنلاحظ زيادة السعة خطيا حسب عدد الهوائيات لنظام التعدد عند القيم الأعلى للنسبة SNR مقارنة بالنظام الأحادي .

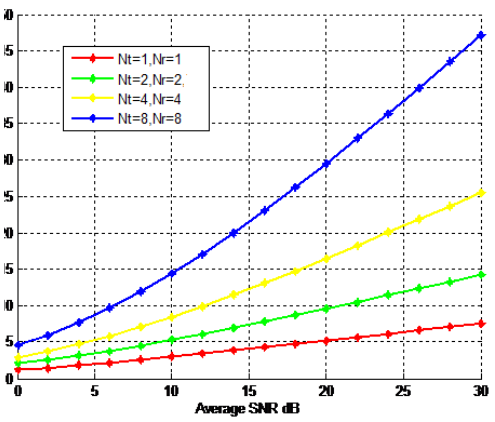

الشكل (2) مقارنة بين سعة النظام الأحادي ونظام التعدد

فمن الشكل يتبين الزيادة المطردة في السعة كلما زاد عدد الهوائيات المستخدمة بكل من المرسل والمستقبل لتكوين نظام التعدد مع زيادة في تعقيد النظام كما هو متوقع , مع افتراض أن الوسط اللاسلكي عديد المسارات حيث تم تمثيل القناة اللاسلكية بالتوزيع الإحصائي ريالاي (Rayleigh) لأنه التوزيع المناسب في هذه الحالة.

كما يوضح الشكل (3) نتائج برنامج المحاكاة بواسطة MATLAB وتظهر النتائج منحنيات لمقارنة وتُوقية نظام التعدد بالنظام الأحادي حيث تم استخدام أعداد مختلفة من هوائيات المرسل والمستقبل لتمثيل نظام التعدد كما تم استخدام هوائي واحد لتمثيل النظام الأحادي مع افتراض التوزيع الإحصائي ريالاي, وتوضح هذه المنحنيات تحسن أداء القناة وزيادة الوثوقية باستخدام نظام التعدد مقارنة بالنظام الأحادي ويقل معدل حدوث الأخطاء للبيانات المرسلة عند القيم الأعلى للنسبة SNR كلما تم استخدام عدد أكثر من هوائيات المرسل والمستقبل وخاصة إذا زاد عدد هوائيات المستقبل عن المرسل لازدياد التنوع الفراغي مع الزيادة في التعقيد باستخدام نظام التعدد كما هو متوقع.

6. الاستنتاج

من خلال النتائج السابقة , فإن استخدام التنوع الفراغي لتقنية التعدد تزيد من نسبة قدرة الإشارة إلى الضوضاء SNR وتقلل من تأثير الخبو في القناة اللاسلكية وتزيد من ووثوقية منظومات الاتصالات اللاسلكية . كما أن استخدام طريقـــــة
الإرسال الفراغي المضاعف SM لتقنية التعدد تعطي زيادة خطية واضحة وكبيرة نسبياً في معدلات إرسال البيانـات أو السعـــة للمنظومـــات

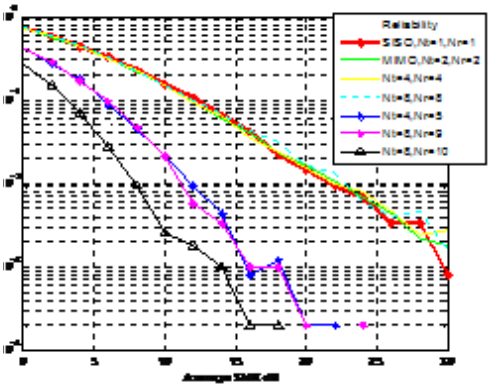

الشكل (3) مقارنة بين احتمالية الخطأ في البتات للنظام الأحادي ونظام التعدد باستخدام أعداد مختلفة لهوائيات المرسل والمستقبل مع استخدام تضمين إزاحة الطور(QPSK).

اللاسلكية وتزيد من كفاءة استعمال الحيز الترددي المتاح وتحسين نسبة الإشارة إلى الضوضاء SNR ووثُوقية المنظومات اللاسلكية وتقليل معدل حدوث الأخطاء للبيانات المرسلة .

7. المراجع

[1] R. Nabar, A. Paulraj, D. Gore, and H. Bolcskei, " An overview of MIMO Communications – a key to gigabit wireless", *Proceedings of the IEEE*, vol. 92, no.2 , pp. 198- 218, February 2004.

[2] E. Telatar, " Capacity of Multi-antenna Gaussian Channels," *Euro. Trans. Telecommun.*, vol. 10, no. 6, pp. 585-95 , Nov.-Dec. 1999.

[3] G.J. Foschini,"Layered SpaceTime Architecture for Wireless Comm-unication in a fading Environment When Using Multiple Antennas", *Bell Labs Technical Journal*,Vol. 1 , No.2 , pp 41-59, Autumn 1996.

[4] G.J. Foschini and M.J. Gans." On limits of wireless communication in a fading environment when using multiple antennas". W*ireless Personal Communi-cations*, 6(3):311–335, 1998.

[5] R. Heath, Jr. and A. Paulraj, "Switching between diversity and multiplexing in MIMO systems,"*IEEE Trans. Commun.*, vol. 53, no. 6, pp. 962-968, June 2005.

[6] A. Sadek, W. Su, and K. J. Ray Liu, "Diversity Analysis For Frequency-Selective MIMO - OFDM Systems With General Spatial and Temporal Correlation Model," *IEEE Transactions on Communications*,

Transaction on Communication, 2000.

[10] Anderea Goldsmith, "WIRELESS Communications," *Cambridge University Press,* 2005.

[11] J. Bach Andersen, "Array gain and capacity for know random channels with multiple element arrays at both ends," *IEEE Journal on Selected Areas in Communications,*2000.

[12] D. Shiu, G. Foschini, M. Gans, and J. M. Kahn, "Fading Correlation and Its Effect on the Capacity of Multielement Antenna Systems*" IEEE transactions on communications, vol. 48, no. 3, march 2000.*

vol. 54, no. 5,pp.878-888, May 2006.

[7] Lizhong Zheng and David N. C. Tse, "Diversity and Multiplexing : A Fundamental Tradeoff in Multiple-Antenna Channels" IEEE Transactions on information theory, vol. 49, No. 5, May 2003.

[8] David Tse and Pramod Viswanath "Fundamentals of wireless communication", *Cambridge University , 2004*

[9] D. Gesbert, H. Boleskei, D. Gore and A. Paulraj, "MIMO Wireless Channel: Capacity and Performance Prediction", *IEEE*

توقعات الربط الراديوي للموجات القصيرة للوصلات القصيرة بين عواصم منطقة شمال أفريقيا للسنوات 2011، 2012

راسم عامر على رقية محمد الباهي علي على عبد الرحمن عكاشة

كلية العلوم الهندسية والتقنية .جامعة سبها

Email: Rasim_63 @yahoo.co.uk

الملخص

في هذا العمل دراسة للربط الراديوي للموجات القصيرة لمنطقة شمال أفريقيا للمسافات القصيرة للسنوات 2011 و 2012 ، وذلك بتعيين موقع كل من المرسل والمستقبل واختيار البارمترات المناسبة لكل منهما وتم دراسة خصائص نظام الاتصالات بين هذه المناطق ومنها ، ارتفاع الإشارة في طبقة الأيونوسفير، والتردد الصالح للاستخدام ، والفقد في النظام ، ونسبة الإشارة إلى الضوضاء ، و ايضا تأثير التشويش على ترددات التشغيل للموجات في المناطق المحددة ، وتم الوصول الى أن ترددات التشغيل تعاني من تشويش أقل عند الساعة الثامنة صباحا وحتى الساعة الثالثة مساءا نتيجة كثافة الإلكترونات العالية بسبب النشاط الشمسي ، أما في الأوقات الأخرى فإن الإشارة تعاني من تشويش أكبر بسبب فقدان الإلكترونات نتيجة لقلة النشاط الشمسي لسنوات الدراسة ، ومن خلال النتائج وجد أن ترددات التشغيل المناسبة تعاني من ضوضاء عند فترات معينة من النهار نتجة التغيرات الشمسية و حركة الأرض وتغير الفصول والمواسم والسنوات.

1- مقــدمة

تعتبر كل من طبقتي التروبوسفير والأيونوسفير أوساط ديناميكية تتغير خواصها الكهربائية مع الزمن وينتج عنها أن فروق زوايا الطور للموجات المختلفة التي تصل هوائي الاستقبال متغيرة مع الزمن، وينتج عنها أن جهد المستقبل بين طرفي هوائي الاستقبال يتغير عشوائيا في سعته وزاوية الطور له

وينتج عن هذا ما يعرف بظاهرة الخبو (Fading) ، وفي بعض الأحوال قد يحدث الانعكاس في الأيونوسفير من طبقة متحركة مما ينتج عنه انحراف دوبلر للتردد وهذا الانحراف يسبب تشوه الإشارات المرسلة ، وقد ينشأ التشوه في هذه الإشارات نتيجة لتغيرات طارئة في الأيونوسفير أو التروبوسفير أو نتيجة لتواجد الشهب أو التفريغ في المناطق ذات السحب الكثيفة [1]. لقد وُجد من القياسات العملية أن الموجات ذات الأطوال الموجية الأكبر من 10 cm لا تعاني تشويش يذكر عند مرورها في التروبوسفير فهي لا تتأثر بالمطر أو الضباب أو الجليد أو البرد(hail) أو العوامل الجوية الأخرى المتواجدة في مناطق التروبوسفير السفلي، ومن ناحية أخرى فقد أثبتت القياسات العملية بأن الموجات ذات الأطوال الموجية الأقصر من 10 cm تعاني توهين عند مرورها في التروبوسفير وفي بعض الأحيان يكون هذا التشويش شديد بحيث يصبح من المتعذر استمرار الاتصال .

منطقة شمال أفريقيا منطقة حيوية تتوسط العالم وبذلك فان دراسة أي نظام اتصالات يعتبر حيوي ومفيد للعالم ، ونظرا لهذه الأهمية باعتبارها وسيلة ربط بين أفريقيا وأوروبا ، عليه كان الهدف لهذا العمل دراسة لتوقعات الربط الراديوي للموجات القصيرة للوصلات القصيرة في منطقة شمال أفريقيا باستخدام الحزمة البرمجية (**ICEPAC** ، **ICEPAC AREA**) ، [9] ، وذلك لتحقيق توقع لهذا النظام للسنوات 2011 و 2012 .

2- الغلاف الجوي وطبقاته

الطبقتان (F,E) تتأثران كثيرا بالنشاط الشمسي والإنفجارات الشمسية المرتبطة بدورة النشاط الشمسي والتي يزيد فيها عدد البقع الشمسية والإنفجارات الشمسية وهذه الدورة تحدث كل 11 سنة [1].

من أهم خصائص الطبقة D هو تركيز صغير للكثافة الإلكترونية في حدود 10^8 لكل متر مكعب و معدل التصادم عالي بين الإلكترونات والجزيئات في حدود (5×10^5 – 5×10^6) لكل متر مكعب لكل ثانية ، ويلاحظ أن التردد الحرج (Critical Frequency) للمنطقة (D) في حدود من 100KHz إلى 700KHz ، تمتاز هذه الطبقة بأن التردد الحرج الأقصى هو حوالي 4 MHz عند تعامد الشمس عليها و 3 MHz عند خطوط العرض القريبة من خط الاستواء ، و تتأثر كثافة الإلكترونات بالدورة الشمسية حيث تكون ذات حد أقصى خلال الذروة الشمسية ويتغير التردد الحرج في حدود 30%

خلال الدورة الشمسية ، كما أن الحد الأدنى للتأين يحدث ليلا نتيجة للإتحاد غير التام بالإضافة للتأين الناتج من الشهب ويكون التردد الحرج في حدود 250 KHz خلال الحد الأدنى للدورة الشمسية و يصل إلى 500 KHz أو 600 KHz نتيجة لكثافة تأين التى تصل الى 10^9 لكل متر مكعب ، تتكون طبقة E نتيجة للتأين بفعل الإشعاع فوق البنفسجي وأشعة X وبواسطة التفاعلات والإتحاد بين الأجسام المشحونة والمتعادلة. طبقة Es غير المستقرة (Sporadic E–layer). الطبقة (F) وهي أعلى طبقة في الأيونوسفير وتتكون من طبقتين F2,F1 ، طبقة F1(The F1–layer) وتقع على ارتفاع حوالي 200 km ومن خواص هذه الطبقة ، الكثافة الإلكترونية خلال النهار تعتمد على زاوية ميل أشعة الشمس، الامتصاص الناتج عن التصادمات صغير في هذه المنطقة. التردد الحرج fc (Critical Frequency) له قيمتان أحدهما في الشتاء والأخرى في الصيف العلاقة بين كثافة الإلكترونات والتردد الحرج بالميجاهرتز في الصيف أو الشتاء

$$N = 1.24 \times 10^{10} f_c^2 \quad \text{..... (1)} \quad m^{-3}$$

حيث f_c التردد الحرج.

التردد الحرج يصل لقيمته القصوى بعد الظهر وهذا لا يحدث بالنسبة لمنطقة E وطبقة F1 . منحنى كثافة الإلكترونات في الشتاء لطبقة F2 له قيمة قصوى أكبر من تلك الخاصة بفصل الصيف وخاصة في نصف الكرة الأرضية الشمالي وتحصل بعد الظهر بقليل مع حدوث قيمة صغرى عميقة قبل الفجر، والهدوء الذي يتصف به منحنى الصيف .

3– الحزمة البرمجية ICEPAC، ICEPAC AREA

مند سنوات عديدة يحاول الباحثون محكاة نظم الاتصالات في الطيف الترددي (HF) للمسافات الطويلة ، ولكن لصعوبات ايجاد موديل رياضي واضح للتغيرات في طبقة الأيونوسفير فقد وجدت صعوبات كثيرة في هذا الجانب [9، 12] ، حيث اصبح نظام الاتصالات يعتمد بشكل كبير على الاختلافات في الأيونوسفيرِ، التي تتغير بشكل سريع مع تغير النشاطِ الشمسيِ، و إلاختلافات الموسميّة والتغيرات اليومية بالإضافة إلى الموقع من حيث خطِّ العرض وخطِ الطول.

طورت العديد من الحزم البرمجية لاجل تحليل وتتبع وتوقع التغيرات المؤترة على نظم الاتصالات(HF) بفعل التغيرات في طبقة لأيونوسفيرِ حيث يمكن تحليل وتنبؤ جدوي نظام الإتصالاتِ الأيونوسفيريِ ، ومن ضمن الحزمة المتاحة **(Ioncap)** حيت تم تطويره واصبح واحداً من النماذجِ المقبولةِ والأكثرِ إستعمالاً لتنبؤاتِ الأيونوسفير(HF). كما وجد من خلال الاختبار ان هذه الحزمة تقدم أداءاً سيّئاً في بعض المناطق القطبيةِ ، ولتَصحيح هذه المشاكلِ في **Ioncap** تم التحول إلى **Icepac** بإضافة التوصيلِ الأيونوسفيريِ وكثافةِ الالكترونات على هذا النمودج حيث النمودج الجديد يقدم ميزّة السعة لنطاق نصف الكرة الأرضيةِ الشماليةِ ، و يَعْرفُ النموذجُ بالعملياتَ الطبيعيةَ المختلفةَ التي تحدث في المناطقِ المختلفةِ للأيونوسفيرِ.

المعلومات العامّة على نموذجِ **Icepac** الجديد جعلت نظام الاتصالات الأيونوسفيريةُ **(Icepac)** للحزمة الترددية **(HF)** اكثر دقة وسعة واكبر في التحليل ، هذه الحزمة مفيدةُ في التخطيط والتوقع لبنا نظام اتصالات متكامل خلال الفصولِ الأربعة وفترة النشاط الشمسي المختلفةِ، واختلاف ساعات النهار، واختلاف الموقع الجغرافي. **Icepac** تَعطي النَتائِجَ المطلوبةَ من خلال اختبار هذه الحزمة ولفترة زمنية طويلة ، ويوجد نوعان من هذه الحزمةِ **Icepac** كامل و **Icepac** لتنبوء من نقطة لنقطة ، يمكن الحصول على النتائج مجدولة وضمن المدي الترددي المحدد وعلى مدي الاربعة والعشرون ساعة ضمن المنطقة المحدد جغرافيا.

مدخلات البرنامج (طريقة الدراسة المستخدمة ، سنة الدراسة والزمن المحدد، قيمة SSN ، احداتيات المرسل والمستقبل ، المسار طويل او قصير ، وزاوية الشعاع وقيمة الضجيج المحتمل ، والقدرة المشعة) ، ويوجد من ضمن القيم المشار اليها قيم قياسية يمكن استخدامها ، اما عن المخرجات فهي جميع البارمترات اللازمة لمنظومة اتصالات متكاملة.

4- حساب وتقييم الأداء المتوقع لموجات HF بين المرسل والمستقبل

تم اختيار طريقة الدراسة **(complete system performance) method 20** [9] ، و سنة الدراسة 2011 و 2012 ، والزمن من الساعة 00:00 إلى الساعة 24:00 بتوقيت غرينتش، الشهر سنة و2012،2011، حيث قيمة الإشعاع الشمسي أخذت على أساس المتوسط الحسابي للإشعاع

الشمسي لسنة 2011 و 2012 وهو من 56 ، 79,5 مأخوذا عن [وتم تحديد موقع جهاز الإرسال وإحداثياته الجغرافية تونس (36°.83 N 10 °.22 E) تحديد موقع جهاز الاستقبال وإحداثياته الجغرافية القاهرة 30 °.05N 31°.25E ، طرابلس 13 ,32 °.88 N 3 ,36 °.70N ، الجزائر 36 °.18E ، الرباط 34°.03N, 6°.85W 36 °.13E ، نواكشوط 15 °.97W ,18 °.15N ، و المسار القصير إلى حدود 19308 كم ، و الطويل إلى حدود 32180 كم، وحددت الترددات على أساس الترددات القياسية المختارة [7] ،

MHz (6.070، 4.580، 9.700، 11.850، 13.700، 4.470 ، 15.350، 17.730، 21.650) ، و تم اختيار هوائي إرسال مثالي له كسب اتجاهي [2] dBi 22.2 ، وقدرة في حدود 500Kw ، ويشع بزاوية 261.7° للفص الرئيسي ، كما تم اختيار هوائي استقبال مثالي له كسب اتجاهي dBi 15.00، ويستقبل الإشعاع بزاوية 78.1° للفص الرئيسي.

بناء على هذه المعطيات تم دراسة الربط الراديوي كل على حدة بين تونس كمرسل، وكل من (القاهرة، طرابلس، الجزائر، الرباط، نواكشوط) كمستقبل، ومن ثم تحليل ومقارنة النتائج ببعضها للوصول إلى تردد التشغيل المناسب الذي يتوقع أن يكون الأفضل في إنجاز الربط الراديوي بين هذه المدن.

أولا:الربط الراديوي بين تونس والقاهرة

المسافة بين تونس والقاهرة 2086 كم وهي بذلك تقع في المسار القصير ، تم دراسة طبقة الإنعكاس وارتفاع الإشارة في الأيونوسفير [6]، الشكل (1أ،ب) يوضح ذلك حيث الترددات المنخفضة مثل (4.580،6.070MHz) تنتشر على ارتفاعات منخفضة وذلك لأن الترددات المنخفضة لاتستطيع اختراق الطبقة E خلال ساعات الذروة الشمسية (8ص – 14 م)، أما بالنسبة لساعات الليل والترددات الأخرى الأعلى (MHz 9.700،11.850،13.700،14.470،15.350،17.730، 21.650) فإنها تعتمد في انتشارها على الطبقة F2 لأنها تستطيع مقاومة الامتصاص الذي يتواجد في الطبقات السفلى D,E وبذلك تخترقها [1، 3]، وكلما زاد التردد قل معامل الامتصاص واستطاعات الترددات أن تصل إلى طبقات الأيونوسفير العليا وتنعكس منها وبذلك يزداد مدى إرسال الإشارات خلال سنة 2011 ، وفي السنة

2012 اتضح أن الترددات المنخفضة مثل (4.580,6.070MHz) يحدث لها توهين كبير في الفترة التي تنتشر فيها في الطبقة Es و يكون ارتفاعها منخفض 100كم في الطبقة E ، أما باقي ساعات النهار عندما تختفي الطبقة E فإنها تنتشر في الطبقة F2 على ارتفاعات منخفضة، أما باقي الترددات فإنها تحقق أعلى ارتفاعاتها في ساعات الذروة الشمسية خصوصا التردد (11.850 MHz)، يليه بقية الترددات تباعا، حيث تخترق الطبقة E لأنها ذات تردد عالي، وينخفض ارتفاعها في آخر ساعات الليل وأول ساعات النهار عن ارتفاعها في ساعات الذروة الشمسية.

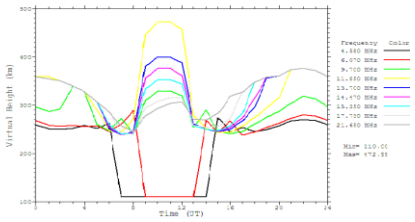

(أ)

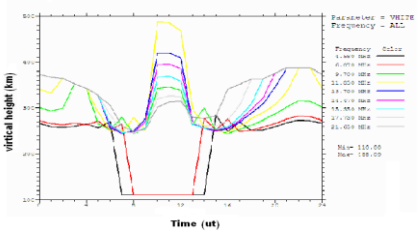

(ب)

الشكل (1) ارتفاع الإشارة في الأيونوسفير
(أ –2011، ب–2012)

عند دراسة التردد الصالح للاستخدام وجد أن قيمة التردد الصالح للاستخدام لسنة 2011 كان في حدود(9.31MHz) ويحدث ذلك عند الساعة (3– 4 ص) ، حيث تنعكس الترددات في هذه الفترة من الطبقة F2 ولكن نظرا لقلة الإشعاع الشمسي في هذه الفترة من النهار وجد أن التردد الصالح للاستخدام ينخفض ، الشكل (2 أ،ب) يبين ذلك ومنه وجد أن أعلى قيمة للتردد الصالح للاستخدام هو (26.44MHz) ويحدث عند الساعة (8 ص) عند ذروة الإشعاع الشمسي وبالتالي يكون التردد الصالح للاستخدام عالي ، و من هنا يكون التردد الذي يجب استخدامه عند إتمام الربط الراديوي بين مدينتي تونس والقاهرة واقع في المدى (9.31–26.44 MHz) للسنة 2011 ، بينما في السنة 2012 الشكل (2ب) كان أقل قيمة (9.62 MHz) ويحدث عند الساعة (4 ص) حيث انخفاض في الكثافة الإلكترونية و يكون أعلى تردد صالح للاستخدام عند الساعة (9 ص) حيث تكون ذروة الإشعاع الشمسي والكثافة الإلكترونية وتنتشر أغلب الترددات في الطبقة F2 في هذه الفترة وعلية يكون التردد الواجب استخدامه عند إتمام ربط راديوي بين تونس والقاهرة في المدى (9.62,29.02 MHz).

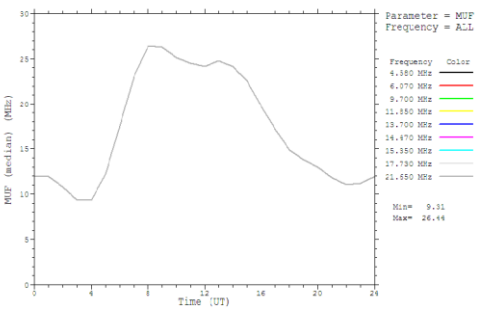

(أ)

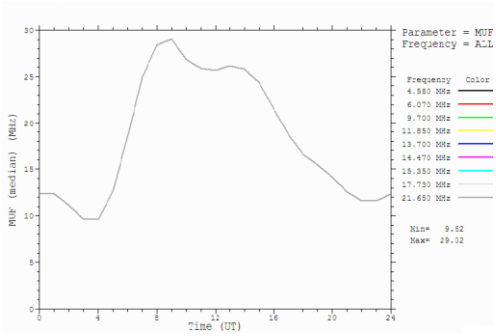

(ب)

شكل(2) التردد الصالح للاستخدام
(أ-2011 ،ب-2012)

عند دراسة نسبة الإشارة إلى الضوضاء ، الشكل (3) يوضح ان نسبة الإشارة إلى الضوضاء في كل الترددات المستخدمة مرتفعة لكل الترددات عند الساعة (6ص-16م) فيما عدا التردد(4.580MHz، 6.070) فيحدث فيها انخفاض شديد لـ SNR في هذه الفترة مقارنة بالترددات الأخرى [4،5] ، وذلك لأنها تعتمد في انتشارها على الطبقة E التي تعمل على امتصاص طاقتها بينما تنخفض قيمة SNR لجميع الترددات تقريبا عند الساعة (4ص، 22م) وكلما زادت قيمة التردد زادت نسبة SNR إلى حد معين بعدها يحدث انخفاض في مستوى الإشارة ، وهذا يتحدد بالتردد الصالح للاستخدام لهذه الوصلة ، ومن الشكل(3-أ) يمكن ملاحظة أن التردد 11.850 MHz هو من أكثر الترددات استقرارا في منحنى SNR حيث أنه يعاني انخفاض بسيط في نسبتها عند الساعة (4ص) ثم يعود للاستقرار، بينما التردد (21.650MHz) هو أقلها من ناحية SNR خلال اليوم لسنة 2011 ، بينما لسنة 2012 شكل (3-ب) يحدث انخفاض في SNRللترددات (4.580,6.070MHz) في ساعات انتشارها في الطبقة E (6 ص-14م) بسبب عمل الطبقة E على امتصاص طاقة الإشارات ذات الترددات المنخفضة ، بينما ترتفع فيها SNR باقي ساعات اليوم وذلك نتيجة انتشارها في الطبقة F2 ، أما بقية الترددات فإن SNR مرتفعة ، ويحدث بها انخفاض بسيط في آخر ساعات الليل وأول ساعات النهار وخصوصا الترددات (17.730, 21.650 MHz) ، فإنها يحدث

بها انخفاض SNR أكبر من الترددات الأخرى خلال ساعات النهار (2–5 ص)، ويحدث انخفاض أقل في آخر ساعات الليل (22– 24 م) ويمكن ملاحظة أن التردد (11.850 MHz) يحقق أعلى قيم SNR ومنحناه يمتاز بالاستقرار خلال ساعات اليوم للسنة 2012 .

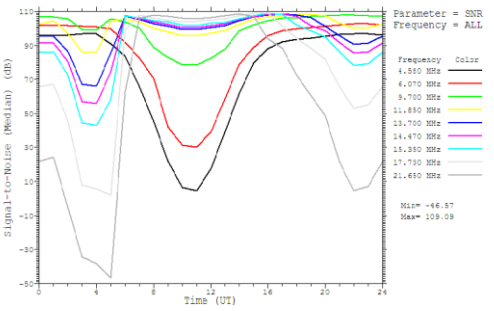

(أ)

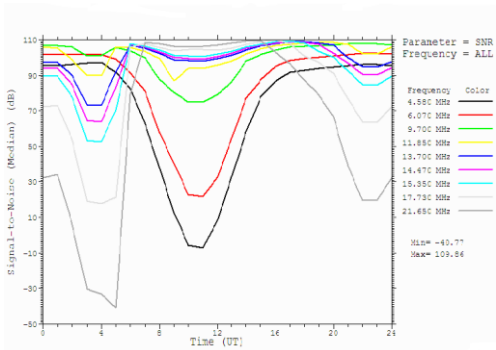

(ب)

الشكل (3) نسبة الإشارة إلى الضوضاء (أ–2011، ب–2012)

عند دراسة الفقد في النظام ، الشكل (4) يوضح الفقد لجميع الترددات كدالة في الزمن والواضح أن جميع الترددات تعاني من فقد أكبر خلال الساعات (6:00–0:00 ص) وكذلك (24:00–16:00م) ، بينما يكون الفقد أقل في الفترة (6:00ص– 16:00 م) ، ويرجع ذلك إلى أن هذه الفترة تتمتع بذروة في الإشعاع الشمسي ، ويقل الفقد نتيجة لجودة الاتصالات خلال هذه الفترة ، أما بالنسبة للترددات (4.580MHz، 6.070) فإنها تعاني فقدا أكبر خلال الساعات (6ص–16م) لأنها تنتشر خلال هذه الفترة في الطبقة E التي تعمل على امتصاص طاقتها ، بينما الفقد فيها أقل خلال الفترة (6:00–0:00ص، 24:00–16:00م) ، لأن الترددات الأقل أنجح في الاتصال خلال ساعات الليل نتيجة لقلة الكثافة الإلكترونية ليلا ، ولنفس السبب وجد أن التردد (21.650MHz) أكثرها فقدا خلال هذه الساعات ، وبالرجوع إلى الشكل(4–أ)، يمكن ملاحظة أن التردد (11.850MHz) هو الأقل في الفقد خلال ساعات اليوم لسنة 2011، بينما للسنة 2012 شكل (4– ب) تكون أعلى قيم الفقد للترددات (4.580,6.070MHz) خلال الساعات (6 ص–14 م) لأنها تنتشر في الطبقة E في هذه الفترة التي تعمل على

امتصاص طاقتها ويزداد الفقد في الإشارات ، بينما يكون الفقد فيها أقل في باقي ساعات اليوم ، أما بقية الترددات فإن قيمة الفقد فيها تكون قليلة أغلب ساعات اليوم وتعاني من ارتفاع بسيط في الفقد في آخر ساعات الليل وأول ساعات النهار نتيجة لقلة الكثافة الإلكترونية في تلك الأوقات ، بينما الترددات (17.730, 21.650 MHz)، يحدث بها أعلى قيم للفقد وخصوصا في أول ساعات النهار بين (2-5 ص)، والتردد (11.850 MHz) يحقق أقل قيم الفقد خلال اليوم.

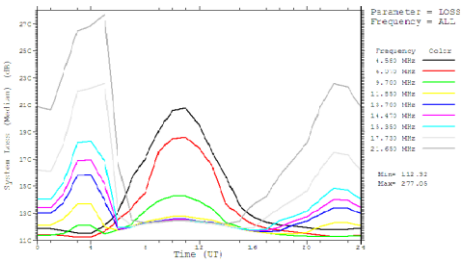

(أ)

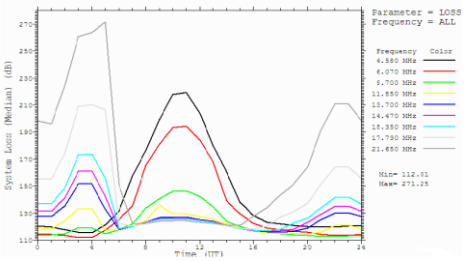

(ب)

الشكل (4) دراسة الفقد في النظام (أ-2011 ، ب-2012)

ومما سبق يمكن القول أن التردد الصالح للاستخدام قيمته بين (9.31-26.44 MHz) ، وتردد التشغيل المناسب لهذه الوصلة هو 10.07MHz لسنة 2011 ، و للسنة 2012 هو 11.850 MHz وهو تردد واقع في مدى التردد الصالح للاستخدام [1،8] (9.62, 29.02 MHz) ، ويكون تردد التشغيل لهذه الوصلة 10.07MHz .

ثانيا: الربط الراديوي بين تونس وطرابلس

المسافة بين مدينة تونس وطرابلس 515 كم وهي بذلك تقع في مدى المسار القصير للموجات القصيرة وعند دراسة طبقة الانعكاس وارتفاع الإشارة في الأيونوسفير وجد أن الترددات (4.580MHz، 6.070) تنتشر صباحا عند الساعة (9:30-1) في الطبقة E وبالتالي تسبب توهينا لهذه الإشارات، بينما بقية الترددات تنتشر طوال اليوم وعلى نفس الارتفاع للسنة 2011 ، و للسنة 2012 لوحظ أن جميع الترددات تنتشر على ارتفاعات متقاربة في F2 عدا الترددات (4.580,6.070MHz) التي تنتشر على ارتفاعات أقل في الساعات (9:30 - 12:30 ص) ،بينما تعود لترتفع باقي ساعات اليوم عند انتشارها في الطبقة F2. الشكل (5-أ) يبين التردد الصالح للاستخدام للوصلة لسنة 2011 ووجد أن أقل

قيمة للتردد الصالح للاستخدام لإنشاء هذه الوصلة هو (4.21MHz) كحد أدنى، وأعلى تردد يمكن استخدامه (11.24MHz) ، وهذا يعتمد على ذروة الإشعاع الشمسي التي يحدث عندها تأين أكثر وبالتالي تسمح باستخدام ترددات أعلى ، بينما فترات انخفاض الإشعاع الشمسي قيمة التردد الصالح للاستخدام تقل نتيجة لقلة كثافة الإلكترونات، وبذلك التردد الصالح للاستخدام للوصلة يكون بين هاتين القيمتين للسنة 2011 ، والسنة 2012 شكل (5– ب) أقل قيمة للتردد الصالح للاستخدام لهذه الوصلة (4.34 MHz) في ساعات الصباح الأولى (4 ص) ، و أعلى قيمة (12.36 MHz) تحدث عند ذروة الإشعاع الشمسي عند الساعة (9 –10 ص) وبالتالي التردد الصالح للاستخدام يكون بين هاتين القيمتين للسنة 2012 .

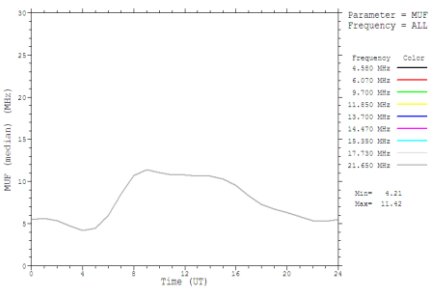

(أ)

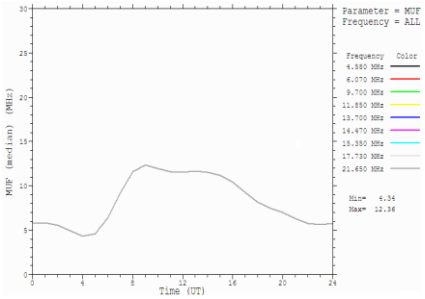

(ب)

الشكل (5) دراسة التردد الصالح للاستخدام (أ–2011 ،ب–2012)

الشكل (6–أ) يوضح نسبة الإشارة إلى الضوضاء لكل الترددات المستخدمة لسنة 2011 ووجد أن التردد (6.070MHz) تحقق أعلى قيم SNR، يليه التردد (4.580MHz) ، وكلما زادت قيم الترددات أصبحت تعاني من فقد أعلى في الفترة بين(8ص–16م) ووجد أن الترددات (17.730MHz، 21.650) تحقق أقل قيم لـ SNR خلال اليوم لأن هذه الترددات تجاوزت الحد الأقصى المسموح به للتردد الصالح للاستخدام لإنشاء هذه الوصلة ،أما بالنسبة لسنة 2012 الشكل (6– ب) يلاحظ أنه يحدث انخفاض في SNR لجميع الترددات خلال آخر ساعات الليل وأول ساعات النهار فالترددات (4.580,6.070MHz) هي أعلى الترددات في قيم SNR خلال اليوم ، وأكبر انخفاض في SNR لها يحدث بها عند الساعة

(12:30–9:30ص) بينما باقي الترددات ترتفع فيها نسبة SNR في هذه الفترة ، بينما آخر ساعات الليل و أول ساعات النهار يحدث انخفاض في SNR ، ويلاحظ أن التردد (21.650 MHz) أقل الترددات في قيم SNR طوال اليوم لأنه يقع خارج مدى التردد الصالح للاستخدام لإنشاء هذه الوصلة ، والتردد (6.070 MHz) من أعلاها قيمة SNR ومنحناه أكثر استقرارا خلال ساعات اليوم.

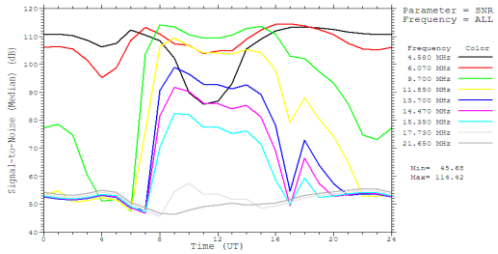

(أ)

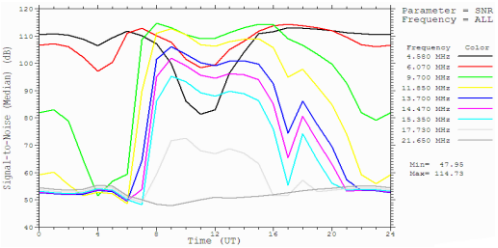

(ب)

الشكل (6) دراسة نسبة الإشارة إلى الضوضاء (أ-2011، ب-2012)

الشكل (7-أ) يبين الفقد لجميع الترددات المستخدمة لسنة 2011 كدالة في الزمن ، حيث أكبر قيمة للفقد تحدث في ساعات النهار ، و تؤثر على الترددات الأخرى ، ويمكن ملاحظة أن الترددات (4.580MHz، 6.070) تحقق أقل فقد في الإشارة خلال اليوم لانها تقع في مدى التردد الصالح للاستخدام و الترددات (17.730MHz، 21.650) تعاني أكبر قيمة للفقد.

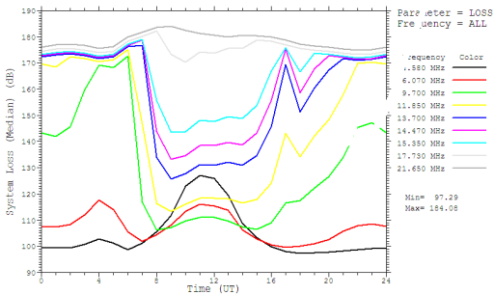

(أ)

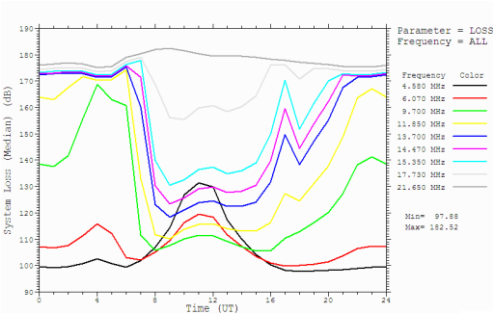

(ب)

الشكل (7) دراسة الفقد في النظام (أ-2011، ب-2012)

من ذلك يمكن القول أن أنسب تردد لإنشاء وصلة الاتصال الذي يقع في مدى الترددد الصالح للاستخدام ، لسنة 2011 هو 6.070MHz ، و تردد التشغيل المناسب لهذه الوصلة هو 5.15MHz ، و لسنة 2012 الشكل (7–ب) هو (6.070 MHz) و تردد التشغيل المناسب لهذه الوصلة هو 5.15 MHz.

ثالثا : الربط الراديوي بين تونس والجزائر

المسافة بين مدينة تونس والجزائر هي 631 كم وهي بذلك تقع في مدى المسار القصير، وعند دراسة خصائص انتشار الموجات القصيرة لطبقة الانعكاس وارتفاع الإشارة في الأيونوسفير لهذه الوصلة لسنة 2011، التردد (4.850MHz) يعتمد في انتشاره على الطبقة E في الساعات (9:30 – 13:30) بينما ليلا على الطبقة F2 ، و باقي الترددات تعتمد في انتشارها طوال اليوم على الطبقة F2 ، الشكل (8–ا) يوضح ذلك وفي سنة 2012 ، جميع الترددات تعتمد في انتشارها على الطبقة F2 على ارتفاع (240–383 كم)، فيما عدا التردد(4.580MHz) الذي ينتشر في الساعات (9ص– 14 م) في الطبقة E بينما باقي اليوم في الطبقة F2 الشكل (8–ب).

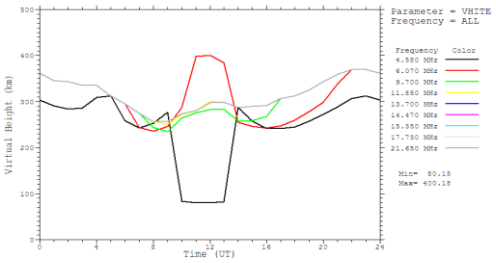

(أ)

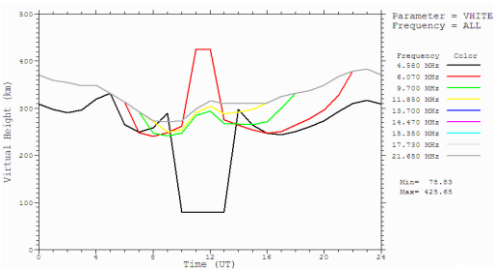

(ب)

الشكل (8) دراسة طبقة الانعكاس وارتفاع الإشارة في الأيونوسفير (أ–2011 ،ب–2012)

الشكل (9–أ) يبين أن أقل قيمة للتردد الصالح للاستخدام الممكن استخدامها لإنشاء هذه الوصلة لسنة 2011 هو (4.52 MHz) وأعلى قيمة (12.24 MHz) حيث أقل قيمة عند ارتفاع الإشارة للترددات المرسلة قليلة في ساعات الصباح الأولى ، بينما عند ارتفاع الإشارة في ذروة الإشعاع الشمسي الساعة (10ص) يكون التردد الصالح للاستخدام أعلى ، وفي سنة 2012 ، الشكل (9–ب) يوضح قيمة التردد الصالح للاستخدام للوصلة حيث أقل قيمة له (4.55MHz) خلال ساعات

النهار الأولى (5ص) وبالتالي الموجات ذات الترددات القليلة تنجح في الانتشار أفضل من الترددات العالية ، وأعلى قيمة (13.19MHz) تحدث عند الساعة (9–10ص) حيث ذروة الإشعاع الشمسي تسمح بانتشار أفضل للترددات الأعلى ، وبذلك يكون التردد الصالح للاستخدام في هذا المدى بين هاتين القيمتين.

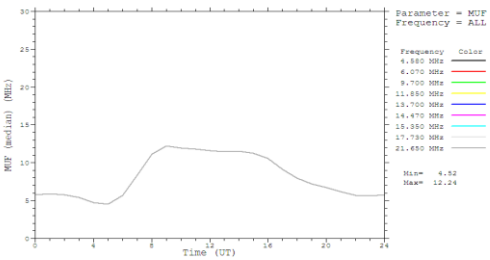

(أ)

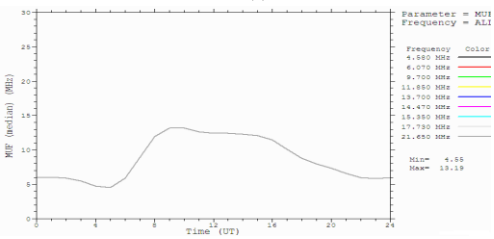

(ب)

الشكل (9) دراسة التردد الصالح للاستخدام (أ–2011 ،ب–2012)

من الشكل (10–أ) و الذي يوضح SNR لكل الترددات لسنة 2011 يمكن ملاحظة أن أعلى قيمة لنسبة SNR تحدث في ساعات بين (9:00ص – 16:00 م). و قيمة SNR تتجه للانخفاض كلما زاد التردد في المدى (4.580MHz، 21.650) خصوصا عند الترددات الصالحة للاستخدام مثل التردد (17.730MHz، 21.650) حيث قيمة SNR بها قليلة جدا ، ووجد أن التردد (4.580,6.070MHz) تحقق أعلى مستوى في SNR ومنحنياتها أكثر استقرارا باختلاف ساعات النهار، وبالنسبة لسنة 2012 وجد من الشكل (10–ب) SNR لجميع الترددات كانت منخفضة (4.580,6.070MHz) و SNR بها خلال اليوم أفضل من الترددات الاخري ولكنها تعاني من انخفاض SNR عند ساعات الصباح الأولى (4 ص) حيث انخفاض الإشعاع الشمسي و عند ساعات الذروة الشمسية بالرغم من أن التردد (6.070MHz) تعتمد في انتشارها على الطبقة F2 إلا أنه يعاني توهينا عند مروره خلال الطبقة E باعتباره من الترددات المنخفضة. بقية الترددات ترتفع بها SNR خلال ساعات الذروة الشمسية (8ص– 14م) بينما تنخفض SNR فيها في ساعات النهار الأولى (1–5ص) وكذلك آخر ساعات الليل (18 –24م) ،بالنسبة للترددات الواقعة في المدى الترددى الصالح للاستخدام وجد انخفاضا واضحا في قيمة SNR طوال اليوم (17.730, 21.650 MHz) و التردد

(4.580MHz) يحقق أعلى قيم SNR خلال اليوم.

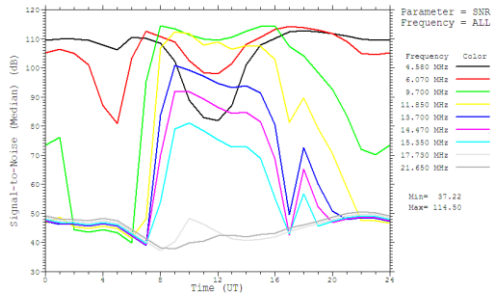

(أ)

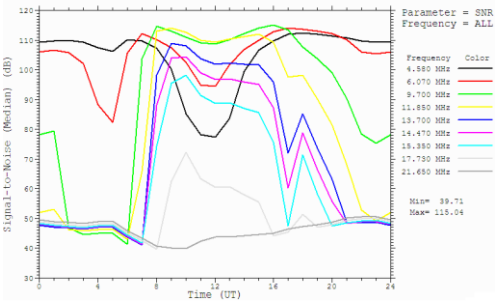

(ب)

الشكل (10) دراسة نسبة الإشارة إلى الضوضاء

(أ-2011، ب-2012)

وجد أن أكثر الترددات فقدا لسنة 2011 هو (21.650 MHz،17.730) طوال اليوم لأنها تبعد كثيرا عن أقصى مدى للتردد الصالح للاستخدام 12.24 MHz، ثم يليها في الفقد الترددات الأخرى باتجاه أقل قيمة للتردد الصالح للاستخدام (4.52MHz) حتى الترددات (4.580,6.070 MHz) التي تحقق أقل قيم للفقد . في سنة 2012 لوحظ أن الترددات (4.580,6.070MHz) يكون فيها الفقد منخفض ، وقيمته أقل من الفقد للترددات الأعلى من ذلك ، ويحدث ارتفاع بسيط مقارنة بالترددات الأخرى عند ساعات النهار الأولى (4ص) (8-14م) نتيجة الانتشار في الطبقة E ، بينما بقية الترددات تكون فيها نسب الفقد قليلة ويلاحظ أيضا أن الترددات (17.730, 21.650 MHz يحدث بها فقد عالي طوال اليوم مما يؤكد أنها تقع خارج مدى التردد الصالح للاستخدام لهذه الوصلة والتردد (4.580MHz) يحقق أقل قيم للفقد خلال اليوم ، لسنة 2012 ، و يلاحظ أن الترددات (4.580,6.070MHz) يكون فيها الفقد منخفض وقيمته أقل من الفقد للترددات الأعلى من ذلك ، ويحدث ارتفاع بسيط مقارنة بالترددات الأخرى عند ساعات النهار الأولى (4ص) ، (8-14م) ، بينما بقية الترددات تكون فيها نسب الفقد قليلة، الترادت(21.650 17.730, MHz) يحدث بها فقد عالي طوال اليوم مما يؤكد أنها تقع خارج مدى التردد الصالح للاستخدام لهذه الوصلة ، ويلاحظ أن التردد (4.580MHz) يحقق أقل قيم للفقد خلال اليوم ، مما سبق يمكن القول بأن أنسب تردد للوصلة بين تونس والجزائر في مدى

التردد الصالح للاستخدام (MHz 12.24، 4.52) لسنة 2011 هو التردد (4.850MHz) ، ويكون تردد التشغيل المناسب لهذه الوصلة 4MHz ، ولسنة 2012 هو التردد 4.580MHz .

رابعا: الربط الراديوي بين تونس إلى الرباط

المسافة بين تونس والرباط هي 1575 كم هي بذلك تقع في مدى المسار القصير، وعند دراسة طبقة الانعكاس وارتفاع الإشارة في الأيونوسفير وجد أنه لسنة 2011 الترددات التي تنتشر في الطبقة Es (6.070,4.850MHz) في الفترة (8:30 ص- 16:30 م) وتكون على ارتفاع متوسط في الطبقة Es التي تساعد في ارتفاع مستوى انتشارها في هذا الوقت ، ويزداد ارتفاع باقي ساعات اليوم عندما تنتشر في الطبقة F2 ، أما باقي الترددات فتنتشر على ارتفاعات متقاربة في الطبقة F2 ، و التردد الصالح للاستخدام يتراوح بين (7.44-22.07MHz) ويحدث أقل MUF خلال ساعات النهار الأولى ، بينما أعلى قيمة عند حوالي الساعة (10:00ص)، وعلية فإن أفضل تردد صالح للاستخدام يكون ضمن هذا المدى ، بينما في سنة 2012 الترددات المنخفضة 4.580 MHz, (6.070MHz) تنتشر على ارتفاعات منخفضة في الأيونوسفير ، بينما باقي اليوم تنتشر في الطبقة F2 ليلا وفي ساعات الصباح الأولى ، باقي الترددات تخترق الطبقة E نهارا وتنتشر طوال اليوم في الطبقة F2على ارتفاعات متقاربة بين (239-393 كم).

من الشكل (11-أ) يتبين أن التردد الصالح للاستخدام لسنة 2011 يتراوح بين (7.44-22.07MHz) يحدث أقل MUF خلال ساعات النهار الأولى ، بينما أعلى تردد عند حوالي الساعة (10:00ص) وعلية فإن أفضل تردد صالح للاستخدام يكون ضمن هذا المدى ، لسنة 2012 الشكل (11-ب) يوضح أن التردد الصالح للاستخدام يقع في المدى بين (4.77MHz - 23.43) ، حيث أقل قيمة في الصباح الباكر (5ص) ، بينما أعلى قيمة له (10 ص) ويكون التردد الصالح لهذه الوصلة في هذا المدى.

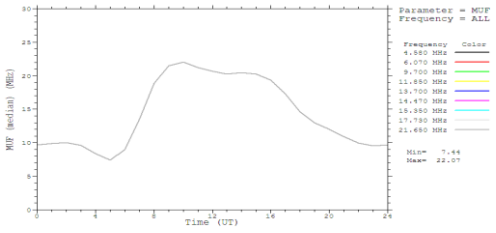

(أ)

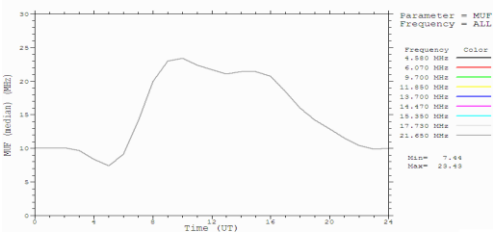

الشكل (11) دراسة التردد الصالح للاستخدام (أ-2011 ،ب-2012)

ويلاحظ من الشكل (12-أ) أن أقل قيمة لـ SNR لسنة 2011 تحدث في آخر ساعات الليل وأول ساعات النهار ، بينما فترة الظهيرة تكون فيها أعلى مستويات لجميع الترددات تقريبا و يعاني التردد (6.070,4.850MHz) من انخفاض في مستوى SNR في الفترة من (10:00ص- 15:00 م) ، وذلك لأنها تنتشر في الطبقة E وبالتالي انخفاض مستوى SNR في هذه الفترة ، ويلاحظ أن التردد (6.070MHz) هو أعلاها وأكثرها استقرارا في SNR ، أما في سنة 2012 فإنه من الشكل (11-ب) ان أقل قيم SNR تحدث في فترات غياب الإشعاع الشمسي بينما في ساعات الإشعاع الشمسي تكون قيمة SNR أعلى ، و أن الترددات(4.580,6.070MHz) يحدث لها انخفاض SNR عند الساعة (8ص- 16م) ، بينما ترتفع SNR باقي اليوم ويمكن ملاحظة أن التردد (9.700 MHz) يحقق أفضل قيم SNR خلال اليوم.

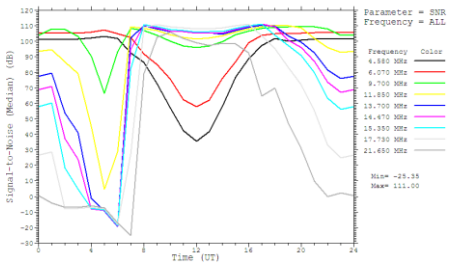

(أ)

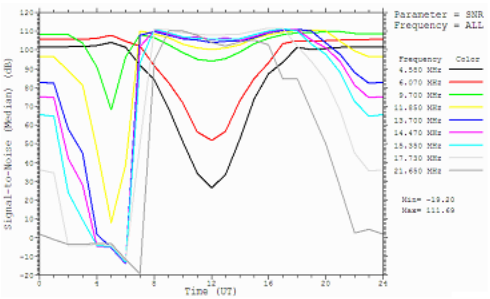

(ب)

شكل(12) دراسة نسبة الإشارة إلى الضوضاء (أ-2011 ،ب-2012)

يوضح الشكل (13-أ) منحنيات الفقد لجميع الترددات المستخدمة لسنة 2011 ويتبين أن الفقد يزداد بزيادة التردد و أعلى قيم للفقد تحدث عند آخر ساعات الليل وأول ساعات النهار. ووجد أن الترددات (4.580,6.070MHz) تحقق أقل قيما للفقد خلال ساعات اليوم فيما عدا فترة انتشارها في الطبقة E (8:00ص- 13:00م) التي تسبب ارتفاعا في نسبة الفقد

مقارنة بالترددات الأخرى ، في سنة 2012 الشكل (13–ب) يوضح منحنيات الفقد لجميع الترددات ويتضح أن قيم الفقد أعلى ما يمكن (الصباح الباكر، آخر الليل) ،هذا بالنسبة للترددات بين(21.650,9.700MHz)، بينما يقل فيها الفقد في ساعات الذروة الشمسية عند الساعة (8ص– 16م) ، بينما الترددات المنخفضة (4.580,6.070MHz) التي تنتشر على ارتفاعات منخفضة تكون أعلى فقد بها نهارا بينما الفقد فيها أقل في آخر الليل وأول النهار مقارنة بالترددات الأخرى ، ويلاحظ أيضا أن التردد (9.700 MHz) يعطي أقل قيم للفقد خلال اليوم.

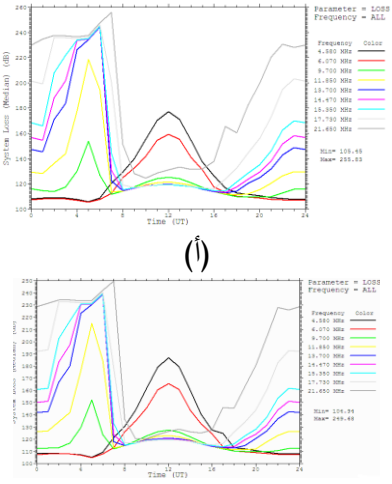

(أ)

(ب)

الشكل (13) دراسة الفقد في النظام (أ–2011 ،ب–2012)

من خلال ما تقدم يمكن القول بأن أنسب تردد صالح للاستخدام للوصلة لسنة 2011 هو 6.070MHz حيث يقع في المدى 7.44– 22.07MHz و تردد التشغيل 5.16 MHz ، أما في سنة 2012 فأن أنسب تردد هو 9.700 MHz ، و يكون تردد التشغيل المناسب 8.2 MHz .

خامسا: الربط الراديوي بين تونس ونواكشوط

المسافة بين تونس ونواكشوط 3294 كم وهي بذلك ضمن المدى القصير، ولدراسة طبقة الإنعكاس وارتفاع الإشارة في الأيونوسفير لسنة 2011 ،الشكل (14–أ) وجد أن الترددات (4.580,6.070MHz) هي أقل الترددات ارتفاعا خصوصا في الفترة (6:00ص–16:00م) ،أما باقي الوقت فتنتشر على ارتفاع منخفض في الطبقة F2، بينما باقي الترددات تعتمد في انتشارها على الطبقة F2 طوال اليوم ، أما في سنة 2012 فإن من الشكل (14–ب) وجد أن الترددات 4.850,6.070,9.700MHz تنتشر على ارتفاعات منخفضة عند الساعة (7ص–16م) على ارتفاعات منخفضة في الطبقة E التي تعمل على امتصاص طاقتها ، أما باقي اليوم فتنتشر في الطبقة F2 على ارتفاع أقل من

ارتفاع الترددات الأخرى. الترددات الباقية (11.850–21.650 MHz) فتنتشر في الطبقة F2 طوال اليوم.

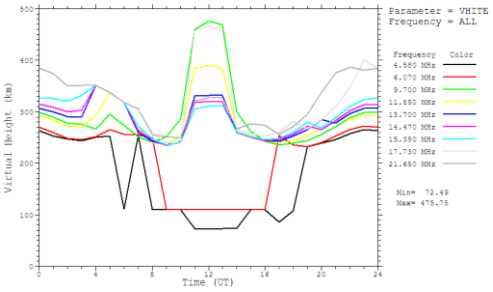

(أ)

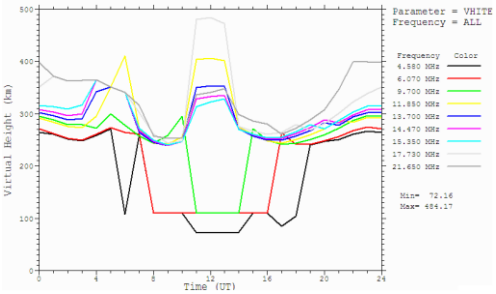

(ب)

الشكل (14) دراسة طبقة الإنعكاس وارتفاع الإشارة في الأيونوسفير (أ–2011 ،ب–2012)

من الشكل (15–أ) يتبين أن أقل تردد صالح للاستخدام لسنة 2011 هو (10.64 MHz) بينما أعلى قيمة للتردد الصالح للاستخدام هي (33.38MHz) حيث أنها تتجاوز مدى الموجات القصيرة علية فإن أعلى قيمة تكون 30MHz ، أما في سنة 2012 فإنه من الشكل (15–ب) يتبين أن أقل قيمة للتردد الصالح للاستخدام (11.10MHz) تحدث عند (5ص) ، وأعلى قيمة له (35.80MHz) وهي تعتبر خارج مدى الموجات القصيرة (3–30 MHz) وبذلك يعتبر أعلى حد لها هو (30 MHz) [1].

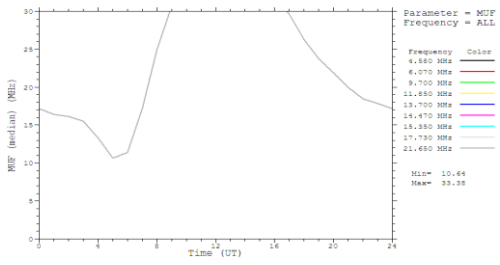

(أ)

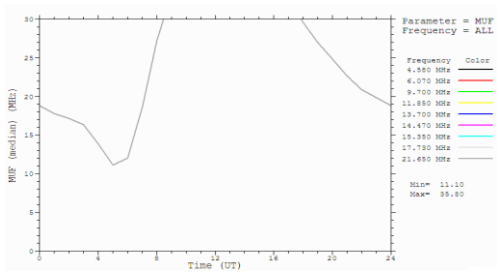

(ب)

الشكل (15) دراسة التردد الصالح للاستخدام (أ–2011 ،ب–2012)

من الشكل (16–أ) الذي يوضح التغيير في SNR لسنة 2011 عند التررددات (4.580,6.070,21.650MHz) تعطي قيم منخفضة لـ SNR في الفترة (13:00–5:00) بينما بقية التررددات تعطي نسب عالية لقيمة SNR طوال اليوم ، ويمكن ملاحظة أن التردد (11.850MHz) هو أكثرها استقرارا ويعطي قيما عالية SNR ،

أما في سنة 2012 الشكل (16–ب) يوضح قيمة SNR لجميع التررددات ، فالتررددات المنخفضة (4.850,6.070MHz) خلال ساعات انتشارها في الطبقة E (8ص–16م) تعاني من انخفاض شديد في SNR ، بينما ترتفع بها SNR كبقية التررددات باقي ساعات اليوم ، و باقي التررددات نسبة SNR تكون متقاربة ا طوال اليوم (21.650,17.730MHz) التي يحدث بها انخفاض SNR عند (5ص) ويلاحظ أن التردد (11.850 MHz) هو من أفضلها في قيم SNR طوال اليوم.

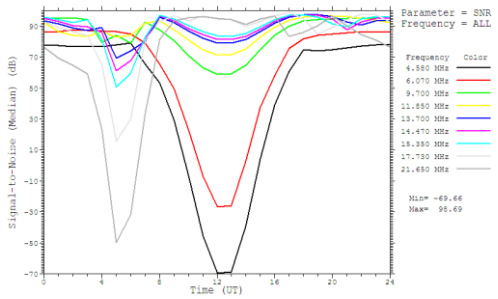

(أ)

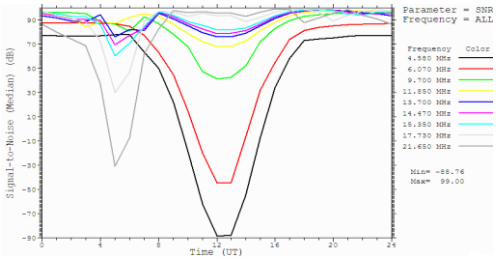

(ب)

الشكل (16) دراسة نسبة الإشارة إلى الضوضاء

(أ–2011 ،ب–2012)

من الشكل(19–أ) الذي يدرس الفقد لسنة 2011 يتضح أن التررددات (6.070,4.580MHz) تعاني أعلى قيم في الفقد أثناء فترة انتشارها (9:00,14:00MHz) ، ويمكن ملاحظة أن التردد (11.850MHz)هو أكثر المنحنيات استقرارا وأقلها فقدا ، و لسنة 2012 حيث قيمة الفقد

للتـرددات المنخفضــة (4.850,6.070MHz) تكون أعلى ما يمكن (8ص–16م) ، بينما بقية الترددات يكون فيها الفقد اكبر خـلال سـاعات الصـــباح (4–6ص). ويلاحظـــه أن التـــردد 11.850MHz يعطـي أقـل قـيم للفقـد مقارنـة بالترددات الأخرى.

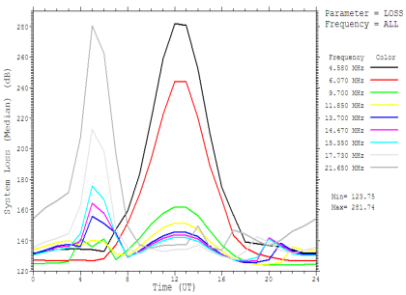

(أ)

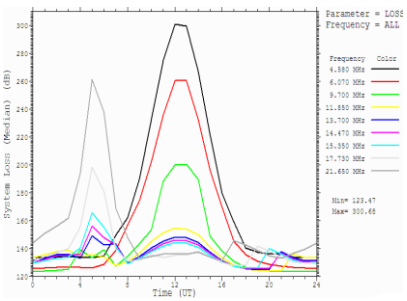

(ب)

الشكل(16) دراسة الفقد في النظام (أ–2011 ،ب–2012)

ومما سبق فإن التردد الصالح للاستخدام لسنة 2011 في المدى بين 33.38MHz –10.64 هو التردد 11.850MHz ويكون تردد التشغيل 10.07MHz، و لسنة 2012 فإن التردد 11.850MHz هو من أفضل الترددات ممكن استخدامها ،علية يكون تردد التشغيل 10.07 MHz.

5–الاستنتاجات

إن طبقـة الأيونوسـفير هـي طبقـة غيـر مستقرة لا يمكن الاعتماد فيها على تردد واحد طوال اليوم حيث أن التردد الذي يحقق أفضل اتصـال قـد لا يعمـل بعـد سـاعة. ومـن خـلال القراءات المتحصل عليها و مقارنته [10 ، 11] يمكن استنتج أن :–

التردد الأقصى الصالح للاستخدام والذي يحقق أفضل انتشار ويضمن وصول الإشارة إلى طرف الاستقبال يتغير باستمرار, حيث تم تحديد التردد الأقصى الصالح للاستخدام عند نقطة الاستقبال لمناطق الدراسة ، الجدول (1) يبين النتائج المتوصل اليها للحصول على نظام اتصالات جيدة خلال فترات ، حيث 1– المسار القاهرة –تونس ، 2– طرابلس –تونس 3– تونس الجزائر ، 4– تونس – الرباط 5– نواكشوط –تونس.

جدول(1) الترددات الصالحة للاستخدام

الوصلة	1	2	3	4	5
التردد MHz 2011	10.07	6.07	4.0	5.16	10.07
التردد MHz 2012	11.85	5.15	4.5 8	8.20	10.07
المسار km	2086	515	631	1575	3294

6-المراجع

[1] د. حســـن الكمشوشـــي , " هندســـة الهوائيات انتشار الموجات والكمبيوتر " , دار الراتب الجامعية , 1990.

[2] Richard C.KIRBY,"Antennas and Wave Propagation", McGraw-Hill, 1975.

[3] Bertoni. H. L,"Propagation of radio wave ", Prentice hall, 2000.

[4]Barclay A. H, "Propagation of radio wave", IEE, 2003.

[5] http://www.khayma.com

[6]http://www.homearab.com /science/4.htm

[7]http://www.astrosurf.com /luxorion/qsl-ssnistory.voacap.htm

[8] Saad Ali El Haj Bakri and Mohamad abderhman El harbi," Introduction to Communication", King Saoud University, 1988.

[9] ITS HF Propagation program, Nittany Scientific, Inc, 2001.

[10]- Rasim A. A, Mona H. R, Amna E. M," Study the linking of the short wave radio in Libyan area 2008, 2009", Sebha University Journal, 2008.

[11]- Aborois M. W, Rasim A. A, "The determinations of operational frequency link in HF between Sebha and Benghazi city", fourth Libyan Arab International conference on Electrical and Electronic Engineering, March 20-23, 2006.

[12] Tascione T.F, Kroehi k.w," A technical description of the ionospheric conductivity and electron density profile model(ICED, version 196-II),syst.Doc.VII,Air Weather Serv.,U.S. Air force, Scott air force base,III, 1987.

فصل مكونات الحمل الكهربائي في منظومة التوزيع العراقية

د. ماجد صالح الحافظ
el_noor2000@yahoo.com

د. أزهر سعيد الفهادي
azheralfahady@yahoo.com

السيد ياسر أحمد محمود
yaser_amm@yahoo.com

قسم الهندسة الكهربائية
جامعة الموصل
موصل – العراق

الخلاصة

يصنف الحمل الكهربائي في العراق عموما والموصل خصوصا ضمن الأحمال الكهربائية المتأثرة بالضروف المناخية. تؤدي عوامل متعددة إلى جعل الحمل الكهربائي لفصل الشتاء أعلى من الحمل الكهربائي لعموم السنة. كذلك فان اعتدال درجة الحرارة في فصلي الربيع والخريف يؤدي إلى حمل كهربائي اقل.

يؤدي عدم وجود قيم دقيقة لمكونات الحمل الكهربائي المتأثرة بالضر وف المناخية والمكونات غير المتأثرة بالضر وف المناخية إلى حصول أخطا كبيرة ومشاكل في التعامل مع الأحمال الكهربائية في الجوانب المختلفة مثل نمو الأحمال وترشيد الاستهلاك وإدارة الأحمال الكهربائية ...الخ.

يعرض البحث الحالي طريقة لفصل مكونات الحمل الكهربائي غيرا لمتأثرة بالضر وف المناخية والمكونات المتأثرة بالضر وف المناخية – فصل الشتاء والمكونات المتأثرة بالضر وف المناخية – فصل الصيف. أعتمدت قراءات الأحمال الكهربائية المسجلة في مدينة الموصل (شمال العراق) في الطريقة المقترحة. تم تسجيل درجة الحرارة الصغرى والعظمى وكذلك الحمل الكهربائي لثلاث مغذيات يوميا ولمدة سنة كاملة. حللت القراءات باستخدام الطريقة المقترحة وعرضت النتائج ونوقشت في الفقرات التالية.

1- المقدمة

يتكون الحمل الكهربائي من مكونات متعددة، لذا فهو يتغير بصورة مستمرة بسبب عوامل كثيرة تؤثر على هذه المكونات. يمكن تصنيف العوامل المؤثرة على الحمل الكهربائي إلى عوامل اقتصادية، تأثيرات سكانية، عوامل الزمن، التأثيرات المناخية، وعوامل عشوائية [3, 2, 1].

تعتمد خصائص الحمل الكهربائي على المستهلك النهائي ونوعية الأجهزة والمستلزمات الكهربائية المستخدمة مثل أجهزة الإنارة وأجهزة التدفئة وأجهزة التبريد والمحركات . . . الخ. تصنف الأحمال الكهربائية إلى أربعة أصناف: التجاري والسكني والزراعي والصناعي [4].

يمثل نموذج الحمل الكهربائي المتأثر بالضر وف المناخية بتقسيمه إلى مركبة تتأثر بالضروف المناخية ومركبة أخرى لا تتأثر بالضر وف المناخية. تتصف الأحمال الكهربائية السكنية والتجارية بالتغير مع فصول السنة و الضر وف المناخية. تكون درجة الحرارة ابرز العوامل المناخية التي تؤثر في تغير الحمل، كذلك فان للرطوبة النسبية وسرعة الرياح بعض التأثير على الحمل الكهربائي.

يتأثر الحمل الكهربائي في العراق بالضر وف المناخية بشدة. يؤدي ارتفاع درجة الحرارة في الصيف إلى زيادة الحمل الكهربائي نتيجة لاستخدام أجهزة التبريد. كذلك فان انخفاض درجة الحرارة في الشتاء يؤدي إلى زيادة الحمل الكهربائي نتيجة لاستخدام أجهزة التدفئة وتسخين المياه. تؤدي درجات الحرارة المعتدلة في فصلي الربيع والخريف إلى حمل كهربائي هو الأقل على امتداد السنة. يتصف الحمل الكهربائي في السنوات الأخيرة بزيادة الحمل الكهربائي لفصل الشتاء عن الحمل الكهربائي لفصل الصيف.

يهدف البحث الحالي إلى فصل مكونات الحمل الكهربائي المتأثرة بالضر وف المناخية ومكونات الحمل الكهربائي غير المتأثرة بالضر وف المناخية. كذلك فصل مكونات الحمل الكهربائي التي تتأثر بانخفاض درجة الحرارة (حمل الشتاء)، ومكونات الحمل الكهربائي التي تتأثر بارتفاع درجة الحرارة (حمل الصيف). استخدمت القراءات المسجلة للأحمال الكهربائية لمدينة الموصل (شمال العراق) في تطبيق الطريقة المقترحة.

2- تسجيل القراءات

يؤثر مستوى الدخل ونمو السكان واستقرار البلاد على الأحمال الكهربائية ونسبة نموها. نظرا لصعوبة تقدير هذه العوامل في العراق في الوقت الحالي, فان البديل المتوفر هو دراسة

وتسجيل الأحمال الحالية , وفق تصنيف مديرية توزيع كهرباء نينوى. تصنف مديرية توزيع كهرباء نينوى المستهلكين وفق معايير هي مسحة الوحدة السكنية وعدد الأفراد والأجهزة المستخدمة من قبل المستهلكين إلى ثلاثة أصناف: الاستهلاك العالي والاستهلاك المتوسط والاستهلاك القليل[5].

تم تسجيل قراءات لأحمال ثلاث مغذيات تمثل نموذج لكل صنف ولمدة عام. كذلك تم تسجيل درجة الحرارة العظمى والصغرى ولمدة عام كذلك. يوضح الشكل رقم 1 درجات الحرارة العظمى والصغرى المسجلة في مدينة الموصل لمدة عام. كذلك يوضح الشكل رقم 2 الحمل الكهربائي للنماذج الثلاثة المسجلة لأصناف المستهلكين الثلاثة.

يتضح من الشكل رقم 2 أن المغذي للمنطقة ذات الاستهلاك العالي أكثر تأثرا بتغير درجة الحرارة. يليه المغذي للمنطقة ذات الاستهلاك المتوسط ، ويكون المغذي للمنطقة ذات الاستهلاك القليل قليل التأثر بتغير درجة الحرارة. كذلك فان الحمل الكهربائي لفصلي الربيع والخريف (فترة الاعتدال الحراري) يكون الأقل على امتداد السنة. يزداد الحمل الكهربائي مع زيادة درجة الحرارة في فصل الصيف. بالإضافة إلى زيادة الحمل الكهربائي عند انخفاض درجة الحرارة في فصل الشتاء. يمثل الحمل الكهربائي لفصل الشتاء الأعلى على امتداد السنة.

يمثل الحمل الكهربائي لفصلي الربيع والخريف اقل القيم لاعتدال درجة الحرارة (20 – 30°) مما يؤدي إلى عدم الحاجة لتشغيل أجهزة تكيف الهواء (تبريد أو تدفئة) وكذلك المراوح ومبردات الهواء والمدافئ الكهربائية . . . الخ. توضح الأشكال 3–6 الأحمال الكهربائية لفصول السنة الشتاء والصيف والربيع والخريف.

3- طريقة التحليل والنتائج

يتضح من الشرح السابق والأشكال المتعددة أن الحمل الكهربائي لفصلي الربيع والخريف يقل عن الحمل الكهربائي لفصلي الشتاء والصيف وذلك لاعتدال درجة الحرارة مما يؤدي إلى عدم استخدام أجهزة التكييف في هذين الفصلين. أي أن الحمل الكهربائي لفصلي الربيع والخريف لا يحوي مركبة تتأثر بالضر وف المناخية.

يمكن إيجاد نموذج رياضي مناسب لتمثل الحمل الكهربائي لفصلي الربيع والخريف. يعطي نموذج الدالة الأسية أفضل النتائج في حالة الأحمال سريعة النمو، وهي الحالة المشابه للأحمال في المنظومة الشمالية عموما ومدينة الموصل خصوصا[6]. ويمكن كتابتها بالشكل الآتي:

$$Y = A * e^{BI/36525}$$

حيث:

Y = الحمل الكهربائي.

A = معامل المركبة غير الحساسة للمناخ.

B = نمو المركبة غير الحساسة للمناخ.

يوضح الشكل رقم 7 المخطط الانسيابي للبرنامج المستخدم في إيجاد قيم الثوابت A&B . يبدأ البرنامج بإدخال المعطيات مثل الحمل الكهربائي الحقيقي وعدد الأيام وتسلسل اليوم وقيمة A&B الابتدائية . . . الخ. يحسب البرنامج قيمة الحمل الكهربائي باستخدام المعادلة الأسية (معادلة رقم 1). يضيف القيمة لمجموع القيم المحسوبة، وكذلك يضيف قيمة الحمل الكهربائي إلى مجموع قيم الحمل الكهربائي الحقيقي. بعد الانتهاء من مجموع الأيام يقارن بين مجموع القيم المحسوبة ومجموع القيم الحقيقية لأجل تعديل قيم A&B أو إحداهما باتجاه تقليل الفرق بين المجموعين. بعد الانتهاء يتم طبع A&B النهائية. تعاد عملية إيجاد قيم A&B للمغذيات الثلاثة.

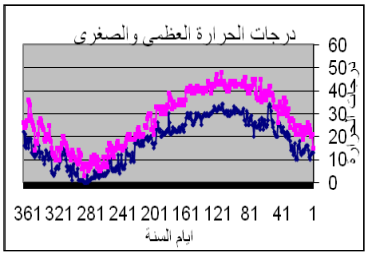

شكل رقم 1 درجات الحرارة العظمى والصغرى لمدة

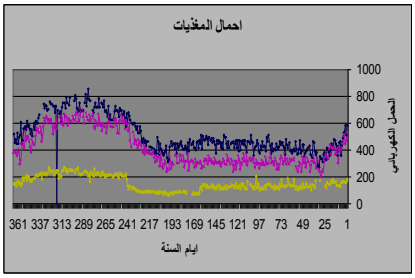

شكل رقم 2 الأحمال الكهربائية

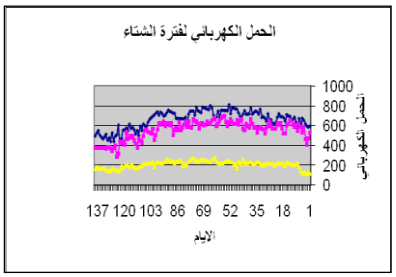

شكل رقم 3 الحمل الكهربائي ل

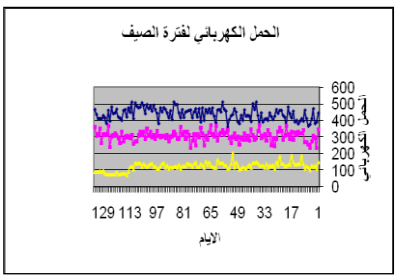

شكل رقم 4 الحمل الكهربائي لفصل

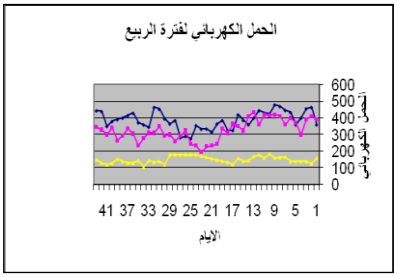

شكل رقم 5 الحمل الكهربائي لفصل

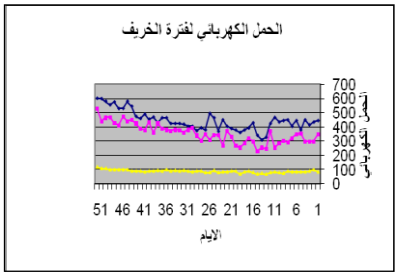

شكل رقم 6 الحمل الكهربائي

يوضح الجدول رقم 1 قيم المعاملات A&B للمغذيات الثلاثة. بعد إيجاد المنحني المناسب لفصلي الربيع والخريف، يمكن تمديد المنحني ليشمل كامل سنة الدراسة. يمثل هذا المنحني المركبة غير الحساسة للمناخ. الفرق بين قيمة المنحني والحمل لفصلي الصيف والشتاء تمثل المركبة الحساسة لارتفاع درجة الحرارة و المركبة الحساسة لانخفاض درجة الحرارة. يمكن إيجاد قيمة هاتين المركبتين للأشهر أو للأسابيع أو مع درجات الحرارة بما يناسب التطبيق المطلوب.

جدول رقم 1 قيم المعاملات A&B للمغذيات الثلاثة.

المغذي	قيمة A	قيمة B
قليلي الاستهلاك	116	0.0585
متوسطي الاستهلاك	341	0.021
عالي الاستهلاك	418	0.0305

استخدمت معادلة مربع الفرق لإيجاد نسبة الخطأ. توضح النسبة القليلة أن المنحني يمثل موائمة جيدة لقيم الأحمال الكهربائية وللمغذيات الثلاثة. يوضح الشكلان 8 و9 المركبات الثلاثة، المركبة غير الحساسة للمناخ، المركبة الحساسة لارتفاع درجة الحرارة و المركبة الحساسة لانخفاض درجة الحرارة ولحالتي المغذي للمستهلكين عالي الاستهلاك وللمستهلكين قليلي الاستهلاك.

4- الاستنتاجات

يمثل إيجاد مكونات الحمل الكهربائي احد طرق إيجاد نماذج مناسبة للتعامل مع الأحمال الكهربائية. شرحت طريقة بسيطة لفصل المركبات الثلاثة، المركبة غير الحساسة للمناخ، المركبة الحساسة لارتفاع درجة الحرارة و المركبة الحساسة لانخفاض درجة الحرارة وطبقت الطريقة على أحمال كهربائية مسجلة لمدينة الموصل (شمال العراق).

شكر وتقدير

يشكر الباحثون إدارة ومهندسو المديرية العامة لتوزيع كهرباء المنطقة الشمالية لما أبدوه من تعاون بناء لإنجاز البحث. ونقدر جهودهم وما تكبدوه في متابعة تسجيل القراءات وإكمال التباحث والمشاورات حول احتياجاتهم من تفاصيل الأحمال ومركباتها للتطبيقات المتعددة.

5- References

1- Salam A. Najim, Zakaria A. M. Al-Omari and Samir M. Said " On the application of artificial neural network in analyzing and studying daily loads of Jordan power system plant" ComSIS Vol.5, No.1, June, 2008, PP 127-136.

2- Mohamed T. Khadir, Damien Fay, John Ringwood and Ahmed Boughrira "Forecasting Electricity Load and Prices in an Algerian Deregulated Market" WWW. Labged.net.

3- Damien Fay, John Ringwood, Marissa Condon and Michael Kelly "Establishing a Solution Strategy for Electrical Demand Forecasting in Ireland" WWW. eprints. nuim.ie.

4- I.Badran, El-Zayyat and G. Halasa "Short-term and medium-term load forecasting for Jordan's power system" American Journal of Applied Sciences 5(7): 2008, PP763-768.

5- M. A. Al-Nama, M S. Al-Hafid and A. S. Al-Fahadi " Estimation of the Diversity Factor for the Iraqi Distribution System Using Intelligent Methods" Al-Rafidain Engineering, Vol.17, No.1, Feb. 2009, PP14-21.

6- M S. Al-Hafid " Modified Model for Long Term Weather Sensitive Load" First Symposium on Electric Power Systems in Fast Developing Countries, March, KSA, 1987, PP122-124.

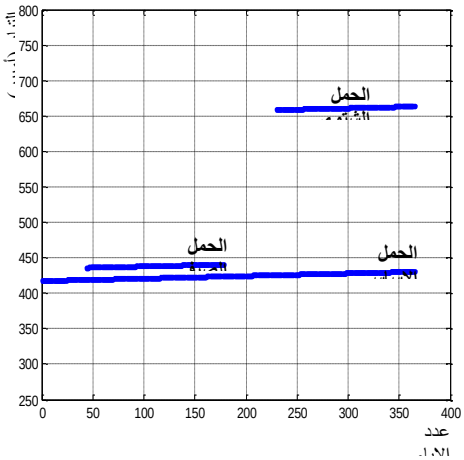

شكل رقم 8 المركبات الثلاثة للمستهلكين عالي

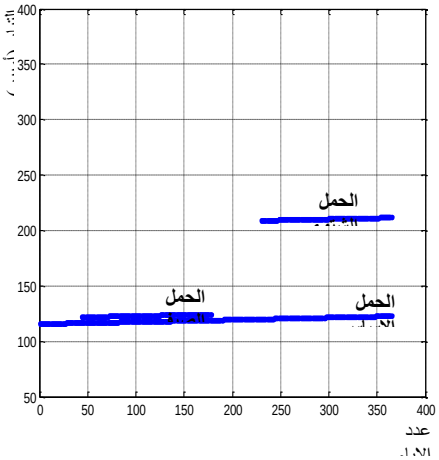

شكل رقم 9 المركبات الثلاثة للمستهلكين

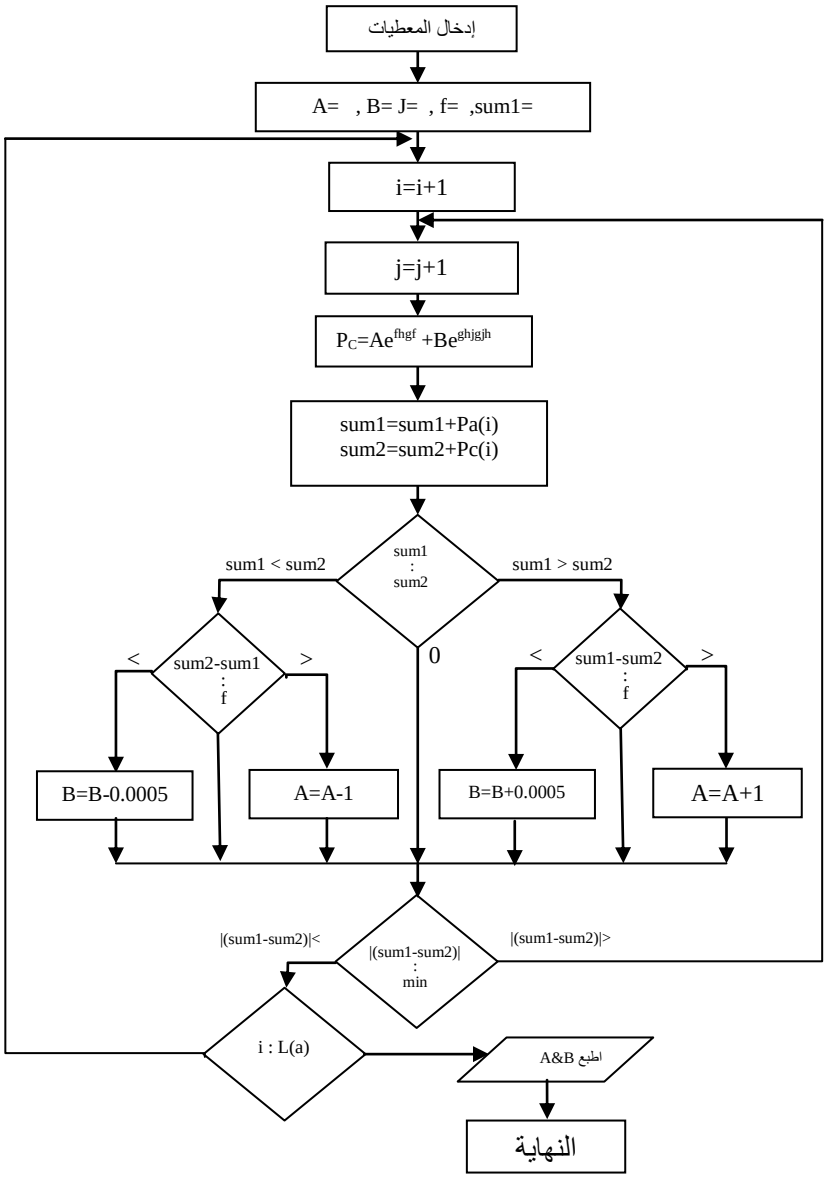

شكل رقم 7 المخطط الانسيابى لإيجاد قيم الثوابت

تعويض التوالي الأمثل باستعمال الخوارزمية الجينية

د. محمد علي عبد الله الراوي السيدة سراء إسماعيل خليل
قسم الهندسة الكهربائية / جامعة الموصل

الملخص

يُعَّد نقل أكبر قدرة في خطوط النقل الكهربائية من الأهداف الرئيسة لشركات التوليد والنقل. تستعمل معوضات التوالي لتحقيق هذا الهدف. يتناول البحث هذه المسألة باستعمال الخوارزمية الجينية Genetic Algorithm وهي إحدى التقنيات البرمجية لإيجاد القيمة المثلى لتعويض التوالي في خط نقل القدرة. تم حساب القيم المثلى لمتسعات التوالي ، وكذلك تأثير زيادة عدد مواقع تعويض التوالي على تقليل الفقد بالقدرة الفاعلة. تم تطبيق الطريقة المقترحة على منظومة IEEE (30 Bus) لحالتين من الحمل.

1.المقدمة Introduction :

إن الهدف الأساسي لمصممي محطات الطاقة الكهربائية هو الحصول على أفضل حالة تشغيل ممكنة وذلك من خلال تقليل مقدار الفقد بالقدرة الفاعلة ، يتم ذلك في بعض الأحيان من خلال إضافة متسعات التوالي في الخط [1]. خطوط النقل في منظومة القدرة تنقل القدرة لمسافات طويلة ، حالياً يتم استخدام تعويض التوالي في الخطوط لزيادة سعة نقل القدرة في خطوط النقل وبالتالي زيادة استقرارية منظومة القدرة [2].

تعمل المعوضات عند دمجها في خطوط النقل على تغير كفاءة النقل وزيادة سعة نقل القدرة ، ونعني بالدمج إضافة معوضات التوالي والتوازي معا.

يمكن اختيار شكل التعويض الأكثر فاعلية للحصول على كفاءة عالية ونقل قدرة أعظم في الخطوط المعوضة وليس بالضرورة أن تكون

القدرة عند الكفاءة العظمى أعلى قدرة يمكن نقلها في الخطوط [2].

وقد تم التعامل مع الموضوع بتقنيات متعددة على مدى العقود الماضية لحل معضلة التشغيل الأمثل لتعويض التوالي والتوازي ومنها استخدام البرمجة الخطية وغير الخطية ... الخ ، وقد استخدمت حديثاً تقنية الخوارزمية الجينية لحل معضلات مشابهة.

أما من الناحية الاقتصادية بالإمكان توضيح فاعلية حشر أو إضافة معوضات التوالي بالكيفية الآتية، على فرض أن كلفة النقل بـ \$/W/m. وأن القدرة المنقولة هي $(P_{max} - P_o)$ ضمن طول الخط البالغ ℓ والفولتية المقننة (V). وأن زيادة حدود القدرة المنقولة تعطى بالمعادلة الآتية [3] :

$$K_{line} = K_{line} * \ell * (P_{max} - P_o) \quad (1)$$

K_{line} : كلفة بـ \$/W/m.

ℓ : طول الخط (m).

P_{max} : أعظم قدرة منقولة (MW).

P_o : القدرة المنقولة (MW).

أما عند إضافة تعويض التوالي ، فإن كلفة التعويض لكل وحدة من القدرة الفاعلة المعوضة هي $K_{condenser}$ بالـ (دولار) لكل (VAR) والتعبير الرياضي المعبر عن الحالة هو :

$$K_{condenser} = K_{condenser} \times Q_c \quad (2)$$

لذلك فان التوفير (S) عندما $K_{ine} >$ $K_{condenser}$ هو:

$$S = K_{ine} \times \ell (P_{max} - P_o) - K_{condenser} \times Q_c \quad (3)$$

حيث أن المعادلة أعلاه تعبر عن مقياس فاعلية تعويض التوالي المستخدم كأداة في زيادة قابلية نقل الخط.

2 . الخوارزمية الجينية :

تعد الخوارزمية الجينية من الطرائق الحديثة المستخدمة لمحاكاة بعض المسائل المعقدة وكبيرة الحجم. وتعد هذه الطريقة أحد أساليب الذكاء الصناعي وتتميز بكفاءتها العالية للإمكانيات الهائلة التي توفرها ومنها كبر حجم فضاء البحث الذي تعمل عليه. وتقوم هذه الخوارزميات بإجراء البحث العشوائي على مجموعة من الحلول والحل الناتج عند تطبيق الخوارزمية الجينية يكون قريب من الحل المثالي (Near Optimal Solution) ويمكن توضيح عمل الخوارزمية الجينية كما يأتي [3, 4].

1 –تبحث عن الحل انطلاقاً من مجموعة من النقاط في فضاء البحث وفي وقت واحد وليس من نقطة واحدة.

ويكون حساب كل عنصر من عناصر حجم المجموعة غير معتمد على الآخر.

2 -تعتمد في عملها على معلومات دالة الهدف (Fitness Function) كأساس للبحث عن الأمثلية ونستطيع التعامل مع جميع الدوال مثل الدوال غير المستمرة والدوال غير التفاضلية (Differential).

3 -تستعمل الخوارزمية الجينية كطرق الانتقال العشوائية ولا تستخدم قواعد محددة لذلك نلاحظ أن مساحة البحث تكون كبيرة جداً وبذلك تكون هنالك سهولة للوصول إلى القيمة المثلى التي تعطي أفضل دالة هدف. لذلك تعد الخوارزميات الجينية أكثر دقة وسهولة من طرائق الأمثلية التقليدية.

1-2 خطوات تطبيق الخوارزمية الجينية :

1-1-2 توليد حجم المجتمع (Generation Population Size):

يتكون المجتمع من عدد من الأفراد ويختار مصمم الخوارزمية حجم المجتمع عادة حسب المسألة المراد حلها ويتم تمثيل كل فرد في المجتمع بسلسلة ثابتة الطول (Constant String) تسمى بالكروموسوم وقد تكون متغيرة الطول (Variable Lengths) والكروموسوم بدوره يتكون من عدد من المواقع تسري الجينات حيث يتم توليد قيم عشوائية من القيم الحقيقة المرشحة لتعويض التوالي. ويمكن أن يكون التعويض في موقع واحد أو عدة مواقع. فإذا كان التعويض في خط واحد فبهذه الحالة يتم جعل كل كروموسوم يتكون من قيمة حقيقية واحدة فقط مرشحة للتعويض وكل كروموسوم من المجتمع يمثل أحد حلول مسألة البحث عن الأمثلية لدالة التعويض [3].

Chromosome = Gene 1 Gene 2 Gene 3 … Gene L

حيث أن :

L : تمثل طول الكروموسوم Chromosome Length.

في البحث الحالي قيمة متسعة التوالي المضافة في خط النقل معطاة في المعادلة الآتية :

$$Z = R + J(XL - X_c) \qquad (4)$$

حيث أن :

X_c : تمثل القيم العشوائية المتولدة في الخوارزمية الجينية.

2-1-2 حساب دالة الهدف (Evaluation of Fitness Function) :

يتم حساب دالة الهدف بعد تكوين المجتمع لكل فرد أي حساب كفاءة كل فرد في المجتمع. وقد تم اعتبار دالة الهدف (Fitness Function) أقل خسارة في القدرة الفاعلة (P) يتم البحث عن القيمة المثلى للتعويض التي تجعل دالة الهدف أقل ما يمكن ، وفي حالة عدم إيجاد القيمة للتعويض فتقوم الخوارزمية الجينية في تطبيق عواملها مثل الانتقاء (Selection) والتداخل الإبداعي (Crossover) والطفرة (Mutation) [4].

$$\text{Fitness Function} = P_{Loss}$$

$$P_{Loss} = \sum_{i=1}^{N}\sum_{j=1}^{N} G_{ij}\left[|V_i|^2 + |V_j|^2 - 2|V_i||V_j| Cos\left(\delta_i - \delta_j\right)\right] \quad (5)$$

حيث أن :

P_{Loss} : مقدار الفقد بالقدرة الفاعلة.

G_{ij} : الجزء الحقيقي لعنصر مصفوفة المسايرة.

V_i : فولتية الإرسال.

V_j : فولتية الاستلام.

δ_i : زاوية الفولتية للعمومي (i).

δ_j : زاوية الفولتية للعمومي (j).

3-1-2 الانتقاء (Selection) :

إن الانتقاء أو تعيين الأفراد للعبور وتحديد كم من الأفراد سيتبع كل فرد مختار ، والآباء يتم اختبارهم وفقاً لدالة الهدف. ويشمل الاختبار الجيد ذات الجهود العالية للانتقاء (High Selection Pressures) حيث جهد الاختبار هو الدرجة أو المستوى لمقياس أفضل للكروموسومات الصالحة التي ينتج عنها دوال هدفها صفري ، ولا يتم اختبار الكروموسومات التي تنتج عنها قيم كبيرة لدالة الهدف. وهذا يعني أن الفقد (الخسارة) في القدرة الفاعلة في البحث يجب أن تكون أقل ما يمكن.

4-1-2 الطفرة (Mutation) :

وهي تغير عشوائي في الكروموسومات وتحدث باحتمالية ضئيلة لكون أغلب الدراسات أقرت أن تكون نسبة الفطرة (Mutation Rate) قليلة جداً لكي لا تؤذي الجيل المتولد وتبعد به عن الحل المطلوب بشكل كبير وأغلب المصادر المتوفرة فضلت أن تكون نسبة الطفرة حوالي (0.5% - 1%) [6].

3 . النتائج ومناقشتها :

تم دراسة وتحليل إضافة معوضات التوالي في خطوط النقل باستخدام الخوارزمية

الجينية (GA) وذلك للحصول على أمثل قيمة لتعويض التوالي عند أقل فقد بالقدرة الفاعلة.

وقد طبقت هذه الخوارزمية على المنظومة (IEEE 30 Bus) ولحالتين من الحمل. الحمل الأدنى (Minimum Load) كانت قيمة الفقد بالقدرة الفاعلة (5.6053 MW) قبل إضافة معوضات التوالي. أما حالة الحمل الأعظم (Maximum Load) فقد كان مقدار الفقد بالقدرة الفاعلة (12.085 MW) ، وتم دراسة الحالات التالية :

4 . الحالات الدراسية Case Studies :

4-1 إضافة معوضات التوالي في حالة أدنى حمل :

4-1-4 إضافة تعويض التوالي في خط واحد عند (أدنى حمل) :

تم الحصول على النتائج المعروضة في الجدول رقم (1) عند إضافة معوضات التوالي لخط واحد. حيث يبين القيم المثلى في الخطوط المضافة إليها معوضات التوالي وكذلك مفاقيد القدرة الفاعلة ودرجة التعويض. ولوحظ أن القيمة المثلى لدرجة التعويض في الخط رقم (12) هي نصف محاثة الخط. وعندها تم الحصول على أقل فقد بالقدرة الفاعلة. وهذا ما يثبت ما ذكر في المصدر [4] حيث يكون الفقد أقل ما يمكن قياساً إلى بقية الخطوط ، وهذا ما يؤكد بأن إضافة متسعات التوالي تقلل من قيمة الفقد والشكل (1-1) يبين علاقة فقد القدرة الفاعلة التي تمثل دالة الهدف مع عدد الأجيال المتولدة.

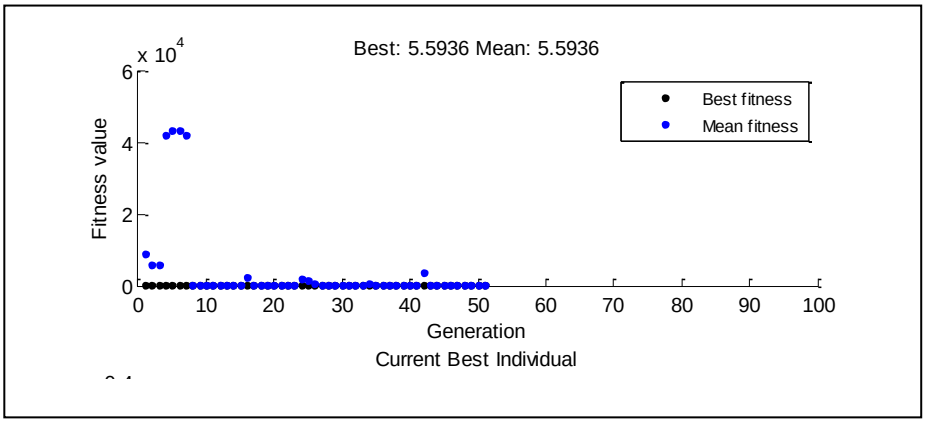

لشكل (1-1) : يبين علاقة عدد الأجيال المتولدة مع دالة الهدف (فقد القدرة الفاعلة) عند الإضافة للخط رقم (12) لحالة الحمل الأدنى

4-1-2 إضافة تعويض التوالي في خطين في آن واحد (أدنى حمل) :

الجدول رقم (2) يبين النتائج التي تم الحصول عليها عند إضافة معوضات التوالي لخطين في آن واحد. حيث أن الجدول يظهر القيمة المثلى في الخطوط المضافة إليها معوضات التوالي ومفاقيد القدرة الفاعلة ودرجة التعويض. وقد تم الحصول على أقل فقد بالقدرة الفاعلة في الخطين (38 , 37) مقارنة مع بقية الخطوط وكانت قيمة الفقد (5.5922 MW) عند درجة تعويض قريبة من نصف محاثة الخط (K_{s1}= 59.8%), (K_{s2} = 64%) ، وهي أقل عن قيمة الفقد ما قبل إضافة المعوضات في الخطين المذكورين أعلاه. والشكل (1-2) يبين علاقة دالة الهدف الفقد في القدرة الفاعلة مع عدد الأجيال المتولدة عند إضافة تعويض التوالي في الخطين (38 ,37) في حالة أدنى حمل.

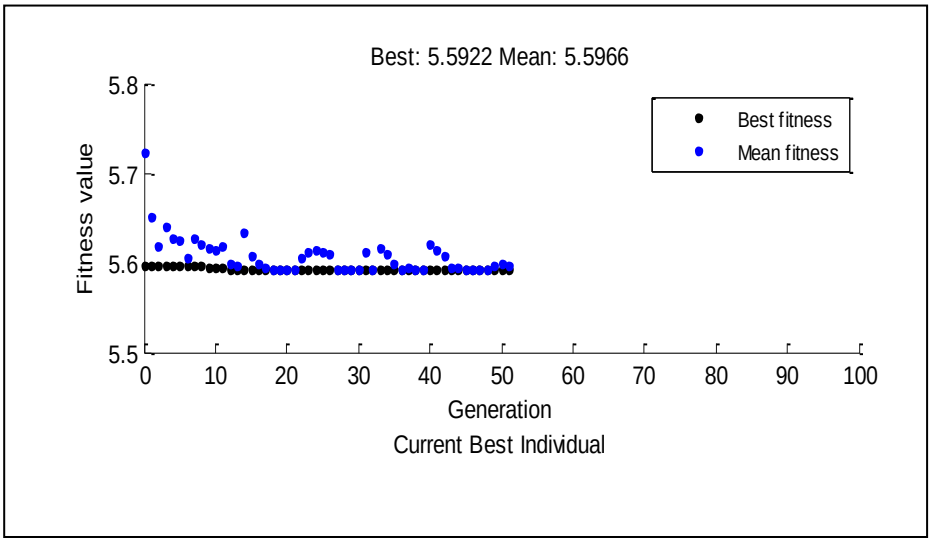

الشكل (1-2) : يبين علاقة عدد الأجيال المتولدة مع دالة الهدف (فقد القدرة الفاعلة) عند الإضافة للخطين (38 ,37) لحالة الحمل الأدنى.

3-1-4 إضافة معوضات التوالي لثلاث خطوط في آن واحد (أدنى حمل) :

يبين الجدول رقم (3) النتائج لإضافة معوضات التوالي لثلاث خطوط في آن واحد. وقد تم الحصول على أقل قيمة فقد حيث كانت قيمة الفقد (5.5856 MW) بينما كانت درجة التعويض والخطين (12, 38) مقاربة من نصف المحاثة الا أن درجة التعويض للخط (39) كانت (11.7%).

ويمكن تحسين درجة التعويض وجعلها مقاربة من نصف المحاثة وذلك من خلال الاستفادة من خاصية الخوارزمية الجينية في اختيار المسارات العشوائية وذلك بتثبيت ممانعة الخط (38 و12) ونرى النتائج الموضحة في الجدول (3) الفقد بالقدرة الفاعلة يبقى ثابت المقدار وهو (5.5856 MW) إلا أن درجة التعويض تم تحسينها وجعلها (K_{S3} = 25%) عند قيمة تعويض التوالي X_c = 0.3999 أي تم تقليل قيمة المتسعة المضافة.

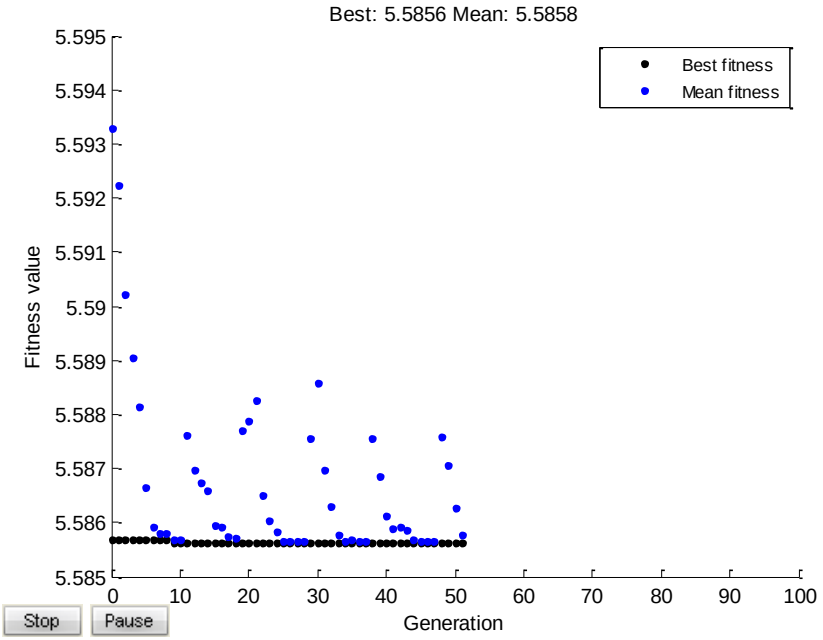

لشكل (3-1) : يبين علاقة الأجيال المتولدة مع دالة الهدف (فقد القدرة الفاعلة) عند الإضافة لثلاث خطوط (39, 12, 38, 37) لحالة الحمل الأدنى.

4-1-4 إضافة معوضات التوالي لأربع خطوط في آن واحد عند (أدنى حمل) :

الجدول رقم (4) يبين النتائج التي تم الحصول عليها عند إضافة معوضات التوالي لأربع خطوط في آن واحد. تم الحصول على القيمة المثلى لمعوضات التوالي للخطوط الأربع في آن واحد وكذلك قيمة الفقد بالقدرة الفاعلة ودرجة التعويض. حيث كانت قيمة الفقد بالقدرة الفاعلة يساوي (5.5795 MW) عند درجات تعويض مثلى مختلفة.

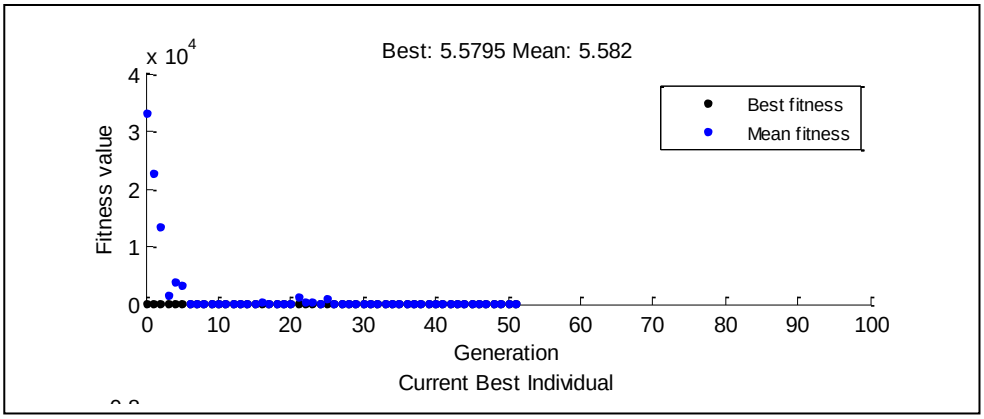

الشكل (4-1) : يبين علاقة عدد الأجيال المتولدة مع دالة الهدف (فقد القدرة الفاعلة) عند الإضافة لأربع خطوط (39, 12, 38, 37) لحالة الحمل الأدنى.

2-4 إضافة معوضات التوالي في حالة أعظم حمل :

يبين الجدول رقم (5) حالات مختلفة لإضافة معوضات التوالي في الخطوط وقد تم الحصول على القيم المثلى لمعوضات التوالي وكذلك قيمة الفقد بالقدرة الفاعلة ودرجة التعويض. نلاحظ من الجدول أنه كلما يتم إضافة متسعات التوالي في الخط كلما تقل قيمة الفقد بالقدرة الفاعلة مع الحصول على أمثل قيمة لمعوضات التوالي وأمثل درجة تعويض وعند الإضافة لأربع خطوط في آن واحد لحالة الحمل الأعظم يقل مقدار الفقد بالقدرة الفاعلة من (12.0857 MW إلى 12.0156 MW) عند أقل قيم لمعوضات التوالي ، ودرجات تعويض مختلفة.

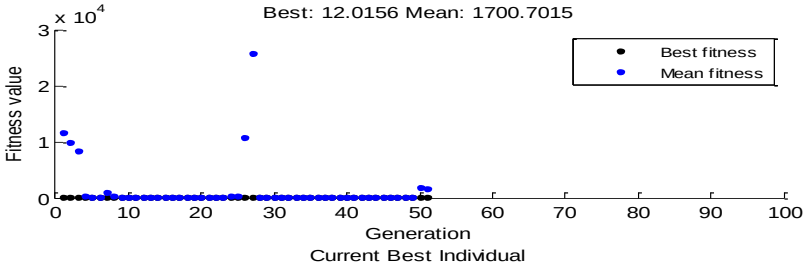

الشكل (1-2) : يبين علاقة عدد الأجيال المتولدة مع دالة الهدف (فقد القدرة الفاعلة) عند الإضافة لأربع خطوط (12, 37, 38, 39) لحالة الحمل الأعظم.

جدول رقم (1) : يبين نتائج تعويض متسعة التوالي لخط واحد لحالة الحمل الأدنى

ت	رقم الخط	أمثل قيمة لـ (X_c)	مفاقيد القدرة الفاعلة (MW)	أمثل درجة تعويض KS%	الفولتية (Bus) (V)	الزاوية (Bus) (δ)
1	38	0.04468	5.604	9.6%	V_5 = 0.9754	δ_5 = - 0.1697
					V_{13} = 0.9425	δ_{13} = - 0.1764
2	12	0.27534	5.5936	50.4%	V_6 = 1.0093	δ_1 = - 0.0936
					V_{10} = 0.9926	δ_{10} = - 0.1435
3	39	0.0537	5.6051	74.37%	V_{11} = 0.9531	δ_{11} = - 0.1944
					V_{13} = 0.9414	δ_{13} = - 0.2080
4	37	0.0497	5.60491	72.9%	V_5 = 0.9743	δ_5 = - 0.1692
					V_{11} = 0.9546	δ_{11} = - 0.1872

جدول رقم (2) : يبين نتائج تعويض متسعة التوالي لخطين في آن واحد لحالة الحمل الأدنى

رقم الخط	أمثل قيمة لـ (X_c)	مفاقيد القدرة الفاعلة (MW)	أمثل درجة تعويض KS%	الفولتية (Bus) (V)	الزاوية (Bus) (δ)
12 & 38	X_{C1} = 0.04527	5.5932	K_{S1} = 71%	V_5 = 0.9745	δ_5 = - 0.1669
	X_{C2} = 0.27578		K_{S2} = 61%	V_{13} = 0.9429	δ_{13} = - 0.1992
				V_6 = 1.0094	δ_1 = - 0.0935
				V_{10} = 0.9914	δ_{10} = - 0.1471
39 & 38	X_{C1} = 0.22631	5.5995	K_{S1} = 62.4%	V_5 = 0.9746	δ_5 = - 0.1693
	X_{C2} = 0.4		K_{S2} = 66%	V_{13} = 0.9441	δ_{13} = - 0.1969
				V_{11} = 0.9543	δ_{11} = - 0.1891
37 & 38	X_{C1} = 0.36694	5.5922	K_{S1} = 59.8%	V_5 = 0.9748	δ_5 = - 0.1693
	X_{C2} = 0.39945		K_{S2} = 64%	V_{13} = 0.9450	δ_{13} = - 0.1947
				V_5 = 0.9748	δ_{11} = - 0.1810
				V_{11} = 0.9570	
39 & 12	X_{C1} = 0.04609	5.5935	K_{S1} = 71.6%	V_6 = 1.0093	δ_6 = - 0.0939
	X_{C2} = 0.27555		K_{S2} = 39.2%	V_{10} = 0.9944	δ_{10} = - 0.1388
				V_{11} = 0.9544	δ_{11} = - 0.1840
				V_{13} = 0.9430	δ_{13} = - 0.1966
37 & 12	X_{C1} = 0.00073	5.5933	K_{S1} = 77.3%	V_6 = 1.0096	δ_6 = - 0.0932
	X_{C2} = 0.11229		K_{S2} = 75.2%	V_{10} = 0.9885	δ_{10} = - 0.1548
				V_5 = 0.9743	δ_5 = - 0.1692
				V_{11} = 0.9546	δ_{11} = - 0.1875
37 & 39	X_{C1} = 0.17335	5.5933	K_{S1} = 61%	V_{11} = 0.9564	δ_{11} = - 0.1723
	X_{C2} = 0.05077		K_{S2} = 27%	V_{13} = 0.9433	δ_{13} = - 0.1968
				V_5 = 0.9747	δ_5 = - 0.1658
					δ_{11} =

جدول رقم (3) : يبين نتائج تعويض التوالي لثلاث خطوط في آن واحد لحالة الحمل الأدنى

رقم الخط	أمثل قيمة لـ (X_c)	مفاقيد القدرة الفاعلة (MW)	أقل درجة تعويض KS%	الفولتية (Bus) (V)	الزاوية (Bus) (δ)
39&12&38	X_{C1} = 0.23104	5.5856	K_{S1} = 61.5%	V_5 = 0.9749	δ_5 = - 0.1658
	X_{C2} = 0.27414		K_{S2} = 50.7%	V_{13} = 0.9454	δ_{13} = - 0.1895
	X_{C3} = 0.4		K_{S3} = 11.7%	V_6 = 1.0094	δ_6 = - 0.0936
				V_{10} = 0.9927	δ_{10} = - 0.1436
				V_{11} = 0.9546	δ_{11} =

الآن نثبت Z_1 و Z_2 ونرى النتائج التعويض أصبحت 25% بدلاً عن 11.7% نلاحظ أن P_{loss} يبقى ثابت لهذه الحالة = P_{loss} وهذا موضح في الجدول (4) وذلك من خلال 5.5856 الذي يتحسن هو (KS) درجة الاستفادة من خاصية الخوارزمية الجينية (GA) التعويض للخط رقم 38 حيث نلاحظ بأن درجة في المسارات العشوائية.

جدول رقم (4) : يبين نتائج تعويض متسعة التوالي لثلاث خطوط في آن واحد لحالة الحمل الأدنى

رقم الخط	أمثل قيمة لـ (X_c)	أقل درجة تعويض KS%	مفاقيد القدرة الفاعلة (MW)	الفولتية (Bus) (V)	الزاوية (Bus) (δ)
31&12&38	X_{C1} = 0.23104	K_{S1} = 61.5%	5.5856	V_5 = 0.9749	δ_5 = - 0.1658
	X_{C2} = 0.27414	K_{S2} = 50.7%		V_{13} = 0.9979	δ_{13} = - 0.1905
	X_{C3} = 0.39999	K_{S3} = 25%		V_6 = 1.0094	δ_6 = - 0.0936
				V_{10} = 0.9927	δ_{10} = - 0.1436
				V_{11} = 0.9452	δ_{11} = - 0.1879

جدول رقم (5) : يبين نتائج تعويض متسعة التوالي لأربع خطوط في آن واحد لحالة الحمل الأدنى

رقم الخط	أمثل قيمة لـ (X_c)	مفاقيد القدرة الفاعلة (MW)	أقل درجة تعويض KS%	الفولتية (Bus) (V)	الزاوية (Bus) (δ)
39&12&38&37	X_{C1} = 0.41538	5.5795	K_{S1} = 30.9%	V_5 = 0.9756	δ_5 = - 0.1657
	X_{C2} = 0.28311		K_{S2} = 49%	V_{13} = 0.9493	δ_{13} = - 0.1760
	X_{C3} = 0.17825		K_{S3} = 60.6%	V_6 = 1.0094	δ_6 = - 0.0937
	X_{C4} = 0.35729		K_{S4} = 21.49%	V_{10} = 0.993	δ_{10} = - 0.1430
				V_{11} = 0.9604	δ_{11} = - 0.1674

جدول رقم (6) : يبين نتائج تعويض متسعة التوالي لحالة الحمل الأعظم

رقم الخط	أمثل قيمة لـ (X_c)	مفاقيد القدرة الفاعلة (MW)	أقل درجة تعويض KS%	الفولتية (Bus) (V)	الزاوية (Bus) (δ)
38	X_C = 0.07412	12.0836	K_S = 46.1%	V_5 = 0.9518	δ_5 = - 0.2530
				V_{13} = 0.9094	δ_{13} = - 0.2839
12 & 38	X_{C1} = 0.7542	12.0655	K_{S1} = 46.2%	V_5 = 0.9525	δ_5 = - 0.2469
	X_{C2} = 0.25552		K_{S2} = 42.8%	V_{13} = 0.9101	δ_{13} = - 0.2777
				V_6 = 1.0032	δ_6 = - 0.1515
				V_{10} = 0.9785	δ_{10} = - 0.2152
12&38&39	X_{C1} = 0.21628	12.0533	K_{S1} = 64.1%	V_5 = 0.9510	δ_5 = - 0.2485
	X_{C2} = 0.25535		K_{S2} = 54%	V_{13} = 0.9099	δ_{13} = - 0.2849
	X_{C3} = 0.39992		K_{S3} = 39.3%	V_6 = 1.0033	δ_6 = - 0.1512
				V_{10} = 0.9760	δ_{10} = - 0.2211
				V_{11} = 0.9197	δ_{11} = - 0.2789
				V_{13} =	
12&37&38&39	X_{C1} = 0.56591	12.0156	K_{S1} = 47.4%	V_5 = 0.9537	δ_5 = - 0.2492
	X_{C2} = 0.24465		K_{S2} = 56%	V_{13} = 0.9154	δ_{13} = - 0.2584
	X_{C3} = 0.39842		K_{S3} = 12.11%	V_6 = 1.0034	δ_6 = - 0.1513
	X_{C4} = 0.39999		K_{S4} = 3.6%	V_{10} = 0.9259	δ_{10} = - 0.2220
				V_{11} = 0.9293	δ_{11} = - 0.2495
				V	

5 . الاستنتاجات :

من خلال الدراسة نستنتج ما يأتي :

1 -أن الفقد بالقدرة الفاعلة يكون أقل كلما زاد عدد الخطوط المضافة إليها معوضات التوالي.

2 -إن الفقد في القدرة الفاعلة أقل ما يمكن عند إضافة معوض التوالي في منتصف الخط في حالة الإضافة لخط واحد ، حيث أن الخط رقم (12) أعطى أقل فقد بالقدرة الفاعلة مقارنة مع بقية الخطوط وكانت قيمة الفقد (5.5936 MW) عند أمثل درجة تعويض Ks = 50.4%.

3 -تم التوصل إلى أقل فقد بالقدرة الفاعلة عند إضافة معوضات التوالي لأربع خطوط نقل قدرة عند حالة الحمل الأدنى ، وكانت قيمة الفقد (5.579 MW) إذا ما قورنت مع بقية حالات الإضافة.

4 -علماً أن الباحث أزهر سعيد قد توصل في أطروحته سنة 1990م إلى أن عناصر تعويض التوالي تعتمد على الزاوية δ فضلاً عن طول خط النقل وهذا ما أثبته البحث الحالي (7).

5 -عند زيادة الأحمال تزداد قيمة الفقد في القدرة الفاعلة.

المصادر :

1- S.E. Khaleel "Reduction of Generation Cost and Losses by Optimal Control of Active and Reactive Power", M. Sc. Thesis, University of Mosul, 2004.

2- M. H. Haque "Maximum Efficiency of Series and Shunt Compensated A.C Transmission Systems", Electrical Power and Energy System, Volume 15, Number 2, 1993, P.P. 79-84.

3- Warqaa. Younis. Ibrahim, "Robotic PCB Soldering with the AID of Genetic Algorithm", M. Sc. Thesis, University of Mosul, 2004.

4 - د. ماجد صالح الحافظ ، بسام فاضل أحمد " تعويض القدرة المفاعلة باستخدام الخوارزمية الجينية " ، (2000). المؤتمر الهندسي الدولي الأول ، حلب ، سوريا ، 2008.

5- Mohamed. Mostafa. Saied, "Optimal Long Line Series

Compensation", IEEE Transaction on Power Systems, Vol. PWRD-1, No. 2, April 1986, P.P. 284-253.

6- Salwan Samie Sabri, "Optimal Fuzzy Controller Design for (CHK) Converter Circuit Using Genetic Algorithm", M. Sc. Thesis, University of Mosul, 2008.

7- Azhar Said AL-Fahady, "New Approaches in Compensation Techniques Applied for INRG System", Ph.D. Thesis, University of Mosul, 1991

ملحق (A)

نتائج سريان الحمل في حالة الحمل الأدنى

عند تطبيق برنامج سريان الحمل على المنظومة (IEEE-30 Bus)

		الفولتية		مقدار التوليد		مقدار الحمل	
رقم العمومي	نوع العمومي	القيمة	الزاوية	الحقيقة (MW)	المتفاعلة (MVAR)	الحقيقة (MW)	المتفاعلة (MVAR)
1	Slack	1.0500	0	99.08	- 2.09	0	0
2	P.Q	0.9452	- 0.1816	0	0	3.5	2.3
3	P.Q	1.0219	- 0.0666	0	0	2.4	1.2
4	P.Q	1.0159	- 0.0798	0	0	7.6	1.6
5	P.Q	0.9741	- 0.1692	0	0	0	0
6	P.Q	1.0096	- 0.0932	0	0	0	0
7	P.Q	1.0008	- 0.1106	0	0	22.8	10.9
8	P.Q	1.0023	- 0.1011	0	0	0	0
9	P.Q	1.0091	- 0.1189	0	0	0	0
10	P.Q	0.9885	- 0.1548	0	0	5.8	2
11	P.Q	0.9531	- 0.1929	0	0	2.4	0.9
12	P.Q	1.0140	- 0.1438	0	0	11.2	7.5
13	P.Q	0.9410	- 0.2100	0	0	10.6	1.9
14	P.Q	0.9964	- 0.1608	0	0	6.2	1.6
15	P.Q	0.9897	- 0.1618	0	0	8.2	2.5
16	P.Q	0.9957	- 0.1535	0	0	3.5	1.8
17	P.Q	0.9850	- 0.1584	0	0	9.0	5.8
18	P.Q	0.9765	- 0.1728	0	0	3.2	0.9
19	P.Q	0.9719	- 0.1756	0	0	9.5	3.4
20	P.Q	0.9752	- 0.1715	0	0	2.2	0.7
21	P.Q	0.9751	- 0.1637	0	0	17.5	11.2
22	P.Q	0.9756	- 0.1636	0	0	0	0
23	P.Q	0.9741	- 0.1689	0	0	3.2	1.6
24	P.Q	0.9622	- 0.1718	0	0	8.7	6.7
25	P.Q	0.9639	- 0.1734	0	0	0	0
26	P.V	1.0450	- 0.0324	80	50.366	21.7	12.7
27	P.V	1.0100	- 0.1138	50	21.3734	94.2	19
28	P.V	1.0100	- 0.0983	20	34.244	30	30
29	P.V	1.0500	- 0.0796	20	21.04	0	0
30	P.V	1.0500	- 0.1175	20	27.30	0	0

ملحق (B)

نتائج سريان الحمل في حالة الحمل الأعظم

عند تطبيق برنامج سريان الحمل على المنظومة (IEEE-30 Bus)

		الفولتية		مقدار التوليد		مقدار الحمل	
رقم العمومي	نوع العمومي	القيمة	الزاوية	الحقيقة (MW)	المتفاعلة (MVAR)	الحقيقة (MW)	المتفاعلة (MVAR)
31	Slack	1.0500	0	178.0593	-17.1404	0	0
32	P.Q	0.9145	- 0.2661	0	0	4	3
33	P.Q	1.0143	- 0.1072	0	0	4	3.5
34	P.Q	1.0079	- 0.1289	0	0	10	3
35	P.Q	0.9505	- 0.2527	0	0	0	0
36	P.Q	1.0035	- 0.1507	0	0	0	0
37	P.Q	0.9960	- 0.1766	0	0	30	11
38	P.Q	0.9935	- 0.1606	0	0	0	0
39	P.Q	0.9984	- 0.1905	0	0	0	0
40	P.Q	0.9701	- 0.2349	0	0	8.5	4.2
41	P.Q	0.9168	- 0.2868	0	0	4.5	2.4
42	P.Q	1.0025	- 0.2213	0	0	14	8.5
43	P.Q	0.9045	- 0.3082	0	0	13	2.2
44	P.Q	0.9778	- 0.2411	0	0	7.5	3
45	P.Q	0.9692	- 0.9692	0	0	10	5.5
46	P.Q	0.9807	- 0.2343	0	0	4.5	1.2
47	P.Q	0.9667	- 0.2399	0	0	11	6.5
48	P.Q	0.9509	- 0.2556	0	0	4.2	2
49	P.Q	0.9456	- 0.2590	0	0	11.5	4.5
50	P.Q	0.9502	- 0.2538	0	0	2.2	2
51	P.Q	0.9533	- 0.2458	0	0	21	14
52	P.Q	0.9540	- 0.2456	0	0	0	0
53	P.Q	0.9516	- 0.2521	0	0	4	1.2
54	P.Q	0.9372	- 0.2553	0	0	10	8
55	P.Q	0.9382	- 0.2573	0	0	0	0
56	P.V	1.0450	- 0.0645	80	73.7685	31	16
57	P.V	1.0100	- 0.1835	50	39.5273	114	26
58	P.V	1.0100	- 0.1612	20	54.0685	37	32
59	P.V	1.0500	- 0.1508	20	26.4633	0	0
60	P.V	1.05z00	- 0.1947	20	35.862	0	0

تصميم وتحليل هوائي تنائى القطبية على شكل حرف S للاستخدام للنطاقات الترددية VHF وUHF

راسم عامر على (*) رجب يوسف صالح(**) حامد عبد الحق سعيد(**)

(*)- كلية العلوم الهندسية والتقنية . جامعة سبها ،(**)-المعهد العالى للمهن الشاملة . سبها

Email: Rasim_63@ yahoo.co.uk

الملخص

في هذه الورقة يقدم نوع من الهوائيات المصنوعة من أسلاك معدنية موصلة على هيئة حرف - S و تسمى الهوائيات الثنائية القطبية . تم دراسة الخواص الإشعاعية لهذه الهوائيات باستخدام إحدى الطرق العددية لحل مسائل الكهرومغناطيسية وتسمى طريقة العزوم وتم استخدام برنامج محاكاة يعتمد هذه الطريقة . من النتائج الحسابية وجد أن هذا الهوائي من الممكن اعتباره ذو نطاق ترددي واسع. المساحة التي يشغلها الهوائي مساحة صغيره تصل لأقل من % 75 من المساحة التي يشغلها الهوائي ثنائي القطبية ، هذا الهوائي المقترح من الممكن استعماله في تطبيقات متعددة وخاصة في النطاقين الترددين العالي والفائق من خلال استعماله فوق سطح موصل او مفرد.

1-المقدمة

الهوائيات السلكية واسعة الاستخدام في مجال الترددات العالية HF والعالية جدا VHF والفائقة UHF ويمكن أن تصمم من موصلات مصمتة أو أنابيب وتعتبر سهلة الفهم نسبيا وسهلة البناء وغير مكلفة وتستخدم على نطاق واسع كهوائيات لأنظمة الاتصالات المتنقلة واللاسلكية.

الهوائي الشهير من هذه الهوائيات Dipole Antenna ، [1،2] ، ويستخدم بشكل واسع كهوائي محطات أساسية Base Station في شبكات الاتصالات المحمولة ، هذه الهوائيات تتميز ببساطة التركيب،واسعة النطاق الترددي نسبيا وصغيرة الأبعاد في الترددات العالية ، الهوائيات الحلقية هي شكل أخر من أشكال الهوائيات السلكية التي تتميز بالبساطة وانخفاض التكلفة ، الهوائي الحلقي يمكن أن ياخد عدة أشكال [1،5] (مربع، دائرة، مثلث، بيضاوي، الخ) وتستخدم بشكل واسع في تطبيقات تصل إلى نطاق UHF

هوائي دايبول على شكل حرف-S يعتبرشكل جديد من الهوائيات السلكية . التحليل الرياضى يعتبر العنصر الاساسي لدراسة خصائص ومواصفات هذه الهوائيات ، وبذلك يتم استخدام طريقة العزوم و هي طريقة تحليل عددي لحل المعادلات التكاملية للمجال الكهربي [1،6].

يتم اختيار الدوال الأساسية Basis functions لتمثل التيارات الغير معروفة على سطح الهوائي ودوال الاختبار يتم اختيارها لتعزيز المعادلة التكاملية على سطح السلك ، و باختيار المعادلات الأساسية ومعادلات الاختيار

يتم اشتقاق مصفوفة تقريبية للمعادلة التكاملية.إذا عكست هذه المصفوفة وتم ضربها بمصادر المجال الكهربي تشتق المقادير المركبة للدوال الأساسية للتيار ، جميع بارامترات أداء الهوائي يمكن أن تحدد من توزيع التيار المشتق . في هذه الورقة تم استخدام الحزمة البرمجية Numerical electromagnetic code, NEC ، [3] ، و التي تعتمد على طريقة العزوم في التصميم والتحليل للحصول على خصائص الهوائي

2- طريقة العزوم

طريقة العزوم طريقة تقنية معروفة لحل المعادلات الخطية ، ويتم استخدم تحويل المعادلات التكاملية للمجال الكهربي إلى مصفوفة معادلات أو منظومة معادلات خطية . يمكن ايجاد معاملات التيار باستخدام تجزئة المصفوفات(LU) , او باستخدام الحدف الجاوسي او بواسطة الطرق الجبرية الخطية . الشكل الأساسي للمعادلة التي تحل بواسطة طريقة العزوم [1،6].

$$L(u) = f, \quad \text{حيث L} \quad \text{.....(1)}$$

البارمتر الخطي ، U دالة غير معرفة ، f- دالة التغذية .

معادلة المصفوفة تكتب وفقا لقانون اوم على الصورة

$$[Z_{m,n}][I_n] = [V_m] \quad \text{.....(2)}$$

حيث مصفوفة الاعاقة تكون على الصورة

$$[Z_{m,n}] = [\langle w_m, L(u_n) \rangle] \quad \text{.....(3)}$$

حيث w_m هي دالة الاختبار او الوزن

بينما مصفوفة التيار العامة تكون :

$$[I_n] = [\alpha_n] \quad \text{.....(7)}$$

و مصفوفة الجهد تكون بالصورة التالية:

$$[V_m] = [\langle w_m, f \rangle] \quad \text{.....(8)}$$

3-الهوائي ثنائي القطبية على هيئة حرف(S):

هذا الهوائي يصنع من سلك أنبوبي رقيق على شكل حرف S كما موضح بالشكل(1) ويتم تغذيته بشكل متماثل بمصدر فولتية صغير بقيمة (1فولت) تقريبا [4].

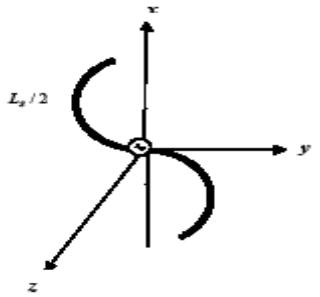

شكل(1) الهوائى على شكل حرف S

يوضع الهوائي في المستوى x ،y .

4-تصميم وتحليل الهوائي S باستخدام الحزمة البرمجية NEC .

تم التصميم وفقا للتردد المختار حيث اختير النطاق التردد من 200-1000MHz ،حيث تم الحصول على الابعاد الاتية

$$Ls = \lambda$$

حيث Ls طول الهوائي

تم تقسيم طول الهوائي الى اجزاء ، حيث طول الجزء $\Delta \le 0.1\lambda$ ، ونصف قطر السلك

$a \le 0.5\Delta$ ، الجـــدول(1) يمثـــل جميـــع البـارامترات الضـرورية للتصـميم وفقـا لبرنـامج NEC

الجدول(1) التصميم وفقا لبرنامج NEC

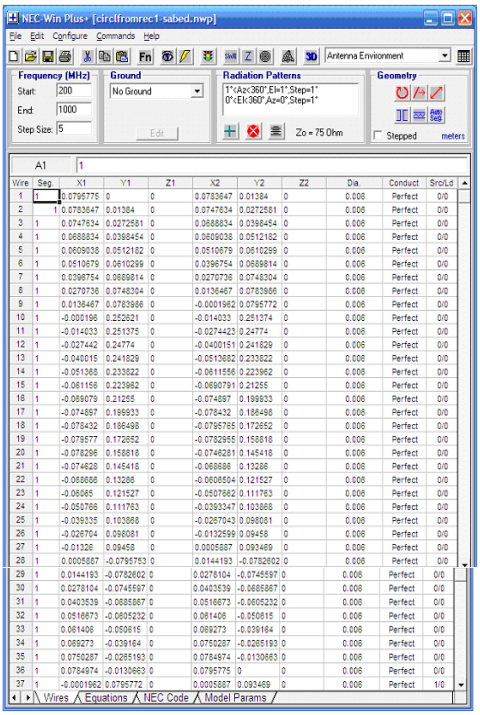

وبناء على هذه المعطيات تم دراسة الخصائص الإشعاعية للهوائي المصمم وذلك على الشكل النحو الاتي:-

اولا: العلاقة بين التغيير في التردد ونسبة فولتية الموجة المستقرة

عند دراسة العلاقة بين التغيير في التردد ونسبة فولتية الموجة المستقرة للهوائى المصمم ، شكل(2) ، وجد انه عند حزمة الترددات من (280-305MHz) تصل نسبة فولتية الموجة المستقرة الى حوالي 1.98:1 عند النهاية السفلى للحزمة ،1.92:1 عند النهاية العظمى للحزمة

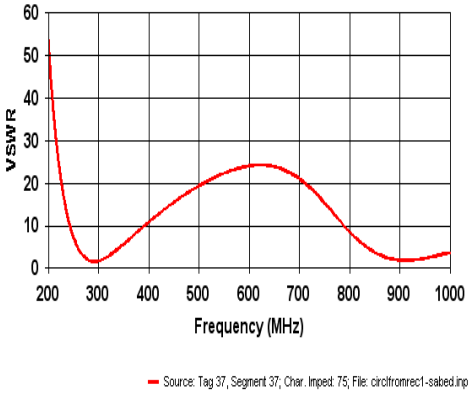

شكل(2) العلاقة بين التردد و نسبة الموجة الواقفة

أما عند حزمة الترددات (895-935MHz) تصل VSWR-voltage standing wave ratio حوالي 1.9:1 عند النهاية السفلى للحزمة ، 1.96:1عند النهاية العظمى للحزمة حيث يكون هناك توافق جيد بين عناصر الهوائي بينما عند باقي الترددات في النطاق يتضح من قيم VSWR إن التوافق بين عناصر الهوائي ضعيف وهذا يسبب فقد كبير للقدرة المشعة حيث يحتاج الهوائي إلى دائرة موائمة للعمل أو تغيير في احد بارمترات الهوائي للعمل عند هذه الترددات ، يمكن ملاحظة التغير في قيمة VSWR حيث التذبذب في قيمتها ، والشكل يبين النمط الإشعاعي للتردد حيث قيمة VSWR مساوية

ثانيا: العلاقة بين معاوقة الدخل و التغيير في التردد

تصمم الهوائيات العملية بمعاوقة دخل أما 50 أو 75 اوم حيث اغلب المكونات الراديوية تبنى عند هذه المعا وقات الشكل (3) ، يبين علاقة الجزء الحقيقي Ra والتخيلي Xa لمعاوقة الدخل للهوائي مع التردد،

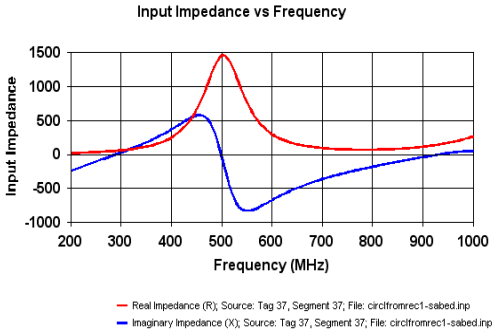

الشكل(3) العلاقة بين التردد ومعاوقة الدخل

حيث تحقق قيم المعاوقة موائمة عند حزمة الترددات (280-305MHz) و عند حزمة الترددات (895-935MHz) حيث تكون قيمة الجزء الحقيقي من المعاوقة اكبر من الجزء التخيلي المسئول عن ضياع الطاقة ، أما عند باقي الترددات في النطاق لا تتحقق شروط الموائمة.

ثالثا:النموذج الإشعاعي للهوائي

تمت دراسة النمط الإشعاعي للهوائي عند حزمتي الترددات (280-305MHz)، (895-935MHz)على التوالي وذلك عند النهاية السفلى والتردد الوسطي والنهاية العظمى لكل حزمة والشكل (4)يوضح ذلك عند ترددات مختارة

305MHz، θ - 1

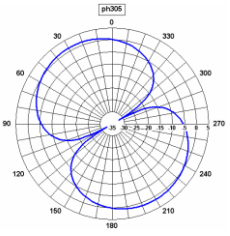

305 MHz ، ϕ - 2

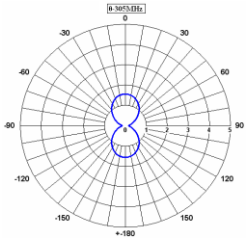

895 MHz، θ -3

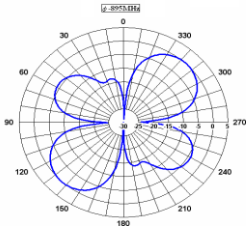

895 MHz ، ϕ – 4

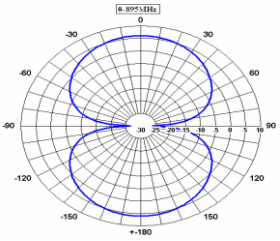

935 MHz، θ -5

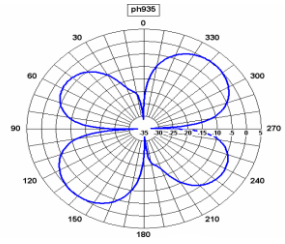

935 MHz، ϕ -6

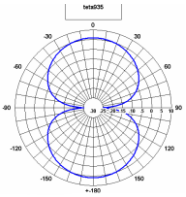

الشكل(4) النمط الاشعاعي لمجموعة من الترددات التى يعمل عندها الهوائى

الخصائص الأساسية للهوائي يمكن تلخيصها في ، الشكل(1) يبين بعض الخصائص للهوائى المصمم ويمكن ملاحظة ان النموذج الإشعاعي في المستوى θ والمستوى ϕ متساوي عند ترددي الحزمة الأولى، و الأمر نفسة بالنسبة للحزمة الثانية ولكن لوحظ الفرق في شكل النموذج الإشعاعي في مجال ϕ بين الحزمتين. من العلاقة بين الكسب والتردد للهوائي فيمكن القول **ان** سلوك الكسب كدالة في التردد موضح في الشكل(5) ، (6) ، وذلك للمستويين θ ، ϕ لكل من حزمتي التردد (280-305MHz) و (895-935MHz) . يلاحظ أن قيم الكسب بالنسبة لحزمة الترددات الأولى تتزايد في المستويين θ ϕ , مع زيادة التردد ، بينما في الحزمة الثانية يلاحظ إنها تتزايد بالنسبة للمستوى ϕ ولكن تتناقص بالنسبة للمستوى θ.

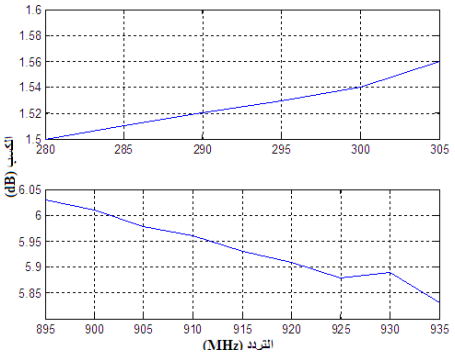

شكل(5) العلاقة بين التردد والكسب للحزمتين الترددیتين عند المستوي θ

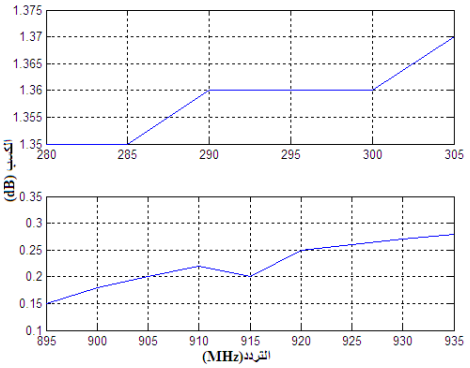

الشكل(6) العلاقة بين التردد والكسب للحزمتين الترددیتين عند المستوي ϕ

5-الاستنتاجات

في هذه الورقة تم تصميم وتحليل هوائي خطي بسيط على شكل حرف S ، عند النطاق الترددي من 1000MHz: 200MHz وتم الحصول على نموذج المجال والكسب في المستويات الرئيسية لمجال من الترددات وكذلك الخصائص الإشعاعية الأخرى مثل ممانعة الدخل والـVSWR كدالة في التردد ، ومن ذلك تم التوصل الى ان الهوائي على شكل حرف-S عند الحزمة الترددية(895-935MHz) وفي المستوى ψ يعطي كسب جيد بالمقارنة مع هوائيات اخري صممت بطرق اخري وبالتالي يمكن القول بان هذا الهوائي يعطي أمكانية كبيرة لاستخدامه في النطاق المحدد والممكن استخدامه في المحطات الأساسية لمنظومة الاتصالات المحمولة.

6-المراجع

[1] C. A. Balanis, Antenna Theory analysis & design, 2nd Ed., John Wiley & Sons, New York, 1997

[2] W. L. Stutzman and G. A. Thiele, Antenna Theory and Design, 2nd Ed., John Wiley & Sons, New York, 1981.

[3] NEC-Win Plus, Version 1.1 copyright 1999. Nittany Scientific, Inc.

[4]Mustafa Abu Nasr & Hassan Elkamchouchi," S-shaped Dipole and Swastika Antennas", Alexandria University, 2008.

[5]Kraus, J. D, "Antenna for all applications", third edition McGraw- Hill companies INS, New York, 2006.

[6] Rajab Y. S," analysis of loop antenna with plane and trough reflector", dissertation for the degree of Masters of science, Sebha University, 2009.

التأكيد الجزئي في منهجية هندسة المتطلبات
Partial Validation in Requirements Engineering Methodology

د. مصطفى عبد العال *قسم الحاسب الآلي /كلية العلوم /جامعة الفاتح*
أ. أمحمد بن زاهية *قسم الحاسب الآلي /كلية العلوم /جامعة الفاتح*

مستخلص

تزخر أدبيات هندسة المتطلبات بالطرق المستخدمة في تأكيد المتطلبات (بمعنى التأكد منها) قبل الاعتماد عليها في تصميم المنظومات البرمجية. وواضح من هذه الأدبيات ومن خبرة العاملين والباحثين في هذا المجال عدم الارتياح لمرحلة تأكيد المتطلبات كمرحلة أخيرة تأتى بعد استنفاذ الطرق واستثمار الوقت وبذل الجهد في جمعها وتحليلها وصياغتها. لأن اكتشاف الخطأ والخلل بعد كل ذلك يكون مكلفاً.

لذلك نقدم في هذه الورقة تعديلاً في منهجية هندسة المتطلبات تجعل عمليات التأكيد مصاحبة لجميع المراحل والطرق المستخدمة في هذه المنهجية من بدايتها، ليتسنى اكتشاف الخلل مبكراً وإكساب المتطلبات درجة كافية من الجودة في مراحل مبكرة. واقترحنا لذلك تطبيق طريقة " التأكيد الجزئي " في كل مرحلة على حده بل وفي كل جزء من المرحلة.

I – مقدمة :

تهتم هندسة المتطلبات Requirement Eng بالطرق والأدوات التي تؤدي أو تساعد على تحديد المتطلبات ذات الجودة العالية التي يمكن الاعتماد عليها في إعداد منظومات برمجية تنال رضا المستفيدين.

وعادة ما يتم ذلك في أربع مراحل [12] وهي :

1) استنباط / تجميع المتطلبات Elicitation
2) تحليل المتطلبات Analysis
3) توصيف المتطلبات Specification
4) التأكيد من المتطلبات Verification and Validation(V&V)

ويمكن توضيح ذلك بالشكل التالي (1) :

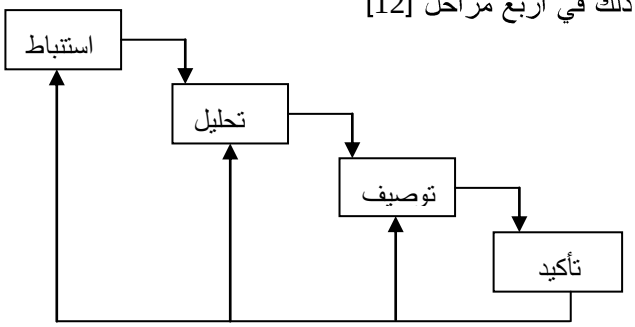

شكل [1] مراحل هندسة المتطلبات /النموذج التسلسلي

والمقصود بالتأكيد الوارد في المرحلة الأخيرة هو التحقق من والمصادقة على بنود المتطلبات التي تم جمعها (استنباطها) وتحليلها وتوصيفها (صياغة مواصفاتها) وأنها حقا تمثل البنود الفعلية التي يجب أن يتم تصميم المنظومة البرمجية على أساسها وقد وضعت جمعية IEEE [1] معايير لذلك وهي أن تكون متطلبات صحيحة وواضحة وكاملة ومتناسقة...الخ.

غير أن التأكيد كمرحلة أخيرة في منهجية هندسة المتطلبات تعتبر مهمة شاقة ومعقدة وغير دقيقة وغير مجدية. وهذا ما يشبه مرحلة التوثيق النهائي في منهجية هندسة البرمجيات. فقد أتضح أنه من الضروري أن تتم أعمال التوثيق الجزئية في كل مرحلة على حدا بل وفي كل خطوة من خطوات المرحلة الواحدة لتكون مرحلة التوثيق النهائية استكمالية ومتيسرة ومعبرة تماماً على جميع مراحل الدورة الحياتية. كذلك هنا فإن نتيجة تأكيد المتطلبات النهائية لا تكون مجدية ومثمرة إلا إذا سبق ذلك تأكيداً جزئياً خاصاً بكل مرحلة من المراحل المذكورة أعلاه ، بل وفي كل خطوة من خطوات كل مرحلة . وواضح من نموذج الشكل (1) أنه إذا كانت نتيجة التأكيد سلبية في أحد بنود المتطلبات فإن الأمر يستدعي المراجعة والتعديل ابتداءً من المرحلة الأولى ثم متابعة التعديلات إلى المراحل التالية وهو أمر معقد ومكلف. لهذا نرى ضرورة تعديل هذه المنهجية وتنفيذ أعمال التأكيد في كل مرحلة من المراحل على حدة لتكون عملية التأكيد الواردة في المرحلة الأخيرة عملية استكمالية ومتيسرة كما هو موضح في شكل (2)

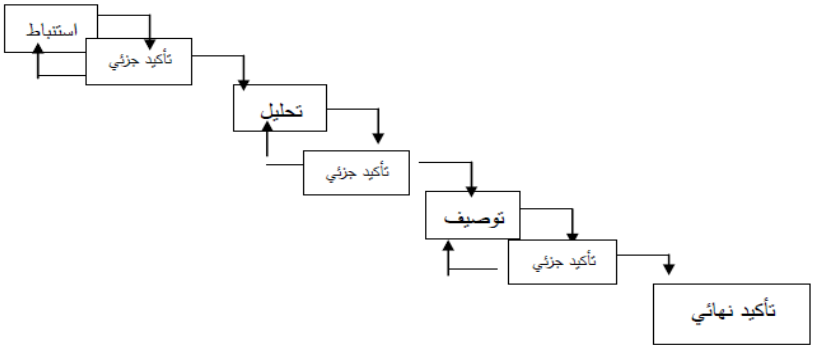

شكل [2] النموذج التسلسلي بالتأكيد الجزئي

ولتوضيح التأكيد الجزئي موضوع هذه الورقة نكتفي بالتركيز على عمليات التأكيد الجزئي الخاص بمرحلة الاستنباط والتجميع التي تتولد فيها جميع بنود المتطلبات والتي يلعب فيها أصحاب الأدوار الرئيسية Stakeholders دوراً جوهرياً. أي أننا في هذه الورقة سنركز على طرق التأكيد الجزئي في المرحلة الأولي.

II) نبذة تاريخية:

أوضح العالم Cleland Huang [2] أن التأكد من جودة المتطلبات يجب أداءه في جميع مراحل إعداد البرمجيات وشدد على مرحلة المتطلبات بصفة خاصة.

إن الوصول إلى متطلبات ذات جودة ليس بالأمر الهين واليسير فقد تعرض العالم Kazmierczak [3] لذلك واستشهد بمشروع Airbus فذكر سلبياً إدماج مرحلتي المتطلبات والتصميم في مرحلة واحدة . أما العالم Boehm [4] فقد ذكر أن مشروع TRW كانت به 85% من الأخطاء سببها عدم جودة المتطلبات بينما الأخطاء البرمجية لم تتعدى 15% وهذا يظهر مدى أهمية التأكيد من المتطلبات مبكراً في مراحل المشروع البرمجي. إن الخلل في بنود المتطلبات من أهم أسباب فشل المشاريع البرمجية حيث ذكر العلماء Hofmann و Lehner [5] أن الحصول على متطلبات صحيحة من أصعب وأهم عناصر المشروع البرمجي وأن في أحد التجارب على التأكيد اتضح أن المشاريع البرمجية الناجحة يكون المجهود المبذول فيها على النحو التالي:

40% جمع المتطلبات
35% توصيف المتطلبات
25% التأكيد مشتملاً V&V

أما العالم Sommerville [6] وهو يعتبر من أشهر علماء هندسة البرمجيات فقد ذكر أن أخطاء المتطلبات ترفع من تكلفة البرمجيات بحوالي 100 ضعف عند اكتشافها متأخرا في مرحلة البرمجة وسانده Kotony [7] حيث ذكر أن الدراسات بينت أن أخطاء المتطلبات مكلفة لأنها تؤثر مباشرة على تصاميم المنظومة المراد إعدادها وأن تكلفة تصحيح هذه الأخطاء تزداد في المراحل اللاحقة. والجدول التالي يوضح التكاليف النسبية لتصحيح الأخطاء:

جدول التكاليف النسبية.

المرحلة	تكاليف تصحيح الخطأ
المتطلبات	1–2
التصميم	5
البرمجة	10
الاختبار	70
الصيانة	500

ولقد ركز أغلب العلماء على التأكيد الكلي للمتطلبات وخصوصاً استخدام طريقة V&V. فقد ذكر Bryan [8] أن التأكيد يقلص تكاليف المنظومة ويحسن مستوى الأداء وشدد هذا العالم على أن تأكيد المتطلبات ليس من الأشياء التي يمكن تأجيلها أو تأخيرها إلى مرحلة متأخرة من المشروع.

. وبخصوص التأكيد الكلي باستخدام V&V ، فقد ذكر العالم Tran [9] إن ذلك أصبح ضرورة ملحة خصوصاً في البرمجيات التي أصبحت أكثر تعقيداً. وخلاصة القول إن الأدبيات المتوفرة على كثرتها إلا أنها تختص بطرق التأكيد كمرحلة نهائية (شكل (1)) مع التعرض كثيراً إلى عدم الارتياح لذلك باعتبار أن التأكيد لا يحتمل التأخير إلى هذه المرحلة. ومن ذلك أتت فكرة هذه الورقة التي تتعلق بالتأكيد المبكر والمصاحب لجميع المراحل والطرق المستخدمة في هندسة المتطلبات.

III) طرق جمع واستنباط المتطلبات:

بما أن هذه الورقة تركز على التأكيد الجزئي الخاص بمرحلة استنباط المتطلبات، رأينا لتسهيل ذلك أن نقدم في هذه الفقرة ملخصاً للطرق المستخدمة في الاستنباط والتي يمكن

تصنيفها وفقاً لبيئة العمل السائد في بلادنا حسب ما يلي[14]:

1) الملاحظة Observation
ويمكن من خلالها تطبيق طرق مثل: جمع العينات Sampling وتعليمات المستخدم User instructions ومخططات حالة الاستخدام Use case diagram والسيناريوهات Scenarios.

2) ورشة العمل Workshop
ويمكن أن يندرج تحتها طرق أخرى مثل: إثارة الأفكار Brainstorming والمتطلبات التفصيلية Detailed requirements والنموذج التجريبي Prototyping.

3) المقابلة الشخصية Interview
وتكون هذه الطريقة مجدية خاصة في المؤسسات التي يتواجد فيها ذوي خبرة بالمنظومات في المجال المطلوب ميكنته ، وفي الحالات التي تستوجب استطلاع رؤية الإدارة العليا (الزبون) وتوقعاتها من المنظومة المطلوبة.

VI) طرق التأكيد الجزئي :

يجدر أن نوضح أن التأكيد الجزئي الخاص بمرحلة جمع واستنباط المتطلبات لا ينتظر إلى نهاية هذه المرحلة بل لابد من تطبيقه على كل طريقة تم استخدامها في هذه المرحلة لاستنباط بنود المتطلبات كما هو موضح في شكل (3):

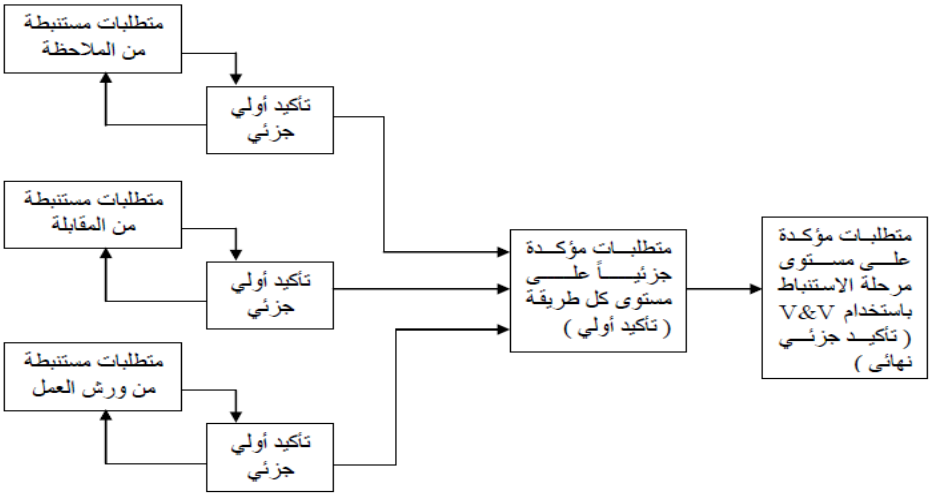

شكل [3] النموذج التسلسلي بالتأكيد الجزئي الأولي

أي أن هناك تأكيد جزئي أولي يتم على مستوى كل طريقة، ثم تأكيد جزئي نهائي يتم على مستوى المرحلة.
وأهم طرق التأكيد الجزئي الأولي فهي:

1 المراجعة غير الرسمية Walkthrough
2 الفحص Inspection

والتي يجدر تنفيذها على مستوى كل طريقة تم استخدامها في جمع المتطلبات مثل المقابلة الشخصية والملاحظة وغيرها. أما طرق التأكيد الجزئي النهائي الخاص بهذه المرحلة فهي(V&V):

3 التحقق Verification.

4 المصادقة Validation.

وهذه لا يمكن تنفيذها بحكم تكلفتها وطول إجراءاتها إلا على مستوى نهاية المرحلة أي بعد جمع واستنباط جميع المتطلبات التي تم تأكيدها أولياً على المستوى الجزئي ، وتسمى " تأكيد جزئي نهائي" كما في الشكل (3) .

وفيما يلي نبذة عن كل من هذه الطرق الجزئية :

1) المراجعة غير الرسمية Walkthrough [10]

هذه الطريقة عبارة عن جلسة (أو عدة جلسات) غير رسمية وغير منتظمة بين محلل النظم الذي قام بجمع واستنباط جزء معين من المتطلبات وبين زملائه من فريق العمل من أجل كشف أي أخطاء أو نواقص أو تناقضات أو غموض في المتطلبات. وهذه الجلسات تكون عفوية وقصيرة ويتم تكرارها لحين الوصول إلى متطلبات شبه خالية من الأخطاء والنواقص والتناقضات والغموض .

2) الفحص Inspection [10]

وهي عبارة عن جلسة أو مجموعة جلسات رسمية (غير عفوية) منظمة بين محللي النظم وفريق فحص متمرس ذو خبرة في كشف الأخطاء. ويستعين هذا الفريق عادة بقائمة من أخطاء تطبيقات سابقة شبيهة بالتطبيق المطلوب. ويتم فحص كل بند من المتطلبات وفقا لقائمة الفحص التي تم إعدادها مسبقا(Check List). ويفضل مشاركة الزبون أو المستخدم خاصة الذي لعب دورا في جمع المتطلبات. وبهذا تكون قائمة المتطلبات في نهاية الجلسات أكثر تنقيحاً وأعلى جودة.

3) التحقق Verification [11]

التحقق هو إجراء عملية التأكيد عن طريق المواد والوثائق التي تم جمعها (استنباطها) وتصنيفها ووضع الأسبقيات لتنفيذها Classify & Prioritize والتي تم التحقق منها مسبقاً بواسطة المراجعة غير الرسمية والفحص. ويفضل أن يقوم بهذا الاختبار استشاري مستقل ويمكن أن يقوم به مهندس المتطلبات التابع لفريق التطوير. ويتم التحقق هنا (من خلال الوثائق فقط) من أن هذه المتطلبات فعلاً مقتبسة من الاحتياجات الفعلية المتعلقة بالزبائن بالإضافة إلى أهمية التأكد من مرجعية كل بنود المتطلبات و أولويتها، وأن التوثيق صالحا للاستخدام في المراحل التالية.

4) المصادقة Validation [11]

ويتم عن طريق ما يعرف بالعرض التجريبي Prototype وهي طريقة تحقق وتأكيد عملي (على جهاز الحاسوب) على المتطلبات المنقحة جزئياً بواسطة الطرق السالفة الذكر وهنا يُفضل الاستعانة بخبرة استشاري مستقل ، ويحضر جلسة العرض التجريبي مهندسي المتطلبات والزبون والمستخدم لمعرفة أي نواقص أو تناقضات أو أخطا أو

غموض في المتطلبات. كما يمكن اقتراح أي متطلبات جديدة خصوصاً بعد التوضيح العملي والمرئي للإمكانيات والوظائف والخيارات . وفائدة العرض التجريبي أنه يحول المتطلبات الغير ملموسة (على الورق) إلى متطلبات واقعية ملموسة يمكن التأكد من صحتها مباشرة على جهاز الحاسوب. وهذا ما يعرف بطريقة المصادقة وهي بالتأكيد ترفع من مستوى الفهم المشترك للمعاني الدقيقة للمتطلبات بين جهة المستفيد وجهة التطوير.

V) مثال تطبيقي للتأكيد الجزئي :

في هذا المثال نتناول كيفية تحديد وظيفة معينة من وظائف قسم الحسابات الجارية بالمصرف. فمحلل النظم يبدأ بمقابلة شخصية مع موظف الشباك حول استفسارات زبائن المصرف عن حساباتهم. كان جواب موظف الشباك أن الزبائن يكثرون من الاستفسار عن أرصدتهم. وقد تم وضع قصاصة لذلك فيما يلي عينة منها:

رقم الحساب :_____ الرصيد _____

طبعاً محلل النظم سيستخدم طرق أخرى ومنها ملاحظة على أرض الواقع ومن خلال مراقبة تعامل الزبائن مع الشباك وجد أن بعض الزبائن يسألون عن مرتبات ، وآخرين يسألون عن صكوك تم إيداعها للتحصيل عن طريق المقاصة، لهذا تم اقتراح نموذج أخر يفي بهذه الأغراض وهو كالآتي :

رقم الحساب :_____

تاريخ آخر صك : _____ قيمة آخر صك : _____

تاريخ آخر مرتب : _____ قيمة آخر مرتب : _____

الرصيد الحالي : _____

وللتحقق من هذا النموذج قام محلل النظم بعرض هذا النموذج على زميل آخر وهو محلل نظم لعمل مراجعة غير رسمية Walkthrough وقام هذا الأخير بتعديل طفيف في هذا النموذج وهو أن كثير من الزبائن لديهم أكثر من مرتب حيث أعمال أخرى. كما أن هناك زبائن تجار قد يستفسرون على مجموعة صكوك تم إرسالها للمقاصة، وقد تم تطوير النموذج وفقا لذلك. طبعاً هناك بعض التحسن ولكن عند الاستعانة بخبير استشاري له خبرة في منظومات المصارف واحتياجات مختلف أنواع العملاء أقترح النموذج التالي:

رقم الحساب :_____ الاسم : _____

☐ الرصيد الحالي :_____

☐ آخر رواتب : _____ العدد: _____

☐ آخر صكوك مقاصة: _____ العدد:_____

☐ آخر حوالات :_____ العدد:_____

☐ آخر إيداعات نقدية:_____ العدد:_____

☐ آخر سحوبات نقدية:_____ العدد:_____

☐ آخر صكوك مصدقة صادرة:_____ العدد:_____

☐

☐

فيختار الزبون المعلومة المطلوبة بوضع إشارة (✓) في المربع مع تحديد العدد الذي يدل مثلا على آخر مرتب أو آخر مرتبين أو ثلاثة أو غير ذلك . وبالتالي تقوم المنظومة بعرض نتائج هذا الاستعلام بالتفصيل.

ويلاحظ هنا أن إجراءات التحقق التي تمت جزئياً لهذه الوظيفة قد أدت إلى تطوير العينة من القصاصة التي تم جمعها من موظف الشباك إلى النموذج الشامل الذي تم تطويره بسهولة ابتداء من خطوة الملاحظة Observation، إلى خطوة المراجعة غير الرسمية Walkthrough، إلى رأي الخبير.
ولو أن خبير المتطلبات المصرفية قد أعطى رأيه في المرحلة الأخيرة بعد برمجة المنظومة بالكامل لكان تعديل النموذج أكثر تكلفة. هذا بالنسبة لبند بسيط من بنود المتطلبات فما بالك بقائمة المتطلبات الطويلة والمعقدة والمتداخلة.

خاتمـــــــــــة

إن الفكرة الرئيسية في هذه الورقة البحثية هي استحداث طريقة "التأكيد الجزئي" وتنفيذها على أي جزأ من المتطلبات وتصحيح أخطائها واستكمال نواقصها والتخلص من تناقضاتها وتوضيح ما يكتنفها من غموض في مرحلة مبكرة من قبل أصحاب الأدوار الرئيسية في المنظومة Stakeholders. فبدلاً من تأجيل التأكيد إلى المرحلة النهائية، نبدأ بالتأكيد الجزئي للمتطلبات المستنبطة من كل طريقة من طرق المرحلة الأولى، ونتبعه بالتأكيد الجزئي النهائي (على مستوى كل مرحلة) وقبل الشروع في المراحل

التالية التي يجدر أن تخضع بالمثل إلى "التأكيد الجزئي". وهذا بدوره يقطع بنا شوطاً هائلاً من التنقيح والتنقية والوصول إلى متطلبات ذات جودة عالية في فترة مبكرة جداً. وبالتالي تكون مرحلة التأكيد النهائية على مستوى منهجية هندسة المتطلبات مرحلة تأكيد شمولية ومتيسرة ومجدية. والهدف دائما أن نتفادى أكثر ما يمكن من تكلفة التعديلات التي تتناسب بزيادة مطردة مع وقت إثارتها وخاصة عند اكتشافها في مراحل متأخرة من تحديد المواصفات أو أثناء التصميم والتطوير البرمجي أو ربما خلال الاختبارات أو التشغيل الحقيقي.

المراجـــــــــع

[1] IEEE standard glossary of software engineering.

[2] Cleland Huang, "Software Requirement" , DePual University, 2004

[3] Kazmierczak, “Requirement Engineering”, University of Melbourne, 2003

[4] B. Boehm, “Software Engineering Economics”, Prentice Hall, 1981

[5] Lehner, Hofmann, "Requirement Engineering as a Success Factor in SW Projects", IEEE Software, 2001

[6] IAN Sommerville, "Requirement Engineering Processes", Software Engineering”, 7th edition 2004

[7] Kotony, G., Sommerville, I. " Requirement Engineering Processes and Techniques", John wiley and Sons, 2000.

[8] Bryan Chojnowski, Reglera : " Software Validation Turning Concepts into Business Benefits", MD & MI 2008.

[9] E. Tran, " Verification & Validation and Certification", Carnegie Mellon University, Spring 1999.

[10] D.P. freedman and G.M. Weiberg, “Handbook of Walkthrough, Inspection and Technical Reviews.”

[11] Andriole Stephen , " Software Validation & Verification & Testing and \Documentation", Princeton, N.J. : Petro Cell; books, 1986.

[12] مصطفى عبد العال وإمحمد بن زاهية ." تكييف منهجيات هندسة المتطلبات للحصول على متطلبات جيدة لتطوير المنظومات البرمجية " المؤتمر الوطني لتقنية المعلومات والاتصالات 2008

المتحكم الأمثل للسيطرة على سرعة محرك التيار المستمر باستخدام الشبكات العصبية المضببة

علي حسين احمد الحديدي
ah_control 2007@ yahoo.com
حميد علي محمد الغثوان
Ham_82_ali@yahoo.com
قسم الكهرباء – كلية الهندسة، جامعة الموصل, موصل - عراق

الملخص:
العمل الحالي يتناول دراسة سرعة محرك تيار مستمر مسيطر عليها باستخدام المغير الخافض الرافع واختبار نظام الحلقة المفتوحة. محكم الشبكات العصبية المضببة صمم باختيار عشوائي لعدد ونوع الدوال العضوية للتحكم بسرعة محرك التيار المستمر. بسبب عدم وجود طريقة واضحة ومعروفة لاختيار عدد ونوع دوال العضوية في حالة استخدام المحكم المضبب,لقد تم تطوير نظام الاستدلال الضبابي المستند على الشبكات العصبية التكيفية والذي يربط بين بنية الاستدلال الضبابي وقابلية التعلم للشبكات العصبية التكيفية وذلك للسيطرة على سرعة محرك التيار المستمر. التقنية استخدمت لاختيار أفضل عدد وأحسن نوع من دوال العضوية للمنظومة المضببة. العملية تمت من خلال اختيار أربعة أنواع من دوال العضوية وبأعداد مختلفة (7,5,3.....الخ) لكل نوع, ثم حساب الخطأ النسبي لكل حاله ومقارنة النتائج لاختيار الأقل من بينهم.ومن ثم استخدام المسار المختار للسيطرة على سرعة المحرك في ما تبقى من وقت العمل. التقنية المطورة استخدمت للسيطرة على سرعة محركين مختلفين في الخصائص ومتشابهين في النوع. النتائج أظهرت بان المحكم المقترح مرن ويمكن استخدامه لأي نوع من الأحمال وليس فقط محرك التيار المستمر,لأنة يحتاج فقط الإخراج الهدف ومن ثم فان المسيطر ذاتيا بأخذ بيانات التدريب للإدخال من نظام الدائرة المفتوحة ويدرب النظام عند كل عدد ونوع من دوال العضوية ومن ثم يختار الحالة الأفضل للسيطرة .

1 - المقدمة:

تلعب محركات التيار المستمر دوراً مهماً في وسائل النقل, حيث تستعمل في السيارات الكهربائية والقطارات والمصاعد . فضلا عن كونها تزود بالقدرة الميكانيكية التي نحتاجها في الكثير من الصناعات , كما أنها تعد جزءاًَ لا غنى عنهَ في حياتنا اليومية حيث أن اغلب الأجهزة المنزلية تعتمد في عملها على المحركات الكهربائية.

تطرق كثير من الباحثين إلى تصميم مسيطر ضبابي يستند على الشبكات العصبية التكيفية (Neuro-Fuzzy Controller) وبمجالات وتطبيقات مختلفة فمثلا قام الباحثان (Jun Oh JANG and Pyeong Gi LEE) بتطوير جهاز سيطرة ضبابي مستند على الشبكات العصبية التكيفية لتعويضِ الاحتكاك في نظام محرك التيار المستمر,حيث تم اختيار خمس

دوال عضوية نوع (Gaussian) وبشكل عشوائي. كما قام الباحثون (Adriana Florescu, Ovidiu Grigore, Dan Alexandru Stoichescu, Alexandru Vasile) بتصميم نظامين للسيطرة أولهما هو المسيطر الضبابي وثانيهما مسيطر الشبكات العصبية المضببة, حيث تم اختيار نوع وعدد دوال العضوية بشكل عشوائي. كما قام الباحثون (Ferenc Farkas, Sandor Halasz, Istvan Kadar) بتصميم مسيطر الشبكات العصبية المضببة للسيطرة على سرعة محرك التيار المستمر نوع الفرشاة , كما في البحوث السابقه فقد تم اختيار نوع وعدد دوال العضوية بشكل عشوائي حيث كانت خمس دوال عضوية من نوع المثلثي في كل من الإدخال والإخراج [1,2,3,4] .

نلاحظ من الأعمال السابقة التي تم استعراضها واعمال كثيرة مثلها لا يسع المجال لذكرها, أن عملية اختيار نوع وعدد دوال العضوية جرت بطريقة عشوائية ومن دون حسابات مدروسة ,أما البحث الحالي فيقترح تقنية جديدة على أساسها يتم اختيار عدد ونوع دوال العضوية للحصول على أحسن استجابة (اقل خطأ ممكن بين السرعة الحقيقية للمحرك والسرعة المرجعية) . إننا في الكثير من التطبيقات بحاجة إلى تثبيت سرعة المحرك عند سرعة معينة وعلى هذا الأساس برزت الحاجة إلى بناء منظومة سيطرة تقوم بهذا العمل, حيث تتكون المنظومة التي تم بنائها من جزأين رئيسيين هما منظومة القدرة ومنظومة السيطرة.

2- منظومة القدرة Power System: تتكون منظومة ألقدرة من محرك التيار المستمر (DC Motor), ومغير التيار المستمر الخافض الرافع **(Buck Boost Converter)** وكما ياتي:

أ- محرك التيار المستمر: في هذا البحث تم اختيار نموذجين من محرك التيار المستمر ذي ألإثارة المنفصلة, حيث الشكل (1) يبين الدائرة الكهربائية المكافئة لكل من المنتج والمجال للمحرك.

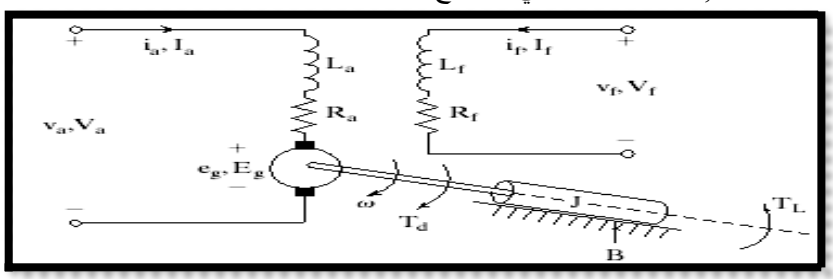

شكل(1) الدائرة الكهربائية المكافئة لمحرك تيار مستمر منفصل الإثارة

وان المصفوفات التي تصف عمل المحرك فهي كما مبين في أدناه:

$$\begin{bmatrix} \dot{i}_a \\ \dot{W}_m \end{bmatrix} = \begin{bmatrix} -R_a/L_a & -K_b/L_a \\ K_b/J & -B/J \end{bmatrix} \begin{bmatrix} i_a \\ W_m \end{bmatrix} + \begin{bmatrix} 1/L_a & 0 \\ 0 & -1/J \end{bmatrix} \begin{bmatrix} v_a \\ T_L \end{bmatrix} \quad \ldots(1)$$

ب- المغير الخافض الرافع Buck Boost Converter: في هذا البحث تم استخدام المغير الخافض- الرافع (Buck-Boost Convertor) وذلك للتحكم بفولتية المنتج عن طريق التحكم بزاوية قدح الترانسيستور لمغير التيار المستمر مما يؤدي إلى الحصول على مدى واسع من الفولتيات . حيث بالإمكان الحصول من خلال المغير على فولتية إخراج Vo أقل أو أعلى من فولتية الإدخال Vs وبقطبيه معاكسة, ويبين الشكل (2) الهيئة العامة للدائرة. وهذا النوع من المغيرات يكون حساسا جدا بتغير قيمة فترة توصيل الترانسستور(α) ، إذ إن معدل فولتية الإخراج هو[5,6,7]:

$$Vo = -\frac{\alpha . Vs}{(1-\alpha)} \quad \ldots.(2)$$

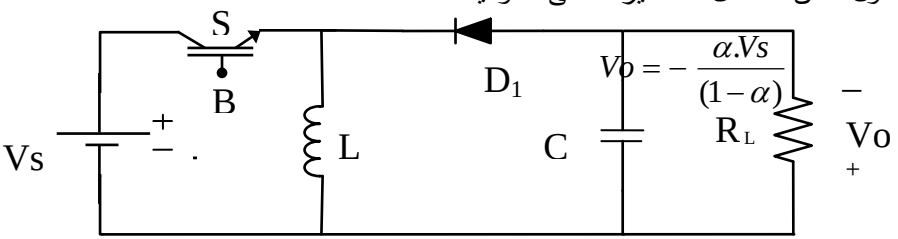

الشكل(2) الهيئة العامة لدائرة المغير الخافض الرافع

إذ بالإمكان كتابة مصفوفات عامة تضم حالتي عمل الترانسيستور وبدلالة نسبة فترة التوصيل(α) كما مبين أدناه [5].

$$\begin{bmatrix} \dot{i}_L \\ \dot{v}_C \end{bmatrix} = \begin{bmatrix} 0 & -(1-\alpha)/L \\ (1-\alpha)/C & -1/RL.C \end{bmatrix} \begin{bmatrix} i_L \\ v_C \end{bmatrix} + \begin{bmatrix} \alpha/L \\ 0 \end{bmatrix} Vs \quad \ldots\ldots(3)$$

ج–المعادلات الرياضية العامة للنظام: يمكن كتابة المعادلات الديناميكية للمنظومة بشكل كامل(محرك التيار المستمر مع المغير الخافض الرافع) بشكل مصفوفات و كما يأتي

$$\begin{bmatrix} \dot{X}_1 \\ \dot{X}_2 \\ \dot{X}_3 \\ \dot{X}_4 \end{bmatrix} = \begin{bmatrix} 0 & -(1-\alpha)/L & 0 & 0 \\ (1-\alpha)/C & -1/RL.C & 0 & 0 \\ 0 & -1/La & -Ra/La & -Kb/La \\ 0 & 0 & Kb/J & -B/J \end{bmatrix} \begin{bmatrix} X_1 \\ X_2 \\ X_3 \\ X_4 \end{bmatrix} + \begin{bmatrix} \alpha/L & 0 \\ 0 & 0 \\ 0 & 0 \\ 0 & -1/J \end{bmatrix} \begin{bmatrix} V_S \\ TL \end{bmatrix}$$

$$y = [0001] \begin{bmatrix} X_1 \\ X_2 \\ X_3 \\ X_4 \end{bmatrix}$$

3

- **استجابة نظام الدائرة المفتوحة:** الشكل (3) يبين المخطط الكتلي لنظام الدائرة المفتوحة والذي يجمع بين محرك التيار المستمر ومغير التيار المستمر(الخافض الرافع) . كما يمكن ملاحظة أن هناك دائرة لتوليد النبضات .إذ تم استخدام نموذجين من نماذج محرك التيار المستمر الموجودة في بيئة (Matlab/Simulink) بأحجام وعناصر مختلفة .

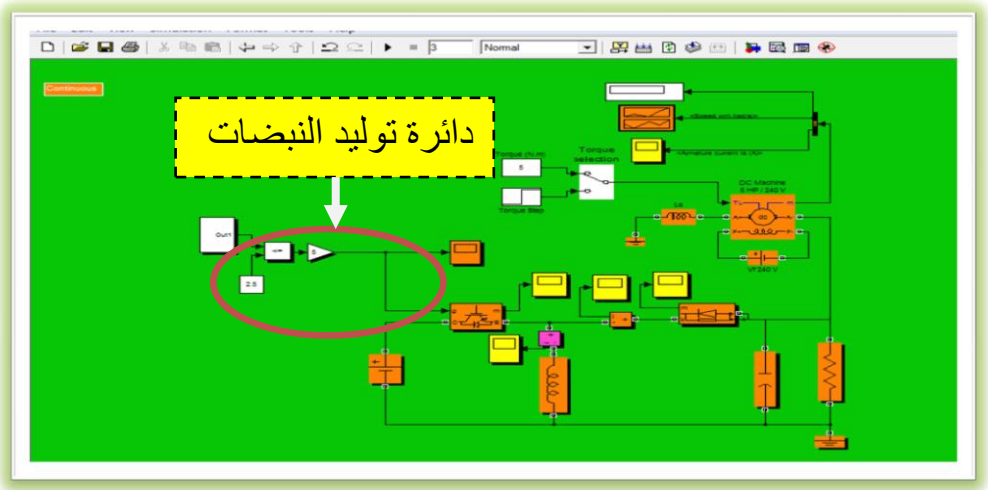

شكل (3)المخطط الكتلي للمحرك مع المغير الخافض– الرافع

الشكل (4) يبين استجابة محرك التيار المستمر كنظام دائرة مفتوحة , فلقد تم تسليط نسبة فترة توصيل بمقدار (50%) حيث نلاحظ أن قيمة تجاوز الحد وصلت إلى (23%) وهذه تعتبر نسبه عالية. كما نلاحظ أن الاستجابة تأخذ وقتا طويلا من أجل أن تصل إلى حالة الثبوت, حيث يحتاج النظام إلى (0.5 sec) وبالتالي فإننا نحتاج إلى نظام سيطرة يحسن من استجابة النظام ويصل به إلى السرعة المطلوبة بأسرع وقت ممكن واقل قيمة لتجاوز الحد .

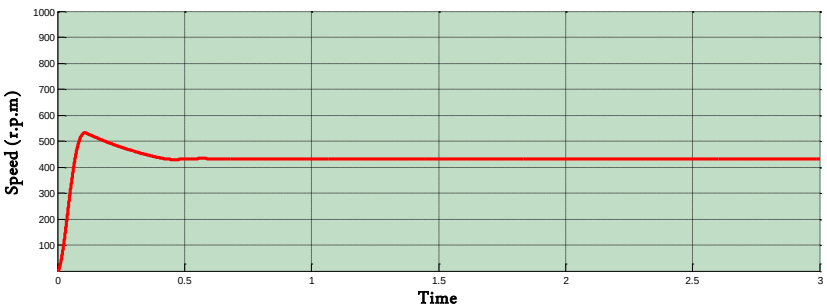

الشكل (4) استجابة سرعة المحرك عند (α=50%)

الشكل (5) يبين استجابة النموذج الثاني لمحرك التيار المستمر, كما تم تسليط نسبة فترة توصيل بمقدار (50%) حيث نلاحظ أن قيمة تجاوز الحد وصلت إلى (43.6%) وهذه تعتبر نسبة

عالية أيضا . و أن الاستجابة وصلت إلى حالة الثبوت بزمن حوالي (0.37 sec).

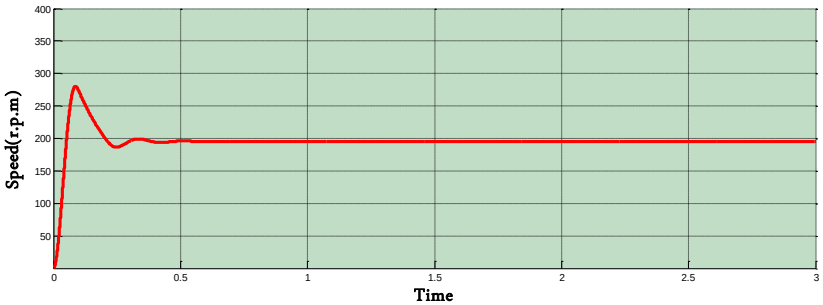

الشكل (5)استجابة سرعة المحرك عند (α=50%)

4

– **منظومة السيطرة:** هناك تقنيات عديدة للسيطرة في هذا المجال وقد تم تناول اثنتان منها في البحث الحالي وكما ياتي:

أ– **نظام السيطرة المضبب Fuzzy Control System:** إن السيطرة المضببة ذات كفاءة عالية, وإنها تستخدم التعابير اللغوية البسيطة بدلاً من المعادلات الرياضية الصعبة المعقدة ولكن من مساوئها صعوبة تضبيط الدوال العضوية لها وصعوبة تضبيط العناصر الخاصة بها ، ومقدار التداخل في ما بينها بحيث إنها تعتمد على خبرة المصمم وهذه تعد من المسائل الصعبة فضلا عن هدر أوقات كبيرة في تضبيط قيم الكسب عشوائيا. والشكل (6) يبين نظام الدائرة المغلقة مع المسيطر الضبابي التي تم بنائها [8,9,10].

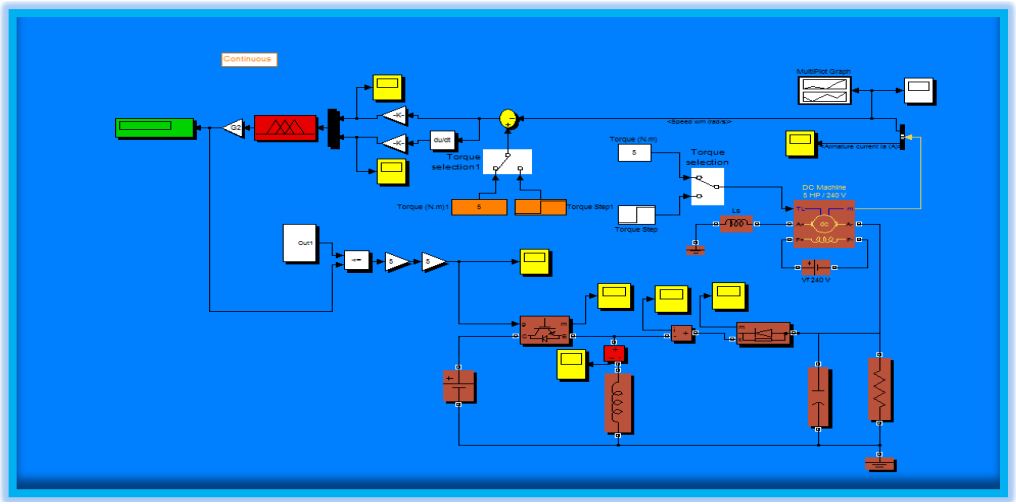

شكل (6) نظام السيطرة المغلقة مع المسيطر الضبابي

الشكل (7) يمثل استجابة السرعة لمحرك التيار المستمر وعند سرعة مرجعية (500), حيث تم تنغيم كل من كسب الإدخال و الإخراج وعند (5N.m إلى 25 N.m) أن المسيطر استطاع أن يرجع بالنظام إلى السرعة المرجعية ويتجاوز التشوه الحاصل في الاستجابة جراء تغيير عزم

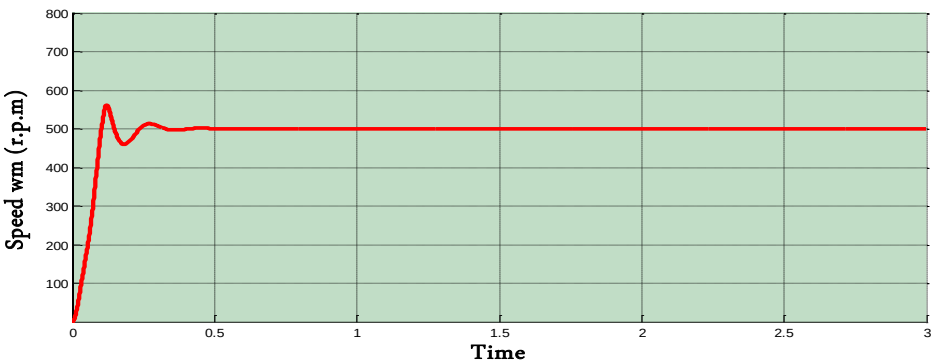

ثلاث دوال عضوية نوع المثلثي . نلاحظ انه الحمل المسلط بشكل جيد . ويلحظ من عند تغيير الحمل الخارجي المسلط (T_L) من

الشكل(7) كذلك أن قيمة تجاوز الحد (12.7 %) وهي نسبة رديئة نوعًا ما .

شكل (7) استجابة السرعة باستخدام المسيطر الضبابي وعند سرعة مرجعية 500(r.p.m)

الشكل (8) يبين استجابة السرعة عند تثبيت قيم الكسب إلى القيم التي تم الحصول من خلالها على السرعة المرجعية (500 r.p.m) ومن ثم تغيير السرعة المرجعية إلى (750 r.p.m) مع الإبقاء على قيم الكسب ثابتة حيث نلاحظ أن الاستجابة تدهورت ولم تصل إلى السرعة المرجعية حيث أصبح خطأ حالة الثبوت مساوٍ لـ (e_{ss}= 28%) كما مبين باللون الأصفر.

أما الاستجابة المبينة باللون الأزرق فتمثل الاستجابة عند تغيير السرعة المرجعية إلى (1000 r.p.m) . حيث نلاحظ أنة عند تغيير السرعة المرجعية تدهورت الاستجابة, وعدم وصولها إلى السرعة المرجعية بحيث أصبح خطأ حالة الثبوت مساوٍ لـ (e_{ss}=45.2%) وهذا يدل على أن المسيطر الضبابي لا يكيف نفسه مع تغيير السرعة المرجعية وهذه الحالة تعد إحدى مساوئ هذا النظام .

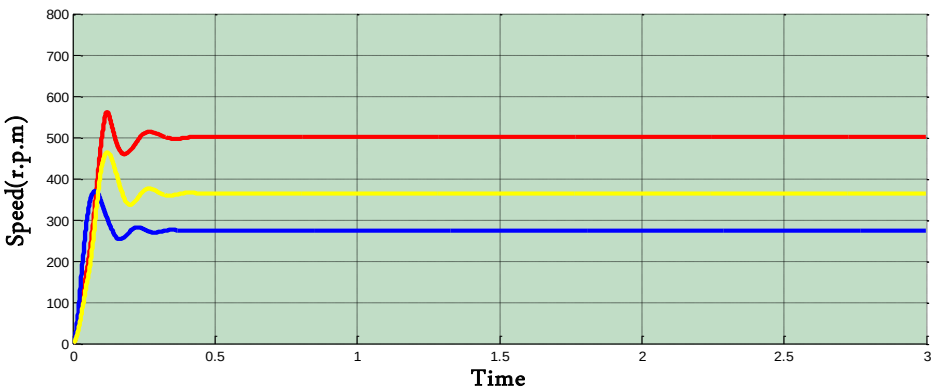

الشكل (8) استجابة سرعة المحرك عند سرع مرجعية مختلفة

الشكل (9) يبين استجابة النظام عند استخدام ثلاث دوال عضوية نوع المثلثي كما مبين باللون الأحمر, وهي الاستجابة نفسها التي تم تنغيم قيم الكسب عندها, ومن ثم تم استخدام أعداد مختلفة حيث كانت الاستجابة باللون الأزرق هي الاستجابة عند خمس دوال عضوية أما الاستجابة باللون الأصفر فهي عند سبع دوال عضوية .

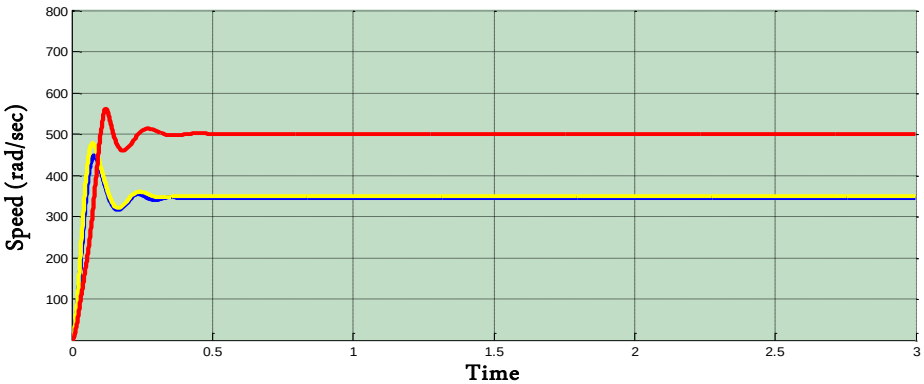

شكل (9) استجابة سرعة المحرك عند أعداد مختلفة من دوال العضوية

من الشكل (9) نلاحظ أن نظام السيطرة الضبابي لا يتكيف مع تغيير عدد دوال العضوية فبتغيير عدد دوال العضوية تختلف قرارات المسيطر الضبابي مما أدى إلى توليد هذه الاستجابات الرديئة .

الشكل (10) يبين استجابات النظام عند ثلاث دوال عضوية وبأنواع مختلفة . حيث الاستجابة باللون الأحمر هي الاستجابة عند دوال عضوية نوع المثلثي وهو النوع الذي تم تنغيم قيم الكسب عنده , أما الاستجابة باللون الأزرق فهي عند دوال عضوية نوع (شبه المنحرف) التي نلاحظ فيها زيادة كبيرة في قيمة خطأ حالة الثبوت. وكذلك الحال بالنسبة للأنواع الأخرى كما مبين بالشكل حيث الاستجابة باللون الأصفر عند دوال عضوية نوع (gbell) و الاستجابة باللون الأسود عند دوال عضوية نوع (Gaussian) . مما سبق نلاحظ أن النظام لا يكيف نفسه مع تغيير نوع دوال العضوية ايضاً.

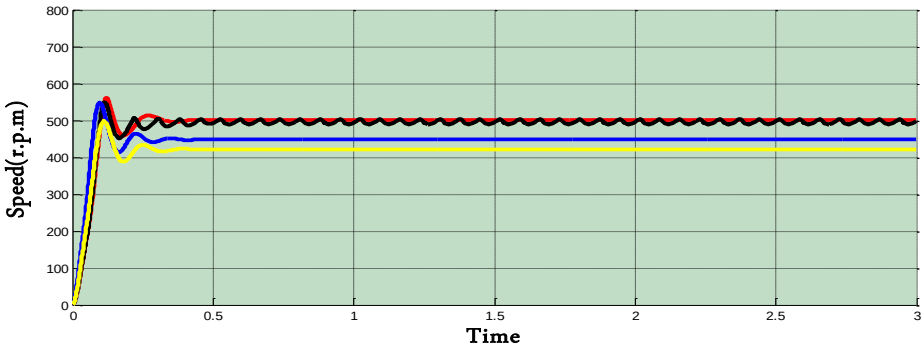

شكل (10) استجابة سرعة المحرك عند أنواع مختلفة من دوال العضوية

نلاحظ مما سبق أن المسيطر الضبابي مسيطر متين حيث قام بتحسين استجابة النظام بشكل جيد كما أنه استطاع أن يحافظ على استقرا رية النظام بعد تسليط عزم حمل أضافي. لوحظ أن المسيطر قام بتقليل خطأ حالة الثبوت إلى قيم قليلة جدا ,مما أدى إلى الوصول إلى السرعة المرجعية المطلوبة, وبالرغم من هذه المحاسن لاحظنا أن المسيطر لم يكيف نفسه مع تغيير السرعة المرجعية أو تغيير نوع أو عدد دوال العضوية .

ب- مسيطر الشبكات العصبية المضببة: في هذا النظام يتم استخدام طريقة الاستدلال الضبابي نوع (Takagi-Sugeno), وإخراج كل قاعدة يمكن أن يكون عبارة عن مركبة خطية لمتغيرات الإدخال مضافاً إليها قيمة ثابتة, أو يكون عبارة عن قيمة ثابتة فقط. والإخراج النهائي هو عبارة عن المعدل الوزني لإخراج كل قاعدة . حيث نفرض أن عندنا تركيب (ANFIS) له ادخالين فقط كما مبين في شكل(11) يحتوي على قاعدتين كما مبين أدناه [10,11,12,13,14,15]:

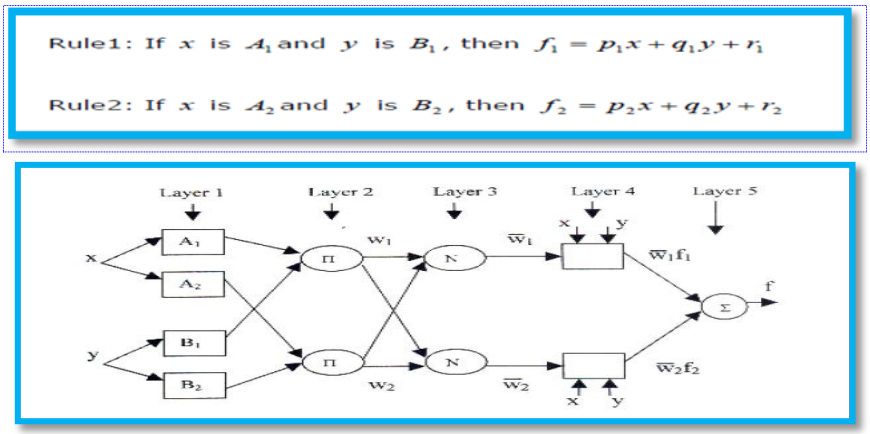

شكل(11) تركيب الـ(ANFIS)

يتكون نظام سيطرة الشبكات العصبية المضببة الذي تم تصميمه من جزأين , جزء برمجي وهو الجزء الذي تتم فيه عملية التدريب وانتقاء النظام الذي يعطي أفضل استجابة . أما الجزء الثاني فهو الـ (Simulink) ويحتوي على الهيكل الأساسي للنظام والمتمثل بمحرك التيار المستمر (*dc motor*) ومغير التيار المستمر (*buck-boost converter*) ,فضلا عن احتوائه على دائرة توليد النبضات .وعند البدء بتشغيل البرنامج يقوم بتشغيل نظام الدائرة المفتوحة واستخلاص بيانات التدريب للإدخال حيث أن عملية التدريب تحتاج إلى زوجين من البيانات (بيانات الإدخال وبيانات الإخراج الهدف) ومن ثم تطبيق الإخراج الهدف وتدريب النظام عند ثلاث دوال عضوية نوع المثلثي ثم يتم تشغيل نظام الدائرة المغلقة وحساب الخطأ النسبي لاستجابة النظام.و بعد ذلك يقوم البرنامج بتغيير عدد دوال العضوية إلى خمس وسبع دوال عضوية ومن ثم تشغيل نظام الدائرة المغلقة وحساب الخطأ النسبي لكل حالة .,ومن ثم يقوم البرنامج بتغيير نوع دوال العضوية إلى شبه المنحرف و (*gbell*) و كاوسيان وبأعداد مختلفة من دوال العضوية و من ثم تطبيق الخطوات السابقة . وبذلك يكون هناك اثنا عشر

استجابة ولكل استجابة هناك خطأ نسبي يختلف عن الاستجابات الأخرى .

بعد ذلك يقوم البرنامج بمقارنة الأخطاء النسبية ألاثنتي عشر واختيار النظام الذي يعطي استجابة بأقل خطأ .ويعد هذا البرنامج برنامج عام لأي حمل, وليس فقط محرك التيار المستمر . في هذا البحث تم التطبيق على نموذجين من محركات التيار المستمر وبإمكان المستخدم تطبيقه على أي حمل آخر حيث انه يحتاج من المستخدم فقط بيانات التدريب للإخراج (الإخراج الهدف). ويمكن تلخيص الخطوات أعلاه بالمخطط الانسيابي المبين في شكل (12):

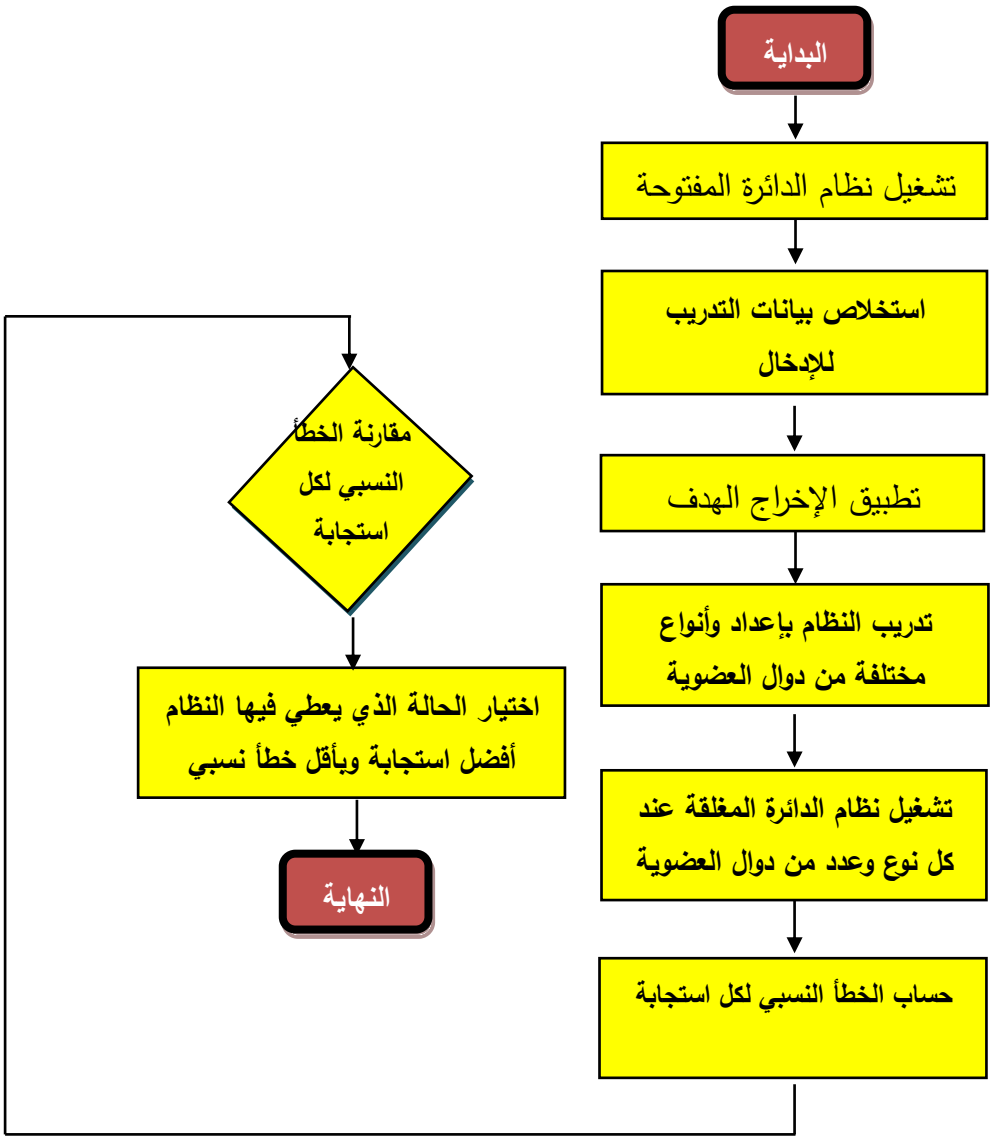

شكل(12) المخطط الانسيابي لآلية عمل مسيطر الشبكات العصبية المضببة

الشكل (13) يبين استجابات محرك التيار المستمر عند أنواع و أعداد مختلفة من دوال العضوية وعند سرعة مرجعية (500 r.p.m), حيث يلاحظ وجود عدد من الاستجابات تتفاوت في ما بينها . هنالك اثنتا عشر نوعاً من الاستجابات إذ يقوم البرنامج بحساب الخطأ النسبي لكل استجابة ومن ثم يقارن بينها ويختار النظام الذي يعطي استجابة بأقل خطأ كما مبين بالشكل أدناه.

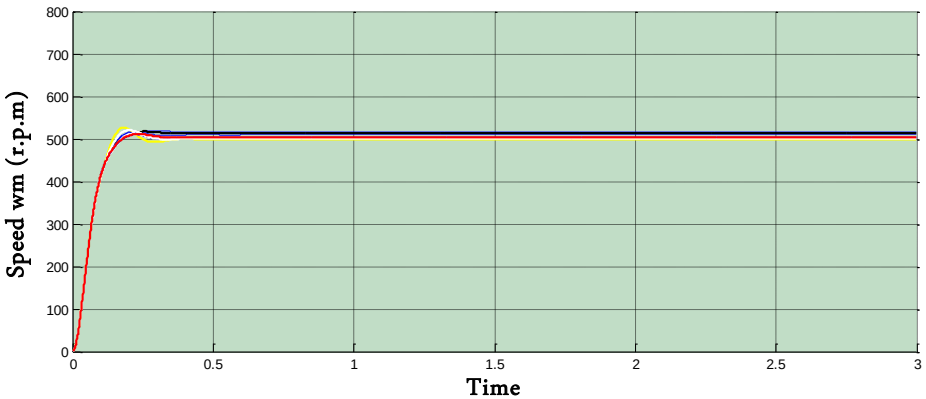

شكل (13) استجابات السرعة مع المسيطر (ANFIS) عند السرعة المرجعية (500 r.p.m)

الجدول (1) يبين عملية المقارنة, يلحظ من الجدول أن النظام الذي له ثلاث دوال عضوية نوع شبه المنحرف (Trapezoidal) يعطي أحسن استجابة وبأقل خطأ كما مبين بالشكل (14).

جدول (1) الأخطاء النسبية لاستجابات المحرك عند السرعة (500 r.p.m)

Wref=500(r.p.m)		Number of membership function		
		3	5	7
Type of membership function	Traingular	0.0778	0.0833	2.312
	Trapezoidal	0.07206	2.602	2.703
	Gbell	0.0788	2.515	0.0991
	gaussian	0.0728	0.08570	0.5289

نلاحظ إن قيمة تجاوز الحد للاستجابة التي تم اختيارها تساوي (Mo.sh=4%) و(e_{ss}=0.0034) وهي نسبة جيدة إذا ما قارناها مع استجابة الدائرة المفتوحة والاستجابة في حالة وجود المسيطر الضبابي كذلك.

شكل (14) يبين الاستجابة التي تم اختيارها بواسطة البرنامج التي تحتوي على اقل خطأ نسبي حيث من الجدول نلاحظ قيمة الخطأ والمساوية لـ(0.07206). وكذلك فلقد تم تسليط عزم حمل خارجي مقداره (20 N.m) كما مبين بالشكل فان النظام قد تغلب على التشوه الناجم من العزم الإضافي المسلط .

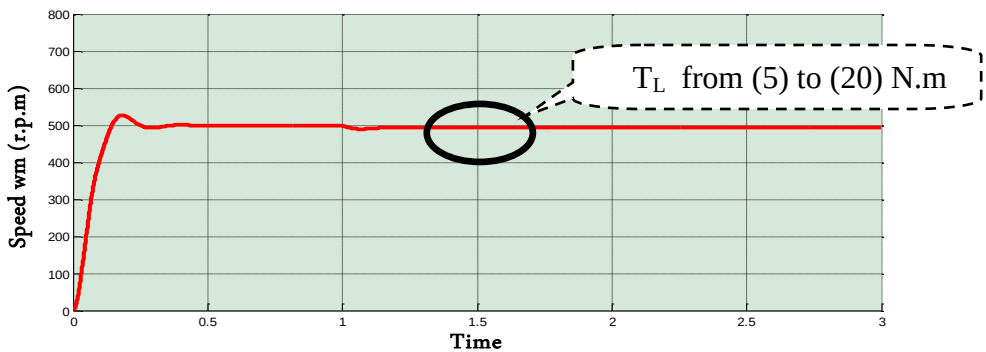

شكل (14) الاستجابة المختارة عند سرعة مرجعية (500 r.p.m)

الشكل (15) يبين استجابات محرك التيار المستمر وعند سرعة مرجعية (750 r.p.m), والجدول (2) يبين عملية المقارنة فمن الجدول نلاحظ أن النظام الذي له ثلاث دوال عضوية نوع (Gbell) يعطي أحسن استجابة وبأقل خطأ وكما مبين بالشكل (16).

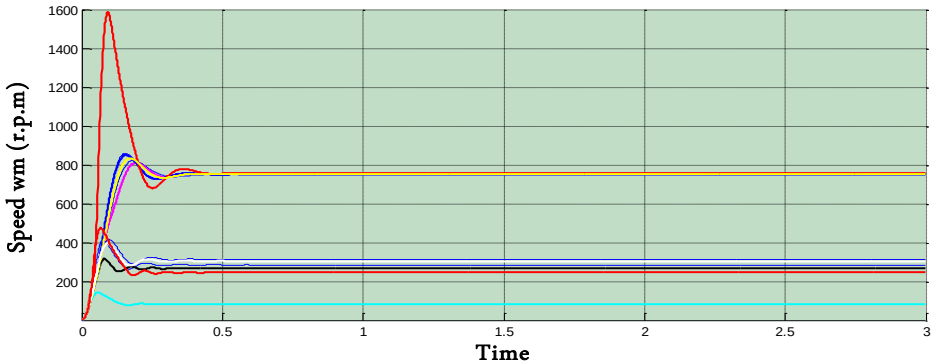

شكل (14) استجابات السرعة للمحرك وعند سرعة مرجعية (750 r.p.m)

جدول (2) الأخطاء النسبية لاستجابات المحرك عند سرعة مرجعية (750 r.p.m)

Relative Error at Wref=750(r.p.m)		Number of membership function		
		3	5	7
Type of membership function	Triangular	0.0855	0.00887	0.1864
	Trapezoidal	0.00835	0.1944	0.2667
	Gbell	0.00817	0.1756	0.0171
	Gaussian	0.00861	0.1791	0.2007

شكل (16) يبين الاستجابة التي تم اختيارها بواسطة البرنامج والتي تحتوي على اقل خطأ نسبي فمن الجدول نلاحظ قيمة الخطأ والمساوية لـ(0.00817) . كذلك تغيير قيمة العزم المسلط كحمل خارجي مقداره من (5 r.p.m) إلى (25 N.m) كما مبين بالشكل إذ تغلب النظام على التشوه الناجم من العزم الإضافي المسلط .

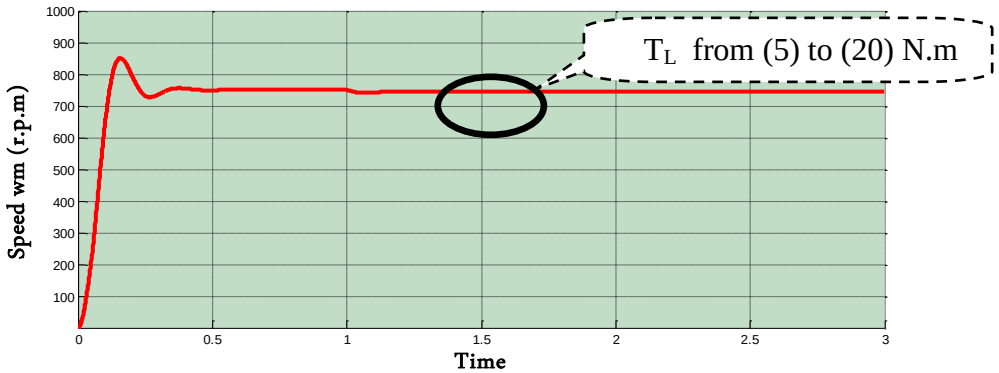

شكل (16) الاستجابة المختارة عند سرعة مرجعية (750 r.p.m)

شكل (17) يبين استجابات محرك التيار المستمر عند سرعة مرجعية (1000 r.p.m) , وفي هذه الحالة تم اختيار النظام الذي له ثلاث دوال عضوية نوع المثلثي والذي أعطى أحسن استجابة وبأقل خطأ نسبي (0.008159) كما موضح في جدول (3) وشكل (18).

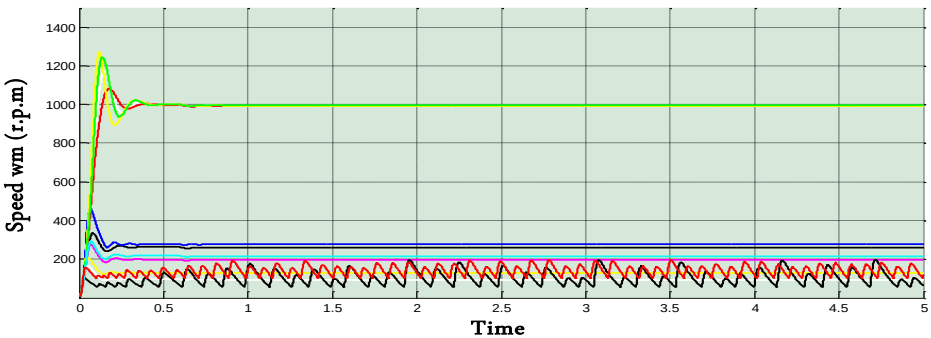

شكل (17) استجابات المحرك عند سرعة مرجعية (1000 r.p.m)

جدول (3) الأخطاء النسبية لاستجابات المحرك عند سرعة مرجعية (1000 r.p.m)

Relative Error at Wref=1000(r.p.m)		Number of membership function		
		3	5	7
Type of membership function	Triangular	0.008159	0.74379	0.7203814
	Trapezoidal	0.079816	0.902507	0.080681
	Gbell	0.8038	0.917884	0.084752
	Gaussian	0.78611	0.87723	0.894

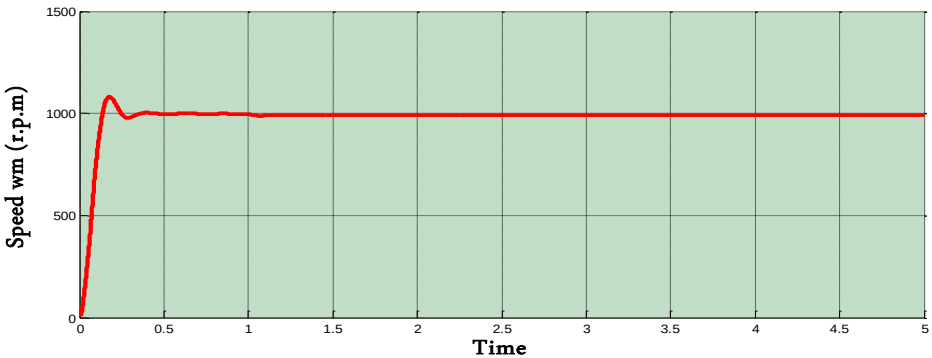

شكل (18) الاستجابة المختارة عند سرعة مرجعية (1000 r.p.m)

كما ذكر سابقا فان مسيطر الشبكات العصبية المضببة المصمم هو مسيطر عام يصلح لأي حمل ولإثبات ذلك تم تغيير نموذج محرك التيار المستمر والموجود ضمن بيئة (Matlab/Simulink). والجدول (4-5) يبين قيم الأخطاء النسبية للنموذج الثاني من محرك التيار المستمر عند ثلاث سرع مرجعية مختلفة ((r.p.m) 1000, 500,750). ومن الجدول

أدناه نلاحظ أنه عند السرعة المرجعية (500 r.p.m) كان النظام الذي له ثلاث دوال عضوية نوع (trapezoidal) هو النظام الذي أعطى أحسن استجابة بأقل خطأ نسبي . و نلاحظ كذلك عند السرعة المرجعية (750 r.p.m) إن البرنامج قام باختيار النظام الذي له خمس دوال عضوية نوع (Gaussian), أما عند السرعة (1000 r.p.m) فقد قام البرنامج اختيار النظام الذي له سبع دوال عضوية نوع (gbell).

جدول (4) يبين الأخطاء النسبية لاستجابات النموذج الثاني لمحرك التيار المستمر عند السرع المرجعية (500 , 750 ,1000 r.p.m)

The second model of dc motor		***Number of membership function***		
		3	5	7
Wref=500 (r.p.m)	Triangular	0.122	0.1588	0.1463
	Trapezoidal	0.0732	0.0754	0.07645
	Gbell	0.865	0.0792	0.0772
	Gaussian	0.0788	*0.0891*	0.0895
Wref=750 (r.p.m)	Triangular	0.1042	1.818	0.0977
	Trapezoidal	0.09245	1.948188	0.087429
	Gbell	0.96388	0.10063	0.14375
	Gaussian	0.0969	0.0911882	1.804
Wref=1000 (r.p.m)	Triangular	0.080859	3.41107	4.55282
	Trapezoidal	2.8232	4.37907	4.54787
	Gbell	2.3847	4.694129	0.0802
	Gaussian	4.07789	4.6681	4.735

5

– **مناقشة النتائج:** تم تصميم المسيطر المنطقي المضبب والذي كان تصميمه ذا تضبيط عشوائي ، تمت دراسة استجابة المنظومة مع المحكم المضبب, إذ كانت النتائج جيدة مقارنة مع (نظام الحلقة المفتوحة) وتبين كذلك وجود تحسن ملحوظ في استجابة النظام, عند السرعة المرجعية (500 r.p.m), ومن ثم احتجنا إلى تغيير هذه السرعة المرجعية إلى (750 r.p.mو1000 r.p.m) فان النظام لم يكيف نفسه مع السرعة المرجعية الجديدة. كما لوحظ انه عند تضبيط قيم الكسب عند ثلاث دوال العضوية نوع المثلثي ومن ثم تغيير نوع أو عدد دوال العضوية بحيث أصبحت الاستجابة رديئة وان المسيطر لم يكيف نفسه مع هذا التغيير. كما أن عمليه اختيارنا لنوع وعدد دوال العضوية كان بشكل عشوائي ولم تكن على وفق حسابات مدروسة وبما أن اختلاف نوع وعدد دوال العضوية وكذلك مدى كل من الإدخال والإخراج و مقدار التداخل في ما بينها له تأثير على استجابة النظام, ولذلك لابد أن تكون هناك طريقة مدروسة وقاعدة يستند عليها النظام في عملية الاختيار.

اما بالنسبة لمسيطر الشبكات العصبية المضببة نلاحظ من النتائج التي تم الحصول عليها إنه عند سرعة مرجعية (500 r.p.m) قام المسيطر باختبار اثنتا عشر نوعاً من دوال العضوية حيث لكل استجابة نوع وعدد خاص من دوال العضوية وقام المسيطر باختيار النظام الذي له ثلاث دوال عضوية نوع المثلثي الذي أعطى اقل خطأ نسبي . ولقد لوحظ من الاستجابة التي تم اختيارها أن المسيطر استطاع أن يتغلب على التشويه الحاصل على استجابة السرعة نتيجةً لتسليط عزم اضافي مقداره (20 N.m) كحمل خارجي. وقد تم تغيير السرعة المرجعية إلى (750 r.p.m) وتدريب النظام على السرعة الجديدة وفي هذه الحالة قام المسيطر باختيار النظام الذي له ثلاث دوال عضوية نوع (Gbell) أما عند تغيير السرعة المرجعية إلى (1000 r.p.m) فقد قام المسيطر باختيار النظام الذي له ثلاث دوال عضوية نوع المثلثي , وقد تم تكرار العملية نفسها على النموذج الثاني لمحرك التيار المستمر وبسرع مرجعية مختلفة, مما سبق نلاحظ أن لكل سرعة مرجعية

وجود نوع وعدد خاص من دوال العضوية يعطي أفضل استجابة .

5- <u>الخلاصة</u>: تناول البحث تصميم نوعين من المسيطرات للسيطرة على سرعة محرك التيار المستمر ذو الإثارة المنفصلة, وذلك بالاعتماد على برمجيات (Matlab/Simulink), حيث تم دراسة استجابة الدائرة (نظام الدارة المفتوحة) و (نظام الدارة المغلقة مع المسيطرين). المسيطران هما المسيطر الضبابي ومسيطر الشبكات العصبية المضببة حيث تم استخدام مغير القدرة الخافض–الرافع للسيطرة على فولطية المنتج للمحرك وبالتالي التحكم بالسرعة. تم تصميم واقتراح ودراسة مسيطر يستند على الشبكات العصبية المضببة ويقوم باختيار عدد ونوع من دوال العضوية التي من خلالها تم الحصول على أفضل استجابة من بين اثنتا عشرة استجابة تم اختبارها, وكذلك فإن هذا المسيطر يمكن أن يكيف نفسه مع تغيير السرعة المرجعية أو تغيير نموذج المحرك حيث أن المسيطر المقترح يعتبر مسيطر عام يمكن استخدامه لأي حمل و ليس فقط محرك التيار المستمر ولا يحتاج من المستخدم سوى الإخراج الهدف, حيث أظهرت النتائج ان مسيطر الشبكات العصبية المضببة يكون ذا كفاءة أعلى ويعطي نتائج أفضل إذا ما قورن بالمسيطر الضبابي

<u>المصادر:</u>

[1] د.مأمون فاضل الكبابجي و د.نبيل محمود عبد القادر "المكائن الكهربائية والكترونيات القدرة" مديرية دار الكتب للطباعة والنشر,جامعة الموصل.العراق 1988 .

[1] Jun Oh JANG and Pyeong Gi LEE, ''Neuro-Fuzzy Control for DC Motor Friction Compensation'' Department of computer control Engineering ,south korea.2000.

[2] Adriana Florescu, Ovidiu Grigore, Dan Alexandru Stoichescu, Alexandru Vasile, ''NEURO-FUZZY DESIGN IN DC MOTOR SPEED CONTROL'' *University of Bucharest, Electronics and Telecommunications Faculty, Bd. Armata Poporului 1-3, Sect. 6, 77206 - Bucharest, Romania .2001.*

[3] Ferenc Farkas, Sandor Halasz, Istvan Kadar,''Speed Sensorless Neuro-Fuzzy Controller for Brush type DC Machine'', Department of Electric power

Mosul/ Iraq, , thesis ,M.Sc. 2004.

[9] Leond Reznik, "Fuzzy Controller", Vectoria University of Technology ,Melbourne, Australia. 1997.

[10] Yodyium Tipsuwan and Saksiri Aiemchareon, "A Neuro-Fuzzy Network-Based Controller for DC Motor Speed Control "Department of Computer Engineering, Kasetsart University, Bangkok, Thailand.2005…….ANFIS

[11] Nada Abd Al-Ghani , "Speaker Recognition Using Neuro-Fuzzy Method", thesis ,M.Sc. University of Mosul/ Iraq,2004.

[12] *Mehamet Akar & Ismail Temiz*, "Motion Controller Design For The Speed Control Of DC Servo Motor "Gaziosmanpasa University & Marmara University, International Journal of Applied Mathmatics and Information.2007

[13] *Heikki Koivo*, "Adaptive Neuro-Fuzzy Inference System " IEEE.2000.

[14] D.C. Theodoridis , Y.S. Boutalis, M.A. Christodoulou, "Indirect Adaptive Neuro-Engineering, Budpest University of Technology ,Hungary.

[4] Salwan Samir Sabri Ali, "Optimal Fuzzy Controller Design For (Cuk) Converter Circuit Using Genetic Algorithm", thesis M.Sc. University of Mosul/ Iraq,2008.

[5] Mohamed H. Rashid, "Power Electronics Circuits , Devices and Applications", Third Edition ,Electrical and Engineering, University of West Florida,2004.

[6] Stanimir Yordanov Yordanov, "An Approach on T-S Fuzzy Model and Control of Buck-boost Converter "Department AIUT, TU Gabrovo, H.Dimitar 4., 5300, Bulgaria,.2004 buck-boost

[7] Nadia Qassim Mohammed, "Neuro Fuzzy Controller For A Four Quadrant Position and Speed Control"University of Baghdad/ Iraq, thesis, M.Sc.2005.

[8] Maher Mohammed Fawzi Saber AL Greer, "Design and Implementation Of Computerized Industrial Fuzzy Control System " University of

Fuzzy Control Based On High Order Neural
[15] Network Function Approximators "cDepartment of Electronic and Computer Engineering, Technical University of Crete, Greece.2008
[16] Ahmed Nasser Bahjat Al-Sammak,'' A Fuzzy Logic Control of Synchronous Motor for Reactive Power Compensation'', University of Mosul/ Iraq, A Ph.D. Thesis.2007.

استخدام التقنية الصوتية في كشف أعطاب محامل المحرك الحثي

ا.د. باسل محمد سعيد
قسم الهندسة الكهربائية
جامعة الموصل
basilms2007@yahoo.com

د.ياسر محمد يونس
قسم الهندسة الكهربائية
جامعة الموصل
yasir_752000@yahoo.com

محمد حامد سعود
قسم الهندسة الكهربائية
جامعة الموصل
msc.panther@yahoo.com

الملخص:-

يقدم هذا البحث نتائج كشف وتشخيص أعطاب المحامل في المحرك الحثي ثلاثي الطور باستخدام التقنية الصوتية. حيث تم اخذ النتائج في حالات كون المحمل سليم وفي حالة وجود عطب عند سرع مختلفة ناتجة عن تغير الحمل، حيث تم فحص عدة عينات من المحامل تحتوي على أعطاب مختلفة ناتجة من استعمالها لفترة طويلة فضلاً عن فحص عينات تم أجراء أعطاب شديدة عليها لغرض دراسة تأثير العطب عند تطوره إلى مراحل متقدمة. كما تمت مراقبة الإشارات في حيز الزمن وفي حيز التردد وفي حيز الزمن – التردد، علاوة على مراقبة مستوى شدة الصوت الناتج عن الماكنة في الحالة السليمة والمعيبة.

وقد بينت الفحوصات أمكانية كشف أعطاب المحامل بصورة مبكرة جداً من خلال مراقبة شدة صوت الماكنة وتحليله وهذا يساعد على اتخاذ التدابير الوقائية كتشحيم المحمل وتقليل العوامل التي تؤدي إلى حدوث العطب كعدم اتزان الحمل الميكانيكي وعدم محاذاة محور الدوران.

1- مقدمة :-

تستخدم المكائن الكهربائية في العديد من التطبيقات الصناعية حيث تمثل العنصر الأساسي في تحويل الطاقة الكهربائية إلى طاقة ميكانيكية وبالعكس, لذلك تستخدم في محطات توليد الطاقة الكهربائية وفي استخراج المنتجات النفطية وفي المعامل, ومن أكثر أنواع المكائن الكهربائية المستخدمة هي المحركات الحثية بحيث تستهلك حوالي 40%-50% من الطاقة المولدة في كل بلد ، ويأتي هذا الاستخدام الواسع بسبب ميزاتها الجيدة من حيث الصلادة والوثوقية العالية وسهولة التركيب وقلة الحاجة إلى الصيانة مقارنة مع المكائن الأخرى, فضلاً

عن سهولة التحكم بسرعتها وخاصة بعد التطور الكبير في مجال اليكترونيات القدرة.

وبالرغم من صلادة هذه المحركات إلا أنها عند استعمالها لفترات طويلة ومع تغير الأحمال المسلطة عليها وتراكم العوامل الأخرى الناتجة إما من المصدر أو من البيئة التي تعمل فيها الماكنة فقد تتعرض لعدة أنواع من الأعطاب الأولية. وهذه الأعطاب عند تطورها مع الزمن ستؤدي إلى خفض كفاءة الماكنة وربما إذا استمرت هذه الظروف فقد تؤدي إلى توقف الماكنة وخروجها عن العمل مما يسبب خسائر كبيرة في الخطوط الإنتاجية فضلاً عن كاف صيانة إضافية.

ان المراقبة المستمرة لحالة الماكنة (On – line condition monitoring) لمعرفة التغيرات التي تحدث خلال فترة التشغيل يساعد على كشف العطب بمرحلة مبكرة وتحديد نوعه وهذا يوفر من الوقت المستغرق للصيانة وتقليل الخسائر في الإنتاج والمحافظة على حياة العاملين.

قام العديد من الباحثين بدراسة أعطاب المحامل في المكائن الدوارة مستخدمين عدة تقنيات ومنهم (R. Saklawi وآخرون) حيث قاموا باستخدام تقنية تحليل فورير السريع (FFT) لتحليل إشارة اهتزاز الماكنة من اجل كشف أعطاب المحامل [2]. كما قام (Mounir Djeddi وآخرون باستخدام تقنية تحليل بصمة التيار في كشف العطب باستخدام تقنية تحويل فورير السريع (FFT) [3].واستخدم (Mohammed A. A. Elmaleeh) تقنية الانبعاث الصوتي لتشخيص أعطاب المحامل من خلال حساب قيمة الانحراف المعياري (Standard Deviation SD) وقيمة عامل الذروة (Crest Factor) للإشارة الصوتية في حيز الزمن [4-5].

إن الهدف من عملية تشخيص أعطاب المحامل هو كشفه في مراحله الأولية قبل تطوره وتفاقمه إلى مراحل متقدمة تؤدي إلى إخراج الماكنة عن العمل حيث ربما تكون مراحله الأولية غير مؤثرة ولكن عند تطوره كزيادة التصدع في المحمل يؤدي إلى ازدياد الاهتزاز في الماكنة وهذا بدوره قد يؤدي إلى خلخلة الربط (structure lossless) في الماكنة مما يؤدي إلى حدوث عدم اتزان الفجوة الهوائية داخل المحرك والذي بدوره يؤدي إلى حدوث دائرة قصر مع الجزء الثابت (rub between stator & rotor).

يستخدم هذا البحث الطريقة الصوتية لكشف أعطاب الماكنة من خلال تحليل الإشارة باستخدام تقنيات تحليل الإشارة في حيز الزمن وتحويلات فورير وتحويلات الموجية. حيث تم تحليل البصمة الصوتية للماكنة لمعرفة

المركبات الموجودة فيها ومن ثم استخلاص مركبات العطب المفيدة في عملية التشخيص.

2- تصنيف مصادر الإشارة الصوتية :-

إن الإشارة الصوتية تنتج من اهتزاز جسم لذلك لابد من معرفة مصادر الاهتزاز والضوضاء الناتجة من الماكنة وهذه المصادر يمكن تصنيفها إلى عدة مجاميع وكما يأتي:

- الاهتزاز أو الضوضاء الكهرومغناطيسي (Electromagnetic Vibration or Noise):

وهي تنتج من المركبات الفراغية والمركبات الزمنية (Time & Space Harmonics) الموجودة في إشارة المصدر المجهز, أو من عدم اتزان الفجوة الهوائية (Air gap Eccentricity) , أو من عدم اتزان فولتية المصدر (voltage unbalance), أو التشبع المغناطيسي في القلب الحديدي (Core Saturation), أو بسبب الفيض المتسرب الناتج من حدوث دائرة قصر في ملفات الجزء الثابت (inter-turn short circuit).

- الاهتزاز أو الضوضاء الميكانيكي (Mechanical Vibration or Noise):

وهي تنتج من الأجزاء الميكانيكية في الماكنة مثل المحامل (Bearing).

- الاهتزاز أو الضوضاء الديناميكي الهوائي (Aerodynamic Vibration or Noise):

وهذا ينتج من أجزاء التبريد في الماكنة كمراوح التبريد.

إضافة إلى إن هناك مصادر للضوضاء ترتبط مع الحمل الميكانيكي وهي:

- الاهتزاز أو الضوضاء الناتجة من المعشق (Coupling) أو من الأحزمة أو السلاسل (belt or chain) أو من صندوق التعشيق (Gear box) وهذه تنتج بسبب عدم محاذاة محور الدوران (shaft misalignment).
- الاهتزاز أو الضوضاء الناتجة بسبب ضعف أو تخلخل ربط الماكنة (Lossless) أو بسبب وضع الماكنة على قاعدة غير ثابتة (Foundation), [6-8].

3- أعطاب المحامل :-

يعتبر هذا النوع من الأعطاب من أكثر الأعطاب شيوعاً حيث تصل نسبة حدوثه إلى حوالي 41% حسب IEEE والى 75% حسب OEM وفي بعض المصادر الأخرى تصل إلى أكثر من 50% من نسبة أعطاب المكائن الدوارة.

يبدأ عطب المحمل عند ارتفاع درجة حرارة الماكنة حيث يؤدي إلى حدوث تغير في التركيب الكيميائي للزيت الموجود داخل المحمل مما يؤدي إلى تغير في لزوجته وهذا يسبب حدوث تماس بين الأجزاء الحديدية مما يؤدي

إلى توليد ترددات فوق الصوتية (>20 KHz). حيث انه في حالة توفر متحسس فوق صوتي (ultrasonic transducer) سيعد هذا من أبكر طرق الكشف. ثم بعد ذلك يؤدي إلى حدوث أعطاب في البنية الداخلية للمحمل أي يؤدي إلى حدوث خدش في الحلقة الخارجية (outer race defect) أو الداخلية (inner race defect) أو الكرات (ball defect) أو الحزام المحيط بالكرات (cage defect) ثم يتطور إلى حدوث تصدع في المحمل وهذه تعتبر من اخطر المراحل وان أي تغير في الحمل أو عدم اتزانه قد يكون كفيل في تكسر المحمل بصورة نهائية مما يؤدي إلى

من خلال ما سبق يتبين أن هناك عدة تقنيات يمكن استخدامها لكشف أعطاب المحامل. حيث طور الباحثون العديد من التقنيات وقاموا بدراسات عديدة حول زيادة كفاءة هذه التقنيات من اجل زيادة كفاءة المنظومة (منظومة الكشف والتشخيص) وتقليل كلف الصيانة والمحافظة على الإنتاج.ومن هذه التقنيات:-

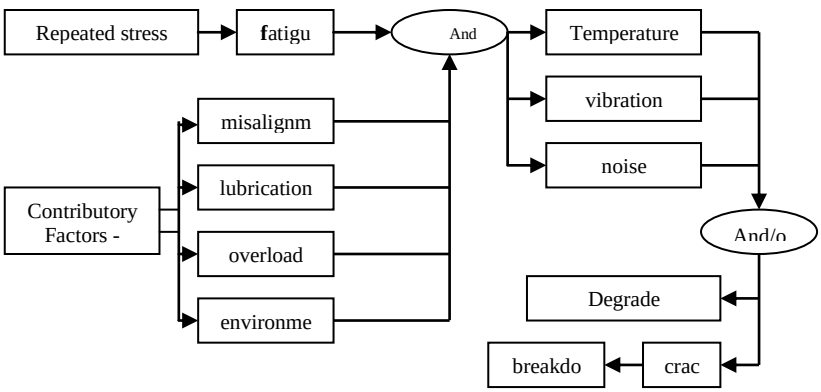

شكل (1) ميكانيكية الانهيار في المحامل

1) تقنية مراقبة درجة الحرارة (Temperature Measurement Monitoring Technique) التي تتضمن قياس درجة الحرارة باستخدام متحسسات حرارية موضوعة داخل الماكنة أو عن طريق الكاميرات الحرارية.
2) تقنية مراقبة الأشعة تحت الحمراء (Inferred Recognize Monitoring Technique).
3) تقنية مراقبة الترددات الراديوية (Radio Frequency Monitoring Technique).
4) تقنية مراقبة الاهتزاز (Vibration Monitoring Technique).
5) تقنية التحليل كيميائي (Chemical analysis Monitoring Technique) لزيت الماكنة أو زيت المحامل.
6) تقنية الانبعاث الصوتية (Acoustic Emission Monitoring Technique) حيث تتضمن استخدام تقنيات صوتية وفوق الصوتية.
7) تقنية تحليل تيار الماكنة (Current Monitoring Technique)
8) تقنية مراقبة بواسطة الليزر (Laser Monitoring Technique)
9) تقنية مراقبة فولتية محور الدوران (Shaft Voltage Monitoring Technique)

إن حدوث تشقق في بنية المحمل سيؤدي إلى توليد ترددات معينة ناتجة من مرور الكرة فوق التصدع. ويمكننا حساب هذه الترددات من العلاقات الآتية [9]:

$$\mathbf{F_{ord}} = (N/2) F_{sh} [1 - D_{ball} \cos (\beta) / D_{cage}]$$

لحساب التردد الناتج في حالة حصول عيب في الحلقة الخارجية.

$$\mathbf{F_{ird}} = (N/2) F_{sh} [1 + D_{ball} \cos (\beta) / D_{cage}]$$

لحساب التردد الناتج في حالة حصول عيب في الحلقة الداخلية.

$$\mathbf{F_{bd}} = (D_{cage} / 2D_{ball}) F_{sh} [1 - (D_{ball} \cos (\beta) / D_{cage})^2]$$

لحساب التردد الناتج في حالة حصول عيب في إحدى الكرات.

$$\mathbf{F_{td}} = (F_{sh} / 2)[1 - D_{ball} \cos (\beta) / D_{cage}]$$

لحساب التردد الناتج في حالة حصول عيب حزام المحمل.

$F_{bd} = (D_{cage} / D_{ball}) F_{sh} [1 - (D_{ball} \cos(\beta) / D_{cage})^2]$

لحساب التردد الناتج في حالة حصول عيب في العناصر الدوارة.

حيث أن:

F_{sh} : يمثل تردد دوران المحور ويقاس ب (دورة\الثانية).

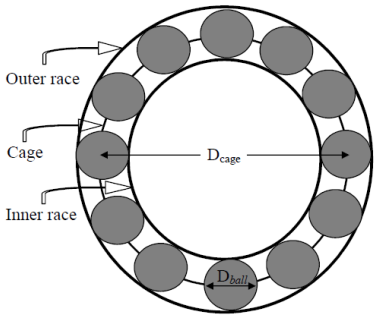

الشكل (2) تركيب المحمل وإبعاده.

4- منظومة الكشف والتشخيص :-

تم بناء وربط منظومة للكشف والتشخيص والتي تتكون من عداد قياس مستوى الاندفاعات الصوتية من طراز (Impulse Precision Sound Level Meter 2209) من شركة Bruel & Kjaer. ومن مقياس رقمي لمستوى الصوت من طراز 407750 لشركة EXTECH. حيث تم إجراء الفحوصات على محرك حثي ثلاثي الطور ذو الخصائص التالية (380 V, 1.3 KW, 4 Pole, 1430 r.p.m). تم إدخال هذه الإشارات إلى الحاسوب باستخدام بطاقة اكتساب البيانات من نوع PCI 1710 , لشركة Advantch ذو تردد تقطيع 100KHz. وتم استخدام برنامج Matlab لبناء البرمجيات اللازمة لعملية تحليل هذه الإشارات المستحصلة باستخدام تقنية تحويل فورير السريع (FFT) وتقنية تحويل المويجة (Wavelet Transform) حيث تم إدخال الإشارات باستخدام تردد اخذ عينات قدره (Sampling Frequency = 4096 Hz) وبعدد عينات (Number of Samples = 32768). ويبين الشكل رقم (3) صورة لمنظومة الكشف والتشخيص المستخدمة.

D_{cage} : يمثل قطر الحزام.

D_{ball} : يمثل قطر الكرة.

β : يمثل زاوية التماس.

N : يمثل عدد الكرات في المحمل.

والشكل (2) يبين تركيب المحمل وإبعاده.

5- النتائج والمناقشة:-

بعد استكمال بناء وربط منظومة كشف وتشخيص الأعطاب تم ربط المنظومة لكشف حالة المحامل حيث تم تشغيل المحرك لمدة ساعتين وأدخلت البيانات من إشارات الصوت

إلى الحاسبة لغرض التعامل معها وتحليلها في خطوات لاحقة. ومن ثم أعيدت عملية الفحص والتشغيل بعد استبدال المحمل وأدخلت البيانات اللازمة إلى الحاسبة أيضا. تم فحص 5 عينات من المحامل المحتوية على مختلف الأعطاب والموضحة في الشكل (4), وتم عرض نتائج بعض العينات في حيزي الزمن والتردد التي تم الحصول عليها من حالات تشغيل مختلفة وكما يأتي:

شكل رقم (4) صورة تبين بعض العينات المستخدمة فى البحث.

5-1- نتائج القياس في حيز الزمن (Time Domain Measurement Results)

عند قياس أعلى قيمة لمستوى شدة الصوت (Maximum Noise) للمحرك كانت النتائج كما مبينة في الجدول (1). حيث تبين النتائج على انه في حالة وجود عطب في المحامل فان مستوى شدة الصوت سيرتفع كما يوضح انه كلما زاد مستوى العطب في المحمل سيزداد مستوى شدة الصوت, كما يلاحظ في العينة رقم (5) والتي تحتوي على عطب شديد متمثل بتصدع كبير في السطح الخارجي والداخلي وحزام الكرات.

شكل رقم (3) صورة لمنظومة الكشف والتشخيص المستعملة.

جدول رقم (1) مستوى شدة صوت لمجموعة من المحامل

Load	Speed (RPM)	Noise Level in (db) for bearing samples					
		Healthy Bearing	Faulty Bearing				
			Sample 1	Sample 2	Sample 3	Sample 4	Sample 5
N.L	1490	76.4	77.6	78.4	79.4	84.3	95
H.L	1450	77.9	77.9	79.3	84.4	88.7	103
F.L	1430	80.3	80.7	81	86	88.8	93.1

5

2- نتائج القياس والتحليل في حيز التردد (Frequency Domain Measurement & Analysis Results)

قبل البدء بدراسة وتحليل الإشارات المدخلة يتوجب حساب الترددات المحتملة الظهور عند حدوث عطب في المحمل. لذلك تم حساب الترددات المحتملة الظهور اعتماداً على العلاقات المذكورة سابقاً اخذين بنظر الاعتبار سرعة الماكنة وأبعاد المحمل المستخدم. و كما موضحة في الجدول رقم (2) والذي يبين نوع المحمل المستخدم و أبعاده حيث تم حساب ترددات الأعطاب عند سرعة دوران تساوي 60 (R.P.M أي (1 Hz و تم حسابها عند تغيير سرعة الماكنة عن طريق تغير الحمل والجدول رقم (3) يوضح هذه الترددات.

جدول رقم (2) أبعاد المحمل المستخدم والتردد الناتج عنه في حالة وجود عطب

Bearing model	6206 2RS, 6206 ZZ
Number of balls	9
Bore diameter	16 mm
Outside diameter	62 mm
Ball diameter	10.2 mm
outer bearing race defect (F_{ord})	3.57 Hz
inner bearing race defect (F_{ird})	5.43 Hz
ball defect (F_{bd})	2.31 – 4.62 Hz
train defect (cage defect) (F_{td})	0.396 Hz

جدول رقم (3) الترددات الناتجة عن المحمل في حالة وجود عطب

Rotational speed (rpm)	F_{ord} (Hz)	F_{ird} (Hz)	F_{bd} (Hz)		F_{td} (Hz)
1490 rpm	88.655	134.845	57.365	114.73	9.834
1480 rpm	88.06	133.94	56.98	113.96	9.768
1470 rpm	87.465	133.035	56.595	113.19	9.702
1460 rpm	86.87	132.13	56.21	112.42	9.636
1450 rpm	86.275	131.225	55.825	111.65	9.57
1440 rpm	85.68	130.32	55.44	110.88	9.504
1430 rpm	85.085	129.415	55.055	110.11	9.438
1420 rpm	84.49	128.51	54.67	109.34	9.372
1410 rpm	83.895	127.605	54.285	108.57	9.306

تم استخدام برنامج لأخذ الإشارة الصوتية في غرفة معزولة (عديمة الصدى), وذلك من اجل تقليل التداخل في الإشارة وتقليل الانعكاسات الحاصلة في البيئة الطبيعية, حيث يقوم البرنامج بتسجيل الإشارة لمدة 16 ثانية ثم يتم تحليل الإشارة باستخدام تحليل فورير السريع (FFT). يبين الشكل رقم (5) عينة من موجة صوتية ناتجة من المحرك في حالة كون المحمل سليم وفي حالة وجود عطب .كما يبين الشكل رقم (6) نتائج تحليل الموجة الصوتية في حيز التردد. ويمكن ملاحظة إن العينة المفحوصة تحتوي على

أعطاب متقدمة ولاجل توضيح النتائج بصورة أكثر دقة تم تحليل الإشارة باستخدام احد البرامج الصوتية حيث تم معالجة الإشارة باستخدام (Low Pass Filter) و (Notch Filter) علاوة على استخدام تقنية تقليل الضوضاء (Noise Reducing). ويوضح الشكل رقم (7) نتائج التحليل في حالة كون المحمل سليم وفي حالة كونه حاوي على أعطاب

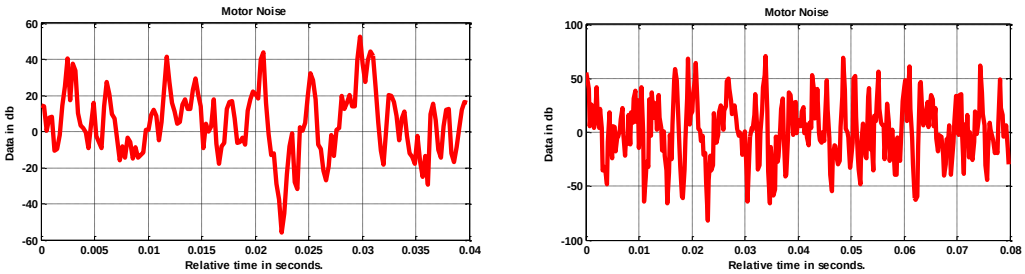

(أ) (ب)

شكل رقم (5) موجة صوتية ناتجة من المحرك في حالة
(أ) كون المحمل سليم , (ب) كون المحمل حاوي على العطب

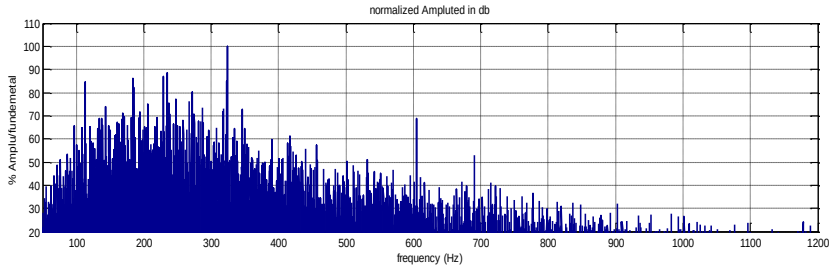

شكل رقم (6) تحليل موجة صوتية ناتجة من المحرك في حالة وجود عطب في المحامل

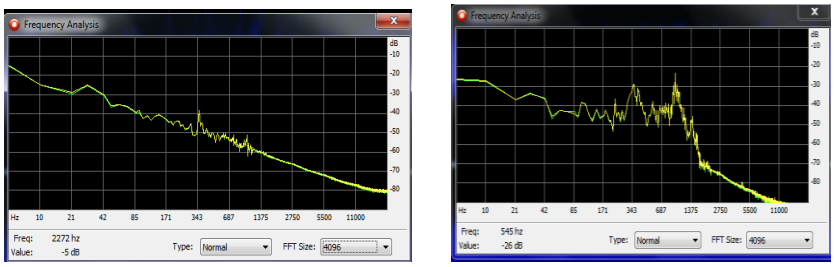

(أ) (ب)

شكل رقم (7) تحليل موجة صوتية لمحمل (أ) سليم و (ب) معطوب

عند ملاحظة تحليل الإشارة الصوتية في حيز التردد في الشكل رقم (6) نلاحظ وجود العديد من المركبات التي تظهر في الإشارة, ومن بينها مركبات عطب المحمل المبينة سابقاً اضافة الى ظهور مركبات أخرى هي توافقيات متزامنة وغير متزامنة لهذه المركبات.

إن ظهور هذا الكم الكبير من المركبات المتوافقة مع مركبات العطب ربما تضعف عملية تشخيص العطب.

5-3- نتائج القياس والتحليل في حيز الزمن – التردد (Time – Frequency Domain Measurement & Analysis Results)

بسبب صعوبة تمييز مركبات العطب تم استخدام تقنية تحليل الإشارة الصوتية في حيز الزمن – التردد باستخدام تقنية تحويل الموجة (Wavelet Transform) حيث تم استخدام دالة أم ديبوجيز من المرتبة الرابعة (db4) عن طريق بناء برنامج فرعي يتم استدعائه عن طريق البرنامج الرئيسي لتحليل الإشارة الصوتية المرسلة إليه إلى 12 مستوى, ويبين الشكل رقم (8) نتائج تحليل الموجة الصوتية باستخدام تقنية تحليل المويجة. وتم حساب معدل الانحراف المعياري (Standard Deviation) لكل مستوى لعدة عينات وقد تم توضيحها في الجدول رقم (4) حيث يوضح قيم معدل الانحراف المعياري لعدة عينات. وبينت النتائج إمكانية كشف أعطاب المحامل باستخدام تقنية تحويل المويجة بصورة أسهل من مراقبة الترددات الناتجة من تحليل الموجة الصوتية في حيز التردد. وذلك عن طريق مراقبة قيم معدل الانحراف المعياري.

جدول رقم (4) قيم معدل الانحراف المعياري لإشارة صوتية ناتجة من المحمل

Standard Deviation Level	Bearing Samples				
	Sample 1	Sample 2	Sample 3	Sample 4	Sample 5
Std1	1.627	1.5085	2.133	7.5714	6.3784
Std2	2.3567	9.9256	3.1942	10.9275	11.2035
Std3	2.6244	12.4855	3.9692	11.8862	13.584
Std4	1.9951	11.8943	3.6619	8.9434	14.9457
Std5	1.0828	8.2125	2.2792	4.6770	13.2084
Std6	0.3791	3.0867	0.9022	1.5913	6.4984
Std7	0.1116	0.8436	0.2631	0.5122	2.8729
Std8	0.0565	0.2341	0.1032	0.3915	0.8729
Std9	0.0578	0.1967	0.1014	0.4359	0.8656
Std10	0.0719	0.2568	0.1225	0.5936	1.0482
Std11	0.099	0.2933	0.1564	0.7491	1.2880
Std12	0.132	0.3916	0.2029	0.9644	1.6781

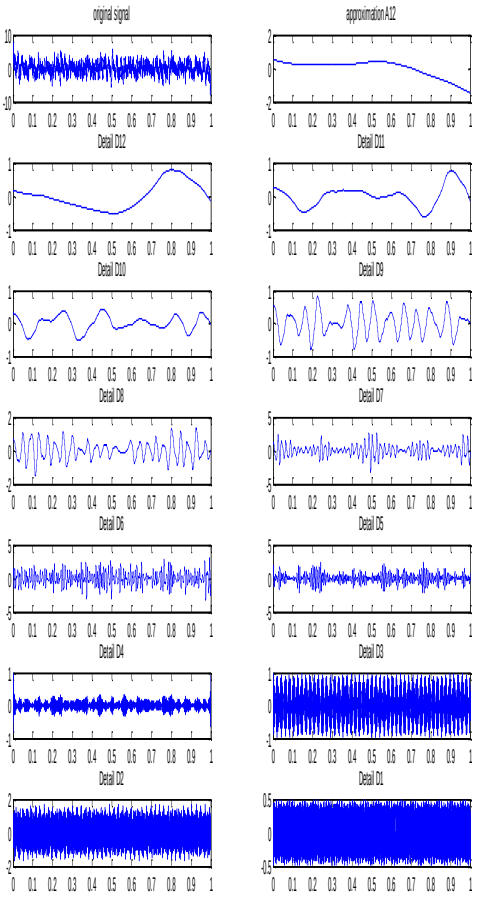

شكل رقم (8) استخدام تقنية تحويل المويجة لتحليل الإشارة الصوتية الناتجة من محرك يحتوي على أعطاب في المحامل

6-الاستنتاجات:-

تعتبر الطريقة الصوتية من أفضل الطرق لكشف أعطاب المحامل في مراحلها المبكرة وخاصة عند توفر متحسس فوق الصوتي حيث بينت الفحوصات أن المحامل تمر بعدة مراحل قبل أن تنهار بصورة نهائية فمثلاً عندما نلاحظ وجود مركبات فوق الصوتية يمكننا إجراء صيانة للمحامل عن طريق تشحيمها. ثم يتطور العطب مما يؤدي إلى توليد ترددات المحامل المذكورة سابقاً وإذا تركت هذه المحامل بدون معالجة سنلاحظ ظهور توافقيات لترددات المحامل وظهور مركبات أخرى يصبح من الصعب معرفة مصدرها. وقد بينت الفحوصات أن المحمل يؤدي إلى ظهور أعطاب أخرى للماكنة بسبب زيادة الاهتزاز حيث أدت بعض العينات إلى ظهور عطب عدم اتزان الفجوة الهوائية الميكانيكي (Dynamic air gap eccentricity) وأدت إحدى العينات إلى حدوث مسح الجزء الدوار مع الجزء الساكن (Rotor Rub) وقد أوضحت النتائج إن المحمل في مراحله النهائية يؤدي إلى توليد عطب عدم محاذاة محور الدوران (Shaft misalignment) ويؤدي إلى خلخلة الربط الماكنة بسبب زيادة مستوى الاهتزاز إلى درجة كبيرة بحيث يتجاوز الحدود المسموحة كما أدى إلى ارتفاع درجة حرارة الماكنة والمعشق وزيادة مستوى الضوضاء إلى درجة كبيرة حيث وصل في إحدى العينات إلى 109 db.

المصادر:-

[1] B. L. Theraja, A.K. Theraja " A Textbook of Electrical technology", volume II, DC & AC Machine, chapter 34, 2005.

[2] Rayyan Saklawi, Assil Smeismeh, and Wissam Yassine, " A Predictive Maintenance Tool: Vibration Analysis to Determine the Condition of Electric Machines ", Electrical and Computer Department, American University of Beirut, Lebanon, ARISER Vol. 4 No. 3 (2008).

[3] Mounir Djeddi, Pierre Granjon, and Benoit Leprettre, " Bearing Fault Diagnosis in Induction Machine Based on Current Analysis Using High Resolution Technique ", IEEE, 2007.

[4] Mohammed A. A. Elmaleeh, N. Saad, " Development of Acoustic Emission Diagnostic System for Condition Monitoring of Rotating Machines", 2nd IEEE International Conference on Power and Energy December 1-3, 2008, Johor Baharu, Malaysia.

[5] Mohammed A. A. Elmaleeh, N. Saad, " A Study of Acoustic Emission Technique on Incipient Detection of Rotating Machine Faults ", Intl. Conf. on Control, Automation, Robotics and Vision Hanoi, Vietnam, 17–20 December 2008.

[6] F. Alton Everest, Ken C. Pohlmann, "Master Handbook of Acoustics" , New York, Chicago, San Francisco, 2009.

[7] Ioan D. Marinescu, Constantin Ispas Dan Boboc, "Handbook of Machine Tool Analysis", Marcel Dekker, Inc. 2002.

[8] *Marlin O. Thurston*, "Noise of Polyphase Electric Motors", Department of

Fault Diagnosis of Electrical Motors—A Review ", IEEE Transactions on energy conversion, Vol. 20, No. 4, December 2005

Electrical Engineering, The Ohio State University, Columbus, Ohio, 2006.

[9] Subhasis Nandi , Hamid A. Toliyat, and Xiaodong Li," Condition Monitoring and

منظومات الخلايا الشمسية ودورها في توسيع قاعدة الاتصالات في شركة المدار

إبراهيم محمد صالح *، خليفة سالم زغب** ، عبد الباسط منير الفورتي**
* جامعة الفاتح ، ** شركة المدار الجديد للهاتف النقال
Ibrahim.saleh@lttnet.net , k.zageb@Almadar.ly , a.forti@almadar.ly

الملخص

لقد كان لاستخدام الطاقة الشمسية في مجال الاتصالات اللاسلكية الأثر الكبير في توسيع دائرة الاتصالات وتراسل المعلومات، إذ أن العقبة الرئيسية في عدم انتشار محطات الاتصالات أو تغطية الهاتف النقال في أي مكان قد يرجع أساسا إلى عدم توفر القدرة الكهربائية اللازمة للتشغيل ، وباستخدام منظومات الخلايا الشمسية التي تستعمل فيها الخلية الشمسية لتحويل الطاقة الشمسية مباشرة إلى طاقة كهربائية دون أي تعقيد في عملية التحويل أو أضرار بيئية يمكن الوصول إلى أماكن الاتصال المعدومة ، وتوفير التغطية الهاتفية للهواتف النقالة. و منظومات الخلايا الشمسية المستخدمة في تغذية محطات الإتصالات والإعادة اللاسلكية هي من أفضل تطبيقات الطاقة الشمسية من حيث الاعتمادية والجدوى الاقتصادية .

تعتبر ليبيا من أوائل الدول التي استخدمت فيها منظومات الخلايا الشمسية في مجال الاتصالات حيث تم تركيب أربعة محطات تجريبية في هذا المجال سنة 1979 ولازالت هذه المحطات تعمل دون توقف.

شركة المدار الجديد هي أقدم شركة للهاتف النقال في ليبيا تسعى دائما إلى توفير تغطية وخدمات الهاتف النقال إلى مشتركيها في جميع أنحاء البلاد، فقد تم تركيب محطتين تجريبيتين تعملان بالطاقة المولدة عن طريق الخلايا الشمسية سنة 1998 ، وبعد أن أثبتت هذه التجربة نجاحها وضعت خطة موسعة لتغطية جميع الطرق ، والحقول النفطية بتغطية الهاتف النقال معتمدة في ذلك على مصدر الطاقات المتجددة .

تم اجراء دراسة لتحديد حجم وقدرة محطات الطاقة الشمسية المطلوبة لتغطية مناطق الطرق والحقول النفطية بخدمات الهاتف النقال ، وتم تصنيف المحطات حسب الأحمال المستهدفة منها ، ومع نهاية سنة 2009 بلغ عدد المحطات العاملة بالطاقة الشمسية إلى 180 محطة بقدرة إجمالية تقترب من 1500 كيلوواط ذروة .

في هذه الورقة سوف نقوم بحصر منظومات الخلايا الشسمية التي تم تركيبها ، وتقييم تجربة شركة المدار الجديد في هذا المجال ، كما سنتطرق إلى الخبرة المكتسبة من هذه المنظومات ، واجمالي الطاقة المنتجة من جميع المحطات وكميات ثاني أكسيد الكربون التي تم منعها من الانبعاث كنتيجة لاستخدام منظومات الخلايا الشمسة بدلا من مولدات الديزل، وكذلك الجدوى الفنية لاستخدام الطاقة الشمسية في هذا المجال.

الكلمات الدالة: منظومات الخلايا الشمسية ، الهاتف النقال ، تقييم منظومات الخلايا الشمسية.

1. المقدمة

استخدمت منظومات الخلايا الشمسية في توليد الطاقة الكهربائية في العديد من الدول المتقدمة والنامية في مجالات الاتصالات كالأقمار الصناعية والهواتف المعزولة ومحطات الإعادة واتصالات القطارات ، وقد أثبتت التجارب العملية اعتماديتها وجدواها الاقتصادية في العديد من الدول ، بل أصبحت منافسة لبعض وسائل توليد الطاقة الكهربائية التقليدية [1].

في ليبيا استخدمت الخلايا الشمسية في مجال الاتصالات من قبل شركة البريد سنة 1979 إلا أن استخدامها بقي محدودا ولم يتم التوسع فيه كما يجب نتيجة لقلة المعرفة في هذا المجال لدى العاملين في شركات الاتصالات. لقد اقتصر استخدام منظومات الطاقة الشمسية على الشركة العامة للبريد والاتصالات السلكية واللاسلكية حتى سنة 1998 عندما استخدمت شركة المدار منظومات الخلايا الشمسية في تغذية محطتي الإعادة والتغطية الهاتفية للنقال في منطقة السدادة ، إلا أن الاستخدام كان محدودا إذ بلغت القدرة الإجمالية المركبة عن طريق شركة البريد 750 كيلواط حتى نهاية 2008 [2،3].

لقد دلت المقارنات الاقتصادية والفنية التي أجريت بين المحطات التي تعمل بمولدات الديزل والمحطات التي تعمل بمنظومات الخلايا الشمسية بالشركة العامة للبريد إلى انخفاض أو انعدام تكلفة التشغيل في محطات الطاقة الشمسية بالمقارنة مع محطات الديزل ، وانعدام انقطاع الاتصالات في الخطوط التي تعمل بالطاقة الشمسية بالمقارنة مع المحطات التي تعمل بمولدات الديزل [4]،وكذلك قلة زيارات الصيانة وعدم تعرض منظومات الطاقة الشمسية إلى التخريب بالمقارنة مع المحطات التي تعمل مولدات الديزل. ولا تزال المحطات التجريبية التي تم تركيبها سنة 1979-1980 تعمل حتى الآن بل أنه لم يتم استبدال أي من المكونات أللإلكترونية المركبة في هذه المحطات [5].

تتمتع ليبيا برقعة واسعة حيث تتناثر القرى والطرق على مساحة 1.75 مليون كيلو متر مربع مع كثافة سكانية لا تزيد عن 6 مليون نسمة ، ومن غير المتوقع ومن غير الاقتصادي مد شبكات الكهرباء على طول البلاد وعرضها أو استخدام مولدات الديزل لتغذية محطات الإعادة أو التغطية الهاتفية البعيدة التي تحتاج إلى رحلات توصيل الوقود والصيانة المستمرة.

وشركة المدار الجديد وهي تسعى إلى تقديم الجديد والأفضل في عالم الاتصالات الهاتفية والهواتف النقالة رأت ضرورة استخدام أفضل السبل لتغطية مناطق الاتصالات المعدومة باستخدام مصادر الطاقات المتجددة، وبالتالي تقرر استخدام منظومات الخلايا الشمسية تحقيقا للأهداف التالية:

1- تغطية رقعة الجماهيرية باتصالات الهاتف النقال.
2- استخدام أكثر طرق التغذية الكهربائية اقتصادا .
3- تجنب مشاكل انقطاع التيار وزيارات الصيانة للمحطات البعيدة.
4- إمكانية استخدام منظومات توليد الطاقة الكهربائية التي تخدم الاهتمامات البيئية.

2. تصميم منظومات الخلايا الشمسية

تختلف طرق تصميم منظومات الخلايا الشمسية بين مصممي منظومات الخلايا الشمسية إلا إنها جميعا تشترك في أهمية تصميم منظومات مثلى تحقق المطلوب بأقل قدرة ممكنة وعند تصميم أية منظومة يتطلب الأمر ما يلي :

1. تحديد الطاقة اليومية المستهلكة.
2. قدرة الحمل المستخدم .
3. نوع التيار

4. الموقع الجغرافي .
5. منحنى قدرة الحمل خلال ساعات اليوم .

تستخدم شركة المدار عدة أنواع من المحطات التي تختلف فيما بينها من حيث الطاقة ونوع التيار ونوع الاستخدام، فبعض المحطات تستخدم للتغطية الهاتفية وكمحطة إعادة ، وبعضها كمحطات إعادة فقط، كما إنها تختلف أيضا من حيث متطلبات الطاقة، وقد اخترنا اكبر أنواع المحطات التي تستخدم كمحطات للتغطية والإعادة ، وهذا النوع من المحطات استخدمت في الطرق من غريان إلى سبها ، وكذلك من نالوت إلى غذامس ، ومن الهيشة الجديدة إلى هون ، ومن أوباري إلى غات، وقد استخدمنا هذا النوع من المحطات كمثال لهذه الدراسة ، هذه المحطات تعمل على جهد 48 فولت والقدرة المطلوبة للتشغيل عالية نسبيا بالمقارنة مع المحطات الأخرى، وهي من النظام المغلق الذي يستخدم مكيف هواء يعمل بالتيار المتردد، وقد تم تحديد سعة البطاريات بخمسة أيام غائمة تفاديا للتوقف الذي قد ينتج عن الغيوم المستمر.

1-2 متطلبات الطاقة الكهربائية لمحطة الإعادة

يتمثل حمل هذه المحطات في حمل المكيف الذي يعمل بالتيار المتردد وحمل الراديو الذي يعمل بالتيار المستمر، كما يجب أخذ حمل المكيف عند بداية تشغيله .

الجدول رقم (1) يبين متطلبات الطاقة التي حددت لهذا النوع من المحطات.

جدول : (1) متطلبات الطاقة للمحطات

الصنف	القدرة	العدد	ساعات التشغيل	التيار	الطاقة [واط ساعة]
الراديو	400	1	20	DC	8000
أجهزة التغطية	1300	1	24	AC	33600
إجمالي	1700				41600

وباستخدام معامل تحويل القدرة من التيار المستمرة إلى المترددة 0.92 فأن إجمالي الطاقة المطلوبة بالتيار المستمر هي

$$\frac{33600}{0.92} + 8000 = 44.5$$ كيلواط ساعة يوميا، وبالتالي يمكن تصميم المحطة بطاقة إجمالية 50 كيلوواط ساعة فى اليوم الواحد ,وبمعامل ضمان قدره 12% . وان أقصى تيار مستمر يمكن حسابه يقدر ب 44 أمبير , وعلى جهد 48 فولت .

بناء على هذه المعلومات قامت الشركات بتصميم محطاتها وقد اخترنا التصميم التالي وهو تصميم أحدى الشركات الموردة:

- القدرة الإجمالية للمحطة 12.88 كيلواط ذ.
- عدد منظمات الجهد 2 بقدرة 2 كيلواط بتيار أقصى 150 أمبير لكل منها .
- عدد محورات التيار 2 بقدرة 2 كيلواط.
- سعة البطاريات الإجمالية 6000 أمبير ساعة

3. حصر منظومات الخلايا الشمسية بشركة المدار

بدأ استخدام منظومات الخلايا الشمسية في شركة المدار بشكل موسع سنة2006 حيث تم تركيب عدد أربعة محطات بمنطقة سوسة وتاكنس وطبرق، من بعدها تم التوسع في

استخدام منظومات الخلايا الشمسية سنتي 2008 و2009 بتركيب محطات التغطية الهاتفية لتغطية جميع الطرق والحقول النفطية ، ومنذ سنة 2006 وحتى منتصف 2010 ، تم تركيب ما يقرب من 170 محطة موزعة على الطرق والجدول رقم (2) يبين خطوط التغطية وعدد المحطات والقدرة الإجمالية لهذه المحطات .

، الشكل رقم 1 يبين تنامي القدرة الإجمالية المركبة من منظومات الخلايا الشمسية التي قامت شركة المدار بتركيبها ما بين سنة 2006و 2010.

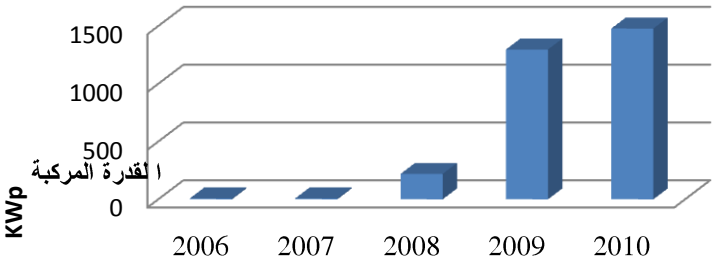

شكل (1) تنامي القدرة الإجمالية المركبة من منظومات الخلايا الشمسية

جدول : (2) عدد المحطات على خطوط النقل والقدرة الإجمالية المركبة

خط التغطية	عدد المحطات	القدرة الإجمالية [KWp]
شحات - درنة	4	25.92
سرت – هون	10	37.8
ودان- زلة	5	17.28
جالو- اجدابيا	6	93.60
جالو- الكفرة	19	107.08
اجدابيا- طبرق	13	42.12
المرج - التميمي	5	14.58
طريق البريقة مرادة	3	11.88
طريق زلة مراده	12	45.36
طريق البريقة	11	17.82

طريق الحرابة -نالوت	4	66.56
طريق درج - غدامس	10	141.68
طريق نالوت وازن	3	42.40
الهيشة- هون	6	77.28
السدادة -الساحلى	5	64.4
طريق الشويرف- سبها	10	128.8
طريق مزدة - الشويرف	9	127.2
سبها - تراغن	4	44.96
محطات متفرقة	6	34.02
طريق اوباري غات	15	187.5
طريق سبها الجفرة	12	150.00
الإجمالي	172	1478.24

بلغ عدد منظومات الخلايا الشمسية التي تم تركيبها من قبل شركة المدار الجديد مع منتصف سنة 2010 عدد 172 محطة ، وبقدرة إجمالية قدرها 1478 كيلو واط ذروة، وبالتالي تحتل شركة المدار الموقع الأول من حيث عدد المحطات والقدرة المركبة في ليبيا إذ تقدر القدرة الإجمالية المركبة من شركة المدار بثلث ما تم تركيبه في جميع أنحاء ليبيا على مدى ثلاثين سنة. هذه المنظومات تعمل بدون توقف منذ تركيبها وباعتمادية عالية وبدون تكاليف تشغيل تذكر.

4. أداء منظومات الخلايا الشمسية

تم اختيار واحدة من المنظومات التي تم تركيبها كحالة دراسية لتقييم أداء منظومات الخلايا الشمسية العاملة في شركة المدار ، المحطة التي تم اختيارها هي المحطة رقم RP02 بمنطقة السدادة وقد تم تركيبها في شهر 8/ 2009 ، هذه المحطات مزودة بوحدة تخزين المعلومات وقد تم تجميع البيانات لمدة عشرة أشهرا وقمنا بتقييم هذه المنظومات بالطريقة التي اعتمدتها وكالة الطاقة الدولية (IEA PVPS) [6] وكذلك معامل الاستخدام [7].

4-1 الطاقة المتاحة Potential Energy

الطاقة المتاحة هي الطاقة التي يمكن الحصول عليها من مسطحات المنظومة .ومن النتائج المسجلة فقد وجدنا أن معدل الطاقة المتاحة من المنظومة هي 58.76 كيلو واط ساعة لكل يوم ، كما ان اقصى طاقة متاحة مسجلة خلال يوم واحد (21-7-2010) هي 82.6 كيلو واط ساعة لليوم الواحد، ومتوسط أقصى طاقة متاحة مسجلة في شهر واحد هو 63.3 كيلو واط ساعة لكل يوم ، ومتوسط الطاقة المتاحة المسجلة خلال شهر 12/2009 هو 50.3 كيلو واط ساعة

لكل يوم. هذه القيم التي تم تسجيلها تعتبر ارقاما عالية في هذا المجال وهذا يدل على أن الطاقة المتاحة باستخدام منظومات الخلايا الشمسية تقدر بحوالي خمسة أضعاف القدرة المركبة.

2-4 طاقة المسطحات Array Energy

طاقة خرج المسطحات هي الطاقة الصادرة من مسطحات المنظومة وهذه الطاقة تعتمد على الطاقة المستخدمة خلال اليوم الواحد ومستوى شحن البطاريات.ومن النتائج المسجلة فقد وجدنا أن معدل طاقة خرج المسطحات من المنظومة 24.9 كيلو واط ساعة لكل يوم ، كما ان اقصى طاقة مسجلة في يوم واحد (27-7-2009) هي 34 كيلو واط ساعة ، ومتوسط أقصى طاقة مسجلة في شهر واحد هي 29.7 كيلو واط ساعة لكل يوم.

3.4 طاقة الحمل Load Energy

طاقة الحمل هي الطاقة الحمل المتصل بالمنظومة وهذه الطاقة تعتمد على الطاقة المستخدمة خلال اليوم الواحد. ومن النتائج المسجلة فقد وجدنا أن معدل طاقة الأحمال من المنظومة خلال العشرة أشهر هي 22.7 كيلو واط ساعة لكل يوم ، كما ان اقصى طاقة الحمل المسجلة في يوم واحد (15-7-2010) هي 30.1 كيلو واط ساعة ، ومتوسط أقصى طاقة مسجلة في شهر (9-2009) واحد هي 25.6 كيلو واط ساعة لكل يوم الشكل (2) يبين منحنى مقارنة الطاقة المتاحة وطاقة خرج المسطحات وطاقة الحمل

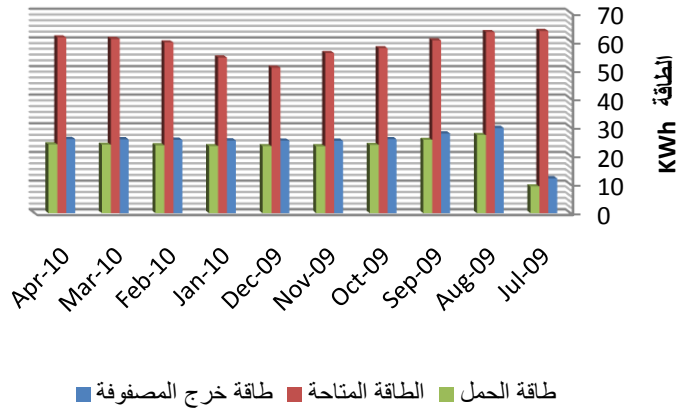

شكل (2) مقارنة الطاقة المتاحة والمنتجة وطاقة الحمل

4.4 معامل الاستخدام Usage factor

هذا المعامل يدل على كيفية استخدام الطاقة المتاحة من المنظومة ، فإذا تم استغلال جميع الطاقة المتاحة فأن معامل الاستخدام يقترب من الواحد، وعند تقييم معامل الاستخدام لمنظومات الخلايا الشمسية المستخدمة في شركة المدار تبين أن معدل هذا المعامل هو 42% وهذا المعامل يعتبر منخفض في مثل هذا النوع من التطبيق ، كما ان اقصى معامل استخدام تم تسجيله في شهر واحد هو 50 %.

5.4 نسبة الأداء Performance Ratio

هذا المعامل يدل على مستوى انتاجية وجودة مصفوفة المسطحات والمنظومة ، فإذا كانت انتاجية المسطحات عالية وكذلك المنظومة، فإن ما يتم انتاجه يتم استهلاكه، وعند تقييم معامل الاستخدام لمنظومة الخلايا الشمسية المستخدمة في شركة المدار تبين أن معدل هذا المعامل هو 31 % وهذا القيمة تعتبر منخفضة في مثل هذا النوع من التطبيق ، كما ان اقصى معامل أداء تم تسجيله في شهر واحد (12-2009)

هو 32%. الشكل رقم (3) يبين معاملا الاستخدام والأداء للمنظومة.

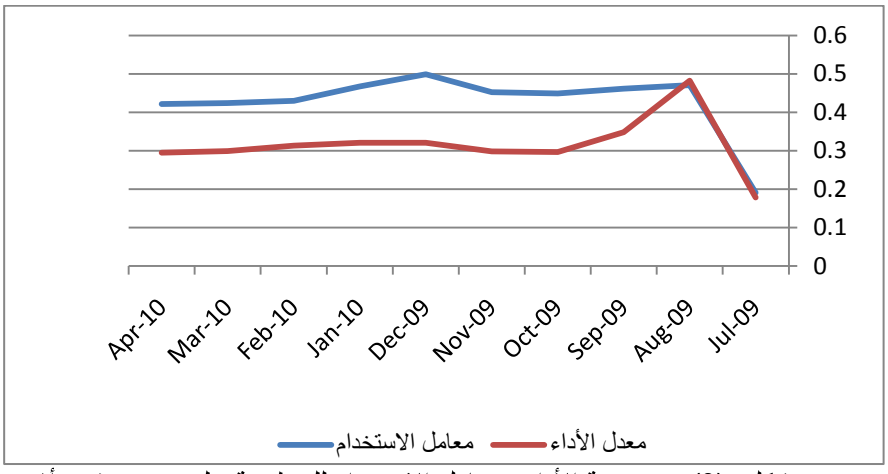

شكل: (3) يبين نسبة الأداء ومعامل الاستخدام للمنظومة على مدى عشرة أشهر

6.4 فقد الاقتناص Capture Loss

معامل فقد الاقتناص يدل على كمية الطاقة التي لم يتم اقتناصها من الطاقة المتاحة التي يمكن إنتاجها من مصفوفة المنظومة، وعند تقييم معامل فقد الاقتناص لمنظومة الخلايا الشمسية المستخدمة في شركة المدار تبين أن معدله هو 3.7 كيلواط ساعة/ كيلواط ذ، أي إن إجمالي الطاقة التي يمكن إنتاجها ولم يتم الاستفادة منها هي 47 كيلواط ساعة لكل يوم، وهذا يدل على أن المنظومة أكبر مما يجب. كما إن أقصى معامل اقتناص تم تسجيله في شهر واحد (10-2009) هو 4.2 كيلواط ساعة/ كيلواط ذ.

7.4 فقد المنظومة System Losses

هذا الفقد يدل على الطاقة المفقودة في مكونات المنظومة والمفقودة نتيجة لعدم موائمة مكوناتها مع بعض، وعند تقييم معامل الاقتناص لمنظومة الخلايا الشمسية المستخدمة في شركة المدار تبين أن معدل هذا المعامل هو 0.16 كيلواط ساعة/ كيلواط ذ، أي أن إجمالي الطاقة التي تفقد في المنظومة ولم يتم الاستفادة منها هي 2.1 كيلواط ساعة لكل يوم، وهذا فقد مقبول. كما أن أقصى معامل فقد تم تسجيله في شهر واحد (10-2009) هو 0.2 كيلواط ساعة/ كيلواط ذ أي 2.5 كيلواط ساعة لكل يوم.

8.4 العائد الطاقي اليومي للمنظومة Daily Energy Yield

الشكل رقم (4) يبين العائد الطاقي اليومي وفقد الاقتناص وفقد المنظومة.

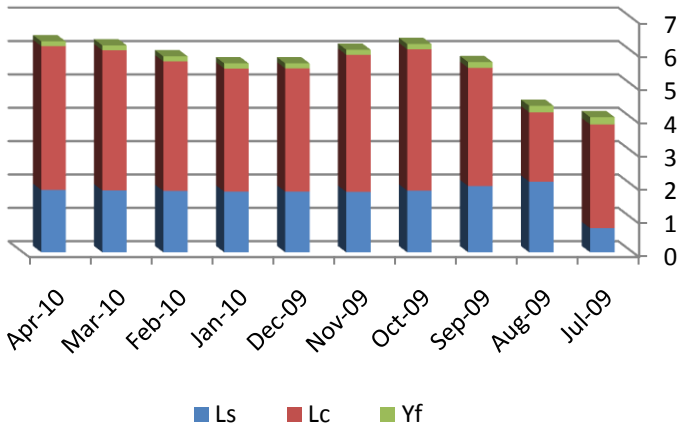

شكل (4) يبين العائد الطاقي Yf اليومي وفقد الإقتناص Lc وفقد المنظومة Ls للمنظومة على مدى عشرة أشهر.

9.4 الكفاءة الكلية Global efficiency

معامل الكفاءة الكلية يدل على كيفية استخدام الطاقة المتاحة من المنظومة ، فإذا تم استغلال جميع الطاقة المتاحة فأن الكفاءة الكلية ستكون أكبر ما يمكن ، وعند تقييم الكفاءة الكلية لمنظومات الخلايا الشمسية وجدنا أن معدل الكفاءة الكلية هو 24.5 % وهذا المعدل يعتبر ضعيفا في مثل هذا النوع من التطبيق ، كما ان اقصى كفاءة كلية تم تسجيلها في شهر واحد هي 29%. الشكل (5) يبين الكفاءة الكلية للمنظومات.

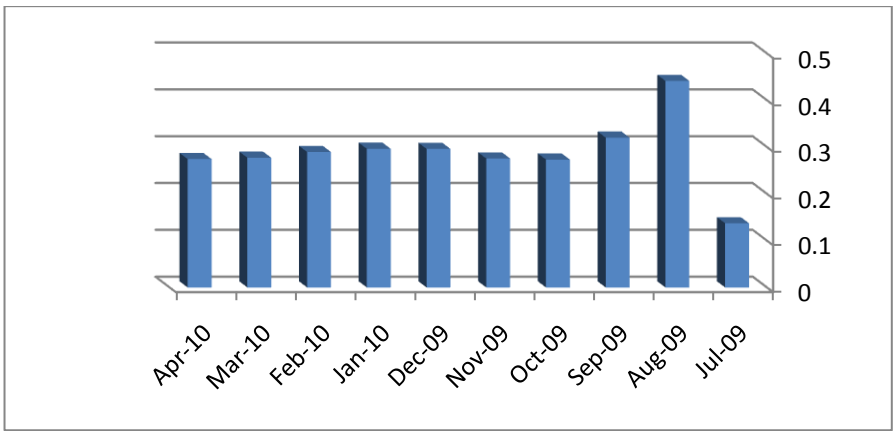

شكل: (5) يبين الكفاءة الكلية للمنظومة على مدى عشرة اشهر

يتبين من منحنيات تقييم الأداء لمنظومة الخلايا الشمسية أن الطاقة المتاحة تقدرب 4.6 ضعف القدرة المركبة وأن أقصى قيمة سجلت هي 6.25 ضعف. وهذا يعني أنه لا يتم استغلال جميع الطاقة المتاحة من المنظومة، وأن اجمالي معدل الفقد في المنظومة هو 50 كيلو واط ساعة لكل يوم وهذا معدلا عالي جدا في هذا النوع من المنظومات المنفردة. وهذا يدل على ان الطاقة المتاحة من المنظومة لم يتم استغلالها ،بل انها لم تستخدم أكثر من نصف طاقتها المتاحة لأن معدل معامل الاستخدام هو 42% ، ومعدل معامل الأداء 31%.

5. الطاقة الكهربائية المنتجة والطاقة المتاحة وكميات ثاني أكسيد الكربون التي تم منعها من الانبعاث باستخدام منظومات الطاقة الشمسية

بناء على ما سبق يمكن تقدير ما يلي:

1. تقدر أيام التشغيل الإجمالية لجميع محطات منظومات الخلايا الشمسية بشركة المدار حتى تاريخ 2010/7/15 ،ب 81411 يوم منظومة أي 223 سنة منظومة.
2. تقدر الطاقة الإجمالية التي تم إنتاجها باستخدام جميع منظومات الخلايا الشمسية على مدى مدة التشغيل حتى تاريخ 2010/7/15، ب 2794.084 ميجاواط ساعة.
3. تقدر الطاقة الإجمالية المتاحة التي يمكن إنتاجها باستخدام جميع منظومات الخلايا الشمسية على مدى مدة التشغيل حتى تاريخ 2010/7/15، ب 4657 ميجاواط ساعة.
4. تقدر كميات ثاني أكسيد الكربون التي تم منعها من الانبعاث باستخدام منظومات الخلايا الشمسية بدلا من الشبكة العامة على مدى مدة التشغيل حتى تاريخ 2010/7/15 1872 طن.
5. تقدر كميات ثاني أكسيد الكربون التي تم منعها من الانبعاث باستخدام منظومات الخلايا الشمسية في حال استعمال مولدات الديزل على مدى مدة التشغيل حتى تاريخ 2010/7/15 4470 طن.

6- الخلاصة

تبرز هذه الورقة أهمية استخدام منظومات الخلايا الشمسية لتوليد الطاقة الكهربائية من الطاقة الشمسية في مجال كهربة محطات تغطية الهاتف النقال في شركة المدار ودورها في توسيع رقعة الاتصالات . يصل عدد المحطات التي تم تركيبها خلال ثلاثة سنوات إلى 172 محطة وبقدرة إجمالية 1478 كيلواط ذ وهذه القدرة تقدر بثلث القدرة الإجمالية المركبة في ليبيا، ساهمت منظومات الخلايا الشمسية التي تم تركيبها في حبس طن من غازات ثاني أكسيد الكربون في حال استخدام مولدات الديزل، المحطات التي تم تركيبها يمكنها تغذية ضعف الأحمال القائمة، أثبتت العديد من المحطات ديمومتها وقد فاقت في ذلك على بعض المحطات العاملة على الشبكة العامة.

7- المراجع

1. Ibrahim Saleh, ..etal, Photovoltaic Power Supplies for Microwave Repeater Stations in Libya, The second world conference on photovoltaic, Vienna, Austria, July 1998.
2. Ibrahim M. Saleh Ibrahim, M. Ali Ekhlat, Rural electrification using photovoltaic for isolated areas in Libya.

The eightieth Arab Conference for Solar Energy, Bahrain 2004

3. **Ibrahim Saleh, ..etal** Experience of standalone photovoltaic systems for telecommunication networks in Libya, The 23th European Photovoltaic Solar Energy Conference, taking place Spain 2008.
4. **Ibrahim Saleh, ..etal** Experience of standalone photovoltaic systems for telecommunication networks in Libya, The 23th European Photovoltaic Solar Energy Conference, taking place Spain 2008.
5. **Ibrahim Saleh, ..etal** Performance of thirty years stand alone photovoltaic system, The 24th European Photovoltaic Solar Energy Conference, taking place in Germany 21-25/9/2009.
6. R. Ramakumar ,Photovoltaic systems IEEE Proceeding Vol. 81 No 3, 1993
7. Didier Mayer, M. Heidenreich, "Performance Analyses of Stand Alone Systems from ay Rational Use of Energy Point of view.

نموذج لتقدير مساهمة تقنية المعلومات والاتصالات في التنمية

د. عبد القادر الصادق عكي د. موسى محمد موسى د. محمد سمير البوني
كلية الهندسة – جامعة الفاتح

ملخص:
تستعرض هذه الورقة بعض الرؤى لمفهوم التنمية ومفهوم تقنية المعلومات والاتصالات ومؤشرات قياسها وتقترح تصوراً لكل منهما مع تحديد الأركان والمحاور الرئيسية لهما والعوامل المؤثرة في تحقيق التنمية الوطنية. كما تقدم تصوراً للعلاقات بين عناصر التنمية وعناصر تقنية المعلومات والاتصالات.
بعدها تقترح نموذجاً رياضياً لتقدير معامل التنمية الوطنية وتقدير مدى مساهمة تقنية المعلومات والاتصالات في التنمية الوطنية. وهذا النموذج يعتمد على عدة عوامل هي نسبة مساهمة أركان التنمية في التنمية الوطنية ومعاملات تنمية أركان التنمية، ومعاملات تنمية القطاعات المختلفة. وقد تم اقتراح منهجية لتحديد معاملات النموذج الرياضي وكيفية استخدامه.
ويعتبر هذا النموذج إطاراً نظرياً يتطلب اختباره وتحسينه تدريجياً من خلال الحصول على المعلومات الأساسية المتعلقة بعناصر التنمية وعناصر تقنية المعلومات والاتصالات للدول المختلفة وذلك من خلال الاستبيانات والمعلومات المتاحة بالمنظمات الدولية ذات العلاقة وبتطبيق هذا النموذج نرى أنه سيساعد الدول في إعداد خططها التنموية واولوياتها كما سوف يساعد الدول والمنظمات المانحة في تحديد أولوية دعمها للمشاريع التنموية للدول المستفيدة.

1 - مقدمة:

من المواضيع الهامة التي استحوذت اهتمام المنظمات والهيئات الدولية مثل الأمم المتحدة والاتحاد الدولي للاتصالات ومنظمة اليونسكو وغيرها هي قياس مساهمة تقنية المعلومات والاتصالات في التنمية الوطنية وقد تم تأسيس شراكة عالمية خلال السنوات الثلاث الماضية لهذا الغرض تضم هذه الشراكة أربع لجان إقليمية للأمم المتحدة هي اللجان الاقتصادية والاجتماعية لكل من غرب آسيا، وافريقيا، وامريكا اللاتينية والبحر الكاريبي وآسيا والمحيط الأطلسي، وكذلك مؤتمر الأمم المتحدة للتجارة والتنمية ومعهد اليونسكو للإحصاء، والمصرف الدولي والاتحاد الدولي للاتصالات ومنظمة التعاون والتنمية في المجال الاقتصادي.

تعتبر هذه الورقة محاولة للوصول إلى نموذج لتقدير مدى مساهمة تقنية المعلومات والاتصالات في التنمية منطلقاً من الأركان الأساسية للتنمية والعناصر الأساسية لتقنية المعلومات والاتصالات، وكذلك من التأثيرات والعلاقات المستنبطة في الدراسات السابقة، وقد تم إعداد هذه الورقة لتشمل تصورات للتنمية وتقنية المعلومات والاتصالات، ثم تقدم بعض

التساؤلات المطروحة على الساحة البحثية، وتقدم تصوراً للعلاقات بين عناصر التنمية وعناصر تقنية المعلومات والاتصالات تم تقدم النموذج المقترح ومنهجية لتكوينه واستخدامه.

2- تصورات لمفهوم التنمية الوطنية:

توجد تصورات متعددة لمفهوم التنمية [1] نذكر منها:

1 -التنمية هي تطوير وتحديث، وتتطلب الآتي:

- استخدام التقنية وامكانياتها.
- توفر رأس المال.
- توفر القوى البشرية الماهرة.
- العزيمة لتحقيق النمو.

ومن خلال التجربة تبين عدم صلاحية مفهوم التنمية كتطوير أو تحديث لأنها لا تأخذ الثقافة والظروف المحلية والاجتماعية في الاعتبار.

2 -التنمية هي تحقيق الاستقلالية أي امتلاك السبل والامكانيات والعمليات المطلوبة للوصول إلى الغنى.

3 -التنمية هي تنمية الموارد البشرية والتي تقاس بعدد من المؤشرات هي:

- معامل تنمية الانسان (HDI) Human Development Index .
- معامل تنمية الجنس (GDI) Gender Development Index.
- مقياس مدى المساواة بين الجنسين (GEM) Gender Equity Measure.
- معامل الفقر البشري (HPI) Human Proverty Index.

ويعتمد معامل تنمية الإنسان على :

أ. طول العمر المتوقع عند الولادة.
ب. مستوى التعليم.
ج. اجمالي الناتج القومي للفرد.

4 -التنمية من خلال منظور توفير آليات التمكين للإنسان مثل:

أ. خيارات التمكين في التعليم والصحة ومستوى المعيشة.
ب. بناء المجتمع الديمقراطي.
ج. ج- تحسين إدارة التصرف والفهم الثقافي.

التصورات المقترحة:

التصور الأول:

التنمية الوطنية هي الانتقال من مستوى معين للوطن إلى مستوى أفضل من حيث:

أ. استغلال الموارد الطبيعية والصناعية والإمكانيات المتاحة.
ب. استغلال وتطوير الموارد البشرية.
ج. مستوى جودة الخدمات.
د. مستوى المعيشة والرفاهية للأفراد.
ه. مستوى الناتج المحلي الإجمالي.

والعوامل المؤثرة في عملية الانتقال هي:

أ. رأس المال.
ب. التقنية والوسائل والأدوات.
ج. السياسات والخطط والبرامج.
د. البنية الأساسية والبيئة المحيطة.
ه. الحكم وإدارة الدولة.

ويوضح الشكل (1) هذا التصور

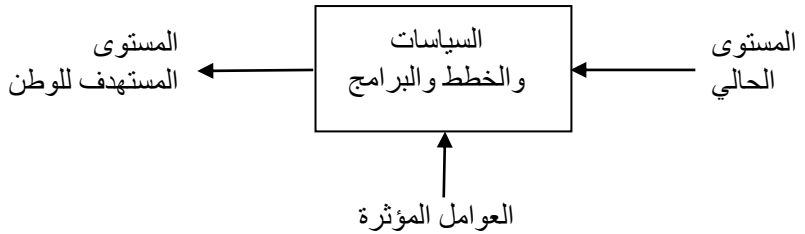

شكل (1) تصور للتنمية الوطنية

التصور الثاني:

التنمية هي استغلال وتطوير الموارد والإمكانيات والقدرات المحلية بما يدعم الاقتصاد ويحسن الخدمات ويعظم إجمالي الناتج المحلي ويحقق الرفاهية والرخاء للمواطن والوطن، ويساهم في تحقيق الاستقلالية والاكتفاء الذاتي. وتتم التنمية من خلال تنمية أركانها ودعائمها الأساسية.

ويمكن تصور التنمية كهيكل يتكون من قاعدة أساسية وأركان أو دعائم رئيسية كما هو موضح بالشكل (2).

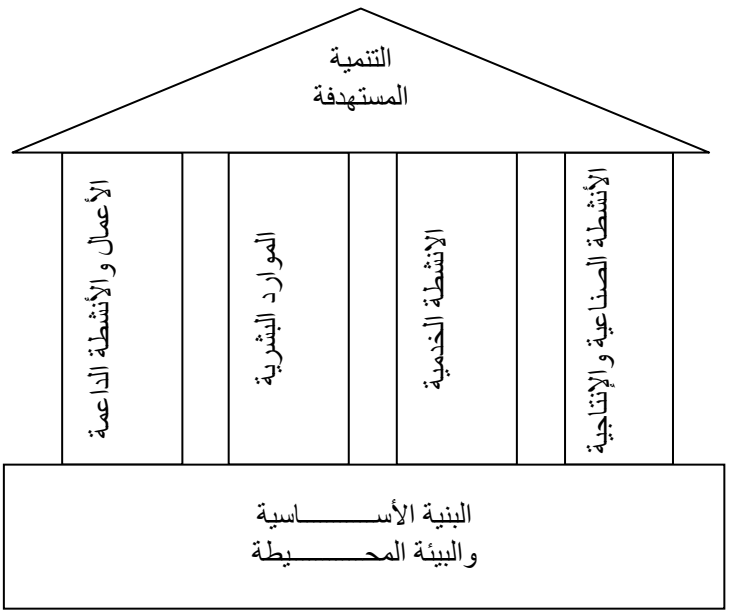

شكل (2) تصور عام لهيكل التنمية

وتتم عملية التنمية من خلال تنمية هيكليتها على النحو التالي:

1 - تنمية البنية الأساسية والبيئة المحيطة.
2 - تنمية الأنشطة الصناعية والإنتاجية.
3 - تنمية الأنشطة الخدمية.
4 - تنمية الموارد البشرية.
5 - تنمية الأعمال والأنشطة الداعمة.

ويتضمن كل من هذه الأركان أو المحاور عدد من القطاعات التي يتطلب تنميتها للوصول إلى تحقيق التنمية في هذه المحاور وهي كما يلي:

1 - تنمية البنية الأساسية والبيئة المحيطة يتطلب تنمية القطاعات الآتية:
- الإسكان والمرافق.
- المواصلات.
- الكهرباء والمياه والغاز.
- الاتصالات.
- البيئة.

2 - تنمية الأنشطة الصناعية والإنتاجية يتطلب تنمية القطاعات الآتية:
- الصناعة.
- الزراعة والثروة الحيوانية.
- الثروة البحرية.
- النفط والغاز.

3 - تنمية الأنشطة الخدمية يتطلب تنمية القطاعات الآتية:
- الصحة.
- الاتصالات وتقنية المعلومات.
- التجارة والسياحة.
- الاقتصاد والمالية.
- الخدمات الاجتماعية.
- الخدمات الإدارية.

4 - تنمية الموارد البشرية يتطلب تنمية القطاعات الآتية:
- التعليم والبحث العلمي.
- القوى العاملة والتدريب.
- الصحة والضمان الاجتماعي.
- الشباب والرياضة.
- الثقافة والإعلام.

5 - تنمية الأعمال والأنشطة الداعمة يتطلب تنمية القطاعات الآتية:
- التخطيط.
- العدل.
- الأمن.
- الاتصال الخارجي والتعاون الدولي.
- الحكم وإدارة الدولة.

ويوضح الجدول (1) ملخص لهذه المحاور ونسب مساهمتها:

جدول (1) محاور التنمية ونسب مساهمتها

م	المحور	نسبة مساهمة المحور	عدد القطاعات والجهات التابعة
1	البنية الأساسية والبيئة المحيطة	A_1	5
2	الأنشطة الصناعية والإنتاجية	A_2	4
3	الأنشطة الخدمية	A_3	6
4	الموارد البشرية	A_4	5
5	الأعمال والأنشطة الداعمة	A_5	5
		%100	25

3 ـ تصورات لتقنية المعلومات والاتصالات

توجد عدة تصورات لتقنية المعلومات والاتصالات فهناك من ينظر إليها كمنتوج من صنع الإنسان، وهناك من يصنفها من منظور البشر إليها أو من خلال استعمالاتها أو من خلال كيفية تأثيرها على التنمية[1].

وهناك من ينظر إليها كأداة أو معدة، أو أجهزة حواسيب، أو وسيلة تمكين أوتخويل لأداء أعمال محددة. وهناك أيضاً من ينظر إليها من خلال استخداماتها والتي يمكن أن تكون كسلعة أو منتوج، مثل الحواسيب وأجهزة ومعدات الاتصالات وشبكات الاتصالات ومعدات تخزين واستخراج المعلومات وغيرها. كما يمكن أن تكون كداعم للأنشطة العامة للتنمية التي تتضمن:

- التخطيط للتنمية.
- إدارة التنمية.
- المشروعات.
- تطوير التدريب.
- دعم المؤسسات المرتبطة بالتنمية.

كما يمكن أن تكون كمحرك للإقتصاد بما يشمل:

- تنمية البنية الأساسية.
- التعليم.
- تنمية القطاع الخاص.
- تحسين الإنتاجية والجودة.

كما يمكن توجيهها لتنمية نشاطات محددة.

المفهوم الواسع لتقنية المعلومات والاتصالات هو كل ما يتعلق بالأجهزة الحاسوبية والمنظومات والبرمجيات والمنتجات والخدمات والأساليب المتعلقة بإنتاج وتجميع وتخزين واسترجاع ومعالجة وتحليل المعلومات وكذلك كل ما يتعلق بالأجهزة والمعدات والشبكات المحلية والوطنية والدولية المطلوبة لنقل وتبادل المعلومات من موقع إلى آخر. واستخدامها في التطبيقات والمجالات المختلفة.

ولذلك فإن قطاع تقنية المعلومات والاتصالات يتضمن كل من قطاع صناعة تقنية المعلومات والاتصالات وقطاع خدمات تقنية المعلومات والاتصالات وقطاع إنتاج المادة (المحتوى) والوسائط.

عناصر وأركان تقنية المعلومات والاتصالات:

يمكن تحديد عناصر وأركان تقنية المعلومات والاتصالات كما يلي:

1 - رأس المال.
2 - الدعم التشريعي والقانوني.
3 - التخطيط والإدارة.
4 - الأجهزة والمعدات والشبكات.
5 - التطبيقات والاستخدامات
6 - العناصر البشرية المؤهلة.

ويمكن تمثيلها على هيئة قاعدة أساسية ودعائم حيث تمثل العناصر الثلاثة الأولى القاعدة الأساسية وتمثل العناصر الثلاثة الأخرى الدعائم الرئيسية كما هو موضح بالشكل (3).

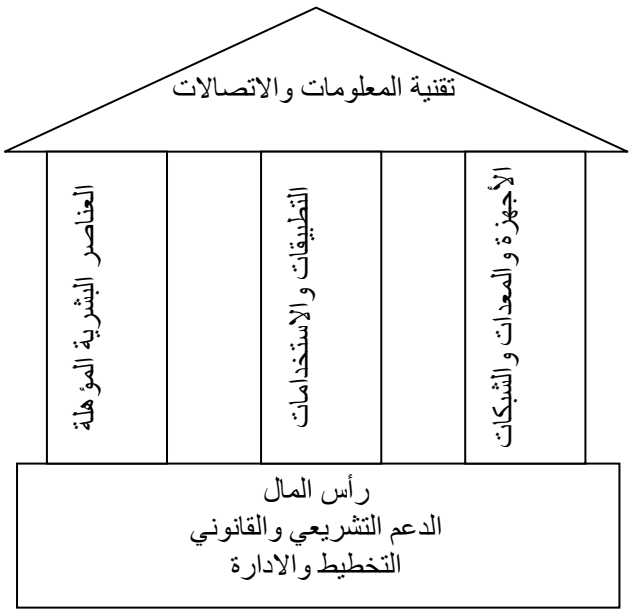

شكل (3) تصور لهيكل تقنية المعلومات والاتصالات

كما يمكن تمثيل تقنية المعلومات والاتصالات على هيئة طبقات حيث تمثل العناصر الثلاثة الأولى الطبقة الأساسية الأولى ويمثل عنصري الأجهزة والمعدات والشبكات والعناصر البشرية المؤهلة الطبقة الثانية ويمثل عنصر التطبيقات والاستخدامات الطبقة الثالثة كما هو

موضح بالشكل (4).

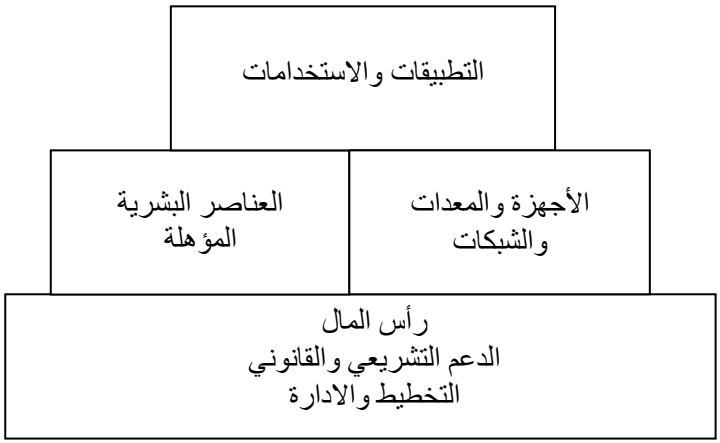

شكل (4) تصور لطبقات هيكل تقنية المعلومات

متطلبات نمو وانتشار تقنية المعلومات والاتصالات

لكي تحقق تقنية المعلومات والاتصالات النمو والانتشار المستهدف لابد من إعداد السياسات والخطط واتخاذ الإجراءات المطلوبة بما يحقق النمو المستمر للأركان الخمسة لتقنية المعلومات والاتصالات المشار إليها أعلاه وكذلك للعوامل الأخرى ذات العلاقة.

والمتطلبات الأساسية لهذا النمو هي كما يلي:

1. توفر الأجهزة والمعدات والشبكات المحلية والوطنية والدولية
2. ضمان جودة خدمات الاتصالات
3. توفر رأس المال المطلوب
4. توفير الدعم التشريعي والقانوني
5. الخطط والبرامج والسياسات والادارة الرشيدة
6. العناصر البشرية المؤهلة
7. توفير المناخ والبيئة المحفزة
8. تسهيل عملية اقتناء واستخدام التقنية

معايير تقييم انتشار تقنية المعلومات والاتصالات

لتقييم مدى انتشار تقنية المعلومات والاتصالات في أي بلد، استحدث الإتحاد الدولي للاتصالات (معامل النفاذ الرقمي (DAI) Digital Access Index والذي يعتمد على الآتي:

1. البنية التحتية للاتصالات المتاحة بالبلد

2. القدرة على اقتناء التقنية
3. المستويات التعليمية المتوفرة
4. جودة خدمات تقنية المعلومات والاتصالات المتاحة
5. مدى استعمال الإنترنت

ويدخل في حساب هذا المعامل العناصر التالية:

1. عدد مشتركي الهاتف الثابت لكل 100 مواطن.
2. عدد مشتركي الهاتف النقال لكل 100 مواطن.
3. تسعيرة استخدام الإنترنت لمدة (20) ساعة في الشهر كنسبة من دخل المواطن الشهري.
4. عرض نطاق الوصلة الدولية للإنترنت لكل مواطن.
5. عدد مشتركي الإنترنت بنطاق واسع لكل 100 مواطن.
6. عدد مستخدمي الإنترنت لكل 100 مواطن.

4- التساؤلات المطروحة على الساحة البحثية:

التساؤلات التي يطرحها الأكاديميون والبحاث والمهتمون بتقنية المعلومات والاتصالات والمؤسسات الدولية والإقليمية حول تأثير تقنية المعلومات والاتصالات على التنمية هي عديدة ومتشعبة ومرتبطة ببعضها، نذكر منها ما يلي:

أ - كيف تحدث التنمية الوطنية؟ وما هي العوامل والعمليات والإجراءات والسياسات والمعايير التي على أساسها نستطيع الحكم بأن دولة ما تتطور وتنمو أو سائرة في طريق النمو؟

ب -كيف نؤثر على هذه العوامل إيجابياً لكي نحدث التنمية الوطنية؟

ج - ما هو دور تقنية المعلومات والاتصالات في تأثيرها على هذه العوامل؟

د - كيف نثبت نجاح تقنية المعلومات والاتصالات في تحقيق التنمية؟

ه - كيف يمكن قياس مدى مساهمة تقنية المعلومات والاتصالات في التنمية الوطنية؟

والدراسات والأبحاث مستمرة لمحاولة الإجابة على هذه التساؤلات.

5- استعراض نتائج بعض الدراسات السابقة:

نستعرض فيما يلي نتائج بعض الدراسات السابقة حول تأثير تقنية المعلومات والاتصالات على التنمية والمجتمع، حيث تم تقسيم هذه النتائج إلى عدة محاور على النحو التالي:

أولاً: التمثيل الرياضي لعملية التأثير

1 - معظم الدراسات المتعلقة بتأثير تقنية المعلومات والاتصالات على التنمية هي دراسات نظرية وتتضمن دراسة لحالات محددة.

2 - توجد مجهودات محدودة لإيجاد إطار نظري لربط تقنية المعلومات والاتصالات مع التنمية على المستوي العام بدون الدخول في خصائص محددة.

3 - لتقدير أجمالي القيمة المضافة (Y) لإجمالي الناتج المحلي (GDP) تم استخدام المدخلات المرتبطة بتقنية المعلومات والاتصالات، والمدخلات الأخرى مثل رأس المال (K) وراس المال البشري (H) والقوى العاملة (N) كما هو مبين بالمعادلة الآتية [2].

$$Y_t = Y(Y_t^{ICT}, Y_t^{O}) = A_t f(C_t, K_t, H_t, N_t)$$

حيث أن t تمثل الزمن و Y^{ICT} هي القيمة المضافة من السلع والخدمات التي سببتها تقنية المعلومات والاتصالات، و Y^0 هي القيمة المضافة من السلع والخدمات التي سببتها المدخلات والمنتجات الأخرى بدون تقنية المعلومات والاتصالات.

4 - استخدمت طريقتين لتقدير تأثير الاستثمار في تقنية المعلومات والاتصالات على النمو الاقتصادي [2] وهي:

أ -طريقة دالة الإنتاج (Production Function Approach).

ب -طريقة حساب النمو (Growth Accounting Approach).

والصيغة العامة لطريقة دالة الإنتاج هي:

$$Y = AC^{\alpha_c} K^{\alpha_k} H^{\alpha_h} N^{\alpha_n}$$

والصيغة اللوغارثمية لها هي :

$$\ln Y = \ln A + \alpha_c \ln C + \alpha_k \ln K + \alpha_h \ln H + \alpha_n \ln N$$

حيث أن الرمز:

A يمثل التغيرات التقنية.

C يمثل الاستثمار في تقنية المعلومات والاتصالات.

K يمثل رأس المال المستثمر.

H يمثل رأس المال البشري.

N يمثل القوي العاملة.

والمعاملات:

α_c يمثل نسبة مساهمة تقنية المعلومات والاتصالات في الدخل الكلي.

α_k يمثل نسبة مساهمة رأس المال المستثمر.

α_h يمثل نسبة مساهمة رأس المال البشري.

α_n يمثل نسبة مساهمة القوي العاملة.

5 - المتغيرات الأساسية في الاقتصاد الكلي (macro) هي [4]:

أ - الناتج المحلي الإجمالي.

ب - الاستثمار.

ج - التوظيف أو التشغيل.

د - الصادرات.

والسؤال المطروح هو: هل مساهمة تقنية المعلومات والاتصالات تتزايد في بعض أو كل من هذه المتغيرات؟

6 - المتغيرات الأساسية في تقنية المعلومات والاتصالات هي:
أ - خدمات تقنية المعلومات والاتصالات مثل الانترنيت والاتصالات.
ب معدات تقنية المعلومات والاتصالات مثل عدد الحواسيب وعدد الخطوط الهاتفية.
ج - التشغيل أو التوظيف لهذه الخدمات والمعدات.

ثانياً: النسق والعلاقات المستنتجة [6،10]

النسق والعلاقات التي تم استنتاجها من دراسات سابقة هي كما يلي:

1 - كلما تحسنت شبكات الاتصالات كلما تم الحصول على دخل عالي، وكلما زاد الدخل تحسنت شبكات الاتصالات.
2 - من خلال دراسات لعدد 92 دولة خلال الفترة من عام 1980 إلى 2003 تبين إن هناك علاقة خطية بين زيادة كثافة مشتركي الاتصالات وإجمالي الناتج المحلي GDP.
3 - تراوح معدل النمو السنوي المركب لإجمالي الناتج المحلي بسبب الاتصالات ما بين 0.2 % في أمريكا إلى 3.3% في ايطاليا.
4 - معدل نمو عدد الهواتف النقالة لكل 100 مواطن خلال السنوات 1996-2003 كان 64% ونمو إجمالي الناتج المحلي كان 2% خلال نفس الفترة.
5 - من خلال دراسة لعدد 38 دولة و260 عملية تقييم تبين أن تضاعف كثافة الهاتف النقال ابتداء من المتوسط العام المعلومات والاتصالات هي: 8% يؤدي إلى زيادة الخرج من نموذج دالة الإنتاج نسبة 10%.
6 - خلال الفترة من 1980 إلى 2003 بينت الدراسات أن زيادة الكثافة الهاتفية بمقدار 10% تعني زيادة في معدل النمو بنسبة 0.6% في الدول المشابهة، وأن تأثير الهاتف النقال في الدول النامية هو ضعف التأثير في الدول المتقدمة.
7 - يمثل قطاع النقل والاتصالات في أوغندا مثلاً 6.3% من إجمالي الناتج المحلي ، وهذا القطاع ينمو بسرعة بسبب الاتصالات.
8 - تتراوح نسبة الاستثمار في تقنية المعلومات والاتصالات في الدول المتقدمة مقارنه بالاستثمار في المجالات الأخرى غير السكن ما بين 10% إلى 33%.
9 - خلال الفترة من 1995 إلى 2002 أظهرت دراسة لدول منظمة التعاون الاقتصادي (OECD) أن الاستثمار في تقنية المعلومات والاتصالات يسبب زيادة في إجمالي الناتج المحلي بنسبة ما بين 0.3% إلى 0.9%
10 - بلغت مساهمة تصنيع معدات تقنية المعلومات والاتصالات في نمو إنتاجية العمال خلال الفترة من 1996 إلى 2002 ما نسبته 0.1% إلى 1%.
11 - الصرف على تقنية المعلومات والاتصالات يعتبر عنصرا مهما جدا في الاقتصاد العالمي، حيث أن ما تم صرفه عليها عام 1997 هو 1800

مليار دولار ويمثل 6% من إجمالي الناتج المحلي العالمي وهذه القيمة اكبر من إجمالي الناتج المحلي لفرنسا مثلا.

12 - في الدول النامية أظهرت الدراسة [10] أن زيادة 10 هواتف نقاله لكل 100 مواطن يزيد معدل نمو إجمالي الناتج المحلي بمقدار 0.6% في السنة.

13 - أظهرت الدراسات أنه كلما زاد مستوى التقنية في الدول النامية كلما زاد إجمالي الناتج المحلي للفرد، أي أن التقنية تلعب دوراً مهما في تنمية الناتج المحلي الإجمالي.

14 - خلال عام 2005 بلغ متوسط نسبة ذوي النشاط الاقتصادي في الوطن العربي ما نسبته 32.7%، وأن معدل البطالة هو مابين 15-20% وهو ضعف المعدل العالمي وتزداد سنويا بمعدل 3%، وأن معدل النمو السكاني خلال الفترة من 1995 إلى 2003 هو 2%.

15 - انخفاض البطالة بنسبة 1% تؤدى إلى زيادة نسبة إجمالي الناتج المحلي بمقدار 3% [9].

16 - تتوفر في الوطن العربي أكثر من 3 ملايين فرصة عمل سنوياً.

ثالثاً: تأثيرات تقنية المعلومات والاتصالات [8,6]

أظهرت الدراسات بأن تقنية المعلومات والاتصالات لها تأثير على الاقتصاد والمجتمع والتنمية كما هو مبين فيما يلي:

1 - التقنيات الجديدة تؤثر على المجتمع من خلال ثلاثة أوجه هي:

أ - التأثير الرئيسي (الأولي) وهو الأبسط ، ينتج عند استبدال التقنيات القديمة بأخرى جديدة وهذا التأثير ضروري لتفعيل التأثيرات الأخرى.

ب - التأثير الثاني هو زيادة استغلال واستخدام التقنيات الجديدة وإمكانياتها.

ج - التأثير الثالث هو توليد الأعمال والوظائف الجديدة المعتمدة على هذه التقنيات الجديدة وإحداث التغيرات الاجتماعية.

2 - تقنية المعلومات والاتصالات تستطيع مساعدة الدول الفقيرة في تجسير مراحل التنمية.

3 - تؤثر تقنية المعلومات والاتصالات على النمو الاقتصادي والإنتاج والإنتاجية من خلال الطرق الآتية:

أ - السلع والخدمات التي تقدمها تقنية المعلومات والاتصالات هي جزء من القيمة المضافة للاقتصاد.

ب - استخدام رأس المال المخصص لتقنية المعلومات والاتصالات من خلال مساهمتها في التطورات والتغيرات التقنية.

ج - تساهم تقنية المعلومات والاتصالات في النمو الاقتصادي من خلال مساهمتها في التطورات والتغيرات التقنية.

واذا اعتمد النمو في انتاج تقنية المعلومات والاتصالات على الاستفادة من الكفاءة الانتاجية للانشطة المختلفة

فإنها ستؤدي إلى الزيادة في نمو الانتاجية على المستوى الاقتصادي العام.

4 - يمكن تلخيص تأثير منظومة الاتصالات فيما يلي:
أ - تنظيم حياة الأسرة والمجتمع.
ب -تنظيم نشاط الأعمال.
ج - زيادة إنتاجية المصانع والقوى العاملة.
د - تقليل تكاليف الإجراءات والعمليات.
ه - توسيع شبكة المزود (البائع) والمشتري.

5 - باستخدام طريقة دالة الإنتاج في تحليل تأثير الاتصالات في دول منظمة التعاون الاقتصادي (OECD) خلال الفترة 1970-1980 تبين إنه يوجد نمو ملحوظ في الناتج المحلي الإجمالي بسبب الاتصالات.

6 - يوجد تأثير تقنية المعلومات والاتصالات على التنمية الاقتصادية من خلال.
أ - تخفيض تكلفة المعاملات التجارية.
ب -زيادة الإنتاجية.
ج - زيادة المنافسة.
د - فرص جديدة للتجارة.
ه - النفاذ إلى المعرفة.
و -تحسين مستوي الاتصالات.

7 - تنمية تقنية المعلومات والاتصالات تؤثر على عدد من العناصر الاجتماعية والاقتصادية التي يمكن تلخيصها في النقاط التالية [8]:
أ - المساهمة في تحسين ودعم الحقوق الإنسانية.
ب -خلق فرص دخل جديدة.
ج - دعم لخدمات البنية الأساسية.
د - دعم الشعور بالإنتماء.
ه - تحقيق الاستمرارية على المدى البعيد.

والقطاعات التي تستفيد من تقنية المعلومات والاتصالات من خلال هذه العناصر موضحة في الجدول (2) .

جدول (2) القطاعات التي تستفيد من تقنية المعلومات والاتصالات [8]

ر.م	القطاع	دعم الحقوق الإنسانية	خلق فرص دخل جديدة	خلق الشعور بالانتماء	دعم خدمات البنية الأساسية	تحقيق الاستمرارية على المدى البعيد
1	النقل	√	√	√	X	X
2	الصحة	X	√	X	X	√
3	التعليم	√	√	√	X	X
4	الزراعة	X	√	X	X	X
5	التصنيع والتجارة	√	√	√	√	√
6	السياحة	√	√	√	√	X
7	المالية والنفط والغاز	X	√	X	√	X

8 - إدخال منظومات الحكومة (الإدارة) الالكترونية هو عنصر أساسي للاستثمار في تقنية المعلومات والاتصالات ووجود هذه المنظومات هو احد الأركان للدول المتقدمة، وقطاعات الحكومة الالكترونية هي التعليم والصحة والعدل والأمن والضرائب وكلها تستهدف تحقيق احتياجات المواطنين.

9 - بينت بعض الدراسات [10] مقدار مساهمة ساعة العمل الواحدة للمواطن على إجمالي الناتج المحلي للدول المختلفة بافتراض أن عدد ساعات العمل السنوية هي 2000 ساعة، أي بمعني إذا قضي المواطن ساعة واحدة في طابور انتظار الحصول على خدمة فإن ذلك المواطن لم يساهم في الناتج المحلى الإجمالي (GDP) ولذلك يمكن القول بأنه فقدت ساعة من المساهمة في الناتج المحلي الإجمالي.
في الدول العشرين في العالم يتراوح الناتج المحلي الإجمالي للساعة الواحدة للفرد ما بين 0.36 دولار في الهند إلى 25.37 دولار في سويسرا [10].

10 - القنوات والمحاور التي تؤثر فيها تقنية المعلومات والاتصالات على التنمية هي:

أ - تأثيرها على التعليم والتعلم أي على طرق وسرعة الحصول على المعرفة لكل القطاعات والمجتمعات.

ب - تأثيرها على الإنتاج وطريقة تنظيم العمليات الإنتاجية وتأثيرها على تنظيم بيئة العمل بما يزيد الإنتاجية وبالتالي زيادة في الدخل والثروة واستحداث طرق جديدة للإنتاج.

ج - تأثيرها على شبكات العمل بما يحسن من طرق أداء الأعمال والأبحاث.

6- العلاقات بين عناصر التنمية وتقنية المعلومات والاتصالات

من خلال الدراسات السابقة تبين وجود علاقة بين عناصر التنمية وتقنية المعلومات والاتصالات ولكي نصل إلى علاقات كمية ومعرفة مدى قوة هذه العلاقة فقد تم أخذ رأي عدد من ذوي الخبرة في المجال وتم التوصل إلى النتائج التالية التي تعبر عن متوسط الأراء.
وقد استخدم التقييم التالي في تحديد مستوى العلاقة:

• علاقة قوية جدا	VH	10 نقاط
• علاقة قوية	H	8 نقاط
• علاقة متوسطة	M	6 نقاط
• علاقة ضعيفة	L	2 نقطة
• لا توجد علاقة	N	0 نقطة

والعلاقات التي أخذت في الاعتبار هي:
أ -علاقة أركان التنمية بمؤشرات التنمية جدول (3):

جدول (3) علاقة أركان التنمية بمؤشرات التنمية

م	مؤشرات التنمية / أركان التنمية	ارتفاع الناتج المحلي الإجمالي	ارتفاع مستوى المعيشة والرفاهية للمواطن	ارتفاع مستوى جودة الخدمات	استغلال وتطوير الموارد والامكانيات	تحقيق الاستقلالية والاكتفاء الذاتي والاستمرارية	الشعور بالحرية والأمن والإنتماء للوطن
1	تنمية البنية الأساسية والبيئة المحيطة						
2	تنمية الأنشطة الصناعية والانتاجية						
3	تنمية الأنشطة الخدمية						
4	تنمية الموارد البشرية						
5	تنمية الأعمال والأنشطة الداعمة						

ب - علاقة مؤشرات التنمية بتقنية المعلومات والاتصالات جدول (4):

جدول (4) علاقة مؤشرات التنمية بتقنية المعلومات والاتصالات

م	مؤشرات التنمية	تقنية المعلومات والاتصالات
1	ارتفاع الناتج المحلي الاجمالي	
2	ارتفاع مستوى المعيشة والرفاهية للمواطن	
3	ارتفاع مستوى جودة الخدمات	
4	استغلال وتطوير الموارد والامكانيات	
5	تحقيق الاستقلالية والاكتفاء الذاتي والاستمرارية	
6	الشعور بالحرية والأمن والانتماء للوطن	

ج -العلاقة بين أركان التنمية وتقنية المعلومات والاتصالات

د - العلاقة بين أركان التنمية وتقنية المعلومات والاتصالات

يتم استنتاج مصفوفة العلاقة بين أركان التنمية وتقنية المعلومات بضرب مصفوفة علاقة أركان التنمية بمؤشرات التنمية [6×5] جدول (3) بمصفوفة العلاقة بين مؤشرات التنمية وتقنية المعلومات والاتصالات [6×1] جدول (4) لكي نحصل على المصفوفة [5×1] الواردة بالجدول (5):

جدول (5) العلاقة بين أركان التنمية وتقنية المعلومات والاتصالات

م	أركان التنمية	تقنية المعلومات والاتصالات
1	تنمية البنية الأساسية والبيئة المحيطة	
2	تنمية الأنشطة الصناعية والانتاجية	
3	تنمية الأنشطة الخدمية	
4	تنمية الموارد البشرية	
5	تنمية الأعمال والأنشطة الداعمة	

د- العلاقة بين قطاعات ركن التنمية بمؤشرات التنمية.

للحصول على علاقة قطاعات ركن من أركان التنمية بمؤشرات التنمية يتم إعداد جدول لكل ركن من أركان التنمية كما هو موضح بالجدول (6) ويتم تعبئته من خلال استبيان لذوي الاختصاص للحصول على مقدار العلاقة.

جدول (6) علاقة قطاعات ركن التنمية (i) بمؤشرات التنمية

	مؤشرات التنمية / القطاع	ارتفاع الناتج المحلي الاجمالي	ارتفاع مستوى المعيشة والرفاهية للمواطن	ارتفاع مستوى جودة الخدمات	استقلال وتطوير الموارد والامكانيات	تحقيق الاستقلالية والاكتفاء الذاتي والاستمرارية	الشعور بالحرية والأمن والانتماء للوطن	مجموع درجات العلاقة	نسبة درجات العلاقة إلى الاجمالي b_{ij}
1									
2									
3									
4									
5									
6									
7									

ويتم تكرار نفس الجدول لكل ركن من أركان التنمية وفق عدد القطاعات التي تكون الركن كما هو موضح في الشكل (5).

هـ- العلاقة بين ركن التنمية وتقنية المعلومات والاتصالات:

يتم استنتاج مصفوفة العلاقة بين قطاعات ركن التنمية وتقنية المعلومات والاتصالات بضرب مصفوفة علاقة قطاعات ركن التنمية بمؤشرات التنمية المبينة في الجدول (6) في مصفوفة العلاقة بين مؤشرات التنمية وتقنية المعلومات والاتصالات المبينة في الجدول (4) لكي نحصل على المصفوف الواردة بالجدول (7) لكل ركن من أركان التنمية.

جدول (7) العلاقة بين قطاعات ركن التنمية بتقنية المعلومات والاتصالات

م	القطاع	درجة العلاقة مع تقنية المعلومات والاتصالات	نسبة درجة العلاقة
1			
2			
3			
4			
5			
6			
7			

7- النموذج المقترح:

للوصول إلى النموذج الرياضي للتنمية المقترح يمكن تصور الموضوع كما هو موضح بالشكل (5) حيث يوضح معاملات أركان التنمية وعلاقاتها بمعاملات القطاعات، وعلاقاتها مع معامل التنمية الوطنية.

لتحويل قيم أي متغير (x) إلى معامل بدون وحدات ($x-index$) نستخدم المعادلة الآتية:

$$x-index=\frac{x-\min(x)}{\max(x)-\min(x)} \quad \ldots\ldots (1)$$

حيث أن $\min(x)$ و $\max(x)$ هما أقل قيمة وأعلى قيمة للمتغير x وتستخدم هذه المعادلة في تحديد معامل نتمية قطاع ما، أو معامل تنمية ركن من أركان التنمية، كما سيرد فيما بعد.

7-1 النموذج الرياضي للتنمية:

نحصل على معامل التنمية الوطنية I_D باستخدام المعادلة الآتية:

$$I_D=\sum_{i=1}^{5} A_i.I_i \quad \ldots\ldots (2)$$

حيث أن I_i هو معامل تنمية الركن i من أركان التنمية

و A_i هو نسبة مساهمة الركن i في التنمية

وللحصول على معامل تنمية ركن التنمية I_i نستخدم المعادلة الأتية:

$$I_i = \sum_{i=1}^{5} b_{ij} x_{ij} \quad .....(3)$$

حيث أن x_{ij} هو معامل تنمية القطاع رقم (j) التابع لركن التنمية (i).

و b_{ij} هو نسبة مساهمة القطاع رقم (j) في ركن التنمية (i).

و n_i هو عدد القطاعات في ركن التنمية (i).

وبالتعويض المعادلة (3) في المعادلة (2) نحصل على المعادلة العامة لمعامل التنمية الوطنية الآتية:

$$I_D = \sum_{i=1}^{n} \sum_{j=1}^{n_i} A_i b_{ij} x_{ij} \quad .....(4)$$

وللحصول على النتيجة النهائية لمعامل التنمية الوطنية I_D يتطلب حساب معامل تنمية كل قطاع من قطاعات التنمية، وتحديد درجة مساهمة ذلك القطاع في تنمية محور التنمية التابع له، وتحديد درجة مساهمة كل محور من محاور التنمية في التنمية الوطنية.

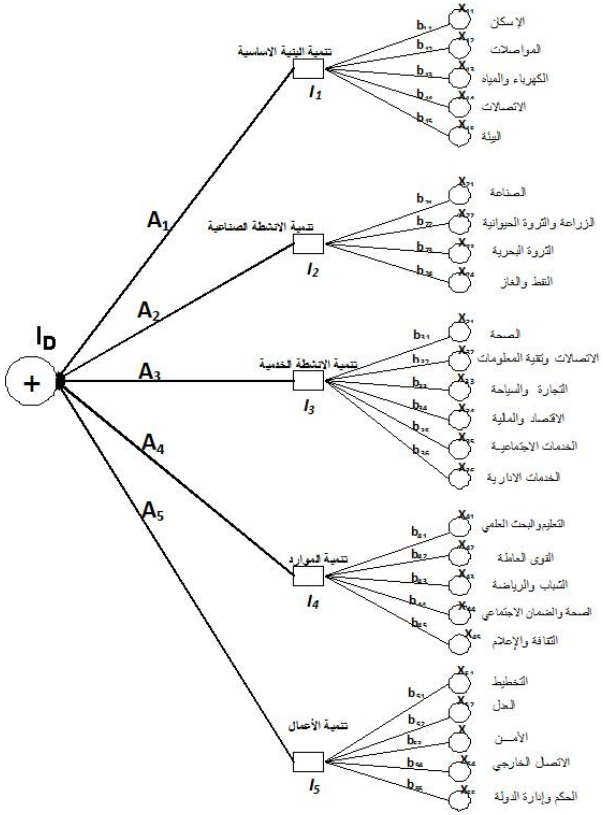

شكل (5) نظرة عامة لمكونات نموذج تقدير معامل التنمية الوطنية

2-7 النموذج الرياضي للتنمية بعد إدخال تأثير تقنية المعلومات والاتصالات

بالرجوع إلى المعادلات (2)، (3)، (4) تكون المعادلة الرياضية لمعامل التنمية الوطنية بعد إدخال تأثير تقنية المعلومات والاتصالات (I_D) كما يلي:

$$I_D' = \sum_{i=1}^{5} A_i . I_i' \quad \ldots\ldots \qquad (5)$$

وأن I_i' هو معامل تنمية ركن التنمية (i) بعد إدخال تأثير تقنية المعلومات والاتصالات والذي نعبر عنه بالمعادلة الاتية:

$$I_i' = \sum_{i=1}^{n_i} b_{ij} x_{ij}' \quad \ldots\ldots \qquad (6)$$

حيث أن x_{ij}' يمثل معامل تنمية القطاع (j) التابع لركن التنمية (i) بعد إدخال تأثير تقنية المعلومات والاتصالات عليه، ويمكن ربط هذا المعامل مع المعامل x_{ij} باستخدام المعادلة الآتية:

$$x_{ij}' = x_{ij} + s_{ij} x_{ij} = x_{ij}(1 + s_{ij}) \quad \ldots\ldots (7)$$

حيث أن معامل s_{ij} هو نسبة زيادة معامل تنمية القطاع (j) التابع للركن (i) نتيجة لتأثير تقنية المعلومات والاتصالات.

وبالتعويض في المعادلة (5)، (6) عن x_{ij}' نتحصل على معامل التنمية الوطنية I_D' بعد إدخال تقنية المعلومات والاتصالات كما يلي:

$$I_D' = \sum_{i=1}^{5} A_i \sum_{j=1}^{n_i} b_{ij} x_{ij} \ (1 + s_{ij}) \ldots\ldots (8)$$

وبذلك نتحصل على نسبة مساهمة تقنية المعلومات والاتصالات في التنمية الوطنية (S) باستخدام المعادلة الاتية:

$$S = \frac{I_D' - I_D}{I_D} = \frac{\sum_{i=1}^{5} A_i \sum_{j=1}^{n_i} b_{ij} x_{ij} \ s_{ij}}{I_D} \quad \ldots\ldots (9)$$

وللوصول إلى هذه النسبة يتطلب الحصول على الآتي:

أ - معاملات النموذج الرياضي وهي A_i التي تمثل نسبة مساهمة المحور (i) في التنمية، و b_{ij} التي تمثل نسبة مساهمة القطاع (j) التابع للمحور (i) في التنمية ويتم الحصول على هذه المعاملات من خلال معلومات واستبيانات لأراء الخبراء المتخصصين يتم اختيارهم على المستوى الدولي.

ب - معاملات تنمية القطاعات x_{ij} ويتم حسابها من واقع المعلومات المتاحة عن كل بلد، ويتم حساب نسبة زيادة هذه المعاملات بسبب تقنية المعلومات s_{ij} من واقع المعلومات المتاحة عن كل بلد.

وبطريقة آخرى مبسطة يمكن التركيز على معامل ركن التنمية I_i' بعد إدخال تأثير تقنية المعلومات والاتصالات والتعبير عنه بالمعادلة الآتية:

$$I_i' = I_i(1+\delta_i) \ldots\ldots (10)$$

حيث أن δ_i هي نسبة زيادة معامل ركن التنمية (i) بسبب تقنية المعلومات والاتصالات وبذلك نستطيع كتابة المعادلة (5) كما يلي:

$$I_D' = \sum_{i=1}^{5} A_i I_i(1+\delta_i) \ldots\ldots (11)$$

وبذلك نتحصل على نسبة مساهمة تقنية المعلومات والاتصالات في التنمية الوطنية (δ) باستخدام المعادلة الآتية:

$$\delta = \frac{I_D' - I_D}{I_D} = \frac{\sum_{i=1}^{5} A_i \delta_i I_i}{I_D} \quad \ldots(12)$$

8- منهجية لاستكمال واستخدام النموذج:

لقد قامت عدة جهات ومنظمات دولية مثل الأمم المتحدة وصندوق النقد الدولي وكتاب الحقائق الصادر من وكالة الاستخبارات الامريكية وغيرها بتصنيف دول العالم ومستويات التنمية فيها ومن هذه التصنيفات:

أ - دول متقدمة (الأعلى نمواً).
ب -دول نامية.
ج - دول في طريق النمو.
د - دول أقل نمواً.

ولتوضيح بعض الاستنتاجات من النموذج المقترح نفترض القيم التالية لمعاملات التنمية لكل صنف من هذه الدول (جدول 8).

جدول (8) معاملات التنمية الافتراضية للدول

م	تصنيف الدول	مقدار معامل التنمية I_D
1	دول متقدمة (الأعلى نمواً)	من 0.8 إلى 1.0
2	دول نامية	من 0.6 إلى 0.80
3	دول في طريق النمو	من 0.4 إلى 0.60
4	دول الأقل نمواً	أقل من 0.4

وقبل أن نصل إلى بعض الاستنتاجات من النموذج سيتم توضيح منهجية للحصول على معاملات النموذج المقترح ومن ثم يسهل استخدام النموذج وتقدير مدى مساهمة تقنية المعلومات والاتصالات في التنمية الوطنية.

وتتلخص خطوات هذه المنهجية فيما يلي:

1 -تشكيل فريق عمل دولي من المتخصصين والمختصين والمهتمين بأمور التنمية الوطنية والتخطيط الاستراتيجي، على أن يضمن هذا الفريق أعضاء من مختلف تصنيفات دول العالم الواردة بالجدول (8) أعلاه. وتوكل لهذا الفريق مهمة الاجابة على الاستبيانات الخاصة بتحديد العلاقات بين مختلف العوامل وفق الجداول المعدة بالخصوص. وبأخذ متوسط آراء الفريق يتم اعداد جداول العلاقات التي تعبر عن متوسط أراء الفريق الدولي كما سيرد فيما بعد.

2 -يتم تحديد نسبة مساهمة كل ركن من أركان التنمية في التنمية الوطنية (A_i) من خلال تعبئة فريق العمل للجدول (3) وأخذ متوسط الاراء وجمع الدرجات التي يتحصل عليها كل ركن من أركان التنمية وقسمة الناتج على إجمالي الدرجات للحصول على نسبة مساهمة الركن (A_i).

3 -يتم تحديد نسبة مساهمة كل القطاع (j) من ركن التنمية (i) في تنمية ذلك الركن (b_{ij}) من خلال تعبئة فريق العمل للجدول (6) وأخذ متوسط الاراء وجمع الدرجات التي يتحصل عليها كل قطاع وقسمة الناتج على اجمالي الدرجات للحصول على نسبة مساهمة ذلك القطاع (b_{ij}).

4 -يتم تحديد علاقة مؤشرات التنمية بتقنية المعلومات والاتصالات من خلال اجابة الفريق على الجدول (4) وأخذ متوسط الاراء للحصول على مصفوفة [1x6] .

5 -الحصول على درجة العلاقة بين أركان التنمية وتقنية المعلومات والاتصالات يتم ضرب المصفوف [6x5] المتحصل عليها من نتائج الجدول (3) في المصفوفة [1x6] المتحصل عليها من الجادول (4) للحصول على مصفوفة [1x5] وهي العلاقة المطلوبة. وبقسمة الناتج في كل صف على إجمالي الدرجات نحصل على نسبة العلاقة δ_i وهي المطلوبة في المعادلة رقم (12) التي تقدم مساهمة تقنية المعلومات والاتصالات في التنمية بدلالة I_i و I_D .

6 -يتم الحصول على علاقة قطاعات ركن التنمية وتقنية المعلومات والاتصالات بضرب النتائج المتحصل عليها بالجدول (6) أي أنها مصفوفة [6x n_i] في المصفوفة [1 x 6] المتحصل عليها من الجدول (4) للحصول على مصفوفة [1 x n_i] حيث أن n_i هي عدد القطاعات في ركن التنمية (i). وبقسمة الناتج في كل صف على اجمالي الدرجات نتحصل على نسبة العلاقة s_{ij} ، حيث أن (j) تساوي من 1 إلى n_i ، وهي المطلوبة في المعادلة رقم (9) التي تقدر نسبة مساهمة تقنية المعلومات والاتصالات في التنمية بدلالة x_{ij} و I_D .

7 -في إطار تقدير نسبة مساهمة تقنية المعلومات والاتصالات في التنمية وفق

8 -المعادلة رقم (12) أو المعادلة رقم (9) يمكن افتراض قيمة لمعامل التنمية I_D وقيمة لمعامل تنمية كل قطاع x_{ij} وذلك لكل صنف من دول العالم كما هو موضح بالجدول (8) ومن تم يمكن الوصول إلى نسبة المساهمة المقدرة لكل صنف من الدول.

9 -يتطلب الأمر القيام باختبار النموذج بصورة مستمرة من خلال دراسات ميدانية وتجميع المعلومات والبيانات الفعلية من مختلف الدول بمختلف الوسائل وتعديل قيم معاملات النموذج بما يحقق التوافق بين نتائج النموذج ونتائج المعلومات الفعلية المجمعة.

مثال استرشادي:

لتطبيق المنهجية المشار إليها نفترض بأننا نسعى لتحديد نسبة مساهمة تقنية المعلومات والاتصالات في التنمية في كل من الدول المتقدمة (الأعلى نمواً) ذات معامل تنمية $I_D = 0.9$ ، والدول الساعية في طريق النمو ذات معامل تنمية $I_D = 0.4$ ، وأن معاملات تنمية قطاعات التنمية متساوية أي أن $X = X_{ij}$ في كل قيم i و j.

بإتباع خطوات المنهجية ثم الوصول إلى النتائج الأتية:

1. بإتباع الخطوة رقم (2) من المنهجية وملئ الجدول (3) تم الوصول إلى نسب مساهمة أركان التنمية في التنمية الوطنية كما يلي:

ركن التنمية	درجات المساهمة	نسبة مساهمة A_i
تنمية البنية الأساسية	54	$0.25 = A_1$
تنمية الأنشطة الصناعية والإنتاجية	52	$0.24 = A_2$
تنمية الأنشطة الخدمية	46	$0.2 = A_3$
تنمية الموارد البشرية	32	$0.15 = A_4$
تنمية الأعمال والأنشطة الداعمة	36	$0.16 = A_5$
الاجمالي	**220**	**1**

2. النتائج المتحصل عليها من الجدول (3) الخاصة بعلاقة أركان التنمية بمؤشرات التنمية هي كما يلي:

أركان التنمية	ارتفاع الناتج المحلي الاجمالي	ارتفاع مستوى المعيشة والرفاهية	ارتفاع مستوى جودة الخدمات	استغلال وتطوير الموارد والامكانيات	تحقيق الاستقلالية والاكتفاء الذاتي والاستمرارية	الشعور بالحرية والامان والانتماء
تنمية البنية الأساسية	M	H	H	M	L	M
تنمية الأنشطة الصناعية والإنتاجية	VH	VH	H	H	VH	H
تنمية الأنشطة الخدمية	VH	VH	VH	H	H	M
تنمية الموارد البشرية	M	H	VH	H	H	M
تنمية الأعمال والأنشطة الداعمة	L	M	M	M	L	VH

حيث تعبر الرموز على درجة العلاقة والتي تم تحديد قيمتها سابقاً.

3. النتائج التحصل عليها من الخطوة رقم (4) من المنهجية والخاصة بالعلاقة من مؤشرات التنمية وتقنية المعلومات والاتصالات هي:

مؤشرات التنمية	ارتفاع الناتج المحلي الاجمالي	ارتفاع مستوى المعيشة	استقلال وتطوير الموارد	ارتفاع مستوى الخدمات	تحقيق الاستقلالية والاستمرارية	الشعور بالحرية والامان والانتماء
تقنية المعلومات والاتصالات	VH	M	H	VH	M	M

4. للحصول على درجة العلاقة بين أركان التنمية وتقنية المعلومات والاتصالات تم إتباع الخطوة رقم (5) في المنهجية بضرب المصفوفتين الواردتين في رقم (2) ورقم (3) أعلاه وتم التوصل إلى الآتي:

أركان التنمية	درجة العلاقة مع تقنية المعلومات والاتصالات	نسبة درجة العلاقة δ_i
تنمية البنية الأساسية	300	$\delta_1 = 0.17$
تنميـــة الأنشـــطة الصـــناعية والإنتاجية	412	$\delta_2 = 0.24$
تنمية الأنشطة الخدمية	408	$\delta_3 = 0.24$
تنمية الموارد البشرية	356	$\delta_4 = 0.20$
تنميـــة الأعمـــال والأنشـــطة الداعمة	236	$\delta_5 = 0.15$
المجموع	1712	1

5. للحصول على نسبة مساهمة تقنية المعلومات والاتصالات في التنمية (δ) من خلال المعادلة رقم (12) نحصل على الآتي:

$$\delta = \frac{I_D^{'} - I_D}{I_D} = \sum_{i=1}^{5} A_i \delta_i I_i / I_D$$

بافتراض أن معاملات تنمية أركان التنمية متساوية أي أن $I = I_i$ لكل قيم (i) لذلك نحصل على:

$$\delta = \frac{I}{I_D} \sum_{i=1}^{5} A_i \delta_i$$

بالتعويض عن A_i و δ_i نحصل على

$$\delta = 0.16 \frac{I}{I_D}$$

لذلك نلاحظ إن نسبة مساهمة تقنية المعلومات والاتصالات في التنمية تساوي 0.16 مضروب في النسبة بين متوسط معاملات تنمية أركان التنمية I ومعامل التنمية الوطنية I_D .

أي أنه إذا افترضنا أن $I_D = I$ فإن نسبة مساهمة تقنية المعلومات والاتصالات في التنمية هي 0.16 أي 16% ، وتتزايد هذه النسبة كلما تزايدت النسبة $\frac{I}{I_D}$ وتتناقص بتناقصها. وتعتمد على الوضع الفعلي للدول المختلفة وفق تصنيفاتها من حيث التنمية ويمكن تقدير قيم I_i من خلال إتباع الخطوات رقم (3)، ورقم (6) في المنهجية.

الخلاصة:

تناولت هذه الورقة موضوعاً من المواضيع التي استحوذت اهتمام المنظمات والهيئات الدولية مثل الأمم المتحدة والاتحاد الدولي للاتصالات ومنظمة اليونسكو وغيرها، وهو موضوع قياس مساهمة تقنية المعلومات والاتصالات في التنمية الوطنية.

تعتبر هذه الورقة محاولة للوصول إلى نموذج رياضي لتقدير مدى مساهمة تقنية المعلومات والاتصالات في التنمية. وقد انطلقت الورقة ابتداءاً من وضع تصور لهيكلية التنمية وهيكلية تقنية المعلومات والاتصالات وأركانها الاساسية، إنطلاقاً من التأثيرات والعلاقات المستنبطة في دراسات سابقة. وقدمت تصوراً للعلاقات بين عناصر التنمية وعناصر تقنية المعلومات والاتصالات.

وبعدها اقترحت الورقة نموذجاً رياضيا لتقدير معامل التنمية الوطنية، ومعاملات تنمية الأركان الرئيسية للتنمية الوطنية، ومعاملات التنمية للقطاعات المختلفة. واقترحت الورقة كذلك منهجية لتحديد معاملات النموذج الرياضي وكيفية استخدامه.

تعتبر هذه الورقة إطاراً نظرياً تنطلق منه دراسات اخرى بهدف اثراء الموضوع واختبار النموذج الرياضي وتحسينه تدريجياً من خلال المعلومات الأساسية المتعلقة بعناصر التنمية وعناصر تقنية المعلومات والاتصالات التي يمكن الحصول عليها من الدول المختلفة وذلك من خلال الاستبيان والمعلومات المتاحة بالمنظمات الدولية ذات العلاقة.

وبتطبيق هذا النموذج الرياضي، نرى أنه سيساعد الدول في إعداد خططها التنموية وأولويها، كما سيساعد الدول والمنظمات المانحة في تحديد أولوية دعمها للمشاريع التنموية للدول المستفيدة.

المراجع:

1- "Conceptualizing the ICT artifact: towards understanding the role of ICT in national development". By maung k. Sein & G. Harindranath the information society 20, p15 – 24, 2004.

2- "The effect of ICT on economic growth: further evidence". Ebrahim Hosseini Nasab & Majid Aghaei
International bulletin of business administration, issue 5, 2009, Eurojournal Inc. 2009
www.eurojournals.com/IBBA.htm.

3- "A review of methodology for assessing ICT impact on development and Economic Transformation" , Samuel Wangwe, contribution to the AERC project on the impact of ICT on Economic development and transformation, July 2007.

4- "Measuring information society", WSIS, Tunis 15 Nov 2005. Partnership on measuring ICT for development.

5- "Core ICT indicators" partnership on measuring ICT for development 2005. http://measuring _ict.unetad.org.

6- ((Mobile telecommunication and economic growth)) , Leonard Waverman, Meloria Meschi & Melvyn Fuss, London Business School, LECG & University of Toronto.

7- ((The impact of ICT on economic performance)) Genevieve Ferand , Marta Perez Cuso. Electronic commerce branch.

8- Booz Allen Hamilton (2005) ICT sector development : Economic of social implication http://www.amcham.org.eg/publications/business monthly/ april%2005/ corporate clinic/ (abstract thought), asp.

9- The impact of ICT investment on economic development in Egypt, Sherif Kamal, Dina Rateb, Mohamed El-Tawil.
The electronic journal on information systems in developing countries 2009.

10- "The Economic impact of interoperability" by Lorenzo Madrid, Microsoft.

استخدام تقنيات معالجة الإشارة الرقمية في كشف و تصنيف و قياس اضطرابات جودة القدرة

باسل محمد سعيد basilms2007@yahoo.com
وائل هاشم حمدون waelhashem_67@yahoo.com
قسم الهندسة الكهربائية
العراق/ جامعة الموصل / كلية الهندسة

الملخص

يقدم هذا البحث دراسة لجودة القدرة الكهربائية (Power Quality) والمشكلات التي قد تحدث وتؤثر عليها من خلال استخدام Yاشارة جودة القدرة المتمثلة بإشارة الفولتية لمنظومة القدرة.إذ يتم إدخال هذه الإشارة الى الحاسبة الرقمية بعد تكييفها وإجراء التحليلات عليها باستخدام تقنيات معالجة الإشارة كتحويل فورير وتحويل الموجية والمقارنة مع التحليل لإشارة مرجعية مثالية خالية من الاضطرابات. لقد تبين من خلال البحث أن استخدام تحويل فورير كان كفوءاً في تحليل الإشارات التي تحتوي على تغيرات متكررة (Stationary Signals) كالإشارات التي تحتوي على التوافقيات أو الضوضاء اما استخدام تحويل الموجية فاظهر كفاءته في تحليل الإشارات التي تحتوي على تغيرات غير متكررة (Non-Stationary Signals) لما يتميز به من عدم فقد الزمن خلال التحليل. فقد تم الاستفادة من ذلك في كشف وتحديد موقع حدوث التغيرات كالحالات العابرة والتغيرات ذوات المدة القصيرة كالانخفاض (Sag) او الارتفاع (swell) او الانقطاع (Interruption) وباستخدام شبكة عصبية مدربة مسبقاً تم قياس قيمة الفولتية اثناء حدوث هذه التغيرات القصيرة. لقد أعطت النتائج تطابقاً وبالتالي يمكن الاعتماد على هذه الطريقة لتشخيص وتحديد نوع الاضطراب الحاصل لجودة القدرة الكهربائية.

1- المقدمة:

إن المتطلبات الرئيسة لمستهلك القدرة الكهربائية من اي مجهز لها هي ثبات قيمة الفولتية وقيمة التردد فضلاً عن كون شكل موجة القدرة الكهربائية جيبية خالصة لكن وبسبب الأحمال الكهربائية المتنوعة كدوائر السيطرة على المحركات ومجهزات القدرة ودوائر الكترونيات القدرة بصورة عامة إضافة إلى دوائر الفتح والغلق للأحمال الكبيرة وتعرض خطوط نقل القدرة الكهربائية للصواعق ودوائر القصر وغيرها فإن موجة القدرة الكهربائية ستتعرض إلى اضطرابات Disturbances مثل التشوهات Distortions أو الانقطاعات Interruptions أو الأحداث العابرة Transient Events. والشكل رقم (1) يوضح نموذج لموجات جودة قدرة كهربائية مضطربة.

إن الاضطرابات أعلاه قد تسبب قطع التجهيز أو فشل في تقديم المتطلبات الرئيسة للمستهلك وإعطاء إشارة خاطئة إلى دوائر الحماية بحدوث خطأ مما قد يسبب فصل قاطع الدورة وقد تؤدي الاضطرابات إلى حدوث أضرار بأحمال المستهلكين ، كذلك التأثير السلبي على كثير من الأحمال وخاصة الأحمال الحساسة منها إضافة إلى أنظمة الفولتية والنقل

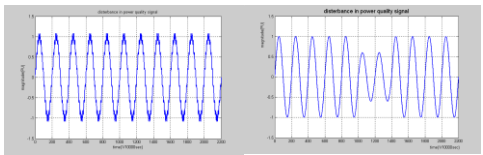

(ب) (ا)

شكل (1) نموذج لموجات جودة قدرة كهربائية مضطربة.

أ- انخفاض في القيمة. ب- تشوه شكل الموجة .

للأسباب السابقة كان من الضروري الحاجة إلى عرض شكل موجة القدرة الكهربائية Electrical Power Waveform Monitoring وجعلها إشارة رقمية لكي يتسنى لنا الكشف Detect والتحليل Analysis والتخمين Estimation والتصنيف Classification للاضطرابات الحاصلة في خط مجهز القدرة.

لقد أصبح عرض جودة القدرة باستخدام الحاسبة الرقمية ضروري للوقوف على نوعية وجودة القدرة الكهربائية لكل من المنتج والمستهلك للطاقة وبالتالي معالجة المشاكل التي تطرأ على جودة القدرة وضمن المعايير المسموح بها. إذ يتم عرض وقياس قيم تمثل متغيرات منظومة القدرة (فولتية ، تيار ، فرق طور ، ... الخ) وأخذ التغيرات المهمة للإشارة من خلال معالجة الإشارات الرقمية.[1]

ومن أهم التقنيات المستخدمة في معالجة الإشارات الرقمية Digital Signal Processing لتقييم وتحليل جودة القدرة الكهربائية هي تحويل فوريير Fourier Transform (FT) وتحويل المويجة Wavelet Transform (WT).[2]

لقد بدأ استخدام تحويل المويجة في مجال جودة القدرة الكهربائية نهاية التسعينات من القرن العشرين لقصور استخدام تحويل فوريير في تحديد موقع وزمن حصول الاضطرابات لموجة جودة القدرة حيث أن استخدام تحويل فوريير السريع ذو النافذة Windowed Fast Fourier Transform. لم يكن الحل المناسب والعملي لهذه المشكلة ، حيث قام الباحث G. T. Heydt (1999) [3] باستخدام هذا النوع من التحليل باختيار نافذة وتحريكها على طول محور الزمن وإيجاد تحويل فوريير لجزء من الإشارة بمقدار النافذة لكشف الاضطرابات في هذا الجزء وكانت الصعوبة في اختيار زمن هذه النافذة للاضطرابات المتعددة ، حيث أن زمن بعض الاضطرابات يكون أكبر من زمن النافذة المختارة أو أقل ، فالصعوبة كانت في اختيار زمن النافذة. وقد قام الباحثان L-Angrisani (1998) و P. Daponte [4] باستعمال تحويل المويجة لتحليل الجودة لأنظمة القدرة الكهربائية حيث ركزا على استخدام تحويل المويجة المتصل (Continuous WT) كما استخدم الباحث A. M. Gaouda (1999) وفريقه [5] تحويل المويجة وتحليل الإشارة متعدد التفاصيل في

حوادث جودة القدرة الكهربائية واستخدم القيمة العظمى للانحراف المعياري (Max. Standard Deviation.) لكشف وتصنيف هذه الحوادث. ومن الاعمال التي سبقت هذا البحث إيجاد برنامج بواسطة البرمجة بلغة الماتلاب يقوم باستخدام تقنية تحويل المويجة في كشف وتصنيف اضطرابات جودة القدرة وقد تبين دقة هذه الطريقة في تشخيص وتصنيف اضطرابات جودة القدرة Basil M. Saied, Wael H. Hamdoon (2007) [6].

في هذا البحث سنتطرق أولاً للتعريف بتقنيات معالجة الإشارة المستخدمة وعرض وتمثيل للخطوات التي اتبعت لكشف وتصنيف بعض اضطرابات جودة القدرة الكهربائية وبعد ذلك تم تقديم ما أستنتج في هذا البحث.

2- التقنيات المستخدمة لتحليل الإشارات (تحويل المويجة وتحويل فوريير) :

إن تحويل فوريير يقوم بتحويل الإشارة إلى عدة مستويات اعتمادا على ما تحويه هذه الإشارة من ترددات مختلفة وممكن التعبير عن تحويل فوريير بشكل آخر على أنه تقنية حسابية لتحويل الإشارة من حيز الزمن إلى حيز التردد. حيث يستخدم الدوال الجيبية كدوال أساسية في تحليل الإشارات وهي مهمة جداً في معرفة ما تحويه الإشارة من ترددات[7].

$$F(\omega)=\int_{-\infty}^{\infty} f(t)\,e^{-j\omega t}\,dt \quad \ldots (1)$$

حيث أن f(t) هي الإشارة في حيز الزمن و F(ω) هي الإشارة في حيز التردد.

ومن الملاحظ أن الإشارة بعد تحليلها بتحويل فوريير لا يحدد زمن وقوع الحدث ولهذا يستخدم تحويل فوريير في الحالات المستقرة المتكررة Periodic Steady State ، أو ما يسمى Stationary Signals. أما في حالات الإشارات التي تحوي على حالات وقتية عابرة (Transitory) أو ما يسمى Non-Stationary Signals فإن تحويل فوريير يكون غير مناسب للتحليل.

ولمعالجة المشكلة أعلاه قام العالم (Gabar) بتجزئة الإشارة إلى نوافذ Windows. وبعد تحليل الإشارة في كل نافذة على حده ، قام بتحويل الإشارة إلى دالة ذات بعدين (Two Dimension) زمن وتردد وهو ما يسمى بـ Windowed F.T أو تحويل فوريير ذو الزمن القصير Short Time FT (STFT). وبهذه الطريقة تم معرفة متى وقع التغيير أو التشوه بالإشارة وما تحويه من ترددات في هذه النافذة. ولكن صعوبة هذه الطريقة كما بُيِّن سابقاً هي كيفية اختيار زمن النافذة المناسب لما يحدث في الإشارة من حوادث.

للأسباب أعلاه كان الحل بتحويل المويجة Wavelet Transform حيث أنه يأخذ تغيير واسع لحجم النافذة. إن تحليل المويجة يستخدم نافذة واسعة عندما يراد معلومات دقيقة عن الترددات المنخفضة ونافذة ضيقة عندما يطلب معلومات دقيقة عن الترددات العالية في الإشارة. والشكل رقم (2) يوضح التقنيات أعلاه [8].

مع ملاحظة أن تحليل المويجة لا يستعمل حيز الزمن - التردد (Time- Frequency) ولكنه يستخدم حيز الزمن - الاتساع (Scale - Time)مع ملاحظة أن الاتساع (Scale) يتناسب عكسياً مع التردد (Frequency) وإن من أهم الميزات الرئيسة لتحليل المويجة هي الحصول على تحليل موقعي مع تحديد موقع حدوث التغيير في الإشارة.

لقد سمي هذا التحليل بتحليل الموجية لكونه يستخدم مويجات مختلفة كدوال أساس في التحليل في المستويات المختلفة.إن الموجات الجيبية تكون غير محدودة المدة أي أنها تمتد من $-\infty \leftarrow +\infty$ وذات طبيعة ناعمة التغيير في حين أن المويجة لها مدة محددة يعتمد على مقياس الاتساع (Scale). وذات طبيعة غير جيبية وغير متماثلة وقد تحوي على تغييرات حادة مما يجعلها أكثر ملائمة لهذا النوع من التطبيق ـ لذا سيتم التركيز على أنواع تحويل المويجة.

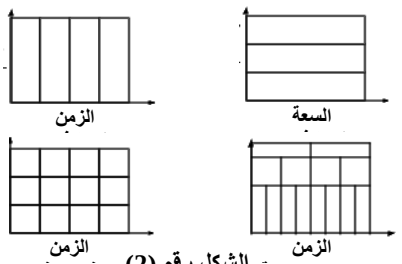

الشكل رقم (2)
التقنيات المستخدمة لمعالجة الإشارة

3- صيغ التحويل المويجي :

1-3 تحويل المويجة المستمر Continuous WT :

يقوم هذا التحويل بتجزئة الإشارة إلى ما لا نهاية من المويجات (المويجة الأم) كدوال للموقع Position والاتساع Scale.

لو كانت $\psi_{a,b}(t)$ تمثل الدالة الأساس للمويجة والمعرفة بمتغيرين هما a,b والتي يمكن التعبير عنها رياضياً كما يأتي :

$$\psi_{a,b}(t)=\frac{1}{\sqrt{|a|}}\,\psi\left(\frac{t-b}{a}\right) \qquad \dots (2)$$

حيث أن a يسمى بعامل التعيير أو التوسيع (Scale Factor or Dilation Parameter) في حين b يمثل الموقع الزمني لدالة المويجة.

يعرف تحويل المويجة المستمر على أنه الضرب الداخلي للإشارة f(t) مع الدالة الأساس للمويجة (المويجة الأم) :

$$WT(a,b)=<f,\psi_{a,b}>=\frac{1}{\sqrt{|a|}}\int_{-\infty}^{\infty} f(t)\,\psi^{*}\left(\frac{t-b}{a}\right)dt \qquad (3)$$

حيث أن $(a\neq 0)$ و $a,b \in R$ ويشير * إلى المرافق المركب Complex Conjugate.

R: تمثل مدى الأعداد الحقيقية [9].

2-3 تحويل المويجة المقطع Discrete WT:

أية إشارة ممكن التعبير عنها بأنها مجموعة من معاملات المويجة التي نحصل عليها من تحويل المويجة المقطع. حيث أن تحويل المويجة المقطع يتعامل مع عينات Samples من الإشارة f(t) أي تكون الدالة مقطعة f(k) كما تكون قواعد التحويل بشكل مقطع أيضاً.

لو كان لدينا إشارة f(t) ينتمي إلى فضاء العينة $L^2(R)$ فإنه ممكن التعبير عنها بدلالة دالتي المويجة Wavelet Function $\psi(t)$ والتوسيع Scaling Function $\phi(t)$ كما يأتي :

$$f(t)=\sum_k C_{j_0}(k)\,\phi(t-k)+\sum_k\sum_j d_j(k)\,2^{-j/2}\,\psi\left(2^{-j}t-k\right) \qquad (4)$$

$$f(t)=\sum_k C_{j_0}(k)\,2^{-j_0/2}\,\phi\left(2^{-j_0}t-k\right)+\sum_k\sum_{j=j_0}^{J-1} d_j(k)\,2^{-j/2}\,\psi\left(2^{-j}t-k\right) \qquad (5)$$

حيث أن C_{jo} معامل التوسيع (Scaling Coefficient) عند المستوى o.

و d_j معامل المويجة (التفصيل) (Detail) عند j.

حيث أن j = 1 أو 2 أو 3 أو .... يمثل مختلف مديات التردد للموجة من التردد الأعلى إلى الأقل و k هو معامل الانتقال Translation Coefficient.

و j_o ممكن أن تكون أي قيمة حقيقية.

يمكن كتابة الدوال الأساس بالشكل الآتي :

$$\phi_{j,k} = 2^{-j/2}\ \phi\left(2^{-j}\, n - k\right) \qquad \ldots (6)$$

$$\psi_{j,k} = 2^{-j/2}\ \psi\left(2^{-j}\, n - k\right) \qquad \ldots (7)$$

يعتبر تحويل المويجة المقطع DWT النوع المناسب من أنواع تحويل المويجة القابل للتطبيق على الحاسبة الرقمية حيث أنه يتعامل مع قيم مقطعة ولا يحوي على عمليات تكامل أو اشتقاق بل عبارة عن عمليات جمع وضرب كما أن هذا النوع يلائم بشكل كبير التطبيقات الهندسية والنتائج العملية المتعاملة مع القيم المقطعة وليس الدوال الأصلية المستمرة[10].

4- <u>التحليل متعدد التفاصيل Multiresolution Analysis(MRA) :</u>

وهو نوع من تحويل المويجة المقطع حيث أنه في التحليل متعدد التفاصيل فإن دوال المويجة ودوال التوسيع يستخدم لبناء منظومة لتحليل وتركيب الإشارة بمستويات تفصيلية متعددة. إن دالة المويجة (ψ) ستولد جزء التفصيل Detail للإشارة المحللة أما دالة التوسيع (ϕ) سوف تولد جزء التقريب Approximate للإشارة المحللة. ويمكن التعبير عن ذلك رياضياً وكما يأتي [11] :

$$f(t) = \sum_k C_{j_o}(k)\,\phi(t-k) + \sum_k \sum_{j=j_o}^{J-1} d_j(k)\, 2^{-j/2}\ \psi\left(2^{-j}\, t - k\right) \qquad (8)$$

ومن أهم الخصائص للتحليل متعدد التفاصيل هي خاصية تحديد الموقع Localization لزمن حدوث أية حالة عابرة في الإشارة المحللة وهو ما سنلاحظه في الفقرة اللاحقة أما الخاصية الأخرى فإن تجزئة الإشارة إلى عدة مستويات (Levels) وبالتالي فإن الطاقة للإشارة سوف تتوزع على هذه المستويات وبمديات تردد محددة ومن معرفة مقدار الطاقة للإشارة ومقارنته مع إشارة خالصة فإننا نستطيع حساب ما تحويه الإشارة من ترددات وكذلك لتصنيف أحداث هذه الإشارة.

5 . الشبكة العصبية الاصطناعية: (Artificial Neural Network ANN):

تعرف على انها مجموعة القواعد والأساليب المتعلقة بنظم معالجة البيانات المكيفة وغير المبرمجة. وفي هذا البحث كانت تركيبة الشبكة العصبية المستخدمة كم يأتي:

- ❖ نوع التغذية : لقد تم اختيار تركيبة التغذية الأمامية .
- ❖ تحديد عدد طبقات الـ ANN: استخدمت شبكة من ثلاث طبقات هي الادخال والاخراج والطبقة المخفية وكان عدد عقد طبقة الإدخال عقدتان وعدد عقد الطبقة المخفية مساويا لـ (عشرين عقدة) أما عقد طبقة الإخراج فكانت مساوية للواحد.
- ❖ تحديد نوع دالة التحويل (Transfer Function): استخدام دالتي (tansig , purelin) بوصفها دوال تنشيط للطبقة المخفية وطبقة الإخراج على التوالي.
- ❖ تحضير جدول لحالات الإدخالات والاخراجات المختلفة .
- ❖ اختيار الخوارزمية المناسبة لإجراء عملية التدريب (Training) وحسب طبيعة التطبيق تم اختيار خوارزمية (Supervised) وفيها نستخدم تقنية

الانتشار العكسي (Back propagation N.N).

تدريب المنظومة أو الشبكة من خلال استخدام الطريقة السابقة وذلك بإدخال مصفوفة الإدخال المتمثلة بقيم كل من المدة الزمنية التي استغرقها الاضطراب الحاصل بإشارة فولتية منظومة القدرة وقيمة الفرق بالانحراف المعياري للمستوى السابع لتحليل هذه الإشارة. ومصفوفة الهدف(Target) المُمَثلة بالقيمة للإشارة المحللة خلال مدة الاضطراب. تم الحصول على جدول الإدخالات والاخراجات من خلال توليد نماذج متعددة لإشارات فيها تغير في قيمة الفولتية نسبة إلى قيمتها المقننة (ارتفاع أو انخفاض) وكذلك تغير المدة الزمنية التي يستغرقها الاضطراب لكل تغير في القيمة. إذ تم توليد (960) إشارة تمثل الحالات المحتملة. حللت الإشارات المولدة بواسطة برنامج تقييم وقياس جودة القدرة وسجلت قيم الفرق بالانحراف المعياري لمستوى التحليل السابع لكل حالة تغير. اصبحت منظومة الشبكة العصبية جاهزة لغرض استخدامها في قياس قيمة فولتية منظومة القدرة اثناء حدوث التغيرات ذوات المدة القصيرة. والشكل رقم (3) يوضح تركيبة الشبكة العصبية المستخدمة.

6- خطوات البحث :

استخدمت البرمجة بلغة الماتلاب في ايجاد برنامج يحقق الخطوات التالية لأجل كشف وتحديد موقع وتصنيف وقياس اضطرابات جودة القدرة.

1. توليد نموذج لإشارة جودة قدرة كهربائية بتردد عينة 8192 Hz وعدد عينات 8192. (أو استخدام اشارات عملية حقيقية لفولتية منظومة القدرة بعد تكييفها وادخالها الى الحاسبة كإشارة رقمية عن طريق كارت اكتساب البيانات (Data Acquisition Card)).
2. قراءة قيم الانحراف المعياري Standard Deviation لجميع تفاصيل الإشارة الجيبية الخالصة (1 P.U., 50 Hz) والمحللة مسبقاً إلى اثني عشر مستوى بالتحليل متعدد التفاصيل (Std pure n) حيث أن n هو مستوى التحليل = n = 1, 2 .. 12.
3. تحليل الإشارة الداخلة باستخدام تحويل الموجية المقطع متعدد التفاصيل إلى اثني عشر مستوى وحساب قيمة الانحراف المعياري لجزء التفصيل (Detail) لكل المستويات (Std sig n).
4. إيجاد قيمة الفرق بين القيمة المقروءة للانحراف المعياري لموجة جيبية خالصة مع القيمة المحسوبة للإشارة الداخلة لتفصيل كل مستوى بمفرده ($\Delta Std\ n = Std\ sig\ n - Std\ pure\ n$).
5. مقارنة أعلى قيمة للفرق $\Delta Std\ n$ مع عتبة محددة

$$Max\ |\Delta Std\ n\ | > Thr$$

Thr: قيمة العتبة (threshold) تم تحديدها من خلال تحليل اشارة فولتية مقبولة ضمن الحدود المسموح بها عالمياً [12]. فاذا كانت قيمة الفرق أعلاه اقل من قيمة العتبة فان الإشارة المحللة تكون مقبولة وضمن الحدود المسموح بها (خالية من الاضطرابات) ويتوقف البرنامج. اما اذا تجاوزت قيمة العتبة فذلك يدل على **كشف** لحالة اضطراب في الإشارة المحللة.

6. عرض شكل إشارة التفصيل للمستوى الأول (d1) من عملية التحليل **لتحديد موقع ومدة** حدوث الاضطراب (**Duration (D)**).

7. عرض شكل قيم الفرق بقيم الانحراف المعياري ΔStd n مع مستويات التحليل.(اعتماداً على موقع أعلى قيمة للفرق ΔStd n وفي أي مستوى حدث يتم **تصنيف** اضطرابات جودة القدرة بالاعتماد على الجدول رقم (1)).

الجدول رقم (1): يوضح مديات التردد لمستويات التحليل متعدد التفاصيل ولتردد عينة 8192 Hz

مستوى التحليل(n)	مدى التردد Hz	مستوى التحليل(n)	مدى التردد Hz
الأول	2048→4096	السابع	32→64
الثاني	1024→2048	الثامن	16→32
الثالث	512→1024	التاسع	8→16
الرابع	256→512	العاشر	4→8
الخامس	128→256	الحادي عشر	2→4
السادس	64→128	الثاني عشر	1→2

8. مقارنة كل من قيم الفرق بالانحراف المعياري لتفاصيل مستويات التحليل مع عتبات محددة هي القيمة المسموح بها للاضطراب بذلك المدى من الترددات وفي حالة تجاوز هذه العتبة في أي مستوى سيتم طبع إن الإشارة المحللة تحوي على ترددات بمقدار مدى التردد لذلك المستوى.

9. إذا كانت أعلى قيمة للفرق في المستوى السابع Max ΔStd n = ΔStd 7 وكانت القيمة موجبة فان الاضطراب ناتج عن ارتفاع في قيمة الفولتية (swell) اما اذا كانت سالبة فان الاضطراب ناتج عن انخفاض في قيمة الفولتية (sag).

10. لأجل **قياس** قيمة الانخفاض أو الارتفاع خلال مدة الاضطراب يتم إدخال مدة الاضطراب (D) وقيمة الفرق بالانحراف المعياري للمستوى السابع ΔStd 7 إلى شبكة عصبية اصطناعية مدربة مسبقا إذ يكون خرجها قيمة اشارة الفولتية خلال مدة الاضطراب نسبة الى القيمة المقننة وكما مبين لاحقاً.

11. إذا كانت أعلى قيمة للفرق ليس بالمستوى السابع

$$\text{Max } \Delta\text{Std n} \neq \Delta\text{Std 7}$$

وكانت المدة الزمنية للاضطراب (D) بمقدار النافذة للإشارة المحللة. فيتم تحليل الإشارة باستخدام تحويل فورير السريع وإيجاد محلل الطيف لها ومن ثم حساب القيمة الكلية للتشوه بالتوافقيات (total Harmonic Distortion (THD)).

7. عرض النتائج:

استخدم برنامج تقييم وقياس جودة القدرة الكهربائية في كشف وتحديد موقع والمدة الزمنية التي استغرقها اضطراب جودة القدرة إن وجد ومن ثم قياس قيمة فولتية منظومة القدرة اثناء الاضطراب في حالة حدوث التغيرات ذوات المدة القصيرة كالانخفاض أو الارتفاع بعد تحليل نماذج لإشارات مولدة تمثل إشارات فولتية منظومة القدرة, إذ تم توليد عدد كبير من نماذج الإشارات التي تحتوي على اضطرابات متنوعة. سيتم عرض نموذجين من الاضطرابات التي قد تحصل على إشارات جودة القدرة.

1. **انخفاض الفولتية** ولمدة قصيرة (أقل من ثانية واحدة) وهو ما يطلق عليه مصطلح **(Sag)**. الشكل (4) يمثل التحليل لإشارة جودة قدرة كهربائية ناتجة عن انخفاض قيمة الفولتية. يلاحظ من (b) أنه هناك اضطراب في جودة القدرة يبدأ من x1 وينتهي بـ x2 إذ يتم تحديد مدة الاضطراب (D) من إيجاد الفرق بين x1 و x2 ومن (c) نلاحظ أن أعلى قيمة للفرق بقيم الانحراف المعياري كان في مستوى التحليل السابع وقيمته سالبة يعني أن تصنيف هذا الاضطراب هو انخفاض قيمة الفولتية.ومن إدخال مدة الاضطراب وقيمة الفرق بالانحراف المعياري لمستوى التحليل السابع إلى الشبكة العصبية يتم معرفة قيمة الفولتية خلال مدة الاضطراب نسبة إلى القيمة المقننة.

2. **تشوه إشارة الفولتية بالتوافقيات** الشكل (5) يمثل التحليل لإشارة جودة قدرة كهربائية مشوهة بالتوافقيات (Harmonics). يلاحظ من (b) أن هنالك كشف لحالات تغير متكررة في الإشارة المحللة. وبالمقابل يلاحظ من الجزء (c) أن أعلى قيمة للفرق بقيم الانحراف المعياري كان في مستوى التحليل الرابع والخامس ومن معرفة مدى التردد لتلك المستويات يمكن الاستنتاج أن تصنيف هذا الاضطراب تشوه إشارة فولتية منظومة القدرة بالتوافقيات التي يكون ترددها ضمن مديات التردد لتلك المستويات. ولكون أعلى قيمة للفرق كانت في المستوى الخامس ومدة الاضطراب بمقدار النافذة للإشارة المحللة فقد تم تحليل الإشارة بتحويل فورير السريع وكما مبين في الشكل (6). إذ أن الجزء (a) يمثل الإشارة المحللة والجزء (b) يمثل محلل الطيف لها. يتضح من الشكل احتواء الإشارة على تردد (150 Hz) وهو تردد التوافقية الثالثة بقيم (26- db) أي ما يعادل (5 %) من قيمة المركبة الأساسية. وكذلك على التردد (250 Hz) وهو تردد التوافقية الخامسة بقيمة (40- db) أي ما يعادل (1 %) من قيمة المركبة الأساسية. وتردد (350 Hz) وهو تردد التوافقية السابعة بقيمة (40- db) أي ما يعادل (1 %) من قيمة المركبة الأساسية وتردد (450 Hz)وهو تردد التوافقية التاسعة بقيمة (34- db) أي ما يعادل (2 %) من قيمة المركبة الأساسية وتردد (750 Hz) وهو تردد التوافقية الخامسة عشرة بقيمة(46- db) أي ما يعادل (0.5 %) من قيمة المركبة الأساسية. وتم حساب القيمة الكلية للتشوه بالتوافقيات (THD) وكانت (5.5736 %).

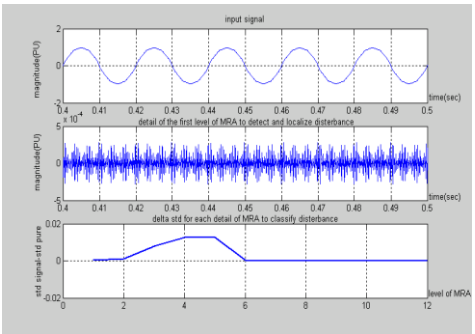

الشكل (5) : يمثل التحليل لإشارة فولتية مشوهة

8. الاستنتاج:

لقد تبين من خلال البحث ما يأتي:

1. ملاءمة استخدام تحويل فورير السريع في تحليل إشارات جودة القدرة التي تحتوي على تغيرات متكررة مستمرة كاحتواء الإشارة على الضوضاء أو تشوهها بالتوافقيات.

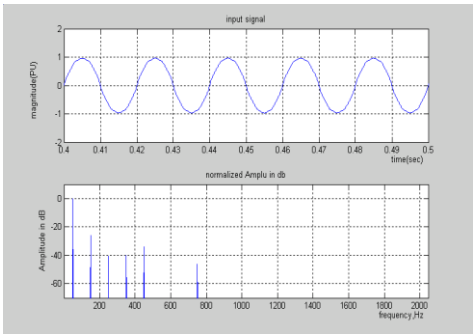

الشكل (6) : يمثل شكل طيف إشارة فولتية مشوهة

2. ملاءمة استخدام تحويل المويجة في تحليل إشارات جودة القدرة التي تحتوي على تغيرات غير متكررة كالحالات العابرة أو التغيرات ذوات المدة القصيرة كالانخفاض في قيمة الفولتية (Sag) أو الارتفاع في قيمة الفولتية (Swell) أو تقطع التجهيز(Interruption) وذلك لعدم فقد الزمن خلال التحليل مما يساعد في تحديد الموقع الزمني لبدء التغييرات التي تحدث على جودة القدرة ومدة حدوثها.

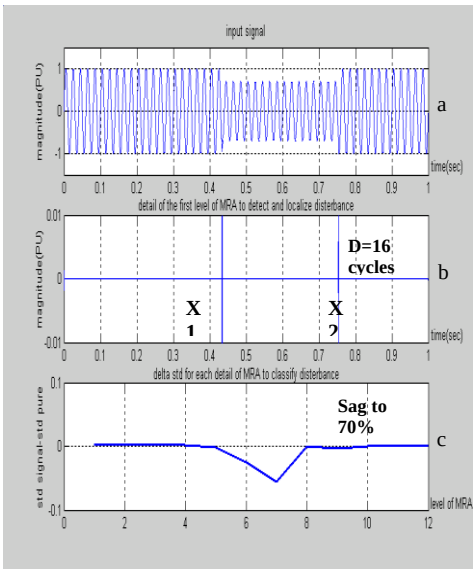

الشكل (4) :يمثل التحليل لإشارة ناتجة عن انخفاض فى قيمة الفولتية (Sag) .

3. ملاءمة استخدام التحليلات الإحصائية للبيانات المستحصلة من عملية التحليل . إذ استخدم في هذا البحث الانحراف المعياري أساساً لتصنيف الاضطرابات الناتجة عن التغيرات المختلفة في إشارات جودة القدرة.

4. ملاءمة استخدام تقنيات الذكاء الصناعي كالشبكات العصبية الاصطناعية في معالجة بعض البيانات لمستحصلة من تحليل الإشارة بتحويل المويجة متعدد التفاصيل.

5. استخدام إشارات التفاصيل لمستويات التحليل المختلفة في تصنيف الاضطرابات التي تحدث على إشارة فولتية منظومة القدرة وذلك بالاعتماد على مديات التردد لتلك المستويات والمعتمدة على تردد العينة.

9. المصادر:

1. Ying-Yi Hong, Cheng-Wei Wang, "Switching Detection / Classification Using Discrete Wavelet Transform and Self-Organizing Mapping Network", IEEE Transactions on Power Delivery, Vol. 20, No. 2, April 2005.
2. Mohammad S. Azam, "A Dependency Model-Based Approach for Identifying and Evaluating Power Quality Problems", IEEE Transactions on Power Delivery, Vol. 19, No. 3, July 2004.
3. G. T. Heydt, P. S. Fjeld, "Applications of the Windowed FFT to Electric Power Quality Assessment", IEEE Transactions on Power Delivery, Vol. 14, No. 4, October 1999.

Duration Variations in Distribution Systems", IEEE Transactions on Power Delivery, Vol. 15, No. 2, April 2000.

12 Group on Monitoring Electrical Power Electrical, IEEE Std 1159-1995, "IEEE Recommended Practice for Monitoring Electric Power Quality".

4. L. Angrisani, P. Daponte, "A Measurement Method Based on the Wavelet Transform for Power Quality Analysis", IEEE Transactions on Power Delivery, Vol. 13, No. 4, October 1998.
5. A. M. Gaouda, M. M. A. Salama, "Power Quality Detection and Classification Using Wavelet-Multiresolution Signal Decomposition", IEEE Transactions on Power Delivery, Vol. 14, No. 4, October 1999.
6. Basil M. Saied, Wael H. Hamdoon,"Using Wavelet Transform Technique to Detect and Classify Power Quality Disturbances", Al-Rafidain Engineering Proceeding, (VOL.16, No. 1, Year 2008).
7. Michel Misiti Yevs Misiti, "Wavelet Toolbox for Use with MATLAB", User Guide, 1996.
8. Olivier Poisson, "Detection and Measurement of Power Quality Disturbances Using Wavelet Transform", IEEE Transactions on Power Delivery, Vol. 15, No. 3, July 2000.

9. وائل هاشم حمدون, "قياس جودة القدرة الكهربائية باستخدام تقنية تحويل المويجة", رسالة ماجستير تموز 2007, كلية الهندسة جامعة الموصل.

10. فراس محمود مصطفى ، "مرشحات المويجة وتطبيقاتها في إزالة الضوضاء من الصور " ، رسالة ماجستير ، تشرين الأول 1999 ، جامعة الموصل.

11 .A. M. Gaouda, M. M. A. Salama, "Application of Multiresolution Signal Decomposition for Monitoring Short